A.J. RINGROSE-VOASE AND G.S. HUMPHREYS
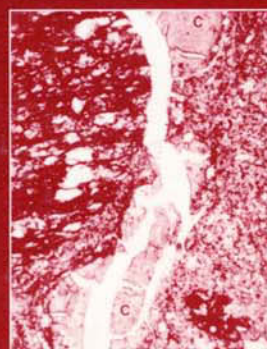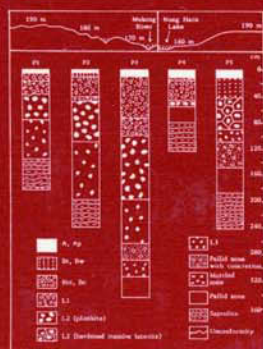
SOIL
MICROMORPHOLOGY:
STUDIES IN MANAGEMENT AND GENESIS

DEVELOPMENTS IN SOIL SCIENCE 22

SOIL MICROMORPHOLOGY:

STUDIES IN MANAGEMENT AND GENESIS

Further Titles in this Series

SOIL MICROMORPOHLOGY:

STUDIES IN MANAGEMENT AND GENESIS

Edited by

A.J. RINGROSE-VOASE

CSIRO Division of Soils, GPO Box 639, Canberra, ACT 2601, Australia

G.S. HUMPHREYS

Research School of Pacific and Asian Studies, The Australian National University, Canberra, ACT 0200, Australia

Proceedings of the IX International Working Meeting on Soil Micromorphology, Townsville, Australia, July 1992

Sub-Commission of Soil Micromorphology International Society of Soil Science

IWMSM-92 Sponsors

International Society of Soil Science
Australian Society of Soil Science
CSIRO Division of Soils
AIDAB (Australian International Development Assistance Bureau)
QANTAS Airways Ltd
Westpac Banking Corporation

Organizing Committee

Chairman	C.J. Chartres	CSIRO Division of Soils
Secretary	A.J. Ringrose-Voase	CSIRO Division of Soils
Programme and Editoral	A.J. Ringrose-Voase	CSIRO Division of Soils
	G.S. Humphreys	Australian National University
Treasurer	I. Salins	CSIRO Division of Soils
Local Arrangements	H.E. Rodd	CSIRO Division of Soils
AIDAB Sponsorship	G.M. Bowman	CSIRO Division of Soils
Field Trips	R.F. Isbell	CSIRO Division of Soils
	R.J. Coventry	CSIRO Division of Soils
	R.S.B. Greene	CSIRO Division of Wildlife & Ecology
	R.J. Gilkes	University of Western Australia

IWMSM 1992
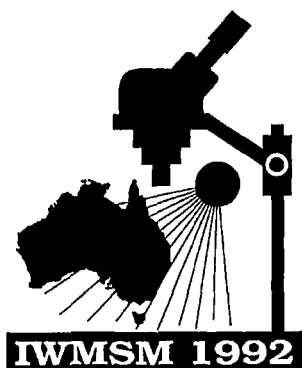
This Page Intentionally Left Blank

Preface

This volume contains refereed papers presented at the IX International Working Meeting on Soil Micromorphology organised under the auspices of Subcommission B of the International Society of Soil Science. The meeting was held in July 1992 in Townsville, Queensland, Australia and was the first meeting of the subcommission to be held not only in the southern hemisphere, but also in a tropical environment. That this was the first meeting of the Subcommission to be held in Australia was also surprising, given the major contribution of Roy Brewer and Jim Sleeman to the development of the discipline over the last 40 years.

In the years since Brewer's seminal work on micromorphological description and terminology (Brewer, 1964) micromorphology has seen several significant advances. Whilst much of the early work was conducted in Europe by Kubiena and his colleagues and then in Australia by Brewer and others, micromorphology was also adopted as a significant pedological tool in the USA and Canada as detailed by Wilding (1990) in the preface to the proceedings of the VIII International Working Meeting. During the last two decades there has been a shift in emphasis of much micromorphological research, with a move away from developing guidelines for description and classification of microstructure, fabric and pedological features towards applications of micromorphology. These applications cover a considerable range of pure and applied research endeavour and applications ranging from pedogenesis to engineering. This shift in emphasis is apparent in the present volume, which contains sections focusing on the contribution of micromorphology to studies on soil genesis, paleosols, soil biota, soil structural measurement, soil management and crusted and indurated soils.

In my view, whilst we will still need to update nomenclature from time-to-time, the increasing emphasis on micromorphological applications is very timely. It will help demonstrate to both scientific colleagues and to users of scientific information that micromorphology is a dynamic discipline which can help provide answers to some of the major environmental, engineering and scientific challenges facing the world today. Applications documenting soil structural changes following cultivation or other land use practices, water flow pathways in the soil and underlying rocks and microelement and pollutant contamination issues are just some of the areas in which micromorphological and electron microscope techniques can contribute to solving specific problems. With the increasing use of powerful computing and image analysis techniques further opportunities exist to shed new light on both these new problems and older issues relating to weathering and soil genesis.

As current Chairman of the Subcommission and in my role of Chairman of the Organising Committee of IWMSM 92, there are several agencies and people who are owed thanks for their assistance with sponsorship and conference planning and management. These include the Australian International Development Assistance Bureau, whose generous sponsorship enabled several scientists from developing tropical countries to attend the meeting and present their work. I also owe a large debt of thanks to all the meeting organising committee in both

Townsville and Canberra and in particular to the editors of this volume, Anthony Ringrose-Voase and Geoff Humphreys, who have turned out a polished product. I would also like to thank Ethel Ringrose-Voase and Claudia Camarotto for assistance with final manuscript preparation and all who reviewed manuscripts.

Colin J. Chartres
Canberra, March 1994.

REFERENCES

Brewer, R., 1964. Fabric and Mineral Analysis of Soils. John Wiley and Sons, New York.

Wilding, L.P. 1994. Preface. In: L.A. Douglas (Editor), Soil Micromorphology: A Basic and Applied Science. Proc. VIII Int. Working Meeting on Soil Mircromorphology, San Antonio, Texas, July 1988. Developments in Soil Science 19, Elsevier, Amsterdam, pp. VII-X.

Contents

(Titles in bold type are review papers)

SOIL STRUCTURE

Quantification

Physical processes

SOIL MANAGEMENT

SURFACE CRUSTS

HARDPANS AND CEMENTED LAYERS

Micromorphology of soils of the humid tropics[*]

G. Stoops[1], V. Marcelino[1], S. Zauyah[2] and A. Maas[3]
[1]Universiteit Gent, Belgium
[2]Universiti Pertanian Malaysia
[3]Universitas Gadjah Mada, Yogyakarta, Indonesia

ABSTRACT

Stoops, G., Marcelino, V., Zauyah, S. and Maas, A., 1994. Micromorphology of soils of the humid tropics. In: A.J. Ringrose-Voase and G.S. Humphreys (Editors), Soil Micromorphology: Studies in Management and Genesis. Proc. IX Int. Working Meeting on Soil Micromorphology, Townsville, Australia, July 1992. Developments in Soil Science 22, Elsevier, Amsterdam, pp. 1-15.

Apart from volcanic or tectonically rejuvenated areas, most soils of the humid tropics are formed on materials preweathered during earlier geological periods. The characteristics of these soils are determined mainly by the type and degree of weathering, the depth of the subsequent erosion and the present position in the landscape. On the basis of three soil sequences the relationship between the micromorphological characteristics of parent material, saprolite, eluvial, colluvial and alluvial soils is discussed, as well as the genesis of the soil material (pedoplasmation) and subsequent changes.

The first sequence is situated in Rwanda and illustrates soil formation in pre-weathered material and in its erosion products. The second sequence is a typical example of a recent incision of an old erosion surface in Zaire; the last sequence, from Indonesia, illustrates the influence of the degree of weathering in volcanic ash soils.

Where possible, soils from the tropics (*e.g.* podzols, andosols) are compared in terms of their micromorphological characteristics with equivalent soils of temperate regions in order to deduce their differentiating characteristics.

INTRODUCTION

In the tropical belt a wide range of climatological, geological and geomorphological situations can be found, including humid, semi-arid and arid environments as well as mountainous areas. This paper deals only with the micromorphological characteristics of lowland soils in the humid tropics.

A review of the micromorphological literature of the last decade shows that few new relevant research results on tropical soils have been published in international journals, except for petrographic studies on weathering and laterites (*e.g.* Nahon, 1991)

The typical characteristics of most tropical soils are not only related to the hot and humid climate in which they occur, but also to the geomorphological history of these areas. Soils of

the humid tropics   occur mainly on old geomorphological surfaces, or are developed in materials derived from their erosion, thus in both cases from a pre-weathered material. Therefore the characteristics of most typical tropical soils (*e.g.* Oxisols and Ultisols) are determined rather by the nature of the saprolite than by the present climate and the parent material. By contrast, in the temperate areas geomorphology is strongly influenced by the different glaciations during the Quaternary: most old surfaces have disappeared or were covered by loess or glacial material. As a result the present surface is formed mainly of fresh rock or recent erosion products and/or glacial loess, derived from the physical disintegration of fresh rocks. Moreover, weathering is relatively slow in these regions, and the soils are forming in fairly fresh material during the first cycle of chemical weathering.

The difference between tropical and temperate areas is further enhanced by the fact that in many cases the geological history is quite different for a large part of the humid tropics and is situated on old continental shields (*e.g.* Central Africa, Brazil, Australia), which were not influenced by the Alpine orogeny. As a consequence much older surfaces are preserved in the tropics and therefore older saprolites too.

Although those soils of the humid tropics that are not formed on pre-weathered materials, such as those found in the mountains or on Holocene volcanic ashes, have more characteristics in common with the soils of temperate regions, they nevertheless have some specific features related to the high rate of weathering. The absence of frost and the intensive biological activity are examples. After dealing with the formation of soil material, the influence of the above mentioned pedogenic factors on the micromorphological characteristics of tropical soils will be discussed on the basis of the study of three sequences from different regions together with some other isolated observations.

FORMATION OF SOIL MATERIAL

In temperate, and especially in arid areas, little difference exists between the composition of the parent material of a soil and the rock from which it was derived, because saprolites are very thin or non-existent. This is not the case in the tropics: here the actual soil is mostly separated from the original rock by a thick saprolite layer, which is thought to result from intense weathering during former geological times. Therefore, the saprolite, not the underlying rock, has to be considered as the soil parent material. In the case of Si-oversaturated (acid) rocks this saprolite layer may be many meters thick, whereas it is generally thin or even absent on neutral or Si-undersaturated (basic) rocks. The transformation of saprolite to soil material, called pedoplasmation by Flach *et al.* (1968), is an essential part of soil formation in the tropics.

In a complete weathering profile, formed on a single geological material, four different zones can thus be considered from bottom to top:

(i) the *fresh rock*; its upper boundary is the *weathering front*;

(ii) the *saprolite*, result of weathering, mainly during an older geological period (referred hereafter as *paleoweathering*); the rock fabric is preserved, although all rock forming minerals may be pseudomorphosed to clay and/or sesquioxides (gibbsite, goethite, hematite); its upper boundary is the *pedoplasmation front*;

(iii) the *undifferentiated soil parent material*, with no evidence of soil forming processes, except for bioturbation and pedogenic weathering; rock fabric is lost, apart from some isolated relics, but some megastructures (*e.g.* pegmatite veins) may remain visible and the new fabric is

characterized by a homogeneous distribution and a random orientation of the rock minerals and weathering products; its upper boundary is the *front of pedogenesis*;

(iv) the *pedogenic soil material*, with evidence of pedogenic differentiation (*e.g.* illuviation, structure, hydromorphism, humification).

The complete profile is observed, in general, on deeply weathered, rather oversaturated rocks (phyllite, sandstone, granite, gneiss). Weathering profiles may be more complicated, *e.g.* when the geological material is not homogeneous (lithological discontinuity) or when layers of lateritic gravel occur within the profile (Stoops, 1967). They may be simpler when one or more zones are missing, *e.g.* on neutral or undersaturated rocks (basalt, gabbro, amphibolite, peridotite) the pedoplasmation front may practically coincide with the weathering front and in conditions of restricted drainage the front of pedogenesis may extend below the pedoplasmation front, and mottles are formed in the undisturbed saprolite.

When the solum is very deep, most factors of pedoplasmation related to climate (wetting and drying, freezing and thawing) can be ruled out, and bioturbation remains the most active factor. This is corroborated by micromorphological observations. From a micromorphological point of view pedoplasmation is characterized by the destruction of the saprolite fabric, as seen by the disappearance of stratification, foliation and clayey pseudomorphs, resulting in the homogenization of the material, the formation of a clayey weathering product (argillization) and a generalized colouration by oxyhydrates. This means that a redistribution and recrystallization of the oxyhydrates has taken place. The first traces of bioturbation/pedoplasmation appear as channels filled with a mixed saprolite material with a crescentic fabric. As their number increases they become interconnected, isolating the spots of *in situ* saprolite, until finally only a few isolated remains of saprolite dispersed through a more or less uniform material may be observed. The complete homogenization and argillization of the material and the uniform reddish or yellowish colouration, typic for oxic materials (Stoops, 1983; Rodriguez-Rodriguez *et al.*, 1988), is only achieved after many cycles of bioturbation (Stoops, 1991).

According to Zauyah (1986) three types of pedoplasmation may be distinguished: (i) the *continuous* pedoplasmation, forming the upper limit of the saprolite, result from the total disintegration of the rock fabric and homogenization of the material, (ii) the *linear* pedoplasmation, penetrating deeper in the saprolite along zones of weakness (*e.g.* former fissures, diaclases, biochannels), as a result of a better drainage and therefore stronger leaching, resulting in an increased rate of weathering, and (iii) the less important *punctual* pedoplasmation, caused by the disintegration of pseudomorphs, forming isolated patches of micromass within the saprolite.

The different processes contributing to pedoplasmation are not yet truly understood, and the influence of pedoplasmation on the physical and chemical characteristics of the material is not well documented. Further experimental work is required on this topic.

SEQUENCES

Three sequences will be discussed, each serving as a central theme for discussing soils in a larger regional context. Sequence A is situated in Rwanda and illustrates the micromorphological characteristics of soils formed in pre-weathered material and in its erosion products. Sequence B is a typical example of a recent incision of an old erosion surface in Lower Zaire: the top of the sequence is formed in an old saprolite and the lower part on fresh
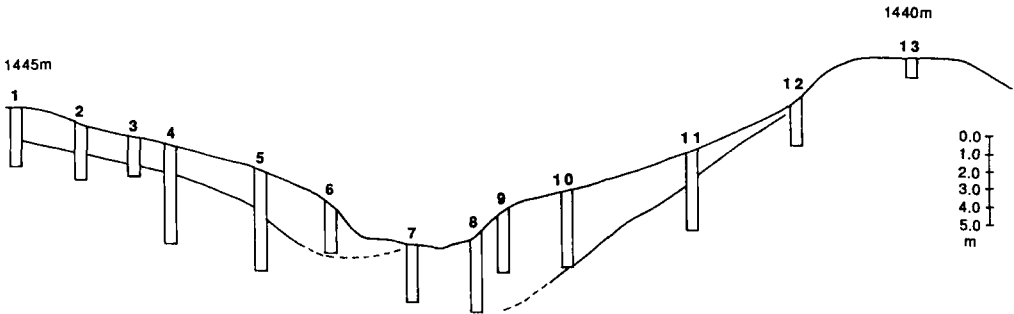
Fig. 1. Topographic position of the profiles of the soil sequence from Akagera National Park (Rwanda), between Kizirakome hill (left) and Kashinuika hill (right). The vertical scale of the profiles (at the right) is exaggerated with respect to that of the relief. Profiles 1 - 6 and 9 - 12 are Ustults developed in the cover, 7 is a Torrert and 8 a Quartzipsamment. The full line gives the observed position of the stone line, the dotted line the suggested.

rock (the contrast between soil material on fresh and preweathered rocks is striking). Finally, sequence C from Indonesia illustrates the influence of the degree of weathering on volcanic ash (here the characteristics of tropical soils not influenced by old pre-weathering can be studied).

The results presented below are based on microscopic studies of thin sections, supported by physical, chemical and mineralogical analyses. Whenever necessary, the method used to obtain a given information is indicated, *e.g.* (XRD) for X-ray diffraction analysis.

Sequence A: soils on saprolite and colluvium

The sequence is located in the Akagera National Park in the North Eastern corner of Rwanda (Chutatis, 1984). The average rainfall varies from 1,000 to 1,400 mm and the dry season lasts 2 to 3 months. The soil temperature regime is isothermic and the soil moisture regime is ustic. The sequence comprises soils from a valley bottom (at 1340 m), two slopes (the top of the hills being situated at 1,445 and 1,440 m) and a foot slope (Fig. 1). The profiles on the slopes are classified as Ustults (1 - 6, 9 - 13), the one on the valley bottom (7) as a Torrert (?) (Black Tropical Soil) and the one on the foot slope (8) as a Quartzipsamment. The substratum is Precambrian metamorphosed (gneissic) granite.

A similar sequence, from the same region also developed on gneiss, was studied by Oyinlola (1988). The micromorphology of many isolated soil profiles has been studied by the senior author in the framework of the "Projet Carte Pédologique du Rwanda".

On the basis of micromorphological characteristics three different soil materials and one rock type are recognized on the slopes. From the bottom to the top of the profiles they are:

a) A saprolite derived from weathered gneissic granite containing quartz, feldspar and biotite, partially weathered to kaolinite. Although the rock structure is still preserved, the influence of soil formation is recognizable by the illuviation of limpid, yellowish clay (kaolinite); this is especially obvious in the weathered perthites (Fig. 2a and b). Pedoplasmation
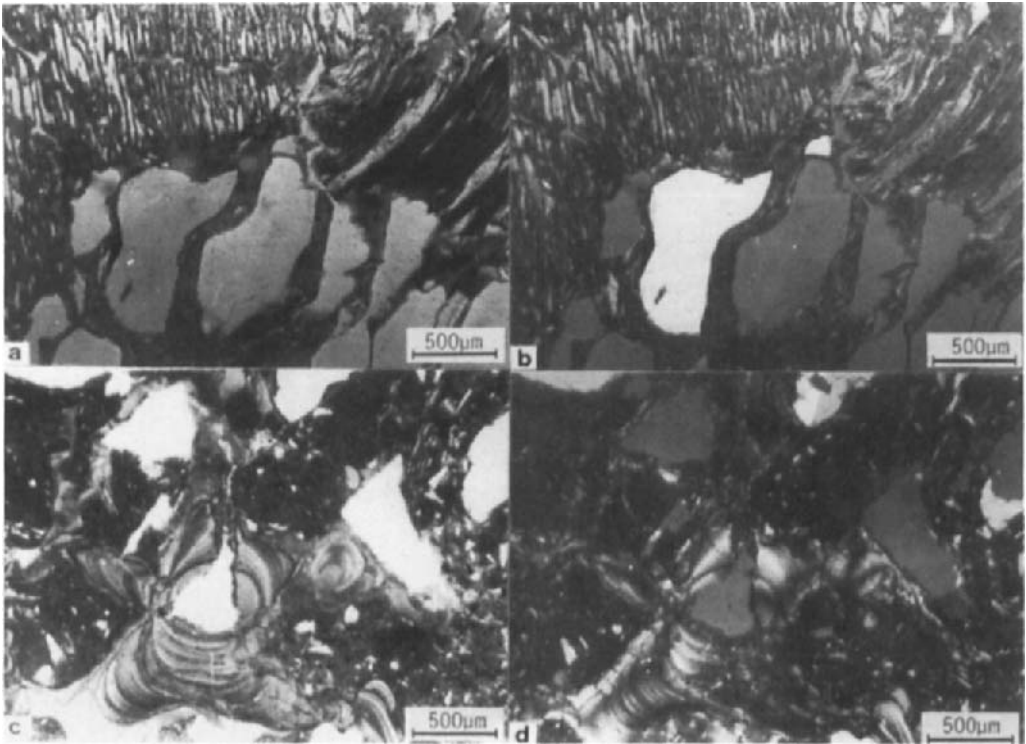
Fig. 2. Akagera National Park.
(a and b) Saprolite: parallel banded weathering of perthite (top) and biotite (right), with partial preservation of the rock structure. Infillings of strongly oriented illuvial kaolinitic clay in the weathered feldspar and between the quartz grains (center). PPL and XP. (c and d) Pedoplasmated material overlying the saprolite: high amount of coatings and infillings of strongly oriented kaolinitic clay (low interference colours). Fragments of weathered perthite are still present (top right). PPL and XP.

seems to be provoked by a collapse of the saprolite fabric mainly due to dissolution of the feldspar.

b) The saprolite is overlain by a completely pedoplasmated material with evidence of soil formation. Porosity (observed in thin sections) is low and consists mainly of channels and vughs. The coarse material is composed of poorly sorted quartz in some cases, or of a mixture of quartz, weathered feldspar and muscovite in other cases. The yellowish to reddish brown speckled micromass (kaolinite) is homogeneous and has a speckled b-fabric when only quartz is present and speckled and weakly striated when feldspar and mica are both present. Small amounts of plinthitic hematite (as defined by Schmidt-Lorenz, 1978) are observed. The c/f related distribution is porphyric. Remarkable is the abundance of coatings and infillings of
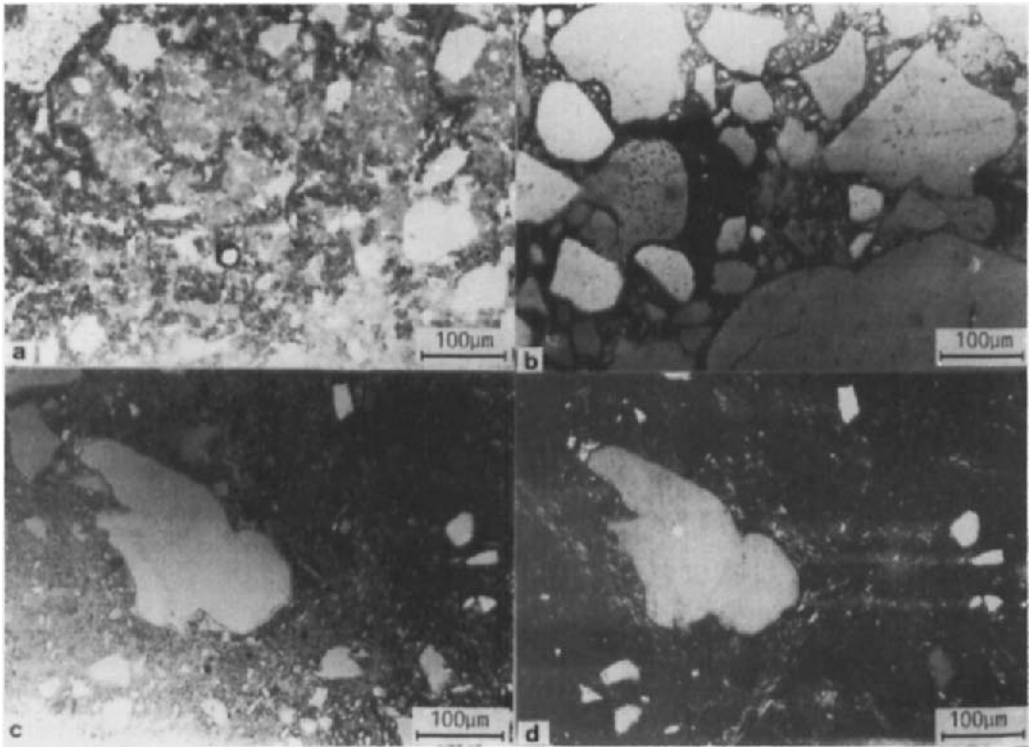
Fig. 3. Akagera National Park.
(a) Flocculated aspect of the micromass in some parts of the cover. PPL. (b) Opaque micromass and clay coatings in the sandy materials at the footslope. (c and d) General aspect of the groundmass of the black clayey soil from the valley. Note presence of numerous phytoliths (all fine sand and silt particles visible) and the granostriated b-fabric. PPL and XP.

strongly oriented yellowish limpid clay, up to 25% by total volume (Fig. 2c and d). The thickness of this material may reach more than 3 m.

A variant of this fabric, found in the stone line, contains coarse polycrystalline quartz grains frequently with hematite inclusions in cracks and concavities (called runiquartz by Eswaran *et al.*, 1975) and laterite nodules.

c) A thick layer or "cover" with a weak granular, crumb or blocky microstructure forms the upper part of the profiles. The coarse material consists of poorly sorted quartz (with runiquartz) and many phytoliths. The yellowish brown to brown, speckled and dotted micromass (kaolinite) has an undifferentiated to weakly speckled b-fabric. It often has a rather flocculated (floccules of 50 μm diameter) appearance, due to small changes in optical density (Fig. 3a). Plinthitic hematite occurs in the groundmass. Although no clay coatings are present, fragments of oriented clay are commonly observed. Roots and partly humified organic material occur near the surface too.

The profile on the valley bottom has a subangular blocky microstructure with vughy and channel intrapedal microstructures. The coarse material consists of poorly sorted grains of quartz, rare microcline, and a high amount of phytoliths (Fig. 3c and d). The homogeneous micromass is a brown to yellowish gray clay (mixture of kaolinite and swelling mixed layers), dotted or speckled, rarely limpid, with a striated (random, parallel, grano- or poro-striated) b-fabric. Locally, coatings and infillings of illuviated yellowish gray kaolinitic clay (as deduced from its low interference colours) occur in channels, but are partly deformed by stress.

On the footslope of the hill a rather sandy material occurs. An intergrain microaggregate structure, mixed with a bridged grain and a pellicular grain structure is observed throughout the profile. The coarse material consists of poorly sorted quartz grains and many phytoliths. The micromass consists of a dark brown to black clay composed mainly of quartz and small amounts of kaolinite (only in the deepest layer do some smectites occur) (XRD). Few laminated coatings of yellowish gray clay are observed; in the deeper part of the profile they commonly appear to be opaque (Fig. 3b).

The profiles on the hill top and on the higher slopes have developed in the residue of a truncated saprolite, as evidenced by the large amount of laterite fragments in the stone line on the slopes and the fact that the stone line reaches the surface on the hill top. As a result of the decreased depth of the soil, the pedoplasmation front coincides with the front of pedogenesis, which is shown by the massive invasion of the saprolite by clay coatings. The *in situ* soil material, overlying the saprolite and sometimes more than 3 m thick, is characterized by an enormous clay illuviation, reaching up to 25% by volume.

The profiles on the slopes can be interpreted as truncated profiles, overlain by a stone line and a "cover". The latter is generally more than one meter thick on the upper slopes, increasing to more than four meters on the lower slopes. It corresponds to the material in which the actual soil profile (according to most classifications) develops. The presence of runiquartz in this layer points to a material derived, at least partially, from the destruction of older surfaces (Eswaran *et al.*, 1975). This is corroborated by the presence of plinthitic hematite (Schmidt-Lorenz, 1978). The abundance of phytolites throughout the layer suggests that it corresponds to a surface accumulation. The speckled and dotted micromass and the absence of a well developed b-fabric is characteristic for such materials. This means that in these Ultisols all micromorphological characteristics of Oxisols are present, except the dominance of fine granular microstructure and the cloudy limpidity.

Surface wash of this material, especially the clay and the lighter constituents, provided the material in which the Black Soil developed, as proved by the very high amount of phytoliths found throughout the profile. Reducing conditions caused the iron oxyhydrates to be removed (even from the runiquartz) and a partial transformation of kaolinite to smectite took place. In similar soils in the Akagera National Park, calcite nodules are commonly found. This material, although strongly transformed, still bears the imprints of the ferrallitic weathering: no weatherable minerals in the coarse fraction, no silt fraction and a very homogeneous micromass. These soils are covered by a thin layer of material identical to the "cover" found on the slopes.

The sandy material at the foot slope is clearly a product of the selective accumulation of the coarse fraction of the slope deposits, rather than an alluvial material (no allochthonous minerals, angular to subangular grains). In a geochemical and micromorphological study of an Oxisol-Spodosol sequence in Amazonia, by Bravard and Righi (1989 and 1990) it is suggested that the sandy texture of the soils on the valley bottoms is not due to a difference in parent
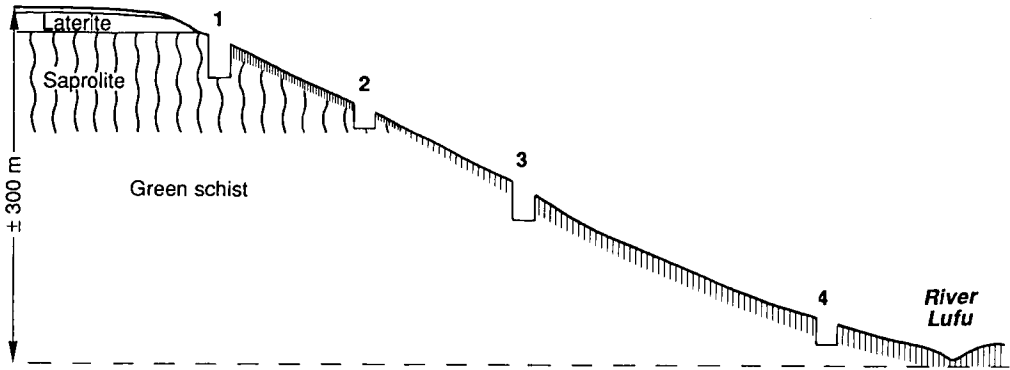
Fig. 4. Topographic position of the profiles of the soil sequence from the Lower Zaire. Profile 1: Ustoxic Dystropept; profile 2: Typic Ustropept; profile 3: Typic Ustropept; profile 4: Lithic Troporthent.

material but is a result of a pedogenic process causing eluviation and destruction of the clays which are abundant in the Oxisols on the slopes. A similar genesis can be postulated for the soil on the footslope of the Rwanda sequence: the opaque aspect of the fine material in the micromass and clay coatings, and its relative depletion of phyllosilicates (the fine material is essentially composed of quartz and few kaolinite (XRD) in the middle and lower part of the profile), can be the result of ferrolysis, as stated by Brinkman (1970). In contrast to the observation by Bravard and Righi (1990) and Chartres (1987), no clear textural differentiation was found in the profile, and the grainy coatings were often covered by hyaline, yellowish brown clay coatings. The latter feature suggests that the hydromorphic conditions, responsible for the ferrolysis and the disappearance of the oxyhydrates and the runiquartz, is a paleofeature. This is in agreement with the topographical position of the profile which is above the present valley floor (terrace ?).

Similar sandy materials in the same area often give rise to very deep podzolic soils with B-horizons characterized by a chitonic related distribution, tending to close porphyric in deeper horizons. The grayish, grainy isotropic micromass also becomes darker with depth. Superimposed upon these materials sepia brown strongly oriented clay coatings occur; their specific colour points to a high content of amorphous organic substances. Over these coatings isotropic iron hydroxides were later deposited. Most probably, the processes of clay illuviation, ferrolysis and deposition of amorphous and cryptocrystalline material alternated.

Comparable horizons of sandy podzols from the tropics and temperate and cool regions have similar micromorphological characteristics (De Coninck and McKeague, 1985), apart from the ferrolysis. The only difference is the absence of weatherable minerals, as both ferrallitic weathering and podzolization have depleted the material. When observed by SEM, the sand grains often show strong corrosion. In temperate regions such extremely weathered sands are found only as polycyclic sediments, and therefore composed only of well rounded grains.

Ortstein layers composed predominantly of isotropic iron oxyhydrates, (without organic material) were sometimes observed in such materials. This feature is most probably not related to podzolization, but rather to oxido-reduction phenomena.

The micromorphological aspects of these lowland podzols are quite different from those of the highland podzols found in the tropics. A few Troporthods studied in the highlands of Burundi showed a granular microstructure in the A horizons, becoming angular blocky in some B horizons. Enaulic related distributions grade into close porphyric ones; in one profile also chitonic related distributions are observed. The micromass is composed of dotted dark brown clay with undifferentiated b-fabric. Phytoliths are common. Some relict gibbsite nodules are observed as well as nodules composed of limpid reddish isotropic material with shrinkage cracks (probably Ortstein fragment). The micromorphological aspects of these soils resemble very much those of Oxisols, except for the high content of organic matter and the absence of hematite. Although having a lower organic matter content, they are similar to the loose spodic horizons of the temperate areas as described by De Coninck and McKeague (1985). These common aspects could probably be attributed to the high biological activity in all these soils.

Sequence B: soils on a recently incised surface

The relatively recent (about 10,000 years BP) and deep incision of the Zaire river in the Lower Zaire resulted in the exposure of the different saprolite layers and even fresh rock, followed by soil formation. The sequence discussed here is situated near Matadi (Zaire), and comprises soils developed on the upper slope of a laterite capped plateau, in the lower part of the saprolite and on the fresh rock (Fig. 4). The geological material is a greenstone rich in epidote, zoisite, actinolite, containing also biotite, magnetite and quartz (De Coninck *et al.*, 1986).

The average precipitation in this region amounts to 1,100 mm; during the long and the short dry season there is practically no rain. The mean annual temperature is 24°C, with a monthly maximum of 31°C in the rainy season, and a monthly minimum of 15°C in the long dry season. The temperature regime is isohyperthermic, the soil moisture regime ustic.

The soil on the upper slope (Ustoxic Dystropept) has a clay fraction containing exclusively kaolinite and goethite (XRD). It has a granular microstructure, typical of Oxic materials (Stoops, 1983) and many granular infillings of biopores (Fig. 5a). The coarse material consists of quartz (partially runiquartz with hematite inclusions), opaques and laterite fragments. The micromass is very homogeneous, contains numerous grains of plinthitic hematite (Schmidt-Lorenz, 1978) and has an undifferentiated to very weakly striated b-fabric (Fig. 5b). There are no specific pedofeatures.

The clay fraction of the soil developed on the middle slope, in the lower saprolite (Typic Ustropept) consists mainly of kaolinite, swelling mixed layer clays (chlorite-vermiculite) and goethite (XRD). The subsurface horizons have a porous or angular blocky microstructure. The coarse material consists of epidote, zoisite, feldspar, quartz and rock fragments; the speckled yellowish brown micromass in the upper layers is rather homogeneous and has a strongly speckled b-fabric; in the lower part it is less homogeneous (Fig. 5c) and has a short striated b-fabric. Pedofeatures are restricted to impregnated iron nodules. Plinthitic hematite is present, although not as much as in the profile on the upper slope.

The profiles formed at the expense of the fresh rock (Typic Ustropept and Lithic Troporthent) have a clay fraction dominated by chlorite-vermiculite mixed layer and smectite
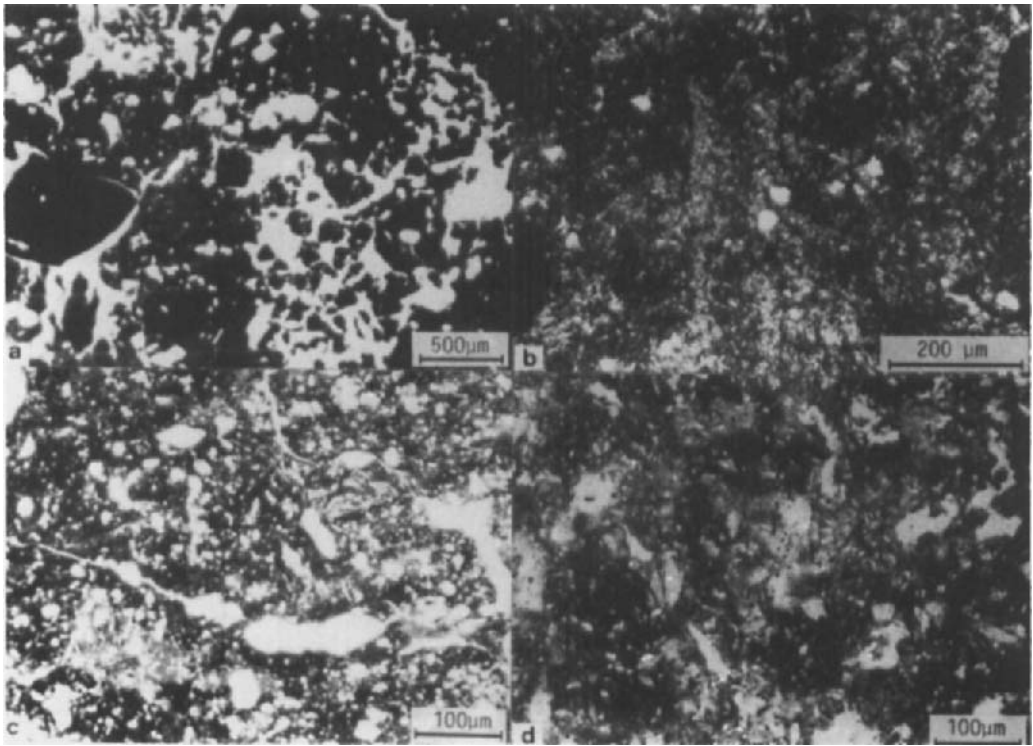
Fig. 5. Lower Zaire.
(a) Ustoxic Dystropept: homogeneous groundmass, granular infillings and laterite fragment (left); PPL. (b) As above: crescent striated b-fabric; XP. (c) Typic Ustropept: channel structure, heterogeneous groundmass; note the presence of rock fragments; PPL. (d) Lithic Troporthent: heterogeneous micromass; coarse, unsorted grains of epidote, zoisite and actinolite (note high relief); PPL.

clays (XRD). Both profiles have a blocky structure. The coarse material consists mainly of epidote, zoisite, few actinolite and quartz grains (Fig. 5d). The grayish to reddish flecked micromass has a speckled limpidity and mosaic speckled to short striated b-fabric. No plinthitic hematite was seen.

Based on this sequence and observations made on a large number of soils from the Lower Zaire by the author and co-workers, the following characteristics can be identified for soils over neutral or Si-undersaturated rocks:
- Soils formed on young geomorphological surfaces directly on weathering rock contain high amounts of weatherable minerals; these minerals have no hematite or goethite inclusions; a close porphyric related distribution is observed, the micromass has a micro-heterogeneous aspect, a rather pronounced striated b-fabric and a generalized deep red or brownish red staining developing early. The front of pedogenesis coincides with that of pedoplasmation.
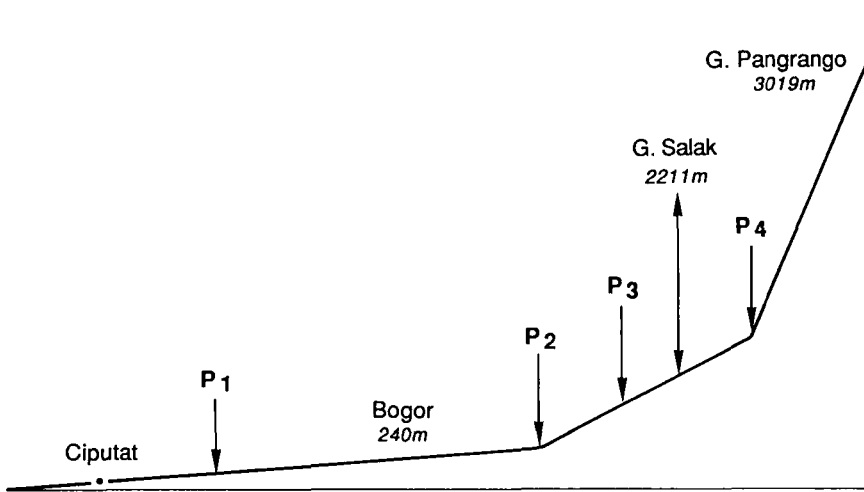
Fig. 6. Topographic position of the profiles of the soil sequence from western Java: P1: Eutrorthox, P2: Typic Eutropept, P3: Typic Humitropept, P4: Andic Humitropept.

Compared to temperate soils on similar materials these recent tropical soils contain a higher quantity of micromass, which is in addition more reddish coloured and has a less flocculated aspect; in temperate soils the porphyric related distribution is also less evident (observations by the authors).
- Soils formed on the lower parts of the saprolite still contain weatherable minerals, but their micromass is more homogeneous and the b-fabric less well expressed.
- Soils formed at the expense of the upper saprolite do not contain weatherable minerals and have a pronounced porphyric related distribution, tending to an open type. The micromass is characterized by a high degree of homogeneity, a red brown colour, a cloudy limpidity and a very weakly developed or undifferentiated b-fabric, i.e. all characteristics of an oxic material.

Sequence C: soils developed on pyroclastic materials

The sequence is situated in the region of Bogor and Jakarta in Java (Indonesia) and comprises four profiles developed on andesitic pyroclastic deposits (Astiana, 1982), and located at an elevation between 140 and 900 m (Fig. 6). The rainfall varies with altitude and the dry season is less than 3 months in the area. Mean monthly maximum and minimum temperatures range between 31.7 - 34.6°C and 20.4 - 23.4°C for Jakarta. The sequence consists of the following soils (Soil Survey Staff, 1975):
  Eutrorthox (elevation 140 m, precipitation 2,636 mm, isohyperthermic; clay fraction containing mainly halloysite);
  Typic Eutropept (elevation 320 m, precipitation 4,422 m; isohyperthermic; clay fraction containing mainly halloysite, with traces of swelling clay and gibbsite);

Typic Humitropept (elevation 450 m, precipitation 4,422 mm, isohyperthermic; clay fraction consisting mainly of halloysite, with relative large amounts of cristobalite); and

Andic Humitropept (elevation 900 m, precipitation 3,344 mm, isohyperthermic; clay fraction containing mainly halloysite).

The profile containing the most weathered material, the Oxisol, has a crumb and fine granular microstructure. The coarse material is rare, and consists essentially of gibbsite pseudomorphs after feldspar. The fine material is a cloudy, brownish red speckled clay with an undifferentiated, locally circular striated b-fabric. Pedofeatures are restricted to nodules of gibbsite and iron oxyhydrates.

Goenadi and Tan (1989) described in the same area red Hapludults and Paleudults which differ micromorphologically from the red soils discussed here, by the presence of feldspar and volcanic glass in the coarse fraction and a B horizon with blocky microstructure and clay coatings and infillings.

In the Typic Eutropept a crumb microstructure is still dominant, but a moderately developed blocky microstructure is also observed in the B_1 horizon. The coarse material of the subsurface layers contains only a few remnants of plagioclase and mainly gibbsitic pseudomorphs; the upper horizon contains hypersthene, plagioclase and volcanic glass, pointing to a rejuvenation by volcanic ash fall. The yellowish brown (brown in the top layer) micromass has an undifferentiated b-fabric; pedofeatures are restricted to gibbsite nodules, and a few gibbsite ped-coatings in the deeper parts.

The Typic Humitropept has a granular microstructure, except for the deeper horizons, where a tendency to blocky microstructure is observed. The coarse material contains plagioclase and pyroxene; the yellowish brown micromass has an undifferentiated b-fabric. In the deeper part of the profiles gibbsitic pseudomorphs after feldspar are common, and even some gibbsite coatings occur.

The Andic Humitropept has a granular microstructure, with many biopores, infilled by granular material, and a blocky microstructure in the IIB_2 horizon. The coarse material contains essentially fresh plagioclase, augite and hypersthene. The micromass has mainly an undifferentiated b-fabric, locally weakly granostriated. Clay coatings are observed throughout the profile; in the IIB_2 horizon gibbsite pseudomorphs occur.

From this sequence a few conclusions can be drawn:

- a granular structure is found in the most weathered, as well as in the least weathered materials. Only in some medium weathered horizons, belonging to buried profiles, a tendency to a blocky microstructure is observed.
- the b-fabric is undifferentiated (except for, locally, a few weak striations) in all horizons of the profiles. There may be some relation with the halloysitic composition (XRD) of the clay fraction.
- the occurrence of gibbsite coatings, especially in the less weathered materials, proves that mobility of Al occurs in the early stages of weathering.

DISCUSSION AND CONCLUSIONS

The first two soil sequences, formed on plutonic and metamorphic rocks, illustrate the influence of pre-weathering and "cover"-formation on the micromorphological characteristics of tropical soils.

In the Akagera sequence the importance of the cover is very clear: all present soils have formed in the cover (on the slopes), or on material derived from it (foot slope and valley bottom). The material of the cover is characterized by a high degree of weathering, a lack or very low amount of silt, a remarkable homogeneity, a practically undifferentiated or weakly developed b-fabric and the omnipresence of phytoliths. Traces of decomposed lateritic layers are present as lateritic nodules, runiquartz (Eswaranan *et al.*, 1975) and plinthitic hematite (Schmidt Lorenz, 1978). Some of these characteristics are inherited from the layers underlying the stone-line: same mineralogical composition, homogeneity and weakly developed b-fabric. The cover originates most probably from the underlying material through biological activity (termites) and colluviation. During these processes the features related to the tremendous clay illuviation, characteristic for the zone below the stone line, were completely destroyed and the present environment of the cover seems not to be suitable for a new phase of clay illuviation. This high amount of clay illuviation, found in many profiles on gneiss and granite in Rwanda, was not always observed in similar profiles of Lower Zaire, Ivory Coast etc.

The material of the clayey soil in the valley was originally similar to that of the cover (same coarse components, presence of phytoliths). As a result of different pedogenic processes other micromorphological characteristics developed: absence of lateritic material (removed by reduction of the iron oxyhydrates) and a better developed b fabric (caused by the synthesis of smectitic clays and the absence of iron oxyhydrates in the micromass).

Also bearing some of the characteristics of the cover are the sandy soils on the footslope: strongly weathered grains derived from granite and large phytoliths. By contrast, the micromass has a totally different aspect: it is locally practically opaque, probably as a result of depletion and destruction of phyllosilicates by ferrolysis, leaving only a micromass of fine quartz, and sometimes TiO_2 minerals. This characteristic of the micromass is also observed in giant podzols of the tropical lowlands.

The highland podzols have, apart from the higher organic matter content, many characteristics in common with the cover material, such as a granular microstructure and undifferentiated b-fabric.

The sequence in the Lower Zaire has one profile formed in the cover, with characteristics comparable to those described for Rwanda, one formed directly on the saprolite and two on fresh rock. Those formed on fresh rock miss several of the characteristics of the cover: many weatherable minerals and silt sized grains are present, the groundmass is less homogeneous and has a better expressed b-fabric. At the same time they differ from temperate soils by having a higher clay content and a reddish colour.

Comparing the two sequences, the most striking difference between soils developed in the cover is the colour: yellow for the soils on granite, red for soils formed on green schist.

The sequence in Java illustrates that on loose neutral or undersaturated pyroclastic material under tropical conditions a red material with stable micromorphological characteristics is formed and only slightly influenced by a further evolution of the soil. The high homogeneity, the undifferentiated b-fabric and the granular structure are common characteristic of all these red soils. Only the amount of weatherable minerals, the presence of *in situ* formed gibbsite coatings and the absence of a cloudy limpidity allow it to be distinguished from less evolved profiles and the oxisol.

REFERENCES

Astiana, 1982. Micromorphological and mineralogical study of a toposequence of latosols on volcanic rocks in the Bogor - Jakarta area (Indonesia). MSc thesis, Universiteit Gent, Belgium, 89 pp.

Bravard, S. and Righi, D., 1989. Geochemical differences in an Oxisol-Spodosol toposequence of Amazonia, Brazil. Geoderma, 44: 29-42.

Bravard, S. and Righi, D., 1990. Micromorphology of an Oxisol-Spodosol catena in Amazonia (Brazil). In: L.A. Douglas (Editor), Soil Micromorphology: A Basic and Applied Science. Proc. VIII Int. Working Meeting on Soil Mircromorphology, San Antonio, Texas, July 1988. Developments in Soil Science 19, Elsevier, Amsterdam, pp. 169-174.

Brinkman, R., 1970. Ferrolysis, a hydromorphic soil forming process. Geoderma, 3: 199-206.

Chartres, C.J., 1987. The composition and formation of grainy void cutans in some soils with textural contrast in southeastern Australia. Geoderma, 39: 209-233.

Chutatis, V., 1984. Micromorphological and mineralogical study of a toposequence in the Akagera Park (Rwanda). MSc thesis, Universiteit Gent, Belgium, 93 pp.

De Coninck, J.F. and McKeague, J.A., 1985. Micromorphology of Spodosols. In: L. Douglas and M. Thompson (Editors), Soil Micromorphology and Soil Classification. Soil Sci. Soc. Am. Special Publ. 15, Madison, Wisconsin, pp. 121-144.

De Coninck, F., Stoops, G. and Van Ranst, E., 1986. Mineralogy and Micromorphology of a Soil Toposequence near Matadi (Lower Zaire) on chloritic green Rocks. In: R. Rodriguez-Clemente and Y. Tardy (Editors), Geochemistry and Mineral Formation in the Earth Surface. CSIC, pp. 57-174.

Eswaran, H., Sys, C. and Sousa, E., 1975. Plasma infusion. A pedological process of significance in the humid tropics. An. Edaf. Agrobiol., 34: 665-674.

Flach, K.W., Cady, J.G. and Nettleton, W.D., 1968. Pedogenic alteration of highly weathered parent materials. In: J.W. Holmes (Editor), Trans. 9th Int. Congr. Soil Sci. Vol IV. ISSS, Angus and Robertson, Sydney, pp. 343-351.

Goenadi, D.H. and Tan, K.H., 1989. Mineralogy and micromorphology of soils from volcanic tuffs in the humid tropics. Soil Sci. Soc. Am. J., 53: 1907-1911.

Nahon, D. B., 1991. Introduction to the Petrology of Soils and Chemical Weathering. J. Wiley and Sons, New York, 313 pp.

Oyinlola, A., 1988. Micromorphological characteristics of a soil sequence in the humid tropics. MSc-thesis, Universiteit Gent, Belgium, 86 pp.

Rodriguez-Rodriguez, C.C., Jimenez Mendoza and Tejedor Salguero, M.L., 1988. Micromorfologia de los suelos Ferraliticos en las Islas Canarias. Anales de Edafologia y Agrobiologia, 47: 409-430.

Schmidt-Lorenz, R., 1978. Soil Reddening through hematite from plinthitized saprolite. Proc. Int. Conf. on Class. and Management of Tropical Soils. Malaysian Soc. Soil Sci. (preprint).

Soil Survey Staff, 1975. Soil Taxonomy. US Dept. Agric. Handb.No. 436. U.S. Gov. Printing Office, Washington,, D.C., 754 pp.

Stoops, G., 1967. Le profil d'altération au Bas-Congo (Kinshasa). Pedologie, 17: 60-105.

Stoops, G., 1983. Micromorphology of the Oxic horizons. In: P. Bullock and C.P. Murphy (Editors) Soil Micromorphology. Vol 2. Soil Genesis. Proc. VI Int. Working Meeting on Soil Micromorphology, London, August 1981, AB Academic Publishers, Berkhamsted, U.K., pp. 419-440.

Stoops, G., 1989. Relict properties in soils of the humid tropical regions with special reference to Central Africa. In: A. Bronger, and J.A. Catt (Editors), Paleopedology. Catena suppl., 16: 95-106.

Stoops, G., 1991. The influence of the fauna on soil formation in the tropics. Micropedological aspects. Meded. Zitt.K. Acad. overzeese Wet., 36: 461-469.

Zauyah, S., 1986. Characterisation of some weathering profiles on metamorphic rocks in Peninsular Malaysia. Ph.D. thesis, Universiteit Gent, Belgium, 388 pp.

This Page Intentionally Left Blank

Biogenic opal as an indicator of mixing in an Alfisol/Vertisol landscape

J.L. Boettinger

Department of Plants, Soils, and Biometeorology, Utah State University, Logan, UT 84322-4820, USA

ABSTRACT

Boettinger, J.L., 1994. Biogenic opal as an indicator of mixing in an Alfisol/Vertisol landscape. In: A.J. Ringrose-Voase and G.S. Humphreys (Editors), Soil Micromorphology: Studies in Management and Genesis. Proc. IX Int. Working Meeting on Soil Micromorphology, Townsville, Australia, July 1992. Developments in Soil Science 22, Elsevier, Amsterdam, pp. 17-26.

Biogenic plant opal distribution and soil morphology were studied to assess the degree of mixing that has occurred in typical red Alfisol and black Vertisol pedons and at the boundary interface between these soils. The contrasting red and black soils are primarily residual, forming on a pediplane-like surface in a highly variable metamorphic and igneous rock complex of subhumid and seasonally dry tropical north Queensland, Australia. Opal phytoliths were concentrated in the surface soil horizon of the low-activity Alfisols, whereas phytoliths occurred throughout the solum of the high shrink-swell Vertisols. Phytolith presence in the lower solum of profiles sampled at the red - black boundary did not correspond completely with morphological evidence of mixing such as slickensides and pockets of different-coloured soil material in the subsoil matrix. This lack of correspondence probably indicates that although shear failure and slickenside formation may be occurring in the lower solum, phytolith mixing does not occur unless desiccation cracks extend into the surface soil material.

INTRODUCTION

Contrasting red and black soils (Alfisols and Vertisols, respectively) occur on a gently undulating residual landscape in the seasonally dry tropics of northeastern Queensland, Australia. The boundary between the low-activity red soils and the high shrink-swell black soils occurs over horizontal distances of as little as 3 m. Detailed studies of soil boundaries are rare, thus a trench was excavated to examine soil morphology and soil mixing along this boundary. This paper reports on the vertical distribution of biogenic plant opal (phytoliths) as an indicator of soil mixing, and relates this evidence to the pattern of soil morphology at the field scale. Phytolith surface micromorphology is used to indicate relative residence time of phytoliths in these soils.

Table 1
Selected morphological properties of the profiles exposed in the Alfisol - Vertisol boundary. The profile at 0.0 m is at the red Alfisol end of the exposed boundary whereas the profile at 6.0 m is located at the black Vertisol end. The greatest morphological change occurs between 1.5 and 3.5 m.

Horizon	Depth cm	Munsell Colour dry (d), moist (m), mottles (mot)	Remarks
0.0 m			
A	0-11	5YR 3/4 d, 5YR 3/3 m	-
BAt	11-25	2.5YR 4/4 d, 2.5YR 3/4 m	-
Bt1	25-35	2.5YR 4/6 d,m	-
Bt2	35-46	2.5YR 3/6 d,m	-
BCt	46-65	2.5YR 4/6 d,m	-
Crt	65-83	10YR 5/8 d, 4/6 m; 2.5YR 5/6 films	Weathered andesite rock
0.5 m			
(Very similar to 0.0 m except that weathered granodiorite gneiss composes Crt layers).			
1.0 m			
(Very similar to 0.0 m except that weathered granodiorite gneiss composes Crt layers).			
1.5 m			
A	0-12	5YR 3/4 d, 5YR 3/2 m	-
BAt	12-25	2.5YR 4/4 d,m	-
Bt	25-51	2.5YR 4/6 d,m; 10YR 5/6, 4/4 mot	2.5YR ped centers
Btss	51-80	2.5YR 4/6 d,m; 10YR 5/6 mot	Slickensides at _68 cm
Crt	80-89	2.5Y 5/4 d, 2.5Y 5/4 m	Weathered porph. andesite
2.0 m			
A	0-14	5YR 3/4 d, 5YR 3/2 m	-
BAt	14-31	5YR 4/6 d,m	-
Bt	31-45	5YR 4/6, 10YR 4/4, 4/6 m	Mottled
Bss1	45-69	10YR 3/3, 7.5YR 4/4 m	Mottled, slickensides
Bss2	69-87	7.5YR 4/4, 5YR 4/4, 10YR 4/3 m	Mottled, slickensides
Crk	87-92	5Y 5/2, 10YR 3/3 m	Weathered andesite and gneiss
2.5 m			
A	0-16	10YR 4/3 d; 10YR 3/3, 3/2 m	-
BAt	16-28	5YR 5/6 d, 4/6 m; 10YR 4/3d, 3/3 m	-
Bt1	28-40	5YR 5/6 d,m; 10YR 5/4 d, 4.4 m mot	Redder matrix, ped interiors
Bt2	40-60	5YR 5/6 d, 4/6 m; 10YR 5/6 m mot	Redder matrix, ped interiors
Btss	60-75	5YR 5/6, 10YR 5/4, 5/3, 7.5YR 5/6 m	Slickensides, soil mixing
Bss	75-90	10YR 3/2 d, 3/1 m; 7.5YR 4/4 m mot	Slickensides in upper part
BCk	90-95	variegated, 10YR 5/3 d, 10YR 4/3 m	Grades to weathered gneiss
3.0 m			
A	0-21	10YR 4/2 d, 3/2 m; 7.5YR 5/6 d, 4/4 m	-
Bt	21-40	10YR 3/3 d,m; 7.5YR 4/6 d,m	Soil mixing, pockets
Bssk	40-75	10YR 3/2 d, 10YR 3/1 m; mottles	Slickensides, mixing
BCk	75-84	2.5 Y 6/4 d; 2.5 Y 5/4 m	Grades to weath. andesite
3.5 m			
A	0-19	10YR 3/2 d, 10YR 2/2 m	Vertical cracks to 71 cm
Bw	19-30	10YR 3/2 d, 10YR 3/1 m	"
Bss	30-53	10YR 3/2 m; 7.5YR 4/4, 4/6 mot	Slickensides, mixing
Bssk	53-73	10YR 3/1 d,m	Red soil in black ped-67 cm
BCk	73-80	2.5Y 6/4 d, 2.5Y 5/4 m	Clay and weath. andesite

Table 1 continued

Horizon	Depth cm	Munsell Colour dry (d), moist (m), mottles (mot)	Remarks
4.0 m			
A	0-17	10YR 3/2 d, 10YR 2/2 m	-
BA	17-34	10YR 3/1 m; 7.5YR 4/4 mot.	Soil mixing
Bss	34-52	10YR 3/1 m; 10YR 4/3 mot	Pockets of higher chroma soil
Bssk	52-72	10YR 3/1 d, 10YR 3/1 m	Slickensides
BCk	72-78	5Y 6/3, 10YR 3/1 d; 5Y 4/3, 10YR 3/1 m	Clay and weath. andesite
4.5 m			
A	0-16	10YR 3/1 d, 10YR 2/1 m	-
Bw	16-37	10YR 3/1 d, 10YR 2/1 m	Many pressure faces
Bssk	37-77	10YR 3/1 d, 10YR 2/1 m	Slickensides
BCk	77-79	2.5Y 4/2 d, 2.5Y 3/2 m	Clay and weath. dike rock

5.0 m, 5.5 m, 6.0 m
(Very similar to 4.5 m except that slickensides and wedge-shaped aggregates become more strongly expressed towards 6.0 m).

MATERIALS AND METHODS

Field Investigations

The red - black (Alfisol - Vertisol) complex occurs on a very gently undulating upland, or pediplane, about 70 km southeast of Townsville, northeastern Queensland, Australia. The soilsare formed in a highly variable metamorphic and igneous rock complex. The dominant rocks on the study area were identified as granodiorite gneiss and andesite. The climate of the study area is warm, subhumid and seasonally dry, with precipitation occurring primarily as monsoonal rains during the summer months. The mean annual precipitation in Clare, located about 4 km west of the study area, is 906 mm, and the mean maximum and minimum temperatures for Clare are 29.1°C and 17.9°C, respectively (Reid and Baker, 1984). Vegetation on the landscape is typified by a low open eucalyptus woodland associated with a tussock grassland. The red and black typical pedons on the landscape are classified as fine, mixed, hyperthermic Udic Paleustalfs and fine, montmorillonitic, hyperthermic Typic Haplusterts, respectively (Soil Survey Staff, 1992).

A typical Alfisol (red) pedon and a typical Vertisol (black) pedon derived from each of the dominant rock types (granodiorite gneiss and andesite) were sampled and characterized. A 6 m long trench was excavated with a backhoe to expose the boundary transition between representative Alfisol and Vertisol soil bodies. Detailed soil morphology was described at every 0.5 m horizontal interval to depths up to 1 m for both faces of the exposure. Field morphological evidence of shearing (slickensides) and mixing (*e.g.* differently coloured soil material in cracks, smeared along slickensides and incorporated into peds) were noted. Five profiles exhibiting the greatest amount of morphological change between the Alfisol and Vertisol were sampled (at 1.5, 2.0, 2.5, 3.0 and 3.5 m from red to black soil) and described. In addition, genetic horizons at about the 50 cm depth from the profiles at 0.0, 0.5, 1.0, 4.0, 4.5, 5.0, and 6.0 m were sampled and described.
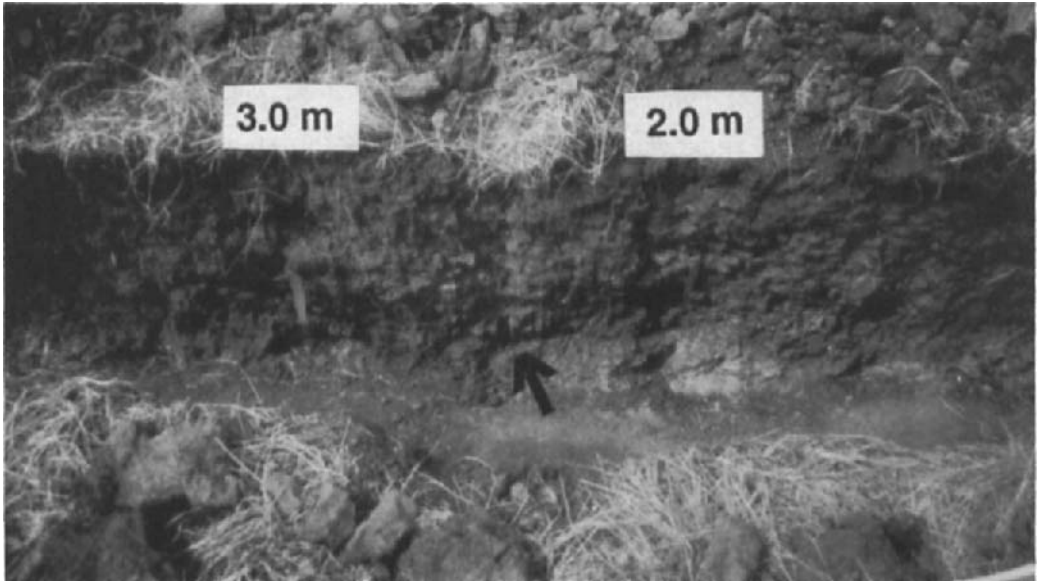
Fig. 1. Photograph of the center of the 6 m-long Alfisol - Vertisol boundary, from about 1.0 m (right) to 4.0 m (left). The end member Alfisol is at 0.0 m, about 1 m beyond the right photograph margin. The end member Vertisol is at 6.0 m, about 2 m beyond the left photograph margin. Soil depth is less than 1 m to saprolite. Arrow indicates slickenside plane exposed in the profile at 2.5 m.

Laboratory Investigations

The presence or absence of opal plant phytoliths was used to assess the extent of mixing in the soils of the Alfisol - Vertisol boundary. Soil samples were fractionated into size separates after the removal of carbonates (Jackson, 1979), organic matter (Lavkulich and Weins, 1972), and free Fe-oxides (Holmgren, 1967). Coarse silt (20-50 μm) grains were immersed in oil with a refractive index of 1.544 on a glass slide. The grain mounts were observed with a petrographic microscope, using crossed polarized light with the first order red plate inserted. Phytoliths were not classified, but general and surface morphology were noted. At least 1000 grains were counted per horizon. Maximum relative abundance equals about 1% of the total number of grains counted.

RESULTS AND DISCUSSION

Soil morphology

Results of detailed morphological descriptions are summarized in Table 1. The excavation between the red Alfisol and black Vertisol bodies exposed a series of profiles that were in transition between the end member soils (Fig. 1). From the Alfisol towards the Vertisol, the
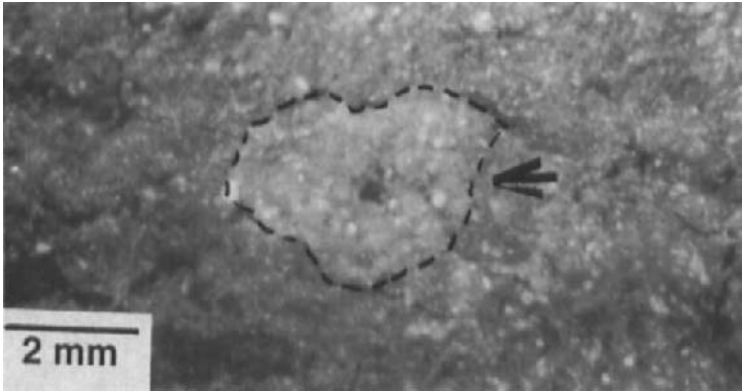
Fig. 2. Dissecting microscope photomicrograph of a pocket of yellow soil (arrow, enclosed within dotted line) in a ped of dark brown soil from the Bss (75-90 cm) horizon of the profile at 2.5 m.

B horizon colours change from 2.5YR to 2.5YR with 10YR mottles, to 5YR with 10YR mottles, to 10YR with 7.5YR mottles , to 10YR with low values and chromas.

From Alfisol to Vertisol, slickenside shear planes first appear in the Btss horizon at 51-80 cm in the profile at 1.5 m (Table 1). The size and abundance of slickensides generally increase towards the Vertisol. The slickensides tend to be associated with 10YR colours (Table 1), presumably because soil horizons dominated by 10YR colours have more smectite and organic C than those with 2.5YR and 5YR colours (Boettinger, 1992).

Physical mixing of a redder (2.5YR to 5YR) material into the darker (10YR) material in the slickenside zones is evident in the exposed profiles at 2.5 through 4.0 m (Table 1). Mixing evidence includes reddish soil material in vertical desiccation cracks (profiles at 3.5, and 4.0); reddish soil material, which had apparently migrated into the subsoil via a crack, smeared along slickenside shear planes (profiles at 3.5 and 4.0 m); and pockets of redder and yellower (7.5YR) material enclosed in peds found in the slickenside zones (profiles at 2.5, 3.0, 3.5, and 4.0 m). In the profiles at 2.0 through 4.0 m, physical mixing in the form of yellower material enclosed in a darker ped, was observed with a dissecting microscope (e.g. Fig. 2).

Opal Phytoliths

In the typical Alfisol (red) pedons derived form both granodiorite gneiss and andesite, opal phytoliths are abundant in the 20-50 μm fraction of the A-horizons at the soil surface (Table 2, Fig. 3A). Phytolith morphology includes rods from fundamental cells, fan-shaped bulliform cells, shield-shaped trichrome cells, dumbbells from silica cells, and helical xylem elements (cf. Drees et al., 1989). In the BAt horizon of the Alfisols, immediately below the A horizon, and in the underlying subsurface horizons, there are practically no phytoliths (Fig. 3B). Considering that biomass turnover of grasses and deposition of eucalyptus leaves occurs mainly at the soil surface and in the surface horizon, subsequent phytolith accumulation is

Table 2
Relative abundance of opal phytoliths in the coarse silt (20-50 μm) fraction of the typical Alfisol and Vertisol pedons.

Pedon	Horizon	Depth (cm)	Phytolith Abundance
Alfisol - Gneiss	A	0-11	XXX
	BAt	11-31	tr
	Bt, BCt, CBt, Crt	31-100	- -
Vertisol - Gneiss	A	0-10	XXX
	Bw	11-28	XX
	Bss	28-46	XX
	Bssk	46-76	XX
	BCk	76-90	X
	Crk	90-108	- -
Alfisol - Andesite	A	0-10	XXX
	BAt	10-28	tr
	Bt1, Bt2, BCt, Crt	28-95	- -
Vertisol - Andesite	A	0-13	XXX
	Bss	13-48	XX
	Bssk	48-87	XX
	BCk	87-104	tr
	Crk	104-115	tr

XXX = most abundant; XX = abundant; X = less abundant; tr = trace amounts.

expected to be in the surface soil. Therefore, the concentration of phytoliths in the surface horizon and the apparent lack of phytoliths in the subsoil of the Alfisols indicate that these soils do not undergo extensive physical mixing.

In contrast to the Alfisols, the typical Vertisol pedons exhibit a more uniform vertical distribution of opal phytoliths (Table 2). Although the 20 - 50 μm-sized phytoliths were most abundant in the A horizons at the soil surface, phytoliths were present throughout the Vertisol solum. The presence of phytoliths in the subsoil of the Vertisols is interpreted to be a result of physical soil mixing. Phytolith distribution in relation to soil morphology observed at the field and meso scales can be invoked to explain the process of phytolith incorporation into the subsoil. Surface soil material containing phytoliths falls down vertical desiccation cracks during the dry season. The phytolith-bearing material is then incorporated into the soil mass: cracks close upon wetting and soil swelling, mass movement occurs along slickenside shear

Fig. 3. Photomicrographs of coarse silt (20 - 50 μm) fractions viewed under cross polarized light with the first order red plate inserted. A) Isotropic opal phytoliths from grasses appear transparent with high relief in contrast to the birefringent crystalline silicates in the A horizon of the typical Alfisol pedon derived from granodiorite gneiss. B) Only a trace amount of opal phytoliths (arrow) can be found in the underlying BAt horizon of the same pedon. C) Photomicrograph of the coarse silt (20 - 50 μm) fraction separated from the Bssk horizon (38-79 cm) of the profile at 5.5 m. Note extensive pitting of the phytolith surface (arrow).
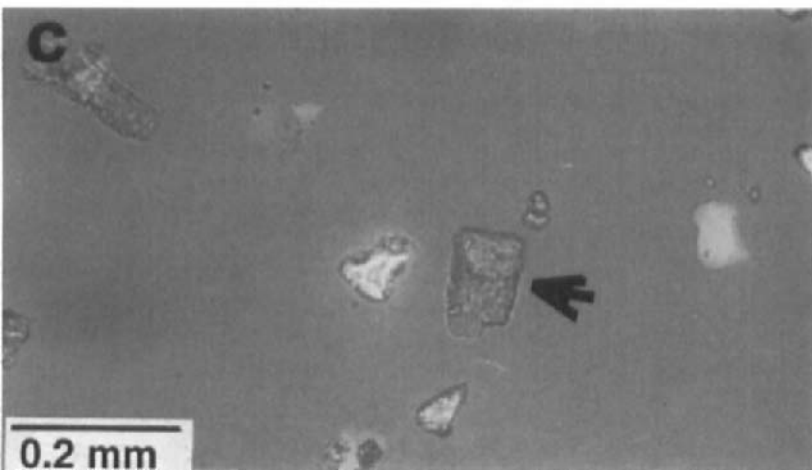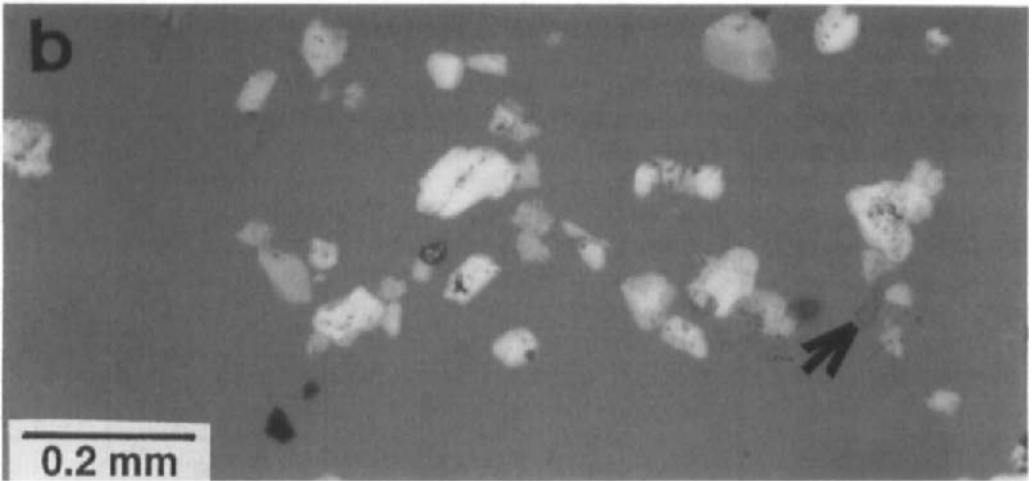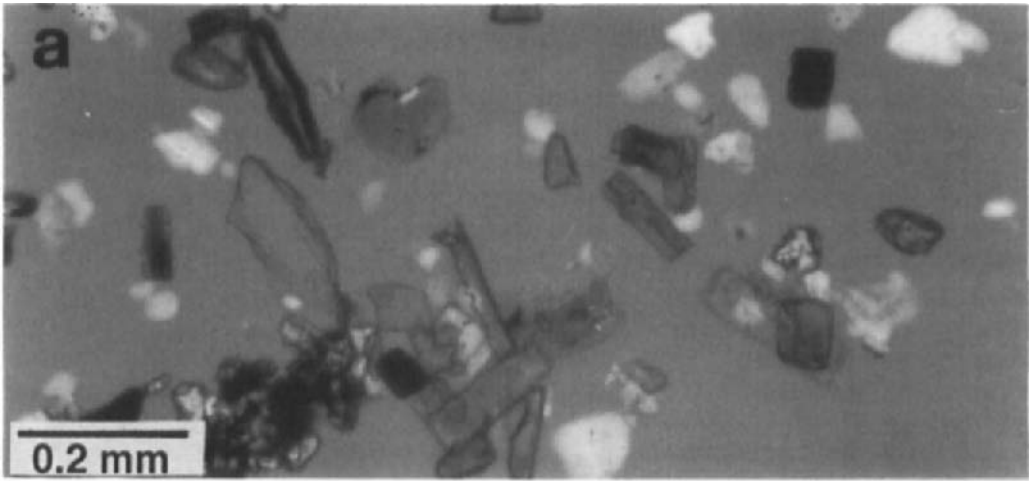
Table 3
Relative abundance of opal phytoliths in the coarse silt (20-50 μm) fraction of the profiles sampled from
the exposed Alfisol - Vertisol boundary. See Table 1 for horizon depths.

Profile	Horizon	Phytolith Abundance
0.0 m	Bt2	- -
0.5 m	Bt2	- -
1.0 m	Bt2	- -
1.5 m	A	XXX
	BAt	tr
	Bt through Crt	- -
2.0 m	A	XXX
	BAt	tr
	Bt1 through Crk	- -
2.5 m	A	XXX
	BAt	tr
	Bt1 through BCk	- -
3.0 m	A	XXX
	Bt	tr
	Bssk	tr
	BCk	- -
3.5 m	A	XXX
	Bw	tr
	Bss	tr
	Bssk	tr
	BCk	- -
4.0 m	Bssk	X
4.5 m	Bssk	X
5.0 m	Bssk	X
5.5 m	Bssk	XX
6.0 m	Bssk	XX

XXX = most abundant; XX = abundant; X = less abundant; tr = trace amounts.

failure planes, new cracks form upon drying and the process is repeated. The mixing of phytoliths into the subsoil is accounted for by the combination of the pedoturbation model and the soil mechanics model of Vertisol genesis described by Wilding and Tessier (1988).

The presence of opal phytoliths in the lower solum of the profiles exposed in the boundary is interpreted as an indicator of soil mixing, given the different vertical phytolith distributions in the contrasting Alfisols and Vertisols. The relative distributions of opal phytoliths in the profiles of the exposed Alfisol - Vertisol boundary are summarized in Table 3. Phytoliths are present in the lower solum of the profiles exposed in the boundary from 3.0 to 6.0 m. In these profiles, the relative abundance of phytoliths in the lower sola (as determined in the genetic horizons sampled at about 50 cm depth) increases from trace amounts in the subsoil of the

profiles at 3.0 and 3.5 m, to higher amounts in the profiles at 4.0, 4.5, and 5.0 m, to the relatively highest amounts in the Vertisol end member at 6.0 m. The increase in the relative abundance of phytoliths from transitional soil to end-member Vertisol indicates the increasing degree to which the soils have been mixed.

In the typical Vertisol pedons and in the end-member Vertisol profiles sampled from the 6 m-long trench, the opal phytoliths found in the lower part of the solum are more pitted and are apparently more weathered than the majority of the phytoliths in the A horizons (Fig. 3C). The higher degree of phytolith weathering in the lower solum probably indicates that the rate of incorporation of surface soil material, which contains a greater abundance of relatively fresh phytoliths, is slower than the rate of phytolith accumulation in the surface soil. If the rates of phytolith accumulation and mixing were similar, they should be uniformly distributed throughout the depth of the Vertisol solum and they should exhibit a similar degree of weathering.

Implications for Soil Genesis

The distribution of opal phytoliths throughout the sola of the typical Vertisols indicates that these soils are subject to physical mixing, which ultimately results in the incorporation of significant amount of surface soil material into the subsoil, in this seasonally dry and subhumid tropical climate. In contrast, red Alfisols do not experience much physical mixing, evinced by the lack of phytoliths in the subsoil. In the profiles exposed at the Alfisol - Vertisol boundary, relative phytolith distribution within profiles indicate that soil mixing has occurred in the profiles at 3.0 through 6.0 m. Mixing based on phytolith content is minimal in the profiles at 3.0 and 3.5 m, greater in the profiles at 4.0, 4.5, and 5.0 m, and is greatest near the Vertisol end-member at 6.0 m. Mixing based on the presence of slickensides and reddish soil incorporated into peds and smeared along shear planes is minimal in the profiles at 1.5 and 2.0 m, greater in the profiles at 3.0, through 4.5 m, with near-typical Vertisol morphology occurring in the profiles at 5.0 and 5.5 m. There is a lack of complete correspondence between phytolith presence in the subsoil and morphological evidence of mixing in the subsoil. This lack of correspondence probably indicates that phytolith mixing does not occur in soils that do not crack to the soil surface, even though some shear failure may be occurring in the lower solum.

Although the phytoliths have been interpreted as indicators of relative extent of soil mixing, the actual rates of soil mixing, or the rates of soil evolution have not been assessed, except that phytolith accumulation is probably more rapid than phytolith mixing into the lower solum. Further research on phytolith stability and experiments on the present day rates of mixing and mass movement must be determined before actual rates of soil mixing and genesis can be assigned.

ACKNOWLEDGEMENTS

REFERENCES

Boettinger, J.L., 1992. Genesis, Mineralogy, and Geochemistry of a Red-black (Alfisol-Vertisol) Complex, Northeastern Queensland, Australia. Ph.D. Dissertation, University of California, Davis.

Drees, L.R., Wilding, L.P., Smeck, N.E. and Senkayi, A.L., 1989. Silica in soils: Quartz and disordered silica polymorphs. In: J.B. Dixon and S.B. Weed (Editors), Minerals in soil environments, 2nd ed. Soil Sci. Soc. Am., Madison, Wisconsin, pp. 913-974.

Holmgren, G.G.S., 1967. A rapid citrate-dithionite extractable iron procedure. Soil Sci. Soc. Am. Proc., 31: 210-211.

Jackson, M.L., 1979. Soil Chemical Analysis - Advanced course. 2nd Ed. Dept. Soil Science, University of Wisconsin, Madison, Wisconsin.

Lavkulich, L.M., and Weins, J.H., 1972. Comparison of organic matter destruction by hydrogen peroxide and sodium hypochlorite and its effect on selected mineral constituents. Soil Sci. Soc. Am. J., 34: 755-758.

Reid, R.E. and Baker, D.E., 1984. Soils of the Lower Burdekin River - Baratta Creek - Haughton River Area, North Queensland. Queensland Department of Primary Industries, Agricultural Chemistry Branch, Technical Report No. 22.

Soil Survey Staff, 1992. Keys to Soil Taxonomy. 5th Ed. SMSS Tech. Monogr. No. 19. Pocahontas Press, Blacksburg, Virginia. 541 pp.

Wilding, L.P., and Tessier, D., 1988. Genesis of Vertisols: Shrink-swell phenomena. In: L.P. Wilding and R. Puentes (Editors), Vertisols: Properties, Classification, and Management. Technical Monograph 18, Texas A&M University, Printing Center, College Station, Texas, pp. 55-81.

Morphology and origin of secondary calcite in soils from Beauce, France

S. Ould Mohamed and A. Bruand

INRA Orléans, Service d'Etude des Sols et de la Carte Pédologique de France, Ardon, 45160 Olivet, France

ABSTRACT

Secondary calcite in soils was studied with optical and scanning-electron microscopes. The observations support a biological origin for the needle and micro-rod calcites: (i) needle calcite forms within mycelian strands; (ii) micro-rods are calcified bacteria that grew in the organic matter of mycelian hyphae; and (iii) needle calcite with a high surface roughness originally had a smooth surface that was subsequently covered by calcified bacteria. As for the rhombohedral and spindle calcites, the observations confirm their non-biological origin. Finally, serrated-edged needle calcite results from the partial dissolution and reprecipitation of needle calcite.

INTRODUCTION

Secondary calcite is known from a wide variety of soil materials and its origin has frequently been discussed in the literature. Certain secondary calcite, like rhombohedral calcite, is now considered to result from physico-chemical processes (Durand, 1979; Dever *et al.*, 1983), but other types of calcite crystals may have had a biological origin, like the subrounded sparitic calcite crystals that result from root-cell calcification (Klappa, 1979; Ducloux and Butel, 1983; Jaillard, 1984). Nevertheless, the origin of many types of secondary calcite, like needle and micro-rod calcites, is still debated, and physico-chemical and biological processes have been proposed, alone or combined (Verges *et al.*, 1982; Ducloux and Butel, 1983; Phillips and Self, 1987). The aim of this paper is to contribute to the discussion of the origin of secondary calcite in soil, by studying the morphology of secondary calcite and its location in different types of soil material.

MATERIALS AND METHODS

The soils studied are located in Beauce, south of Paris, France (Fig. 1a). They developed on a lacustrine limestone (Miocene) that was cryoturbated in its upper part during the ice age (Menillet, 1980; Ould Mohamed, 1991). Morphological field studies showed three superposed units from the soil surface downward (Fig. 1b): (i) a Cambisol consisting of clayey-loam materials, in which the main pedological evolution is a decarbonation of the upper horizons and
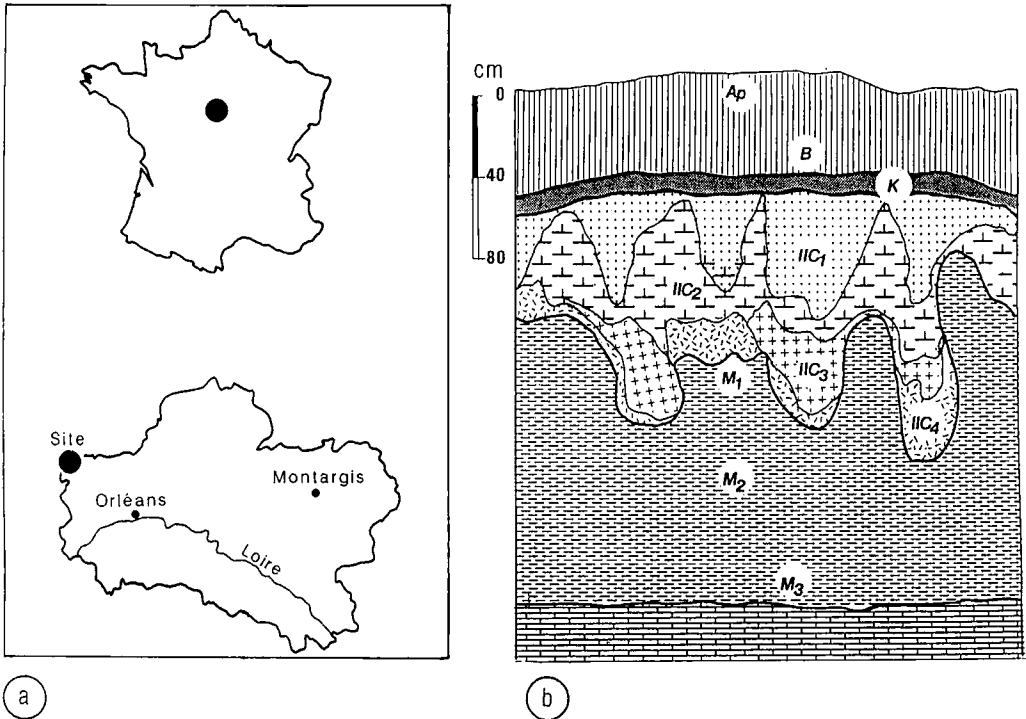
Fig. 1. a) Location of the site and b) schematic diagram of the profile showing the three superposed units: the Cambisol with the A, B and K horizons; the cryoturbated unit with the IIC_1, IIC_2, IIC_3 and IIC_4; and the fragmented powdery limestone with the M_1, M_2 and M_3 horizons.

the formation of a calcareous crust (K horizon) at its base; (ii) a calcareous and loamy material resulting from Quaternary cryoturbation; and (iii) a fragmented powdery limestone with fine ovoid fragments that become scarce with depth.

Samples were collected from horizons in these three units and were impregnated with polyester resin that was diluted with styrene monomer (30% volume). Thin sections, 6.8 × 14 cm and 4.5 × 6 cm in size, were prepared respectively for optical and scanning electron microscopy (SEM). In the latter case, the thin sections were automatically polished with diamond grains (0.3 μm in size) sprayed on polishing sheets and coated with carbon prior to SEM observation in the backscattered-electron mode.

Some samples were collected for SEM observation on aggregates in the secondary-electron mode.

RESULTS

Needle calcite

Needle calcite was originally termed pseudomycelium by Kubiena (1938), but other terms include "lublinite" (Stoops, 1976) or "whisker crystals" (Calvet, 1982). Needle calcite has been observed in many geological units (James, 1972; Knox, 1977; Klappa, 1980; Ducloux and Butel, 1983; Wright 1984) and soils (Bocquier, 1973; Durand, 1979; Bruand 1980, Verges *et al.*, 1982; Phillips and Self, 1987; Kaemmerer *et al.*, 1991). Such needle calcite is elongated in shape, but shows different types of morphology at high magnification.

Needle calcite occurs in all sampled horizons except in the A horizon. In the B horizon calcite needles are 10 - 60 μm long and 1 - 3 μm wide, and their number increases with depth. They are mainly located along the walls of cavities and around calcareous pebbles at the bottom of the B horizon, but they are not observed within the common tubular voids. In the K horizon, needle-shaped calcite is mainly located within both cavities and voids resulting from the packing of limestone pebbles (Fig. 2 a, b, c and d). The needle-calcite fabric shows square or circular mesh-structures called 'alveolar texture' (Esteban, 1973) or 'bird-nest fabric' (Ould Mohamed, 1991) (Fig. 3a and b). Generally, needle calcite is associated with both micro-rods and calcified biological filaments, as will be discussed later. At high magnification, needle calcite shows a large range of morphology according to its surface roughness (Fig. 3c, d and e) and the shape in cross-section (Fig. 3c). The cross-section may be disc-, cross- or dumbbell-shaped and would correspond to a single needle, or to the association of two or four needles, respectively, as earlier discussed by Verges *et al.* (1982).

In cryoturbated horizons, needle calcite fills the numerous voids due to gravel packing (Fig. 3f). The needles are longer (10 - 100 μm long and 1 - 3 μm wide) than in the B and K horizons, and they generally have smooth surfaces (Fig. 4a). A few long fibre calcites are observed (> 150 μm long) but, unlike the 10 - 60 μm long needles, they are curved (Fig. 4b).

In the powdery limestone, needles are mainly located in large voids that result from ovoid fragment packing. There is no difference in morphology from the needles described in the cryoturbated unit, except that needles in the limestone show smoother surfaces.

Serrated-edged needle calcite

Serrated-edged needle calcites were first described by Stoops (1976), who showed that needle- and fibre-calcite crystals, known earlier as "lublinite", consist of short, individual, stacked crystals with parallel c-axes, forming a needle or fibre shape. Serrated-edged needle calcite was identified subsequently by several authors (Verges *et al.*, 1982; Phillips and Self, 1987), but individual crystals were not identified. In the samples studied, serrated-edged needle calcites are mainly observed in the cryoturbated unit, where they are located along the walls of packing voids. A few serrated-edged calcite needles are also seen in the K horizon. Two types are distinguished: (i) long and fine serrated-edged needle calcite (10 - 100 μm long and 1 - 3 μm wide) with smooth or slightly rough surfaces, and single or coalesced forms that occur throughout the cryoturbated unit and in the K horizon (Fig. 4c); (ii) short and wide serrated-edged calcite needles (10 - 25 μm long and 4 - 6 μm wide) in IIC_4 that have a morphology similar to the needle calcite studied by Stoops (1976), consisting of single crystals with parallel c-axes (Fig. 4d).
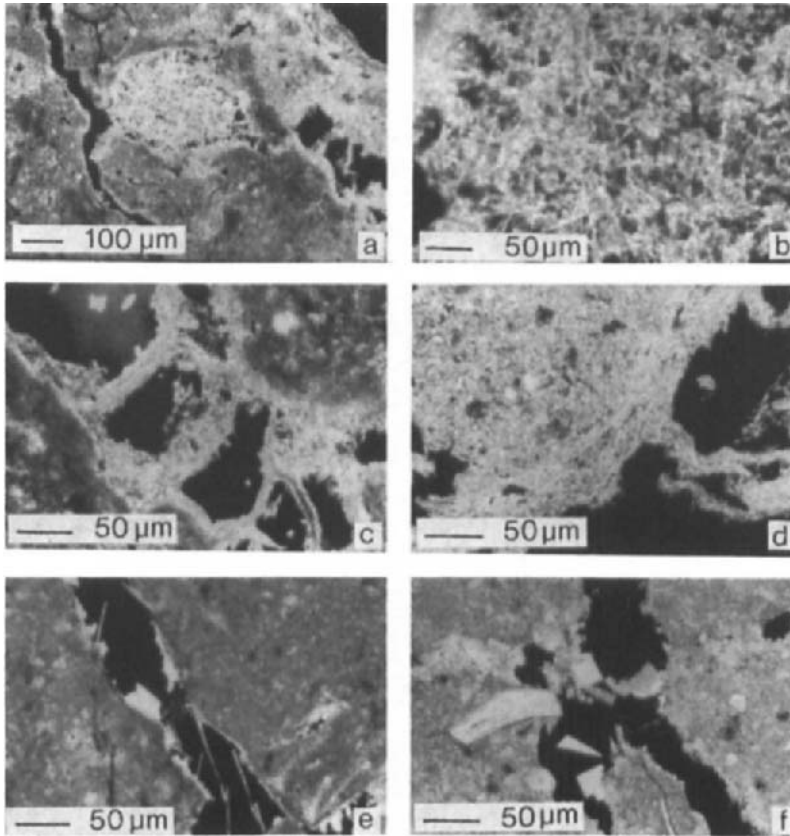
Fig. 2. Observations with optical microscope in cross polarized light: a, b, c and d) needle calcite in the K horizon; e) spindle calcite in the M_3 horizon and f) rhombohedral calcite in the M_3 horizon.

Micro-rod calcite

Micro-rod calcite was described by Verges *et al.* (1982), Ducloux and Butel (1983) and Phillips and Self (1987). The micro-rods are 1 - 3 μm long and 0.1 - 0.5 μm wide, and were observed in the B, K and IIC_1 horizons where they are usually associated with needles (Figs 3d, e, and 5a). At high magnification, needles with a high surface roughness appear to be partly formed by micro-rods. In the K horizon micro-rods fill the voids, creating bonds between needles.

Calcified filaments

Calcified filaments 5 - 10 μm in external diameter were reported by many authors (Durand, 1979; Bruand, 1980; Klappa, 1980; Calvet, 1982; Ducloux and Butel, 1983; Phillips *et al.*,
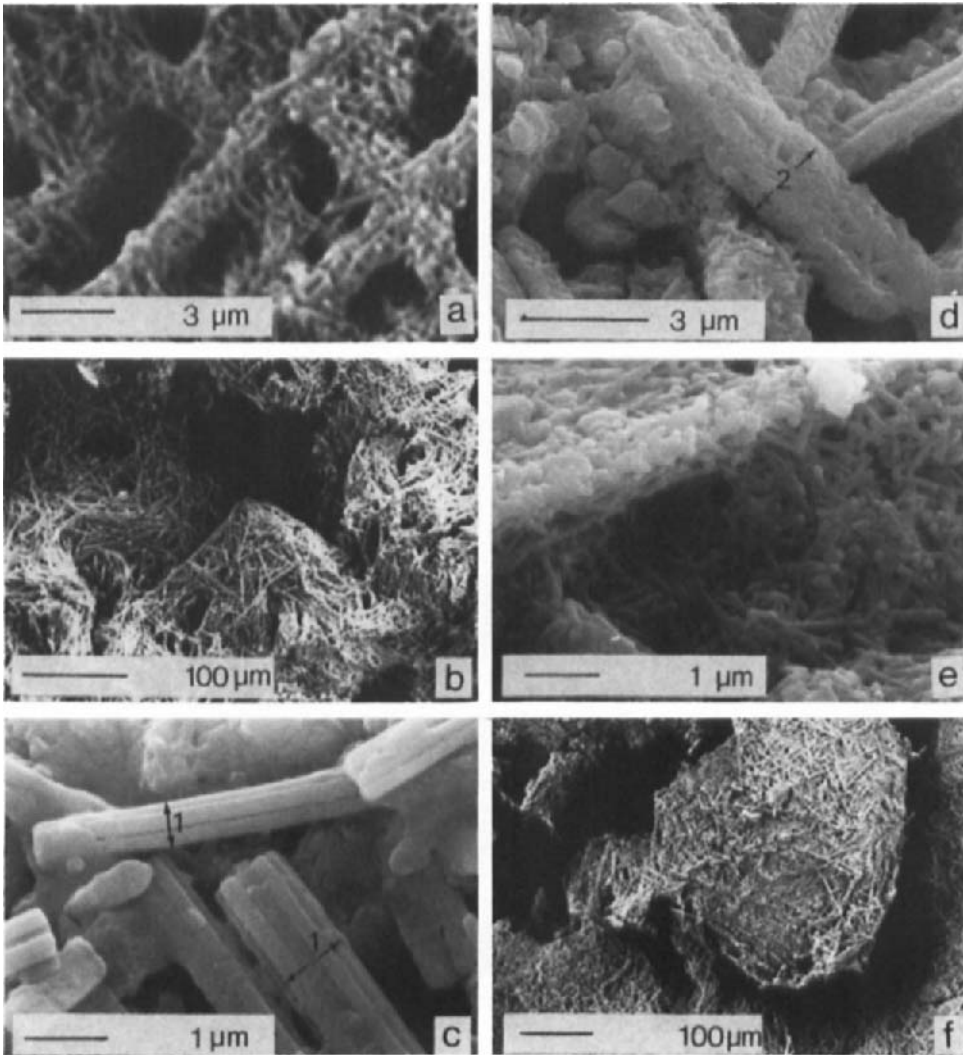
Fig. 3. SEM Observations in the secondary-electron mode: a) needle calcite showing circular meshed structures in the K and b) IIC_1 horizons; c) needle calcite with a smooth surface (1) in the B horizon; and d and e) with a high surface roughness (2) in the K horizon; and f) needle calcite wrapping calcareous pebbles of the IIC_1 horizon.

1987). They are present in the K horizon and the cryoturbated unit (Fig. 4e and f). The size and morphology of the calcite crystals forming their walls are close to those studied by Phillips *et al.* (1987). In the K horizon, smaller calcified filaments were found. They are 1 - 2 µm in external diameter (calcified micro-filaments) and their walls are partly made of micro-rod
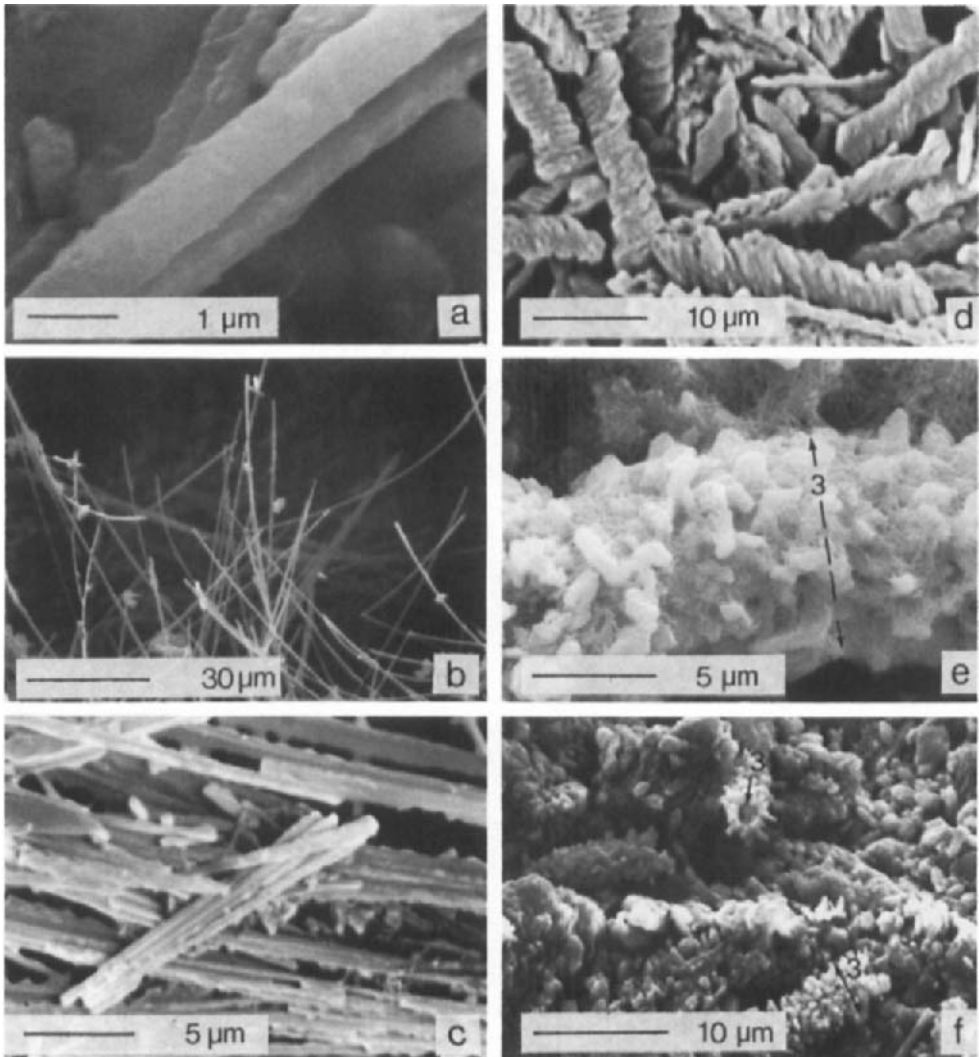
Fig. 4. SEM observation in the secondary-electron mode: **a**) long needles in the IIC_3; and **b**) IIC_4 horizon long; **c**) fine serrated-edged needle calcite in the IIC_3 horizon; **d**) short and wide serrated-edged needle calcite in the IIC_4 horizon and **e** and **f**) calcified filaments (3) in the K horizon.

calcite (Fig. 5a and b). Their central void is 0.5 - 1 μm in diameter and many of these voids are shown in backscattered-electron mode in thin section (Fig. 5c and d).
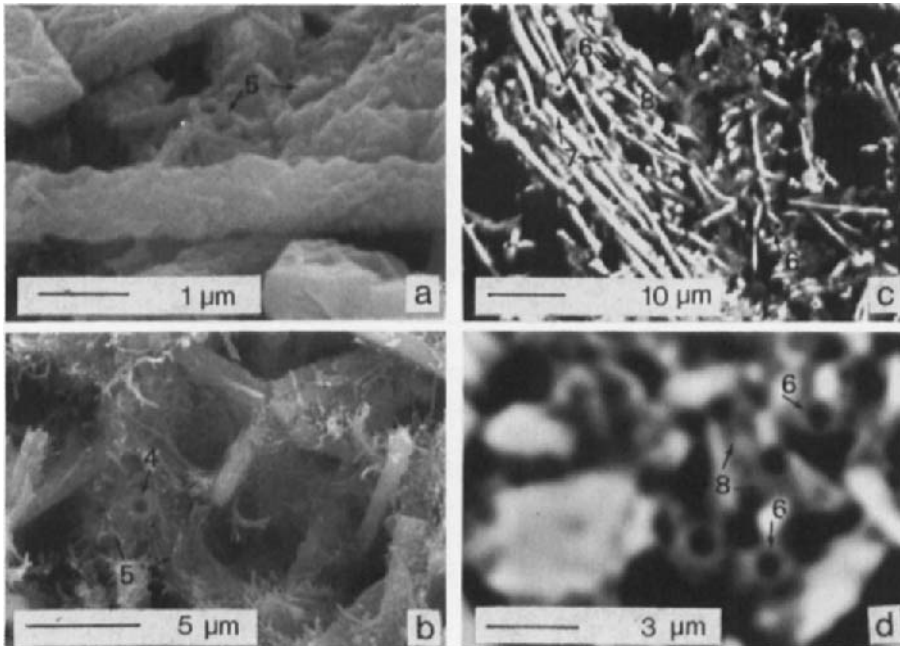
Fig. 5. SEM observation: calcified micro-filaments (4) and micro-rods (5) in the K horizon (a, b, c and d). The micrographs c and d were obtained in the backscattered-electron mode on a thin section, and show a close association of rounded voids (6) needle calcite (7) and micro-rods which corresponding to the fuzzy grey zones (8).

Rhombohedral and spindle calcites

Rhombohedral crystals were studied by Durand (1979) and Dever *et al.*, (1983). Rhombohedral (30 - 50 μm long and 15 - 20 μm wide) and spindle (100 - 200 μm long and 10 - 15 μm wide) calcites are observed in the M_3 horizon, where they are mainly located in narrow planar voids (Fig. 2e and f). Some spindle calcite is also seen in the IIC_1 horizon.

DISCUSSION

Calcified micro-filaments, 1 - 2 μm in diameter (Figs 4f and 5b), and filaments, 5 - 10 μm in diameter (Fig. 4e), respectively correspond to individual hyphae and mycelial strands as earlier shown by Callot *et al.* (1985a), Phillips *et al.* (1987) and Phillips and Self (1987). Calcite crystals radiating from a central hollow are sufficiently developed to be easily seen around strands and individual hyphae (Figs 4f and 5b). Backscattered-electron scanning images (BESI) show numerous small rounded voids, 0.5 - 1.5 μm in diameter in the K horizon (Fig. 5c and d), which correspond to the central hollow of micro-filaments. BESI also show the close association of these voids with micro-rod and needle calcites (Fig. 5c). Individual micro-rods

are too small to be distinguished on the BESI, but they correspond to the grey zones between calcified micro-filaments and needle calcite. The micro-rods are easily seen in the secondary electron mode (Figs 3d and e and 5a), but their association with micro-filaments cannot be seen as the latter are covered by micro-rods. Micro-rod calcite is assumed to be the remains of rod-shaped calcified bacteria that developed in the organic matter of the hyphae, as proposed by Phillips and Self (1987) and according to the work of Boquet *et al.* (1973). These authors obtained micro-rod calcite corresponding to calcified bacteria from *in vitro* experiments with soil bacteria.

For needle calcite, Callot *et al.* (1985b) showed that needles are closely related to fungal hyphae, and proposed that needle differentiation takes place within such hyphae. Phillips and Self (1987) published SEM observations that strongly support this hypothesis. We did not observe the filament structures made of needle calcite that are reported by Callot *et al.* (1985b) and Phillips and Self (1987), but we did observe many needle calcite crystals that are wrapped by micro-rods (Fig. 3d and e). The bacterial action causing lysis of the hyphae walls might explain the disorganization of filament structure and the large number of needle-calcite crystals covered by micro-rods.

The close association between calcified micro-filaments, needle calcite and micro-rods in the K horizon, is assumed to result from the development of fungal hyphae at a depth where the $CaCO_3$ concentration in soil solution is high. Fungal hyphae concentrate $CaCO_3$ around individual hyphae and within hyphae in the mycelial strands. Bacteria developing in the organic matter of the hyphae release needle calcite from mycelial strands, explaining the infilling of pores by micro-rod and needle calcite, and the resulting cementation of the K horizon.

The long and fine serrated-edged needle calcite (Fig. 4c) presumably resulted from a secondary evolution of needle calcite by partial dissolution and reprecipitation. Such serrated-edged calcite does not show any intermediate facies with the single micro-rods, indicating that the differentiation between serrated-edged and needle calcites is primarily governed by physico-chemical processes. On the other hand, the short and wide serrated-edged needle calcite, whose needles consist of individual rhombohedric crystals (Fig. 4d), may have had a non-biological origin. Rhombohedral calcite is interpreted as resulting from the slow crystallization of calcite in a pure super-saturated $CaCO_3$ solution (Durand, 1979; Dever *et al.*, 1983), which is consistent with the location of rhombohedra in small voids, as indicated above. The spindle calcite that is seen in both small and large voids can be interpreted as resulting from faster super-saturation of the solution than was the case for rhombohedra.

CONCLUSION

Our observations of secondary calcite show that needle and micro-rod calcites probably resulted from mycelial hyphae activity. Micro-rods are calcified bacteria, which developed in the mycelial strands and individual hyphae of fungi. Needles are formed within hyphae in the mycelial strands, as proposed by Callot *et al.* (1985a and b) and Phillips and Self (1987). Assuming that such hyphae concentrate calcium carbonate, the lysis of hyphae walls would form needle calcite covered by micro-rod calcite. On the other hand, the individual fungal hyphae concentrate calcium carbonate on their outer walls and give empty calcified micro-filaments. Calcified micro-filaments and needle calcite could also have formed from various fungi that behave differently when exposed to varying $CaCO_3$ concentrations.

Rhombohedral, spindle and serrated-edged calcites are interpreted as being indirectly or not at all related to biological activity. Dissolution and reprecipitation phenomena and super-saturation conditions explain the variations in morphology. The location of rhombohedral and spindle calcites in soil pores is consistent with the physico-chemical conditions required for their formation.

ACKNOWLEDGEMENTS

REFERENCES

Bocquier, G., 1973. Génèse et évolution de deux toposéquences de sols tropicaux du Tchad. Interprétation biogéodynamique. Doctoral Thesis, Univ. of Strasbourg, 364 pp.

Boquet, E., Boronat, A. and Ramos-Cormenzana, A., 1973. Production of calcite (calcium carbonate) crystals by soil bacteria is a general phenomenon. Nature, 246: 527-529.

Bruand, A., 1980. Analyses de la Superposition de Profils en Vallée Sèche de Champagne Crayeuse. Mem. D.E.A. in Soil Science 7, Univ. of Paris, 50 pp.

Callot, G., Mousain, D. and Plassard, C., 1985a. Concentrations de carbonate de calcium sur les parois des hyphes mycéliens. Agronomie, 5: 143-150.

Callot, G., Guyon, A. and Mousain, D., 1985b. Inter-relations entre aiguilles de calcite et hyphes mycéliens. Agronomie, 5: 209-216.

Calvet, F., 1982. Constructive micrite envelope developed in vadose continental environment in Pleistocene eoliantes of Mallorca (Spain). Acta Geol. Hisp., 17: 169-178.

Dever, L., Durand, D., Fontes, J.C. and Vachier, P., 1983. Etude pédogénétique et isotopique des néoformations de calcite dans un sol sur craie. Caractéristiques et origines. Geochim. et Cosmochim. Acta, 47: 2079-2090.

Ducloux, J. and Butel, P., 1983. Micromorphology of calcretes in a slope deposit in the Poitevine plain, France. In: P. Bullock and C.P. Murphy (Editors), Soil Micromorphology, volume 2. Soil Genesis. Proc. VI Int. Working Meeting on Soil Micromorphology, London, August 1981, AB Academic Publishers, Berkhamsted, U.K., pp. 637-646.

Durand, R., 1979. La pédogenèse en pays calcaire dans le nord-est de la France. Sci. géol., Mem., 55, 198 p.

Esteban, M., 1973. Caliche textures and 'microcodium'. Bull. Soc. Geol. It., 92 (supp): 105-125.

Jaillard, B., 1984. Mise en évidence de la néogenèse de sables calcaires sous l'influence des racines : incidences sur la granulométrie du sol. Agronomie, 4: 91-100.

James, N.P., 1972. Holocene and Pleistocene calcareous crust (caliche) profiles: criteria for subaerial exposure. J. Sediment. Petrol., 42: 817-836.

Kaemmerer, M., Revel, J.C., Berrier, J., Bruand, A. and Lefèvre, D., 1991. Dissolution et précipitations de carbonates dans des sols (Calcrètes) en zone aride, Bassin de Ksabi, moyenne Moulouya, Maroc: Conséquences sur la désertification. Arid Soil Res. and Rehab., 5: 105-126.

Klappa, C.F., 1979. Calcified filaments in Quaternary calcretes: organo-mineral interactions in the subaerial vadose environment. J. Sediment. Petrol., 49: 955-968.

Klappa, C.F., 1980. Rhizoliths in terrestrial carbonates: classification, recognition, genesis and significance. Sedimentology, 27: 613-629.

Knox, G.J., 1977. Caliche profile formation, Saldanha Bay (South Africa). Sedimentology, 24: 657-674.

Kubiena, L.W., 1938. Micropedology. Collegiate Press, Ames, Iowa. 235 pp.

Menillet, F., 1980. Les lithofaciès des calcaires de Beauce (Stampien ... Aquitanien) du Bassin de Paris (France). Bull. B.R.G.M, IV, (1): 15-25.

Ould Mohamed, S., 1991. Prise en Compte de l'Organisation du Sol dans l'Étude des Transferts d'Eau et de Solutés. Mem. D.E.A. in Soil Science I, Univ. of Nancy, 55 pp.

Phillips, S.E., Milnes, A.R. and Foster, R.C., 1987. Calcified filaments: an example of biological influences in the formation of calcrete in South Australia. Aust. J. Soil Res., 25: 405-428.

Phillips, S.E. and Self, P.G., 1987. Morphology, crystallography and origin of needle-fibre calcite in Quaternary pedogenic calcretes of South Australia. Aust. J. Soil Res., 25: 429-444.

Stoops, G.J., 1976. On the nature of "lublinite" from Hollanta (Turkey). Am. Mineral., 61: 172.

Verges, V., Madon, M., Bruand, A. and Bocquier, G., 1982. Morphologie et cristallogenèse de microcristaux supergènes de calcite en aiguilles. Bull. Minéral., 105: 351-356.

Wright, V.P., 1984. The significance of needle-fibre calcite in a Lower Carboniferous paleosol. Geol. J., 19: 23-32.

Phases of calcrete (Nari) development as indicated by micromorphology

M. Wieder[1], M. Sharabani[1] and A. Singer[2]
[1]Department of Geography, Bar-Ilan University, Ramat-Gan, Israel
[2]Faculty of Agriculture, The Hebrew University, Rehovot, Israel

ABSTRACT

Wieder, M., Sharabani, M. and Singer, A., 1994. Phases of calcrete (Nari) development as indicated by micromorphology. In: A.J. Ringrose-Voase and G.S. Humphreys (Editors), Soil Micromorphology: Studies in Management and Genesis. Proc. IX Int. Working Meeting on Soil Micromorphology, Townsville, Australia, July 1992. Developments in Soil Science 22, Elsevier, Amsterdam, pp. 37-49.

A calcareous crust of 1 to 2.5m thickness, known locally as Nari, often covers the chalky hills of semi-arid and arid areas of Israel. The formation of this crust has been attributed in the past to upward water movement from the water table or to descending water during the course of pedogenesis. A comparative study of this phenomena in arid and semiarid areas, supported by micromorphological analysis, has shown that the Nari develops within the host chalky material or calcareous sandy material and not in the soil material. Three phases have been distinguished in the formation of the Nari: (i) a subterraneous phase when Nari developed below a soil cover, (ii) a surface phase when Nari developed after the erosion of the soil material, and (iii) an alteration phase. During the subterraneous phase pedogenic, biogenic and hydrological factors induce morphological differentiation in the host material. Characteristic of the subterraneous phase is the presence of a discontinuous layer of blocky fragments disintegrated *in situ* from the top part of the upper layer. The broken fragments are covered with a dense thin brown crust, 1 cm thick, produced by roots and subsurface water flow. This crust does not have an internal laminar structure. The main development of Nari occurs during the surface phase without pedogenic involvement. The morphological differentiation of a Nari profile shows a surface with a laminar crust produced by lichens which trap airborne dust particles. This crust overlies a very hard consolidated upper layer formed by direct precipitation and recrystallization processes and a lower, moderately indurated layer, with platy structure produced by subsurface water flow. The third alteration phase is characterized by the formation in the upper part of the hard layer of a mosaic like layer consisting of dark reddish brown zones of intercalated laminar crust fragments and light white zones of host material. During this phase the lower platy layer weathers forming large solution pockets. Consequently, the upper hard layer often collapses into large blocks.

INTRODUCTION

A particular type of calcrete called "Nari" occurs locally in the semiarid region of Israel, an area that is subjected to continuous dust deposition. It is widespread in the semiarid areas on porous calcareous substrates, particularly on chalk and calcareous sand. A typical developed

Fig. 1. Location map.

Nari profile has a depth of about 1.5 - 2.5 m and is divided into three layers: a laminar crust, capping the Nari, a hard upper layer of about 1 m thickness termed upper-Nari, which overlies a softer, partly indurated layer termed lower-Nari (Yaalon and Singer, 1974). In more arid or in more humid areas the Nari is shallower and less developed. The origin of the Nari has been the considered by others. According to Goldberg (1958), Nari was considered to be a product of diagenetic changes caused by capillary water rise from the water table. Later the Nari was thought to have a pedogenic origin. Thus, Yaalon and Singer (1974) considered the Nari as an indurated petrocalcic horizon formed by carbonate infilling and recrystallization of the host material, whereas Dan (1977) considered the Nari as a secondary carbonate segregation in soil material, following the morphogenetic sequence of Gile et al. (1966). In a recent study Verrechia (1990) concluded that Nari is an alteration product which formed previously in the soil material in which Bca horizon and argillic features are preserved.

To help resolve these differences a detailed comparative study was initiated in different climates and host materials. The first part of the study, based on field observations and micromorphological characteristics, is presented here.

THE SITES STUDIED

Three representative profiles were described and sampled. Two of them in the semiarid Judean foothills (Fig. 1), one on Eocene chalk of the Zora Formation (Buchbinder, 1969) near Bet Guvrin (BG) and the other on calcareous sand of the Pleshet Formation near Kefar Menachem (KM). The mean annual rainfall is about 400 mm at both sites. The third profile is situated in the arid area of the northern Negev on Eocene chalk near Shivta (SH) with a mean annual rainfall of 150 mm.

METHODS

The profiles were described in the field at exposed sites after mechanical cleaning. Thin sections were prepared after polyester resin impregnation. The terms used in descriptions are from sedimentary petrography and from Brewer's (1964) nomenclature. Values of ^{14}C for dating and stable isotopes of ^{13}C and ^{18}O were determined at the Weizmann Institute, Israel.

Fig. 2. a) Morphological characteristics of the Shivta Nari
  A. laminar-like crust   B. broken fragments in situ
  C. initial upper-Nari   D. lower-Nari   E. bedrock
  b) Morphological characteristics of the Bet Guvrin Nari
  A. mosaic layer   B. upper-Nari   C. lower-Nari   D. bedrock

RESULTS

Macroscopic characteristics

Profile SH

(Fig. 2a). The landscape is slightly undulated with a continuous shallow, desert, skeletal soil consisting of fragments derived by disintegration of calcareous bedrock and mixed with fine material of eolian origin overlying Eocene chalk.

0-40 cm: Surficial, skeletal material mixed with calcareous yellow-brown loessial material with an abrupt lithic transition.

40-55 cm: Blocky *in situ* fragmented layer. The size of the blocks is 10 - 20 cm and some are capped by a dense brown thin layer 0.5 cm thick.

55-80 cm: Moderately indurated layer which consists of plates about 20 cm thick.

80-100 cm: Soft platy structure 1 - 2 cm thick.

100 cm+:   Massive chalk.
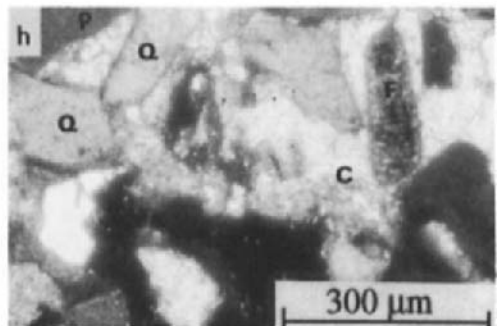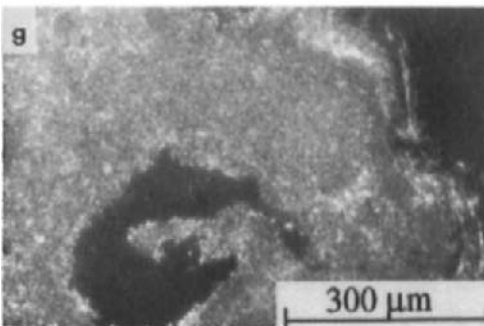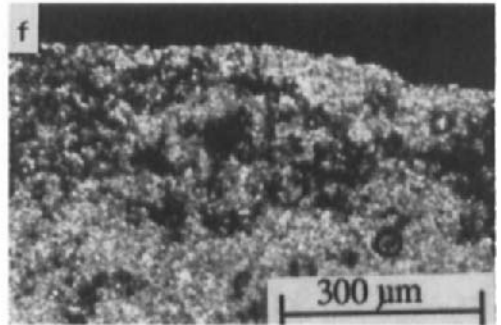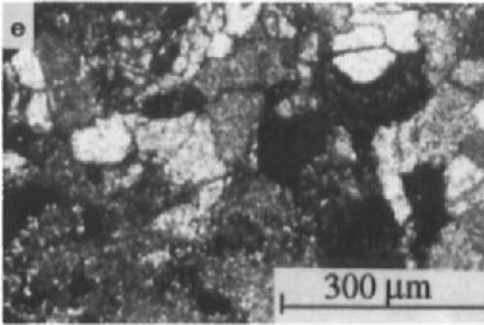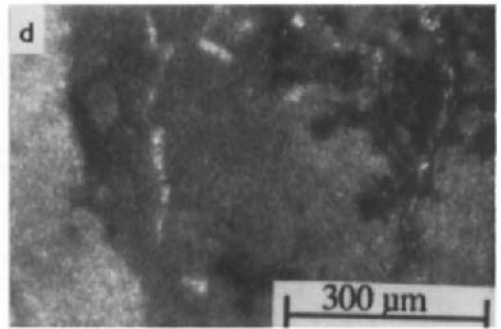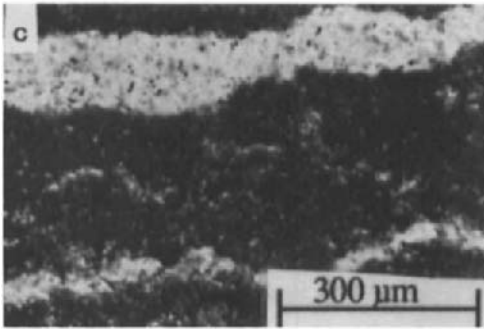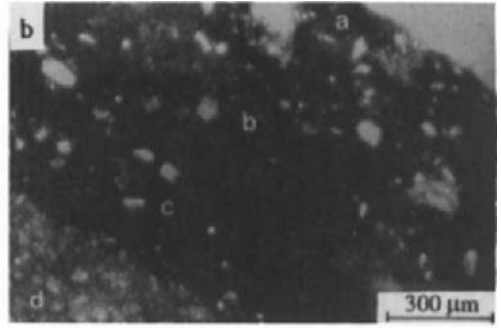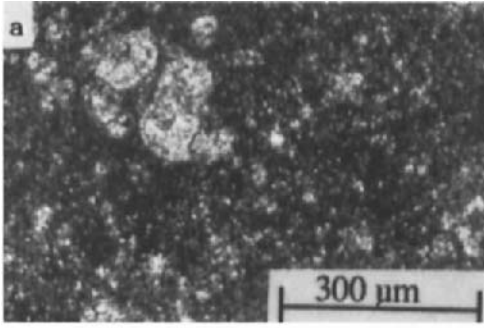
Profile BG

(Fig. 2b). The landscape of the surrounding area show large expanses of exposed Nari on chalk with some brown soil material, mainly of eolian origin, accumulated in pockets.

0-1 cm:	Dense, brown, laminar layer showing alteration features of biogenic dissolution and exfoliation.
2-30 cm:	Strongly indurated layer which consists of white zones and brown zones, 1 - 5 cm thick, showing a mosaic-like fabric.
30-80 cm:	Strongly consolidated hard layer.
80-110 cm:	Moderately indurated platy nodular structure 2 - 5 cm thick.
110-140 cm:	Soft platy structure, 1 - 4 cm thick.
140 cm+:	Massive chalk.

The overall thickness of the upper-Nari is 80 cm and that of the lower-Nari is 60 cm. The lower-Nari frequently shows signs of strong alteration due to intensive dissolution in the form of large cave-like pockets. Without solid support from below, the upper-Nari collapses into large blocks.

Profile KM

Large exposed Nari surfaces on calcareous sand or on calcareous sandstone. Soil material occurs in some pockets.

0-2 cm:	Well developed laminar crust.
2-40 cm:	Strongly indurated mosaic-like fabric composed of brown and white zones of 5 cm thick.
40-80 cm:	Strongly indurated homogeneous layer.
80-120 cm:	Slightly indurated platy structure 1 - 5 cm thick.
120 cm+:	Loose to partly consolidated calcareous sand.

Fig. 3. a) Microfabric of the upper initial Nari of Shivta profile. The rock fabric with Foraminifera is well preserved (crossed polarized light, XPL)

b)Microfabric of the laminar-like crust of the Shivta Nari. From the right upper corner to the left down corner the following zones occur: (a) a soil fabric rich in decomposed roots. (b) soil fabric without root remnants. (c) a transition dense layer to the rock fabric. (d) rock fabric (plane polarized light, PPL)

c) Microfabric of the platy structure of the Shivta Nari (PPL)

d) Microfabric of the mosaic layer of Bet Guvrin Nari. Note lichen remnants on the right side (characteristic to the brown zone) and Foraminifera fossils on the left side (characteristic to the white zone) (XPL)

e) Microfabric of sparitic cementation in the mosaic layer of Bet Guvrin Nari (XPL)

f) Microfabric of the laminar crust of the Kefar Menachem Nari with laminae of lichen remnants (XPL)

g) Microfabric of the Kefar Menachem upper-Nari with micritic calcite crystals and oriented clay in the cracks (right edge) (XPL)

h) Microfabric of the host material of Kefar Menachem Nari. Note the large quartz grains (Q), mollusk fossils (F), pellets (P) and large calcite crystals (C) (XPL)

Micromorphological Characteristics

Profile SH

40-55 cm: The blocky units show a chalky rock fabric which consist of micritic crystals and large rounded grains of Foraminifera (Fig. 3a). The matrix is free of organic remnants. The thin dense brown layer consists of three zones (Fig. 3b). The outer zone shows a brown plasma which includes silt sized grains, mainly quartz and some hornblende and plagioclase grains. The plasmic fabric is calciasepic. Many decomposed organic remnants occur, probably originating from decomposed roots. This zone passes gradually into a middle zone with a similar microfabric but with less decomposed root remnants. The third zone is dense and represents the transition from the soil fabric to the rock fabric. The microfabric of the thin layer differs from that of the laminar crust of the exposed Nari and, therefore, it is defined as a laminar-like layer.

55-80 cm: Similar to the layer above. It has a chalky fabric but with some narrow cracks oriented parallel to the surface. Brownish spots occur within some of the cracks.

80-100 cm: A chalky fabric with a more greyish color which indicates a higher content of organic components. Many laterally oriented voids of about 50 - 300 μm width occur (Fig. 3c). Alongside the planes the color is lighter.

100 cm+:   Typical chalk fabric with a dark-grey color.

Profile BG

0-1 cm: Brownish micritic fabric with laminae of decomposed lichens. On calcrete this fabric is due to lichen stromatolites (Klappa, 1979a). Silt-sized quartz grains of eolian-dust origin frequently occur in the material. Dissolution voids, partly filled by sparry calcite crystals, appear in the crust.

2-30 cm: Two different zones are recognized. A brownish zone in which silt-size grains and lichen remnants are included and a greyish zone which shows remnants of Foraminifera (Fig. 3d). Directly precipitated sparite crystals occur along many planes (Fig. 3e) and convolute fabric often occurs in association with biogenic root channels. A rock nodular fabric, formed by disintegration, occurs in both zones.

30-80 cm: The fabric is micritic with some altered Foraminifera grains. Convolute fabrics occur with root channels. Recrystallized spars and microspars occur in some voids and the micritic fabric shows areas of darker and lighter zones.

80-110 cm: Greyish micritic fabric with more Foraminifera than in the upper layer and it is also less altered. In lateral oriented planes recrystallized microspars occur. Along the planes the micritic fabric has a lighter color.

110-140 cm: Like the above layer

140 cm+:   Dark greyish micritic fabric rich in organic matter and Foraminifera grains.

Profile KM

0-2 cm: In the upper part has a dense micritic fabric, with many partially decomposed lichen laminae and silt-size grain inclusions (Fig. 3f); in the middle part. A gradual transition to a zone with more sandy grains occurs in the middle part. A

convolute fabric, caused by root penetration occurs below the crust in the lower part.

2-40 cm: Micritic fabric with very few sand sized, quartz grains. In the brownish zones lichen remnants and silt-size quartz grains occur.

40-80 cm: Micritic fabric with very few sand-size grains and micritic zones free of sand-size grains (Fig. 3g). In some laterally-oriented planes well oriented clay deposition has occured.

80-120 cm: Microsparitic fabric with many sand size grains.

120 cm+:   Sand size grains with carbonate fossils and pellets. The packing voids between grains are partly filled by sparry calcite crystals (Fig. 3h).

Carbon isotopes

^{14}C values and stable isotopes of profiles SH and BG are presented in Table 1. There is no great age difference between the two profiles or between the layers. ^{13}C is highly depleted in profile BG which was located in the semiarid climate but not depleted in profile SH, which had an arid climate and scarce vegetation. In the deep bedrock of profile BG, where the roots do not penetrate the ^{13}C represents the background value inherited from marine deposition conditions.

PHASES OF NARI FORMATION AND DISCUSSION

Subterraneous phase

Numerous field observations indicate that when Nari occurs below a continuous soil cover it is relatively shallow and undeveloped if the climate is arid or semiarid whereas, when exposed, Nari crusts are thick and well developed. Some particular characteristics of the former case, *i.e.* Nari-below-soil cover, should be emphasized. The main feature is an *in situ* discontinuous layer of broken fragments (Fig. 2a) that is often covered by a thin, dense brown layer. The break-down of these fragments occurred along zones of weakness following plane-surfaces that developed during partial induration of the upper part of the rock.

The thin, dense brown layer is a characteristic feature also and results from dissolution, by root activity, and subsequent cementation at the soil-rock interface. This layer is defined as laminar-like because macroscopically it is very similar to the laminar crust of exposed Nari. The microfabric of the moderately indurated layer shows a slight micritic recrystallization of older, dissolved micritic material. This change is indicated by the light color and the absence of dark grey color caused by organic matter preserved from the original deep seated mud (Folk, 1965). The foraminifera are only slightly altered (Fig. 3a) and convolute fabrics do not appear, as in the case of the indurated petrocalcic horizons in Texas (Rabenhorst and Wilding, 1986), presumably because the water regime is less favorable for root penetration. Cementation caused by large calcite crystals was not observed and it seems that the elimination of the organic matter by carbonate recrystallization favored improved binding among the partly recrystallized micritic grains. The microfabric suggests that the moderate induration is the result of alteration of the host material rather than by translocation of secondary carbonates.

Another characteristic is the thin platy structure below the moderately indurated layer. Water penetrating through the cracks of the upper layer changes the flow direction in the
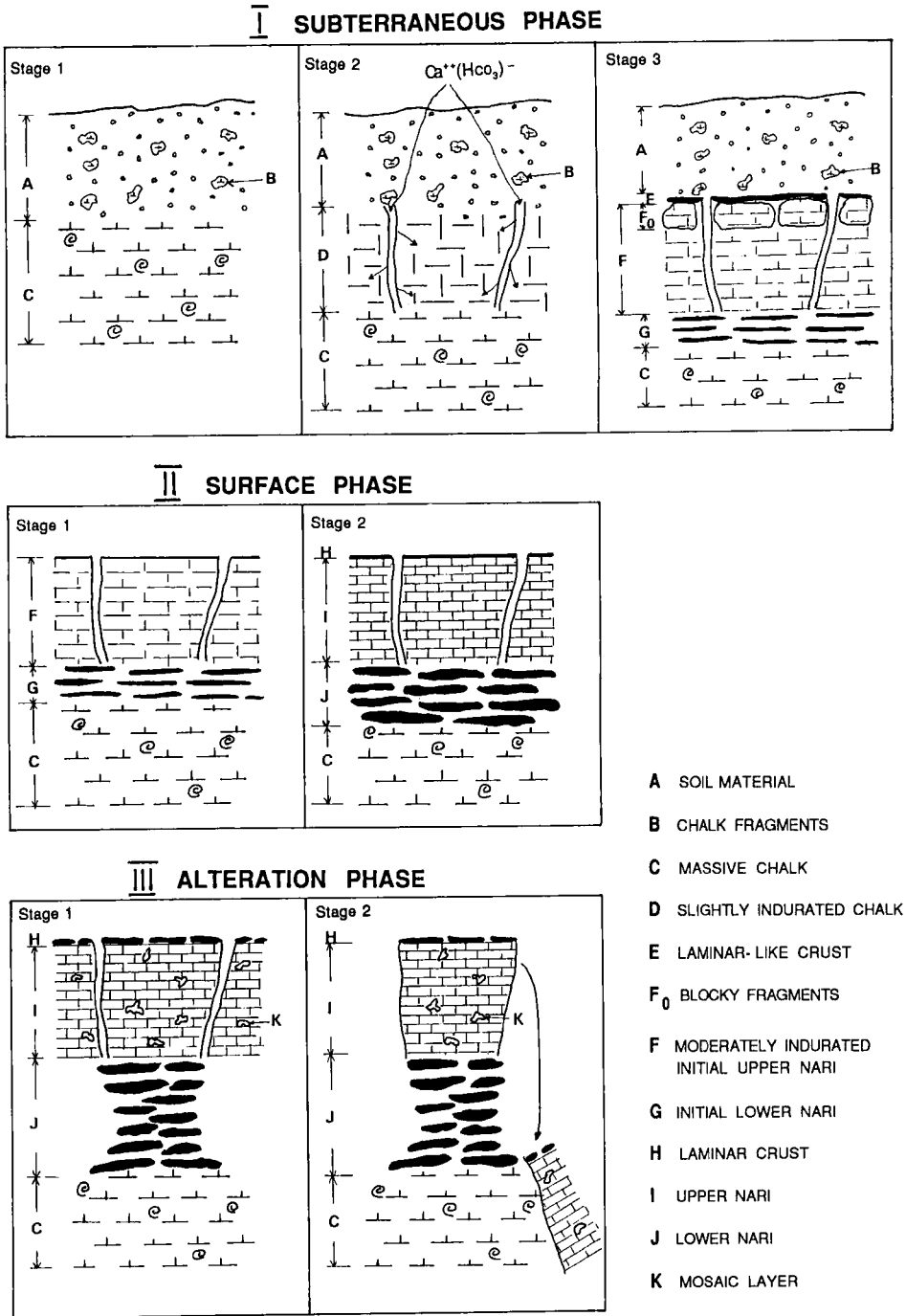
Fig. 4. Model of phases and stages of Nari formation.

Table 1
^{14}C ages and stable isotopes of two Nari profiles

Profile	Layer	^{14}C age	^{13}C	^{18}O
BG	Laminar crust	22,200	-8.11	-3.30
BG	Upper-Nari	26,400	-7.97	-3.60
BG	Lower-Nari	24,500	-7.07	-4.30
BG	Bedrock	>50,000	-0.18	-0.30
SH	Laminar-like crust	25,900	-0.27	-3.16
SH	Upper initial Nari	29,500	-0.48	-4.35
SH	Lower-Nari		-0.34	-5.44
SH	Bedrock	>50,000	+0.29	-4.62

impermeable chalky material to a lateral flow which in turn induces a platy type structure. A very similar situation was reported previously (Wieder and Lavee, 1990).

In view of these findings the stages of Nari formation during the subterraneous phase could be reconstructed as follows (Fig. 4):

Stage 1.   Soils develop and by biophysical alteration of chalk an A/C type soil results (Pale Rendzina in the semiarid climate and Brown Lithosol and Desert Lithosols in the arid climate). Rock fragments occur in the soil material.

Stage 2.   Soil solution penetrating into the rock causes slight induration by carbonate recrystallization and cementing processes.

Stage 3.   The trend at this stage is the differentiation, with depth, of the host material which leads to the appearance of an initial Nari profile. This stage is represented by the following layers downwards:

(i)   A dense, discontinuous brown laminar-like crust (E) 5 - 10 mm thick at the soil rock interface.

(ii)   A layer of blocky *in situ* disintegrated fragments (Fo) 10 - 20 cm in size, consisting of an upper moderately indurated material.

(iii) A dense moderately indurated, massive layer (F) which occasionally cleaves horizontally into thick plates 10 - 25 cm thick.

(iv)   A soft layer, built of thin horizontal plates (G) 0.5 - 2 cm thick. The differentiation took place simultaneously over about 30,000 years (Table 1).

Thus for the development of the subsurface Nari phase below a continuous soil cover, the following can be concluded: (1) the Nari is not the result of pedogenic translocation, (2) the Nari is not formed by secondary carbonate segregation in soil material, and (3) the Nari is an alteration product and can be defined as a petrocalcic horizon formed by alteration in which biogenic and hydrologic factors are involved.

Surface phase

Following exposure Nari develops specific characteristics. The laminar crust consists of decomposed laminae of lichens, and the organic-rich cryptocrystalline laminae are considered to be calcified lichens (Klappa, 1979b). Lichen metabolism requires sunlight, and this means

that for about 22,000 years the laminar crust must have remained exposed and not covered by soil material. Hence, during this period of exposure the differentiation of the Nari cannot be considered as pedogenic. Eolian dust is trapped by lichens and thus most of the insoluble residue of the laminar crust is contributed by the deposited silt-size grains.

An important characteristic is the continuity of the Nari surface in the form of massive blocks and cementation of the smaller fragments or blocks. The intensive cementation occurs after exposure and not before. This feature adds to the basic characteristic of the upper-Nari, namely its very high degree of induration. According to the micromorphological evidence, the main processes which lead to induration were micritization by dissolution and recrystallization of the host material. The process can be easily followed in the case of profile KM developed on calcareous sandstone. Following micritization the sand grains disappear almost completely (Fig. 3g versus Fig. 3h). Possibly, displacement is involved also during the recrystallization to small crystals (Wieder and Yaalon, 1974). Following all stages of micritization it is clear that in this case the convolute fabric is only partly due to micritization. The convolute fabric is biogenic in nature (Danin et al., 1987) and its appearance depends on the intensity of root activity. In the chalky host material micritization is associated with the elimination of organic matter that was preserved in the chalk from the original deep sea, mud material. Large crystals, showing recrystallization features, occur mainly in cracks.

The next characteristic feature is the platy structure of the moderately indurated lower-Nari. The platy structure is caused also by subsurface water flow. The water comes from the surrounding area by runoff and not from a soil solution in the upper surface soil. The descending water flow through the Nari imports carbonate from an external source (Yaalon and Singer, 1974) and this enhances the alteration process. Such a translocation is not pedogenic, even in the case of transported colloidal clay which can be deposited in cracks of the Nari (Fig. 3g). Blümel (1982) proposed in such cases to use the term "per descensum" without the term "pedogenic".

Based on the above characteristics, a model for the surface phase formation can be presented (Fig. 4). The first stage is represented by surface erosion of the soil material which covered original upper-Nari. Erosion also removed the upper blocky fragments. The second stage operated over a long period and led to an increase in thickness of the initial Nari, from about 50 - 80 cm to 1.5 - 2.5 m. Differentiation is gradual and simultaneous in all the layers and results from various factors. The laminar crust is produced by biogenic alteration, the upper-Nari mainly by chemical alteration and the lower-Nari by hydro-physical alteration. The result of the differentiation is a thicker profile with better expression of the characteristic features of all layers. The laminar crust is not the last stage of the induration process as proposed by Gile et al.(1966) for its age is no more advanced than that of the other layers (Table 1).

It can be concluded that the surface phase does not have a pedogenic component and the main development during this phase is produced by alteration of the host material in which biological, chemical and hydrological factors are involved.

Alteration phase

In this phase well developed Nari has been subjected to alteration by weathering. Alteration features can be observed in all layers. The laminar crust of well developed Nari displays feaures of dissolution, disintegration and exfoliation. The lichens built the crust at a stage when

the substrate was softer. Later, when a high degree of induration was attained, the lichens provoked biogenic alteration. The disintegrated laminar crust fragments are gradually imbedded into the upper part of the Nari to about 30 cm depth and become strongly cemented. As a result of this incorporation, the fabric of the top part of the upper-Nari changed to a mosaic-like fabric. The dark-brown to reddish-brown zones show a fabric similar to the laminar crust with silt-size grains and decomposed lichen remnants.

Within this phase weathering is best developed in the lower-Nari. The material contains large and small pores which, together with the available water, create optimal conditions for weathering. The carbonates from this layer are subjected to strong dissolution and the residual material is released. Material from eolian dust and from other released residual material accumulates in some pockets. Intensive alteration leads to the formation of very large solution pockets below the upper-Nari. The large dislocated blocks in the area are the result of this weathering. Detailed data about the weathering process will be published elsewhere.

The model of Nari alteration is presented in Fig. 4. There are two main stages. In the first, the formation of the mosaic layer and partial alteration of the lower-Nari prevail. In the second large cave-like pockets are formed associated with collapse of the upper-Nari into large blocks.

Goudie (1983), in a comprehensive review on calcrete, presented various pedogenic and non-pedogenic models of calcrete formation. In the present study the subterraneous phase is in good agreement with the pedogenic in situ model. This model was adopted by Blank and Tyner (1965) and Rabenhorst and Wilding (1986). The surface phase, however, is not in agreement with other published models. Blümel (1982) presented a model based on a subterraneous stage and a subaerial stage. The subterraneous stage is formed by carbonate translocation from eolian dust into granitic sands and basaltic debris free of carbonates. Blümel considers the subterraneous stage as having formed in semihumid conditions with a dry season with an annual rainfall range of 300 - 600 mm and the subaerial stage formed in arid and semiarid conditions with 100 - 300 mm annual rainfall. The assumption of this model is that in an arid environment the soil cover is eroded and subaerial weathering in arid conditions generates the formation of the upper indurated crust. These postulated environmental conditions are very different from the models presented here. In our situation the Nari is better developed between 400 - 500 mm rainfall and less developed in the arid regions both below soil cover or when exposed. In the more humid areas exposed Nari prevails whereas in the arid areas subterraneous Nari dominates. This is the reverse of postulated by Blümel (1982). The laminar crust of the exhumed calcrete is considered by him as being produced by runoff whereas in our case it is a product of lichen growth. Verrechia (1990) considers the Nari a *per descensum* Bca horizon which was eroded but is still partly preserved within it. In this study no evidence was found for an eventual Bca segregation in a former soil.

The impact of possible climatic changes during the development of the Nari should be taken into consideration also. It is known that fully developed Nari requires semiarid conditions (Yaalon and Singer, 1974). Therefore, the presence of well developed Nari in the semiarid area of Israel suggests that only slight climatic fluctuations occurred throughout the late Pleistocene. This is consistent with stable isotope data from loess-derived paleosols reported by Goodfriend and Magaritz (1989), who found that the climatic fluctuations during the late Pleistocene did not exceed 100 mm mean annual rainfall. Furthermore, the low values of ^{13}C in profile SH could not have occurred if there had been abundant vegetation during the development of the Nari. Finally, these results indicate that the climatic fluctuations during the late Pleistocene did not include a moist phase.

CONCLUSIONS

Three phases are involved in the development of Nari: a subterraneous phase, a surface phase and an alteration phase. Each of these phases has specific characteristics allowing their identification. The Nari is the result of subterraneous pedogenic alteration and surface non-pedogenic alteration of the host material. The main development of the Nari takes place during the surface phase.

REFERENCES

Blank, H.R. and Tyner, E.W., 1965. Formation of caliche *in situ*. Bull. Geol. Soc. Am., 75: 1387-1391.

Blümel, W.D., 1982. Calcretes in Namibia and SE-Spain relations to substratum, soil formations and geomorphic factors. In: D.H. Yaalon (Editor), Aridic Soils and Geomorphic Processes. Catena Suppl. 1, pp. 67-82.

Brewer, R., 1964. Fabric and Mineral Analysis of Soils. Wiley, New York, 470 pp.

Buchbinder, B., 1969. The geological map of the Shephela region, Israel. Israel Geol. Survey Report, OD/168, 13 pp. and maps.

Dan, J., 1977. The distribution of nari and other lime crusts in Israel. Israel J. Earth-Sci., 26: 68-83.

Danin, A., Wieder, M. and Magaritz, M., 1987. Rhizofossils and rootgroves in the Judean desert and their paleoenvironmental significance. Israel J. Earth-Sci., 36: 91-99.

Folk, R.L., 1965 Some aspects of recrystallization in ancient limestones. In: C. Pray and R.C. Murray (Editors), Dolomitization and Limestone Diagenesis. Soc. Econ. Paleontol. Mineral., Special Publ., 13: 14-18.

Gile., L.H., Peterson, F.F. and Grossman, R.B., 1966. Morphological and genetic sequences of carbonate accumulation in desert soils. Soil. Sci., 101: 347-360.

Goldberg, A.A., 1958. Contributions of the study of nari in Israel. Ph.D. thesis, Hebrew University Jerusalem, 162 pp., [in Hebrew].

Goodfriend, A. and Magaritz, M., 1988. Paleosols and late Pleistocene rainfall fluctuations in the Negev desert. Nature, 332: 144-146.

Goudie, A.S., 1983. Calcrete. In: A.S. Goudie and K. Pye (Editors), Chemical Sediments and Geomorphology. Academic Press, pp. 93-131.

Klappa, C.F., 1979a. Lichen stromatolites: criterion for subaerial exposure and a mechanism for the formation of lamina calcretes (caliche). J. Sed. Petrology, 49:389-400.

Klappa, C.F, 1979b. Calcified filaments in Quaternary calcretes: organo-mineral interactions in the subaerial vadose environment. J. Sed. Petrology, 49: 955-968.

Rabenhorst, M.C. and Wilding, L.P., 1986. Pedogenesis on the Edwards Plateau, Texas,III. New model for formation of petrocalcic horizons. Soil Sci. Soc. Am. J., 50: 693-699.

Verrechia, E.P., 1990. New micromorphological interpretation of nari-calcrete (Israel). In: L.A. Douglas (Editor), Soil Micromorphology: A Basic and Applied Science. Proc. VIII Int. Working Meeting on Soil Mircromorphology, San Antonio, Texas, July 1988. Developments in Soil Science 19, Elsevier, Amsterdam, pp. 677-682.

Wieder, M. and Lavee, H., 1990. Micromorphological characteristics induced by subsurface flow in the Judean desert. In: L.A. Douglas (Editor), Soil Micromorphology: A Basic and Applied Science. Proc. VIII Int. Working Meeting on Soil Mircromorphology, San Antonio, Texas, July 1988. Developments in Soil Science 19, Elsevier, Amsterdam, pp. 235-243.

Wieder, M. and Yaalon, D.H., 1974. Effect of matrix composition and carbonate nodule crystallization. Geoderma, 11: 95-121.

Yaalon, D.H. and Singer, S., 1974. Vertical variations in strength and porosity of calcrete (nari) on chalk, Shephela, Israel and interpretation of its origin. J. Sed. Petrology, 44: 1016-1023.

This Page Intentionally Left Blank

Fabric features of laterite and plinthite layers of ultisols in northeast Thailand

A. Suddhiprakarn and I. Kheoruenromne

Department of Soil Science, Kasetsart University, Bangkok 10903, Thailand

ABSTRACT

Suddhiprakarn, A. and Kheoruenromne, I., 1994. Fabric features of laterite and plinthite layers of ultisols in northeast Thailand. In: A.J. Ringrose-Voase and G.S. Humphreys (Editors), Soil Micromorphology: Studies in Management and Genesis. Proc. IX Int. Working Meeting on Soil Micromorphology, Townsville, Australia, July 1992. Developments in Soil Science 22, Elsevier, Amsterdam, pp. 51-64.

A study of fabric features of laterite and plinthite layers of Ultisols in northeast Thailand was conducted on samples collected from five soil profiles including two Typic Plinthustults, two Typic Plinthaquults and a Petroferric Haplustult. Petrographic (thin section) and scanning electron microscopic (SEM) analytical techniques were employed in the study. X-ray diffraction (XRD) analysis was also used to identify mineral components of the samples. Petrographic analysis of plinthite layers of the Plinthustults has revealed a fabric having mainly a ferri-argillan groundmass embedded with impregnated nucleic nodules of iron oxides, subangular quartz fragments and some vughs. Material interpreted to be lepidocrocite exists in the samples as dark orange patches in the fabric groundmass. Argillans occur on pore walls, rock fragment surfaces and some nodule surfaces. For laterite layers of the Plinthaquults and Petroferric Haplustult, some differences in the fabric components was noted among profiles. Relationships of coarse and fine materials in the fabric range from open to close spacing of skeleton materials embedded in the groundmass, inclusive of the nodules of iron oxides. The nature of the nodules ranges from impregnated nucleic to concentric and concentric nucleic. Other minerals identified include hematite and goethite. Scanning electron microscopic analysis of the samples has revealed distinctive forms of goethite, hematite, quartz, kaolinite and possibly lepidocrocite. Based on the morphological features and mineral assemblages in these laterite and plinthite layers their profile types and mode of formation can be differentiated.

INTRODUCTION

Northeast Thailand lies between latitudes 14°10' and 18°10' North, and between longitudes 101°30' and 105°40' East. Physiographically, it is a plateau underlain by various clastic sedimentary rocks including sandstone, siltstone and shale. This entire northeast plateau is separated into two broad basins by the Phu Pan mountain range. The upper basin is called the Sakon Nakhon basin and the lower one is generally known as the Khorat basin. Elevation in this region, excluding high hills and mountains, ranges between 150 and 250 m (a.s.l.); being highest in the western fringe and descending towards the northeast and east.
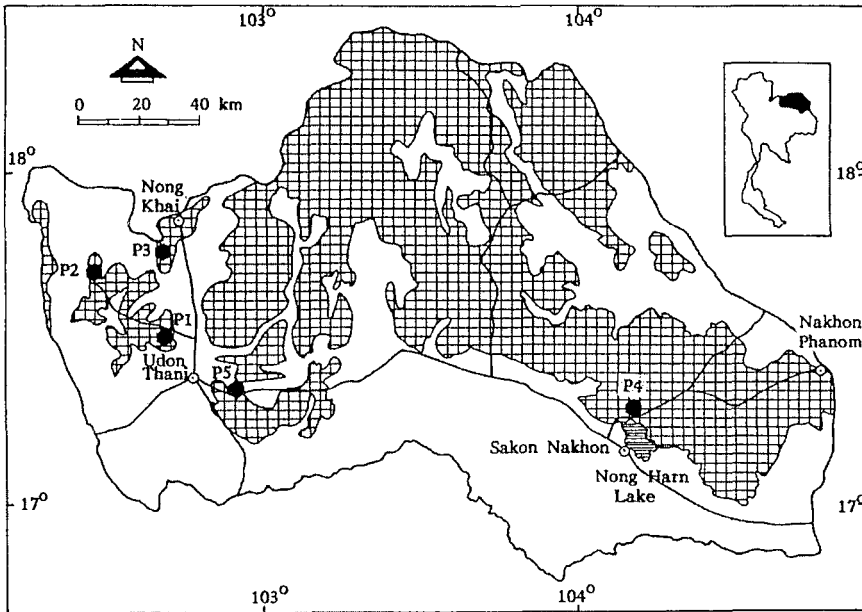
Fig. 1. Location map of the Sakon Nakhon basin and sampling sites. Shaded area indicates Ultisols with laterite or plinthite layers, P1 and P2 are Plinthustults, P3 and P4 are Plinthaquults and P5 is a Petroferric Haplustult.

The area is subject to a tropical savanna (Aw) broad climatic regime (Koppen, 1931) having a long and pronounced dry season. Mean annual rainfall varies from approximately 1,000 mm in the west to 1,800 mm in the northeast and east. Land use of the area, at present, is characterized by remnants of deciduous forest, upland field crops of mainly cassava and sugarcane and transplanted rice on the lowlands. The most extensive soils found in the area are Ultisols (Kheoruenromne and Kesawapitak, 1989; Moncharoen *et al.*, 1987). Plinthustults, Haplustults and Plinthaquults which have plinthite and hardened (petro) plinthite (ferricrete or laterite) layers in their profiles are quite extensive in the Sakon Nakhon basin, bordered by the Mekong river. This area has a mean annual rainfall of approximately 1,400 mm and a mean temperature of 28° Celsius. The objectives of this paper are to discuss (i) some features of the laterite and plinthite layers in these soils that have been used to differentiate them, and (ii) elucidate their genesis and stages of development.

MATERIALS AND METHODS

Ultisols in the study included two Plinthustults (P1 and P2), two Plinthaquults (P3 and P4) and a Petroferric Haplustult (P5). Their locations are shown in Fig. 1.

Field studies included the morphological analysis of soil profiles from the surface down to the saprolite or to a depth of 3.5m. Disturbed (39 samples) and undisturbed (24 samples) soil

Table 1

Morphology of Ultisols with plinthite or laterite layer in Sakhon Nakhon Basin, Northeast Thailand.

Horizon	Depth (cm)	Colour; Mottles	Texture	Structure	Consistence	pH (1:1 H$_2$O)	Other Features
P1 (Typic Plinthustult)							
A	0-5	10YR6/4	SL	sbk	SH, S, SS/SP	7.0	Few iron oxide nodules; clear; smooth boundary
Btc	5-17	10YR6/8, 10YR7/1	GSL	sbk	H, Fri, SS/SP	5.5	Common iron oxide nodules; clear and smooth boundary
L1	17-35/38	10YR6/4	EGSCL	sbk	Moderately packed, partially cemented	5.5	Irregular shaped nodules and concretions (0.4-1 cm) embedded in matrix; clear and smooth boundary
L2	38-70/78	10YR7/1, 10R3/4	VGC	sbk	Strong and partially cemented	5.5	Common iron oxides nodules and concretions (0.3-0.7 cm); abrupt and wavy boundary
L3	78-128	10YR7/1; 75YR5/8, 10R4/8	C	sbk	F, S/P	5.5	Zone of sesquioxides and clay separation with common irregular shaped nodules and concretions (0.3-0.7 cm); clear and smooth boundary
S	128-180	2.5YR4/8	Saprolite	rs	F	5.5	Bedding of sandstone
P2 (Typic Plinthustult)							
A	0-3/4	7.5YR4/6	SL	sbk	S,V.Fri, SS/NP	6.0	Few nodules and concretions; clear and smooth boundary
Bt	4-12	10YR5/8	L	sbk	SH, Fri, SS/SP	6.0	Few nodules and concretions (0.3-0.5 cm); abrupt and smooth boundary
Btc	12-30/40	10YR6/8	GL	sbk	F, SS/SP	5.5	Manganocretes mixed with iron oxide nodules; clear and wavy boundary
L1	40-50	10YR5/8, 10R3/2	EGCL	sbk	Moderately weakly and partially cemented	5.5	Irregular shaped hardened sesquioxides (1-2 cm) mixed with manganiferrous nodules; abrupt and smooth boundary
L21	50-80/90	10YR7/4, 2.5YR4/6	EGCL	sbk	Moderately strongly and partially cemented	5.5	Few manganiferrous nodules mixed with sesquioxide nodules and concretions (0.2-0.4 cm); clear and wavy boundary
L22	90-105/110	10YR7/1, 10R3/3, 10YR6/8	VGCL	sbk	Moderately weakly cemented, argillaceous and ferri-argillaceous cementation	5.5	Common semi-platy to subrounded iron and aluminum oxide nodules and concretions (0.3-2 cm); clear and wavy boundary
L3	110-200	10YR7/1; 7.5YR5/8	C	sbk	F, S/P	5.0	Common partially hardened iron oxide nodules (0.5-1 cm) of irregular shape; abrupt and smooth boundary
S	200-240	10R4/8, 10YR7/1	Saprolite	rs	F	5.5	Highly weathered red siltstone mixed with clay

P3 (Typic Plinthaquult)

A	0-10	10YR6/4	GSL	sbk	SH, VR, NS/NP	6.5	Common subrounded concretions (0.2-0.5 cm); clear and smooth boundary
Bc1	10-40	10YR6/3	GSL	sbk	SH, V.Fri, NS/NP	6.5	Common subrounded concretions (0.4-1 cm); clear and smooth boundary
Bc2	40-70/75	10YR6/2	VGSL	sbk	VH, Fri, SS/NP	6.0	Many concretions of various sizes; abrupt and wavy boundary
L1	75-90/100	10YR7/6	EGCL	m	Moderately weakly packed	6.0	Few manganiferrous nodules mixed with many subrounded and irregular shaped hardened iron-aluminum oxide concretions (1-1.5 cm); abrupt and wavy boundary
L2	100-190/100	10YR7/4	EGL	m	Very strongly cemented	6.0	Practically consisting of semi-platy hardened vermicular iron-aluminum oxide concretions and nodules (2-4 cm), massively cemented; abrupt and wavy boundary
L3	200-260/270	10YR7/1; 10YR7/8	EGCL	m	Moderately cemented	6.0	Many irregular shaped concretions (2-8 cm) embedded in clay matrix; clear and wavy boundary
Pc	270-295	10YR7/1	EGCL	sbk	F, SS/SP	6.0	Many irregulur shaped iron-aluminum oxide concretions and nodules (2-3 cm); clear and smooth boundary
M	295-320	10YR7/1; 10R3/3, 10R4/8	CL	sbk	SF, SS/SP	6.0	Few irregular shaped iron-aluminun oxide concretions and nodules; clear and smooth boundary
P	320-350	10YR7/1; 10R4/8, 10R6/8	SiL	sbk	SF, SS/SP	6.0	Semi-massive clay layer

P4 (Typic Plinthaquult)

Ap	0-10	10YR4/4	GSL	sbk	Fri, SS, SP	6.5	Common rounded iron-aluminum oxide concretions (0.2-0.4 cm); abrupt and smooth boundary
Bc	10-15	10YR4/3	EGSiL	sbk	Fri, SS/SP	7.0	Many rounded iron-alumium oxide concretions (0.2-0.4 cm); clear and smooth boundary
L1	15-30/45	10YR5/4, 10R5/8, 10R3/2	EGSL	sm	Loosely packed, partially cemented	7.0	Many rounded and subrounded hardened iron-aluminum oxide concretions, some enriched with manganese 0.2-4 cm mainly; abrupt and wavy boundary
L2	45-50/55	2.5Y6/4, 5YR3/3, 2.5YR4/8; 7.5YR5/8	EGC	m	Moderately strongly cemented	6.0	Many rounded and subrounded iron-alumium oxide concretions (0.3-0.6 cm) with few aggregates of 1-2 cm; abrupt and wavy boundary
P	55-75/80	5Y7/1; 7.5YR4/8	C	m	F, S/P	6.0	Common rounded and subrounded iron-aluminum oxide concretions, some enriches with manganese (<0.3 cm); clear and wavy boundary

S1	80-90	5Y7/1; 2.5YR4/8, 10R4/6, 7.5YR5/8	SiC	m	F	6.0	Many fragments of highly weathered siltstone; clear and smooth boundary
S2	90-125	5Y7/1, 2.5YR3/6	Saprolite	rs	F	6.0	Moderately weathered siltstone with bedding

P5 (Petroferric Haplustult)

Ap	0-5/10	10YR7/3; 7.5YR5/8	SiL	abk-sbk-sm	VH, Fri, SS/NP	6.5	Streak mottles; clear and wavy boundary
Bw	10-20/40	10YR6/1	SiL	sbk	VH, Fri, SS/NP	6.5	Common trace of dead roots; few rounded concretions (0.4 cm); abrupt and wavy boundary
L2	40-75/90	7.5YR5/8,7.5YR4/6,- 5YR4/8, 10R3/4		m	Strongly cemented	7.0	Massively cemented hardened iron-aluminum oxide and manganiferrous concretions; clear and wavy boundary
L3	90-102/110	10YR7/2; 2.5YR4/8,- 10YR5/6, 2.5YR3/0		sm	Partially but mainly strongly cemented	7.0	Platelike and irregular shaped concretions and nodules (mainly 0.4-1 cm); abrupt and wavy boundary
Pc1	110-125	10YR7/1	EGC	sm	Moderately cemented	6.0	Ootithic iron-aluminum oxide concretions (0.2-0.4 cm); clear and smooth boundary
Pc2	125-150	5Y7/1; 7.5YR5/8	GC	m	F, S/P	6.0	Few irregular shaped hardened iron-aluminum oxide concretions (0.2-0.4 cm); abrupt and wavy boundary
P	150-190	5Y7/1; 10YR6/8	SiC	sm	F, S/P	6.5	Common cracks and few iron-aluminum oxide concretions (0.2-0.4 cm); abrupt and smooth boundary
S1	190-225/230	5Y7/2; 2.5YR4/6	Saprolite	rs	F	6.5	Patches of iron oxide concentrations; clear and wavy boundary
S2	230-245	5Y7/2	Saprolite	rs	F	6.5	Bedding of sandstone

Texture	C	= clay		SiC	= silty clay		GSiL	= gravelly silt loam
	L	= loam		SiL	= silt loam		VGCL	= very gravelly clay loam
	CL	= clay loam		GSL	= gravelly sandy loam		VGSL	= very gravelly sandy loam
	SL	= sandy loam		VGC	= very gravelly clay		EGSL	= extremely gravelly sandy loam
	GC	= gravelly clay		EGC	= extremely gravelly clay		EGCL	= extremely gravelly clay loam
	GL	= gravelly loam		EGL	= extremely gravelly loam		EGSiL	= extremely gravelly silt loam
							EGSCL	= extremely gravelly sandy clay loam
Structure	sbk	= subangular blocky		sm	= semi-massive		rs	= rock structure
	abk	= angular blocky		m	= massive			
Consistence	Fri	= friable		VH	= very hard		NS	= nonsticky
	V.Fri	= very friable		S	= soft		SS	= slightly sticky
	H	= hard		F	= firm		NP	= nonplastic
	SH	= slightly hard		VF	= very firm		SP	= slightly plastic
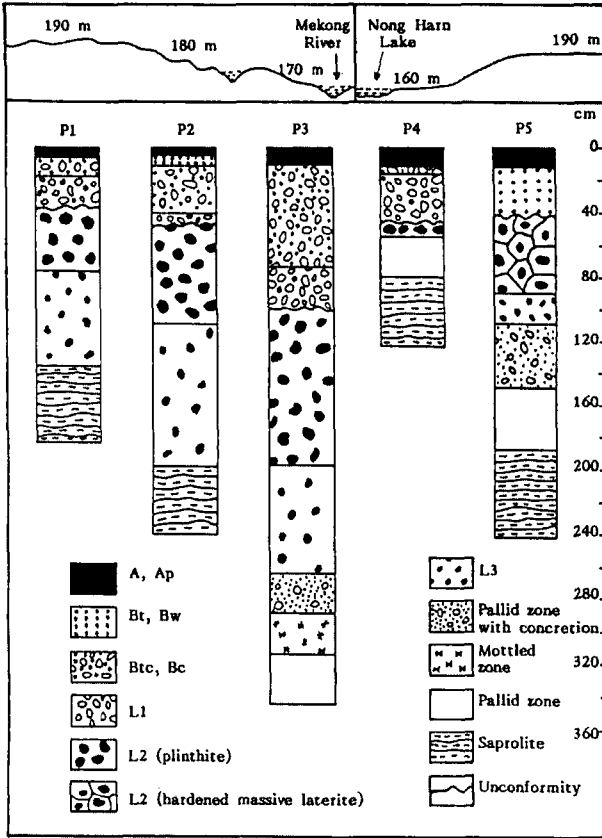
Fig. 2. Topographic position, elevation and schematic models of Ultisols having a laterite or plinthite layer in their profiles. P1 and P2 are Plinthustults, P3 and P4 are Plinthaquults and P5 is a Petroferric Haplustult.

samples, including laterite or plinthite, were collected from each genetic horizon for laboratory analysis. Results of 14 samples of laterite and plinthite layers are reported in this paper.

Laboratory work included mineralogical analysis and fabric analysis of each sample in triplicate. Mineralogical analysis employed the use of powder XRD of oriented clay samples on glass slides and disoriented powder samples of laterite or plinthite materials in an Al-holder (Jackson, 1969; Whittig, 1965) using Shimadzu XRD model XD-5A. Fabric analysis consisted of two parts: (i) a study of thin sections of impregnated samples using a petrographic microscope (Brewer, 1964), (ii) using a Jeol SEM model JSM-35CF with samples being gold coated and mounted on a stub with silver paint.

RESULTS AND DISCUSSION

Field Morphology and Profile Models of Ultisols with Laterite or Plinthite Layers

Results of the study of field morphology (Table 1) revealed that all of these soils have the L layer at a shallow depth (<1 m). Soil horizons above the L layer include A or Ap, Bw or Bt, and Bc or Btc. Most of these soils have a loose laterite layer (L1) on top of the main laterite or plinthite layer (L2). Clay coatings occur in the Bt and Btc horizons of these soils indicating

their relatively well developed stage of soil formation (Buol *et al.*, 1989). The L layers in these soils are of variable thickness and most of the soils have a saprolite layer at a shallow depth (<2 m) (Fig. 2).

The nature of the L layers in these soils varies. For P1 and P2 the main L layers fit the definition of plinthite in Soil Taxonomy (Soil Survey Staff, 1975, 1990) and laterite as described in earlier studies (Alexander and Cady, 1962; Gidigasu, 1976; Goudie, 1973; McFarlane, 1976; Sivarajasingham *et al.*, 1962). The layers have a massive appearance. A major part of each layer is composed of clay patches mixed with nodules and concretions of concentrated iron oxides with some manganese oxides. These nodules and concretions are linked or cemented by iron oxides mixed with clay to form various network patterns. However, any cementation is weak because the layers can be cut with a spade. The clay matrix in the L2 layers of P1 and P2 generally has high chroma (>4). The L2 layers in P3 and P4 have a similar appearance to those of P1 and P2 but are relatively harder, particularly in P3. Their clay matrix has a low chroma (≤2) and they have some mottles with high chroma indicating episodic wet and dry conditions in the soil profile. The L2 layer in P5 is a massive, hardened plinthite with few clay patches. Both the nodules and concretions and the cementing materials in the layers are hardened and cannot be cut by a spade in the field. The L2 layers in P5 have red and reddish brown colours.

From the schematic profiles shown in Fig. 2 it is evident that four of these five profiles (except P5) have L1 layers (loose laterite layers) and Btc or Bc layers. The presence of these layers indicates both erosion and deposition of materials while the absence of them (as in P5) indicates only erosion of the surface. Since erosional features on the surface of the L2 layers are so pronounced it is apprarent that they mark a discontinuity or unconformity in these profiles.

Mineralogy of Laterite or Plinthite Layers

Results obtained from XRD analysis of the clay fraction of L layers of these soils are summarized in Table 2. For P1, P2 and P3, kaolinite and sometimes illite are the major clay minerals with the former dominating. This is usual in well developed soils in the tropics (Sanchez, 1976). The presence of illite suggests the influence of water transported materials and is consistent with the presence of loose transported laterite layers in these soils. Traces of smectite, vermiculite and chlorite occur in P1 and P2. Though their quantities are very small their presence suggests the continuation of weathering processes within the laterite or plinthite layers. The presence of lepidocrocite in P1 and gibbsite in P2 suggests a drier moisture regime in P1 (Schwertmann, 1988). The general mineral assemblage in P3 is similar to that in P2. However, the absence of weatherable minerals such as smectite, chlorite and feldspar indicates a more advanced stage of weathering and soil formation in P3 (Buol *et al.*, 1989). Traces of quartz in the clay fraction of most L layers in these soils conform well with results of other studies of soils in Northeast Thailand (Sindhusen, 1984; Suddhiprakarn *et al.*, 1985) where an abundance of sandstone-derived materials is present. For P4, the mineralogy of the clay fraction presents a different picture. Moderate amounts of illite, along with the thick L1 layer indicate the strong influence of alluvium in the present day environment. This profile occupies a lower part of the landscape and has been more influenced by seasonal waterlogging for a long period each year. This condition appears to retard the formation of kaolinite (Buol *et al.*,

Table 2

Mineral composition of the clay fraction in the laterite or plinthite layers. (IS clay=Interstratified clay, 1+1.4 nm).

Horizon	Depth (cm)	Kaolinite	Illite	Smectite	Vermiculite	Chlorite	IS clay	Quartz	Feldspar	Goethite	Gibbsite	Hematite	Lepidocrocite
P1 (Typic Plinthustult)													
L1		xx	xx	tr	tr	-	tr	tr	tr	tr	-	tr	-
L2	38-70/78	xxx	xx	tr	tr	-	tr	tr	-	tr	-	tr	-
L3	78-128	xx	xx	tr	tr	-	tr	-	tr	-	-	tr	-
P2 (Typic Plinthustult)													
L1	40-50	xx	xx	-	tr	tr	tr	tr	-	tr	tr	-	-
L21	50-80/90	xxx	xx	-	tr	tr	tr	tr	-	-	tr	-	-
L22	90-105/110	xxx	xx	-	tr	tr	tr	tr	tr	tr	tr	-	-
L3	110-200	xx	xx	-	tr	tr	tr	tr	tr	tr	tr	-	-
P3 (Typic Plinthaquult)													
L1	75-90/100	xxx	tr	-	tr	-	tr	tr	-	tr	tr	-	-
L2	100-190/200	xxxx	tr	-	x	-	tr	tr	-	tr	tr	-	-
L3	200-260/270	xxxx	x	-	tr	-	tr	tr	-	tr	tr	-	-
P4 (Typic Plinthaquult)													
L1	15-30/45	x	xx	-	tr	-	tr	tr	-	tr	-	-	-
L2	45-50/55	x	xx	-	tr	-	tr	-	-	-	tr	-	tr
P5 (Petroferric Haplustult)													
L2	40-75/90	Massive laterite horizon											
L3	90-102/110	Mainly cemented and pisolitic laterite horizon											

xxxx = dominant (>60%)	xxx = large (40-60%)	xx = moderate (20-40%)	
x = small (5-20%)	tr = trace (<5%)	- = not detected	

1989). The L layers in P5 are consolidated without a free clay fraction. They indicate a long period of exposure in the past (McFarlane, 1976).

The silt fraction of the L layers of these soils contains much quartz. Other minerals in this fraction are present in very small quantities. They include feldspar, mica, goethite, hematite and kaolinite. Traces of hematite occur in all L layers of P2. However, the presence of feldspar and mica in the L layers indicates a relatively immature weathering status and the influence of alluvium in their formation.

The mineral composition of nodules or concretions in the laterite and plinthite layers of these soils is given in Table 3. Only three major minerals occur consistently in these lateritic materials. They are quartz, goethite and hematite. Even in the hardened L layers in P5, moderate amounts of quartz exist. From Table 3, a generalization can be drawn that the typical mineral composition of the lateritic nodules and concretions in this region should consist of quartz, goethite and hematite in approximately equal amounts. In drier conditions, with some loss of water, the nodules and concretions would become aged and their mineral composition would evolve to have more hematite than goethite (Fitzpatrick, 1987). The aged nodules or concretions may have more hematite than goethite whereas under moister conditions more goethite and less hematite occur. The amount of quartz varies from place to place and with the development stages of the laterite or plinthite layer.

Fabric Features of Laterite and Plinthite Layers

Micromorphological features in thin section

Fig. 3 illustrates features of the undisturbed fabric of laterite or plinthite layers in some of these Ultisols. In the L1 layer of P1 (Fig. 3A), the fabric features show impregnated nucleic nodules, ferri-argillan groundmass, subangular quartz grains in the nodule and large voids (vughs). This kind of fabric, with nodules of various shapes embedded in the clay-iron oxide groundmass, indicates the unconsolidated nature of the layer. Actually, lateritic nodules, which account for approximately 25% by volume in L1, are partially cemented. In the L2 layer of P1 the lateritic nodules account for approximately 50% by volume and though they are generally cemented, they are not hard. The fine earth in the matrix comprises clay and a small amount of fine grained quartz with approximately 5% clay coatings on pore walls. Iron oxide coatings on quartz grains generally act as the cementing material of the lateritic nodules. In the L3 of P1, partial leaching is quite evident being indicated by the pale brown colour of the clay matrix. In this layer, fewer iron oxide nodules occur. The iron oxide coating around quartz grains indicates *in situ* weathering. The orange colour of the iron oxide accumulations in these layers may be lepidocrocite.

Fabric features in the L layers of P2 are similar to those of P1. L1 consists mostly of loose lateritic nodules with a very small amount of cemented materials and with a similar fabric to that of L1 in P1. In L21, lateritic nodules are abundant. They are partially compacted and partially cemented by clay and iron oxides and also have layered features which indicate flow in the matrix. Most lateritic nodules (>50% by volume) are nucleic ferruginous nodules of reddish brown to dark brown colour. Cementing materials are composed of silt-sized quartz embedded in a matrix of clay and iron oxides. Ferri-argillans are also present. In L22, most of the fabric shows similar features to that of L21 but only about 50% by volume of the lateritic nodules are cemented. The fabric of this L22 layer is shown in 3B. It consists of impregnated shale that is rich in iron oxides, nucleic nodules, ferri-argillan cementing material and subangular quartz grains. This kind of fabric is typical of the major plinthite section of P1, P2 and P3. The cementing materials have considerable contents of iron and manganese oxides but the degree of hardening in most cases is not sufficient in natural field conditions to form massive hardened plinthite or laterite layers. However, upon exposure due to forest clearing or erosion of the overburden materials the hardening process can proceed rapidly. Ironstone gravels and boulders in the vicinity of these pits support this interpretation. The L3 layer in some of these profiles can be characterized by a light coloured clay matrix with some high chroma iron oxides and ferri-argillans. Lateritic nodules are also present in low amounts in this layer which is considered a transitional zone in the profile.

The degree of sphericity of the nodules and concretions in the L1 layers varies and it probably depends mainly on the transportation of these materials before redeposition to form a layer of loose lateritic materials. Fig. 3C shows the fabric features of L1 in P4. Embedded in the groundmass of clay and iron oxides is a concentric nodule with a high degree of roundness. However, subrounded quartz fragments occur inside the nodule. This profile appears to consist of appreciable quantities of water transported materials. As a consequence the lateritic nodules or concretions in the L1 layer of this soil are generally spherical.

The fabric of the laterite and plinthite layers in P5 as shown in Fig. 3D is very similar to that of P2. It is composed mainly of concentric nucleic nodules and subangular quartz, but with hardened cementing materials. This type of fabric represents a hard plinthite layer (laterite) or

Table 3
Mineral composition of nodules or concretions in laterite or plinthite layers.

Horizon	Depth (cm)	Quartz	Feldspar	Goethite	Hematite	Mica
P1 (Typic Plinthustult)						
L1	17-38	xx	-	tr	xx	-
L2	38-70/78	xxx	tr	tr	x	tr
L3	78-128	xxx	-	-	tr	tr
P2 (Typic Plinthustult)						
L1	40-50	x	-	x	x	-
L21	50-80/90	xx	-	x	x	-
L22	90-105/110	x	-	tr	x	-
P3 (Typic Plinthaquult)						
L1	75-90/100	x	-	x	x	-
L2	100-190/200	x	-	x	x	-
L3	200-260/270	xx	-	x	xx	-
P4 (Typic Plinthaquult)						
L1	15-30/45	tr	-	xx	x	tr
L2	45-50/55	x	-	xx	x	-
P5 (Petroferric Haplustult)						
L2	40-75/90	xxx	-	x	x	-
L3	90-102/110	xx	-	x	x	-

xxx = large (40-60 %)   xx = moderate (20-40 %)   x = small (5-20 %)
tr = trace (<5%)   - = not detected

ironstone. Its presence indicates that erosion occurred in the area in the past and the plinthite layer has hardened irreversibly as a result.

Scanning electron microscopic features of minerals

Some results of SEM study of minerals in the laterite or plinthite layers of these Ultisols are summarized in Fig. 4. Major minerals in these laterite or plinthite layers are goethite, hematite, quartz, kaolinite and with some material interpreted as lepidocrocite. Goethite in these layers takes many forms, including poorly developed plates and granular or lenticular aggregates. Figs 4A and 4B illustrate lenticular goethite in P3 (Plinthaquult) and P5 (Petroferric Haplustult) respectively. The difference in size and form of this lenticular goethite is interpreted as being determined by available moisture within each environment. The larger size and better defined form in P3 is due to moister conditions favoring the stability of goethite. The form of goethite in Fig. 4B is grading towards the form of hematite shown in Fig. 4C. Hematite in the form of botryoidal columns is very characteristic of all profiles. Forms of a mineral interpreted as lepidocrocite in P1 is shown in Fig. 4D. It has a poor platy form resembling goethite. However, further studies are needed to verify the habit of this mineral in lateritic profiles. It should be noted here that P1 is under a remnant of dry dipterocarp forest with drier climatic conditions than the other profiles. Forms of kaolinite in P1 and quartz in P2 are shown in Figs 4D and 4E. The tabular form of kaolinite and sharp-hexagon edge of quartz are readily recognizable under the electron microscope (Fig. 4F). Their presence also indicates conditions of stability in the soils.
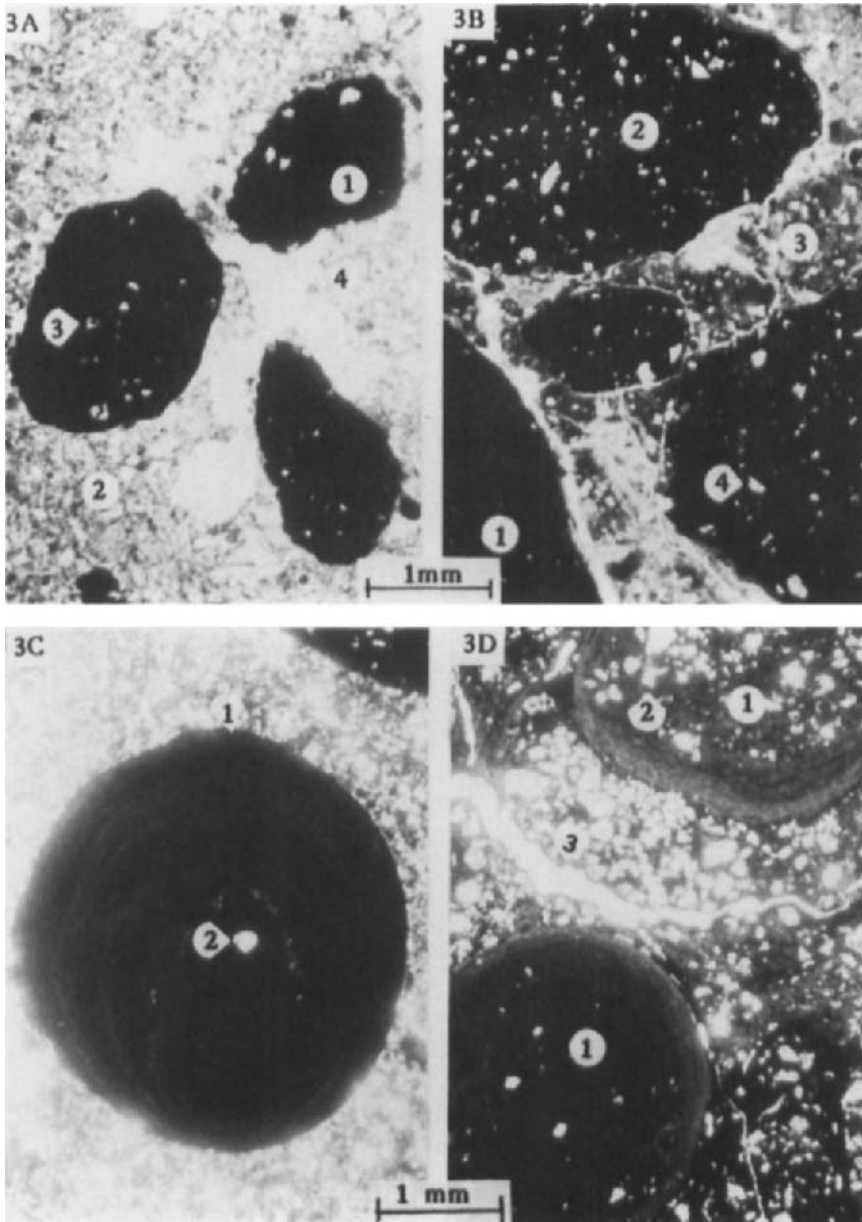
Fig. 3. Petrographic micrographs of laterite or plinthite layers of Ultisols in Northeast Thailand. **A)** Fabric of L1 in P1: 1=impregnated nucleic nodule; 2=ferri-argillan groundmass; 3=subangular quartz grain in nodule and 4= vugh (plane light). **B)** Fabric of L22 in P2: 1=impregnated shale fragment rich in iron oxides; 2=nucleic nodule; 3=ferri-argillan cementing materials and 4=subangular quartz (plane light). **C)** Fabric of L1 in P4: 1=concentric nucleic nodule and 2=subangular quartz fragment in nodule (crossed polarized light). **D)** Fabric of L2 in P5: 1=concentric nucleic nodules; 2=subangular quartz and 3=channel (plane light).
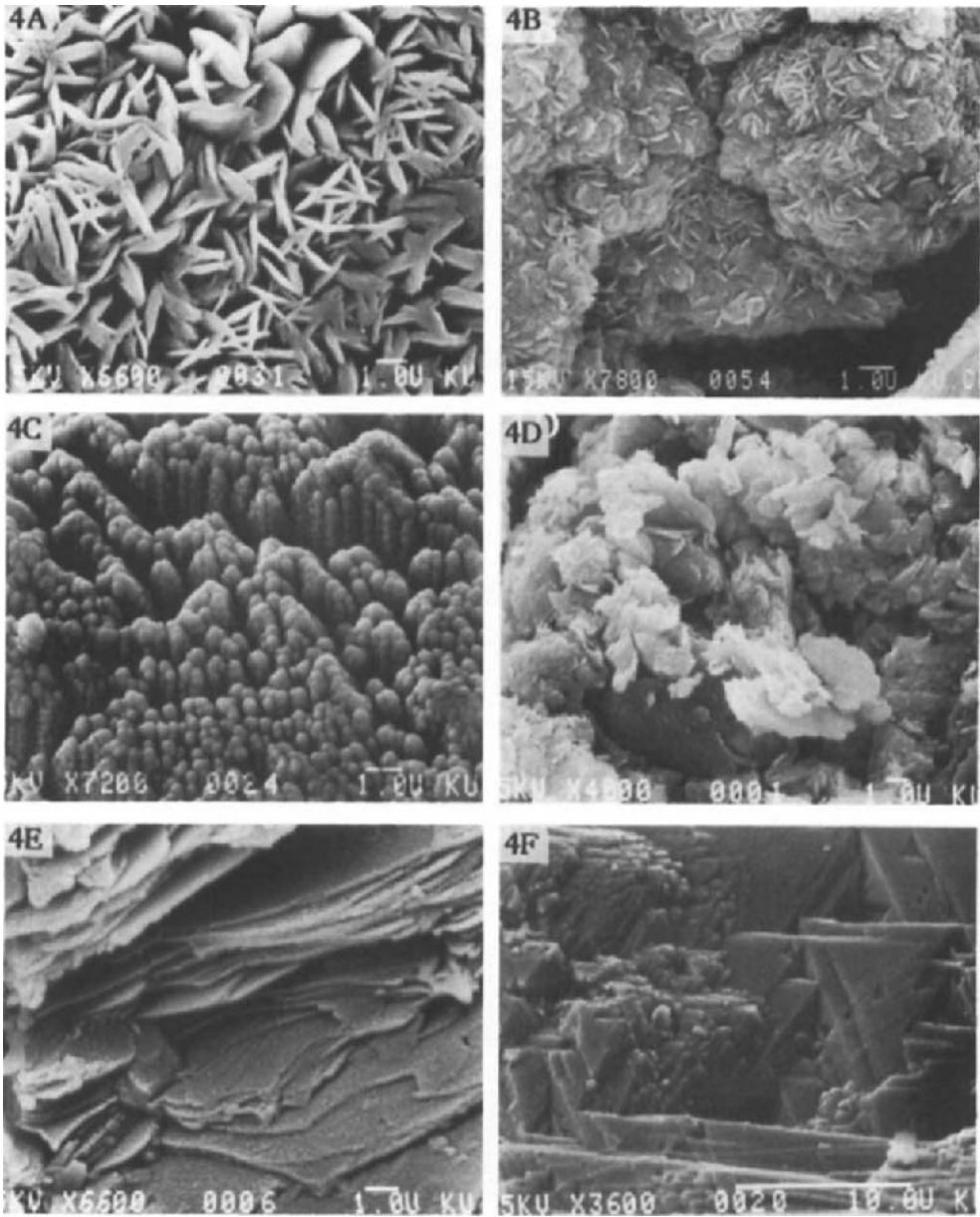
Fig. 4. Scanning electron micrographs of major minerals in laterite or plinthite of Ultisols in Northeast Thailand: A) lenticular goethite in P3; B) lenticular goethite in P5; C) botryoidal columns of hematite in P2; D) possible platy lepidocrocite in P1; E) tabular sheets of kaolinite in P1; F) hexagonal edges of quartz in P2. (A-E: bar=1 μm; F: bar=10 μm).

CONCLUSION

Based on the profile features, mineral assemblages, fabric features and forms of minerals in their laterite or plinthite layers, these soils can be grouped into four profile types.

The Type I profile includes the two Plinthustults of P1 and P2. It illustrates a profile of mature development on relatively well-drained undulating terrain at a higher elevation (180 - 190 m a.s.l.). Pedogenic processes are active and weatherable minerals are still present. Plinthite fabric in the profile consists of cemented nucleic nodules of iron oxides and patchy accumulations of kaolinite. The lateritic nodules are composed mainly of quartz, goethite and hematite in relatively equal proportions. The Type II profile is characterized by the Plinthaquult (P3), an old and well differentiated profile on moderately well-drained terrain showing a more complete lateritic horizonation. It developed on a gently undulating surface connected to the area of Type I profile but at a lower elevation (170 m a.s.l.) and a lower position in the same landscape continuum. It contains a mature and thick layer of a harder plinthite with less kaolinite. The proportions of quartz, goethite and hematite are approximately equal throughout the semi-hardened plinthite layer. The fabric of laterite or plinthite also has similar features to that of Type I, but the main laterite or plinthite layers are generally hard. The Type III profile is the shallow Plinthaquult of P4. It occupies a lower part of the landscape, *i.e.* a depression area at lower elevation (160 m a.s.l.). It is characterized by having a thick layer of loose laterite nodules and concretions, and a thin layer of weakly recemented lateritic nodules and concretions, showing a degree of vertical sorting, resting unconformably on an *in situ* pallid zone derived by weathering of clastic sedimentary rock. The lateritic nodules and concretions generally have equal proportions of quartz, goethite and hematite but the soil matrix also has substantial amounts of illite. The profile has poor internal drainage though it is well developed.

The Type IV profile is markedly different from the others. It is represented by the Petroferric Haplustult (P5) occupying a gently undulating plain at higher elevation (190 m a.s.l.) and with obvious evidence of past severe erosion. Its laterite layers have hardened completely forming a hardpan near the soil surface. The laterite layer has equal proportions of quartz, goethite and hematite. The fabric features in the laterite layer are no different from those of Types I and II but the entire layer has hardened.

ACKNOWLEDGEMENTS

REFERENCES

Alexander, L.T. and Cady, J.G., 1962. Genesis and Hardening of Laterite in Soils. Soil Conservation Service, U.S. Dep. Agric. Technical Bulletin No. 1282, 90 pp.

Brewer, R., 1964. Fabric and Mineral Analysis of Soil. John Wiley and Sons, New York, 470 pp.

Buol, S.W., Hole, F.D. and McCracken, R.J., 1989. Soil Genesis and Classification. Iowa State University Press, Ames, Iowa, 403 pp.

Fitzpatrick, R.W., 1987. Iron compounds as indicators of pedogenic processes: Examples from the Southern Hemisphere. In: J.W. Stucki, B.A. Goodman and U. Schwertmann (Editors), Iron in Soils and Clay Minerals. D. Reidel Publishing, Dordrecht, Netherlands, pp. 351-396.

Gidigasu, M.D., 1976. Laterite Soil Engineering, Pedogenesis and Engineering Principle. Elsevier, Amsterdam, 544 pp.

Goudie, A., 1973. Duricrust in Tropical and Subtropical Landscapes. Oxford University Press, London, 174 pp.

Jackson, M.L., 1969. Soil Chemical Analysis - Advanced Course. 2nd Edition, 8th printing, 1973. Dept. of Soil Sci., Uni. of Wisconsin, Madison, 895 pp.

Kheoruenromne, I. and Kesawapitak, P., 1989. Management of acid soils for food crop production in Thailand. In: E.T. Craswell and E. Pushparajah (Editors), Management of Acid Soils in the Humid Tropics of Asia. ACIAR Monograph No. 13, Canberra, Australia, (IBSRAM Monograph No. 1), pp. 100-109.

Koppen, W., 1931. Grundrisz der Klimakunde. Walter de Gruyster, Leipzig, Berlin, 388 pp.

McFarlane, M.J., 1976. Laterite and Landscape. Academic Press, London, 149 pp.

Moncharoen, L., Vearsilp, T. and·Eswaran, H., 1987. Benchmark Soils of Thailand. Dept. of Land Development, Ministry of Agriculture and Cooperatives, Bangkok, Thailand, and SMSS, Washington, D.C., USA, 77 pp. + Appendix 99 pp.

Sanchez, P.A., 1976. Properties and Management of Soils in the Tropics. John Wiley and Sons, New York, 618 pp.

Schwertmann, U., 1988. Occurrence and formation of iron oxides in various pedoenvironments. In: J.W. Stucki, B.A. Goodman and U. Schwertmann (Editors), Iron in Soils and Clay Minerals. D. Reidel Publishing, Dordrecht, Netherlands, pp. 267-308.

Sindhusen, P., 1984. Mineralogy and Chemistry of Selected Red and Yellow Soils in Thailand. Masters Thesis, Kasetsart University, Bangkok, 193 pp. [in Thai].

Sivarajasingham, S., Alexander, L.T., Cady, J.G. and Cline, M.G., 1962. Laterite. Advances in Agronomy, 14: 1-60.

Soil Survey Staff, 1975. Soil Taxonomy: A Basic System of Soil Classification for Making and Interpreting Soil Surveys. U.S. Government Printing Office, Washington, D.C., 754 pp.

Soil Survey Staff, 1990. Keys to Soil Taxonomy, 4th edition. SMSS Technical Monograph No. 6. Virginia Polytechnic Institute and State Univ., Blacksburg, Virginia, 422 pp.

Suddhiprakarn, A., Kheoruenromne, I., Sindhusen, P. and Yoothong, K., 1985. Clay minerals and iron oxides of selected red and yellow soils in Northeast Plateau and Southeast Coast, Thailand. Kasetsart J., 19: 265-271.

Whittig, L.D., 1965. X-ray diffraction techniques for mineral identification and mineralogical composition. In: C.A. Black (Editor), Methods of Soil Analysis, Part 1. Am. Soc. Agron., Madison, Wisconsin, pp. 671-698.

Darwinian zircons as provenance tracers of dust-size exotic components in laterites: mass balance and SHRIMP ion microprobe results

G.H Brimhall[1], W. Compston[2], I.S. Williams[2], R.F. Reinfrank[2] and C.J. Lewis[1]

[1]*Department of Geology and Geophysics, University of California, Berkeley 94720 USA*
[2]*Research School of Earth Sciences, Australian National University, Canberra ACT 0200, Australia*

ABSTRACT

Brimhall, G.H., Compston,W., Williams, I.S., Reinfrank, R.F. and Lewis, C.J., 1994. Darwinian zircons as provenance tracers of dust-size exotic components in laterites: mass balance and SHRIMP ion microprobe results. In: A.J. Ringrose-Voase and G.S. Humphreys (Editors), Soil Micromorphology: Studies in Management and Genesis. Proc. IX Int. Working Meeting on Soil Micromorphology, Townsville, Australia, July 1992. Developments in Soil Science 22, Elsevier, Amsterdam, pp. 65-81.

At the lateritic bauxite deposit at Jarrahdale, Western Australia we quantify micromorphological evidence of an excess cumulative detrital soil component and relate its presence and accommodation in the subsurface to the combined effects of long-term, eolian deposition and progressive, dilational mixing induced by biological activity. The subsurface entry mechanism involves a repeated sequence of void space creation through root decay, detrital translocation, pore infilling, and renewed root growth. This process is evident as a multitude of oriented, geopetal, microsedimentary pore deposits cross-cutting still older in-filled voids along arcuate, concave-up unconformities observed in ultra-thin (5-micron) sections. Tubular root voids controlling invasive translocation penetrate even the most indurated of duricrusts and hence provide effective pathways for detritus to descend from the surface down to the top of saprolite. In comparison to this detrital transport, we show that *in situ* residual enrichment, viewed conventionally as the principal mechanism of bauxitization, dominates only the lowest, most primitive part of the soil above bedrock where tubular voids are uncommon. The horizontal interface separating detrital (plus minor residual) and purely residual components below is critical to mapping and understanding the exposure level of laterite profiles. This two-part soil package, previously referred to by Ollier and Galloway (1990) as detrital ferricrete overlying saprolite, was interpreted by them as being subdivided by a sedimentary unconformity. However, we conclude that the Jarrahdale lateritic bauxite has no unconformity but instead is differentiated *internally* into a composite but *continuous* biomechanical system with two distinct compartments defined by the penetration depth of exotic detritus mixed into the subsurface by pedoturbation and bioturbation. While the upper bio-active part is contaminated by surficial detritus and biochemically-cycled components like carbon and sulfur, the lower cell receives only organic acid decay products. We integrate these micromorphologic features of the soil profile with their broader geological context by application of SHRIMP ion microprobe zircon geochronology which is a new, preferred

technique in provenance studies. This proved the exotic character of detrital zircons and also established preliminary age constraints on their ultimate provenance. From comparison of ages of rounded zircons in bauxite with dated in-place zircons in bedrocks exposed regionally, we infer the detrital source regions to be disrupted kaolinitic-laterite mantles developed earlier on eroded paleo-orogenic mountain belts surrounding the Yilgarn and/or younger sedimentary basins containing kaolinitic erosional detritus.

INTRODUCTION

The purpose of this paper is to interpret micromorphological evidence of exotic cumulative soil components in lateritic bauxite deposits which is inconsistent with the prevailing view of a simple *in situ* residual origin. Rather than fuel continued debate over merits of conflicting models of residual versus transported detrital origin, we set out here instead to apply definitive new analytical methods to determine where, how and why either or both of these contrasting enrichment mechanisms occur. The techniques we employ to resolve these issues involve both elemental and isotopic mass analysis and in combination afford unique capabilities of first discerning and then quantifying the effects of these discrete processes. We measure the mass contribution of the detrital laterite component by elemental mass balance and constrain its provenance using isotopic tracers. These new techniques make it possible to unequivocally differentiate detrital additions (aeolian, colluvial and alluvial) from residual components. Thus we can begin to integrate complex small-scale microscopic soil features with the broader long-term geological context of surficial transport processes in cratons. Here, processes occurring at ground level uniquely reflect subdued peneplained landscapes where erosion is minimal and the biota inevitably plays an important role in development of a composite weathering mantle by complex internal ordering at the interface of the biosphere with the geosphere.

ANALYTICAL STRATEGY AND FIELD SITE SELECTION

We have applied elemental mass balance and isotopic methods to the Jarrahdale lateritic bauxite deposit in the Darling Range of Western Australia (Fig. 1). This deposit has been studied by Sadleir and Gilkes (1976), Smurthwaite (1990) and Anand et al., (1991) and besides excellent mineralogical profile descriptions, offers the potential advantage of having developed locally over a late Archean (2.6 Ga) granitic parent material making it possible to eliminate its variability as a cause of diversity in soil profile characteristics or a significant factor in its pedogenic evolution. Although a lingering controversy persists as to the igneous or sedimentary character of the parent material (Grubb, 1971) this issue is resolved here in a later section.

Analytical sequence

Using fresh granitic gneiss parent material exposed in a deep rail cutting as the state of comparison, we proceed through a sequence of analytical steps in a well-proven mass balance strategy (Brimhall and Dietrich, 1987; Brimhall et al., 1988, 1991, 1992). First, volume change induced by weathering and pedogenesis is determined directly rather than assuming an isovolumetric process. Second, using the calculated volume changes or strains, we determine the absolute chemical gains and losses of elements in individual samples of the
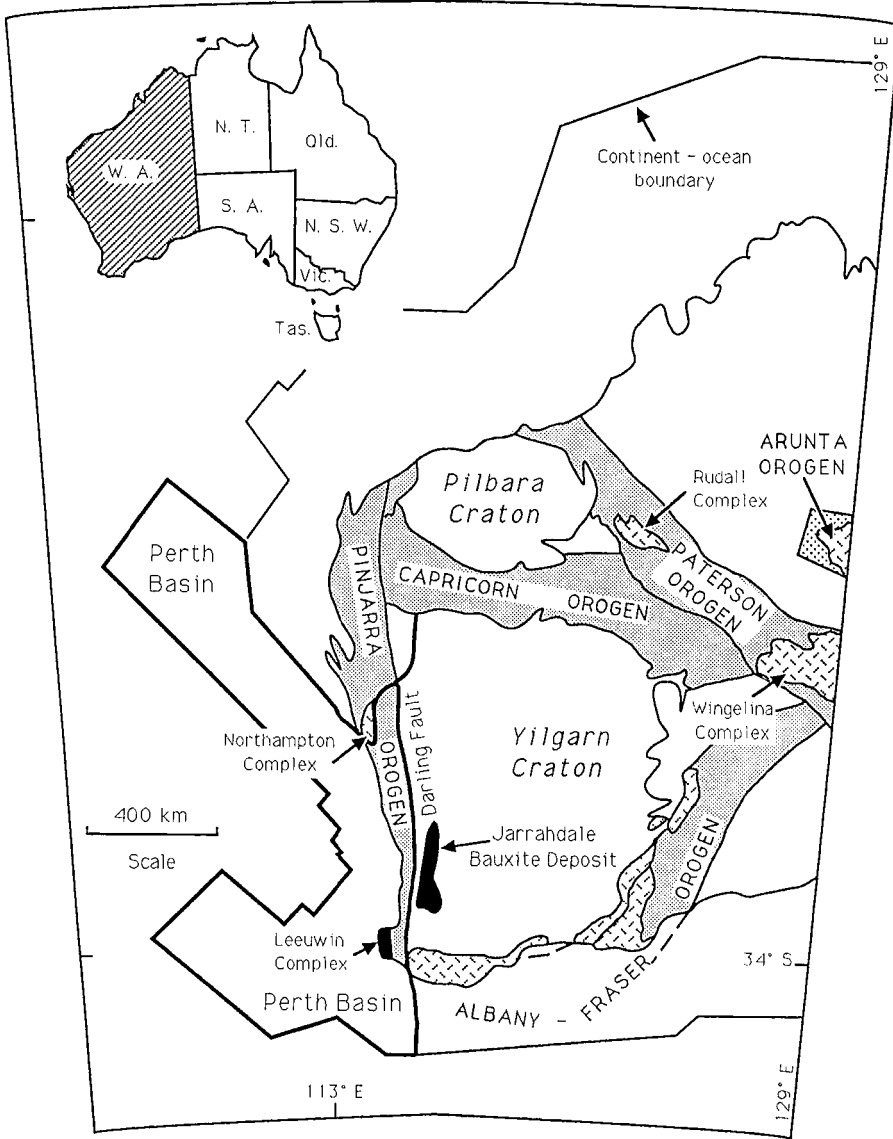
Fig. 1. Location map of Jarrahdale lateritic bauxite deposit in Western Australia in the Darling Ranges near Perth at the western edge of the late Archean Yilgarn Craton. Ancient, now eroded, Pinjarra, Albany-Fraser, Patterson and Arunta orogen mountain belts are shown modified from Myers (1990) and Trendall (1990) in relation to the Perth sedimentary Basin (Trendall and Cockbain, 1990). The Leeuwin Complex, interpreted here as the principal source of rounded exotic zircons in the Jarrahdale bauxite, is shown on the southwest corner of Australia within the Pinjarra orogen.

porous medium. From these true *transported* mass profiles we evaluate each zone of mass accumulation. For those with a related zone of depletion, local profile-scale migration is inferred. Zones of accumulation lacking internal source regions require influx from external sources. Thirdly, we evaluate the total enrichment factor of each element in terms of component enrichment mechanisms: residual accumulation, deformation and transport. Finally, SHRIMP (sensitive high-resolution ion microprobe) (Compston *et al.*, 1984) zircon dating is used to verify the identity of the parent material, establish its upward continuity and to constrain the provenance of dateable exotic detrital minerals associated with aluminous and ferruginous detritus shown by mass balance to have been derived from sources external to the profile.

Incompleteness of the in situ residual and detrital origin models

Basically three laterite genesis models have been advanced that differ principally in the mode of accumulation of aluminous and ferruginous minerals and in the interpretation of the relevant parent material. These models can be categorized as (1) *in situ* residual enrichment of granitic gneiss parent material, (2) detrital transport and (3) weathering of sedimentary parent material rather than granitic gneiss. Each of these models, while making important advances in understanding bauxite genesis, are incomplete and leave essential features of the profiles unexplained. The prevailing *in situ* residual model of the genesis of the Jarrahdale bauxite deposit (Sadleir and Gilkes, 1976; Davy, 1979, Smurthwaite, 1990; and Anand *et al.*, 1991) cites the similarity between chemical, mineralogical and physical characteristics of bauxite including textures and structures with specific underlying igneous rocks (generally late Archean granites or more rarely younger dolerite dikes of the Yilgarn Craton). Ollier and Galloway (1990), addressing laterite genesis in general, prefer a strict detrital origin of ferricrete occurring above saprolite and interpret the contact as being a depositional sedimentary unconformity of presumably-transported material overlying an indigenous substrate.

An alternative and controversial weathering model invoking an arkosic fluviatile sedimentary parent material instead of local granitic gneisses, was proposed by Grubb (1971) to explain the presence of a rounded abraded suite of heavy accessory minerals (zircon, rutile, ilmenite, monazite and tourmaline) in the uppermost zones of certain bauxites, including Jarrahdale. This interpretation of Grubb's "mineralogical anomalies" was refuted by Baker (1972), Sadleir and Gilkes (1976) and also Davy (1979). Davy (1979), who while also favoring a residual weathering mechanism, pointed out that the origin of the exotic accessory minerals and the means of their incorporation into the "caprock" had not been clearly identified. Davy also pointed out that windblown materials would be expected over the expanses of the Yilgarn under desert conditions inferred earlier by Killigrew and Glassford (1976).

MASS BALANCE STUDIES

By making the first application of mass balance techniques fully-integrating chemical composition with physical properties and volume change (Brimhall *et al.*, 1985; Brimhall and Dietrich, 1987) to the Jarrahdale bauxites, Brimhall *et al.* (1988) were able to use chemical elements as geochemical tracers which reveal their own history of transport. Thus, effective discrimination between residual accumulation and transport was made possible. This study of
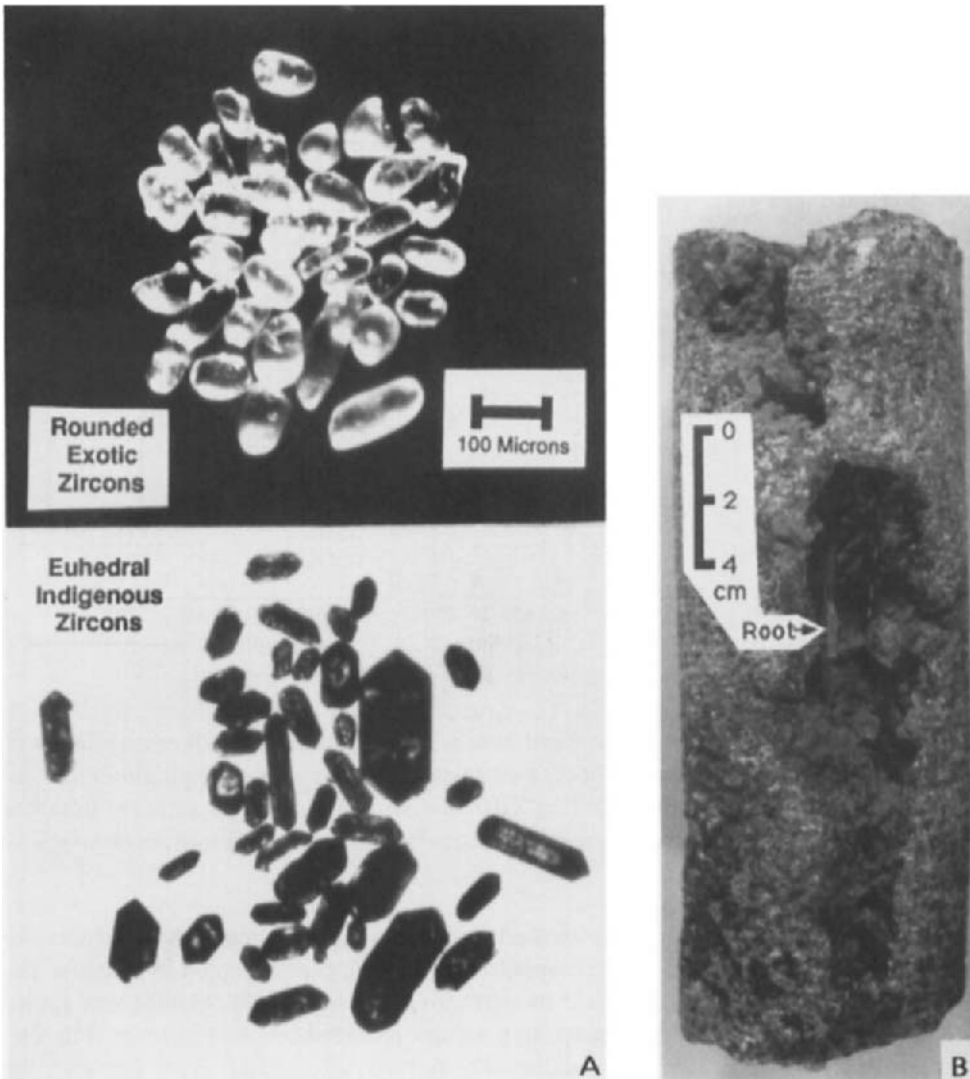
Fig. 2. (A) Comparison of clear rounded exotic Darwinian zircons (top) with cloudy euhedral indigenous zircons (bottom) from the Jarrahdale bauxite. (B) Example of a modern root occupying an older void in which detrital translocation occurs.

Jarrahdale reconciled several features of the previously contradictory interpretations and showed that the widespread but vertically-localized surficial detrital suite of accessory minerals, including rounded zircon (Fig. 2A), was in fact introduced from the top of the profile possibly after eolian transport responsible for grain abrasion. The decreasing abundance of the detrital suite with depth does not support Grubb's contention that it is derived from a fluviatile
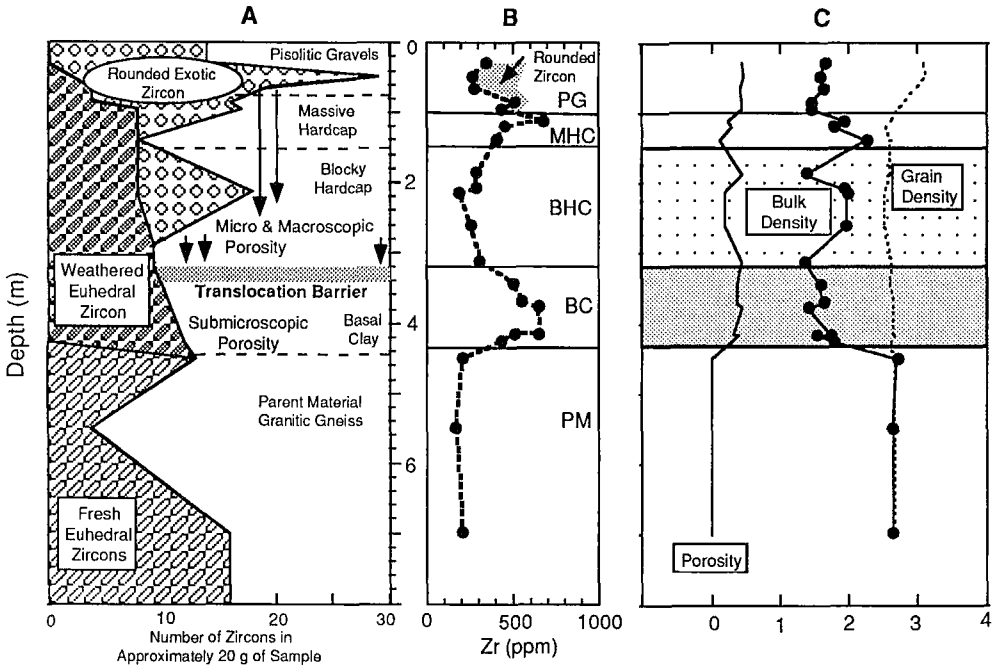
Fig. 3. **A)** Vertical distribution of zircon types in relation to laterite zones showing number of grains in each type recovered from about 20 g samples using heavy liquid separation methods. **B)** Zirconium concentration profile based on XRF analysis of pressed pills showing influence of exotic zircons. **C)** Dry bulk density (g/cm^3), porosity and grain density profiles (g/cm^3).

deposit. Instead, Brimhall *et al.* (1988) showed that size sorting of grains through pores of decreasing size with depth lent additional support to the exotic contamination hypothesis. The mechanism whereby foreign material made its way into and through soil columns was shown further to be controlled by translocation through tubules provided by decayed roots (Fig. 2B) (Brimhall *et al*, 1991 and 1992). Hence, exotic detritus is excluded from entering the submicroscopic pore system of the basal clay after passage through the pisolitic gravel, massive hardcap and blocky hardcap zones (Fig. 3A). With this interpretation, debate over *in situ* versus detrital origin became unnecessary as both processes were proven to occur but to dominate differentially with depth within the same profile for reasons governed by complex interfacial activity of biological and geological systems perturbed by major additions of detrital material.

Volumetrics of weathering

   Explicit mass balance composition/density/volume relations were applied to chemical and physical data on Jarrahdale (Figs 3B and 3C). The central goal was to characterize the transport, deposition and deformation processes responsible for the formation of a multitude of oriented, geopetal, microsedimentary pore deposits cross-cutting a sequence of still older
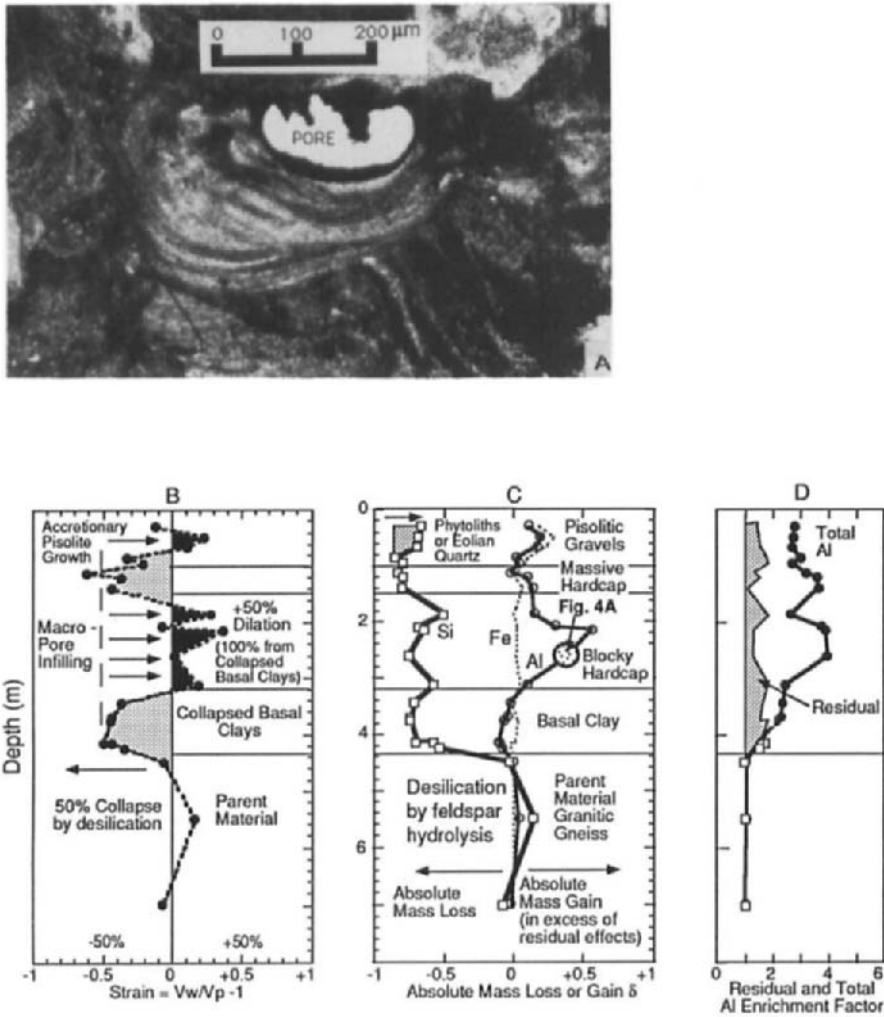
Fig. 4. **A)** Oriented ultra-thin section 5 μm thick showing in-filled pore with clay skins in blocky hardcap beneath open pore lined with chemical precipitates. **B)** Strain profile computed using zirconium concentrations corrected for the presence of rounded zircons (3B). Initial volume change is collapse related to desilication as feldpars weathered at the bedrock/saprolite interface. Expansion from this collapsed state occurs in the blocky hardcap and pisolitic gravels by macro-pore infilling and accretionary growth respectively. **C)** Absolute transported mass gains and losses for Si, Fe and Al. Note the accumulation of Al within the blocky hardcap for the same sample shown in Fig. 4A. Minor Si accumulation is evident at very top of profile, perhaps related to eolian quartz or phytoliths. Si analysis is by XRF of fused glass plate and Fe and Al are by AAS. **D)** Residual enrichment factor compared with overall enrichment factor showing residual effects account for only one-third of total Al enrichment.

in-filled voids along arcuate concave-up unconformities that were observed in ultra thin (5 μ) sections (Fig. 4A).

A Zr mass balance-based strainometer was used for the most basic component in the analytical strategy. Volume change during weathering, $\varepsilon_{Zr,w}$ (Fig. 4B) was computed using:

$$\varepsilon_{Zr,w} = \frac{V_w - V_p}{V_p} = \frac{V_w}{V_p} - 1 = \frac{\rho_p}{\rho_w} \frac{C_{Zr,p}}{C^*_{Zr,w}} - 1 \tag{1}$$

This method uses Zr as an immobile reference element after correcting its total concentration for introduced morphologically-distinct rounded zircon to yield $C^*_{Zr,w}$. Symbols V and ρ refer to volume and bulk dry density, and subscripts p and w refer to parent material and weathered samples respectively. Our technique has similarities to other approaches as reviewed recently by Moran et al., (1988) which use zircon as an index of volume change. However, unlike these other studies we are not limited by the assumption of no loss of zircon and through SEM morphology and quantitative modal analysis, the movement of zircon into the soil profile is evaluated. Furthermore, after heavy liquid separation is used to concentrate zircons quantitatively, we measure modes of morphological groups of zircon using a computer-assisted line integration counting method which is statistically more accurate than point counting (Brimhall and Rivers, 1985).

Mass gains and losses

After determining volume changes, evaluation of absolute mass gains and losses during weathering, $\delta_{j,w}$ for an element, j, are computed using Eq. 2 where $m_{j,flux}/V_p$ is the overall difference in mass of element j between a modern sample in the deformed weathered state and its parent material per cm^3(Brimhall et al., 1992).

$$\delta_{j,w} = \frac{m_{j,flux}}{V_p} = \frac{V_w \rho_w C_{j,w}}{V_p 100} - \frac{\rho_p C_{j,p}}{100} = \left(\varepsilon_{Zr,w} + 1\right)\frac{\rho_w C_{j,w}}{100} - \frac{\rho_p C_{j,p}}{100} \tag{2}$$

In Fig. 4C showing results for Si, Fe and Al, a value of $\delta_{j,w}$ equal to 0 signifies no transport and indicates that only residual and deformational effects have occurred while a positive value proves accumulation by transport. A negative value shows the amount of removal. Notice that there are no source regions internal to the weathering profile for the excess transported Al and Fe evident in the blocky hardcap and pisolitc gravels. Both these elements were introduced from above the present soil profile. The in-filled pore, rich in gibbsite from the blocky hardcap shown in Fig. 4A, is depicted again by a large rounded symbol on the Al profile line in Fig. 4C to demonstrate the correspondence of micro-structure with dilation and Al accumulation by transport.

Correlated mass accumulation and inflation

The basal clay unit, developed by incongruent dissolution and desilication of feldspars (Fig. 4C), is in a highly collapsed state representing the primitive condition of *in situ* weathering from which all the upper zones have evolved. In contrast, the pisolitic gravels and blocky

hardcap zones have experienced volumetric expansion related to the excess mineral volume of introduced detrital Al and Fe species by pore infilling and accretionary growth mechanisms respectively. The entire weathering column is however developed from a single continuous permeable medium which is differentiated internally by migration through the variably-permeable porous medium.

Contribution of residual in situ processes to ore-grade Al enrichment

The individual contributions of *in situ* residual and transported Al to the total concentration are distinguished by use of the enrichment factor which is the ratio of the Al concentration in a weathered sample divided by the concentration in the parent material (Eq. 3).

$$
\begin{array}{ll}
(1) & (2) \\
\text{Closed} & \text{Open} \\
\text{System} & \text{System}
\end{array}
$$

$$
\frac{C_{Al,w}}{C_{Al,p}} = \frac{\rho_p}{\rho_w}\frac{V_p}{V_w}\left(1+\frac{100\delta_{Al,w}}{C_{Al,p}\rho_p}\right) = \frac{\rho_p}{\rho_w}\frac{1}{\left(\varepsilon_{Zr,w}+1\right)}\left(1+\frac{100\delta_{Al,w}}{C_{Al,p}\rho_p}\right)
\tag{3}
$$

Terms 1 and 2 in Eq. 3 represent these two distinct contributions to the enrichment factor and are referred to here as the "closed" and "open" system parts. Term 1 describes the enrichment of Al as an immobile element. It is a product of ρ_p/ρ_w the pure residual enrichment factor multiplied by a second factor, $1/(\varepsilon_{Zr,w}+1)$ which is the same as the volume ratio, V_p/V_w. Residual enrichment results from simple removal of mobile elements with a corresponding reduction in bulk density and a corresponding increase in porosity (Brimhall and Dietrich, 1987) with volume change expressed by a separate factor. Term 2 gives the *transported* part of the enrichment factor. Notice in Eq. 3 that the residual factor affects even the transported component. An important conclusion of this analysis at Jarrahdale is that *in situ* residual concentration of Al given as ρ_p/ρ_w accounts for only one-third of the total enrichment with the remaining two-thirds being due to transport (Fig. 4D).

Inferred composition of exotic detritus

It is evident from Fig. 4C that the detrital contaminant enriching the bauxite to several times residual levels is a chemically-mature, previously weathered suite rich in aluminum and to a lesser extent iron, but is surprisingly quartz deficient. A likely source of such fine-grained argillaceous material is older deeply weathered terrains disrupted by uplift, erosion and ablation. More than 60 km east of the Darling Scarp, the lateritic cover has been partially stripped exposing the lower kaolinite-rich zone referred to as a semi-stripped etchplain by Finkl (1979) and Hocking and Cockbain (1990). These source regions are probably similar to regions described in South Australia by Milnes *et al.* (1985) supplying highly kaolinitic clastic material in the Eromanga Basin. This erosion and sedimentation history is interpreted as involving repeated exhumation and re-burial processes. The morphodynamic pattern is referred to as the "cratonic regime" by Fairbridge and Finkl (1980) where poly-cyclic topographic inversion results from escarpment retreat.

Profile evolution above and below the midprofile boundary

We have shown that under the influence of surficial deposition, the bauxite profile has evolved as a unit and has become differentiated into two principal parts comprising a composite but continuous system with an internal boundary. The lower part of the weathering system was shown to be a primitive basal residual clay regime developed *in situ* from weathering of bedrock. The contaminated system near surface slowly transforms the primitive basal saprolite or clay zone system by bioactivation, a process involving translocation of indigenous and foreign detritus through open and connected root tubules (Brimhall *et al.*, 1991 and 1992). The base of the upper system is defined essentially by the average depth of root penetration which limits the depth of translocation and hence bioactivation. Since root tubules penetrate even the most indurated of hardcaps and can be maintained in an open state by roots, this subsurface evolution proceeds even within and beneath duricrusts.

The subsurface acquisition mechanism proceeds by repeated cycles of void space creation by root decay and pore infilling, followed by renewed root growth evident in the numerous oriented, geopetal, microsedimentary pore deposits. Spatial accommodation of this excess volume of exotic detritus is through deformation developed by episodic root growth stresses causing an incremental dilational mixing which progressively inflates the soil (Brimhall *et al.*, 1991, 1992). We infer that this dilational mixing mechanism defines and is an integral part of the upper portions of lateritic weathering systems developed on rocks exposed on tectonically-stable cratons where low erosion rates ensure local retention of the clay and iron oxide products of weathering.

With these conclusions, we interpret the mid profile boundary of lateritic bauxites at Jarrahdale not as an unconformity separating two distinct materials, the overlying one having been deposited on top of the other by superposition as described by Ollier and Galloway (1990) for laterites elsewhere, but rather as simply being the internal boundary recognized here separating the basal clay system from the superadjacent zone of bioturbation and dilational mixing. Instead of stratigraphic superposition (Finkl, 1980) and aggradation above the exposed surface, we interpret the detrital deposition to occur *within* a continuum by migration down into and *through* the laterite rather than accumulate on top of it. We do not refute that unconformities do exist in laterites, but show that at least in the profile studied here, the rate of deposition of detritus must not have exceeded the capacity of bioturbation to accommodate the excess mass in the subsurface. Unquestionably, more rapid deposition of eolian detritus can literally bury laterites as in the migration of sand dunes.

Additional evidence against the midprofile boundary being an unconformity at Jarrahdale is that parent materials, differing greatly in composition and mineral assemblages, can survive and impart their character throughout the laterite profile even into surficial pisolites with little lateral dispersion (Sadleir and Gilkes, 1976). This occurs even with intense contamination, physical mixing and deformation within the upper soil system. Vivid examples of these effects are: the higher abundance of quartz in pisolites over granites in contrast to those over dolerites (Smurthwaite, 1990), lateritic enrichment of gold over primary mineralization (Davy and El-Ansary, 1986; Brimhall *et al.*, 1991), and geological mapping of inferred bedrock contacts on the basis of laterite features (Smurthwaite, 1990).

SHRIMP ION MICROPROBE ZIRCON STUDIES

While mass balance results allow unique inferences to be made about the involvement of pedogenic material from sources internal or external to the existing weathering profile, one of its limitations is that it does not discriminate between parautochthonous material translocated downward by regolith reduction into the existing soil column and truly allocthonous material of external derivation. The mineral zircon serves as a tracer useful in resolving this dilemma and has been used elsewhere in provenance studies in sedimentary rocks with unparalleled success. The utility of zircon stems from the fact that it is not only a chemically resistant mineral surviving pedogenesis but it is also dateable. Upon formation, its crystal structure accepts uranium substituting in small quantities (generally less than several thousand ppm) for zirconium. The uranium undergoes decay to radiogenic lead. An additional advantage is that during its original growth, zircon tends to exclude common (mostly non-radiogenic lead) thereby facilitating accurate U-Pb dating and minimizing the magnitude of the necessary corrections.

Ireland (1992) showed that not only can individual zircon age components be dated, but the relative proportions of age components of crustal sources may be determined. Previously, zircon occurring in Jamaican bauxites was studied successfully using fission track ages to demonstrate that bauxite formed by lateritic weathering of volcanic ash (Comer *et al.*, 1980). Our SHRIMP dating of zircons here, however, is focused on verification of the proposed exotic character of the rounded zircons and associated aluminous material.

To resolve this issue, we apply the SHRIMP to (1) check the continuity of the granitic gneiss parent material, (2) verify the foreign character of the abraded mineral suite by using zircon as a datable pathfinder mineral, and (3) provide some constraints on the provenance of the complete exotic suite including its aluminous components.

SHRIMP capabilities and analytical conditions

Using the SHRIMP it is possible to determine Pb-U and Pb/Pb ages as well as elemental concentrations of U and Pb rapidly on individual zircons as small as 50 μm in diameter and to do so on sufficiently large numbers of grains as to generate population statistics useful in provenance analysis. Efficiency was improved in this study by automatic peak centering of the ^{204}Pb peak on Zr_2O, and ^{207}Pb and ^{208}Pb on ^{206}Pb. This helped to reduce analysis times while U, UO and ThO peaks were centered independently. We performed five scan sets on rounded zircons and seven scan sets on euhedral zircons using the following counting times: UO$^+$ for 2 seconds; ^{238}U$^+$ for 5 seconds; ^{204}Pb, ^{206}Pb, ^{208}Pb and background for 10 seconds; and ^{207}Pb for 40 seconds. A secondary beam current of 3 nanoamps was normal. A 572 Ma gem-quality zircon from Sri Lanka analyzed conventionally with solid source mass spectrometry was used as a standard. Standards have been ^{208}Pb corrected and unknowns ^{204}Pb corrected using Broken Hill composition lead.

Continuity of the granitic gneiss parent material

We first established the age of the granitic gneiss parent material by probing 33 fresh untransported euhedral zircons (Fig. 5A). Although generally discordant, their age is clearly late Archean near 2650 Ma (Fig. 6A). In comparison, analysis of 44 weathered
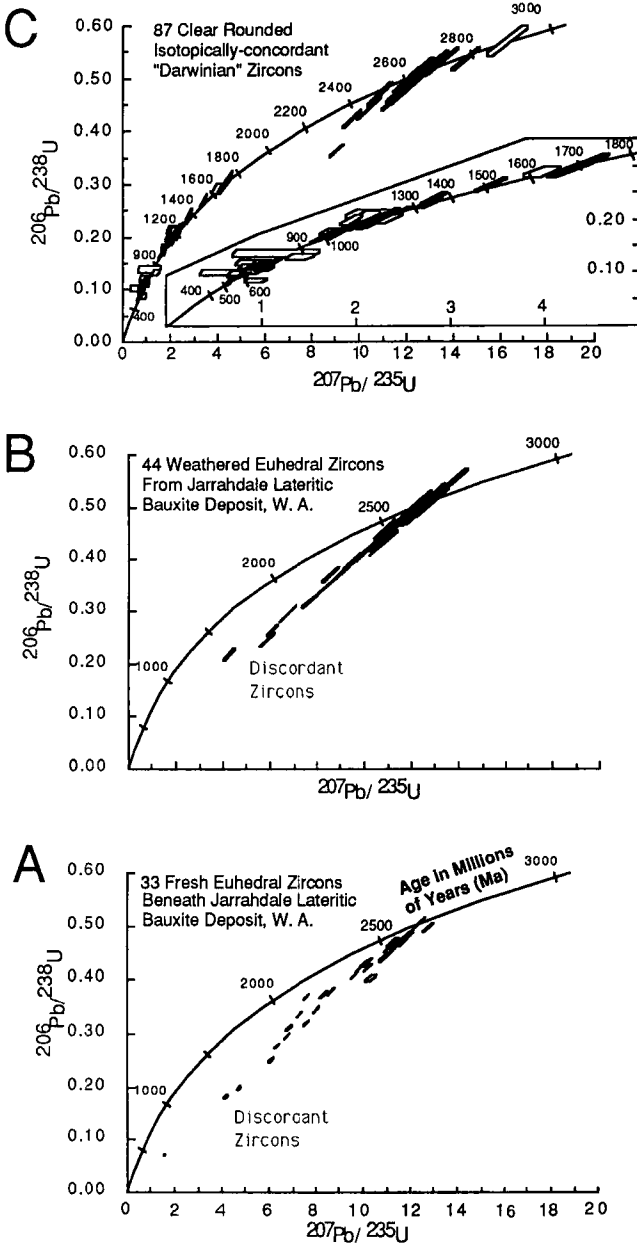
Fig. 5. SHRIMP data showing "Concordia" plot of **A)** 33 fresh unweathered euhedral zircon grains occurring at depth in the gneissic granite parent material. **B)** 44 weathered euhedral zircons in the bauxite. **C)** 87 rounded abraded exotic Darwinian zircons falling on or near "Concordia" indicating closed ^{238}U-^{206}Pb and ^{235}U-^{207}Pb systems. Ages fall into several groups between 500 to 2900 million years (Ma).
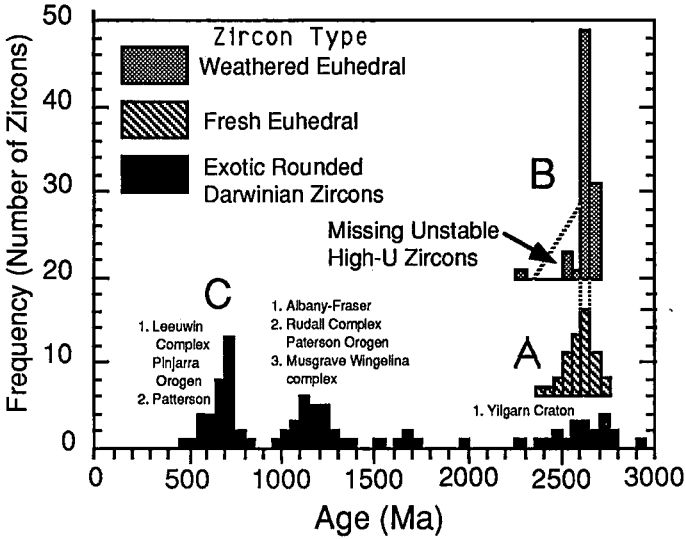
Fig. 6. **A)** $^{207}Pb/^{206}Pb$ age histogram of fresh euhedral zircons and **B)** weathered euhedral zircons. $^{207}Pb/^{206}Pb$ ages approach the ages of zircons unaffected by Pb loss as they do not rely on either Pb or U concentrations and instead use only Pb isotope ratios. Unstable high U and Th zircons with alpha track damage of the crystal structure appear to be missing in the weathered zircon population (B). **C)** $^{238}U-^{206}Pb$ age histograms of rounded exotic Darwinian zircon grains showing four age populations.

zircons, spanning the bauxite profile from immediately above the fresh gneiss to within a few centimeters of the surface, have a similar age and a discordancy pattern indicative of either recent lead loss or uranium gain without fractionation of isotopes (Figs 5B and 6B) as do the fresh unweathered zircons of the bedrock (Figs 5A and 6A). These two features strongly suggest upward continuity of Archean bedrock granitic gneiss parent material through what is now the bauxite profile and establish continuity of the gneiss parent material.

The age histogram for the weathered euhedral zircons (Fig. 6B) appears skewed towards older ages. We interpret this to be due to an absence of grains younger than 2600 Ma (a few grains do occur and have high U) having become more susceptible to breakdown because of their more metamict (alpha decay)-damaged character. We conclude that this is evidence of *in situ* selection of low U rounded grains and their preservation even within the weathering profile.

Exotic character and provenance of rounded zircons

Our main objective of dating rounded zircons in the bauxite was to test the hypothesis advanced by Brimhall *et al.*, (1988) that the abraded mineral suite was exotic. The secondary objective was to constrain possible source regions. Eighty seven clear rounded (abraded) zircons contained in the upper 2.2 meters of bauxite were analyzed (Fig. 5C). From the surface

downward, these rounded zircons decrease in abundance in relation to weathered euhedral zircons which increase (Fig. 3A). Within the hardcap (duricrusts), rounded zircons are subequal in number to local weathered euhedral (unabraded) zircon but below, in the saprolite, they are essentially absent. Beneath the saprolite only fresh euhedral zircons occur in the granitic bedrock.

Our SHRIMP data show that in contrast to euhedral zircons, rounded zircons are distinctly concordant (Fig. 5C). Their low uranium content indicates that survival of only the most robust, unmetamict grains are left since they are relatively undamaged by alpha particle radiation effects. As observed with the euhedral grains (Fig. 6B), this selection process may actually begin in the subsurface in the source region but undoubtedly occurs during eolian grain impact and abrasion during eolian transport episodes. Because of the remarkable survival of this robust mineral fraction during weathering, erosion, transport and redeposition, we refer to these isotopically-concordant rounded grains as "Darwinian zircons" in deference to Darwin's recognition in 1846 of the importance of atmospheric transport of land-derived dust to long-term offshore sedimentation.

An age histogram (Fig. 6C) reveals four well-defined age groups with modes near 700, 1150, 1700, and 2600 to 2750 Ma contributing 39%, 30%, 6% and 24% each to the total number of rounded zircons. Hence, the youngest age group, 700 Ma is by far the dominant contaminant of the lateritic bauxites followed by the 1150 and 2600-2750 Ma age groups.

Constraints on possible source regions of these detrital zircons are made using published compendia of major Australian Precambrian orogenic provinces (Page et al., 1984) but principally from more recent published and unpublished mapping in Australia and Antarctica where age assignments have been based upon reliable conventional solid source (U/Pb and Rb/Sr) mass spectrometry or SHRIMP (U/Pb and Pb/Pb) geochronology (Shaw et al., 1984; Nelson et al., 1989; Wilde and Murphy, 1990; McNaughton and Goellnicht, 1990; Goellnicht et al., 1991; Young and Black, 1991; Sheraton et al., in press).

We have interpreted the provenance of the 700 Ma zircons as shown in Fig. 6C as having come principally from the Leeuwin complex southwest of the Jarrahdale bauxites (Fig. 1). The Darling Fault separates the Pinjarra Orogen containing the Leeuwin Complex from the Yilgarn Craton to the east and formed the eastern margin of a major rift zone by which Greater India was split from Australia and the western margin of Australia was defined (Veevers and Cotterill, 1978; Myers, 1990). Most of the rocks formed in collisional tectonic regimes and were accreted to the Yilgarn craton with the most recent collisional episode inferred to be near 0.75-0.65 Ga old. Leeuwin Complex rocks are intensely-deformed and consist of granite metamorphosed to granulite facies grade and include granulite, granite gneiss, and lesser anorthosite occurring as remnants of anorthosite-gabbro intrusions. The Pinjarra Orogen, while appearing as only a small potential source region, is a small fragment of a much larger plate (Wilde and Murphy, 1990).

The subordinate source regions are interpreted as being the orogens surrounding the Yilgarn Craton on its southern, eastern and northern, and/or sedimentary sequences of intermediate age containing detritus derived from them. The 1150 Ma group is interpreted as having a principal source in the Albany-Fraser Orogen in Australia and Bunger Hills of East Antarctica as is the minor 1700 Ma age component. The 2600-2750 Ma age group we assign to transport of material derived directly from the local surrounding Yilgarn block of granites and granitic gneisses.

CONCLUSIONS

In cratons, because of long-term tectonic quiescence over periods on the order of billions of years, uplifted regions are levelled and erosion eventually becomes sufficiently slow that the products of weathering accumulate in deep soil columns. Continued weathering produces a nearly indestructible, chemically-mature, eclectic continental residuum composed of (1) local *in situ* residual products of weathering and stable accessory minerals, (2) local detritus accessed by regolith reduction from above a present exposure by escarpment retreat and topographic inversion, and (3) admixed exotic minerals derived from several distant weathered source regions elsewhere.

The regional topographic levelling process may be dominated by redistribution of this eclectic mixture in contrast to earlier mass removal in outflowing rivers when topographic gradients may have been higher. During the cratonal stage of soil evolution, deposition of a previously minor dust component may become a significant contributor to mass accumulation in the evolving continental residuum. It can serve to dilute indigenous elemental abundances although metal anomalies in the parent material still persist into the regolith and may even be concentrated by regolith reduction. While lateritic terrains may appear static in comparison to landscapes with greater relief and dust deposition may seem an inconsequential process, slow transmigration by escarpment retreat, colluviation, topographic inversion and regolith reduction (Ollier and Galloway, 1990; Brimhall, *et al.*, 1991) eventually desegregates even the most indurated duricrusts. By these mechanisms thorough mixing of both local and exotic detrital components occurs through repeated exposure to the rigors of the surficial environment.

Repeated re-introduction of this eclectic, chemically-mature suite back into the porous subsurface occurs through pathways open for translocation provided by connected pore networks in the loose pisolitic gravels and the tubular cavities below exploited and maintained by roots. Faunal burrows, transport and dissaggregation of termite mounds provide further mixing processes. *In situ* residual weathering is only the first step in this evolution. Sources and mechanisms of accommodation of this indigestible excess mass directly influence the fabric of cratonal soils and reflect complex interfacial activity of biological and geological systems perturbed by major additions of exotic material.

ACKNOWLEDGMENTS

REFERENCES

Anand, R.R., Gilkes, R.J. and Roach, G.I.D., 1991. Geochemical and mineralogical characteristics of bauxites, Darling Range, Western Australia. Applied Geochemistry, 6: 233-238.
Baker, G.F.U., 1972. Origin of Darling Range bauxites, Western Australia. Econ. Geol., 67: 981.
Brimhall, G.H. and Dietrich, W.E., 1987. Constitutive mass balance relations between chemical composition, volume, density, porosity, and strain in metasomatic hydrochemical systems: Results on weathering and pedogenesis. Geochem. et Cosmochim. Acta, 51: 567-587.
Brimhall, G.H and Rivers, M.L., 1985. Semi-automated optical scanning device, United States Patent No. 4, 503-555.
Brimhall, G.H., Alpers, C., and Cunningham, A.B., 1985. Analysis of supergene ore-forming processes using mass balance principles. Econ. Geol., 80: 1227-1254.
Brimhall, G.H., Lewis, C.J., Ague, J.J., Dietrich, W.E., Hampel, J. and Rix, P., 1988. Metal enrichment in bauxites by deposition of chemically mature aeolian dust. Nature, 333: 819-824.
Brimhall, G., Lewis, C., Ford, C., Bratt, J., Taylor, G., and Warin, O., 1991. Quantitative geochemical approach to pedogenesis: Importance of parent material reduction, volumetric expansion, and eolian influx in lateritization. Geoderma, 51: 51-91.
Brimhall, G.H, Chadwick, O., Lewis, C., Compston, W., Williams, I., Danti, K., Dietrich, W., Power, M., Hendricks, D. and Bratt, J., 1992. Deformational mass transport and invasive processes in soil evolution. Science, 255: 695-702.
Comer, J.B., Naeser, C.W. and McDowell, F.W., 1980. Fission-Track ages of zircon from Jamaican Bauxite and Terra Rossa. Econ. Geol., 75: 117-121.
Compston, W., Williams, I., and Meyer, C.J., 1984. U-Pb geochronology of zircons from lunar breccia 73217 using a sensitive high mass-resolution ion microprobe. Jour. Geophys. Research, 89: Supp., pp. B525-B534.
Darwin, C., 1846, An account of the fine dust which often falls on vessels in the Atlantic Ocean. Q. J. Geol. Soc. Lond., 2: 26-30.
Davy, R., 1979. A study of laterite profiles in relation to bed rock in the Darling Range, near Perth, W. Australia: Western Australia. Geol. Surv. Report 8.
Davy, R. and El-Ansary, M., 1986. Geochemical patterns in the laterite profile at the Boddington Gold Deposit, Western Australia. J. Geochemical Exploration, 26: 19-44.
Fairbridge, R.W. and Finkl, C.W., 1980, Cratonic erosional unconformities and peneplains. J. Geol., 88: 69-86.
Finkl, C.W., 1979. Stripped (etched) land surfaces in southern Western Australia. Australian Geographical Studies, 177: 1, 33-52.
Finkl, C.W., 1980, Stratigraphic principles and practices as related to soil mantles. Catena, 7: 169-194.
Goellnicht, N.M., Groves, D.I. and McNaughton, N.J., 1991. Late Proterozoic fractionated granitoids of the mineralized Telfer area, Paterson Province, Western Australia. Precambrian Res., 51: 375-391.
Grubb, P.L.C., 1971. Mineralogical anomalies in the Darling Ranges bauxites at Jarrahdale, Western Australia. Econ. Geol., 66: 1005-1016.

Hocking, R.M. and Cockbain, A.E., 1990. Regolith. In: Geology and Mineral Resources of Western Australia.Geol. Surv. of Western Australia, Memoir 3, 592pp.

Ireland, T.R., 1992. Crustal evolution of New Zealand: Evidence from age distributions of detrital zircons in Western Province paragneiss and Torlesse greywacke. Geochem. et Cosmochim Acta, 56: 911-920.

Killigrew, L.P. and Glassford, D.K., 1976. Origin and significance of kaolin spherites in sediments of south-western Australia. Search, 7: 393-394.

McNaughton, N.J. and Goellnict, N.M., 1990. The age and radiothermal properties of the Mt. Crofton Granite, Telfer area, Western Australia. Aust. J. Earth Science, 37: 103-106.

Milnes, A.R., Bourman, R.P. and Northcote, K.H., 1985. Field relationships of ferricretes and weathered zones in southern South Australia: A contribution to "laterite" studies in Australia. Aust. J. Soil Res., 23: 441-465.

Moran, C.J., McBratney, A.B. and Koppi, A.J., 1988. A micromorphometric method for estimating change in volume of soil induced by weathering. J. of Soil Sci., 39: 357-373.

Myers, J.S., 1990. Pinjarra Orogen in Geology and Mineral Resources of Western Australia, Geol. Surv. of Western Australia, Memoir 3, pp. 265-274.

Nelson, D.R., Black, L.P. and McCulloch, M.T, 1989. Nd-Sm isotopic characteristics of the Mordor Complex, Northern Territory: Mid-Proterozoic potassic magmatism from an enriched mantle source. Aust. J. of Earth Sci., 36: 541-551.

Page, R.W., McCulloch, M.T. and Black, L.P., 1984. Isotopic record of major Precambrian events in Australia. Precambrian Geology, 5: 25-72.

Ollier, C.D. and Galloway, R.W., 1990. The laterite profile, ferricrete and unconformity. Catena, 17: 97-109.

Sadleir, S.B. and Gilkes, R.J., 1976. Development of bauxite in relation to parent material near Jarrahdale, Western Australia. J. Geol. Soc. Aust., 23: 333-344.

Shaw, R.D., Stewart, A. and Black, L.P., 1984. The Arunta Inlier: a complex ensialic mobile belt in central Australia. Part 2: Tectonic history: Aust. J. Earth Sci., 31: 457-484.

Sheraton, J.W., Black, L.P. and Tindle, A.G., ( ) Petrogenesis of plutonic rocks in a Proterozic granulite-facies terrane in the Bunger Hills, East Antarctica. Chem. Geol., (in press).

Smurthwaite, A.J., 1990. Alumina. In: Geology and Mineral Resources of Western Australia. Geol. Surv. of West. Australia, Memoir 3, pp. 615-624.

Trendall, A.F., 1990. Orogens. In: Geology and Mineral Resources of Western Australia, Geol. Surv. of Western Australia, Memoir 3, p. 196.

Trendall, A.F. and Cockbain, A.E., 1990. Basins, Geology and Mineral Resources of Western Australia, Geol. Surv. of Western Australia, Memoir 3, p. 289.

Veevers, J.J. and Cotterill, D., 1978. Western margin of Australia - evolution of a rifted arch system. Geol. Soc. Amer., 89: 337-355.

Wilde, S.A. and Murphy, D.M.K., 1990. The nature and origin of Late Proterozoic high-grade gneiss of the Leeuwin Block, Western Australia. Precambrian Res., 47: 251-270.

Young, D.N. and Black, L.P., 1991. U-Pb dating of Proterozoic igneous charnokites from the Mawson coast, East Antarctica. Antarctic Science, 3: 205-216.

This Page Intentionally Left Blank

Iron oxides in iron-rich nodules of sandy soils from Alberta (Canada)

J.M. Arocena, S. Pawluk and M.J. Dudas

Department of Soil Science, University of Alberta, Edmonton, Canada T6G 2E3

ABSTRACT

Arocena, J.M., Pawluk, S., and Dudas, M.J. 1994. Iron oxides in iron-rich nodules of sandy soils from Alberta (Canada). In: A.J. Ringrose-Voase and G.S. Humphreys (Editors), Soil Micromorphology: Studies in Management and Genesis. Proc. IX Int. Working Meeting on Soil Micromorphology, Townsville, Australia, July 1992. Developments in Soil Science 22, Elsevier, Amsterdam, pp. 83-97.

A large proportion of Fe oxide in some Alberta soils is "naturally concentrated" in the form of nodules. An *in situ* investigation of these nodules was carried out through X-ray microdiffraction and electron microscopy to study the spatial distribution, mineralogy and micromorphology of the common Fe oxides.

The typical X-ray microdiffraction patterns of the nodules consist of several smooth and continuous Debye Scherrer rings. This indicates that within the 50 μm collimation of the microcamera, the normally large (100 - 300 μm) Fe nodule is a conglomeration of very fine particles of Fe oxide minerals in random orientation. Goethite was the most common Fe oxide with morphologies ranging from "flake-like" crystals about 2 μm wide, 1 μm long and 0.25 μm thick, "block-like" crystals about $2 \times 2 \times 4$ μm and aggregates of fine crystals. The Al for Fe substitution, calculated from the *c*-dimension, ranged from as low as 2 to as high as 28 mole% Al. The low amount of Al for Fe substitution usually occurred in the C and Ae horizons while highly substituted goethite was found in the B horizons. Goethite was also present in association with hematite and/or lepidocrocite in some of the nodules in the B and C horizons. Other minerals identified in the nodules were quartz and various phyllosilicates. The presence of ferrihydrite in the bulk samples of the sola is suggested by the high Fe*o*/Fe*d* ratio.

The variety of Fe oxide associations within the sola reflects the variable environmental conditions that existed during their formation (*e.g.*, goethite with hematite is typical for well-drained conditions while the formation of goethite and lepidocrocite association is common in reductomorphic environments). The different degree of Al for Fe substitution in goethite even within the same horizon, probably reflects the influence of variation in microenvironments. The *in situ* approach used in this study and the resolution achieved is considered an improvement over the conventional use of bulk samples analysis where the average value is determined and the heterogeneity within the horizon is often not established.

INTRODUCTION

Apart from the high pigmenting ability of Fe oxides, the presence of Fe-rich nodules in many sola indicates its importance in most pedogenic studies. The nature of iron oxides reflects the "environmental conditions under which they formed" (Schwertmann and Taylor,

1989). For example, the extent of Al for Fe substitution in goethite is related to the activity of Al in the environment (Fitzpatrick and Schwertmann, 1981; Schwertmann *et al.*, 1987).

Most mineralogical investigations of soil Fe oxides usually start with concentration techniques such as magnetic separation (Schulze, 1988), ore separation (Schwertmann *et al.*, 1987), chemical treatment (Norrish and Taylor, 1961) or particle size and density separation (Jackson, 1969). It should be realized, however, that a large proportion of Fe oxide in soils are "naturally concentrated" in the forms of mottles, nodules, or coatings and through *in situ* investigation, concentration is not necessary. Investigation *in situ* also provides important information such as spatial distribution and avoids the "averaging" effects of concentration procedures where one normally obtains the "mean information" about the different Fe oxides phases present as nodules, mottles or coatings.

In situ investigation of soil Fe oxides has been attempted previously mainly through selective dissolution in thin section (*e.g.*, Bullock *et al.*, 1975; De Geyter *et al.*, 1982) where the mineralogical composition is correlated to differential solubility by specific extractants. This technique has proven useful in the study of the spatial distribution of ferrihydrite based on its preferential dissolution with acid ammonium-oxalate although not when the ferrihydrite was present with siderite and vivianite because these Fe minerals are also soluble in acid ammonium-oxalate.

The objective of this study was to characterize the mineralogy of Fe-rich nodules in sandy soils from Alberta. X-ray microdiffraction methods were employed to assist in the *in situ* characterization of these materials. This technique has been successful in the study of serpentine minerals (Wicks and Zussman, 1975) and selected pedological features in some Alberta soils (Brewer and Pawluk, 1975; Pawluk, 1983).

MATERIALS AND METHODS

The study area, Fe extraction, and microscopy

The three sandy soils used for the study are situated at 1,150 m a.s.l. in the Wildhay benchland near Hinton, Alberta (pedon 1: 53°46'24 ± 15"N, 117°37'37 ± 30"W; pedon 2: 53° 44'21 ± 15"N, 117°39'11 ± 30"W) and at 850 m a.s.l. in the Alberta plateau benchland along the Forestry Trunk Road (pedon 3: 54°31'32 ± 15"N, 118°9'57 ± 30"W). The pedons are classifed as transitional between Luvisolic and Podzolic orders in the Canadian system of soil classification (Canadian Soil Survey Committee, 1978). The field morphological descriptions for each pedon are described in Arocena *et al.* (1992).

Soil samples of about 5 kg were collected and subsequently air-dried and passed through a 2 mm sieve for bulk chemical analyses. The amounts of various forms of free Fe were measured by extracting the soil with dithionite-citrate-bicarbonate (Mehra and Jackson, 1960), sodium-pyrophosphate (McKeague, 1967) and acid ammonium-oxalate (Schwertmann, 1964). The extracts were analyzed for Fe by atomic absorption spectrophotometry. Total carbon was determined using a carbon analyzer and total Fe was determined following the microwave dissolution technique outlined by Warren *et al.* (1990).

Three soil monoliths, measuring 6 × 8 × 24 cm taken from each profile, were impregnated with electrical resin and 30 μm thick 8 × 5 cm thin sections were prepared and described following the methods and terminologies of Brewer and Pawluk (1975), Brewer (1976) and
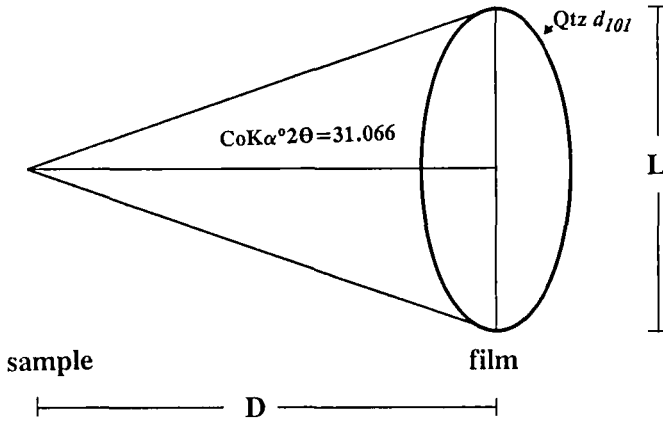
Fig. 1. The arrangement of the sample, the film and the quartz d_{101} spacing in the microcamera. The geometry is used to calculate the corrected specimen to film distance. The corrected distance (D) is given by: D=L/(2 tan 31.066°) where, L is the diameter of the quartz d_{101} and 31.066° is the Bragg angle of quartz d_{101} for Co Kα.

Bullock *et al.* (1985). Morphometric analysis of the distribution of the nodules was conducted using a computerized image analysis system. The sub-microscopic morphology and the amounts of Fe and Al in selected Fe-rich nodules were determined with the aid of a scanning electron microscope (SEM) equipped with an energy dispersive X-ray analyzer.

X-ray microdiffraction and Al for Fe substitution in goethite

In situ mineralogical determination of Fe-rich nodules was conducted by removing portions of the thin section containing the nodule of interest from the glass slide. Mounted glass slides were heated at 80°C for 10 minutes and thin sections were peeled while hot with a razor blade. The peel was then mounted on a transmission type microcamera (Chesley, 1947) equipped with a 50 µm collimator. Alignment of the sample with the collimated X-ray beam was achieved by ensuring that the light from a petrographic microscope passed through the 50 µm aperture and illuminated the nodule of interest. The camera was attached to a X-ray generator. The unit was equipped with an Fe filter and was operated at 30 kV and 20 mA to generate Co-Kα radiation. The X-ray diffraction pattern composed of several Debye Scherrer rings was recorded on a 35 × 40 mm photographic film after exposure times of 8 - 12 hours.

The strong, spotty, and discontinuous Debye Scherrer ring produced by the d_{101} reflection of quartz (Qtz) in almost every nodule examined provided the internal standard for the determination of the exact specimen-to-film distance, a critical factor in the calculation of the *d*-spacings. The distance was calculated from the geometrical arrangement of sample, film and Qtz d_{101} reflection (Fig. 1). The corrected distance (D) is given by:

$$D = \frac{L}{2 \tan 31.066°} = \frac{L}{1.204} \qquad 1$$

where, *L* = diameter of Qtz d_{101} ring and 31.066° = Bragg angle of Qtz d_{101} for Co Kα.

The corrected D is used to determine the Bragg angle corresponding to the diameter of each Debye Scherrer ring recorded from the diffraction of a particular lattice of the unknown Fe oxide. The use of Qtz d_{101} ring as an internal standard enabled accurate measurements of

Table 1
Total and free iron contents of the soil materials.

Sample	Fe_p	Fe_o	Fe_d (g kg^{-1} soil)	Fe_t	(Fe_{t-d})	$Fe_{(d-o)/d}$	$Fe_{o/d}$
			Pedon 1				
Ae	0.2	0.5	0.6	2.4	1.8	0.17	0.83
Bfj	2.3	9.0	11.9	13.6	1.7	0.24	0.76
Bt	0.9	5.0	8.2	11.0	2.8	0.39	0.62
C1	0.2	0.9	3.5	29.9	26.4	0.74	0.26
			Pedon 2				
Ae	0.4	0.5	0.6	4.3	3.7	0.17	0.86
Btf	4.4	11.5	15.1	22.6	7.5	0.24	0.76
Btj	1.4	5.6	7.9	16.0	7.1	0.22	0.71
IIC1	1.4	3.6	5.6	18.3	12.7	0.36	0.63
			Pedon 3				
Ae	0.2	0.7	0.9	2.3	1.4	0.22	0.83
Btf	3.3	9.6	14.3	14.9	0.6	0.32	0.67
C1	0.5	1.0	4.7	10.9	6.2	0.79	0.22

Fe_p pyrophosphate extractable Fe_d dithionite-citrate-bicarbonate extractable

Fe_o ammonium-oxalate extractable Fe_t total dissolution

d-spacings and the calculation of unit cell parameters for goethite using the Applemans and Evans computer program for indexing powder patterns and refining unit cell parameters by least square procedures as adapted to personal computers by Benoit (1986). The Al for Fe substitution based on the measured c-unit cell dimension was estimated using the relationship *mole% Al = 1730 - 572 c-unit cell dimension* (Schulze, 1981).

Iron nodules around 100 μm in diameter and 10 μg in weight collected from bulk samples by density separation were also exposed to X-ray microdiffraction similar to the nodules in thin section. Fig. 1 showed the location of the sample in the camera. Selected nodules from B horizon were likewise subjected to infrared analysis using a FTIR spectrometer in which the pellets were prepared from a 1:300 mixture of sample and KBr.

RESULTS AND DISCUSSION

Distribution of Fe and Fe nodules

The total free Fe (Fed) and the pyrophosphate extractable Fe (Fep) show maximum values in the B horizons and lowest values in the Ae horizons (Table 1) which is characteristic of Fe accumulation in Spodosol profiles (McKeague *et al.*, 1983). The amount of oxalate extractable Fe (Feo) in the B horizons is more than double that in the Ae horizons and is additional evidence for the presence of a spodic horizon (ICOMOD, 1990). The high Feo/Fed ratios within the solum of all the pedons suggest that most of the free Fe is present as less-ordered Fe oxyhydroxides (Schulze, 1981; De Geyter *et al.*, 1982). The ratio is about twice

Table 2
Frequency, size of and area occupied by Fe nodules.

Parameter	Ae	B	C
Frequency (#/100 cm^2)	300	1200	2500
Range in size (×100 cm^2)	3-27	5-56	2-10
Mean size (×100 cm^2)	4.0	5.0	1.0
(standard deviation)	(0.4)	(0.4)	(0.1)
Area occupied by nodule (%)	14	58	27
Number of nodules measured	34	119	254

that of (Fed-Feo)/Fed, a ratio taken as the measure of crystalline free Fe. The higher proportion of total Fe (Fet) over Fed in the C horizons reflects the presence of magnetite, unweathered Fe-containing silicates and probably some lithogenic hematite which is claimed to resist extraction with dithionite-citrate-bicarbonate (Campbell and Schwertmann, 1984).

The Fe nodules investigated are mostly the typic type (Bullock et al., 1985) characterized by a round shape and undifferentiated internal fabric. The distribution of the nodules within the profile indicates an accumulation of Fe in the B horizon as suggested by the occurrence of an average of 12 nodules ($\approx$ 0.005 cm^2 size) in every cm^2 area in the thin section of B horizon and an average of 3 nodules ($\approx$ 0.004 cm^2 size) in a similar area in the Ae horizon (Table 2). Moreover, the Fe nodules occupied a smaller portion (14%) of the total area in the Ae horizons when compared to the B horizons where nodules occupied about 58% of the area. The large area occupied by the nodules in the latter is attributed mainly to the accumulation of free Fe but also includes weathered mineral grains that are completely coated with Fe oxyhydroxides. The Fe nodules in the C horizon are numerous at about 25 nodules per cm^2 but are small in size ($\approx$ 0.001 cm^2) and are probably inherited. The wide range in sizes of the nodules in the B horizons suggests a history of Fe oxide formation. The small nodules probably represent the unaltered allogenic iron nodules similar to those present in the C horizons. The big nodules may have started forming early in the genesis of the soils and continued up to the present day.

Occurrence and morphology of Fe oxide minerals

The presence of ferrihydrite in the bulk samples of the sola of all the pedons is suggested by the high Feo/Fed ratio (Table 1) because neither Fe carbonate nor Fe phosphate is present in the samples (De Geyter et al., 1982). Ferrihydrite is also found to be thermodynamically stable as indicated by the positive values for the saturation index (SI) based on Fox (1988): $SI = \log(a(Fe^{3+})(a(OH))^{2.35})/\log 10^{-31.7}$ where $a(Fe^{3+})$ and $a(OH)$ measured in natural solution (Arocena, 1991). Saturation index values of zero, positive and negative denote equilibrium, oversaturation (stability) and undersaturation (instability) with respect to the mineral of interest, respectively. The Ae horizons (SI=2.9 - 5.6) show higher SI values compared to those for B horizons (SI=0.6 - 2.0).

The X-ray microdiffraction pattern shown in Fig. 2 is typical for all the nodules and consists of smooth and continuous Debye Scherrer rings and indicates that within the 50 μm collimation of the microcamera, the normally large (100 - 300 μm) Fe nodule is actually a
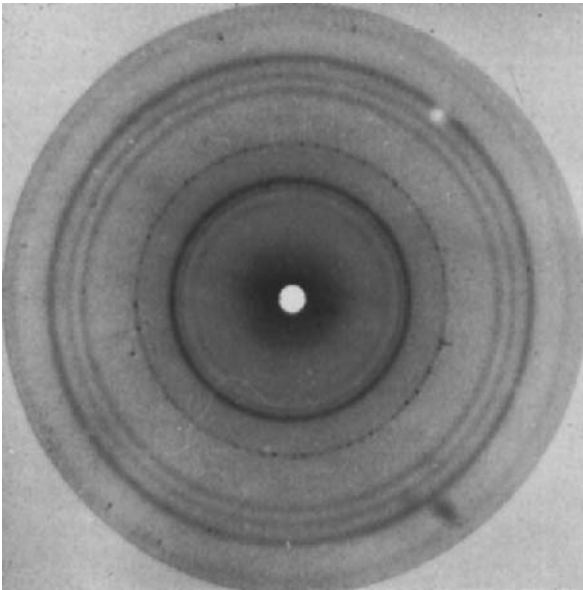
Fig. 2. Typical example of X-ray microdiffraction pattern of Fe-rich nodules. The strong, spotty and discontinuous Debye Scherrer ring is the quartz d_{101} spacing and the remaining smooth and continuous rings are for iron oxides and associated phyllosilicates.

conglomeration of very fine particles of Fe oxide minerals in random orientation (Cullity, 1959). In addition, the strong, spotty and discontinuous reflections around 0.334 nm is the d_{101} spacing of ubiquitous quartz. The presence of quartz suggests it plays a role in the formation of the nodules. It is proposed that the larger quartz grains, evident from their spotty reflections, attracted the very fine Fe oxide particles through van der Waals attraction onto quartz surfaces and thus initiated the accumulation of Fe oxides into nodules. Quartz grains frequently showed etched and altered surfaces which would facilitate the adsorption and binding of colloidal iron oxyhydroxides.

Goethite was the most common Fe oxide and was usually the sole Fe oxide mineral in nodules throughout the soil sola. Some samples of goethite appear to have "flake-like" units of about 2 µm wide, 1 µm long and 0.25 µm thick (Figs 3D, 3F, 3G and 3H). A vertical cut through these flakes resembles the "fan-like" morphology reported earlier for goethite in Belgium (Stoops, 1983). Block-like crystals of about 2 µm × 2 µm × 4 µm are also observed (Figs 3A, 3B and 3C). The surfaces of these goethite specimens are smooth and free of etching and corrosion indicative of their neosynthesis. A portion of the nodules however, shows neither the "flake-like" nor the "block-like" morphologies but appears as aggregates of fine crystals of goethite (Figs 3C, 3D and 3E). These randomly oriented aggregates of goethite are probably the major contributors to the smooth and continuous Debye Scherrer rings of the *in situ* XRD patterns.

In a few cases, goethite is present in association with hematite in the same nodules in the B and C horizons (Fig. 4A). In such associations, the estimates of the *Gt/Gt+Hm* ratios (Boero and Schwertmann, 1989) is higher in the B horizon (0.61) compared to C horizon (0.37) (Table 3). The high amount of goethite in the B horizons can be attributed to several factors such as the "anti-hematitic" effect of the high organic carbon content in the B horizons where
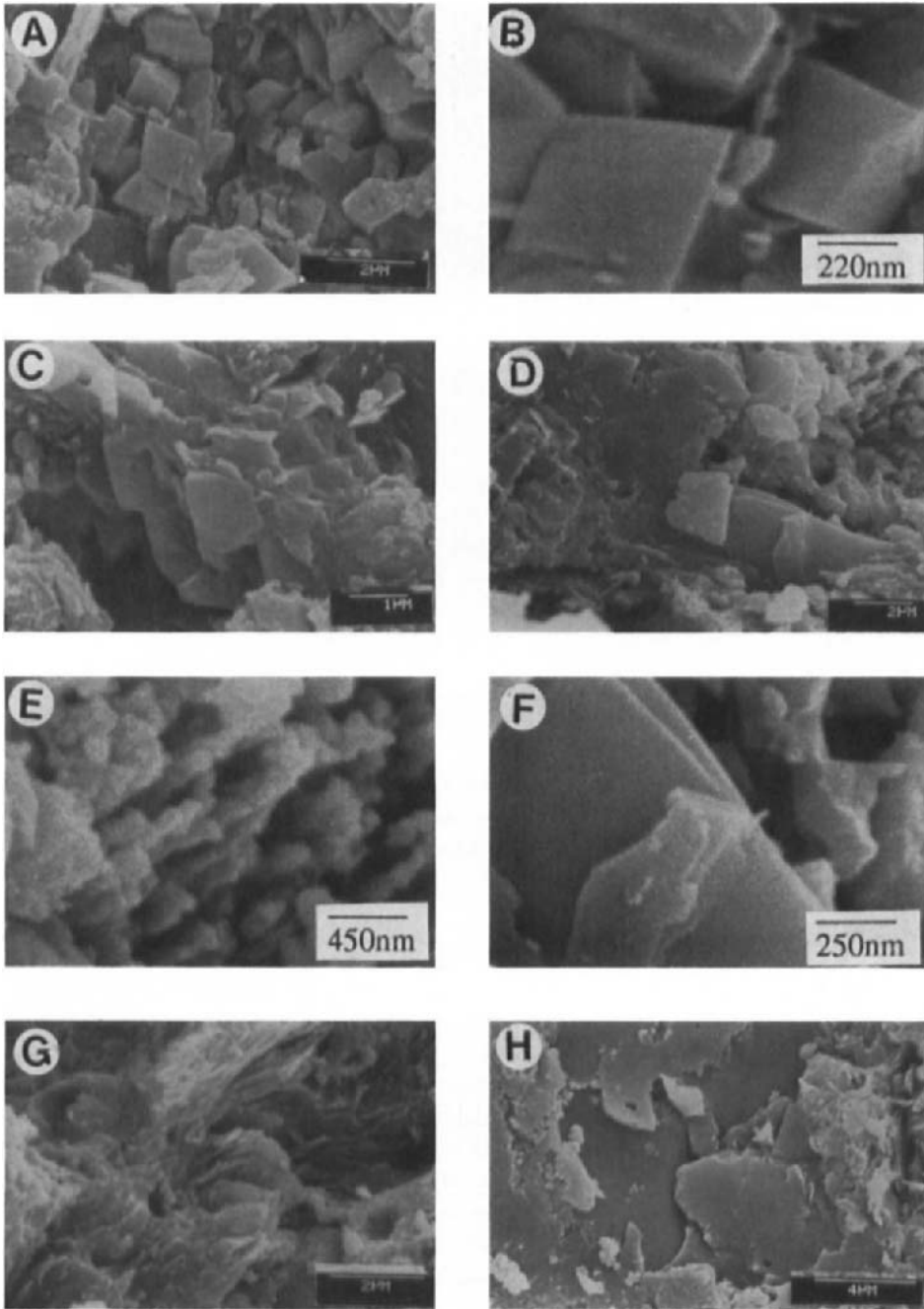
Fig. 3. Scanning electron micrographs of the different morphologies of goethite. (A and B) "block-like" crystals (C) "block-like" crystals and aggregates (D) aggregates and "flake-like" crystals (E) close-up micrograph of aggregates (F) close-up micrograph of "flake-like" crystals and (G and H) "flake-like" crystals.
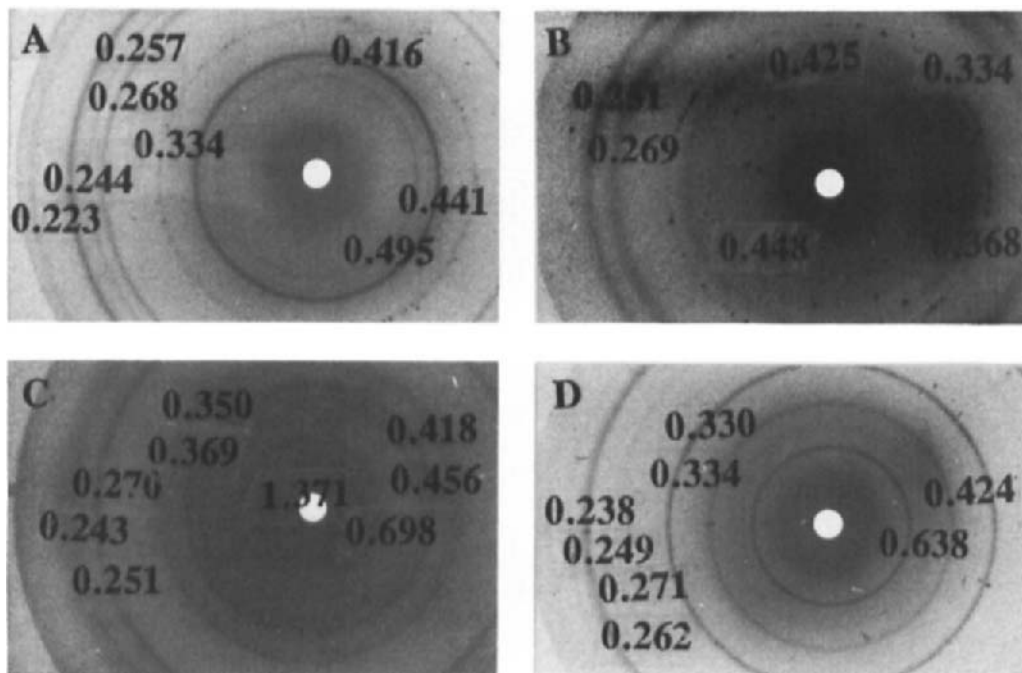
Fig. 4. *In situ* X-ray microdiffraction patterns of the different Fe oxides (A) goethite in association with hematite (B) hematite (C) goethite in association with phyllosilicates and (D) goethite in association with lepidocrocite. Quartz is present in almost every nodule.

the organic ligands effectively tie up the Fe^{3+} such that its concentration is rendered below the solubility product for ferrihydrite, a necessary precursor for hematite formation (Schwertmann and Taylor, 1989; Cornell *et al.*, 1989). Another factor is the high free Al content that results from the accumulation of weathering products in the B horizons as compared to C horizons (Table 3). Moreover, complexing of Al by organic acids decreases the polymerization of hydrous-aluminum species, leaving more Al available for other reactions (April and Keller, 1990) such as Al for Fe substitution during goethite formation. It should be mentioned that the reported values for carbon and Al are given for bulk samples of the horizons and not for individual nodules; however, the values are thought to be reliable expressions of the differences between microenvironments where the nodules formed. The competitive formation of goethite and hematite is also affected by soil temperature, soil pH, moisture and rate of release of free Fe (Schwertmann and Taylor, 1989).

Other nodules in the B horizon are composed of goethite in association with lepidocrocite (Fig. 4D). The formation of lepidocrocite is often associated with reductomorphic environments (Pawluk, 1971; Campbell and Schwertmann, 1984). In contrast, Tarzi and Protz (1978) reported the occurrence of lepidocrocite in well-drained Ontario soils developed on a

Table 3
Carbon and aluminum contents, Gt/(Gt+Hm) ratio and Al for Fe substitution in the B and C
horizons.

Sample	Carbon	Ald (g kg^{-1} soil)	Gt/(Gt+Hm)	Al subs (mole %)
B horizon	5.1	8.3	0.61	28
C horizon	1.8	0.5	0.37	12

Ald	dithionite-citrate-bicarbonate extractable
Gt/(Gt+Hm)	goethite and hematite present in same nodule

granite and granite-gneiss. Lepidocrocite in those soils may be relicts of a previous reducing
environment. The presence of high Al activity is also reported to favor the formation of
goethite over lepidocrocite (Schwertmann and Taylor, 1989).

Goethite is also associated with 2:1 phyllosilicates as indicated by the reflections around
1.378, 0.712 and 0.441 nm (Fig. 4C). Hematitic nodules (Fig. 4B) observed in the Ae
horizons have weathered surfaces and edges and are believed to be the remnant of allogenic
hematite or the authigenic hematite formed early in the genesis of these soils which are now no
longer stable.

The calculated SIs for hematite, goethite and lepidocrocite show that these oxides are
unstable in the Ae horizons (SI<0) but not in the B horizons (SI>0) (Arocena, 1991).

Aluminum for iron substitution in goethite

One of the properties of goethite that is most sensitive to conditions of formation is the Al
for Fe substitution (Norrish and Taylor, 1961; Fitzpatrick and Schwertmann, 1981; Schulze,
1984) where the Al is present as an elemental constituent in the solid solution series between
the isomorphs goethite and diaspore (Yapp, 1983). The smaller radius of Al^{3+} (0.053 nm)
compared to Fe^{3+} (0.065 nm) cause the linear decrease of the unit cell parameters according to
Vegard's rule (Cullity, 1959). In this study, there is a positive linear relation ($r=0.951$)
between the Fe/Al weight ratio determined by energy dispersive analysis and the measured c-
axis (Fig. 5) which is consistent with the findings of Schulze (1984). The c-axis dimension
appears to be a good measure of Al content in goethite (Schulze, 1984). The correlation
between the Fe/Al weight ratio and the unit cell volume is slightly lower ($r=0.718$) than the
relation to c-axis dimension.

The Al for Fe substitution (mole% Al) calculated from the c-dimension ranged from as low
as 2 to as high as 28 mole% Al (Table 4), indicative of the solid solution series involving
goethite and diaspore. For discussion purposes, the substitution was grouped into <15 mole%
Al ("low goethite") and >15 mole% Al ("high goethite"), similar to the division used by
Fitzpatrick and Schwertmann (1981). The substitution in the Ae and C horizons is limited to
low goethite with values from 2 to 14 mole% Al. In the B horizon, substitution ranged from
low (2 mole% Al) to high goethite (28 mole% Al). The proportion of high goethite in B
horizons accounts for about 38% of the nodules (Fig. 6).

The low goethite phase was observed in the Ae, B and C horizons and probably represents
the original goethite present in the parent material or the goethite formed early in the genesis of
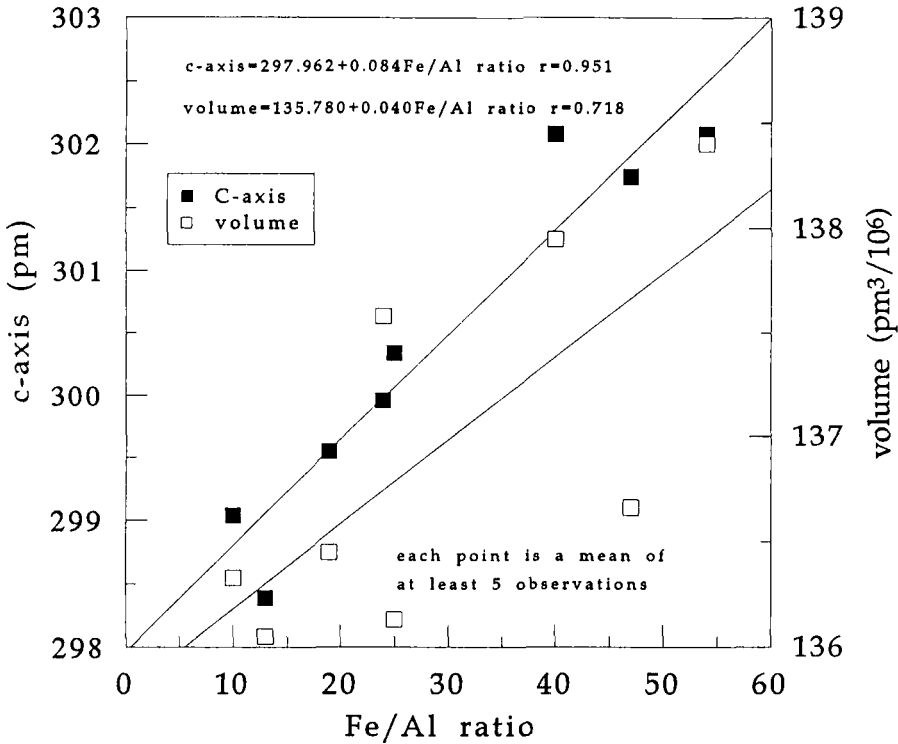
Fig. 5. The positive linear relationships between the measured c-axis, the calculated cell volume and the Fe/Al weight% ratio of goethite.

these soils. The high goethite phase probably represents the pedogenic goethite that resulted from the weathering and reorganization of earlier formed goethite as a result of concurrent soil processes characterized by high Al activity in the soil solution. In the reorganization of goethite, the low goethite can provide the seeding effect (Schwertmann, 1988) for the recrystallization of weathered goethite to form the larger and highly substituted pedogenic goethite. The presence of high goethite is also suggested by the wide separation at about 96 cm^{-1} of the IR absorption bands observed for δOH at 893 cm^{-1} and of τOH at 797 cm^{-1} (Schwertmann et al., 1987) in goethite from the B horizons. The high goethite is most often associated with the 2:1 phyllosilicates and is similar to some of the goethite in Finland (Schwertmann et al., 1987).

Implications to soil heterogeneity and pedogenesis

The occurrence of several Fe oxide associations within the sola points to the various and changing conditions that existed during their formation. The association of goethite with hematite is typical for well-drained conditions while the formation of goethite and lepidocrocite association is common in reductomorphic environments. The presence of hematitic nodules in the Ae horizons is interpreted to represent the region of less aggressive conditions in the

Table 4
Unit cell parameters and Al for Fe substitution in goethite.

Sample	Cell dimension (nm)			Al-subs (mole%)
	a-axis	*b*-axis	*c*-axis	
		Ae horizon		
311BFe	0.46063	0.99615	0.30185	3.43
41Fe	0.45897	1.00020	0.30215	1.70
41HFe3	0.45796	0.98631	0.30074	9.76
41HFe4	0.45498	0.99360	0.29997	14.14
41-3	0.45773	0.98646	0.29994	14.38
41-4	0.45657	0.98142	0.30006	13.68
41-6	0.45538	0.99125	0.30043	11.56
41-7	0.45921	0.99157	0.30042	11.60
41-2c	0.45980	0.99235	0.30098	8.40
41-1	0.46428	0.93635	0.30090	8.82
		B horizon		
312A	0.45840	0.99291	0.30035	11.99
312RCO	0.46400	0.98512	0.30046	11.70
34HFe2	0.46084	0.99461	0.29986	14.81
34HFe1	0.46292	0.99140	0.30028	12.39
34HFe3	0.45957	0.98389	0.29833	23.56
MAT1IN	0.46695	0.99168	0.30127	6.76
MAT2OUT	0.46683	0.98588	0.30043	11.50
42-4	0.46251	0.99160	0.30170	4.29
42-3	0.46614	0.98868	0.29985	14.89
42-5	0.45910	0.99543	0.29965	15.99
422HFe	0.45959	0.99045	0.30111	7.63
422HFe1	0.46316	0.99645	0.29997	14.19
422HFe5	0.45882	0.99042	0.30158	4.95
4231O3a	0.46207	0.99993	0.30105	7.97
4231O3b	0.46031	0.98983	0.29889	20.36
312Nod5	0.46076	0.99679	0.30208	2.10
312Nod1	0.45809	0.99254	0.29754	28.05
312AB2	0.45946	0.99957	0.29957	16.46
422-1	0.46092	0.98922	0.29839	23.19
422-3	0.46444	0.98106	0.29955	16.56
422-5a	0.460392	0.98743	0.29990	19.49
		C horizon		
45HFe5	0.45564	0.99399	0.30174	4.03
45HFe6	0.46240	0.98723	0.30038	11.83
45Fe	0.46193	0.99270	0.30115	7.45
320Fe	0.46004	0.98951	0.30006	13.66
46Fe4	0.45897	0.98752	0.30034	12.06
46Fe5	0.45564	0.99399	0.30174	4.03
46Fe6	0.46240	0.98792	0.30038	11.82
46Fe1	0.46447	0.98986	0.30019	12.90
46-2	0.45766	0.99546	0.30170	4.29
46-5	0.45748	0.98589	0.30050	11.15
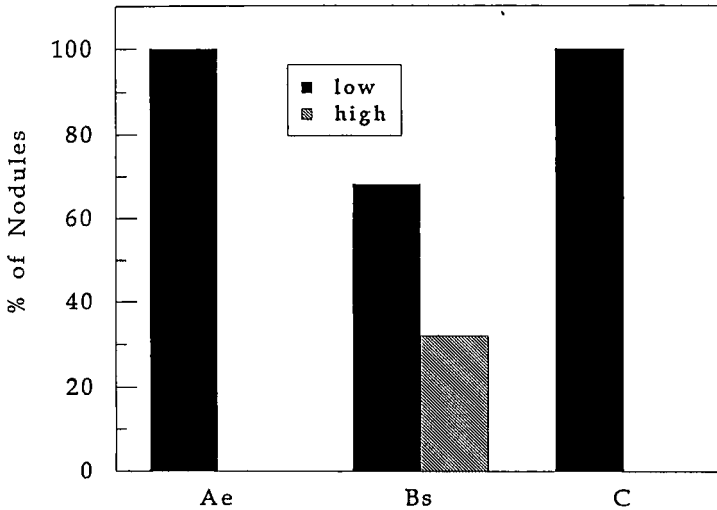
Fig. 6. Class distribution of the degree of Al for Fe substitution in goethite in the various horizons. The low goethite has substitution of <15 mole% Al and the high goethite has >15 mole% Al.

eluvial horizon although the high degree of crystallinity in most of the allogenic hematite can also be a factor in its stability.

The identification of different degrees of Al for Fe substitution in goethite within the same horizon is considered an improvement on the conventional use of bulk samples where the average value is determined (Schwertmann and Taylor, 1989) and the heterogeneity within the horizon is often not established. In the B horizon, the wide range of Al for Fe substitution (2 to 28 mole% Al) suggests the existence of various microenvironments and temporal changes where Al activity (Campbell and Schwertmann, 1984) and the amounts of organic ligands differ widely. For instance, the high goethite may have formed in an environment of high biological activity such as in the indurated nodules in the B horizon where the fungal population was found to be higher than that in the matrix (Arocena and Pawluk, 1991).

The nature, occurrence and characteristics of Fe oxides also provide information about the pedogenesis of these soils. In the early stage of soil formation, where mineral weathering is dominated by the dissolution of Fe-bearing minerals like olivines, high amounts of Fe^{3+} and low amounts of Al^{3+} are released into the soil solution and lead to the the possible formation of hematite and goethite, and particularly low goethite. With time, most of these Fe minerals are weathered and the dissolution shifts to the Fe and Al containing silicates. The chemistry of the soil solution at this point is different from the early stage because it has high amounts of Al as well as Fe. High concentrations of organic acids resulting from increased vegetative growth and decomposition is another characteristic of the soil solution. These conditions are conducive to the formation of high goethite. The formation of large goethite nodules can be

the result of the dissolution of the earlier formed small goethite nodules and their subsequent recrystallization although cumulative crystallization may also be a cause.

The dominance of goethite over lepidocrocite suggests the prevalence of an oxidizing environment in the pedogenesis of the soils which may be expected in a coarse textured well drained soil. Reductomorphic conditions necessary for the formation of lepidocrocite is likely to occur only under certain microenvironmental conditions such as the interphase between the spongy LFH layer and the Ae horizon, or some isolated period of flooding, during the period of soil genesis.

REFERENCES

April, R. and Keller, D., 1990. Mineralogy of the rhizosphere in forest soils of the eastern United States. Biogeochemistry, 9: 1-18.

Arocena, J.M., 1991. Microstructures of Some Podzolic Soils from Alberta: Genesis and Mineral Transformation. Ph.D. Thesis, University of Alberta, Edmonton, Canada.

Arocena, J.M. and Pawluk, S., 1991. The nature and origin of nodules from podzolic soils from Alberta. Can. J. Soil Sci., 71: 411-426.

Arocena, J.M., Pawluk, S. and Dudas, M.J., 1992. Genesis of selected sandy soils in Alberta, Canada as revealed by microfabric, leachate and soil composition. Geoderma, 54: 65-90.

Benoit, P.H., 1986. A Computer Package for Indexing and Least Square Refinements of Powder Diffraction Data Written by D.E. Appleman and H.T. Evans: Microcomputer Version. Lehigh University, Bethlehem, Pennsylvania.

Boero, V. and Schwertmann, U., 1989. Occurrence and transformations of iron and manganese in a colluvial terra rosa toposequence of Northern Italy. Catena, 14: 519-531.

Brewer, R., 1976. Fabric and Mineral Analysis of Soils. 2nd ed. R.E. Krieger Publishing Co. Huntington, New York, 482 pp.

Brewer, R. and Pawluk, S., 1975. Investigation of some soils developed in hummocks of the Canadian sub-Arctic and southern Arctic regions. I. Morphology and micromorphology. Can. J. Soil Sci., 55: 301-319.

Bullock, P., Fedoroff, N., Jongerius, N., Stoops, G. and Tursina, T., 1985. Handbook for Soil Thin Section Description. Waine Research Publications, Wolverhampton, U.K., 152 pp.

Campbell, A.S. and Schwertmann, U., 1984. Iron-oxide mineralogy of placic horizons. J. Soil Sci., 35: 569-582.

Canadian Soil Survey Committee, 1978. The Canadian System of Soil Classification. Agriculture Canada, Supplies and Services Canada, Ottawa, Ontario Canada.

Chesley, G.F., 1947. X-ray diffraction camera for micro-techniques. Rev. Sci. Instr., 18: 422-424.

Cornell, R.M., Schneider, W. and Giovanalli, R., 1989. The transformation of ferrihydrite to lepidocrocite. Clays and Clay Miner., 24: 549-553.

Cullity, B.D., 1959. Elements of X-ray Diffraction. Addison-Wesley Publ., London.

De Geyter, G., Hoste, S., Stoops, G., Vandenberghe, R. and Verdonck, L., 1982. Mineralogy of the ferriferous soil materials in the source area of Blanchimont (Province of Liege), Belgium. Pedologie, 32: 349-366.

Fitzpatrick, P.W. and Schwertmann, U., 1981. Al-substituted goethite - an indicator of pedogenic and other weathering environments in South Africa. Geoderma, 27: 335-347.

Fox, L.E., 1988. Solubility of colloidal ferric hydroxide. Nature, 333: 442-444.

ICOMOD, 1990. International Committee on the Classification of Spodosols, Circular Letter #9, 23 March 1990.

Jackson, M.L., 1969. Soil Chemical Analysis - Advanced Course, second edition. Dept. of Soils, Univ. of Wisconsin, Madison, USA.

McKeague, J.A., 1967. An evaluation of 0.1M pyrophosphate and pyrphosphate-dithionite in comparison with oxalate as extractants of the accumulation products in podzols and some other soils. Can. J. Soil Sci., 47: 95-99.

McKeague, J.A., De Coninck, F. and Franzmeier, D.P., 1983. Spodosols. In: L.P. Wilding, N.E. Smeck, and C.F. Hall (Editors), Pedogenesis and Soil Taxonomy: II. The Soil Orders. Developments in Soil Science IIB, Elsevier, Amsterdam, pp. 217-248

Mehra, O.P. and Jackson, M.L., 1960. Iron removal from soils and clays by dithionite-citrate system buffered with sodium bicarbonate. In: A. Swineford (Editor), Proc. 7th Nat. Conf. Clays and Clay Miner. Monograph 5. Pergamon Press, New York, pp. 317-327.

Norrish, K. and Taylor, R.M., 1961. The isomorphous replacement of iron by aluminum in soil goethites. J. Soil Sci., 12: 294-306.

Pawluk, S., 1971. Characteristics of Fera Eluviated Gleysols developed from acid shales in northwestern Alberta. Can. J. Soil Sci., 51: 113-124.

Pawluk, S., 1983. Fabric sequences as related to genetic processes in two Alberta soils. Geoderma, 30: 233-242.

Schulze, D.G., 1981. Identification of soil iron oxide minerals by differential X-ray diffraction. Soil Sci. Soc. Am. J., 45: 437-440.

Schulze, D.G., 1984. The influence of aluminum on iron oxides. VIII. Unit cell dimensions of Al-substituted goethites and estimation of Al from them. Clays and Clay Miner., 32: 36-44.

Schulze, D.G., 1988. Separation and concentration of iron-containing phases. In J.W. Stucki, B.A. Goodman, and U. Schwertmann (Editors), Iron in Soils and Clay Minerals. D. Reidel Publishing, Dordrecht, The Netherlands, pp. 63-81.

Schwertmann, U., 1964. Differenzierung der Eisenoxide des Bodens durch Extraktion mit Ammoniumoxalat Losung. Z. Pflanzehernähr., Dung. Bodenkunde, 105: 194-202.

Schwertmann, U., 1988. Occurrence and formation of Fe oxides in various pedoenvironments. In J.W. Stucki, B.A. Goodman, and U. Schwertmann (Editors), Iron in Soils and Clay Minerals. D. Reidel Publishing Co, Dordrecht, The Netherlands, p. 893.

Schwertmann, U. and Taylor,R. M., 1989. Iron oxides. In: J.B. Dixon and S.B. Weed (Editors), Minerals in Soil Environments. 2nd ed. Soil Sci. Soc. Am. Book Series # 1., Madison, Wisconsin, pp.379-427.

Schwertman, U., Carlson, L. and Murad, E., 1987. Properties of iron oxides in two Finnish lakes in relation to the environment of their formation. Clays and Clay Miner., 35: 297-304.

Stoops, G., 1983. SEM and light microscopic observations of minerals in bog-ores of the Belgian Campine. Geoderma, 30: 179-186.

Tarzi, J.G. and Protz, R., 1978. The occurrence of lepidocrocite in two well-drained Ontario soils. Clays and Clay Miner., 26: 448-451.

Warren, C.J., Xing, B. and Dudas, M. J., 1990. Procedure for microwave digestion and total dissolution of inorganic soil and clay minerals. Can. J. Soil Sci., 70: 617-620.

Wicks, F.J. and Zussman, J., 1975. Microbeam X-ray diffraction patterns of the serpentine minerals. Can. Miner., 13: 244-258.

Yapp, C., 1983. Effects of AlOOH-FeOOH solid solution on Gt-Hm equilibrium. Clays and Clay Miner., 31: 239-240.

This Page Intentionally Left Blank

Iron-rich peds near a volcanic mudpool, Mt. Makiling (Philippines)[*]

J.M. Arocena[1], C. Landuydt[2], G. De Geyter[2] and G. Stoops[2]
[1]Dept. of Soil Science, University of Alberta, Canada T6G 2E3
[2]Laboratory of Mineralogy, Petrography and Micropedology, State University of Gent, Belgium

ABSTRACT

Arocena, J.M., Landuydt, C., De Geyter, G. and Stoops, G., 1994. Iron-rich peds near a volcanic mudpool, Mt. Makiling (Philippines). In: A.J. Ringrose-Voase and G.S. Humphreys (Editors), Soil Micromorphology: Studies in Management and Genesis. Proc. IX Int. Working Meeting on Soil Micromorphology, Townsville, Australia, July 1992. Developments in Soil Science 22, Elsevier, Amsterdam, pp. 99-105.

Samples of peds around a volcanic mudpool of the solfataric Mt. Makiling in the Philippines were investigated to determine the nature of selected minerals with emphasis on the formation of iron oxides. The results of mineralogical and micromorphological studies show that iron oxides crystallize to hematite in the mudpool edges and to goethite further away from the pool. These oxides occurred as coatings, infillings and nodules. Other secondary minerals formed include alunite, sulfur, opal and kaolinite. The acidity produced from present-day solfataric activity of the volcano is believe to be the driving force in most of the observed mineral transformations.

INTRODUCTION

Mt. Makiling, a solfataric volcano (14°08'N, 121°11'E) lies on the western belt of Quaternary volcanism associated with the tectonics of the Manila trench in the Philippines. Its volcanic ejecta belong to a calc-alkali suite composed mainly of andesite with small proportions of dacite and basalt dated between 0.18 to 0.51 million years BP (Bureau of Mines and Geosciences, 1981). Related to this volcanism is solfataric activity as indicated by the occurrence of a number of mudpools, fumaroles, and hot springs scattered around the volcano. An area near a mudpool on the eastern side of the mountain, at 27 m elevation, was selected for the study. The objective of the study was to describe the micromorphology and to characterize the minerals with emphasis on the formation of iron oxides in the vicinity of the mudpool.

MATERIALS AND METHODS

Iron-rich surface soil peds were collected from the mudpool area of Mt. Makiling. Sampling distances from the pool were set arbitrarily and coincide with the color gradation of

---

[*] Contribution from the International Training Centre No. 092/055.

Table 1
Location, redness index, pH, iron and mineralogical analyses of peds from the mudpool of Mt. Makiling (Philippines).

| | Samples | | |
	P20	P21	P22
Distance from pool edge (m)	0	50	100
Redness Index	2	4	0
pH	3.5	4.7	4.7
Feo (%)	1.34	0.38	0.61
Fed (%)	21.53	19.42	14.53
Feo/d	0.6	0.02	0.04
XRD*	Kt, Gt, Hm, Qtz, S	Kt, Gt, Hm, Qtz, Al	Kt, Gt, Hm, Qtz, Al
Hm/Hm+Gt	0.70	0.37	0.34

*Kt-kaolinite; Gt-goethite; Hm-hematite; Qtz-quartz; S-sulfur; Al-alunite

the peds starting from yellow (10YR 3/4; sample P22 at 100 m away from the edge of the pool), to yellowish red (7.5YR 6/6; sample P21 at 50 m away from the edge of the pool), and to red (2.5YR 5/8; sample P20 at the edge of the pool). Brief descriptions of the samples with the calculated redness rating according to Torrent *et al.* (1983) are given in Table 1.

Thin sections were prepared from polyester resin-impregnated peds and described according to the terminology of Bullock *et al.* (1985). Iron, both from ground samples and uncovered thin sections, was extracted using acid ammonium oxalate (Schwertmann, 1964) and dithionite-citrate-bicarbonate (DCB) (Mehra and Jackson, 1960). *In situ* extraction of iron was carried out according to the technique proposed by Arocena *et al.* (1989). "Feo" and "Fed" designate the oxalate and DCB extractable iron, respectively.

The mineralogy of randomly oriented ground samples of the bulk material was investigated by a Philips X-ray diffractometer using Co-Kα (40kV and 20mA). Infrared (IR) spectra of the samples were determined from pellets prepared by 1:400 soil to KBr ratio. Differential thermal analysis (DTA) was employed in sample P22 to identify whitish concretions at heating rate of 10°C per minute. Heavy minerals were separated using heavy liquid and quantified, where possible, by point counting under a polarizing microscope.

Iron oxide mineralogy was investigated using X-ray diffraction. The amounts of hematite and goethite were estimated from their prominent peak heights; the intensity of Gt d_{111} was multiplied by 1.25 and the Hm d_{110} by 1.41 as suggested by Boero and Schwertmann (1989). The morphology and chemistry of iron accumulation in sample P20 were studied using a scanning electron microscope with energy dispersive X-ray analyzer (SEM-EDS).

RESULTS AND DISCUSSION

Iron content and iron minerals

Table 1 shows that all the samples contain high amount of free iron (Fed) with values ranging from 14.53% (P22) to 21.53% (P20). The oxalate extractable iron (Feo) is of minor

Wavenumber (cm⁻¹)
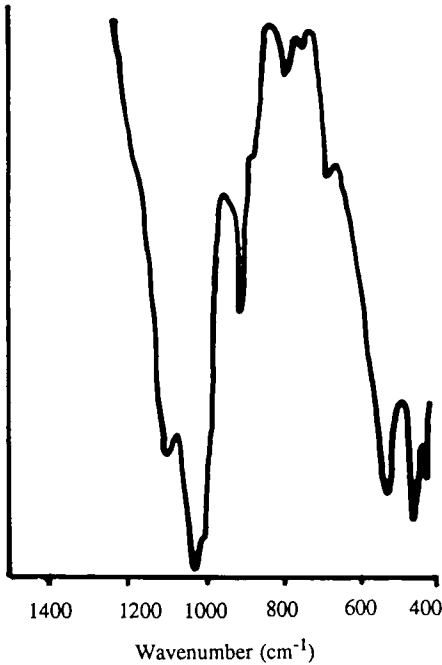
Fig. 1. Infrared spectrum of sample (P20) containing Fe oxides as revealed by the IR absorption for vibrational mode of Fe-containing groups at 400-700 cm^{-1} and the O-H bending vibration at 795 and 890 cm^{-1} regions.

importance in all samples, showing the dominance of crystalline iron minerals. X-ray diffraction patterns show distinct reflections at 0.418 , 0.269 , 0.245 nm for goethite and at 0.270, 0.252, and 0.169 nm peaks for hematite. Infrared spectrum of the samples in Fig. 1 showed a strong IR absorbance at 400-700 cm^{-1} indicating the presence of vibrational mode of Fe-containing groups. Adsorption is strong at 470 and 540 cm^{-1} and confirms the presence of hematite identified from XRD results. The presence of goethite is also confirmed by its O-H bending vibration at 795 and 890. Moreover, optical investigations also revealed that interference color of these oxides are in the second order red comparable to those of goethite and hematite.

The ratio Hm/Hm+Gt (Table 1) is higher in P20 than in P21 and P22 and indicates the dominance of Hm in the mudpool itself. This is consistent with the findings of Schwertmann (1985) stating that Hm formation is favored at higher temperature. The temperature near the pool could reach about 90°C and is significantly higher than in the area 50 m away from it. The high redness index of P20 (Table 1) also points to dominance of Hm (Torrent *et al.*, 1983).

Table 2 shows the properties of these oxides. They accumulate in a variety of forms such as nodules, infillings and coatings. Radiating pattern of hematite coatings in sample P20 is shown in the SEM micrograph (Fig. 2). Free iron can also impregnate the whole groundmass (P20). *In situ* iron removal effectively removed these oxides and revealed the secondary blocky structure. The infillings are quite dense especially along planar voids that they completely mask the microstructure. Infillings can also occur in association with opal. The nodules are mostly typic about 0.2 mm in diameter.

Table 2
Micromorphology of the iron-rich peds from the mudpool of Mt. Makiling (Philippines).

| | Samples | | |
	P20	P21	P22
Microstructure	vughy	angular blocky	sub-angular to angular blocky
Porosity (%)	25	15	15
C/F limit (ratio)	5μm (1:9)	5μm (2:8)	5μm (3:7)
C material*	Qtz, Op	Qtz, Gl	Qtz, Opl, Gl, rock fragments
F material	similar among the three samples: clay, Fe-oxide		
Related distribution	heterogenous, (some parts open porphyric)	open porphyric	open porhyric
Pedofeatures	(similar among samples: Fe nodules, infillings, and coatings; clay coatings and infillings and opal accumulations)		
	nodules of sulfur		nodules of alunite
Organic material	(none observed)	root fragments	plant remains

*Qtz-quartz; Op-opaque; Gl-volcanic glass; Opl-opaline materials

The iron is derived from the breakdown of silicate minerals, and perhaps some volcanic glass, that are exposed to an aggressive weathering environment in the mudpool and its surrounds. Oxidation of H_2S results in acid formation, creating a very low soil pH favorable for the release of iron.

Mineralogy

Powder diffraction patterns obtained from bulk samples reveal the presence of kaolinite, quartz, goethite and hematite. Infrared spectrum shows the presence of O-H bending vibrations in 1630 and 3420 cm^{-1} wavenumber regions that relate to water associated with the kaolinite structure. The Si-O absorption band at around 1010 cm^{-1} also indicates the presence of kaolinite. Thin sections show that the clays form part of the groundmass and accumulate as coatings and infillings. *In situ* removal of the iron, shows clearly that whenever these clays are present in the microstructure, they are situated along the edges of the blocks and have extinction lines parallel to the planar voids. Dessication of the percolating water carrying the peptised clays may have caused the orientation (Theochrapolus and Dalrymple, 1987) and the formation of the cracks. Clay also occurs associated with other pedofeatures such as void infillings in the iron-oxide and alunite nodules.

In P20, the weak reflections at 0.47, 0.38, 0.33 and 0.32 nm are interpreted to be due to elemental sulfur. The hand specimen shows scattered yellowish accumulations which are indicative of the presence of sulfur. The precipitation of sulfur requires a very high total sulfur
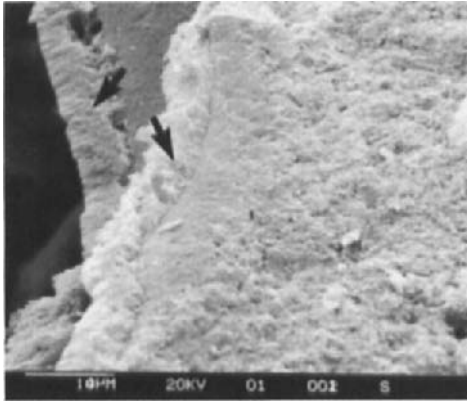
Fig. 2. Scanning electron micrograph of the radiating pattern of hematite accumulation (with the arrow) as coatings on voids in sample P20.
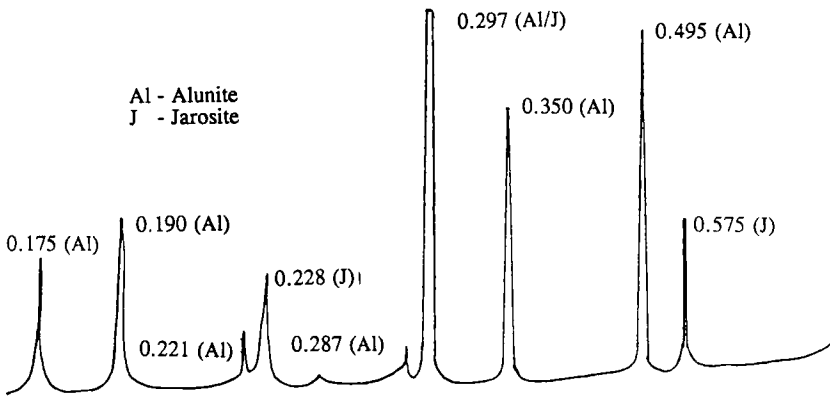
Fig. 3. X-ray diffraction pattern of randomly oriented powder sample of P21 showing the presence of alunite group of minerals (the units in nanometer).

supply, a low pH and an intermediate Eh. These conditions are satisfied in the study areas where emission of H_2S gas is constantly occurring due to the solfataric activity that initiates aggressive chemical weathering of the minerals, particularly silicates. In P20, sulfur accumulations may result from the incomplete oxidation of this gas into the mudpool. The intensive weathering has resulted in a very low reserve of weatherable minerals and high free iron content. The soil parent material represented by sample P22 contains augite (48%), hornblende (18%), hypersthene (16%), staurolite (13%) and opaques (18%). The same heavy minerals occur in insufficient abundance for quantitative estimate in sample P21, and only opaques were separated from P20 at the pool edge.

Another secondary mineral observed as whitish nodules (in P21) has XRD pattern shown in Fig. 3. It has well defined XRD reflections at 0.30, 0.50, 0.35, 0.23, 0.19, and 0.18 nm which are attributed to the member(s) of the alunite group, a series of basic sulfates with alunite,

$A\text{Fe}_3(\text{SO}_4)_2(\text{OH})_6$ and jarosite, $A\text{Al}_3(\text{SO}_4)_2(\text{OH})_6$ as end members, where A can be K, Na, Pb, NH_4, Ag or B (Stephen *et al.*, 1988; Brophy, *et al.*, 1962, 1965). Using the lattice-variation diagram of Brophy *et al.* (1962), the measured unit cell dimension a ($a=4d_{2240}$) is 0.699 nm and corresponds to Al/Al+Fe ratio of 0.96. This indicates the predominance of alunite. Endothermic peaks at 538° and 755°C on the DTA pattern further support the presence of alunite. X-ray fluorescence analysis of the nodules also show the presence of S, K, Al and iron which are the main constituents of the mineral. Silica was also detected together with traces of P and Ca.

The main rock type in the study area is andesite (Bureau of Mines and Geosciences, 1981), and is the necessary starting materials (mainly feldspars) required for the formation of alunite. The formation of alunite from feldspars is well documented (*e.g.*, Harvey and Vitaliano, 1964; Holler, 1967) and the proposed reaction can liberate silica. In the mudpool sample we did find porous opaline accumulations and locally silicified plant fragments with distinct cellular structure. In acid sulfate soils where similar silicate weathering takes place under acid conditions, jarosite is usually present and occasional concentrations of secondary silica and opal-C are observed (van Breemen, 1979).

CONCLUSIONS

Chemical, mineralogical and micromorphological results suggest that an aggressive chemical weathering of the primary ferro-magnesian minerals of the andesitic parent material is the principal soil forming process in the area. The high soil acidity caused by the oxidation of the H_2S gas, high rainfall and warm temperatures in the area provide the main driving forces to the weathering process. Intense weathering of minerals is suggested by the high amount of free iron and opaque minerals, low amount of weatherable minerals, neoformation of alunite, opal and elemental sulfur. Free iron crystallizes to hematite in the mudpool edges and to goethite at greater distance away from the mudpool.

ACKNOWLEDGEMENTS

REFERENCES

Arocena, J.M., De Geyter, G., Landuydt, C. and Schwertmann, U., 1989. Dissolution of soil iron oxides with ammonium oxalate: comparison between bulk samples and thin section. Pedologie, 39: 275-297.

Boero, V. and Schwertmann, U., 1989. Occurrence and transformations of iron and manganese in a colluvial terra rosa toposequence of Northern Italy. Catena, 14: 519-531.

Brophy, G.P., Scott, E.S. and Snellgwice, R.A., 1962. Sulfate studies: solid solution between alunite and jarosite. Amer. Miner., 47: 112-126.

Brophy, G.P. and Sheridan, M.F., 1965. The jarosite-hydronium-jarosite solid solution series. Amer. Miner., 50: 1595-1607.

Bullock, P., Fedoroff, N., Jongerius, N., Stoops, G. and Tursina, T., 1985. Handbook for soil thin section descriptions. Waine Research Publications, U.K., 152 pp.

Bureau of Mines and Geosciences (Philippines), 1981. Geology and Minerals Resources of the Philippines. Vol I: Geology. Govt. Printing Press, Manila, 406 pp.

Harvey, R.D. and Vitaliano, C.J., 1964. Wall rock alterations in the Goldfield District, Nevada. J. Geol., 72: 569-579.

Holler, M., 1967. Experimentelle bildung von alunit-jarosit durch die einwirkung schwefelsaure auf mineralen en gesteine. Contr. Mineral. and Petrol., 15: 309-329.

Mehra, O.P. and Jackson, M.L., 1960. Iron removal from soils and clays by dithionite-citrate system buffered with sodium bicarbonate. In: A. Swineford (Editor), Proc. 7th Nat. Conf., Clays and Clay Miner. Monograph 5. Pergamon Press, New York, pp. 317-327.

Schwertmann, U., 1964. Differenzierung der Eisenoxide des Bodens durch photochemische Extraktion mit saurer Ammoniumoxalat-Lösung. Z. Pflanzenernähr. Düng. Bodenkunde., 105: 194-202.

Schwertmann, U., 1985. Occurrence and formation of iron oxides in various pedoenvironments. In: A NATO Advanced Study Institute on Fe, Iron in Soils and Clay Minerals. Bad Windsheim, Germany, 1-3 July 1985, pp. 682-736.

Stephen, P., Altarar, J., Fitzpatrick, J., Dennis Khan, M., Bethke, P.M., Haban, D.O., Gos, J. A. and Brown, Z.A., 1988. Ammonium alunites. Amer. Miner., 73: 145-152.

Theochrapolous, S.P. and Dalrymple, D.G., 1987. Experimental construction of illuvial cutans (channel argillans) with differing morphological and optical properties. In: N. Fedoroff, L.M. Bresson and M.A. Coutry (Editors), Soil Micromorphology. Proc. VII Int. Working Meeting of Soil Micromorphology, Paris, July 1985. Association Française pour l'Etude du Sol, Plaisir, France, pp. 245-250.

Torrent, J., Schwertmann, U., Fechter, H. and Alferez, F., 1983. Quantitative relationships between soil color and hematite content. Soil Sci., 136: 354-358.

van Breemen, N., 1979. Genesis, morphology and classification of acid sulfate soils in coastal plains. In: J.J. Kittrick, D.S. Fanning and L.R. Hassner (Editors), Acid Sulfate. Soil Sci. Soc. Am. Spec. Publ. No. 10. Madison, Wisconsin, pp. 95-108

This Page Intentionally Left Blank

Light and electron microscopy studies of uranium distribution in the regolith at Koongarra, N.T.

A.J. Koppi and D.A. Klessa

Dept. of Agricultural Chemistry and Soil Science, University of Sydney, NSW, 2006

ABSTRACT

Autoradiographs of thin sections from the M2 core in the regolith (about 25 m thick) of the Cahill Schist Formation at Koongarra, Northern Territory, revealed that relatively large amounts of U as an α-particle emitter occurred in Fe-rich and Mn-rich areas. Electron microprobe analysis (EMA) and X-ray maps showed that within the Fe-rich areas ($\leq 60\%$ Fe), U ($< 4\%$) is associated diffusely with Fe. Within Mn-rich areas there were smaller areas with high concentrations of U ($\leq 17\%$) in intimate association with Ce ($\leq 61\%$). XRD of Mn-rich areas at 10 m depth identified the Mn mineral as lithiophorite and this was confirmed by EDS on the SEM. The lithiophorite crystals have a prismatic morphology. The Ce/U association is in the form of balls (1 – 2 μm diameter) consistent with a mixture of microcrystalline Ce and U oxides as identified by electron diffraction.

INTRODUCTION

The geology of the uranium deposit at Koongarra (225 km east of Darwin in the Northern Territory of Australia) has been extensively described (Foy and Pedersen, 1975; Snelling, 1980a and 1989) together with uranium minerals in the unweathered quartz-chlorite-schist of the Cahill Formation (Snelling, 1980a and b). Secondary uranium mineralisation is present from the surface to the base of weathering, approximately 25 m depth, and forms a tongue-like body of ore material, dispersing laterally about 80 m from the primary zone.

During weathering, uranium distribution follows the formation of various iron phases. Oxides of iron and manganese appeared to dominate scavenging of radionuclides (Edghill, 1991) and a large proportion of total U is associated with various Fe-rich phases in the weathered zone at Koongarra (Nightingale, 1986). At the nearby Ranger deposit, U is concentrated in iron minerals (Davey and Gray, 1986). Mn is a well-known scavenger of numerous trace elements (McKenzie, 1975 and 1989).

The purpose of this study was to examine the nature and role of Fe- and Mn-rich areas in the mobilisation and retardation of naturally occurring U in the weathering environment at Koongarra. This paper presents the association of U with Fe, Mn, P and Ce in an intact drill core (labelled "M2" in the drilling program) from the regolith. The location of relatively high U

concentrations associated with Fe and Mn in thin sections were defined by α-track autoradiography prior to further detailed analyses.

MATERIALS AND METHODS

Samples (about 120 × 80 × 50 mm) for thin sections (ultimately, 100 mm × 65 mm × 25 μm) were cut from intact drill cores, air-dried at 30°C and impregnated under vacuum with a low viscosity equal volume mixture of Modar 835S polyester resin (ICI) and acetone. After evaporation of the acetone (about 15 days at 20°C), resin polymerisation and curing was accomplished by 7·5 kGy γ-irradiation (^{60}Co) (Gray, 1986). Thereafter, thin sections were prepared from the hard block in the usual manner (FitzPatrick, 1984).

Autoradiographs (to locate the U-rich areas) were prepared from the thin sections using Tastrak film (diethylene glycol bis (allyl carbonate) polymer) as a solid state nuclear track detector. The film was etched in 6·25 M NaOH for 6 hours at 75°C (Gray, 1986). Areas with high α-particle emission were almost always opaque in transmitted light and therefore were also examined in reflected light whereupon the black Mn-rich material could be distinguished from red or yellow Fe-rich areas.

To locate the U and ascertain its chemical associations, representative high α-particle emission areas from each thin section were studied using an ETEC Autoprobe (electron probe microanalyser) operated at 15 kV accelerating voltage and a beam current of 50 nA. Elements present were identified qualitatively by energy dispersive spectrometry (EDS) and measured quantitatively by wavelength dispersive spectrometry (WDS). Analyses were corrected for matrix effects (atomic number (Z), absorption (A) and fluorescence (F)) using a standard ZAF routine (Reed, 1975). The spatial association of elements was determined from X-ray maps.

Mn-rich areas contained the greatest accumulation of U, thus the crystal form and composition had to be ascertained. Mn-rich areas were therefore hand-picked from a sample at 10 m depth and examined on a Philips 505 SEM with an EDS detector and multi-channel analyser (MCA). The picked samples were ground and also examined by X-ray diffraction on a Philips X-ray diffractometer, and by electron diffraction on a Philips EM 430 300 kV transmission electron microscope (TEM) with EDS detector and Tracor Northern 5500 MCA.

RESULTS

The association of high density α-tracks with red-brown or yellow Fe-rich, or black Mn-rich material was limited in distribution and often confined to infilled pores, cracks, or lined fractures within the weathered rock. Rarely was localised high density α-particle emission sourced to remnants of primary minerals.

Fe-rich areas

Most of the high density α-tracks associated with the iron-rich areas in the core samples were yellow under reflected light indicative of a goethite dominant phase. Elemental X-ray maps of a typical area from 21 m depth (Fig. 1) show a clear spatial association of U, Fe and P. (In the centre and bottom left of this figure, the occurrence of two bright areas containing U, P and Th indicates the presence of rarely encountered remnant monazite.) When the microprobe
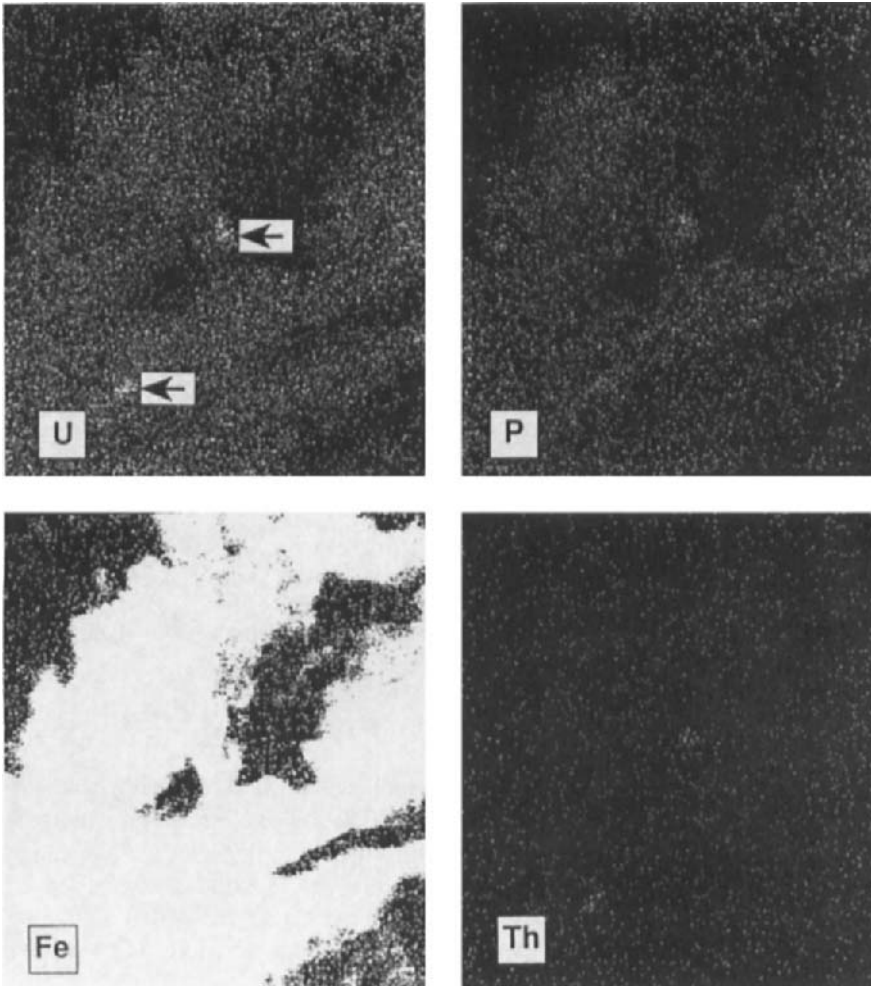
Fig. 1. X-ray maps of U, P, Fe and Th from a goethite-rich area at 21 m depth. Arrows indicate remnant monazite. The width of each photograph is 125 μm.

data of the Fe-rich zones from 17, 21 and 25 m depths are combined, Fe (≤ 60 %) is positively ($P < 0.001$) correlated with U (≤ 4%), and P (≤ 1.5 %) is not correlated with either U or Fe.

The U concentration is relatively low (< 4 %) and appears to be distributed throughout the secondary Fe depositions in a diffuse fashion. This suggests an adsorption process of UO_2^{2+} onto oxy-hydroxide surfaces. This adsorbed U would become progressively occluded as further Fe is deposited or as the crystalline structure of these Fe minerals transform whilst aging. This would account for the strong extractant required to remove U from the weathered
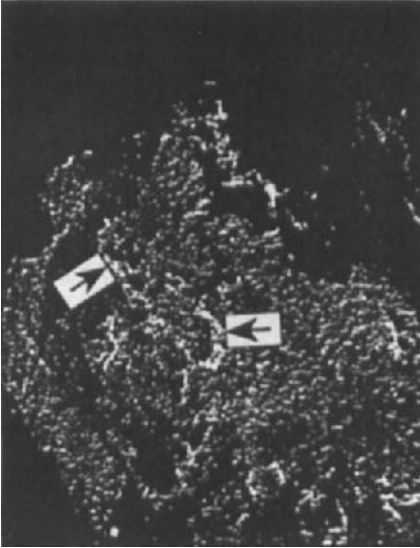
Fig. 2. Back-scattered electron image of a Mn-rich area at 8 m in the M2 core showing discrete small bright U-rich areas (arrowed). The width of the photograph is 500 μm.

material as part of a sequential extraction procedure as reported by Edis (1991). Uranium is unlikely to replace Fe in the crystal structures of Fe-minerals (Gerth, 1987).

Mn-rich areas

Fig. 2 shows a typical back-scattered electron image of a black, opaque Mn-rich area at 8 m depth associated with relatively high α-emissions. The U was found to be localised within the many small bright areas shown in this figure and not throughout the Mn area. X-ray maps (Fig. 3) show that the Mn and U are in juxtaposition and that the U is intimately associated with Ce. Microprobe data gave U concentration up to 17% and Ce up to 61% and a strong correlation of the two elements. In these Mn-rich areas, U concentrations were always associated with Ce. Where Ce and U occur together, Fe seems to play no role (Fig. 3).

Fig. 4 shows a SEM secondary electron image of a Mn-rich area from 10 m depth that had been treated with 20% hydrogen peroxide for 2 hours to remove amorphous coatings. Prismatic rods and smaller (1 – 2 μm) individual balls or clusters of balls can be seen. A typical EDS trace of the rods (Fig. 5) shows them to be Mn- and Al-rich and devoid of U and Ce. X-ray diffraction indicated lithiophorite ($(Al, Li) MnO_2 (OH)_2$). A typical EDS trace of the balls (Fig. 6) showed them to be dominated by Ce and U. Other elements are also present on the trace probably because of the small size of the balls relative to the area of X-ray detection.

The Ce/U balls have a composition different to that of published U or Ce containing minerals (Frondel, 1958; Vlasov, 1966; Cordfunke, 1969) and have an almost fixed Ce:U ratio (7:1 – 9:1). TEM electron diffraction investigations of a ground sample from 10 m depth revealed that the composition of the Ce/U balls is consistent with a microcrystalline mixture of Ce and U oxides.
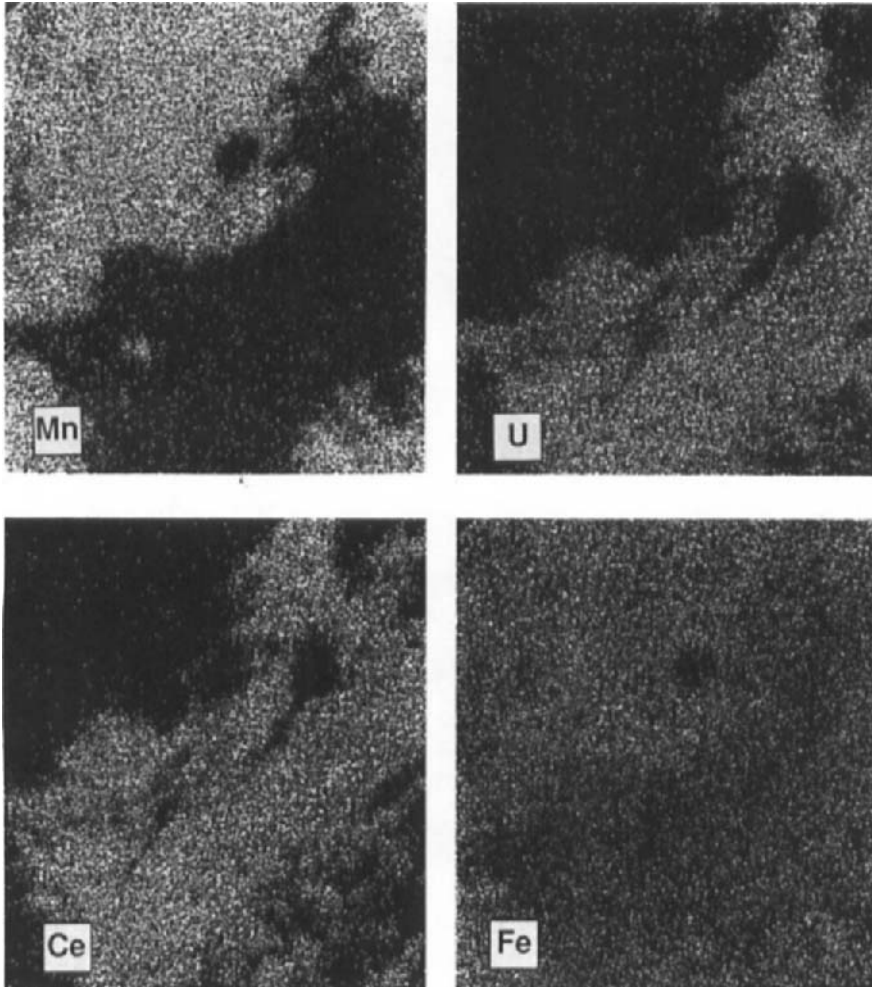
Fig. 3. X-ray maps of Mn, U, Ce and Fe from a Mn-rich area at 17 m depth. The width of each photograph is 62·5 μm.

DISCUSSION

At the scale of the light microscope, U (indicated by the α-tracks) was observed in thin section to be in intimate association with Fe and Mn accumulations. Electron microprobe analysis (1) confirmed the presence of the U in these zones, (2) quantitatively showed that U concentrations were much greater with Mn associations than with Fe and (3) revealed that Ce was always present in appreciable quantities in association with U and Mn but never with U and Fe. X-ray maps showed the intimate spatial relationship of U and Fe and revealed that Ce

Fig. 4. Scanning electron photomicrograph of a Mn-rich area from 10 m depth in the M2 core showing rods of lithiophorite ((Al, Li) MnO_2 $(OH)_2$) crystals and balls of intimately mixed Ce/U oxides. Scale bar is in 10 µm sections.

and U were spatially inseparable and in juxtaposition to Mn. The SEM showed that the Mn was in the form of rod-like lithiophorite crystals, and that the Ce and U were together in the form of small (1 – 2 µm) balls attached to the mineral surfaces. EDS confirmed that the balls were composed dominantly of Ce and U, although it was impossible to obtain an analysis of the balls exclusively because of their diminutive size (small amounts of Si, Al, Mn and P were usually also detected). Electron diffraction and EDS on the TEM showed the chemical purity of the Ce/U balls and that their diffraction pattern was consistent with a microcrystalline mixture of Ce and U oxides.

The phase of U, Fe, Mn and Ce in the regolith depends on the prevailing Eh-pH conditions. As Eh rises, U, Fe, Mn then Ce become oxidised progressively in accordance with the
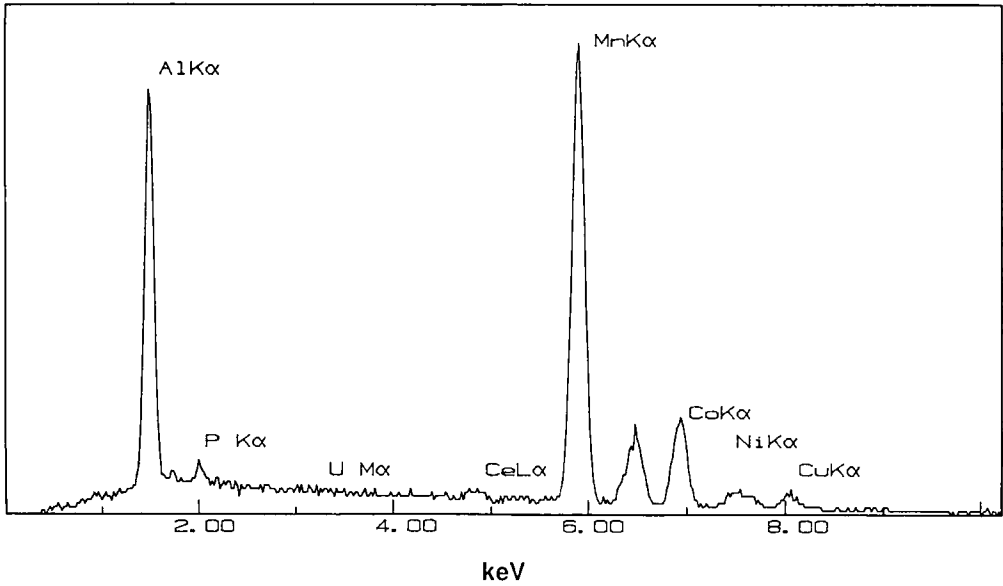
Fig. 5. Typical EDS of the Mn rods shown in Fig. 4. The Al and Mn peaks confirm the presence of lithiophorite (Li is not detectable by this technique). U and Ce were not detected; the peak to the left of the main Mn peak is also Mn.
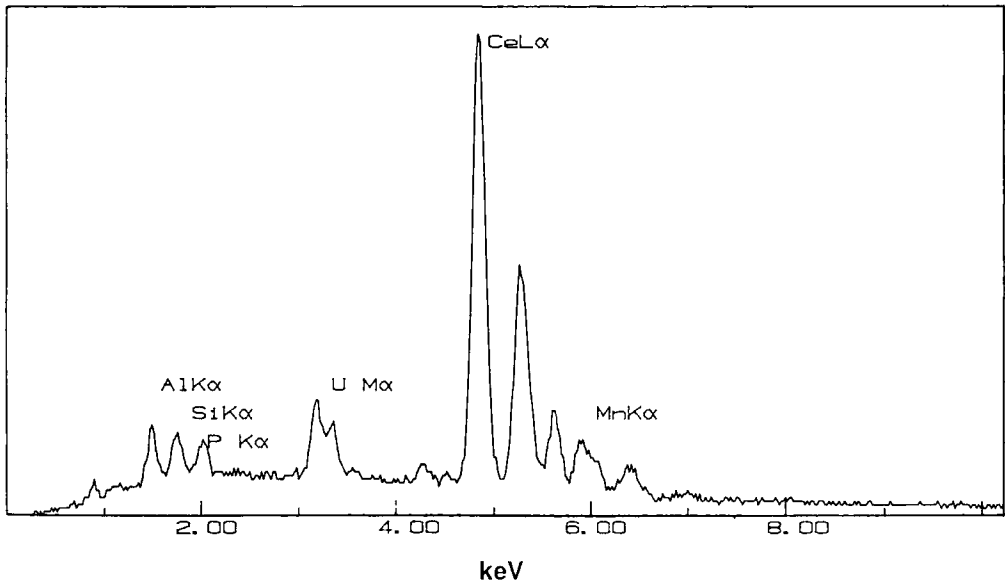
Fig. 6. Typical EDS of the Ce/U balls shown in Fig. 4. Two overlapping peaks of U and the Ce triplet of peaks (the main peak and two to the left) are shown.

electrochemical series (Weast, 1981). Oxidised forms of Fe (III), Mn (IV) and Ce (IV) are insoluble. However, under certain conditions of Eh and pH, Fe and Mn are present as oxides or oxy-hydroxides while U (VI) and Ce (III) are soluble. U (VI) will exist as such under conditions normally encountered in the regolith. In the shallow groundwaters of the Koongarra regolith, the chemical conditions (pH 5·5–7; Eh 100–400 mV, (Australian Nuclear Science and Technology Organisation ANSTO, 1992) permit Ce to occur as either Ce (III) or (IV) whereas Mn will be reduced (Brookins, 1988).

Manganese oxy-hydroxides have a high sorption capacity for heavy metals in the weathering environment (McKenzie, 1989). Oxidised Mn (lithiophorite) was found in veins and fissures indicating that these localities were more aerobic than the measured Eh of the groundwater and that the lithiophorite provided a surface for the sorption of Ce and U from solution. The marked seasonality of the rainfall in the northern part of Australia produces large changes in the depth to groundwater in the region. Consequent alternating reducing and oxidising conditions about the solid Mn surfaces would permit regular partial dissolution and mobilisation of the Mn, U and Ce thereby facilitating the growth of Ce/U balls containing large amounts of Ce and U ($\leq 17\%$). Indeed, the lithiophorite surfaces may act as a catalyst for the agglomeration of Ce and U oxides.

Under the prevailing conditions in the Koongarra regolith, iron oxy-hydroxide surfaces clearly behave in a different manner to those of Mn. U concentrations associated with Fe were always found to be lower ($< 4\%$) and without Ce. In the absence of adsorbed Ce, it seems that a mechanism does not exist for increasing the U concentration upon partial dissolution of the Fe minerals in response to seasonally changing redox conditions.

CONCLUSIONS

In the M2 core from Koongarra, uranium concentrations were associated mainly with Fe and Mn oxy-hydroxides. With Fe, U was present apparently as surface adsorption; within Mn-rich areas (containing the rod-shaped Mn mineral, lithiophorite), relatively large concentrations of U were associated with Ce in balls on mineral surfaces. The Ce/U balls appear to be a microcrystalline mixture of Ce and U oxides.

ACKNOWLEDGMENTS

REFERENCES

ANSTO (Australian Nuclear Science and Technology Organization), 1992. Alligator Rivers Analogue Project. Groundwater Data 1990 and 1991. P. Duerden (Editor). Progress report, 1 March 1991–31 August 1991. ANSTO, Lucas Heights, Sydney, pp. 311–349.
Brookins, D.G., 1988. Eh-pH Diagrams for Geochemistry. Springer-Verlag, Berlin, 176 pp.
Cordfunke, E.P.H., 1969. The Chemistry of Uranium Including its Applications in Nuclear Technology. Elsevier, Amsterdam, The Netherlands, 237 pp.

Davey, B.G. and Gray, D., 1986. Mineralogical studies. In: P.L. Airey, D. Roman, C. Golian, S. Short, S.T. Nightingale, T. Payne, R. Lowson and P. Duerden. Radionuclide Migration Around Uranium Ore Bodies – Analogues of Radioactive Waste Repositories. Ann. Rep. 1984–85, AAEC Rep. C45, pp. 119–141.

Edghill, R., 1991. The redistribution of uranium with weathering in the Koongarra Uranium Deposit. Radiochimica Acta., 52/53: 381–386.

Edis, E., 1991. The Effect of Weathering on the Distribution of Uranium and Associated Elements at Koongarra, Northern Territory, Australia. M.Sc.Agr. Thesis, University of Sydney.

FitzPatrick, E.A., 1984. Micromorphology of Soils. Chapman and Hall, London, 433 pp.

Foy, M.F. and Pedersen, C.P., 1975. Koongarra uranium deposit. In: C.L. Knight (Editor), Economic Geology of Australia and Papua New Guinea, Vol. 1 Metals, The Austalasian Institute of Mining and Metallurgy. Melbourne, pp. 317–321.

Frondel, C., 1958. Systematic Mineralogy of Uranium and Thorium. Geological Survey Bulletin 1064. U.S. Gov. Printing Office, Washington, D.C., 397 pp.

Gerth, J., 1987. Role of Iron Oxides in the Retention of Trace Metals and Radionuclides. Australian Institute of Nuclear Science and Engineering Research Fellowship Project, Final Report. (Unpublished, ANSTO)

Gray, D.J., 1986. The Geochemistry of Uranium and Thorium During Weathering of Chloritic Schists at the Alligator Rivers Uranium Province, N.T. Australia. Ph.D. thesis, University of Sydney.

McKenzie, R.M., 1975. An electron microprobe study of the relationships between heavy metals and manganese and iron in soils and ocean floor nodules. Aust. J. Soil Res., 13: 177–188.

McKenzie, R.M., 1989. Manganese oxides and hydroxides. In: J.B. Dixon and S.B. Weed (Editors), Minerals in Soil Environments, Soil Sci. Soc. of Am. Madison, Wisconsin, pp. 439–465.

Nightingale, J.T., 1986. Distribution of uranium series nuclides throughout the Koongarra deposit. In: P.L Airey, D. Roman, C. Golian,S. Short, T. Nightingale, T. Payne, R. Lowson, and P. Duerden, (Editors). Radionuclide Migration Around Uranium Ore Bodies-Analogues of radioactive waste repositories. Ann. Rep. 1984–85, AAEC Rep. C45, pp 41-64

Reed, S.J.B., 1975. Electron Microprobe Analysis. Cambridge University Press.

Snelling, A.A., 1980a. A Geochemical Study of the Koongarra Uranium Deposit Northern Territory, Australia. Ph.D. Thesis, University of Sydney.

Snelling, A.A., 1980b. Uraninite and its alteration products, Koongarra uranium deposit. In: J. Ferguson and A.G. Goleby (Editors), Uranium in the Pine Creek Geosyncline. International Atomic Energy Agency, Vienna, pp. 487–498.

Snelling, A.A., 1989. Koongarra uranium deposits, In: F.E. Hughes (Editor) The Geology of the Mineral Deposits of Australia and Papua New Guinea. The Austalasian Institute of Mining and Metallurgy, Monograph 14, Melbourne, Australia, pp. 807-812.

Vlasov, K.A., 1966. Geochemistry and mineralogy of rare elements and genetic types of their deposits. In: K.A. Vlasov (Editor), Volume II. Mineralogy of Rare Elements, Israel Program for Scientific Translations, Jerusalem, pp. 249–266.

Weast, R.C., (Editor), 1981. Handbook of Chemistry and Physics. 61st Edition, Electrochemical Series B1-B411, CRC Press, Boca Raton, Florida.

This Page Intentionally Left Blank

Aquic conditions for Soil Taxonomy: concepts, soil morphology and micromorphology

M.J. Vepraskas[1], L.P. Wilding[2] and L.R. Drees[2]

[1]*North Carolina State University, Soil Science Department, Raleigh, North Carolina, U.S.A.*
[2]*Texas A&M University, Soil and Crop Sciences Department, College Station, TX, U.S.A.*

ABSTRACT

Vepraskas, M.J., Wilding, L.P. and Drees, L.R., 1994. Aquic conditions for Soil Taxonomy: concepts, soil morphology and micromorphology. In: A.J. Ringrose-Voase and G.S. Humphreys (Editors), Soil Micromorphology: Studies in Management and Genesis. Proc. IX Int. Working Meeting on Soil Micromorphology, Townsville, Australia, July 1992. Developments in Soil Science 22, Elsevier, Amsterdam, pp. 117-131.

Aquic moisture regimes have been redefined in Soil Taxonomy and are now called aquic conditions. The new system uses micromorphological concepts to define macroscopic indicators that show that a soil has been saturated and reduced. *Aquic conditions* are defined on the basis of three criteria which must be documented separately: saturation, reduction, and redoximorphic features. Saturation must be confirmed by using piezometers or tensiometers to record water table levels to a depth of 2 m. Reduction implies that reduction of Fe occurs. This can be confirmed by using dyes or Pt microelectrodes. No minimum period of reduction is required. Low (< 2) chroma colours and mottles have been replaced in Soil Taxonomy by *redoximorphic features* which are features formed by the reduction, translocation, and oxidation of Fe and Mn compounds. Three major groups of redoximorphic features have been identified: redox concentrations, redox depletions, and reduced matrices. Within the first two groups there are several specific kinds of features that will be discussed. The redox depletions and concentrations have been defined on the basis of micromorphological concepts, but features were named using terminology of the new Soil Survey Manual. Description of redoximorphic features can be done with the naked eye or a hand lens, and should emphasize the relationship of the features to macropores. The descriptions should identify where oxidation and reduction occur in the soil horizon, and show how water and air move through the horizon during both infiltration and drainage. Additional research is needed in order to utilize more fully redoximorphic features in defining *aquic conditions*. Ways must be found to identify relict features. The relation of the abundance of features to lengths of saturation and reduction are not well understood and require more work. Models should be developed that describe formation of redoximorphic features on the bases of fundamental physical and chemical processes. Such models should enable us to estimate rates of formation of redoximorphic features and to better understand their genesis.

INTRODUCTION

The aquic soil moisture regime that is used in Soil Taxonomy pertains to soils that are saturated with water and chemically reduced such that the soil water contains no dissolved oxygen (Soil Survey Staff, 1975). At the suborder level of the classification, soils that have an aquic moisture regime are saturated and reduced from the soil surface to a depth of 2 m. If used at the subgroup level, only the lower soil horizons need to be saturated and reduced.

While the aquic moisture regime is defined on the basis of saturation and reduction, the occurrence of these phenomena often cannot be verified before a soil is classified. Instead, soil colours are used to infer that the soils are saturated and reduced at some time during the year, unless the soil has been artificially drained. Generally, low ($\leq$ 2) chroma or grey colours are used as indicators of saturation and reduction, but in some soils hues of 2.5Y or 5Y are used when high chroma mottles are present.

The aquic moisture regime can be applied to all soil orders and it may be the most widely used moisture regime of those defined in Soil Taxonomy. Since it was originally defined, it has become clear that the aquic moisture regime is not precisely defined and an unequivocal identification of it in the field has been difficult (Bouma, 1983; Wilding and Rehage, 1985). The International Committee on Aquic Moisture Regime (ICOMAQ) has been examining the limitations of the aquic moisture regime since 1978 and has suggested improvements. Its final recommendations were made in 1991 and took effect in 1992 (Bouma, 1991; Soil Survey Staff, 1992). The modified aquic moisture regime has been named *aquic conditions*.

The purpose of this paper is: 1) to describe the requirements for aquic conditions; 2) to discuss the micromorphological aspects of aquic conditions and 3) to identify topics where more micromorphological research is needed to further improve the identification of soils with aquic conditions.

This paper will discuss the classification of hydromorphic mineral soils. Organic soils will not be considered because aquic conditions do not have to be confirmed for the Histosols as defined in Soil Taxonomy. Excellent reviews of the micromorphology of organic soils are available elsewhere (Fox, 1985; Bouma *et al.*, 1990). The term aquic conditions has a well-defined meaning which pertains only to Soil Taxonomy. It is not a general term for hydromorphic soils. Recent comprehensive reviews on the micromorphology of hydromorphic soils are also available (Stoops and Eswaran, 1985; Bouma *et al.*, 1990).

AQUIC CONDITIONS

Aquic conditions must be identified by determining three separate properties for every soil: duration and depth of saturation; occurrence of Fe reduction and presence redoximorphic features. These three properties must be measured to make certain that saturation and reduction do occur in a specific soil series at some locations. Once duration of saturation and occurrence of reduction have been determined at one site, the data can be extrapolated to other soils of the same series using redoximorphic features. This approach calibrates the redoximorphic features of each soil series to specific periods of saturation in particular and ensures that the features are not relict.

Saturation

A horizon is saturated when the soil water pressure is zero or positive (greater than atmospheric pressure). Water will run into an unlined auger hole when a horizon is saturated, but piezometers or tensiometers should be used to evaluate saturation.

Three different types or patterns of saturation were defined:
1. Endosaturation - occurs in soils having permanent water tables. The soil is saturated in all horizons that lie between the upper boundary of saturation and a depth of 2 m.
2. Episaturation - occurs in soils having perched water tables. The soil is saturated in one or more horizons that overlie one or more unsaturated horizons within a depth of 2 m from the surface.
3. Anthric saturation - occurs in rice paddies. This is similar to episaturation with the difference being that saturation is produced by controlled flooding for wetland rice.

Saturation can occur at any time during the year, not just during the growing season or when soil temperatures exceed biological zero.

Reduction

The definition of aquic conditions requires the reduction of Fe rather than simply oxygen. Any method that shows Fe (II) is present is considered suitable for assessing reduction. Reduction can be measured using Pt microelectrodes. Critical oxidation-reduction potentials (Eh values) needed for Fe reduction are pH dependent and should be determined from an Eh-pH diagram (Collins and Buol, 1970). Two dyes, potassium ferricyanide and α α' dipyridyl, can also be used in the field to confirm that Fe reduction has occurred (Childs, 1981). No minimum time period for reduction is required. Reduction must only be confirmed once, using either dyes or electrodes.

Redoximorphic Features

"Mottles and low chroma colours" will be replaced in Soil Taxonomy by *redoximorphic features* which are formed by the reduction, translocation and oxidation of Fe and Mn oxides. "Mottles" technically could consist of carbonates or organic stains which are not indicative of saturation and reduction.

Redoximorphic features were defined for the most part using micromorphological concepts. Most of the features are pedofeatures that were formed by either the concentration or removal of Fe or Mn oxides. The features are visible to the naked eye or using a hand lens such that they can be described by soil mappers in the field. It was assumed that thin sections would not be used routinely to identify or describe redoximorphic features, and that microscopic examination of features was also not practical.

New terms were invented to name redoximorphic features. The new terms conform to those already in use in the new Soil Survey Manual (Soil Survey Staff, 1993). They are also simple and descriptive so that they can be easily remembered by soil mappers who have widely different backgrounds and training. A new terminology also had to be used because some pedofeatures (*e.g.* coatings and hypocoatings of Bullock *et al.*, 1985; cutans and subcutans of Brewer, 1976; or orthocutans and metacutans of Brewer and Sleeman, 1988) were simply considered as one kind of feature (pore linings) if they could not be distinguished except by microscopic examination.

Categories of Redoximorphic Features

Three major categories of redoximorphic features were defined: 1) redox concentrations, 2) redox depletions and 3) reduced matrices. The first two categories consist of pedofeatures that micromorphologists will recognize, while the third category has no micromorphological counterpart.

1. *Redox Concentrations* are zones of apparent concentration of Fe-Mn oxides. Three types of redox concentrations are recognized:

    a) *Nodules and concretions* (Fig. 1A) are firm irregularly-shaped bodies with diffuse boundaries when formed *in situ*, or with sharp boundaries after transport or pedoturbation. The terms nodules and concretions are considered to be two names for the same feature, because the concentric banding of concretions may not always be visible to the naked eye or when a hand lens is used.

    b) *Masses* (Fig. 1B) are soft bodies within the groundmass whose shape is variable.

    c) *Pore linings* (Fig. 1C) are zones of accumulation along pores which may be either coatings on the pore surface or impregnations of the matrix adjacent to the pore. They include coatings and hypocoatings (cutans and neocutans) because both features can form around aerated macropores. Pore linings do not include quasicoatings (Bullock *et al.*, 1985) which are considered Fe masses.

2. *Redox Depletions* are zones of low ($\leq$ 2) chroma where Fe-Mn oxides alone have been removed, or where both Fe-Mn oxides and clay have been removed. Two basic kinds of redox depletions are recognized:

    a) *Iron depletions* (Fig. 2A) are zones which contain low amounts of Fe and Mn oxides, but have clay contents similar to that of the adjacent matrix. These features have been called albans and neoalbans when they were found around macropores (Veneman *et al.*, 1976). They may also be found within the matrix. When the entire matrix is low in Fe (*i.e.* is an Fe depletion) this can be described as an Fe depleted matrix.

    b) *Clay depletions* (Fig. 2B) are zones which contain low amounts of Fe, Mn and clay. They have also been called "neoskeletans". These are believed to only occur along macropores.

3. *Reduced Matrices* are soil matrices that contain reduced or ferrous Fe. Such matrices may have a low chroma *in situ*, but the hue or chroma will increase when a sample is exposed to air. The change in colour should occur within 30 minutes of a freshly broken surface of a field-moist sample being exposed to air. The change in colour occurs because Fe (II) in the matrix is being oxidized to Fe (III).

Description of Features

Descriptions of redox concentrations and redox depletions should identify type, colour and abundance. Whether the features lie along macropores or within the matrix must also be described. For reduced matrices, the time required for the colour change to occur can be noted.

Exceptions

When nodules or concretions are the only redoximorphic features present, they should be considered relict features which are not representative of current conditions. These features are resistant to decomposition and may be more properly considered as gravels rather than redoximorphic features. Organic stains also should not be considered to be redoximorphic
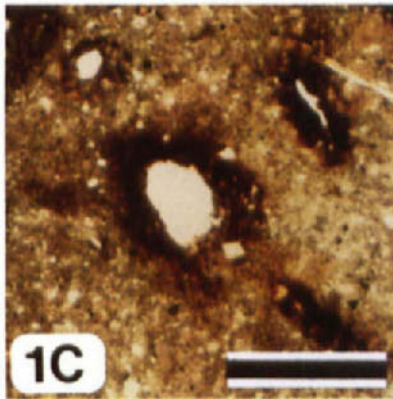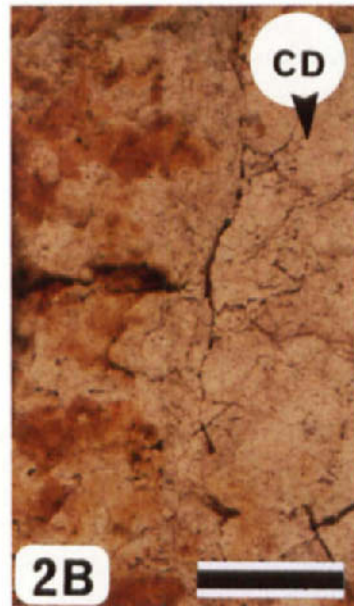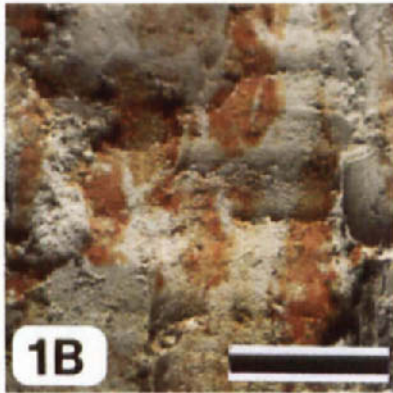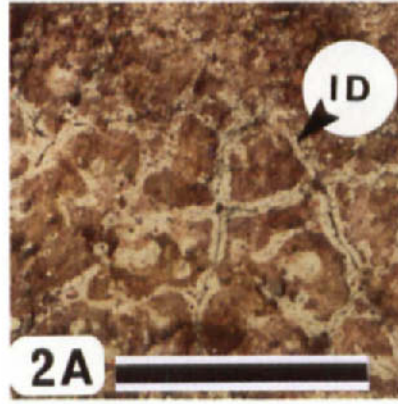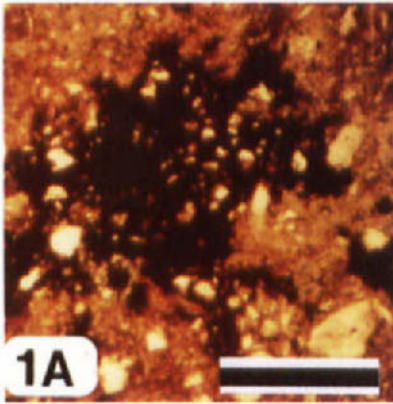
Fig. 1. Examples of redox concentrations: **A**) Fe-Mn nodule seen in thin section (plane light), **B**) Fe masses seen in a pit wall, and **C**) pore linings seen in thin section (plane light). Scale bars represent 2 mm in A, 50 mm in B, and 4 mm in C.

Fig. 2. Examples of redox depletions: **A**) Fe depletions (ID) occur around ped surfaces and root channels in this horizontal section, and **B**) clay depletions (CD) along prismatic ped surfaces. Scale bars represent 150 mm in A, and 50 mm in B.

features. It has been suggested that features having both values and chromas of less than 4 not be considered a redoximorphic feature.

INTERPRETATIONS OF REDOXIMORPHIC FEATURES

During the field testing of the proposals for aquic conditions, it was found to be impossible to define characteristic sets of redoximorphic features that clearly identified endosaturation separately from episaturation (Hudnall *et al.*, 1990; Wilding and Griffin, 1990). Despite reports to the contrary (*e.g.* Blume and Schlichting, 1985; Bouma *et al.*, 1990), the same kinds of features were found to occur with either type of saturation. Part of the reason for this is related to how the different kinds of saturation are defined. For example, perched water tables develop on top of slowly permeable layers when surface water infiltrates, moves downward in the soil, and accumulates on top of the slowly permeable layer. Blume and Schlichting (1985) suggested that in these cases redox depletions will develop around macropores while redox concentrations develop within peds or in the groundmass away from the macropores. When the impermeable layer is within 2 m of the soil surface, the soil will have episaturation by definition. However, if the slowly permeable layer occurs below a depth of 2 m, the soil will have endosaturation by definition. The same pattern of redoximorphic features would be expected in either case because in both instances surface water flows downward along macropores which terminate on top of the slowly permeable layer. Because of such problems, redoximorphic features must be interpreted as indicators of where reduction and oxidation occur within a soil horizon rather than as indicators of the kind of saturation that occurs. Redox depletions generally show where reduction occurs, while redox concentrations show where oxidation occurs within horizons. The relationship of redox depletions to redox concentrations can then be used to indicate how water and air move through the macropores and matrix of a soil horizon.

Such interpretations should be based around our concepts as to how specific features form. The simplest cases occur where macropores are well-defined and stable because features that form around the macropores can increase in size from one year to the next around the same macropore. In cases where macropores are not stable, such as in sandy soils or horizons having much biological activity, the distribution of redoximorphic features may appear to be random with regard to root channels, structural planes and matrix.

Formation of iron and clay depletions

Formation of these two features is similar and the two kinds of redox depletions may occur within the same or adjacent horizons. Field studies of the features indicate that they are best expressed in dense horizons having a low saturated hydraulic conductivity (Daniels *et al.*, 1968; Ransom *et al.*, 1987; Vepraskas and Wilding, 1983a). They are found in the horizons that perch water (Blume and Schlichting, 1985).

Roots growing along a structural crack or channel provide the energy source (organic matter) needed by microbes for Fe-reduction (Fig. 3). When the root dies and the macropore is filled with water, bacteria will consume the root tissue and utilize oxygen in the water if soil temperatures are above biological zero. During this process, Fe (III) in the soil along the channel will be reduced to Fe (II). The dissolved Fe (II) ions may move into the matrix where they can be oxidized (if air has been entrapped) to form a redox concentration which may be a
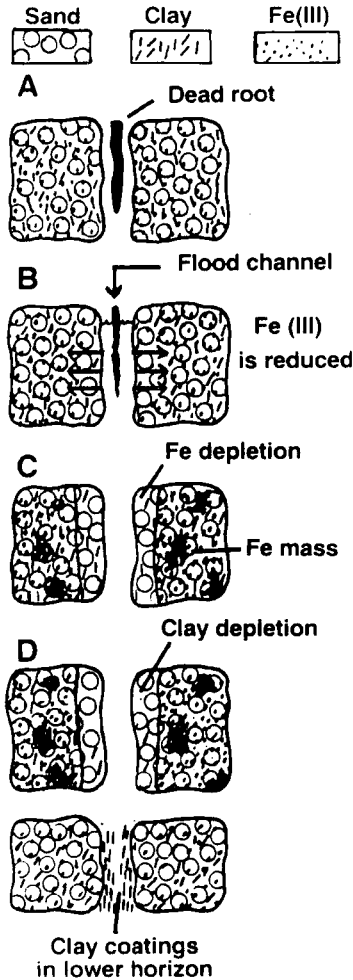
Fig. 3. Schematic illustration showing the formation of redox depletions. The process begins with: **A)** a decomposing root lying in a channel. **B)** When the channel fills with water, Fe in soil along the channel is reduced when the root's decomposition occurs anaerobically. The reduced Fe (II) may diffuse into the soil matrix. An Fe depletion occurs along the channel when enough Fe has been lost to produce a color chroma of 2 or less. **C)** Iron masses form when the Fe (II) in the matrix oxidizes to Fe (III). The loss of Fe makes clay along the channel dispersible, and water moving along the channel may illuviate this clay to a lower horizon. **D)** Clay depletions form where the clay has been removed.

mass of Fe oxides or a nodule. The newly formed bleached layer along the void is a redox depletion, specifically a Fe depletion. The Fe depletion differs from the soil matrix primarily in its lower content of Fe and Mn.

Removal of Fe oxides may make the clay in the Fe depletion dispersible. During movement of water along the macropore, clay may be removed and eluviated to a lower horizon (Wilding and Rehage, 1985). The feature which has had its clay removed is a clay depletion. Often, grey clay coatings occur in horizons below those with clay depletions.

Because of the need for an energy source to enhance reduction, it appears that Fe depletions and clay depletions will form along macropores such as root channels and ped surfaces where roots grow. Iron depletions may also form within the soil matrix if carbon-rich waters flow through the soil matrix and produce reducing conditions there.

Formation of redox concentrations

Pore linings
These occur along ped surfaces and root channels (Fig. 4). Pore linings form when reduced Fe and Mn ions diffuse toward aerated macropores and then oxidize and precipitate adjacent to the macropores. They are also found along or on the roots of plants such as rice, that can a lower Eh value than will Mn (Collins and Buol, 1970). Therefore, pore linings may appear to consist of clearly separated Mn oxides and Fe oxides.aerate their roots and adjacent soil surfaces in saturated soils (Fisher and Stone, 1991). If both Fe and Mn are in solution, the Fe tends to oxidize and precipitate first because it will oxidize at a lower Eh value than will Mn (Collins and Buol, 1970). Therefore, pore linings may appear to consist of clearly separated Mn oxides and Fe oxides.

Masses, nodules, and concretions
Formation of these features *in situ* is not well understood. The features are similar and differences between masses and nodules or concretions may depend on how fast air penetrates into a reduced horizon. It has been proposed that when a horizon that is saturated and reduced drains, masses will form when the air penetrates into the horizon quickly (Blume and Schlichting, 1985). Nodules and concretions may form when air penetrates slowly into the wet matrix containing Fe (II) and Mn (II).

Interpretations for water movement

Movement of water within horizons, at the scale of peds and macropores, can sometimes be traced or inferred from the relationship between redox depletions and redox concentrations. In general, it can be assumed that water has moved from redox depletions into or toward redox concentrations. Inferring movements between or among horizons may be difficult except where the same features extend across horizons.

Inferring the movements is simplest when redoximorphic features show a consistent relationship to the soil structure and macropores. For redoximorphic features to have a consistent relationship to macropores (*e.g.* redox depletions occur only along ped surfaces) the macropores must be stable and spaced widely enough that redoximorphic features along adjacent macropores do not overlap. Basic principles will be illustrated with four examples. In all cases, the redoximorphic features are assumed to be contemporary.

Example 1: Redox depletions occur around macropores, and redox concentrations occur within the matrix (Fig. 2A).
This arrangement of redoximorphic features indicates that water infiltrates the horizon along macropores and reducing conditions develop within the macropores. Air can be entrapped within the matrix, in part because water-filled macropores surround an air-filled matrix.

As noted earlier, this morphology occurs in soils with perched water tables, and is found within and above the slowly permeable horizon that is perching water. Thus, this morphology pattern can occur in dense horizons whose matrix has a low saturated hydraulic conductivity. The morphology is found with either episaturation or endosaturation depending on whether the perching layer lies above or below a depth of 2 m. Detailed descriptions have been given by Fanning and Fanning (1989, mottling model II), Vepraskas and Wilding (1983a), and Blume and Schlichting (1985) among others.
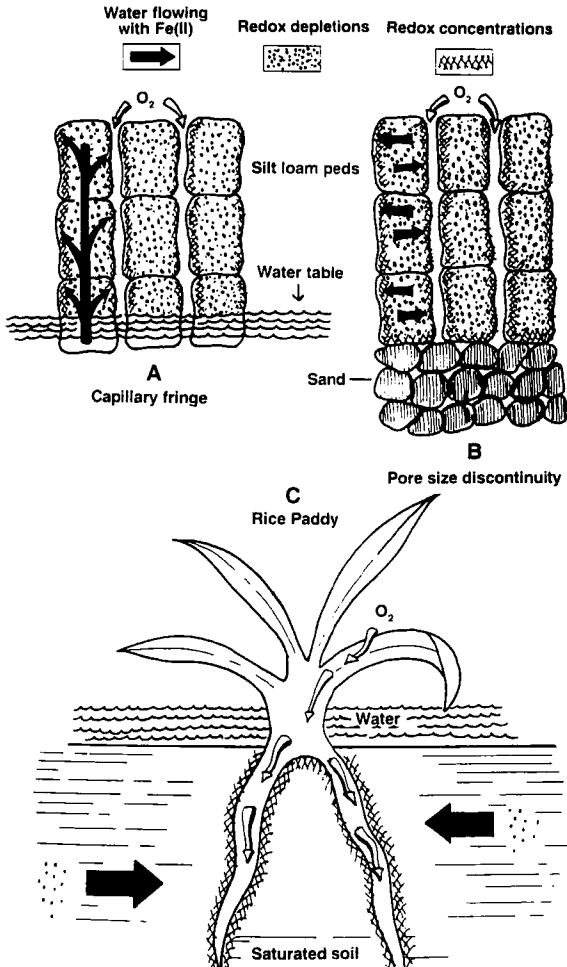
Fig. 4. Different hydrologic settings that create a pattern of redoximorphic features where redox concentrations occur around macropores and redox depletions occur within the matrix: A) capillary fringe of a water table; B) stratified sediments having different pore sizes and C) saturated soils having plants with aerated roots.

Example 2: Redox concentrations occur around macropores, redox depletions occur within matrix.

This arrangement of redoximorphic features indicates that the matrix is wet for periods long enough for reducing conditions to be maintained within the matrix. The macropores are aerated while the matrix is reduced. The movement of water and reduced substances is from the matrix toward the macropores. Horizons with this morphology may be unsaturated or saturated. Unsaturated horizons are found in at least two cases (Figs 4A and B). The horizon can be saturated and still have aerated macropores if plants grow in the saturated horizon and transport air to their roots (Fig. 4C). This morphology has been found with episaturation, endosaturation and anthric saturation.

Example 3: Redox depletions and concentrations have no consistent relationship to macropores.

This example can be found in sands or materials with small aggregates where macropores such as channels or planes are either not stable or are relatively small and closely spaced such

that water and air movement into the horizon does not follow the same macropores after each infiltration event. Water and air may also move through both macropores and matrix. This pattern of features is difficult to interpret except to say that reduction and oxidation occur at different locations throughout the horizon over time. This example may occur with either episaturation or endosaturation.

Example 4: Redoximorphic features have a distribution that combines two of the three examples.

The above examples are idealized versions of well-recognized morphological patterns. Soils can have one horizon with one type of pattern of features that is overlain or underlain by a horizon containing another type. This has to be expected and, therefore, it is important to describe the features individually and not try to expect "sets" of features to occur throughout the soil.

RESEARCH NEEDS

Relationships of the abundance of features to lengths of saturation and reduction

Redoximorphic features form by reduction and oxidation of Fe and Mn. Therefore, the abundance of redox depletions for example, is generally related to how long a soil is reduced (Moorman and van der Wetering, 1985). Feature abundance is **not** directly related to how long a soil horizon is saturated (Vepraskas and Wilding, 1983a). Vepraskas and Guertal (1992) compared the abundance of clay depletions found in five different soils to periods of saturation and reduction. These redoximorphic features were selected because they were clearly identified in each study and their abundance was measured. Data came from different investigators, but in general the abundance of clay depletions ranged from 18 to 79% (by weight) for the different soils. All horizons were found to be saturated for up to 6 months during some years. During "dry" years they were saturated for 3 months or less. Clearly, the length of time a horizon was saturated could not be predicted by measuring the abundance of redox depletions along macropores. It was noted, however, that in the horizon with the fewest clay depletions (18%) the oxidation-reduction potential measurements (Eh values) showed Fe reduction was occurring for less than 1 month during the year of measurement, while the horizon with the most clay depletions was reduced for up to 4 months of the year. The data were not extensive nor complete across broad soil regions, but they do suggest that the abundance of redox depletions will be more closely related to how long soils are reduced rather than how long they are saturated.

It has also been found that in some landscapes horizons can be reduced without being saturated (Vepraskas and Wilding, 1983b). Alternatively, other landscapes have been found where soils may be saturated and not reduced (Daniels and Buol, 1992; Griffin *et al.*, 1992). More work needs to be done showing how the abundance of redox depletions is related to periods of saturation and Fe reduction. Studies should consider different landscape positions, because it appears different relationships will be found at different positions.

Relict redoximorphic features

A major problem that remains unsolved is how to identify relict redoximorphic features. Whenever redoximorphic features are described for determining aquic conditions it is assumed

that the features represent current conditions of saturation and Fe reduction. Unfortunately, there is no known way to ensure that the features being described represent contemporary conditions unless saturation and reduction have been determined to occur.

Micromorphologists must determine if it is possible to identify relict redoximorphic features using simple techniques that can be used in the field by soil scientists. Work on this topic indicates that several feature characteristics show promise for determining whether features are relict or contemporary:

1. Feature boundary characteristics

Fe-Mn nodules and concretions that are actively forming *in situ* probably have irregular surface outlines and gradual or diffuse boundaries with the soil matrix. In some cases these diffuse boundaries may be described as haloes or glaebular haloes (Bullock *et al.*, 1985; Brewer and Sleeman, 1988). Nodules or concretions that are not forming currently tend to have smoother more rounded outlines, sharp boundaries with the matrix, and may show many grains protruding from the surface. Such nodules may be dissolving, particularly when they occur in eluvial E horizons. Dissolution should smooth the nodule surface, create sharp boundaries, and cause included grains to protrude.

2. Relation to macropores

Some features only form along macropores. For example, clay depletions have been described as forming along stable macropores through which roots repeatedly grow. Clay depletions that represent current conditions must occur along macropores, and must not be overlain by Fe-rich clay coatings which indicate that Fe is not being stripped from around the macropore any longer (Rehage, 1985; Vepraskas and Guertal, 1992).

3. Feature colour

Redox concentrations generally consist of the Fe minerals goethite, lepidocrocite, ferrihydrite or jarosite. These Fe minerals can form through oxidation of Fe (II) (Schwertmann and Taylor, 1989). Redox concentrations should not consist of hematite. Hematite has been associated with hot, dry climates where periodic saturation and reduction have not occurred recently (Schwertmann and Taylor, 1989). Because each type of Fe oxide mineral has a characteristic range of hues, the colours of features might be used to identify those that could be contemporary from those that are probably relict. Examples of diagnostic hues, values, and chromas are given in Table 1, and were developed by personal communication with Dr. R. W. Fitzpatrick.

4. Skeleton grain inclusion

A micromorphic aid to determining whether a redox concentration has formed in place is to determine whether the size, shape, mineralogy and abundance of occluded skeleton grains is similar to that of the host matrix. If not, then it is probable that the concretion or nodule is allogenic rather than authigenic. Further, evidence of transport of a concretion from external soil or geological environments may be present in the form of beveled or truncated zones of the concretion (Wilding *et al.*, 1983). In this case the growth pattern will be continuous over part of the concretion but will be abruptly interrupted over another portion of it.

Table 1.
Colour characteristics of relict and contemporary redox concentrations (R.W. Fitzpatrick, personal communication).

Fe Mineral	Hue
Relict Redox Concentrations	
Hematite	10R, 5R, 2.5YR
Contemporary Redox Concentrations	
Ferrihydrite	5YR
Lepidocrocite	7.5YR
Goethite	7.5YR, 10YR
Jarosite	2.5Y

Rates of feature formation

As noted earlier, the mechanisms by which most redoximorphic features form is relatively straightforward. Vepraskas and Bouma (1976) reproduced some mechanisms in laboratory experiments to show quickly how different kinds of features form. A reasonable next step is to begin to develop simple mathematical models to help understand how fast features form in the field and to identify the most important variables that govern feature formation. Vepraskas and Guertal (1992) proposed a simple model for the formation of an Fe depletion along a root channel. Their results showed that the Fe loss from the depletion would most likely occur by diffusion rather than mass flow. The time required to form an Fe depletion that was 2 mm thick varied from < 1 year to more than 100 years depending upon how long reducing conditions occurred within the channel and how much Fe was in solution each day. These results are encouraging, but much more work needs to be done. Rates of formation of redoximorphic features will be influenced by how fast Fe oxide minerals can be dissolved by reduction reactions, and how fast Fe (II) can be transported through the soil and oxidized. Factors affecting the dynamics of reduction reactions include the specific types of Fe minerals present in the soil parent material, the amount of Al substitution in the Fe minerals, crystal size and surface area, and the amount and kind of organic material present (Wilding and Rehage, 1985). The dynamics of some of these reactions have been quantified by Ahmad and Nye (1990) and Kirk *et al.* (1990).

Redoximorphic features found under anthric saturation

Aquic conditions include anthric saturation which is found under controlled flooding for rice production. The redoximorphic features that have been discussed were not tested for rice paddies. While there is no reason to expect different kinds of features will be found under anthric saturation than have been identified for endosaturation and episaturation, this should be confirmed.

CONCLUSION

Micromorphology has made a large contribution to the development of the definition of aquic conditions. Most of the newly defined redoximorphic features have been studied intensively by micromorphologists. All indications are that these features are going to be quickly adopted by field soil scientists for immediate use. This again confirms that micromorphological concepts can be widely used at the macroscopic level, particularly where simplified terms are substituted for the standard micromorphological terms.

While micromorphologists can be proud of this contribution, more work needs to be done. There is presently no reliable way to identify relict redoximorphic features. Our understanding of how Fe masses, nodules, and concretions form is sketchy at best. Probably most important, the relationship of the abundance of redoximorphic features to the specific lengths of time horizons are saturated and reduced is not known for different landscapes or landscape positions. Micromorphologists are well-positioned to address these problems. To do so, they must recognize that quantitative data are needed and that the conditions under which features form must be documented. Description of features are useful only if feature abundance and the length of time horizons are saturated and reduced are known.

REFERENCES

Ahmad, A.R. and Nye, P.H., 1990. Coupled diffusion and oxidation of ferrous iron in soils. I. Kinetics of oxygenation of ferrous iron in soil suspension. J. Soil Sci., 41: 395-409.

Blume, H.P. and Schlichting, E., 1985. Morphology of wetland soils. In: S.J. Banta (Editor), Wetland Soils: Characterization, Classification, and Utilization. Proc. of a Workshop held March 26 to April 5, 1984. Int. Rice Res. Inst., Los Baños, Philippines, pp. 161-176.

Bouma, J., 1983. Hydrology and soil genesis of soils with aquic moisture regimes. In: L.P. Wilding, N.E. Smeck and G.F. Hall (Editors), Pedogenesis and Soil Taxonomy. I. Concepts and Interpretations. Developments in Soil Science 11A, Elsevier, Amsterdam, pp. 253-281.

Bouma, J., 1991. Final report of the International Committee for the Classification and Management of Wet Soils. ICOMAQ Circular 11, March 15, 1991. Agric. Univ., Wageningen, The Netherlands.

Bouma, J., Fox, C.A. and Miedema, R., 1990. Micromorphology of hydromorphic soils: applications for soil genesis and land evaluation. In: L.A. Douglas (Editor), Soil Micromorphology: A Basic and Applied Science. Proc. VIII Int. Working Meeting on Soil Micromorphology, San Antonio, Texas, July 1988. Developments in Soil Science 19, Elsevier, Amsterdam, pp. 257-278.

Brewer, R., 1976. Fabric and Mineral Analysis of Soils. Krieger, Huntington, New York 482 pp.

Brewer, R. and Sleeman, J.R., 1988. Soil Structure and Fabric. CSIRO (Australia) Division of Soils, Adelaide, 173 pp.

Bullock, P., Federoff, N., Jongerius, A., Stoops, G. and Tursina, T., 1985. Handbook for Soil Thin Section Description. Waine Research Publications, Wolverhampton, U.K., 152 pp.

Childs, C.W., 1981. Field test for ferrous iron and ferric-organic complexes (on exchange sites or in water-soluble forms) in soils. Aust. J. Soil Res., 19: 175-180.

Collins, J.F. and Buol, S.W., 1970. Effects of fluctuations in the Eh-pH environment on iron and/or manganese equilibria. Soil Sci., 110:111-118.

Daniels, R.B., and Buol, S.W., 1992. Water table dynamics and significance to soil genesis. In: J.M. Kimble (Editor), Proc. Eighth Int. Soil correlation Meeting (VIII ISCOM): Characterization, Classification, and Utilization of Wet Soils. USDA, Soil Cons. Serv., Nat. Soil Survey Center, Lincoln, Nebraska, pp. 66-74.

Daniels, R.B., Gamble, E.E. and Bartelli, L.J., 1968. Eluvial bodies in B horizons for some Ultisols. Soil Sci., 106: 200-206.

Fanning, D.S. and Fanning, M.C.B., 1989. Soil morphology, genesis and classification. J. Wiley and Sons, New York, N.Y., 395 pp.

Fisher, H.M. and Stone, E.L., 1991. Iron oxidation at the surfaces of slash pine roots from saturated soils. Soil Sci. Soc. Am. J., 55: 1123-1129.

Fox, C.A., 1985. Micromorphological characterization of Histosols. In: L.A. Douglas and M.L. Thompson (Editors), Soil Micromorphology and Soil Classification. Soil Sci. Soc. Am., Spec. Publ. No. 15, Madison, WI, USA, pp. 85-104.

Griffin, R.W., Wilding, L.P. and Dress, L.R., 1992. Relating morphological properties to wetness conditions in the Gulf Coast Prairie of Texas. In: J.M. Kimble (Editor), Proc. Eighth Int. Soil Correlation Meeting (VIII ISCOM): Characterization, Classification and Utilization of Wet Soils. USDA Soil Cons. Serv., Nat. Soil Survey Center, Lincoln, Nebraska, pp. 136-147.

Hudnall, W.H., Szogi. A., Touchet, B.A., Diagle, J., Edwards, J.P. and Lynn, W.C., 1990. VIII Int. Soil Correlation Meeting, Classification and Management of Wet Soils. Guidebook for Louisiana. Louisiana State Univ., Baton Rouge, 195 pp.

Kirk, G.J.D., Ahmad, A.R. and Nye, P.H., 1990. Coupled diffusion and oxidation of ferrous iron in soils. II. A model of the diffusion and reaction of O_2, Fe^{2+}, H^+, and HCO^- in soils and a sensitivity analysis of the model. J. Soil Sci., 41: 411-431.

Moormann, F.R. and van de Wetering, H.T.J., 1985. Problems in characterizing wetland soils. In: S.J. Banta (Editor), Wetland Soils: Characterization, Classification, and Utilization. Proc. of a Workshop held March 26 to April 5, 1984. Int. Rice Res. Inst., Los Baños, Philippines, pp. 53-68.

Ransom, M.D., Smeck, N.E., and Bigham, J.M., 1987. Micro-morphology of seasonally wet soils on the Illinoisan till plain, U.S.A. Geoderma, 40: 83-100.

Rehage, J.A., 1985. Hydrology and Genesis of Clay Pans Soils in East Central Texas. Ph.D. Dissertation. Texas A & M Univ., College Station.

Schwertmann, U. and Taylor, R.M., 1989. Iron oxides. In: J.B. Dixon and S.B. Weed (Editors), Minerals in Soil Environments, Second Ed., Soil Sci. Soc. Am., Madison, Wisconsin, pp. 379-438.

Soil Survey Staff, 1975. Soil Taxonomy: A Basic System of Soil Classification for Making and Interpreting Soil Surveys. U.S. Dep. Agric. Hndb. No. 436. U.S. Gov. Printing Office, Washington, D.C., 754 pp.

Soil Survey Staff, 1992. Keys to Soil Taxonomy, fifth edition. SMSS Tech. Monogr. No. 19, Pocahontas Press, Blacksburg, Virginia, 541 pp.

Soil Survey Staff. Soil Survey Manual. U.S. Gov. Printing Office, Washington, D.C. (In press).

Stoops, G. and Eswaran, H., 1985. Morphological characteristics of wet soils. In: S.J. Banta (Editor), Wetland Soils: Characterization, Classification, and Utilization. Proc. of a Workshop held March 26 to April 5, 1984. Int. Rice Res. Inst., Los Baños, Philippines, pp. 177-190.

Veneman, P.L.M., Vepraskas, M.J. and Bouma, J., 1976. The physical significance of soil mottling in a Wisconsin toposequence. Geoderma, 15: 103-118.

Vepraskas, M.J. and Bouma, J., 1976. Model experiments on mottle formation simulating field conditions. Geoderma, 15: 217-230.

Vepraskas, M.J. and Guertal, W.R., 1992. Morphological indicators of soil wetness. In: J.M. Kimble (Editor), Proc. Eighth Int. Soil Correlation Meeting (VIII ISCOM): Characterization, Classification, and Utilization of Wet Soils. USDA, Soil Conservation Service, National Soil Survey Center, Lincoln, Nebraska, pp. 307-312.

Vepraskas, M.J. and Wilding, L.P., 1983a. Albic neoskeletans in argillic horizons as indices of seasonal saturation and iron reduction. Soil Sci. Soc. Am. J., 47: 1202-1208.

Vepraskas, M.J. and Wilding, L.P., 1983b. Aquic moisture regimes in soils with and without low chroma colors. Soil Sci. Soc. Am. J., 47: 280-285.

Wilding, L.P. and Griffin, R.W., 1990. VIII Intern. Soil Correlation Meeting, Classification and Management of Wet Soils. Guidebook for Texas. Texas A & M Univ., College Station, 269 pp.

Wilding, L.P., Milford, M.H. and Vepraskas, M.J., 1983. Micromorphology of deeply weathered soils in the Texas coastal plains. In: P. Bullock and C.P. Murphy (Editors), Soil Micromorphology. Vol. 2: Soil Genesis. Proc. VI Int. Working Meeting on Soil Micromorphology, London, August 1981. A.B. Academic Publishers, Berkhamsted, Herts., U.K., pp. 567-574.

Wilding, L.P. and Rehage, J.A., 1985. Pedogenesis of soils with aquic moisture regimes. In: S.J. Banta (Editor), Wetland Soils: Characterization, Classification, and Utilization. Proc. of a Workshop held March 26 to April 5, 1984. Int. Rice Res. Inst., Los Baños, Philippines, pp. 139-157.

This Page Intentionally Left Blank

Saprolite influence on formation of well-drained and hydromorphic horizons in an acid soil system as determined by structural analysis

P. Curmi[1], Widiatmaka[2], J. Pellerin[3] and A. Ruellan[4]

[1]*INRA-ENSA Laboratoire de Science du Sol, 65 rue de Saint Brieuc, 35042 Rennes Cedex, France*
[2]*Bogor Agricultural University, Dept. of Soil Science, 1 Jl. Pajajaran, Bogor 16144, Indonesia*
[3]*CNRS, Centre de Géomorphologie, rue des Tilleuls, 14000 Caen, France*
[4]*CNEARC, 1101 Av. Agropolis B.P. 5098, 34033 Montpellier Cedex 1, France*

ABSTRACT

Curmi, P., Widiatmaka, Pellerin, J. and A. Ruellan, A., 1994. Saprolite influence on formation of well-drained and hydromorphic horizons in an acid soil system as determined by structural analysis. In: A.J. Ringrose-Voase and G.S. Humphreys (Editors), Soil Micromorphology: Studies in Management and Genesis, Proc. IX Int. Working Meeting on Soil Micromorphology, Townsville, Australia, July 1992. Developments in Soil Science 22, Elsevier, Amsterdam, pp. 133-140.

A landscape unit was studied on both macroscopic and microscopic scales - emphazising the 3-D relationships between horizons - to understand soil distribution and their genetic and functional relationship.

On a granitic saprolite with a silty loam cover in the Armorican Massif (France), associations of Dystrochrepts, Hapludalfs and Glossaqualfs had developed. Structural analysis of a landscape unit showed these soils form two types of pedological system. In this paper, only systems of one type are studied. They occur upslope and along the slope and associate well drained and hydromorphic soils.

In these systems, the following features occur: 1) Thickness of the loamy layer varies independently of topography. 2) Clay migration takes place in this loamy layer. When the layer is thin, clay accumulation forms banded horizons a few centimetres thick within the saprolite, whereas, when the layer is thick enough, clay accumulation develops a textural B horizon inside it. 3) Granite saprolite has sandy and clayey facies which are probably of lithological origin and have an inverted inclination compared to the topographic slope. 4) The distribution of clayey facies of the saprolite induces development of local perched water tables. 5) Groundwater emergence transforms the upper loamy horizons from their base by hydromorphic and degradation processes.

INTRODUCTION

In the Armorican Massif (France), associations of soils referred to as "Alocrisols", "Luvisols" and "Luvisols-Redoxisols Degrades", according to the Pedological Reference Base (AFES., 1992) (Dystrochrepts, Hapludalfs and Glossaqualfs, Soil Survey Staff, 1975), are commonly observed in the loamy layer on granite, schist or sandstone (Curmi, 1979a; Roussel,

1980, 1983; Al Siddik, 1983). A landscape unit was studied to understand the distribution of soils and their genetic and functional relationships - emphazising geometric relations between horizons - on both macroscopic and microscopic levels.

MATERIAL AND METHODS

The "la Touche" site, near Quintin (Côtes d'Armor, France) is on a granitic saprolite with a silt loam cover. Mean annual precipitation is about 1000 mm with a regular distribution and mean annual temperature is 11°C. This site was selected after a 1:25000 soil survey of the whole watershed (600 ha) (Buson, 1982), because of the occurrence of hydromorphic soils spotted along the slope. A 3 ha area was studied which extended from a plateau, down a 6° convex slope, where hydromorphic soils appear locally, to a flat narrow thalweg. In this area, 14 pits were dug along 2 toposequences and 150 auger holes were made. Distribution of these punctual observations (Fig. 1c) was not done following a regular or stochastic grid but focused on the boundaries between horizons to better analyse their geometry (Boulet *et al.*, 1982, 1989; Ruellan *et al.*, 1989).

Bulk samples were collected from the main horizons for physicochemical and mineralogical analysis. A Siemens diffractometer was used to determine the mineralogy of the clay fraction (prepared according to Robert and Tessier, 1974). Large thin sections (160 x 90 mm) impregnated with polyester resin after dehydration by acetone exchange (Delaye, 1984) were performed on each horizon. Thin section descriptions were made using Bullock *et al.* (1985) terminology.

RESULTS AND DISCUSSION

Structural analysis of the landscape unit shows these soils may be distinguished according to two types of pedological systems (Fig. 1a). The first type includes upslope and slope systems and consists of both well drained and hydromorphic soils. The second type is a colluvio-alluvial system which occurs downslope and is characterised by hydromorphic soils and locally by histic horizons. In this paper, only systems of the first type are considered.

Systems of the first type consist of two domains: a well drained domain and a hydromorphic and degraded one (Fig. 1a). Twelve horizons were identified and labelled according to the Pedological Reference Base (AFES, 1992). The symbols used were the following: L (from French Labouré) for ploughed horizons, S (from Structural) for cambic horizons, E for eluvial horizons, BT for illuvial horizons, FEm (from pétro-ferrique) for horizons cemented by iron, C for saprolite, -al (from aluminique) for dystric properties, -a for albic properties, -t for evidences of clay accumulation, -d (from dégradé) for bleaching and tonguing features, -g for pseudogleyic features, -G for gleyic features and -o for oxidized macropores in gleys. Their respective distribution in relation to topography is established. Analytical data and mineralogy of the clay fraction for most horizons are given in Table 1.

The well drained domain

In this domain, the granitic saprolite (Ct) is sandy. Over the saprolite, the silty horizons of the Alocrisol and the Luvisol occur and consist of a yellowish brown microgranular Sal horizon (Fig. 2d), a yellowish brown polyhedral E horizon and a reddish brown BT horizon.
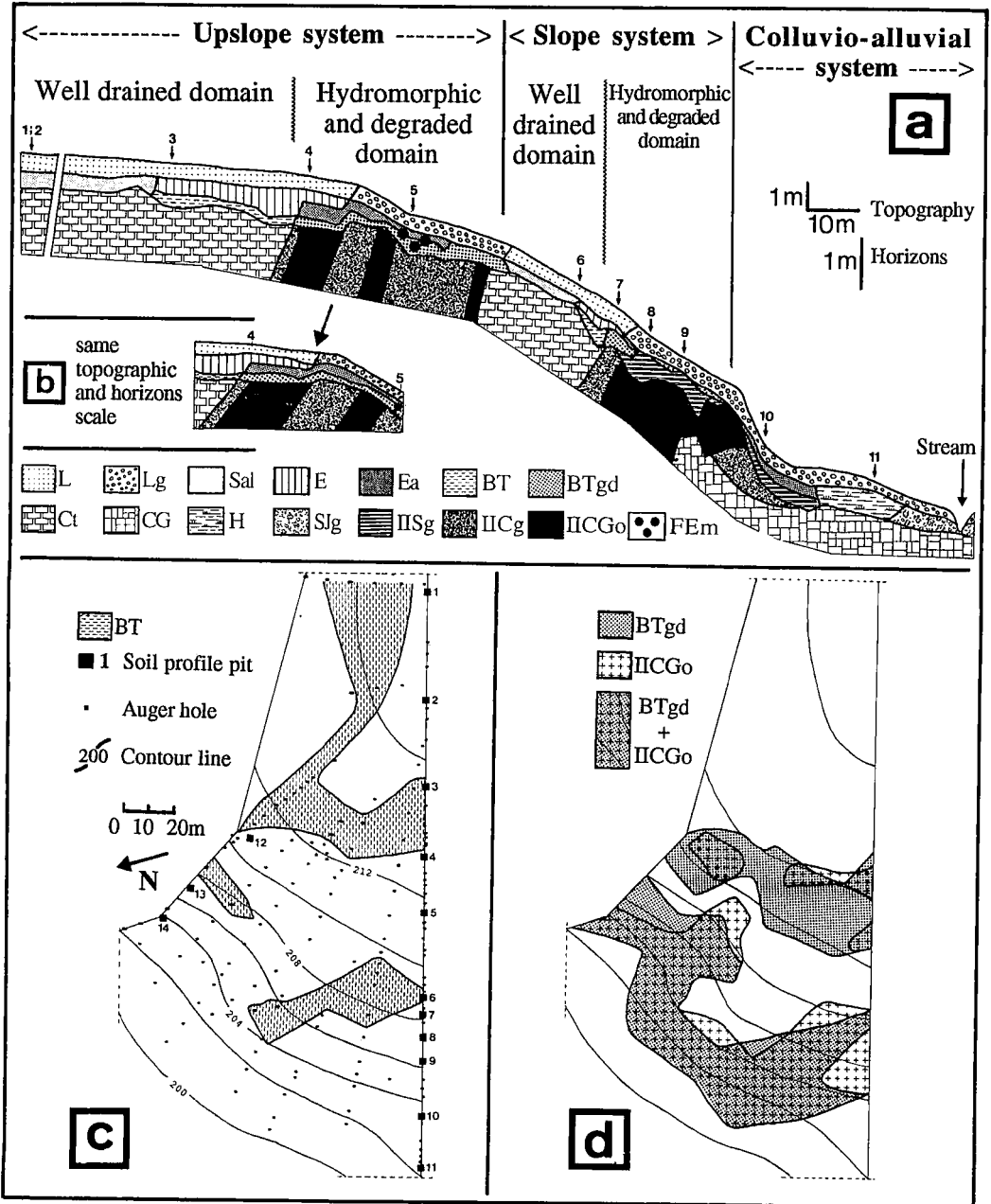
Fig. 1. Vertical and horizontal representation of the soil cover: **a)** vertical cross section; **b)** relative inclination of horizons in relation to topographic slope; **c)** location of profile pits and auger holes, and extension of BT horizon in relation to topography; **d)** map of relative extension of IICGo in the top 1.2 m and Btgd horizons.

Table 1
Physico-chemical data and clay fraction mineralogy of the main horizons

Horizon	Particle size analysis %			pH	CEC	Base sat.	Clay fraction mineralogy[*]							
	clay $\langle 2\mu m$	silt 2-50μm	sand 50-2000 μm	H$_2$0	meq/ 100g soil	%	Q	K	M	VM	V1	V2	S	C
Sal	7.9	57.4	34.7	5.8	7.1	39	4	2	3	2	-	2	-	1
E	8.2	77.0	14.8	6.1	3.5	59								
BT	16.4	69.6	14.0	5.1	7.6	54	3	4	3	2	1	2	-	-
Ct	1.2	6.3	92.5	5.0	6.8	10	2	4	3	1	2	2	-	-
Ea	5.1	51.6	43.3	6.2	5.2	67	4	2	2	1	-	3	-	-
BTgd	13.1	66.3	20.6	5.7	4.7	72	4	3	2	2	1	3	-	-
IISg	24.5	30.2	45.3	5.1	9.4	82	3	4	2	2	-	-	3	-
IICGo	25.6	32.4	42.0	4.1	5.9	39	2	4	1	1	-	1	2	-

[*]*Mineral codes:* Q, quartz; K, kaolinite; M, mica; VM, interstratified mica/vermiculite; V1, s.s. vermiculite; V2, hydroxyaluminous vermiculite; S, smectite; C, chlorite. *Abundance (X-Ray):* 1, rare, to 4, very abundant.

Thickness of the loamy layer and BT occurrence

A survey of the area shows that the BT horizon occurs when the thickness of the loamy layer is more than 0.5 m (Fig. 1a, positions 3 and 6) and that the thickness of the loamy layer varies independently of topography (Fig. 1c).

Clay migration

Coatings of illuvial clay developed in subhorizontal bands (several centimeters thick) in the upper part of the Ct saprolite (Fig. 2a). These coatings occurred within the well drained domain even under Alocrisols (Curmi, 1979a and b; Aurousseau *et al.*, 1985).

Therefore, clay migration takes place in the whole well drained domain. When the loamy layer is thin, clay accumulation forms subhorizontal bands within the Ct saprolite whereas a textural BT horizon (Fig. 2c) develops inside the loamy layer when it is thick enough. The morphological expression of the clay migration appeared to be lithodependent.

Transition between the two domains

Distribution of saprolite and upper horizons

Granitic saprolite shows different sandy and clayey facies which are probably of lithological origin. In the clayey saprolite, a IICGo horizon has a c/f ratio of 40/60 with a predominant cross striated weathering micromass (Fig. 2b). The boundary between these sandy and clayey facies has an inverted inclination compared to the topographic slope (Fig. 1b). Moreover, in the above silty horizons, hydromorphic and degradation features appear successively, emphazised by the development of a BTgd horizon at the base of the BT and then of an Ea horizon at the base of the E horizon.

Relative distribution of clayey saprolite and BTgd horizon

There is a good correlation between the distributions of clayey saprolite, IICGo, in the top 1.2 m of the surface and development of a BTgd horizon in the loamy layer (Fig. 1d). The clayey saprolite extends upslope or along the extension of BTgd horizon.

This distribution suggests that the clayey facies of the saprolite induce development of local perched water tables. Groundwater emergence transforms the upper loamy horizons from their base by hydromorphic and degradation processes.

The hydromorphic and degraded domain

Clay migration and chronology of hydromorphic processes

In brown mottles in the BTgd horizon iron concentrations overlie clay coatings. In grey mottles, there is no secondary accumulation of clay or iron (Fig. 2g). Iron redistribution related to hydromorphism is therefore more recent than clay migration.

Absolute oxide concentrations (Bog ores)

Absolute iron and manganese concentrations occur over limited areas (50 m^2) downslope of the clayey saprolite (IICGo). These oxide concentrations cement Ea (Fig. 2h) and BTgd horizons into FEm horizons. This horizon is called "grison" locally and seems similar to the "bog ores" of the Belgian Campine area (Landuydt, 1990). In addition to greater impregnation and extension of brown and black mottles, fan-like goethite crystals (Fig. 2i) and black manganese coatings line the pores (Curmi *et al.*, 1994). This absolute concentration may be due to groundwater emergence from the gley clayey saprolite (IICGo) which is rich in ferrous iron that precipitates in more oxidizing conditions near the surface.

Development of degradation processes

Grey mottles in the Ea and BTgd horizons have a monic fabric of silt-size quartz with a scarce, pale speckled micromass (Fig. 2e). The transition between brown and grey mottles in BTgd horizon is produced by the decrease in micromass and its bleaching and the break up of clay coating over 50-100 μm (Fig 2f). This suggests that the monic fabric of silt-size quartz results from a relative accumulation of resistant particles. Moreover, loss of the clay fraction is accompanied by an evolution in its mineralogy. When comparing Sal and BT to Ea and BTgd clay fractions, quartz and hydroxyaluminous vermiculite increase whilst kaolinite or micaceous clay decrease (Table 1). Therefore, degradation processes in these soils involve weathering of clay minerals, shown by the decrease of kaolinite and micas and the increase of residual quartz, and the aluminisation of clay, shown by the increase of hydroxyaluminous vermiculite (Aurousseau, 1990; Aurousseau and Curmi, 1992).

This degradation successively transforms BT and E horizons from their base and occurs in acid and reducing conditions. This is in contrast to the degradation process following intense clay translocation and soil acidification (De Coninck & Herbillon, 1968; Jamagne, 1973; Chartres, 1987; Ransom *et al.*, 1987), and may correspond to the "hydromorphic degradation", of Eimberck-Roux (1977) which " ... results in a gradual and ascending destruction of the BT horizon".
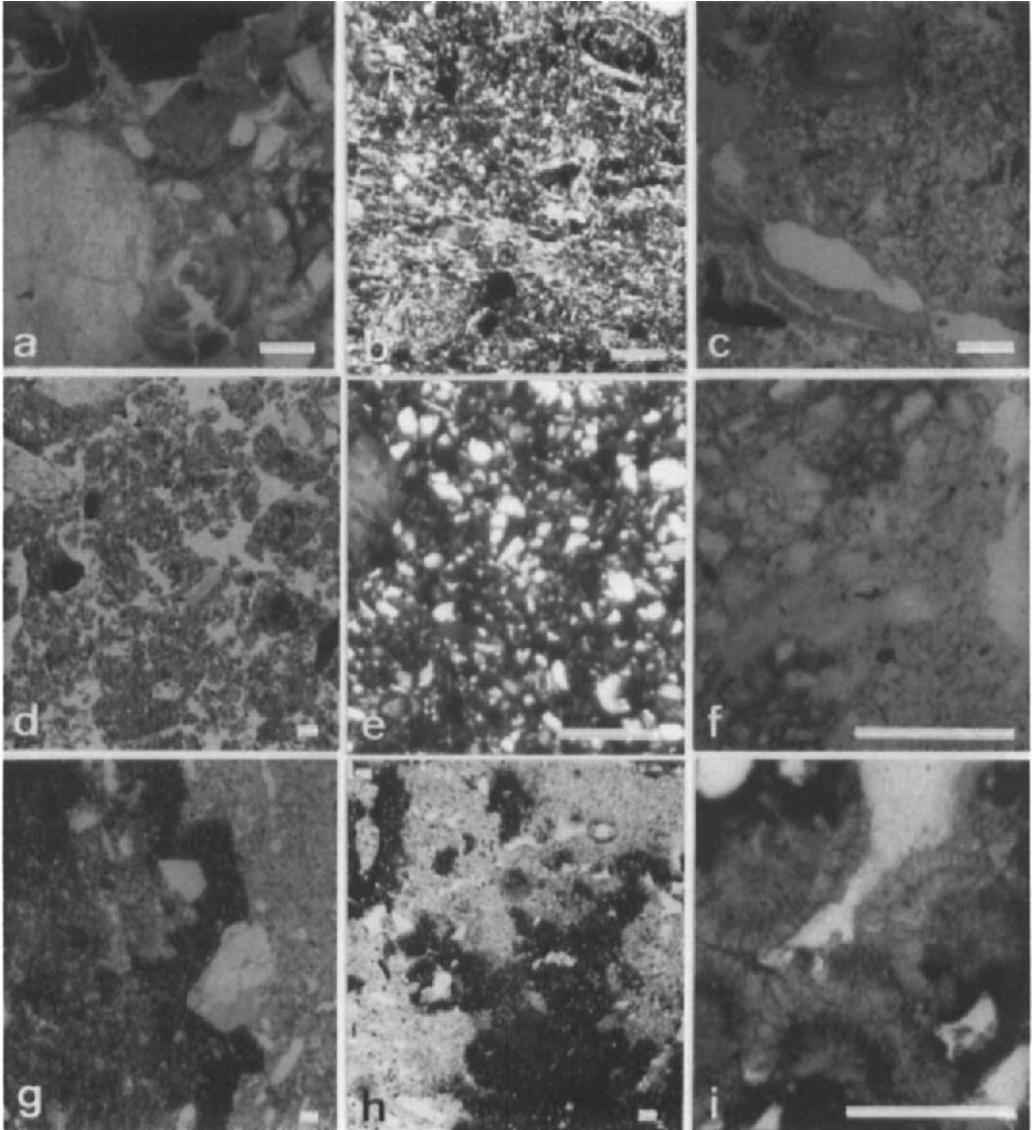
Fig. 2. Micrographs of the main horizons. Bar=250 μm. **a)** Ct sandy saprolite, thick clay coatings between grains (PPL); **b)** IICGo clayey saprolite, cross striated b-fabric of micromass (XPL); **c)** BT horizon, silty clay coatings in channels and vughs (PPL); **d)** Sal horizon, compound packing voids between granular and intergrain microaggregate structure (PPL); **e)** Ea horizon, monic fabric of silt-size quartz with a scarce speckled micromass (XPL); **f)** BTgd horizon, transition between bleached and brown mottles (PPL); **g)** FEm horizon, absolute iron accumulation in a Btgd matrix (PPL); **h)** FEm horizon, absolute iron accumulation in an Ea matrix (PPL); **i)** Fan-like goethite crystals lining large channels (PPL).

CONCLUSIONS

The importance of the characteristics and distribution of deep saprolite horizons on genesis and water behaviour of superficial loamy horizons was shown by structural analysis of a landscape unit. The nature, distribution and boundaries between different volumes were studied at various scales. At the microscopic scale, the boundaries studied were between different fabrics. At the macroscopic scale, they were: (1) between organizations, (2) between horizons, (3) between horizons and topographical slope on 2-D transects, and (4) between pedological volumes in a 3-D context. This allowed identification of pedological systems and therefore the understanding of the different organizational levels of the pedological cover. This approach demonstrates that the transformation of the upper loamy horizons by hydromorphic and degradation processes originate in the lower clayey saprolite.

ACKNOWLEDGEMENTS

REFERENCES

AFES, 1992. Référentiel Pédologique. Principaux Sols d'Europe. Coll. Techniques et Pratiques, INRA Editions, Paris, 222 pp.

Al Siddik, M.A., 1983. La Couverture Pédologique en Forêt de Rennes: Analyse Morphologique de Séquences et Cartographie en Courbes d'Isodifférenciation à Grande et Petite Echelle. Thèse Ing. Doct. ENSA Univ. Rennes, 125 pp.

Aurousseau, P., 1990. A microscopic and mineralogical study of clay degradation in acid and reducing conditions. In: L.A. Douglas (Editor), Soil Micromorphology: A Basic and Applied Science. Proc. VIII Int. Working Meeting on Soil Mircromorphology, San Antonio, Texas, July 1988. Developments in Soil Science 19, Elsevier, Amsterdam, pp. 245-255.

Aurousseau, P. and Curmi, P., 1992. Transformation structurale et géochimique dans les couvertures pédologiques du Massif Armoricain. In: J.M. Wackerman (Editor), Organisation et Fonctionnement des Altérites et des Sols, Séminaire ORSTOM Bondy, 5-9 Fév. 1990. Colloques et Séminaires, ORSTOM éditions, pp. 103-104.

Aurousseau, P., Curmi, P. and Bresson, L.M., 1985. Microscopy of the cambic horizon. In: L.A. Douglas and M.L.Thompson (Editors), Soil Micromorphology and Soil Classification. Soil Sci. Soc. Am. Spec. Publ. no 15, Madison, Wisconsin, pp. 49-61.

Boulet, R., Humbel, F.X. and Lucas, Y., 1982. Analyse structurale et cartographie en pédologie: II - Une méthode d'analyse prenant en compte l'organisation tridimensionnelle des couvertures pédologiques. Cah. ORSTOM, sér. Pédol., 4: 323-339.

Boulet, R., Curmi, P., Pellerin, J. and Queiroz Neto J.P., 1989. Distribution spatiale des horizons dans un versant: apport de l'analyse de leurs relations géométriques. Science du Sol, 27 : 53-56.

Bullock, P., Fedoroff, N., Jongerius, A. and Tursina, T., 1985. Handbook for Soil Thin Section Description. Waine Research Publications, Wolverhampton, U.K., 152 pp.

Buson, C., 1982. Etude pédologique du bassin versant de la Noé Sèche: contribution à l'étude de la pollution diffuse. Résumé des principaux résultats. G.E.S. 133.

Chartres, C.J., 1987. The composition and formation of grainy void cutans in some soils with textural contrast in southern Australia. Geoderma, 39: 209-233.

Curmi, P., 1979a. Altération et Différenciation Pédologique sur Granite en Bretagne. Etude d'une Toposéquence. Thèse Ing. Doct. ENSA Rennes, 179 pp.

Curmi, P., 1979b. Différenciation pédologique dans une arène granitique bretonne. Science du Sol, 1: 1-15.

Curmi, P. Soulier, A. and Trolard, F., 1994. Forms of iron in hydromorphic soil environment. Morphology and characterization by selective dissolution. In: A.J. Ringrose-Voase and G.S. Humphreys (Editors). Soil Micromorphology: Studies in Management and Genesis. Proc. IX Int. Working Meeting on Soil Micromorphology. Developments in Soil Science 22. Elsevier, Amsterdam, pp. 141-148.

De Coninck, F. and Herbillon, A.J., 1968. Evolution minéralogique et chimique des fractions argileuses dans les Alfisols et les Spodosols de la Campine (Belgique). Pédologie, XIX: 159-261.

Delaye, R., 1984. Notes techniques sur la préparation des lames minces dans les matériaux meubles. Bull. Inst. Géol. Bassin d'Aquitaine, Bordeaux, 35: 153-158.

Eimberck-Roux, M., 1977. Les sols lessivés glossiques à pseudogley de l'Argonne méridionale: Caractérisation micromorphologique et minéralogique. Bull. Ass. Fr. Et. Sol, 2: 81-94.

Jamagne, M., 1973. Contribution à l'Etude Pédogénétique des Formations Loessiques du Nord de la France. Thèse Fac. Gembloux, Belgique, 445 pp.

Landuydt, C.J., 1990. Micromorphology of Iron Minerals from Bog Ores of the Belgian Campine Area. In: L.A. Douglas (Editor), Soil Micromorphology: A Basic and Applied Science. Proc. VIII Int. Working Meeting on Soil Mircromorphology, San Antonio, Texas, July 1988. Developments in Soil Science 19, Elsevier, Amsterdam, pp. 289-294.

Ransom, M.D., Smeck, N.E. and Bigham, J.M., 1987. Micromorphology of seasonally wet soils on illinoian till plain, U.S.A. Geoderma, 40: 83-99.

Ruellan, A., Dosso, M. and Fritsch, E., 1989. L'analyse structurale de la couverture pédologique. Science du Sol, 27 : 319-334.

Robert, M. and Tessier, D., 1974. Méthode de préparation des argiles des sols pour les études minéralogiques. Ann. Agron., 25: 859-882.

Roussel, F., 1980. Etude d'une Toposéquence sur Schistes Pourprés de Montfort. Application aux Problèmes de Mise en Valeur Forestière sur les Sols Dégradés dans la Région de Rennes.Thèse Doct. Ing., Rennes, 215 pp.

Roussel, F., 1983. Horizon and microscopic organisations characteristic of degraded soils on cambrian schist in central Brittany. In: P. Bullock and C.P. Murphy (Editors) Soil Micromorphology, volume 2: Soil Genesis. Proc. VI Int. Working Meeting on Soil Micromorphology, London, August 1981, AB Academic Publishers, Berkhamsted, U.K., pp. 559-565.

Soil Survey Staff, 1975. Soil Taxonomy. U.S. Dept. Agric. Handb. 436, U.S. Gov. Printing Office, Washington, D.C., 754 pp.

Forms of iron oxides in acid hydromorphic soil environments. Morphology and characterization by selective dissolution

P. Curmi, A. Soulier, and F. Trolard

INRA-ENSAR, Laboratoire de Science du Sol, 65 rue de Saint Brieuc 35042 Rennes Cedex, France

ABSTRACT

Curmi, P., Soulier, A. and Trolard, F. 1994. Forms of iron oxides in acid hydromorphic soil environments. Morphology and characterization by selective dissolution. In: A.J. Ringrose-Voase and G.S. Humphreys (Editors), Soil Micromorphology: Studies in Management and Genesis. Proc. IX Int. Working Meeting on Soil Micromorphology, Townsville, Australia, July 1992. Developments in Soil Science 22, Elsevier, Amsterdam, pp. 141-148.

Spatial distribution, pedological and chemical characteristics of some oxide concentrations were studied using selective dissolution on both thin sections and bulk samples. The reagents used for selective dissolution were citrate-bicarbonate (CB) and dithionite-citrate-bicarbonate (DCB). At each stage of the reaction, the nature and amount of the dissolved elements were determined by spectrophotometry and remnant oxides by optical microscopy and X-ray diffraction (XRD).

Selective dissolutions on bulk samples of the different pedofeatures confirm the observations on thin sections. Four categories of iron compounds were defined with respect to their differential solubilities: (i) iron complexed by citrate without reduction, (ii) "amorphous" iron forms, (iii and iv) more or less crystallized iron oxides. The different pedofeatures can be classified according to the relative importance of these categories depending on the degree of hydromorphism.

INTRODUCTION

Some elements such as iron and manganese play an important part in the expression of the hydromorphic and degraded morphological features. Thus, the study of these oxide concentrations constitutes an important step in understanding the genesis and the current behaviour of hydromorphic soils. A previous study (Maître, 1991) made on an acid pedological system showed variations in the bulk composition of free water and in the behaviour of dissolved iron in different hydromorphic horizons. Therefore it becomes necessary to link these results with the nature of the solid compounds and the hydrological behaviour of the system.

The main goal of this work was to study the spatial distribution and the pedological and chemical characteristics of oxide accumulations using kinetic selective dissolutions on bulk samples and thin sections. These pedological features were observed in a landscape unit described by Curmi *et al.* (1994) in terms of the mineral constitution and spatial organization of the soils and the quality of the free waters (Maître, 1991).
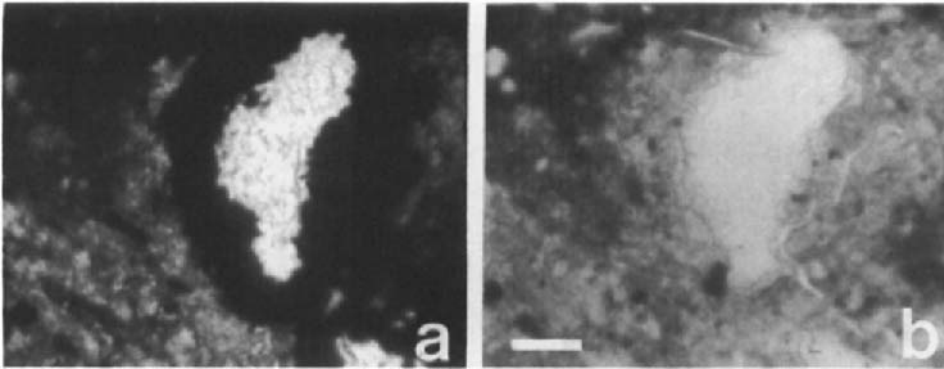
Fig. 1. Black coatings in FEm horizon. Thin section treated with DCB. a) untreated; b) after 45 minutes. Bar = 100 µm.

MATERIALS

The soils are developed in a loamy cover overlying a granite saprolite. They change over a short distance from Alocrisol (AFES, 1992) (Dystrochrept, Soil Survey Staff, 1975) upslope to Luvisol-redoxisol degrade (Glossaqualf) downslope. Samples were taken from connected horizons in the same pedological system in contrast to many others studies on iron compounds. Our *in situ* observations indicate that different iron forms distributed in different pedological volumes can be distinguished. Coatings localized around root channels were observed in gleyed clayey saprolite with a grey or blue matrix (IICGo). Other quasicoatings (Bullock *et al.*, 1985) around root channels and diffuse mottles in the groundmass were sampled in the IISg prismatic clayey horizon. Finally, different pedological features were distinguished in a FEm horizon (AFES, 1992) with absolute iron accumulation, which occurred locally above a clayey saprolite of limited spatial extent.

METHODS

Selective dissolution of the iron compounds was applied with control of the concentrations *versus* time. The two chemical reagents used were dithionite-citrate-bicarbonate (DCB) and citrate-bicarbonate (CB). The DCB reagent (Mehra and Jackson, 1960) combines the strong reductive action of dithionite with the strong complexation capacity of the citrate anion. This allows dissolution of iron mineral forms excluding iron bonded by the crystal lattices of silicates. The CB reagent (Jeanroy *et al.*, 1991) allows only dissolution by complexation. It extracts iron available without reduction, *i.e.* adsorbed or lightly complexed on minerals. These selective dissolution procedures make it difficult to identify the mineralogical structure of the iron minerals but permit distinction of several categories of different reactivity (Borggaard, 1988).

To take into account the behaviour of each selected location, we combined bulk samples and thin sections to monitor dissolution kinetics and accompanying optical changes like

Arocena *et al.* (1989). Thin sections without cover ships were used to observe the behaviour of the different pedological features during treatment in relation to the horizon organisation (Bullock *et al.*, 1975). Well defined time durations were used to give control at each step of the dissolution. Optical observations were made after each treatment. Thin sections were immersed in CB, then in DCB reagent, at room temperature, for periods ranging from 10 minutes to 150 hours. Additional data were obtained on the composition of some features by microprobe analysis.

Small bulk samples were taken from selected features *in situ* in order to concentrate the features. Selective dissolutions were carried out for 1, 2, 4, 48 and 150 hours. After each extraction, chemical analyses of the solution allowed distinction of various categories of iron forms. In the same way, the crystalline minerals present in the samples were recognized by X-ray diffraction. In addition, a control of the dissolved part of the crystallized minerals was attempted by differential X-ray diffraction (Schulze, 1981).

RESULTS

Uncovered thin sections

Hydromorphic horizons (IICGo and IISg)

Two kinds of pedological features in these horizons were studied. Quasicoatings around root channels impregnated the matrix and were 1 to 2 mm thick. They were occasionally bordered with a darkened edge and separated from the root by a bleached zone. Rusty mottles formed from diffuse iron in the groundmass were approximately equidimensional and more clayey than the contiguous bleached zones. Although these two features were morphologicaly different, they showed similar dissolution behaviour. In both cases, all the iron was extracted after 150 hours of DCB treatment, but none after 150 hours of CB treatment.

Nodular horizons (FEm)

Under the optical microscope, black void coatings with mamillated boundaries were identified. Microprobe analyses showed high amounts of manganese (between 40 to 70%). Dissolution of these sites occurred very rapidly after only 45 minutes of DCB treatment suggesting that the coatings are poorly crystalline (Fig. 1).

In addition, large formations of goethite crystals were observed filling up some pores. These coatings occurred as acicular fan-shaped aggregates radiating out from the pores (Landuydt, 1990). Several layers of aggregates can overlap one another. Although well crystalline, these goethites are completely dissolved after 150 hours of DCB treatment. Nevertheless, an isotropic "print" is still visible using an optical microscope (Fig. 2).

Other data obtained by microprobe analyses of such goethites (Fig. 3) show the occurrence of iron, silicon, aluminium and phosphorus. The distribution maps show that silicon and aluminium are associated and that phosphorus is associated with iron (Fig. 4). From similar situations, Jonasson *et al.* (1988) has suggested that this phosphorus is adsorbed on the iron oxide surfaces. Distribution maps of silicon and aluminium are complementary to those of phosphorus and iron. This indicates that alumino-silicate clays overlie fans of goethite.

Besides these two kinds of pedological features, the thin sections also showed brown and black mottles of variable sizes between mm^2 and cm^2. Their dissolution behaviour is a function of their colour. Like the black coatings, the black mottles dissolved rapidly within one hour.
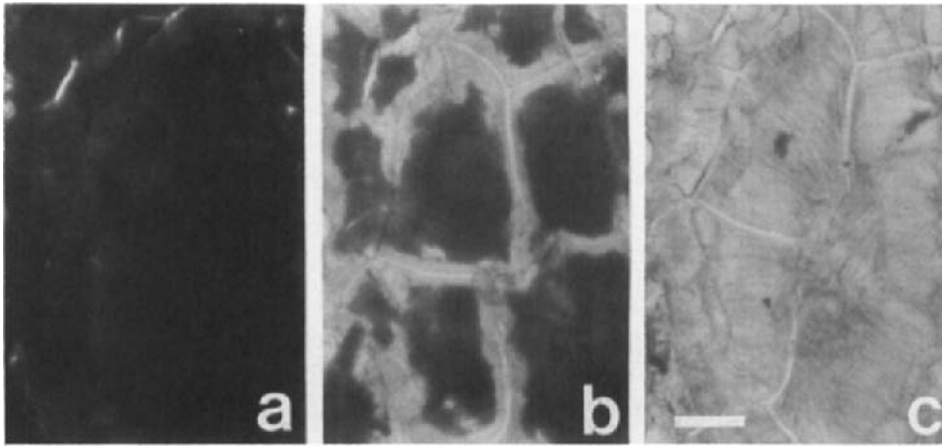
Fig. 2. Aggregates of radiating acicular goethite. Thin section treated with DCB. Progressive discoloration of the mineral. **a)** untreated; **b)** after 4 hours; **c)** after 150 hours. Bar = 100 μm.
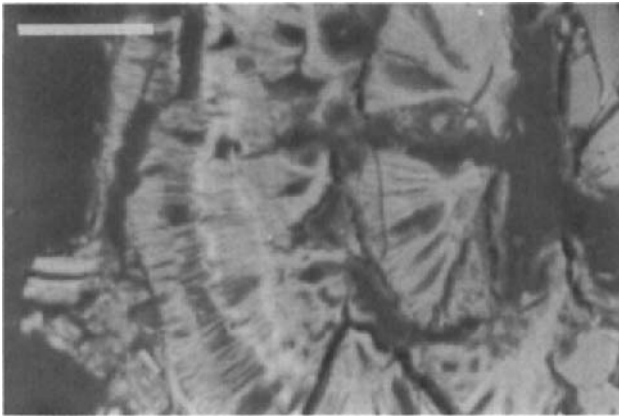
Fig. 3. Backscattered electron micrograph of aggregates of radiating acicular goethite from the FEm horizon. Bar = 20μm.

Dissolution of the brown mottles was slower but complete after 150 hours of DCB treatment. This made it possible to observe the spatial distribution of iron and manganese oxides (Arocena *et al.*, 1990). The CB treatment did not induce any modification to thin sections in any of above cases.

Bulk samples

Data obtained from the bulk samples (Table 1) confirmed the results deduced from the uncovered thin sections (Trolard *et al.*, in press). They indicate that the different pedofeatures
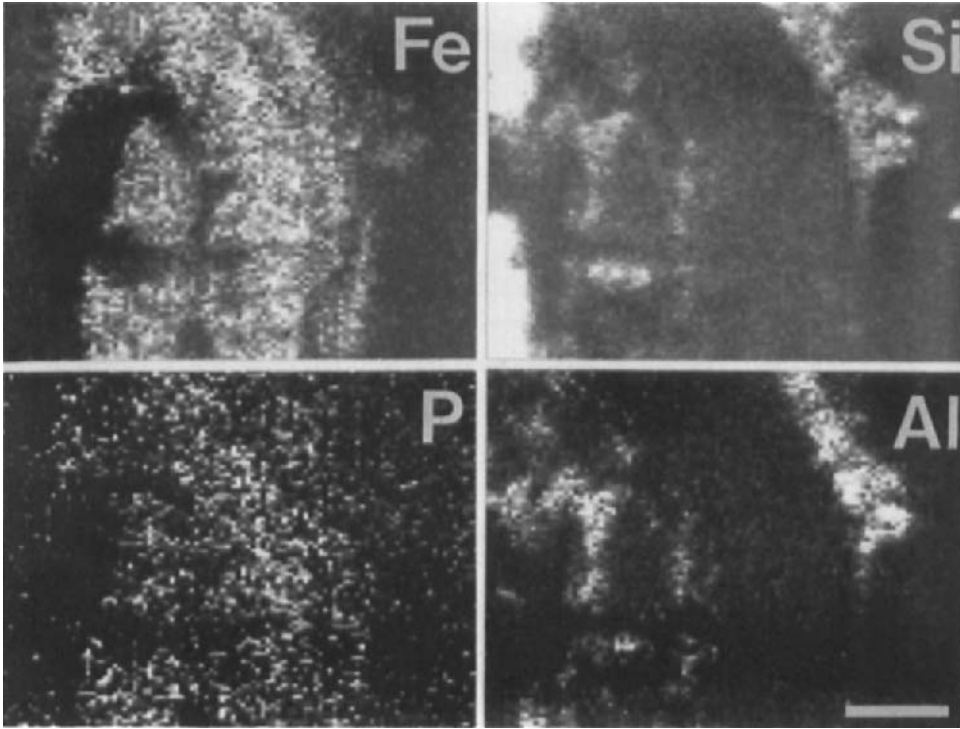
Fig. 4. Element maps of Fe, P, Si and Al in the aggregates of goethite shown in Fig. 3. Bar = 20 μm.

ranked according to decreasing resistance to dissolution: rusty coatings around root channels from the IICGo blue gleyey saprolite (sample 1) > rusty coatings from the IICGo grey gleyey saprolite (sample 2) > rusty quasicoatings (sample 3) and iron from groundmass (sample 4) from the IISg clayey pseudogleyey prismatic horizon > black nodules in FEm horizon (sample 6) > ochre nodules in FEm horizon (sample 5).

DISCUSSION

The use of both DCB and CB reagents with kinetic control and X-ray diffraction makes it possible to distinguish four categories of different reactivity (Table 2). The first includes adsorbed or complexed iron extracted by citrate without reduction (CB treatment). The second category corresponds to "amorphous" iron forms. These forms are rapidly dissolved by DCB reagent within a few hours. The third category is composed of crystalline forms identified by XRD which are dissoved after 150 hours of DCB treatment The last one is composed of crystalline forms identified by XRD which resist DCB treatment. Thus, with the blue or grey gleyey saprolites (IICGo) are associated high amounts of adsorbed and complexed iron soluble without reduction, "amorphous" or poorly crystallized oxides available after reduction and well

Table 1
Dissolved iron fraction per total amount of iron (%) after 150 hours of treatment.

Pedofeatures	Horizons	CB	DCB
1. rusty coatings	blue IICGo	9.1	56.2
2. rusty coatings	grey IICGo	10.9	69.0
3. rusty quasicoatings	IISg	1.6	74.5
4. diffuse mottles	IISg	1.2	74.8
5. black nodules	FEm	2.8	79.0
6. ochre nodules	FEm	1.9	81.8

Table 2
Partition of the solid forms of iron in various features.

Pedofeatures	Horizons	Iron Forms			
		Complexed by citrate without reduction	"Amorphous"	Crystallized goethite dissolved by DCB	undissolved treatment (150h)
1. rusty coatings	blue IICGo	+++	+	0	+
2. rusty coatings	grey IICGo				
3. rusty quasicoatings	IISg	+	++	+	0
4. diffuse mottles	IISg				
5. black nodules	FEm	+	+++	+	0
6. ochre nodules	FEm				

Legend: decreasing abundance (+++), (++), (+); absence (0)

crystallized goethites, dissolution-proof. With the prismatic clayey horizon (IISg) are associatied low amounts of adsorbed and complexed iron available without reduction, "amorphous" or poorly crystallized oxides and crystallized goethites available with reduction. With the FEm horizon are associated adsorbed and complexed iron available without reduction, high quantities of "amorphous" or poorly crystallized iron and manganese oxides and crystallized goethites highly soluble with reduction.

CONCLUSION

   In these acid hydromorphic environments where constituants and organisation vary over very short distances within horizons, it is important to work at the microsite scale on thin section. Thus, it is possible to study pedofeatures associated with porosity, where constituants are in contact with circulating solutions. When the soil environment favours reduction, amorphous and well crystallized solid iron forms are dominant together with adsorbed or complexed iron, whereas, when oxidation is favoured, large amounts of amorphous or poorly crystallized iron minerals are observed.

REFERENCES

AFES (Association Française pour l'Etude du Sol), 1992. Référentiel Pédologique. Principaux Sols d'Europe. Coll. Techniques et Pratiques, INRA Editions, Paris, 222 pp.

Arocena, J.M., De Geyter, G., Landuydt, C. and Schwertmann, U., 1989. Dissolution of soil iron oxides with ammonium oxalate: comparison between bulk samples and thin sections. Pedologie, 3: 275-297.

Arocena, J.M., De Geyter, G., Landuydt, C. and Stoops, G., 1990. A study on the distribution and extraction of iron (and manganese) in soil thin sections. In: L.A. Douglas (Editor), Soil Micromorphology: A Basic and Applied Science. Proc. of the VIII Int. Working Meeting of Soil Micromorphology, San Antonio, Texas, July 1988. Developments in Soil Science 19, Elsevier, Amsterdam, pp. 621-626.

Borggaard, O.K., 1988. Phase identification by selective dissolution techniques. In: J.W. Stucky, B.A. Goodman and U. Schwertmann (Editors), Iron in Soils and Clays Minerals. Riedel, Dordrecht, Switzerland, pp. 83-98.

Bullock, P., Loveland, P.J. and Murphy, C.P., 1975. A technique for selective dissolution of iron oxides in thin sections of soils. J. Soil Sci., 26: 247-248.

Bullock, P., Fedoroff, N., Jongerius, A. and Tursina, T., 1985. Handbook for Soil Thin Section Description. Waine Research Publishers, Wolverhampton, U.K., 152 pp.

Curmi, P., Widiatmaka., Pellerin, J. and Ruellan, A., 1994. Saprolite influence on formation of well-drained and hydromorphic horizons in an acid soil system as determined by structural analysis. In : A.J. Ringrose-Voase and G.S. Humphreys (Editors). Proceedings of 9th International Working Meeting on Soil Micromorphology. Developments in Soil Science, 22. Elsevier, Amsterdam, pp. 133-140.

Jeanroy, E., Rajot, J.L., Pillon, P. and Herbillon, A.J., 1991. Differential dissolution of hematite and goethite in dithionite and its application on soil yellowing. Geoderma, 50: 79-94.

Jonasson, R.G., Martin, R.R., Giuliacci, M.E. and Tazaki, K., 1988. Surface reactions of goethite with phosphate. J. Chem. Soc., Faraday Trans. I, 84, 7: 2311-2315.

Landuydt, C.J., 1990. Micromorphology of iron minerals from bog ores of the Belgian Campine area. In: L.A. Douglas (Editor), Soil Micromorphology: A Basic and Applied Science. Proc. of the VIII Int. Working Meeting of Soil Micromorphology, San Antonio, Texas, July 1988. Developments in Soil Science 19, Elsevier, Amsterdam, pp. 289-294.

Maître, V., 1991. Géochimie des Eaux Libres Extraites de Sols Hydromorphes sur Granite dans le Massif Armoricain. Mobilité et Dynamique Saisonnière. Thèse de doctorat, Université Paris 6, 230 pp.

Mehra, O.P. and Jackson, M.L., 1960. Iron oxide removal from soils and clays by a dithionite-citrate system buffered with sodium bicarbonate. Clays and Clay Miner., 7: 317-327.

Schulze, D.G., 1981. Identification of soil iron oxide minerals by differential X-ray diffraction. Soil Sci. Soc. Am. J., 45: 437-440.

Soil Survey Staff, 1975. Soil Taxonomy. U.S. Dept. Agric. Handb. 436, U.S. Gov. Printing Office, Washington, D.C., 754 pp.

Trolard, F., Soulier, A. and Curmi, P., Les formes solides du fer en milieu hydromorphe acide: une approche compartimentale par dissolution sélective. C.R. Acad. Sci. Paris, t. 316, Série II. (In press).

Signposts old and new: active and inactive redoximorphic features; and seasonal wetness in two Alfisols of the gulf coast region of Texas, U.S.A.

R.J. Tucker[1], L.R. Drees[2] and L.P. Wilding[2]

[1]*Department of Primary Industries, Box 1143 Bundaberg, Queensland, 4670, Australia*
[2]*Department of Soil and Crop Sciences, Texas A&M University, College Station, Texas, 77843-2474, USA*

ABSTRACT

Tucker, R.J., Drees, L.R. and Wilding, L.P., 1994. Signposts old and new: active and inactive redoximorphic features; and seasonal wetness in two Alfisols of the gulf coast region of Texas, U.S.A. In: A.J. Ringrose-Voase and G.S. Humphreys (Editors), Soil Micromorphology: Studies in Management and Genesis. Proc. IX Int. Working Meeting on Soil Micromorphology, Townsville, Australia, July 1992. Developments in Soil Science 22, Elsevier, Amsterdam, pp. 149-159.

Two Alfisols, an Aquic Paleudalf (Katy soil) and a Plinthic Paleudalf (Wockley soil) were examined to see if redoximorphic features were relict or contemporary. Currently there is little information available about distinguishing between these features. Relict features included: Fe-Mn nodules which had sharp boundaries to the matrix or were covered by clay coatings; mangans, skeletans and colour depletion zones which did not relate to current voids. Contemporary features included: macroscopic sand-silt coats on ped faces, nodules undergoing dissolution as shown by sand grains protruding from the nodules, and diffuse boundaries to the matrix; pore linings, patches of iron, and soft agglomerations of iron. Relict and contemporary features could occur in the one horizon. Saturation was more pronounced where nodules were dissolving and sand-silt coats were evident. However, nodules were also dissolving in areas with little saturation, suggesting that rare very wet periods may contribute more to the saturation and reduction.

INTRODUCTION

It is a recurring desire to predict wetness in soils just by looking at them. Precise universal predictions of where, when, and for how long water tables will be found would make life a lot easier for soil surveyors and their clients. Alas, we must shuffle back into the shadows of conjecture, best-bets and probability, using the imperfect signs at our disposal.

Yet, having recognised the limitations now arms us for objective approaches to solving the riddles. We report here on efforts to relate features in soils, marked by water tables and seasonal wetness, to observed conditions; concentrating on micromorphology of these features. The presence of active and inactive features in a pedon can tell us about the pattern of water movement within it - and challenge our expectations of what the water does once it arrives.
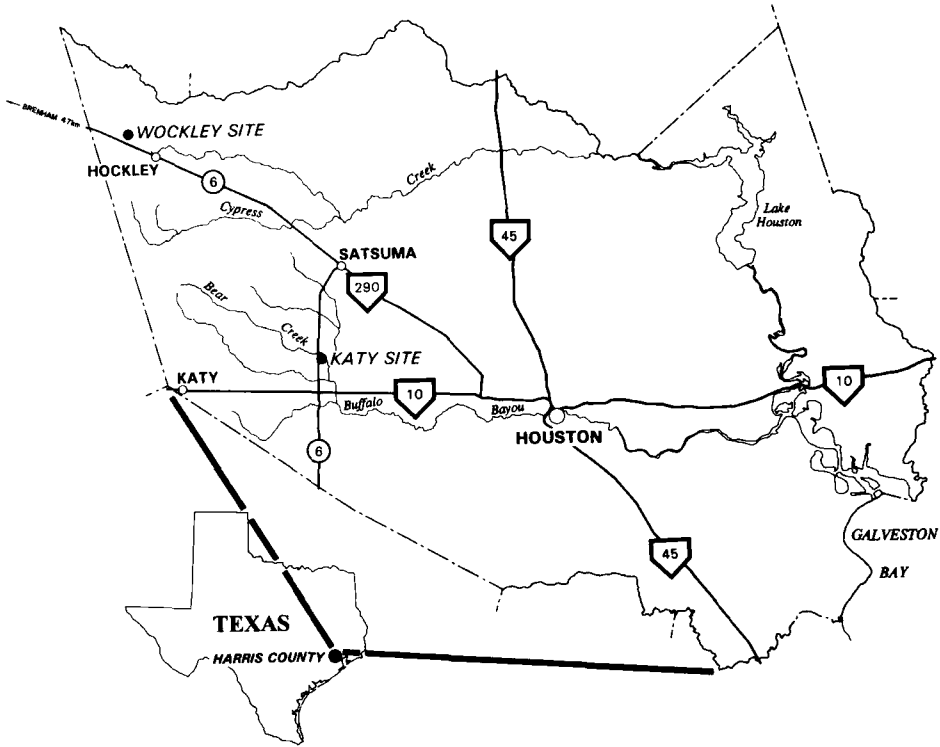
Fig. 1. Location of Katy and Wockley Soil Research Sites, Harris County, Texas, USA.

Seasonal wetness in soils refers to the complete saturation of soils on a periodic basis. This may indeed be "seasonal" but often relates to less frequent events. Seasonal wetness and saturation have been inferred from soil morphological features which result from reduction processes induced by anaerobic respiration of bacteria which become active in saturated anoxic soil. These "redoximorphic features" develop if chemical reduction occurs, and manganese and/or iron are reduced, mobilised, translocated and concentrated. For reduction to occur, there needs to be saturation, anaerobic conditions and sufficient organic matter. The movement and loss of iron, translocation and precipitation may be over distances as short as a ped or several metres within a profile. Redoximorphic features consist of:
- reduced matrices (completely saturated and reduced zones which are pale in colour, but regain colour on exposure to air if sufficient iron is retained in the matrix);
- redox depletions (zones depleted of Fe-Mn minerals or clay); and
- redox concentrations (concentrations of Fe-Mn minerals as nodules, concretions, pore linings, soft masses or coatings on pores, voids and ped surfaces; and soft masses).

Soil colours can relate to all three types of redoximorphic features, because the iron minerals haematite and goethite are the main soil-colouring minerals. Haematite imparts reddish colours and goethite yellow to brown colours (Barrón and Torrent, 1986). Loss of these iron minerals results in paler colouration.

Apart from observing morphological features induced by reduction, there are few means of deducing that saturation has occurred. Saturation without reduction is caused principally by: influxes of oxygenated water, inhibition of bacterial action through lack of organic matter or low temperature, high pH and high carbonate content.

Soils which have been reduced considerably in the past may show all the evidence of redoximorphic processes. However, reducing conditions may not be occurring at the present, and the redoximorphic features are relics from a previous climatic era. Monitoring and modelling are then needed to discover whether or not the features have relevance. Difficulty is also encountered when active features are superimposed on relict features. (Vepraskas and Wilding, 1983; Vepraskas et al., 1994).

Currently, there is little information available on gauging whether redoximorphic features are relict or contemporary. Two sites in the Gulf Coast region of Texas, USA, whose soil morphology suggested that they are subject to seasonal wetness, were selected for monitoring, characterisation and detailed microscopic examination. Part of this exercise was to see if observed redoximorphic features are relict or contemporary.

MATERIALS AND METHODS

Two sites were established in Harris county, Texas, (Fig. 1). One site was on Katy fine sandy loam soil which classifies as a fine-silty, siliceous, thermic Aquic Paleudalf (Soil Survey Staff, 1992). The surface horizons are fine sandy loams from 57 to 66 cm. Subsoils are grey clay loams, with red and/or yellow mottles, to 205 cm, overlying grey sandy clay loam with yellow mottles to 345 cm. This grades into grey fine sandy loam to loam fine sandy horizons to 500 cm, in turn overlying red clay with grey mottles. Traces of carbonate occur at 275 - 245 cm and 560 - 610 cm. The other site was on a Wockley fine sandy loam soil; a fine-loamy, siliceous, thermic Plinthic Paleudalf. It qualifies as a plinthic subgroup because of the presence of 10% plinthite in the Btv horizon. The surface horizons are fine sandy loams and depth to the Bt horizons usually varies from 40 to 53 cm but is occasionally 100 cm. The surface soils overlie a grey fine sandy loam BE horizon with yellow mottles, then a series of mottled grey and yellow sandy clay loam to clay loam subsoils to 400 cm, which overlie grey and red silty clay buried soils. High contents of iron nodules are found in the upper Bt horizons.

Both soils formed in fluvio-deltaic sediments ranging in age from 150,000 YBP (Katy site) to 2 million YBP (Wockley site) (Aronow, 1990). Mean annual rainfall in the vicinity of the Katy site is 1046 mm; and near the Wockley site is 1035 mm. Rainfall is rather uniform throughout the year, but May and September usually have higher rainfalls. Land use at the Katy site is currently pasture, but was formerly farmed. At the Wockley site, the land is used for row-cropping and occasional grazing, but was previously used for rice cultivation.

At each site, soils were described as per routine soil survey procedures from a pit dug to 2 m and a single 5 cm core beyond 2 m; and then sampled for laboratory characterisation and micromorphology. Thin sections for most major horizons were prepared from samples which were impregnated with a polyester resin diluted 2:1 with acetone. Horizontal and vertical thin sections were cut from the blocks and described according to Brewer (1976). Replicated piezometers and tensiometers were installed at 25, 50 and 100 cm at each site. Replicated piezometers were also installed at 200 cm depth and single piezometers to 5.9 m at the Katy site and 7.5 m at the Wockley site. Each piezometer had an intake zone of 15 cm at the base.

Field measurements collected on a bi-weekly basis included rainfall, soil moisture tension and depth to free water in the piezometers. A water table was considered to be present when water levels in replicate piezometers were within 15 cm of each other. At particular depths, the soil was considered to be "saturated" if water was present in all three piezometers at that depth and soil moisture potentials (from tensiometers) were ≥ 0 kPa. Soil redox potentials (Eh) and soil pH (1:1) were measured when soils were either saturated or near-saturated, or on other occasions as required, using a freshly-extracted soil core. The onset of reduction was determined by comparing Eh - pH values against redox stability diagrams. Readings commenced on December 30, 1988, and are continuing to be read at the Wockley site. Data collection ceased at the Katy site on November 15, 1991.

RESULTS AND DISCUSSION

Macroscopic Redoximorphic Features

Katy Site
The Katy soil has chromas of 2 or less through most of the solum, either as matrix or mottle colours. In the subsoils, 57 - 610 cm, these low-chroma colours all have values of 6. Vepraskas *et al.* (1994) point out that values >4 are required to distinguish redoximorphic colours from organic colouration. High-chroma mottles occur in association. Pale (10YR 7/2-3) sand-silt coats are evident in the field in the Btg1 - Btg4 horizons, 57 - 205 cm. A few ironstone nodules were found in the Btg1 horizon, 57 - 84 cm, and Mn/Fe Mn stains appear in the 2C horizons, 500 - 610 cm. The sand-silt coats in the Btg horizons strongly suggest contemporary reduction and thus saturation.

Wockley Site
The Wockley soil has chromas of 2 and values of 5-6 in the BE and upper Bt horizons, as well as high-chroma mottles (10YR 5/6-8), iron nodules and plinthite. In the horizons below, high-chroma matrix colours and low-chroma mottles occur. Distinct iron-manganese stains were observed in the Bt6 horizon, 300 - 370 cm.

Current estimates of wetness for the soil series as a whole suggest that perched watertables should be expected between 0 and 75 cm in the Katy soil for December and January and between 0 and 60 cm in the Wockley soil from November to March (Wheeler 1976).

Microscopic Redoximorphic Features

Details are given in Tables 1 and 2 for Katy and Wockley soils respectively.

Katy Site.
Ferrans in the E horizon of the Katy soil (Table 1) suggest recent mobilisation of iron; otherwise these features would be lost because of pedoturbation. The stripping of colour from the E horizon (Fig. 2A) further suggests that there has been active reduction. In contrast, Fe-Mn nodules have abrupt boundaries suggesting stability, since nodules alone are now being interpreted as relict features (Vepraskas *et al.*, 1994). The smooth sides of the nodules in this case most likely result from movement of soil around the nodules after formation, and lack of active accretion or dissolution.

Active dissolution of Fe-Mn nodules in the Btg1-Btg4 horizons of the Katy soil is suggested by the presence of ragged to diffuse boundaries to the matrix. Accretion of mobilised iron is suggested by the few soft masses of iron (Fig. 2B) and by ferrans lower in the Btg horizons (Table 1). However some nodules in these horizons show no signs of activity. The specimen in Fig. 2C is surrounded by a thin argillan, which is indicative of stability. If the nodule were dissolving, then there should be some evidence of iron spreading into the argillan and the matrix. Further, if iron was being lost through the argillan, there should be evidence of loss of volume due to removal of iron, such as formation of a cavity between the argillan and the nodule; stripped skeleton grains or a discontinuous broken argillan. None of these are apparent. On the other hand, evidence for the active accretion of iron is also lacking since the argillan has not been impregnated or covered with iron nor destroyed through a build up of iron on the surface of the nodule. Argillans covering nodules then imply either that they protect the nodule or that the nodule has not experienced fluxes of reduced water since being covered by the argillan.

Cutans of iron and manganese lower in the profile, weak nodules and iron impregnation (Table 1) result from the oxidation of Fe-Mn from reduced water. Some of these features are relict, as they do not relate to current voids. The red and grey colouring in the 2C horizons would have resulted from historic uneven reduction, with the grey areas being depletion zones (Fig. 2D). These are traversed by a contemporary void which has been in place for some time, shown by the presence of void argillans.

Wockley Site

In the Wockley soil, ferrans, neoferrans and nodules with diffuse boundaries in the E horizon demonstrate active dissolution, movement and re-oxidation of iron (Table 2, Fig. 2E and F). Similar features have been recorded in the BE horizon. With depth, there are fewer ferrans and some nodules become covered with argillans (Fig. 2G) or protected by thick plugs of clay (Fig. 2H). However there is also evidence of nodules disintegrating in the Bt horizons (Table 2). In the lower Bt horizons and the 2C horizon, the ferrans, neoferrans and mangans demonstrate the re-oxidation of iron and manganese. The compound ferrans/ferriargillans indicate deposition of iron following illuviation of clay, and suggest recent reduction and re-oxidation.

Rainfall, Soil Water Levels, and Saturation

Dry conditions in 1988 proceeded the observation period, with rainfalls 40 - 60% of mean annual rainfall at nearby weather stations. In 1989 and 1990, rainfalls at the sites were between 85 and 101% of mean annual rainfall. By contrast, in 1991, rainfalls were higher with record or near-record rainfall in January, April and December. At the Katy site, the total rainfall for 1991 up to the end of observations was over 17% above the annual mean, while the total for 1991 at the Wockley site was 33% above the mean. The durations of saturation which resulted from water tables in the soils are presented in Table 3.

Katy Site

In the Katy soil water tables were often present between 50 and 100 cm and rarely at 50 cm or less (Table 3). Water never showed in all three 200-cm piezometers at the same time. This shows that water tables did not occur at 200 cm and that water perching above 200 cm drains

Table 1
Active and inactive microscopic redoximorphic features in Katy Soil, Bear Creek, Harris Co, Texas.

Horizons	Active features	Inactive features
Ap, 0-10 cm		Few very fine Fe-Mn nodules.
E, 35-57 cm	Few metavughs with vugh ferrans; common Fe nodules with abrupt boundaries.	Common Fe nodules with abrupt boundaries to matrix.
Btg1-Btg4, 57-205 cm	Common Fe-Mn nodules with ragged to diffuse boundaries; common planar voids with few ferrans; common metavughs with common ferrans	Nodules lower in horizons covered by ferriargillans.
Btkg, 205-275 cm	Accumulations of iron in some areas.	Common Fe-Mn nodules (probably protected by argillans).
BCg-Cg1 275 - 345 cm	Few ferrans and neoferromangans in BCg; some iron accumulation and occasional, weakly developed nodules.	
2Css-2Ckss, 500-610 cm	Common void mangans, few void ferrans; neoskeletans along some voids.	Common, very fine, irregular glaebules of Mn; quasi-mangans and quasi-skeletans which do not relate to voids; depletion colours which do not relate to current voids.

via specific pathways to greater depths. No water was observed in the single deep piezometer, showing that water tables did not exist at depth, and that the drainage paths did not intercept this particular piezometer. Water is probably perching in the Btg1-Btg3 horizons (57 - 170 cm).

Wockley Site

At the Wockley site, water was found mainly between 100 and 200 cm (Table 3). Water was sometimes found at the 100 cm level, and rarely between 10 and 50 cm (Table 3). Water was found in the single deep piezometer in one series of consecutive sampling periods. Water levels had parallel response patterns to those of the 200 cm piezometers, though they occurred at greater depths and showed a time lag; indicating a draining regime. Uneven water levels were also detected in the piezometers, with plots of water levels indicating draining of water along specific pathways, and sometimes a rising watertable. Water is perching on a restrictive layer below 200 cm, probably the Bt5 horizon (250 - 300 cm) and/or the Bt6 horizon (300-370 cm).

Reduction

Redox potentials (only measured in early 1990) showed that in both soils, reducing conditions for manganese were prevalent whenever the Katy soil was saturated; and in both soils even when the soils were below saturation. The potential for reduction of manganese is

Table 2
Active and inactive microscopic redoximorphic features in Wockley soil, near Hockley, Harris Co., Texas

Horizons	Active features	Inactive features
Ap, 0-11 cm.		Few fine to large Fe-Mn nodules.
E, 22-45 cm.	Common vugh ferrans and neoferrans; few medium Fe-Mn nodules; common large Fe nodules with occluded quartz grains. Protrusion of skeleton grains into matrix and diffuse boundaries of nodules indicate loss of iron.	
BE, 45-73 cm.	Common meta channels and vughs with ferrans, weak neoferrans and quasiferrans; many Fe-Mn nodules with occluded quartz grains; sharp to diffuse nodule boundaries with protruding skeleton grains.	Very few strong continuous ferriargillans embedded in nodules.
Btv, 73-96 cm.	Common vugh ferrans, neoferrans and quasiferrans. Some nodules showing evidence of degradation with iron spreading into the matrix. Portions of matrix pale (grey material) and devoid of iron straining.	Many small to large Fe-Mn nodules with occluded quartz grains; ferriargillans covering some nodules, especially on under-surface.
Bt1-Bt2, 96-188 cm.	Common ferromangans. Some nodules appearing to disintegrate in grey areas of matrix.	Many Fe-Mn nodules with occluded quartz grains; clay plugs covering nodules.
Bt3, 188-224 cm.	Common void ferromangans and mangans; common vugh ferrans and neoferrans; common to many quasiferrans; few vugh mangans and neomangans; diffuse boundaries to some nodules.	Many Fe-Mn nodules with occluded quartz grains; some sharp boundaries, but without quartz grains protruding into matrix.
Bt4-Bt6, 224-370 cm.	Many neo/quasiferrans; many strong continuous ferrans; common compound ferrans / ferriargillans or ferrans / neoferrans; few Fe-Mn nodules with diffuse boundaries in Bt6 horizon.	Clay plugging in Bt4 horizon probably covers some nodules.
2C2-2C3, 400-600 cm.	Common planar voids with continuous ferrans and quasiferrans; accumulation of Fe-Mn in red isotic zones with diffuse boundaries to matrix; few channel ferrans/neoferrans in 2C3.	

limited as low levels of dithionate-citrate extractable Mn are present in the soils, and there would be limited movement of Mn under sub-saturation. Mangans have only been recorded at depth (Tables 1 and 2).
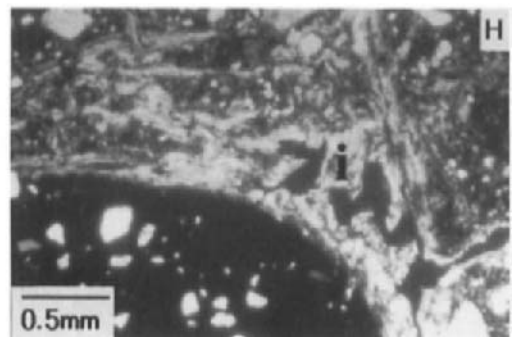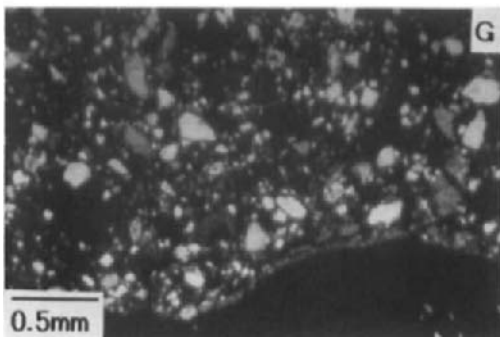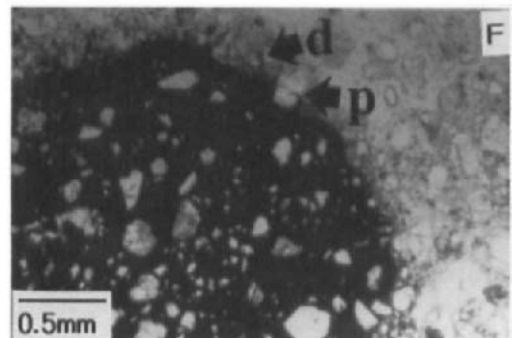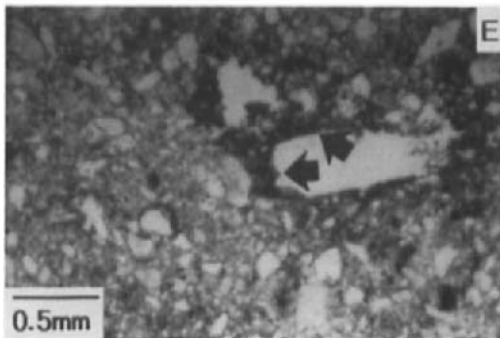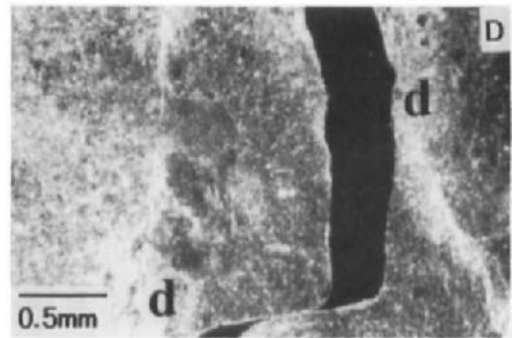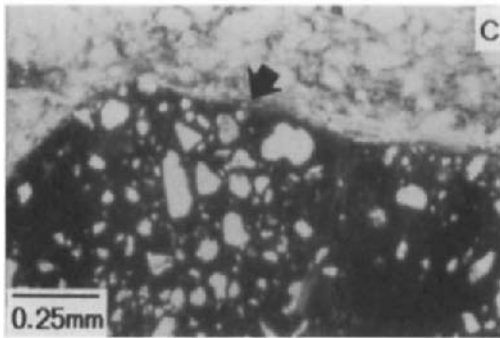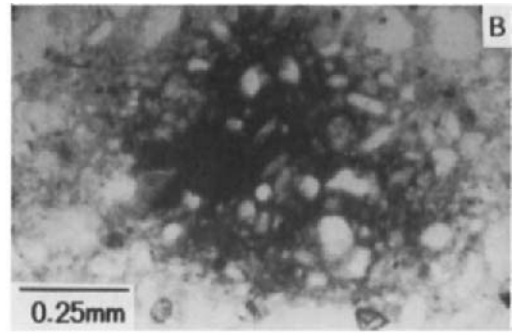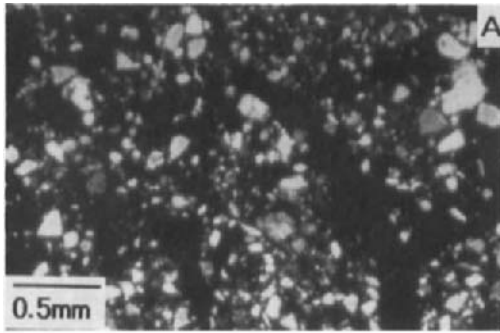
Redox potentials showed that, in early 1990, iron was never reduced in either soil. However, reduction was nearly achieved in the E horizon of the Katy soil on one occasion. With greater degrees of saturation shown later in 1990 and in 1991, reduction most likely would have occurred, particularly in the E horizon.

DISCUSSION

Both active and inactive redoximorphic features occur in the Katy soil and the Wockley soil. Dissolution of Fe-Mn nodules is prevalent in the upper Btg horizons of the Katy soil and in the Bt horizons of the Wockley soil. The macroscopic sand-silt coats in the Btg horizons of the Katy soil also demonstrate active stripping of Fe on the larger ped faces. Other active features are mainly pore linings and relate to the re-oxidation of Fe-Mn following reduction and movement. Inactive redoximorphic features are mainly nodules with abrupt boundaries to the matrix or covered by clay coats or clay plugs. These can occur in the same horizons as active features. There are also some relict coloured redox concentrations and depletions which do not relate to contemporary voids.

The higher frequencies of saturation recorded (Table 3) correspond to some extent with active dissolution of nodules in the upper Btg horizons of the Katy soil, around 100 cm, and in the Bt3-Bt6 horizons of the Wockley soil, around 120-300+ cm (assuming saturation also occurs below 200 cm). However, active dissolution of nodules higher in the Wockley soil does not relate so well to the lower frequency of saturation measured at 50 cm (Table 3).

There is some uncertainty about the degree of iron reduction associated with the saturation given in Table 3. Reduction seemed more likely to occur in the E horizons of the Katy soil, going on what little Eh data is available. However, active dissolution and stripping of iron is apparent in the B horizons. In these horizons, iron reduction is more likely to occur along root channels and ped faces where organic matter is present. This would not have been detected in Eh measurements because they were made in the matrix of the soils. At the moment this can not be verified. However, water draining into and perching in these horizons could introduce accessions of organic matter which would be readily consumed under anoxic saturated conditions.

A causal relationship should not be unequivocally drawn between the saturation in Table 3 and the active redoximorphic features. Observations of extremely wet events which have subsequently occurred in 1992 and 1993 are still being evaluated. These events may have a

Fig. 2. Micrographs of: **A)** Katy E horizon, 35-57 cm, showing coarse texture and clean sand grains (loss of Fe); crossed polarised light (XPL); **B)** Katy Btg2 horizon, 84-120 cm, showing diffuse nodule/soft mass; Plane polarised light (PPL); **C)** Katy Btg3 horizon, 120-170 cm, nodule protected by argillan (arrowed); PPL; **D)** Katy 2Css horizon, 500-560 cm, showing relict redox depleted zones (d) which do not correspond with contemporary void; XPL; **E)** Wockley E horizon, 22-45 cm, showing void ferran (arrowed); PPL; **F)** Wockley E horizon, 22-45 cm, showing nodule with diffuse boundary (d) and protruding sand grains (p); PPL; **G)** Wockley Btv horizon, 73-96 cm, showing nodule covered by thin clay coating; XPL; **H)** Wockley Bt2 horizon, 127-188 cm,showing nodule in void plugged with illuviated clay (i); PPL.

Table 3
Proportion of time that Katy and Wockley soils were saturated, between December 1988 and January 1992.

Site and Duration of Observations	Proportion of time soil was saturated at depths of:					
	0 cm	10 cm	25 cm	50 cm	100 cm	200 cm
Katy Site 30 December 1988 -15 November 1991	nil	nil	1%	4%	19%	nil
Wockley Site 30 December 1988 -9 January 1992	nil	1%	1%	1%	6%	19%

Notes: 1. Proportion calculated from observations of watertables at 14 day intervals.
2. Saturation in the matrix at 25, 50 and 100 cm confirmed by tensiometers.
3. The proportion of time saturated at the Katy site is underestimated in relation to the Wockley site because significant rainfall and hydrologic events occurred between 15 November, 1991 and 9 January 1992.

greater effect on saturation and reduction than those reported here. In particular, longer periods of saturation in the surface may have induced greater reduction in the upper parts of the profiles, which will have had a greater effect on redoximorphic features.

Ponding of water for rice culture at the Wockley site in the past could have enhanced the potential for the reduction through higher saturation and the contribution of organic matter thereby causing the development of some contemporary redoximorphic features in the Wockley soil. However, this does not explain the similar features seen in the Katy soil where no rice has been grown.

ACKNOWLEDGMENTS

REFERENCES

Aronow, S., 1990. Geology of the West Gulf Coastal Plain. Unpubl. report, Lamar University, Beaumont, Texas. (Prepared for the Tour Guide, Aquic and Seasonally Wet Soils of the Coast Prairie Land Resource Area, Louisiana-Texas, International Soils Correlation Meeting VIII, October, 1990, Soil Management Support Services, USDA-SCS, Washington, DC.)

Barrón, V. and Torrent, J., 1986. Use of the Kubelka-Munk theory to study the influence of iron oxides on soil colour, J. Soil Sci. 37: 499-510.

Brewer, R., 1976. Fabric and Mineral Analysis of Soils. R.E. Krieger, Huntington, New York.

Soil Survey Staff, 1992. Keys to Soil Taxonomy. 5th editon. SMSS Tech. Monogr. no. 19. Pocahontas Press, Blacksburg, Virginia.

Vepraskas, M.J. and Wilding, L.P., 1983. Albic neoskeletans in argillic horizons as indices of seasonal saturation and iron reduction. Soil Sci. Soc. Am. J. 47: 1202-1208.

Vepraskas, M.J., Wilding, L.P. and Drees, L.R., 1994. Micromorphology of soils with aquic conditions. In: A.J. Ringrose-Voase and G.S. Humphreys (Editors), Soil Micromorphology: Studies in Management and Genesis. Proc. IX Int. Working Meeting on Soil Micromorphology. Developments in Soil Science, 22. Elsevier, Amsterdam, pp. 117-131.

Wheeler, F.F., 1976. Soil Survey of Harris County, Texas USDA-SCS, Washington, DC.

This Page Intentionally Left Blank

Micromorphology of an aquic paleudult developed in clayey, kaolinitic, coastal plain sediments in Maryland, U.S.A.

D. P. Wagner[1] and M. C. Rabenhorst[2]
[1]Geo-Sci Consultants, Inc., College Park, MD, USA
[2]University of Maryland, College Park, MD, USA

ABSTRACT

Wagner, D.P. and Rabenhorst, M.C. 1994. Micromorphology of an aquic paleudult developed in clayey, kaolinitic, coastal plain sediments in Maryland, USA. In: A.J. Ringrose-Voase and G.S. Humphreys (Editors), Soil Micromorphology: Studies in Management and Genesis. Proc. IX Int. Working Meeting on Soil Micromorphology, Townsville, Australia, July 1992. Developments in Soil Science 22, Elsevier, Amsterdam, pp. 161-169.

Fundamental to understanding the genesis of a soil formed in clayey sediments is the ability to distinguish properties attributable to pedogenesis from those essentially inherent to the geologic material. The Christiana soil examined in this study is developed in reddish (2.5YR) Cretaceous sediments in which free Fe oxides are abundant (>4%); concentrations of weatherable minerals are low and mostly kaolinitic clay comprises nearly 40% of the parent material. Although the soil is classified as a Paleudult, common field and laboratory techniques did little to confirm the identification of argillic horizons. Clay films are not readily discernible in field examinations of upper subsoil horizons, and fine clay/total clay ratios do not vary appreciably throughout the solum. However, other features such as strong structural development, a thick solum, and pronounced Fe losses from ped faces are suggestive of an advanced stage in soil genesis. In an effort to reconcile these seemingly discordant traits, micromorphology was employed. Thin illuvial clay coatings were identified to a depth of 3 m, with maximum expression in the lower Bt and upper BC horizons (120 - 220 cm). Continuously oriented argillans occur principally on or near well defined channels or ped faces presumably due to the dense nature of the clayey parent sediments (bulk density 1.7 to 1.9). In addition, roots were concentrated in these interpedal voids and gray redox-induced Fe oxide depletions were confirmed in them. Although the soil has been classified as a Paleudult, these diagnostic properties may have been largely inherited from the highly weathered and clayey parent material, rather than forming through intense and prolonged pedogenesis.

INTRODUCTION

This paper presents findings from two investigations. These comprise a broad reconnaissance study of reddish Cretaceous clay soils (Wagner, 1976) as well as follow-up efforts undertaken in 1991-92 that were directed specifically toward the micromorphology of a representative Cretaceous clay soil. Although an interpretation of soil genesis was among the principal goals of the initial characterization effort, the highly weathered nature of the parent material rendered the findings inconclusive. Examination of micromorphology was not
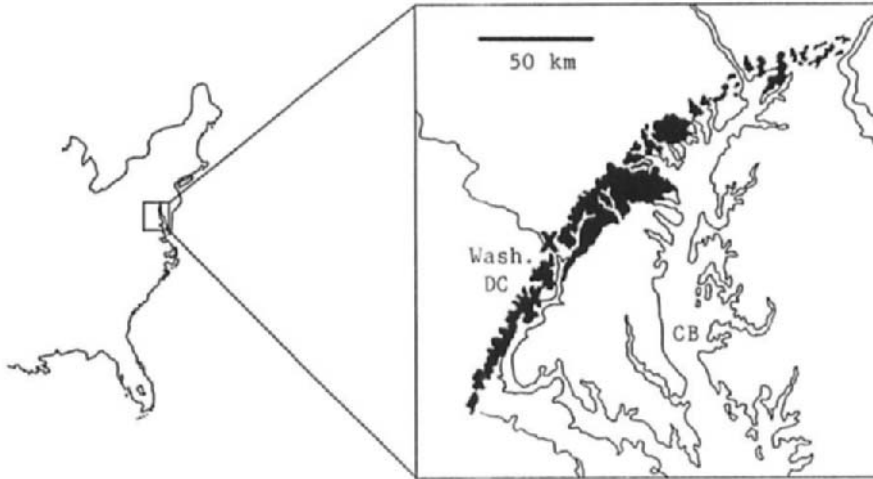
Fig. 1. Outcrop belt of Lower Cretaceous sediments defining the western limit of the Maryland Coastal Plain; metamorphic crystalline rocks of the Piedmont occur to the west. The deposits run through Washington, DC and near to Chesapeake Bay (CB). After Glaser (1969).

attempted in the earlier study, but was undertaken in the follow-up investigation in an attempt to more fully decipher the weathering history of a Cretaceous clay soil.

SOILS

Soils developed from reddish clays of Lower Cretaceous age are widespread throughout western portions of Maryland's Coastal Plain. Among the oldest of the unconsolidated deposits forming the Coastal Plain in the Mid-Atlantic region of the United States, Cretaceous sediments adjoin much more ancient metamorphic rocks of the Piedmont along an arc known as the "Fall Line". Historically important in the development of several major East Coast cities, this line marks the landward extent of navigable waters where flow patterns shift from sluggish Coastal Plain estuaries to tumbling, rock strewn rivers of the Piedmont. Despite these differences in geology and hydrology, upland landscapes on opposing sides of the line are markedly similar and display little topographic variation to distinguish the two physiographic provinces. Fig. 1 shows the distribution of Cretaceous sediments defining the western margin of the Coastal Plain.

Clayey Cretaceous sediments are considered to have been laid down in a fluvial-deltaic, subtropical environment in which clayey deposits were accumulated in shallow back swamp basins (Groot and Penny, 1960; Glaser, 1969). Much later Plio- Pleistocene fluvial systems then produced a discontinuous veneer of sand and gravel over much of the Coastal Plain (Schlee, 1957; Cooke, 1958), and these deposits, often partially reworked during the Holocene, commonly account for lithologic discontinuities in the upper levels of soils otherwise formed in Cretaceous clay sediments.

Cretaceous clay strata are fine-textured, dense, extremely acid (pH 4.5) and intensely weathered. The sediments typically contain about 40% clay and 35% silt, and have bulk densities ranging from 1.7 to 1.9 (Wagner, 1976). Mineralogical composition tends to reflect sediment source areas. As determined by mineralogy of gravel deposits, the headwaters of the Lower Cretaceous deltaic complex were mostly in the adjacent Piedmont, and less commonly extended to the more distant Appalachian Mountains (Cleaves, 1968; Glaser, 1969). Therefore, mineralogy of finer textured strata would presumably tend to resemble the predominant soils of the Lower Cretaceous Piedmont.

Some similarities between Piedmont and Cretaceous clay soils exist even today. Although most contemporary Piedmont soils are loamy-textured, clay mineralogy of the predominantly schist-derived soils is, like Cretaceous clays, dominated by mica and kaolinite. In addition, landscapes in both areas are likely to have similar weathering histories. Since the region is nearly 200 km south of the glacial boundary, soil ages could potentially extend well into the Pleistocene. However, Cretaceous clays are much more weathered than modern Piedmont soils. Even though both are reddish in colour, Cretaceous clay soils are more red (2.5YR versus 7.5YR) and have an average free Fe oxide content of about 4.5%, which is two to three times higher than most Piedmont soils. Also, whereas modern Piedmont soils may have combined feldspar and muscovite contents as high as 15 to 20%, weatherable mineral contents well below this level are more typical for Cretaceous clay deposits. Feldspars and muscovite account for about 6% of the silt fraction, but fall to less than 2% in the sand fraction (Rabenhorst, 1991).

Given the inherent properties of Cretaceous clay parent materials, pedogenic assessments of soil age and degree of development can rely on few of the normal developmental benchmarks. Such features as high clay content, low weatherable mineral content and high Fe content are characteristic properties of the sediments even before the initiation of soil genesis. These common indices demonstrate the degrees of soil development in both Piedmont and more coarse-textured Coastal Plain soils of the region. However, in the absence of discernible differences between sola and clayey parent materials, they do not adequately assess soil formation in previously weathered, fine-textured sediments.

Cretaceous clay soils such as the Christiana series are mainly classified as Paleudults due to uniform high clay content with depth. A Kandiudult classification would also be possible, but implications of extreme age and more intense weathering suggested by these great taxa may be inconsistent with the genesis of these soils. If some of the Cretaceous clay soils are indeed of extreme age, then indicators must be sought of prolonged weathering, other than those discussed above.

METHODS

A number of the reported results are taken from the Wagner (1976) study of Cretaceous clay soils. In that study soil profiles or parent materials were examined at 58 locations throughout the Cretaceous belt (Fig. 1). Laboratory analyses were focused primarily on five representative Christiana pedons to determine their main physical, chemical and mineralogical properties. From the five pedons analyzed in detail, one was chosen for the micromorphological analyses reported herein. The pedon, originally described and sampled in 1974, was re-sampled and a revised description compiled in 1991 (Table 1).

Table 1.
Description of a Christiana soil profile located in Beltsville, Maryland. The soil was classified as a clayey, kaolinitic, mesic Aquic Paleudult.

| Horizon	Lower depth, cm	Description
A	5	Very dark gray (10YR 3/1) to very dark grayish brown (10YR 3/2) fine sandy loam; weak, fine granular with weak, medium platy structure in the lower part of the horizon; friable; abrupt smooth boundary.
E	20	Yellowish brown (10YR 5/4 and 10YR 5/6) fine sandy loam; weak, medium to coarse platy structure; friable, clear, smooth boundary.
BE	32	Strong brown (7.5YR 5/6) to yellowish red (5YR 5/6) loam; common medium and fine yellowish brown (10YR5/6) mottles; weak, medium to fine subangular blocky structure; friable, clear, smooth boundary.
2Bt1	58	Yellowish red (5YR 4/6) clay loam; many medium distinct reddish brown (2.5YR 4/4), common medium distinct brown (7.5YR 5/4), and few fine distinct yellowish red (5YR 5/8) mottles; moderate, medium subangular blocky structure; firm; thin patchy clay films on ped faces; clear, smooth boundary.
2Bt2	80	Reddish brown (2.5YR 4/4) and red (2.5YR 4/6) clay; 5% fine distinct yellowish red (5YR 5/8) and strong brown (7.5 YR 5/8) mottles on ped faces; 15% medium and large prominent pinkish gray (7.5 YR 7/2) and light gray (10 YR 7/1) mottles on ped faces and root channels in ped interior; moderate to strong medium and coarse prismatic parting to moderate medium subangular blocky structure; very firm; thin, nearly continuous clay films on ped faces; gradual boundary.
2Bt3	102	Reddish brown (2.5YR 4/4) and red (2.5YR 4/6) clay; 25% prominent mottles of pinkish gray (7.5YR 7/2), light gray (10YR 7/1) and light reddish brown (5YR 6/3) mainly along ped faces; moderate coarse prismatic structure parting to moderate, medium to coarse subangular blocky and weak, medium and coarse platy structure; firm; thin nearly continuous clay films; gradual wavy boundary.
2Bt4	140	Red (2.5YR 4/6) clay; common prominent mottles of pinkish gray (7.5YR 7/2) to light gray (10YR 7/1) along ped faces, and common distinct mottles of strong brown (7.5YR 5/8) and yellowish red (5YR 5/6); moderate to weak, coarse and very coarse prismatic structure, parting to moderate to weak, medium and fine subangular blocky and weak, medium platy structure; firm; moderately thick continuous reddish brown (5YR 4/4) clay films on ped faces; gradual, wavy boundary.
2BC1	220	Red (2.5YR 4/6) ped interiors with reddish brown (2.5YR 4/4) faces; common large prominent light gray (10YR 7/1) mottles on ped faces; moderate to strong medium and fine subangular blocky structure with some moderate medium prismatic structure; very firm; common thin continuous clay films on ped faces; approximately 15% comprised of gently dipping (10%) bands of light gray (10YR 7/1) very fine sandy loam with few fine and medium distinct brown (7.5YR 5/4) and yellowish red (5YR 5/8 and 5YR 4/6) mottles; common continuous yellowish red (5YR 5/6) clay films on ped faces; wavy diffuse boundary.
2BC2	300	Fifty percent of horizon: red clay loam with colours and properties similar to horizon above; fifty percent of horizon: light gray (10YR 7/1) very fine sandy loam; the latter with approximately 40% yellow (10YR 7/6) mottling and 2% yellowish red (5YR 5/8) and strong brown (7.5 YR 5/8) clay films.
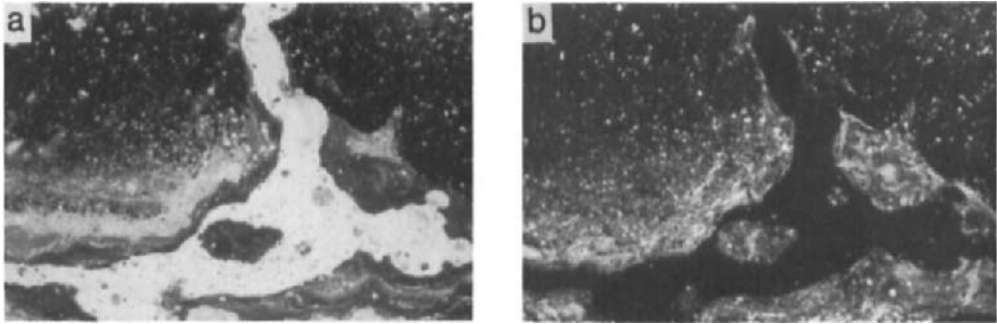
Fig. 2. Micrograph of the Bt4 horizon showing depletion of Fe oxides from a 1 mm zone at the ped face with Fe-rich materials remaining in the interior of the ped; note the presence of laminated illuvial clay coatings exterior to the zones of Fe depletion; frame length 5mm: a) plane polarized light; b) cross polarized light.

Particle size analyses were determined using the pipette method following dispersion with sodium hexametaphosphate. Free Fe oxide was measured using a dithionite-citrate-bicarbonate extraction. Elemental analyses of coarse and fine silt fractions were determined by X-ray fluorescence spectroscopy. Oriented air dried clods were impregnated under vacuum using a 60:40 mixture of polyester resin:styrene. After 2 weeks, the plastic was hardened using 5Mrads of γ radiation. Owing to the high density and low conducting porosity of the clayey samples, they were not well impregnated. Therefore, the cut blocks were surface impregnated with an epoxy resin to obtain an impregnated zone of sufficient thickness for thin section preparation.

RESULTS

The description of the Christiana soil profile given in Table 1 reveals several major features typical of soils formed in Cretaceous clay sediments. Upper horizons in these soils are often formed in a veneer of coarser materials that is occasionally thick enough to influence the taxonomic classification of the soil. In this case a sandy surface mantle constituting the upper 32 cm of the profile is readily distinguishable from the underlying Cretaceous clay. The 2Bt1 horizon beneath the surficial sands is partially influenced by mixing of the clay and overburden, but below this horizon's lower boundary at 58 cm depth the profile is entirely within Cretaceous clay.

Other than the fine textures of Cretaceous clay soils, perhaps the next most characteristic feature is the predominantly red (2.5YR 4/6) colour. Red colours typify subsoil horizons as well as deep sediments of the substrata, but, in striking contrast to the red matrix colour, prominent light gray (10YR 7/1) mottling is present in most soils. This mottling is normally concentrated along ped faces in the solum (Fig. 2). When gray colours are present in the substrata, they appear to be related to sediment rather than pedologic structure (Table 1, BC2 horizon). The light gray ped faces are apparently caused by localized reduction and loss of Fe in the solum and correspond to major avenues of root penetration (providing a C source for microbial reduction of Fe). In most soils the Fe stripping results from reducing conditions of

Fig. 3. Micrograph of the upper BC1 horizon showing zones of redox depletion which do not appear to be related to soil structural features; these are interpreted as inherited from the time of deposition or post-depositional diagenesis; frame length 5 mm; plane polarized light.

an epiaquic nature. Deeper in the soil, irregular zones of Fe oxide depletions (or absence) were identified which showed no relation to soil structure (Fig. 3). These gray zones are interpreted to be inherited from the time of deposition or during post-depositional diagenesis.

Free iron, with an average concentration of 4.7%, is abundant in the Cretaceous clay portion of the subsoil, and on a whole soil basis is nearly constant with depth. Iron is not, however, uniformly distributed within soil structural units. Analyses of samples separately collected from gray prism faces, red ped interiors well removed from faces, and brownish rinds transitional between the bleached faces and ped interiors, revealed Fe concentrations ranging from 0.32% to 5.48% and 2.53%, respectively (similar to Fig. 2). The data demonstrate a progressive loss of Fe from ped faces. Since the ped interiors away from the gray faces exhibit relatively uniform red colouration, there is little to indicate that localized reprecipitation occurs. The pedon appears to be undergoing a net loss of Fe.

The solum described is deep, extending beyond 3 m, and is somewhat thicker than the average Cretaceous clay soil. Field evidence of soil development at such depth relies mainly on structure and the presence of ped coatings tentatively identified as clay films. Very thin and superimposed against a clayey fabric, clay films are not readily verifiable in the field. Those most discernible are often at levels above Cretaceous clay horizons in coarse-textured surface mantles that have sufficient thickness and age to support argillic horizon development. Fig. 4 shows the cumulative distribution of particle size fractions with depth. The lithologic discontinuity at 32 cm depth as well as the zone of mixing extending to 58 cm are well marked by sand contents five to ten times higher than that of the underlying Cretaceous clay. Cretaceous clay materials normally have sand contents of less than 20%, with most of the sand concentrated in the very fine and fine fractions. Interestingly, the lowest 2BC2 horizon is distinctly higher in sand content, demonstrating that, even though this horizon is undoubtedly formed in Cretaceous materials, stratigraphic variability is a nearly unavoidable complicating factor in the interpretation of Coastal Plain soil genesis.

The distribution of clay content with depth again clearly defines stratigraphic changes in the profile, but within the 162 cm Cretaceous clay increment encompassing the 2Bt2 through 2BC1 horizons, clay content varies only slightly. Discounting differences attributable to either the upper lithologic discontinuity or the deep stratigraphic variability, no subsoil horizon in the Cretaceous clay shows a sufficiently high comparative clay increase to qualify clearly as argillic according to Soil Taxonomy (Soil Survey Staff, 1992). In addition, the fine clay content, even when compared in ratio with total clay, is virtually unchanged throughout the Cretaceous clay portion of the profile and does not indicate sufficient illuviation to document an argillic
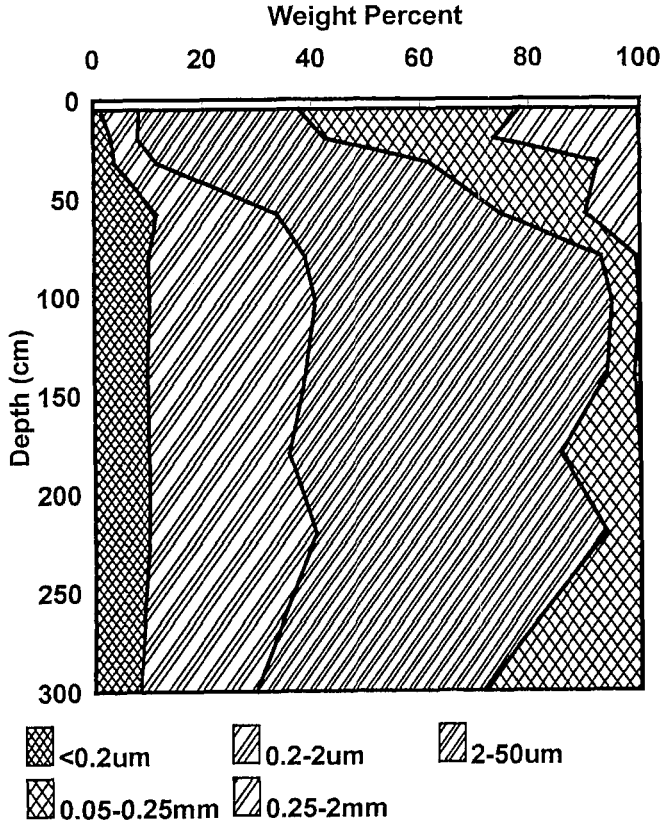
Fig. 4. Cumulative weight distribution of particle size fractions with depth in the Christiana soil profile derived from a thin (30 - 60 cm) mantle of sandier material overlying clayey Cretaceous sediments.

horizon. However, the pedon does meet textural requirements for a Paleudult because total clay content does not decrease from the maximum by more than 20% within 1.5 m of the top of the field-described argillic horizon. Micromorphological examination did reveal common illuvial clay coatings throughout the argillic horizon. The clay coatings were usually restricted to ped faces or occasional intrapedal conducting voids. They were commonly thin (<0.2 mm) (Fig. 5) although in portions of the lower Bt horizon, some laminar clay coatings were observed up to 0.6 mm in thickness (Fig. 2). These observations confirm that illuvial processes have been somewhat active during the pedogenic history of this soil. However, the magnitude of this process seems much less than might be expected for a clayey Paleudult with mixed mineralogy.

Elemental analyses of silt fractions were found to be inconsistent indices of soil weathering. As shown in Fig. 6, the profile distributions of Zr, Ca, K, and Ti in the coarse silt fraction provide mixed results. Whereas the upper discontinuity is readily apparent, the only weathering trends indicated in the Cretaceous clay are suggested by the distributions of K and

Fig. 5. Micrograph of a gray sandy stratum from the lower BC2 horizon showing thin (50 - 75 μm) well oriented coatings of illuvial clay lining pores; frame length 1.2 mm; circularly polarized light.

possibly Ti. Very low concentrations of Ca in these sediments may largely preclude any utility for Ca in this approach, and interpretations of K and Ti should be tempered with other findings by Wagner (1976). In that study of five Christiana profiles, no single elemental trend was consistently suggestive of deep weathering in all of the profiles. Most elemental distribution patterns were either erratic or even contrary to normal weathering trends. By and large, these appear to be better related to stratigraphic variation than to deep pedogenic weathering.

CONCLUSIONS

Clayey sediments of Cretaceous age are a widespread soil parent material along the western border of Maryland's Coastal Plain. These kaolinitic-illitic sediments were apparently derived from the erosion of soils in the adjacent Piedmont and are inherently highly weathered. Although commonly overlain by thin surficial mantles of much younger and more coarse-textured deposits, the major features of the Cretaceous sediments include clay textures, red colours, high Fe oxide contents and very low concentrations of weatherable minerals.

The main characteristics of the sediment similarly account for the dominant properties of soils formed in Cretaceous clay, but obvious pedological features are also exhibited by these soils that occupy landscapes potentially dating to the Pleistocene. Field features described in a Christiana soil include soil structure extending to depths of up to 3 m, thin ped coatings later confirmed to be of illuvial origin and prominent gray mottling derived from the reduction and loss of Fe from ped faces. Some of the Fe oxide segregations appear to predate pedogenesis and were probably associated with the original parent material. The soil is classified as a Paleudult due to uniform clay content with depth, but this was due primarily to the highly weathered and clayey nature of the parent material, rather than intense and prolonged pedogenesis.

REFERENCES

Cleaves, E.T., 1968. Piedmont and Coastal Plain geology along the Susquehanna Aqueduct, Baltimore to Aberdeen, Maryland. Maryland Geol. Survey Rept. Inv. 8, 45 pp.

Cooke, C.W., 1958. Pleistocene shore lines in Maryland. Geol. Soc. Amer. Bul., 10: 1-53.

Glaser, J.D., 1969. Petrology and origin of Potomac and Magothy (Cretaceous) sediments, Middle Atlantic Coastal Plain. Maryland Geol. Survey Rept. Inv. 11, 101 pp.

Groot, J.J. and Penny, J.S., 1960. Plant microfossils and age of nonmarine Cretaceous sediments of Maryland and Delaware. Micropalontology, 6: 225-236.

Elemental Analyses of Coarse Silt Fraction

Percent Zr and Ca
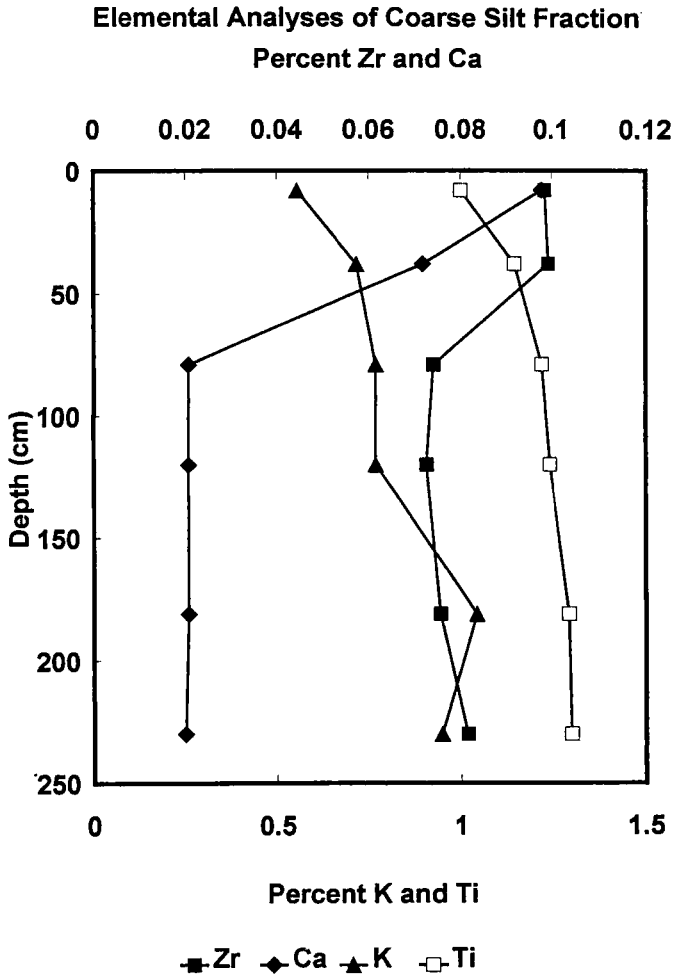
Fig. 6. Elemental analyses of the coarse silt fraction with depth in the Christiana soil profile.

Rabenhorst, M.C., 1991. Soils Data. In: Maryland Critical Loads Study, Vol. III. Input Data. Maryland Department of Natural Resources, Chesapeake Bay Research & Monitoring Div. Annapolis, MD, pp. 1-32.

Schlee, J., 1957. Upland gravels of Southern Maryland. Geol. Soc. Amer. Bul., 68: 1371-1410.

Soil Survey Staff, 1992. Keys to Soil Taxonomy. 5th editon. SMSS Tech. Monogr. no. 19. Pocahontas Press, Blacksburg, Virginia.

Wagner, D.P., 1976. Soils Associated with the Reddish Cretaceous Clays of Maryland. M.S. Thesis. Univ. Maryland, College Park.

This Page Intentionally Left Blank

Micromorphological interpretation of redox processes in soils derived from triassic redbed parent materials

M.P. Elless[1] and M.C. Rabenhorst[2]
[1]Oak Ridge National Laboratory, Oak Ridge, TN, USA
[2]University of Maryland, College Park, MD, USA

ABSTRACT

Elless, M.P. and Rabenhorst, M.C. 1994. Micromorphological interpretation of redox processes in soils derived from triassic redbed parent materials. In: A.J. Ringrose-Voase and G.S. Humphreys (Editors), Soil Micromorphology: Studies in Management and Genesis. Proc. IX Int. Working Meeting on Soil Micromorphology, Townsville, Australia, July 1992. Developments in Soil Science 22, Elsevier, Amsterdam, pp. 171-178.

There are problems assessing the degree of wetness of soils derived from certain red parent materials because they resist formation of field-identifiable redoximorphic features. Such soils occur within the Triassic Culpeper Basin, found in the Piedmont physiographic province of the Mid-Atlantic region of the USA. A micromorphological examination of soils along two topohydrosequences within this area was conducted to evaluate microscopic redoximorphic features. Distinct nodules of iron and manganese oxides were observed in the Ap horizons of somewhat poorly and poorly-drained soils. Redox driven depletions of iron oxides commonly occurred behind (subjacent to) argillans in horizons associated with a seasonally high water table. Within the better-drained soils, the iron oxides appeared to remain more evenly dispersed throughout the matrix. However, segregation of manganese oxides as stains occurred within the matrix or upon shale and sandstone fragments in the lower solum of the better-drained soils. This indicates that the redox conditions in these horizons become sufficiently reducing to mobilize manganese but not iron.

INTRODUCTION

There are problems assessing the degree of wetness of soils derived from certain red (2.5YR to 5YR 3/4 or 4/4) parent materials because they resist formation of field-identifiable redoximorphic features. The inhibition of gleying of red Triassic sediments was recently demonstrated in a three-month incubation study involving red C-horizon material derived from red shale and using glucose as a C source for microbes (G. Niroomand and J.C.F. Tedrow, pers. comm., 1991). The inhibition of such soils and sediments against the formation of distinct redoximorphic features may lead to erroneous interpretations for a variety of purposes.

In Maryland, such red sediments occur in the Triassic Culpeper Basin. This basin is one member in a series of Triassic-aged basins which occur in the Mid-Atlantic region of the USA (Fig. 1). These basins formed as a result of tensional forces created during the breakup of the supercontinent Pangaea II at the start of the Triassic Period (Levin, 1978). Alluvial sediments subsequently infilled each basin, resulting in the occurrence of sandstones, siltstones, and
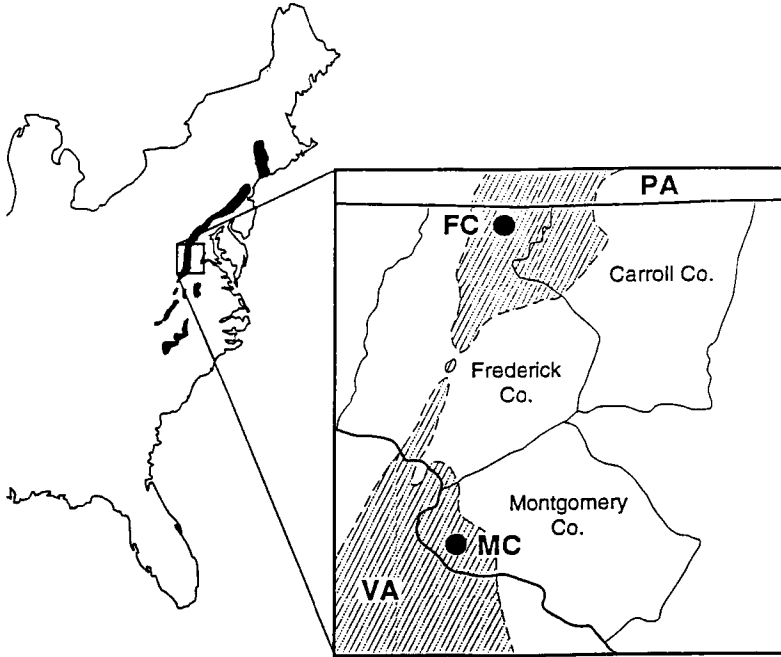
Fig. 1. Location of Triassic basins occurring along the Mid-Atlantic region of North America and location of sample sites (FC and MC) within the Culpeper basin of Maryland. (After Levin 1978).

shales. A reconnaissance survey showed the dominant geologic parent material of this basin was dusky red (2.5YR to 5YR 3/4 or 4/4) shales with lesser amounts of fine-grained sandstones.

Because the development of redoximorphic features appears to be inhibited in these soils, the objective of this research is to determine the nature of redox-driven pedogenic processes from examination of microscopic features.

MATERIALS AND METHODS

Two representative topohydrosequences (THS) were selected for study within the Triassic Culpeper Basin in Maryland. One THS was located in Montgomery County (MC) and the other THS was located in Frederick County (FC)(Fig. 1). Along these THS, eleven pedons were examined. Each pedon was classified according to Soil Taxonomy (Soil Survey Staff, 1990). Detailed soil descriptions are given in Elless (1992). Field moist Munsell colours were recorded for soil matrices, mottles and coatings. Precipitation for both sites is evenly distributed throughout the year in this region. However, a "wet" season is noted during winter and early spring when precipitation exceeds evapotranspiration.

Table 1.
Classification and landscape element of each pedon of both topohydrosequences.

Pedon	Landscape Element	Classification*
MC5	Summit	coarse-loamy Alfic Hapludult
MC4	Upper Backslope	fine-loamy Aquic Fragiudalf
MC3	Lower Backslope	fine-loamy Aeric Fragiaqualf
MC2	Footslope	fine-loamy Typic Fragiaqualf
MC1	Toeslope	fine-loamy Typic Ochraqualf
FC5	Summit	fine-loamy Ultic Hapludalf
FC4	Upper Backslope	fine-loamy Typic Eutrochrept
FC3	Lower Backslope	fine-loamy Aquic Hapludult
FC2	Footslope	fine-loamy Aquic Fragiudalf
FC1A	Lower Footslope	fine Aeric Fragiaqualf
FC1	Toeslope	fine Ultic Ochraqualf

*All soils have mixed mineralogy and occur in the mesic soil temperature regime.

To determine the hydrological status of soils along each THS, a combination of both open boreholes and water table wells was installed near to where each pedon was described and sampled. Water table levels were recorded in each well on a biweekly basis from September 1, 1989 to August 31, 1991.

Undisturbed, oriented clods were sampled from each horizon in every pedon. Following air-drying, oriented clods were impregnated under vacuum using a 60:40 polyester:styrene mixture. After 1-2 weeks, the impregnated clods were hardened using a 5 Mrad dose of γ-radiation. Horizontal and vertical thin sections were prepared and described according to Bullock *et al.* (1985). Other laboratory determinations included particle-size analyses by the pipette method (Gee and Bauder, 1986) and extraction of Fe/Mn oxides using both sodium dithionite citrate buffer (DCB) (Kittrick and Hope, 1963) and acid ammonium oxalate in the dark (Schwertmann, 1964). Iron and manganese were determined in all extracts by atomic absorption spectroscopy.

RESULTS AND DISCUSSION

Soil Classification and Hydrology

The classification and landscape element of the soils along both THS are given in Table 1. These soils tend to be high base-status soils and are generally fine-loamy to fine within the particle size control section. With the exception of pedon FC4, argillic horizons were observed in all pedons of both THS. Internal drainage is restricted during the "wet" season in more poorly-drained soils of each THS either by argillic horizons or fragipans which commonly occur. This seasonal perching of the water table promotes the development of redoximorphic features above these water-restricting layers.

Results of the hydrological investigation demonstrate similar hydrological characteristics among the more poorly-drained pedons of the FC site (FC1 and FC2), namely a high frequency
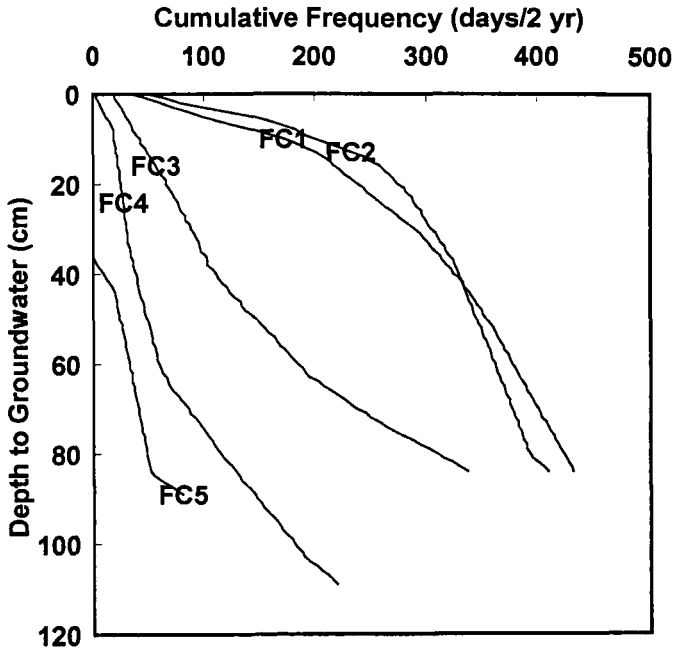
Cumulative Frequency (days/2 yr)

Fig. 2. Cumulative frequency curves of the water table heights associated with the pedons of the Frederick County (FC) Maryland site as observed between Sept. 1989 and Aug. 1991.

of upper sola saturation and a long duration of the water table within their profiles (Fig. 2). As expected, the hydrology of the better-drained pedons (FC3, FC4, and FC5) show a lower frequency of saturation in the upper sola and a shorter duration of the water table within the profile of these soils. Similar results were observed for the MC site pedons. Perched water tables (overlying argillic horizons and/or fragipans) were observed during the monitoring of the wells, particularly during the warmer and drier portions of the "wet" season.

Redox Depletion Features

Low chroma (≤ 2) mottles and low chroma matrix colours (gleying) were observed mainly in the soils in lower landscape positions or in lower soil horizons. Grey (2.5Y 5/2) prism faces are commonly observed in fragipans and argillic horizons which retain reddish colours of the parent materials in the prism interiors. As expected, these depletion features contain less Fe_d and Mn_d than the redox concentration features (Table 2). The iron oxides which remain are rather poorly crystalline ($Fe_o/Fe_d=0.27$). In the field, clay films (2.5Y 6/2 to 5Y 6/1) were also observed along the same grey prism faces in B horizons. Therefore, there was a question as to whether the grey colours on the ped faces were due to a redox-induced depletion of Fe oxides from the red hematitic soils or whether the grey colours were simply due to the illuviation of grey clays which previously had been depleted in Fe. Fig. 3a shows a section through a ped face from an argillic horizon. The ped interior remains pigmented with Fe oxides but has been depleted in Fe oxides around the exterior of the ped. Also in this Fe-depleted zone, illuvial clay coatings have been identified which are relatively low in Fe oxides. This indicates that the grey ped faces have in fact been altered by reduction and depletion of Fe oxides and are not simply the result of illuvial coatings of grey clay. These depleted zones, however, are rather

Table 2
Mean and standard deviation (sdv) values for iron and manganese in redoximorphic features of various colours collected from soils of both topohydrosequences.

Feature		Fe_d	Fe_o	Mn_d	Fe_o/Fe_d	Colours
				g/kg		
Fe/Mn Nodules	mean	97.9	29.7	39.6	0.32	N 2/0
(n=9)	sdv	32.6	9.2	15.3	0.10	
Black Stains	mean	27.3	4.6	8.6	0.17	N 2/0 - N 3/0
(n=4)	sdv	8.4	1.8	3.2	0.22	
Brown Redox	mean	24.9	2.6	0.0	0.08	10YR - 7.5YR hues and
Concentration	sdv	16.5	3.6	0.1	0.07	chroma $\geq$3
Features (n=19)						
Red Redox	mean	30.2	2.2	0.2	0.07	5YR - 2.5YR hues and
Concentration	sdv	14.3	1.5	0.4	0.04	chroma $\geq$3
Features (n=19)						
Redox Depletion	mean	10.4	1.7	0.0	0.27	varying but typically grey or
Featureas (n=19)	sdv	7.3	2.1	0.1	0.52	pale brown with yellowish hues (7.5YR - 5Y) and/or chroma $\leq$3

thin and rarely exceed 0.5 mm in thickness. Further confirmation that the hematite within these soils does become reduced is found in Fe oxide depleted exteriors of shale fragments (Fig. 3b).

Redox Concentration Features

Three types of redox concentration features were observed in these soils, namely rounded Fe/Mn nodules, high chroma ($\geq$4) matrices and mottles, and black Mn stains and hypocoatings. The rounded Fe/Mn nodules were observed in the somewhat poorly to poorly-drained pedons (MC1, MC2, MC3, FC1, FC1A, FC2) where reducing conditions frequently occur. The nodules occurred primarily at the Ap/Bt boundary at depths ranging from 22 to 25 cm in pedons MC1, MC2, and MC3 and from 25 to 33 cm in the pedons FC1, FC1A and FC2. These nodules exhibited a black colour (N 2/0) and varied in both size (0.5 to 10 mm in diameter) and abundance (up to 10% by horizon volume). Although these nodules may be interpreted as relict features which had formed in the B horizon and are now lag gravels, the current hydrological/morphological characteristics of both THS also favour the development of such nodules. The underlying argillic horizon perches the water table within the OM-rich plough layer during a saturation episode. The restricted drainage is thought to induce reduction of the metal oxides and mobilization of the Fe and Mn, while at the same time preventing the mobile metals (especially Mn) from being leached from the system. Therefore, the reduced iron and manganese are vulnerable to reoxidation and reprecipitation during the next drying episode. Successive wetting/drying episodes apparently cause segregation and favour formation of such nodules. The formation of Fe/Mn nodules has been reported under similar situations of restricted internal drainage conditions over other types of parent materials (Schwertmann and Fanning, 1976; Richardson and Hole, 1979).
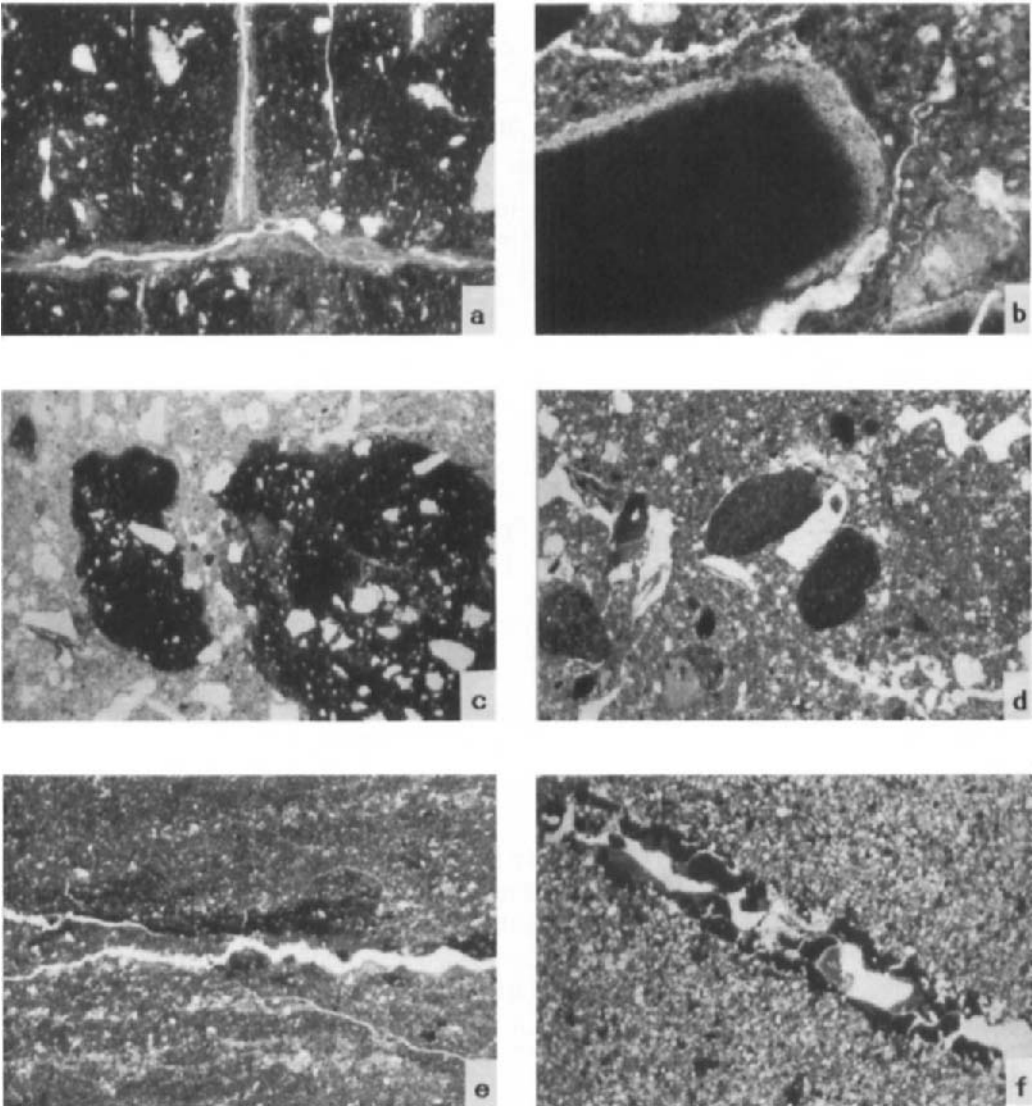
Fig. 3. Micrographs (plane polarized light; frame lengths 2.5 mm except 3b which is 1.2 mm) of:
a) ped faces in an argillic horizon (Bt2, 54-74 cm) of pedon FC1A showing lighter zone of Fe oxide depletion adjacent to the ped faces;
b) Fe oxide depletion from the outer rim of a shale fragment in the 2Bx horizon (74-158 cm) of pedon FC1A;
c) typic orthic Fe/Mn nodules from the Ap horizon of pedon MC2 showing undifferentiated internal fabric and protruding framework sand grains;
d) dark shale fragments from the Ap horizon (0-19 cm) of pedon FC4, which can be confused in the field with orthic nodules, showing absence of framework sand grains;
e) Mn hypocoatings adjacent to ped face in the 2BCt1 horizon (110-132 cm) of pedon FC5;
f) black Mn coatings along conducting channel which has been coated with laminated illuvial clay in 3BCt2 horizon (132-158 cm) of pedon FC5.

The nodules possessed very high levels of DCB extractable Fe (Fe_d) and Mn (Mn_d) (Table 2). They also had high oxalate extractable iron (Fe_o) and Fe_o/Fe_d ratios, which indicates that the iron oxides are poorly crystalline, probably due to their development under alternating wet/dry conditions and the higher organic matter content in the horizons where they form. The nodules were typic and possessed an undifferentiated fabric. They were interpreted to be orthic because the distribution of sand-sized framework grains within the nodules was the same as that in the surrounding matrix (Bullock *et al.*, 1985) (Fig. 3c). In addition, framework grains were observed protruding from the edges of the nodules, which would have been unlikely to survive transport. Features which appear similar by field examination were observed in the A horizons of better drained soils. However, when examined in thin section, it was evident that these dark coloured, sand-sized features lacked the framework sand grains of the surrounding matrices and were in fact Fe oxide-rich shale fragments rather than redox-induced concentrations of Fe and Mn (Fig. 3d).

Other redox concentration features include: a) high chroma (≥ 4) mottles in a brown or grey matrix, b) high chroma matrix which contains low chroma mottling, and c) black, neutral-hued manganese stains. In this order, these three features are commonly observed in the toeslope, backslope, and shoulder positions in both THS, respectively. In horizons with a low chroma matrix which overlie a water-restricting layer (*i.e.* gleyed argillic horizons overlying red fragipans in pedons MC1, MC2, and FC1), brown or red high chroma mottles typically occur in the ped interiors. Because conditions which favour pedogenic hematite formation, such as pH 7 to 8 (Schwertmann and Taylor, 1989), are absent within these soils, the red and brown mottles represent remnants of formerly coloured matrices rather than metal oxide concentrations formed from the reprecipitation of previously reduced iron in a more oxygenated zone. Soils with brown or red matrices and low chroma mottling typically occur in those horizons which experience saturation/reduction episodes too limited to cause gleying of the horizon (*i.e.* fragipans having gleyed prism faces in pedons MC3, MC4, FC1A, and FC2). Black Mn stains typically occur in the lower sola of the better drained (moderately well) soils (pedons MC4, FC3, and FC4). This indicates that the redox conditions in these horizons become sufficiently reducing to mobilize Mn but not Fe. These three types of redox concentration features had similar levels of Fe_d (Table 2). The black Mn stains possessed higher Fe_o levels which resulted in a higher Fe_o/Fe_d ratio. Significant Mn_d levels were found only within the black stains.

The Mn stains may also exist as hypocoatings on ped faces and occur commonly in lower horizons where solubilized Mn moves toward the ped surface through moisture or diffusion gradients (Fig. 3e). Fig. 3f illustrates the accumulation of Mn oxides as coatings which have been subsequently covered by illuvial clay. This suggests that the mobilization of Mn may occur early in the genesis of these soils, prior to the transport and accumulation of clay during argillic horizon formation.

CONCLUSIONS

Experience of field soil scientists and recent experimental work has shown that soils formed in the red Triassic parent materials are less apt than other soils to express redox-induced low chroma colouring. While low chroma colours do not form as readily, this study has identified redox segregations in soils formed in these parent materials. In the more poorly drained soils these features occur principally as orthic typic nodules and as Fe depletions near conducting

voids. In better drained soils, Mn coatings and hypocoatings are common in lower horizons where Fe does not seem to be mobile. Additional correlative work is necessary in order to properly interpret the hydrology of these soils from the redox-induced segregations.

REFERENCES

Bullock, P., Fedoroff, N., Jongerius, A., Stoops, G., and Tursina, T., 1985. Handbook for Soil Thin Section Description. Waine Research Publications, Wolverhampton, U.K., 152 pp.

Elless, M.P., 1992. Morphology, mineralogy, and hydrology of soils in the Triassic Culpeper Basin of Maryland. Ph.D. Diss. Univ. of Maryland, College Park (Diss. Abstr. 92-34559).

Gee, G.W. and Bauder, J.W., 1986. Particle-size analysis. In: A. Klute (Editor), Methods of Soil Analysis. Part 1. Second Edition. Agronomy, 9: 383-412.

Kittrick, J.A. and Hope, E.W., 1963. A procedure for the particle size separation of soils for XRD analysis. Soil Sci., 96: 319-323.

Levin, H.L., 1978. The Earth Through Time. W.B. Saunders, Philadelphia, Pennsylvania, 530 pp.

Richardson, J.L. and Hole, F.D., 1979. Mottling and iron distribution in a Glossoboralf-Haplaquoll hydrosequence on a glacial moraine in northwestern Wisconsin. Soil Sci. Soc. Am. J., 43: 552-558.

Schwertmann, U., 1964. Differenzierung der eisenoxide des bodens durch photochemische extraktion mit saurer ammoniumoxalate-losung. Z. Pflanzenernahr. Dueng. Bodenk., 105: 194-202.

Schwertmann, U. and Fanning, D.S., 1976. Iron-manganese concretions in hydrosequences of soils in loess in Bavaria. Soil Sci. Soc. Am. J., 40: 731-738.

Schwertmann, U. and Taylor, R.M., 1989. Iron Oxides. In: J.B. Dixon and S.B. Weed (Editors), Minerals in Soil Environments. Second Edition. Soil Sci. Soc. Am., Madison, Wisconsin, pp. 379-438.

Soil Survey Staff. 1990. Keys to Soil Taxonomy, 4th edition. SMSS Technical Monograph no. 6. Virginia Polytechnic Institute and State Univ., Blacksburg, Virginia.

Micromorphology of spodic horizons in a Psamment - Aquod toposequence on the Atlantic coastal plain of Maryland, U.S.A.

M.A. Condron[1] and M.C. Rabenhorst[2]
[1] Office of Surface Mining and Reclamation, Denver, CO, USA
[2] University of Maryland, College Park, MD 20742, USA

ABSTRACT

Condron, M.A. and Rabenhorst, M.C., 1994. Micromorphology of spodic horizons in a Psamment - Aquod toposequence on the Atlantic coastal plain of Maryland, U.S.A. In: A.J. Ringrose-Voase and G.S. Humphreys (Editors), Soil Micromorphology: Studies in Management and Genesis. Proc. IX Int. Working Meeting on Soil Micromorphology, Townsville, Australia, July 1992. Developments in Soil Science 22, Elsevier, Amsterdam, pp. 179-186.

Micromorphological features were examined in soils with spodic horizon characteristics along two topo-hydrosequences on the coastal plain of Maryland, U.S.A. The soils were classified according to Soil Taxonomy as (siliceous, mesic,) Typic Quartzipsamment, Typic Endoaquod, and Typic Alaquod. Better drained soils showed evidence of clay translocation in B and BC horizons through thin clay coatings on grains and in voids. Somewhat poorly drained transitional soils contain polymorphic organic-sesquioxide material in the voids of the spodic horizon. The upper zone of spodic horizons in the very poorly drained soils had enaulic-gefuric related distribution with aggregates of organic material in the voids; the lower zones had gefuric-chitonic related distribution with cracked monomorphic coatings on grains. Weak clay orientation around grains in some spodic horizons implies that podzolization took place after an earlier episode of clay translocation.

INTRODUCTION

On the Coastal Plain of Maryland, U.S.A. soils with spodic horizon morphology have formed in late Pleistocene or early Holocene dune deposits in areas which have seasonally high water tables.

A study of the genesis of spodic horizon formation was undertaken in soils along two topo-hydrosequences in the Pocomoke State Forest on the coastal plain of the Delmarva Peninsula in Eastern Maryland, U.S.A (Fig. 1). The study area has a humid temperate climate with an annual rainfall of 1250 mm per year and an average annual air temperature of 13.7° C. The predominant vegetation is Loblolly pine (*Pinus taeda*) with a greenbrier (*Smilax rotundifolia*) understory.

Soils with spodic horizons have been studied extensively and a combination of chemical, morphological and microscopic features have been used as criteria to classify spodosols. Sodium pyrophosphate extracts humic and fulvic acids and organic aluminum complexes. Ammonium oxalate extracts aluminum and iron organic complexes and poorly crystalline minerals. The optical density of oxalate extracts (ODOE) at 430 nm (Daly, 1982) is an
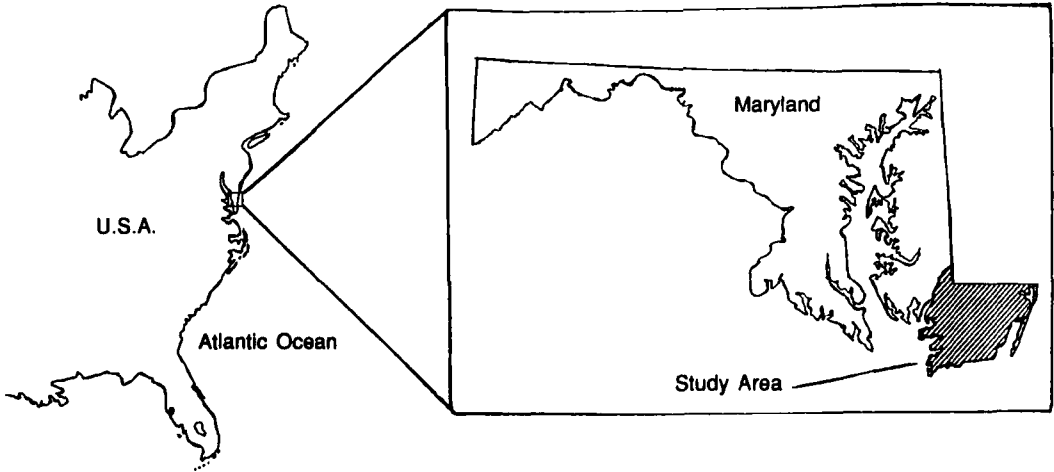
Fig. 1. Locations of study area and sampling sites in Maryland, U.S.A.

indicator of translocated organic material. Dithionite citrate bicarbonate (DCB) is used as an extractant of organically complexed iron and aluminum, amorphous aluminosilicates and noncrystalline hydrous oxides. Another procedure, NaF pH is used to estimate the presence of paracrystalline and noncrystalline materials in the soil. NaF pH $\geq$ 9.4 is considered a strong indicator that amorphous material dominates the exchange complex.   The main features which have been noted in micromorphological studies of spodic horizons are monomorphic, a continuous mass with uniform colour and density, and polymorphic, a discontinuous mass with variable colour and density.   Cracked coatings found on grains in spodic horizons are considered to be composed of translocated organic matter, aluminum and iron.   Another feature often found in spodic horizons is a pellety microstructure (McKeague *et al.*, 1983; McSweeney and FitzPatrick, 1990).

This paper, which is part of a larger study of pedogenic processes in soils along two topo-hydrosequences, focuses on the micromorphological features of the soils and their varying degrees of spodic horizon expression.

METHODS

Site Description and Sampling

A topographic transect representing the soil morphology and sequence of drainage classes at one of the study sites is shown in Fig. 2. Chemical data from three pedons at both sites are given in Table 1. These pedons were chosen because each represents the different degrees of spodic horizon development found in the toposequences, ranging from no expression to strongly expressed. They also represent a range of drainage classes from excessively drained in the summit position to very poorly drained in the depressional footslope position.

Transects were run along two topo-hydrosequences in the Pocomoke State Forest, Maryland. Groundwater monitoring wells made of perforated PVC pipes (7.6 cm diameter)
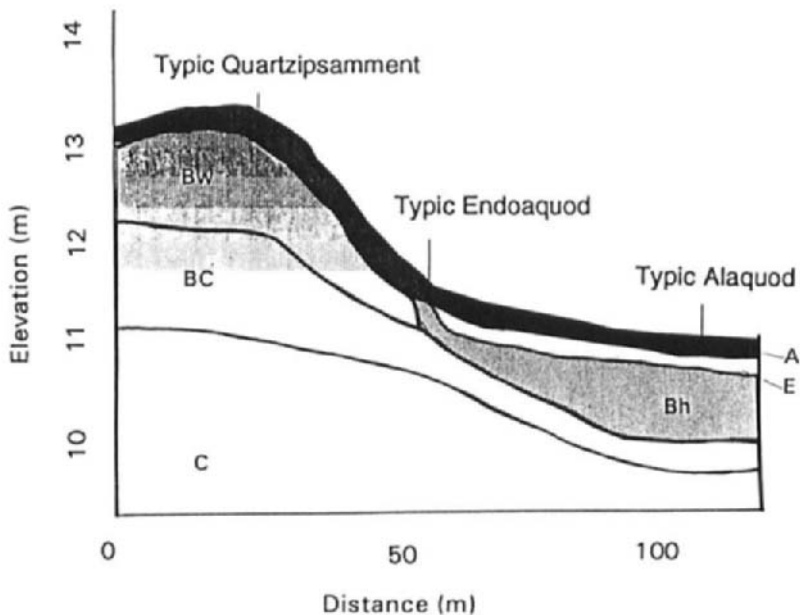
Fig. 2. Locations and classifications of three pedons along the transect at Study Site 2, Atlantic Coastal Plain, Maryland, U.S.A.

were placed along the transects, and the depth of the ground water from the soil surface was measured using a weighted wire connected to an electronic multitest meter. Pits were opened adjacent to five wells at Site 1 and four wells at Site 2, and the pedons were described and sampled using standard SCS procedures (USDA Soil Conservation Service, 1992).

The relation between landscape position and water table depth appears to be an important influence on the formation of spodic horizons in the soils at both sites. The soil in the highest landscape position is at the summit of a dune formation. The water table is deeper than 159 cm in this soil, and there is no evidence of spodic horizon development. In both transects spodic horizon morphology starts to appear in the lower landscape positions where the water table comes closer to the surface (29 - 48 cm). The most strongly expressed spodic horizons are in the lowest landscape positions (depressional footslope) where the water table is at the soil surface or above during the wet season (Condron, 1990).

Analytical Methods

Thin sections were prepared from air dried, undisturbed clods and were described according to Bullock *et al.* (1985). A 60:40 solution of Castolite and styrene was used to impregnate the clods which were then hardened using 5 Mrad of gamma radiation. Sections were cut from the clods, mounted on glass slides with epoxy and ground to approximately 30 microns.

Table 1
Chemical data from three pedons representing different degrees of spodic horizon expression,
Atlantic coastal plain, Maryland.

Horizon	Depth	Fed	Fep	Feo	Ald	Alp	Alo	Ct	Cp	ODOE	pH (NaF)
	(cm)				(g/kg)						
Tyic Quartzipsamment, Site 2											
Oe	1-0										
A1	0-9	0.4	0.2	0.2	0.1	0.2	0.1	7.3	1.1	0.010	7.70
A2	9-20	1.6	0.6	0.5	0.3	0.5	0.4	4.2	1.4	0.008	8.12
BA1	20-44	2.2	0.7	0.4	0.8	0.8	0.9	2.2	0.8	0.013	9.70
BA2	44-69	3.0	0.7	0.3	0.6	0.6	0.5	2.2	0.8	0.017	6.90
Bw	69-98	4.5	1.1	0.5	0.8	2.6	0.8	1.0	0.6	0.020	9.12
CB1	98-149	1.0	0.2	0.1	0.1	0.4	0.2	0.3	0.2	0.011	7.95
CB2	149-194	1.2	0.3	0.1	0.1	0.5	0.3	0.3	0.3	0.008	8.05
C1	194-249	1.2	0.3	0.1	0.1	0.3	0.2	0.3	0.3	•0.008	8.00
C2	249-284	1.0	0.2	0.1	0.1	0.3	0.2	0.0	0.3	0.007	8.10
C3	284-313	1.3	0.4	0.4	0.1	0.3	0.2	0.4	0.3	0.009	8.20
C4	313-354	1.1	0.4	0.3	0.1	0.3	0.2	0.2	0.3	0.008	8.20
Typic Endoaquod, Site 2											
Oe	4-0										
A	0-7	1.3	0.8	1.2	0.3	0.4	0.3	11.9	2.6	0.047	7.75
Ap	7-15	1.8	1.2	1.8	0.7	1.1	0.7	11.8	4.9	0.083	8.10
Bh	15-26	3.3	2.4	2.8	3.2	4.8	4.5	13.4	7.7	0.136	11.05
Bs	26-39	4.2	2.4	2.9	2.1	3.0	3.6	4.8	2.8	0.032	10.65
BC1	39-53	3.2	1.7	1.9	1.3	1.8	1.8	1.6	0.8	0.012	9.70
BC2	53-91	6.6	2.9	1.1	1.9	5.5	1.0	1.2	0.4	0.011	9.55
C1	91-105	0.4	0.2	0.1	0.0	0.1	0.0	0.0	0.0	0.007	8.05
Typic Alaquod, Site 1											
Oe	6-0										
A	0-22	0.3	0.2	0.2	0.3	0.6	0.4	21.1	7.2	0.014	6.95
E	22-50	0.0	0.0	0.0	0.0	0.0	0.0	1.8	1.0	0.008	7.70
Bh1	50-58	0.1	0.1	0.1	2.7	4.4	3.2	35.4	25.7	0.801	7.82
Bhsm	58-81	0.1	0.2	0.2	4.8	7.5	5.5	28.0	25.0	0.748	11.14
Bh2	81-114	0.1	0.0	0.0	0.7	3.7	0.8	9.5	7.7	0.221	7.65
Bh3	114-164	0.0	0.0	0.0	0.4	0.8	0.5	6.2	5.5	0.110	7.95
Bhs	164-209	0.0	0.0	0.0	0.4	0.7	0.5	4.2	4.2	0.101	8.45
Bs	209-254	0.0	0.0	0.0	0.6	0.8	0.7	4.2	4.4	0.132	9.33
BC	254-290	0.0	0.0	0.0	0.2	0.6	0.4	1.8	2.2	0.040	9.05

Samples for chemical analyses were air dried, crushed and passed through a 2 mm sieve.
Organic C was measured by dry combustion. Fe and Al were extracted using sodium

pyrophosphate (Method 6C5, USDA Soil Conservation Service, 1992), dithionite citrate bicarbonate (Fanning *et al.*, 1970) and ammonium oxalate (McKeague and Day, 1966), and measured by atomic absorption spectroscopy. Pyrophosphate C was determined with a Dohrmann Carbon Analyzer. Duplicate extractions of each sample were made and reported as averages. Optical density of oxalate extract (ODOE) was read with a spectrophotometer (Method 8J, USDA Soil Conservation Service, 1992). Whole soils were treated with NaF to estimate the presence of paracrystalline and noncrystalline materials in the soil (Method 8C1d, USDA Soil Conservation Service, 1992).

RESULTS

Psamments

The soil in the summit position, a Typic Quartzipsamment (Soil Survey Staff, 1992), has a thin A horizon which, in thin section, has gefuric related distribution with few organic aggregates in voids and on mineral grains. Fungal hyphae and root tissue are present. Quartz is the dominant mineral with a few weathered grains of microcline and plagioclase. There is no evidence of spodic horizon development, but there are indications of clay illuviation. In the B horizon the related distribution is chitonic with thin clay coatings occurring on sand grains (Fig. 3a). The upper walls of the voids are more thinly coated than the lower walls and a few voids have crescentic coatings. Although field observations suggested this profile has a Bt horizon, particle size analysis revealed that the clay increase in the horizon was insufficient to be an argillic horizon.

Endoaquods

The soil in the lower backslope position (a Typic Endoaquod) is an example of a transitional soil which has a weakly expressed spodic horizon. In the field the spodic horizon was seen to be thin, though continuous, with some reddish, brittle zones. Fe and Al are present in measurable amounts in all three extractants, and pyrophosphate-extractable C is greatest in the spodic horizon. The micromorphology of the A horizon is similar to that in the soil on the summit position, but the related distribution and other features of the B horizon are characteristic of spodic horizons. The upper part of the B horizon has enaulic related distribution with polymorphic material forming intergranular aggregates in voids and occasionally coating grains. The related distribution pattern in the lower zone of the spodic horizon is chitonic. Organic material appears as coatings (not cracked) around grains rather than as aggregates.

Alaquod

The soil in the depressional footslope position (a Typic Alaquod, Soil Survey Staff, 1992) is very poorly drained and has an umbric epipedon with an organic carbon content almost triple the amount in the surface horizon of the excessively drained Typic Quartzipsamment. In thin section the A horizon has enaulic related distribution with aggregates of black polymorphic organic material in the voids and as coatings on some grains. The E horizon is grayish and
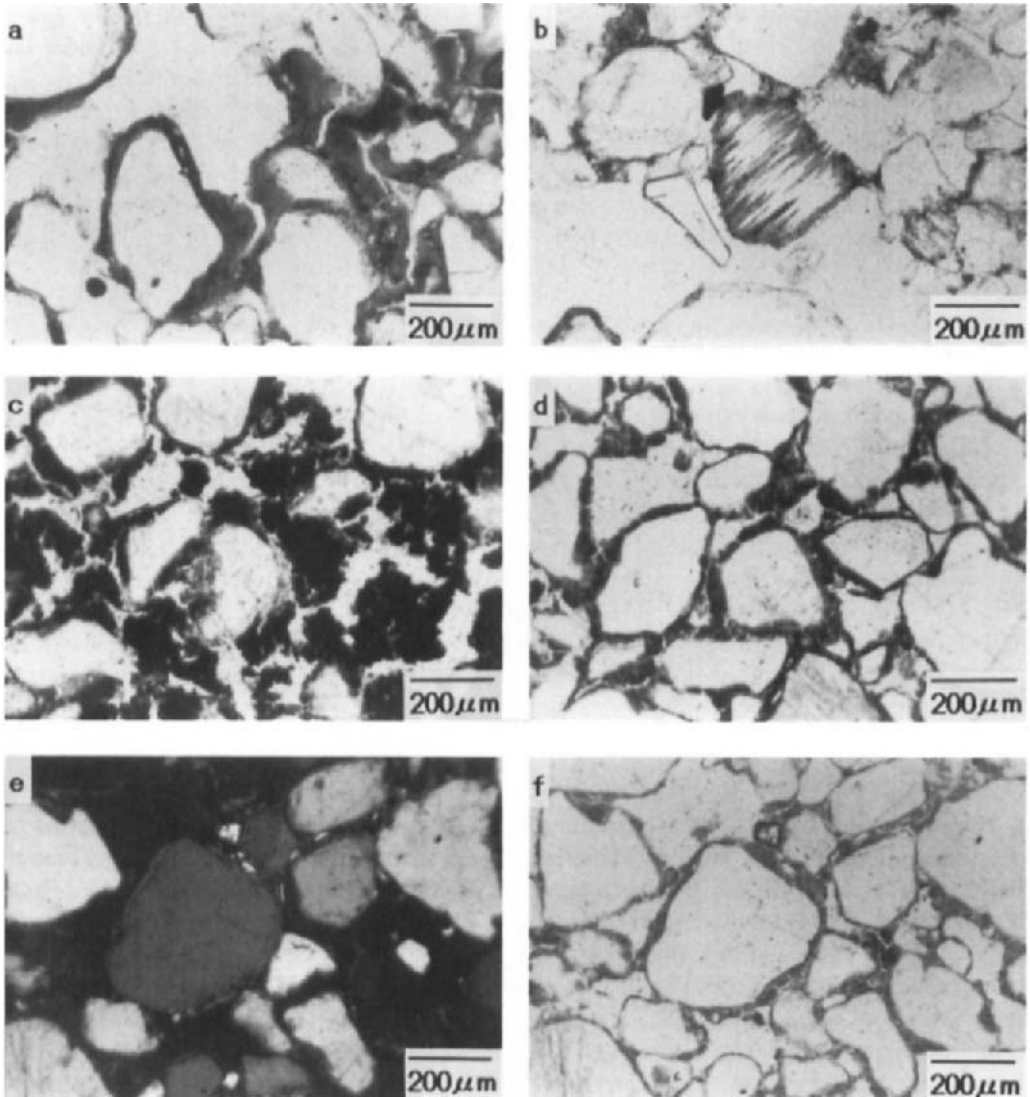
Fig. 3. Micrographs of: a) Typic Quartzipsamment, Bt horizon, showing crescentic coatings in voids; plane polarized light (PPL); b) Typic Alaquod, E horizon, showing weathered feldspar grain; PPL; c) Typic Alaquod, Bh horizon, showing pellety microstructure; PPL; d) Typic Alaquod, Bhsm horizon, showing cracked coatings on sand grains; PPL; e) Typic Alaquod, Bhsm horizon, showing weakly oriented clay around sand grains; crossed polarized light; f) same frame as e) showing complex organic coating with oriented clay; PPL.

very distinct from the surface and spodic horizons with speckled amorphous organic material forming braces between some grains in thin section. The A and E horizons contain weathered

feldspar grains with cross banded and cross linear alteration which illustrate that weathering of the mineral has taken place and suggest the loss of structural aluminum from the upper horizons of the soils (Fig. 3b). X-ray diffraction of the sand and silt fractions in these horizons showed the presence of potassium feldspar (orthoclase and microcline) and, in lesser amounts, albite (Condron, 1990). The micromorphological evidence of feldspar weathering in conjunction with an earlier study (Condron 1990) supports the hypothesis that weathering of feldspar in the surface horizons is a source of the Al accumulated in the spodic horizon.

The micromorphology of the spodic horizons differs between the upper and lower horizons. The upper Bh horizons have enaulic-gefuric related distribution with polymorphic organic matter in the voids ("pellets") and as coatings on grains (Fig. 3c). This black isotropic material has a globular to blocky shape with rough surfaces, and ranges in size from 40 - 160 μ. This part of the spodic horizon has more organic C than in the surface horizons and the proportion of organic C that is pyrophosphate extractable is greater than in the surface horizon, indicating that organic matter translocation may be taking place. The lower zones of the spodic horizon are characterized by gefuric-chitonic related distribution with cracked monomorphic coatings on the grains (Fig. 3d). In addition to polymorphic and monomorphic coatings, some of the sand grains in the upper and lower parts of the spodic horizon have compound coatings of clay and monomorphic material. Striated clay is moderately oriented around sand grains with monomorphic coatings occurring outside the clay (Fig. 3e and f).

DISCUSSION

The presence of pellets in spodic horizons has been reported by others (Flach, 1960; DeConinck and McKeague, 1985). In the past Soil Taxonomy (Soil Survey Staff, 1975) has used the presence of "pellets of coarse silt-size or larger" as a criterion for spodic horizon identification. McSweeney and FitzPatrick (1990) pointed out that the criterion lacked the specificity to distinguish pellets associated with spodic horizons from other types of pellets, such as concretions or biological features, and suggested that cracked coatings are more suitable than pellets for identification of spodic horizons. Cracked monomorphic coatings are thought to be evidence of translocated organic matter (De Coninck and McKeague, 1985) and/or amorphous Al-Si complexes (Farmer *et al.*, 1984).

The results of pH_{NaF} indicate the presence of paracrystalline or noncrystalline Al/Fe minerals in the spodic horizons of the soils studied. A $pH_{NaF} > 9.4$ can indicate the presence of aluminum hydroxide groups (Wada, 1980) either as organic aluminum hydroxide or allophane-imogolite complexes. The predominance of pyrophosphate extractable aluminum coupled with the virtual absence of extractable Si (Condron, 1990) suggests that amorphous aluminum organic complexes, rather than Al-Si compounds, form in these soils. This evidence and the presence of weathering feldspar in the surface horizons of all soils along the transects suggest that accumulations of aluminum in the spodic horizons may be due to movement of soluble organo-aluminum complexes within pedons (Condron, 1990).

In a discussion of compound coatings in spodic horizons, De Coninck and McKeague (1985) proposed that the compound coatings may be formed in separate illuvial events. Silt and clay and/or illuvial clay from the E horizon can become more or less oriented on the sand grains in the spodic horizon. In a later episode, organo-metal compounds accumulate as monomorphic coatings around the previously translocated silt and clay. A similar model could be used to explain the formation of spodic horizons in the soils of this study. The moderately

oriented clay in the spodic horizons implies that clay translocation took place prior to podzolization and the formation of the monomorphic outer coatings.

CONCLUSIONS

In this landscape, spodic horizons form in low-lying areas and are most strongly expressed in the lowest landscape positions. They are characterized by accumulations of amorphous aluminum-organic complexes. Cracked coatings and polymorphic material ("pellets") in the spodic horizons are similar to micromorphological features reported in other studies of spodosols. The presence of compound coatings, however, suggest that clay translocation took place prior to the process of podzolization in these soils.

REFERENCES

Bullock, P., Federoff, N., Jongerius A., Stoops G., Tursina T., and Babel U., 1985. Handbook for Soil Thin Section Description. Waine Research Publ., Wolverhampton, 152 pp.

Condron, M.A., 1990. Soils with Spodic Characteristics on the Eastern Shore of Maryland. M.S. thesis, Univ. of Maryland, U.S.A.

Daly, B.K., 1982. Identification of podzols and podzolised soils in New Zealand by relative absorbance of oxalate extracts of A and B horizons. Geoderma, 29: 139-55.

De Coninck, F. and McKeague, J.A., 1985. Micromorphology of Spodosols. In: L.A. Douglas and L.M. Thompson (Editors), Soil Micromorphology and Soil Classification. Soil Sci. Soc. Am. Special Publ. 15, Madison, Wisconsin, pp. 121-144.

Fanning, D.S., Korcak, R.F., and Coffman, C.B., 1970. Free iron oxides: Rapid determination using x-ray spectroscopy to determine iron in solution. Soil Sci. Soc. Am. Proc., 34: 941-946.

Farmer, V.C., Fraser, A.R., Robertson, L. and Sleeman, J.R., 1984. Proto-imogolite allophane in podzol concretions in Australia: possible relationships to aluminous ferrallitic (lateritic) cementation. J Soil Sci., 35: 333-340.

Flach, K.W., 1960. Sols bruns acides in Northeastern United States: Genesis, morphology and relationship to associated soils. Ph.D. diss., Cornell Univ. (Diss. Abstr. 21-283).

McKeague, J.A. and Day, J.H., 1966. Dithionite and oxalate extractable Fe and Al as acids in differentiating various classes of soils. Can. J. Soil Sci., 46: 13-22.

McKeague, J.A., De Coninck, F. and Franzmeier, D.P., 1983. Spodosols. In: L.P. Wilding, N.E. Smeck and G.F. Hall (Editors), Pedogenesis and soil Taxonomy, II: The soil orders. Elsevier, Amsterdam.

McSweeney, K. and FitzPatrick, E.A., 1990. Microscopic characterization of the spodic horizon. In: Proceedings from the Fifth International Soil Correlation Meeting (ISCOM IV): Characterization, Classification, and Utilization of Spodosols. USDA, SCS, Lincoln, NE.

Soil Survey Staff, 1975. Soil Taxonomy: A basic system of soil classification for making and interpreting soil surveys. USDA-SCS Agric. Handb. 436. U.S. Govt. Print. Office, Washington D.C.

Soil Survey Staff, 1992. Keys to Soil Taxonomy, 5th edition. Pocahontas Press, Inc., Blacksburg, VA, U.S.A.

USDA Soil Conservation Service, 1992. Soil Survey Laboratory Methods Manual. Soil Survey Investigations Report No 42, ver 2.0. U.S. Gov. Printing Office, Washington, D.C., 400

Micromorphology of paleosols - genetic and paleoenvironmental deductions: Case studies from central China, south India, NW Morocco and the Great Plains of the USA

A. Bronger[1], N. Bruhn-Lobin[1] and Th. Heinkele[2]

[1]Department of Geography, University of Kiel, D-24098 Kiel, Germany
[2]Department of Soil Conservation and Recultivation, Techn. University of Cottbus, D-03044 Cottbus, Germany

ABSTRACT

Bronger, A., Bruhn-Lobin, N. and Heinkele, Th., 1994. Micromorphology of paleosols - genetic and paleoenvironmental deductions: Case studies from central China, south India, NW Morocco and the Great Plains of the USA. In: A.J. Ringrose-Voase and G.S. Humphreys (Editors), Soil Micromorphology: Studies in Management and Genesis. Proc. IX Int. Working Meeting on Soil Micromorphology, Townsville, Australia, July 1992. Developments in Soil Science 22, Elsevier, Amsterdam, pp. 187-206.

Paleosols are grouped into relict and buried soils. Buried soils in loess are mostly truncated and recalcified. Micromorphology can distinguish between secondary and, if still present, primary carbonates and therefore can be used to separate pedogenic from postpedogenic processes. This has some very important paleoclimatic implications. In addition, micromorphology can be used to identify clay illuviation which allows, under certain restrictions, additional paleoenvironmental inferences. This method, together with (clay) mineralogical investigations, is used as the basis for deducting a detailed climatic history of the last 2.5 Ma, including the interglacials, from a loess-paleosol sequence in central China.

Relict micromorphological features occur in semiarid tropical Alfisols with distinct kaolinitic clay maxima in the Bt horizon. These include runiquartzes with hematitic infillings and some hematitic iron concretions or kaolinized feldspars, biotites and hornblendes, which are viewed as evidence of a more humid climate probably dating back to the Neogene. In contrast, the accumulation of secondary carbonates refers to the present day climate. This result implies that the efficiency of weathering under a tropical climate is often overestimated. In the central and northern part of the Great Plains of the USA, many soils such as Borolls, Ustolls and even Aridisols have subsoils enriched with ≥20% clay. This Bt horizon is referred to genetically as a horizon of clay illuviation, or an argillic horizon. However, micromorphological evidence from over 20 principle soil series, does not indicate clay illuviation. Additional investigations of the quantitative composition of the primary and clay minerals show that the main cause of the clay maximum in the subsoil is a lithologic discontinuity in the parent material. Selected soils of the short-grass prairie with much higher clay contents in the B horizons are polygenetic soils or paleosols in the sense that the subsoils are the result of much older soil forming processes probably occuring during a period with moister climate.

INTRODUCTION

The term paleosol is used either for a soil "formed in a landscape of the past" (Ruhe, 1956; Yaalon, 1971) or formed under changing environmental conditions, especially climatic and associated changes. According to these definitions paleosols can be grouped into *buried* or *fossil soils* and *relict soils*. Relict soils began forming when soil forming conditions were different from those of the present but are still close enough to the surface to continue developing today. Difficulties connected with this definition, notably the problem of a minimum age limit, are discussed in a previous paper (Bronger and Catt, 1989). On the other side, there is a considerable measure of agreement over what is meant by a fossil soil. It is a soil buried by younger sediment sufficiently thick that any subsequent pedogenesis has not affected its entire thickness or, therefore, the buried soil. But difficulties can remain in separating the two groups of paleosols such as the buried Holocene soil in the Loess Plateau in central China (to be discussed later).

Micromorphology can give important information on the genetic and paleoenviromental interpretation of buried and relict soils. However, many open questions remain and this paper only focuses on some of them. Special attention is drawn to the use of Soil Taxonomy, first because this classification is used as an international reference system in many countries where relict soils are widespread, mainly in the tropics and subtropics. Second, Soil Taxonomy has strong genetic implications because many of its diagnostic horizons are thought to be the result of soil genesis (Smith, 1983). Out of this complex we focus our attention mainly on the argillic horizon which is referred to genetically as a horizon of clay illuviation (Soil Survey Staff, 1975, 1990; Smith, 1983). This process can be unequivocally demonstrated by micromorphology and allows, with some restrictions, certain paleoenvironmental conclusions. For further genetic and paleoclimatic interpretations of buried and relict soils, mineralogical investigations, especially of clay, are necessary to indicate the nature and intensity of weathering. Therefore, additional (clay) mineralogical results are given in some of our examples. Excluded in this paper are micromorphological aspects of many other important paleopedological features such as various duricrusts in relict soils or lithified and metamorphosed paleosols (Retallak and Wright, 1990).

BURIED OR FOSSIL SOILS

General remarks

This section focuses on paleosols developed from loess because loess-paleosol sequences can provide detailed records of Pleistocene climatic changes. As such they are well studied and several recent comprehensive articles, with extended references, can be cited *e.g.* for the central part of the USA (Olson, 1989), UK (Catt, 1988, 1989), Italy (Cremaschi, 1987), Central Europe (Semmel, 1989; Bronger and Heinkele, 1989b; Smolikova, 1990) and central China (Bronger and Heinkele, 1989a; Heinkele, 1990; Guo *et al.*, 1991).

It is often difficult to classify buried soils genetically for paleoclimatic deductions. First, they are mostly truncated (see above), and second, several important diagnostic features which can be recognized in modern soils, *e.g.* chemical properties, have disappeared or have been changed because of postpedogenic alteration of the paleosols. One example is the progressive decomposition of organic matter with advancing age not only during the Upper Pleistocene (Bronger, 1966, 1974) but also in the Early Holocene (Bronger and Heinkele, 1989a). This

prevents designating most buried Chernozems (see below) as Mollisols after the Soil Taxonomy. Another example in loess areas is that all fossil soils are more or less recalcified from the overlying loess. Thus, in contrast to modern soils, pH or base saturation values, although published until recently (Guo *et al.*, 1991), are of little use. It is therefore necessary to study the sequence of *processes* in buried soils to provide information about pedogenesis as well as diagenesis. Micromorphology is of special significance, for it provides a complete view of soil development through different stages even in polygenetic pedocomplexes (Kubiena, 1959, 1964; Smolikova, 1967, 1971, 1990; Bronger, 1969/70, 1976) and often reveals the effects of post-pedogenetic processes after burial. Micromorphology can, for example, distinguish between secondary carbonates and, if still present, primary carbonates. *Secondary carbonates* occur as fine calcite concentrations in voids (micrite and microsparite after Courty *et al.*, 1987), as accumulations of coarse calcites in root channels, or as calcite needles in finer pores (Figs 1a-c: see also Bronger, 1966, Photos 9-12 and 1976, Photos 10, 18, 19; Bronger *et al.*, 1987; Bronger and Heinkele, 1989a, Fig. 9; and Wieder and Yaalon, 1982). However, individual carbonate clasts, irregularly distributed in the soil matrix, can be regarded as *primary* (*cf.* Bronger, 1976, Photos 9, 17 and 23). This genetic distinction between carbonate constituents is of special importance, because one can distinguish between Degraded Chernozems and Chernozems with the presence of primary carbonates, the latter developing in a shorter time and under a drier climate (see below).

Furthermore, micromorphology makes it possible to demonstrate the process of *clay illuviation* unequivocally. This soil forming process takes place in the pH range 4.5 - 6 (0.1M KCl or $CaCl_2$) in climaphytomorphic soils (Schroeder, 1984) in a plateau position far above the groundwater table and without the influence of Na^+ ions. It is associated with a temperate climatic belt and forest vegetation under a udic soil moisture regime but not under steppe vegetation with a ustic soil moisture regime (for definitions see Soil Survey Staff, 1975, pp. 51-57). This regular relationship has been found in many Holocene loess soils in east Central Europe, in the western part of the Central Lowlands and in the Great Plains of the USA (Bronger, 1976, pp. 35-106; 1991). Even when the illuviation argillans (Brewer, 1964; Bullock *et al.*, 1985), as unequivocal signs of clay illuviation, are transformed by changing environmental conditions in buried or relict soils, they remain visible as a very stable element of the fabric. For example, they are even found in the excrements of earthworms (*e.g.* Zachariae, 1964; Bronger, 1976, Photo. 3; Catt, 1989, Photo. 1A) and in "Fließerde" (geliflucted soil) material from a buried Mid-Pleistocene Udalf (Bronger, 1969/70, Fig. 2A and B; Catt, 1989, Photo. 1: B-D). Other features of illuvial clay may be less clear for interpretations are often subjective (McKeague, 1983; Bullock and Thompson, 1985; Bronger 1991, p. 44). However, it is necessary to separate the basically climatogenic process of clay illuviation (in the form of illuviation argillans) from the process of argillipedoturbation (in the form of oriented birefringence, see Fig. 5d), which is predominantly a lithogenic process determined by the soil material (Bronger, 1977) especially in vertic soils *sensu lato*.

Buried Holocene soils in central China

For paleoclimatic deductions from buried soils (see above), the comparison with the climaphytomorphic Holocene soil of the specific area is necessary. The difficulties both in
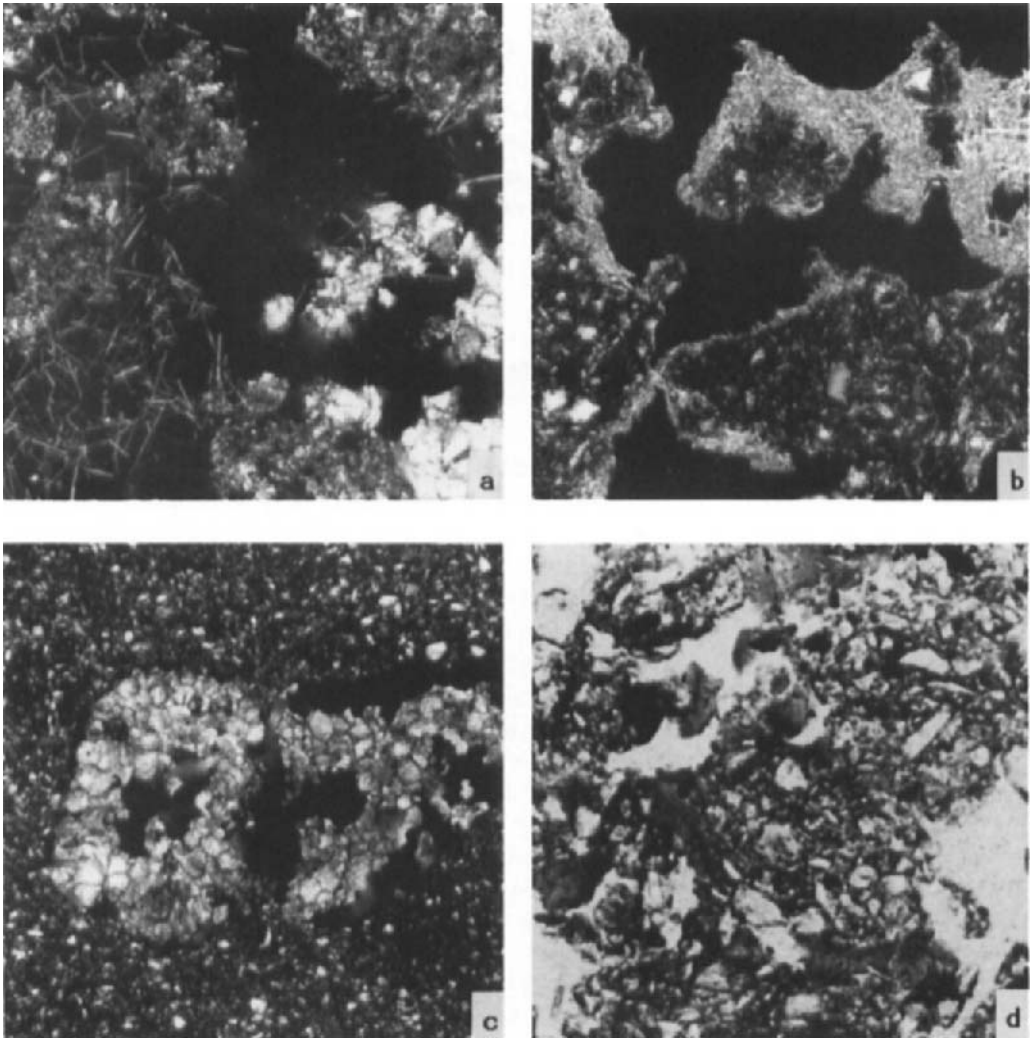
Fig. 1. **a)** Calcite needles and larger clastic calcite with soil aggregates partly impregnated with micritic calcite are forms of secondary carbonate in the Ahb horizon of a buried Holocene Chernozem near Luochuan in the Loess Plateau of central China; crossed polarised light (XPL); frame width (FW) 1.33 mm. **b)** Micritic and microsparitic calcites, with needles in voids or around aggregates occur as secondary carbonates in the Ahb horizon; Same soil as a). XPL; FW 1 mm. **c)** Clastic carbonates mainly in the coarse silt fraction in a root channel, a kind of macroscopically visible pseudomycel in the AC horizon; Same soil as a); XPL; FW 3 mm. **d)** Traces of illuviation argillans in the fine spongy fabric of the lower soil of the S1-pedocomplex in the Potou section near Luochuan, Shaanxi, China (*cf*. Fig. 3). Plane light (PL); FW 1.33 mm.

separating the two groups of paleosols and also the use of soil classification systems, notably the "Soil Taxonomy", can be demonstrated by the buried Holocene soils near Luochuan in the Loess Plateau of central China (*cf.* Introduction). These soils on the relatively small loess plateaus called "yuans" (the remnants of the now dissected loess plateau) were previously named "yellow" and "black loessical soils" with "carbonates present throughout the profiles" (Zhu *et al.*, 1983). Our investigations (Bronger and Heinkele, 1989a; Heinkele, 1990, pp. 14-48) showed that a soil with the typical horizon sequence Ahb (45 - 100 cm) - AC (100 - 120 cm) - Ck (>120 cm), probably truncated, is buried by an anthropogenic Ap horizon. It consists of a mixture of loess, farmyard manure and other residues containing pieces of brick and charcoal, placed on top of the soil as a fertilizer over a period of about one thousand years. Until recently the Ap horizon (10YR 6/4, when dry) of this area was considered in the chinese literature (Liu *et al.*, 1985, p. 53) to have originated from the accumulation of young Holocene airborne dust and not by human activity. Our micromorphological investigations of four selected pedons showed that the Ahb horizons (10YR 4/3 to 5/3, when dry) had a fine, spongy fabric rich in aggregates and voids which is a result of high biological activity and is typical of a steppe soil. This microstructure was apparent in the Ap horizon too, but was less well expressed. The Ap horizon still contained primary carbonates but not so the Ahb horizon. This indicates that the carbonate content results from recalcification of the overlying Ap horizon (Figs 1a and b). Guo *et al.* (1991) has come to a very similar conclusion regarding the genesis of a Holocene soil in the Xifeng area which has the same soil moisture regime (*cf.* Fig. 2). The Ahb horizon of one of the selected Holocene pedocomplexes contains traces of illuviation argillans in thin seams along a few pores, indicating that clay illuviation had just started before burial. However, the very small amounts do not justify its designation as an argillic horizon.

To summarize, the pedogenesis of the lower part of this polygenetic soil ("SO-complex") was formed in the Early and Middle Holocene under a natural tall grass steppe (Zhu *et al.*, 1983; Liu, 1985, pp. 146 and 224; Walter, 1974; Nat. Atlas P. R. China, 1984, Map 15). This resulted in a *Degraded Chernozem* with an Ah-AC-Ck horizon sequence, comparable with a Hapludoll in the Soil Taxonomy, and probably close to the udic/ustic boundary. After burial by the Ap horizon, decomposition of this soil's organic material started and it was also recalcified from the overlying material. The classification of these polygenetic soils, particularly according to the Soil Taxonomy, is inadequate from a genetic point of view. Although the Ah-AC-Ck horizon sequences have typical features of a steppe soil (*e.g.* thickness of the remaining Ah horizon, structure, microfabric, colour and krotovinas) they no longer meet the requirements of Mollisols because of the low organic carbon content. Accordingly they must be classified as Eutrochrepts. In some places the overlying Ap horizon exceeds 50 cm and these soils are Plaggepts. In which direction soil development would have continued without man's activity must remain an open question. Would soil development have remained at the stage of a Hapludoll or proceeded towards an Argiudoll? However, the present day soil moisture regime after the Newhall Simulation Model (Van Wambeke, 1985) is still "typic udic", without any water surplus during the year (*cf.* Fig. 2).

Buried Pleistocene soils in central China

The loess-paleosol sequence below the described Holocene SO-pedocomplex in the well known Potou section near Luochuan extends through the entire Pleistocene back to 2.5 Ma in
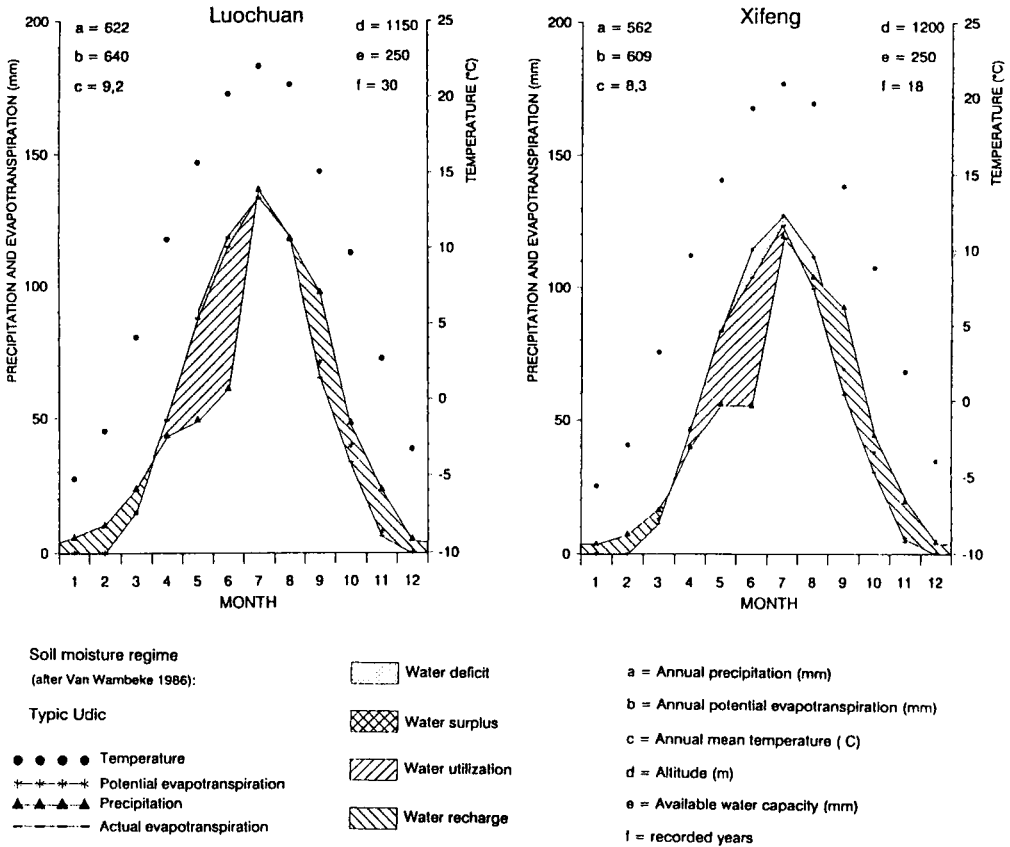
Fig. 2. Climatic data and soil water balance at Luochuan and Xifeng, Loess Plateau of central China.

a much more complete sequence than any known from Europe or North America. Micromorphological investigations in particular allow reconstruction of the genesis of the paleosols or pedocomplexes and, therefore, provide specific information regarding the paleoclimate, notably the interglacial periods (Fig. 3; see Bronger and Heinkele, 1989a; Heinkele, 1990). The last four paleosols represented by the two soils of the "S1" pedocomplex, the upper soil of the "S2" pedocomplex and the "S3" are genetically comparable to the natural Holocene soil in that they have a fine, spongy fabric and are rich in aggregates and voids, because of high biological activity. They are also free of primary carbonates. Thus these paleosols indicate a climate similar to that of the Holocene with a tall grass steppe vegetation. The lower soil of the "S1" pedocomplex shows traces of illuviation argillans as does one of the Holocene pedons mentioned above (Fig. 1d). The paleosols "S6", the "S11" and "S13", the latter two being older than the Brunhes/Matuyama boundary, are also free of primary carbonates and developed under steppe vegetation. The fine, spongy fabric is even preserved below the "S13" at 74 m depth (Heinkele, 1990, Photo. 3) which corresponds to an
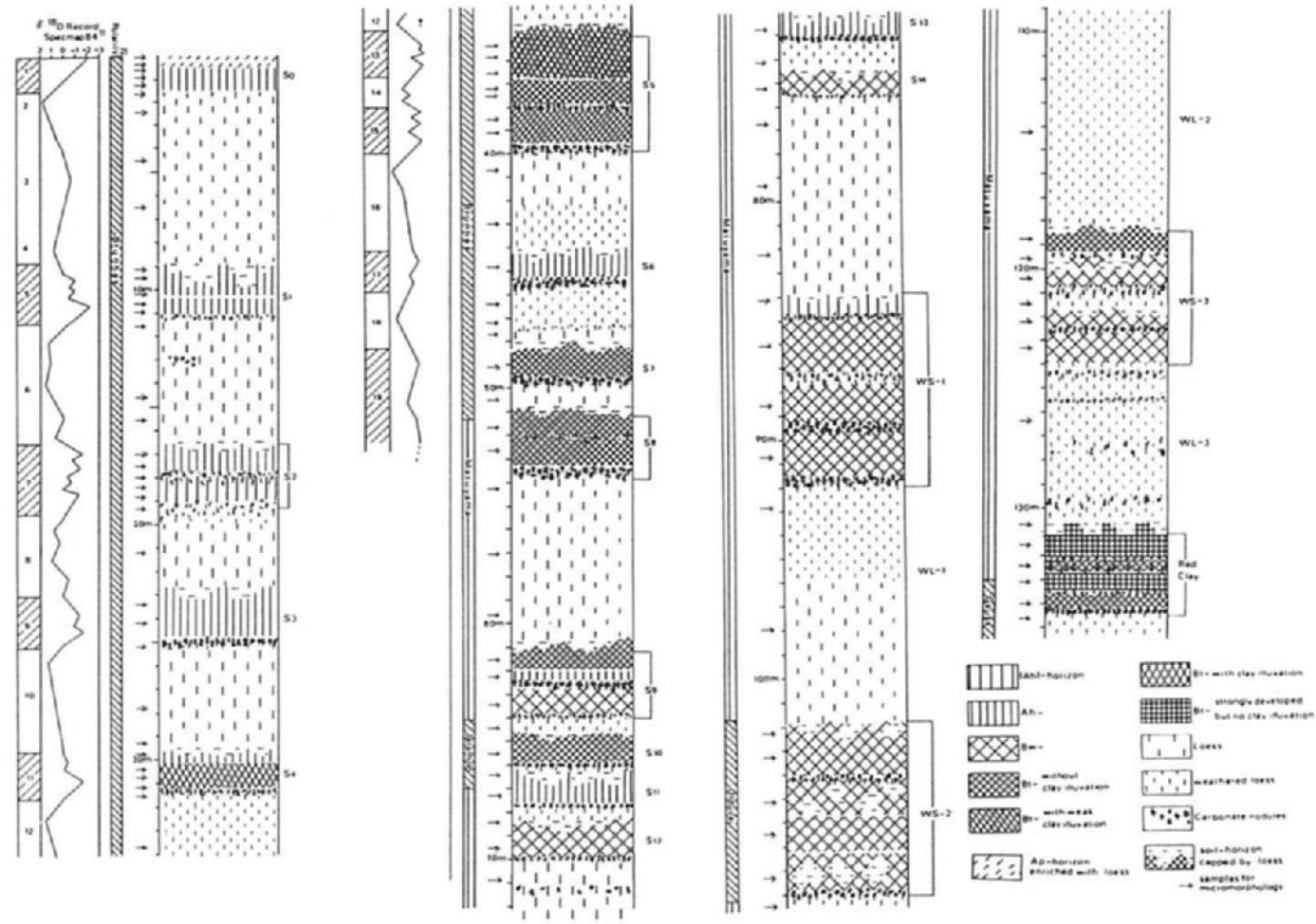
Fig. 3. Buried Holocene soil (S0) and Paleosols in the Luochuan Loess Profile (Potou section), China.

age of about 1.2 Ma according to paleomagnetic investigations (Heller and Liu, 1982, 1984). In contrast, the "S4", the three paleosols of the "S5"-complex, the "S7", the two soils of the "S8"-complex, the uppermost soil of the "S9" and the "S10" have a much denser fabric with very few aggregates though some conductive channels occur. Only the Bt horizon of the "S4" and the uppermost soil of the "S5"-complex reveal distinct illuviation argillans though there are fewer in the former than the latter, whilst in the lower soil of this pedocomplex there are very few. All other Bt horizons (in a genetic rather than a diagnostic sense, Soil Survey Staff, 1990, pp. 413 and 419) are free of illuviation argillans. The most pronounced micromorphological features are illustrated in Bronger and Heinkele (1989a, Figs 4-9) and Heinkele (1990, Photos 1-8). Nevertheless, these paleosols must be regarded as forest soils with a much denser fabric and very few aggregates presumably because of less biological activity. This compares to the fine, spongy fabric rich in aggregates and pores typical of steppe soils. The forest soils indicate more moist and somewhat warmer interglacials than the Holocene. On this basis it is difficult to understand why most of the paleosols in the loess profile in Xifeng with a similar soil moisture regime of today ("typic udic", *cf.* Fig. 2), were classified by Guo *et al.* (1991) as "Kastanozems" according to the FAO system (FAO-Unesco, 1974). It is stated that "humification is relatively weak in most of the paleosols" because the "summer temperature was too high for humus accumulation" (Guo *et al.,* 1991, p. 101). Furthermore, the authors stressed "that the lower humus contents in the paleosols are unlikely to be explained only by the humus decomposition as the time goes on" (p. 101). In all of the subtypes of their Kastanozems "a dense steppe was dominant during the soil formation" and in two of them ("Chromic luvic" and "Luvic Kastanozem") the steppe vegetation was "replaced during a short humid climatic optimum by forest cover" (p. 106). The concept of a Kastanozem, however, is that of a soil developed in a short grass steppe (or short grass prairie) and with an aridic soil moisture regime in the sense used in the "Soil Taxonomy" without a continuous vegetation cover.

For further genetic and paleoenvironmental interpretation of buried soils, and also of relict soils, *mineralogical*, especially *clay mineralogical* investigations, are necessary to indicate the nature and intensity of weathering. This provides data to distinguish relict from recent soil forming processes.

RELICT SOILS

A relict soil contains two or more sets of properties which can be related to different combinations of soil forming factors through sets of often incompatible soil-forming processes. Incompatibility of processes implies two or more environmentally different periods of soil development (Bronger and Catt, 1989).

In contrast to most mid-latitude regions large areas in the tropics are covered with very old soils, often with deep weathered profiles, dating back to the Tertiary (Schmidt-Lorenz, 1986). During soil development over such a long period, the soil forming factor of climate, and with it vegetation, must have changed considerably, especially in the present day semiarid tropics. However, not very much is known regarding the polygenesis of the soils in these climatic regions, especially of the Alfisols (Allen and Fanning, 1983). The micromorphology of the main soils in tropudic climates, notably the Ultisols and Oxisols, is better known and includes some discussion of their relict features (Fedoroff and Eswaran, 1985; Stoops and Buol, 1985; Stoops, 1989).
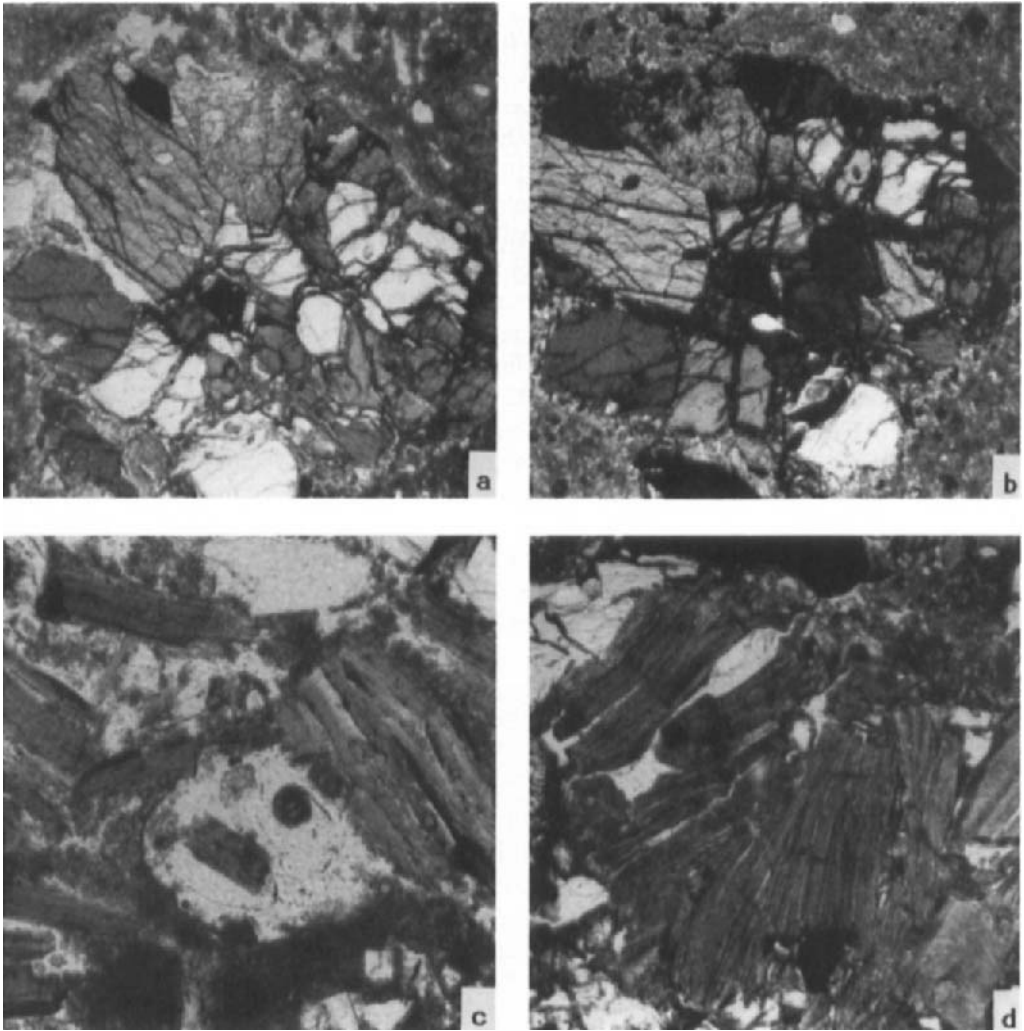
Fig. 4. **a)** Strongly weathered hornblendes in a secondary $CaCO_3$ accumulation. CrkB horizon of an Aridic Rhodustalf (Patancheru I Soil); PL; FW 3.33 mm. **b)** as a); XPL. **c)** Weathered biotites with secondary $CaCO_3$ accumulation mainly in the lower right part; Crk horizon of a Typic Ustropept (Palathurai Soil); PL; FW 2 mm. **d)** Strongly weathered biotite and hornblende with small illuviation argillans inside the minerals; CrB horizon of an Udic Rhodustalf (Palghat Soil); PL; FW 2 mm.

"Red Soils" in south India

In India, tropical Alfisols, the so called *"Red Soils"*, cover an area of about 720,000 km^2 (Krantz *et al.*, 1978) mainly in the southern part. Most of them are classified as *Udic, Typic*

and *Aridic Rhodustalfs* according to the Soil Taxonomy which reflect, the present day climate, notably rainfall. Most Alfisols from south India are formed in saprolitically weathered "Peninsular Gneiss". As a fragment of the old Gondwana continent, the southern part of the Indian plate crossed the equator to reach its present day position in the Miocene. According to paleomagnetic data (Klootwijk and Peirce, 1979; Somayajulu and Srinavasan, 1986; Molnar, 1986) the whole of the Indian plate was probably subjected to a hot, wet tropical climate for about 15 - 20 million years. Due to northward drift beyond the equatorial zone most of the Indian subcontinent became drier. This effect was fortified by the uplift of the West Ghats since the late Tertiary (Kale, 1983) as major parts of south India are now in the rainshadow of this mountain range.

A climatic sequence of nine Alfisols and Ultisols, where possible Benchmark soils (Murthy *et al.*, 1982), representing rainfall conditions from 2500 mm/year (10 humid months) to 590 mm/year (1 humid month) were investigated (Bruhn, 1990; Bronger and Bruhn, 1989, Figs 2-10, Photos 1-8). The results show that only soils with a base saturation <35% display *recent weathering features*. A Typic Rhodudult and a neighbouring Typic Hapludox from the humid West Ghats (10 humid months) show evidence of recent deep weathering, *i.e.* low base saturation, gibbsitisation of plagioclase, kaolinization of biotite, boxwork-pseudomorphs of weathered almandine and hypersthene. The soils formed in this highly preweathered material are kaolinitic with various amounts of gibbsite. These soils seem to be in equilibrium with the recent climatic environment, so they are not paleosols although they are quite old and may be polygenetic.

The climatic threshold for sufficient leaching capacity of recent weathering is about 2000 mm rainfall (about 6 humid months). In a Udic Rhodustalf no gibbsites are formed anymore but deep weathering results in the formation of kaolinites and 2:1 clay minerals occur in the solum. Below the 2000 mm threshold in two Typic Rhodustalfs, one of them close to an Aridic Rhodustalf, the base saturation of the saprolite increases as do the amounts of 2:1 clay minerals in the saprolite and the soil. No fresh weathering features on micas and feldspars are visible. Despite the decreased weathering intensity, a broad spectrum of weathering features is present in the soils, *e.g.* kaolinized biotite flakes, boxwork of strongly weathered hypersthene, garnet or hornblende and single quartz grains with hematitic fillings ("runiquartz" of Eswaran *et al.*, 1975; Eswaran, 1979; Schnütgen and Späth, 1983; Stoops, 1989). These features, including the juxtaposition of kaolinites and illites with no intergrades obviously do not fit into the recent soil environment. In two Aridic Rhodustalfs pedogenic kaolinites still dominate. However, in these two soils and in a Typic Ustropept we found increasing amounts of smectite, illite-smectite intergrades and illite. This succession of clay minerals seems to reflect a process of climatic desiccation in the past. In the present day climate illites are being formed, but smectites and mixed-layer minerals are apparently relict features. In three soils secondary calcite has accumulated in the saprolite and lower B horizons. In contrast to the kaolinites this carbonate accumulation is good evidence for a significant change of the soil environment (Figs 4a-c).

Most of the soils we studied are classified as Rhodustalfs due to an often distinct clay maximum in the Bt horizons (*cf.* Bronger and Bruhn, 1989, Figs 4-8) which implies clay illuviation as a dominant soil forming process (Soil Survey Staff, 1975, p. 19). However, only in the Udic Rhodustalf under 2115 mm rainfall is clay translocation an intense and recent process. In two other soils argillans with lower birefringence can be found in very small amounts (*c.*1%) (Fig. 4d, see also Bronger and Bruhn, 1990, Photos 1 and 2). In all other soils
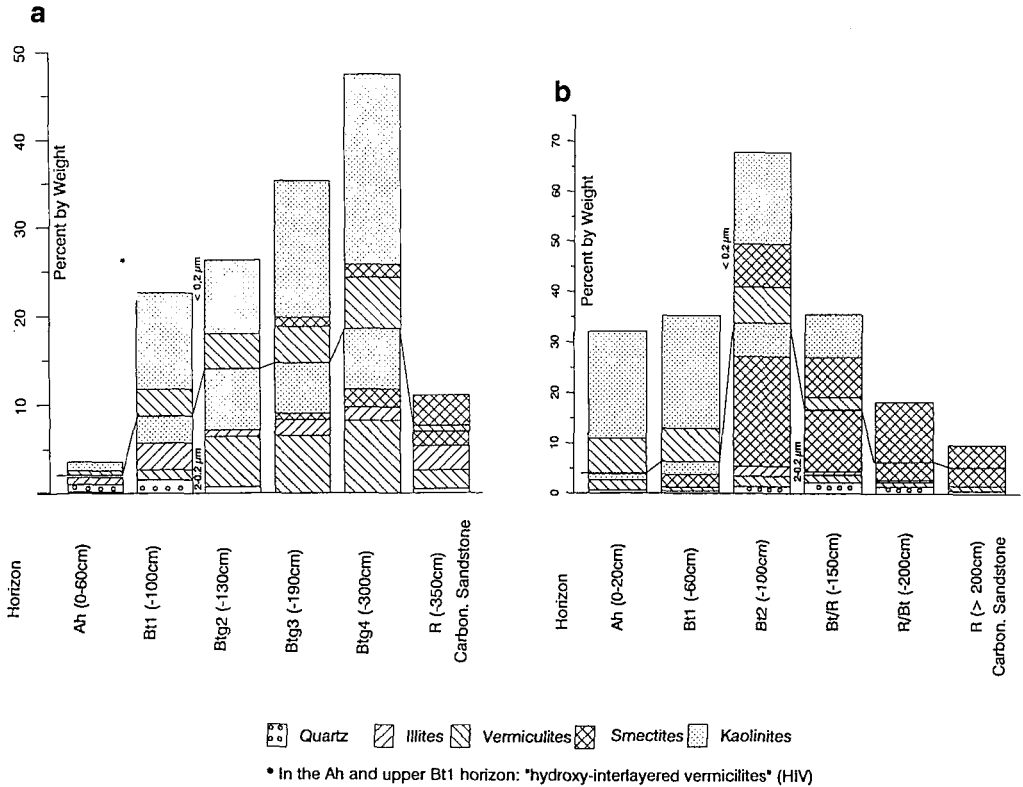
Fig. 5. Clay mineral composition of a Typic Rhodoxeralf. a) Sidi Chaffi/Rabat, Morocco; b) Tal'at Ach Chwar/Rabat, Morocco.

the b-fabric is mainly granostriated with almost no illuviation argillans. Two explanations are possible. First, reworking into the matrix may have destroyed the argillans and, second, the increase in clay content in the profiles could be due to higher *in situ* clay formation in the Bt horizons. On this basis a new concept of defining Alfisols was proposed as soils with significant clay *formation* expressed by an increase in clay of >10% from the C to the Bt horizon (Bronger and Bruhn, 1990).

Relict features in soils of the western Mediterranean area

Within the Mediterranean climatic region red soils, *i.e.* Terra Rossa-Rhodoxeralfs, occur over a broad lithologic spectrum, but mainly on carbonatic rocks. A xeric soil moisture regime (winter moisture surplus and summer drought) leads to the bright red soil colour (hue < 5YR) and a distinct argillic horizon. Due to their patchy distribution in the Mediterranean landscape as well as their frequently truncated character they are often considered to be relict soils (Kubiena, 1970, p. 174; Fanning and Fanning, 1989, p. 286). According to Kubiena (1970) precipitation in the Mediterranean today is not sufficient to form these soils, although Meyer and Kruse (1970) were able to show that rubification, due to iron release from carbonate

solution, was the only significant pedogenic process in Pleistocene coastal dunes in Morocco. Based on extensive investigations on Terra Rossas, in eastern and southern parts of Spain, Skowronek (1978) concluded that rubification and strong mineral weathering including the formation of 2:1 clay minerals but not kaolinites was in equilibrium with the Holocene climate. On the other hand Bronger *et al.* (1983; 1984) have shown that all mineralogical properties, except the formation of hematite, of a Terra Rossa karst pocket infilling in Slovakia were *inherited* from travertine of Pliocene age.

Another example, as to whether Mediterranean Terra Rossas are relict or modern soils, is given by Bruhn-Lobin and Bronger (1991). Pliocene (Moghrebien) to Mid- or even Late Pleistocene beach ridge complexes around Rabat/Morocco, running parallel to the present coast, are covered by red Mediterranean soils ("Formation rouge"). The beach ridge complexes with eolian and marine sedimentary cycles were studied by Gigout (1958), Choubert and Faure-Muret (1959), André and Beaudet (1967, 1980), Beaudet (1969), Stearns (1978), Weisrock (1980), Lefevre *et al.* (1985) and Aberkan (1987). Recently, some of these Pleistocene eolian sequences were dated (Brückner *et al.*, in press). The Terra Rossas are not only intensively rubified (about 2.5YR) but also strongly weathered. The calcarenites display a mineral composition of quartz, plagioclase, pyroxenes, micas, chlorites and magnetite in the fractions >2 µm; and illites, vermiculites and smectites in the clay fractions. With depth the weatherable minerals decline and the clay content increases markedly showing a dominantly *kaolinitic* mineralogy (*cf.* Fig. 5a and b). The pedogenically formed kaolinites are mostly of a disordered structure (DMSO-test) and low crystallinity with some halloysite. Soil micromorphology indicates that in these soils clay illuviation is a significant process, but the clay is usually translocated into the carbonatic Bk or R horizon, forming well developed illuviation argillans around solution channels (Fig. 6a) and ped surfaces. Only a few soils show distinct illuviation argillans in the Bt horizon, like in a Typic Rhodoxeralf in Sidi Chaffi, about 15 km east of Rabat. Here the maximum clay illuviation is in the red-yellow mottled Btg2 horizon, displayed by large, mostly well laminated illuviation argillans (Fig. 6b). Others, however, are already aged in most parts (Fig. 6c). The amount of clay illuviation is less in the Btg3 and even less in the Btg4 horizon, as indicated by rapidly decreasing amounts of illuviation argillans, although the clay content increases markedly with depth (*cf.* Fig. 5a). The Typic Rhodoxeralf is superimposed by a 60 cm thick dune sand (A horizon, Fig. 5a). Its lower part contains artefacts and was recently TL-dated at 20-22 ±2ka (Brückner *et al.*, in press). Most other soils despite often having a distinct clay maximum in the B horizon, like in Tal'at Ach Chwar about 15 km south of Rabat (Fig. 5b), have only traces of illuviation argillans, if any. Probably argillipedoturbation has reworked them into the matrix which often exhibits a cross-and grano-striated b-fabric. A very weakly rubified Rendzina (7.5YR 3/2 when dry) on top of the second youngest beach ridge complex about 10 km southwest of Rabat and 2 km east of the coast shows no micromorphological evidence of clay illuviation even though the Ck horizon underneath has a TL-age of >100ka (Brückner *et al.*, in press). With respect to our results the Terra Rossas in this area are relict polygenetic soils.

Relict features in soils of subtropical and temperate regions in the USA

Nettleton *et al.* (1989) summarize concepts and ideas regarding recent and relict features in soils of subtropical regions of the United States and present new results for five selected soils
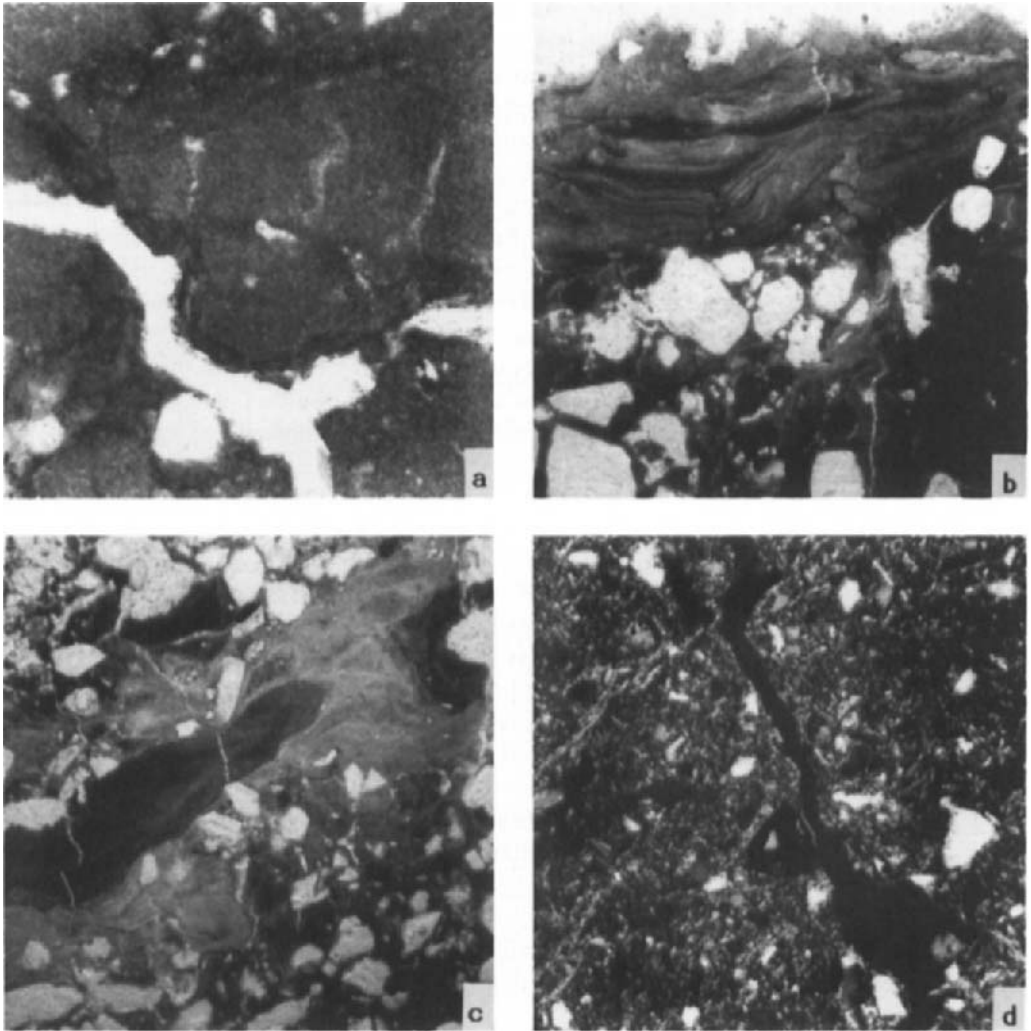
Fig. 6. **a)** Illuviation argillans, mostly laminated in a solution channel surrounded by secondary micritic calcites in the CkB horizon of a Petrocalcic Rhodoxeralf south of Rabat/Morocco; PL; FW 2 mm. **b)** Large illuviation argillans, mostly well laminated; Btg2 horizon of a Typic Rhodoxeralf, Sidi Chaffi, east of Rabat/Morocco; PL; FW 3mm; **c)** Large illuviation argillans, mostly aged although laminations occur in small areas;. Darker parts rubified, lighter parts yellow; same horizon as b); PL; FW 3.3 mm. **d)** Conductive channel, free of any illuvation argillans; oriented birefringence, probably caused by argillipedoturbation in a "Bt" horizon of an Abruptic (Aridic) "Argi"boroll (Shaak series, Montana, USA, *cf.* Bronger, 1991, Fig. 10); XPL; FW 1.33 mm.

on geomorphic surfaces of Middle Pleistocene to Pliocene age. Examples of relict features or relict horizons, related to a much more humid environment in the past, are: plinthite in a Plinthic Kandiudult in North Carolina, petrocalcic horizons in a Typic Paleorthid in southern Nevada and argillic horizons in an Aridic Paleustalf on the High Plains of Texas, in a Typic Haplargid in Arizona and in an Abruptic Durixeralf in southern California. The strongly developed argillic horizon in the last soil contains in its lower part a distinct Btqm (duripan) horizon. The source of the silica cement is thought to be the result of weathering of feldspar and other minerals to kaolinite during a long time span in more humid environments of the past. The feature that best supports these conclusions is the movement of pedogenic carbonates and clays to a depth that extends well below the depth of wetting expected in the present day dry xeric, aridic and ustic soil moisture regimes. It may, however, be added that the strong increase of clay content in the Abruptic Durixeralf from 11% in the A horizon to 37% in the Bt1 to 60% in the Bt2 horizon could be the result of a distinct *lithologic discontinuity* also. This soil is one of the examples where the concept of "argillic horizons without clay skins" (Nettleton *et al.*, 1969) was developed.

In the central and northern part of the Great Plains Borolls, Ustolls and even Aridisols with a $\geq 20\%$ higher clay content in the subsoil are widespread. This "Bt" horizon is considered to be one of clay illuviation, or an argillic horizon. However, from the micromorphological study of about 300 thin sections (Bronger, 1978, 1991), it was concluded that the clay maximum in more than 20 widespread soil series could not be explained properly by clay illuviation. The soils examined in this study were from uneroded stable surfaces and included Typic and Aridic Argiborolls, Udic, Typic and Aridic Argiustolls and Ustollic Haplargids, which were all free of Na^+ ions. Only traces of illuviation argillans could be detected in a few Bt horizons, though oriented birefringence can often be observed and is probably caused by argilliturbation (Fig. 6d) especially in subsoils with high clay content rich in smectites (Bronger, 1991, Figs 7-15). Additional investigations of the quantitative composition of the primary and clay minerals, including the fine-clay fraction ($<0.2\ \mu m$) of nine selected soils showed that the cause of the clay maximum in the subsoil was most likely in a *lithologic discontinuity* in the parent material. This is demonstrated by the extremely variable content of quartz, which is a stable mineral in the temperate climatic zone. At least four soils of the short-grass prairie with a much higher clay content in the Bt horizons are *polygenetic soils* or *paleosols* in the sense that the subsoils are the result of much older soil forming processes which probably occurred during a period of moister climate.

DISCUSSION AND CONCLUSION

Buried soils in loess are mostly truncated and recalcified. Micromorphology can distinguish between secondary and, if still present, primary carbonates and therefore can be used to separate pedogenic from postpedogenic processes having important paleoclimatic implications. Second, micromorphology can confirm the process of clay illuviation which allows, under certain restrictions, paleoenvironmental conlusions. In the temperate climatic belt this soil forming process is associated with a forest vegetation and udic soil moisture regime and not with a steppe vegetation and ustic soil moisture regime in the sense of the Soil Taxonomy. Therefore, micromorphology together with (clay) mineralogical investigations allows, for instance from the loess-paleosol sequence in central China (Fig. 3), the deduction of a detailed climatic history over the last 2.5 Ma. In particular, specific information on the

paleoenvironment of the interglacial periods can be deduced. In this sense micromorphology is much more than a tool (Wilding, 1990).

An open question remains as to why illuviation argillans, as based on present day knowledge from loess profiles in China and in Central Europe (Bronger, 1966, 1969/70, 1976) are well expressed in forest soils in the Brunhes chron but hardly visible in the Matuyama chron, although the illuviation argillans are a very stable element in the fabric. This observation may indicate that illuviation argillans, especially when laminated, are rather young, as in the relict Petrocalcic Rhodoxeralf (Fig. 6a) or visible almost only in the upper Btg horzon in the Typic Rhodoxeralf (Fig. 6b). In most relict Terra Rossas illuviation argillans are almost absent perhaps because these soils may date back to the Matuyama chron. Paleomagnetic investigations are required to provide information on the approximate age of these soils. In relict Rhodustalfs in semiarid south India, with a distinct clay maximum in the Bt horizon pedogenesis occurred in a much more humid climate probably dating back to the Neogene. Only a Udic Rhodustalf, with 5 - 6 humid month, displays laminated illuviation argillans in its upper part as a recent process. On this basis, Bronger and Bruhn (1990) redefined Alfisols to include soils with significant clay *formation* expressed by an increase in clay content of >10% from the C to the B horizon. According to this definition, Alfisols can easily be separated from the Inceptisols and even the Brown Forest Soils as the higher weathering intensity in the mid-latitudes would fit into this concept.

The genetic classification of more than 20 widespread soil series with a much higher clay content in the "Bt" horizon in comparison to the A horizon in the Central and Northern Great Plains of the USA as *Argi*borolls, *Argi*ustolls and Hapl*argids* revealed only traces of illuviation argillans, if any, and must be reconsidered. The micromorphological and clay mineralogical investigations show that it is not sufficient merely to identify an increase in clay *content* of ≥20% to designate a horizon *genetically* as an argillic horizon resulting from the process of clay illuvation.

ACKNOWLEDGEMENTS

REFERENCES

Aberkan, M., 1987. Étude des formations quaternaires des marges du Bassin du Rharb (Maroc Nord-Occidental). Université de Bordeaux.

Allen, B.L. and Fanning, D.S., 1983. Composition and soil genesis. In: L.P. Wilding, N.E. Smeck and G.F. Hall (Editors), Pedogenesis and Soil Taxonomy, Part I: Concepts and Interactions, Developments in Soil Science II, Amsterdam, Elsevier, pp. 141-192.

André, A. and Beaudet, G., 1967. Observations nouvelles sur les dépôts quaternaires des environs de Rabat. Revue de Géographie du Maroc, 11: 77-98.

André, A. and Beaudet, G., 1980. Formations marines et tectonique plio-quaternaires du NW Atlantique. In: Colloque: Niveaux marins et tectonique quaternaires dans l'aire méditerranéenne. Paris, pp. 449-477.

Beaudet, G., 1969. Plateau Central Marocain et ses Bordures. Étude Géomorphologique. Thèse, Imprimeries Françaises et Marocaines, Rabat, 478 pp.

Brewer, R., 1964. Fabric and Mineral Analysis of Soils. John Wiley and Sons, New York, 470 pp.

Bronger, A., 1966. Lösse, ihre Verbraunungszonen und fossilen Böden - ein Beitrag zur Gliederung des oberen Pleistozäns von Südbaden. Schriften d. Geograph. Instit. d. Universität Kiel, 25/2: 1-113.

Bronger, A., 1969/70. Zur Mikromorphologie und zum Tonmineralbestand quartärer Lößböden in Südbaden. Geoderma, 3: 281-320.

Bronger, A., 1974. Zur postpedogenen Veränderung bodenchemischer Kenndaten insbesondere von pedogenen Eisenoxiden in fossilen Lößböden. Trans. 10 Int. Cong. Soil Sci., Moscow, VI (II): 429-441.

Bronger, A., 1976. Zur quartären Klima- und Landschaftsgeschichte des Karpatenbeckens auf paläopedologischer und bodengeographischer Grundlage. Kieler Geographische Schriften, 45: 1-268.

Bronger, A., 1978. Die Sequenzen Braunerde (-Lessivé) - erdiger Braunlehm (-Lessivé). Tonverlagerung als Klimaindikator? In: M. Delgado (Editor), Micromorfolgia del Suelos. Proc. V Int. Working Meeting on Soil Micromorpology, Granada, Spain, Univeristy of Granada, pp. 303-323.

Bronger, A., 1978. Climatic sequences of steppe soils from eastern Europe and the USA with emphasis on the genesis of the "argillic horizon". Catena, 5: 33-51.

Bronger, A., 1991. Argillic horizons in modern loess soils in an ustic soil moisture regime? Comparative studies in forest-steppe and steppe areas from Eastern Europe and the USA. Advances in Soil Science, 15: 41-90.

Bronger, A. and Bruhn, N., 1989. Relict and recent features in tropical Alfisols from south India. In: A. Bronger and J. Catt (Editors), Paleopedology - Nature and Application of Paleosols. Catena Suppl. 16: 107-128.

Bronger, A. and Bruhn, N., 1990. Clay illuviation in semiarid- tropical (SAT) Alfisols? A first approach to a new concept. In: L.A. Douglas (Editor), Soil Micromorphology: A Basic and Applied Science. Proc. VIII Int. Working Meeting on Soil Mircromorphology, San Antonio, Texas, July 1988. Developments in Soil Science 19, Elsevier, Amsterdam, pp. 175-181

Bronger, A. and Catt, J., 1989. Paleosols: problems of definition, recognition and interpretation. In: A. Bronger and Catt, J. (Editors), Paleopedology - Nature and Applications of Paleosols, Catena Suppl. 16: 1-7.

Bronger, A., Ensling, J., Gütlich, P. and Spiering, H., 1983. Mössbauer studies on the rubification of terrae rossae in Slovakia. Clays and Clay Minerals, 31: 269-276.

Bronger, A., Ensling, J. and Kalk, E., 1984. Mineralverwitterung, tonmineralbildung und rubifizierung in terrae calcis der Slowakei. Ein beitrag zum paläoklimatologischen aussagewert von Kalkstein-Rotlehmen in Mitteleuropa. Catena, 11: 115-132.

Bronger, A. and Heinkele, T., 1989a. Micromorphology and genesis of paleosols in the Luochuan loess section, China: pedostratigraphical and environmental implications. Geoderma, 45: 123-143.

Bronger, A. and Heinkele, T., 1989b. Paleosol sequences as witnesses of Pleistocene climatic history. In: A. Bronger, and J. Catt (Editors), Paleopedology - Nature and Application of Paleosols. Catena Suppl., 16: 163-186.

Bronger, A., Pant, R.K. and Singhvi, A.K., 1987. Pleistocene climatic changes and landscape evolution in the Kashmir Basin, India: paleopedologic and chronostratigraphic studies. Quartemary Research, 27: 167-181.

Brückner, H., Halfar, R.A., Hambach, U., Laouina, A., Bensaad, N., Tailassane, M., Watfeh, A. Dating marine and eolian sequences in the Rabat region, Marocco. In: H. Brückner and B. Harrison (Editors) Time, Frequency and Dating in Geomorphology. Proc. COMTAG Symp., Tatranská Lomnica, CSFR, June 1992. Catena, Suppl.-Bd. (in press).

Bruhn, N., 1990. Substratgenese - Rumpfflächendynamik. Bodenbildung und Tiefenverwitterung in saprolitisch zersetzten granitischen Gneisen aus Südindien. Kieler Geographische Schriften, 74: 1-189.

Bruhn-Lobin, N. and Bronger, A., 1991. Mineralverwitterung und Tonmineralbildung in rezenten und reliktischen Terrae calcis im Raum Rabat/Marocco. Mitteilgn. Dtsch. Bodenkdl. Gesellsch. 66/ II, 1069-1072.

Bullock, P., Federoff, N., Jongerius, A., Stoops, G., Tursina, T. and Babel, U., 1985. Handbook for Soil Thin Section Description. Waine Research Publications Wolverhampton, 152 pp.

Bullock, P. and Thompson, M.L., 1985. Micromorphology of Alfisols. In: L.A. Douglas, and M.L. Thompson (Editors), Soil Micromorphology and Soil Classification, Soil Sci. Soc. Am. Spec. Publ. No. 15, Madison, Wisconsin, pp. 17-47.

Catt, J.A., 1988. Soils of the Pliocene-Pleistocene: do they distinguish types of interglacial? Trans. Roy. Soc. London, 318: 539-557.

Catt, J.A., 1989. Relict Properties in Soils of the Central and North-West European Temperate Region. In: A. Bronger and J.A. Catt (Editors), Paleopedology, Nature and Application of Paleosols. Catena Supplement, 16: 41-58.

Choubert, G. and Faure-Muret, A., (1959). Note au sujet du Pléstocène de la région de Rabat Maroc.-Comptes Rendus de la Société Géologique de France, 1: 19.

Courty, M.A., Dhir, P. and Raghavan, M., 1987. Microfabrics of calcium carbonate accumulation in arid soils of western India. In: N. Fedoroff, L.M. Bresson and M.A. Coutry (Editors), Soil Micromorphology. Proc. VII Int. Working Meeting of Soil Micromorphology, Paris, July 1985. Association Française pour l'Etude du Sol, Plaisir, France, pp. 227-234.

Cremaschi, M., 1987. Paleosols and Vetusols in the Central Po Plain (Northern Italy) - A Study in Quaternary Geology and Soil Development. Edizioni Unicopli, Milano, 306 pp.

Eswaran, H., 1979. Micromorphology of Oxisols. In: F.H. Beinroth and S. Paramananthan (Editors), Second International Soil Classification Workshop Part I: Malaysia. Bangkok: Soil Survey Division, Land Development Department, pp. 61-74.

Eswaran, H., Sys, C. and Sousa, E.C., 1975. Plasma infusions -a pedological process of significance in the humid tropics. Anales de Edafologia y Agrobiologia, 34: 665-674.

Fanning, D.S. and Fanning, M.C.B., 1989. Soil - Morphology, Genesis and Classification. John Wiley and Sons, New York, 395 pp.

FAO-Unesco, 1974. Soil Map of the World, Vol. I (Legend), Paris.

Fedoroff, N. and Eswaran, H., 1985. Micromorphology of Ultisols. In: L.A. Douglas and M.L. Thompson (Editors), Soil Micromorphology and Soil Classification. Soil Science Soc.of Am. Spec. Publ. No. 15, Madison,Wisc., pp. 145-164.

Gigout, M., 1958. Sur le Pliocène et le Quaternaire de Rabat et Salé. Comptes Rendus de l'Académie des Sciences, Paris, t. 247, no. 17.

Guo, Z., Fedoroff, N. and An, Z., 1991. Genetic Types of the Holocene Soil and the Pleistocene Paleosols in the Xifeng Loess Section in central China. In: T.S. Liu (Editor), Loess, Environment and Global Change. Science Press, Beijing, pp. 93-111.

Heinkele, T., 1990. Bodengeographische und paläopedologische Untersuchungen im zentralen Lößplateau von China - ein Beitrag zur quartären Klima- und Landschaftsgeschichte. Schriftenreihe Instf. Pflanzenernährung und Bodenkunde d. Universität Kiel, 9: 1-120.

Heller, F. and Liu, T.S., 1982. Magnetostratigraphical dating of loess deposits in China. Nature, 300, pp. 431- 432.

Heller, F. and Liu, T.S., 1984. Magnetism of Chinese loess deposits. Geophys. J. R. Astr. Soc. 77: 125-141.

Kale, V.S., 1983. The Indian Peninsular movements, Western Ghat formation and their geomorphic repercussions - a geographical overview. Trans. Inst. Indian Geographers, 5: 145- 155.

Klootwijk, C.T. and Peirce, J.W., 1979. India's and Australia's pole path since late Mesozoic and the India-Asia collision. Nature, 282: 605-607.

Krantz, B.A., Kampen, J. and Russell, M.B., 1978. Soil Management Differences of Alfisols and Vertisols in the Semiarid Tropics. In: M. Stelly (Editor), Diversity of Soils in the Tropics. Am. Soc. Agron. Spec. Public. No 34. Madison, Wisconsin, pp. 77-95.

Kubiena, W.L., 1959. Prinzipien und Methodik paläopedologischer forschung im dienste der stratigraphie. Z. deutsch. Geol. Ges., 111: 643-652.

Kubiena, W.L., 1964. Zur Mikromorphologie und Mikromorphogenese der Lößböden Neuseelands. In: A. Jongerius (Editor), Soil Micromorphology, Proc. II Int. Working Meeting on Soil Micromorphology. Arnhem, The Netherlands Sept. 1964. Elsevier, Amsterdam, pp. 219-235.

Kubiena, W.L., 1970. Micromorphological Features of Soil Geography. Rutgers Univ. Press, New Brunswick, 254pp.

Lefevre, D., Rayanal, J.P., Texier, J.P., 1985. De la fin du Villafranchien au début du Soltanien. Colloque héritages géomorphologiques et paléoenvironnments du Quaternaire moyen méditerranéen, Paris.

Liu, T.S., (Editor) 1985. Loess and the Environment. Beijing, 251 pp.

McKeague, J.A., 1983. Clay Skins and Argillic Horizons. In: P. Bullock and C.P. Murphy (Editors), Soil Micromorphology, volume 2. Soil Genesis. Proc. VI Int. Working Meeting on Soil Micromorphology, London, August 1981, AB Academic Publishers, Berkhamsted, U.K., pp. 367-387.

Meyer, B. and Kruse, W., 1970. Untersuchungen zum Prozess der Rubefizierung (Entkalkungsrötung) mediterraner Böden am Beispiel kalkhaltiger marokkanischer Küsten-Dünen. Göttinger Bodenkundliche Berichte, 13: 77-140.

Molnar, P., 1986. The geologic history and structure of the Himalaya. American Scientist, 74: 144-154.

Murthy, R.S., Hirekerur, L.R., Deshpande, S.B. and Venkata Rao, B.V., 1982. Benchmark Soils of India. Morphology, Characteristics and Classification for Resource Management. Nat. Bureau of Soil Survey and Land Use Planing (ICAR), Nagpur.

National Atlas of the Peoples Republic of China, 1984. Atlas Publishing Company, Beijing.

Nettleton, W.D., Flach, K.W. and Brasher, B.R., 1969. Argillic horizons without clay skins. Soil Sci. Soc. Am. Proc., 33: 121-125.

Nettleton, W.D., Gamble, E.E., Allen, B.L., Borst, G. and Peterson, F.F., 1989. Relict Soils of Subtropical Regions of the United States. In: A. Bronger and J. Catt (Editors), Paleopedology: Nature and Application of Paleosols. Catena Suppl., 16: 59-93.

Olson, C.G., 1989. Soil Geomorphic Research and the Importance of Paleosol Stratigraphy to Quaternary Investigations, Midwestern USA. In: A. Bronger and J. Catt (Editors), Paleopedology: Nature and Application of Paleosols. Catena Suppl., 16: 129-142.

Retallak, G.J. and Wright, V.P., 1990. Micromorphology of Lithified Paleosols. In: L.A. Douglas (Editor), Soil Micromorphology: A Basic and Applied Science. Proc. VIII Int. Working Meeting on Soil Mircromorphology, San Antonio, Texas, July 1988. Developments in Soil Science 19, Elsevier, Amsterdam, pp 441-452.

Ruhe, R.V., 1956. Geomorphic surfaces and the nature of soils. Soil Sci., 82: 441-455.

Schmidt-Lorenz, R., 1986. Die Böden der Tropen und Subtropen. In: S. Rehm (Editor), Handbuch der Landwirtschaft und Ernährung in den Entwicklungsländern: Band 3: Grundlagen des Pflanzenbaus in den Tropen und Subtropen. Eugen Ulmer, Stuttgart, pp. 47-92.

Schnütgen, A. and Späth, H., 1983. Mikromorphologische Sprengung von Quarzkörnern durch Eisenverbindungen in tropischen Böden. Z. Geomorph. N.F. Suppl. Bd., 48: 17-34.

Schroeder, D., 1984. Soils - Facts and Concepts. International Potash Institute, Bern, 140 pp.

Semmel, A., 1989. Paleopedology and Geomorphology: Examples from the Western Part of Central Europe. In: A. Bronger and J. Catt (Editors), Paleopedology -Nature and Application of Paleosols. Catena Suppl., 16: 143-162.

Skowronek, A., 1978. Untersuchungen zur terra rossa in E- und S- Spanien - ein regionalpedologischer Vergleich. Würzburger Geographische Arbeiten, 47: 1-272.

Smith, G.D., 1983. Historical Development of Soil Taxonomy - Background. In: L.P. Wilding, N.E. Smeck and G.F. Hall (Editors), Pedogenesis and Soil Taxonomy Part I: Concepts and Interactions. Elsevier, Amsterdam, pp. 23-49.

Smolikova, L., 1967. Polygenese der fossilen Lößböden der Tschechoslowakei im lichte mikromorphologischer Untersuchungen. Geoderma, 1: 315-324.

Smolikova, L., 1971. Gesetzmäßigkeiten der Bodenentwicklung im Quartär. Eiszeitalter u. Gegenwart, 22: 156-177.

Smolikova, L., 1990. Problematika paleopedologie. Regionalni paleopedologie. In: J. Nemecek, L. Smolikova and M. Kutilek, (Editors): Pedologie a paleopedologie, Praha, pp. 381-479.

Soil Survey Staff, 1975. Soil Taxonomy. U.S. Dept. Agric. Handb. 436, U.S. Gov. Printing Office, Washington, D.C., 754 pp.

Soil Survey Staff, 1990. Keys to Soil Taxonomy. SMSS Technical Monograph No.6, 4th editon. Virginia Polytechnic Institute and State University, Blacksburg, Virginia, 422 pp.

Somayajulu, B.L.K. and Srinivasan, M.S., 1986. Indian Ocean Floor: Evolution and Palaeoenvironment. In: The Indian Lithosphere. Indian National Science Academy, Kapoor Art Press, New Delhi, pp. 124-133.

Stearns, C.E., 1978. Pliocene-Pleistocene emergence of the Morocan Meseta. - Geological Society of America, Bulletin, 89: 1630-1644.

Stoops, G., 1989. Relict properties in zonal soils of humid tropical regions with special reference to Central Africa. In: A. Bronger and J.A. Catt, (Editors), Paleopedology - Nature and Application of Paleosols. Catena Suppl., 16: 95-106.

Stoops, G.J. and Buol, S.W., 1985. Micromorphology of Oxisols. In: L.A. Douglas, and M.L. Thompson (Editors), Soil Micromorphology and Soil Classification. Soil Sci. Soc. Am. Spec. Publ. No. 15, Madison, Wisconsin, pp. 105-119.

Van Wambeke, A., 1985. Calculated Soil Moisture and Temperature Regimes of Asia Soil Management Support Services Tech. Monograph No.9, Ithaca, N.Y., 144 pp.

Walter, H., 1974. Die Vegetation Osteuropas, Nord- und Zentralasiens. Fischer, Stuttgart pp. 1-452.

Wieder, M. and Yaalon, D.H., 1982. Micromorphological fabrics and developmental stages of carbonate nodular forms related to soil characteristics. Geoderma, 28: 203-220.

Weisrock, A., 1980. Géomorphologie et paléoenvironnements de l'Atlas atlantique, Maroc. Thèse, Paris, 981 pp.

Wilding, L., 1990. Preface. In: L.A. Douglas (Editor), Soil Micromorphology: A Basic and Applied Science. Proc. VIII Int. Working Meeting on Soil Mircromorphology, San Antonio, Texas, July 1988. Developments in Soil Science 19, Elsevier, Amsterdam, pp. viii-x.

Yaalon, D.H., 1971. Soil-forming processes in time and space. In: D.H. Yaalon (Editor), Paleopedology. Origin, nature and dating of paleosols. ISSS and Israel Univ. Press, Jerusalem, pp. 29- 39.

Zachariae, G., 1964. Welche Bedeutung haben Enchytraeen im Waldboden? In: A. Jongerius (Editor), Soil Micromorphology. Proc. II Int. Working Meeting on Soil Micromorphology Arnhem, The Netherlands, September 1964, Elsevier, Amsterdam pp. 57-68.

Zhu, X., Li, Z., Peng, X. and Zhang, S., 1983. Soils of the Loess Region in China. Geoderma, 29: 237-255.

Pedosedimentary fabrics of soils within loess and colluvium in southern England and southern Germany

R.A. Kemp[1], H. Jerz[2], W. Grottenthaler[2] and R.C. Preece[3]

[1]*Department of Geography, Royal Holloway London University, Egham, United Kingdom*
[2]*Bayerisches Geologisches Landesamt, Munich, Germany*
[3]*Department of Zoology, Cambridge University, United Kingdom*

ABSTRACT

Kemp, R.A., Jerz, H., Grottenthaler, W. and Preece, R.C., 1994. Pedosedimentary fabrics of soils within loess and colluvium in southern England and southern Germany. In: A.J. Ringrose-Voase and G.S. Humphreys (Editors), Soil Micromorphology: Studies in Management and Genesis. Proc. IX Int. Working Meeting on Soil Micromorphology, Townsville, Australia, July 1992. Developments in Soil Science 22, Elsevier, Amsterdam, pp. 207-219.

The necessity of accounting for not only pedogenic, but also sedimentary, geomorphic and diagenetic processes when attempting to interpret buried soils within aeolian and colluvial sequences is demonstrated by reference to three sites in England and Germany. Micromorphology has underpinned these detailed studies and helped to unravel complex pedosedimentary and diagenetic relationships. The buried soil at Northfleet (England) formed over a significant period of time at a stable landsurface in a parent material containing transported relicts of an older soil. Many of its most notable characteristics reflect processes active at the time of, or subsequent to, burial. The vertical succession of Late-Glacial colluvial materials at Ventnor (England) represents a single thick accretionary soil, although a laterally-extensive, well-developed humic horizon over a metre below the present surface relates to a period when conditions temporarily favoured establishment of a more stable landsurface. The buried pedocomplex at Attenfeld (Germany) is interpreted in terms of at least two phases of pedogenesis preceded, separated and postdated by sediment deposition. Insufficient thicknesses of material were deposited during the middle sedimentary phase to isolate the underlying soil horizons from effects of pedogenesis associated with the next major stable landsurface. A buried welded soil therefore has eventuated.

INTRODUCTION

Vertical stacks of pedogenically-altered units within sedimentary sequences in mid-latitudes are frequently interpreted as representing 'stable' phases of soil formation interspersed with 'unstable' phases of sediment deposition (Morrison, 1978). This model has led to the widespread use of buried soils as stratigraphic units representing regionally-extensive depositional hiatuses (*e.g.* Rose *et al.*, 1985; Liu Tungsheng *et al.*, 1985). Valuable information has been derived from such buried soils on environmental conditions during periods of geological time unrepresented within the depositional record.

Fig. 1. Location of study sites.

The polycyclic nature (Duchaufour, 1977) of some buried soils has provided the basis for relatively complex reconstructions of palaeoenvironmental change within 'soil-forming intervals', notably across interglacial/glacial transitions (*e.g.* Federoff and Goldberg, 1982; Kemp, 1987a). Difficulties in ascertaining and interpreting the environmental significance of buried soils, whether monocyclic or polycyclic in terms of climatically-induced pedogenic pathways, are often a consequence of complications brought about by diagenetic changes (*e.g.* compaction or groundwater reactions) **after** burial (Catt, 1990; Retallack, 1990) or geomorphic modifications **before** (complete) burial. Erosion, for instance, frequently results in profile truncation and hiatuses within the pedosedimentary record and/or mixing and deposition of transported soil material within covering sediments (Thompson and Smeck, 1983; Kemp, 1987 a and b).

The notion of landscape 'stability' with complete cessation of erosion and deposition processes during 'soil-forming intervals' represented by the buried soils, although attractive in principle, is frequently difficult to accept. Periodic or continual additions of thin layers of alluvial, colluvial or aeolian sediments may lead to accretionary soils with pedological features extending throughout much of the vertical column (Catt *et al.*, 1987; Catt, 1990; McDonald and Busacca, 1990). Some entire loess, colluvial and alluvial sequences therefore may be considered as pedocomplexes (Kukla, 1977; Kraus and Bown, 1986). Even when mature (non-accretionary) soils do form, subsequent phases of sedimentation are often insufficient to bring about true burial and isolation from the effects of pedogenesis associated with the next major 'stable' landsurface (Catt, 1990). Overlapping or 'welded' soils (Ruhe and Olson, 1980) then eventuate within the sequence, characterised by complex depth distributions of superimposed pedological features (Federoff and Goldberg, 1982; Cremaschi *et al.*, 1990).

Field work by itself is often unable to unravel the types of complexities discussed above: micromorphology is increasingly being used to aid the interpretation. This paper aims to illustrate the usefulness of the technique in elucidating pedosedimentary and diagenetic histories of buried soils within colluvial and aeolian sequences by reference to three current studies in England and Germany (Fig. 1).
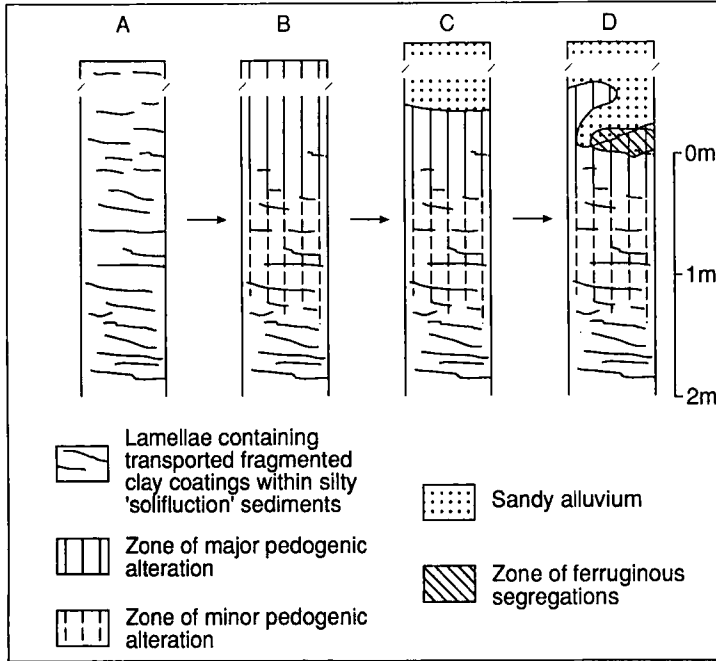
Fig. 2. Schematic summary of the main sequence of pedosedimentary and diagenetic events responsible for the buried soil at Northfleet. **A)** Deposition of silty 'solifluction' sediments. **B)** Soil formation. **C)** Truncation and deposition of sandy alluvium. **D)** Slumping or loading of alluvium into soil: mobilisation of iron oxides by groundwaters. Original thickness of sandy alluvium is unknown due to its partial removal by archaeologists earlier this century.

METHODS

The basic stratigraphy at each site had been established by previous fieldwork. Undisturbed blocks were removed in Kubiena tins from relevant units within the vertical successions: sampling intervals varied between 0.1 and 0.4 m. Blocks were acetone-dried, impregnated with polyester resin and made into thin sections (70 × 50 mm) according to standard techniques (Lee and Kemp, 1992). Thin sections were described using the terminology of Bullock *et al.* (1985). The proportion of thin section area covered by illuvial clay was estimated by comparison to point-counted reference thin sections (Murphy and Kemp, 1984).

NORTHFLEET

The existence of a soil developed in calcareous solifluction deposits infilling a river channel, and buried beneath fluvial sediments containing molluscan and mammalian assemblages characteristic of a temperate environment, was first noted at Northfleet in Kent, U.K. (Fig. 1) by Burchell (1957) and Zeuner (1959). Kemp (1991) re-examined the buried soil, concentrating particularly on its micromorphology, and was able to demonstrate a more complex pedosedimentary history than envisaged by earlier workers (Fig. 2).
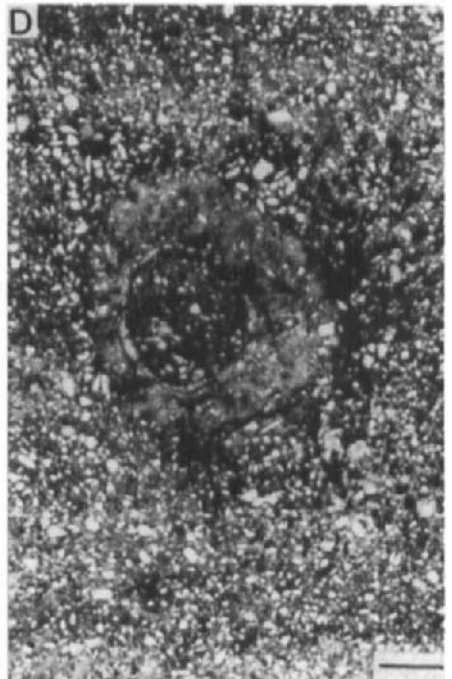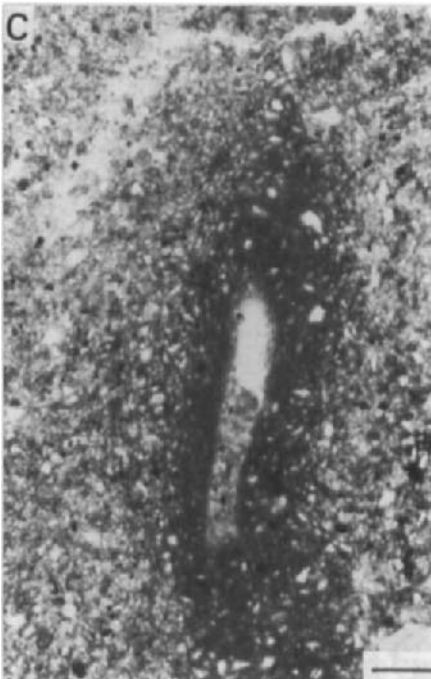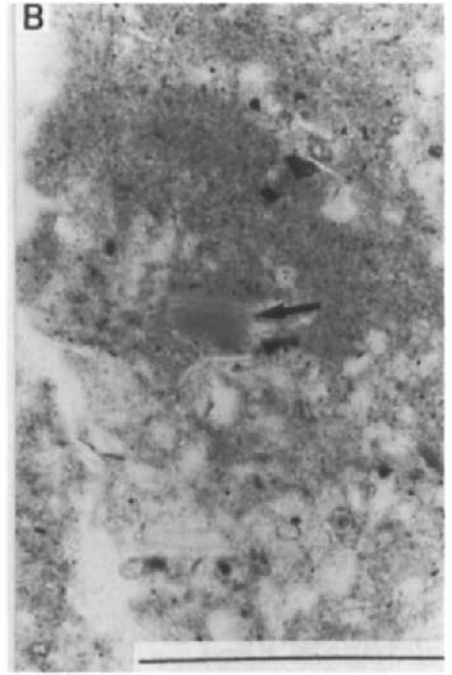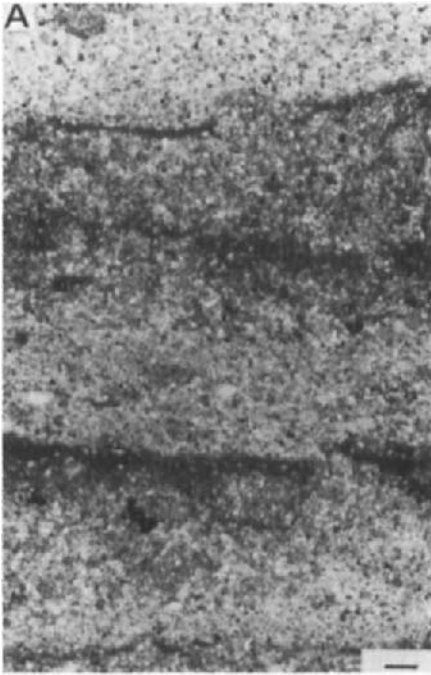
The silty parent material contains a series of discontinuous, sorted fine- and coarse-textured lamellae (Figs 2A and 3A) in which rare, rounded, fragmented clay coatings are embedded (Fig. 3B). These features indicate that the sediment was at least partially derived from a soil elsewhere and transported to the present location by water, possibly by sheet or overland flow. The lamellae become increasingly disrupted and eventually cannot be recognised towards the top of the soil, a depth distribution attributable to the effects of pedoturbation processes associated with a single landsurface that was stable for a substantial period of time (Fig. 2B). During this 'soil-forming interval', the upper horizons were decalcified and some of the solute reprecipitated lower down in the form of calcitic hypocoatings and coatings around channels.

The re-establishment of a river channel led to truncation of the soil and deposition of fluvial sediments (Fig. 2C). Silty clay coatings, which postdate the calcitic features in the soil (Fig. 3C), probably accumulated relatively rapidly at this stage due to infiltration of suspended sediment load and/or translocation of slaked soil material. The boundary between the soil and covering sediments is very irregular (Fig. 2D) with structures not dissimilar to those attributed to cryoturbation elsewhere by Van Vliet-Lanoe (1988). The absence of associated cryogenic features and the temperate nature of the molluscan fauna in the overlying sediments, however, provide no justification for invoking a periglacial formative environment at this stage. A more plausible interpretation for the structures is that they are diagenetic, formed by slumping or loading of the sandy alluvium into the underlying saturated, fine-textured soil (Fig. 2D). Post-burial processes are also largely responsible for the reddish (5YR) hues of the upper horizons of the soil. Initially interpreted as evidence for intense *in situ* weathering 'in a climate somewhat warmer than at present' (Zeuner, 1959, p. 165), the colours are clearly associated with ferruginous segregations which are frequently superimposed on calcitic and silty clay coatings (Fig. 3D) and extend across the boundary between the truncated soil and burying sediment (Fig. 2D).

In summary, the buried soil at Northfleet has a more complex history than initially conceived. Formed over a significant period of time at a stable landsurface, yet in a parent material containing transported relicts of an older soil, many of its most notable characteristics appear to reflect processes active at the time of, or subsequent to, burial.

VENTNOR

A laterally-extensive section at the base of a dry valley near Ventnor on the Isle of Wight, UK (Fig. 1) consists of a clearly-defined pale brown (10YR 6/3) 'humic' soil horizon up to 35 cm thick developed within, and covered by, poorly sorted colluvial sediments derived primarily from the local chalk bedrock. A radiocarbon date of 11690 ± 120 BP from charcoal within the humic horizon is comparable to that obtained from buried soils within dry valley colluvial sequences in Kent (Preece, 1991). These dates correspond to the so-called 'Allerod interstadial'

Fig. 3. Photomicrographs from thin sections at Northfleet. Plane polarized light. Scale bar: 0.25mm. **A)** Fine- and coarse-textured lamellae towards base of buried soil. **B)** Fragmented clay coating (arrowed) embedded within fine-textured lamellae. **C)** Calcitic hypocoating around a channel postdated by a partial infilling of silty clay. **D)** Ferruginous segregation postdating a calcitic hypocoating and a silty clay infilling.
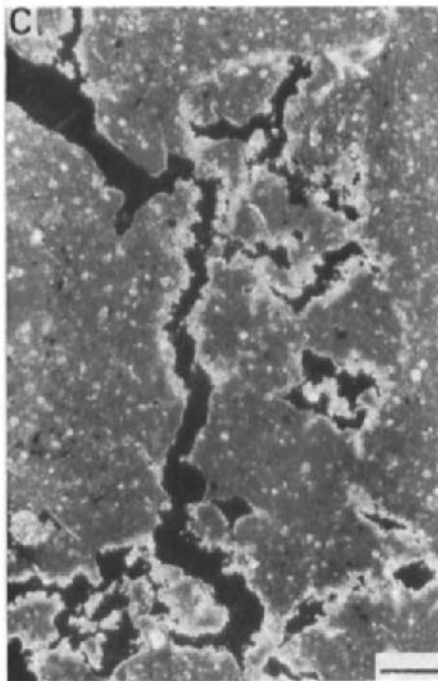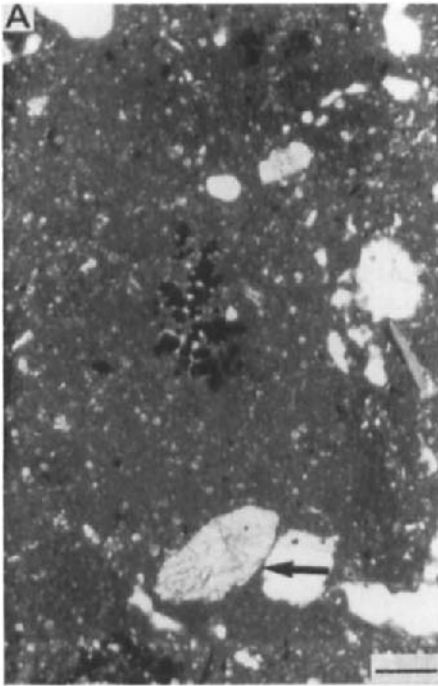
of the Late-Glacial when there was a period of regional landscape stability of sufficient duration to allow soil horizonation to develop.

Micromorphological analysis confirms the pedogenic origin of the humic horizon at Ventnor: its colouration is due to concentration of organic components, mainly cell residues, amorphous fine material, punctuations and groundmass pigments (Fig. 4A). Additionally there are numerous biological channels, many of which contain calcitic root pseudomorphs or faunal excrements coated by (microbially-formed?) needle fibre calcite (Fig. 4B). Nodules of interlinked, euhedral microsparite and sparite crystals (Fig. 4A) are also prevalent: these bear close resemblance to those apparently produced in the calciferous gland of earthworms (Bal, 1977).

Similar biological features, although less numerous, occur at all levels within the sequence. Some of these features above the humic horizon could have been eroded from the soil upslope, and transported, mixed and deposited within the colluvial material. Their presence below along with the ubiquitous *in situ* calcitic concentration and depletion features (Fig. 4C), however, suggest that the complete Late-Glacial sequence should be considered as a single thick accretionary soil. Increments of colluvial material would have been periodically added to the surface whilst the soil was continuing to form (Fig. 5). Micritic, speckled/impure clay coatings (Fig. 4D) on clast and void surfaces throughout this accretionary soil therefore formed during, or just after, colluvial events by rapid vertical migration of mobile slurries or suspensions of clay and very fine silt. The accretionary soil 'grew upwards' without developing discrete horizons (Figs $5A_n$, $5A_{n+n}$ and $5C_n$), except during the Allerod when conditions favoured establishment of a more stable landsurface. The dominance of pedogenic over geomorphic inputs during this period of relative landsurface stability encouraged the formation of a discrete 'humic' horizon (Fig. 5B). The subsequent deterioration in environmental conditions after the interstadial led to renewed accretionary pedogenesis and burial of the horizon (Fig. $5C_n$).

Molluscan evidence at this and other sites (Preece, 1991) indicate that climatic conditions were not constant during the Late-Glacial. Rates, if not types, of soil processes presumably varied in response to these changes. The fact that the molluscan data appear to provide a relatively continuous record of environmental change during this time period is in itself independent confirmation of the accretionary nature of the soil. Molluscan species typical of Mid-Holocene environments (Preece, unpublished data) occur in the sediments immediately above those attributable to the Late-Glacial. The absence of intervening Early Holocene sediments is presumably due to erosion between the Late Glacial and Mid-Holocene (Fig. 5D). The A, B, BC and C horizons of the well developed soil at the present surface extend through the Holocene into the Late-Glacial materials (Fig. 5E). It is therefore difficult to differentiate between some of the Post- and Late-Glacial pedological features. On this basis, it could be argued that the 'humic' horizon at Ventnor is not a 'buried' soil in the strictest sense (Catt, 1990), but that it is part of a vertical sequence representing a single complex soil with

---

Fig. 4. Photomicrographs from thin sections at Ventnor. PPL: plane polarized light; XPL: crossed polarized light. Scale bar: 0.25 mm. **A)** Amorphous organic fine material (black) and a nodule of interlinked, euhedral calcite crystals (arrowed). PPL. **B)** Needle fibre calcite on surface of excrements. XPL. **C)** Calcitic depletion hypocoatings along planar void and vugh surfaces. XPL. **D)** Micritic, speckled/impure clay coating on surface of chalk clasts. PPL.
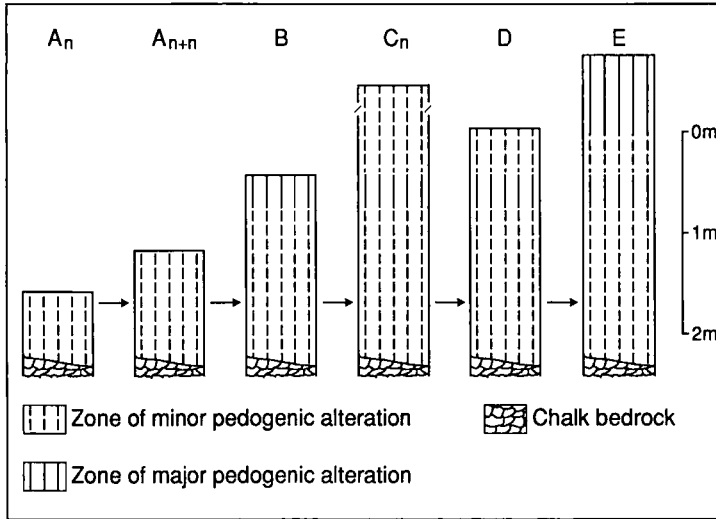
Fig. 5. Schematic summary of the main sequence of pedosedimentary events responsible for the accretionary soil profile at Ventnor. A) Weak pedogenesis simultaneous with deposition of colluvial sediments leading to the formation of an accretionary soil. A_n and A_{n+n} represent arbitrary moments in time during this stage illustrating the 'upward growth' of the soil. B) Establishment of a stable landsurface and development of the 'humic' horizon. C) Renewed accretionary soil development. C_n represents an arbitrary point in time during this stage. D) Truncation of accretionary soil. E) Deposition of colluvial sediments, establishment of a stable landsurface and soil development.

transported, accretionary and welded (Ruhe and Olson, 1980) components. Such a conclusion, however, should not reduce the important stratigraphic significance attached to this regionally-extensive soil horizon.

ATTENFELD

A series of buried interglacial and interstadial soils have been recognised within thick sequences of loess and solifluction deposits on low-angled interfluves in the Bavarian Alpine Foreland of Germany (*e.g.* Brunnacker, 1964). Thin sections from some of the soils at a few sites contain disrupted argillic fabrics indicative of complex pedogenic and environmental histories (Léger, 1987). A new exposure at Attenfeld, north-west of Munich (Fig. 1), consists of over 8.5 m of loess and solifluction deposits overlying Tertiary sands (Jerz and Grottenthaler, in press). Three soils occur within the Quaternary sediments, the oldest developed in "pre-Riss solifluction deposits" derived primarily from loess (Loess Loam A and Loess Loam B) or Tertiary sands (reworked Tertiary deposits) (Fig. 6). This basal soil is truly 'buried' in the sense that it was covered by sufficient thickness of material to isolate it from subsequent pedogenesis (Catt, 1990). There is no evidence for appreciable diagenetic alteration, whilst any weak accretionary pedological depth functions, which might have developed particularly during incremental loess accumulation, were masked and nullified by more intense pedogenesis associated with long-term landsurface stability. This buried soil at
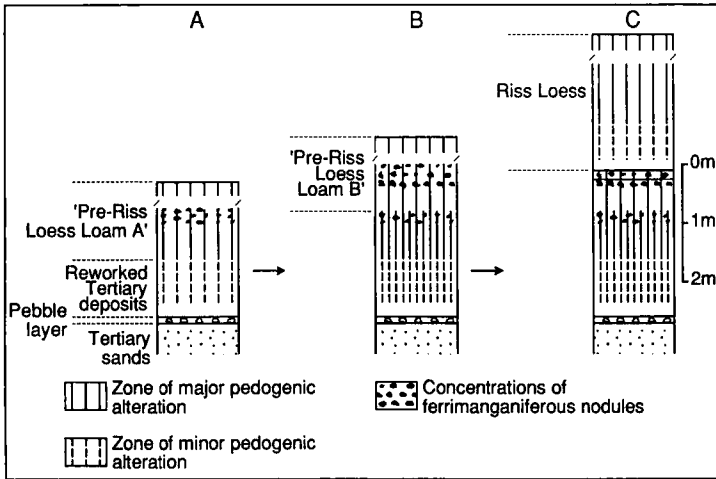
Fig. 6. Schematic summary of the main sequence of pedosedimentary events responsible for the buried pedocomplex at Attenfeld. A) Deposition of solifluction deposits (reworked Tertiary deposits and Loess Loam A, establishment of a stable landsurface and soil development. B) Truncation, deposition of Loess Loam B, establishment of a stable landsurface and soil development. Pedogenic activity extended throughout the Loess Loam B and into the underlying truncated soil developed in Loess Loam A. C) Truncation and deposition of units of calcareous loess. Pedogenic processes associated with major phases of landsurface stability between deposition of the different loess units did not extend into the truncated pedocomplex.
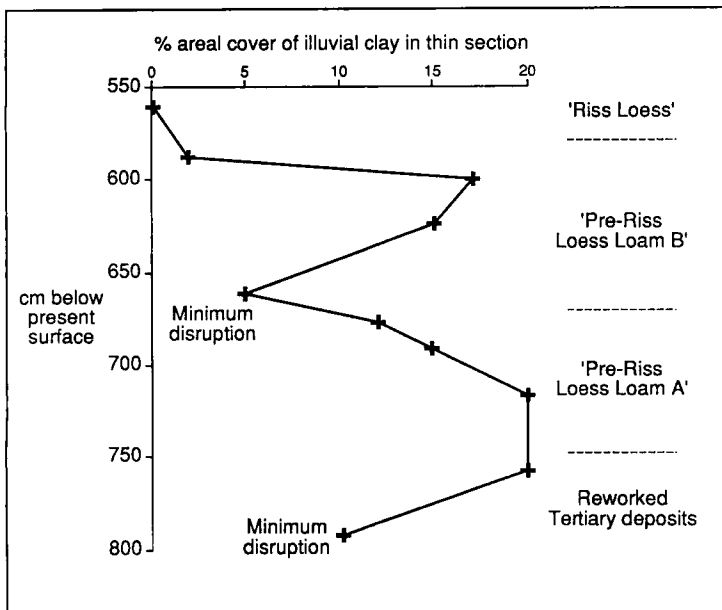
Fig. 7. Depth function of estimated illuvial clay content for the buried pedocomplex at Attenfeld.
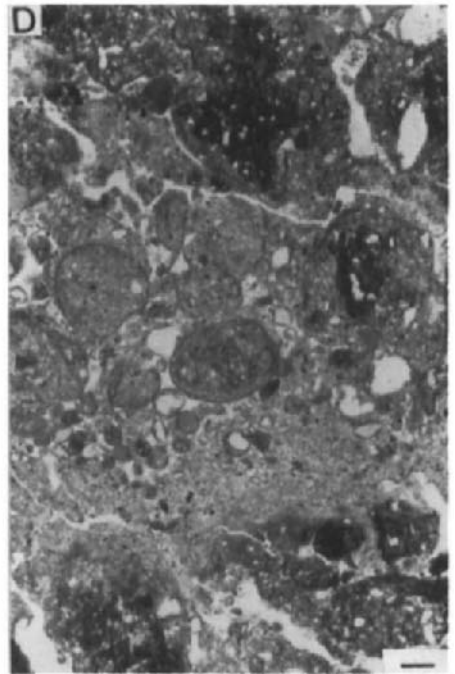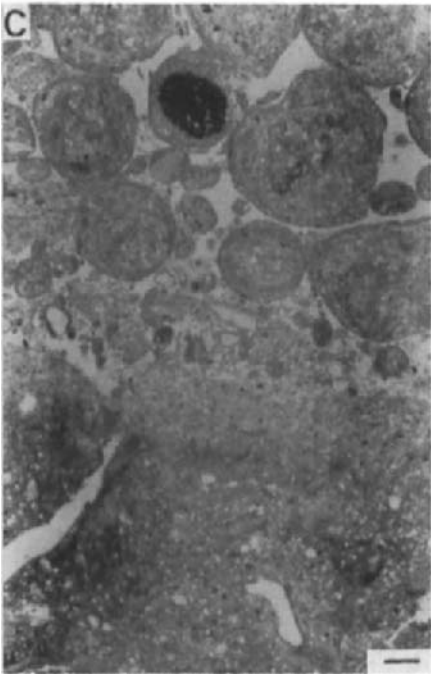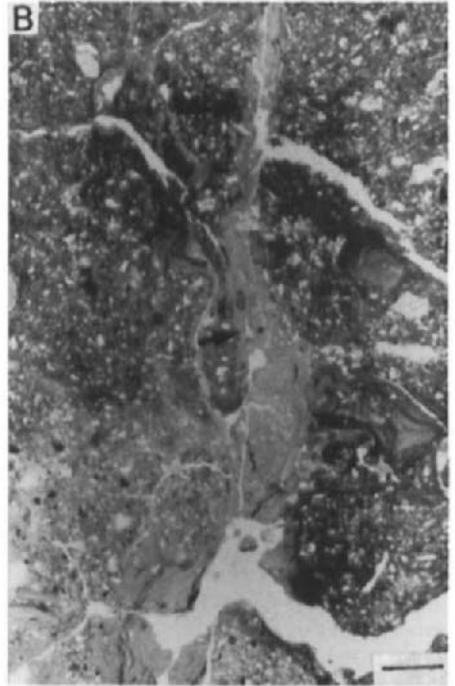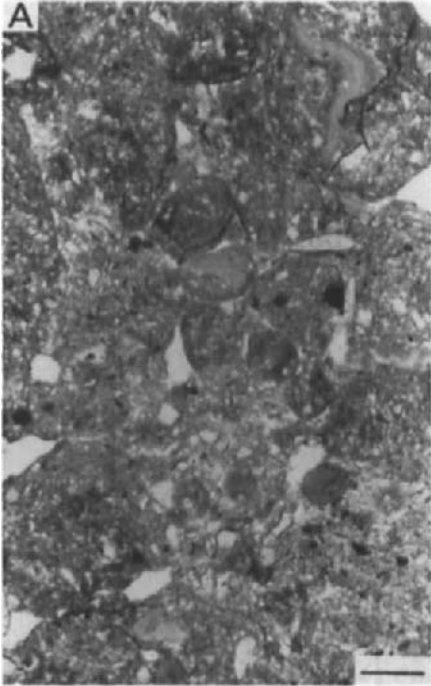
Attenfeld, however, is in many respects more complicated than the examples previously discussed from Northfleet and Ventnor. Detailed descriptions of thin sections throughout the unit have highlighted complex depth functions of total illuvial clay contents (Fig. 7) and individual or superimposed pedofeatures. Careful consideration and interpretation of these patterns have allowed a detailed pedosedimentary history to be reconstructed (Fig. 6).

Deposition of the reworked Tertiary deposits and Loess Loam 'A' was followed by a 'stable' landscape phase of sufficient duration for a well-developed soil to form (Fig. 6A). Fine, coarse and silty clay was translocated from the surface horizons along channels and planar voids into the subsoil: the lower peak in the illuvial-clay depth function (Fig. 7) is largely attributable to this phase. Many of the textural coatings, particularly in the upper parts of this illuvial horizon, were subsequently disrupted by freeze-thaw activity. Supporting evidence for such a cryogenic environment is provided by the remnants of a sorted platy structure and granular aggregates (Fig. 8A) which are similar to those reported forming at the present in the Arctic by Van Vliet-Lanoe (1985, 1988). At some stage during this first phase, drainage deteriorated to such an extent that iron and manganese were redistributed and concentrated in the form of superimposed ferrimanganiferous mottles and nodules within the upper parts of the argillichorizon (Fig. 6A). Renewed geomorphic activity then led to truncation of the soil and deposition of the Loess Loam B (Fig. 6B).

The second phase of soil development associated with a new landsurface (Fig. 6B) was characterised by further translocation of fine, coarse and sometimes silty clay. Maximum illuviation was at the level of the upper peak shown on the illuvial clay depth function (Fig. 7), although fine clay also accumulated lower down within the Loess Loam A and reworked Tertiary deposits. Recognition of these undisturbed limpid clay coatings are important with regards to the proposed pedosedimentary sequence as they are superimposed upon, and thus clearly postdate, the disrupted argillic and Fe/Mn-impregnated fabric of stage A (Fig. 8B). Ferrimanganiferous nodules and concentration or depletion mottles also developed higher up the profile within the Loess Loam B during stage B (Fig. 6B). Major cryogenic disruption in the upper part of the soil resulted in fragmentation and deformation of clay coatings, fracturing and rounding of aggregates and formation of reverse-sorted cappings (Figs 8C and 8D).

Truncation of the soil, and possible mixing and redeposition of remnants of eluvial and illuvial horizons, was followed by deposition of over 5 m of calcareous loess. The present surface soil and two buried soils are developed within this aeolian unit (Jerz and Grottenthaler, in press). The basal part of the loess is not decalcified, however, and contains no micromorphological evidence of significant pedogenic alteration. It can be concluded, therefore, that the pedocomplex developed in solifluction deposits was effectively buried by the

---

Fig. 8. Photomicrographs from thin sections at Attenfeld. PPL. Scale bar: 0.25 mm. A) Clustering of rounded aggregates and fragmented clay coatings in part of pedocomplex developed in Loess Loam A. B) Clay coatings and infillings (arrowed) postdating Fe/Mn-impregnated fabric in part of pedocomplex developed in Loess Loam A. C) Reverse-sorted capping comprising rounded sand-size aggregates overlying progressively smaller aggregates and grains in part of pedocomplex developed in Loess Loam B. D) Melange of rounded aggregates, fragmented clay coatings, nodules and coated grains in part of pedocomplex developed in Loess Loam B.

loess and isolated from the major effects of soil processes associated with subsequent landsurfaces (Fig. 6C).

SUMMARY AND CONCLUSIONS

These selected examples from England and Germany have demonstrated the potential role and value of micromorphology in helping to reconstruct the succession of pedogenic, geomorphic, sedimentary and diagenetic processes responsible for buried soils within colluvial and aeolian sequences. Such an approach complements, but clearly does not replace, detailed field-based studies.

ACKNOWLEDGEMENTS

REFERENCES

Bal, L., 1977. The formation of carbonate nodules and intercalary crystals in the soil by the earthworm *Lumbricus rubellus*. Pedobiologia, 17: 102-106.

Brunnacker, K., 1964. Der Ablauf und Alterstellung altquartärer Verschüttungen im Maintal und nächst dem Donautal bei Regensburg. Eiszeitalter und Gegenwart, 15: 72-80.

Bullock, P., Federoff, N., Jongerius, A., Stoops, G. and Tursina, T., 1985. Handbook for Soil Thin Section Description. Waine Research Publications, Wolverhampton, 152 pp.

Burchell, J.P.T., 1957. A temperate bed of the last interglacial period at Northfleet, Kent. Geological Magazine, 94: 212-214.

Catt, J.A., 1990. Paleopedology manual. Quaternary International, 6: 1-95.

Catt, J.A., Bateman, R.B., Wintle, A.G. and Murphy, C.P., 1987. The 'loess' section at Borden, Kent, SE England. Journal of Quaternary Science, 2: 141-147.

Cremaschi, M., Federoff, N., Guerreschi, A., Huxtable, J., Colombi, N., Castelletti, L. and Maspero, A., 1990. Sedimentary and pedological processes in the Upper Pleistocene loess of Northern Italy. The Bagaggera sequence. Quaternary International, 5: 23-38.

Duchaufour, P., 1977. Pedology. George Allen and Unwin, London.

Federoff, N. and Goldberg, P., 1982. Comparative micromorphology of two Late Pleistocene paleosols (in the Paris Basin). Catena, 9: 227-251.

Jerz, H. and Grottenthaler, W. Quaternary sections with palaeosols in southern Bavaria, Germany. In: C. Turner (Editor), The Early Middle Pleistocene in Europe. Balkema, Rotterdam, in press.

Kemp, R.A., 1987a. The interpretation and environmental significance of a buried Middle Pleistocene soil near Ipswich Airport, Suffolk, England. Philosophical Transactions of the Royal Society of London, B317: 365-391.

Kemp, R.A., 1987b. Genesis and environmental significance of a buried Middle Pleistocene soil in eastern England. Geoderma, 41: 49-77.

Kemp, R.A., 1991. Micromorphology of the buried Quaternary soil within Burchell's 'Ebbsfleet Channel', Kent. Proceedings of the Geologists' Association, 102: 275-287.

Kraus, M.J. and Bown, T.M., 1986. Paleosols and time resolution in alluvial stratigraphy. In: V.P. Wright (Editor), Paleosols, their Recognition and Interpretation. Blackwell Scientific, Oxford, pp. 180-207.

Kukla, G.J., 1977. Pleistocene land-sea correlations. 1. Europe. Earth Science Reviews, 13: 307-374.

Lee, J.A. and Kemp, R.A., 1992. Thin Sections of Unconsolidated Sediments and Soils: a Recipe. Centre for Environmental Analysis and Management Technical Monograph, Royal Holloway, University of London.

Léger, M., 1987. Micromorphologie de loess et paléosols intraloessiques en Souabe et Bavière. In: N. Fedoroff, L.M. Bresson and M.A. Coutry (Editors), Soil Micromorphology. Proc. VII Int. Working Meeting of Soil Micromorphology, Paris, July 1985. Association Française pour l'Etude du Sol, Plaisir, France, pp. 611-618.

Liu Tungsheng, An Zhisheng, Yuan Baoyin and Han Jiamao, 1985. The loess-paleosol sequence in China and climatic history. Episodes, 8: 21-28.

McDonald, E.V. and Busacca, A.J., 1990. Interaction between aggrading geomorphic surfaces and the formation of a Late Pleistocene paleosol in the Palouse loess of eastern Washington state. Geomorphology, 3: 449-470.

Morrison, R.B., 1978. Quaternary soil stratigraphy - concepts, methods and problems. In: W.C. Mahaney (Editor), Quaternary Soils. Geo Abstracts, Norwich, pp. 77-108.

Murphy, C.P. and Kemp, R.A., 1984. The over-estimation of clay and the under-estimation of pores in soil thin sections. J. Soil Sci., 35: 481-496.

Preece, R.C., 1991. Accelerator and radiometric radiocarbon dates on a range of materials from colluvial deposits at Holywell Coombe, Folkestone. In: J.J. Lowe (Editor), Radiocarbon Dating: Recent Applications and Future Potential. Quaternary Proceedings No 1, Quaternary Research Association, Cambridge, pp. 45-53.

Retallack, G.J., 1990. Soils of the Past. Unwin Hyman, Boston, 520 pp.

Rose, J., Boardman, J., Kemp, R.A. and Whiteman, C.A., 1985. Palaeosols and the interpretation of the British Quaternary stratigraphy. In: K.S. Richards, R.R. Arnett and S. Ellis (Editors), Geomorphology and Soils. George Allen and Unwin, London, pp. 348-375.

Ruhe, R.V. and Olson, C.G., 1980. Soil welding. Soil Sci., 130: 132-139.

Thompson, M.L. and Smeck, N.E., 1983. Micromorphology of polygenetic soils in the Teays River Valley, Ohio. Soil Sci. Soc. Am. J., 47: 734-742.

Van Vliet-Lanoe, B., 1985. Frost effects in soils. In: J. Boardman (Editor), Soils and Quaternary Landscape Evolution. John Wiley and Sons, Chichester, pp. 117-158.

Van Vliet-Lanoe, B., 1988. The significance of cryoturbation phenomena in environmental reconstruction. Journal of Quaternary Science, 3: 85-96.

Zeuner, F.E., 1959. The Pleistocene Period: Its Climate, Chronology and Faunal Successions. Hutchinson, London, 447 pp.

This Page Intentionally Left Blank

Soil and landscape processes evident in a hydromorphic grey earth (Plinthusalf) in semiarid tropical Australia

H.J. Mücher[1] and R.J. Coventry[2]

[1]*Laboratory of Physical Geography and Soil Science, University of Amsterdam, Nieuwe Prinsengracht 130, 1018 VZ Amsterdam, The Netherlands and Visiting Scientist, CSIRO Division of Soils, Townsville, Australia.*

[2]*CSIRO Division of Soils, Private Mail Bag, P.O. Aitkenvale, Townsville, Queensland 4814, Australia.*

ABSTRACT

Mücher, H.J. and Coventry, R.J., 1994. Soil and landscape processes evident in a hydromorphic grey earth (Plinthusalf) in semiarid tropical Australia. In: A.J. Ringrose-Voase and G.S. Humphreys (Editors), Soil Micromorphology: Studies in Management and Genesis. Proc. IX Int. Working Meeting on Soil Micromorphology, Townsville, Australia, July 1992. Developments in Soil Science 22, Elsevier, Amsterdam, pp. 221-231.

This micromorphological study supports previous field-based conclusions for polycyclic soil and landscape processes operating in profiles from a toposequence of red, yellow, and grey earth soils (Paleustalfs, Plinthustalfs, and Ochraqualfs) at Torrens Creek, North Queensland. These processes have resulted in hydromorphic grey and yellow soils lying upslope of a well-drained red earth.

The focus of this paper is on the grey earth component of the soil sequence which demonstrates the main elements of the genesis of the toposequence by displaying clear evidence of sedimentary layering, and of episodic soil development in superimposed slope deposits. Our pedogenetic interpretations have been derived from studies of the distribution and degree of development of a range of soil micromorphological features, including: preserved fragments of an original red or brown s-matrix, biological features (especially termite-produced pedotubules), yellow or grey mottles indicative of redoxymorphic conditions, iron-manganese nodules, illuviated clay, sand laminae, charcoal, and fragments of weathered sandstone.

There are indications of red soils forming initially in the lower layers of the soil profile. Subsequent hydromorphism led to reducing conditions with the mobilisation of iron and clay in the development of pseudogley features. Iron segregation and biological (termite) activity increased towards the surface in each of the three superimposed soils evident within the studied grey earth profile, in which evidence of alternating periods of oxidation and reduction are preserved in ferriargillans and argillans respectively.

Strong clay illuviation in the grey earth, after the original red soil development, suggests significant climatic change over the period during which the soils formed in the successive slope deposits.
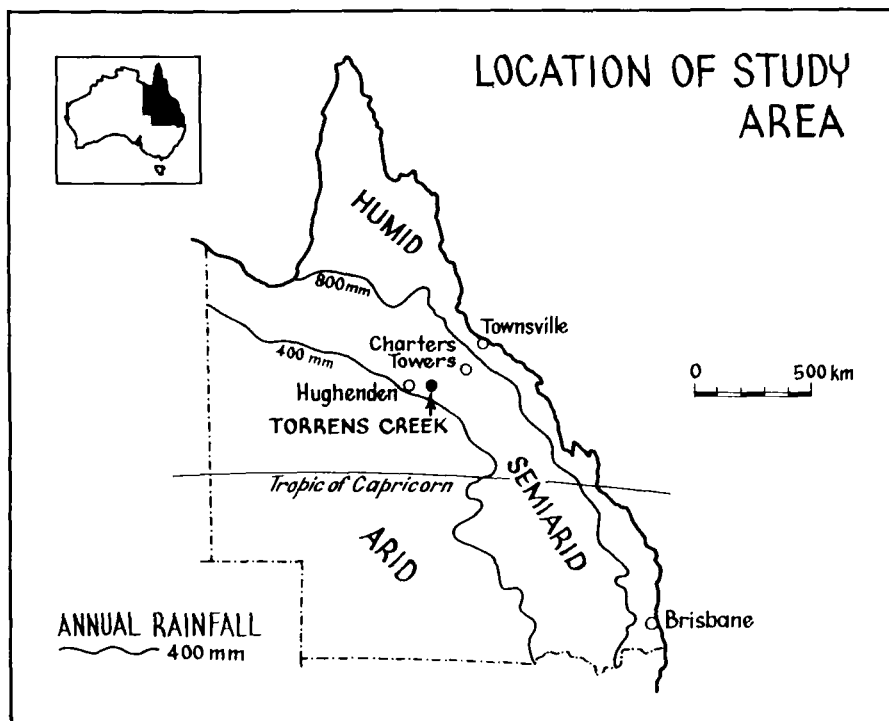
Fig. 1. Location of the Torrens Creek area with respect to the annual rainfall over Queensland. Data from the Commonwealth of Australia, Bureau of Meteorology (1977).

INTRODUCTION

Red, yellow, and grey earth soils (Stace *et al.*, 1968) or Oxic Paleustalfs, Plinthustalfs and Ochraqualfs (Soil Survey Staff, 1975), are widespread in the semiarid tropics of northern Australia. They are non-calcareous, and have massive structure, earthy fabric, mineralogy dominated by quartz, kaolin, iron oxides and oxyhydroxides, low natural fertility, and gradual texture changes through the sola of most profiles (Coventry, 1982).

Coventry (1978, 1982) found that grey and yellow earths (profiles usually less than 1.5 - 3 m deep with varyingly abundant mottles and ironstone gravels), have formed in erosional parts of the study area near Torrens Creek, Queensland (Fig. 1) on broad low ridges, where weathered bedrock lies close to the surface. The red earths (much thicker sola, 5 m to > 20 m) have formed in the lower, depositional parts of the landscape. Relationships between soils, landforms, and isotopically-dated basalt flows suggest that soil forming processes have been active in the region since the Mid to Late Tertiary (Coventry, 1978; Coventry *et al.*, 1985).

There are few field macroscopic indicators of the pedogenetic processes that are currently active in these soils or have contributed to past phases of soil formation. Nevertheless, our study of the micromorphological features of one of these soils, a grey earth profile, has revealed clear evidence of redoxymorphic, illuviation, and biological (termite) processes

operating in a superimposed sequence of colluvial slope deposits that constitute the parent materials of the soil.

An aridic soil moisture regime prevails in the semi-arid tropical study area. The mean annual rainfall of 585 mm at Torrens Creek falls in a marked wet season between December and April. There is no month in the year when the mean rainfall exceeds the potential evapotranspiration, which implies that a water surplus in the soil profile should not, therefore, occur. Nevertheless, hydromorphic grey and yellow earths occur in positions upslope of well-drained red earths. The hydromorphism results from contrasting, shallow groundwater soil hydrologies, which have been monitored and interpreted by Coventry and Williams (1984) and Williams and Coventry (1979, 1981).

MATERIALS AND METHODS

The Soil

The grey earth soil of this study (Profile T222) is located 19 km east of Torrens Creek and 280 km southwest of Townsville, Queensland (Fig. 1). The soil lies near a broad ridge crest with a slope of less than 1%. It is underlain by poorly sorted, coarse grained, quartzose sandstone of Triassic age (the Warang Sandstone; Evans, 1980) which contains minor beds and lenses of quartzitic conglomerate.

The main features of the field morphology of the soil are summarised in Table 1; a full profile description and particle size analysis are given in Coventry and Fett (1982, pp. 50-52). The soil is classified as a grey earth (Stace *et al.*, 1968), Gn 2.85 (Northcote, 1979), Plinthustalf (Soil Survey Staff, 1975), and as a Grey Petroferric Kandosol (Isbell, 1993).

Soil samples and their description

Undisturbed samples from 10 cm diameter soil cores provided almost continuous, vertical thin sections, 6×5 cm, down the grey earth profile to weathered bedrock. Thin sections were described using the terminology of Brewer (1976) and Brewer *et al.* (1983), supplemented by Barratt (1969) and Mücher *et al.* (1981).

The main micromorphological features of Profile T222, and of its component soils and sedimentary layers, are also summarised in Table 1. The sedimentary units that constitute the weathered sandstone and the successive, superimposed slope layers have been numbered starting at the surface with 1.

Full descriptions of each thin section are available from the authors on request. In the following descriptions, the colours of features have been observed in plane polarised light; those observed in incident reflected light are indicated in brackets.

DESCRIPTION AND INTERPRETATION

The grey earth (Profile T222) is a polygenetic soil consisting of 5 successive sedimentary layers and 3 superimposed soil profiles (Table 1). In the following section, the soil profile has been described systematically from the base of the profile up to the ground surface so as to observe the nature of the soil parent materials and their progressive modification by pedological processes.
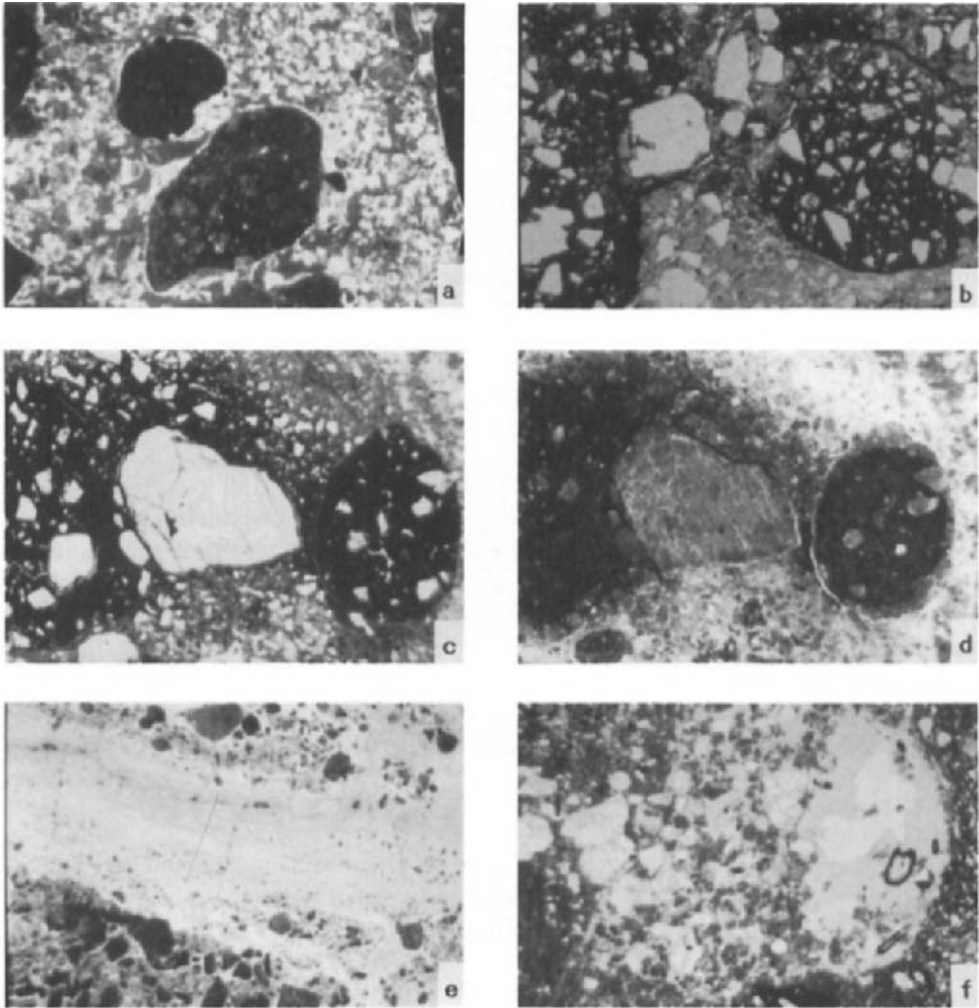
Fig. 2. Thin section micrographs. All frame lengths are 7.2 mm. a) Redeposited brown (red brown) ferric nodule above a brown one of different composition surrounded by brown (grey) matric fecal pellets in the reduced, grey soil matrix. *Incident reflected light; thin section 10; horizon 3Ccb; mean profile depth 81 cm.* b) Oxidised brown (red and brown in incident reflected light) matrix preserved as vein-like patterns within the left part of the photomicrograph and extending towards and above a brown ferric nodule that is embedded in the pale brown (grey), reduced soil matrix. *Incident reflected light; thin section 14; horizon 4Btcb; mean profile depth 117 cm.* c) Brown ferric nodules formed *in situ* in the soil matrix that have been partly reduced at the rims forming pale brown (yellow in incident reflected light) haloes in a reduced, grey matrix; gravel-sized fragment of polycrystalline quartz in centre of photomicrograph. *Plane light (1N); thin section 13; horizon 4Btcb; mean profile depth 110 cm.* d) As for (a), *incident reflected light.* e) Thick, light brown (grey), channel argillan. *Plane light (1N); thin section 22; horizon 5Bt(r)b; mean profile depth 185 cm.* f) Loosely packed aggrotubule produced by termites and containing a rootlet fragment within the denser, reduced pale brown (grey) soil matrix. *Plane light (1N); thin section 10; horizon 3Ccb; mean profile depth 100 cm.*

Sedimentary Units 5 and 4 (170 - 83 cm; Table 1)

The lowest unit, 5, is a poorly sorted, fine sandy material indicating a weathered sandstone provenance. However, there are a few indications of reworking of the weathered sandstone in this unit. They include lithorelicts with an iron-impregnated sandstone fabric, mainly composed of polycrystalline quartz up to 6 mm in diameter, and several kinds of ferric glaebules. The glaebules are thought to be redeposited because of their sharp boundaries, and their contrasting lithologies (differences in size distributions and mineralogy of included particles), and their different colours in incident light (Fig. 2a). Other ferric nodules have clearly formed *in situ* in the soil matrix and have undergone subsequent reduction as shown by the yellow rims and haloes surrounding them (Fig. 2c, 2d).

Unit 4 differs from the underlying layer in that it has a greater number and variety of redeposited ferric nodules, lithorelicts of increased size and number, and its grey matrix contains more argillicol than below.

Pedogenesis in Units 5 and 4

Soil formation proceeded in Units 4 and 5 by three successive stages of reduction, pseudogley, bioturbation and oxidation to produce horizons recognised as 5Bt(r)b and 4Btcb (Table 1).

The first phase of pedogenesis developed primarily as a red soil with little evidence now preserved of clay illuviation and ferran development. Remnants of the oldest, red soil are recognised in the field often as brown to red "mottles", and in thin sections as brown to red-brown (red) matrix; they diminish in numbers up the profile.

The second phase of pedogenesis in Units 4 and 5 is characterised by strong reduction accompanying pseudogley development and intense clay illuviation. A consequence of the reducing conditions was the change in the brown to red-brown matrix in incident reflected light from the unaltered central parts of "mottles" to yellow and grey colours at their edges (Fig. 2b). These hydromorphic processes were accompanied by strong clay illuviation giving rise to light coloured and pale brown (grey) argillans in the reduced areas (Fig. 2e), and brown to red-brown in the similarly coloured soil matrix.

Two phases of clay illuviation are evident from the intersecting relationships within the cutans (Fig. 3a and b). Separate phases of oxidation and reduction are recorded in the red and brown colours of the oxidised soil matrix and illuviated clay features and in the paler, yellow and grey colours of the reduced areas (Fig. 3c and d). The reduction started from planes, cracks and channels and developed into the surrounding matrix. The original brown matrix is reduced from about 60% of Unit 5 to less than 5% by volume of the upper part of Unit 4.

The third stage soil formation occurred under aerobic conditions in which a part of the reduced soil matrix was oxidised again. Very thin ferrans have formed in microcracks of the illuviation argillans. In incident reflected light they are bright red and less yellow, resulting in the formation of brown "matrix" or brown mottles.

Evidence for bioturbation processes is restricted to the grey, reduced parts of the s-matrix, particularly in the upper part of 4Btcb horizon. Loosely packed aggrotubules showing infillings of rounded to subrounded soil aggregates, probably the results of termite activity, were derived from grey, yellow and red matrix materials (Fig. 2f). The fine granular structure of the aggrotubule fillings supports the suggestion of termite activity (Fitzpatrick, 1984).

Table 1
Soil properties and inferred pedological processes, grey earth (Profile T222)

FIELD DESCRIPTION	MICROMORPHOLOGICAL DESCRIPTION AND INTERPRETATION			
	Soil Horizon*	Properties of Sedimentary Layers**	Micromorphological Characteristics of Soils	Inferred Pedological Processes
A1 (0 - 10 cm): Dark greyish brown (10YR 4/2m); sandy loam; gravel is rounded ironstone nodules and quartz pebbles (5-15 mm); massive; earthy fabric; hard-setting surface; abundant rootlets; pH=6.5; clear change to:	**0 cm** 1A1 ts: 1,2 **15 cm** 1A2 ts: 3	Unit 1: Silt -fine sand surface seal; ferric glaebules and lithorelicts. Gravel=12-25%; Sand = 90%; Clay = 4 - 7%.	Very little plasma; packing voids (<0.3mm) abundant; charcoal fragments; some granotubules; some matric faecal pellets; few channels.	Minor accumulation of organic matter; weak soil biological activity.
A2 (10 - 60 cm): Very pale brown (10YR 6/3m); loamy sand to sand; gravel as above; massive; sandy fabric; rootlets common; pH=5.8 - 6.7; gradual change to:	**22 cm** 2Ccb ts: 4 - 7	Unit 2: Many ferric glaebules and lithorelicts. Gravel=65-76%, Sand = 85-90%, Clay = 3 - 9%.	Little plasma; packing voids common; silt cappings on coarse grains; channels; aggrotubules; mullicol and organic faecal pellets.	Weak soil biological activity
A3 (60 - 65 cm): As above but texture increasing with depth to sandy clay loam; gravel mainly ironstone nodules; massive; sandy fabric; pH=6.2; diffuse change to:	**60 cm** 3B(t)cb ts: 8 **70 cm** 3Ccb ts: 9,10	Unit 3: Mainly reworked ferric glaebules. Gravel=80%, Sand = 80%, Clay = 16-25%.	**TOP OF A TRUNCATED, BURIED SOIL** Few argillans; many aggrotubules in sandy matrix; little plasma; compound packing voids between glaebules.	**TOP OF A TRUNCATED, BURIED SOIL** Strong soil biological activity (termites)
B2 (65 - 120 cm): Light yellowish brown (2.5Y 6/4m) with red (2.5YR 4/6m) mottles that increase in size and number with depth; light - medium sandy clay; gravel as above with few rounded quartz pebbles (50 mm); massive; earthy fabric; lower boundary irregular and broadly tongued between 108 cm and 120 cm; pH=5.5; clear change to:	**83 cm** 4Btcb ts:11-14	Unit 4: Similar to Unit 5 but has more abundant and smaller, redeposited ferric glaebules with contrasting colours, fabrics, and lithologies. Gravel=53-75%, Sand = 50-70%, Clay = 36-41%.	**TOP OF A TRUNCATED, BURIED SOIL** 1. Thin, red-brown ferrans in microcracks in pale argillans. 2. Loose aggrotubules; mullicol; faecal pellets. 3. Pale argillans in reduced areas; brown argillans in red-brown soil matrix. 4. Brown and red-brown matrix of mottles with pale and yellow edges.	**TOP OF A TRUNCATED, BURIED SOIL** 1. Oxidation 2. Bioturbation in loose areas (termites, earthworms) 3. Clay illuviation. 4. Reduction.
C (120 - 198 cm): Strong brown (7.5YR 5/6m), red (10R 4/6m), and light grey (10YR 7.5/1m) subhorizontal mottles 10 - 30 mm wide; light sandy clay; gravel is mainly quartz (10-50mm) with minor ironstone nodules;massive; earthy fabric; pH=6.0-6.4; clear change to very hard, conglo-meratic sandstone at 198 cm.	**120 cm** 5Bt(r)b ts:15-22	Unit 5: Redeposited weathered sandstone with siliceous pebbles and reworked ferric glaebules. Gravel=34-51%, Sand = 55-68%, Clay = 29-39%.	1. Thick, brown argillans - some covering pale argillans; red ferrans in microcracks in grey argillans; few aggrotubules. 2. Pedorelicts of original red soil with few ferrans preserved as areas of brown or red "mottles".	1. Strong clay illuviation; reduction; minor oxidation. 2. Oxidation and iron mobilisation; little clay illuviation.

* Depth (cm) of upper boundary of the soil horizon; soil horizon nomenclature from McDonald *et al.* (1990); "ts" indicates thin section number.

** Gravel content as wt % of whole soil; sand (0.02-2 mm) and clay (<0.002 mm) as wt % of <2 mm fraction.

An increasing number of pedotubules, mullicol, and mullicol fecal pellets, produced by earth worms, occur in the upper part of Unit 4 where bioturbation increases so strongly that only about 10% of the matrix material has been left unmodified. This suggests that a former A horizon was once not far above the now-truncated surface of Unit 4.

The bioturbation occurs only in the grey matrix material, implying that the soil animal activity was largely restricted to the reduced parts of the soil profile. The end product of such bioturbation is the development of an intersecting set of aggrotubules which give the soil a loose fabric (Fig. 3e and f).

The original soil, preserved in the lowest part of the studied profile, was truncated by erosion at what is now the top of the 4Btcb horizon at a depth of 83 cm.

Sedimentary Unit 3 (83 - 60 cm; Table 1)

The parent material of Unit 3 differs significantly from that of Unit 4 below. It consists of 70 - 80% redeposited ferric nodules and concretions up to 25 mm in diameter with a silty argillaceous matrix in between the glaebules. The soil matrix was probably derived from a reduced, pale-coloured soil that had a low clay content and contained little illuviated clay. The sediment is poorly sorted and appears to have been deposited by turbulent overland flow.

Pedogenesis in Unit 3

The style of soil formation within the second of the superimposed soils of the studied profile resembles that of the soil in Units 4 and 5 below, but is much more weakly developed.

The fine matrix of the soil has been almost completely biologically reworked by termites into aggrotubules. The increasing number and size of macrovoids in the upper part of the unit, has resulted in a high water infiltration capacity for the soil. The small component of the fine, grey matrix material that has not been biologically reworked (< 5% by volume of Unit 3) shows evidence for reduction, and also very few illuviation argillans in the 6 cm thick 3Bc(t)(r) horizon. Reduction phenomena that have formed *in situ* were only observed in the weakly developed 3Bc(t)(r) horizon. These features include ferric glaebules whose colour varies in incident reflected light from red-brown interiors to yellow near the rims; they are surrounded by grey, reduced matrix material.

The second soil, limited to Unit 3, has been truncated by erosion at 60 cm at the top of what is currently the 3B(t)(r)cb horizon.

Sedimentary Units 1 and 2 (60 - 0 cm; Table 1)

The colluvial material of Unit 2 differs from Unit 3 below in the composition, size, and number of ferric glaebules, and has a more abundant fine and coarse sand matrix with little argillicol; aggrotubules are less abundant and are difficult to identify. The unit was probably deposited under less turbulent conditions than those prevailing for deposition of the underlying sediment.

Unit 1 is very similar to Unit 2 but has less frequent and smaller ferric glaebules of different composition, more lithorelicts, and a compact sand matrix that comprises up to 90% of the layer.
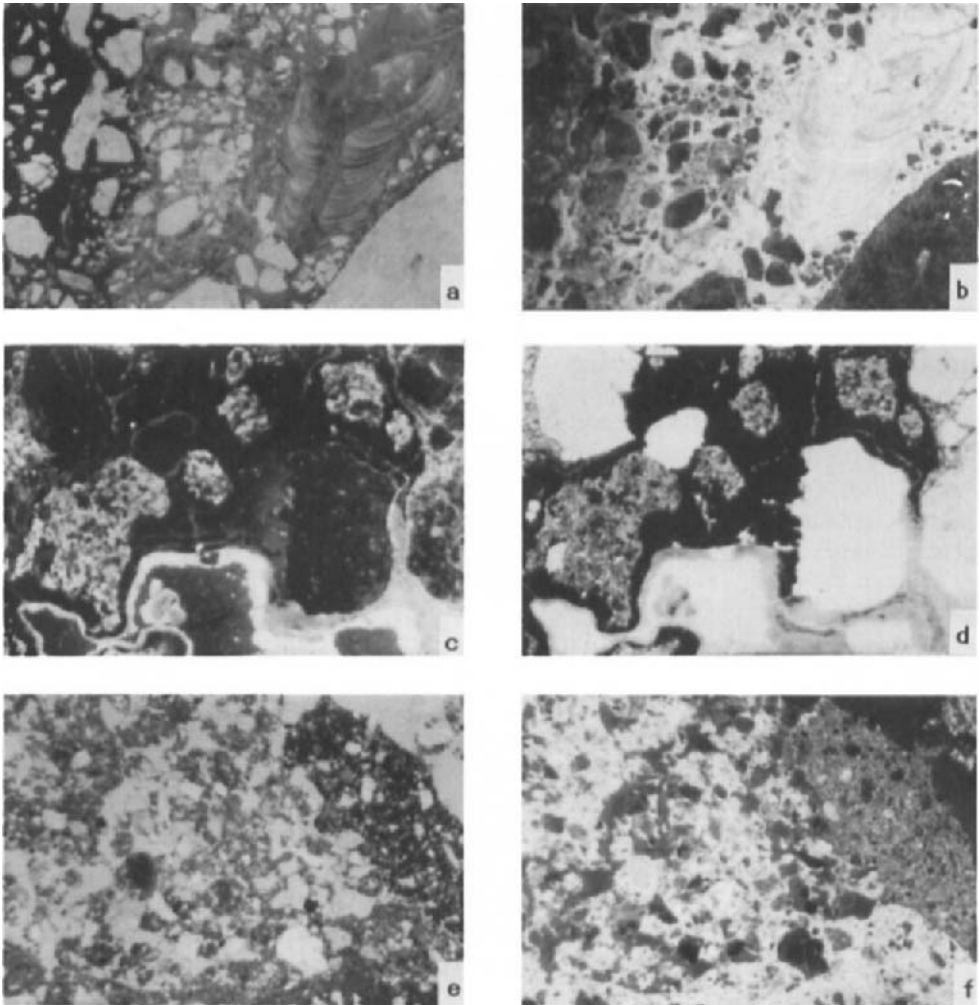
Fig. 3. Thin section micrographs. All frame lengths 7.2 mm. **a)** Strong clay illuviation giving rise to two generations of pale brown (grey) argillans in the soil matrix whose colour varies from dark brown (yellow, at left edge), to brown, and yellow (grey; at right edge) as a consequence of variable iron reduction. *Plane light (1N); thin section 18; horizon 5Bt(r)b; mean profile depth 153 cm.* **b)** As for c), *incident reflected light.* **c)** Several phases of reduction of dark brown (orange) ferriargillans to yellow argillans within an extensive void infill. The variably reduced soil matrix is preserved as speckled remnants. *Plane light (1N); thin section 15; horizon 5Bt(r)b; mean profile depth 129 cm.* **d)** As for e), *incident reflected light.* **e)** Channel with dark brown (light brown) mullicol plaster (upper right) crossing an aggrotubule of termite origin in reduced pale brown (grey) soil matrix. *Plane light (1N); thin section 13; horizon 4Btcb; mean profile depth 110 cm.* **f)** As for 3(e), *incident reflected light.*

Pedogenesis in Units 1 and 2

The third and uppermost of the superimposed soils within the studied profile formed within Sedimentary Units 1 and 2. It is characterised by a very sandy fabric with the accumulation of a little organic matter in the upper part of the 1A1 horizon, and the formation of a few silt/clay cappings over lithorelicts and ferric glaebules. Soil biological activity was largely restricted to the formation of a few channels, aggrotubules, and granotubules, and the production of a few mullicol matric fecal pellets and very fine brown organic fecal pellets, produced by worms, collembola, and/or enchytrae.

The horizon between depths of 10 cm and 65 cm, designated A2 in the field (Table 1) could be interpreted to indicate a thick zone of apparent eluviation within the profile. However, this is inconsistent with the underlying thin illuviation horizon 3B(t)(r)bc (Table 1). The relatively thick zone of apparent eluviation is probably the result of a combination of the following factors: an originally low content of clay in the colluvial deposits of Units 1 and 2 that, themselves, were probably derived from pre-existing A2 soil horizons; and any remaining clay in the sediments may have been eluviated in vertical or lateral directions. The thick apparently "eluviated" horizon is therefore best regarded as a 2Ccb horizon (Table 1).

Soil Porosity

The greatest porosity in the soil profile is 15 - 30% by volume and occurs in Units 1 to 3. As a result of crust formation in the upper parts of the 1A1 and 2Ccb horizons, there are less voids. The porosity is less than 13% in the lower Units 4 and 5. The water storage capacity of the profile above 83 cm reaches a maximum of 0.21 m^3/m^2 but, below this depth, does not exceed 0.09 m^3/m^2.

If the soil were to hold the annual rainfall of the Torrens Creek area of 500 mm, it would need a porosity of 0.5 m^3/m^2. This implies that the profile saturation is mainly the result of the lower water storage capacity of the underlying, reduced soil below 83 cm depth. This is in agreement with the averaged duration of profile saturation for the grey earth of more than 9 weeks below 60 cm (Coventry and Williams, 1984).

CONCLUSIONS

The grey earth profile is a polygenetic soil profile consisting of 5 successive sedimentary layers and 3 superimposed soil profiles. The paleosols were truncated to varying extents after each phase of soil formation, but none of the original A horizons of the paleosols have been identified.

The characteristic grey colour of this soil profile in the lower part, below 83 cm, is the result of reduction by pseudogley of a former red soil. In the upper part of the profile, above 83 cm, the grey colour has mainly been inherited from the source areas of the colluvial material and, to a much lesser extent, to reduction *in situ*. The profile saturation is mainly due to the high infiltration capacity of Units 1 to 3 and the low water storage capacity of the polygenetic red soil in Units 4 and 5 below.

Interpretation of the distribution and degree of development of micromorphological features has provided clear evidence for sedimentary layering, and of episodic soil development in the

superimposed slope deposits. Soil forming processes have proceeded intermittently in the deposits and have been interrupted by phases of landscape instability and erosion.

The polygenetic grey earth profile is characterised by five unstable periods with colluviation and deposition of slope deposits as an active force. A stable period with weathering and soil formation followed the deposition of Sedimentary Units 4, 3, and 1. Biological activity has kept pace with the colluviation processes and has destroyed any original sedimentary structures.

Each soil carries an imprint of the red soil development as the first stage of pedogenesis in the oldest (*i.e.* lowest) slope deposits. This original red soil was progressively modified by processes of reduction and pseudogley that were marked by the segregation and mobilisation of iron and clay in the soil. Pale-coloured soil features such as reduction mottles and argillans developed. Alternating periods of oxidation were recorded by the deposition of redder mottles and ferriargillans, often in transecting relationships with the older reduction features.

Subsequent biological activity, and very limited clay illuviation, increased the porosity and permeability of the soil. These processes have played a major role in developing the present hydraulic characteristics of the soil. Consequently, it is possible to relate very closely the observed field saturation behaviour and distribution of aerobic conditions in the sequence to the degree of modification of the soil fabric by soil animals, particularly termites.

The fact that the original red soil has been so strongly reduced in the grey earth soil profile suggests that there has been a significant increase in profile hydromorphy with the passage of time. Strong clay illuviation in the soil profile, after the prior red soil development, also suggests significant hydromorphic change over the period during which the profile's constituent soils formed, and were buried by successive slope deposits. The most reasonable explanation for these phenomena is a climatic change, perhaps towards more humid conditions, since soil forming processes began operating in this area (*i.e.* since the Mid-Miocene; Coventry *et al.*, 1985).

ACKNOWLEDGEMENTS

REFERENCES

Barratt, B.C., 1969. A revised classification of microscopic soil materials with particular reference to organic components. Geoderma, 2: 257-272.

Brewer, R., 1976. Fabric and mineral analysis of soils. R.E. Krieger, New York, 482 pp.

Brewer, R., Sleeman, J.R. and Foster, R., 1983. The fabric of Australian soils. In: Soils, An Australian Viewpoint. CSIRO Melbourne/Academic Press, London, pp. 439-476

Commonwealth of Australia, Bureau of Meteorology, 1977. Climatic Atlas of Australia, Map 5: Rainfall. Aust. Gov. Publ. Serv., Canberra, Australia.

Coventry, R.J., 1978. Late Cainozoic geology, soils, and landscape evolution of the Torrens Creek area, North Queensland. J. Geol. Soc. Aust., 25: 415-427.

Coventry, R.J., 1982. The distribution of red, yellow, and grey earths in the Torrens Creek area, central North Queensland. Aust. J. Soil Res., 20: 1-14.

Coventry, R.J., and Fett, D.E.R., 1982. Morphology and particle-size characteristics of the red, yellow, and grey earths and associated soils of the Torrens Creek area, central North Queensland. CSIRO (Australia) Division of Soils, Divisional Report No. 60.

Coventry, R.J., Stephenson, P.J. and Webb, A.W., 1985. Chronology of landscape evolution and soil development in the upper Flinders River area, Queensland, based on isotopic dating of Cainozoic basalts. Aust. J. Earth Sci., 32: 433-447.

Coventry, R.J. and Williams, J., 1984. Quantitative relationships between morphology and current soil hydrology in some Alfisols in semiarid tropical Australia. Geoderma, 33: 191-218.

Evans, P.R., 1980. Geology of the Galilee Basin. In: R.A. Henderson and P.J. Stephenson, (Editors), The Geology and Geophysics of Northeastern Australia. Geological Society of Australia, Queensland Division, Brisbane, pp. 299-305.

Fitzpatrick, E.A., 1984. An Introduction to Soil Science. Longman Scientific and Technical, Harlow, Essex, England, 255 pp.

Isbell, R.F., 1993. A Classification System for Australian Soils (3rd approximation). CSIRO (Australia), Division of Soils, Technical Report, 2/1993.

McDonald, R.C., Isbell, R.F., Speight, J.G., Walker, J. and Hopkins, M.S. 1990. Australian Soil and Land Survey Field Handbook. Second Edition. Inkata Press, Melbourne, 198 pp.

Mücher, H.J., De Ploey, J. and Savat, J., 1981. Response of loess materials to simulated translocation by water: micromorphological observations. Earth Surface Processes and Landforms, 6: 331-336.

Northcote, K.H., 1979. A Factual Key for the Recognition of Australian Soils, 4th Edition. Rellim Technical Publications, Glenside, South Australia, 124 pp.

Soil Survey Staff, 1975. Soil Taxonomy. US Dep. Agric., Handb. 436, U.S. Gov. Printing Office, Washington, D.C., 754 pp.

Stace, H.C.T., Hubble, G.D., Brewer, R., Northcote, K.H., Sleeman, J.R., Mulcahy, M.J., and Hallsworth, E.G., 1968. A Handbook of Australian Soils. Rellim Technical Publications, Glenside, South Australia, 429 pp.

Williams, J. and Coventry, R.J., 1979. The contrasting soil hydrology of red and yellow earths in a landscape of low relief. In: The Hydrology of Areas of Low Precipitation. Proc. Canberra Symposium. (Int. Assoc. Sci. Hydrol.), Publ., 128: 385-395.

Williams, J. and Coventry, R.J., 1981. The potential for groundwater recharge through red, yellow, and grey earth profiles in central North Queensland. In: Groundwater Recharge. Australian Water Resources Council, Conf. Series, pp. 169-181.

This Page Intentionally Left Blank

An exploratory examination of some relict hardpans in the coastal lowlands of southern Queensland

C.H. Thompson[1], E.M. Bridges[2] and D.A. Jenkins[3]

[1]*CSIRO Cunningham Laboratory, 306 Carmody Road, St. Lucia, 4067, Queensland, Australia*

[2]*ISRIC, PO Box 353, 6700 AJ Wageningen, the Netherlands*

[3]*School of Agricultural and Forest Sciences, University College, Bangor, Gwynedd, LL57 2UW, U.K.*

ABSTRACT

Thompson, C.H., Bridges, E.M. and D.A. Jenkins. 1994. An exploratory examination of some relict hardpans in the coastal lowlands of southern Queensland. In: A.J. Ringrose-Voase and G.S. Humphreys (Editors), Soil Micromorphology: Studies in Management and Genesis. Proc. IX Int. Working Meeting on Soil Micromorphology, Townsville, Australia, July 1992. Developments in Soil Science 22, Elsevier, Amsterdam, pp. 233-245.

An exploratory examination of samples from six exposures of relict hardpans has been made using simple laboratory tests, optical microscopy and SEM equipped with an energy-dispersive X-ray. Five of the hardpan sites are associated with rivers upon an old coastal plain; their relationships to the present streams, land surfaces and overlying soils implies that these hardpans formed before the streams responded to the low sea levels of the Pleistocene; so a Pliocene age is inferred. One of the hardpans has formed in Pleistocene dune sands of the Cooloola coastal sandmass and underlies Holocene dunes and soils.

The lack of dispersion during 48 hours immersion in either H_2O or N HCl indicates that the induration is not due to particle packing alone, that the materials are cemented, and that the cement is not $CaCO_3$. Two samples gave a positive response to the rapid test for allophane indicating the presence of an imogolite/ allophane complex. SEM photomicrographs show an amorphous material blanketing the skeletal quartz grains as well as fine grains in the matrix. However, microprobe analysis of this material shows that strong Si peaks are always accompanied by Al and, in the case of the Cooloola sample, with Al in excess of Si. Thus, deposition of amorphous Si as a coating upon, or laminated with, kaolinite clays appears to form the cementing agent in four samples and an imogolite/allophane complex is involved in the other two.

The pans underlie a range of contemporary soils - red podzolic soils, red earths, gleyed soloth and solodic soils - and contribute to problems of land use. Obviously, they restrict both vertical drainage and rooting depth. On the coastal plain, where the hardpans are less than 2 m below the surface, their presence contributes to salinisation and solonization of the soils. Knowledge of the cementing mechanism, and the environmental conditions which promote its development would help to throw light upon past climatic conditions.

INTRODUCTION

In Australia, and many other countries, soils with lower horizons hard enough to withstand a blow with a hammer occur. Such hardened or cemented horizons in or below the soil profile are referred to as 'hardpans or pans' (McDonald *et al.*, 1984). Although much speculation has taken place about the mechanism causing the hardening, it remains far from clear what processes are involved and what environmental conditions are necessary for these features to develop. The aim of this paper is to use micromorphological techniques in combination with simple laboratory tests in an attempt to find an answer. The investigation reported here is concerned with an exploratory examination of six samples of hardpans from three different environments within the coastal lowlands of southern Queensland, between Gympie and Bundaberg (Fig. 1). Several kinds of hardpans have been observed during soil surveys in the coastal lowlands. Some are associated with remnants of soils and landforms of Tertiary age; others have formed in Quaternary deposits and soils. Apart from the geological descriptions of the Elliott Formation (Ridley, 1957; Ellis, 1968; Robertson, 1979) to the north of Howard, there are no other published data characterising the hardpans affecting soils in this section of the coastal lowlands of southern Queensland. The nearest studies of somewhat similar hardpans are those of Van Dijk and Beckmann (1978) west of Toowoomba in southern Queensland, and Chartres (1985) in north-western New South Wales. Of these, there appear to be closer affinities between the Yuleba hardpan (Van Dijk and Beckmann, 1978) and the materials we have investigated in the Cherwell, Isis and Gregory Rivers area, north of Howard.

Of the six sites sampled, two are associated with an ancestral (Pliocene) Mary River - one from an old alluvial fan, graded to the ancient river alluvium and the other in saprolite underlying deposits interpreted as ancient river alluvium. Both of these sites show evidence of intense weathering (lateritization) and the development of pans before the Mary River cut its present inner valley in response to the low sea levels of the Pleistocene. Three sites are associated with the short coastal Cherwell, Isis and Gregory Rivers and are exposures of a very extensive hardpan underlying the soils of a large part of the adjacent coastal plain. This hardpan has formed in Tertiary alluvium which is regarded by geologists as a southern extension of the Elliott Formation. Since the hardpan developed, the area has been strongly eroded, covered by a veneer of younger sediments and the present streams have cut through the hardpan to underlying country rock.

At one of the sites, Cooloola, south of Rainbow Beach, a hardpan has been exposed by both wind and water erosion of the high coastal dunes. This pan has formed in Pleistocene aeolian sands and extends under Holocene dune sands. It is rather different in character and is not as strongly indurated as the other pans.

METHODS

The six pans were examined and sampled in road cuttings at: 1) Bell's Bridge, 2) Owanyilla, 3) Cherwell River, 4) Isis River, 5) Gregory River, and 6) Cooloola Ledges (Fig. 1). Freshly broken samples were taken from large blocks for description and analyses. Other samples were ground to < 2 mm for determination of field pH (Raupach and Tucker, 1959) and response to allophane test (Fieldes and Perrot, 1966). Two pieces, of approximately 2 or 4 cm size, from each sample were tested for dispersion in demineralized water or N HCl over 48 hours.
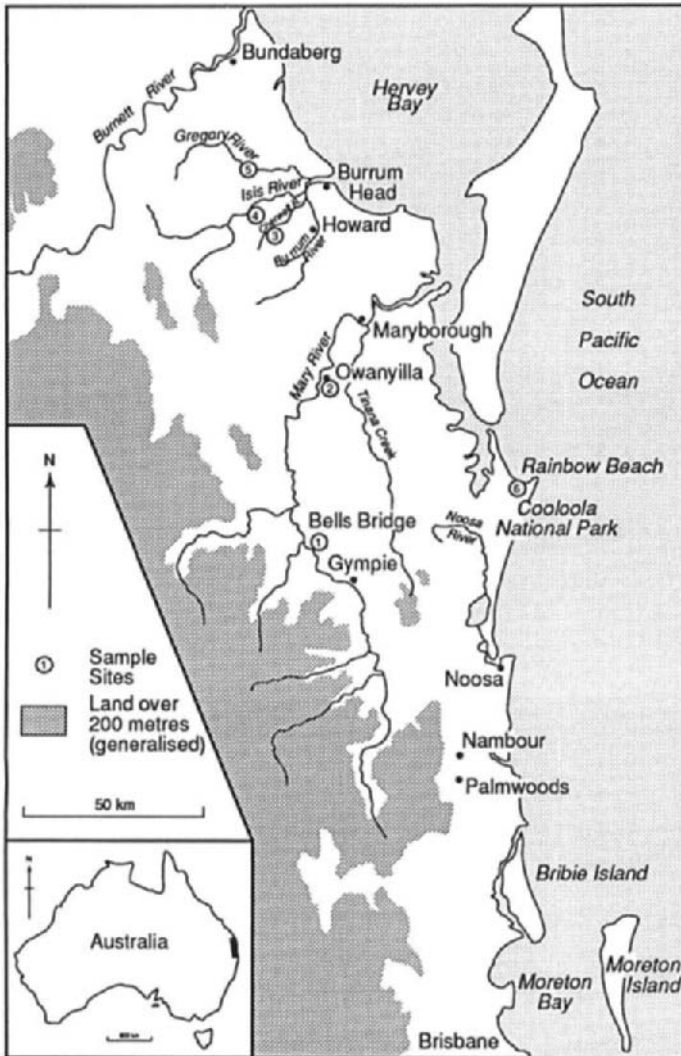
Fig. 1. Coastal Lowlands of Southern Queensland showing sites examined.

Small subsamples from each site were coated with carbon and examined in a scanning electron microscope equipped with an energy dispersive X-ray analyser (SEM-EDXRA). Qualitative chemical analysis by X-rays was achieved using the LINK 290 system. Duplicates from some subsamples were set in Metsett SW, polished and given two coats of carbon before analysis at 30 kV using a JEOL 35C scanning electron microscope. Uncovered thin sections, 30 μm thick, were prepared from resin-impregnated samples (acetone-diluted "crystic" styrene system) and examined by normal polarising microscope techniques, supplemented where necessary by phase contrast (Leitz Heine) and UV-autofluorescence (Leitz Hg lamp; 5 mm BG12/K530 filtres). Selected areas from these sections were then examined under a Hitachi S520 SEM fitted with a LINK QX2000I/LZA detector system. XRD traces were obtained for the powdered samples using Fe_{Ka} in a Philips 1140/1048 system.
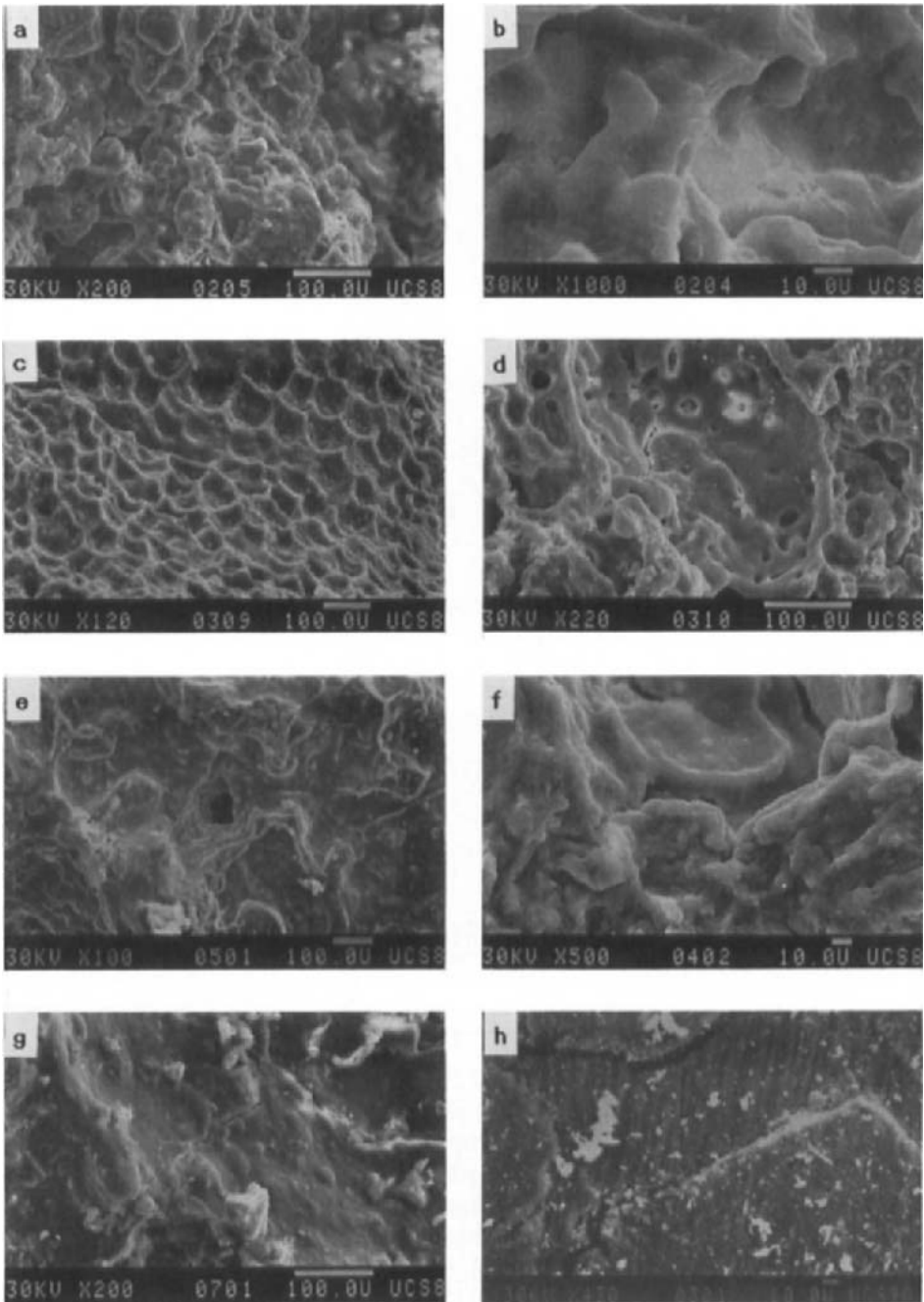
Fig. 2. SEM micrographs of: the: **a)** and **b)** Bell's Bridge hardpan; **c)** and **d)**Owanyilla hardpan; **e)** Cherwell river site; **f)** hardpan at the Isis river site; **g)** hardpan at the Gregory river site; **h)** hardpan at the Cooloola Ledges site. Scale bar: 100 μm a, c, d, e, g; 10 μm b, f, h.

The soils overlying the hardpans were classified by inspection and extrapolation of chemical data from similar soils nearby and have been provisionally classed according to the Australian Great Group scheme (Stace *et al.*, 1968) and Soil Taxonomy (Soil Survey Staff, 1990).

DESCRIPTION OF MATERIALS STUDIED

Bell's Bridge - western side of road cutting, near Gympie

Sample 1 is from an old fan alluvium derived from the sedimentary rocks of the underlying and adjacent Permian Tamaree and nearby Rammutt Formations (Runnegar and Fergusson, 1969). The old fan alluvium is, in the lower part, interleaved with ancient (Pliocene) alluvium of an ancestral Mary River and both occupy a high terrace level relative to the present stream (Bridges *et al.*, 1990). A red podzolic soil (Ultic Paleustalf) overlies the hardpan which is underlain by coarsely mottled light grey and red clays. The soil and hardpan materials have been strongly weathered to depth, and the reticulate coarse mottles of both hardpan and clays implies oscillating conditions of oxidation and reduction in the past, and is interpreted as the impress of lateritization during the late Tertiary.

Field morphology
The indurated layer is 1 - 2 m thick, approximately parallel to and 1.5 - 2 m below the surface. It is confined to the fan alluvium and does not extend into the soils overlying Rammutt shales. The hardpan in coarsely mottled brownish grey (10YR 5/1 to 6/1), reddish brown (5YR 4/6) and brown (10YR 4/4) with light grey (5Y 7/1) or grey-brown (5YR 5/2) colouring along fracture lines. It contains numerous subangular and angular clasts of green shale, siltstone, silicified argillite, greywacke and quartz 2 - 80 mm across. The material is massive, very hard, requires hammer blows to break it and fractures along the coarser gravel margins. It is moderately acid, does not disperse during prolonged soaking in water or N HCl and is unresponsive to the allophane test.

Micromorphology
Low SEM magnification (30 kV × 200) images recorded for the Bell's Bridge samples show a characteristic cellular appearance with frequent pores (Fig. 2a). At higher magnifications (30 kV × 1000) samples have grain surfaces which appear to be strongly coated with an amorphous material and there is much bridging between grains (Fig. 2b). With a polished sample, quartz grains with a conchoidal fracture can be seen to be set in a matrix which has a stronger X-ray fluorescence from silicon than aluminium. The micro-probe shows the consistent presence of both silicon and aluminium peaks showing that the cementing matrix of the bridging material could be a clay mineral (Fig. 3a). Even at the highest magnification available, it was not possible to see whether the silicon and aluminium are present as a clay mineral, or as a combination of clay mineral and amorphous silica.

Owanyilla - western side of road cutting near Maryborough

Sample 2 is from an irregular hardpan exposed adjacent to and downslope of a red earth (Kandiustalf), formed in a (Pliocene) alluvium of an ancestral Mary River and occupying a high terrace level relative to the present stream. The hardpan is associated with the underlying rocks
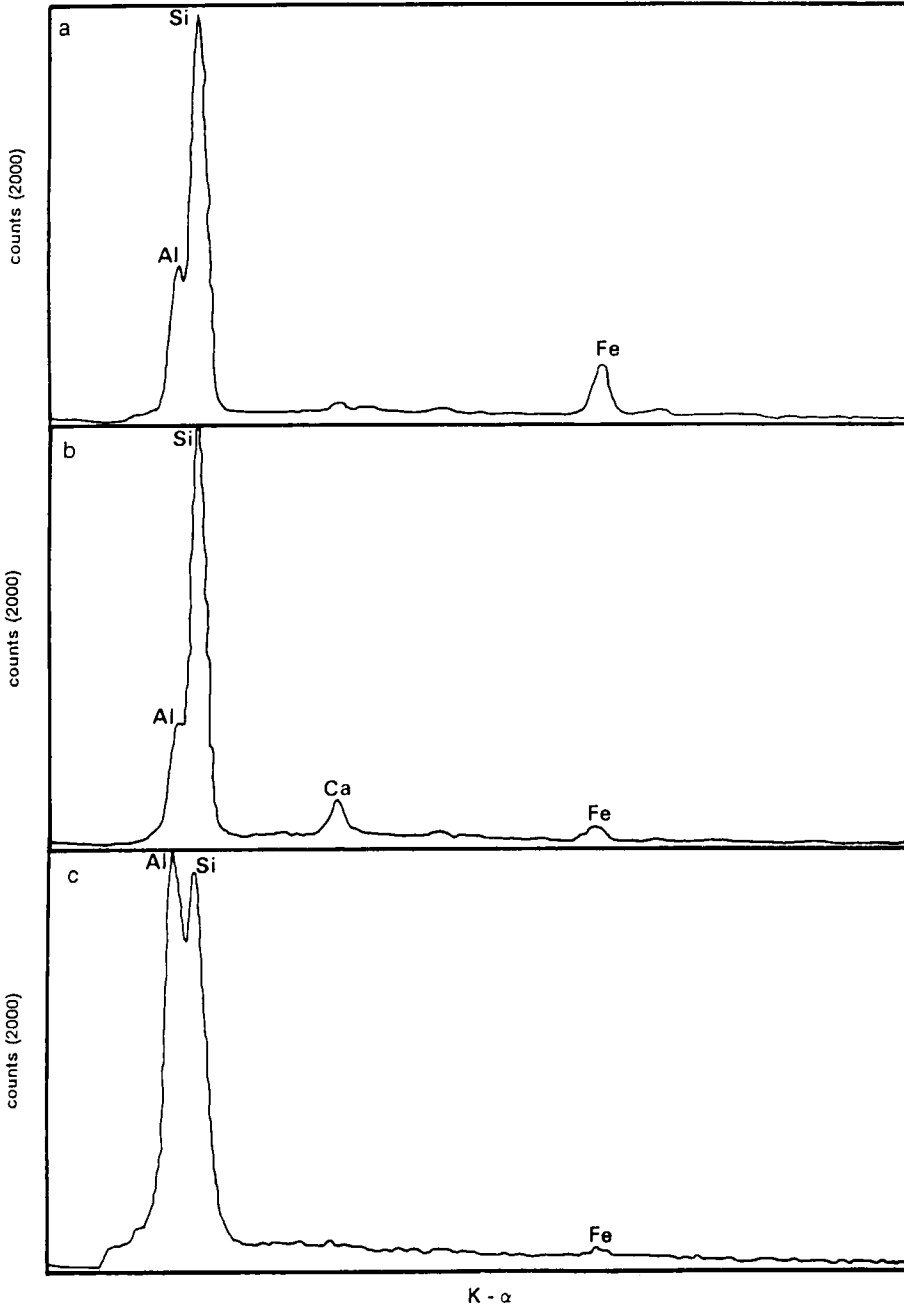
Fig. 3 **a)** Microprobe trace of the Bell's Bridge hardpan; **b)** Microprobe trace of the Owanyilla hardpan; **c)** Microprobe trace of the Cooloola Ledges hardpan.

which appear to be strongly weathered tuffs or tuffaceous siltstones of the Cretaceous Grahams Creek formation of Ellis (1968). It appears that the hardpan has been exposed by truncation and may underlie the red earth on the crest, as well as a red podzolic soil (Durustalf) on the upper slope.

Field morphology

The indurated layer is very light grey (2.5Y 7/2) with coarse reticulate red-brown (2.5YR 4/8) or dusky red (2.5YR 4/2 to 5/2) mottles. When fractured it is seen to have red-brown lines (1 mm or less) forming a fine network and lining fine pores. Old 8 - 10 mm channels with very light grey vermiform casts and finer 4 - 6 mm channels with red-brown clay coatings and vermiform fill are evident through the mass and indicate that the material was once soft and easily penetrated. The indurated zone requires hammer blows to shatter it and breaks with a very irregular fracture which, under the hand lens, has a fine lumpy appearance. The material is strongly acid, does not disperse during prolonged immersion in water or N HCl, but in some parts gives a weak or moderate response to the allophane test.

Micromorphology

In thin section, the fabric of this sample tended to be composed of poorly sorted 20 -100μm quartz grains, but mica and fine cherty fragments also occur. The matrix forms over 80% of the the sample, comprising a fine (5 - 10 μm), dense quartzose intergrowth with linear cracks and rare irregular vesicles. Some cracks appear to be infilled with a mosaic of finer material with low positive relief and low birefringence. Some smaller voids contained dusty argillans (Bullock et al., 1985). XRDA of polished surfaces again gave very weak traces dominated by quartz, but microanalysis of crack infillings revealed Al and Si in a ratio comparable to that of kaolinite. Analysis of the argillans gave similar results.

Under the SEM, at low magnification, a cleanly broken fragment of this pan was seen to have a well-developed "honeycomb" morphology; structure with cells 40 - 50 μm across (Fig. 2c). A similar structure has been described by FitzPatrick (1984) as "egg box" morphology. At high magnification (30 kV × 1000) this structure appears to be formed of small particles of weakly crystalline or amorphous material building-up into ridges about 10 μm wide. Elsewhere, similar honeycomb morphology merges into a cradle-shaped hollow of amorphous material which presumable held a larger quartz grain (Fig. 2d).

Analysis by micro-probe shows a strong silica peak with a clear, but partly obscured, aluminium peak (Fig. 3b). Examination of a polished sample revealed the larger silica grains to be embedded in a densely packed matrix of fine crystalline material which responds equally well to silicon and aluminium when subject to X-ray fluorescence. Thus, there appears to be a strong case for the presence of kaolin in the cementing material. Except for the Cooloola sample, this was the only one to have a weak response to the allophane test which implies that the bonding agency could in part be an aluminium silicate complex of the allophane group (possibly imogolite or proto-imogolite, Farmer et al., 1980) and probably relates to a volcanic origin of part of the underlying parent material.

Cherwell, Isis and Gregory River sites

The hardpans at sites 3, 4 and 5, sampled from the banks of the Cherwell, Isis and Gregory rivers, have several features in common. They occur on the coastal plain (about 30 m a.s.l.) to
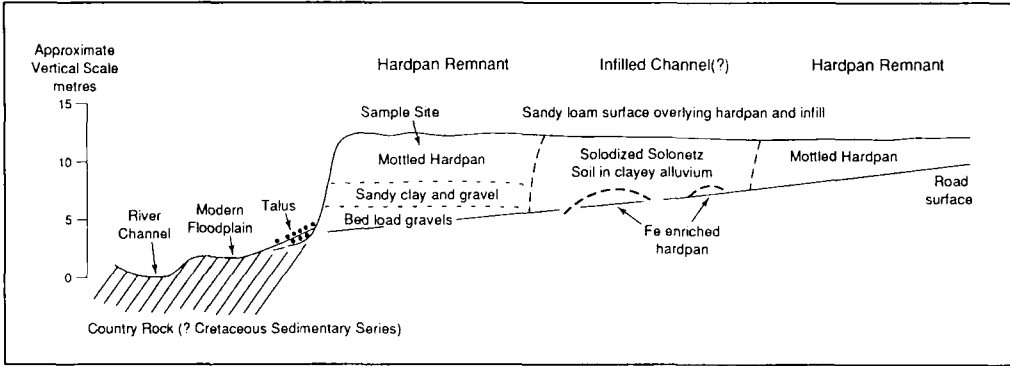
Fig. 4. Relationship of the hardpan at the Cherwell, Isis and Gregory river sites to present topography and surficial deposits.

the north of Howard (Fig. 1), occupy a terrace level well above the floodplains of the present streams, extend laterally between the streams, and are regarded by geologists as silicified beds of a truncated southern extension of a local sequence of Tertiary sediments (Elliott Formation), described as consisting of sandstone and siltstone with some conglomerate and shales (Ridley, 1957; Ellis, 1968). To the north of Howard, it is represented by thin (<6 m thick) discontinuous outliers between the coastal streams. Ridley (1957) recorded it in the Gregory River area, 'as very much like a type of siliceous hardpan, 2 - 3 feet below the surface' and, at the Isis River crossing, as 'undoubtedly sandstone'. He noted that the sandstone was frequently mottled and where exposed weathers irregularly forming a large cellular pattern.

The relationship of the hardpan to the present streams and the surficial deposits of the coastal plain is evident at Gregory River crossing (Fig. 4). Here the river has cut through the hardpan and underlying sediments to flow over Cretaceous country rock, but old channels cut through the hardpan have been filled with clay alluvium, and both channel fill and hardpan are covered by a thin veneer of sandy alluvium. The hardpan is about 2 m thick and is underlain by sandy clays with gravel lenses. The gravels appear to be bedload sediments of the formative stream and contain clasts that may be related to the Permian and Mesozoic rocks in the headwaters of the stream to the west.

Field morphology

The Cherwell hardpan, sample 3, is exposed where the Cherwell River has cut through the old coastal plain to the underlying Cretaceous country rock. The indurated material extends laterally beneath gleyed soloth and solodic soils (Glossic Natraqualfs or Aquic Natrustalfs and also appears to underlie earthy yellow podzolic soils (Kandiustalfs) of the slightly higher and better drained parts of the old coastal plain. The Cherwell hardpan is brownish grey (10YR5/1 to 6/1) with coarse brown (10YR4/3) and dark reddish brown (5YR4/4) mottles. It is massive, very hard, requires hammer blows to shatter it and breaks with a highly irregular and rather wedge shaped fracture. Under a hand lens most of the freshly fractured faces appear as a brownish grey amorphous mass with few sand grains evident *i.e.* most of the grains and pores

of the sandstone appear to be blanketed by the hard amorphous material which may be secondary silica. Some old fracture lines are also evident, distinguished by few very fine plant roots and thin grey-brown coatings along the partings. Occasional 5 mm channels with grey-brown (10YR5/2) vermiform fill have been observed in places. The material is mildly acid, does not disperse during prolonged immersion in water or N HCl and does not respond to the allophane test.

The Isis hardpan, sample 4, exposed on the high southern bank of the rivers is brownish grey (10YR5/1) with coarse pale yellowish brown (2.5Y6/4) and brown (7.5YR5/6) mottles. It is similar in hardness and fracture to the samples from Cherwell River but under a hand lens it is much more porous with many sand grains evident (*i.e.* fabric of sandstone), including a few lithic grains, but some areas are denser, and completely amorphous. No channels or vermiform fill were observed in the samples.

The Gregory hardpan, sample 5, is light grey-brown (10YR6/2) with coarse grey-brown (10YR5/3) and brown (10YR5/8) mottles. The material is very similar to that of the Isis River with similar fabric evident under a hand lens. Thin brown coatings line what appear to be old fracture lines but no old channels with vermiform fill were observed. The material is moderately acid, does not disperse during prolonged immersion in H_2O or N HCl and is unresponsive to the allophane test.

Micromorphology

At low and medium magnifications 30 kV × 300-500) the individual grain boundaries of the Cherwell sample within a broken fragment of this pan are not clearly visible (Fig. 2e). Crystals appear to have an overgrowth of amorphous material and in places, a transition towards the honeycomb pattern of morphology seen in the Owanyilla sample. Examination of bridging material from the Cherwell sample with the micro-probe indicates a strong silica peak with a less obvious aluminium peak to its left. When examined by X-ray fluorescence, polished samples indicate widespread presence of silicon, obvious in the larger quartz grains, but a response to aluminium also occurs throughout the matrix. X-ray fluorescence examination of the brown mottles show a strong coincidence of iron and silicon in the matrix material.

With a polished sample of the Isis hardpan, the coated nature of the interstitial grains may be seen and in places the X-ray fluorescence displays a significant response to barium and sulphur, the latter implying some residual presence of material accumulated in evaporative conditions. These coatings give a strong response to silicon with X-ray fluorescence, but aluminium also gives a widespread signal. Although individual grains of quartz can be distinguished, they appear to be extensively coated with secondary material giving smoothed outlines to the grains (Fig. 2f). Pore spaces between the grains are rare. Examination of fracture surfaces on a subsample of the Gregory hardpan showed larger quartz crystals set in a matrix of smaller, more angular grains. In places, there is evidence of extensive coating of amorphous material, covering matrix and larger quartz grains alike (Fig. 2g). Examination of this bridging material by the electron microprobe reveals a strong silicon peak with minor amounts of aluminium and iron.

This hardpan has been recorded during soil surveys on the plain both north-east and south-east of the Gregory River site, near Childers, at 75 cm under a gleyed solodic soil (Typic Natraqualf). Here the pan was described as a light brownish grey with yellow-brown mottled silica pan with occasional channels with 3 - 5 mm vermiform fill.

Cooloola Ledges - eroded track bed in high dunes near Wide Bay

The hardpan from Cooloola Ledges, site 6, exposed in the bed of a track in high dunes near Wide Bay, has formed in Pleistocene dune sands at 120 m a.s.l., in the Cooloola sandmass, south of Rainbow Beach. It is exposed where vehicular/water erosion has cut through the old dunes to the indurated layer. To the south it extends under Holocene dune sands in which podzols (Quartzipsamments and Troporthods) have formed.

Field morphology

The indurated layer is a very pale brown (10YR 8/3 to 8/2) massive, fine to medium grained, sandy material. It breaks readily with a hammer blow to an irregular fracture. Under a hand lens, the fracture surface shows clean quartz grains set in a fine matrix; there is an occasional dark fine grain of a heavy mineral (ilmenite or rutile) but very few fine pores are evident. The matrix material appears to fill all of the voids between the grains and looks like precipitation between, rather than around, grains. There is much evidence of grains plucked out of the matrix during fracture.

Micromorphology

Examination of thin sections revealed a well-sorted sand with rounded grains (50 - 250 μm) of quartz embedded in a uniform matrix of low positive relief and effectively isotropic between crossed polars. Distinctive rounded voids were present with diameter of 100 - 200 μm. Phase contrast was required to bring out any detail, but viewed under UV the matrix is strikingly autofluorescent in pale green, suggestive of 'active' aluminium. XRDA of both surface and powdery matrix gave very weak traces with only traces of kaolinite and gibbsite being detectable in addition to quartz. These properties are consistent with those of an allophanic or imogolitic material.

SEM examination of a polished sample shows fine amorphous fill between the quartz grains and no evidence of pores (Fig. 2h). X-ray fluorescence of the matrix shows approximately equal amounts of aluminium and silicon. This is confirmed by micro-probe analysis which shows strong peaks for aluminium and silicon and virtually nothing else (Fig. 3c).

DISCUSSION

The relict nature of the pans along the coastal streams (sites 1 - 5) is clearly evident from their relationships to the present streams, land surfaces and overlying soils. These imply that none of these hardpans are currently forming and that all have been inherited from pre-Pleistocene environments. The reticulate mottling of the pans, particularly those along the Mary River implies a past history of repeated reduction and oxidation (seasonal saturation) so the pans may represent part of a mottled zone formed during lateritization and since hardened. The presence of fine cylindrical channels with vermiform fill in samples from Owanyilla, Cherwell River, and north-east of Gregory River indicate that these materials were once soft and easily penetrated sediments.

The large erosion channels through the hardpans and underlying materials seen at Owanyilla, near Maryborough, and at the Gregory River) and the sharp boundaries between the hardpan and clayey channel fill indicate that hardening occurred before the downcutting of the streams in response to the low sea levels of the Pleistocene. On this basis, the formation of

the hardpans along the coastal streams is seen to pre-date the Pleistocene and to be most likely of Pliocene age.

Although different grain sizes are clearly evident and their packing probably contributes to the overall resistance of the six hardpans to deformation, the lack of dispersion during 48 hours immersion in H_2O or N HCl shows that they are not "densipans" (Smith *et al.*, 1975) and that a cementing agency other than calcium carbonate is involved. The lack of dispersion also points to a bonding agent other than clay because most clays tend to swell and so disrupt the sample when wetted. The lack of response to sodium fluoride in the allophane test (other than in the samples from Owanyilla and Cooloola) indicates that the bonding agent in the hardpans is not an amorphous aluminium silicate complex of the imogolite/allophane group; conversely the positive response of samples from Owanyilla and Cooloola Ledges implies that such a compound is present. The presence of an imogolite/allophane complex in the sample from Cooloola Ledges is not surprising, given its known association with podzol development overseas (Farmer *et al.*, 1980; Childs *et al.*, 1983) and Australia (Skjemstad *et al.*, 1992) and the opportunity in high Pleistocene dunes for allophanic material to move and separate at considerable depth below giant podzol profiles. However, a weak response to the sodium fluoride test in the Owanyilla sample was unexpected. It is possible that the "egg box" structure may relate to the volcanic origin of the underlying parent material, although this is doubtful. The positive response to NaF allophane test, indicating an imogolite/allophane complex in mottled zone material is certainly surprising and difficult to explain other than it has been inherited from the parent rocks below depths affected by lateritization.

Examination of the SEM images from both fracture and polished surfaces of the samples show considerable variation in the micro-morphology of the matrix and cementing materials in the hardpans. In all cases, an amorphous (at the micron level) material rich in silicon appears to coat both the larger quartz grains and the finer grains of the matrix, given a visual impression of melted candle wax poured over them. All samples showed coatings and fillings of amorphous material that gave a strong silicon peak, but the evidence also indicated the presence of kaolinite. Only the Owanyilla sample showed a strong development of the egg box structure. Other elements are present in much smaller amounts and do not appear to influence induration except perhaps in some of the iron-rich red or yellow patches. The trace from the micro-probe shows that the silicon is always accompanied by aluminium in the coatings although in some cases, e.g. Cooloola Ledges, aluminium may be in excess of silicon. However, only at the Owanyilla and Cooloola Ledges is the aluminium and silicon likely to have formed an imogolite/allophane complex. Presumably the cementing agent at the other sites, is fine-grained kaolinite, possibly accompanied by silica. It will require a greater order of resolution at the submicron level to resolve this question satisfactorily.

None of the pans could be regarded as classical 'grey billy' or silcrete of inland Australia because of their greater porosity, lower hardness, and different fracture. The pans associated with the old terrace of the Mary River (sites 1 and 2) have reticulate red mottling and occur in what appear to be lateritized profiles. They could be regarded as 'weakly silicified mottled zone' of a laterite profile as described by Connah and Hubble (1960) and their apparent pre-Pleistocene age would lend some support to this. The hardpans under the coastal plain (sites 3, 4, 5) are similar in colour, and their associations with younger soil mantles and ancient remnants, to the Yuleba hardpan of central southern Queensland (Van Dijk and Beckmann, 1978). However, they differ in thickness and local undulations. For example, the Yuleba hardpan may vary 1 - 50 cm in thickness over 5 m laterally with marked undulations and

discontinuities. None the less, similarity in field relationships and bonding materials (dominantly clay mineral with some silicon) points to contemporaneous development. Similarity between these pans and those described in north-west New South Wales (Chartres, 1985) is less evident although again silica with some clay is seen as the cementing materials.

The hardpan in the sand dunes (site 6) is most interesting in that Al-exceeds or equals Si (Fig. 8b) and the SEM micrograph shows that the space between the quartz grains is completely filled with amorphous material. This is identified as imogolite/allophane complex by the NaF test, consistent with its strong autofluorescence. The lack of voids other than vesicles in the matrix implies precipitations from solution between rather than around the coarser grains.

Zabowski and Ugolini (1992) have shown that mineral stability is influenced by seasonal changes. In the sub-alpine podzol studied, they found that the soil solution remained unsaturated with respect to silica throughout the year. However, as the content of soil water dropped in summer, leaching losses are minimised and equilibrium conditions are approached. At the same time, it was observed that the clay minerals, smectite and kaolinite together with amorphous silica were being formed in the E horizon. Lower in the profile, the soil solution becomes saturated with kaolinite and leaching losses are limited by the presence of imogolite and quartz. Although the soil studied by these researchers occurs in a different environment, they have shown that further investigations into the stability of minerals in different soil environments could help provide an answer to the questions which have begun to be addressed in this paper.

Although the pans have developed in and persisted from an earlier environment, they affect the soils of the present land surface and where they occur at depths of < 2 m, need to be recognized in soil classification. The Australian great groups described by Stace *et al.* (1968) do not mention pans in the red podzolic, red earth, soloth or solodic soil groups, and no provision for pans has been made in Gn2, Dr or Dy categories of A Factual Key (Northcote, 1979). Presumably the pans at Sites 1, 3, 4 and 5 meet the criteria of a duripan in Soil Taxonomy (Soil Survey Staff, 1990) and where the pans are within 100 cm of the surface the soils should be classified as Durustalfs.

ACKNOWLEDGEMENT

REFERENCES

Bridges, E.M., Ross, D.J. and Thompson, C.H., 1990. Soils of the Mary River alluvia near Gympie, Queensland. CSIRO Australia, Division of Soils Divisional Report No. 109.

Bullock, P., Fedoroff, N., Jongerius, A., Stoops, G., and Tursina, T., 1985. Handbook for Soil Thin Section Description. Waine Research Publications, Wolverhampton, U.K., 152 pp.

Chartres, C.J., 1985. A preliminary investigation of hardpan horizons in north-west New South Wales. Aust. J. Soil Res. 23: 325-337.

Childs, C.W., Parfitt, R.L. and Lee, R., 1983. Movement of aluminium as an inorganic complex in some podzolized soils, New Zealand. Geoderma 29: 139-155.

Connah, T.H. and Hubble, G.D., 1960. Laterites. In: D. Hill and A.K. Denmead (Editors). The Geology of Queensland. Geological Society of Australia. Melbourne University Press, Melbourne, pp. 373-386.

Ellis, P.L., 1968. Geology of the Maryborough 1:250,000 sheet area. Geological Survey, Queensland Report No. 26. Queensland Department of Mines, Brisbane.

Farmer, V.C., Russell, J.D. and Berrow, M.L., 1980. Imogolite and proto-imogolite allophane in spodic horizons: evidence for a mobile aluminium silicate complex in podzol formation. Journal of Soil Science 31: 673-684.

Fieldes, M. and Perrot, K.W., 1966. The nature of allophane in soils, Part 3. Rapid field and laboratory test for allophane. New Zealand Journal of Science, 9: 623-629.

FitzPatrick, E.A., 1984. The Micromorphology of Soils. Chapman and Hall, London. 433 pp.

McDonald, R.C., Isbell, R.F., Speight, J.G., Walker, J. and Hopkins, M.S., 1984. Australian Soil and Land Survey Field Handbook. Inkata Press, Melbourne, 160 pp.

Northcote, K.H., 1979. A Factual Key for the Recognition of Australian Soils. 4th Edition Rellim Technical Publications, Glenside, South Australia, 124 pp.

Raupach, M. and Tucker, B.M., 1959. The field determination of soil reaction. J. Aust. Inst. Agric. Sci. 25: 129-133.

Ridley, W.F., 1957. A sedimentary formation of Tertiary age, between Maryborough and Bundaberg. Proc. Royal Soc. Queensland, 68: 11-16.

Robertson, A.D., 1979. Revision of the Cainozoic geology between Kolan and Elliott Rivers. Queensland Government Mining Journal 80: 350-363.

Runnegar, B. and Fergusson, J.A., 1969. Stratigraphy of the Permian and Lower Triassic marine sediments of the Gympie District. Queensland University Department of Geology Papers Vol.6 No. 9, University of Queensland Press, Brisbane.

Skjemstad, J.O., Fitzpatrick, R.W., Zarcinas, B.A., and Thompson, C.H., 1992. Genesis of podzols in coastal dunes in southern Queensland. II Geochemistry and forms of elements as deduced from various soil extraction procedures. Aust. J. Soil Res. 30: 615-644.

Smith, G.D., Ayra, L.M. and Stark, J., 1975. Densipan, a diagnostic horizon of Densiaquults for Soil Taxonomy. Soil Sci. Soc. Am. Proc., 39: 369-370.

Soil Survey Staff, 1990. Keys to Soil Taxonomy. SMSS Technical Monograph No.6, 4th editon. Virginia Polytechnic Institute and State University, Blacksburg, Virginia.

Stace, H.C.T., Hubble, G.D., Brewer, R., Northcote, K.H., Sleeman, J.R., Mulcahy, M.J. and Hallsworth, E.G., 1968. A Handbook of Australian Soils. Rellim Technical Publishers, Glenside, South Australia, 435 pp.

Van Dijk, D.C. and Beckmann, G.G., 1978. The Yuleba hardpan, and its relationship to soil geomorphic history, in the Yuleba-Tara region, south-east Queensland. In: T. Langford-Smith (Editor), Silcrete in Australia. Department of Geography, University of New England, Armidale, pp. 73-91.

Zabowski, D. and Ugolini, F.C., 1992. Seasonality in the mineral stability of a subalpine podzol. Soil Science, 154: 497-507.

This Page Intentionally Left Blank

Micromorphology of polygenetic soils in a small watershed, north central Kansas, U.S.A.

W.A. Wehmueller[1], M.D. Ransom[2], and W.D. Nettleton[3]

[1]USDA Soil Conservation Service, Manhattan, Kansas, USA
[2]Department of Agronomy, Kansas State University, Manhattan, Kansas, USA
[3]USDA Soil Conservation Service, National Soil Survey Laboratory, Lincoln, Nebraska, USA

ABSTRACT

Wehmueller, W.A., Ransom, M.D. and Nettleton, W.D. 1994. Micromorphology of polygenetic soils in a small watershed, north central Kansas, U.S.A. In: A.J. Ringrose-Voase and G.S. Humphreys (Editors), Soil Micromorphology: Studies in Management and Genesis. Proc. IX Int. Working Meeting on Soil Micromorphology, Townsville, Australia, July 1992. Developments in Soil Science 22, Elsevier, Amsterdam, pp. 247-255.

The Konza Prairie Research Natural Area (KPRNA) in north central Kansas is the largest parcel of native, tallgrass prairie preserved for ecological research in the U.S. The micromorphology of three polygenetic soils (designated as Pedons 6, 8, and 9) from a 125 ha watershed within KPRNA was examined as part of a larger study of soil genesis and geomorphology. The objectives of this study were to use micromorphology to: (1) evaluate the parent material stratigraphy; and (2) investigate processes of clay illuviation, and calcium carbonate and gypsum accumulation. The study area has a mesic temperature regime, and the moisture regime is transitional from udic to ustic. Pedon 6 occurred in a small depression along a summit (bench) position and classified as a Typic Natrustoll. Pedon 8, on a shoulder of an interfluve, was a Udertic Argiustoll. Pedon 9, a Udertic Paleustoll, was on a summit position along the interfluve. All three pedons developed in a thin mantle of Wisconsin loess overlying welded paleosols formed in hillslope sediment (colluvium) over residuum from Permian cherty limestone. The Bt horizons that were formed in loess and hillslope sediment exhibited skel-masepic and lattisepic plasmic fabrics indicative of high shrink-swell activity. Illuvial void argillans were occasionally found in abundance. Clusters of pedogenic, lenticular gypsum were identified in the paleosol formed in hillslope sediment on the summit and summit-depression. The horizons in which gypsum occurred also had high contents of exchangeable Na. For Pedons 8 and 9, the paleosol developed in cherty limestone residuum was truncated and well developed with continuous, thick illuvial ferriargillans. The extent of weathering observed in this paleosol suggests a longer period of soil formation than that of the composite modern soil and paleosol formed in hillslope sediment.

INTRODUCTION

The Konza Prairie Research Natural Area (KPRNA) is a 3400 ha native, tallgrass prairie in north central Kansas that is preserved for long term ecological research (Fig. 1). It is part of the International Network of Biosphere Reserves. Soils on the Konza Prairie and throughout
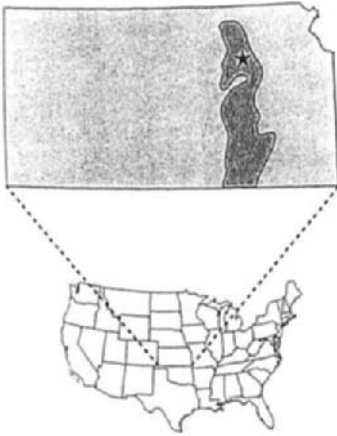
Fig. 1. Location of the Konza Prairie Research Natural Area. The darker shaded portion of Kansas is the Bluestem Hills land resource area.

the surrounding Bluestem Hills area of Kansas are developed in a variety of parent materials including loess, residuum from Permian shale and cherty limestone, colluvium, and alluvium.

As part of an investigation of a 125 ha watershed within KPRNA by ecologists, geomorphologists, and pedologists, a detailed soil map, made at a scale of 1:2000, and transects within the watershed were used to select nine pedons for soil characterization and micromorphological analyses. These pedons represented typical landscape positions and included soils formed in various parent materials in the watershed. In the present paper, we will report results for three pedons occurring on the summit and shoulder positions. These soils formed in multiple parent materials and have more complex stratigraphy of parent materials than recognized by the existing soil survey (Jantz *et al.*, 1975), which was made at a scale of 1:24,000. According to Jantz *et al.* (1975), soils on summit and shoulder positions in the watershed developed in residuum or sediments from clayey shales. Therefore, the objectives of this paper were to conduct soil characterization and micromorphological investigations of selected pedons from summit and shoulder positions to (1) evaluate parent material stratigraphy and (2) investigate processes of soil genesis, especially clay illuviation and calcium carbonate and gypsum accumulation.

The 125 ha watershed is within the Bluestem Hills land resource area of the Central Great Plains region (Soil Conservation Service, 1981). In the watershed, elevations above sea level range from 364 to 432 m. The climate is continental with a normal annual precipitation of 800 mm and a mean annual air temperature of about 13°C. The moisture regime is transitional from udic to ustic.

METHODS

Field investigations made during the soil survey of the watershed were used to select three representative pedons from summit and shoulder positions. At each site, a 1 × 2 m pit was excavated to bedrock in order to describe and sample the pedons. Samples were collected from each horizon and analyzed for routine soil characterization and clay mineralogy by the methods described by the Soil Survey Laboratory Staff (1992). For thin section analysis, undisturbed, oriented clods from selected horizons were collected, air-dried, and impregnated

with polyester resin. Horizontal sections from each clod were mounted on 27 × 46 mm petrographic slides and polished to an approximate thickness of 30 μm. The thin sections were then described using the nomenclature of Brewer (1976).

RESULTS AND DISCUSSION

Soil Classification and Parent Material Stratigraphy

Table 1 shows selected soil characterization data for the study pedons. Pedon 9 is a fine, montmorillonitic, mesic Udertic Paleustoll.   This pedon contained high contents of exchangeable Na (Table 1), but it was too deep in the profile to meet natric horizon requirements (Soil Survey Staff, 1992). The summit on which this pedon occurred was the highest topographic position in the watershed. This summit is on a broad interfluve with a thicker loess mantle than the other two pedons. Field observations and laboratory data (including clay mineralogy and clay-free particle size distribution data that are not shown) indicate lithologic discontinuities at 58 and 107 cm. The upper 58 cm was identified as loess based on the high silt and low coarse fragment content (Table 1). According to Ruhe (1984), the loess mantle across the eastern part of Kansas and Nebraska is Wisconsin (Peoria), and the maximum age of soils developed in this material is about 14,000 years. The material from 58 to 107 cm was identified as colluvium or hillslope sediment as defined by Daniels and Hammer (1992). The upper horizon of this material from 58 to 71 cm exhibited an increase in coarse fragment content (Table 1) and contained a stone line. Transect work showed that this hillslope sediment could be traced across most of the erosional landscape of the small watershed. The high content of chert fragments and high clay content suggests that the material from 107 to 148 cm was formed in residuum weathered from the underlying cherty limestone. A strongly-developed paleosol with continuous ferriargillans occurred in this material.

Pedon 6 was classified as a fine, montmorillonitic, mesic Typic Natrustoll. This pedon had a natric horizon (Soil Survey Staff, 1992) as indicated by (i) exchangeable Na percentages ≥15 (Table 1) within 40 cm of the upper boundary of the Btn1 horizon, (ii) columnar structure in the Btn horizons, and (iii) sufficient clay increase for an argillic horizon. This pedon occurred in a small, irregularly shaped depression on the summit of a bench that was topographically about 25 m lower than the summit of Pedon 9. The upper 43 cm was identified as Wisconsin loess based on the high silt content and low content of coarse fragments (Table 1). The material from 43 to 73 cm was identified as hillslope sediment similar to that of the second parent material of Pedon 9. The material from 73 to 77 cm was identified as residuum weathered from the underlying limestone. Particle size distribution on a clay-free basis (data not shown) also supports the identification of the lithologic discontinuities.

Pedon 8 occurred on a shoulder slope below the summit of Pedon 9 and was classified as a clayey-skeletal, montmorillonitic, mesic Udertic Argiustoll. At this location, the interfluve is more sloping and narrower than that of Pedon 9. The upper 18 cm was identified as Wisconsin loess based on high silt content and low content of coarse fragments (Table 1). The second parent material from 18 to 37 cm was identified as hillslope sediment based on subrounded coarse fragments that were mostly chert. An abrupt boundary at 37 cm marked the top of a truncated paleosol formed in residuum similar to the paleosol developed in residuum in Pedon 9. The limestone and chert fragments in the 3Bt horizon were less angular than those in the 2Bt horizon and were coated with thick, continuous ferriargillans.

Table 1
Selected physical and chemical characterization data for the study pedons.

Horizon	Depth (cm)	>2mm (%)	Sand (%)	Silt (%)	Clay (%)	COLE[1] (cm/cm)	pH 1:1 H2O	Elec. Cond. mmhos/cm	Na Sat- uration (%)	Ext.[2] Fe (%)
Pedon 6 (Summit-depression)										
A	0-9	0	7.7	64.0	28.3	-	5.6	1.37	1	0.9
Btn1	9-20	0	6.3	51.1	42.6	0.03	6.4	0.69	10	1.1
Btn2	20-31	0	4.8	46.1	49.1	0.11	7.8	1.17	16	1.2
Btkn1	31-42	1	4.5	51.5	44.0	0.13	8.2	2.36	27	1.1
2Btkn2	42-57	1	9.4	48.7	41.9	0.09	8.2	4.23	35	1.2
2Btkny	57-73	<1	6.0	47.8	46.2	0.14	7.8	8.48	36	1.3
3Bkn	73-77	39	31.2	37.8	31.0	0.12	8.3	7.74	45	0.3
3R	77-80	-	-	-	-	-	-	-	-	-
Pedon 8 (Shoulder)										
A1	0-9	2	11.1	60.0	28.9	-	6.3	-	<1	1.0
A2	9-18	9	10.8	53.1	36.1	0.04	5.8	-	<1	1.2
2Bt1	18-28	6	10.0	46.5	43.5	-	5.9	-	<1	1.5
2Bt2	28-37	19	9.0	45.1	45.9	0.06	6.0	-	<1	1.6
3Bt3	37-66	84	15.7	33.2	51.1	-	6.0	-	<1	1.6
3Bt4	66-79	10	4.6	32.6	62.8	0.14	7.1	-	<1	2.2
3Bt5	79-90	8	3.4	26.4	70.2	-	7.5	-	<1	2.2
3R	90-93	-	-	-	-	-	-	-	-	-
Pedon 9 (summit)										
A1	0-10	0	7.2	66.8	26.0	0.04	6.3	0.73	1	0.8
A2	10-17	<1	6.5	62.9	30.6	0.04	5.6	-	3	0.9
Bt1	17-33	<1	3.7	47.4	48.9	0.10	6.9	0.53	6	1.2
Bt2	33-41	<1	2.8	54.1	43.1	0.09	7.6	0.90	8	1.1
Btk1	41-58	3	4.8	59.3	35.9	0.06	8.2	0.85	10	1.0
2Btk2	58-71	7	7.1	60.8	32.1	-	8.2	1.29	17	1.0
2Btky	71-86	3	9.1	56.6	34.3	0.06	7.6	5.73	20	1.2
2Bt1	86-97	4	9.0	51.9	39.1	0.08	7.7	5.06	20	1.4
2Bt2	97-107	12	10.5	46.8	42.7	0.09	7.7	3.63	23	1.5
3Bt3	107-127	58	11.0	34.8	54.2	-	7.7	3.17	26	1.7
3Bt4	127-148	75	3.8	27.1	69.1	-	7.7	1.34	17	1.6
3R	148-150	-	-	-	-	-	-	-	-	-

[1]COLE=Coefficient of Linear Extensibility (Soil Survey Staff, 1992).
[2]Extractable in Na citrate-dithionite.
N.B. Gravel fraction (>2mm) on a whole soil basis. Sand, silt and clay content as a proportion
of the fine earth fraction (<2mm).

Clay Movement and Orientation

All three pedons have complex, welded paleosols (Ruhe and Olson, 1980). The depth distribution of clay in Pedon 6 is bisequal with maxima in both the loess and the underlying hillslope sediment (Table 1). Pedon 9 had maximum values in clay content in the Bt1 horizon of the loess and the 3Bt4 horizon developed in cherty limestone residuum. In contrast, the loess mantle for Pedon 8 was much thinner, and the clay content increased uniformly with depth. All three pedons exhibited vertic characteristics and high COLE values (Table 1).

The paleosol formed in residuum of Pedons 8 and 9, which exhibited clay contents of about 70% (Table 1), contained common papules of weathered biotite and omnisepic and lattisepic plasmic fabrics. Such features are common in soils with vertic properties (Nettleton and Sleeman, 1985). Chert fragments in the paleosol were rounded with thick ferriargillans on all surfaces and in cavities (Fig. 2A). Dithionite-citrate extractable Fe (Table 1) was higher in the paleosol suggesting that it was more weathered than the modern soil developed in the overlying parent materials. The lack of an A horizon, abrupt textural difference, and change in fabric to skel-masepic plasmic fabric in the lower horizon of the hillslope sediment suggests that the paleosol developed in residuum for Pedons 8 and 9 was truncated before deposition of the hillslope sediment.

The residuum of Pedon 6 was much thinner and higher in carbonate than the residuum of Pedons 8 and 9. This residuum is from the Schroyer Limestone, which is less cherty and more resistant to weathering than the Florence Limestone (Jewett, 1941) underlying Pedons 8 and 9. The strongly-developed paleosol observed in Pedons 8 and 9 may not have been as strongly developed at this location. Alternatively, the paleosol formed in residuum for Pedon 6 may have been truncated before deposition of the overlying hillslope sediment.

The hillslope sediment in Pedon 9 had distinct argillans in the 2Bt2 horizon (Fig. 2B). Although this horizon had high shrink-swell potential and a COLE of 0.09 (Table 1), stress had not been sufficient to disrupt the argillans. At this depth, the soil may not dry enough to experience the full range of linear extensibilities that disrupt argillans as reported by Nettleton *et al.* (1969). The upper part of the hillslope sediment (*e.g.* the 2Btk2 horizon) had fewer illuvial argillans and exhibited increasing amounts of stress-oriented features including areas of lattisepic plasmic fabric.

The horizons formed in hillslope sediment of Pedons 6 and 8 also exhibited illuvial argillans. For all three pedons, clay illuviation in the hillslope sediment could have occurred before or after deposition of loess. For Pedons 6 and 9, the sequence of clay illuviation into the hillslope sediment can be determined using micromorphology. The hillslope sediment of these two pedons contained argillans superimposed with pedogenic carbonate and gypsum (Fig. 2C), which probably originated during the weathering of the Wisconsin loess. This indicates that clay illuviation occurred in the hillslope sediment before deposition of Wisconsin loess. Since the loess mantle of Pedon 8 is so thin, determining the sequence of clay illuviation into the 2Bt horizon is difficult.

Occasional argillans in voids and channels provided evidence of clay illuviation in the upper argillic horizon formed in loess in Pedons 6 and 9. In addition to these illuvial argillans, embedded grain argillans were also observed in the upper argillic horizon. These grain argillans were thin, exhibited a rather diffuse boundary, and coated the grains with uniform thickness on all sides. Such grain argillans may result from stress rather than illuviation (Rabenhorst and Wilding, 1986; Ransom and Bidwell, 1990).
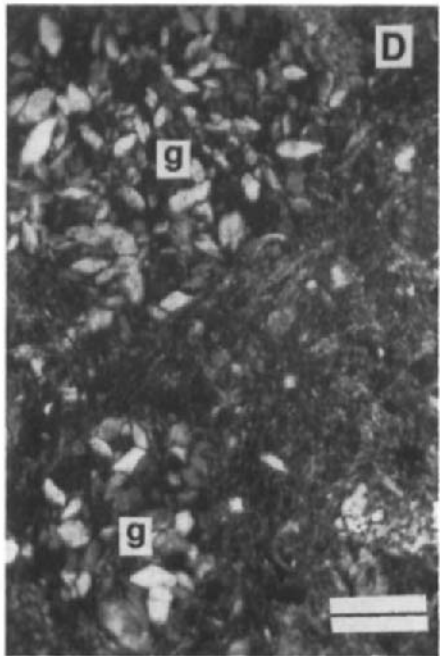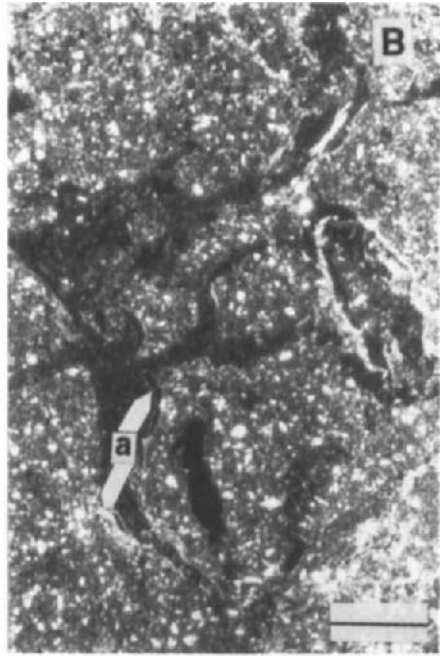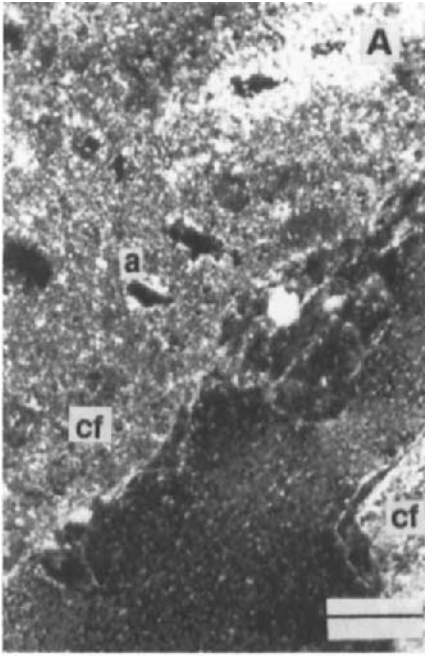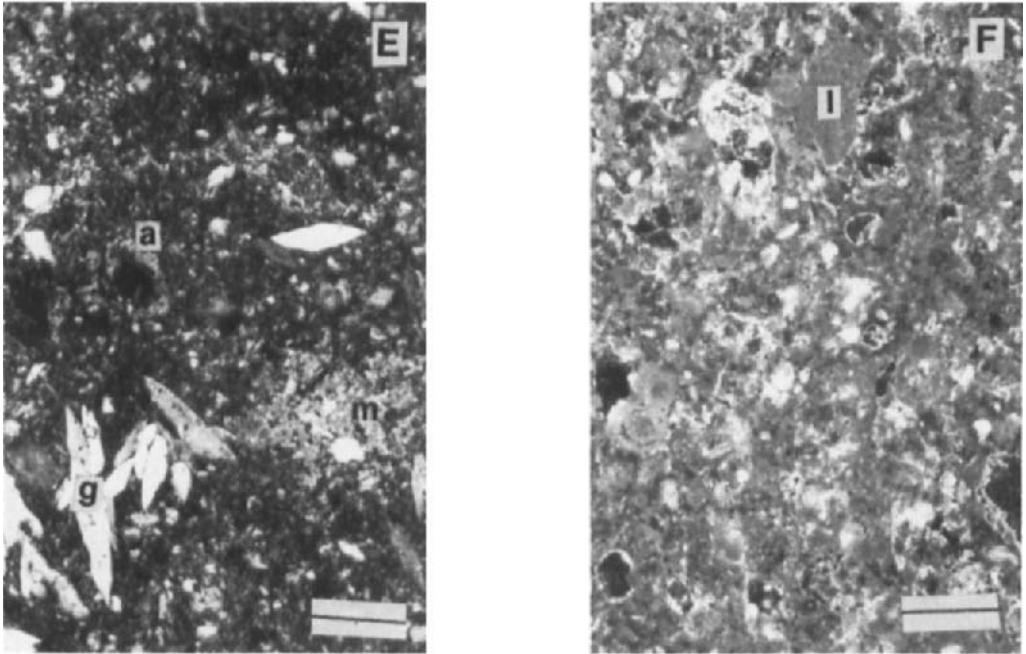
Fig. 2. Thin section photomicrographs of the study pedons. Crossed-polarized light: **A)** Chert fragments (cf) in the 3Bt3 horizon of Pedon 8 with thick argillans (a) on surfaces and in cavities. Bar scale=200 μm. **B)** Thick ferriargillans (a) on the wall of a vugh in the 2Bt2 horizon of Pedon 9. Bar scale=500 μm. **C)** Illuvial argillan (a) superimposed with pedogenic gypsum crystals (g). Bar scale=200 μm. **D)** Clusters of lenticular gypsum crystals (g) in the 2Btkny horizon of Pedon 6; plasmic fabric is lattisepic in the surrounding s-matrix. Bar scale=200 μm. **E)** Accumulations of gypsum (g) and micrite (m) in the 2Btky horizon of Pedon 9. A ferriargillan (a) is also evident on the wall of the void. Bar scale=200 μm. **F)** Crystic plasmic fabric of the 3Bk horizon of Pedon 6 showing highly weathered limestone fragments (l) within micrite-rich fabric. Bar scale= 500 μm.

CaCO₃ and Gypsum Accumulation

Gypsum clusters occurred in the 2Btky and 2Btkny horizons of Pedons 9 and 6, respectively. This gypsum was in the form of lenticular-shaped euhedral grains (Fig. 2D), which according to FitzPatrick (1984) and Porta and Herrero (1990), are characteristic of pedogenic gypsum. The parent material for both horizons containing gypsum was hillslope sediment. Nettleton *et al.* (1982) found that gypsum accumulates in soils near the maximum depth of wetting in semiarid soils. Pedogenic gypsum typically forms in soils where there is minimal water movement through the soil profile because of low precipitation or because of slowly permeable subsoils (Allen and Hajek, 1989). In Pedons 6 and 9, gypsum occurred at

about the same depth and in proximity to a lithologic discontinuity that would restrict water movement. Dispersion caused by the high Na contents in these two horizons may be responsible for restricting water movement that caused gypsum accumulation. Marine shales and mudstones are interbedded with the limestone in the area (Jewett, 1941) and are the most probable source of Na^+ and SO_4^{2-} in these pedons. We believe the source of Ca^{2+} and CO_3^{2-} was the weathering of the overlying Wisconsin loess that was probably calcareous when first deposited.

Pedon 8 did not exhibit any gypsum accumulation, and the exchangeable Na content was low in all horizons. This pedon was more freely drained because of the large amount of coarse fragments in the 2Bt horizon developed in hillslope sediment; it also occurred on a more sloping shoulder slope and had a much thinner loess mantle than the other two pedons.

Pedons 6 and 9 exhibited pedogenic $CaCO_3$ accumulations in the horizons containing gypsum (Fig. 2E) as well as in the horizon above. The carbonate forms included neocalcans and micritic nodules and accumulations. In the horizon formed in residuum in Pedon 6, the carbonate morphology was more complex (Fig. 2F). Crystic plasmic fabrics, abundant micrite, limestone fragments coated with micritic calcans, and void neocalcans suggest that much dissolution, redistribution, and reprecipitation of carbonate had occurred (Sobecki and Wilding, 1983; West et al., 1988). Pedon 8 contained pedogenic carbonate in the 3Bt5 horizon in the form of soft masses as a weathering rind between the peds and limestone fragments.

CONCLUSIONS

The three pedons contained sufficient oriented clay to meet the requirements of an argillic horizon. Pedon 6 also had enough exchangeable Na for a natric horizon. All three pedons are polygenetic in that the modern soil development extends through the loess into the underlying material. Pedons 8 and 9 had a paleosol developed in residuum that exhibits lattisepic and omnisepic plasmic fabrics. The plasmic fabrics, high clay content, and higher extractable Fe suggest a long period of soil development. Horizons formed in the hillslope sediments had patchy illuvial argillans. Argillans superimposed with pedogenic carbonate and gypsum in the upper part of the hillslope sediments of Pedons 6 and 9 suggest they are being recharged with carbonate from the loess. Pedon 8 was more freely drained; carbonate and gypsum did not accumulate in the hillslope sediment of this pedon. Pedon 6 did not have the strongly developed paleosol in residuum. Because the limestone beneath this pedon was more resistant to weathering, the strongly-developed paleosol may not have formed, or it may have been truncated before deposition of the hillslope sediments.

REFERENCES

Allen, B.L. and Hajek, B.F., 1989. Mineral occurrence in soil environments. In: J.B. Dixon, and S.B. Weed (Editors), Minerals in Soil Environments. Soil Sci. Soc. Am. Book Series No. 1, Madison, Wisconsin, pp. 199-278.

Brewer, R., 1976. Fabric and Mineral Analysis of Soils. R.E. Krieger Publishing Company, Huntington, New York, 482 pp.

Daniels, R.B. and Hammer, R.D., 1992. Soil Geomorphology. John Wiley and Sons, Inc., New York, 236 pp.

FitzPatrick, E.A., 1984. Micromorphology of Soils. Chapman and Hall, London, 433 pp.

Jantz, D.R., Harner, R.F., Rowland, H.T. and Gier, D.A., 1975. Soil Survey of Riley County and Part of Geary County, Kansas. Soil Conserv. Serv., U.S. Dept. Agric., Washington, D.C., 71 pp.

Jewett, J.M., 1941. The Geology of Riley and Geary Counties, Kansas. Kansas Geological Survey Bull. 39, 164 pp.

Nettleton, W.D., Flach, K.W. and Brasher, B.R., 1969. Argillic horizons without clay skins. Soil Sci. Soc. Am. Proc., 33: 121-125.

Nettleton, W.D., Nelson, R.E., Brasher, B.R. and Derr, P.S., 1982. Gypsiferous soils in the western United States. In: J.A. Kittrick *et al.* (Editors), Acid Sulfate Weathering. Soil Sci. Soc. Am. Spec. Publ. 10, Madison, Wisconsin, pp. 147-168.

Nettleton, W.D. and Sleeman, J.R., 1985. Micromorphology of Vertisols. In: L.A. Douglas and M.L. Thompson (Editors), Soil Micromorphology and Soil Classification. Soil Sci. Soc. Am. Spec. Publ. 15, Madison, Wisconsin, pp. 165-196.

Porta, J. and Herrero, J., 1990. Micromorphology and genesis of soils enriched with gypsum. In: L.A. Douglas (Editor), Soil Micromorphology: A Basic and Applied Science. Proc. VIII Int. Working Meeting on Soil Mircromorphology, San Antonio, Texas, July 1988. Developments in Soil Science 19, Elsevier, Amsterdam, pp. 321-339.

Rabenhorst, M.C. and Wilding, L.P., 1986. Pedogenesis on the Edwards Plateau, Texas: II. Formation and occurrence of diagnostic subsurface horizons in a climosequence. Soil Sci. Soc. Am. J., 50: 687-692.

Ransom, M.D. and Bidwell, O.W., 1990. Clay movement and carbonate accumulation in Ustolls of central Kansas, U.S.A. In: L.A. Douglas (Editor), Soil Micromorphology: A Basic and Applied Science. Proc. VIII Int. Working Meeting on Soil Mircromorphology, San Antonio, Texas, July 1988. Developments in Soil Science 19, Elsevier, Amsterdam, pp. 417-423.

Ruhe, R.V., 1984. Soil-climate system across the prairies in midwestern, U.S.A. Geoderma, 34: 201-219.

Ruhe, R.V., and Olson, C.G., 1980. Soil welding. Soil Sci., 130: 132-139

Sobecki, T.M. and Wilding, L.P., 1983. Formation of calcic and argillic horizons in selected soils of the Texas Coast Prairie. Soil Sci. Soc. Am. J., 47: 707-715.

Soil Conservation Service, 1981. Land Resource Regions and Major Land Resource Areas of the United States. U.S. Dep. Agric. Handb. 296, U.S. Gov. Printing Office, Washington, D.C.

Soil Survey Laboratory Staff, 1992. Soil Survey Laboratory Methods Manual. Soil Survey Investigations Report No. 42. USDA Soil Conservation Service, National Soil Survey Center, Lincoln, Nebraska.

Soil Survey Staff, 1992. Keys to Soil Taxonomy. 5th editon. SMSS Tech. Monogr. no. 19. Pocahontas Press, Blacksburg, Virginia. 541 pp.

West, L.T., Drees, L.R., Wilding, L.P. and Rabenhorst, M.C. 1988. Differentation of pedogenic and lithogenic carbonate forms in Texas. Geoderma, 43: 271-287.

This Page Intentionally Left Blank

Micromorphology of a Cambrian paleosol developed on granite: Llano Uplift region, Central Texas, U.S.A.

R.C. Capo

Jet Propulsion Laboratory and Division of Geological & Planetary Sciences, 170-25, California Institute of Technology, Pasadena, CA, 91125, USA

ABSTRACT

Capo, R.C., 1994. Micromorphology of a Cambrian paleosol developed on granite: Llano Uplift region, Central Texas, U.S.A.. In: A.J. Ringrose-Voase and G.S. Humphreys (Editors), Soil Micromorphology: Studies in Management and Genesis. Proc. IX Int. Working Meeting on Soil Micromorphology, Townsville, Australia, July 1992. Developments in Soil Science 22, Elsevier, Amsterdam, pp. 257-264.

The micromorphology, mineralogy and geochemistry of a Cambrian paleosol developed on Grenville-aged granite in Central Texas suggest that pedogenic processes similar to modern ones were active before the advent of vascular land plants. The clay-rich horizon of the weathering profile exposed along Squaw Creek has cutans (argillans, ferrans and ferri-argillans) and well developed sepic plasmic fabric (vosepic, skelsepic and masepic). Development of the profile resulted in depletion of alkalis and alkaline earths, Fe^{2+}, Mn and Si, and enrichment in Fe^{3+}, Cu and Zn. Comparisons with modern soils suggest that expanding clays were present during formation of the profile, and support other evidence for a hot semiarid climate in parts of equatorial coastal Laurentia during the Middle Cambrian.

INTRODUCTION

Two of the most difficult aspects of studying pre-Quaternary soils are recognition and accurate age determination of preserved weathering profiles (Yaalon, 1971; Holland and Zbinden, 1988; Retallack, 1988). The Squaw Creek Paleosol (SQP) is part of a stratigraphically well constrained weathering profile developed on Precambrian granite in Texas over 500 Ma ago. The SQP provides a record of the terrestrial environment during the Cambrian and also provides a rare opportunity to study surficial weathering processes in the absence of vascular plants, which were not present on land until mid-Ordovician time, and which are a major factor in soil-forming processes today.

GEOLOGIC AND GEOMORPHIC SETTING

The Llano Uplift region in Central Texas, U.S.A. is an exposure of Paleozoic and Grenville-aged Precambrian rocks rimmed by the Cretaceous Edwards plateau. Large granite plutons were intruded into the area ~1.1 Ga ago; this was followed by regional uplift, exposure and erosion. During the Cambrian, the landscape was dominated by granite inselbergs; local relief exceeded 250 m. This irregular surface was then buried by the tidally influenced or estuarine

sediments of the Riley Formation as seas transgressed over the Texas craton in the Late Middle Cambrian, ~520 Ma (Barnes and Bell, 1977).

The weathering profile is exposed along Squaw Creek in Mason County at the southwestern rim of the uplift (Barnes and Bell, 1977). The parent material is a buried exfoliation dome of pink Town Mountain granite (1.06 Ga; Garrison *et al.*, 1979; Walker, 1992) that forms a 6 m escarpment. The overlying Hickory Sandstone Member of the Riley Formation, a beige kaolinitic coarse sandstone, forms a prominent ledge 4 m high. The contact appears as a distinct recess between the two lithologies. Alteration of the granite increases upward toward the Cambrian nonconformity, and white-mottled, deep red *in situ* paleosol material caps the profile. Reworked and stratified material of a similar nature is deposited nearby along one flank of the dome. In other outcrops of the Cambrian-Precambrian contact in the area, no paleosol material is preserved; this is not surprising, since there were no vascular plants to anchor soil material to the granite domes. The *in situ* Squaw Creek paleosol was probably preserved due to its location in a shallow depression on top of a dome, which protected it from the influx of external material and prevented it from being completely eroded.

METHODS

Samples were chipped from the outcrop with rock hammers and chisels and selected to avoid contamination from modern surficial weathering, as exemplified by the thin yellow-orange coating of limonite on the exposed outer surface of the profile. Modal abundances were determined by standard point-counting techniques. Clay minerals were identified by XRD of oriented clay mounts according to the methods described by Carroll (1970). Major element oxide and trace element abundances were obtained by wet chemical analysis and inductively coupled plasma atomic emission spectroscopy analysis. Biotite and plagioclase compositions were determined by electron microprobe (Capo, 1984).

THE SQUAW CREEK WEATHERING PROFILE

In both its physical and micromorphological aspects, the SQP exhibits a gradual change from the Cambrian-Precambrian contact downward to the unweathered parent granite. A zone of relatively fresh granite at the base of the profile is transitional into an intensely altered oxidized horizon, which grades upward into a laterally discontinuous, 1.5 m thick horizon characterized by angular blocky peds, a deep red clay-rich matrix, iron and clay coatings, and white mottles of kaolinite and Ti-oxide. The deep purple-red (7.5R 4/3) color and induration of this horizon contrasts with the orange to brown color and uncemented nature of modern soils developed on the Town Mountain granite, but such a color is not unusual for sediments of Paleozoic age (Folk, 1976; Folk and Patton, 1982).

This clay-rich horizon is abruptly truncated by the basal Hickory Sandstone, which constrains a Cambrian minimum age for the soil. Thin bands of red material similar to that in the clay and iron-oxide horizon are entrained within the sandstone; this is evidence that this material was unconsolidated and present prior to deposition of the sandstone, and that the profile observed is not simply the result of post-depositional burial diagenesis. In addition, thicker and more extensive deposits of stratified reworked material (pedolith) are found nearby along paleoslopes and between corestones.

Micromorphological evidence for the pedogenic origin of the SQP includes the development of plasmic fabric, coatings of clay and Fe- and Ti-oxides around grains and along voids, and shrink-swell textures. Spallation of quartz grains has occurred and some shifting of grains is evident, but the preservation of delicate textures and grain relationships rules out wholesale compaction and post-burial deformation. The chemical trends in the weathering horizon are similar to trends observed in modern soils developed on granite. The constancy of immobile elements such as Zr and Ti between parent material and soil argues that the profile has not been strongly affected by an influx of allochthonous material. Work by Maynard (1992) suggests that the Ti/Zr ratios of *in situ* soils do not deviate by more than 40% from their parent material values; Ti/Zr ratios of the SQP and of the stratified soil material deposited nearby are within 10% of the fresh granite. In addition, there is no evidence of external addition of K by metasomatism or of significant Fe loss, which often alter ancient paleosols (Holland and Zbinden, 1988).

DESCRIPTION OF THE PALEOSOL

Having established a case that the SQP is in fact an ancient soil, it is useful to identify the horizons in analogy with modern soils. The assignment of soil horizon names to these zones is based on the criteria and terms for paleosols discussed in Retallack (1988); micromorphological terminology is based on Brewer (1964).

R horizon

The pink coarse-grained microcline perthite granite of the R horizon near the base of the exposed profile contains ~40% euhedral perthite, 15% euhedral plagioclase (An 10-23), 33% anhedral quartz, 5-8% biotite and 4-6% chlorite, sericite, kaolinite and accessory zircon and apatite. Plagioclase shows minor vacuolization and alteration to clay, although microcline is quite fresh. Albite stringers within perthite are turbid, and all plagioclase crystals exhibit some alteration, particularly along twin planes and within calcic cores, probably enhanced by dissolution features present in the grains prior to subaerial exposure.

C horizon

About 3 m below the unconformity, numerous fractures subparallel to the surface cut across grain boundaries. This is probably due to biotite weathering and laterally confined expansion (Folk and Patton, 1982). Biotite exhibits bloating, fraying and expansion along the edges of its basal cleavage planes, and shows replacement by Fe and Ti oxides, chlorite, kaolinite and illite (Fig. 1). In the indurated and oxidized C horizon 1.5 - 2 m below the unconformity, secondary clays and iron oxide increase to ~35%. Numerous white kaolinite pseudomorphs after plagioclase are present in this horizon, but plagioclase is completely absent. Much of the biotite is intensely altered, which may have been the source for iron oxides that stain nearby microcline perthite grains. The breakdown of albite stringers in the perthite left behind lenticular islands of more resistant microcline which are surrounded by clay and Fe-oxides (Fig. 2). Even quartz shows signs of weathering by dissolution and spalling.
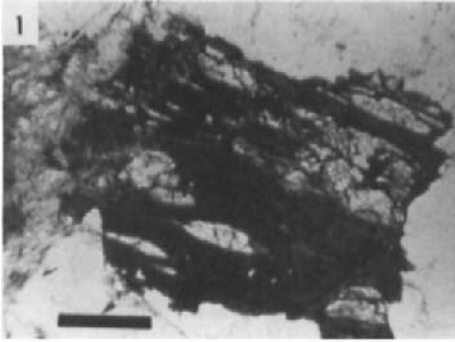
Fig. 1. Photomicrograph of biotite (plane polarized) from the lower C horizon. Note fraying along edges; bloating occurs between basal planes due to replacement by kaolinite (white) and hematite (black). Length of bar = 0.5 mm.
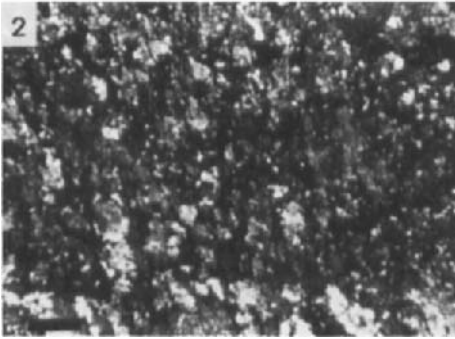
Fig. 2. Photomicrograph (crossed polars) from oxidized C horizon. Microcline "islands" (cross-hatched twinning) are surrounded by kaolinite (white) and hematite (black). Length of bar = 1mm.

B horizon

Original granitic textures are obliterated in the ~1.5 m thick, indurated but friable argillic B horizon, which consists of ~50% porphyroskelic primary residual quartz (0.5-12 mm long), 3% biotite and 47% authigenic clays and Fe- and Ti-oxides. Clay minerals present include illite (~2-3%) and kaolinite (~30%); expandable clays such as smectite were not found in XRD analysis. The increase in modal abundance of quartz suggests a net volume loss as feldspars (absent in this horizon) were replaced by clay and oxides. This horizon contains common white kaolinitic mottles with dark green biotite centers (2-6 mm total diameter) in a dark red clay and iron oxide matrix, which tends to break into slickensided medium angular blocky peds. Micromorphologic features diagnostic of soil development such as sepic plasmic fabric and cutans (Brewer, 1964; Retallack, 1988) are present. Numerous cracks and veins outline ped surfaces. Stress cutans are also present and are associated with the slickensides visible in hand sample. The texture is porphyroskelic (quartz grains float in a clay-rich matrix).

Within peds, iron oxide and birefringent clay as well as combinations of both coat residual grains (ferrans, argillans, and ferri-argillans) and line planar voids (Fig. 3). Authigenic clay and hematite are also draped around or forcing apart fractured primary quartz grains and crenulated biotite flakes. Packing between grains is loose; there appears to be displacive growth of clay and hematite cement between fractured quartz grains (Fig. 4). Patches of

Fig. 3. Photomicrograph of plasmic fabric in the B horizon (crossed polars). Matrix consists of kaolinite, illite and hematite. Patches of birefringent clay (illite) are oriented within the matrix and along planes oriented at 30° to each other (masepic fabric). Note birefringent clay lining fracture at upper right (vosepic fabric). Length of bar = 0.1 mm.
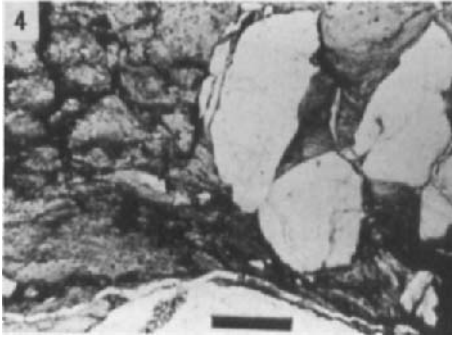
Fig. 4. Photomicrograph of porphyroskelic texture in the argillic B horizon (plane polarized). Hematite (black) coats skeletal quartz grains. Note glaebules of kaolinite surrounded by hematite (lower right), spalling of quartz crystals, and displacement of grains by clay. Length of bar = 1 mm.

birefringent clay (sericite/illite) within the matrix show a parallel orientation. Clusters of vermicular kaolinite glaebules ~1 mm in diameter are surrounded by dark red hematite. They are similar in size and shape to the microcline islands of the C horizon; however, in this horizon, all feldspar is absent. This suggests that the texture formed as the result of replacement of microcline. The lenticular shapes may also be a relict of clay expansion.

Surprisingly, intensely weathered and crenulated biotite is still preserved. Its color change from black to greenish or reddish brown in this horizon represents loss of Fe^{2+} and Ti^{4+} during weathering. It has also undergone a 7% loss of K_2O and 23% loss of MgO. The biotite is invariably surrounded by a thick cutan of clays and oxides which probably formed an impermeable barrier that inhibited cation exchange and prevented further degradation (Bohn *et al.*, 1979; Nahon, 1991).

No organic A is observed. Although vascular plants would not make their appearance on land for another 100 Ma, terrestrial cyanobacteria (blue-green algae) and other bacteria had evolved by the Cambrian (Margulis, 1982) and could have affected surficial weathering processes. The hematite of the paleosol is distinctive in that it is very fine grained (0.2-0.5 μm). Other workers have suggested that aging of sediments would result in the dehydration and recrystallization of amorphous oxides into crystals which coarsen with time (Folk, 1976; Walker, 1976). Residue from Fe-oxidizing bacteria may have prevented grain coarsening since organic material inhibits the crystallization of Fe-hydrates (Duchafour, 1982). However, if a

discrete zone of organic-rich material was present in the SQP, it was eroded during or prior to the deposition of the Hickory sandstone.

Pedolith

The sampled pedolith material was found 10 m laterally and downslope from the B horizon. It is very similar in color, composition and induration to the *in situ* B horizon, but is stratified. In addition, the orientation of the matrix is disrupted; many fine spalled quartz fragments have been separated from their parent grains. Clay is oriented only within small (<2 mm) domains. Another difference is the absence of birefringent argillans, slickensides and biotite; mottles are similar in size to those of the B horizon, but consist solely of white kaolinite and leucoxene. The B horizon was subject to the same burial history as the pedolith; this supports the origin by pedogenesis rather than by post-burial compaction or diagenesis of those features present in the B horizon but absent in the pedolith. They were probably disrupted or removed due to exposure and winnowing when the soil washed downslope prior to burial by the Cambrian sandstone. Transport was most likely not more than a few tens of meters, since delicate quartz shards and some small-scale soil fabrics (sepic plasmic fabric) are still intact.

GEOCHEMISTRY

Major and trace element patterns within the profile and pedolith correspond to the variation in mineralogy and follow the trends observed for modern weathering profiles (Wahlstrom, 1948; Harriss and Adams, 1966; Nesbitt *et al.*, 1980). In the B horizon, when normalized relative to TiO_2, alkalies and alkaline earth elements are depleted by 30 to 99%, water is enriched, and ferric iron is enriched at the expense of ferrous iron, relative to the parent granite; total iron is highest in the upper part of the profile. Over 90% of the Na and Ca were removed with plagioclase breakdown in the C horizon. K depletion is less marked until the B horizon where microcline disappears; Mg decreases also, reflected in the decrease in MgO in the biotite. Mg and K were probably first incorporated into 2:1 clays such as illite or smectite; with increased leaching these cations would be removed as clays degraded further into more stable 1:1 clays such as kaolinite. Si is depleted by ~20% and Al by ~25% between the parent and the B horizon. Although feldspar makes up ~55% of the parent granite and is absent in the B, some of the silica and alumina released by feldspar breakdown was retained in the soil by the formation of secondary clays.

DISCUSSION AND CONCLUSIONS

Central Texas (part of Laurentia) was located within 600 km of the equator during the Middle Cambrian, and ventifacts, sand dunes, evaporite pseudomorphs and fresh feldspar in the Riley Formation suggest hot and semiarid conditions at this time (Scotese *et al.*, 1979; Chafetz, 1980). Modern soils developed on granitic parent material in semiarid to arid environments are usually dominated by expandable clays such as smectite (Barshad, 1966; Tardy *et al.*, 1973). Angular blocky peds and slickensides, which are observed in the Squaw Creek Paleosol, are commonly associated with soils with expandable clays (Buol *et al,*. 1980). Although illite is still present in the SQP, no other 2:1 clays were identified. This may be related to the intensity and length of time involved in weathering; clays such as smectite are

unstable and over time would recrystallize to 1:1 clay such as kaolinite. The textures observed in the transition from fresh granite to soil strongly suggest that some of the clay in the argillic B horizon formed *in situ*. However, optically-oriented clay coatings in voids within peds and around grains, as well as the gains and losses of cations provide evidence that some physical and chemical illuviation has also taken place.

The suggested weathering history for the Squaw Creek Paleosol is as follows: Soil formed on the irregular, weathered surface of the Precambrian granite, in a hot, semiarid tropical environment. Plagioclase weathered first, followed by microcline, which resulted in the formation of expandable clays, with subsidiary illite and kaolinite. Biotite breakdown resulted in the formation of Fe and Ti-oxides and clay. Over the next 10^3-10^6 years, increased leaching led to the decomposition of 2:1 clays to form stable kaolinite. Porphyroskelic primary quartz and biotite remained in a matrix of clay and sesquioxides. Some soil material washed downslope and was redeposited nearby (with loss of biotite in the process). Erosion and burial followed as the Cambrian seas transgressed over the craton. Reddening deepened and induration increased as iron oxides dehydrated and recrystallized.

Textural, mineralogical and chemical variations within the Squaw Creek Paleosol indicate that Cambrian weathering and soil-forming processes were similar to modern ones, despite the absence of vascular land plants. Pedogenic features of the paleosol are consistent with their development upon granite in an arid or semi-arid tropical environment.

ACKNOWLEDGEMENTS

REFERENCES

Barnes, V.E. and Bell, W.C., 1977. The Moore Hollow Group of Central Texas. Bureau of Econ. Geol. Rept. of Invest., 88, 169 pp.

Barshad, I., 1966. The effect of a variation in precipitation on the nature of clay mineral formation in soils from acid and basic igneous rocks. Proc. Int. Clay Conf. Jerusalem, Israel, 1: 167-173.

Bohn, H.L., McNeal, B.L. and O'Connor, G.A., 1979. Soil Chemistry. John Wiley and Sons, New York, 329 pp.

Brewer, R., 1964. Fabric and Mineral Analysis of Soils. John Wiley and Sons, New York, 470 pp.

Buol, S.W.,, Hole, F.D. and McCracken, R.J., 1980. Soil Genesis and Classification, 2nd ed. Iowa State Univ. Press, USA, 404 pp.

Capo, R.C., 1984. Petrology and geochemistry of a Cambrian paleosol developed on Precambrian granite, Llano Uplift, Texas. M.A. thesis Univ. of Texas at Austin, 111 pp.

Carroll, D., 1970. Clay minerals: a guide to their X-ray identification. Geol. Soc. Amer. Sp. Paper 126, 80 pp.

Chafetz, H.S., 1980. Evidence for an arid to semi-arid climate during deposition of the Cambrian System in central Texas, USA. Palaeogeog., Palaeoclim., Palaeoecol., 30: 83-95.

Duchafour, P., 1982. Pedology. Paton, T.R. (Transl.), George Allen and Unwin, London, 448 pp.

Folk, R.L., 1976. Reddening of desert sands: Simpson desert, N.T. Australia. J. Sed. Petrol., 46: 604-615.

Folk, R.L. and Patton, E.B., 1982. Buttressed expansion of granite and development of grus in central Texas. Zeit. Geomorph. N.F., 26: 17-32.

Garrison, J.R., Long, L.E. and Richmann, D.L., 1979. Rb-Sr and K-Ar geochronologic and isotopic studies, Llano Uplift, Central Texas. Contrib. Mineral.Petrol., 69: 361-374.

Harriss, R.C., and Adams, J.A.S., 1966. Geochemical and mineralogical studies on the weathering of granitic rocks. Am. J. Sci., 264: 146-173.

Holland, H.D. and Zbinden, E.A., 1988. Paleosols and the evolution of the atmosphere: Part I.In: A. Lerman and M. Meybeck (Editors), Physical and Chemical Weathering in Geochemical Cycles., Kluwer Academic, Dordrecht, pp 61-82.

Margulis, L., 1982. Early Life. Science Books International, Boston, 160 pp.

Maynard, J.B., 1992. Chemistry of modern soils as a guide to interpreting Precambrian paleosols. J. Geology, 100: 279-289.

Nahon, D.B., 1991. Introduction to the Petrology of Soils and Chemical Weathering. John Wiley and Sons, New York, 313 pp.

Nesbitt, H.W., Markovics, G., and Price, R.C., 1980. Chemical processes affecting the alkalies and alkaline earths during continental weathering. Geochem. et Cosmochim. Acta, 44: 1659-1666.

Retallack, G., 1988. Field recognition of paleosols. In: J. Reinhardt, W.R. Sigleo (Editors), Paleosols and weathering through time. Geol. Soc. Amer. Spec. Paper 216, pp. 1-21.

Scotese, C.R., Bambach, R.K., Barton C., Van der Voo, R., and Ziegler, A.M., 1979. Paleozoic base maps. J. Geol., 87: 217-277.

Tardy, Y., Bocquier, G., Paquet, H. and Millot, G, 1973, Formation of clay from granite and its distribution in relation to climate and topography. Geoderma, 10: 271-284.

Wahlstrom, E., 1948. Pre-Fountain and recent weathering on Flagstaff Mountain near Boulder, Colorado. Geol. Soc. Amer. Bull., 59: 1173-1190.

Walker, T.R., 1976. Diagenetic origin of continental redbeds In: H. Falke (Editor), The Continental Permian of Central, Western, and Southern Europe. H. Reidel, Holland, pp. 240-282.

Walker, N.J., 1992. Middle Proterozoic geologic evolution of Llano Uplift, Texas: evidence from U Pb zircon geochronometry. Geol. Soc. Amer. Bull., 104: 494-504.

Yaalon, D.H., 1971. Criteria for the recognition and classification of paleosols. In: D.H. Yaalon (Editor), Paleopedology: origin, nature and dating of paleosols. Halsted Press, New York, pp. 153-158.

Micromorphological evaluation of loess deposits and paleosols on Crowley's Ridge, Arkansas, U.S.A.

L.T. West[1] and E.M. Rutledge[2]
[1]University of Georgia, Athens, Georgia, USA
[2]University of Arkansas, Fayetteville, Arkansas, USA

ABSTRACT

West, L.T. and Rutledge, E.M., 1994. Micromorphological evaluation of loess deposits and paleosols on Crowley's Ridge, Arkansas, U.S.A. In: A.J. Ringrose-Voase and G.S. Humphreys (Editors), Soil Micromorphology: Studies in Management and Genesis. Proc. IX Int. Working Meeting on Soil Micromorphology, Townsville, Australia, July 1992. Developments in Soil Science 22, Elsevier, Amsterdam, pp. 265-276.

Three loess deposits, Peoria associated with late Wisconsin glaciation, Roxana associated with middle Wisconsin glaciation, and Loveland/Sicily Island associated with Illinoian or early Wisconsin glaciation, are generally recognized within the lower Mississippi River Valley of the U.S.A. At localized sites within the region two additional silty deposits, designated as Crowley's Ridge and Marianna, have been observed underlying the loess deposits. These deposits have particle-size properties typical of loess and have been assumed to be loess. Their sporadic occurrence, however, precludes tracing the deposits across the landscape to evaluate thickness and particle-size characteristics that would provide firm evidence of eolian deposition. The objectives of this study were to evaluate micromorphological properties of the Crowley's Ridge and Marianna deposits at a site on Crowley's Ridge to determine if they were similar to those of the overlying loess deposits and to evaluate relative development of Bt horizons among the deposits. The site was described and sampled to 17.5 m from three 65 mm diameter continuous cores. Undisturbed samples were collected from the interior 30 mm of one core, impregnated, and thin sections prepared by standard techniques. All horizons within the Crowley's Ridge and Marianna deposits had <10% sand and relative proportions of silt fractions were uniform throughout each deposit indicating no coarse stratification. Relatively unweathered horizons from all deposits had close porphyric related distribution patterns with thin clay coatings on coarse grains. Other microfabric features were also similar among the deposits and no evidence of fine stratification that would suggest alluvial deposition was observed in thin sections from these horizons. The surface soil and paleosols at the surface of the Loveland/Sicily Island, Crowley's Ridge and Marianna deposits had illuvial clay coatings on planar voids and channels. Structural development and amount and thickness of the illuvial clay coatings indicated that the paleosols in the Loveland/Sicily Island and the Crowley's Ridge loesses had undergone similar amounts of development which appeared to be greater than that in the surface soil. The paleosol in the Marianna loess had the weakest development.
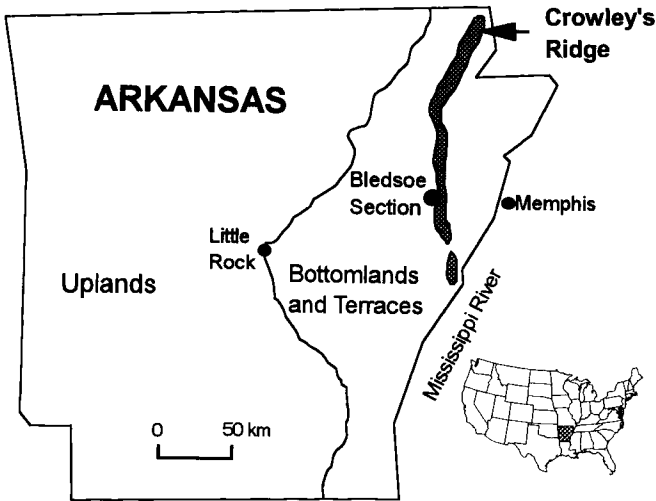
Fig. 1. Location of the Bledsoe Section.

INTRODUCTION

Crowley's Ridge is a long and narrow ridge standing 30 to 60 m higher than the surrounding lowlands that extend from southeastern Missouri through much of eastern Arkansas (Fig. 1). The core of this ridge is composed of Tertiary-aged, unconsolidated Coastal Plain sediments left behind as the ancestral Mississippi and Ohio Rivers formed the lowlands on either side of the ridge (Fisk, 1951). Only during the mid to late Pleistocene did the Mississippi River divert eastward and join the Ohio River at its current location north of Crowley's Ridge. Thus, during much of the Pleistocene, active floodplains were available on either side of Crowley's Ridge to serve as source areas for loess deposits.

Loess has been recognized on Crowley's Ridge since the late 1800's (Call, 1891), and numerous workers have since observed and described the loess on this ridge (Wascher et al., 1947; Leighton and Willman, 1950; West et al., 1980). Each of these reports described at least three loess deposits on Crowley's Ridge; a thick surficial deposit containing the modern soil, a thin middle deposit with weak soil development, and a thick third loess with a well-developed paleosol. West et al. (1980) determined that the source area for the upper two loesses was in the lowlands east of Crowley's Ridge, and the third deposit had source areas in the lowlands on both sides of the Ridge. Though the terminology was different, both Leighton and Willman (1950) and West et al. (1980) correlated these loesses with those in the midwest U.S.A.: the upper loess as Peoria Loess (late Wisconsin age), the middle loess as Roxana Silt (mid to late Wisconsin age), and the third loess as Loveland Silt (Illinoian age).

In addition to the three loesses commonly identified on Crowley's Ridge, a fourth silty deposit has been described on Crowley's Ridge and at other locations within the Lower Mississippi Valley (Leighton and Willman, 1950; Miller et al., 1986; McCraw and Autin, 1989). Miller et al. (1986) have termed this fourth silty deposit "Crowley's Ridge Loess." At one site on Crowley's Ridge (Fig. 1; site CS04 of West et al. (1980) herein referred to as the Bledsoe Section), a fifth silty deposit is present which has been termed "Marianna Loess" (Miller et al., 1986; McCraw and Autin, 1989). Both the Crowley's Ridge and Marianna

deposits commonly contain buried soils and have low sand contents and other characteristics typical of loess deposits. Neither deposit, however, has been identified at enough locations to determine particle-size and thickness relationships with distance from a source area that would provide firm evidence of a loessial origin. Establishment of such relationships is unlikely because of deep burial and isolated occurrence of the deposits. Thus, this study was initiated to (1) compare the micromorphological characteristics of the Crowley's Ridge and Marianna deposits at the Bledsoe Section on Crowley's Ridge with those of the overlying loess deposits in order to elucidate their mode of deposition (loess or alluvium), and (2) to compare the relative degree of development of the paleosols in each deposit at this site.

METHODS AND MATERIALS

Field Methods

The Bledsoe Section is located on the western edge of Crowley's Ridge (Fig. 1). This site was described from the surface to 17.5 m from three relatively undisturbed, continuous 65 mm diameter cores using standard terminology (Soil Survey Staff, 1951). Bulk samples were collected by horizon for particle size and chemical analysis. Horizons thicker than 40 cm were sub-sampled. Intact core samples about 10 cm long were collected from selected horizons for thin section preparation and evaluation.

Laboratory Methods

Particle-size distribution was determined by the hydrometer method described by Day et al. (1956). In addition to expressing the particle-size data on a fine-earth basis (<2 mm), the data were converted to a clay-free basis to reduce effects of pedogenic clay translocation on particle-size distribution (Kellogg, 1962). Abrupt changes in clay-free silt separate distribution were interpreted as evidence for a change in loessial parent materials (West et al., 1980). The outer 1-2 cm of the intact core samples were removed to avoid material that may have been disturbed during sample collection, and the remaining central part of the sample was impregnated with epoxy resin. Thin sections (0.03 mm thick) were prepared by standard techniques (Murphy, 1986) and evaluated for microfabric and pedological features. Terminology used to describe microfabric and other features was that of Bullock et al. (1985). No evidence of disturbance from sample collection was observed in any of the thin sections.

RESULTS AND DISCUSSION

Differentiation of Deposits

Morphology, clay distribution, and clay-free particle-size distribution indicated that five silty deposits were present at this site. Below the surface soil, three buried soils with soil structure and evidence of clay translocation were observed (Table 1). Associated with each of these buried soils was a pedogenic clay maximum (Fig. 2). The lowest of the paleosols had two clay maxima at 11.5 and 13.5 m (Fig. 2) suggesting that two soils in two separate deposits may be present. Lack of any other evidence of a lithologic discontinuity between these two clay maxima and the relatively minor changes in clay content led to the interpretation that only one deposit was present.

Table 1
Abbreviated description of Bledsoe Section.

Horizon	Depth, cm	Color	Texture[1]	Structure[2]	Clay Films
Ap	0-13	7.5YR 3/2, 5/6	sicl	2mgr & sbk	
Bt	13-46	7.5YR 4/4	sicl	2msbk	medium continuous
Btx	46-160	7.5YR 4/4	sil	1mpr - 2mabk	medium discontinuous
BC	160-221	7.5YR 4/4	sil	1msbk	
C	221-292	10YR 4/4	sil	ma	
2Ab	292-389	7.5YR 4/4	sil	ma & 1csbk	
3BAtb	389-417	5YR 4/4	sil	1mpr - 2msbk	thin patchy
3Btb1	417-472	5YR 4/4	sicl	2mpr - 2mabk	thick continuous
3Btb2	472-599	7.5YR 5/6	sil	1mpr - 2mabk	thin to medium discontinuous; clay in pores
3BCtb	599-650	7.5YR 5/6	sil	1cpr	few clay lined pores
4Ab	650-676	7.5YR 5/6	sil	ma	few clay lined pores
4BAtb	676-704	7.5YR 5/6	sil	1csbk	thin patchy clay films
4Btb	704-864	5YR 5/6	sicl	1mpr - 2mabk	medium to thick discontinuous
4Ctb	864-1003	7.5YR 6/6	sil	ma	common clay lined pores
5Ab	1003-1029	10YR 6/3	sil	1mpr	common clay lined pores
5Btb	1029-1234	10YR 6/4, 6/6	sil	1mpr	thin discontinuous; clay lined pores
5Btgb	1234-1325	10YR 6/2	sil	1mpr - 2mabk	common clay lined pores
5Bgb1	1325-1732	2.5Y 7/2	sil	1mpr	few black concretions
6Bgb2	1732-1758	2.5Y 7/2	sl	1mpr	

[1]Texture abbreviations: sil = silt loam; sicl = silty clay loam; sl = sandy loam.
[2]Structure abbreviations are: 1 = weak; 2 = moderate; m = medium; c = coarse; gr = granular; sbk = subangular blocky; abk = angular blocky; pr = prismatic; ma = massive; *i.e.* 2mpr - 2msbk = moderate medium prismatic parting to moderate medium subangular blocky structure.

This sequence of horizon development and clay distribution suggests that the silty materials at this site are the product of at least four episodes of deposition separated by periods of soil development. The relative amount of clay increase in Bt horizons of the paleosols and the presence of clay films suggests that these periods were relatively long or that soil development progressed at a rate greater than that currently observed.

At 2.9 m, an abrupt color change was observed, and the color, structure, and other properties of the materials between this depth and the subjacent 3Btb horizon suggest that these materials could be the A and upper B horizons associated with the paleosol. An abrupt change in dominant clay-free silt fraction from medium to coarse silt at 3.9 m indicates, however, that the materials between 2.9 and 3.9 m comprise a separate deposit. This interpretation agrees with other reports on Crowley's Ridge of a thin loess subjacent to a thick surface loess and overlying a paleosol in a thick third loess deposit (Wascher *et al.*, 1947; Leighton and Willman, 1950; West *et al.*, 1980).

% Fraction
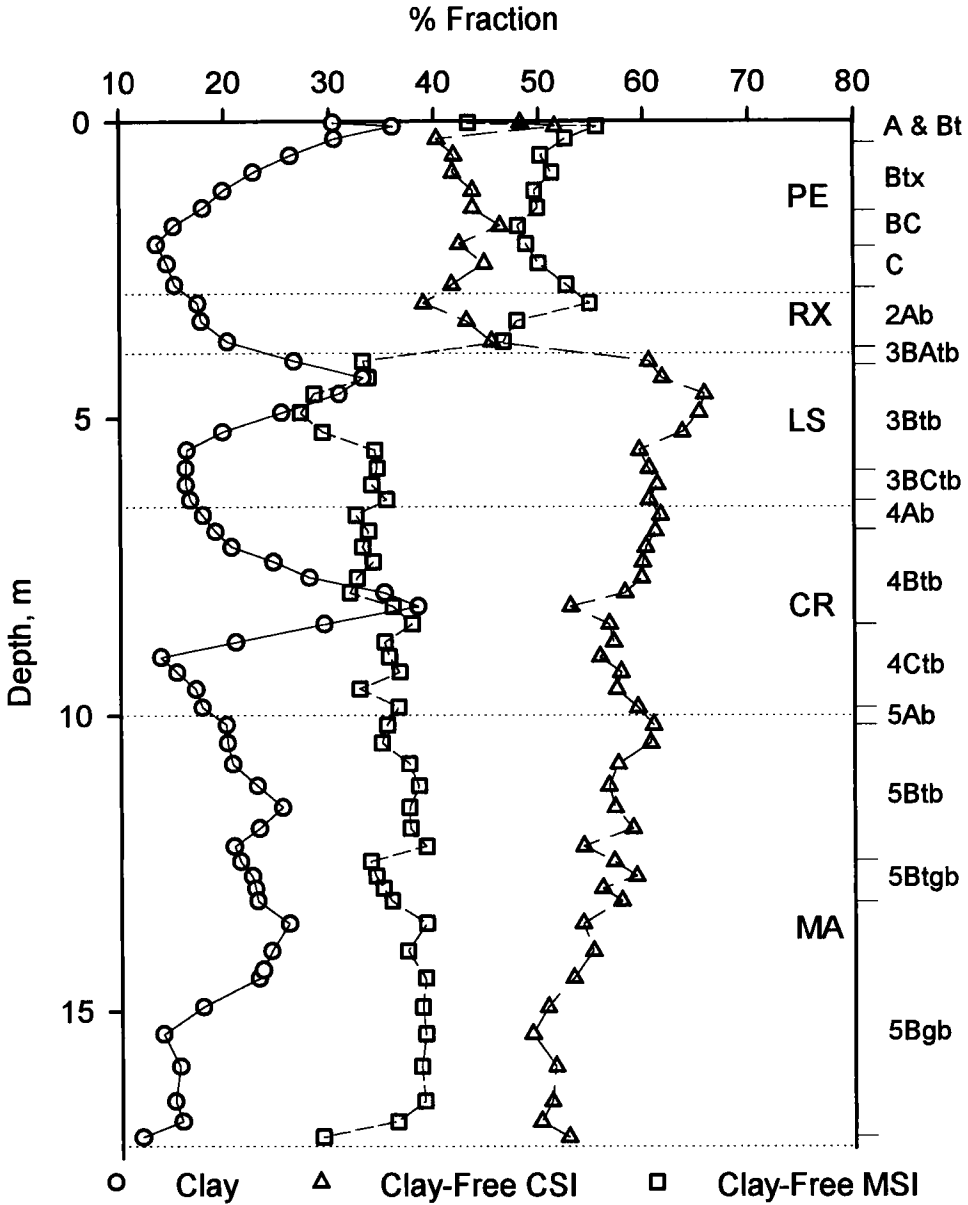
Fig. 2. Clay distribution and clay-free silt separate distribution with depth. PE = Peoria Loess, RX = Roxana Silt, LS = Loveland/Sicily Island Loess, CR = Crowley's Ridge Loess, MA = Marianna Loess; MSI = 0.005-0.02 mm silt separate, CSI = 0.02-0.05 mm silt separate.

West *et al.* (1980) correlated the surface, middle and lowest of the upper three deposits at this site as Peoria Loess, Roxana Silt, and Loveland Silt respectively. No radiocarbon dates

were available for any of the loesses at that time. Thus, the correlations followed those of earlier workers in the region (Leighton and Willman, 1950) and the terminology used in the midwest U.S.

Subsequently, at a site on Crowley's Ridge, Canfield (1985) reported thermoluminescence (TL) dates of 19,200 ± 2,650 years for the base of the Peoria Loess, 45,600 ± 9,000 years for the base of the Roxana Silt, and 85,300 ± 7,200 years for the lower part of the Loveland Silt. The dates for the upper two loesses support their correlation as Peoria Loess and Roxana Silt. The date for the lowest deposit, however, suggests that the deposit may be early Wisconsin rather than Illinoian and thus, would correlate with the Sicily Island Loess identified in other parts of the Lower Mississippi Valley (Miller *et al.*, 1985, 1986; McCraw and Autin, 1989). However, a data of 111,550 ± 11,600 years was obtained for this deposit using total bleach TL methodology (Canfield, 1985), and an Illinoian age was also suggested by amino acid ratios from gastropod shells. Because of conflicting ages for this deposit, it is currently referred to as Loveland/Sicily Island Loess.

The fourth silty deposit at this site, Crowley's Ridge Loess, has been reported to occur at other locations on Crowley's Ridge and at other sites in the Lower Mississippi Valley. This deposit has been dated at a site near Vicksburg, Mississippi as 125,000-135,000 BP (Johnson *et al.*, 1984) and is considered to be Illinoian in age (Miller *et al.*, 1985, 1986; McCraw and Autin, 1989). The fifth silty deposit, Marianna Loess, has only been identified at the Bledsoe Section, and though no dates are available, this deposit was considered to be early to middle Pleistocene in age (Miller *et al.*, 1986).

Depositional Mode

All five silty deposits at the Bledsoe Section were high in silt, had <10% sand, lacked any evidence of textural or color stratification, and generally had properties typical of loess deposits in the region. Even though Crowley's Ridge and Marianna deposits have morphological and particle-size properties typical for loess, additional evidence is needed to confirm this mode of deposition. On a Pleistocene terrace in the lowlands west of Crowley's Ridge, silty deposits with properties typical of loess did not conform to expected relationships with distance from a proposed source area and were identified as silty alluvial deposits (West and Rutledge, 1987). The upper three loess deposits, however, provide a benchmark to which the macro and micromorphological properties of the Crowley's Ridge and Marianna deposits can be compared to evaluate their depositional mode: loess or silty alluvium.

The C horizons of the Peoria Loess and the BC horizons of the Loveland/Sicily Island Loess were friable silt loam textured and massive or had weak very coarse prismatic structure (Table 1). These horizons had close porphyric related distribution patterns, primarily simple packing voids, and little evidence of pedality (Fig. 3A and C). The 2Ab horizon in the Roxana Silt had more evidence of structure, but otherwise was similar to C horizons of the other

---

Fig. 3. Thin section micrographs of least weathered horizons of each deposit; **A)** C horizon of Peoria Loess; **B)** 2Ab horizon of Roxana Silt; **C)** 3BCtb horizon of Loveland/Sicily Island Loess; **D)** 4Ctb horizon of Crowley's Ridge Loess; **E)** 5Btgb horizon of Marianna Loess; **F)** 5Bgb horizon of Marianna Loess; Crossed polarized light; Bar length 1 mm.
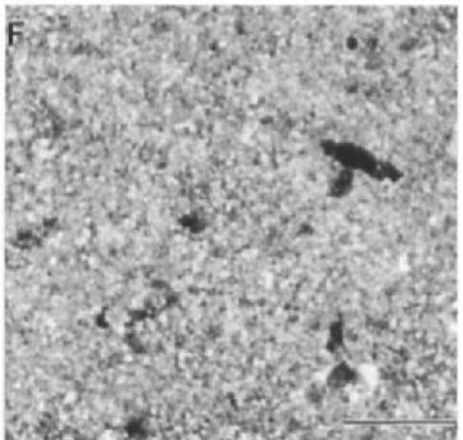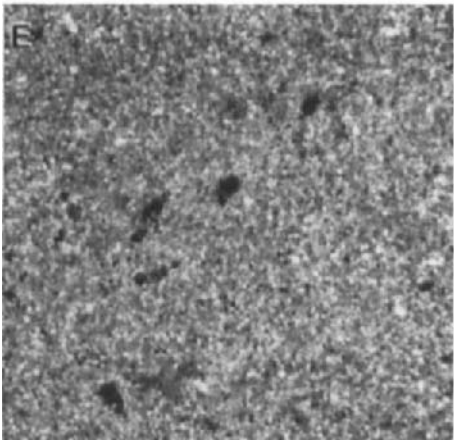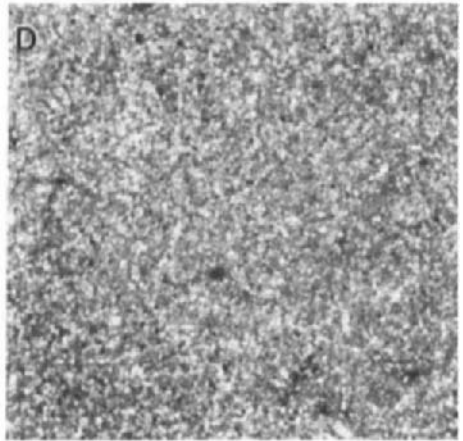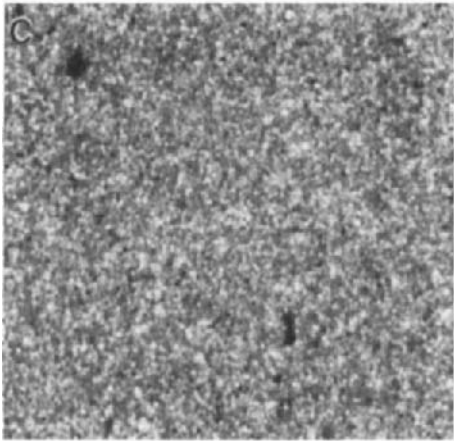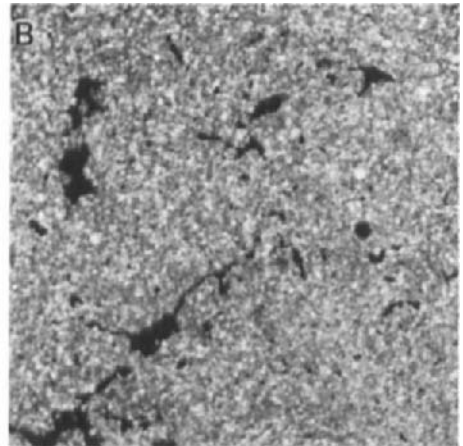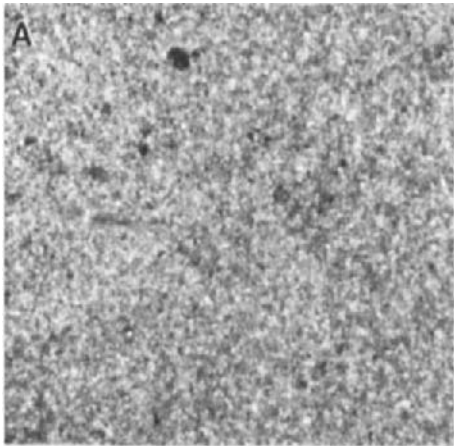
loesses (Fig. 3B). No evidence of color or textural stratification was observed in any of these horizons either at a macro scale or in thin section. If it is assumed that these characteristics are typical for loess in the region, then the presence of similar macro and micromorphological characteristics in the slightly weathered horizons in the subjacent Crowley's Ridge and Marianna deposits can be interpreted as indicating a loessial origin.

The C horizons of the Crowley's Ridge deposit were similar to C and BC horizons of the Peoria and Loveland/Sicily Island Loesses. These horizons were silt loam textured, friable and massive (Table 1). Related distribution patterns for these horizons were close porphyric with primarily simple packing voids (Fig. 3D). The C horizons in the Crowley's Ridge deposit were described in the field as having thin clay films in coarse pores (Table 1), and illuvial clay coatings were observed in coarse vughs (channels) in thin section. No evidence of stratification was observed either at a macro or micro-scale that would indicate deposition as alluvium or water reworking of a loess deposit (Mücher and De Ploey, 1977, 1984). Because of the similarities both macromorphically and micromorphically between C horizons of the Crowley's Ridge deposit and C horizons of overlying loess deposits, the Crowley's Ridge deposit is interpreted to be loess.

No C horizons were present in the Marianna deposit. Even though all horizons were weathered, zones in many of the horizons did not appear to have been appreciably modified by pedogenic processes and were used as comparators to C horizons of the overlying loesses. These zones had close porphyric related distribution patterns similar to that of the overlying loess deposits. No evidence of vertical stratification was observed (Fig. 3E and F). Because of the similarity of the microfabric of these lesser weathered zones to unweathered horizons of overlying loess, and the other properties of the deposit (high silt, low sand and friable consistence), this deposit is also interpreted as loess.

The lower horizons (5Btg and 5Bgb) of the Marianna deposit were gleyed, and coarse zones depleted in clay and Fe could be observed both macromorphically and in thin section. In addition, circular bodies suggestive of coarse channels occurred occasionally in these horizons and appeared to be infilled with coarser silt than that in the groundmass (Fig. 4E). The origin of these bodies is unclear, but they may represent biological channels that were infilled with coarser silt than that in the groundmass.

Thin zones with a concentration of weakly-striated clay, either surrounding infilled channels or occurring as elongate bodies (Fig. 4F) were also observed in these horizons. The origin of these zones cannot be conclusively determined from available data, but one hypothesis is that they were illuvial clay coatings on channel walls and ped faces that have been disrupted by reduction and deep burial. If the clay in these zones was illuvial, the degree of pedogenesis associated with clay translocation and processes that have subsequently altered the illuvial clay

---

Fig. 4. Thin section micrographs of Bt and Bg horizons; **A)** Btx horizon of surface soil, showing clay coating (arrow); **B)** 2Ab horizon of Roxana Silt, showing thin clay coating (arrow); **C)** 3Btb1 horizon of Loveland/Sicily Island Loess, showing clay coating (arrow); **D)** 4tb horizon of Crowley's Ridge Loess, showing clay coating (arrow); **E)** 5Btb horizon of Marianna Loess, showing apparent filled channel with thin clay coating on channel wall (arrow); **F)** 5Bgb horizon of Marianna Loess, showing concentration of weakly-striated clay (arrow); crossed polarized light; Bar length 0.5 mm.
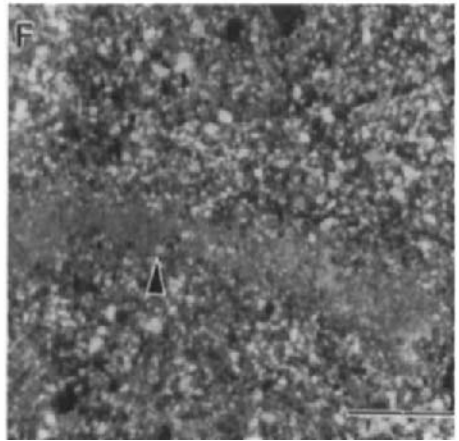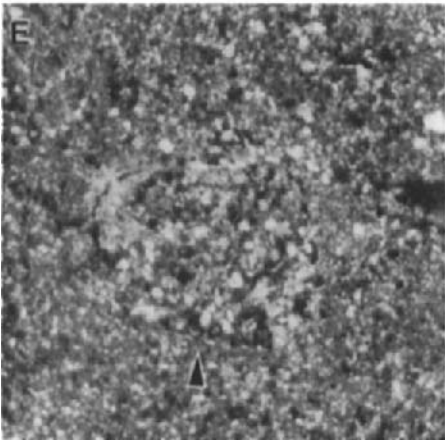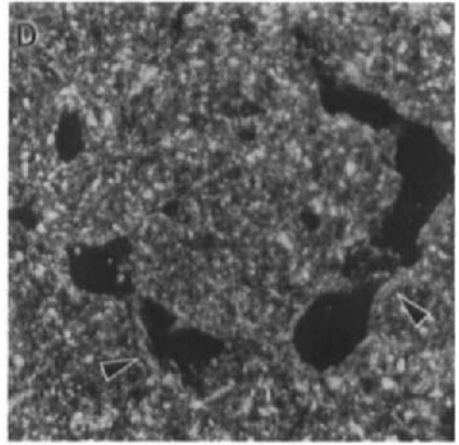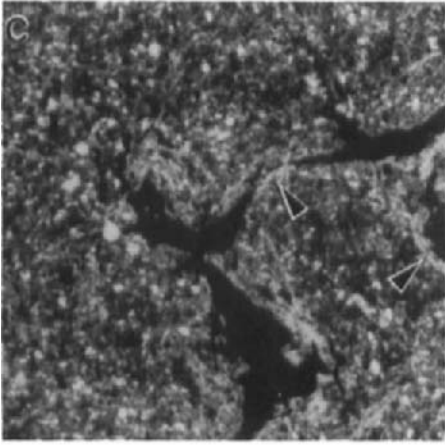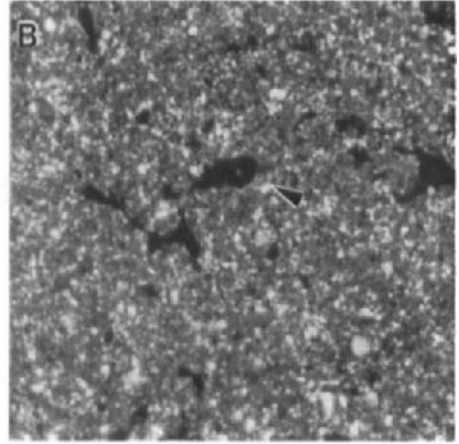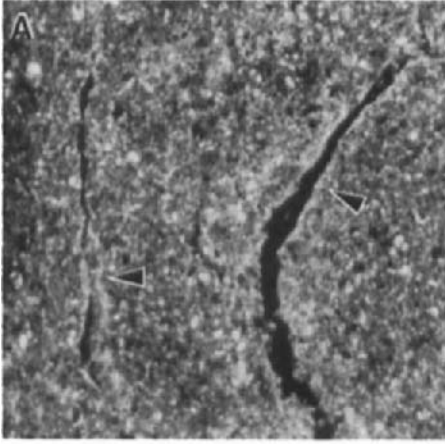
coatings would most certainly have altered the microfabric of the horizon and destroyed any stratification that may have been present in the original unaltered deposit. Thus, identification of this deposit as loess is tenuous.

The Bgb horizons of the Marianna also had vertically oriented zones (or pockets) with a slightly greater concentration of subrounded fine sand grains than was present in the groundmass. These zones of slightly elevated fine sand may be due to admixing of sand from underlying sandy Coastal Plain deposits during deposition or by burrowing fauna after deposition. However, no evidence was observed that these zones of higher sand were due to alluvial deposition.

Relative development of paleosols

The paleosols in the Loveland/Sicily Island and Crowley's Ridge Loesses had the highest clay contents and reddest colors of the soils in this section (Table 1; Fig. 2). These buried soils also had the thickest and most abundant illuvial clay coatings of the soils (Fig. 4A, B, C, D and E). The surface soil had slightly higher clay contents and more abundant clay coatings than were observed in the Marianna paleosol (Table 1; Figs 2, 4A and E). The paleosol in the Roxana Silt had the lowest clay contents and least abundant clay coatings of the soils in this section (Fig. 4B).

As indicators of soil development, these properties suggest that the paleosols in the Loveland/Sicily Island and Crowley's Ridge Loesses have undergone similar amounts of pedogenic development, and that development in these paleosols was greater than that in the surface soil. Similarly, the surface soil exhibits greater development than the Marianna paleosol. The buried soil in the Roxana Silt was the least developed of the soils in this section.

Relative degree of soil development does not always correspond to length of time that the material was exposed at the surface. In addition to time, soil development is a function of temperature, rainfall, and other climatic factors, and these factors may not have been similar during each interglacial stage. Norton *et al.* (1988) suggested that weak development in Roxana Silt may be related to a cold dry climate rather than short time of exposure.

Thickness of Bt horizons was similar in the surface soil, the Loveland/Sicily Island paleosol and the Crowley's Ridge paleosol. Again, this may not be related to the degree of pedogenic development as erosion and loss of material from the paleosols before burial cannot be evaluated. The paleosol in the Marianna Loess was the thickest soil in this section (7.0 m). Such a thickness is greater than would be expected for a soil with relatively weak development under current climatic conditions. Even if soil development was proceeding at a greater rate than today while this deposit was exposed, greater amounts of clay translocation than that observed would be expected to correspond to this depth of weathering. One hypothesis for the thickness of the soil in the Marianna deposit is that it is composed of two soils in two deposits that became merged as the soil in the upper deposit developed. The double clay maximum and differences in properties between 5Btb and 5Bgb horizons could be interpreted as supporting this hypothesis (Fig. 2). Alternately, the overly thickened soil could have developed if deposition was slow and occurred over a long period during which soil development proceeded at a rate similar to the deposition rate.

CONCLUSIONS

Morphology, clay distribution and clay-free silt distribution indicated five silty deposits were present at the Bledsoe Section on the western margin of Crowley's Ridge in Arkansas. The upper three deposits are relatively continuous across Crowley's Ridge, have been shown to have particle-size relationships with distance from source areas expected of loess, and have been correlated from top to bottom as Peoria Loess, Roxana Silt, and Loveland/Sicily Island Loess. The lower two deposits have been correlated as Crowley's Ridge Loess and Marianna Loess. Relatively unweathered horizons from these lower two deposits had low sand contents, massive or weak structure and porphyric related distribution patterns similar to unweathered horizons in overlying loess deposits. These similarities and lack of evidence of stratification lead to the interpretation that these deposits were also loess.

Maximum clay contents and thickness and abundance of illuvial clay coatings suggested that the paleosols in the Loveland/Sicily Island and Crowley's Ridge Loesses were the most developed soils in the section. The surface soil was less developed than these paleosols but more developed than the paleosol in the Marianna Loess. The Roxana Silt had the least pedogenic development.

REFERENCES

Bullock, P., Fedoroff, N., Jongerius, A., Stoops, G. and Tursina, T., 1985. Handbook for Soil Thin Section Description. Waine Research Publications, Wolverhampton, U.K., 152 pp.

Call, R.E., 1891. The geology of Crowley's Ridge. Geol. Sur. of Arkansas Annual Report (1889), Vol. 2, Little Rock, Arkansas.

Canfield, H.E., 1985. Thermoluminescence dating and the chronology of loess deposition in the central United States. M.S. Thesis. University of Wisconsin, Madison, 159 pp.

Day, P.R., Van Bavel, C.H.M., Jamison, V.C., Dohnke, H., Lutz, J.F., Miller, R.D., Page, J.B. and Peele, T.C., 1956. Report of the committee on physical analysis. 1954-1955. Soil Sci. Soc. Am. Proc., 20: 167-169.

Fisk, H.N., 1951. Loess and Quaternary geology of the Lower Mississippi Valley. J. Geol., 59: 333-356.

Johnson, R.A., Pye, K. and Stipp, J.J., 1984. Thermoluminsecence dating of southern Mississippi loess: American Quaternary Association, Program and Abstracts, 8th Biennial Meeting, Boulder, CO.

Kellogg, C.E., 1962. The place of the laboratory in soil classification and interpretation. USDA-SCS, Washington, D.C.

Leighton, M.M. and Willman, H.B., 1950. Loess formations of the Mississippi Valley. J. Geol., 58: 599-63.

McCraw, K.J. and Autin, W.J., 1989. A review of historic and modern concepts of Lower Mississippi Valley loess stratigraphy. In L.R. Follmer (editor) Lower Mississippi Valley Loess: A Field Guide. Louisiana Geol. Survey, Baton Rouge.

Miller, B.J., Day, W.J. and Schumacher, B.A., 1986. Loesses and loess-derived soils in the Lower Mississippi Valley. Guidebook for Soils-Geomorphology Tour. Am. Soc. Agron., New Orleans, 144 pp.

Miller, B.J., Lewis, G.C., Alford, J.J., and Day, W.J., 1985. Loesses in Louisiana and at Vicksburg, Mississippi. Guidebook for Friends of the Pleistocene Field Trip. South-Central Friends of the Pleistocene, Baton Rouge, 126 pp.

Mücher, H.J., and De Ploey, J., 1977. Experimental and micromorphological investigation of erosion and redeposition of loess by water. Earth Surface Processes, 2: 17-24.

Mücher, H.J. and De Ploey, J., 1984. Formation of afterflow silt loam deposits and structure modification due to drying under warm conditions: An experimental and micromorphological approach. Earth Surface Processes and Landforms, 9: 523-531.

Murphy, C.P., 1986. Thin Section Preparation of Soils and Sediments. AB Academic Publishers, Berkhamsted, U.K.

Norton, L.D., West, L.T., and McSweeney, K., 1988. Soil development and loess stratigraphy of the midcontinental USA. In D.N. Eden and R.J. Furkert (Editors), Loess: Its Distribution, Geology, and Soils. Proc. Int. Sym. on Loess. A.A. Balkema, Rotterdam, pp. 145-159

Soil Survey Staff, 1951. Soil Survey Manual. U.S. Dept. Agric. Handb. 18. U.S. Gov. Printing Office, Washington, D.C., 503 pp.

Wascher, H.L., Humbert, R.P., and Cady, J.G., 1947. Loess in the Southern Mississippi Valley, identification of the loess sheets. Soil Sci. Soc. Am. Proc., 12: 389-399.

West, L.T., and Rutledge E.M., 1987. Silty deposits of a low, Pleistocene-age terrace in Eastern Arkansas. Soil Sci. Soc. Am. J., 51: 709-715.

West, L.T., Rutledge, E.M., and Barber, D.M., 1980. Sources and properties of loess deposits on Crowley's Ridge in Arkansas. Soil Sci. Soc. Am. J., 44: 353-358.

Micromorphological characteristics and paleoclimatic implications of lower cretaceous paleosols in southern Israel

M. Wieder[1], G. Gvirtzman[1,2] and T. Weissbrod[2]

[1]Department of Geography, Bar-Ilan University, Ramat Gan, Israel
[2]Geological Survey of Israel, Jerusalem, Israel

ABSTRACT

Wieder, M., Gvirtzman, G. and Weissbrod, T., 1994. Micromorphological characteristics and paleoclimatic implications of lower cretaceous paleosols in southern Israel. In: A.J. Ringrose-Voase and G.S. Humphreys (Editors), Soil Micromorphology: Studies in Management and Genesis. Proc. IX Int. Working Meeting on Soil Micromorphology, Townsville, Australia, July 1992. Developments in Soil Science 22, Elsevier, Amsterdam, pp. 277-284.

Mineralogical, chemical and micromorphological analyses of several samples from the Lower Cretaceous of southern Israel indicate that they are all Oxisols that developed under terrestrial tropical conditions. The very low ratio of silica versus sesquioxides and the high proportions of kaolinite and hematite indicate advanced soil weathering. The soil material of the alluvial-derived paleosols is rich in fine- to coarse quartz grains; whereas those intercalated within basalt flows originated from the parent rock under relatively stable conditions.

The alluvial Oxisols contain several ferruginous, massive, brick-like pedogenic siliceous plinthites with a high proportion of fine-grained quartz in the clay fraction, which was probably inherited from the parent sediment, although some if it might be authigenic. Where exposed it is extremely hard and forms a ledge with a dark carapace.

Since the paleosols are rich in hematite, and without gibbsite, they were apparently formed under tropical conditions with periodic short dry seasons in the outer tropical belt.

INTRODUCTION AND GEOLOGICAL BACKGROUND

Makhtesh Ramon is a large elongated erosive cirque which developed on the crestal area of one of the central Negev anticlines (Fig. 1). It exposes Triassic to Lower Cretaceous rock units which are bounded by cliffs of Upper Cretaceous carbonates. Within this sequence soils developed under seemingly different environmental conditions and some of them have been studied by Singer (1975), Goldbery (1982) and Buchbinder and Le Roux (1990). The present-day climate in the Negev is that of a dry desert.

The Lower Cretaceous in Makhtesh Ramon (Hatira Formation) is a dominantly siliciclastic sequence, 220 m thick, consisting of continental sediments, occasionally intercalated by partly carbonatic marine tongues. In the eastern part of Makhtesh Ramon the lower part of the Hatira Formation, the very distinct Red Valley Member consists of 20 - 30 m thick variegated silty clays interspersed with siliceous-ferruginous crusts. Well-preserved leaves and trunks of fossil plant remains (*e.g. Weichselia reticulata*) are abundant throughout the section. Baer *et al.* (1989) suggested that the parent material of this section was actually basic pyroclastic or
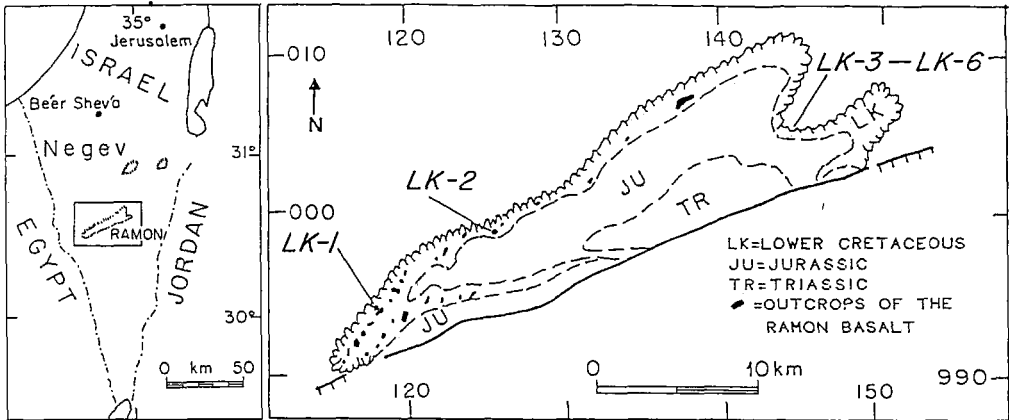
Fig. 1. Makhtesh Ramon. Location map and sampling sites.

volcanic rocks, whereas Ben-David and Goldbery (1990) interpreted it as bleached red clays which may originally have been low-energy overbank deposits that underwent lateritization.

The Red Valley Member passes laterally westward into a continental, fluvial sandstone unit and an overlying marine intercalation which consists of fossiliferous shale, siltsone and dolomitic sandstone of Late Barremian (?) to Early Aptian age (Zuweira marine tongue). The latter is overlain by thick basalt flows (Ramon Basalt) dated 118 Ma BP, which are separated by paleosols.

The present study deals with the nature of the paleosols comprising most of the Red Valley Member and those within the Ramon Basalt and their paleoclimatic implications.

MATERIALS AND METHODS

Six types of material were studied. Two samples (LK-1,2) were taken from the earthy intercalations within the basalt flows. Both consist of angular to subangular, blocky, reddish brown material sampled in the western part of Makhtesh Ramon (Fig. 1). Four other samples are from the Red Valley Member of the Hatira Formation in the eastern part of Makhtesh Ramon. These include: an extremely hard dusky red homogenous material (LK-3), red material with white-greyish mottles and gypsum efflorescences (LK-4), a hard crust (LK-5) and a moderately indurated red material (LK-6). In order to avoid the effect of present-day climatic conditions, the samples were collected from the inner non-weathered zone, after removing the outer exposed surface. Sample LK-4, however, still bears modern gypsum efflorescences.

The samples were impregnated with polystyrene and thin sections (7 x 5 cm) were prepared in duplicate and described according to Brewer (1964).

The chemical analyses were carried out by melting with lithium-metaborate and determined by ICP-AES. Na_2O and K_2O were determined by AAS. The mineralogy was determined using a Phillips X-ray diffractometer with Cu $K\alpha$ radiation.
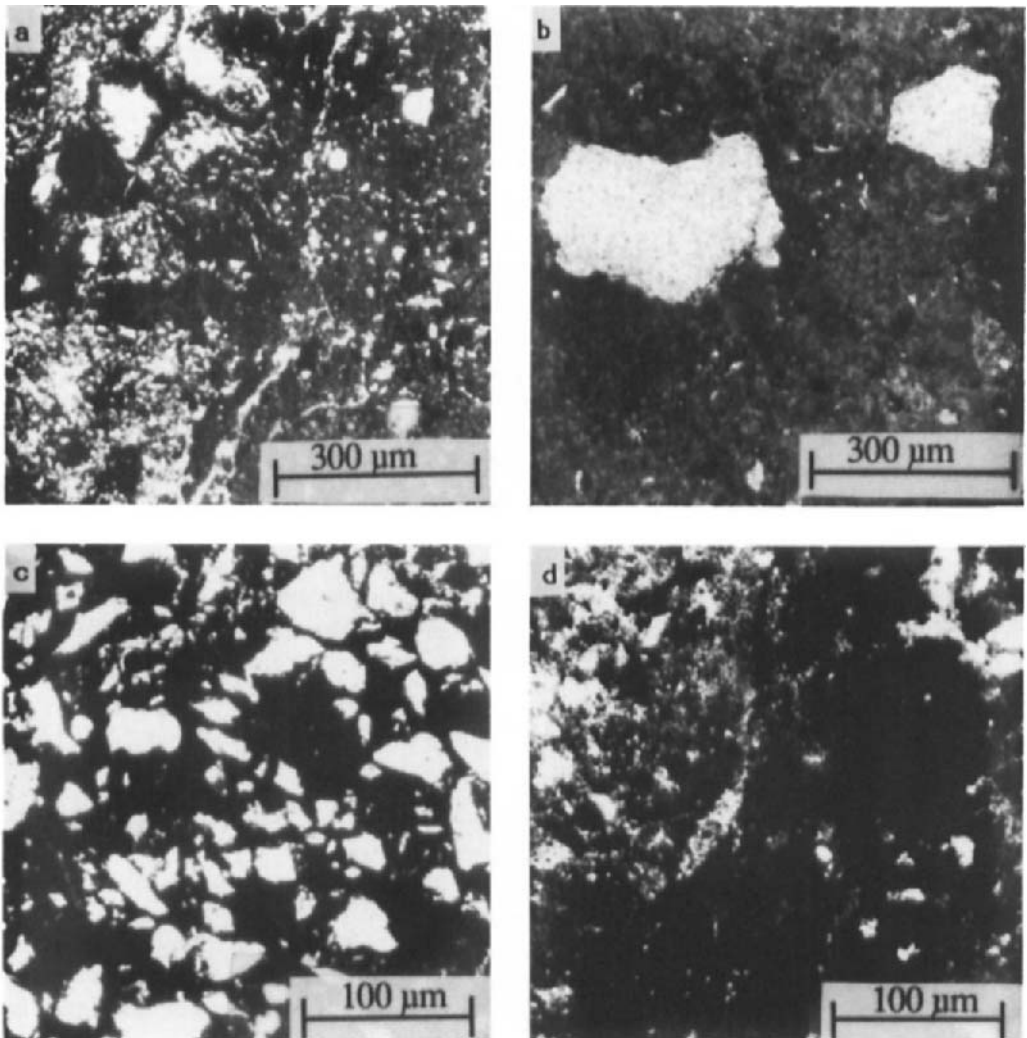
Fig. 2. Micrographs in plane polarized light of : a) weathered basalt fragment (left side) in LK-1; b) coarse quartz grains in the basalt-derived soil, LK-2; c) microfabric of the plinthite crust (LK-3) showing a porphyric fabric of iron impregnation, salt and fine quartz grains d) microfabric of iron seggregation in LK-4.

RESULTS

Micromorphological characteristics

Ramon Basalt Paleosols

LK-1:   The plasma is red with iron oxyhydrate inclusions. The plasmic fabric is asepic, with some vughs and short narrow craze planes. There are a few skeleton grains of iddingsite,

strongly weathered basalt rock fragments (Fig. 2a), and many small papules of weathered primary minerals. The related distribution is argillamatric.

LK-2: The plasma is red with iron oxyhydrate inclusions. Frequently coarse quartz (*ca.* 1 mm) grains occur (Fig. 2b) with some strongly weathered basalt fragments. The plasmic fabric shows a striated masepic and mosepic pattern. Voids appear as skew planes. Some iron hypocoating occurs beside the grains.

Red Valley Member Paleosols

LK-3: The plasma is dark red to black ferruginous. More than 60% of the material consists of silt and very fine (*ca.* 0.1 mm) quartz grains (Fig. 2c) which displays a porphyric fabric. There are also a few unidentifiable, strongly weathered primary minerals and coarse quartz grains. The voids are filled with iron oxyhydrates.

LK-4: The plasma is red and yellow-brown. The latter color corresponds to the white-greyish spots and represent iron depleted zones. The skeleton grains comprise very fine quartz and some silt. The plasmic fabric is asepic to isotic. Voids are mainly skew planes. Many iron oxide nodules occur (Fig. 2d) and there are very few illuviation argillans.

LK-5: The fabric is similar to LK-3. Some vugs of surface weathering occur.

LK-6: The plasma is mainly ferruginous, mostly dark red with some yellowish-brown zones. Juxtaposition of yellow-brown to red and black material is present. The skeleton grains consist of silt and very fine-grained quartz. Some large (0.3 mm) quartz grains are of the runiquartz type (Stoops and Buol, 1985). There are some vughs and narrow planes. Silica coats some of the voids (quartzan).

Chemical and Mineralogical Data

The chemical results are presented in Table 1 and the mineralogical results in Table 2 and Fig. 3 (sample LK-5 was not analyzed).

Besides iddingsite, which replaces olivine, and the absence of quartz grains in the clay fraction of the basalt-derived samples, there is no difference between the mineralogy of the latter and that of the alluvial-derived paleosols. Most samples have a very low silica/sesquioxides ratio and kaolinite and hematite are the dominant minerals. The amount of kaolinite in LK-3, however, is low. Unlike the other samples, LK-3 contains quartz in the clay fraction and has a high amount of silica and low amount of alumina (Table 1).

DISCUSSION

The microfabric of the samples studied shows features which are characteristic of soils in the tropical belt, and the chemical and mineralogical composition likewise corresponds to highly weathered conditions. The micromorphological features reflects the different local environmental conditions in which each of the soils were formed.

LK-1 has a typical Oxisol fabric with an argillamatric related distribution (Eswaran, 1972), *i.e.* a highly weathered soil material in which the plasma dominates and with very few skeletal grains present. The plasmic fabric in LK-1 is weakly expressed, which is typical of Oxisols (Stoops and Buol, 1985).

Table 1
Chemical Composition of the Lower Cretaceous Paleosols (by weight %).

	LK-1	LK-2	LK-3	LK-4	LK-6
SiO_2	31.0	35.5	65.5	34.0	27.0
Al_2O_3	24.3	25.5	5.8	28.0	22.0
Fe_2O_3	27.0	22.5	16.0	16.6	22.0
TiO_2	4.4	3.9	6.3	5.3	4.3
CaO	0.7	0.2	0.9	<0.1	0.2
MgO	0.6	0.1	0.2	0.4	1.1
MnO	0.1	0.08	0.04	0.04	0.05
P_2O_5	0.3	-	0.1	0.4	0.7
Na_2O	0.4	0.8	0.1	1.9	1.2
K_2O	0.1	<0.1	0.1	<0.1	<0.1
SO_3	-	-	0.8	0.4	0.5
LOI	9.6	9.9	3.8	12.6	12.6
Total	98.5	98.6	99.7	99.8	99.2
SiO_2/Al_2O_3	1.27	1.39	11.0	1.21	1.22
SiO_2/Al_2O_3(Mol.)	2.26	2.36	18.6	2.07	2.14
$SiO_2/Sesquioxides$	0.60	0.73	3.2	0.76	0.52
$SiO_2/Sesq.$(Mol.)	1.20	1.51	7.5	1.51	1.15

Table 2
Relative Mineralogical Distribution of the Clay Fraction of the Lower Cretaceous Paleosols.

	LK-1	LK-2	LK-3	LK-4	LK-6
Kaolinite	++++	++++	+	++++	++
Anatase	++	+	++	++	+
Hematite	+++	+++	+++	+++	++++
Quartz	-	-	+++	-	++
Halite	-	-	-	++	++

Legend: ++++ (>50%); +++ (20-50%); ++ (<20%); + (<5%); - (<2%)

This is not the case with the LK-2 paleosol, which has a birefringent plasma. A similar fabric sometimes occurs in tropical soils (Bennema et al., 1970) during an early stage of pedogenesis. The birefringence is probably due to the poor drainage conditions which often prevail in weathered basalt substrates. The birefringence can be easily seen in this basalt-derived paleosol due to the absence of continuous iron oxide segregation, which would normally mask the other plasmic features. Possibly the iron segregation in these relatively shallow basalt-derived paleosols is inhibited compared to the deep tropical soils.

The main difference between the LK-1 and LK-2 samples is that the former was developed from pure basalt parent material whereas the latter was formed from two different parent materials - from a weathered basalt and from an overlying sandy alluvium veneer. The alluvial
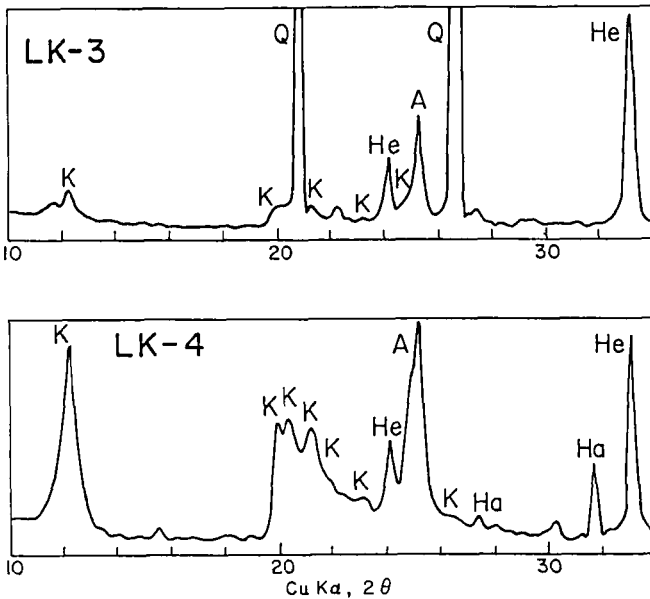
Fig. 3. X-Ray diffractogram
of a paleosol (LK-4)
and plinthite (LK-3).
Red Valley Member,
Lower Cretaceous, Negev
(A=anatase; Ha=halite;
He=Hematite; K=Kaolinite;
Q=quartz).

character is expressed by the large quartz grains which occur in the material (Fig. 2b). The weathering process of the two basalt-derived soils was associated with strong kaolinite reformation from plagioclase (Singer, 1973).

The paleosols of the Red Valley Member originated in the weathering of alluvial sediments, as indicated by the appearance of runiquartz (Stoops and Buol, 1985) which is characteristic of transport of the sandy material. Such grains have features with inherited fill which does not correspond to any material of the surrounding environment. Desilification of the clay minerals led to a relative accumulation of iron and strong iron impregnation. Indeed, all samples exhibit strong iron accumulation on the clay minerals, which can be seen under condensed light. LK-6 represents a moderate stage of iron segregation, preliminary to plinthite formation. In addition to iron segregation random depletion of iron occurred in LK-4 as evidenced by the light mottles.

A very intensive accumulation of iron led to the formation of plinthite (LK-3) in which the amount of the clay minerals and alumina content is low (Tables 1 and 2). Such an accumulation is characteristic of residual plinthite (McFarlane, 1976). The higher amount of titanium in the plinthite also supports its residual origin. The possibility of the formation of plinthite by capillary seasonal fluctuation from a high water table is, in this case, less feasible since the substrate is a permeable sand which presumably avoids water accumulation close to the surface. Moreover, the high degree of crystallinity of the kaolinite points to good drainage conditions (Craig and Loughman, 1964).

Polyphase features as usually found in tropical soils were not observed in any of the studied samples. Even the plinthite crusts, which are usually very complex in this local environment, have a homogeneous pattern of iron impregnation. No concretions or pisolites, which are often found in oxisols, were identified. The monogenetic appearance of the local plinthites is attributed to the preservation of the paleosols under cover of the overlying sediment.

Consequently they were not subjected to surface erosion and weathering processes, particularly during the Tertiary, as is the case in Africa and Australia.

PALEOLATITUDE IMPLICATIONS

Segalen (1971) has classified the warm humid areas of the world into three zones, namely, equatorial, tropical and subtropical, according to the global distribution of diagnostic minerals.

The equatorial zone is characterized by soils with a high amount of gibbsite and geothite, in which hematite is lacking since a short annual dry season is required for its accumulation. The studied paleosols, therefore, were not formed in this climatic zone.

The conditions best fitting the Negev paleosols are found in the tropical zone, which is very humid but has relatively short annual dry season. These conditions favour hematite release and plinthite formation (D'Hoore, 1954). The very high rate of weathering as expressed by the very low silica/sesquioxides ratio and the main micromorphological features suggest that the Makhtesh Ramon paleosols were located during Early Cretaceous times closer to the equatorial zone, within the limit of 10° paleolatitude.

The fern *Weichselia*, found in the Red Valley Member, was distributed in a belt about 30° wide on either side of the paleoequator during Early Cretaceous times (Barnard, 1973). In various reconstructed paleogeographic maps, based on paleomagnetic data (*e.g.* Smith *et al.*, 1973), the Negev is located some 5° away from the paleoequator. Hence, both the paleobotanic and paleomagnetic models support the interpretation deduced from the micromorphology of the Negev paleosols.

CONCLUSIONS

The unconsolidated terrestrial material of the Lower Cretaceous Red Valley Member and the basalt-derived materials from the same period are paleosols. They were formed during a tropical climate with a short annual dry season.

Kaolinitization was very intensive in all the paleosols. In the alluvial-derived paleosols iron segregation was stronger than in the basalt-derived paleosols, leading to pedogenic monophase plinthite formation. Where exposed, the plinthite appears in the landscape in the form of a "carapace".

REFERENCES

Baer, G., Frieslander, U. and Goldman, M., 1989. The Red Valley - an Early Cretaceous caldera in eastern Makhtesh Ramon. Isr. J. Earth Sci., 38: 163-171.

Barnard, P.D.W., 1973. Mesozoic floras. In: N.F. Hughes (Editor), Organisms and Continents Through Time. Paleont. Assoc., Spec. Publ. No. 12, London, pp. 175-188.

Ben-David, R. and Goldbery, R., 1990. Arod Conglomerate and the Red Valley Member (Hatira Formation) - reconstruction of the sedimentological environment. Isr. Geol. Soc. Ann. Mtg, Elat 1990, pp. 16-17.

Bennema, J., Jongerius, A. and Lemos, R.C., 1970. Micromorphology of some oxic and argillic horizons in south Brazil in relation to weathering sequences. Geoderma, 4: 333-355.

Brewer, R., 1964. Fabric and Mineral Analysis of Soils. John Wiley and Sons, New York, 470 pp.

Buchbinder, B. and Le Roux, J.P., 1990. Sedimentological analysis of the Ardon Formation (Lower Jurassic) in the Makhtesh Ramon and its correlation with borehole sections to the north. Isr. Geol. Surv., Rep. GSI/14/90, 30 pp.

Craig, D.C. and Loughman, F.C., 1964. Chemical and mineralogical transformations accompanying the weathering of basic volcanic rocks from New South Wales. Aust J. Soil Res., 2: 218-234.

Eswaran, H., 1972. Micromorphological indicators of pedogenesis in some tropical soils derived from Nicaragua. Geoderma, 7: 15-31.

Goldbery, R., 1982. Palaeosols of the Lower Jurassic Mishhor and Ardon formations (laterite derived facies), Makhtesh Ramon, Israel. Sedimentology, 29: 669-690.

D'Hoore, J., 1954. L'accumulation des sesquioxides libres dans les sols tropicaux. Publ. Inst. Nation. Etude Agron. Congo Belge, Ser. Sci., 62, 132 pp.

McFarlane, M.J., 1976. Laterite and Landscape. Academic Press, London, 151 pp.

Segalen, P., 1971. Metallic oxides and hydroxides in soils of the warm and humid areas of the world: formation, identification, evolution. In: Soils and Tropical Weathering. UNESCO Public., Paris, 149 pp.

Singer, A., 1973. Weathering products of basalt in the Galilee and Menashe. Vesicular and saprolitic weathering. Isr. J. Earth Sci., 22: 229-249.

Singer, A., 1975. A Cretaceous laterite in the Negev desert, southern Israel. Geol. Mag., 112: 151-162.

Smith, A.G., Briden, J.C. and Drewry, G.E., 1973. Phanerozoic world maps. In: N.F. Hughes (Editor), Organisms and Continents Through Time. Paleont. Assoc., Spec. publ. No. 12, London, pp. 1-42.

Stoops, G. and Buol, S.W., 1985. Micromorphology of Oxisols. In: C.A. Douglas and M.L. Thomson (Editors), Soil Micromorphology and Soil Classification. Soil Sci. Soc. Am. Spec. Publ No. 15, Madison, Wisconsin, pp. 105-119.

Micromorphology and submicroscopy of isotropic and anisotropic Al/Si coatings in a Quaternary Allier terrace, (France)

A.G. Jongmans[1], F. van Oort[2], P. Buurman[1], and A.M. Jaunet[3]

[1]*Dept. of Soil Science and Geology, Agricultural University, PO Box 37, 6700 AA Wageningen, The Netherlands*

[2]*INRA, Station Agropedoclimatique, BP 1232, F-97185, Pointe à Pitre Cédex, Guadeloupe, France*

[3]*INRA, Station Science du Sol, Route de St-Cyr, 78026 Cédex, Versailles, France*

ABSTRACT

Jongmans, A.G, Oort, van F., Buurman, P. and Jaunet, A.M. 1994. Micromorphology and submicroscopy of isotropic and anisotropic Al/Si coatings in a Quaternary Allier terrace, (France). In: A.J. Ringrose-Voase and G.S. Humphreys (Editors), Soil Micromorphology: Studies in Management and Genesis. Proc. IX Int. Working Meeting on Soil Micromorphology, Townsville, Australia, July 1992. Developments in Soil Science 22, Elsevier, Amsterdam, pp. 285-291.

Optical studies of a middle Pleistocene Allier river terrace in France reveal the occurrence of isotropic non-laminated coatings and anisotropic non-laminated coatings with a stipple-speckled b-fabric in a buried paleosol, rich in trachytic pumice fragments. Optical and scanning electron energy dispersive X-ray analyses (SEM-EDXRA), *in situ* microdrilling for step scan X-ray diffraction, and transmission electron microscope (TEM) analyses of undisturbed parts of the coatings were used to establish their chemistry, mineralogy and internal microfabric. Micromorphological observations indicate that both coatings are genetically identical. Both kinds were formed by clay neoformation rather than by clay illuviation. The isotropic type consists of amorphous material with a low molar Al/Si ratio, and is the first step in clay neoformation. These coatings contain minor amounts of 2:1 clay. The anisotropic type is formed by recrystallization of isotropic coatings, and consists of unoriented domains of 2:1 clay. The formation of the coatings and their typical chemical and mineralogical characteristics are due to: (1) weathering of trachytic pumice fragments, and (2) occurrence of restricted leaching conditions during coating formation.

INTRODUCTION

Non-crystalline material, appearing as neoformed coatings and infillings, is produced upon weathering of volcanic components in the middle and early Pleistocene Allier river terraces (Jongmans *et al.*, 1991). The occurrence of isotropic non-crystalline coatings under different climatic conditions in soils developed in parent material containing pyroclastic components has been reported previously (*e.g.* Dalrymple, 1964; Chartres *et al.*, 1985). Recrystallization of such coatings was reported by Buurman and Jongmans (1987) in soils with pyroclastic components from Indonesia. Veldkamp and Jongmans (1991) studied the occurrence and weathering of pumice clasts in a paleosol found at 5 m in depth in the middle Pleistocene

Allier terrace deposits, and observed partially altered trachytic pumice fragments together with isotropic and anisotropic coatings. In the present paper the morphology, chemistry, and mineralogy of these coatings are studied, to determine their genesis and relationships. Micro fabrics of the coatings were examined by transmission electron microscope (TEM) to assess the distribution pattern of the individual clay domains. Together, these analyses should provide some insight into the formation of these coatings in relation to the environmental conditions of the paleosol.

SOIL SITE CHARACTERISTICS

The paleosol is approximately 1 m thick, grey (10YR 5/1) and consists of cryoturbated sand and clay bodies (Veldkamp and Jongmans, 1991). The clayey parts show a distinct angular blocky structure, whereas the sandy parts are structureless and massive. Soft, white (10YR 8/2), rounded, trachytic pumice fragments (up to several mm, Al/Si ratio = 0.36) and fresh and partially weathered volcanic and granitic fragments are present. Many biogenic channels occur, surrounded by a clear porostriated birefringent fabric. Cryoturbation features, pedal structures, and channels are absent in the 4 - 5 m thick gravel sediment that overlies the paleosol. A stratified gravel deposit with a firm consistence, as a result of close packing of different grain sizes, underlies the paleosol.

ANALYTICAL METHODS

Undisturbed samples (8 × 8 cm) from the sandy and clayey parts of the paleosol, and the directly adjacent underlying and overlying sediments were taken, and thin sections were made according the method of FitzPatrick (1970). For thin section description the terminology of Bullock et al. (1985) was used. In situ microchemical analyses on isotropic and anisotropic coatings were performed in uncovered thin sections with a Philips scanning electron energy dispersive X-ray analyser (SEM-EDXRA). Four coatings of both kinds were analysed, and five block (12 μm^2) analyses were made of every coating (n=20). The peak to background heights of the EDXRA signal were linearly transformed to element percentages by comparison with standard minerals of a known chemical composition, analysed in the same measurement. Isolation of microquantities of coatings from uncovered thin sections was performed with a microscope-mounted drill (Verschuren, 1978), and X-ray diffraction patterns of this material were obtained by step scan X-ray diffraction (SSXRD) (Meunier and Velde, 1982). Undisturbed sections of 50 nm thickness, cut from undisturbed fragments (±100 μm^2) of both coating types were prepared according the method of van Oort et al. (1990), and analysed with a Philips 420 TEM. A Link AN 10000 EDS analyser permitted microchemical analysis.

RESULTS

Micromorphological observations show that isotropic (A) and anisotropic (B) coatings (Fig. 1) are found in the paleosol, and in the upper part of the underlying sediment. They are absent in the overlying deposit. Coatings are common around partially altered pumice fragments. The pale yellow, isotropic coatings are unoriented and non-laminated. Locally, anisotropic spots occur with a weak stipple-speckled b-fabric. Anisotropic coatings are unoriented, non-laminated, pale yellow, and display a stipple-speckled b-fabric. Both variations
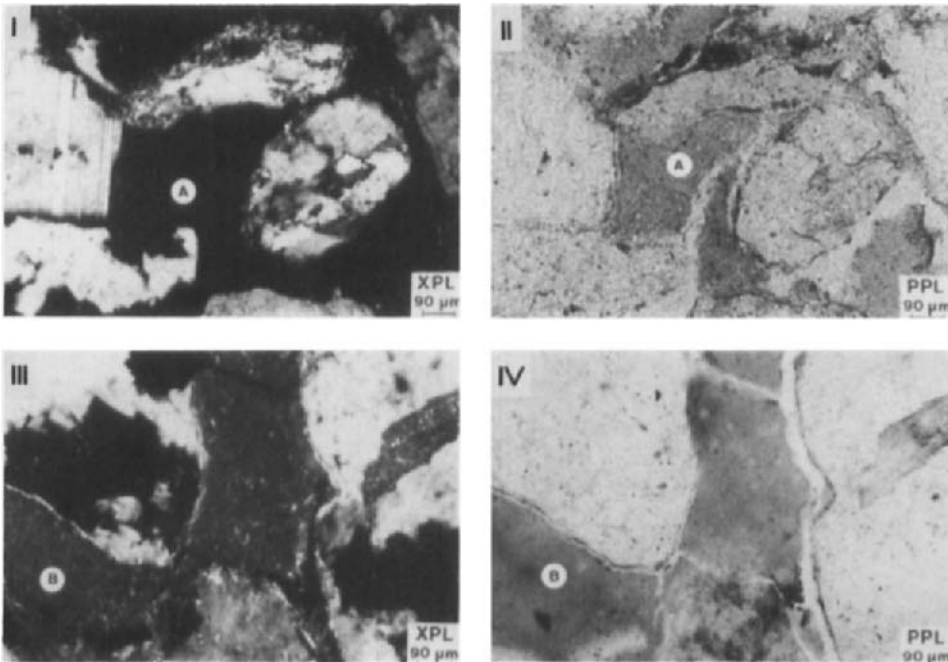
Fig. 1. Micromorphological characterization of: I) and II) the isotropic coatings (label A) and III) and IV) the anisotropic coatings (label B) in I) and III) crossed polarized light (XPL) and II) and IV) plane polarized light (PPL).

frequently occur within one coating and cannot be distinguished in plane polarized light. They may be weakly impregnated by ferruginous hypocoatings. Muscovite grains (10×3 μm) are sometimes enclosed in both types. Fig. 2 shows the results of SSXRD of both coating types. Anisotropic coatings show a clear broad peak at 1.9 nm (expanded smectite) and small peaks at 1 nm (mica) and 0.7 nm (kaolinite/halloysite). No peaks occur in the diffractogram of the isotropic coatings.

Table 1 shows SEM-EDXRA analyses of the isotropic coating (A) and anisotropic (B) coatings. Mg, Ca, and K contents are very low in the isotropic type. Ca and K tend to be higher in the anisotropic type but concentrations are still low. Some coatings contain minor amounts of Ti. Al is slightly lower in the anisotropic type B, while Si and Fe are somewhat higher. The molar Al/Si ratios in both coating types are lower than normal allophane values; type B has the lowest value.

Fig. 3 shows the TEM images of the studied coatings. In Fig. 3I the isotropic coating (A) consists of amorphous material with some randomly distributed 2:1 clay-domains. The anisotropic coating (B in Fig. 3II) consists of randomly distributed domains of 2:1 clay. High resolution lattice-fringe imaging (Fig. 3III and IV) reveals basal spacings of 1.4 nm. Microchemical analyses of individual clay-domains in the anisotropic type B show high Si and low Al contents and an inverse relationship between Al and Fe (Fig. 3V).
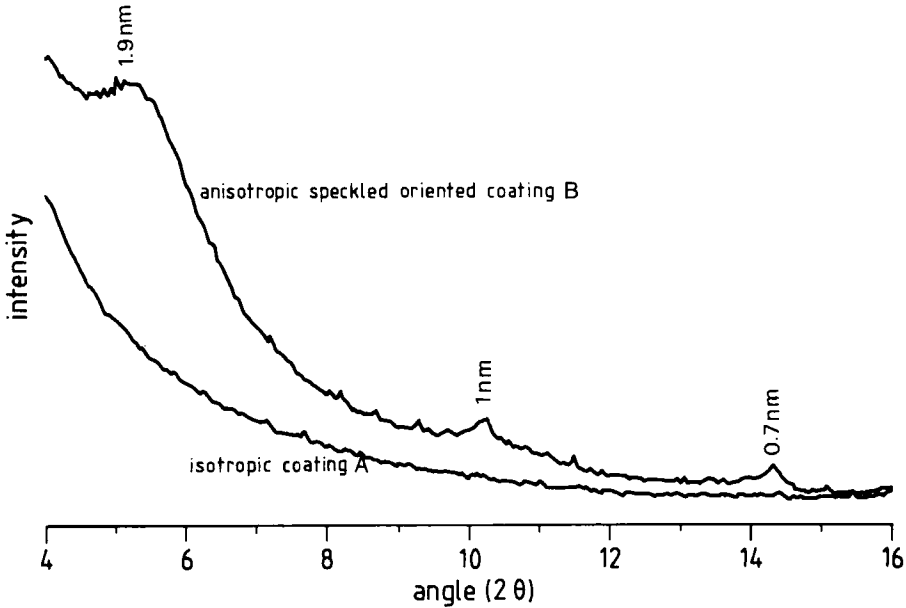
Fig. 2. Step scan X-ray diffractograms (Co-Kα radiation) of microquantities of the isotropic (A), and anisotropic (B) coatings obtained by microdrilling.

Table 1
SEM-EDXRA analyses of isotropic coatings (A) and anisotropic coatings (B) (wt%; N=20).

	coating A	coating B	t value	significance
Mg		0.06 ± 0.06	1.86	*
Al	5.3 ± 0.8	4.1 ± 0.9	4.56	**
Si	12.4 ± 1.4	14.3 ± 2.2	-3.23	**
K	0.004 ± 0.1	0.2 ± 0.3	-1.81	*
Ca	0.6 ± 0.4	1.1 ± 0.2	-3.39	**
Fe	7.2 ± 1.2	9.6 ± 1.8	-5.84	**
Al/Si molar	0.5		0.3	

*,**, Significant at P <0.05 and 0.01, respectively

DISCUSSION

The presence of isotropic (A) and anisotropic parts (B) within one coating and their similarity in plane polarized light indicate that they are genetically related. The limpid texture and non-laminated internal fabric of the coatings, and the occurrence of types A and B within one coating suggest that A and B are due to clay neoformation rather than clay illuviation.
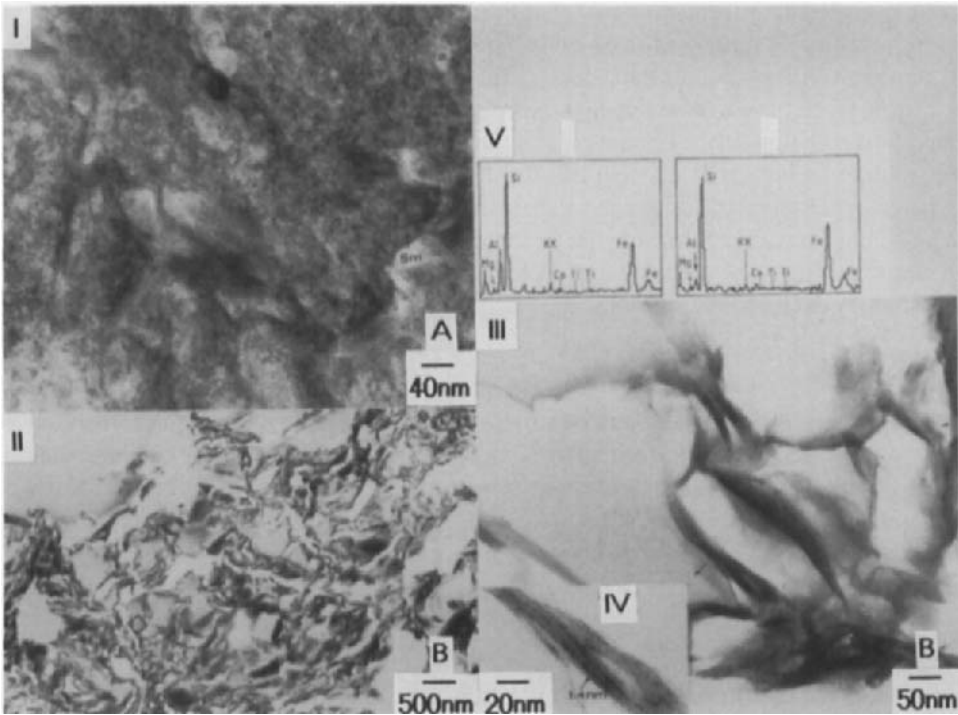
Fig. 3. TEM observations of undisturbed parts of: **I**) the isotropic coatings (A) showing allophane (a) and smectite (Sm); **II**) the anisotropic coatings (B); **III**) and **IV**) the anisotropic coating (B) by high resolution lattice-fringe imaging; **V**) micro-chemical analyses of clay domains in the anisotropic coatings.

Moreover, clay illuviation coatings should be anisotropic because they always consist of crystalline clay minerals, while an isotropic character points to amorphous material (Bullock *et al.*, 1985). SSXRD shows that the isotropic type A is X-ray amorphous, while TEM observations demonstrate occurrence of small amounts of 2:1 clay domains in an amorphous groundmass. Anisotropic coatings B predominantly consists of crystalline 2:1 phyllosillicates. TEM analyses show absence of preferred orientation patterns between the clay domains, which is in agreement with the micromorphologically observed stipple-speckled b-fabric. This suggests that the precipitation of the amorphous, isotropic coatings is the first step, and recrystallization of these coatings to anisotropic coatings is the second step in clay neoformation. The isotropic coatings may be allophane-like, although they are relatively rich in silica. Parfitt and Kimble, (1989) reported Al/Si ratios of allophane are usually around 2, but variations may occur between 0.5 and 4. These values are strongly influenced by the chemical composition of the parent material and its resistance against weathering, and the prevalent leaching/drainage conditions (Parfitt, 1989; Singleton *et al.*; 1989). As a result, the weathering of trachytic pumice fragments (Al/Si ratio 0.36) in the paleosol, and restricted leaching

conditions during coating formation are thought to be the main sources of large amounts of liberated Si, resulting in formation of Si-rich allophanes and subsequent formation of 2:1 clay minerals rich in Si. After burial of the paleosol, the coatings were preserved.

Both coating types have a relatively high Fe content, probably due to iron impregnation, but partial incorporation of variable amounts of iron in the smectite lattice cannot be excluded. The observed muscovite in type B may explain the 1.0 nm diffraction peak, and are parts of the adjacent parent material mixed in the gels during transport.The difference between the SSXRD diagram and TEM images, as shown by the measured basal spacings of the smectite, might be a result of the use of acetone during sample preparation (swelling), and/or high vacuum used during TEM analysis (partial collapsing).

CONCLUSIONS

Weathering of trachitic pumice under restricted leaching conditions in a Quaternary river terrace in France resulted in the formation of optically isotropic allophanic coatings with a Al/Si ratio up to 0.5. With time, these coatings may partially crystallize to anisotropic coatings consisting predominantly of randomly distributed smectitic clay domains. Although such coatings may still form in similar environments they are believed to be preserved by burial in the case reported here.

REFERENCES

Bullock, P., Fedoroff, N., Jongerius, A., Stoops, G., and Tursina, T., 1985. Handbook for Soil Thin Section Description. Waine Research Publications, Wolverhampton, U.K., 152 pp.

Buurman, P. and Jongmans, A.G., 1987. Amorphous clay coatings in a lowland Oxisol and other andesitic soils of West-Java, Indonesia. Pemberitaan Penelitian Tanah Dan Pupuk, 7: 31-41.

Chartres, C.J., Wood, A. and Pain, C.F., 1985. The development of micromorphological features in relation to some mineralogical and chemical properties of volcanic ash soils in highland Papua New Guinea. Aust. J. Soil Res., 23: 339-345.

Dalrymple, J.B., 1964. The application of soil micromorphology to the recognation and interpretation of fossil soils in volcanic ash deposits from the north Island, New Zealand. In: A. Jongerius (Editor), Soil Micromorphology, Proc. II Int. Working Meeting on Soil Micromorphology. Arnhem, The Netherlands Sept. 1964. Elsevier, Amsterdam, pp. 339-349.

FitzPatrick, E.A., 1970. A technique for the preparation of large thin sections of soils and consolidated material. In: D.A. Osmond and P. Bullock (Editors), Micromorphological Techniques and Application. Soil Survey Technical Monograph 2, Rothamsted Experimental Station, Harpenden, U.K., pp. 3-13.

Jongmans, A.G., Fijtel, T.C., Miedema, R., van Breemen, N. and Veldkamp, A., 1991. Soil formation in a Quaternary terrace sequence of the Allier, Limagne, France. Macro- and micromorphology, particle size distribution, chemistry. Geoderma, 49: 216-239.

Meunier, A. and Velde, B., 1982. X-ray diffraction of oriented clays in small quantities (0.1 mg). Clay Miner., 17: 259-262.

Oort, van F., Jongmans, A.G., Jaunet, A.M., van Doesburg, J., and Feijtel, T., 1990. Andesite weathering and halloysite newformation in a ferralitic soil environment in Guadeloupe. In situ study of different halloysite facies on thin sections by SEM-EDXRA, microdrilling, step scan XRD and TEM. C.R. Acad. Sci. Paris, t. 310, Series II, pp. 425-431.

Parfitt, R.L. and Kimble, J.M., 1989. Conditions for formation of allophane in soils. Soil Sci. Soc. Am. J., 53: 971-977.

Singleton, P.L., Mcload, M. and Percival, H.J., 1989. Allophane and halloysite content and soil solution silicon in soils from Rhyolitic volcanic material, New Zealand. Aust. J. Soil Res., 27: 67-77.

Veldkamp, A. and Jongmans, A.G., 1991. Trachitic pumice clasts in Middle Pleistocene Allier terrace deposits, Limagne, France: A chronostratigapic marker. In: A. Veldkamp, Quaternary River Terrace Formations in the Allier Basin, France. Thesis, Wageningen Agricultural University, pp. 27-35.

Verschuren, R.H., 1978. A microscope-mounted drill to isolate microgram quantities of mineral material from polished thin sections. Mineral. Mag., 42: 499-503.

This Page Intentionally Left Blank

Interpretation of interglacial cave sediments from a hominid site in North Wales: translocation of Ca-Fe-phosphates

D.A. Jenkins
Soil Science, SAFS, University of Wales, Bangor, U.K.

ABSTRACT

Jenkins, D.A., 1994. Interpretation of interglacial cave sediments from a hominid site in North Wales: translocation of Ca-Fe-phosphates. In: A.J. Ringrose-Voase and G.S. Humphreys (Editors), Soil Micromorphology: Studies in Management and Genesis. Proc. IX Int. Working Meeting on Soil Micromorphology, Townsville, Australia, July 1992. Developments in Soil Science 22, Elsevier, Amsterdam, pp. 293-305.

Pontnewydd Cave is one of only two Lower Palaeolithic hominid sites in the U.K. dating to the temperate Oxygen Isotope Stage 7 (*c.* 225 ka). Fossiliferous beds occur within a thick sequence of "debris slide" sediments and include a thin stratum distinguished by its yellow brown pigmentation and originally interpreted as an interglacial soil transported into the cave. Detailed mineralogical analysis of sand and clay fractions has clarified the provenance of the sediments and confirmed the relatively strongly weathered nature of this stratum. Micromorphological analysis revealed weathered clasts, a distinctive "pellety" microfabric and also distinctive orange-brown isotropic cutans overlain by later argillans. Microchemical analysis using EDXRA showed the cutanic material to be a Ca-Fe phosphate with a composition approaching that of the mineral calcioferrite $(Ca_2Fe_2[PO_4]_3(OH).7H_2O)$; its origins could be traced back to a progressive alteration of fossil bone in the overlying horizons, and probably involved translocation as a colloid. Whilst conclusions as to the pedogenic origins of this stratum remain the same, care must clearly be taken in the interpretation of pigmented horizons in archaeological contexts involving original bone material. The distinctive nature and composition of the cutanic material opens up a new area of phosphorus geochemistry in archaeological sites.

INTRODUCTION

Evidence for the earlier periods of human activity diminishes progressively, and consequently achieves greater significance, with age. This is especially so for the Lower Palaeolithic in a glaciated terraine such as the British Isles where succeeding phases of glacial and interglacial conditions lead to the disturbance and/or removal of evidence by erosion or to its burial by deposition; survival and discovery tend to rest on special circumstances. To enhance our knowledge about early man and his environment it is therefore necessary that, once identified, the maximum information is gleaned from such deposits, and soil mineralogy and micromorphology have the potential to play important roles in this process (Bullock, 1985; Jenkins, 1985).

Fig. 1. Location of site in relation to glaciations and distribution of Lower Palaeolithic artefacts in the British Isles. (After Wymer, 1968; West, 1977; Lowe and Walker, 1984).

This paper will illustrate the problems and contributions of such techniques by reference to the interpretation of deposits in Pontnewydd cave, an important Lower Palaeolithic hominid site in North Wales (Green, 1984).   Here initial interpretation of the sequence of dominantly glacially derived strata was influenced by the orange-brown pigmentation of one stratum which was interpreted as arising from intense weathering and related to interglacial pedogenesis (Jenkins, 1984).   Subsequently, more detailed micromorphological and microchemical analysis has shown that this first interpretation was somewhat naive. The story is more complicated, involving translocation and redeposition of phosphate in an unusual Ca-Fe form, which in turn opens up an interesting area of soil chemistry. The palaeoenvironmental conclusions, however, remain essentially the same.

The archaeological context

To explain the context for this micromorphological study it will be necessary to give a brief description of the sites. The cave at Bontnewydd is exposed half way up a steep valley side cut into Carboniferous Limestone by the river Elwy.   It is a fragment of a phreatic tube some 50 m long left by the progressive downcutting of the river, and truncated by cliff recession. However the entrance was apparently favoured for habitation by Lower Palaeolithic man whose remains have been discovered in deposits carried deeper into the cave and thus protected from subsequent phases of glacial erosion. Preserved by these special circumstances the site is therefore unique in Wales, and one of the few to have been identified in upland Britain (Fig. 1). The cave was well known for its fossil bones in the last century, having been examined by Boyd Dawkins in 1874, but because of its significance it has recently been subjected to a detailed and intensive re-examination by Stephen Green of the National Museum of Wales (Green, 1984; Greene *et al.*, 1989). This report forms one component of that inter-disciplinary programme of research.
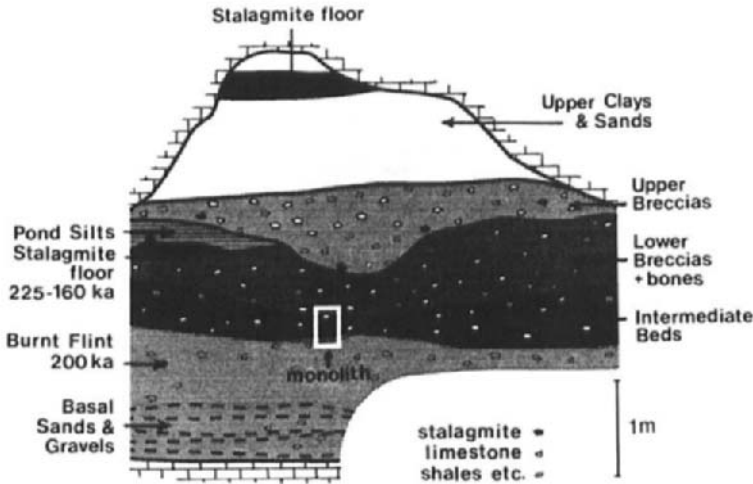
Fig. 2. Composite section of deposits in Pontnewydd Cave (after Green, 1984).

Excavation in the cave has revealed a complex sequence of deposits mostly thought to have been slumped in from the cave entrance by debris flow (Collcutt, 1984). The stratigraphy is summarised in Fig. 2 and commences with a basal sequence of brown (10YR 5/3) Sands and Gravels up to 3 m thick which is barren with respect to fossil bone or artefacts. This is succeeded by the thin (<0.5 m) loamy Intermediate Beds, distinguished by their dark yellowish brown colour (10YR 5/6-5/8) and carrying a few artefacts together with fauna (wood mouse, bear, roe deer, beaver, *etc.*) indicative of warm, open woodland conditions: in places silty deposits at the top of the underlying Sands and Gravels have also been stained a distinctive brown (7.5YR 5/4). These Intermediate beds are capped by stalagmites which began to form *c.* 225 ka ago, and they pass up into the brown (10YR 5/3) Lower Breccia which carries the bulk of the artefacts together with faunal remains (hyaena, Norway lemming, Northern vole, *etc.*) indicative of a cool, open steppe environment. Overlying these beds is a sequence of brown/light brown (10YR 5/3 - 7.5YR 6/4) clays, sands, breccias and silt beds, including intact and fragmented stalagmitic floors: they are thought to be Late Devensian and Postglacial and contain only the occasional derived artefact.

The artefacts recovered from the Intermediate Beds and Lower Breccias number several hundred. They are dominated by handaxes and the products of a "Levallois" technology. The human remains discovered in the recent excavations comprise mostly teeth and jaw fragments derived from at least one adult and two children, and show features ("taurodontism" of the teeth) characteristic of early Neanderthals. These remains have been dated to around 200 - 225 ka BP by U-Series techniques applied to stalagmites which seals the deposits (Schwarcz and Ivanovich: in Green, 1984) and by Thermoluminescence of both stalagmites and of a burnt

flint core (Debenham and Huxtable: in Green, 1984), a date consistent with the archaeological interpretation. The relevant sequence of beds has therefore been tentatively correlated with oxygen isotope stages 7c (Intermediate - warm), 7b (Lower Breccias - cool) and 7a (stalagmite seal - warm) possibly corresponding to the penultimate interglacial (Green *et al.*, 1989). This site with human remains is thus the earliest in Wales and one of only two in Britain, the other being at Swanscombe. Any information relating to the palaeoenvironment that can be obtained by analysis of the deposits therefore assumes importance, and in particular from the nature of the yellow-brown Intermediate Beds.

MATERIALS AND METHODS

During archaeological excavation, loose sediment samples were collected for laboratory analysis from several sections exposed in the cave, and in particular from a 3 m deep fissure some 5 m in from the entrance ("deep sounding") and from a 1.5 m section (Site D) a further 5 m into the cave passage. The latter included a conveniently compact and strongly pigmented section through the "Intermediate Complex" ("buff-orange"; 10YR 5/6-5/8) selected for micromorphological study. The fine sand and clay fractions (<2 μm esd.) were separated and analysed by the usual techniques of optical microscopy, XRDA and SEM/EDRA, and chemical analyses (differential extraction of Al, Fe and Mn, *p*H, % $CaCO_3$, *etc.*) were also carried out by routine procedures which, although referred to below, are to be described in detail elsewhere.

Routine sampling for micromorphology of the loose, stony material proved impossible by use of the "kubiena tin". An intact monolith some 20 cm deep had to be sculpted and encased in plaster-of-paris before it could be extracted. This was air-dried, impregnated with an acetone-diluted monostyrene system and a series of large and small uncovered thin sections prepared. For more detailed optical and SEM/EDXRA examination, slides were cleaned ultrasonically and polished successively with 6, 3 and 1 μm diamond pastes. Slides were examined optically under temporary oil-mounted cover-slips on a Leitz Ortholux- pol using also UV fluorescence (Hg-lamp with 5 mm BG12 exciter filter and K530 barrier filter). Samples selected for SEM/EDXR analysis were first photographed, then trimmed down to a 1.5 cm square from the slide, cleaned ultrasonically in ether and coated with carbon. They were then examined in a Hitachi S520 Microscope fitted with a LINK QX2000-I system (LZ4 detector), the selected areas located, and elemental X-ray spectra and distribution maps obtained. A preliminary analysis was made on 5 point samples and also by scanning over 10 20 × 30 μm homogenous areas for 50sec (realtime) at 14 kV beam voltage. The method was calibrated for P, Ca, Fe, Si, Al and K from a sequence of prepared $FePO_4$/$CaHPO_4$/kaolinite/ muscovite standards abutting the sample. These produced smooth curves for Ca, P, Si., Al and K but not for Fe, and for this reason only "semiquantitative" values are quoted at this stage.

RESULTS

Mineralogy

In order to establish the provenance of the sequence of sediments, quantitative heavy mineral and clay mineral analyses were made on 10 strata, and the morphology of individual species examined by SEM. Only a summary of these data will be presented here as a detailed account will be presented elsewhere. Variation in heavy mineral assemblages can be linked
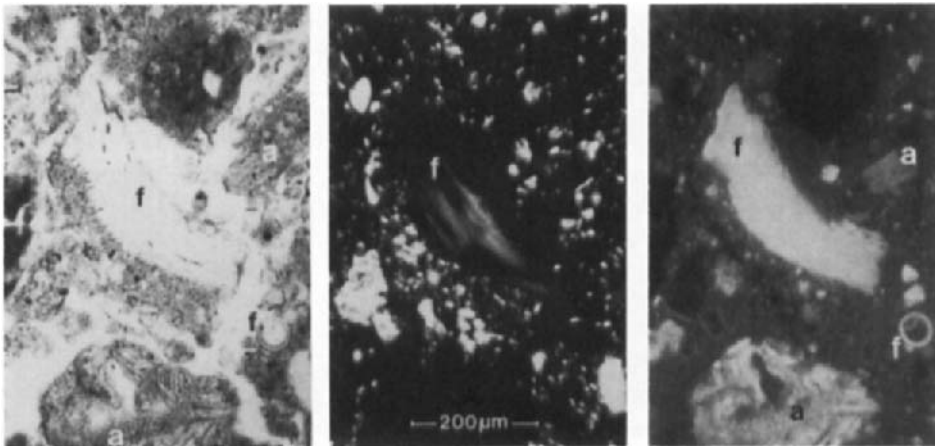
Fig. 3. Bone in a thin section of the Lower Breccia showing (f) fresh clear birefringent, fluorescent fragments, and (a) altered, isotropic, and weakly fluorescent fragments; as seen: (left) in plane polarised light, (centre) between crossed polars, and (right) using UV-autofluorescence.

with recognisable sources. The Basal Sands and Gravels are dominated (80-90%) by a pale chlorite characteristic, together with minor tourmaline, of the Silurian mudstones of Hiraethog, 15 km to the west. These are accompanied by small amounts of clinopyroxenes, amphiboles and clinozoisite from the igneous rocks of the Snowdonian Mountains a further 40 km to the west. The Intermediate Beds show a change to minimal Silurian material (chlorite <0.1 - 30%) which is replaced by resistate minerals (zircon, rutile, tourmaline, garnet *etc.*) typical of the Carboniferous strata outcropping along the coast immediately to the north, together with traces of Triassic-derived glacial material from the Irish Sea further to the north indicated by the presence of staurolite and kyanite. In the overlying strata (Breccias, Upper Sands and Gravels, *etc.*) there is an admixture of these materials with the Silurian again assuming importance (chlorite 41 - 77%).

There is therefore a change of provenance from local sources to the west in the basal beds to local and extraneous sources to the north in the Intermediate Beds and back to a mixture in the upper strata. The Intermediate Beds appear to have derived mainly from material on the landsurface to the north of the escarpment, probably by temperate slope processes supplemented by aeolian deposition, whilst the beds above and below reflect the influence of Lower Palaeozoic outcrops to the west, consistent with local glaciation. A change of environment is also distinctly apparent in the greater degree of etching seen by SEM in the more susceptible mineral species (*i.e.* chlorite and clinopyroxene) from the Intermediate Beds, consistent with temperate (interglacial) as compared to glacial conditions. The same trends are seen in the inherited mineralogy of the clay fractions where Silurian sources are represented by hydrous mica and chlorite (together with derived vermiculite and inter-stratified material), while Carboniferous sources contribute hydrous mica and kaolinite. The Intermediate Beds are
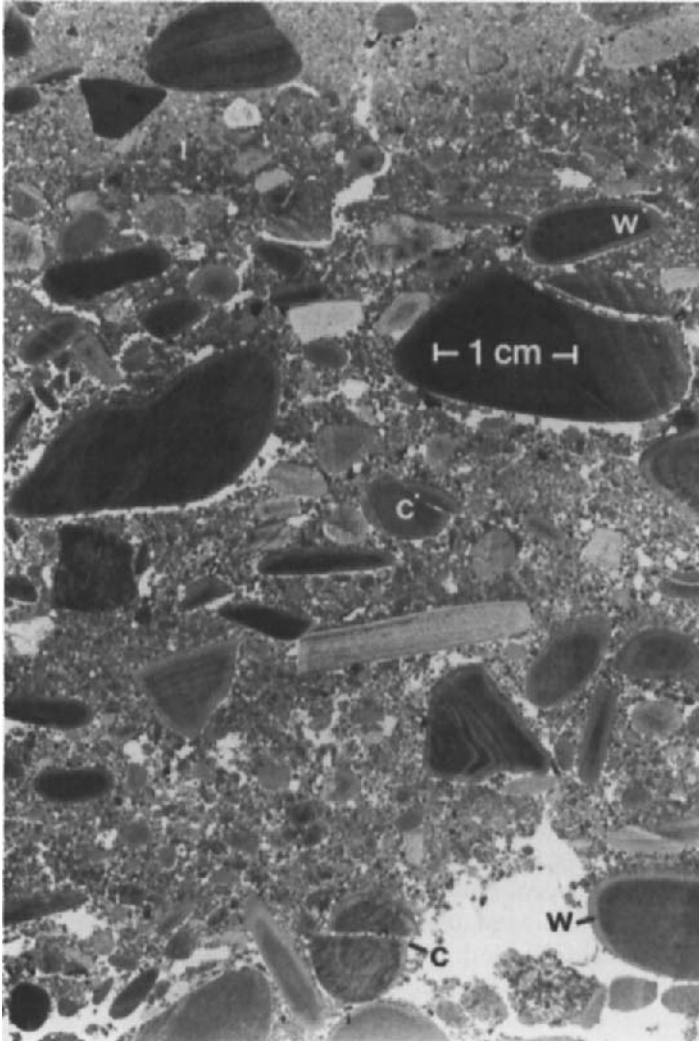
Fig. 4. Vertical section through Intermediate Beds showing very fine "pellety" fabric, and clasts with cracks (c) and weathered rims (w).

marked by an assemblage depleted of chlorite and vermiculites but with smectites making an unusual appearance. Overall the impression therefore remains of these fossiliferous Beds being derived from a more weathered terraine, consistent with selective destruction under interglacial conditions, rather than of an unaltered assemblage inherited under glacial conditions.

A conscious search was made by magnetic fractionation and by DXRDA for crystalline iron hydroxides/oxides, but no particular concentration was found in the Intermediate Beds whose distinctive pigmentation is therefore ascribed to amorphous materials. A search was also made for pollen and, in the light (SG<2.3) 20 - 200 μm fraction, for opaline silica bioliths but none was detected, although the alkaline environment (*p*H ≥8) would mitigate against their preservation in these deposits.

Micromorphology

A progressive trend was observed on passing down from the Lower Breccias into the underlying Intermediate Beds and "purple-stained" beds (5YR-7.5YR 5/4) below. In the Lower Breccias the numerous rounded shale and sandstone fragments are supported in a matrix with a relatively uniform, strongly developed, very fine to fine granular microstructure, with simple and complex packing voids. The groundmass shows a uniform speckled b-fabric ("silasepic") with a related distribution ranging from enaulic to porphyric (Bullock *et al.*, 1985). A feature of this horizon is the presence of numerous small bone fragments. Some of these are relatively unaltered, being a pale brown, and retaining a vesicular structure. They display a weak birefringence (length fast), and show strong green autofluorescence in UV (blue - BG12) light. These grade progressively into less well defined orange brown fragments which are structureless, isotropic and showing no autofluorescence (Fig. 3).

On passing down into the Intermediate Beds certain trends are apparent (Fig. 4). Firstly, the rounded shale fragments display a more obvious bleached weathering rind, up to 2 - 3 mm thick, and are occasionally fragmented, whilst identifiable bone fragments are absent. Secondly, the fine granularity (500 μm) of the microfabric breaks down into ultrafine granules (50 μm) whilst there is an increasing chitonic character to the related distribution which, in places, takes the form of distinct silt cappings. Rare pedofeatures in the form of discrete uniform grey silty coatings also occur.

At the base of the Intermediate Beds these trends are accentuated and, in particular, there is a development of a distinctive pattern of coatings. This starts with uniform typic coatings 50 - 200 μm thick of a transparant orange brown material on voids and in aggregates, sometimes infilling the voids, giving a chitonic/gefuric character to the related distribution. The material shows distinctive shrinkage cracks, and is mostly isotropic but sometimes develops a weak streaky birefringence (length-slow) (Fig. 5). In a few places this is overlain by a sharply defined grey brown silty argillan up to 500 μm thick, which may show weak micro-lamination; it displays strong aggregate birefringence (length-slow) and even, on occasions, a distinct pleochroism in a shade of brown. It is, however, the nature of the underlying orange "colloidal" coating which is of particular interest, since it is presumably an important contributor to the distinctive colour of these deposits. Samples were therefore prepared for microanalysis by EDXRA in the SEM.

Spectral analysis of the material indicated its composition to be dominated by Ca, Fe and P. These elements are accompanied by minor but variable amounts of Si, Al and K which were interpreted as associated clay (hydrous mica). No other elements (Mg, Na, Ti *etc.*) were detectable except occasionally for S which is atributed to the impregnating resin. The spatial distribution of elements in relation to matrix, Ca-Fe-P cutan and argillan is illustrated in Fig. 6. For the "semiquantitative" EDXRA, spots (5) and areas (10) in the colloid were selected as far as possible on the basis of minimal birefringence to reduce the effect of possible dilution by
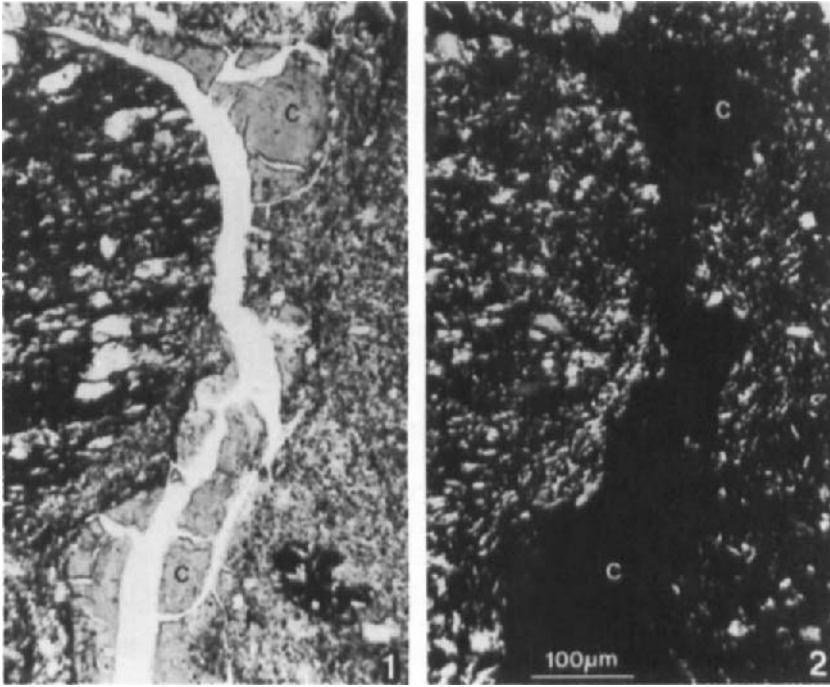
Fig. 5. Orange brown cutan (c) in a thin section from the base of the Intermediate Beds showing, in plane polarised light (left) the distinctive cracking, and between crossed polars (right) its essentially isotropic nature.

clay minerals. Nevertheless, K, Al and Si were present in all the analyses in proportions that were generally consistent with small amounts of hydrous mica ($\pm 10\%$), supplemented occasionally with quartz. To obtain an estimate of the possible composition of the colloid, an average was taken of the five analyses with maximal values for P and minimal values for Si+Al+K (the latter equivalent to some 5% of hydrous mica - 0.6% K). These values indicate a relatively narrow range of Ca:P:Fe for the 15 analyses (*ie*. $1.00(\sigma=0.10):1:1.26(\sigma=0.50)$) and are given below in Table 1 together with those of some known Ca-Fe phosphates and also one K (4.4%)-Ca-Fe phosphate (Lindsay and Vlek, 1977). From this it would appear that the material is a Ca-Fe phosphate which approaches the composition of the mineral calcioferrite, but possibly with lower hydration.

The composition of other components was also checked by EDXRA. That of the brown matrix underlying the orange cutanic material was, predictably, dominated by Si, Al, Fe and K with detectable Ca, Na, Mg and Ti; P however was present only in trace amounts or not detectable. The composition of the silty argillan overlying the orange cutanic material was dominated by Si, Al and K in proportions that suggest hydrous mica with minor quartz; again, P was not detectable.
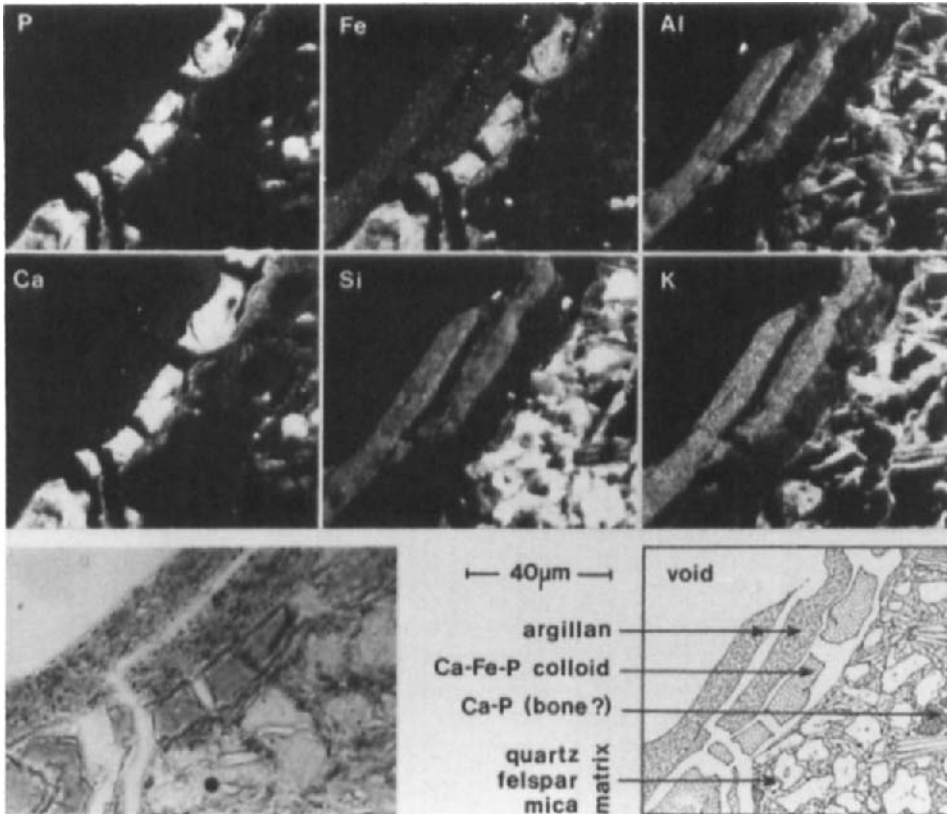
Fig. 6. X-ray images for P, Fe, Ca, Si, Al and K in an argillan/colloid cutan at the base of the Intermediate beds.

DISCUSSION

The initial purpose of this study was to obtain information relevant to the origin of the Intermediate Beds. The problem is one of distiguishing features within the sediments that survived from their original subaerial environment (pedogenic?) from those that were developed after deposition within the cave (diagenic). From the former it may prove possible to diagnose the external palaeo-environment, whilst the latter may have developed at any point over a long period of changing conditions. Arising from this study, the translocation of phosphate subsequently became a feature of specific interest. These two aspects will be discussed in turn.

Palaeo-environmental considerations

The Intermediate Beds are distinguished by their colour which was initially attributed to some form of ferric oxide/hydroxide and thus to an increased degree of oxidation/weathering.

Table 1
Chemical composition of the colloidal coatings

| | | wt.% | | |
		Ca	Fe	P
Average of 5 "semiquantitative" EDXRA analyses				
of colloid with highest P and low Si/Al/K		14.5	20.0	14.5
(analysis with highest P and low Si/Al/K		15.0	21.5	17.5)
(Hydroxyapatite	$Ca_5[PO_4]_3(OH)$	39.9	-	18.5)
Xanthoxenite	$Ca_4Fe_2[PO_4]_4(OH)_2.3H_2O$	21.6	15.1	16.8
Calcioferrite	$Ca_2Fe2[PO_4]_3(OH).7H_2O$	12.9	18.1	15.0
Mitridatite	$Ca_2Fe_3[PO_4]_3(OH)_4.2H_2O$	13.3	28.0	15.0
(Fe-englishite[*]	$K_2Ca_4Fe_8[PO_4]_8(OH)_{10}.9H_2O$	9.0	25.8	13.9)
(Fe-crandallite[*]	$CaFe_3[PO_4]_2(OH)_5.H_2O$	8.0	33.6	12.4)
(Fe-foucherite[*]	$CaFe_4[PO_4]_2(OH)_8.7H_2O$	5.6	31.3	8.7)
Borickite	$CaFe_5[PO_4]_2(OH)_{11}.3H_2O$	5.3	37.3	8.3
Richellite	$Ca_3Fe_{10}[PO_4]_89OH)_{12}.nH_2O$	5	20	12
Dufrenite	$CaFe_6[PO_4]_4(OH)_6.2H_2O$	4.5	37.6	13.9
Eguëite	$CaFe_{14}[PO_4]_{10}(OH)_{14}.21H_2O$	1.9	36.5	32.9
(Strengite	$FePO_4.2H_2O$	-	29.9	34.1)

( ) Ca and Fe end members
(*) theoretical Fe end members of Ca-Al/Fe phosphates

This is certainly confirmed in an increase from 0.9% to a peak of 4.9% for dithionite-extractable iron in these Beds, but no concentration of specific iron minerals (*e.g.* haematite) was detectable by enhanced XRD techniques that could be specifically linked with more extreme weathering regimes. Nevertheless, after taking account of possible differences in provenance, the inherited mineral assemblages would suggest a greater intensity of prior pedogenic weathering in these Beds, and this is supported by the degree of etching on susceptible mineral species such as chlorite and clinopyroxene. The disappearance of unstable chlorite and vermiculite from the clay fraction, together with the appearance of smectites, adds further weight to this interpretation.

Micromorphology revealed well developed rinds to the rounded clasts in the Intermediate beds again indicating strong weathering prior to deposition. Some of these had been fractured *in situ*, suggesting thermoclastic processes following deposition; this feature was also recorded by Collcutt (1984) who noted its increase upward through the sediment column. The sediments also displayed a distinctive pellety fabric which is reminiscent of those of podzolic Bs horizons (Clayden, 1970) such as occur in upland Wales today. It would be surprising if such a pedogenic fabric were to survive any prolonged transportation into the cave system, and indeed the structure of present-day Bs material can be seen to be susceptible to rapid destruction by reduction of the iron under wet conditions. Alternatively this distinctive

microfabric could have been generated differentially within one stratum of the sediments within the cave, presumably in the period immediately after emplacement and prior to deposition of the overlying Lower Breccias. Post depositional modification certainly did occur in the Intermediate Beds. This is evident from the cappings of fine granular material on the clasts in the Intermediate Beds, and from the two phases of cutans to be seen below, the silty argillans indicating a phase of illuviation of fine sediment that succeeded one of colloidal material; the latter certainly involved some chemical redistribution and will be discussed further below.

On balance, however, it seems probable that the Intermediate Beds originated as strongly weathered soils in the immediate vicinity of the cave entrance, possibly from the cliff top above as suggested by their particular heavy mineralogy. This would correspond to pedogenesis during the penultimate Interglacial suggested by dates from these deposits. The contemporary soils of the same parentage at this altitude are brown earths rather than podzolic (Ball, 1960) implying that the environment was the result of stronger weathering than that of today. This conclusion is thus essentially the same as that reached in the initial study.

Nature of the cutans

The orange brown (7.5YR 5/8) isotropic cutans that occur at the base of the Intermediate Beds raise separate and interesting problems. The material exists as a distinctive and sharply defined illuviation pedofeature whose distribution contributes to the orange tinge in these beds. A first problem is that of composition, and a second that of origins. As to composition it would appear from initial EDXRA that a mixed 1:1 Ca-ferric phosphate is involved. It is relatively uniform and mostly isotropic with distinctive shrinkage cracks and presumably was an amorphous colloid. There are birefringent streaks and although these might be interpreted as the development of a crystalline Ca-Fe-P phase, they could also arise from occluded hydrous micas which would account for the persistent traces of Si, Al and K that were detected. Further characterisation will first require physical concentration of the pure material from the deposit followed by full chemical analysis, XRDA, SAED, IRA, *etc.*: this is planned.

The source of this material is not difficult to identify. The overlying strata are rich in bones as reflected in their very high P contents (3 - 4% P as compared to 0.1% in the sediments above and below). The bone fragments are identifiable in thin section where a progressive transformation from fresh pale to amorphous orange brown material can be observed: this is the most likely source. The P and Ca may then have been translocated after release from hydroxyapatite (or dahlite) into ionic solution with subsequent readsorption onto "active" ferric hydrous oxides in the horizon below to give the Ca-Fe-P material analysed. However, in view of (i) the observed alteration of bone to orange material in the source beds, (ii) the narrow range of composition of the cutans and their possible incorporation of hydrous mica, and (iii) the lack of P in the matrix which would have resulted from diffusion, it seems more likely that a discrete Ca-Fe-P colloid was translocated.

Translocation appears to have occured as a single event, and to have been followed by an abrupt change to clay illuviation during a wet phase following deposition of later sediments. The conditions under which formation, translocation and deposition (flocculation) of such colloids might occur are difficult to define. At present the sediment column has a pH in the range 8.4 - 8.9, characteristic of $CaCO_3$ buffered systems and consistent with the presence of later stalagmitic deposits in the overlying beds, but pH may well have been lower immediately

following deposition of the bone rich beds. Further chemical and experimental studies will be needed to resolve this process.

There have been numerous studies reported on phosphate chemistry. These relate to both to fertiliser practices in soils (*e.g.* Lindsay *et al.*, 1989) and also to bone in archaeological contexts (*e.g.* Price, 1989), although the latter are concerned rather specifically with the diagenic changes in intact bone that are relevant to dating or to the interpretation of the individuals diet. The particular phenomenon of Ca-Fe-P translocation observed in this micromorphological study does not appear to have been recorded. Nevertheless, the same orange brown (7.5 YR 5/8) colloidal infilling of voids is, in hindsight, also familiar from the separate study of thin sections of sherds from cinerary urns. It is now intended to investigate these features by EDXRA to see whether they too comprise a Ca-Fe-P rich material, representing the last chemical vestiges of the original occupant of the urn. However, in the broader context of investigating archaeological deposits, it is clear that care must be taken to avoid the simplistic interpretation of colour in terms of only pedogenic ferric hydrous oxides which was originally made in this study.

ACKNOWLEDGEMENTS

REFERENCES

Ball, D.F., 1960. The Soils and Land Use of the District around Rhyland Denbigh. Soil Survey of England and Wales, Harpenden, Herts., U.K.

Bullock, P., 1985. The rôle of micromorphology in the study of Quaternary soil processes. In: J. Boardman (Editor), Soils and Quaternary Landscape Evolution. John Wiley and Sons, pp.45-68.

Bullock, P., Federoff, N., Jongerius, A., Stoops, G., Tursina, T. and Babel, U., 1985. Handbook for Soil Thin Section Description. Waine Research, Wolverhampton, U.K., 152 pp.

Clayden, B., 1970. The micromorphology of the ochreous B horizons of sesquioxidic brown earths developed in upland Britain. In: D.A. Osmond and P. Bullock (Editors), Micromorphological Techniques and Applications. Soil Survey Technical Monograph No.2, Rothamsted Experimental Station, Harpenden, U.K., pp. 53-67.

Collcutt, S.N., 1984. The sediments. In: H.S. Green (Editor), Pontnewydd Cave. A Lower Palaeolithic Hominid Site in Wales. The First Report. National Museum of Wales, Cardiff, pp. 31-76.

Green, H.S., 1984. Pontnewydd Cave. A Lower Palaeolithic Hominid site in Wales. The First Report. National Museum of Wales, Cardiff, 227 pp.

Green, H.S., Bevins, R.E., Bull, P.A., Currant, A.P., Debenham, N.C., Embleton, C., Ivanovich, M., Livingston, H., Rae, A.M., Schwarcz, H.P. and Stringer, C.B., 1989. Le site acheuéen de Grotte de Pontnewydd, Pays de Galles; géomorphologie, stratigraphie, chronologie, faune, hominidés fossiles, geologie et industrie lithique dans le context paléoélogiqueian. L'Anthropologie, 93: 3-19.

Jenkins, D.A., 1984. Sand and Clay Mineralogy. In: H.S. Green (Editor), Pontnewydd Cave. A Lower Palaeolithic Hominid site in Wales. The First Report. National Museum of Wales, Cardiff, pp. 181-185.

Jenkins, D.A., 1985. Chemical and mineralogical composition in the identification of palaeosols. In: J. Boardman (Editor), Soils and Quaternary Landscape Evolution. John Wiley and Sons, pp. 23-44.

Lindsay, W.L., Vlek, P.L.G. and Chien, S.H., 1977. Phosphate minerals. In: J.B. Dixon and S.B. Weed (Editors), Minerals in Soil Environments. 2nd ed. Soil Sci. Soc. Am., Madison, Wisconsin, U.S.A., pp. 1089-1130.

Lowe, J.J. and Walker, M.J.C., 1984. Reconstructing Quaternary Environments. Longman Scientific and Technical, Harlow, U.K., 389 pp.

Price, T.D., (Editor) 1989. The Chemistry of Prehistoric Human Bone. Cambridge University Press, Cambridge, 325 pp.

West, R.G., 1977. Pleistocene Geology and Biology. 2nd Edn. Longman, London and New York, 440 pp.

Wymer, J., 1968. Lower Palaeolithic Archaeology in Britain as Illustrated by the Thames Valley. John Baker, London, 429 pp.

This Page Intentionally Left Blank

Source materials, micromorphology, and the provenance of the storage jars from Roman Galilee

M. Wieder[1], D. Adan-Bayewitz[1] and F. Asaro[2]

[1]Bar-Ilan University, Ramat-Gan, Israel
[2]Lawrence Berkeley Laboratory, Berkeley, California, USA

ABSTRACT

Wieder, M., Adan-Bayewitz, D. and Asaro, F., 1994. Source materials, micromorphology, and the provenance of the storage jars from Roman Galilee. In: A.J. Ringrose-Voase and G.S. Humphreys (Editors), Soil Micromorphology: Studies in Management and Genesis. Proc. IX Int. Working Meeting on Soil Micromorphology, Townsville, Australia, July 1992. Developments in Soil Science 22, Elsevier, Amsterdam, pp. 307-316.

Identifying the local origins of common household pottery, an important objective in the study of archaeological ceramics, is one of the most elusive goals of pottery analysis. Chemical analysis has been used effectively for localizing origin when appropriate reference material, such as waste from pottery manufacture, is available. In most instances, however, such material is not available, and there is no indication, other than sheer quantity, of the provenance of the wide array of wares recovered from any one excavation. The goal of the present study was to characterize and determine the provenance of the common storage jars of Roman age from the Galilee and Golan. Analysis of the storage jars by neutron activation distinguished a number of distinct chemical compositional groups, but a specific provenance could be assigned to only two of those groups.

Micromorphological investigation of these storage jars showed, on the one hand, characteristics common to certain vessels, and, on the other, their distinguishing features. The source of the soil material used to make the jars was from different soil types, and the kinds and quantities of temper added were found to be related to the respective soil types. The largest amount of temper, of mostly calcareous material, was added to Grumusol type soils of the Galilee and Golan. A small amount of calcareous material was added to kaolinitic Terra Rossa soils, while both calcareous material and sand were added as temper for storage jars made from smectite-rich Terra Rossa and Grumusolic Terra Rossa soil material. Storage jars made from Rendzina soil types, in contrast, contained sufficient calcareous material, which served as natural temper. Identification of the soil material and the nature of the added temper in each case, enabled the assignment of a relatively limited geographical procurement area for each of the analyzed storage jars.

INTRODUCTION

In previous studies on common pottery of the Roman period from Galilee and Golan, micromorphological analysis indicated that local soil materials were used in their manufacture and the principal soil types used were identified. It was found that for certain pottery groups
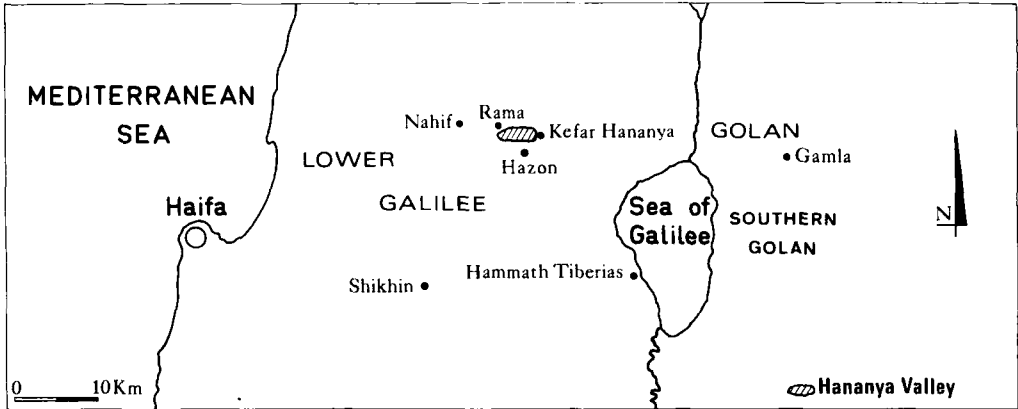
Fig. 1. Map showing regions and sites mentioned in text.

temper had been added while others lacked additional temper (Adan-Bayewitz and Wieder, 1992; Wieder and Adan-Bayewitz, 1993).

Subsequent examination of the various functional vessel types and of other Galilean and Golan pottery of the Roman period showed that the common storage jars of this region could be distinguished by a variety of temper-adding practices. These jars were therefore selected for further study, with a twofold purpose: firstly, to determine the soil types from which the storage jars were made and the relationship between these soils and the kind and amount of temper added and, secondly, to provide supplementary data to those obtained from chemical analysis by neutron activation on the provenance of the storage jars.

METHODS

Thin sections were prepared from thirteen storage jars recovered from six archaeological sites in the Galilee and the Golan (Nahif, Rama, Hazon, Gamla, Hammath Tiberias, and Shikhin, see Fig. 1; the identification of the Shikhin site is in Strange, *et al.*, in press) and analysis was performed in the same manner as for micromorphological analysis of soil materials. Although pottery preparation induced changes in the original microfabric of the soil materials, the method developed by Brewer (1964) could be effectively adapted for the description of the pottery samples, bearing in mind changes resulting from manufacturing processes. The soil groups were defined according to the Israel soil classification (Dan *et al.*, 1972) and the American soil taxonomy (Soil Survey Staff, 1975). Thin section descriptions are presented in Table 1.

The chemical compositions of the storage jars were determined using neutron activation analysis (Perlman and Asaro, 1969). The chromium abundance in Standard Pottery has been revised downward by 11.4% (Alvarez *et al.*, 1982, p. 887, Table 1), while the ytterbium abundance has been revised upward by 5.7% (Asaro *et al.*, in press). Cr and Yb abundances obtained at The Hebrew University and the Lawrence Berkeley Laboratory before the corrections have been modified accordingly.

Table 1

Thin-section description of representative storage jar samples.

Sample	Plasma characteristics	Skeleton grains	Plasmic fabric	Voids	Temper	Related distribution (%)	Other features
378	grey	Qs (F) P and H (R); C (C)	isotic	Vs; Pn	chalky material	P =50; S = 20 V = 10; T = 20	
327	grey	Qs (F) P and H (R)	isotic	Vs; Pn	calcareous material of fine crystals	P =50; S = 20 V = 10; T = 20	
547	black	Qs (F)	isotic	VES	chalky material	P = 30-35; S+T=5-10; V=60	Diag.
535	reddish brown homogeneneous	A, I, P, and B (O to C); QS (R)	asepic	Vs to VS	calcareous material	P = 30; S = 10 V = 10; T = 50	
33	red and homogeneous	Qs (F)	asepic	Vs; VEs	calcareous material	P = 50; S = 20-25 V = 20-25; T = 5	
52	red and homogeneous	Qs (F)	asepic	Vs; VEs	small amount of calcareous material	P = 52; S = 20 V = 25; T = 1-3	Ir. Nod.
305	red homogeneous	Qs (F) QS (C)	asepic	Ves; Pn	chalky material	P = 55; S = 10 V = 15; T = 20	Ill.
307	red homogeneous	Qs (F) QS (O)	asepic to mosepic	Vs; Pn	chalky material	P = 50; S = 5-10 V = 25; T = 15-20	Ill.
310	brown homogeneous	Qs (F) QS (F)	asepic	Vs to VS; Pn to PW	calcareous material	P = 50; S = 30 V = 15; T = 3-5	S. Nod.
311	brown homogeneous	Qs (F) QS (O)	asepic	Vs; Pn	calcareous material	P = 50; S = 15 V = 10; T = 25	S. Nod.
306	very dark brown (edges), dark red (core)	Qs (F) QS (O)	isotic (edges) asepic to isotic (core)	Vs; VEs; Pn	calcareous material	P = 50; S = 20 V = 20; T = 10	S. Nod.
309	dark brown to dark red	Qs (F) QS (O)	asepic to isotic	Vs	calcareous material	P = 50; S = 15 V=25-30;T=5-10	S. Nod.
34	red (edges), dark grey (core)	Qs (F)	calci-asepic	Vs; Pn	natural calcareous material	P= 40; S = 25-30 V= 10; T = 20-25 (natural)	

Legend:

Skeleton grains: Qs = quartz grains of silt size; QS = quartz grains of sand size; P = plagioclase; I = iddingsite; H = hornblende; A = augite; C = calcite; B = basalt fragments. F = frequent; C = common; O = occasional; R = rare

Voids: Pn = short narrow planes; PW = wide planes; Vs = small vughs; VS = large vughs; VEs = small vesicles; VES = large vesicles.

Related distribution: P = plasma; S = skeleton; V = voids; T = temper.

Other features: Ill. = clay illuviation remnants; S. Nod. = brown or dark brown soil nodules with silt grain inclusions; Diag. = diagenetic features of wavy extinction; Ir. Nod. = pedogenic iron nodule remnants.

Table 2
Compositional and micromorphological grouping of sampled pieces

Sample No.	Site Recovered	Chemical Compositional Group	Micromorphological Group
378	Gamla	Shikhin	(1) Grumusol
327	Hammath Tiberias	Shikhin	(1) Grumusol
547	Shikhin	Shikhin	(1) Grumusol
535	Gamla	Gamla storage jars	(2) basalt-derivedGrumusol
33	Rama	Storage jar 1	(3a) kaolinitic Terra Rossa
52	Hazon	Storage jar 1	(3a) kaolinitic Terra Rossa
305	Nahif	Nahif	(3b) Galilean Terra Rossa
307	Nahif	Nahif	(3b) Galilean Terra Rossa
310	Nahif	Nahif	(4) Grumusolic Terra Rossa
311	Nahif	Nahif	(4) Grumusolic Terra
306	Nahif	Nahif	(4) Grumusolic Terra Rossa
309	Nahif	Nahif	(4) Grumusolic Terra Rossa
34	Rama	Storage jar 1	(5) Rendzina

CHEMICAL COMPOSITIONAL GROUPS

Based on compositional data, the thirteen storage jars studied by micromorphological analysis were assigned to four distinct chemical compositional groups, called Shikhin, Nahif, Storage jar 1, and Gamla storage jars (see Table 2). Mean abundances for 18 elements of each of the four compositional groups are given in Table 3, Columns 1 and 3-5. The data for only a representative part of the Shikhin chemical compositional group, Shikhin 1, is shown in Column 1 (see Adan-Bayewitz and Perlman, 1990). Chemical elements that distinguish these groups include Cr, Hf, La, Lu, Th, U, Yb and the abundance values for additional chemical elements obtained by X-ray fluorescence by Robert D. Giauque, Lawrence Berkeley Laboratory further distinguish the Shikhin and Nahif groups.

The abundances of individual pieces in each compositional group, together with a statistical treatment of the data and a typological and chronological discussion of the jars, will be presented in separate studies.

REFERENCE MATERIAL AND PROVENANCE

Chemical analysis can be effectively employed for determining pottery provenance when appropriate reference material such as waste from pottery manufacture (*i.e.* ceramic "wasters") is available. When the chemical composition of the pottery matches that of the reference material it shows that the pottery was made from the same raw material and suggests a locale of manufacture for the vessels. In some cases, a match in chemical composition with reference material has made it possible to assign a site-specific manufacturing provenance for certain ceramic wares (Adan-Bayewitz and Perlman, 1985; 1990; Adan-Bayewitz, 1993). For most wares, however, adequate reference material is not available and there is no indication, other than limited information on the distribution of the vessel types, of the provenance of the wide array of pottery recovered from any one excavation.

Table 3*
Element abundances of storage jar compositional groups and storage jar waster

	Shikhin1 group abundances 38 samples		Storage jar waster ADAN-547 1 sample		Nahif group 9 samples		Storage jar1 group 3 samples		Gamla storage jar group 2 samples	
Ca%	8.0	±2.0	-- --		10.2	±1.4	7.1	±0.8	18.0	±2.5
Ce	107.1	±7.1	99.5	±1.0	109.4	±7.8	117.1	±5.2	40.3	±2.8
Co	29.6	±4.5	27.0	± .3	26.7	±2.0	32.1	±2.2	21.8	±2.1
Cr	188.6	±11.8	172.0	±1.7	202.0	±9.5	232.9	±11.0	105.3	±1.1
Cs	2.67	±0.28	2.85	± .06	3.24	±0.35	3.23	±0.30	1.07	±0.07
Eu	2.07	±0.08	2.03	± .03	2.38	±0.19	2.56	±0.05	1.11	±0.01
Fe%	5.70	±0.21	5.60	± .06	6.19	±0.29	6.35	±0.21	4.07	±0.04
Hf	11.37	±0.87	11.07	± .15	8.65	±0.74	11.17	±0.60	3.49	±0.32
La	45.0	±1.9	44.6	± .5	51.4	±3.2	58.2	±1.1	20.1	±0.4
Lu	0.63	±0.03	0.62	± .02	0.68	±0.05	0.85	±0.04	0.273	±.004
Na%	0.32	±0.07	0.288	±.006	0.25	±0.06	0.24	±0.03	0.32	±0.08
Sc	18.78	±0.63	18.38	± .18	20.86	±1.25	21.66	±0.44	12.11	±0.30
Sm	8.35	±0.32	8.12	± .08	9.36	±0.69	10.19	±0.24	3.81	±0.04
Ta	1.75	±0.09	1.70	± .04	1.83	±0.11	1.90	±0.05	0.71	±0.02
Th	10.90	±0.41	10.84	± .11	11.40	±0.60	12.06	±0.28	3.66	±0.05
Ti%	0.82	±0.05	-- --		0.82	±0.07	0.79	±0.04	0.53	±0.03
U	3.91	±0.57	3.47	± .05	5.87	±0.77	5.97	±0.75	4.53	±1.46
Yb	4.59	±0.26	4.33	± .12	4.93	±0.36	6.11	±0.05	1.96	±0.08

*All elements are in units of parts-per-million unless indicated by the % sign. Entries after ± signs are measurement errors (one sigma value) for 1 sample or standard deviations for multiple samples. Column 1 contains selected pottery pieces from 15 sites in Galilee and the Golan. Column 2 is a storage jar waster recovered at Shikhin. Columns 3 and 4 each include selected storage jars from two Galilean sites, while column 5 contains storage jars from Gamla.

In the present study, the available reference material made it possible to assign a site-specific provenance to one of the compositional groups (at Shikhin, see Fig. 1), and to suggest a likely provenance for another (at Nahif). Reference material for the Shikhin group included kiln wasters recovered at Shikhin and pottery vessels of limited distribution. The chemical composition of one of these wasters, the warped handle of a storage jar, is given in Table 3, Column 2. Comparison of these data with those of Shikhin 1 (Table 3, Column 1) shows a close match. Additional evidence for the site-specific provenance of this group is provided in rabbinic texts of the Roman period (Adan-Bayewitz and Perlman, 1990). A provenance at Nahif could be suggested for the Nahif group, whose composition is shown in Column 3, on the following evidence. Two pottery kilns were unearthed in archaeological excavations at Nahif which shows that pottery was made at that site. Second, storage jars of distinct form and decoration were the most common single vessel type recovered in the excavations of these

kilns (Vitto, 1986); and all six analyzed storage jars of this type from Nahif match in chemical composition.

For two other compositional groups, (*i.e.* Storage jar 1 and the Gamla storage jars), reference material was not available and the only indication of the source of this pottery was limited evidence on the distribution of the vessel types, the three pieces of Storage jar 1 were all found in the same vicinity (Table 2), and the Gamla storage jars are the most common storage vessels in early Roman contexts at that site. It was thought that identification of the soil materials and the nature of the temper added for the manufacture of each of these wares might enable the assignment of a relatively limited procurement area for the raw materials used to make these two compositional groups, and also shed further light on the manufacture of the Shikhin and Nahif groups.

MICROMORPHOLOGY

The thirteen analyzed storage jars could be assigned to five distinct micromorphological groups based on the soil types from which the vessels were made.

1. The Grumusol group (Vertisols) includes samples 327, 378 and 547. This soil type commonly occurs in the valleys of Galilee. The intensive shrinking and swelling of this soil material requires the addition of a large amount of temper to make it more suitable for pottery making. This temper was added in the form of calcareous material of Eocene chalky origin which occurs in the vicinity of Shikhin (Sample 378, Fig. 2a), or Miocene lacustrine calcareous material mixed with chalk, occurring in the eastern Lower Galilee (sample 327). Sample 547, a storage jar waster, was subjected to very high temperatures resulting in: (a) numerous very large vesicles, and (b) zones with strongly oriented clay fabric similar to sediments subjected to diagenesis; the oriented clay shows striated orientation and wavy patterns.

2. The basalt-derived Grumusol group (Chromoxererts) includes sample 535. This soil type occurs in the southern Golan. A very large amount of calcareous temper (*i.e.* about 50%) was added for the manufacture of this group despite the many basalt fragments found in the soil material which act as natural temper (Fig. 2b). The combination of the smectite clay mineral with a large amount of iron oxides probably necessitated large amounts of temper. It is noteworthy that no temper was added in the manufacture of cooking ware from basalt-derived soil material (Adan-Bayewitz and Wieder, 1992).

3. The Terra-Rossa group (Rhodoxeralfs; Xerochrepts). Most of the moderately deep soils that developed on hard limestone or on dolomitic limestone in the Galilee are Terra-Rossa soils. These soils contain a large amount of silt-size grains from airborne dust. The microfabrics of these soils show some variation according to depth and lithology and these can be considered as subgroups. On hard limestone red Terra-Rossa soils develop with kaolinite as the dominant clay mineral, while on dolomitic limestone reddish brown Terra Rossa soils develop with smectite as the dominant clay mineral (Koyumdjisky, 1972). Ceramic manufacture depends much on the occurrence and ratio of these two minerals.

Samples 33 and 52 represent the former case (kaolinitic Terra Rossa; micromorphological group 3a), with a very small amount of added calcareous temper. Near Kefar Hananya in the Hananya Valley a rare Lower Cretaceous outcrop occurs. The limestone residue of this geological formation releases the kaolinite found in this soil material. It is noteworthy that
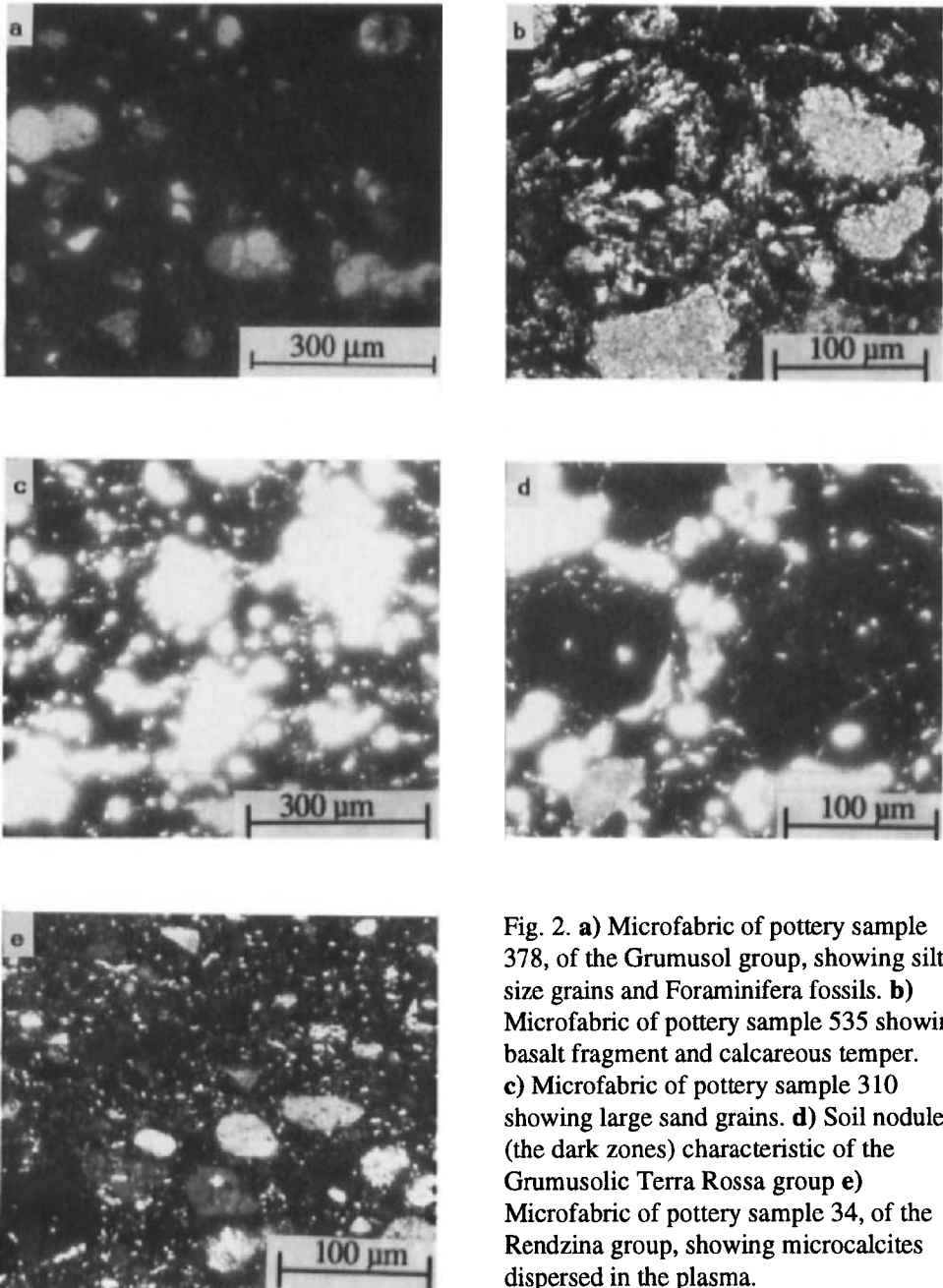
Fig. 2. a) Microfabric of pottery sample 378, of the Grumusol group, showing silt-size grains and Foraminifera fossils. b) Microfabric of pottery sample 535 showing basalt fragment and calcareous temper. c) Microfabric of pottery sample 310 showing large sand grains. d) Soil nodules (the dark zones) characteristic of the Grumusolic Terra Rossa group e) Microfabric of pottery sample 34, of the Rendzina group, showing microcalcites dispersed in the plasma.

cooking vessels prepared from soil material from the vicinity of Kefar Hananya do not contain added temper (Adan-Bayewitz and Wieder, 1992).
Samples 305 and 307 represent the latter case (smectite-rich Galilean Terra Rossa;

micromorphological group 3b), with a larger amount of added temper, including both calcareous material and a small amount of sand from the central coast of Israel. Smectite-rich Terra Rossa soils commonly occur throughout the Galilee.

4. Grumusolic Terra Rossa group (Vertic Rhodoxeralfs). These are deeper soils occurring on the lower part of slopes. The high deposition rate of the soil material has prevented the development of typical Grumusol soil. The smectite clay mineral is dominant, however, and this soil material therefore requires added temper for pottery making. Both calcareous material and sand were added to this soil for the manufacture of storage jars. Samples 310 and 311 are characteristic of this group: Sample 310 contains less calcareous material but more sand (Fig. 2c) while sample 311 contains more calcareous material and less sand. Furthermore, soil material appears as small nodules that contain only silt-size grains (Fig. 2d), was also added to the material used to make this group. This soil, apparently added to improve the quality of the raw material, may have come from the vicinity of the kaolinite-rich Lower Cretaceous outcrop mentioned above. Samples 306 and 309 that are classified with this group also contain such nodules.

The microfabric of the pottery specimens to which calcareous material and sand were added is similar to the Brown Grumusolic soil type that occurs in the semiarid area of southern Israel. Grumusols of the Sharon region along the central sea coast of Israel (about 45 km southwest of Shikhin) to which a small amount of calcareous material is added are quite similar as well. Distinguishing between these different materials presents a considerable challenge to the soil micromorphologist for it is necessary to become familiar with all the soils of the area when evaluating the relationship between ancient pottery and soil materials. The microfabric of pottery made from Terra Rossa soil material includes very large limestone fragments with opaline silica inclusions as characteristic features of this soil material. Brown Grumusolic soil material, on the other hand, does not include limestone fragments. The sand grains in the pottery, however, are similar to sand grains from the central coast of Israel. It is likely, therefore, that the small amount of added sand was brought to the Galilee.

5. The Rendzina group (Rendolls). Characteristic of the Rendzina soils of Israel are fine microcalcite grains dispersed within the plasmic fabric (Fig. 2e). This soil is suitable for pottery making providing that it does not contain too much calcareous material. The carbonate in the soil material acts as natural temper. Sample 34 represents this group. The Lower Cretaceous outcrop in the Hananya Valley is partly soft limestone upon which Rendzina type soil locally appears. These soils are very similar to Terra Rossa soils developed on hard limestone of the Lower Cretaceous, the two differing mainly in calcareous material content.

THE RELATIONSHIP BETWEEN SOIL TYPES AND TEMPER

The amount of temper added to soil material for the manufacture of the Galilean and Golan storage jars of the Roman period was found to depend on the properties of the individual soil material. The greatest amount of temper, in the form of calcareous material, was added to the Grumusol soil types particularly Grumusols developed on basalt. Storage jars made from Terra Rossa soils had less temper when kaolinite was present in the soil and more temper when smectite was the dominant clay mineral. Vessels made from Grumusolic Terra Rossa and smectite-rich Terra Rossa soils contained two kinds of added temper, sand as well as

calcareous material. Both types of temper were apparently needed and were added in varying proportions. Finally, additional temper was not needed in storage jar manufacture from calcareous Rendzina soils.

The common cooking pots of this region and period, in contrast with the storage jars, do not contain added temper; the rock fragments and silt-size quartz grains naturally present in the soils used to made these cooking wares serve as natural temper, preventing cracking from shrinkage, and additional temper was not needed (Adan-Bayewitz and Wieder, 1992). Differences in the functional requirements of these wares, and the fact that Galilean and Golan cooking and storage wares of known provenance were made by different manufacturers using different raw materials (Adan-Bayewitz and Perlman, 1990), may help to explain these different tempering practices. This topic warrants further study, however.

It should also be noted that the intended primary function of the storage jar may have influenced tempering practices. Jars used as containers for olive oil, for example, may have required a different kind of temper than those used for wine, while a different fabric, perhaps requiring little or no temper, may have been adequate for solid foodstuff such as grains and legumes (Landgraf, 1980, p. 80). Storage jars were often reused, however, so the relationship between the fabric and the function of these vessels is not easily investigated, even when the contents of a jar are preserved or are otherwise attestable (Adan-Bayewitz and Perlman, 1990, p. 171).

THE PROVENANCE OF THE STORAGE JARS

Identification of the soil types used to make the Gamla storage jar and Storage jar 1 compositional groups makes it possible to suggest raw material procurement areas for these two pottery compositional groups. The basalt-derived Grumusol soil material (micromorphological group 2) from which the Gamla storage jars were made occurs in the southern Golan, in the vicinity of Gamla, while the calcareous temper added in large quantity to this soil material is also available in the same area. It should be noted that the large quantity of added calcareous material dilutes considerably the abundances of all measured chemical elements (except for calcium) in the Gamla storage jar group.

The three vessels of the Storage jar 1 compositional group were made from kaolinitic Terra Rossa (micromorphological group 3a) or Rendzina (micromorphological group 5), which are two very similar soils that differ mainly in calcareous content. These two similar materials cannot be separated by neutron activation analysis. A source, in the vicinity of the Lower Cretaceous outcrop near Kefar Hananya, can be suggested for both soil types.

Micromorphological analysis has also shed light on the ceramic resources used to make the Shikhin and Nahif pottery compositional groups. Grumusol soils, occurring in the valleys of the Galilee, along with added calcareous temper, also locally available, served as raw material for the Shikhin group.

The vessels of the Nahif compositional group were all made from the same parent material, Galilean Terra Rossa (micromorphological group 3b) and Grumusolic Terra Rossa (micromorphological group 4), both of which contain smectite as the dominant clay mineral. Additional soil material added to some of the Nahif jars may have come from the vicinity of the Lower Cretaceous outcrop near Kefar Hananya. Micromorphological analysis has shown that all storage jars of this compositional group contain as added temper both locally available calcareous material and a small amount (about 1 - 5%, except for sample 310 which contains

about 15%) of quartz sand from the central coast. Both of these added materials are essentially sterile to neutron activation analysis. This practice of adding marine sand as temper was found to distinguish the Nahif compositional group from all other analyzed storage jar compositional groups of the Galilee and Golan. This evidence from thin-section analysis, therefore, further supports the archaeological and compositional evidence for a distinct manufacturing center for this group.

ACKNOWLEDGEMENTS

REFERENCES

Adan-Bayewitz, D., 1993. Common Pottery in Roman Galilee: A Study of Local Trade. Bar-Ilan University Press, Ramat-Gan, 304 pp.

Adan-Bayewitz, D. and Perlman, I., 1985. Local pottery provenance studies: A role for clay analysis. Archaeometry, 27: 203-217.

Adan-Bayewitz, D. and Perlman, I., 1990. The local trade of Sepphoris in the Roman period. Israel Exploration Journal, 40: 153-172.

Adan-Bayewitz, D. and Wieder, M., 1992. Ceramics from Roman Galilee: A comparison of several techniques for fabric characterization. Journal of Field Archaeology, 19: 189-205.

Alvarez, W., Asaro, F., Michel, H.V. and Alvarez, L.W., 1982. Iridium anomaly approximately synchronous with terminal Eocene extinctions. Science, 216: 886-888.

Asaro, F., Salazar, E., Michel, H.V., Burger, R.L. and Stross, F.H. Equadorian obsidian sources used for artifact production and methods for provenance assignments. Latin American Antiquity, [in press].

Brewer, R., 1964. Fabric and Mineral Analysis of Soils. John Wiley and Sons, New York,

Dan, J., Yaalon, D.H., Koyumdjisky, H., and Raz, Z., 1972. The Soil Association Map of Israel (1:1,000,000). Israel Journal of Earth-Sciences, 21: 29-49.

Koyumdjisky, H. 1972. Behavior of magnesium during weathering of carbonate and silica rocks and its influence on soil formation in Israel. Ph.D. dissertation, The Hebrew University, Jerusalem. [in Hebrew with English summary].

Landgraf, J. 1980. Keisan's Byzantine pottery. In: J. Briend and J-.B. Humbert (Editors), Tell Keisan (1971-1976) une cité phénicienne en Gallilee. Paris, pp. 51-99.

Perlman, I. and Asaro, F., 1969. Pottery analysis by neutron activation.Archaeometry,11:21-52.

Soil Survey Staff, 1975. Soil Taxonomy. U.S. Dept. Agric. Handb. 436, U.S. Gov. Printing Office, Washington, D.C., 754 pp.

Strange, J.F., Groh, D.E. and Longstaff, T.R.W. University of South Florida excavations at Sepphoris: The location and identification of ancient Shikhin. Israel Explor. J., (in press).

Vitto, F., 1986. A potter's kiln at Nahif. In: M. Yedaya (Editor), The Western Galilee Antiquities. Misrad HaBitahon, Tel-Aviv, pp. 451-456 (in Hebrew).

Wieder, M. and Adan-Bayewitz, D., 1993. Thin-section analysis. In: D. Adan-Bayewitz, (Editor), Common Pottery in Roman Galilee: A Study of Local Trade. Bar-Ilan University Press, Ramat-Gan, pp. 193-200.

Soil thin section description: higher levels of classification of microfabrics as a tool for interpretation[*]

G. Stoops

Laboratorium voor Mineralogie, Petrografie en Micropedologie, Universiteit Gent, Belgium

ABSTRACT

Stoops, G., 1994. Soil thin section description: higher levels of classification of microfabrics as a tool for interpretation. In: A.J. Ringrose-Voase and G.S. Humphreys (Editors), Soil Micromorphology: Studies in Management and Genesis. Proc. IX Int. Working Meeting on Soil Micromorphology, Townsville, Australia, July 1992. Developments in Soil Science 22, Elsevier, Amsterdam, pp. 317-325.

The current internationally accepted systematic terminologies for soil thin section descriptions are restricted to the lowest fabric members. Comparing and evaluating these descriptions is difficult and time consuming. Therefore a need is felt for a classification of higher levels of soil fabrics. In this paper an attempt is made to develop a higher level classification.

The nature of the constituents, comprising both the mineralogical composition (*e.g.* a granitoidic mineral association) and its geological origin (weathering residuum, alluvium) is the first of the three basic criteria used. A second is grain size distribution (as evaluated in thin sections) which is related to parent material, weathering stage, classification and fertility of the soil. Similar classes are necessary for organic material when dominant. The third, but most important criterium are the features (including both pedofeatures and fabrics of the groundmass), grouped in significant natural combinations, called "formations". Features which occur as an overprint on those of the main genetic processes form a "syndrome". The relative importance of these criteria depends upon the type of soil material. Additional characteristics are expressed as "phases". Based on these criteria types of soil material are named using specific composed terms.

It is not possible to classify all soil materials in a simple system, but it is believed that the most important and most frequent materials can be easily characterized this way.

INTRODUCTION

During the short history of soil micromorphology, two different ways of thin section description have been promoted: a morphoanalytical and a morphogenetic (Stoops and Eswaran, 1986).

The morphogenetic system of Kubiëna (1948, 1953) is more synthetic than analytic for it is based upon some specific aspects of the groundmass and other selected features. In this system a name is given to the whole fabric (*e.g.* Rotlehm, Braunlehm, Braunerde, Iwatoka Rotlehm,

---

Moder, Mor). This name reflects, in the opinion of Kubiëna, the position of the material in his evolutionary genetic system. The system, therefore, can be applied only to a limited number of soil materials described in the works of Kubiëna (mainly temperate and some tropical soils, but not arid soils). The use of these terms directly implies a unique genetic interpretation, which may or may not correspond to the ideas of the user and to reality. For these reasons, the system has not been used since the end of the sixties.

In a morphoanalytical system, in contrast, the fabric of the soil is analyzed, starting from its lowest level, *i.e.* dealing with the basic components of the soil such as mineral grains, clay matrix, plant remains, nodules and coatings. Examples of such systems are those of Kubiëna (1938), Brewer (1964), Bullock *et al.* (1985), FitzPatrick (1984) and partially Brewer and Sleeman (1988). A description made according to these systems gives a simple enumeration of morphological characteristics that appear unrelated in many cases. Such descriptions are time consuming and frustrating, both to prepare and to read, and therefore lessen the impact of micromorphology in soil characterization and classification. These systems, however, have been an essential step in the development of more synthetic micromorphological systems and will remain necessary for a complete fabric analysis of known materials, and for the first analysis of new materials.

As mentioned before, the existing morphoanalytical systems deal with the *lowest level* of classification of soil fabrics and were most useful for genetic purposes (including the study of the impact of cultivation and soil management on fabric). They are also useful in providing insight into the diversity of soil materials and into the relation between some specific features. It is now an opportune time to establish *higher levels* of classification, thus allowing soil scientists to characterize the essential micromorphological aspects of a soil thin section by a few terms, rather than by lengthy description. This can be compared to the difference between describing a profile horizon by horizon, or by giving it a name according to an accepted classification system. Care should be taken, however, to make such a micromorphological classification morphosynthetic and not morphogenetic, although genetic considerations may be used in elaborating it. A first attempt to such a system was proposed by Brewer (1964) in his *basic structure*, but it did not become popular as it consists merely of an accumulation of terms of the lowest level of classification (*e.g.* channeled agglomeroplasmic s-matrix). For the same reason, and because of the complicated artificial terminology, a new attempt (Brewer, 1983 and Brewer and Sleeman, 1988) has met with limited success.

In this paper an attempt is made to propose principles for a higher level classification of soil microfabrics and a few examples are used to illustrate this. The units for this type of classification should not be an enumeration of observations, rather it should represent the concept of "Gestalt" (*i.e.* the configuration of phenomena so integrated as to constitute a functional unit with properties not derived from the summation of its parts of that soil material). It should be emphasized, however, that this is only a first approximation, which probably will be developed and refined later. The system has to be elaborated separately for the different soil materials that need to be distinguished and it should be sufficiently flexible to include new data. It, therefore, cannot be comprehensive from the beginning. The main objective of this paper is to open a discussion on this topic. All names used in the examples are therefore tentative.

Apart from a function in communication, the system is also a tool to assist observation for it creates the need to recognize systematically the relationship between different features and

other fabric elements, not only on the scale of a thin section, but on the scale of a worldwide
variety of soils.

CRITERIA OF CLASSIFICATION

Although micromorphology as such deals only with morphology, including fabric, it is clear
that composition plays an important role in distinguishing different soil materials also, *e.g.* in
the case of a calcic or gypsic horizon. Therefore this classification should be considered as
micropedological, rather than purely micromorphological.

According to the experience gathered at the International Training Centre for Post Graduate
Soil Scientists in Gent (Belgium), three factors dominate the micropedological aspects of a
soil: *grain size distribution*, *nature of the constituents* and *features* (including both
pedofeatures and fabrics of the groundmass). Which one is dominant depends upon the type of
soil material. This situation is comparable to that of Soil Taxonomy where some soils are
grouped according to climate (Aridisols), others according to diagnostic horizons (Alfisols),
others according to the epipedon (Mollisols) and still others according to parent material
(Andisols).

Grain size distribution

The importance of grain size distribution in soil fabric has been emphasized by Eswaran and
Banos (1976) in their paper on related distributions. According to our experience the
micromorphological expression of an argillic horizon will be quite different in a sand than in
loam or clay material. The same is true for the spodic horizon, which does not occur in clays,
and the oxic horizon, which does not exist as such in sands.

Essentially five types of grain size distribution should be taken into account: gravel, sand,
silt, clay and loam. An additional one reflecting the reality of specific soils can be added also
viz. "loess".

Gravely, sandy, silty and loess-like materials are characterized by the presence of a
microscopically visible, inherent microporosity, resulting from the packing of the grains (simple
packing pores), which makes them different from the other materials (loam, clay), in which
such a porosity does not exist.

The large inherent porosity in coarse sand and gravel may give rise to special fabrics. The
introduction of a gravel class is necessary because it quite often contains specific features, such
as gypsum or calcite pendants, or clay cappings.

Estimation of textural classes in thin sections involves identification of the grain size,
frequency and sorting. A material will be considered as sandy or silty when the majority of the
grains is respectively larger or smaller than 50 μm, and simple packing voids are preserved.
The term clay refers to materials mainly composed of particles not recognizable as individuals
in thin sections; packing pores are not visible. Loam is used to indicate mixtures of sand, silt
and clay with no simple packing pores visible. The term loess will be used here to indicate a
very well sorted material of coarse silt or fine sand size, with simple packing pores, either of
eolian origin or not. For the gravel it is of primary importance that packing pores should not be
filled by finer particles and in the latter case terms such as gravely sand, gravely loam *etc.*
should be used. Special textural classes, for micromorphological uses only, are suggested in
Fig. 1. This may not be completely satisfying to all workers but a more suitable proposal can
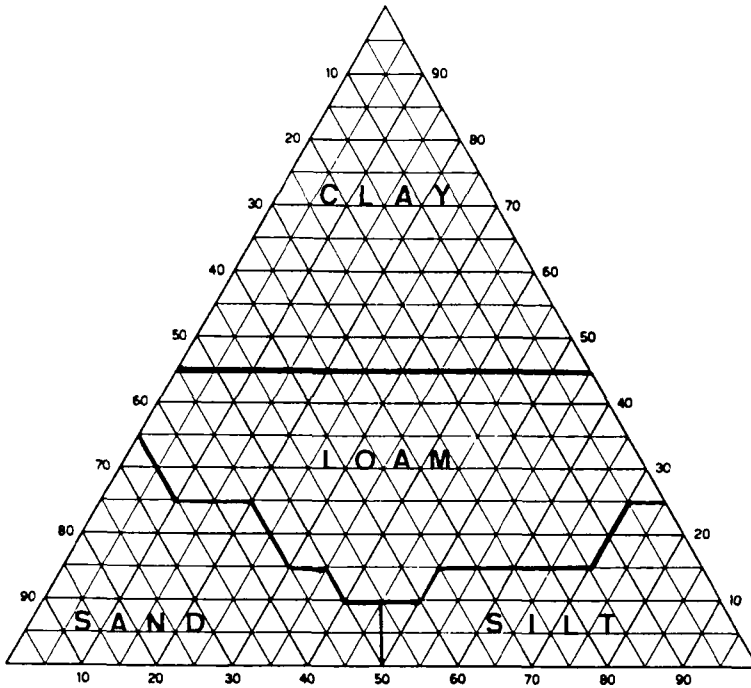
Fig. 1. Proposed textural classes.

only be obtained after a systematic, and probably experimental study of the relationship between textural classes and microfabrics.

Tentatively, sand, silt and clay could be delimited according to the U.S.D.A. triangular textural diagram: "sand" would correspond then to sand, loamy sand and sandy loam, "silt" to silt and silt loam, and "clay" to clay, all the other classes being grouped as "loam". According to the I.S.S.S. system "sand" would correspond to sand, loam sand, sand loam and loam, "silt" to silty loam and silty clay loam and "clay" to heavy clay.

The grain size classes refer essentially to the actual groundmass of the soil. For example, a soil material will be called sandy, even if all packing voids are filled by illuvial clay, newly formed calcite or amorphous organic material. This means that pedofeatures are not taken into consideration and this approach implies the adoption of a genetic interpretation from the beginning. Textural classes as described will therefore, in many cases, not always correspond to the textural classes determined on bulk samples by routine methods.

Nature of the constituents

This item deals essentially with the nature of the groundmass, especially that of the coarse material. Several criteria have to be taken into consideration: the mineralogical nature of the constituents, their relationship to rock types and their origin (*e.g.* eluvium of magmatic or metamorphic rocks, colluvium or sedimentary material).

As far as mineral grains and rock fragments are considered, the following scheme is proposed :

Monomineralic: The name of the mineral is given in its adjective form such as quartzitic, calcitic, vitric. Example: quartzitic sand in the E horizon of a Podzol, vitric silt in an Andisol.

Mineral associations: In weathering profiles, or colluvia, or alluvia derived from a single geological material, specific mineral associations may be observed: *e.g.* granitoidic, (quartz, alkali-feldspar, biotite and/or muscovite, a few grains of zircon and tourmaline). Other examples are gneissic (similar to granitoidic, except for the type of quartz and fabric), dioritoidic, gabbroidic, phyllitic, andesitic (see textbooks of petrography). Combinations of associations are also possible, *e.g.* granitoidic-vitric. A distinction between grains derived from metamorphic and from plutonic rocks is not always easy, nor relevant. The names of large groups of plutonic rocks (*e.g.* granitoid) seem therefore the most suitable to use (terms according to Streckeisen, 1976).

Polymictic: a mixture of minerals of different origin. Within this class it is useful to distinguish between a calcareous and a non-calcareous subclass, based on the presence of carbonaceous minerals in the dominant size fraction.

Three classes of weathering are proposed: (i) *strongly weathered* when only quartz and more resistant minerals are preserved; (ii) *moderately weathered* when the most unstable minerals (*e.g.* calcite) have disappeared, the metastable minerals show evidence of weathering; and (iii) *fresh* when minerals show practically no chemical weathering.

The origin of the material may result from *in situ* weathering, indicated by the prefix *orthic* (*e.g.* moderately weathered orthic dioritoidic sand, *i.e.* a sand composed of quartz, partly weathered plagioclases and amphiboles or pyroxenes), or transported, indicated by the prefix *anorthic* (*e.g.* a fresh anorthic granitoidic sand means a sand composed of unweathered but transported grains of quartz, alkali-feldspar, biotite and/or muscovite).

In a similar way different types of organic components can be distinguished on the basis of structure and degree of humification.

Features

The concept of features, as used here, includes both pedofeatures and fabrics of the groundmass. In principle, these ideas can be expressed in two ways; single features or significant combinations of features. In order to reduce the number of variables in descriptions the latter has been adopted for this is also closer to the aim of expressing the "Gestalt" of the material. Such a combination of features is called a "formation" (*i.e.* a persistent body of soil with a common genetic background). Formations are defined both by a combination of features present, and by their degree of development. In many cases, the latter can be indicated by the prefix eo- (early, *i.e.* weakly developed), no prefix (normal development), hyper- (strongly developed) and holo- (the soil material consists practically only of the feature or combination of features). Quantitative limits have yet to be elaborated. Two examples help to illustrate this. In the first an eocalcic horizon represents the first stage of pedogenic calcite precipitation in a soil material - a loamy material with calcite hypocoatings and diffuse impregnative nodules are observed and the soil material mostly has a channel or vughy or weakly pedal microstructure. The second example is a beta-argillic formation (observed in beta-horizons, Bartelli and Odell,

1960) which has, typically, a channel microstructure, important coatings of limpid strongly oriented fine clay, that is undisturbed by stress and locally has more organic-rich illuviations.

Whereas the type and degree of development of features determine the formation, their specific characteristics determine the *subformations*. For example, an eogypsic formation in loamy materials comprises the early stages of gypsum deposition in a soil which is characterized by gypsum infillings in voids (mainly channels). The material has mostly a vughy, channelled or weakly developed pedal structure. Due to biological activity some of the infilling material may be mixed with the groundmass since isolated gypsum crystals may be observed in the groundmass. The morphology of the infillings determines the subformation such as lenticular (loose, lenticular gypsum crystals) or petric (compact xenotopic gypsum infillings) (Stoops and Poch, 1994).

For each formation and subformation a typic description has to be made of the typic features or combinations of features; atypic features, such as the presence of biocalcite in an eogypsic horizon, are not part of its definition. If observed frequently, an additional subformation could be made.

Features which occur as an overprint on those of the main genetic processes are called a *syndrome*. This term was used by Buol and Eswaran (1978), but in the meaning comparable to "formations" in this paper. A common example of a syndrome is the hydromorphic one such as an *argillic formation* (coatings and infillings of strongly oriented fine clay) with an *eoaquic syndrome* which means that some manganese hypocoatings and diffuse nodules are superposed on the fabric, and that the chroma of the groundmass is not affected by reduction. Another example is that of the *holoargillic* formation (all pores filled with illuvial clay) where a *vertic syndrome* is quite often observed, shown by the stress deformation of the coatings and infillings, and a well developed striated b-fabric in the groundmass.

When the relative importance of two or more superposed processes cannot be separated clearly, different authors will provide different names, depending on which association of features is considered as determining the formation and which belongs to the syndrome. In such cases the choice will be influenced by the experience and interest of the describer. One must be aware that only a perception of reality is provided. Later it may be necessary to add a key (*e.g.* argillic keys out before hydromorphic).

Other characteristics

This new system makes it possible to express, in a relatively short way, a number of micromorphological aspects of the soil. The system can be extended in future by adding criteria to express other properties besides those implicit in the name, *e.g.* the degree of pedality, relative importance of constituents compared to adjacent horizons, intensity of processes *etc.*

TERMINOLOGY

As mentioned earlier, the classification systems takes into account the following elements in order of importance: features, grain size distribution, composition and other criteria.

The features determine the *formations*, *subformations* and eventually the *syndromes* which result from pedogenic processes. For the same process different formations can be distinguished, depending upon the degree of evolution. For example, eogypsic (< 10% gypsum), gypsic (10 - 60%), hypergypsic (60 - 90%) and hologypsic (> 90%) (Stoops and
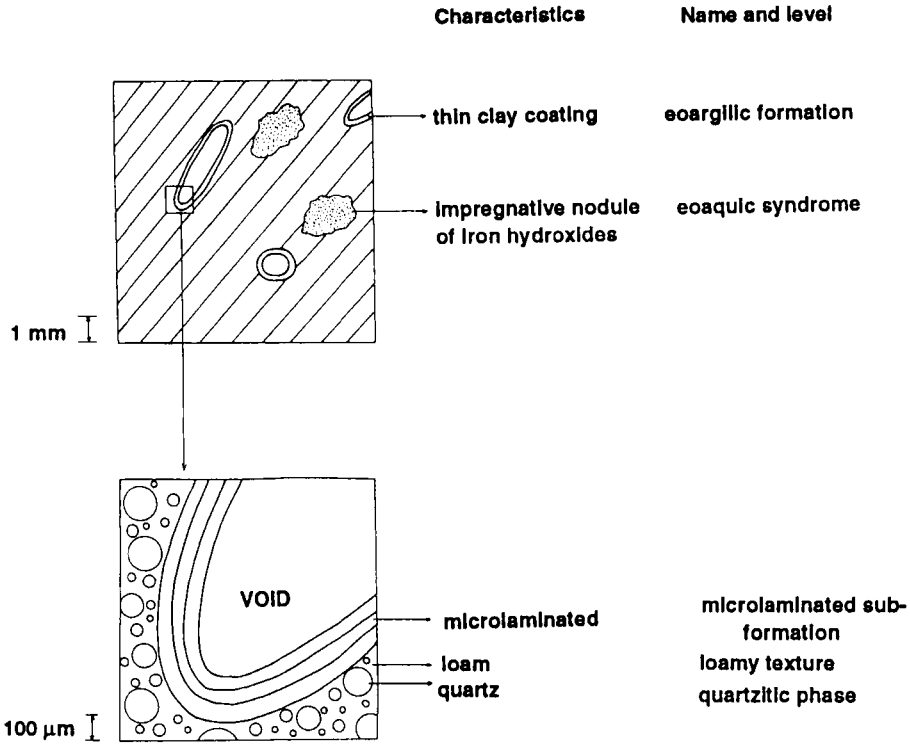
Fig. 2. Example of a loamy (texture), quartzic (phase), microlaminated (subformation) eoargilic formation with eoaquic syndrome.

Poch, 1994). In a similar way eoargillic, argillic, hyperargillic and holoargillic can be recognized (compare for instance with classes of clay illuviation proposed by Miedema and Slager, 1972). The subformations are determined by specific characteristics of the features, *e.g.* in the case of gypsic the crystal morphology and in the case of argillic by the internal fabric and/or mineralogy of the illuviation features.

Features of a relatively less expressed or superimposed processes are introduced as a syndrome though in theory practically all formations can be syndromes also. For example, hydromorphic features reflecting the main pedological processes active in a material will be called a formation; the same features occurring as an overprint on clay illuviation features are considered as a syndrome. The same criteria and terminologies are used in both cases, *e.g.* an eoaquic (syndrome) argillic formation (Fig. 2). Conflicting situations may arise when both processes interact such as when an argillic formation in strongly hydromorphic conditions gives rise to a fabric which is much more than just a superposition of mottling over clay illuviation. In this case a specific hydrargillic formation has to be considered.

The grain size distribution determines the *texture* as the impact of a process can be quite different depending upon the texture of the parent material. For example, in a sandy or gravely

eoargillic formation the illuviated clay occurs only as grain coatings but in a loamy eoargillic formation it can occur as pore coatings only.

The composition of the material determines the *phase*. In many cases the phase may seem less important to many soil scientists, but such a view is countered by the following example. A gabbroidic (phase), sandy (texture), eoargillic formation compared to a quartzic, sandy, eoargillic formation will have a much higher nutritive reserve, and most probably a different genesis. In the first case, clay may be formed in the profile by weathering of plagioclases and pyroxenes. In the second case, clay must be supplied from another source.

CONCLUSIONS

The outline of a higher level classification system for micromorphological aspects of soil materials is presented. The system is based mainly on three criteria: features, resulting from the principal active pedogenic processes which determine the *formation* and *subformation*; grains size distribution of the parent material which determines the *texture*; and composition of the detrital material which determines the *phase*. Features of less pronounced processes appearing as an overprint on the fabric are called *syndromes*.

The author is aware that this proposal is a first approximation and requires considerable discussion and testing. Formations and subformations are yet to be defined and a concise description of the (combination of) features is required. This future research must take into account the texture from a wide range of soils from all over the world. In particular an adequate terminology has yet to be developed for humus materials.

It is not possible to create from the beginning an all encompassing classification of all materials, and it is questionable if this is even necessary, since it would complicate the system. If the majority of soil materials can be classified using this new system it will be a great help to soil science. Moreover, the author is convinced that the elaboration of such a higher level classification of microfabrics of soils will not only contribute to easier description, comparison and classification of soil materials, but also to more systematic study and cataloguing that will serve micromorphology and soil science in general. "Language is indeed the first step in scientific endeavour" (Nietzsche).

REFERENCES

Bartelli, L.J. and Odell, R.T., 1960. Laboratory studies and genesis of a clay enriched horizon in the lowest part of the solum of some brunizem and gray-brown podzolic soils in Illinois. Soil Sci. Soc. Amer. Proc., 23: 390-395.

Brewer, R., 1964. Fabric and Mineral Analysis of Soils. John Wiley and sons, New York, 470 pp.

Brewer, R., 1983. A petrographic approach to soil classification. Sciences Géologiques Mém., 73: 31-40.

Brewer, R. and Sleeman, J.R., 1988. Soil Structure and Fabric. CSIRO, Australia, 173 pp.

Bullock, P., Fedoroff, N., Jongerius, A., Stoops, G., and Tursina, T., 1985. Handbook for Soil Thin Section Description. Waine Research Publications, Wolverhampton, U.K., 152 pp.

Buol, S.W. and Eswaran, H., 1978. The micromorphology of Oxisols. In: M. Delgado (Editor), Micromorfolgia del Suelos. Proc. V Int. Working Meeting on Soil Micromorpology, Granada, Spain, Univeristy of Granada, pp 325-347.

Eswaran, H. and Banos, C., 1976. Related distribution patterns in soils and their significance. Anal. Edafol. y Agrobiol., 35: 33- 45.

FitzPatrick, E.A., 1984. Micromorphology of Soils. Chapman and Hall, London, 433 pp.

Kubiëna, W.L., 1938. Micropedology. Collegiate Press, Ames, Iowa, 242 pp.

Kubiëna, W.L., 1948. Entwicklungslehre des Bodens. Springer Verlag, Vienna, 215 pp.

Kubiëna, W.L., 1953. The Soils of Europe. Thomas Murby and Co., London, 314 pp.

Miedema, R. and Slager, S., 1972. Micromorphological quantification of clay illuviation. J. Soil Sci., 23: 309-314.

Stoops, G. and Eswaran, H., 1986. Soil Micromorphology. Van Nostrand Reinhold, New York, 345 pp.

Stoops, G. and Poch, R.M., 1994. Micromorphological classification of gypsiferous soil materials. In: A.J. Ringrose-Voase and G.S. Humphreys (Editors), Soil Micromorphology: Studies in Management and Genesis. Proc. IX Int. Working Meeting on Soil Micromorphology. Developments in Soil Science, 22. Elsevier, Amsterdam, pp. 327-332.

Streckeisen, A., 1976. To each plutonic rock its proper name. Earth-Science Reviews, 12: 1-33.

This Page Intentionally Left Blank

Micromorphological classification of gypsiferous soil materials

G. Stoops[1] and R.M. Poch[2]

[1]Lab. Mineralogy, Petrography and Micropedology, University of Ghent, Belgium
[2]Dept. Environment and Soil Science, University of Lleida, Spain

ABSTRACT

Stoops, G. and Poch, R.M., 1994. Micromorphological classification of gypsiferous soil materials. In: A.J. Ringrose-Voase and G.S. Humphreys (Editors), Soil Micromorphology: Studies in Management and Genesis. Proc. IX Int. Working Meeting on Soil Micromorphology, Townsville, Australia, July 1992. Developments in Soil Science 22, Elsevier, Amsterdam, pp. 327-332.

The present approach to soil thin section description, based on a morpho-analytical study, deals with the lowest level of classification of materials, i.e. with the basic components of the soil and their fabric. The relation of such descriptions to soil characterization and classification is difficult and therefore a higher level of classification, using a more morpho-synthetic approach, is necessary to obtain insight into the diversity of soil materials and in the relationships between some specific features. An application of these new concepts to gypsiferous soils is presented.

The micromorphological characteristics of gypsiferous soil materials have several features in common which often appear together and can be related to genetic, climatic and plant growth conditions. For these reasons an attempt has been made to classify the materials in terms of the proposed criteria.

Initially, materials are classified according to their volumetric gypsum content. A further subdivision depends on the shape and appearance of gypsum and the composition of the micromass. The main crystal habits of gypsum in the soil (lenticular, fibrous, microcrystalline) and the degree of intergrowth are taken into account. Finally the particle size class and hydromorphic or decarbonation features are also considered.

INTRODUCTION

This paper is an example of the classification of microfabrics of Stoops (1994), applied to soils with gypsum.

The process of gypsification, or progressive enrichment of gypsum in the soil, has been recognized as such by several researchers (Barzanji and Stoops, 1974; Herrero et al., 1992), consisting of the crystallization of gypsum in pores and subsequent mixing within the gypsum-free groundmass. This process gives rise to soil materials with increasing amounts of gypsum showing characteristic fabrics, depending on the particle size distribution and structure characteristics of the host material. The last stage consists of horizons made almost completely of sand-sized lenticular gypsum crystals, which correspond to hypergypsic horizons (ICOMID, 1989; Eswaran and Zi-Tong, 1991). In other cases, when the soils are formed on gypsum rock, in margins of playa-like enviroments or in some gypsum desert crusts another type of

Table 1.
Micromorphological classification of gypsiferous materials.

Formation	Subformation	Phase	Syndrome
Eogypsic	lenticular petric fibrous	calcareous non-calcareous	decarbonated hydromorphic
Gypsic	lenticular petric fibrous	*id.*	*id.*
Hypergypsic	lenticular petric microcrystalline	*id.*	*id.*
Hologypsic	lenticular microcrystalline petric		

Texture: sand, silt, loam, clay, gravelly.

hypergypsic horizon consisting mainly of silt-sized microcrystalline gypsum may occur (Warren, 1982; Watson, 1988; Herrero *et al.*, 1992). Higher degrees of crystal intergrowth leading to cementation, decarbonatation of the gypsum-free groundmass, or hydromorphic features are phenomena frequently encountered in these materials.

The micromorphological classification presented here takes into account all of these factors in a hierarchical way, classifying them into formations, subformations, texture and phases. Other processes recognized as overprints are designated as syndromes.

THE CLASSIFICATION SYSTEM

The proposed classification system is summarized in Table 1 and additional details are presented below.

Formations

Materials (whole thin sections or parts of it) are first classified into formations according to their gypsum content, since this is a parameter that is associated with other characteristics. The presence of gypsum restricts the range of possible formation processes of soil to certain genetic conditions and it constitutes a major constraint for plant growth. Furthermore it can be correlated with the results of chemical analyses.

The indicated percentages of gypsum are given in volume, *i.e.* surface estimations over the area of the thin section occupied by solid material. It is a direct estimator of the bulk content of gypsum in the soil.

Eogypsic   gypsum content <10%
Gypsic   gypsum content 10-60%
Hypergypsic   gypsum content 60-90%
Hologypsic   gypsum content >90%

The criteria for these limits are:

10%: A smaller content is considered not to affect the plant growth.

60%: Limit for the Hypergypsic Horizon (ICOMID 1989) although it is referred to as a weight percentage by that committee.

90%: Separates hypergypsic materials from pure gypsum crusts.

Subformations

Subdivision of formations depends on the morphology of the gypsum.

Eogypsic:

Lenticular:	Infillings and/or coatings of loose lenticular crystals, coarse to fine sand in size; occurs in channels and chambers or as poikilotopic aggregations of gypsum and sand (Fig. 1a).
Petric:	Infillings of pores by xenotopic/hypidiotopic gypsum intergrowths (Fig. 1b).
Fibrous:	Fibrous gypsum (satin spar) occurs as continuous infillings in planar voids (mainly in clayey soils).

Gypsic:

Lenticular:	Idiomorphic/hypidiomorphic lenticular gypsum is found in channels, chambers and fissures, as infillings and/or coatings, and also in the groundmass; irregularly distributed. Some regions of the groundmass may show isles fabric (Herrero *et al.*, 1992) *i.e.,* fragments of groundmass, deformed by biological activity, completely surrounded by loose gypsum. Gypsum crystals often have a crescent, bow-like distribution. Nests of celestite needles may be found (Fig. 1c).
Petric:	As above, but with xenotopic/hypidiotopic crystal intergrowths. In the case of gravels they may form pendants of xenotopic lenticular gypsum "in palisade" (Fig. 1d).
Fibrous:	As for eogypsic (Fig. 1e).

Hypergypsic:

Lenticular:	As for Gypsic, but isles fabric (Herrero *et al.*, 1992) more developed. Microcrystalline gypsum (silt size) may be found as nodules or infillings (Fig. 2a).
Petric:	As for gypsic, but with more gypsum. Microcrystalline gypsum may be present as nodules or infillings (Fig. 2b).
Microcrystalline:	Silt-sized microcrystalline gypsum constitutes most of the thin section, appearing as faint yellow masses in PPL and almost isotropic in XPL. The isotropic quality is due to the presence of low amounts of very fine dispersed insoluble material and to the superposition of the small crystals (Fig. 2c).

Hologypsic:

Lenticular:	Sand-sized lenticular gypsum, idio- or hypidiotopic, predominant in the thin section (Fig. 2d).
Microcrystalline:	Silt-sized microcrystalline gypsum predominant (Fig. 2e).
Petric:	Gypsum crystals, mostly sand size, are hypidio- or xenotopic, forming frequent intergrowths (Fig. 2f).
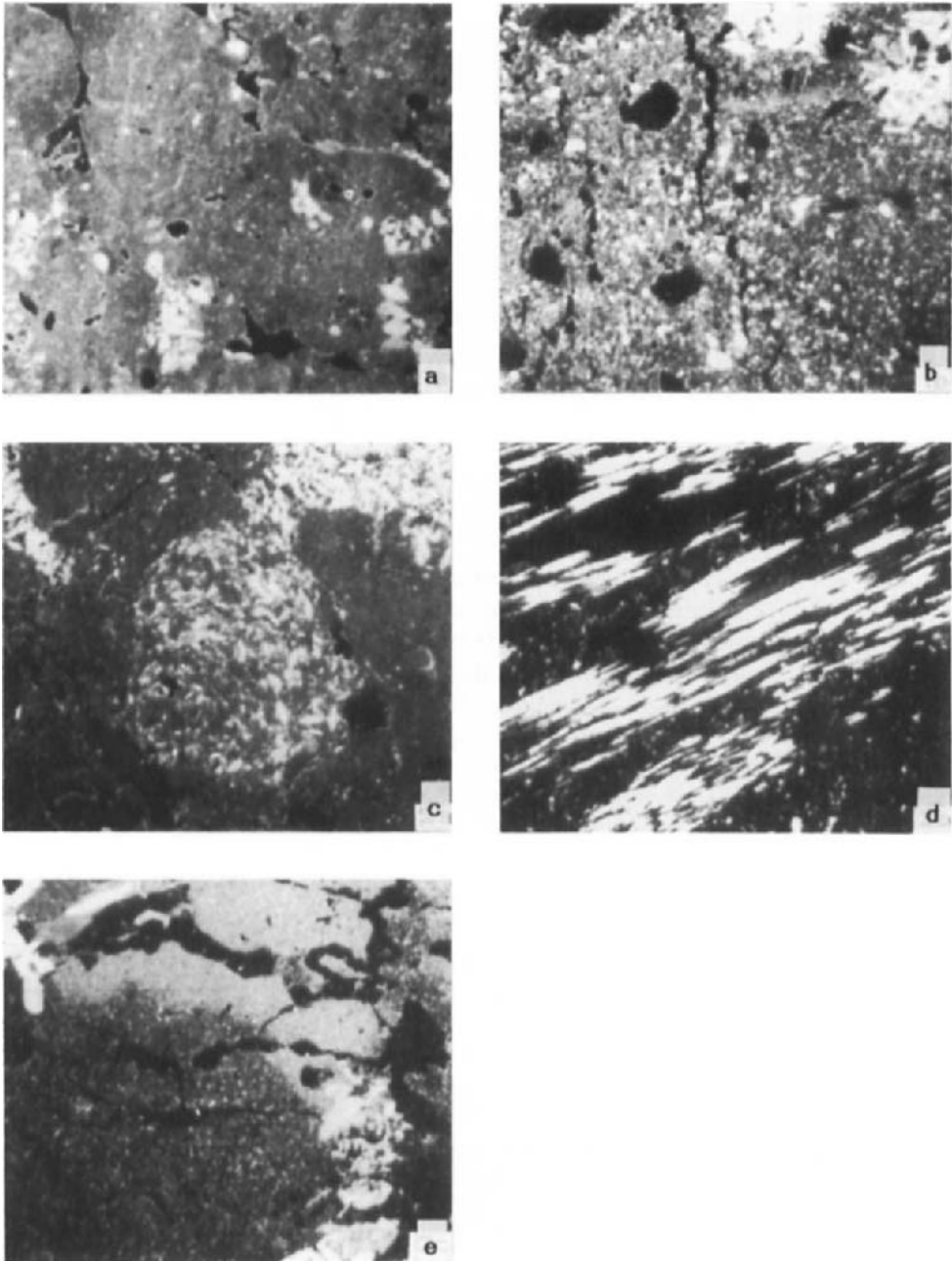
Fig. 1. **a)** Lenticular Eogypsic, loam, calcareous (Spain); **b)** Petric Eogypsic, loam, calcareous (Spain); **c)** Lenticular Gypsic, loam, calcareous (Spain); **d)** Petric Gypsic, loam, calcareous, decarbonated syndrome (Syria); and **e)** Fibrous Gypsic loam, non-calcareous (Egypt). Frame length 10.3 mm.
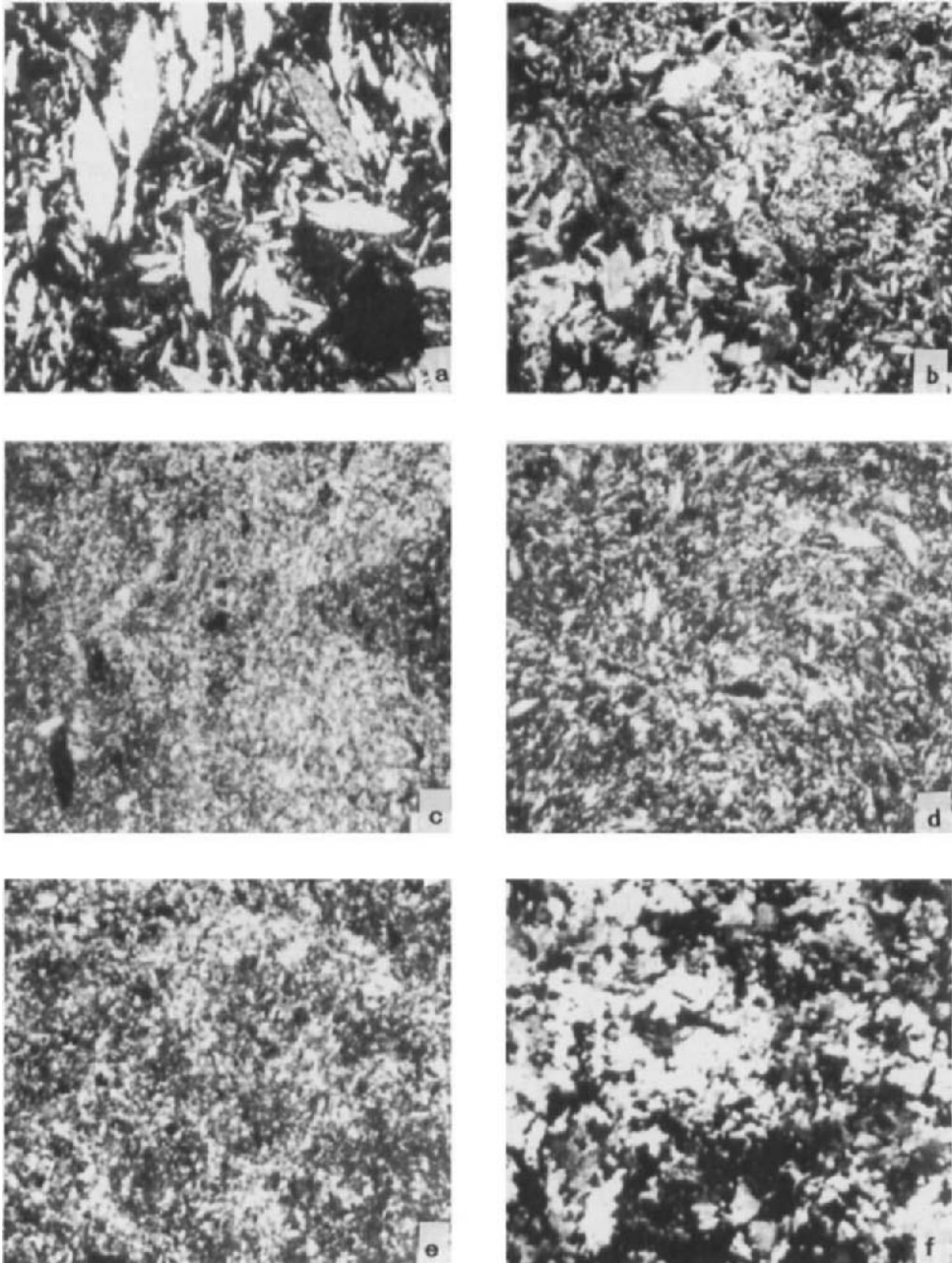
Fig. 2. a) Lenticular Hypergypsic, sand, calcareous (Spain); b) Petric Hypergypsic, non-calcareous (Syria); c) microcrystalline Hypergypsic, sand, calcareous (Spain); d) Lenticular Holoypsic, sand (Syria); e) Microcrystalline Holoypsic, loam (Spain); and f) Petric Hologypsic (Syria). Frame length 10.3mm.

Texture

The nomenclature for texture classes as suggested by Stoops (1994) may be applied. It can be used for the groundmass in the case of eogypsic and gypsic, and for a whole range of materials, including gypsum crystals, in hypergypsic and hologypsic types. It gives a better approximation to field texture than laboratory results. Moreover, in these cases an indication of the texture of the gypsum-free material would not have any meaning.

Especially in the eogypsic and gypsic materials, a clear difference can be observed between clayey and loamy texture at one side and sandy at the other. In the former gypsum crystallizes in the biopores forming rather pure crystals, whereas in the latter larger crystals are found in the packing pores, often enclosing the sand grains (poikilotopic crystals).

Phases

Calcareous: The gypsum-free groundmass consists of a mixture of micritic calcite, clay and silt. The coarse elements are often polymictic.
Non-calcareous: Micritic calcite is missing.

Syndromes (tentative)

Hydromorphic: Nodules, hypocoatings or punctuations of Fe-oxihydroxides, intercalations or hypocoatings of Fe-depleted groundmass.
Decarbonated: CaCO₃-depleted patches of groundmass, as intercalations or hypocoatings, showing stipple-speckled or granostriated b-fabric.

REFERENCES

Barzanji, A.F. and Stoops, G., 1974. Fabric and mineralogy of gypsum accumulations in some soils of Iraq. Proc. 10th Int. Congress Soil Science (Moscow), Vol. VII: 271-277.

Eswaran, H. and Zi-Tong, G., 1991. Properties, genesis classification and distribution of soils with gypsum. In W.D. Nettleton (Editor), Occurrence, Characteristics and Genesis of Carbonate, Gypsum and Silica Accumulation in Soils. Soil Sci. Soc. Am. Publ., 26, pp. 89-119.

Herrero, J., Porta, J. and Fedoroff, N., 1992. Hypergypsic soil micromorphology and landscape relationships in Northeastern Spain. Soil Sci. Soc. Am. J., 56: 1188-1194.

ICOMID - International Committee in Aridisols, 1989. Aridisols, Version 6.0. Draft.

Stoops, G., 1994. Soil thin section description: higher levels of classification of microfabrics as a tool for interpretation. In: A.J. Ringrose-Voase and G.S. Humphreys (Editors), Soil Micromorphology: Studies in Management and Genesis. Proc. IX Int. Working Meeting on Soil Micromorphology. Developments in Soil Science, 22. Elsevier, Amsterdam, pp. 317-325.

Warren, J.K., 1982. The hydrological setting, occurrence and significance of gypsum in Late Quaternary Salt Lakes in South Australia. Sedimentology, 29: 609-637.

Watson, A., 1988. Desert gypsum crusts as palaeoenvironmental indicators: A micropetrographical study of crusts from Southern Tunisia and the Central Namib Desert. J. of Arid Environments, 15: 19-42.

Proposals for classifying and describing secondary micro-structures observed within completely weathered minerals

J. E. Delvigne

ORSTOM. Géosciences de l'Environnement, Université, Aix-Marseille III, Marseille, France

ABSTRACT

Delvigne, J.E., 1994. Proposals for classifying and describing secondary micro-structures observed within completely weathered minerals. In: A.J. Ringrose-Voase and G.S. Humphreys (Editors), Soil Micromorphology: Studies in Management and Genesis. Proc. IX Int. Working Meeting on Soil Micromorphology, Townsville, Australia, July 1992. Developments in Soil Science 22, Elsevier, Amsterdam, pp. 333-342.

A specific and concise terminology does not exist for describing, at the scale of the optical microscope, the micromorphology of secondary structures derived from complete weathering of primary minerals in the weathering mantle. Some attempts have been made to classify partly-weathered mineral structures in which both residual and supergene products are considered. Such classifications, however, remain unsatisfactory. To fill this gap, the author proposes a coherent series of new terms composed from Greek and Latin roots commonly used in Earth Sciences. Definition, description and explanation of proposed terms are given and illustrated by some natural examples of weathering structures.

The author proposes the replacement of the formerly used, ambiguous and restrictive word pseudomorph by the more general and broader term alteromorph. Subclassifications are made according to geometrical criteria based on the extent of preservation of the original shapes. The alteromorphs are subdivided into iso-, meso- and katamorphs, complemented by more specific terms such as pseudo-, crypto-, echino-, and phantomorphs. According to increasing importance of secondary intramineral voids, the alteromorphs are subdivided into holo-, poro- and koilomorphs. The complementary distribution of voids and solid within the poromorphs is responsible for their further subdivision into either, alveoporo-, phylloporo- and retiporomorphs where the void distribution is the easiest key for classification or, into botryo-, glomero- and septomorphs where the solid phase microstructure is responsible for the differential criteria. Alteromorphs having complex mineralogy can be classified according to genetic criteria into polygenic or polyphased alteromorphs. The term cumulomorph is restricted to initially porous alteromorphs whose residual porosity is infilled by further accumulated materials of allochtonous origin.

INTRODUCTION

The term *pseudomorph* is commonly used when a primary mineral, identified by its specific shape, is replaced by a secondary mineral (or by an aggregate of secondary minerals) with preservation of the characteristic shape of the former whatever the mineralogical and chemical composition of the latter. According to the etymology of the term (from Greek ψευδης =

wrong, which is not what it seems to be, and μορφη = shape) and according to the above definition, the term pseudomorph should be used only when an automorphous (from Greek αυτος = own, particular, from it self) primary mineral, with characteristic and well developed crystalline faces, is weathered and replaced by secondary material, with preservation of the shapes and outlines of the automorphous primary mineral.

Automorphous (or euhedral) rock-forming minerals are generally very rare and their weathering does not play an important role in the bulk rock transformation. Most primary minerals exhibit poorly developed crystalline faces and their shapes are uneven and not characteristic. These are *Xenophormous* minerals (from Greek ξενος = foreign). In most cases, the use of the term pseudomorph is thus wrong, improper or excessive for describing the secondary products derived from xenomorphous primary minerals. Under these conditions, it is necessary to define a new terminology. On one hand, it should be strongly related to the observed micromorphological structures and shapes and, on the other hand, it should be based on generalities, particularities or restrictions capable of specification, in a concise and unequivocal way. The micromorphological aspect of the internal secondary materials, whatever their origin, complexity, history or later evolution is central to this. The aim of this paper is to propose such a system of classification.

THE PRESERVATION OF SHAPES AND VOLUMES

The general term *Alteromorph* (from Latin alter = other and from Greek μορφη = shape) is proposed for all cases of transformation of primary minerals into secondary products which result in distinct bodies. They are limited by more or less conspicuous, generally inherited, outlines and identified by recognizable internal microstructures and by specific mineralogical content, whatever may be the extent of preservation of the original shapes and volumes. This definition excludes forms and entities which are the result of the infilling of the genetically independent external voids such as open fractures, vesicles and other voids of pedological or biological origin.

Alteromorphs do not always exactly exhibit the shapes, sizes and volumes of the replaced primary minerals (Fig. 1a). According to the preservation extent of these original features, terms such as isomorphous, mesomorphous and katamorphous alterations were proposed (Stoops *et al.*, 1979). Using the same etymological roots and maintaining the content of the definition given by these authors, three new terms are proposed :

Isomorph (from Greek ισος = similar, and μορφη = shape) (Fig. 1b) which corresponds to the result of a transformation with preservation of external outlines and sizes of the primary mineral or, at least, with modification imperceptible at the scale of the optical microscope. The isomorphs are the main structural components of isalterites (Chatelin, 1974).

Mesomorph (from Greek μεσος = middle) (Fig. 1c) where the general shape of the original mineral is preserved but with modifications to its size in one, two or three dimensions. Non equant modifications in one or two dimensions may introduce perceptible and measurable deformations of the secondary structures. They are frequently observed in the weathering of some groups of minerals such as, for example, the phyllosilicate group.

Katamorph (from Greek κατα = downward) (Fig. 1d) when the alteromorph is completely distorted under the influence of external processes such as fracturing, dislocation, swelling and shrinkage, dissemination, assimilation and pedoturbation. Outlines are no longer clear nor

continuous but the position of the original mineral is still recognizable. Katamorphs are frequently observed in alloterites (Chatelin, 1974) and their importance increases towards the pedological horizons.

SPECIFIC CASES

An additional four particular cases of alteromorphs are frequently observed whose patterns are strongly related to this first level of classification. Four specific terms are proposed.

Pseudomorph (from Greek ψευδης = wrong) (Fig. 1e) is a particular case of alteromorph resulting from the isomorphous weathering of a euhedral mineral exhibiting well developed and characteristic crystalline faces. Pseudocubic crystals of goethite after pyrite, or iddingsitized euhedral crystals of olivine in a basaltic rock, are fairly common examples of pseudomorphs.

Echinomorph (from Greek εχινος = urchin) (Fig. 1f) is a particular case of mesomorphous weathering in which part of the secondary material, mainly smectitic clays, protrude outside the original mineral outlines by infilling radiating intermineral fractures opened by internal swelling of the secondary mineral phase. Infillings of nontronitic clays expelled outside an alteromorph after pyroxene are commonly observed within the adjacent intermineral fractures.

Phantomorph (from Greek φαντασμα = phantom, ghost) (Fig. 1g) is a particular case of katamorphous weathering in which traces of secondary products or structures, with irregular or diffuse outlines, are observed within a matrix with which they contrast by their colour, density, crystallinity, shape or internal structure. The original limits are no longer recognizable because they are progressively shaded off and assimilated by the surrounding matrix. Thread-shaped or foliated relicts after micas or septaric structures after feldspars, wholly embedded in an hematitic or gibbsitic matrix, commonly observed in old iron-crusts and bauxites, are good examples of phantomorphs.

Kryptomorphs (from Greek κρυπτειν = to hide, to mask, to conceal) result from an assemblage of adjacent isomorphs whose individual original limits, although maintained, are no longer clearly identified under the microscope, because all the primary minerals composing the assemblage are weathered together into similar secondary minerals which do not exhibit particular characteristic nor specific crystalline orientation. This case is frequently observed in monomineralic and agglomeromineralic rocks but it appears also when different associated primary minerals are weathered into the same secondary products: both olivine and pyroxene, in a doleritic rock, can be replaced by iron oxihydrates alteromorphs and sanidine; plagioclase and nepheline, in alkaline rocks, can be weathered into gibbsitic complex secondary structures in which internal limits of each primary mineral component have become indistinct.

COMPLETE ALTEROMORPHS

The previous proposals by Stoops *et al.* (1979) and Bullock *et al.* (1985) are quite satisfactory for describing partially developed alteromorphs (classes of alteration 1, 2 and 3) in which recognizable primary mineral residues are still embedded within secondary products, but these authors have not proposed a way of describing the completely developed alteromorphs (class of alteration 4). The following new proposals are an attempt to fill this gap and to facilitate the micromorphological descriptions of isalteritic and alloteritic weathered materials.

Fig. 1 : Schematic sketches of the most commonly observed secondary microstructures formed in the wholly weathered primary minerals.

a PRIMARY MINERAL

b ISOMORPH
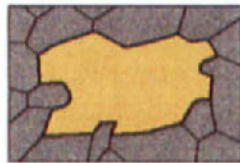
c MESOMORPH

d KATA MORPH

e PSEUDOMORPH

f ECHINOMORPH

g PHANTOMORPH
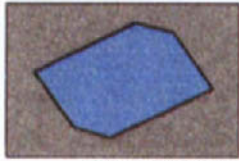
h HOLOMORPH
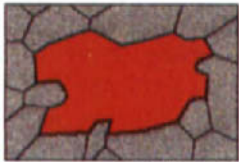
i POROMORPH

j KOILOMORPH

k PHYLLOPOROMORPH

l ALVEOPOROMORPH

m RETIPOROMORPH

n BOTRYOMORPH
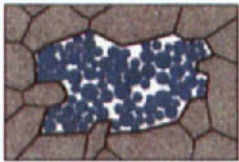
o GLOMEROMORPH
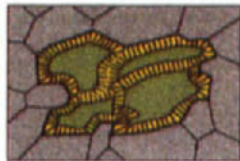
p SEPTOMORPH

q POLYPHASED ALTER.

r POLYGENIC ALTER.
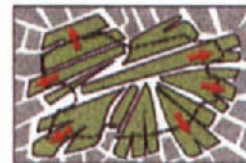
s CUMULOMORPH

Alteromorphs exibit regular or irregular internal structures that are independent of the degree of preservation of the shape and size of the original primary minerals. These structures are closely related either to the dissolution processes, which determine the volumes of secondary products and complementary secondary voids, or related to the internal patterns of primary structures (fractures, cleavages, twinning, *etc.*) which influence both the weathering progression into the primary mineral and the micromorphology of the secondary products.

The wholly developed alteromorphs can be classified, first according to the total volume of the secondary voids whatever their distribution and organization and second, according to their inherited or neoformed internal structures which control the complementary distribution of the solid neoformed phase and the residual voids.

Holomorph (from the Greek ολος = whole, complete and μορφη = shape) (Fig. 1h) corresponds to an alteromorph in which the volume of the secondary minerals is apparently equal to the original volume of the replaced mineral. The volume of the secondary voids is not discernible at the scale of the optical microscope and the secondary solid phase exhibits a dense and homogeneous aspect. Holomorphs correspond generally to peripheral centripetal weathering patterns in poorly cleaved and unfractured minerals. They form also when drainage conditions do not cause lixiviation of the original soluble constituents. For example, complete weathering of olivine or pyrite grains, and pyroxenes under low leaching conditions, induces the formation of dense, non porous, holomorphs composed of iddingsite, goethite and smectites respectively.

Koilomorph (from the Greek κοιλος = empty, hollow and μορφη = shape) (Fig. 1j), corresponds to an empty alteromorph, without any secondary mineral. It results from weathering of a very soluble mineral (*e.g.* calcite) or by slow and congruent dissolution of a less soluble mineral (*e.g.* quartz) exposed to intense leaching conditions. The external outlines of koilomorphs are generally well preserved because they are composed of outlines of adjacent mineral grains. Koilomorphs may contain small quantities of residual or newly formed minerals corresponding to primary mineral inclusions or to insoluble impurities originally contained within the solubilized host mineral.

Poromorphs (from the Greek οιπορροι = pores and μορφη = shape) (Fig. 1i) form a group of alteromorphs, transitional between the two former extreme cases, in which the ratio of discernible voids is important compared with the volume of newly formed minerals. This word is used to introduce the next items, (Figs 1k-p). Depending on the complementary proportions of the solid phase and included voids, poromorphs can be described either according to the void pattern, if these are few or small within an important continuos solid phase, or according to the solid phase pattern if its volume is smaller or equal to that of the voids.

Phylloporomorph (from the Greek φυλλον = sheet) (Fig. 1k): the volume of the voids is somewhat smaller than that of the solid phase. The pores are elongated, planar and parallel, continuous and their distribution is regular. They are very often interconnected with the trans- and intermineral porosity and can consequently be filled up by allochtonous deposits. This particular foliated microstructure is frequently observed either in weathered sheet silicates, or in alteromorphs in which well oriented secondary smectitic clays are the main constituents. This kind of porosity can also result from the artificial shrinkage of a foliated secondary phase during the preparation of the thin section.

Alveoporomorph (from the Latin *alveolus* = alveolus, cell, small cavity) (Fig. 1l). The volume of the discernible voids, at the scale of the optical microscope, is considerably smaller

than that of the solid phase and its distribution is generally irregular and random with uneven shapes (circular, lenticular, denticulated) and is located within an abundant, continuous solid phase. These pores generally result from weathering, under average leaching conditions, of uncleaved and unfractured minerals and represent the final stage of evolution of perinuclear and interplasmamineral pores (Bisdom, 1967) appeared in partly weathered minerals. This internal porosity is generally not connected to intermineral porosity and, consequently, is rarely filled up by later deposits of allochtonous origin. This intramineral porosity can also result from later degradation and solubilisation of the secondary solid phase itself.

Retiporomorph (from the Latin *reticulum* = network) (Fig. 1m) is a kind of alteromorph in which voids are distributed according to a tridimensional network of planar open fractures, exhibiting constant or hierarchized thickness, which divide the solid phase into polyhedral isolated volumes. This particular microstructure is the result of the natural dehydration, shrinkage and partition of an originally continuous and homogeneous hydrated solid phase. For example, nepheline can be replaced, during the first step of weathering, by an homogeneous, continuous, isotropic phase which later divides into isolated polyhedral volumes by the formation of a reticulated polygonal network of shrinkage fissures.

Botryomorph (from the Greek βοτρυς = grape, cluster) (Fig. 1n) is a kind of alteromorph whose internal microstructure is determined by the distribution of the solid components although the volume of voids may still be important. The isolated and well formed secondary crystalline components are homogeneously distributed in the whole alteromorph. They are stacked side by side, such as in a cluster, leaving between them small interstitial interconnected voids morphologically similar to packing voids. For example, the complete weathering of a felspar grain can produce a botryomorph in which isolated kaolinite booklets are clustered in such a way that they leave between them small polyhedral "packing" voids.

Glomeromorph (from the Latin *glomerare* = to agglomerate) (Fig. 1o) is a kind of alteromorph somewhat similar to the previous one but in which the volumes of voids are more important because the individual crystals of supergene origin show a tendency to agglomerate together into small compact and irregular areas separated by large interconnected vughs. Within the solid volumes, the individual crystals are assembled into a poreless microgranulated structure. The weathering of felspar, under strong leaching conditions which promote marked lixiviation of the original chemical components, provides a good example of a glomeromorph composed of agglomerated gibbsite crystals associated with large interconnected vughs.

Septomorphs (from the Latin *septum*, pl. *septa* = partition, compartment) (Fig. 1p) are the most characteristic and frequently observed alteromorphs, mainly in lateritic isalterites. The secondary minerals are distributed in banded structures between which empty, isolated polyhedral voids are enclosed. The layout of these banded structures is influenced by the regular (cleavage and twinning planes) or irregular (fissures and cracks) discontinuities which have controlled the first step of the weathering in the pre-existing primary mineral. The orientation of the elementary monocrystals, which compose a septum, can be uneven and, in this first case, this lack of preferential optical orientation is observed in all septa and through the whole septomorph. Their orientation can be also perpendicular to the middle plane of the septum. Their orientation can also be controlled by the crystalline orientation of the primary mineral itself and, in this case, all secondary crystals of a given septomorph are extinguished simultaneously under crossed polars. The first two cases are commonly observed in gibbsitic septomorphs after feldspars whereas the third case is more frequently observed in ferruginous

septomorphs derived from weathered pyroboles. The thickness of the septa is generally proportional to the original insoluble sesquioxide content of the primary mineral (Delvigne, 1965). The progressive thickening of the septum is the result of nanotransfers of chemical elements over very short distances, from the isolated primary remnants to the growing secondary crystals (Nahon and Bocquier, 1983).

According to the original network of fissures, cracks, cleavages and other preferential directions pre-existing in the primary minerals, and according to the previous classification of partly weathered minerals (Stoops *et al.*, 1979), the septomorphs can be described as :

Irregular Septomorphs; when the septa arrangement is uneven without any particular distribution or orientation and it is controlled by the fissure and crack patterns appearing in the uncleaved primary mineral. These discontinuities commonly correspond to trans- and intramineral fissures. A continuous polygonal and peripheral septum generally surrounds the septomorph and corresponds to the intermineral suture planes. This kind of irregular septomorph is frequently observed in alteromorphs after olivine or garnet and, generally, after other uncleaved but fractured primary minerals.

Regular Septomorphs; when the septa are clearly oriented parallel to the cleavage planes of the primary mineral. According to the orientation of these planes with respect to the plane of the thin section, a single network of parallel or a double network of crossed cleavages may appear. This can be further subdivided into an *Orthogonal* network (in the case of pyroxenes and alkaline feldspars) and into a *Crossed* network (in the case of amphiboles). It is obvious that more complex septomorphs may be formed, for example, by combination of irregular fractures and regular cleavage networks.

All these structures correspond to the so-called "boxwork structures". They are well supported by a strong tridimensional network of stable secondary minerals, mainly sesquioxides. Most of these septomorphic structures are mechanically and chemically resistant and can persist in alloterites and even in soil horizons or within ferruginous and bauxitic duricrusts. At these different levels of weathering, the interseptal porosity can be filled by later crystallization or deposition of solubilized or transported material coming from long distances (from upper horizons or from upper parts of the landscape).

THE COMPOSITE ALTEROMORPHS

The composite alteromorphs are composed of two or more associated secondary minerals (or secondary solid phases) of hypogene and/or supergene origin. The primary mineral remnants, temporarily maintained within the alteromorph, are not taken into account for the definition of this kind of microstructure. The composite character of these alteromorphs is independent of their external shapes and internal morphology but the orientation pattern of one component with respect to the other can be uneven, parallel or crossed, whereas, the concentration pattern within the alteromorph, can be uniform, clustered, peripheral, central or otherwise. The composite alteromorphs can originate from polygenic or polyphased processes.

Polygenic alteromorphs (Fig. 1r) are formed in two or more successive steps, very often according to different alteration processes, of hypogene and/or supergene origins, though separated in time. During the first step, alteration has not transformed the whole primary mineral and, during the second step, the primary remnants are transformed into different secondary minerals without affecting the first formed secondary products. For example: (1) during a first step, an olivine crystal has been partly altered to serpentine (hypogene alteration)

whereas, later, during the second step, the olivine remnants are replaced by iddingsite (deuteric process) without any modification of the first formed serpentine; (2) during a first step, a feldspar grain has been partly replaced by inclusions of sericite and zoisite (hydrothermal process) whereas during a later weathering process, the felspar remnant is weathered to kaolinite without modifying the internal inclusions; (3) a pyroxene grain is partly weathered (supergene process) to a banded structure of smectite enclosing weathered pyroxene remnants which will later be weathered into iron oxyhydrates whereas the smectitic component is temporarily maintained in the composite alteromorph.

Polyphased alteromorphs (Fig. 1q) are formed during a single step of hypogene alteration or of supergene weathering (they are monogenic alteromorphs), but the result consists of an association of two or more secondary products due to exsolution processes or to gradual transformation processes. Generally the internal distribution of the neoformed products is not uneven but exhibits an organized and hierarchized structure as one of the two secondary components is always situated close to the eventual primary remnants whereas the other secondary components are always more distant and separated from them by the first one. For example (1) supergene weathering with an exsolution process such as weathering of an aluminous hornblende to a septomorph composed of goethitic septa covered by small isolated crystals of gibbsite; (2) supergene weathering with a gradual transformation process such as a plagioclase (Plg) grain, partly transformed to optically isotropic secondary material (IM) which progressively evolves into gibbsite (G) crystals, while plagioclase residues convert to isotropic material. In this case, the alteromorph after plagioclase is successively composed of (Plg + IM), (Plg + IM + G), (IM + G), (G). Such polygenic or polyphased alteromorphs, when not carefully observed in thin section, may induce false interpretations concerning the nature of the weathered primary mineral or concerning the chronology of its alteration steps (Delvigne, 1965).

WEATHERING AND ACCUMULATION

All porous and empty alteromorphs can be later infilled by further crystallizations, or deposits of allochtonous origin, coming either from adjacent weathered minerals by transmineral diffusion of elements, or from the upper parts of the profile or landscape by long distance transport processes. Situated in absolute accumulation sites, these partly or completely filled, but initially porous alteromorphs are *Cumulomorphs* (from the Latin cumulare = to accumulate) (Fig. 1s). These cumulomorphs are polygenic alteromorphs (two successive steps of supergenic processes). The accumulated minerals are generally quite independent upon the secondary products which constitute the reception structure although, under certain circumstances, both materials can be constituted by similar mineral species. For example, gibbsitic septomorph after feldspar whose residual voids are later filled up by a second generation of gibbsite of allochtonous origin.

Authigenic and allogenic materials occurring in a given cumulomorph generally exhibit rather different microstructures. Allogenic transported material forms complete or crescentic coatings whose individual particles are parallel to the walls of the former voids: discordance of the optical and crystalline orientations result between authigenic and allogenic materials. Allogenic crystallizations from solubilized material grow outwards perpendicularly to the walls of voids and frequent concordance of the optical and crystalline orientations between both crystal generations is observed. In the latter case, if both generations of crystals are built up of

the same mineral species, it may be difficult to distinguish the cumulomorphic character of the observed alteromorph. Some frequently occurring examples include: koilomorph after quartz which is later filled up by gibbsite in a bauxitic horizon; gibbsitic septomorph after felspar filled up by clay coatings in a ferrallitic soil; and gibbsitic glomeromorph after felspar filled up latter by iron oxyhydrates in a ferruginous duricrust.

CONCLUSIONS

The above proposed classification of alteromorphs is independent of the mineralogical composition of both primary and secondary materials. It has several entries. According to the aim of the micromorphological descriptions, the alteromorph can be successively subdivided according to following criteria:
- Geometric criteria essentially based on the extent of conservation of shapes and sizes of the primary minerals. To this first criteria corresponds a simple classification into iso-, meso- and katamorphs to which are added specifically new coined terms of pseudo-, echino-, phanto- and cryptomorphs.
- Microstructural criteria, based on the related and complementary distribution of the secondary solid products and of the associated residual voids: no apparent pores (holomorph) or none or very little solid material (koilomorph). Between these two extreme cases, the poromorphs exhibit an important solid volume and a subordinate but structured pore volume (alveoporo-, phylloporo- and retiporomorphs) whereas very porous alteromorphs are classified according to the structural patterns of the solid phase (botryo-, glomero- and septomorphs).
- Genetic criteria based on history and on the mineral content of composite alteromorphs. They are either polygenic or polyphased alteromorphs. Initially porous alteromorphs, whose residual porosity is infilled by further accumulated material of allochtonous origin, are cumulomorphs.

New terms have been composed from Greek and Latin roots commonly used in Earth Sciences and their use should not introduce any difficulty because they are simple and often self-explanatory. Concerning the composite alteromorphs with complex origin, it seems unnecessary to introduce new terms: the qualifying words such as polygenic or polyphased are sufficient.

Mixed roots among the proposed new terms can be combined for describing particularly complex alteromorphs. Only the infillings of allochtonous material within porous alteromorphs are sufficiently frequent to justify the use of the new term cumulomorph.

ACKNOWLEDGEMENTS

REFERENCES

Bisdom, E.B.A., 1967. Micromorphology of a weathered granite near the Ria de Arosa (NW Spain). Leidse Geol. Meded., 37: 33-67.

Bullock, P., Fedoroff, N., Jongerius, A., Stoops, G., and Tursina, T., 1985. Handbook for Soil Thin Section Description. Waine Research Publications, Wolverhampton, U.K., 152 pp.

Chatelin, Y., 1974. Les Sols Ferrallitiques. III L'Altération. Initiations - Documentations Techniques n°24.ORSTOM, Paris, 144 pp.

Delvigne, J., 1965. Pédogenèse en Zone Tropicale. La Formation des Minéraux Secondaires en Milieu Ferrallitique. Mem. ORSTOM n°13, Paris, Dunod Ed., 177 pp.

Nahon, D. and Bocquier, G., 1983. Petrology of elements transferred in weathering and soil systems. Mem. Sci. Géol., Strasbourg, 72: 111-121.

Stoops, G., Altemuller, H.J., Bisdom, E.B.A., Delvigne, J., Dobrovolsky, V.V., Fitzpatrick, E.A., Paneque and G., Sleeman, J., 1979. Guidelines for the description of mineral alterations in soil micromorphology. Pedologie, XXIX: 121-135.

The normal related distribution pattern of soils developed in volcanic ash in the humid tropics

K.H. Tan[1] and D.H. Goenadi[2]
[1]Agronomy Dept., University of Georgia, Athens, GA, USA
[2]Bogor Research Institute For Estate Crops, Bogor, Indonesia

ABSTRACT

Tan, K.H. and Goenadi, D.H., 1994. The normal related distribution pattern of soils developed in volcanic ash in the humid tropics. In: A.J. Ringrose-Voase and G.S. Humphreys (Editors), Soil Micromorphology: Studies in Management and Genesis. Proc. IX Int. Working Meeting on Soil Micromorphology, Townsville, Australia, July 1992. Developments in Soil Science 22, Elsevier, Amsterdam, pp. 343-351.

An investigation was conducted to study differences in related distribution patterns (NRDP) of selected tropical soils derived from dacito-andesitic tuffs. Samples were taken from genetic horizons of two Andosols, a Hapludult and a Haplorthox, for thin section, chemical and mineralogical analyses. The Andosols were strongly acid soils, had high organic matter contents, and exhibited CEC's ranging from 21.9 to 39.8 cmol+kg^{-1}. The clay fraction was dominated by allophane and imogolite. The Hapludult and Haplorthox were very strongly to strongly acid soils. They were low in organic matter content, and CEC ranged from 9.4 to 19.0 cmol+kg^{-1} in the Hapludult, and from 7.5 to 9.5 cmol+kg^{-1} in the Haplorthox. Kaolinite and sesquioxide minerals were major clay minerals in the soils. Some proto-imogolite was detected in the BC and C horizons of the Hapludult. In terms of NRDP, the two Andosols were characterized by porphyric to porphyri-phyric fabrics. A strongly developed granular structure was noticed, showing features of a congelic SRDP (specific related distribution pattern). According to the c/f relation, these soil fabrics were open porphyric RDP's. It was concluded that the Andosols fabric was formed under the influence of high humic matter content, and micro-organisms activity. Such a fabric created a microclimate more humid than the climate above the soil surface. This is one of the reasons why Andosols were frequently oversaturated with water without causing poor drainage conditions. In contrast, the dense fabric in the Bt horizon of the Hapludult was expected to affect drainage and water percolation.

INTRODUCTION

Large areas in Sumatra and Java, Indonesia, are covered by volcanic ash and tuff from Pleistocene volcanic eruptions. Depending on local conditions, this volcanic ash has given rise to the development of a variety of soils. At altitudes above 600 m a.s.l. Andosols have formed, whereas below 600 m a.s.l. Latosols occur on volcanic ash (Dudal and Supraptohardjo, 1961, 1975), though some Andosols have been reported in the lowlands of Indonesia (Tan, 1960, 1984). These Latosols are now classified as Ultisols and Oxisols in the American system.

The micromorphology of Ultisols and Oxisols has recently received considerable research attention (Fedoroff and Eswaran, 1985; Stoops and Buol, 1985). A review of the earlier

research on micromorphology of Oxisols was reported by Buol and Eswaran (1978) and Stoops (1983). Such studies have shown that soil fabrics can be used for the identification of argillic and oxic horizons in Ultisols and Oxisols, respectively. In particular, the micromorphological criteria for identifying an oxic horizon were reported by Buol and Eswaran (1978), and Paramananthan and Eswaran (1980). However, Stoops and Buol (1985) indicated that only oxic soil constituents, and not oxic horizons, could be identified by micromorphological methods.

Although data have started to accumulate recently, comparatively less is known on the micromorphology of Andosols. The term Andosols is used here as in the FAO-Unesco soil classification. Kawai (1969) has reported that Andosols in Japan exhibited blocky and loose to fine grained porous soil fabrics. According to Pain (1971), isotic plasmic fabrics were indicative of soils derived from volcanic ash (Kandepts) in Papua New Guinea. Such a fabric was reported to be associated with allophane-organic matter complexes (Chartres *et al.*, 1985). More information appears to be needed on the micromorphology of Andosols in other regions. It is expected that differences in properties between Andosols, Ultisols and Oxisols will be reflected in the nature of soil fabrics. In addition, most of the fabric analyses of Oxisols and Ultisols were from soils not derived from volcanic ash (Bennema *et al.*, 1970; Eswaran, 1972). Therefore, this investigation was conducted to (i) study differences in NRDP between Andosols, Ultisols and Oxisols, derived from volcanic ash, in Indonesia, and (ii) determine their mineralogical and chemical properties.

MATERIALS AND METHODS

The soils used in this investigation included two Andosols, a Hapludult and a Haplorthox, representing two dark coloured and two red coloured soils, respectively. The soils are derived from dacito-andesitic tuffs from Pleistocene eruptions of the volcanos in West Java. The mineral composition of the tuffs are mostly andesitic with slight dacitic properties. One Andosol was located at 600 m a.s.l. on the slope of the Salak volcano near the village Ciapus, and is referred to as Andosol/Ciapus. The area has a mean annual precipitation of 4880 mm, and a mean annual temperature of 20°C (Schmidt and Ferguson, 1951). Vegetation in the area is composed of clove trees (*Syzygium aromaticum* (L.) Merrill and L.M. Terry) and grasses (*Paspalum* spp.). Another Andosol, referred to as Andosol/Pengalengan, is located in a tea (*Camellia sinensis* (L.) O. Kuntze) plantation at 1500 m a.s.l. on the slope of the Wayang volcano near the town Pengalengan. The area has a mean annual precipitation of 2564 mm, and a mean annual temperature of 18°C. The Hapludult was selected in an oil palm (*Elaeis guineensis* Jacq.) plantation near the town Rangkasbitung at 100 m a.s.l. The region has a mean annual rainfall of 2842 mm, and a mean annual temperature of 26°C. The vegetation underneath the oil palm consists of grasses (*Imperata cylindrica* (L.) Rausch, and *Paspalum* spp.). The Haplorthox is located at 50 - 100 m a.s.l. near the town of Depok under grasses (*Paspalum* spp.). The mean annual rainfall is 3130 mm with a mean annual temperatureof 26°C.

Samples were taken from genetic horizons for thin section, chemical and mineralogical analysis. Thin sections were prepared using the technique of Fitzpatrick (1980), by which drying of the samples was avoided and the water replaced with acetone prior to impregnation. Thin sections showing artifical cracking, as noted by Chartres *et al.* (1985) because of drying,

Table 1
Physico-chemical properties of the soils.

	Sand	Silt	Clay	pH		Corg	CEC	Base sat.
	2-0.005mm	0.005-0.002mm	<0.002mm	H₂O	KCl			
		%				%	cmol+/kg	%
				Andosol/Ciapus				
Ap	15.6	62.5	21.9	4.9	4.7	15.2	26.4	7.9
Bw	13.0	68.5	18.5	4.8	4.5	13.5	20.9	4.1
C	12.0	72.8	15.2	5.3	5.0	4.1	-	-
				Andosol/Pengalengan				
Ap	42.6	33.2	24.2	4.71	4.5	13.4	24.4	-
Bw	32.4	43.9	25.2	4.9	4.5	3.3	23.4	-
				Hapludult				
Ap	20.4	28.4	51.1	3.8	3.5	2.0	9.4	6.2
Bt	15.4	24.7	59.9	3.6	3.4	1.0	19.0	4.2
C	28.1	31.2	42.7	4.0	3.5	0.2	21.3	3.3
				Haplorthox				
Ap	13.0	12.2	74.8	4.9	4.0	1.7	10.6	7.0
B	12.8	4.8	82.4	4.8	3.7	0.6	12.3	8.5

were discarded. Fabric analysis was done by employing the normal related distribution pattern (NRDP), specific related distribution pattern (SRDP; Eswaran and Banos, 1976), and the c/f related distribution pattern concept (c/f RDP; Stoops and Jongerius, 1975). Organic C was determined by the Walkley-Black method (Nelson and Sommers, 1982), and pH was measured in water and KCl suspensions using a soil/solution ratio of 1:1 (McLean, 1982). Exchangeable bases and CEC were determined by the neutral 1 M NH₄OAc method (Jackson, 1958). Particle size distribution analysis was conducted by the centrifugation procedure (Jackson, 1956), after ultrasonic dispersion at 20 kHz and 125 W for 30 minutes. It is thought that this method ensures complete dispersion. Clay was collected and extracted for allophane and imogolite (Yoshinaga and Aomine, 1962). Identification of clay minerals was performed by x-ray diffraction (XRD) analysis and transmission electron microcoscopy (TEM) including EDAX (energy dispersive analysis by X-rays; see Goenadi and Tan, 1989, 1991).

RESULTS AND DISCUSSION

The Andosols were strongly acid soils, with loam to silt loam textures (Table 1). They have high organic matter contents, and exhibit CEC's ranging from 20.9 to 26.4 cmol+kg⁻¹. The Hapludult and Haplorthox were very strongly to strongly acid soils, with clayey textures. These soils were low in organic matter content. The CEC ranged from 9.4 to 21.3 cmol+kg⁻¹ in the Hapludult, and from 10.6 to 12.3 cmol+kg⁻¹ in the Haplorthox. The base saturation in all profiles was very low, which is an indication of the drastic leaching attributed to the very humid condition.
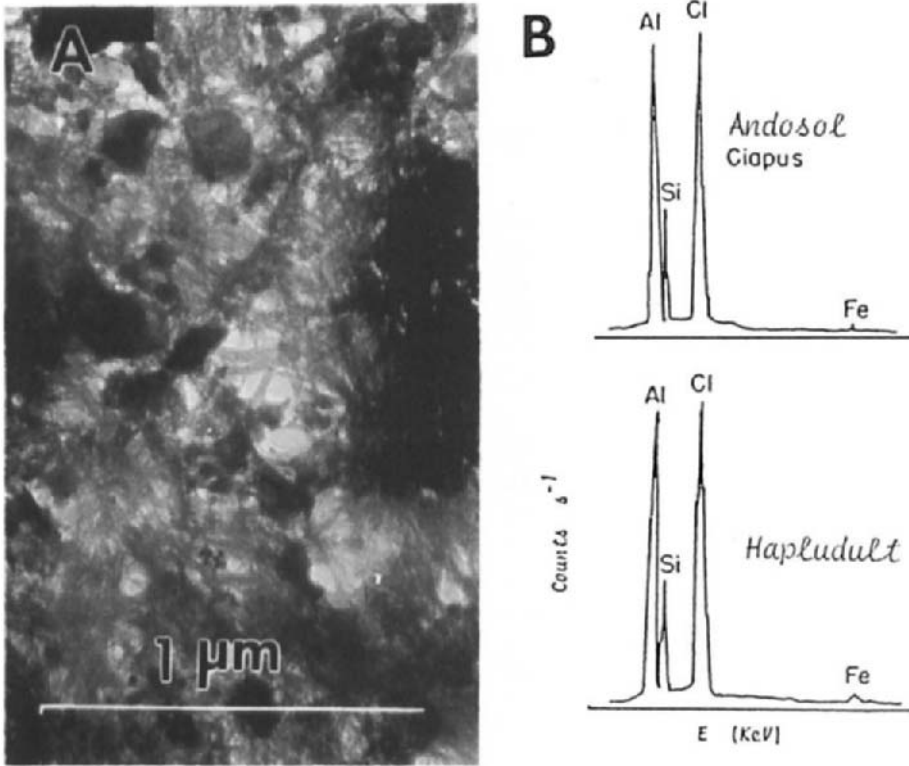
Fig. 1. A) TEM micrograph of imogolite in the clay fraction of Andosol/Ciapus. B) Elemental composition of an imogolite strand as determined by EDAX, showing and Al/Si ratio of 2:1. The presence of Cl is attributed to the NaCl used in the extraction method.

Allophane and imogolite were the dominant clay minerals in the Andosols (Fig. 1). The fibrous strands of imogolite varied in diameter from 0.010 to 0.015 µm (Goenadi and Tan, 1991). Elemental analysis of the imogolite strands by EDAX yielded a composition with an Al/Si ratio of 2:1, which was within the limits of imogolite clays. Allophane and imogolite were also detected in Andosols of the Bukit Tungul volcano north of the city of Bandung (Chartres and Van Reuler (1985). This Andosol is located at 100 km east from the Ciapus/Andosol. Kaolinite, halloysite, iron oxide minerals and gibbsite were the major clay minerals in the Hapludult and Haplorthox (Goenadi and Tan, 1991). Some fibrous clay was detected in the BC and C horizon of the Hapludult (Fig. 2). It was closely associated with allophane, and exhibited a structure characteristic of an imogolite-allophane mixture called proto-imogolite (Yoshinaga and Aomine, 1962).

In terms of the c/f RDP, all the soils were characterized by an open porphyric fabric (Table 2). However, when projected in the NRDP triangle, different types of soil fabrics are inferred. The Andosol/Ciapus had a porphyri-phyric NRDP, whereas the fabric of Andosol/Pengalengan was porphyric in nature (Fig. 3). The plasmic fabrics in Andosols noted by Chartres et al.

Fig. 2. TEM micrograph of proto-imogolite in the BC horizon clay of the Hapludult.

Table 2.
Summary of soil fabric analysis.

Soil	NRDP Eswaran & Banos	RDP Stoops & Jongerius	SRDP Eswaran & Banos
Andosol-Ciapus	Porphyri-phyric	Open porphyric	Congelic
Andosol-Pengalengan	Porphyric	Open porphyric	Congelic
Hapludult	Plasmi-porphyric to Porphyri-plasmic	Open porphyric	-
Haplorthox	Plasmic	Open porphyric	Agglutinic

(1985), and the high clay content resulting in the development of Bt horizons in the Bukit Tungul Andosol (Chartres and Van Reuler, 1985) are exceptions rather than the norm in Andosols. The Hapludult exhibited a plasmi-porphyric to porphyri-plasmic NRDP. Only in the C horizon, where the fabric skeleton is at a minimum, does a porphyric NRDP occur. The solum of the Haplorthox was characterized by a plasmic NRDP, because of the high plasma content. Typical examples of the NRDPs discussed above are shown in Fig. 4A to D. The Andosol fabric (Figs 4A and 4B) was strongly influenced by the high humic matter content. It exhibited a strong granular structure, which was attributed to the activity of soil organisms, such as earthworms. These organisms contributed to aggregation of the large amounts of silt
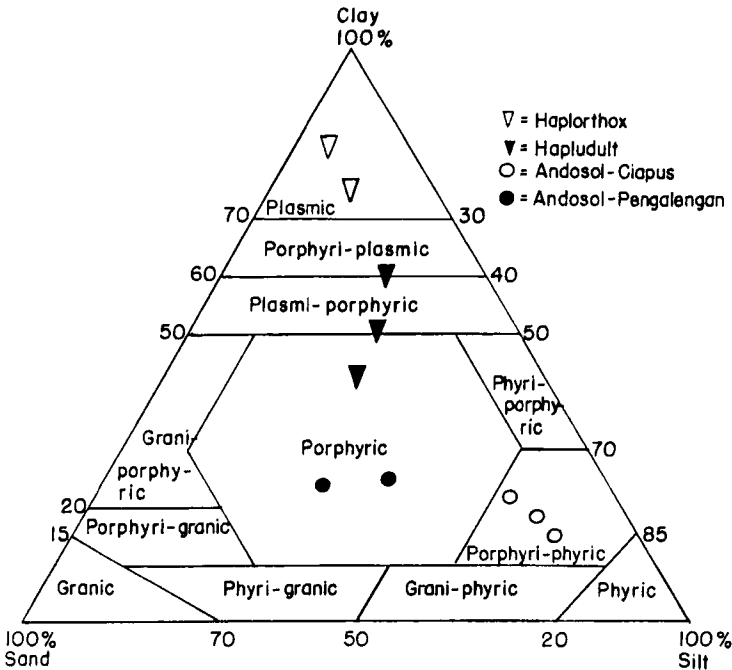
Fig. 3. The NRDP's of the soils determined by employing the NRDP triangle of Eswaran and Banos (1976).

with humic matter and plasma, resulting in formation of features of a congelic SRDP. Such a fabric would be formed only if the NRDP was in the phyric category, and the plasma was high in amorphous clays (Eswaran and Banos, 1976). Due to the extremely high humic matter content, the resulting soil fabric had a very high water holding capacity, high porosity and rapid internal permeability. In contrast, the fabrics of the Hapludult and Haplorthox (Fig. 4C and D) were affected more by a high plasma content. Fabric skeletons were at a minimum, and only the initial development of granular structures was noticed. In the Oxisol fabric, the plasma aggregated together with sand and silt to form granular structures with features characteristic of an agglutinic SRDP (Eswaran and Banos, 1976).

CONCLUSIONS

In conclusion, it can be stated that the c/f RDP approach is too coarse in that discrete differences in soil fabric cannot be recorded. On the other hand, the NRDP concept appears to be more capable in detecting detailed differences. In terms of NRDP, the Andosols were characterized by a porphyric to porphyri-phyric fabric, and the Hapludult by a plasmi-porphyric to porphyri-plasmic fabric, which are NRDP intergrades. The Haplorthox was distinguished by a plasmic soil fabric. The high humic matter and amorphous clay content, together with high activity of micro-organisms, contributed towards formation of the Andosol fabric with its high water holding capacity and porosity. Such a fabric is the reason for Andosols becoming frequently oversaturated with moisture without causing the development of poor drainage. On the other hand, the high plasma and low organic matter content in the Hapludult are conducive to the formation of a dense fabric. This has affected water percolation, especially in the Bt
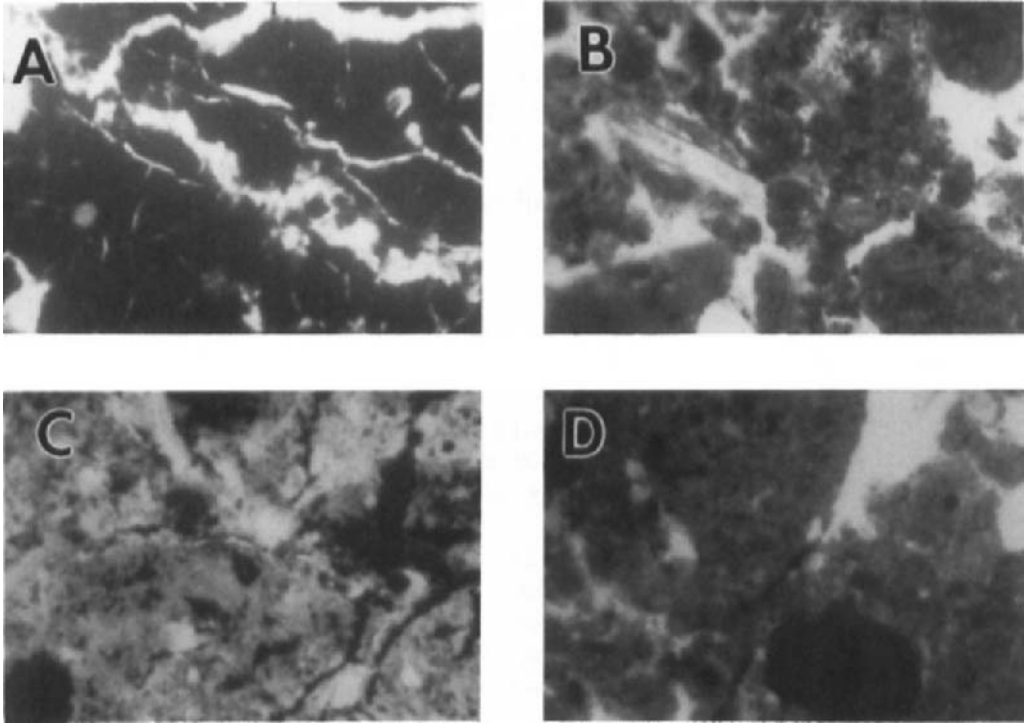
Fig. 4. Thin section micrographs (magn. 30×; plane polarized light.): **A)** A horizon of Andosol/Ciapus; **B)** A horizon Andosol/Pengalengan; **C)** Bt horizon of Hapludult; and **D)** B horizon of Haplorthox.

horizon, where signs of some mottling indicate the presence of impeded drainage. This was not a serious problem in the Haplorthox because aggregation of plasma into granular structures, forming features of an agglutinic SRDP, maintains a permeable characteristic.

REFERENCES

Bennema, J., Jongerius, A., and Lemos, R., 1970. Micromorphology of some oxic and argillic horizons in south Brazil in relation to weathering sequences. Geoderma, 4: 333-355.
Buol, S.W., and Eswaran, H., 1978. The micromorphology of Oxisols. In: M. Delgado (Editor), Micromorfolgia del Suelos. Proc. V Int. Working Meeting on Soil Micromorpology, Granada, Spain, Univeristy of Granada, 325-347.
Chartres, C.J., and Van Reuler, H., 1985. Mineralogical changes with depth in a layered Andosol near Bandung, Java (Indonesia). J. Soil Sci., 36: 173-186.

Chartres, C.J., Wood, A., and Pain, C.F., 1985. The development of micromorphological features in relation to some mineralogical and chemical properties of volcanic ash soils in highland Papua New Guinea. Aust. J. Soil Res., 23: 339-354.

Dudal, R., and Supraptohardjo, M., 1961. Some consideration on the genetic relationship between Latosols and Andosols in Java. Trans. VII Int. Cong. Soil Sci., Madison, WI, USA, 4: 229-233.

Dudal, R., and Supraptohardjo, M., 1975. Soil classification in Indonesia. Contrib. Gen. Agric. Res. Stn., Bogor, Indonesia, 148: 1-23.

Eswaran, H., 1972. Micromorphological indicators of pedogenesis in some tropical soils derived from basalt of Nicaragua. Geoderma, 7: 15-31.

Eswaran, H., and Banos, C., 1976. Related distribution patterns in soils and their significance. Anales de Edafologia y Agrobiologia, 35: 33-45.

Fedoroff, N., and Eswaran, H., 1985. Micromorphology of Ultisols. In: L.A. Douglas and W.L. Thompson (Editors), Soil Micromorphology and Soil Classification. Soil Sci. Soc. Am. Special Publ. No. 15, Madison, Wisconsin, USA, pp. 145-164.

FitzPatrick, E.A., 1980. Micromorphology of Soils. Dept. Soil Sci., Univ. Aberdeen, Aberdeen, UK, 227 pp.

Goenadi, D.H. and Tan, K.H., 1989. Mineralogy and micromorphology of soils from volcanic tuffs in the humid tropics. Soil Sci. Soc. Am. J., 53: 1907-1911.

Goenadi, D.H. and Tan, K.H., 1991. The weathering of paracrystalline clays into kaolinite in Andisols and Ultisols. Indon. J. Trop. Agric., 2: 56-65.

Jackson, M.L., 1956. Soil Chemical Analysis-Advanced Course. Dept. Soils, Univ. Wisconsin, Madison, WI, USA, 991 pp.

Jackson, M.L., 1958. Chemical Analysis. Prentice Hall, Engelwood Cliffs, NJ, USA, 498 pp.

Kawai, K., 1969. Micromorphological studies of Andosols in Japan. Bull. Nat. Inst. Agric. Sci., Series B, 20: 77-154.

McLean, E.O., 1982. Soil pH and lime requirement. In: A.L. Page, R.H. Miller, and D.R. Keeney (Editors), Methods of Soil Analysis, 2nd edition. Agronomy series 9. Am. Soc. Agronomy, and Soil Sci. Soc. Am., Madison, Wisconsin, USA, pp. 199-224.

Nelson, O.W., and Sommers, L.E., 1982. Total carbon, organic carbon and organic matter. In: A.L. Page, R.H. Miller, and D.R. Keeney (Editors), Methods of Soil Analysis, 2nd edition. Agronomy series 9. Am. Soc. Agronomy and Soil Sci. Soc. Am., Madison, WI, USA, pp. 539-580.

Pain, C.F., 1971. Micromorphology of soils developed from volcanic ash and river alluvium in the Kokoda Valley Northern District, Papua. J. Soil Sci., 22:275-80.

Paramananthan, S., and Eswaran, H., 1980. Morphological properties of Oxisols. In: B.K.G. Theng (Editor), Soils with Variable Charge. Soils Bureau, DSIR, Lower Hutt, New Zealand, pp. 35-43.

Schmidt, F.H. and Ferguson, J.A.H., 1951. Rainfall types based on wet and dry period ratios for Indonesia with Western New Guinea. Publ. 42. Java. Geophys. Meteor., Jakarta, 231 pp.

Stoops, G., 1983. Micromorphology of the oxic horizon. In: P. Bullock and C.P. Murphy (Editors) Soil Micromorphology, volume 2: Soil Genesis. Proc. VI Int. Working Meeting on Soil Micromorphology, London, August 1981, AB Academic Publishers, Berkhamsted, U.K., pp. 419-440.

Stoops, G.J., and Buol, S.W., 1985. Micromorphology of Oxisols. In: L.A. Douglas and W.L. Thompson (Editors), Soil Micromorphology and Soil Classification. Soil Sci. Soc. Am. Special Publ. No. 15, Madison, Wisconsin, USA, pp. 105-119.

Stoops, G. and Jongerius, A., 1975. Proposal for a micromorphological classification of soil materials I. A classification of the related distributions of fine and coarse particles. Geoderma, 13: 189-199.

Tan, K.H., 1960. The black dust soil of Deli (Sumatra). Tehnik Pertanian, 9: 77-93. In Indonesian with English summary.

Tan, K.H. (Editor), 1984. Andosols. Van Nostrand Reinhold, 418 pp.

Yoshinaga, N., and Aomine, S., 1962. Imogolite in some Ando-soils. Soil Sci. Plant Nutr., 8: 114-121.

This Page Intentionally Left Blank

Quantitative relationships between net volume change and fabric properties during soil evolution

O.A. Chadwick[1] and W.D. Nettleton[2]

[1]*JPL, California Institute of Technology, Pasadena, Califironia, USA*
[2]*USDA-SCS National Soil Survey Laboratory, Lincoln, Nebraska, USA*

ABSTRACT

Chadwick, O.A. and. Nettleton, W.D, 1994. Quantitative relationships between net volume change and fabric properties during soil evolution. In: A.J. Ringrose-Voase and G.S. Humphreys (Editors), Soil Micromorphology: Studies in Management and Genesis. Proc. IX Int. Working Meeting on Soil Micromorphology, Townsville, Australia, July 1992. Developments in Soil Science 22, Elsevier, Amsterdam, pp. 353-359.

The state of soil evolution can be charted by net long-term volume and elemental mass changes for individual horizons compared with parent material. Volume collapse or dilation depends on relative elemental mass fluxes associated with losses from or additions to soil horizons. Volume collapse occurs when minerals are weathered followed by leaching of elements, volume dilation occurs when carbon or other elements are introduced into a horizon in greater abundance than loss through weathering and leaching. For selected soil parent materials, the related-distribution-pattern of plasma and skeleton grains provide a parallel description of these pedological changes that can be quantified through image analysis. Here, we investigate relationships between chemical/mineralogical and micromorphological measures of volume change during pedogenesis. For coarse-textured, arkosic, fluvially laid parent materials, fabrics progress from monic to porphyric related-distribution-patterns as new elements are introduced into a horizon or as secondary products form due to primary mineral weathering. Porphyric related-distribution-patterns evolve from single-space to open with increasing dilation or collapse, because in either case plasma is augmented relative to skeleton grains. Since coarse-textured soils evolve to the same fabrics under differing intensities of additions from external sources and accumulation of weathering products, a true understanding of the state of soil evolution implied by observation and classification of fabric properties requires quantification of both net volume change and net mass change during soil development.

INTRODUCTION

In microscopic studies of soil, the relationship between fine and coarse constituents (*i.e.* plasma and skeleton grains) is termed 'related-distribution-pattern' (hearafter shortened to RDP) and is accorded special importance (Kubiena, 1938; Brewer, 1964; Brewer and Pawluk, 1975; Stoops and Jongerius, 1975; Bullock *et al.*, 1985). In essence, micromorphologic classification schemes recognize that plasma may fill voids between skeleton grains, coat grains, or compose the matrix within which skeleton grains are distributed. RDPs are useful

for studying soil evolution where parent material composition, grain size, and mode of deposition are kept constant. In this case, it is desirable to relate changes in RDPs to quantitative measures of soil development.

Evolution of RDPs from parent material to soil horizon implies changes in soil volume caused by the combined effects of pedogenesis (Brewer, 1964; Stoops and Jongerius, 1975; Bullock *et al.*, 1985). Thus, a quantitative measure of volume change between parent material and the horizon being described microscopically has special interest (Haseman and Marshall, 1945; Brewer, 1964; Brimhall and Dietrich, 1987; Chadwick *et al.*, 1990; Brimhall *et al.*, 1992). In an ideal situation, we should be able to ascribe a volume-change value to the RDP described for each horizon. If this is possible, soil fabric observation would provide a visualization of a quantified value and would be a more robust tool in studying soil genesis. Here, we investigate the possibility of developing quantitative relationships among RDPs, plasma content, and volume change in coarse-textured, arkosic, fluvially laid parent material that has evolved to form soil horizons.

METHODS

We selected examples from soil profiles whose characterization database resides in previously published papers or in the USDA National Soil Survey Laboratory (referenced by laboratory number in Table 1). Samples were selected to represent a range of horizon types, but are not inclusive; results are presented as an example of our approach that is constrained by a specified set of initial conditions. Standard procedures were used for chemical and physical characterization and preparation of thin sections (USDA Soil Conservation Service, 1992). RDP descriptions follow the classification of Stoops and Jongerius (1975) and Bullock *et al.*, (1985). Areas of skeleton grains (> 50 μm in diameter), plasma and void space (> 50 μm in diameter) were measured for five fields in thin sections using an Olympus C-2 Image Analyser[1] and are reported as a mean. The coefficient of variation ranges from 10 - 40% for skeleton grains.

We quantify volume change (strain) in soil ($\varepsilon_{i,w}$) by identifying bulk density (ρ_w) (g cm^{-3}) and the mass of an immobile component ($C_{i,w}$) (wt.% or ppm) in a soil horizon and compare it with bulk density (ρ_p) and the mass of an immobile component ($C_{i,p}$) in the soil parent material as follows (Brimhall and Dietrich, 1987; Brimhall *et al.*, 1992):

$$\varepsilon_{i,w} = \frac{\rho_p C_{i,p}}{\rho_w C_{i,w}} - 1 \qquad\qquad \text{Eqn. 1}$$

Positive volume changes represent dilations; negative volume changes represent collapse. Collapse occurs when the increase in concentration of an immobile element ($C_{i,w}$) caused by loss of mobile constituents is not exactly compensated by an inversely proportional decrease in bulk density (ρ_w) due to increasing porosity. This formulation is derived under the constraints of mass conservation in deformable media and is functionally similar to one derived by Brewer (1964, p. 81).

---

[1] Given for the convenience of the reader and does not imply endorsement by JPL or USDA-SCS.

Table 1
Related Distribution Patterns, Strain, and Areal Measurements for Soil Horizons Plotted in Fig. 1.

Related Distribution Patterns[1]	$\varepsilon_{i,w}$[2]	Area[3](%)			Horizon	Reference
		Skeleton Grains	Plasma	Void Space		
MN	0	42	—	58	[parent material]	Chadwick et al., 1990
GF	0.2	16	73	11	2Bs1	Pedon 1 – Merritts et al., 1991
EU	0.2	20	68	12	2Bs1	Pedon 1 – Merritts et al., 1991
CT	0.4	43	48	9	ABs	Pedon 1 – Merritts et al., 1991
EU–CT	0.5	37	53	10	2Bs1	Pedon 1 – Merritts et al., 1991
PS	0.2	32	68	—	A1	Pedon 4b – Merritts et al., 1991
PD	0.1	17	83	—	A2	Pedon 4b – Merritts et al., 1991
PD	0	12	88	—	AB	Pedon 4b – Merritts et al., 1991
PO	-0.2	7	93	—	Bw1	Pedon 4b – Merritts et al., 1991
PS	0.3	30	70	—	Bw3	Pedon 4b – Merritts et al., 1991
PO	0.1	6	94	—	AB1	Chadwick et al., 1990
PD	-0.3	12	88	—	Bw	Chadwick et al., 1990
PD	-0.3	13	87	—	Bt	Chadwick et al., 1990
PS	-0.3	18	82	—	Bt	Chadwick et al., 1990
PO	-0.2	8	92	—	Bo2	Chadwick et al., 1990
PS	0.1	14	86	—	A1	118 ka Soil, Fig. 1 – Brimhall et al., 1992
PS	-0.1	18	82	—	Bw	118 ka Soil, Fig. 1 – Brimhall et al., 1992
PS	-0.3	19	81	—	BC	118 ka Soil, Fig. 1 – Brimhall et al., 1992
GF	0	43	46	11	C	118 ka Soil, Fig. 1 – Brimhall et al., 1992
PD	1.1	14	86	—	K22m	Soil Number 3 – Gile et al., 1965
PS	0.3	29	71	—	Bt2	Lab Number 81P4572
PO	1.2	10	90	—	Bt1	Lab Number 64658
PO	2.0	3	97	—	Bt2	Lab Number 64651
PO	0.7	15	85	—	Bt2	Lab Number 66727
PD	2.2	13	87	—	Bt2	Lab Number 66649
PS	0.4	30	70	—	Bt2	Lab Number 40A1794

[1]MN = Monic; GF = Gefuric; EU = Enaulic; CT = Chitonic; PS = Single-Space Porphyric;
PD = Double-Space Porphyric; and PO = Open Porphyric.
[2]$\varepsilon_{i,w}$ calculated using Eqn. 1.
[3] Cross-Sectional area of thin section.

In these calculations, we use either the mass of Zr as an immobile element, or for selected soils from the NSSL database, the mass of the medium sand size fraction. We evaluated the validity of immobility assumptions on a case-by-case basis.
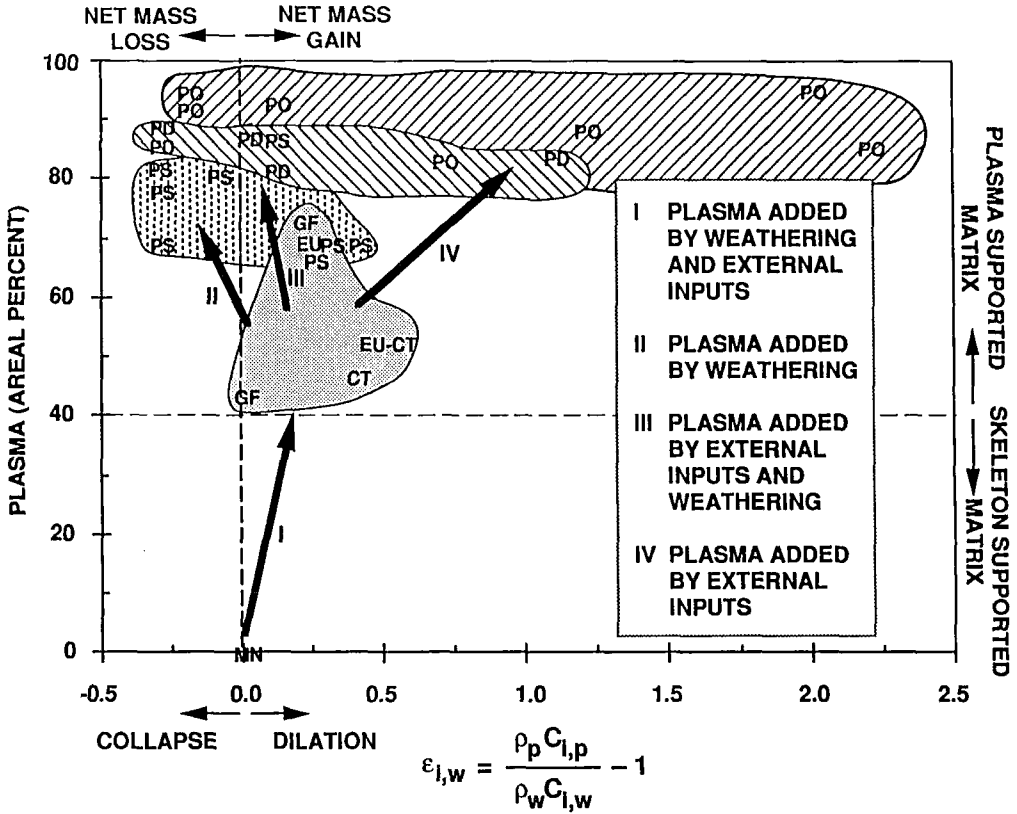
Fig. 1. Relationship among volume change ($\varepsilon_{i,w}$), soil plasma, and related-distribution-patterns (RDPs) for soil horizons listed in Table 1. RDP abbreviations are: MN=monic, EU=enaulic, CT=chitonic, GF=gefuric, PS=single-space porphyric, PD=double-space porphyric, PO=open porphyric. Shaded areas and arrows are explained in the text.

RESULTS

We classified RDPs, measured areas of fabric components in thin sections, and calculated volume change ($\varepsilon_{i,w}$) for 26 horizons (Table 1), and plotted each RDP into a graphical field defined by the numerical volume change and % plasma (Fig. 1). The graph is separated into four regions (dashed lines) defined by collapse or dilation along the x-axis which is controlled by the net mass loss or gain within each horizon and the change from skeleton supported matrix to plasma supported matrix along the y-axis which is interpreted from the RDPs. By our selection criteria, all soil parent material has monic RDP and zero volume change; they evolve in the direction of increasing plasma with either positive or negative volume change.

The RDPs plot into four overlapping fields shown as shaded areas in Fig. 1. Enaulic (EU), chitonic (CT), and gefuric (GF) RDPs (stippled field) range from 0 to 50% dilated and contain

40 to 70% plasma. Single-space porphyric (PS) RDPs (vertical dashes) range from 30% collapsed to 50% dilated and contain 70 to 85% plasma. Double-space porphyric (PD) RDPs (left slant lines) range from 30% collapsed to 100% dilated and contain 80 to 90% plasma. Open-space porphyric (PO) RDPs (right slant lines) range from 20% collapsed to over 200% dilated and contain 85 to 95% plasma.

Essentially, each of the fields in Fig. 1 represents stages of plasma accumulation along different soil evolutionary trajectories. We interpet the processes involved in plasma accumulation based on the observation that dilation results from net mass addition to soil horizons and collapse results from net mass loss from soil horizons (Brimhall and Dietrich, 1987; Chadwick *et al.*, 1990; Brimhall *et al.*, 1992; Merritts *et al.*, 1992). We infer that as these soils evolve from a monic starting point, they gain plasma forming either enaulic, chitonic, or gefuric RDPs where voids are infilled and/or skeleton grains are coated (path I, Fig. 1). In this case, plasma is derived from external inputs such as organic carbon and from weathering of nonresistant minerals. In humid environments, the coatings are usually composed of iron and aluminum oxides, and organic compounds; in arid environments, they are usually composed of calcite or gypsum (Chadwick and Nettleton, 1990). Though excluded by our selection criteria, we note that E horizon formation occurs through a reversal of path I.

There are three possible evolutionary pathways leading from the RDPs defined by plasma coatings on skeleton grains or plasma infillings (EU, CT, GF) to the more plasma-rich fields shown on Fig. 1. They are defined by the balance between leaching of elements that results in net mass loss, and external inputs of elements into the soil column that results in net mass gain. Where weathering of minerals, leaching of mobile elements, and accumulation of the less mobile elements as plasma is the dominant pedogenic process (path II, Fig. 1), soil horizons collapse even as plasma is accumulating. Along path II, the single-space, double-space, and open porphyric RDPs result from mass transfer between the skeleton and plasma fractions of the s-matrix. At the opposite extreme, where weathering and leaching are less important than external inputs such as silicate and carbonate dust or calcium in rainwater (path IV, Fig. 1), soil horizons may more than double in volume as plasma from external sources is incorporated by deformational mass transport (Brimhall *et al.*, 1992). The double-space and open porphyric RDPs result from floating of skeleton grains in the increased plasma (a generalization of the K-fabric concept (Gile *et al.*, 1965). Commonly, where external inputs are balanced partly by leaching losses (path III, Fig. 1), soil horizons are slightly dilated even though much plasma has accumulated. Along path III, the single-space, double-space, and open porphyric RDPs result from both accumulation of externally derived plasma and weathering derived plasma.

DISCUSSION AND CONCLUSIONS

The relationship between RDPs and volume change is summarized by the diagrams in Fig. 2. Two diagrams are shown, one for cases where cohesive forces dominate and the other case where adhesive forces dominate. Cohesive forces occur in humid environments when covalently bonded silica, iron, aluminum, and organic matter form the non-silicate clay portion of the plasma and adhesive forces dominate in arid environments when ionically bonded salts form the non-silicate clay portion of the plasma (Chadwick and Nettleton, 1990). The diagrams show the progression of fabrics from monic (the orthogranic of Brewer and Pawluck, 1975) to open porphyric. In the cohesive case, the progression is through gefuric and chitonic to close porphyric, whereas, in the adhesive case the progression is through enaulic and
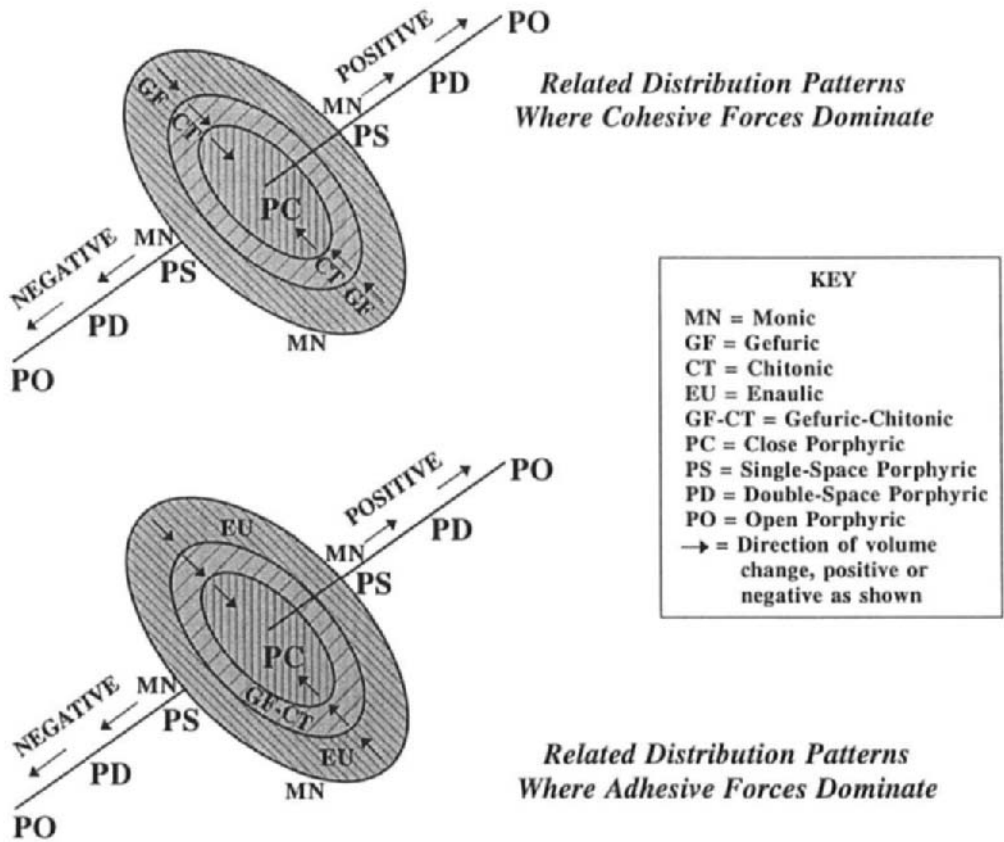
Fig. 2. Relationship of soil fabrics to soil volume changes where either cohesive or adhesive forces dominate.

gefuric-chitonic to close porphyric. The enaulic to close porphyric pathway occurs in the adhesive case because irregularly shaped aggregates first accumulate in the spaces between grains. In this case, continued plasma addition fills the spaces that develop between grains such that former grain-to-grain contacts are forced apart to produce a close porphyric RDP. None of the categories defined by Bullock *et al.*, (1985) describe this intermediate class very well. It best fits the plectic class of Brewer and Pawluck (1975).

Progressive filling of inter-skeleton grain voids by plasma drives an inward movement along the discs in Fig. 2 and produces small dilations. Once soil evolution produces a plasma supported matrix, the same sequence of fabrics can develop from either dilation or collapse as shown by progression from single-space to open porphyric along both ends of the orthogonal line through the discs. Thus, while it is possible to relate RDPs to quantitative volume change and plasma content, it is not possible to develop a cause and effect relationship between these measures of soil evolution. To relate RDPs, volume change, and soil plasma uniquely, it is also

necessary to calculate net mass-balance change during soil evolution (see Chadwick *et al.*, 1990).

REFERENCES

Brewer, R., 1964. Fabric and Mineral Analysis of Soils. John Wiley and Sons, New York. 470 pp.

Brewer, R. and Pawluck, S., 1975. Investigations of some soils developed in hummocks of the Canadian sub-artic and southern-artic regions 1. Morphology and Micromorphology. Can. J. Soil Sci., 55: 301-319.

Brimhall, G.H and Dietrich, W.E., 1987. Constitutive mass balance relations between chemical composition, volume, density, porosity, and strain in metasomatic hydrochemical systems: results on weathering and pedogenesis. Geochim. Cosmochim. Acta, 51: 567-587.

Brimhall, G.H, Chadwick, O.A., Lewis, C.J., Compston, W., Dietrich, W.E., Power, M., Hendricks, D.M., and Bratt, J., 1992. Deformational mass transport and invasive processes in soil evolution. Science, 255: 695-702.

Bullock, P., Fedoroff, N., Jongerius, A., Stoops, G., and Tursina, T., 1985. Handbook for Soil Thin Section Description. Waine Research Publications, Wolverhampton, U.K., 152 pp.

Chadwick, O.A. and Nettleton, W.D., 1990. Micromorphologic Evidence of Adhesive and Cohesive Forces in Soil Cementation. In: L.A. Douglas (Editor), Soil Micromorphology: A Basic and Applied Science. Proc. VIII Int. Working Meeting on Soil Mircromorphology, San Antonio, Texas, July 1988. Developments in Soil Science 19, pp. 207-212.

Chadwick, O.A., Brimhall, G.H. and Hendricks, D.M., 1990. From a black to a gray box - a mass balance approach to understanding soil processes. Geomorphology, 3: 369-390.

Gile, L.H., Peterson, F.F. and Grossman, R.B., 1965. The K horizon: a master soil horizon of carbonate accumulation. Soil Science, 99: 74-82.

Haseman, J.F. and Marshall, C.E., 1945. The use of heavy minerals studies of the origin and development of soils. Missouri Agricultural Experimental Station Research Bulletin 387.

Kubiena, W.L., 1938. Micropedology. Collegiate Press, Inc., Ames, Iowa, 243 pp.

Merritts, D.M., Chadwick, O.A., and Hendricks, D.M., 1991. Rates and processes of soil evolution on marine terraces, northern California. Geoderma, 51: 241-275.

Merritts, D.M., Chadwick, O.A. Hendricks, D.M., Brimhall, G.H. and Lewis, C.J.,   1992. The mass balance of soil evolution on late Quaternary marine terraces, northern California. Geological Society of America Bulletin, 104: 1456-1470.

Stoops, G. and Jongerius, A., 1975. A proposal for a micromorphological classification of soil materials. I. A classification of the related distributions of fine and coarse particles. Geoderma, 13: 189-199.

USDA Soil Conservation Service, 1992. Soil Survey Laboratory Methods Manual. Soil Survey Investigations Report No 42, ver 2.0. U.S. Gov. Printing Office, Washington, D.C., 400 pp.

This Page Intentionally Left Blank

Silt flow in soils

W.D. Nettleton[1], B.R. Brasher[1], O.W. Baumer[1], and R.G. Darmody[2]

[1]USDA-SCS, NSSC, Soil Survey Laboratory, Federal Building, Lincoln, NE, USA
[2]Department of Agronomy, University of Illinois, Urbana, IL, USA

ABSTRACT

Nettleton, W.D., Brasher, B.R., Baumer, O.W. and Darmody, R.G., 1994. Silt flow in soils. In: A.J. Ringrose-Voase and G.S. Humphreys (Editors), Soil Micromorphology: Studies in Management and Genesis. Proc. IX Int. Working Meeting on Soil Micromorphology, Townsville, Australia, July 1992. Developments in Soil Science 22, Elsevier, Amsterdam, pp. 361-371.

Silts and very fine sands, although considered to be skeleton grains, behave as soil plasma when they are moved and reorganized or concentrated in soil crusts, fragipans, and buried paleosols. We investigated the sizes of the voids through which the silt and very fine sand have moved and infer conditions responsible for formation of silty pedogenic features such as pedotubules and silt and very fine sand cutans. Soils which have both argillic horizons with illuviation argillans and underlying horizons with the silty pedogenic features were selected from Indiana, Illinois, Missouri, and Idaho. The average minimum diameters of these features, measured by image analysis, were 0.074 mm for voids with illuviation argillans and 0.402 mm for the silty pedogenic features. Most of the silty pedogenic features are striotubules. The voids, and former voids, are all < 3 mm in diameter and water flow in them theoretically has been mostly laminar. Under special cases, such as rapidly wetting of dry soil, the draining of saturated soil, or thawing of frozen soil, silty pedogenic features form as a result of detachment, transport, and deposition of silt and very fine sand. The deposition process is favoured by pore size discontinuities, low Ca and Mg content, low Fe content of prism coatings, high silt content, low aggregate stability, and by low organic carbon content. Because of the accumulated, silty pedogenic features most of the horizons have the lowest total porosity and the highest ratio of pores filled to those drained at 0.03 MPa. Besides producing root restricting horizons in soils and impeding drainage in tile lines and septic tank drain fields, silt and very fine sand movement and accumulation are involved in subsurface tunnel erosion or piping.

INTRODUCTION

Plasma as defined by Brewer and Sleeman (1960) includes colloidal-size mineral and organic material, as well as relatively soluble material not bound up in skeleton grains. Plasma is capable of being moved, or has been moved and reorganized or concentrated by soil forming processes. Silt, although not of colloidal size and subsequently excluded from plasma by Brewer (1976, pp. 11-12), is reported to have moved in the formation of surface crusts in soils (Falayi and Bouma, 1975; Boiffin and Bresson, 1987; Arshad and Mermut, 1988; and West *et al.*, 1990), in vesicular layers (Sullivan and Koppi, 1991), in cryoturbated features such as silt

cappings and distorted horizons (Tarnocai and Valentine, 1989; Romans et al., 1966; Catt, 1989; Bronger, 1969/1970), in fragipan horizons (Carlisle, 1954; Nettleton et al., 1968; Miller et al., 1971; De Kimpe and McKeague, 1974; Fitzpatrick, 1974; Van Vliet and Langohr, 1981; Anderson and Darmody, 1989; and Habecker et al., 1990), and in buried paleosols (Ransom, 1984; Ransom et al., 1987; and Fedoroff et al., 1990; Thompson, 1986; Thompson and Smeck, 1983).

In this paper we investigate the size of the voids through which clay and silt move in soils and infer the kind of water movement responsible for formation of the silty pedogenic features.

METHODS AND MATERIALS

Fifteen soils with argillic horizons and underlying Btx horizons with pedotubules, or other evidence of silt and very fine sand movement were selected. Fragipans were recognized in some of them and all of them formed in loess over paleosols. The soils occur in Indiana, Illinois, Missouri and Idaho in association with other loessial soils that have argillic horizons, but do not have Btx horizons or fragipans (see the review by Franzmeier et al., 1989). These associated soils formed in deeper loess or in loess over calcareous till. The soils selected in Indiana and Illinois formed in Peorian loess over Illinoian paleosols which formed in drift or pedisediment. The soils in Missouri were formed in loess over paleosols which had developed in moderately weathered local colluvium from limestone and dolomite. The soil from Idaho was formed in loess over a paleosol which had developed in loess also. Eluvial horizons formed at the loess paleosol boundaries in each of the soils.

Unoriented thin sections of pairs of horizons from each soil were mounted on 27 × 46 mm glass slides. The pairs included a Bt horizon with mostly illuviation argillans in voids in the overlying loess and a Btx horizon with mostly pedotubules in the underlying paleosol. These features were studied with the Cue-2 Image Analysis System[1]. The smallest Martin's radius from the shape analysis was used to estimate the minimum diameter of the voids and pedotubules. The smallest radius was recorded because it is a measurement not influenced by the orientation of the thin section. Ten voids with argillans or 10 pedotubules were selected by transecting and were analyzed for each of the two horizons. In all 300 observations were made, 150 in each kind of horizon.

The soil characterization data were obtained by methods described in Soil Survey Investigations Report No. 42 (USDA Soil Conservation Service, 1992) and identified herein by codes. The pore volume ratio was calculated from the volume of pores filled at 0.033 MPa divided by those drained at this suction. Statistics were performed using SAS (1988).

RESULTS

The minimum diameter of the voids and pedotubules ranged in size from a few micrometers up to slightly more than 1 mm (Fig. 1a and Table 1). Two diameters dominated, one at 0.080 mm and the other at 0.320 mm. About half of the voids with illuviation argillans had minimum diameters of <0.065 mm (Fig. 1b).

---

[1]Olympus Corporation, 4 Nevada Drive, Lake Success, NY 11042-1179, U.S.A. Name and address of manufacturer is given for the convenience of the reader and does not imply endorsement by the USDA Soil Conservation Service.
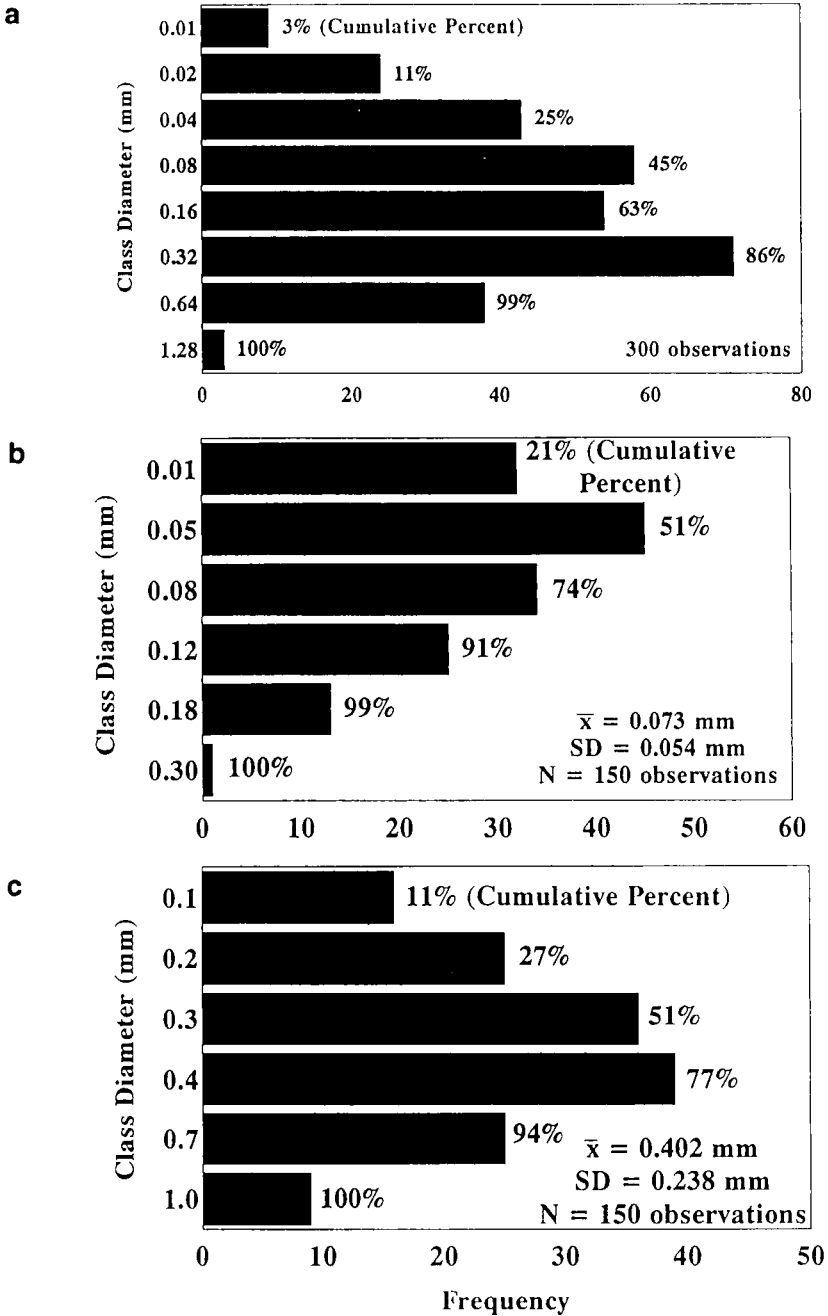
Fig. 1. Frequency of the minimum diameter of: **a)** voids with illuviation argillans and pedotubules; **b)** voids with illuviation argillans and **c)** pedotubules.

Table 1.
Some statistics for the minimum diameter of voids with illuviation argillans and those with pedotubules in the horizon-pairs of the fifteen soils.

| | | Diameter of the features, mm | | | |
Variable	N	Minimum	Maximum	Mean	Std. dev.
Voids with illuviation argillans	150	0.004	0.332	0.0735	0.0541
Pedotubules	150	0.030	1.035	0.4032	0.2378
				Difference of means	Std. error of difference
Difference				0.3288*	0.0209

*A t-test shows this difference has a t-ratio of 15.72 and is significant at the 0.01% level (SAS Institute, 1988).

The average minimum diameter, 0.074 mm (Table 1), shows that the distribution is skewed toward the smaller diameters. About half of the pedotubules had silt and very fine sand filled voids, with a minimum diameter of < 0.350 mm (Fig. 1c). The average minimum diameter, 0.402 mm, showed that this distribution was also skewed towards the smaller diameters. Selected characterization data for the horizon-pairs of the fifteen soils are shown in Table 2.

Some of the silt flows are coatings along void channels or on coarse fragments and consist of finely stratified silts and clays with a few very fine and fine sands like the one in Fig. 2. Most, however, are striotubules. Figs 3a and b are of a silty pedogenic feature like a pedotubule except that this one has a void. Some are outlined by well oriented, ansiotropic clays but consist of silts without apparent order (Figs 3c and d).

DISCUSSION

The minimum diameters of the former voids filled with silt and clay (Figs 2-3), are significantly larger than those outlined with illuviation argillans (Table 1). Some overlap of diameter sizes occur as shown in Fig. 1a. Because the microscope and image analyzer system we used is limited to widths of <2 mm, our study was limited to channel voids and pedotubules of this size range. Furthermore, the program could not cope with complex shapes encountered and hence, no measure of tortuosity of the channel voids was attempted.

The voids observed in this study were mostly in the micro to meso range (Brewer, 1964), which is the range for water storage and transmission (Greenland, 1977) and for gravitation (Luxmoore, 1981). At normal temperature and pressure these are the ranges for capillary pores, <3 mm diameter (Hamblin, 1985), in which flow is assumed to be laminar.

Theory

The pedotubules are evidence that silts and very fine sands move in soils. This requires detachment, transport, and then deposition in a new location. Transport occurs because gravity acts on the particles once they are in suspension. The particles drop out of suspension

Table 2. Comparison of physical and chemical data and the minimum pore diameters of horizons with mostly illuviation argillans (Bt) and those with mostly pedotubules (Btx) from fifteen Alfisols, Mollisols, and Udults (Soil Survey Staff, 1992). (Sand, 2 - 0.05 mm; silt, 0.05 - 0.002mm; clay, <0.002mm).

	Horizon	Volume >2mm	Particle Size Analysis % <2mm soil by weight			Analysis of <2mm soil			Min. Pore Diameter	Al Saturation	Aggregate Stability
						Organic C	ρ_b (30kPa)	COLE			
		%	Sand	Silt	Clay	dg kg^{-1}	g cm^{-3}	cm cm^{-1}	mm	%	%
Aeric Ochraqualf	Bt	0	4	70	26	0.11	1.47	0.05	0.090	35	4.7
	Btx	2	31	42	27	0.08	1.57	0.03	0.272	0	0.3
Typic Natraqualf	Bt	0	4	72	24	0.44	1.50	0.02	0.092	0	5.8
	Btx	0	8	69	23	0.09	1.51	0.04	0.209	0	0.7
Mollic Albaqualf	Bt	0	7	69	24	0.37	1.56	0.01	0.114	41	20.1
	Btx	0	10	66	24	0.10	1.59	0.00	0.302	0	2.0
Typic Albaqualf	Bt	0	4	53	43	0.43	1.50	0.02	0.082	46	NA
	Btx	0	12	60	28	0.13	1.52	0.03	0.414	9	NA
Typic Hapludalf	Bt	1	26	39	35	0.15	1.56	0.05	0.097	7	NA
	Btx	1	63	24	14	0.06	1.89	0.01	0.315	0	NA
TypicFragiudalfs	Bt	1	23	52	25	0.20	1.49	0.03	0.070	41	NA
	Btx	1	31	45	24	0.14	1.61	0.04	0.387	19	NA
Typic Fragiudalfs	Bt	0	13	61	26	0.21	1.50	0.01	0.080	20	NA
	Btx	1	30	52	18	0.06	1.75	0.01	0.263	29	NA
Aquic Fragiudalf	Bt	0	16	59	25	0.13	1.54	0.02	0.103	42	NA
	Btx	3	28	50	22	0.06	1.63	0.02	0.476	1	NA
Mollic Fragiudalfs	Bt	9	5	56	39	1.02	1.33	0.04	0.030	31	NA
	Btx	81	11	57	32	0.55	1.70	0.00	0.728	52	NA
Mollic Fragiudalfs	Bt	8	6	51	43	0.67	1.36	0.04	0.021	57	NA
	Btx	82	21	40	39	0.26	1.68	0.01	0.640	49	NA
Mollic Fragiudalfs	Bt	1	4	55	41	0.91	1.37	0.01	0.038	34	NA
	Btx	7	6	59	35	0.23	1.59	0.02	0.484	41	NA
Mollic Fragixeralf	Bt	1	7	75	18	0.85	1.36	0.01	0.086	0	NA
	Btx	0	6	65	29	0.34	1.55	0.05	0.218	0	NA
Argic Cryoboroll	Bt	62	67	21	12	0.33	1.49	0.01	0.086	0	19.9
	Btx	70	73	17	10	0.18	1.66	0.01	0.342	0	26.9
Typic Fragiudults in fine-	Bt	20	10	54	36	0.31	1.51	0.02	0.046	49	23.4
loamy, siliceous mesic families	Btx	28	18	49	33	0.18	1.41	0.00	0.561	75	27.9
Typic Fragiudults in fine-	Bt	12	7	59	34	0.21	1.50	0.02	0.043	57	48.6
loamy, siliceous mesic families	Btx	13	10	66	24	0.06	1.51	0.01	0.418	80	15.1
Horizon Mean± S.D.	Bt	8±16	14±16	56±14	30±9	0.42±0.30	1.47±0.08	0.02±0.01	0.072±0.03	31±20	20.4±15.9
	Btx	19±31	24±20	51±15	25±8	0.17±0.14	1.61±0.12	0.02±0.01	0.402±0.15	24±29	12.2±13.0

Fig. 2. Photomicrograph of a thin section of the BC horizon of the Argic Cryoboroll in plane polarized light. The feature consists of finely stratified silt and clay bridging between two coarse fragments.

when the water flow slows upon reaching a pore size discontinuity or where the water infiltrates ped interiors leaving the particles at the interface.

The size of the voids with illuviation argillans (0.007 cm, see Table 1) suggests that for turbulent flow to be responsible for detachment of particles, the discharge velocity would need to be at the high rate of 1.4 cm sec^{-1}. We arrived at the rate by rearranging the equation for Reynold's number (Harr, 1962) and solving for the discharge velocity, v in cm s^{-1}:

$$v = (R\eta)/(dD) \tag{Eqn. 1}$$

where R is the Reynold's number, here set to its minimum of 1 (Muskat, 1946), η the viscosity of water, 0.01 g s cm^{-2}, d the average minimum diameter of voids with illuviation argillans, 0.007 cm, and D the density of water, 1 g cm^{-3}.

However, if we accept that only laminar flow occurs through the fine pores just mentioned, detachment can still be explained by the stress on the pore walls, τ, created by shear. Thus:

$$\tau = F/A = \eta (dv/dr) \tag{Eqn. 2}$$

where F is the force, A the area, r the pore radius and dv/dr the change of velocity in the direction of the increasing radius. Changes in pore water velocity will cause corresponding changes in stress. If stress exceeds a critical value, particles will be detached from the pore wall. Sufficient stress to detach particles may be produced during wetting. The upper, slower conducting layer will become saturated, and as the water breaks into preferred passages of the faster conducting, lower layer, pore water velocity in the larger pores of the upper layer increases. This increases the stress on the pores walls so that detachment of particles occurs. In the drying cycle, stress increases as water from the larger pores drains first and water from the soil matrix enters larger pores through the pore walls. We have noted clays and silts in the
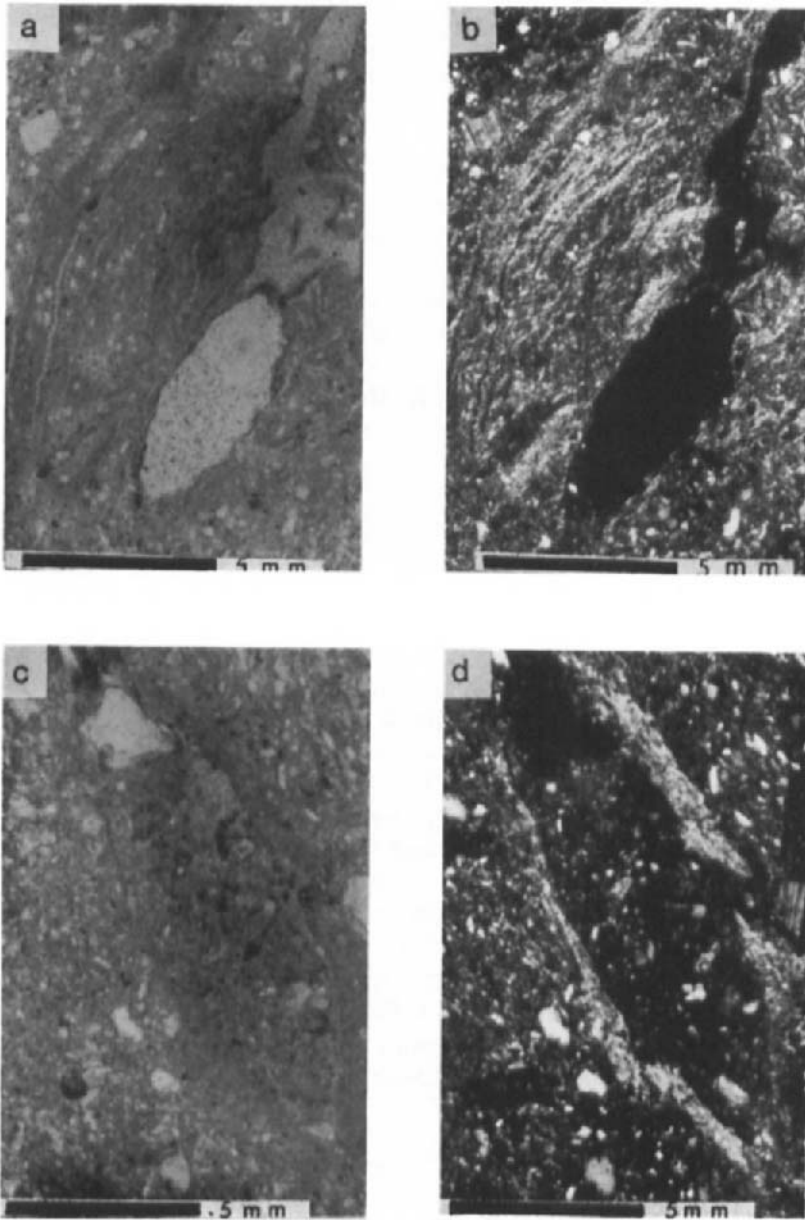
Fig. 3. Photomicrographs of thin sections of: **a**) the 2Btg5 horizon, 140 - 160 cm depth, of the Mollic Albaqualf in plane polarized light, showing layers of silt and clay around an elliptical void; **b**) as a) but in crossed polarized light; **c**) the 2Btx horizon, 94 - 125 cm depth, of the Aeric Ochraqualf in plane polarized light showing the clay layers outlining the mostly silt filled voids; **d**) as c) but in crossed polarized light, showing the orientation of the clays that outline the island of silt and the small void in the upper part.

water draining from soil cores at the end of hydraulic conductivity studies. Measurement of stress, however, is beyond the scope of our study.

Supporting Observations

Silt and very fine sand have been translocated and deposited as silty pedogenic features in Btx horizons of each of the 15 soils. Physical and chemical data show that the overlying Bt horizons have some features in common that help explain the silt movement. All except the Argic Cryoboroll have at least one horizon with >50% silt (Table 2) so material was available to be moved if conditions were favourable. Each of the soils has a particle size discontinuity with finer-textured material overlying coarser-textured material and hence smaller diameter voids overlying larger diameter silt-filled voids (Table 2). We infer that the silty pedogenic features formed below the contact occupy former voids. The larger diameter voids in these lower horizons would have favoured formation of near saturated conditions in overlying Bt horizons before the wetting front could break through to the lower horizons. As the wetting front passes across the pore-size discontinuity occurring at the contact, strain develops in the pores at the base of the overlying horizon. Clay, silt, and very fine sand particles are detached from the walls of these channel voids, and are carried into the lower horizons to form pedotubules (see Figs 3a and b for an incomplete pedotubule) and other silty pedogenic features.

Particles in weak soil aggregates are more easily detached from pore walls than particles in well aggregated material. These particles then, may be moved by processes described herein into lower horizons. In our study, most of the Bt and Btx horizons have weak soil aggregates, *i.e.* aggregate stabilities are <30% (Table 2 and R. Grossman, pers. commun., 1993). Several of their attributes help explain this weak aggregation. Low Ca and Mg saturation of some of the soils and high Na percentages in others (Table 2) tend to produce weak aggregation (Hamblin, 1985). Low organic carbon content of these horizons tends to produce weak aggregation (Table 2) (Emerson, *et al.*, 1986; McKeague *et al.*, 1986; Mbagwu and Piccolo, 1989). Dithionite-citrate Fe contents of <0.2 dg kg^{-1} in ped coatings and prism faces in and above the fragipans and other horizons in which the silty pedogenic features occur (Unpublished data from the Soil Survey Laboratory) are believed to be too low to stabilize soil aggregates (Panayiotopoulos and Kostoponlou, 1989; Columbo and Torrent, 1991). All 15 soils are subject to freezing and thawing, an action also known to weaken soil aggregates (Bisal and Nielsen, 1967; Hinman and Bisal, 1968; Sillanpaa and Webber, 1961; and Mbagwu and Bazzoffi, 1989).

Application

The understanding of the process of silt flow and deposition developed herein helps explain the high bulk density of soil horizons such as fragipans and aids in the design of agricultural subsurface drainage systems, lined irrigation ditches, earthen dams, and structures for the control of gully erosion. The design of drainage lines should include encasement by envelopes of material to receive all incoming water without developing flow velocities high enough to detach and move particles into the drains (Willardson, 1974). Our results suggest that one way to control the flow velocity would be to change the particle size of the envelope material gradually from the soil to the coarse material at the drain so as to avoid pore-size

discontinuities. To avoid piping and subsurface erosion the design of structures should avoid development of strong hydraulic gradients in soil adjacent to the structures.

CONCLUSIONS

The occurrence of pedotubules and other silty pedogenic features in soils is evidence that silt and very fine sand move downward. This requires particle detachment, transport, and deposition in a new location. Particles are detached when shear stress forces developed by laminar flow in a pore or by the surge of suspended water across a pore size discontinuity exceed the forces that retain a particle in the soil mass. Detachment can also occur as water in the soil matrix drains through the pore wall under suction induced by drying. Once in suspension, a particle moves with the water until the flow slows enough for deposition to occur. This happens where the water is suspended above a discontinuity or where it slows after flowing across a discontinuity. Deposition also occurs as water infiltrates ped interiors, and the particles are sieved out of suspension. These deposits are in the form of pedotubules, coarse cutans, and related features.

REFERENCES

Anderson, E.R. and Darmody, R.G., 1989. Origin of silt coatings in a Typic Fragiudalf. Agronomy Abstracts. 1989 Annual Meeting of the Soil Science of America. Las Vegas, NV, USA, pp. 4.

Arshad, M.A. and Mermut, A.R., 1988. Micromorphological and physio-chemical characteristics of soil crust types in northwestern Alberta, Canada. Soil Sci. Soc. Am. J., 52: 724-729.

Bisal, F. and Nielsen, K.F., 1967. Effect of frost action on the size of soil aggregates. Soil Sci., 104: 268-272.

Boiffin, J. and Bresson, L.M., 1987. Dynamique de formation des croutes superficielles: apport de l'analyse microscopique. In: N. Fedoroff, L.M. Bresson and M.A. Coutry (Editors), Soil Micromorphology. Proc. VII Int. Working Meeting of Soil Micromorphology, Paris, July 1985. Association Française pour l'Etude du Sol, Plaisir, France, pp. 393-399.

Brewer, R., 1964. Fabric and Mineral Analysis of Soils. John Wiley and Sons, New York, 470 pp.

Brewer, R., 1976. Fabric and Mineral Analysis of Soils. Krieger, New York, 482 pp.

Brewer, R. and Sleeman, J.R., 1960. Soil structure and fabric: their definition and description. J. Soil Sci., 11: 172-185.

Bronger, A., 1969/1970. Zur mikromorphogenese und zum tonmineralbestad quartarer lossboden in sudbaden. Geoderma, 3: 281-320.

Carlisle, F.J., 1954. Characteristics of Soils with Fragipans in a Podzol Region. Ph.D. diss. Cornell Univ., Ithaca, New York (Diss. Abstr. 14: 1861-1862).

Catt, J.A., 1989. Relict properties in soils of the central and north-west European temperate region. In: A. Bronger and J.A. Catt (Editors), Paleopedology, nature and application of paleosols. Catena Supplement 16: 41-58.

Columbo, C. and Torrent, J., 1991. Relationships between aggregation and iron oxides in Terra Rossa soils from Southern Italy. Catena, 18: 51-59.

DeKimpe, C.R. and McKeague, J.A., 1974. Micromorphological, physical, and chemical properties of a podzolic soil with a fragipan. Can. J. Soil Sci., 54: 29-38.

Emerson, W.W., Foster, R.C. and Oades, J.M., 1986. Organo-mineral complexes in relation to soil aggregation and structure. In: P.M. Huang and M. Schnitzer (Editors), Interactions of soil minerals with natural organics and microbes. Soil Sci. Soc. Am. Spec. Publ. 17., Madison, Wisconsin, pp. 521-548.

Falayi, O. and Bouma, J., 1975. Relationships between the hydraulic conductance of surface crusts and soil management in a Typic Hapludalf. Soil Sci. Soc. Am. J., 39: 957-963.

Fedoroff, N., Courty, M.A. and Thompson, M.L., 1990. Micromorphological evidence of paleoenvironmental change in Pleistocene and Holocene paleosols. In: L.A. Douglas (Editor), Soil Micromorphology: A Basic and Applied Science. Proc. VIII Int. Working Meeting on Soil Mircromorphology, San Antonio, Texas, July 1988. Developments in Soil Science 19, Elsevier, Amsterdam, pp. 653-665.

Fitzpatrick, E.A., 1974. Cryons and isons. Proc. of the North of England Soils Discussion Group, No. 11, Penrith, pp. 31-43.

Franzmeier, D.P., Norton, L.D. and Steinhardy, G.C., 1989. Fragipan formation in loess of the midwestern United States. In: N.E. Smeck and E.J. Ciolkosz, (Editors), Fragipans: Their Occurrence, Classification and Genesis. pp. 69-97.

Greenland, D.J., 1977. Soil damage by intensive arable cultivation: temporary or permanent? Phil. Trans. R. Soc. Lond. B, 281: 193-208.

Habecker, M.A., McSweeney, K., and Madison, F.W., 1990. Identification and genesis of fragipans in Ochrepts of North Central Wisconsin. Soil Sci. Soc. Am. J., 54: 139-146.

Hamblin, A.P., 1985. The influence of soil structure on water movement, crop root growth, and water uptake. In: N.C. Brady (Editor), Advances in Agronomy. Vol. 38. Academic Press, New York, pp. 95-158.

Harr, M.E., 1962. Mechanics of Particulate Media, a Probalistic Approach. McGraw-Hill Book, 543 pp.

Hinman, W.C. and Bisal, F., 1968. Alterations of soil structure upon freezing and thawing and subsequent drying. Can. J. Soil Sci., 48: 193-197.

Luxmoore, R., 1981. Micro-, meso-, and macroporosity of soil. Soil Sci. Soc. Am. J., 45: 671-672.

Mbagwu, J.S.C. and Bazzoffi, P., 1989. Effect of antecedent matric potential on the stability of soil aggregates subjected to cyclic freezing and thawing as evaluated by three structural indices. Soil Technology, 2: 59-70.

Mbagwu, J.S.C. and Piccolo, A., 1989. Changes in soil aggregate stability induced by amendment with humic substances. Soil Technology, 2: 49-57.

McKeague, J.A., Cheshire, M.V., Andreux, F. and Berthelin, J., 1986. Organo-mineral complexes in relation to pedogenesis. In: P.M. Huang and M. Schnitzer (Editors), Interactions of soil minerals with natural organics and microbes. Soil Sci. Soc. Am. Spec. Publ. No. 17. , Madison, Wisconsin, USA, pp. 549-592.

Miller, F.P., Wilding, L.P. and Holowaychuk, N. , 1971. Canfield silt loam, a Fragiudalf: II Micromorphological, physical, and chemical properties. Soil Sci. Soc. Amer. Proc., 35: 324-331.

Muskat, M., 1946. The flow of homogeneous fluids through porous media. McGraw-Hill Book, New York,, 1937; reprinted by J.W. Edwards, Publisher, Ann Arbor, Michigan, 737 pp.

Nettleton, W.D., McCracken, R.J. and Daniels, R.B., 1968. Two North Carolina coastal plain catenas: II Micromorphology, composition, and fragipans genesis. Soil Sci. Soc. Am. Proc., 32: 582-587.

Panayiotopoulos, K.P. and Kostopoulou, S., 1989. Aggregate stability dependence on size, cultivation and various soil constituents in Red Mediterranian soils (Alfisols). Soil Technology, 2: 79-89.

Ransom, M.D., 1984. Genetic processes in seasonally wet soils on the Illionian till plain in southwestern Ohio. Ph.D. dissertation, The Ohio State Univ., Columbus, Ohio, 355 pp.

Ransom, M.D., Smeck, N.E. and Bigham, J.M., 1987. Micromorphology of seasonally wet soils on the Illinoian till plain, USA. Geoderma, 40: 83-99.

Romans, J.C.C., Stevens, J.H. and Robertson, L., 1966. Alpine soils of north-east Scotland. J. Soil Sci., 17: 184-199.

SAS Institute, 1988. SAS/STAT User's Guide, release 6.03 ed. SAS Inst., Cary, North Carolina, 1027 pp.

Sillanpaa, M. and Webber, L.R., 1961. The effect of freezing-thawing and wetting-drying cycles on soil aggregation. Can. J. Soil Sci., 41: 182-187.

Soil Survey Staff., 1992. Keys to Soil Taxonomy. SMSS Technical Monograph No. 19. Fifth Ed. Pocahontas Press, Blacksburg, Virginia, 541 pp.

Sullivan, L.A. and Koppi, A.J., 1991. Morphology and genesis of silt and clay coatings in the vesicular layer of a desert loam soil. Aust. J. Soil Res., 29: 579-586.

Tarnocai, C. and Valentine, K.W.G., 1989. Relict soil properties of the arctic and subarctic regions of Canada. In: A. Bronger and J.A. Catt (Editors), Paleopedology, nature and application of paleosols. Catena Supplement 16. Catena Verlag, Cremlingen-Destedt, Germany, pp. 9-39.

Thompson, M.L., 1986. Morphology and mineralogy of a pre-Wisconsinian paleosol in Iowa. Soil Sci. Soc. Am. J., 50: 981-987.

Thompson, M.L. and Smeck, N.E., 1983. Micromorphology of polygenetic soils in the Teays River Valley, Ohio. Soil Sci. Soc. Am. J., 47: 734-742.

USDA Soil Conservation Service., 1992 (rev). Soil Survey Laboratory Methods Manual. Soil Survey Investigations Report No. 42, Version 2.0, U.S. Gov. Printing Office, Washington, D.C., 400 pp.

Van Vliet, B. and Langohr, R., 1981. Correlation between fragipans and permafrost with special reference to silty Weichselian deposits in Belgium and northern France. Catena, 8: 137-154.

West, L.T., Bradford, J.M. and Norton, L.D., 1990. Crust morphology and infiltrability in surface soils from the southeast and midwest U.S.A. In: L.A. Douglas (Editor), Soil Micromorphology: A Basic and Applied Science. Proc. VIII Int. Working Meeting on Soil Mircromorphology, San Antonio, Texas, July 1988. Developments in Soil Science 19, Elsevier, Amsterdam, pp. 107-113.

Willardson, L.S., 1974. Envelope materials. In: J. Van Schilfgaarde (Editor), Drainage for Agriculture. Agron. Series 17. Am. Soc. Agron. Madison, Wisconsin, pp. 179-200.

This Page Intentionally Left Blank

Clay coating formation on impermeable materials: deposition by suspension retention

L.A. Sullivan

*Resource Science and Management, University of New England-Northern Rivers,
PO Box 157, Lismore, NSW 2480, Australia*

ABSTRACT

Sullivan, L.A., 1994. Clay coating formation on impermeable materials: deposition by suspension retention. In: A.J. Ringrose-Voase and G.S. Humphreys (Editors), Soil Micromorphology: Studies in Management and Genesis. Proc. IX Int. Working Meeting on Soil Micromorphology, Townsville, Australia, July 1992. Developments in Soil Science 22, Elsevier, Amsterdam, pp. 373-380.

The formation of optically-oriented illuviation clay coatings on impermeable surfaces was investigated by passing clay suspensions (smectitic and ranging in concentration from 0.5% to 29.4%) through columns of coarse quartz sand. Following drainage and drying, suspensions retained on sand grain surfaces formed clay coatings with a high degree of optical orientation: these clay coatings were not removed by the subsequent passage of water through the columns. Clay coatings occurring at points of contact between sand grains were thicker than those occurring away from contact points. Most of the clay in suspensions retained within the columns could be removed by a subsequent passage of water suggesting that the dominant clay deposition mechanism involved the retention of suspensions on sand surfaces by capillarity and adsorption forces. The results show that the formation of optically-oriented illuviation coatings does not require the presence of a dry soil layer for clay deposition and can result from the flow of clay suspensions within initially wet soil materials.

INTRODUCTION

Optically-oriented clay coatings on impermeable surfaces

Soil micromorphology literature contains many examples of optically-oriented clay coatings around non-porous materials: for example, around quartz sand grains (FitzPatrick, 1984), around sand grains, rock fragments, silica coatings and glaebules (Chartres, 1985), and around quartz sand grains and chalcedony coatings (Bullock *et al.*, 1985). In a detailed micromorphological study of a desert loam (Haplic Durargid; Soil Survey Staff, 1975) Sullivan (1988) found that clay coatings with a high degree of optical orientation occurred on the vertically-oriented surfaces of sand grains and gravel protuding into vesicles as well as on the vertical surfaces of non-porous silica coatings.

Pore surfaces such as those described above would not allow appreciable water absorption. Thus, clay coating formation by filtration of clay suspensions flowing across the pore surface into adjacent dry soil materials would not have been possible. As the clay within these coatings has a high degree of optical orientation it is probable that the clay within these features has not

been deposited by flocculation (Brewer and Haldane, 1957). In addition, the coated surfaces are vertically-oriented, so deposition of the clay by sedimentation due to gravity - as in the formation of clay plugs (Eswaran and Sys, 1979) - is unlikely.

Formation of optically-oriented clay coatings on impermeable surfaces

In order to satisfactorily explain the characteristics of the above clay coatings a new process for the formation of optically-oriented clay coatings on vertically-oriented impermeable surfaces is required. Such a process is examined below and involves two separate stages.

Stage 1: Retention of clay suspensions by impermeable surfaces.
Two possible mechanisms were considered:
Mechanism A. During the flow of clay suspensions down pores surrounded by impermeable surfaces clay may be deposited by the mechanism proposed by Hunter and Alexander (1963). These authors examined the flow of kaolinite clay suspensions through saturated columns of silica sand grains and found that during the flow of these suspensions some of the clay was deposited within the columns causing reductions in column permeability of up to 80%. The possibilities of the kaolinite clay having been deposited within the column by sedimentation, flocculation or interstitial straining were discounted by these authors who proposed that the clay suspensions situated in 'dead' spaces (*e.g.* near sand grain surfaces) would act as Bingham liquids and exhibit a certain strength which could "resist the shearing force of the moving liquid. It will then behave as a rigid deposit" (Hunter and Alexander, 1963). Subsequently, Hunter (1989) showed that clay suspensions often act like Bingham liquids when the suspension remains rigid with increasing shear stress until a small but distinct threshold limit (termed the 'yield stress') is reached after which the liquid behaves like a Newtonian liquid (*i.e.* where the coefficient of viscosity is virtually independant of the rate of shear. In the experiments of Hunter and Alexander (1963) the clay materials within the sand columns were removed when the hydraulic gradient across the column was increased and indirect observations indicated that the deposited clay was evenly distributed within the column.
Mechanism B. In this mechanism clay suspensions are retained on impermeable pore surfaces within a soil when drainage of those pores ceases or is virtually negligible. This suspension retention mechanism is, in effect, governed by the same physical forces responsible for the retention of water within soils at 'field capacity' (*i.e.* the capillarity and adsorption forces involved in the matric potential). The amount of clay retained on the impermeable pore surfaces by this mechanism would be a direct function of the concentration of the clay suspension and the amount of suspension retained.
One difference between the above two clay suspension retention mechanisms is that for clay suspensions to be retained on pore surfaces under mechanism A the suspensions would have to exhibit an initial yield stress and thus would have to behave as Bingham-like liquids, whereas for Mechanism B to operate the clay suspensions retained would not need to have an initial yield stress and could thus exhibit a wide range of colloidal suspension behaviour (*e.g.* they could exhibit Newtonian, pseudoplastic, dilatant, or Bingham plastic behaviour, Hunter, 1989).

Stage 2: Orientation of clay particles to coated surfaces.
Although not considered by Hunter and Alexander (1963), the deposited clay would most probably become strongly oriented (in a face-to-face pattern) upon drying (Williamson, 1960)

thus forming oriented clay coatings where ever clay supensions had been retained. Depending upon the nature of the clay, oriented clay coatings can resist dispersion when subsequently wetted (Emerson, 1960). In this situation a mechanism is required that allows even thick optically-oriented clay coatings to form on impermeable materials, presumably by repeated wetting (with clay suspensions) and drying.

This paper (1) examines optically-oriented clay coatings on non-porous soil surfaces where clay deposition by the filtering mechanism could not operate, (2) proposes possible mechanisms for clay deposition on these surfaces, (3) examines experimentally the retention of clay suspensions flowing through columns of coarse quartz sand, and (4) examines the morphology of clay coatings formed by drying suspensions retained on the sand grains.

METHODS AND MATERIALS

The clay suspension (<2 μm) was obtained from the B horizon (30 - 45cm layer) of a yellow podsolic soil (Stace *et al.*, 1968) near Casino (lat. 28°55'S., long. 153°E.) in New South Wales by sedimentation after shaking the soil in water for 5 minutes. The water used in these experiments was tap water (electrolytic conductivity of 0.10 mS cm^{-1}). This clay suspension was then concentrated by further sedimentation and decantation and remained stable (*i.e.* in a dispersed state) for several months. X-ray diffraction determined that this clay was mainly smectitic with smaller amounts of kaolinite and lepidocrocite. All experiments were carried out at 20°C.

Experiment No. 1

The porous medium consisted of columns (0.85 cm diameter) of washed angular quartz sand (0.5 - 2.0 mm in diameter). Air-dried sand (2.74 g) was quickly poured into each column and the column brought into close packing by gently tapping the sides of the column twenty times. The bulk density of the sand in the column after this procedure was 1.41 g cm^{-3} resulting in a total pore space within the sand column of 0.91 cm^3. The following concentrations of the clay suspensions (in g of clay per 100 cm^3 of suspension) were used: 0.46, 0.92, 1.84, 3.68, 7.35, 14.70, 19.57, 24.44 and 29.40. A volume of clay suspension equivalent to three times the total pore space within the sand column (*i.e.* 2.73 cm^3) was passed though a column at the rate of 0.30 cm^3 min^{-1} (equivalent to a flow rate of 25 cm hr^{-1}) using a peristaltic pump. A new sand column was used for the passage of each clay suspension. After the passage of the clay suspension each column was drained on blotting paper to a moisture potential of -8.0 cm of water and the weight of retained suspension was determined. Each column was then dried in a fan-forced oven at 40°C and weighed. The weight of clay retained within each column was then calculated by subtraction.

Experiment No. 2

The porous medium consisted of columns (0.85 cm diameter) of washed angular quartz sand (0.5 - 2.0 mm in diameter). Air-dried sand (4.11 g) was quickly poured into each column and brought to close packing as in Experiment No. 1. The bulk density of the sand in the column after close packing was 1.41 g cm^{-3} thus resulting in a total pore space within the sand column of 1.36 cm^3.

In Experiment No. 2 four treatments were used:

Treatment 1. The passage of 4.08 cm^3 (equivalent to three times the total pore space within the sand column) of a 5% clay suspension.

Treatment 2. The passage of 4.08 cm^3 of water followed immediately by the passage of 4.08 cm^3 of a 5% clay suspension.

Treatment 3. The passage of 4.08 cm^3 of water followed immediately by the passage of 4.08 cm^3 of a 5% clay suspension followed immediately by the passage of 4.08 cm^3 of water.

Treatment 4. The passage of 4.08 cm^3 of a 5% clay suspension followed immediately by the passage of 4.08 cm^3 of water.

The rate of application of the clay suspensions and water was 0.15 cm^3 hr^{-1} (equivalent to a flow rate of 12.5 cm hr^{-1}). After the passage of the final volume of liquid each column was drained to moisture potential of -10 cm on a Buchner funnel, then dried in a fan-forced oven at 40°C and weighed.

Each treatment was repeated ten times (*i.e.* there were ten leaching cycles) with the amount of clay that had been deposited within each column after each leaching cycle being determined by weighing each column after oven-drying.

Micromorphological examination of the columns

Both experiments were duplicated. Selected sand grains from each column in one the duplications were examined under a JEOL 35C scanning electron microscope (SEM) following gold coating and mounting onto aluminium discs. The other duplicates were impregnated with epoxy resin and thin sections prepared through these columns using the method of FitzPatrick (1984).

RESULTS AND DISCUSSION

Experiment 1

The clay coatings formed in this experiment were found to bridge sand particles and to spread over other sand grain surfaces (Fig. 1b). The coatings between contact points between sand grains (hereafter called 'bridge clay coatings' and indicated by arrow B in Fig. 1b) were, however, thicker than those over the rest of the sand grain surfaces (hereafter called 'non-bridge clay coatings' and indicated by arrow N in Fig. 1b). The maximum thickness of the non-bridge clay coatings ranged from 40 μm when the 29.4% suspension was used down to 2 μm when 0.5% suspensions were used.

Fig. 1. a) Micrograph of thin sections through a sand column through which a 24.44% clay suspension had been passed, in crossed polarised light (note: the dark central areas of the coatings displayed dark red and green interference colours). Scanning electron photomicrographs of: b) a fracture surface across a sand column through which a 29.4% clay suspension had been passed; c) a fracture across a clay coating from the sand column shown in (b); d) a fracture surface across a non-bridge clay coating on a sand grain from a column through which a 7.35% clay suspension had been passed; e) a fracture surface across a non-bridge clay coating on a sand grain from a column through which a 29.4% clay suspension had been passed; f) detail of d); g) detail of e).
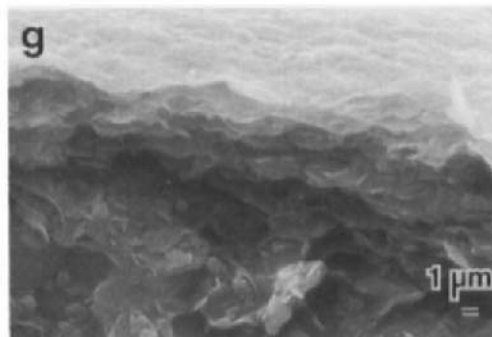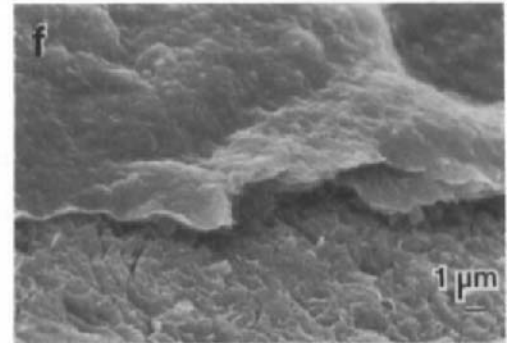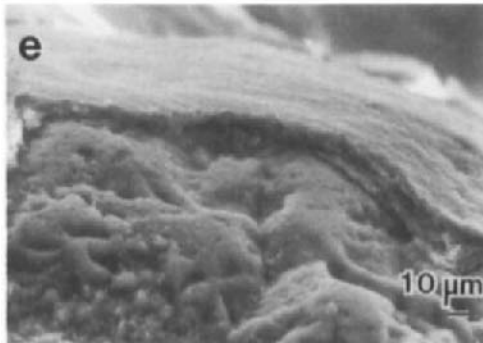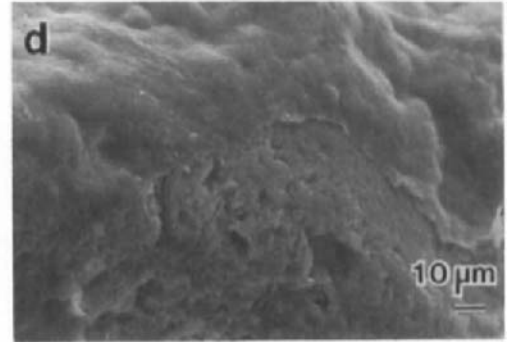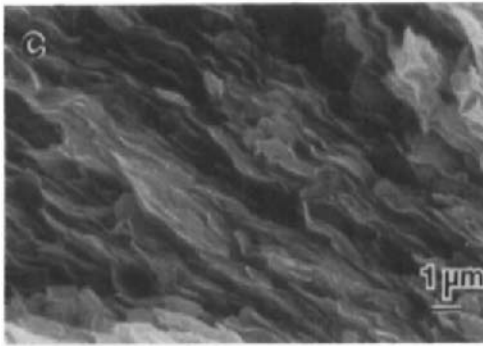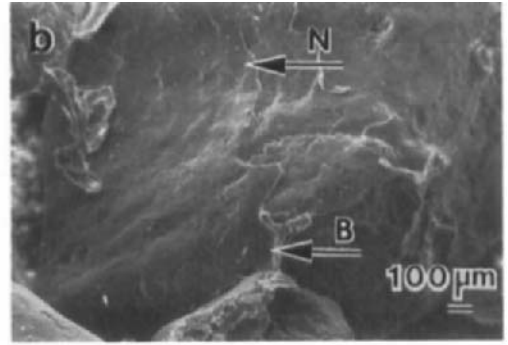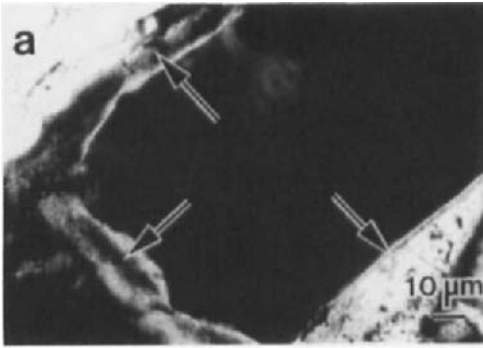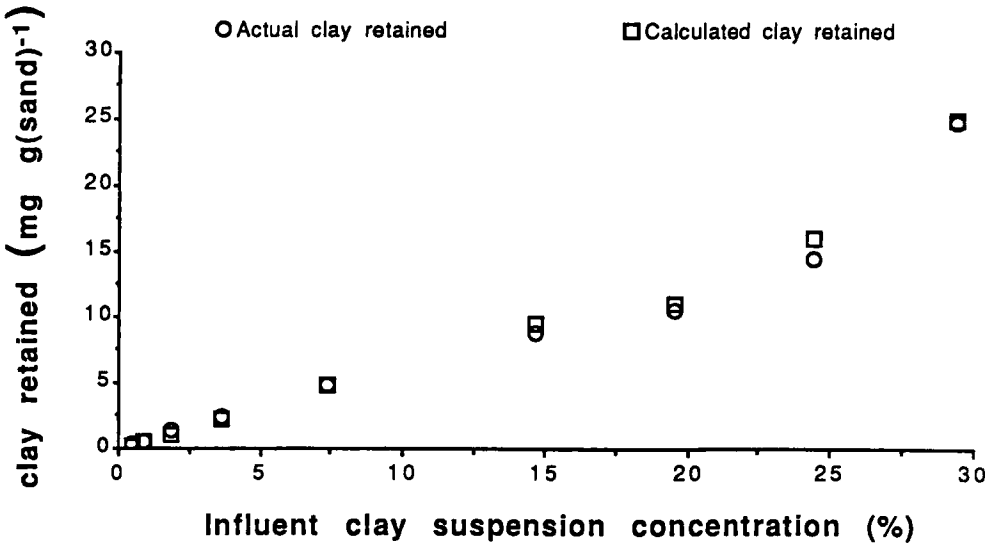
Fig. 2. The amount of clay retained within the sand columns in Experiment 1 at each influent clay suspension concentration.

Clay coatings were detected over most but not all sand grain surfaces within the columns. This was probably due to the unsaturated flow conditions during the experiments resulting in the suspensions bypassing some sand grain surfaces. The clay within the coatings exhibited a high degree of preferred optical orientation even when the influent clay suspensions were concentrated to 29.4% (clay coatings are indicated by arrows in Fig. 1a). The SEM morphology of fractures across the clay coatings (Fig. 1c) support this with the sheet-like clay platelets showing a strong preferential orientation parallel to the sand grain surfaces.

Fig. 2 shows that the amounts of clay retained within the sand columns were equivalent to the product of the concentration of the influent clay suspension and the volume of suspension retained (note: each volume was calculated by assuming that the density of the retained suspension was equivalent to that of the influent clay suspension). Thus, under these experimental conditions the amounts of clay retained on the surfaces of sand grains were equal to those that would be expected if mechanism B alone was responsible for clay retention. In line with the clay retention results shown in Fig. 2, the lower the suspension concentration the thinner the clay coatings formed on the sand grain surfaces. For example, the non-bridge clay coatings formed using a suspension concentration of 7.35% (Fig. 1d and f) were much thinner than those formed using a suspension concentration of 29.4% (Fig. 1e and g).

Experiment 2

The morphology and optical properties of the clay coatings formed in treatments 1 and 2 were similar to the coatings formed by the retention of the 29.4% clay suspension in Experiment 1 (*i.e.* as shown in Fig. 1e and g, and described in the above section), whereas the

morphology and optical properties of the clay coatings formed in treatments 3 and 4 were similar to the coatings formed by the retention of the 7.35 % clay suspension in Experiment 1 (*i.e.* as shown in Fig. 1d and f, and described in the above section). The maximum thickness of the non-bridge clay coatings ranged from 30 µm in treatment 2 down to 4 µm in treatment 4.

As for the clay coatings formed in Experiment 1, the clay within the coatings formed in treatments 1 and 2 exhibited a high degree of preferred optical orientation. Clay accumulated within each column at a constant rate over the ten leaching cycles. The mean rates of clay accumulation (in mg clay accumulated per gram of sand per leaching cycle) and standard deviations, respectively, were as follows: Treatment 1, 2.40, 0.23; Treatment 2, 2.68, 0.56; Treatment 3, 0.23, 0.10 and Treatment 4, 0.37, 0.05. From these results it is apparent that much greater amounts of clay were retained on the sand surfaces (after drainage) when the last liquid passing through the column was a clay suspension (*i.e.* in Treatments 1 and 2) rather than water (*i.e.* Treatments 3 and 4). The large difference in the amounts of clay retained on the sand surfaces (after drainage) between Treatments 1 and 4 indicates that much of the clay suspension retained within the column after the passage of clay suspensions was subsequently removed by the passage of water. This suggests that clay deposition by mechanism B was more important than by mechanism A under the experimental conditions employed.

The clay-in-flakes manufactured by air-drying clay suspensions would not disperse even when immersed in distilled water so it is most likely that once deposited on the sand surfaces and dried, the clay coatings could not be removed by subsequent passage of either clay suspensions or water. This is supported by the constant and similar accretion of clay over the ten leaching cycles within the sand columns in Treatments 1 and 2.

CONCLUSIONS

The results of this study show that:
1. Coatings of clay with a high degree of optical orientation can form on impermeable pore surfaces by drying of clay suspensions retained on these surfaces after the flow of both concentrated (up to 29.4%) and dilute (down to 0.5%) clay suspensions.
2. Clay coatings occurring at points of contact between sand grains were thicker than those occurring away from contact points.
3. Most of the clay in suspensions retained by the impermeable surfaces could be subsequently removed by the passage of water. This suggests that, under the experimental conditions employed, the probable dominant clay deposition mechanism involved the retention of suspensions on sand surfaces by the same physical forces responsible for the retention of water within soils at 'field capacity' (*i.e.* the capillarity and adsorption forces involved in the matric potential).
4. The formation of optically-oriented illuviation coatings does not require the presence of a dry soil layer for clay deposition: clay deposition leading to the formation of such coatings can result from the flow of suspensions within initially wet soil materials.

REFERENCES

Brewer, R. and Haldane, A.D., 1957. Preliminary experiments in the development of clay orientation in soils. Soil Sci., 84: 301-309.

Bullock, P., Fedoroff, N., Jongerius, A., Stoops, G., and Tursina, T., 1985. Handbook for Soil Thin Section Description. Waine Research Publications, Wolverhampton, U.K., 152 pp.

Chartres, C.J., 1985. A preliminary investigation of hardpan horizons in north-west New South Wales. Aust. J. Soil Res., 23: 325-337.

Emerson, W.W., 1960. Factors affecting the strength of soil crumbs. In: Interparticle Forces in the Clay-Water-Electrolyte Systems. CSIRO, Melbourne, pp. 34-39.

Eswaran, H. and Sys, C., 1979. Argillic horizon in LAC soils; formation and significance to classification. Pedologie, 29: 175-190.

FitzPatrick, E.A., 1984. Micromorphology of Soils. Chapman and Hall, London, 433 pp.

Hunter, R.J., 1989. Fundamentals of Colloid Science. Vol. 2. Clarendon Press, Oxford, 441 pp.

Hunter, R.J. and Alexander, A.E., 1963. Surface properties and flow behaviour of kaolinite. Part III. Flow of kaolinite sols through a silica column. J. Colloid Sci., 18: 846-862.

Soil Survey Staff, 1975. Soil Taxonomy. U.S. Dept. Agric. Handb. 436, U.S. Gov. Printing Office, Washington, D.C., 754 pp.

Stace, H.C.T., Hubble, G.D., Brewer, R., Northcote, K.H., Sleeman, J.R., Mulcahy, M.J. and Hallsworth, E.G., 1968. A Handbook of Australian Soils. Rellim Technical Publications, Glenside, South Australia, 429 pp.

Sullivan, L.A., 1988. Surfaces and Pedological Features Associated with Planar Pores, Channels, Chambers, Vesicles and Cavities. Ph.D. Thesis, University of Sydney, Sydney, N.S.W., 355 pp.

Williamson, W.O., 1960. Particle orientation in a kaolinite-illite clay caused by deposition or deformation; some shrinkage and mechanical properties of the aggregates so formed. In: Interparticle forces in the Clay-Water-Electrolyte Systems. CSIRO, Melbourne, pp. 40-65.

The ultramicromorphology of soil biota *in situ* in natural soils: a review

R.C. Foster

*CSIRO Division of Soils and CRC for Soil and Land Management, Private Bag No. 2,
Glen Osmond, SA 5064, Australia*

ABSTRACT

Foster, R.C., 1994. The ultramicromorphology of soil biota *in situ* in natural soils: a review. In: A.J. Ringrose-Voase and G.S. Humphreys (Editors), Soil Micromorphology: Studies in Management and Genesis. Proc. IX Int. Working Meeting on Soil Micromorphology, Townsville, Australia, July 1992. Developments in Soil Science 22, Elsevier, Amsterdam, pp. 381-393.

Soil microbiota, located *in situ* within and between soil aggregates, can be studied using electron optical methods (TEM, SEM, ESEM and EPMA). ESEM and TEM of ultrathin sections of soils show that microaggregates are penetrated by fungal hyphae, which binds them together to form macroaggregates. Hyphae at the centre of aggregates are often collapsed and have degenerate cytoplasm whereas those at the aggregate surface have normal ultrastructure. Bacteria occur in plant and animal residues, including faecal material, and in the microvoids within microaggregates. Soil microfauna can ingest soil micro-organisms *in situ* within the intermacroaggregate voids.

Different types of soil organics (carbohydrates, humic materials, enzymes) in aggregates and microaggregates, can be distinguished by ultrahistochemical methods, so that sites of aggregate stabilisation by mechanical interlinking by cell wall remnants can be separated from those due to gluing by root derived mucigel or microbial ECP. These tests also distinguish empty microvoids (between micro-aggregates) from microvoids filled with organic matter (within microaggregates). EPM shows that amorphous organic matter nearly always contained Fe and Al. Histochemical tests for soil organics suggest that most microaggregates have an organic core composed of either root mucilage, microbial ECP or cellular remnants. Ultrahistochemical tests for enzymes suggest that not all micro-organisms in a microsite have the same function, and that some soil enzyme activity is outside of the biomass where it is associated with organic remnants of nanometre size.

INTRODUCTION

It is the presence of the soil biota and the organic matter they produce, consume and transform, which distinguishes a soil from a mere heap of minerals. The soil flora produce materials which stabilise aggregates, and the soil fauna and flora together are involved in nutrient recycling. Where precisely in aggregates and microoggregates are the various types of soil biota located?

If the roots of plants are included, the soil biota comprise representatives of all the phyla of plants and micro-organisms, and representatives of all but a few exclusively marine phyla of

animals. The soil fauna proper range in size from earthworms that may be >1 m long and >20 mm diameter and weighing >500 g, down to protozoa <5 μm in diameter and weighing <10^{-10} g, (Lee and Foster, 1991). The soil flora ranges in size from major secondarily thickened tree roots 50 cm in diameter, down to bacteria <0.3 μm (Foster, 1985b) and virus particles 0.01 μm diameter (Foster and Rovira, 1978; Foster et al., 1983). The size range of soil organisms that can be practically investigated by transmission electron microscopy (TEM) is, however, limited to organisms <1 mm and mainly to organisms <100 μm diameter.

Traditional ultrastructural studies of the *soil fauna* have ranged in scale and complexity from the general morphology of soil arthropods using scanning electron microscopy (SEM) (Eisenbas and Wicherd, 1987), TEM studies of the fine structure of worms (Jamieson, 1981), worm burrows (Jeanson, 1971; Kretzschmar, 1982) and worm casts (Barois, 1987; Lee and Foster, 1991), to the detailed ultrastructure of soil amoebae (Ogden and Pitta, 1990; Foster and Dormaar, 1991) and the flagellae of commensal spirochaetes in the hindgut of termites (Breznak, 1984).

Ultrastructural studies of the *soil flora* have largely concentrated on the fine structure of roots and rhizospheres, (Foster et al., 1983; Foster, 1985a and b, 1986, 1988; Bottner and Billes, 1987; Robert and Chenu, 1992) and on bacteria, actinomycetes and fungi of economic importance, such organisms which cause root disease or form mycorrhizas (Massicotte et al., 1989; Moore et al., 1989; Scales and Peterson, 1991; Giannazzi-Pearson et al., 1990).

In many ultrastructural studies the biota have been extracted from the soil and studied in isolation. This paper, however, is confined largely to *in situ* studies of the ultrastructure of soil biota in their normal microenvironments within natural soils, and to the effects of soil biota on *soil ultrastructure*, that is to effects that require electron microscopy for their elucidation. Because this is a comparatively new and of research many of the results are still in the realm of tentative conclusions. Nevertheless, they are presented here to convey some notion of the type of results that have been reported and no attempt is made to expose any contradictory lines of evidence.

This paper does not attempt to review the methods used to prepare soil biota for *in situ* electron microscopy. Nevertheless, it is important to note that special techniques are often required for fixation, embedment and histochemistry (*e.g.* Foster and Marks, 1967; Kilbertus and Reisinger, 1975; Foster and Martin, 1981; Foster, 1983; Santos et al., 1989; Newman and Briarty, 1990).

POPULATION SIZE OF SOIL BIOTA

The most numerous soil biota on which *in situ* ultrastructural observations have been made are plant roots, mesofauna (mainly microarthropods and worms) and micro-organisms. Except for the first few centimetres below a pasture, which may be nearly all roots and rhizosphere, the numerous roots, occupy only about 6% of the soil volume.

The most common microarthropods are the mites and collembola which may both number >100,000 per m^2 of the soil surface. Both groups are confined to the top few centimetres of the soil and their cast-off exuviae are therefore not uncommon in ultrathin sections of surface soils (Foster, 1985a). In comparison, earthworm numbers vary from 100-2000 per m^2, and in temperate grasslands they can deposit up to about 40-50 t of casts ha^{-1} y^{-1} at the soil surface (Lee, 1985).

The total number of species of soil organisms has been estimated to be 2.2 million, comprising 30,000 bacteria, 1,500,000 fungi, 60,000 algae, 100,000 protozoa and 500,000 nematodes (Hawksworth and Mound, 1991). The use of RNA probes has shown that 1 g of soil may contain over 4000 species of bacteria.

Although a fertile agricultural soil contains large numbers of microbiota (bacteria 10^7 - 10^9, actinomycetes 10^6, fungi 10^5, algae 10^4 colony forming units (CFU) g^{-1} and 10^4 -10^5 protozoa g^{-1} dry weight of soil, Alexander, 1977), the soil biomass occupies only 0.001% of the soil volume (Sparling, 1985), so that a large volume of soil must be processed to obtain an overall view of their distribution. The soil is generally regarded as an oligotropic medium, largely devoid of readily metabolisable, energy-rich materials (Poindexter, 1981). The great majority of micro-organisms in the bulk soil are therefore small (>63% of soil bacteria are <0.3μm in diameter, Bae *et al.*, 1972), have long generation times (2.5 yr), or are in a quiescent or dormant state, (Sparling, 1985). It is important to notice that, because of their small size, most bacteria are difficult to resolve by light microscopy of thin sections of soil, even when they are adequately fixed and stained.

THE DISTRIBUTION OF MICROBIOTA

Soil biota are neither randomly nor uniformly distributed through the soil. They show a clumped distribution to sites with a compatible pH, water potential and oxygen concentration in or near food materials (Hattori and Hattori, 1976; Foster, 1988).

Bacteria and actinomycetes

Bacteria and actinomycetes occur mainly in rhizospheres, faecal pellets, organic (plant and animal) debris and in the interiors of microaggregates. Many microaggregates have an organic core (Jocteur Monrosier *et al.*, 1991; Ladd *et al.*, 1992) which provides suitable substrates for microbiota, as well as gluing the components of the microaggregate together.

Numbers of microbiota are generally higher in localised energy-rich microhabitats such as faecal deposits and rhizospheres, where populations may rise to 10^{10} - 10^{12} bacterial cells cm^{-3} (Foster, 1988). Individual cells are generally larger in these nutrient rich sites compared to the bulk soil. Thus in rhizospheres only 20% of bacteria are <0.3 μm and >30% are >0.5 μm diameter, (Foster, 1985b).

In rhizospheres where substrates are not limiting, numerous small colonies of many different kinds of actinomycetes and bacteria contribute to the large populations of micro-organisms observed (Foster and Rovira, 1978; Foster *et al.*, 1983). Many colonies (and individuals) produce their own extracellular polysaccharides (ECP) which can be distinguished ultrastructually and histochemically from the root surface ECP. Often the microbial ECP becomes coated with clay particles. Indeed, bacterial colonies frequently form the core of nascent microaggregates in rhizospheres (Dormaar and Foster, 1991).

In ultrathin sections of the interior of large aggregates the micro-organisms are small, Gram positive and devoid of storage materials such as polysaccharide granules, polyhydroxybutyrate (PHB) and polyphosphate (PP) (Foster, 1988). In contrast, the near surface of aggregates have micro-organisms that are large, Gram negative and often contain PHB and PP granules. Similarly, the cells of fungi in the interior of large aggregates are often collapsed and devoid of cytoplasm or the cytoplasm is dense and disorganised. Those near the surface of the aggregate,

however, have normal organelles. This suggests that the interior of large aggregates may be microaerophyllic or even anaerobic. Also, when rain follows a dry period that was severe enough to cause cell death, there may be a transient flush of soluble organic materials. These materials may all be intercepted by micro-organisms on the surface of the aggregate, before reaching the interior (Killham *et al.*, 1993). In this situation the cells have no opportunity to deposit reserves.

Although bacteria occur in micropores *near the surface* of microaggregates and aggregates, environmental SEM (ESEM) studies indicate that they seldom occur *on the actual surface*, except in sites rich in organic matter. Conversely fungi often occur in the pores between the aggregates of surface soils. Macropores between aggregates drain more quickly than the micropores within them and fungi will continue to grow at much lower water potentials (to *ca.* -40 bar) than bacteria, and bacteria may be limited by water potentials to micropores. However, it is also possible that bacteria on the surface of aggregates are removed by amoebae browsing through the interaggregate micropores, (Hattori, 1988; Foster and Dormaar, 1991). Rutherford and Juma (1992) showed that when protozoans were added to soils they reduced the bacterial populations by up to 75% and that within 7 days most protozoans had encysted for want of food. Moreover, the rate of removal of bacteria was markedly influenced by the texture of the soil, suggesting that access to bacteria was a limiting factor.

Fungi and protozoa

Fungi are also common in rhizospheres, as commensals, symbionts in mycorrhizas and as root pathogens. In the bulk soil fungi generally colonise the pores between aggregates, with occasional branches into adjacent microaggregates. Fungi penetrate the microaggregates by inserting wedge shaped hyphae between the various components. These vacuolate, swell and push the soil minerals and organic matter aside. Thus, as with mycorrhizal roots, penetration of aggregates appears to be mechanical rather than by enzymatic or chemical lysis (Foster and Marks, 1967). Macroaggregates are often composed of microaggregates which are linked together by the hyphae of soil fungi, especially mycorrhizal fungi (Tisdall and Oades, 1988).

Protozoa similarly accumulate in regions rich in bacteria, actinomycetes and fungi. One example is the region of the rhizosphere where the root hairs and the outer rhizodermal cells are undergoing autolysis. The concomitant release of lystes results in a population explosion of the rhizosphere microflora, which in turn is accompanied by an increase in numbers of soil protozoa such as ciliates and amoebae (Foster, 1985a), which feed on bacteria (Foster and Dormaar, 1991). The presence of protozoa may markedly alter the physiology of the root and rhizosphere, inducing increases in the turnover of both P (Gould *et al.*, 1979) and N (Kuikman *et al.*, 1990).

EFFECTS OF THE BIOTA ON SOIL STRUCTURE

Mesobiota

Lee and Foster (1991) have recently undertaken an overview of the effects of the mesofauna on soil structure. Neglecting the gross effects of mammals, the fauna most active in modifying soil structure are worms and soil arthropods, particularly ants and termites.

The mesofauna affect soil structure by the following: burrowing in search of food or for the construction of living spaces; transporting excavated and ingested soil materials; modifying plant litter *etc.* by digestive processes which are subsequently deposited as faecal pellets; and locally incorporating excreta, mucus and salivary materials into linings on burrows and galleries. Thus, in case of some worm burrows, the surrounding soil may be modified up to a distance of 2 mm or more to form the *drilosphere* (Bouché, 1975). In another situation, electron probe microanalysis (EPM), has been used to show that worm burrow walls can contain higher concentrations of Fe and Mn than the surrounding soil. This technique also showed that these elements were evenly distributed along the burrow, whereas calcium was found as discrete granules (Jeanson, 1971). Additional detail was provided by Kretzschmar (1987) who showed that the burrow is lined with a multilamellate layer 30-80 μm thick composed of mucus secreted by the worm epidermis. In the same way, materials lining termite galleries contain enhanced concentrations of organic matter, mainly plant cell wall debris and larger numbers of bacteria than the nearby soil.

Faecal deposits often have a characteristic morphology in SEM and a characteristic internal ultrastructure in TEM. In general, faecal materials have a chaotic ultrastructure (Foster and Martin, 1981; Foster, 1985a) though organised cell wall remnants and even subcellular organelles such as chloroplasts may be recognised (Foster and Martin, 1981; Foster *et al.*, 1983). Arthropod faecal pellets are recognised by their dense staining by heavy metals, by the fact that they are almost entirely organic and by the large numbers of bacteria they contain (Foster, 1988; Lee and Foster, 1991).

In some temperate soils up to 50% of aggregates in the surface layers of soils may be recognisable as derivatives of worm casts and casts may form a layer of 15-20 cm thick in tropical wooded savannas (see review by Lee and Foster, 1991). In contrast to arthropod droppings, worm casts are largely composed of clay minerals and soil organic matter, and although many micro-organisms (*Frankia*, VAM) survive passage through the worm digestive tract (Reddell and Spain, 1991a and b) the bacteria and fungi comprise a relatively small proportion of the cast volume (Lee and Foster, 1991). Most living micro-organisms in worm casts (*i.e.* those with intact subcellular organelles) are protected by being enclosed either in plant residues or cutans of clay. In contrast, micro-organisms in more open textured cast material are represented by empty ghosts of cell wall material devoid of organelles (Lee and Foster, 1991).

Roots tend to grow in pre-existing pores or are attached to ped surfaces where nutrients such as P and S accumulate (Quereshi and Jenkins, 1987). Where they grow into soil fabrics they modify the soil structure by physical displacement of nearby soil components and by rhizodeposition (Martens, 1990). Small roots do not necessarily fill the pore in which they grow and part of the pore may be occluded by mucigel (Robert and Chenu, 1992). If a root enters a small pore, the stele retains its normal diameter but the cortex may be locally crushed or missing. Physical expansion of roots longitudinally results in the lateral displacement of soil particles. Radial expansion, especially by secondary thickening, results in the reorientation and compression of nearby soil so that mineral grains round roots are often aligned tangential to the root's surface (Foster and Rovira, 1978; Foster, 1983; April and Keller, 1990), which also results in the soil near roots having a greater density than the bulk soil (the minimal voids zone) (Foster, 1983; Foster and Rovira, 1978).

Rhizodeposition (Martens, 1990) is the addition of organic matter to the soil by roots, as cast off tissues (bark, cortical cells, lateral roots, root hairs, root cap cells), exudates

(mucilages, enzymes, sugars, organic acids, polyphenolics, *etc.*) and the breakdown products of cell autolysis (lysates). Root surface gels penetrate the soil to about 100-200 μm and hold soil to the root surface. Gel composition and amount vary between species, and even between cultivars of the same species. This may account for the fact that some species (*e.g. Lolium perenne* L.) generate water stable aggregates near their roots, especially when their transpiration dries the rhizosphere, whereas the aggregates associated with other species growing in the same soil (*e.g.* tomato) slake on wetting (B. Cockcroft, pers. comm.).

The secretion of organic acids and polyphenolics may directly promote accelerated weathering of soil minerals near roots by the selective chelation of metal ions (Tributh *et al.*, 1987; April and Keller, 1990), so that clay platelets in rhizospheres may show characteristic etch pits. Hence, soil in the immediate vicinity of roots can show marked differences in physical characteristics, mineralogy and weathering compared to the bulk soil, (Leyvak *et al.*, 1991) including the disassociation of grains (April and Keller, 1990). However there is no general agreement as to whether rhizosphere soils are more or less stable than the bulk soil, though differences between crops are commonly observed (Reid and Goss, 1981; Reid *et al.*, 1982; Pojasok and Kay, 1990; Ellsworth *et al.*, 1991). In addition, exudates and lysates affect soil structure by encouraging the growth and development of rhizosphere micro-organisms, which in turn may modify rates of decomposition of soil organic matter (Reid and Goss, 1982; Reid *et al.*, 1982; Rasolomanana and Balandreau, 1987; Dormaar, 1988). One key to sustainable agriculture in the future may be the selection of crops and rhizosphere micro-organisms which increase aggregate stability.

Microbiota

It is generally assumed that microbiota are passive inhabitants of the soil, which confine themselves to the available pore space. Thus, amoebae *in situ* in rhizospheres appeared to have adapted their morphology to the shape of the macropore in which they are found, probing connected fine micropores with elongated pseudopodia in order to reach bacterial prey (Foster, 1985a, 1988; Foster and Dormaar, 1991).

However, recent ultrastructural work has shown that during differentiation and growth in soil micropores, both individual fungal hyphae and bacterial colonies may increase in size to such an extent that they displace nearby soil components. This displacement may include both reorientation and compaction of the nearby clay platelets as the result of pressure exerted by the expanding micro-organism(s). *Reorientation* results in clay platelets arranged parallel or tangential to the surface of the microbial cells or their ECP instead of assuming a random orientation, as in the bulk soil (Foster *et al.*, 1983; Emerson *et al.*, 1986; Robert and Chenu, 1992) .

Expansion of hyphae and microbial colonies may also *compress* the nearby soil, so that the packing density in the cutan surrounding the colony or hypha is increased compared with that of the bulk soil. This gives rise to a compact, wall-like layer of clay enclosing the colony or hypha which is readily distinguished in both SEM (Robert and Chenu, 1992) and TEM (Foster *et al.*, 1983; Emerson *et al.*, 1986). These clay cutans protect the micro-organisms within from bacterial or virus attack, (Roper and Marshall, 1974), the digestive enzymes of soil animals (Foster and Lee, 1991) and possibly desiccation.

ULTRASTRUCTURAL EVIDENCE OF ORGANIC MATTER TURN OVER BY SOIL BIOTA

Physical Breakdown of cellular remnants

By the time they reach the forest floor, many leaves are well colonised by micro-organisms (Foster, 1985a). The same is true of dead lateral roots. Recently deposited materials may display the multilamellate structure characteristic of parenchyma or stelar tissues. The parenchyma cell remnants may contain remnant plasmodesmata and the stelar tissues may reveal carbohydrate rich, secondary cell wall layers, which are electron transparent, contained between electron dense middle lamella, primary cell wall and terminal lamella layers (Foster *et al.*, 1983; Rasolmanana and Balandreau, 1987). Such tissues are soon comminuted by grazing soil animals to fine fragments of wall material, which quickly become coated with cutans of clay (Emerson *et al.*, 1986).

Chemical modification

At the same time microbial decay results in the formation of characteristic lysis holes in cellular debris and microbial enzymes breakdown the readily metabolisable wall components (*e.g.* carbohydrates). This unmasks the polyphenolic groups of the lignins, so that older materials are often highly electron dense after heavy metal fixation and staining. Cell wall remnants may ultimately be reduced to the resistant middle and terminal lamellas which probably compose the fine, electron dense layers which sometimes link aggregate components together.

The death of plant cells results in membrane breakdown so that vacuolar polyphenolics are released to tan the cytoplasm. These materials, together with cell wall components may be reworked by soil micro-organisms to produce the amorphous electron dense masses especially common in composts, worm casts *etc.* Specific tests for carbohydrates and polyphenolics reveal the various stages of humification of such materials.

Some of the enzymes involved in nutrient cycling and humification processes can be detected ultra-histochemically. Phosphatases can be located in rhizodermal cells, root surface mucilages, fungi, bacteria and their ECP and on fragments of microbial membranes as small as 0.01 µm long and 7-10 nm thick, (Foster and Dormaar, in press).

ROLE OF BIOTA IN STABILISING AGGREGATES AND MICROAGGREGATES

Much microaggregate stability is due to the mechanical interlocking of the various mineral components and to the cross linking of soil components by amorphous materials. A combination of histochemistry (to identify soil organic matter) and EPM suggests that much of this amorphous material contains both organic matter and Fe, Si and Al (*i.e.* they are organo-mineral complexes rather than being composed of purely organic or inorganic materials).

However soil stability at the aggregate level correlates highly with the organic matter content of the soil, and particularly with the concentration of soil polysaccharides. Electron micrographs of sections of aggregates and microaggregates reveal four main mechanisms in which soil biota contribute to aggregate stability.

Mechanical stabilisation by entanglement in fungal hyphae and roots

Apart from members of a very few plant families such as the Brassicaceae, all commercial crops, including tree species, have mycorrhizas, so mycorrhizal fungi are ubiquitous components of surface soils. The sand grains near *Casuarina* trees growing on the Caloola sands are bound together in long chains by mycorrhizal fungi. These do not penetrate the grains but are associated with deep etch pits in their surface. Similarly, SEM of surface soil layers (*i.e.* just below the litter) from radiata pine plantations show microaggregates linked together by fungi.

Sections of large aggregates often have planar voids which contain hyphae, and these may represent the junction between two aggregates which have subsequently become united mechanically. Branch hyphae enter the microaggregates so that these are linked together to form macroaggregates. Hence aggregate stability can be correlated with length of hyphae Oades (1987).

Mechanical stabilisation by remnants of plant cells

Many microaggregates contain sections of plant cell walls or convoluted sheets of cellular materials in which various lamellae and even plasmodesmata can still be recognised by their substructure characteristics. These sheets of cell wall are bonded with nearby clay minerals, micro-organisms and amorphous organic and mineral soil materials. Indeed, most cell wall materials in soils are coated with a cutan of clay which varies in thickness from a few manometres to several microns in size.

Carbohydrate gels gluing aggregate components together.

Roots, root hairs, many bacteria and fungi secrete ECP as granular or fibrous gels. Root surface gels penetrate the soil for distances up to 100 µm from the rhizodermis and stabilise the nearby soil fabric. Root and microbial gels can be detected by using histochemical techniques for carbohydrates. These histochemical tests allow open micropores to be distinguished from micropores which are occluded by gel. They also allow pure clay fabrics to be distinguished from clays impregnated with polysaccharide, and amorphous deposits of iron and aluminium compounds to be separated from organomineral complexes.

Freshly deposited root surface gels are relatively soluble in water, but in some circumstances the gel becomes irreversibly denatured so that the soil is retained on the surface as a *rhizosheath*, even after prolonged washing (Goodchild and Myers, 1987; McCully and Canny, 1988). It is these denatured gels which form the core and stabilise the microfabrics of microaggregates.

Some soil fungi also secrete ECP which appear to attach the hyphae to mineral surfaces. In the planar voids between some microaggregates most of the space not occupied by the hyphae is filled with ruthenium/osmium reactive ECP, and this serves to glue the two parts of the macroaggregate together. Chenu (1989) deals with the effects of fungal polysaccharides on aggregate stability.

Many soil bacteria secrete extensive coats of ECP. These also stain with ruthenium red and hold nearby minerals to the surface of both individual bacteria and microcolonies. The ECP may persist after the death of the micro-organisms which secreted it, and continue to link one

part of the microaggregate to another in the absence of viable micro-organisms. Hence, microbial ECP content is highly correlated with aggregate stability (Lynch and Bragg, 1985).

Stabilisation of worm casts

Worm casts are generally more stable than the surrounding soil as measured by various tests of soil stability including wet sieving (Marinissen and Dexter, 1990). This results partly from the preferential selection by worms of soil which is rich in plant and other organic debris, and poor in large mineral grains. Worm casts are also richer in soluble nutrients such as N and P than the ingested soil, so that as well as an increased abundance of plant cell wall remnants, casts contain fungal hyphae and bacterial ECP. In addition casts contain mucins secreted by the worm gut (Foster and Lee, 1991).

POSSIBLE DIRECTIONS OF FUTURE RESEARCH.

The last 10 years has seen the development of techniques for electron microscopy of biological tissues which, if applied to ultrathin sections of soils, will revolutionise the *in situ* study of the soil biota and the processes they mediate. For example, incorporation of ^{14}C-labelled plant residues into soils followed by sampling at known time intervals and *autoradiography* of ultrathin sections, will precisely identify sites where organic matter residues at different stages of comminution and mineralisation reside. This will differentiate between stages in which the organic matter is vulnerable to microbial lysis from stages in which it is chemically or physically protected. In particular, *pulse labelling* of soils with specific radioactive substrates, followed by ultrastructural autoradiography, will allow the localization of microsites where particular biochemical transformations occur.

In addition, *gold labelling of antibodies* to particular enzymes or metabolites will identify which organisms or parts of organisms (*e.g.* cellular membranes) are mediating particular events of organic matter breakdown or resynthesis *in situ* in soils. Gold labelling of genetic markers will allow particular micro-organisms (*e.g.* biocontrol agents) to be identified and localised. EPM will allow the specificity of all these techniques to be verified. Hence for the first time, it will be possible to follow particular processes in soils, from the deposition of specific types of residue to their breakdown to the submicron and even nanometre size.

ACKNOWLEDGEMENTS

REFERENCES

Alexander, M., 1977. Introduction to Soil Microbiology. John Wiley and Sons, New York.
April, R. and Keller, D., 1990. Mineralogy of the rhizosphere in forest soils of the eastern United States. Biogeochem., 9: 1-18.
Bae, H.C., Cota-Robles, E.H. and Casida, L.E., 1972. Microflora of soil as viewed with transmission electron microscopy. Appl. Microbiol., 23: 637-48.

Barois, I., 1987. Intéractions entre les vers de terre (Oligocheta) tropicaux géophages et la microflore pour l'exploration de materielles organiques du sol. Trav. Cheurch. Stat. LAMTO, 7: 1-15.

Bottner, P. and Billes, G., 1987. La rhizosphere:site d'interactions biologiques. Rev. Ecol. Biol. Sol., 24: 369-388.

Bouché, M.B., 1975. Action de la faune sur les états de la matière organique dans les écosytèmes. In: G. Kilbertus, O. Reisinger, A. Mourey and J.A. Cancela de Fonseca (Editors), Biodégredation et Humification. Sarreguemines, Pierron, pp. 157-168.

Breznak, J.A., 1984. Hindgut spirochetes in termites and *Cryptocercus punctatus* In: N.R. Krieg and J.G. Holt (Editors), Bergey's Systematic Bacteriology, Vol.1. Williams and Wilkins, Baltimore, pp. 67-70.

Chenu, C., 1989. Influence of a fungal polysaccharide, scleroglucan on clay microstructure. Soil Biol. Biochem., 21: 229-305.

Dormaar, J.F., 1988. Effect of plant roots on chemical and biochemical properties of surrounding soil. Can. J. Soil Sci., 68: 233-242

Dormaar, J.F. and Foster, R.C., 1991. Nascent aggregates in the rhizosphere of perennial ryegrass (*Lolium perenne* L.). Can. J. Soil Sci., 71: 465-474.

Eisenbas, G., and Wicherd, W., 1987. Atlas on the Biology of Soil Arthropods. Springer Verlag, Berlin.

Ellsworth, T.R., Clapp, C.E. and Blake, G.R., 1991. Temporal variations in soil structural properties under corn and soybean cropping. Soil Sci., 151: 405-416.

Emerson, W.W., Foster, R.C. and Oades, J.M., 1986. Organo-mineral complexes in relation to soil aggregation and structure. In: P.M. Huang and M. Schnitzer (Editors.), Interactions of Soil Minerals with Natural Organics and Microbes . Soil Sci. Soc. Am. Spec. Publ. 17, Madison, Wisconsin, pp. 521-548.

Foster, R.C., 1983. The plant root environment. In: Soils: An Australian Viewpoint. CSIRO, Melbourne/Academic Press, London, pp. 673-684.

Foster, R.C. 1985a. *In situ* localization of organic mattter in soils. Quaestiones Entomologicae, 21: 609-633.

Foster, R.C., 1985b. The Biology of the Rhizosphere. In: C.A. Parker , A.D. Rovira, K.J. Moore, P.T.W. Wong and J.F. Kollmorgen (Editors), Ecology and Management of Soil Borne Plant Pathogens. Am. Phytopath. Soc., St. Paul, Minnesota, pp. 75-79.

Foster, R.C., 1986. The ultrastructure of the rhizoplane and rhizosphere. Ann. Rev. Phytopath., 24: 211-234.

Foster, R.C., 1988. Microenvironments of soil microorganisms. Biol. Fert. Soils, 6: 189-203.

Foster, R.C. and Dormaar, J.F., 1991. Bacteria grazing amoebae *in situ* in the rhizosphere. Biol. Fert. Soil, 11: 83-87.

Foster, R.C. and Dormaar, J.F. Phosphatases in the rhizosphere: Sites of secretion in young roots of *Lolium Perenne* L. Biol. Fert. Soil, (in press).

Foster, R.C. and Marks, G.C., 1967. Observations on the mycorrhizas of forest trees II The rhizosphere of *Pinus radiata* D.Don. Aust. J. Biol. Sci., 29: 915-926.

Foster, R.C. and Martin, J.K., 1981. *In situ* analysis of soil components of biological origin. In: E.A. Paul and J.N. Ladd (Editors), Soil Biochemistry, Vol 5. Marcel Dekker, New York, pp. 75-110.

Foster, R.C. and Rovira, A.D., 1978. The ultrastructure of the rhizosphere of *Trifolium subterraneum* L. In: M. Loutit (Editor), Proc. Int. Symp. Microbial Ecology. Springer Verlag, Berlin, pp. 278-289.

Foster, R.C., Rovira, A.D. and Cock, T.W., 1983. Ultrastructure of the root-soil interface. Am. Phytopath. Soc., St Paul, Minnesota, 157 pp.

Gianinazi-Pearson, V., Smith, S.E., Gianiazzi, S. and Smith,F.A., 1990. Enzymatic studies on the metabolism of vesicular-arbuscular mycorrhizas.New Phytol., 117: 61-74.

Goodchild, D.J and Myers, L.F., 1987. Rhizosheaths a neglected phenomonon in Australan Agriculture. Aust. J. Agric. Res., 38: 559-563.

Gould, N.D., Coleman, D.C. and Rubink, A.J., 1979. Effect of Bacteria and Amoebae on rhizosphere phosphatase activity. Appl. Envir. Microbiol., 37: 943-946.

Hattori 1988. Soil aggregates as microhabitats of microorganisms. Rep. Inst. Agric. Res. Tohoku Univ., 37: 23-36.

Hattori, T. and Hattori, R., 1976. The physical environment in soil microbiology. An attempt to extend the principles of microbiology to soil microorganisms. Crit. Rev. Microbiol., 4: 423-461.

Hawksworth, D.L. and Mound, L.A., 1991. Biodiversity databases: the critical significance of collections. In: D.L. Hawksworth (Editor), The Biodiveristy of Microorganisms and Invertebrates: Its Role in Sustainable Agriculture. CAB International, Wallingford, U.K., pp. 17-29.

Jamieson, B.G.M., 1981. The Ultrastructure of the Oligochaeta. Academic Press, London.

Jeanson, C., 1971. Structure d'une galerie de lombric à la microsonde électronique. In: J. D'Aguilar (Editor), IV Colloquium Pedobiologiae. Institut National des Recherches Agronomiques, Publ. No. 71-7, Paris, pp. 513-525.

Jocteur-Monrosier, L., Ladd, J.N., Fitzpatrick, R.W., Foster, R.C. and Raupach, M., 1991. Components and microbial biomass content of size fractions in soils of contrasting aggregation. Geoderma, 49: 37-62.

Kilbertus, G. and Reisinger, O., 1975. Dégredation du matèrial vegital activité in vitro et *in situ* de quelques microorganisms. Rev. Ecol. Biol. Sol, 12: 363-374.

Killham,K., Amato, M. and Ladd, J.N., 1993. Effect of substrate location in soil and soil pore water regime on carbon turnover. Soil Biol. Biochem., 25: 57-62.

Kretzschmar, A., 1982. Description des galiers de vers de terre et variation saisonière des réseaux (observations en conditions naturelles). Rev. Ecol. Biol. Sol, 19: 579-591.

Kretzschmar, A., 1987. Caractérisation microscopique de l'activité des lombriciens endoginés. In: N. Fedoroff, L.M. Bresson and M.A. Coutry (Editors), Soil Micromorphology. Proc. VII Int. Working Meeting of Soil Micromorphology, Paris, July 1985. Association Française pour l'Etude du Sol, Plaisir, France, pp. 325-330.

Kuikman, P.J., Jansen, A.G., van Veen, D.A. and Zehnder, A.J., 1990. Protozoan predation and the turnover of soil organic carbon and nitrogen in the presence of plants. Biol Fert. Soil 10:22-28.

Ladd, J.N., Jocteur Monrizier, L. and Amato, M., 1992. Carbon turn over and nitrogen transformations in an Alfilsol and a Vertisol amended with [U-14C] glucose and [15N] ammonium sulfate. Soil Bio. Biochem., 24: 359-372.

Lee, K.E., 1985. Earthworms: Their Ecology and Relationships with Soils and Land Use. Academic Press, Sydney, 411 pp.

Lee, K.E. and Foster, R.C., 1991. Soil fauna and soil structure. Aust. J. Soil Res., 29: 745-775.

Leyval, C., Laheunte, F., Belay, G. and Berthelin, J., 1991. Weathering of Micas in the rhizospheres of maize, pine and beech seedlings influenced by mycorrhizal and bacterial innoculation. Symbiosis, 9: 105-109.

Lynch, J.M. and Bragg, E., 1985. Microorganisms and soil aggregate stabiliy. Adv. Soil Sci., 2: 133-171.

Marinissen, J.C.Y. and Dexter, A.R., 1990. Mechanisms of stabilization of earthworm casts and artificial soils. Biol. Fert. Soils, 9: 163-167.

Martens, R., 1990. Contribution of rhizodeposits to maintenance and growth of soil microbial biomass. Soil Biol. Biochem., 22: 141-147.

Massicotte, H.B., Peterson, R.L. and Melville, L.H., 1989. Hartig net structure of ectomycorrhizae synthesised between *Laccaria bicolor* (Tricholomataceae) and two hosts: *Betula alleghaniensis* (Betulaceae) and *Pinus resinosa* (Pinaceae). Amer. J. Bot., 76: 1654-1667.

McCully, M.E. and Canny, M.J., 1988. Pathways and Processes of water and nutrient movement in roots. Plant and Soil, 111:159-170.

Moore, A.E.P., Massicotte, H.B. and Peterson, R.L., 1989. Ectomycorrhiza formation between *Eucalyptus pilularis* Sm. and *Hydnangium carneum* Wallr. in Dietr. New Phytol., 112: 193-204.

Newman, T. and Briarty, L.G., 1990. The use of Vapour phase fixation for the investigation of fully hydrated living plant material. Ann. Bot., 64: 305-334.

Oades, J.M., 1987. Aggregation in soils In: P. Rengasamy (Editor), Soil Structure and Aggregate Stability. Proc. of a Seminar, Tatura, Vic, August 1986. Conference Proceedings 12, Victorian Dept. Agriculture and Rural Affairs, pp. 74-101.

Ogden, C.G. and Pitta, P., 1990. Biology and ultrastructure of mycophageous soil testate amoeba *Phrygamella acropodia* (Rhizopodia,Protozoa). Biol. Fert. Soils, 9: 101-109.

Poindexter, J.S., 1981. Oligotrophy: Fast and famine existence. In: M. Alexander (Editor), Advances in Mcrobial Ecology, Vol. 5. Plenum Press, New York, pp. 63-89.

Pojasok, T. and Kay, B.D., 1990. Effect of root exudates from corn and bromegrass on soil structural stability.Can. J. Soil Sci.,70: 351-362.

Quereshi, R.H. and Jenkins, D.H., 1987. Concentration of phosphorus and sulphur at soil ped surfaces. J. Soil Sci., 38: 255-265.

Rasol0manana, J.L. and Balandreau, J., 1987. Rôle de la rhizosphere dans la biodégradation des composes recalcitrants: cas d'une rhizère poluée par des residus petroliers. Rev. Ecol. Biol. Sol, 24: 443-457.

Reddell, P. and Spain, A.V., 1991. Transmission of infective *Frankia* (Actinomycetales) propargules in thje casts of the endogeic earthworm *Pontoscolex corethrus* (Oligochaeta: Glossoscoliectidae), Soil Biol. Boiochem., 23: 775-778.

Reddell, P. and Spain, A.V., 1991. Earthworms as vectors of viable propargules of mycorrhizal fungi. Soil Biol. Biochem., 23: 767-774

Reid, J.B. and Goss, M.J., 1981. Effect of living roots of different plant species on the aggregate stability of two arable soils. J. Soil Sci., 32: 521-541

Reid, J.B., Goss, M.J., 1982. Supression of decomposition of ^{14}C labelled plant roots in the presence of living roots of maize and perennial rye grass. J. Soil Sci., 33: 287-295.

Reid, J.B, Goss, M.J. and Robertson, P.D., 1982. Relationship between decreases in soil stability effected by the growth of maize roots and changes in organically bound alumium. J. Soil Sci., 33: 397-410.

Robert, M. and Chenu, C., 1992. Interactions between soil minerals and microorganisms.In: G. Stotzky and J.-M. Bollag (Editors), Soil Biochemistry, Vol. 7. Marcel Dekker, New York, pp. 307-404.

Roper, M.M. and Marshall, K.C., 1974. Modification of the interaction between *Escherichia coli* and bacteriophage in a saline sediment. Microb. Ecol., 1:1-13.

Rutherford, P.M. and Juma, N.G., 1992. Influence of texture on habitable pore space and bacterial-protozoon populations in soil. Biol. Fert. Soils, 12: 221-227.

Santos, M.C.D., Mermut, A.R. and Ribeiro, M.R., 1989. Submicroscopy of clay microaggregates in an Oxisol from Pernambuco Brazil. Soil Sci. Soc. Am. Proc., 53: 1895-1901.

Scales, P.F. and Peterson, R.L., 1991. Structure and developmenmt of Pinus banksiana-Wilcoxina ectencomycorrhizae. Can. J. Bot., 69: 2135-2148.

Sparling, G.P., 1985. The soil biomass. In: D. Vaughn and R.E. Malcolm (Editors), Soil Organic Matter and Biological Activity. Martinus Nijhoff Junk, Dortrecht, pp. 223-262.

Stout, J.D. and Heal, O.W., 1967. Protozoa. In: A. Burges and F. Raw (Editors), Soil Biology. Academic Press, London, pp. 149-195.

Tisdall, J. and Oades, J.M., 1979. Stabilization of soil aggregates by root systems of rye grass Aust. J. Soil Sci., 17: 429-441.

Tributh, H., Bognslawski, E.v., Lieris, A.v., Steffens, D. and Mengill, K., 1987. Effect of potassium removal by crops on the transformation of illitic clay minerals. Soil Sci., 143: 404-409.

This Page Intentionally Left Blank

Morphological aspects of microorganism habitats in a vertisol

J.L. Chotte[1], G. Villemin[2], P. Guilloré[3] and L. Jocteur Monrozier[4]

[1]ORSTOM, BP 8006 97259 Fort de France cédex, France, Martinique, French West Indies
[2]U.P.R. 6831 CNRS associée à l'Université de Nancy I, BP 5, 54501 Vandœuvre les Nancy Cédex, France
[3]Institut National Agronomique Paris-Grignon, INRA, 78850 Thiverval-Grignon, France
[4]Université Lyon I, URA CNRS 1450, 69622 Villeurbanne cédex, France

ABSTRACT

Chotte, J.L., Villemin, G., Guilloré, P. and Jocteur Monrozier, L., 1994. Morphological aspects of microorganism habitats in a vertisol. In: A.J. Ringrose-Voase and G.S. Humphreys (Editors), Soil Micromorphology: Studies in Management and Genesis. Proc. IX Int. Working Meeting on Soil Micromorphology, Townsville, Australia, July 1992. Developments in Soil Science 22, Elsevier, Amsterdam, pp. 395-403.

The aim of this study, was to determine the distribution of soil microorganisms with respect to soil fabric, and to obtain morphological indications on microorganism habitats in a heavy smectitic clayey soil.

The top layer (3 - 8 cm) of a vertisol under a 7 years old pasture was taken with a soil ring sampler. An undisturbed soil sample was submersed in cold water for 36 h without agitation. Soil was fractionated by gentle wet sieving and sedimentation to isolate coarse roots (diameter >500 μm) and aggregates of size >2,000 μm, 200 - 2,000 μm, 50 - 200 μm, 20 - 50 μm, 2 - 20 μm and 0 - 2 μm. Microbial biomass of the total soil amount and of the different size aggregates were determined by a fumigation-extraction method. Thin sections were made on undisturbed wet aggregates, size >2,000 μm and 200 - 2,000 μm that were dehydrated by the acetone exchange process and embedded in polyester resin. Ultrathin sections were made on undisturbed wet aggregates of size >2,000 μm, 200 - 2,000 μm and 0 - 2 μm, dehydrated by acetone exchange process and embedded in epon's medium. Polysaccharides were revealed by Thiery's reaction. Ultrathin sections were observed with a TEM.

Clay fraction isolated by this method represented only 20% of the clay content obtained by mechanical analysis. Only 14% of the total soil biomass was located in the fraction <2 μm composed of dispersed clay or clay particles aggregated around organic amorphous compounds. Most of the biomass was associated with aggregates of size >2,000 μm and 200-2,000 μm (30% and 18% of the total biomass respectively). These aggregates amounted to 45% and 11% of the soil total weight respectively. They were composed of fine roots (diameter <500 μm) coated with an organo-mineral plasma consisting of birefringent minerals and clay. TEM observations indicated that microorganisms colonized organic skeleton and clay plasma. Polysaccharides may represent the glue permitting the cohesion of micro-fabrics.

INTRODUCTION

Soil is composed of an assemblage of solid particles and voids and represents the most complex habitat for microorganims. The distribution of microorganisms throughout the soil is controlled by the concentration in assimilable carbon (Gray and Williams, 1971), soil water regime (Griffin, 1981), and soil structure (Elliott and Coleman, 1988; Hattori, 1988) as defined by Brewer (1964). Conversely the size of soil particles and the surrounding water-film control the microbial activity (Tiedje *et al.*, 1984; Elliott, 1986) and the ability of microorganisms to decompose soil organic matter (Adu and Oades, 1978 a and b).

Much of the difficulty in studying the relationships between soil structure and soil microbial distribution and activity is based on our lack of knowledge of microorganims in undisturbed soil habitats. Most of the research involved on the characterization of soil microorganism habitats employed physical soil fractionation (Kanazawa and Filip, 1986; Gupta and Germida, 1988; Jocteur Monrozier *et al.*, 1991). However, the energy deployed during soil fractionation modified the aggregate size distribution (Oades and Waters, 1991), the biological properties of the aggregates (Elliott, 1986), and distribution of soil microorganisms and the morphological characteristics of the aggregates (Chotte *et al.*, 1993). In the latter work, the agitation of the soil in the presence of agate marbles (5 pieces, diameter = 1 cm) before soil fractionation induced the total disappearance of soil aggregates >250 µm, in comparison with the agitation without marbles. Their breakdown produced the dispersion of primary particles (mineral and organic) and associated microorganisms.

This paper is an attempt to determine the macro-, micro-, and ultramicro- morphological characteristics of undisturbed soil microorganism habitats of a smectitic clayey soil. In this study, undisturbed soil cores were sampled, submersed in water, and fractionated by wet sieving without prior agitation. Attention will be given to the coarsest aggregate size fraction.

MATERIAL AND METHODS

Material

The soil used in this study is a vertisol developed on volcanic ashes, and situated at Sainte-Anne in the south-east of Martinique (Lesser Antilles). This tropical region is characterized by annual rainfall of 1,300 mm, and a dry season of four months (March to June). Undisturbed topsoil (layer 3 - 80 cm) samples (10 replicates) under a seven years old pasture (*Digitaria decumbens*) were taken with a soil ring sampler (volume = 98 cm^3). At sampling, water tension was about pF 2.5.

Methods

Physical soil fractionation

Each undisturbed soil sample was submersed in water (250 ml 100 g^{-1} dry soil) for 36 hours before physical soil fractionation. Water saturated samples were fractionated without shaking. Plant roots (diameter = 500 µm) were separated from soil samples by hand fractionation. Soil was then fractionated by wet sieving, and by sedimentation to obtain 6 size fractions: >2,000 µm, 200 - 2,000 µm, 50 - 200 µm, 20 - 50 µm, 2 - 20 µm and 0 - 2 µm. All procedures were performed at 4°C to avoid biological modification. Care was taken during physical soil
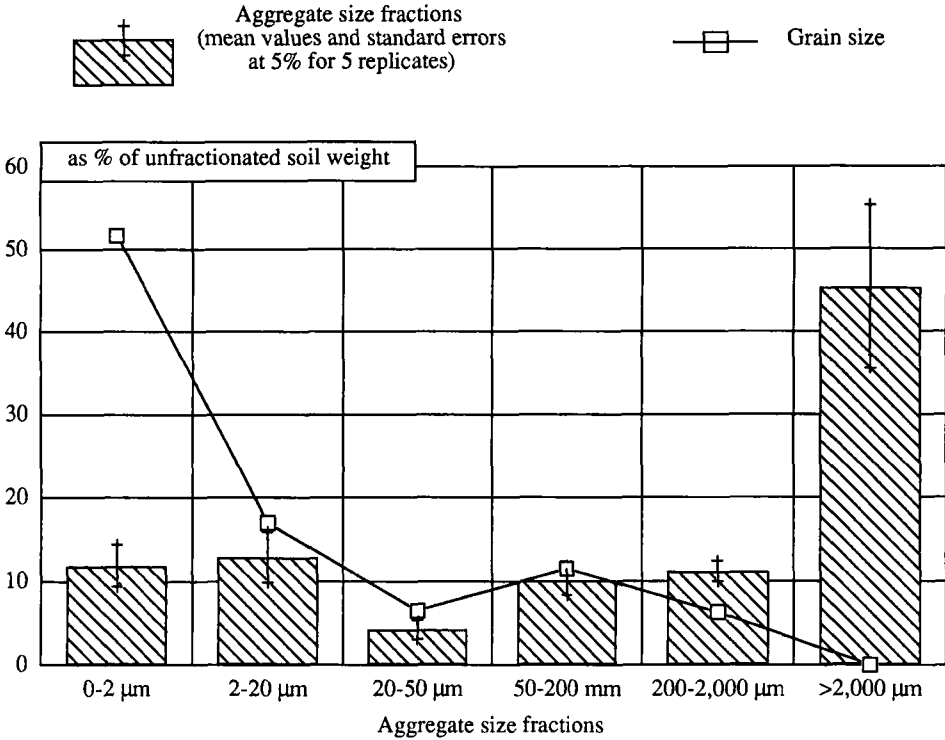
Fig. 1. Distribution of the aggregate size fractions separated by physical fractionation method.

fractionation to split the soil along planes of weakness and to remove small aggregates adhering to roots. Composite samples were prepared by mixing each wet fraction from 5 of the 10 replicates for analysis (microbial biomass, micro and ultramicromorphology). The other 5 replicates were air dried for macromorphological observations.

Grain size distribution was determined after removal of soil organic matter by treatment with hydrogen peroxide. Grain sizes >50 μm were obtained by sieving, and grain sizes <50 μm were analysed by a laser diffraction analyser (Malvern Mastersizer/E instrument).

Total Microbial biomass assay

Microbial biomass of the unfractionated soil and of the size fractions was determined in duplicate by a fumigation extraction method (Amato and Ladd, 1988). This method involves fumigation with chloroform of wet soil samples (unfractionated soil and particle size fraction subsamples) to kill the biomass. Biomass C was assessed using 2M KCl as soil extractant and expressed as leucine/NH4+ equivalents as following: Biomass C = 21 X (ninhydrin-reactive nitrogen after 10 days fumigation less ninhydrin-reactive nitrogen before fumigation).
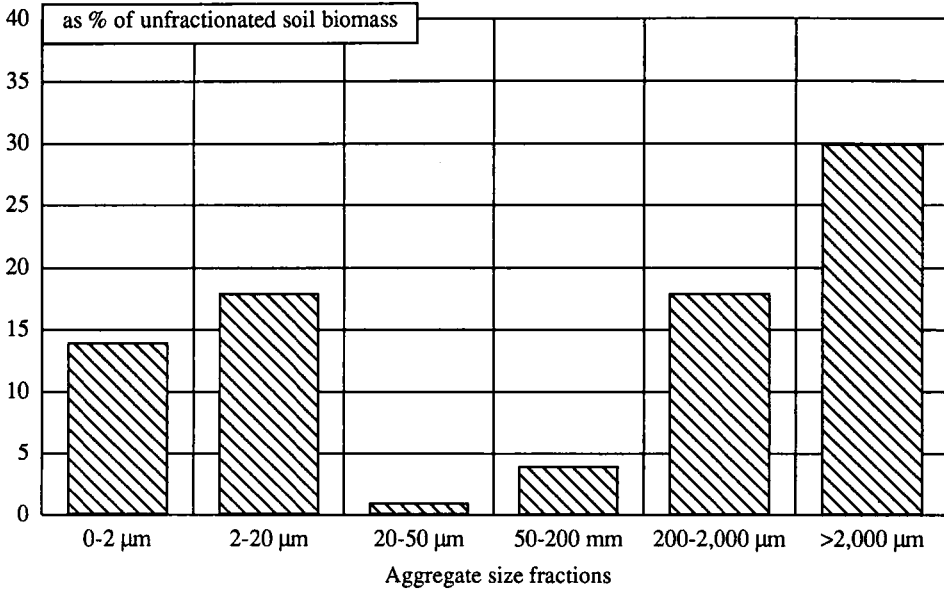
Fig. 2. Biomass-C distribution within the aggregate size fractions (results expressed as % of the unfractionated soil biomass-C).

Morphological observations

Macromorphological observations: Air-dried fractions >2,000 μm were observed and classified according to the shape classification (in Brewer ,1964, p. 21) which is based on the ratios of the long, intermediate, and short axes of the particles. Their axes were measured with a digital caliper.

Micromorphological observations: Undisturbed wet subsamples of fractions (>2,000 μm) were dehydrated by solvent exchange, impregnated, hardened with a polyester resin, and prepared as thin sections (Guilloré, 1983). Thin sections were examined with a stereo microscope (Wild M420).

Ultramicromorphological observations: Wet fraction subsamples for TEM were fixed in buffered 1% OsO_4 for 16 hours (Villemin and Toutain, 1987). After washing the buffer, the samples were enclosed in 2% agar, dehydrated by solvent exchange and embedded in Epon's medium. Ultrathin sections were stained successively in uranyl acetate and lead citrate solutions. Polysaccharides were revealed by Thiery's reaction (Thiery, 1967). Ultrathin sections were examined with a Zeiss EM 95-2 at 60 Kv.

RESULTS

Weight distribution of the aggregate size fractions

Clay fraction (<2 μm) isolated by the physical fractionation method represented only 11% of the unfractionated soil weight (Fig. 1). This fraction amounted to only 20% of the clay

Table 1

Macromorphological characteristics of the aggregate size fractions >2,000 μm according to their long axis (size in mm). Statistical analyses were made on classes of 0.2 mm width.

Replicate	Total number	Length		Median class	Modal class(es)
		min	max		
1	274	2.63	14.88	5.0-5.2	(3.8-4.0); (4.2-4.4); (4.6-4.8)
2	344	2.01	18.89	4.6-4.8	4.0-4.2
3	365	2.08	18.45	4.2-4.4	3.6-3.8
4	260	2.05	19.92	3.6-3.8	3.6-3.8
5	307	2.05	18.59	4.2-4.4	4.2-4.4
1+2+3+4+5	1550	2.01	19.92	4.4-4.6	3.6-3.8
Mean	310				
CV%	14				

Table 2

Distribution of the aggregate size fraction >2,000μm within the different shape classes (after Brewer, 1964). Results expressed as % of the total particle number.

Replicate	Total number	Shape classes						
		Acicular-Planar	Acicular	Planar	Triaxial	Prolate	Oblate	Equant
1	274	0	0	0	1.5	23.5	11.0	64.0
2	344	0	0	0	3.5	30.5	17.0	49.0
3	365	0	0	0	5.0	27.0	22.0	46.0
4	260	0	0	0	4.0	35.0	17.0	44.0
5	307	0	0	0	7.0	28.0	20.0	45.0
Mean	310	0	0	0	4.2	28.8	17.4	49.6
CV%	14	0	0	0	48	15	24	17

particle content of the total soil. The aggregate size fractions 2 - 20 μm, 20 - 50 μm, 50 - 200 μm and 200 - 2,000 μm represented 13%, 4%, 10% and 11% of the unfractionated soil weight respectively. The aggregate size fraction >2,000 μm was the most abundant fraction. This fraction represented about 45% of the total soil weight although there is no sand grain >2,000 μm: it seems obvious that this fraction was constituted by aggregated simple particles.

Distribution of biomass-C within the aggregate size fractions

Biomass-C of the unfractionated soil was equal to 4,750 μg g^{-1} soil. Slightly less than 15% of biomass-C of the unfractionated soil was dispersed with the clay fraction (Fig. 2). Biomass-C associated with the fraction 2 - 20 μm was as important as the biomass-C located in the aggregate size fraction 200 - 2,000 μm. They each represented 18% of the unfractionated soil

biomass-C. The lowest proportion of the total soil biomass-C was associated to the aggregate size fractions 20 - 50 μm, and 50 - 200 μm (1% and 4% of the unfractionated soil biomass-C respectively). These fractions did not represent habitats for soil microorganisms. In contrast, about 30% of the unfractionated soil biomass-C was found in the fraction >2,000 μm. The aggregates larger than 200 μm (>2,000 μm + 200 - 2,000 μm) were the most important soil microorganism habitats (30% and 18% of the unfractionated soil biomass-C respectively).

Morphological characteristics of the aggregate size fraction >2,000 μm

Macromorphological characteristics

The size of the long axis of the aggregate size fraction >2,000 μm varied from 2.01 mm to 19.92 mm (Table 1) with a median class equal to 5.0 - 5.2 mm, 4.6 - 4.8 mm, 4.2 - 4.4 mm, 3.6 - 3.8 mm, and 4.2 - 4.4 mm for the replicate 1, 2, 3, 4, and 5 respectively. The distribution of the size of their long axis was tri-modal for the replicate 1. For the others, the distribution was uni-modal. For the whole replicates (1+2+3+4+5), the classes 4.4 - 4.6 mm, and 3.6 - 3.8 mm were the median and modal classes respectively. About 50% of the aggregates were classified in the equant shape class (Table 2). About 30%, less than 20% and, less than 5% of these aggregates were classified in the prolate, oblate and, triaxial class respectively. There were no acicular-planar, acicular and planar aggregates. The aggregates were smooth and their physical stabilization could be performed by plant roots encrusted in it.

Micromorphology

The observations under plane light revealed the abundance of manganiferous glaebules randomly distributed within the S-matrix ranging in size up to 1,000 μm (Fig. 3a). Intra-aggregate planar voids 150 μm to 50 μm wide and, 500 μm to 4,000 μm long can be distinguished. Under crossed polarized light birefringent mineral skeleton grains randomly distributed within the S-matrix can be observed (Fig. 3b). The black area represents a planar void. There was no plasma separation in the wall of the plane. Observations under episcopic light allowed the recognition of organic skeleton grains (Fig. 3c). These organic skeletons were fresh or partly humified and randomly distributed within the S-matrix.

Ultramicromorphology

Ultramicromorphology of these aggregates larger than 2,000 μm were revealed by TEM observations (Fig. 3d-g). Using these observations, it was not possible to determine a significant influence of the soil water submersion on bacteria morphology. These aggregates

---

Fig. 3. **a)** to **c)** Thin section micrographs (aggregate size fraction >2,000 μm). **a)** General trend, plane light. **b)** Detail of S-matrix, crossed polar light. **c)** Detail of S-matrix, episcopic light. G: manganiferous glaebule, Pv: planar void, R; root, oS: organic skeleton, mS: mineral skeleton, M: magnetite.

d) to **g)** TEM micrographs (Aggregate size fraction >2,000μm, uranyl acetate and lead citrate stained). **d)** and **e)** S-matrix. **f)** Clay plasma grouped along organic skeleton decomposed by bacteria. **g)** Clay plasma encrusted around a bacterial colony. B: bacteria, Q: quartz, C: clas plasma, oS organic skeleton, hO: humified organic matter.
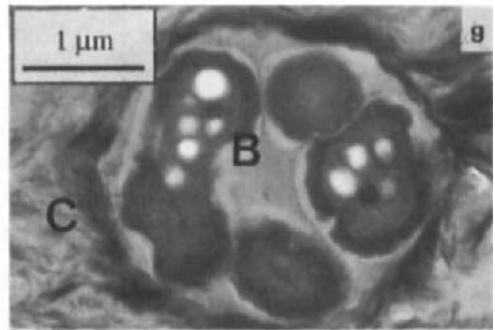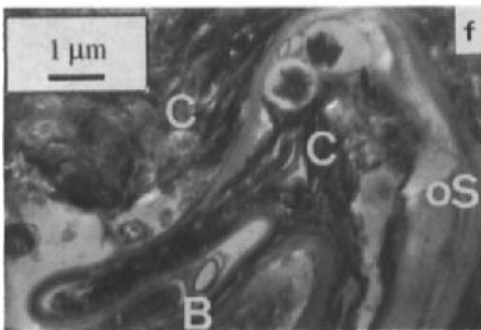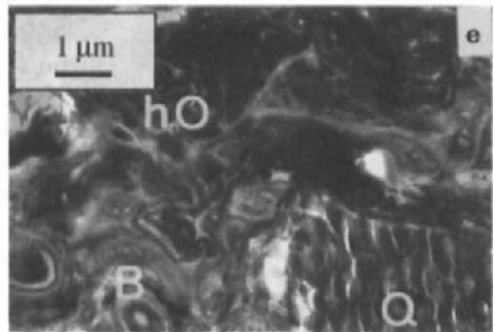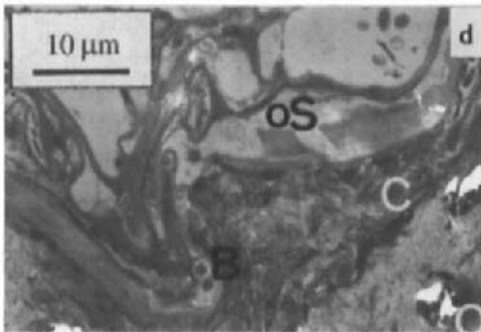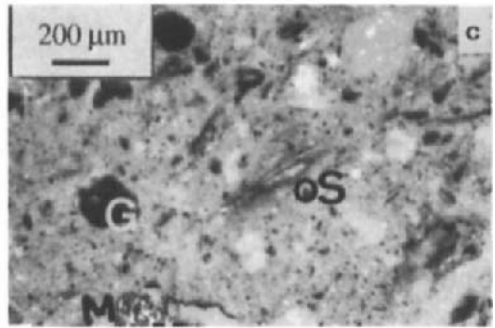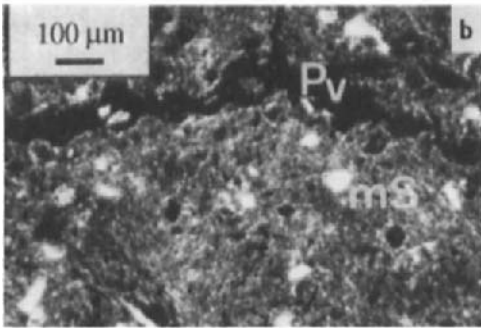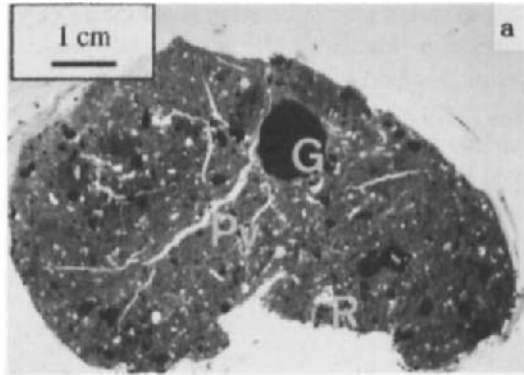
were constituted by organic skeleton grains coated in an abundant clay plasma (Fig. 3d) and by mineral skeleton grains (quartz) (Fig. 3e). The relationship between organic skeleton and bacteria and between clay plasma and bacteria could be seen. Most of bacteria were located with organic skeletons and clay plasma grouped along these organic skeletons (Fig. 3d). Most ultra-microvoids of this compacted clay zone were occupied by bacteria (Fig. 3e and f). These bacteria may have survived the chloroform treatment (Martin and Foster, 1985). Clays were also concentrated around bacterial colonies (Fig. 3g). Bacteria were very active since their cytoplasm was filled by polyphosphate granules (black dashes) and by polyhydroxybutyrate granules (white dashes). Clay cutans may protect bacteria from lysis by bacteriophage (Foster, 1986) and soil dessication (Kilbertus et al., 1979).

DISCUSSION

The aggregates larger than 2,000 μm, isolated by wet sieving without agitation, represented, with the aggregates 200 - 2,000 μm, the most abundant soil microorganism habitat. These aggregates amounted to slightly less than 50% and 10% of the total soil weight and, they contained 30% and 18% of the total soil biomass respectively. Morphological observations revealed that aggregates larger than 2,000 μm were smooth and, constituted by manganiferous glaebules, mineral (birefringent mineral and magnetite) and organic (fresh or partly decomposed) skeletons. Intra-aggregate voids (planes and chambers) could be observed. The microorganisms located in these aggregates colonized organic skeleton and clay plasma. These aggregates represented an energy environment as rich as the rhizosphere since bacteria cytoplasm was filled by large amounts of storage materials (Foster et al., 1983). The cohesion of these microstructures could be due to bacterial polysaccharides as discussed by Robert and Chenu (1992).

CONCLUSION

To investigate the morphological characteristics of soil microorganism habitats in a vertisol, the relationship between soil microorganisms and organic skeleton, and between soil microorganisms and clay plasma have been emphazised. However, further important studies are required of the distribution of soil microorganisms within soil pores and the relationship between microorganisms and mineral skeleton. These studies will allow us to assess the interactions of microbiotic processes with soil structure.

REFERENCES

Adu, J.K. and Oades, J.M., 1978a. Physical factors influencing decomposition of organic materials in soil aggregates. Soil Biol. Biochem., 10: 109-115.

Adu, J.K. and Oades, J.M., 1978b. Utilization of organic materials in soil aggregates by bacteria and fungi. Soil Biol. Biochem., 10: 117-122.

Amato, M. and Ladd, J.M., 1988. Assay for microbial biomass based on ninhydrin-reactive nitrogen in extracts of fumigated soils. Soil Biol. Biochem., 20: 107-114.

Brewer, R., 1964. Fabric and Mineral Analysis of Soils. John Wiley and Sons, New York, 470 pp.

Chotte, J.L., Jocteur Monrozier, L., Villemin G. and Albrecht, A., 1993. Study of soil microhabitats. Importance of the fractionation method. In: K. Mulongoy and R. Merckx (Editors), Soil Organic Matter Dynamics and Sustainability of Tropical Agriculture. John Wiley and Sons, London, pp. 39-45.

Elliott, E.T., 1986. Aggregate structure and carbon, nitrogen, and phosphorus in native and cultivated soils. Soil Sci. Soc. Am. J., 50, pp. 627-633.

Elliott , E.T. and Coleman, D.C., 1988. Let the soil work for us. Ecol. Bull., 39: 23-32.

Foster, R.C., 1986. The utlrastructure of the rhizoplane and rhizosphere. Ann. Rev. Phytopatholo., 24: 211-234.

Foster, R.C., Rovira, A.D. and Cock, T.W., 1983. Ultrastructure of the Root-Soil Interface. The American Phytopathological Society, St Paul, U.S.A., 157 pp.

Gray, T.R.G. and Williams, S.T., 1971. Soil Micro-organisms. Oliver and Boyd, Edinburgh, 240 pp.

Griffin, D.M., 1981. Water potential as a selective factor in the microbial ecology of soils. In: J.F. Parr, W.R. Gardner and L.F. Elliott (Editors), Water Potential Relations in Soil Microbiology. Soil Sci. Soc. Am., Madison, Wisconsin, pp. 141-151.

Guilloré, P., 1983. Méthode de fabrication mécanique et en série de lames minces (2ème éd.) Institut National Agronomique Paris-Grignon, Département des Sols, 22 pp.

Gupta, V.V.S.R. and Germida, J.J., 1988. Distribution of microbial biomass and its activity in different soil aggregate size classes as affected by cultivation. Soil Biol. Biochem., 20, pp. 777-786.

Hattori, T., 1988. Soil aggregates as microhabitats of microorganisms. Rep. Inst. Agr. Res. Tohoku Univ., 37: 23-36.

Jocteur Monrozier, L., Ladd, J.N., Fitzpatrick, R.W., Foster, R.C. and Raupach, M., 1991. Components and microbial biomass content of size fractions in soils of contrasting aggregation. Geoderma, 49: 1-10.

Kanazawa, S. and Filip, Z., 1986. Distribution of microorganisms, total biomass, and enzyme activities in different particles of brown soil. Microb. Ecol., 12: 205-215.

Kilbertus, G., Proth, J. and Vervier, B., 1979. Effets de la dessiccation sur les bactéries gram-négatives d'un sol. Soil Biol. Biochem., 11: 109-114.

Martin, J.K. and Foster R.C., 1985. A model system for studying the biochemistry and biology of the root/soil interface. Soil Biol. Biochem., 17: 261-269.

Oades, J.M. and Waters, A.G., 1991. Aggregate hierarchy in soils. Aust. J. Soil Res., 29, 815-828.

Robert, R. and Chenu, C., 1992. Interactions between soil minerals and microorganisms. In: G. Stotzky, J.M. Bollag (Editors), Soil Biochemistry. Marcel Dekker, New York.

Thiery, J.P., 1967. Mise en évidence des polysaccharides sur coupes fines en microscopie électronique. J. Microscopie, 6: 987-1017.

Tiedje, J.M., Sextone, A.J., Parkin, T.B., Revsbech, N.P. and Shelton, D.R., 1984. Anaerobic processes in soil. Plant and Soil, 76: 197-212.

Villemin, G. and Toutain, F., 1987. Méthode de fixation d'échantillons organo-minéraux de sols pour la microscopie électronique à transmission. In: N. Fedoroff, L.M. Bresson and M.A. Coutry (Editors), Soil Micromorphology. Proc. VII Int. Working Meeting of Soil Micromorphology, Paris, July 1985. Association Française pour l'Etude du Sol, Plaisir, France, pp. 43-47.

This Page Intentionally Left Blank

The influence of fungus-cultivating ants (Hymenoptera, Formicidae, Attini) on the morphology of andosols in Martinique

V. Eschenbrenner

ORSTOM, BP 8006, 97259 Fort-de-France Cédex, Martinique, French West Indies

ABSTRACT

Eschenbrenner, V., 1994. The influence of fungus-cultivating ants (Hymenoptera, Formicidae, Attini) on the morphology of andosols in Martinique. In: A.J. Ringrose-Voase and G.S. Humphreys (Editors), Soil Micromorphology: Studies in Management and Genesis. Proc. IX Int. Working Meeting on Soil Micromorphology, Townsville, Australia, July 1992. Developments in Soil Science 22, Elsevier, Amsterdam, pp. 405-410.

Andosols are formed on volcanic ash and pumice in high rainfall areas in Martinique (French West Indies). A common morphological feature of these soils is the occurrence, at depths of 0.2 to 3 m, of numerous smooth-walled chambers and galleries: the chambers are ellipsoidal with flat floors, (length 4 - 12 cm, breadth 3 - 6 cm, and height 2 - 5 cm); and the galleries are cylindrical and 1 - 4 mm in diameter. Both the chambers and the galleries are formed by attine ants which cultivate fungi gardens in the chambers using insect faeces, and plant debris (60 - 200 µm) as the nutritive source for the fungi.

Most of the soil material excavated by these ants is not translocated above the soil surface, but is packed into pre-existing chambers and galleries (previously excavated by these ants), giving rise to pedotubular features, *viz.*, chambers and channels aggrotubules.

INTRODUCTION

Animals that affect the soil have received inadequate attention from pedologists (Hole, 1961,1981). In particular there are few publications on the effects of ants on tropical and subtropical soils (Petal, 1978; Cowan *et al.*, 1985; Lobry de Bruyn and Conacher, 1990).

The attine, or fungus-growing ants, comprise a tribe of eleven genera containing 200 species (Weber, 1982; Holldobler and Wilson, 1990). All of them occur in the New World (from 44°S in Argentina to 40°N in the U.S.A.) and have been considered the ecological equivalent of the African fungus-cultivating termites (Weber, 1972).

Some of these fungus-growing ants (or major Attini) grow their fungi on fragments freshly-cut from living plants. These are the so-called "leaf-cutting ants". Since their colonies may be very large (up to several million workers), they are considered as agricultural pests, and some attention has been given to their effects on soils (Moser, 1963; Jonkman, 1979, 1980; Alvarado *et al.*, 1981). However, most of the fungus-growing ants cultivate their fungi on different substrates, *viz.*, insect faeces and cuticles, rotting wood and other plant debris. Because their colonies are small and they are not considered as pests, very little is known on the influence of these minor Attini on the soil morphology.

Fig. 1. Distribution of the genus *Mycocepurus* (Formicidae, Myrmicinae, Attini), "primitive" fungus growing ants (after Weber, 1972; modified).

Leaf-cutting ants do not occur in Martinique although minor attines have been found (A. Kermarrec, pers. comm., 1992). As part of an ongoing project aimed at assessing the importance of soil fauna on soil properties, we have examined the influence of ants of the genus Mycocepurus on the morphology of andosols.

STUDY AREA AND METHODS

The study was conducted near Sainte-Marie, in the central northern part of Martinique, French West Indies. The site, covering one square kilometer, is located 14°46'15" N, 61°03'W (Fig. 2), and it lies between 300 m and 400 m a.s.l. Mean annual precipitation is 2500 - 3000 mm with a drier period between January and April. The soils are perhydrated (water retention at 1/3bar >100%) Andosols (Hydrandepts) developed from andesitic to dacitic ashes and pumices. Within this area, eight plots representing different land-uses (rain forest, mahogany forest plantations of different ages, banana and sugarcane permanent cultures, traditional yam-taro-grazed fallow rotations) have been investigated for evidence of ant activity, both above and below ground. Their influence on the subsoil was estimated on the basis of eight pits dug to a depth of 2 - 3.5 m. Observations were made of the pit walls using a hand lens and serial sections were taken from the walls. Undisturbed soil samples ranging up to some decimetres in size were taken and dissected under a stereo microscope (magnifications from 3.6 to 175× (Macroscop Wild M 420; objectives 0.5×, 1× and 2×; wide field oculars 10× and 20×, and Apozoom 1: 6).

RESULTS

Evidence of the activities of the fungus-cultivating ants was noted in each of the eight plots. The burrow system consists of open galleries, backfilled galleries and chambers, and chambers
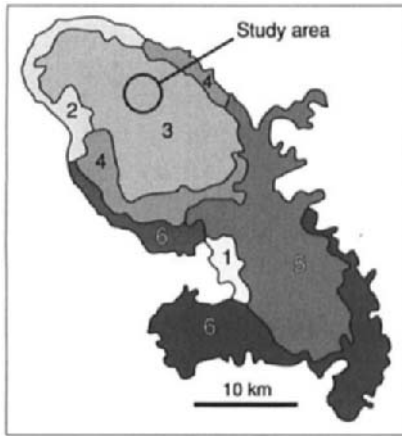
Fig. 2. Schematic soil map of Martinique. 1: "Sols peu évolués" on alluvial material (Tropofluvents); 2: "Sols peu évolués" on ashes and pumices (Vitrandepts); 3: Andosols (Eutrandepts and Hydrandepts); 4: "Sols brun-rouille à halloysite" (Tropudalfs); 5: "Ferrisols" (Tropudults); 6: Vertisols (Pellusterts).

with the fungus gardens. Soil materials transported to the surface were observed less commonly. Ants collected from these sites, in the above ground soil material and within chambers with fungus gardens, were identified by Dr. Kermarrec (INRA, Guadeloupe, F.W.I.) as belonging to the genus *Mycocepurus*. They have a small size (body length *ca.* 2 mm), with dull reddish brown colouring and the workers are monomorphic. The genus has a wide distribution througout the Caribbean area, Central and Southern America (Fig. 1).

Fungus gardens

The fungus gardens consist of 3 to 15 elongated ellipsoidal units (vertical long axis 2 - 5 cm; horizontal short axis 0.2 - 1 cm) that hang from the ceilings of the chambers (Fig. 3). Each individual unit is composed of insect faeces and wood fragments, 100 - 400 μm long, loosely embedded in a hyphal network (Fig. 4). Eggs and brood occur within the fungus garden.

Empty chambers and access galleries

Chambers occur from 0.2 to more than 3 m in depth and their basic distribution pattern is generally random, but locally clustered. These chambers are ellipsoidal in shape with the horizontal long axis 4 - 12 cm, the horizontal short axis 3 - 6 cm and the vertical axis 2 - 5 cm. The walls are smooth (metachambers), but locally, unweathered pumices that are too hard to be broken up by the ants or too large to be translocated protrude (Fig. 5) or lie on the floors of the chambers.

Four to fifteen access galleries open onto the floor and the walls of each chamber (Fig. 6). The galleries are cylindrical, 1 - 4 mm in diameter and smooth-walled (metachannels).

Soil material translocated above ground

The soil materials translocated by *Mycocepurus* ants consists of very loosely packed mineral soil aggregates and skeleton grains ranging in size from 80 - 1000 μm. They form very small conical mounds (basal diameter 2 - 4 cm, height 1 - 2 cm).
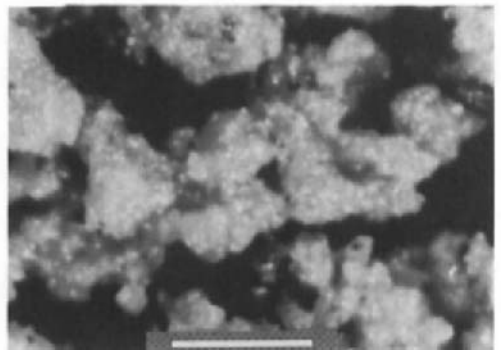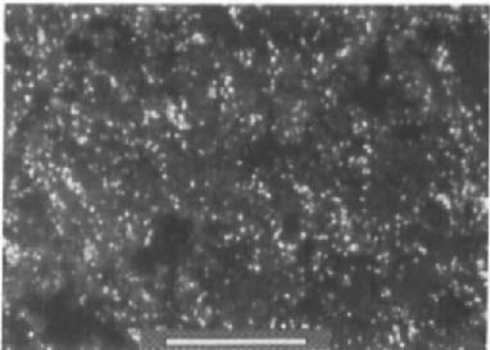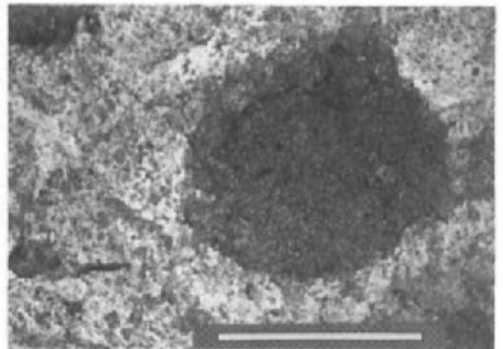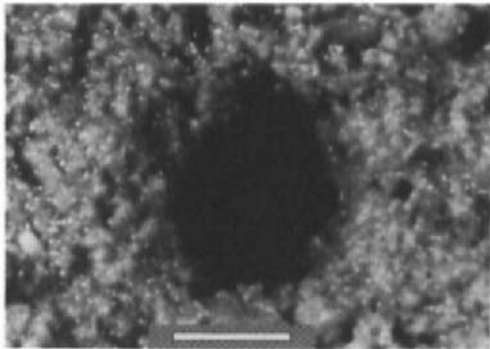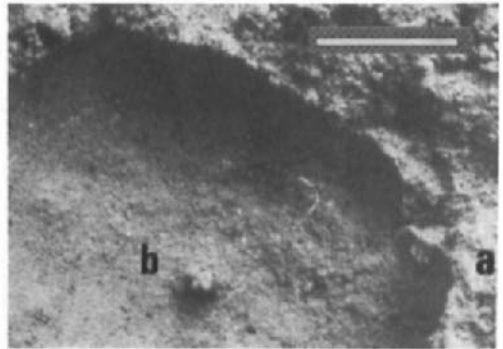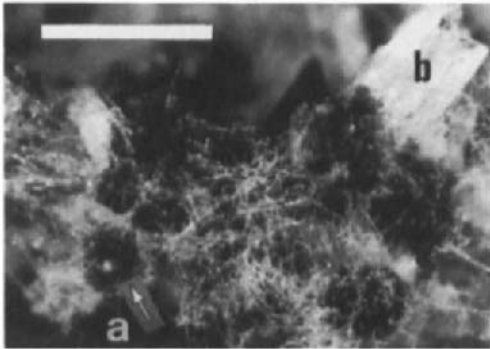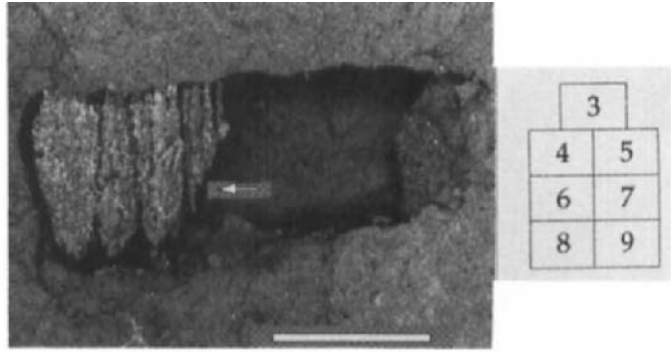
Backfilled chambers and access galleries

Backfilled chambers and galleries have the same shape and size as their empty equivalents. The granular backfilling material (Fig. 9) contrasts strongly with massive surrounding soil material (Fig. 8) and the boundary between the two phases is sharp (Fig. 7). The backfill material consists of loosely packed mineral soil aggregates and free skeleton grains ranging in size from 80 - 1000 µm and is similar to that translocated above ground. The macroporosity of this backfilled phase (interconnected mammilated vughs and compound packing voids, Fig. 9), is very high and its cohesion is low. These backfilled chambers and galleries are chambers and channel aggrotubules.

CONCLUSION

Excavation and backfilling of channels and chambers result directly from the activities of ants of the genus *Mycocepurus*. Part of the mineral soil material excavated by these minor attine fungus cultivating ants is translocated above ground; most, however, is translocated within the soil giving rise to chamber and channel pedotubular features.

It is possible that these ants have a considerable effect on the soil in Central and South America.

ACKNOWLEDGEMENTS

REFERENCES

Alvarado, A., Berish, C.W. and Peralta, F., 1981. Leaf-cutter ant *(Atta cephalotes)* influence on the morphology of Andepts in Costa Rica. Soil Sci. Soc. Am. J., 45: 790-794.

Fig. 3. Fungus garden: individual unit (arrow) hanging from the ceiling of a chamber. Scale bar 2 cm.

Fig. 4. Detail of an individual unit of a fungus garden. Insect faeces (a) and wood fragment (b). Scale bar 200 µm.

Fig. 5. Horizontal section of an empty chamber. Surrounding soil material. (a) Smoothed chamber floor with protruding unweathered pumices and openings of access galleries. (b). Scale bar 1 cm.

Fig. 6. Access gallery opening on the floor of a chamber. Scale bar 1 mm.

Fig. 7. Backfilled chambers (chamber aggrotubules) enclosed in massive undisturbed s-matrix. Scale bar 5 cm.

Fig. 8. Massive soil material surrounding the aggrotubule in Fig. 7. Scale bar 200 µm.

Fig. 9. Loosely packed granular backfilling in the aggrotubule in Fig. 7. Scale bar 200 µm.

Cowan, J.A., Humphreys, G.S., Mitchell, P.B. and Murphy, C.L., 1985. An assesment of pedoturbation by two species of mound-building ants, *Camponotus intrepidus* (Kirby) *and Iridomyrmex purpureus* (F. Smith). Aust. J. Soil Res., 22: 95-107.

Hole, F.D., 1961. A classification of pedoturbation and some other processes and factors of soil formation in relation to isotropism and anisotropism. Soil Sci., 91: 375-377.

Hole, F.D., 1981. Effects of animals on soil. Geoderma, 25: 75-112.

Holldobler, B. and Wilson, E.O., 1990. The Ants. Springer-Verlag, Berlin, 732 pp.

Jonkman, J.C.M., 1979. Distribution and densities of nests of the leaf-cutting ant Atta vollenweideri Forel 1893 in Paraguay. Zeit. ang. Ent., 88: 27-43.

Jonkman, J.C.M., 1980. The external and internal structure and growth of nests of the leafcutting ant Atta vollenweideri Forel 1893 (Hym.: Formicidae). Zeit. ang. Ent., 89: 158-173 (part I), 217-246 (part II).

Lobry de Bruyn, L.A. and Conacher, A.J., 1990. The role of termites and ants in soil modification: a rewiew. Aust. J. Soil Res., 28: 55-93.

Moser, J.C., 1963. Contents and structure of *Atta texana* nest in summer. An. Entomol. Soc. Amer., 56: 286-291.

Petal, J., 1978. The role of Ants in Ecosystems. In: M.V. Brian (Editor), Production Ecology of Ants and Termites. Cambridge University Press, Cambridge, pp. 293-325.

Weber, N.A., 1972. Gardening Ants, the Attines. Memoirs of the American Philosophical Society, 92. American Philosophical Society, Philadelphia, xvii + 146 pp.

Weber, N.A., 1982. Fungus ants. In: H.R. Hermann (Editor), Social Insects. Academic Press, New York, vol. 4, pp. 255-363

Variability in the growth of *Faidherbia albida* near Niamey, Niger, Africa: micromorphological aspects of termite activity*

R. Miedema[1], J. Brouwer[1,2], S.C. Geiger[2] and R.J. Vandenbeldt[2]

[1]Dept. of Soil Science and Geology, Agricultural University, PO Box 37, 6700 AA Wageningen, The Netherlands
[2]ICRISAT Sahelian Center, B.P. 12404, Niamey, Niger

ABSTRACT

Miedema, R., Brouwer, J., Geiger, S.C. and Vandenbeldt, R.J., 1994. Variability in the growth of *Faidherbia albida* near Niamey, Niger, Africa: micromorphological aspects of termite activity. In: A.J. Ringrose-Voase and G.S. Humphreys (Editors), Soil Micromorphology: Studies in Management and Genesis. Proc. IX Int. Working Meeting on Soil Micromorphology, Townsville, Australia, July 1992. Developments in Soil Science 22, Elsevier, Amsterdam, pp. 411-419.

Spatial variability in the growth of *Faidherbia albida* over distances of only 5 - 20 m was observed on sandy soils (Psammentic paleustalfs) at the ICRISAT Sahelian Center in Niamey, Niger, Africa. The differences in growth have been related to pre-existing differences in soil chemical and physical properties. The hypothesis that these soil differences can be related to the level of termite activity was investigated using three sites: a site with poor growth; a site with good growth, but without evidence of termite activity at the surface; and a site with very good growth surrounding an abandoned *Macrotermes* mound. However the mound itself showed poor growth.

A higher level of termite derived pedofeatures (termite infillings) and termite amended groundmass features (bridged grain microstructure) occurs at the good growth site. This was quantitatively demonstrated using micromorphology in conjunction with a macromorphological study. The termite mound itself shows very frequent infillings. Contrasting partial fabrics suggest that the termites have explored underlying strata. Results of this study indicate that termite amended soil material in the good growth site and the very good growth site, which was relatively enriched with organic matter and clayey fine material, caused the better fertility status and a better water holding capacity.

INTRODUCTION

Spatial variability in the growth of crops over distances of only 5 - 20 m is widespread in the Sahelian zone of West Africa. This effect is largely due to pre-existing variability in soil chemical and physical properties (Scott-Wendt *et al.*, 1989; Manu *et al.*, 1990), which in turn may be related to termite activity (*e.g.* Lee and Wood, 1971; Lal, 1987). Such relationships led Geiger *et al.* (1992) to hypothesize present or previous higher levels of termite activity had

---

caused the locally more favourable soil conditions for the growth of *Faidherbia albida*. Brouwer *et al.*, (1992) tested this hypothesis by studying three soil profiles in a three-year-old *F. albida* plantation at the ICRISAT Sahelian Centre near Niamey, Niger, West Africa. The profile pits extended to laterite at 4 - 5 m depth. Site 1 was in an area of poor growth of *F. albida*; site 2 was in an area of good growth but had no evidence of termite activity at the surface; and site 3 was located at an abandoned *Macrotermes* mound, with poor growth on the remnants of the mound itself, but very good growth (actual sampling site) surrounding it. This study had shown that macromorphological evidence of (previous) termite activity, soil chemical and physical fertility, and growth of *F. albida* were positively correlated. In addition, *F. albida* growth and macromorphological evidence of termite activity were quantified along two 1.5 m deep trenches through the plantation. Again, tree growth and level of termite activity were positively correlated (Brouwer *et al.*, 1992). This paper focuses on the micromorphological aspects of the termite activity at the study sites and discusses the significance of the micromorphological data in conjunction with the macromorphology.

SITE DESCRIPTION AND METHODS

The average yearly rainfall at Niamey (13°N, 2°E), close to the investigated site, is 562 mm (80 year average). Virtually all the rain occurs between May and September. Monthly mean temperatures (average of daily minima and maxima) vary from 34°C in May to 24°C in January (Sivakumar, 1986). The soils are deep red aeolian sands occurring on very gently undulating terraces underlain by an indurated laterite layer. They have been classified as Psammentic Paleustalfs (West *et al.*, 1987). Prior to establishment of the *F. albida* trial the land had lain fallow for at least five years and before this the site had supported mixed cropping of millet and cowpea. The sites studied will be referred to as a poor growth site, good growth site and mound site (very good growth). Details on textural and chemical characteristics are given in Geiger *et al.* (1992) and Brouwer *et al.* (1992).

Macromorphologic evidence of biological activity was mapped in the pits using a 1 × 1 meter square metal frame, subdivided into 10 × 10 cm squares. Countings included size and number of open and back-filled channels of termites. The minimum diameter of macromorphologically detectable open and infilled channels is approximately 1 mm (see Fig. 3). Gentle brushing with a soft brush made the infillings visible because the infilling itself and the immediate surrounding of the infilled channel is somewhat cemented. Micromorphological samples (7 × 7 × 7 cm) were taken from all horizons from the upper 2 - 3 m of each pit. The 19 samples were impregnated according to FitzPatrick (1970). The thin sections were studied with a petrographic microscope and described according to Bullock *et al.* (1985). Quantification of features was achieved by point counting some 500 points from a 3 × 3 mm grid.

RESULTS

Parent material

All three profiles have similar parent material consisting of relatively well sorted, rounded rather fine quartz sand (compare Figs 1 and 2). Almost all of the sand grains have a (dis)continuous primary coating (De Coninck and Laruelle, 1964) consisting of clay and fine

Table 1

Point count quantification of porosity and coating thickness ratio (20 - 50μm / <20 μm) thickness in the good growth site and the poor growth site.

Good growth site				Poor growth site			
Depth cm	Pts	Pores % v/v	Ratio thickness	Depth cm	Pts	Pores % v/v	Ratio thickness
14-27	477	24.5	1.18	20-30	440	29.8	0.52
44-63	435	27.8	1.01	57-67	514	27.8	0.46
131-148	489	25.2	1.03	91-102	478	25.1	0.38
233-251	499	27.7	1.17	175-190	488	33.8	0.34
				245-255	304	33.2	0.14 groundmass
				245-255	209	36.4	0.96 termite infilling

silt with very little organic matter. The thickness of these coatings is generally less than 10 μm, though thicker patches (up to 20 μm) occur in microhollows on the surface of grains (*e.g.* Fig. 1B-C).

The surface soil

Micromorphologically the top few centimeters of the non-mound sites shows discontinuous stratification (differences in sand size and relative amount of organic matter). These washed-in layers are clearly more evident at the poor growth site. The sampled mound site with very good growth demonstrates a continuous stratification (laminated crust), which appears to be extremely dense. Core samples from the mound itself (poor growth site) demonstrated very high bulk densities up to 1680 kg/m^3, however.

Microstructure and pedofeatures

Single grain microstructure of sand grains with primary coatings (Fig. 1A-C) predominates in the poor growth site with infrequent patches of bridged grain microstructure with thicker coatings whereas bridged grain microstructure is predominant in the good growth site (Fig. 1D-F). This is shown by the ratio of bridged grain to single grain microstructure (expressed on solid matter basis to account for the differences in pore space between the samples) which on the good growth site is about double the value on the poor growth site (Table 1).

Another clear difference between the two non-mound sites are fabric pedofeatures and infillings. In the good growth site complete infillings are commonly encountered. They are surrounded by a darker and denser lining consisting of repacked sand grains fused together with fine material containing some organic matter (Fig. 2A-B) though fragmented infillings predominate. In the poor growth site, however, such infillings and fragmented infillings are scarce. Occasionally at both sites, round to ovoid and sometimes squashed groundmass pellets (oral and/or faecal; 100 - 400 μm diameter) occur in conjunction with the areas with bridged grain microstructure.
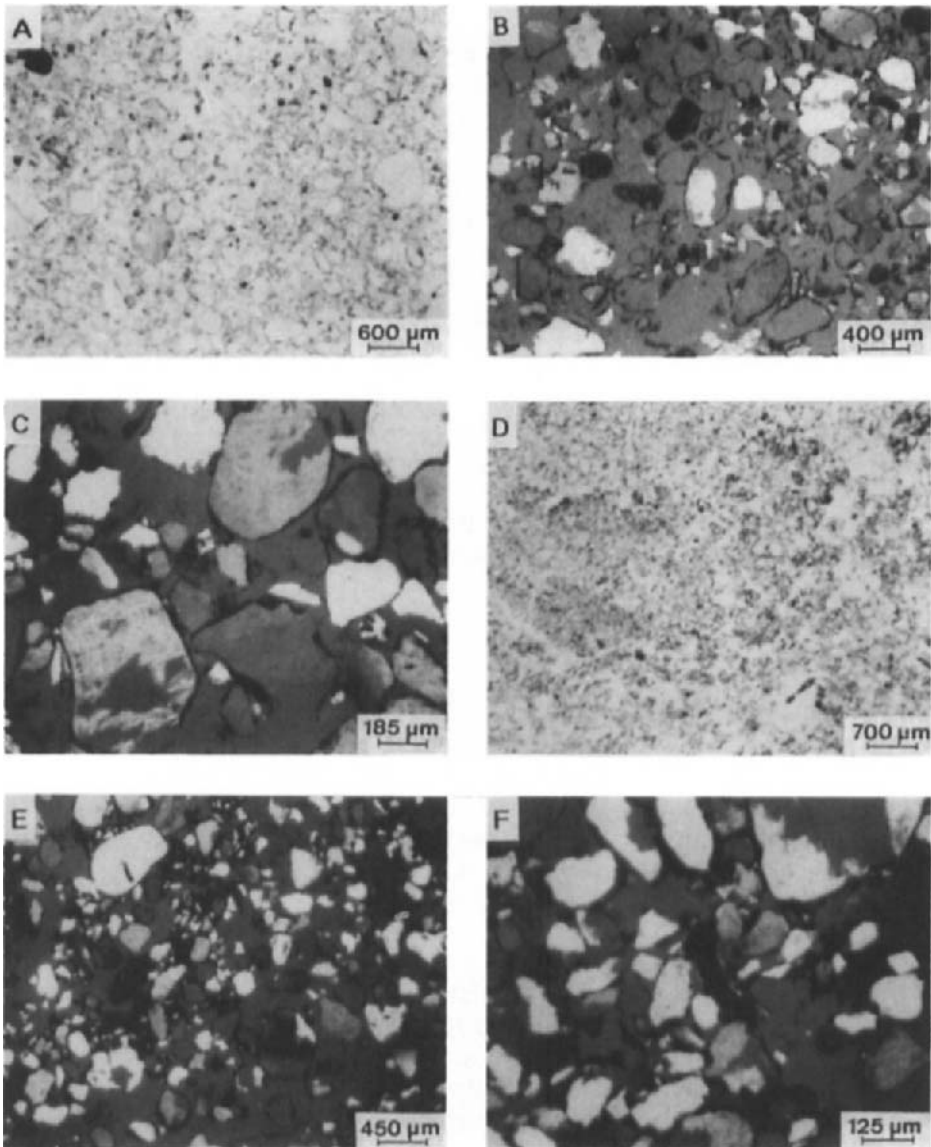
Fig. 1. A-C) Single grain microstructure with primary coatings (term according to De Coninck and Laruelle, 1964) in the poor growth site. A) Plane polarized light (PPL); B) and C) partly crossed polarizers (PXPL).
D-F) Bridged grain microstructure due to termite activity in the good growth site. D) PPL; E) and F) PXPL.
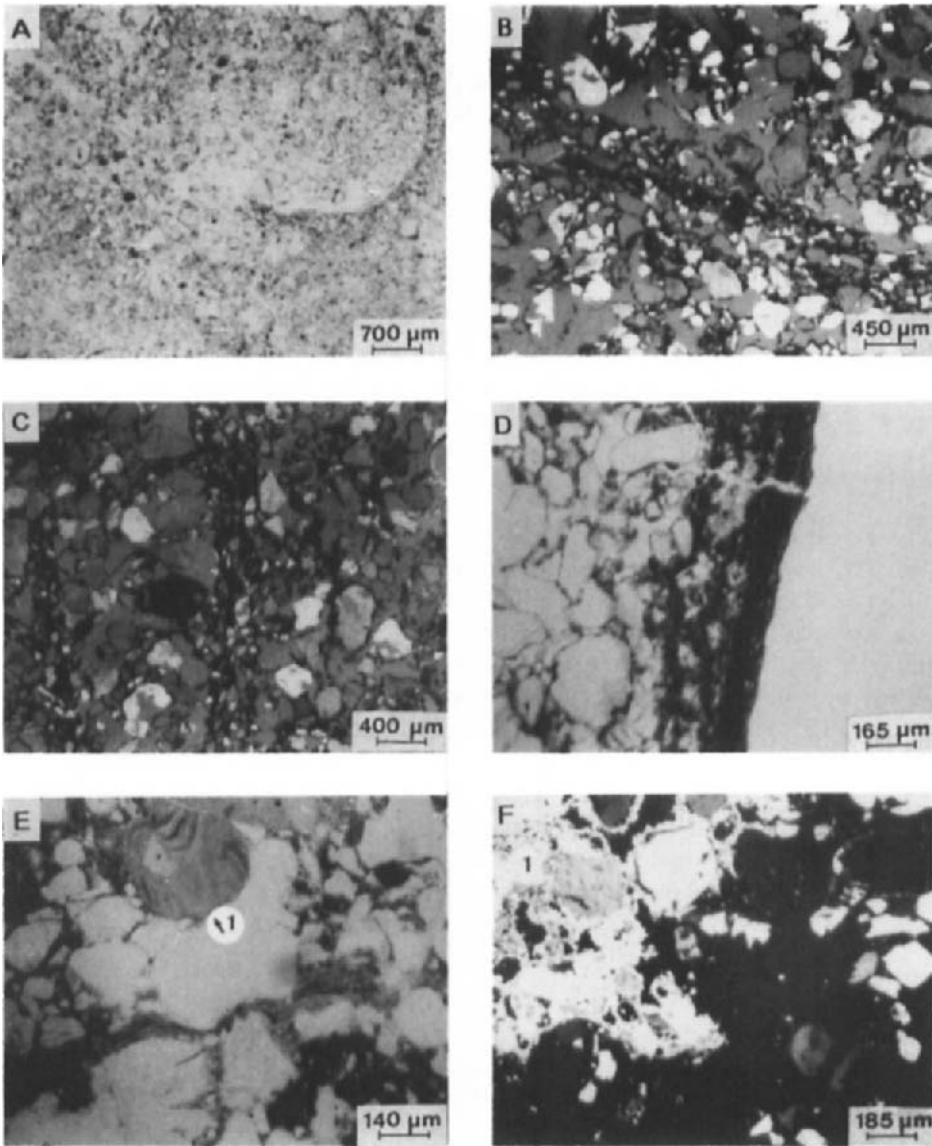
Fig. 2. **A-C)** Complete infilling with darker and denser lining; **A)** good growth site; PPL.
B) good growth site; PXPL. **C)** mound (very good growth) site; PXPL.
D-F) Pedofeatures exclusively observed in the mound site. **D)** coarse/fine laminated channel
coating; PPL. **E)** Pellety contrasting partial fabric with remnants of clay illuviation features,
probably from deeper strata (1). Notice also differences in organic matter content of building
material used by termites; PPL. **F)** secondary calcite nodules (1); Almost completely XPL.

The mound site

Micromorphologically the mound site (very good growth site) shows a great diversity of pedofeatures. Very conspicuous infilled channels with dense and dark linings (Fig. 2C) are similar to the ones observed at the good growth site. Associated with these lined infillings are round to ovoid and sometimes squashed groundmass pellets (oral and/or faecal; 100 - 200 μm diameter). However, subrounded to angular faecal pellets (10 - 50 μm diameter) have been observed too. Separation of groundmass components (textural pedofeatures) is visible in the laminated crust and fine to coarse laminated coatings (Fig. 2d) have been observed. Contrasting partial fabrics occur in the mound that consist of round pellets (100 - 400 μm diameter) of saprolitic material (mudstone, siltstone?) with fragments of illuvial clay coatings (Fig. 2E-I). Occurrences of (secondary) carbonates (around 3 m depth) have also been found (Fig. 2F-I).

Macromorphology

From Fig. 3 it is evident that the good growth site has a much larger areal extent and average size of macroscopically detectable (visible with the naked eye) infilled termite tunnels (channels) compared to the poor growth site. Infilled tunnels predominate in both non-mound sites and open tunnels are infrequent in both sites. The top 50 cm at both non-mound sites show less tunnels than the deeper layers (between 100 and 250 cm depth). This could be due to redeposition by wind and water destroying existing tunnels (see surface soil). Also the stronger drying of the topsoil may play a role. The mound site shows many more open tunnels, also in the very top part. This points to a high level of termite activity. The termite mound section in Fig. 3 also shows white (W), black (B) and red (R) spots within the mound. However, the relationship of these to micromorphological features is not clearly established. Dark coloured infillings and white spots of secondary carbonates might account for (at least part of) the B and W. Extended discussion on spatial variability along the investigated trenches is published elsewhere: Brouwer *et al.* (in press, a, b).

DISCUSSION

The micromorphology demonstrates few discrete pellets in the mound and even less in the two non-mound sites. This is contrary to literature results (Stoops, 1964; Sleeman and Brewer, 1972; Mermut *et al.*, 1984; Wielemaker, 1984; Eschenbrenner, 1986; Kooyman and Onck, 1987). The lack of pellets (oral and/or faecal) is most likely due to their rapid disintegration in these very sandy soils as they contain very little clay and organic carbon. The studies published in literature all pertain to much more clayey soils in which pellets would not be expected to disintegrate as quickly. The features attributed to termite activity in the good growth and poor growth site (infilled channels, bridged grain microstructure) are similar to features observed in the thin sections of the mound site. This suggests a strong termite influence. Multiple cycles of subsequent termite activity including species of smaller termites (probably *Microtermes* - Kooyman, personal comm., 1993) have destroyed previous lined passageways in the upper 1.5 m and fragments thereof are now found randomly spread in the groundmass in the good growth site. In the poor growth site this subsequent high level of termite activity probably never occurred, though there are still some lined channels and a few fragments in the
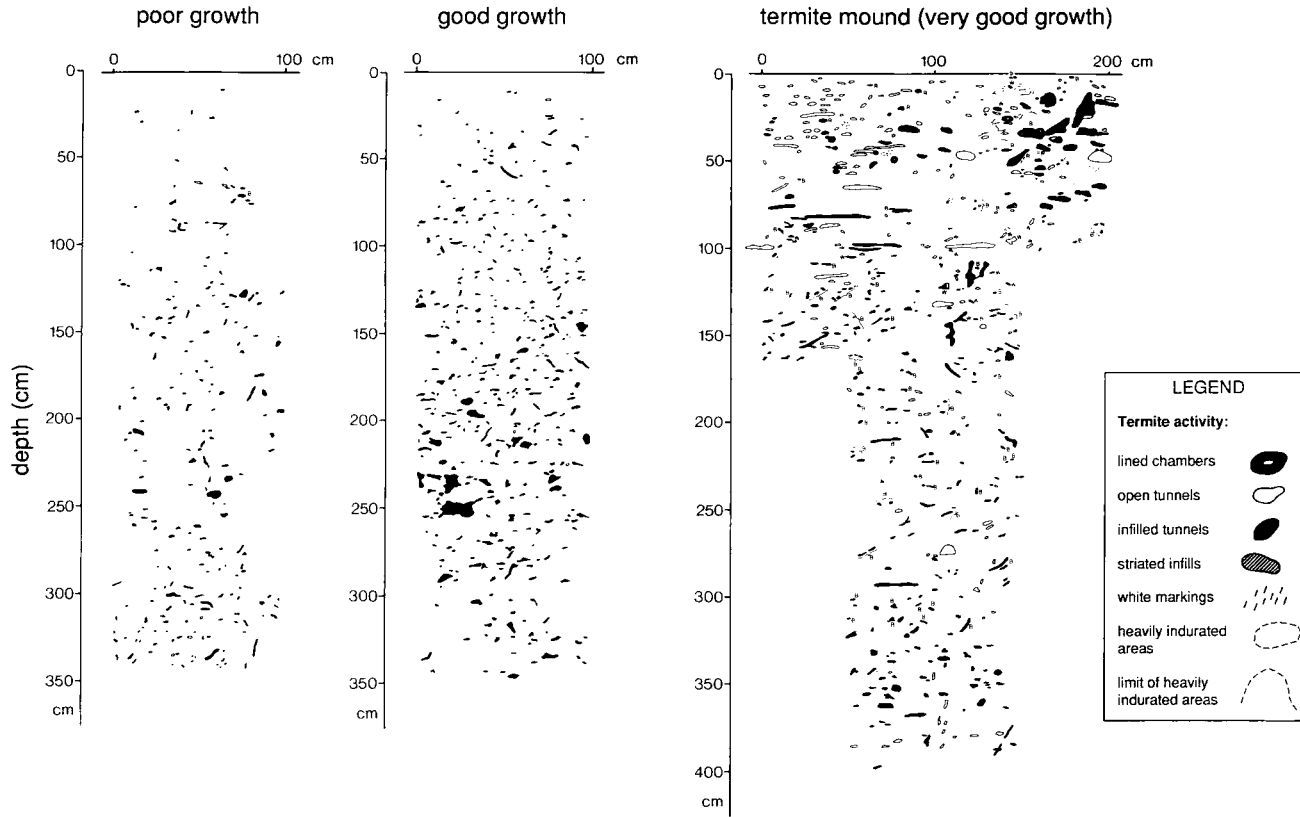
Fig. 3. Macroscopically detectable termite activity in the very good growth site around termite mound, the good growth site and the poor growth site. Note the small sysmbols of B (black), R (red) and W (white) especially on the termite mound section. (Source: Brouwer *et al.*, in press, a, b).

groundmass. The contrasting, pellety partial fabrics in the mound are thought to be due to building behaviour of the termites who incorporate material gathered from strata from the very deep subsoil. The very small pellets probably result from other insects or smaller termite species co-inhabiting the now abandoned *Macrotermes* mound. By themselves the macromorphological differences between the sites (Fig. 3; Brouwer *et al.*, 1992) in top 150 cm may not seem sufficient to explain the differences in tree growth. This micromorphological study, however, confirms that, in the top 150 cm, considerable differences in the extent of termite activity exist. Due to termite activity the contents of clay, organic carbon, exchangeable cations, free iron, P-Bray and total N are higher, whilst lower values occur for sand (fraction 105 - 250 μm) and exchangeable acidity (Al + H). In all these respects the good growth site is intermediate between the poor growth site and the very good growth around the termite mound (Brouwer *et al.*, 1992; Brouwer *et al.*, in press, a, b).

CONCLUSIONS

A higher level of termite activity over the sampled depth at the site with good growth is micromorphologically evident from termite derived pedofeatures and termite amended microstructure. This supplements the results of the macromorphological quantification. The better fertility status is caused by termite altered soil material being relatively enriched with organic matter and clayey material. This is also beneficial for the water holding capacity. The differences in growth of *F. albida* at the three sites can be attributed to different levels of previous termite activity. This conclusion is supported by transect data from Brouwer *et al.* (1992) and Brouwer *et al.* (in press, a, b). Therefore, in low external input agroecosystems these termite-caused "islands of fertility" should be used and maintained (Miedema and Van Vuure, 1977; Brouwer *et al.*, 1992; Geiger *et al.*, 1992). Agricultural measures detrimental to this termite activity should be kept to a minimum in these circumstances.

REFERENCES

Brouwer, J., Geiger, S.C. and Vandenbeldt, R.J., 1992. Variability in the growth of *Faidherbia albida*: a termite connection? In: R.J. Vandenbeldt (Editor), *Faidherbia albida* in the West African Semi-arid Tropics: Proceedings of a Workshop, 22-26 April 1991, Niamey, Niger. International Crops Research Institute for the Semi-arid Tropics, Patancheru, India and International Centre for Research in Agroforestry, Nairobi, Kenya.

Brouwer, J., Vandenbeldt, R.J., Geiger, S.C. and Miedema, R. Effects of antecedent construction activity of moundbuilding termites on early growth of *Faidherbia albida*. Agroforestry Systems, (in press, a).

Brouwer, J., Geiger, S.C, Vandenbeldt, R.J. and Miedema, R. Effects of moundbuilding termites on fertility of a sandy soil in the Sahel. J. Ecol., (in press, b).

Bullock, P., Fedoroff, N., Jongerius, A., Stoops, G., and Tursina, T., 1985. Handbook for Soil Thin Section Description. Waine Research Publications, Wolverhampton, U.K., 152 pp.

Coninck, F. de and Laruelle, J., 1964. Soil development in sandy materials of the Belgian Campine. In: A. Jongerius (Editor), Soil Micromorphology. Elsevier, Amsterdam, London, New York, pp. 169-189.

Eschenbrenner, V., 1986. Contribution des termites à la micro-aggrégation des sols tropicaux. Cahiers ORSTOM - Pédologie 22: 397-408.

FitzPatrick, E.A., 1970. A technique for the preparation of large thin sections of soils and unconsolidated materials. In: D.A. Osmond and P. Bullock (Editors), Micromorphological Techniques and Applications. Technical Monograph 2, Rothamsted Experimental Station, Harpenden, Herts, U.K., pp 3-13.

Geiger, S.C., Vandenbeldt, R.J. and Manu, A., 1992. Pre-existing soil fertility and the variable growth of *Faidherbia albida*. In: R.J. Vandenbeldt (Editor), *Faidherbia albida* in the West African Semi-arid Tropics: Proceedings of a Workshop, 22-26 April 1991, Niamey, Niger. International Crops Research Institute for the Semi-arid Tropics, Patancheru, India and International Centre for Research in Agroforestry, Nairobi, Kenya.

Kooyman, Chr. and Onck, R.F.M., 1987. The interactions between termite activity, agricultural practises and soil characterisitics in Kisii District, Kenya. Agricultural University Wageningen Papers, 87-3, 120 pp.

Lal, R., 1987. Termites. In: R. Lal (Editor) Tropical Ecology and Physical Edaphology. J. Wiley and Sons, Chichester, U.K., pp. 337-421.

Lee, K.E. and Wood, T.G., 1971. Termites and soils. Academic Press, London, New York, 251 pp.

Manu, A., Geiger, S.C., Berrada, A. and Scott-Wendt, J.W., 1990. Microvariabilité dans le Sahel: un apercu général. In: A. Berrada, I. Mahaman and M. Gandah (Editors), Actes du Séminaire sur l'Aménagement des Sols, la Conservation de l'Eau et la Fertilisation, Tahoua, Niger, Fevrier 1989. (INRAN).

Mermut, A.R., Arshad, M.A. and St. Arnaud, R.J., 1984. Micropedological study of termite mounds of three species of *Macrotermes* in Kenya. Soil Sci. Soc. Am. J., 48: 613-620.

Miedema, R. and Van Vuure, W., 1977. The morphological, physical and chemical properties of two mounds of *Macrotermes bellicosus* (Smeathman) compared with surrounding soils in Sierra Leone. J. Soil Sci., 28: 112-124.

Scott-Wendt, J.W., Chase, R.G. and Hossner, L.R., 1989. Soil chemical variability in sandy Ustalfs in semi-arid Niger, West Africa. Soil Sci., 145: 414-419.

Sivakumar, M.V.K., 1986. Climat de Niamey. International Crops Research Institute for the Semi-arid Tropics Centre, Sahélien, Niamey, Niger, Africa.

Sleeman, J.R. and Brewer, R., 1972. Micro-structures of some Australian termite nests. Pedobiol., 12: 347-373.

Stoops, G., 1964. Application of some pedological methods to the analysis of termite mounds. In: Colloque Int. Termites Afr. UNESCO, Leopoldville, pp. 379-398.

West, L.T., Wilding, L.P. and Calhoun, F.G., 1987. Argillic horizons in sandy soils of the Sahel, West Africa. In: N. Fedoroff, L.M. Bresson and M.A. Coutry (Editors), Soil Micromorphology. Proc. VII Int. Working Meeting of Soil Micromorphology, Paris, July 1985. Association Française pour l'Etude du Sol, Plaisir, France, pp. 221-227.

Wielemaker, W.G. 1984. Soil Formation by Termites. A Study in the Kisii Area, Kenya. Dr. thesis, Wageningen Agricultural University, 132 pp.

This Page Intentionally Left Blank

Bioturbation, biofabrics and the biomantle: an example from the Sydney Basin

G.S. Humphreys

Research School of Pacific and Asian Studies, Australian National University, Canberra, ACT 0200, Australia

ABSTRACT

Humphreys, G.S., 1994. Bioturbation, biofabrics and the biomantle: an example from the Sydney Basin. In: A.J. Ringrose-Voase and G.S. Humphreys (Editors), Soil Micromorphology: Studies in Management and Genesis. Proc. IX Int. Working Meeting on Soil Micromorphology, Townsville, Australia, July 1992. Developments in Soil Science 22, Elsevier, Amsterdam, pp. 421-436.

The characteristics, distribution and origin of a variety of channels, chambers and pedotubules produced by mesofauna, often to species level, was determined at two locations in the Sydney Basin. This was achieved by combining field observations on different types of mesofauna together with a wide range of soil fabric techniques including: casting and latex peels of nests; mapping serially sectioned impregnated blocks of undisturbed soil; and thin section analysis.

The study showed that most mesofauna activity is confined to coarse textured topsoils with about 8% of the A and E horizons comprising fauna-produced channels, chambers and pedotubules. However, it is suggested that the surrounding soil material or s-matrix, in which these features are embedded, represents the remnants of re-bioturbated pedotubules to which the term maculae has been applied. In this sense the bulk of the topsoil consists of biofabrics and hence defines a biomantle.

In addition the study shows that whilst most mesofauna activity is confined to topsoil horizons, a small but potentially significant component is directed to the subsoil. In texture contrast soils it appears that the E - B horizon interface is being mined, *i.e.* it is being lowered by mesofauna.

INTRODUCTION

Previous research into the origin of texture contrast and other soil types in the Sydney Basin established that considerable amounts of material are brought to the surface by organisms such as ants, earthworms and termites (Humphreys, 1981; Humphreys and Mitchell, 1983; Humphreys, 1985; Mitchell, 1985, 1988). In the case of texture contrast soils this situation provides an apparent paradox since it is widely assumed in general soil science literature that the main effect of soil mesofauna is to homogenize the soil. To help resolve this issue it is necessary to establish the horizons where soil-transporting fauna are most active, the destination of excavated soil, and to assess the relative importance of various transporting processes including: the movement of particles or aggregates within the soil (*e.g.* by biota),

over the soil surface (*e.g.* by rainwash), *en masse* (*e.g.* by soil creep), and via intervoid transport (*e.g.* by illuviation and pervection *cf.* Paton, 1978).

In an attempt to resolve part of this issue, a study was initiated at two locations to gain a better understanding of the origin and subsequent history of pedotubules and associated features (or biofabrics *cf.* Johnson, 1990) formed by the dominant soil-transporting fauna.

STUDY SITES

Soils were examined from two localities within the Sydney Basin: Cattai and Cordeaux, 39 km NW and 64 km SW of Sydney respectively (See Humphreys, 1994 for location figure). Both sites are positioned on upper ridge crests of quartzose Hawkesbury Sandstone and support open forest dominated by *Eucalyptus* spp. with an understorey of proteaceae shrubs. Rainfall averages 900 - 1,000 mm annually but is highly variable on a yearly basis. The topsoil at both sites consists of 200 - 400 mm of apedal, loamy fine sand to fine sandy loam which can be subdivided into an upper A horizon and an E horizon or bleached layer. This overlies either clayey or loamy saprolitic subsoils (B horizon) to produce texture contrast soils (Haplohumult, Soil Survey Staff, 1975; Yellow Podzolic, Stace *et al.*, 1968) and shallow earths (Quartzipsamments, Soil Survey Staff, 1975; Earthy Sands, Stace *et al.*, 1968). As will become apparent the A and E horizons constitute a distinct biomantle (*cf.* Johnson, 1990) even though the E horizon in the texture contrast soil exhibits a hardsetting condition. Additional site details are contained in Humphreys and Mitchell (1983).

APPROACH

The selection of particular species for study was based on their importance as mounders and/or burrowers. The choice of the former was determined from field experiments aimed at quantifying mounding rates (Humphreys and Mitchell, 1983) and the latter on their apparent frequency of occurrence in the soil. Because of the high species diversity only the most prominent mesofauna were considered.

Initial examination concentrated on active burrow systems in which the species occupying the burrow could be observed and identified and where the dimension, shape and other characteristics of the burrow could be described. This was pursued by careful field observations (*e.g.* Humphreys, 1989) and by a variety of fabric techniques including: latex peels of dissected nests (method of Mitchell and Paton, 1988); casting with white gypsum (plaster-of-paris); examination of undisturbed and impregnated (polyester resin) soil samples (collected in Kubiena-tins, $150 \times 80 \times 50$ mm) under a dissecting microscope at magnifications up to 80×; and analysis of thin sections (30 μm thick and from 20×40 to 70×100 mm in size) with a petrological microscope and large field polarizing microscope. In total, biofabrics were examined from 44 Kubiena-tin samples (of which 29 were from the A and E horizons) and over 120 thin sections from 6 texture contrast and two earth profiles. To determine the proportion and distribution, by horizon, of different types of pedological features - especially those of a biological origin - three sections from each impregnated block were mapped and the areas of these features calculated (minimum size of features mapped was about 3 - 4 mm^2). This facet of the study concentrated on the texture contrast soil in which > 0.85 m^2 was mapped. The terminology of Brewer (1976) was used in the description of various fabrics and pedological features.

CHARACTERISTICS OF BURROW SYSTEMS

For each species an attempt was made to determine the shape and dimensions of the burrow system, the type of burrow wall alteration, the fabric of infills (pedotubules), the burrowing method, the size of soil aggregates and particles that had been transported, and the destination of excavated soil. This information is summarized in Table 1 and additional details are presented below.

*Funnel ant (*Aphaenogaster longiceps*)*

This species contributes over 80% of the total amount of soil transported to the surface by mesofauna at the study sites (Humphreys and Mitchell, 1983; Humphreys, 1985). The subterranean nest system consists of a labyrinth of channels (Fig. 1A), 5 - 10 mm in diameter and connected to the surface by vertical shafts. This pattern developed in an artificial nest within a few days but it was also apparent in natural settings. In addition, the excavation of nest systems, in which white plaster was used as a tracing medium, established that many channels follow roots and that the vertical shaft was often funnel shaped with an entrance hole at the surface mound 10 - 20 mm in diameter and tapering over a depth of 150 - 300 mm. No chambers could be detected despite tracing over 25 m of casted-channel.

In thin section it is evident that the burrow walls preserve the arrangement of the surrounding s-matrix (Figs 1B and C). Pedotubules could be recognised with certainty only when part of an existing channel was infilled. The enclosed material is very similar to the surrounding soil with little if any colour contrast. In summary, the funnel ant forms ortho-channels with a sharp, irregular surface and ortho-isotubules. However, it is not certain that infilling is due to this ant since mounds are composed of discrete aggregates (0.5 to 1.5 mm in size) derived from the A and E horizons and occasionally also from the saprolitic subsoil. These observations suggest that this species excavates soil material by extracting suitable sized aggregates and transporting them directly to the surface, with any infilling resulting from the collapse of channel walls or by activities incidental to tunnelling.

*Sugar ant (*Camponotus consobrinus*)*

This species was found at the Cattai site only but it did not form mounds. The subterranean nest consists of a smooth-walled near-vertical shaft (smooth-metachannel), 15 - 17 mm in diameter, that extends from the surface into the A and E layers and to the top of the saprolitic-B. Several chambers occur as off-shoots to the shaft. These have smooth flat floors 10 - 20 mm wide and 20 - 30 mm long and arched roofs 10 mm high (smooth-metachambers) (See Humphreys, 1994, Fig. 1B).

Two types of lining occur. The first consists of a thin 100 μm band of yellow clayey material bordering the s-matrix of the topsoil. This is capped by a layer, up to 2 mm thick, of clayey plasma which holds plant fragments up to 600 μm in length and quartz grains up to 100 μm in size. These grains are finer than the modal size of 100 - 270 μm in the topsoil and subsoil. This layered material occurs on the chamber floor and sometimes on the arched roof (Fig. 1D). The lining is probably emplaced by gunarding mineral soil and macerated plant fragments onto the excavated face. The particle size distribution indicates that finer particles are selected for this role. The other type of lining is a dark brown opaque material which, in

Table 1

Comparison of the main burrow types of the principal soil moving fauna and roots at the study sites. (See text for additional information).

Fauna type (Species names given in text)	Type of burrow (branching)[1]	Cross-section of burrow		Burrowing method[2]	Type of alteration to burrow walls[3]	Size of aggregates carried in soil and/or deposited at surface, mm	Destination of excavated and/or ingested soil
		Max. width (mm)	Ratio max:min width				
Funnel ant	complex	5-10	≈1	excavation	none	0.5-1.5	mound
Sugar ant	simple (?)	≈15	"	"	gunarded, secreted	2-3	soil
ant (*C. intrepidus*)	"	"	"	"	gunarded	"	soil; mound
Bulldog ant	simple	20-30	"	"	"	3-6	"
Termite	complex; also dendroid	3-5	mostly >3	excavation	secreted (compacted?)	0.5-1.5 (carried)	soil; in trees, logs and mounds
Earthworm	simple to complex	3-5	≈1	ingestion	partial	1-2.5 (3-6 for Notoscolex)	soil; surface cast
Cicada	unbranched	25-40	"	excavation	compacted and gunarded	pellets 4-6	soil; turrets
Trap-door spider	unbranched	"	20-30	"	web lined; gunarded? compacted?	?	scattered on surface?; perhaps in soil
Roots	dendroid	variable	"	pushing	compacted	-	-

Notes:
1. Type of burrow refers to the overall shape.
   - Unbranched: no off-shoots.
   - Simple branched: main shaft with one or more off-shoots (frequently chamber).
   - Complex branched: burrows interconnect in an irregular pattern or more than one shaft with off-shoots joined to more than one other part of the burrow system.
   - Dendroid branched: simple or complex variety with a recognisable pattern.
2. Method of burrowing.
   - Excavation: soil extracted with legs and/or mouth parts.
   - Ingestion: soil taken in through the mouth and passed through the body.
   - Pushed: soil forced away from the perimeter of the organism such as in root growth.
3. Type of alteration of burrow wall.
   - None: no change in fabric of the surrounding soil at the edge of the burrow.
   - Smoothed: no effective change in fabric but wall shows slight smearing.
   - Compacted: soil material forced into the surrounding soil thereby locally reducing porosity, but no change in particle size or composition of the material.
   - Gunarded; as for compacted except using finer material, usually imported from another soil layer, so that the wall is sometimes lined with several layers.
   - Secreted: excrement as a thin continuous layer and not as faecal pellets (brown to dark brown material in termite and sugar ant burrows).
   - Web: thin layer of silk web lining the burrow to form a sack or stocking-like structure.
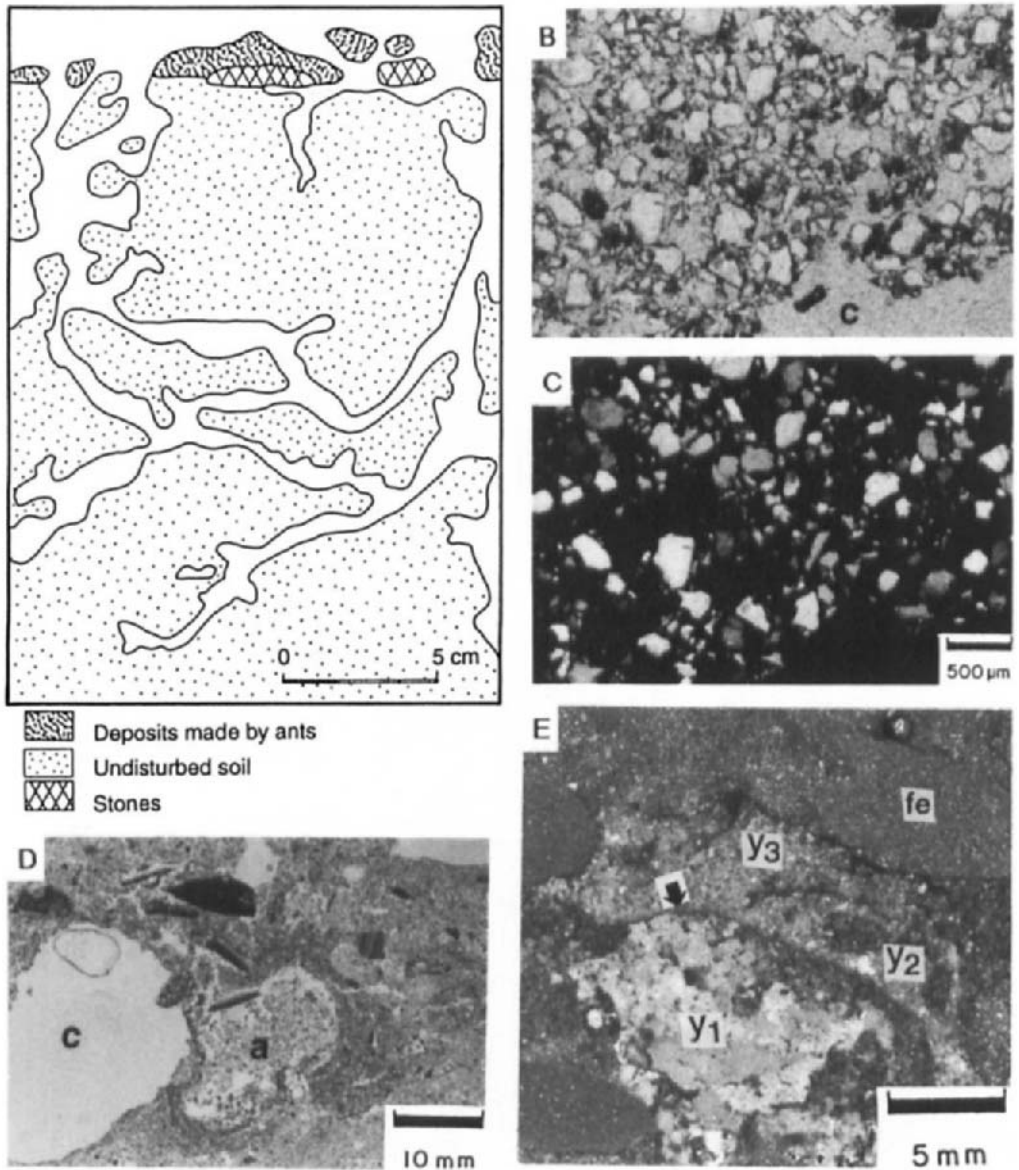
Fig. 1. A) Channel pattern in a laboratory ant nest after 8 days of burrowing by *Aphaenogaster longiceps* with all excavated soil deposited on the surface to bury a layer of stones. B) and C) Edge of an orthochannel (c) and part of the nest system of *Aphaenogaster longiceps* (lower left) showing no sign of compaction or gunarding in the s-matrix bordering the channel; E horizon, 20 cm depth; plane polarized light (PPL) and cross polarized light (XPL) respectively. D) Smooth-metachamber (c) and a meta-aggrotubule (a) formed by *Camponotus consobrinus*; A horizon (PPL). E) Successive stages of infill of yellow clay (saprolitic-B) (y_1-y_3), the most recent (y_1) being a brighter yellow than the others (y_2 and y_3), with each stage separated by a thin dark brown organic border (arrow); ironstones (fe); E horizon; polished impregnated section. B)-E), Yellow Podzolic at Cattai.
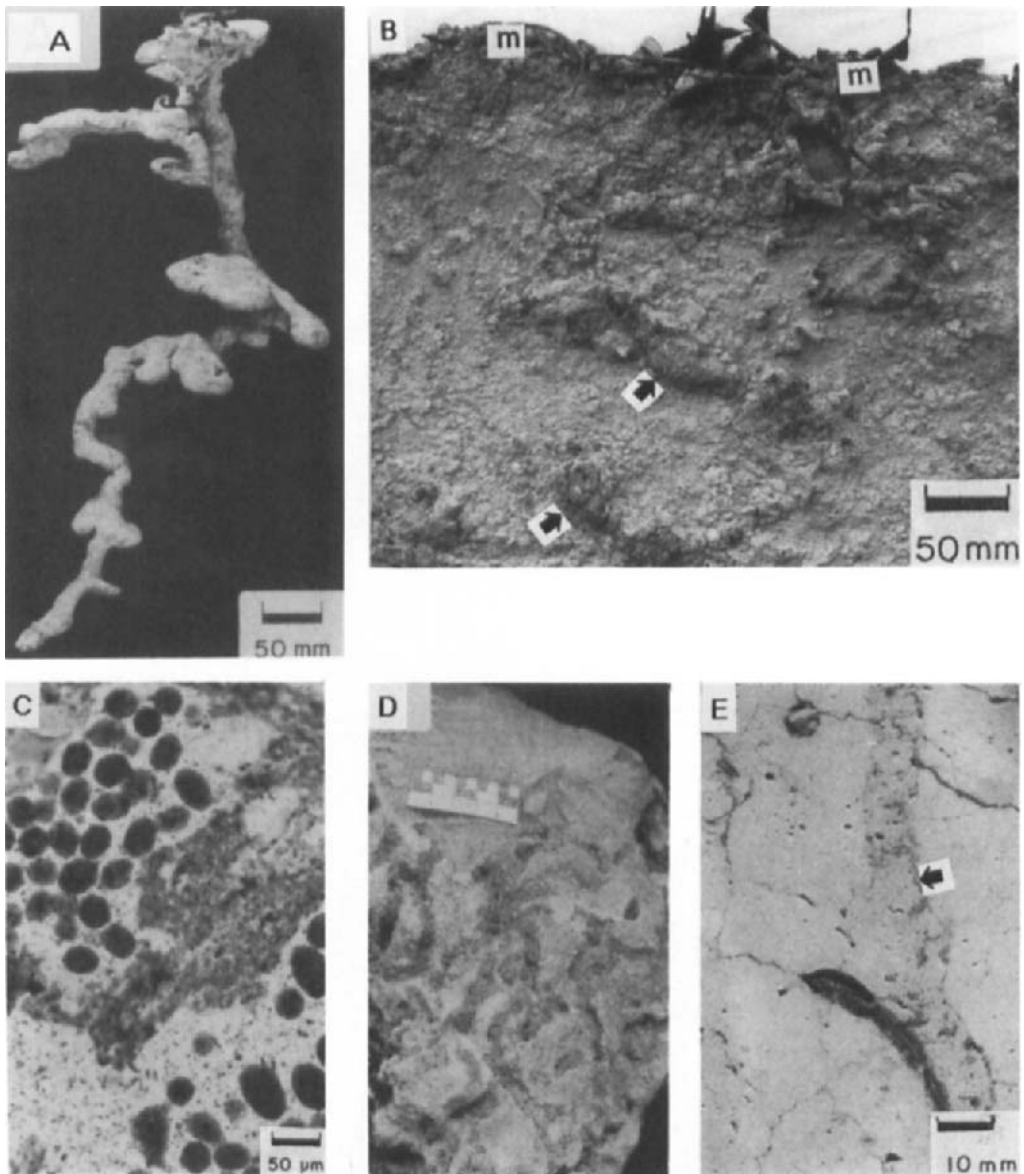
Fig. 2. A) Cast of a subterranean nest of a bulldog ant, *Myrmecia forficata,* showing a single main shaft with wider horizontal off-shoots or chambers; vertical depth 52 cm; volume 787 cm^3. B) Cross-section latex peel through a decaying nest of *Myrmecia forficata* showing remnants of the mound (m) and infilling of the original burrow system (arrows). C) Discrete circular elliptical faecal pellets composed of weakly anisotropic material within a termite channel-tubule. D) Termite tunnelled sandstone from Cordeaux (species unknown). In the Cattai area, *Nasutitermes fumigatus* has been found in similar tunnels in sandstone benches and cliff faces. Scale 50 mm long. E) Example of an orthotubule (arrow) in the saprolitic-B horizon due to *Notoscolex* sp. A)- C) & E), Yellow Podzolic at Cattai.

thin section, comprises domains of weakly anisotropic material 30 - 40 μm long and quartz grains up to 30 μm in size. This material forms a 100 - 500 μm thick border and seems to be used to line channels and seal infilled chambers. The exact origin of this dark material is uncertain, but it may be regurgitated masticated plant fragments and/or faecal material that is smeared over the soil. Infilled channels and chambers (Fig. 1D) contain aggregates, 750 - 2,000 μm in size, of A, E and saprolitic-B material that is loosely packed in mixtures of varying proportions (*i.e.* meta-aggrotubules). A well defined lining separates this material from the enclosing s-matrix or the existing nest system. In some pedotubules progressive infilling occurs (Fig. 1E). This can be best seen where the aggregates are mostly derived from the yellowish brown saprolitic-B. Older infills, separated by a brown lining, are paler in colour which may suggest aging.

Another ant of this genus encountered at both sites, *Camponotus intrepidus,* constructs tunnels and chambers of a similar size and shape in the soil, but they are always associated with mounds (Cowan *et al.,* 1985). These authors reported that the galleries in the mounds have a 2 - 3 mm thick dark lining composed partly of finely macerated leaves and rootlets.

*Bulldog ants (*Myrmecia spp.*)*

Though this genus frequently constructs sizeable mounds, > 0.2 m^3, the rate of mound growth is low (< 30 g m^{-2}y^1) and contributes less than 5% of the total amount of mounded soil. Subterranean nest systems were similar for the four species examined: *M. forficata, M. gulosa, M. nigriceps* and *M. pyriformis.* The nests consist of a smooth-walled single prominent shaft, mostly 20 - 30 mm in diameter (*i.e.* smooth-metachannel), from which a number of chambers emanate (Fig. 2A). These chambers are oriented approximately parallel to the surface, have flat floors up to 50 mm wide and 100 mm long, and have somewhat arched roofs about 20 to 30 mm high (*i.e.* smooth-metachambers). The walls within the subterranean nest and mound are frequently lined with layers of predominantly clayey material that appear to have been emplaced by gunarding. Infilling of channels and chambers occurs during the life of an active nest and these features may be preserved even after the extinction of the colony. Figure 2B shows a latex peel through a defunct mound and subterranean nest of *M. forficata.* This peel was made two years after the nest had been abandoned, by which time the mound was partly eroded. The nest was infilled with a porous mixture of aggregates from the s-matrix of the A, E and B horizons and sometimes empty cocoon sacks (15 mm long and 5 mm in diameter) to form distinct meta-aggrotubules. This suggests that infilling occurred prior to final abandonment.

Termites

Four species occur between the sites: *Coptotermes acinaciformis, Heterotermes ferox, Nasutitermes exitiosus* and *N. fumigatus.* Collectively they appear to be more important as sub-surface bioturbators than as mounders. Even with this small number of species, however, it was not always certain whether or not the species occupying the structure also built it. For example, *H. ferox* was found at the Cattai site in low disc-shaped mounds, 50 mm high and 340 - 480 mm wide. These mounds had a hard outer casing, a few centimeters thick, covering an extensive gallery system. Ratcliffe *et al.* (1952, p. 96) questioned whether or not this type of mound and gallery system is constructed by this species, noting that it resembled the outer wall

region of a *Coptotermes* mound. However, the only other mound-building species in the area was *N. exitiosus* and its mound is very different to *Coptotermes* (*cf.* Lee and Wood, 1971).

Despite this uncertainty, the tunnel or channel system within the soil for these species appear to be similar. They tend to have trellised or dendroid shaped branching patterns, oriented for the most part perpendicular or parallel to the surface, so that several centimeters of channel may occur within a confined area of soil (Fig. 3). Those with a dendritic branching pattern are, or appear to have been, associated with roots. The channels are mostly linear with cross-sections varying from circular/elliptical to slot-like with heights of 3 - 5 mm and widths up to about 20 - 30 mm (*i.e.* smooth-metachannels). Where channels are surrounded by s-matrix there is little indication of compaction or gunarding. Evidence for the mining of soil can be seen in Fig. 2D which shows sandstone riddled with termite channels. In thin section it appears that quartz grains have been plucked from the rock.

Channel walls are commonly coated with a thin (40 - 250 μm) brown substance thought to be faecal material. This lining commonly occurs in the A and E horizons but not in the denser saprolitic-B. Two types of lining were observed in fresh hand specimens: a darker brown type with a fairly uniform colour and a speckled type. The latter is characteristic of some, if not all, *Coptotermes* including *C. lacteus* and *C. frenchi* (Ratcliffe and Greaves, 1940) and *C. acinaciformis* (Greaves, 1962) and possibly *H. ferox* (Ratcliffe *et al.*, 1952), whilst the former type is recorded for *N. exitiosus* (Ratcliffe and Greaves, 1940) and probably occurs in *N. fumigatus* as well. This distinction is not apparent in thin section which shows that the brown to dark brown linings consist of weakly anisotropic domains, 10 - 35 μm long, of what appears to be plant fragments. Such material is similar to that observed in faecal pellets found with root fragments within termite pedotubules. These pellets were circular to elliptical in shape and 30 - 70 μm across, with weakly anisotropic domains about 10 μm long (Fig. 2C). However, these domains are smaller than those found in the lining, and despite other similarities, it is possible that the pellets are due to a microarthropod (*c.* Lee and Foster, 1991) rather than termites.

Infill material within termite channels is either homogenized with a uniform colour (ortho to meta-isotubules) or consists of individual aggregates mostly less than 1 mm derived from topsoil and subsoil material to give a distinct speckled appearance (meta-aggrotubules) (Fig. 3A). Occasionally a sequence of backfilling leads to a striated appearance with infill being arranged in arcuate patterns (striotubules).

*Earthworms (*Cryptodrilus, Notoscolex *and* Oreoscolex*)*

At Cordeaux, casting by *Cryptodrilus* sp. and/or *Oreoscolex* sp. contributed to about 10% of the total amount of soil material deposited at the surface. Rates of casting were not measured at Cattai, but during excavation of soil pits earthworms (*Notoscolex* sp.) were commonly found near the base of the E horizon moving towards the surface only during wetter conditions.

The tunnel system at Cattai consists of mostly single sinuous channels which may intersect when infilled, thus giving a branched appearance. There is no preferred orientation. The tunnels are mostly 3 - 5 mm in diameter, but this figure can reach 7 mm, and the walls are somewhat smooth. In thin section this smoothness appears as a smear of mostly clayey plasma, varying in thickness up to 250 μm around the tunnel perimeter. However, there is no preferred location for the thickest part of the smears. The infills of earthworm tubules are noted for their
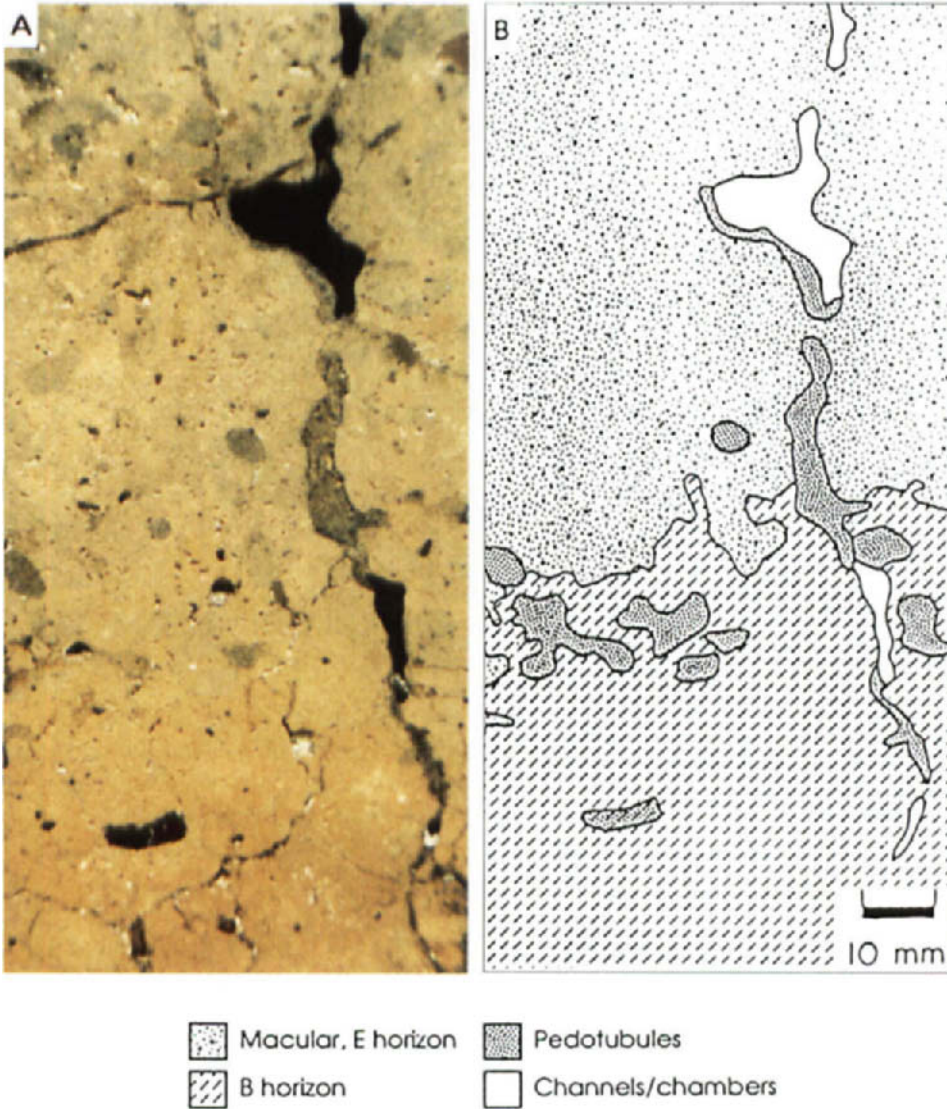
Fig. 3. A) and B) A prominant vertical, smooth-metachannel with partial infilling (meta-aggrotubule) by termites passes from the E horizon into the saprolitic-B along a planar void in a Yellow Podzolic at Cattai. The bulk of the E horizon consists of maculae which define the macular colour pattern. The irregular but sharp boundary between the E and B horizons is attributed to mesofauna mining the lower horizon. Polished impregnated section (3A), sketch of same (3B).

uniformity in colour and fabric, but often change gradually with depth as different soil horizons are encountered (*i.e.* ortho to metatubules) (Fig. 2E).
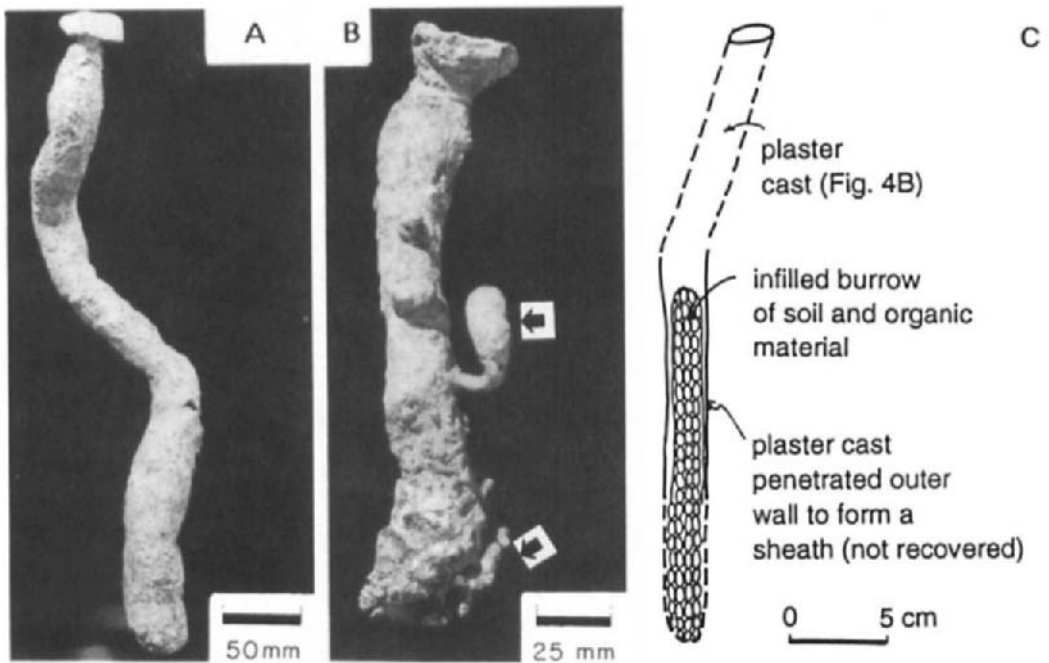
Fig. 4. A) Cast burrow of the cicada nymph, *Macrotristia angularis*; vertical depth 39 cm; volume 581 cm³; A-E horizon, Red Podzolic at Epping. B) Partial cast of a burrow of a trap-door spider *Arbanitus* sp. or *Dyarcyops* sp. showing protruberances on the right side (arrows); A-E horizon, Yellow Podzolic at Cattai; cast volume 104 cm³. C) Outline of full extent of spider burrow shown in B) the lower half of which contained surface derived detritus.

These observations indicate that the earthworms mine the soil by ingestion, and cause little if any compaction in the surrounding s-matrix. The zones of thicker smearing may be related to changes in direction during tunnelling since at a bend the earthworm's movement could be expected to exert a greater force on the side of the tunnel with the maximum arc of curvature.

Cicadas and spiders

Examples of a complete cicada (*Cyclochilia australiasiae*) and an incomplete spider (*Arbanitis* sp. or *Dyarcyops* sp.) burrow are shown in Fig. 4A and B. Excavation of several burrows of both invertebrates, especially of the cicada *Psaltoda moerens* in the Cattai region, indicate that they are very similar in terms of overall shape and dimension. They consist of a single shaft up to 500 mm long and 20 - 40 mm in diameter though the cicada burrows tend to be the widest. The burrow is oriented perpendicular to the surface but commonly contains at least one bend.

Recently abandoned burrows of cicada nymphs and trap-door spiders can be distinguished from one another. The latter is lined with a fine coating of silk web and exoskeleton remains of invertebrates (food source) occur at the base and/or against the side (*cf.* Main, 1976). Both

features are absent in cicada nymph burrows. Furthermore, there is a basic difference in the method of burrow construction. The adult trap-door spider excavates from the surface downwards, but it is not certain whether the loosened soil is actually removed from the burrow or compacted into the surrounding soil. No evidence of compaction was detected in hand specimens, implying that the excavated soil was discarded at the surface well away from the entrance hole since no mound occurs.

In comparison, a cicada burrow can only be constructed by compaction of the soil into any available void space. This must occur since cicada eggs are laid in trees and the very small newly hatched nymph begins the next phase of life by dropping to the surface and burrowing down to a suitable root (Marlatt, 1907; Myers, 1929). At the root, where it occupies a chamber, the nymph stays for several years (about 5 y for Sydney species; McKeown, 1944) slowly increasing in size. Only as it approaches maturity is a large burrow constructed towards the surface. The formation of a burrow has been described by Snodgrass (1921, pp. 384-386): "the nymph scrapes away at the soil, raking it into a small lump and then, with the use of the legs, mashes the lump into the surrounding soil". This results in some compaction and in particular the development of a gunarded layer, which in one pedotubule was about 5 mm thick.

Roots

The common association of roots with channels occupied by termites and some ant species raises the proverbial question as to which came first. Though it is often impossible to provide a definitive answer it is, nevertheless, possible to reduce the level of uncertainty in some instances.

Channels formed by small roots normally have a smooth lining and cause some compaction of the surrounding soil. In some hand specimens well formed channels were observed which were originally thought to be due to earthworms or termites. However, close inspection commonly revealed traces of epidermis or the imprint of the epidermis onto the channel wall. Small decayed roots are rarely found in the soils at the study site, presumably because such material would be fed upon by termites or earthworms. Likewise larger roots and remnant stumps are only preserved if they have been burnt to form charcoal.

THE FATE OF ABANDONED BURROWS

In many of the active nest systems partial infilling of the tunnels and chambers occurs (*e.g.* Figs 1D and 3A). However, abandoned nests are also infilled. For example, incomplete infill was encountered during the excavation of some trap-door spider burrows. Figure 4C is a sketch of one such burrow. At the time of sampling the channel was opened at the surface and found to be empty down to the first bend. On the assumption that it was an intact burrow, casting was attempted. The result is shown in Fig. 4B. In the lower half plaster penetrated close to the burrow wall to partly enclose the infill and form a discontinuous sheath. The enclosed infill consisted of A horizon material with charcoal, capsules, twigs and leaf fragments. This type of infill can best be explained by surface material dropping into the hole under conditions of rainwash (Humphreys, 1994).

Figure 4B also shows two protuberances. That on the centre right consists of a smooth conical chamber 30 mm long and with a maximum diameter of 15 mm. It is oriented vertically

with a narrow (5 mm diameter) connecting tunnel to the main burrow. The other consists of a narrow irregular channel that is very contorted in shape. Neither of these features can be attributed to the original spider, both being too small. The lower one is probably due to earthworms or termites (see previous description) but the origin of the upper one is uncertain. Apart from showing that burrows can be infilled by other mechanisms it reveals that whether occupied, abandoned or infilled they can be re-excavated by other soil fauna. Additional evidence for re-bioturbation was observed in narrow 30 mm diameter auger holes filled with dyed soil that had been established as part of an experiment to measure soil creep (*cf.* Humphreys and Mitchell, 1983). In the topsoil of these columns, pedotubules of dyed soil could be traced into the adjacent soil, and tubules of normal (undyed) soil could be followed into these columns.

MACULAE

Apart from the presence of a variety of channels, chambers and pedotubules the s-matrix of the bioturbated layers *viz.* the A and E horizons has a distinctive pattern (Fig. 3A). This pattern consists of patches, spots and/or blotches that are commonly less than 5 mm in diameter and have somewhat sharp boundaries. They are circular/elliptical to irregular in cross-sectional shape, but with a faint colour contrast to the adjacent patches. Individual patches of the same colour are usually randomly distributed though some clustering may occur. Nevertheless, it is the faint colour contrast that is the diagnostic feature. Collectively, these colour shapes are termed *maculae* and s-matrix consisting of maculae is referred to as having a *macular colour pattern*. This contrasts to a whole-coloured pattern in the pedal saprolitic-B horizon (Fig. 3A).

The close association of maculae with pedotubules suggests that they may have a similar origin. Thus, repeated intersections of a pedotubule will result in smaller and smaller portions of the original. It is these remnants that become maculae. This hypothesized close association between pedotubules and maculae raises the valid issue as to how they can be separated, especially if the infill has the same colour as the s-matrix. In this context, any feature that can be differentiated from the s-matrix using criteria such as continuity of shape is treated as a pedological feature, normally a pedotubule. The faint colour contrast between maculae may be due to mesofauna depositing locally derived material (*e.g.* Fig. 2E). Alternatively, it may be due to aging (*cf.* Bal, 1973, p. 82) by oxidation and leaching. Organic rich, and hence darker soil materials, normally "age" in this fashion. Undoubtedly, both processes occur in these soils.

The requirement of a faint colour has meant that maculae are frequently difficult to distinguish and their identification is dependent on the method of observation. In the field, especially when the soil is in a dry state, the identification of maculae is difficult and in many situations they are overlooked. However, wetting the surface of impregnated soil sections, > 1 - 2 mm thick revealed maculae. In thin section, maculae could not normally be detected and, in many cases, even pedotubules were difficult to distinguish from the s-matrix unless steps were taken to ensure their location (*e.g.* marking slides). Consequently, it is not surprising that the full significance of maculae has not been reported previously.

The term maculae has been chosen to avoid any confusion with similar phenomena. For example, within the soil descriptive system of the Soil Survey Staff (1951, 1975), maculae could be described as "many fine, faint mottles". However, the term "mottle" is frequently associated with poor drainage, and this certainly does not apply to the soils dealt with in this paper. Secondly, in Australia, mottles (as defined by Northcote, 1979) have a definite colour

Table 2
Proportion of pedotubules, chambers, channels and macular colour pattern in the s-matrix in texture contrast soils at Cattai (composite of six profiles).

Soil type	Horizon	Depth	Feature (% of area)			
		(cm)	Pedotubules	Channels and chambers	Macular colour	Total
Texture	A	0-15	4.8	3.4	71.8	80.0
contrast	E	15-37	6.6	1.5	90.5	98.6
	B	37-66	2.3	1.2	6.3	9.8
	C	66-81	1.0	0.2	0.0	1.2
	C_r	81-100	0.9	tr	0.0	0.9

Cr = altered bedrock (argillaceous sandstone) and the C is intermediate to the B and Cr.

contrast to the surrounding soil. Maculae, as used here, are not mottles in Northcote's terms. A macular colour pattern does conform to Northcote's whole colour pattern, but on the basis of the hypothesis presented here, there is good justification for considering it as a separate colour pattern. In addition, the term mottle has been used in the sedimentological literature, in this context, to refer to remnants of bioturbated stratified deposits in which 'distinct mottles' are equivalent to pedotubules and 'indistinct mottles' are equivalent to maculae (Pettijohn, 1975 after Moore and Scruton, 1957).

DISTRIBUTION OF PEDOTUBULES, CHAMBERS AND CHANNELS

The above description indicates that much of the activity of the mesofauna at the study sites is confined to the topsoil (A and E horizons). This association was tested by calculating the proportion of soil, as viewed in vertical sections, that was unequivocally pedotubule, channel and chamber from 6 texture contrast profiles (Table 2). This shows that about 8% of the topsoil consists of recent bioturbation products. There is also a reasonable proportion in the saprolitic-B horizon of which a quarter is confined to the uppermost 5 cm where mesofauna appear to be actively mining. This is indicated in Fig. 3 which displays a sharp but irregular boundary between the E and B horizons. A macular colour pattern dominates the bulk of the A and E horizons but constitutes only 6.3% of the B horizon, though the majority (four-fifths) is confined to the upper 5 cm of this horizon. The remainder of the topsoil consists of bowl-structures in the top of the A horizon (Humphreys, 1994) and organic remains. In the subsoil the bulk of material consists of s-matrix derived from *in situ* alteration of the bedrock in which biological activity below the B horizon forms a very minor component.

DISCUSSION AND CONCLUSION

In the study sites bioturbation generates a variety of channels, chambers and pedotubules. Burrows left open to the soil surface may be infilled by sediment transported by rainwash, and by litter fall before being subjected to bioturbation. Abandoned and infilled burrows are re-bioturbated by the same or different species, including species from other types of mesofauna.

This observation lead to the recognition of maculae, the macular colour pattern and to the hypothesis that maculae are remnants of former pedotubules. If this interpretation is correct it suggests that soil layers consisting of biologically produced channels, chambers, pedotubules and maculae are in a state of continuous bioturbation and it is on this basis that a biomantle (cf. Johnson, 1990) can be best defined.

From the viewpoint of pedogenesis this study indicates that active bioturbation occurs even though the topsoil maintains two horizons, an A and E, and that a strong texture contrast is preserved where bioturbated material overlies clayey saprolite. This implies that either the rates of bioturbation are much slower than other horizon-maintaining processes or that bioturbation aids the formation of distinct layers.

Previously, Humphreys and Mitchell (1983) argued that a combination of shallow mixing, active mounding and effective rainwash would tend to yield texture contrast soils providing the soil is derived from material capable of being sorted. The efficacy of mounding and rainwash has been demonstrated previously at these sites (Humphreys and Mitchell, 1983; Mitchell and Humphreys, 1987) and this study has shown that most of the bioturbation is confined to the existing topsoil (Table 2) but with evidence of fauna mining the subsoil, especially at the E - B interface. The saprolitic-B horizon of these texture contrast soils has a sandy clay field texture and it has been noted elsewhere that aggregates of B s-matrix at the surface are disrupted by rainwash with the clays transported away from the mounds as suspended load (Mitchell and Humphreys, 1987), leaving the coarser particles to form a topsoil. It would appear, therefore, that these texture contrast soils are to a large extent a by-product of bioturbation and rainwash. Nevertheless, important issues remain, including the preservation or development of A and E horizons in a realm of active bioturbation. Finally, the origin of many of the burrow linings reported in this paper have yet to be resolved. In this context, the examination of ultrastructures as advocated by Lee and Foster (1991) may prove useful.

ACKNOWLEDGMENTS

REFERENCES

Bal, L., 1973. Micromorphological Analysis of Soils. Lower Levels in the Organization of Organic Soil Materials. Soil Survey Paper No. 6. Soil Survey Institute, Wageningen, The Netherlands, 174 pp.

Brewer, R., 1976. Fabric and Mineral Analysis of Soils. Reprinted by R.E. Kreiger Co., New York, 482 pp.

Cowan, J.A., Humphreys, G.S., Mitchell, P.B. and Murphy, C.L., 1985. An assessment of pedoturbation by two species of mound-building ants, Camponotus intrepidus (Kirkby) and Iridomyrmex purpureus. Aust. J. Soil Res., 22: 95-107.

Greaves, T., 1962. Studies of the foraging galleries and the invasion of living trees by Coptotermes acinaciformis and C. brunneus (Isoptera). Aust. J. Zool., 10: 630-651.

Humphreys, G.S., 1981. The rate of ant mounding and earthworm casting near Sydney, New South Wales. Search, 12: 129-131.

Humphreys, G.S., 1985. Bioturbation, Rainwash and Texture Contrast Soils. Ph.D. thesis. Macquarie University, Sydney, 2 Vols.

Humphreys, G.S., 1989. Earthen structures built by nymphs of the cicada *Cyclochila Australasiae (Donovan) (Homoptera: Cicadae).* Aust. Ent. Mag., 16: 99-108.

Humphreys, G.S., 1994. Bowl-structures: a composite depositional crust. In: A.J. Ringrose-Voase and G.S. Humphreys (Editors), Soil Micromorphology: Studies in Management and Genesis. Proc. IX Int. Working Meeting on Soil Micromorphology, Townsville, Australia, July 1992. Developments in Soil Science 22, Elsevier, Amsterdam, pp. 787-798.

Humphreys, G.S. and Mitchell, P.B., 1983. A preliminary assessment of the role of bioturbation and rainwash on sandstone hill-slopes in the Sydney Basin. In: R.W. Young and G.C. Nanson (Editors), Aspects of Australian Sandstone Landscapes. Aust. and NZ Geom. Gp. Spec. Publn. No. 1, pp. 66-80.

Johnson, D.L., 1990. Biomantle evolution and the redistribution of earth materials and artifacts. Soil Sci., 149: 84-102.

Lee, K.E. and Foster, R.C., 1991. Soil fauna and soil structure. Aust. J. Soil Res., 29:745-755.

Lee, K.E., and Wood, T.G., 1971. Termites and Soils. Academic Press, London, 251 pp.

Main, B.Y., 1976. Spiders. Collins, Sydney, 296 pp.

Marlatt, C.L., 1907. The Periodical Cicada. U.S. Dept. Agr. Bur. Ent. Bull., 71: 1-181.

McKeown, K.C., 1944. Australian Insects. Royal Zool. Soc. NSW, Sydney, 303 pp.

Mitchell, P.B., 1985. Some aspects of the role of bioturbation in soil formation in southeastern Australia. Ph.D. thesis, Macquarie University.

Mitchell, P.B., 1988. The influences of vegetation, animals and micro-organisms on soil processes. In: H.A. Viles (Editor), Biogeomorphology, Basil Blacwell Inc., New York, U.S.A., pp. 43-83.

Mitchell, P.B. and Humphreys, G.S., 1987. Litter dams and microterraces formed on hillslopes subject to rainwash in the Sydney Basin, Australia. Geoderma, 39: 331-357.

Mitchell, P.B. and Paton, T.R., 1988. A simple technique for collecting large soil profiles for display. Aust. J. Soil Res., 26: 439-442.

Moore, D.G. and Scruton, P.C., 1957. Minor internal structures of some recent unconsolidated sediments. Bull. Amer. Assoc. Petrol. Geol., 41: 2723-2751.

Myers, J.G., 1929. Insect Singers. A Natural History of Cicadas. G. Routledge and Sons, London, 285 pp.

Northcote, K.H., 1979. A Factual Key for the Recognition of Australian Soils, 4th Ed. Rellim Technical Publ., Glenside, South Australia, 124 pp.

Paton, T.R., 1978. The Formation of Soil Material. George Allen and Unwin, London, 143 pp.

Pettijohn, F.J., 1975. Sedimentary Rocks. 3rd Ed. Harper and Row, New York, 628 pp.

Ratcliffe, F.N. and Greaves, T., 1940. The subterranean foraging galleries of *Coptotermes lacteus* (Frogg). J. Coun. Sci. Ind. Res. Aust., 13: 150-161.

Ratcliffe, F.N., Gay, F.J. and Greaves T., 1952. Australian Termites. CSIRO Aust., Melbourne, 120 pp.

Snodgrass, R.E., 1921. The seventeen-year locust. In: Ann. Rep. Smithsonian Instit. 1919, pp. 381-409.

Soil Survey Staff, 1951. Soil Survey Manual. U.S. Dept. Agric. Handb. 18, U.S. Gov. Printing Office, Washington D.C., 503 pp.

Soil Survey Staff, 1975. Soil Taxonomy. U.S. Dept. Agric. Handb. 436, U.S. Gov. Printing
    Office, Washington D.C., 754 pp.
Stace, H.T.C., Hubble, G.P., Brewer, R., Northcote, K.H., Sleeman, J.R., Mulcahy, M.J. and
    Hallsworth, E.G., 1968. A Handbook of Australian Soils. Rellim Technical Publications,
    Glenside, South Australia, 435 pp.

Investigations on distribution patterns in soil: basic and relative distributions of roots, channels and cracks

M. Krebs[1], A. Kretzschmar[2], U. Babel[1], J. Chadœuf[3] and M. Goulard[3]

[1]Institut f. Bodenkunde und Standortslehre, Universität Hohenheim (310), 70593 Stuttgart, Germany
[2]INRA, Zoologie, Laboratoire de Physique et Biologie des Sols, BP 91, 84140 Montfavet, France
[3]INRA, Station de Biométrie, BP 91, 84140 Montfavet, France

ABSTRACT

Krebs, M., Kretzschmar, A., Babel, U., Chadœuf, J. and Goulard, M., 1994. Investigations on distribution patterns in soil: basic and relative distributions of roots, channels and cracks. In: A.J. Ringrose-Voase and G.S. Humphreys (Editors), Soil Micromorphology: Studies in Management and Genesis. Proc. IX Int. Working Meeting on Soil Micromorphology, Townsville, Australia, July 1992. Developments in Soil Science 22, Elsevier, Amsterdam, pp. 437-449.

Different root systems of different plant species may result in different soil fabrics. This might be an important aspect of spatial variability in soils.

A method is described to observe the individual fabric units of six different partial fabrics (small and large roots, small and large channels, cracks and "other pores") on polished blocks, prepared from places where two plant species (*Poa trivialis* and *Rumex obtusifolius*) formed pure stands, respectively. Data were obtained by projecting the screen of a computer into the path of rays of a fluorescence microscope, so that the screen and microscopic images were visible in one plane; x/y-coordinates of fabric units could be stored directly.

Results are presented as digitized drawings ("maps") of the 6 separate partial fabrics (basic distribution patterns) and their combinations (relative distribution patterns), so that their degree of randomness and their spatial relationships could be studied. This opens a wide field for the interpretation of the functions and development of soil fabrics.

INTRODUCTION

Investigations into the relationships between root systems and soil fabrics leads to the question on how a root system or an individual root reacts on a given soil fabric. Whiteley and Dexter (1984) have stated that the geometry of soil crack patterns is likely to have a significant effect on the morphology of the plant root systems. Bengough and Mullins (1990) and Passioura (1991) reviewed the possible responses that an individual root can have on different soil fabric features (pores, dense zones *etc.*). On the other hand, since the experiments of Pfeffer (1893) on the hydrostatic pressures of roots, it is obvious that roots also have a mechanical effect on the soil such as by deforming the soil or pushing aggregates aside (Blevins *et al.*, 1970; Altemüller and Haag, 1983; Bengough and Mullins, 1990; Passioura, 1991). The review by Helal (1991) takes other biological and chemical aspects of root induced fabric

genesis into account also. Earlier, Geyger (1964) presented an example of how different soil fabrics are created by different plants. Such studies suggest that different root system patterns of different plant species may be a major factor in explaining spatial variability in soil organisation. The hypothesis is, that different morphologies of root systems (together with other factors influencing fabric, *e.g.* earthworm activity, Babel *et al.*, 1992) can create different soil fabrics. A combination of qualitative and quantitative morphological studies, applied to topsoil below different plant species, seemed to show a correlation between finely branched root systems and finely arranged soil fabrics (Babel and Krebs, 1991). This paper attempts to explore this relationship in greater detail.

Simple stereological measurements of volume density (V_V) and surface density (S_V) of voids compared with the length density (J_V) of roots (Weibel, 1979) give a first impression about relationships between root systems and soil fabric. However, in most cases, they give an unsatisfactory quantitative confirmation of qualitative observations on polished blocks. This approach may become more specific when the measurements take depth gradients within the polished blocks into account (McBratney and Moran, 1990; McBratney *et al.*, 1992).

Information about the distribution of the fabric components within the section plane is missing in nearly all morphometric estimations. Relative distributions between pores and roots were estimated by Babel (1990) and Van Noordwijk (1993). To observe basic distributions (Brewer, 1964) and relative distributions (extending Brewer's definition for basic distributions for the relation of at least two different kinds of fabric units), a partition into the individual partial fabrics with their individual fabric units is necessary.

MATERIALS AND METHODS

Site

The samples were taken from a conventionally and intensively managed meadow near Hohenheim, Southwestern Germany (altitude: 330 m; mean annual temperature: 8.5°C; annual precipitation: 687 mm). The soil type is Vega (German classification) or Fluvic Mollic Gleysol (FAO classification). The top soil (0 - 8 cm) is a loamy silt (21% clay, 75% silt, 4% sand), the content of organic carbon is 5.3%.

Sampling

Under two different plant species, each forming almost a pure stand at this place (>90% of the above ground green mass, stand diameter >25 cm), four vertical polished blocks (6 × 8 cm) per species were prepared from the top soil (depth: 0 - 8 cm; dehydration: acetone replacement (Miedema, *et al.*, 1974; Murphy, 1982); polyester resin: Vestopal 120L). The surface of the polished blocks was etched with fluoric acid (10%) to improve the contrast between pores and solid material (Krause and Babel, 1984) (Fig. 2a and b). The plant species were the grass *Poa trivialis* and the dicotyledon plant *Rumex obtusifolius*. The date of sampling was 8 May 1989.

General micromorphological description

For the whole polished block area, pore volume densities (V_V), pore surface densities (S_V) and length densities (J_V) of roots were obtained by point counting, intersection counting and profile counting respectively, using a stereo microscope (magnification 32×, oblique incident

light) with quadratic eyepiece testgrids (3.1×3.1 mm in the object) which were continuously situated along six vertical test lines per polished block. Stereological calculations were done according to Weibel (1979), assuming isotropy in the case of S_V and J_V, which may be justified at least for a first approach.

Investigations on distribution pattern

Fluorescence microscopy

To ensure that each root could be identified and distinguished from other organic material, fluorescence microscopy was necessary (short arc mercury lamp for coaxial incident light excitation, filter for violet and blue excitation 420 - 490 nm; dichromatic beam splitter 520 nm; barrier filter 515 nm).

Prior to measurement polished blocks were stained with the fluorochrome Acridine Orange (solution 1:1000 in $HCl_{10\%}$) according to Altemüller and van Vliet-Lanoe (1990). Simultaneously with the excitation light, a normal oblique incident light was used for accurate discrimination of the different pore types (it becomes possible to observe the third dimension within the pores) and other fabric components. For maintaining the optimum contrast of the fluorescent organic objects under the excitation light, the oblique incident light could be "switched off" at any time by covering the light source. Magnification was 25× (160× for checking in doubtful cases).

Evaluation and "hand-scanning"

The method of Vogel et al. (1993) was modified slightly and applied to fluorescence microscopy. The screen of a personal computer was projected into the path of rays of the fluorescence microscope by using a drawing device. In this way, the microscopic image of the polished block and the screen were visible in one plane in the microscope. Controlled by a computer mouse, one of six partial fabrics could be chosen from a menu that appeared on the screen. "Scanning" of the polished block and tracing of the individual fabric units was achieved by using a mouse button (by clicking while looking through the microscope), so that the coordinates could be stored. To cover areas of several cm^2 on the polished block with the storing procedure, coherent moves of polished block and screen image could be controlled by motors connected with the computer, also executed with the mouse. The procedure resulted in digitized drawings ("maps") of the evaluated polished block area (4.5×3.5 cm at a depth of 3 to 6.5 cm) (Fig. 2c and d). From this, maps of each of the six individual partial fabrics (Figs 3 and 4) could be obtained as well as maps of every possible combination of the partial fabrics (Fig. 5). Printing of the maps (Figs 3 to 5) and calculations (numbers of partial fabrics units, boundary lengths (Table 2)) from the stored coordinates were done by the programme S-Plus.

The six observed partial fabrics were:
- small roots (<200 µm, stored as discrete x/y-coordinates)
- small channels (<200 µm, stored as discrete x/y-coodinates)
- cracks (stored as a series of x/y-coordinates in the middle of the cracks, open polygon)
- "other pores" (stored as a series of x/y-coordinates on their boundary, closed polygon)
- large roots (>200 µm, stored as a series of x/y-coordinates on their boundary, closed polygon)
- large channels (>200 µm, stored as a series of x/y-coordinates on their boundary, closed polygon)

Table 1

Volume density (V_V), surface density (S_V), and ratio S_V/V_V of pores; and length density (J_V) of roots in the top soil of a meadow under *Poa trivialis* and *Rumex obtusifolius*, obtained on vertical polished blocks (depth 0 - 5 cm, averages of 4 polished blocks per species).

Plant species	Pores			Roots
	V_V, cm^3 cm^{-3}	S_V, cm^2 cm^{-3}	S_V/V_V, cm^{-1}	J_V, cm cm^{-3}
P. trivialis	16.0	13.9	94.9	146.5
	(s=5.29)	(s=1.97)	(s=34.6)	(s=29.7)
R. obtusifolius	14.2	13.0	91.5	141.7
	(s=2.24)	(s=3.51)	(s=22.7)	(s=15.7)

s = standard deviation

Small roots and small channels were stored as one point only, because their thickness was considered as negligible at the given magnification. As usual for hand drawings, all available information of the microscopic image was considered for the decision on the classification of the individual fabric units and for the tracing of their boundaries. Discrimination of the different pore types was undertaken using the approach described by Vogel *et al.* (1993).

It is essential to remember that all these fabric units are not the units of the respective partial fabrics in the 3D-space, but just profiles of them in the given vertical soil sections. For studies in 3D, as estimated from vertical sections, see Vogel and Babel, (1994).

RESULTS AND DISCUSSION

General micromorphological description

Table 1 shows no significant differences between *P. trivialis* and *R. obtusifolius* for pore-V_V, -S_V, -S_V/V_V and root-J_V, regarding the whole polished block area (average for 4 blocks per plant species). However, there are differences in pore-V_V, -S_V in the upper 2 cm of the polished blocks and for root-J_V at lower depth classes (Fig. 1). This indicates an influence of depth.

Further numerical results

Table 2 shows cumulative data of the individual partial fabric maps (Figs 3 and 4). For the evaluated area the root system of *P. trivialis* appears to be denser than that of *R. obtusifolius* (small root transections are 635 and 392, respectively, Fig. 3a and b; Table 2). This corresponds with the results for root densities (J_V) in Fig. 1 at a depth of 3-5 cm.

The number of small channel transections (4114 and 2766, respectively, Table 2) also indicates, also, higher channel length densities under *P. trivialis* than under *R. obtusifolius* (Fig. 3c and 3d). Because of the assumption that small channels are created by small roots, the ratio of channel and root transections (Table 2) raises the issue about age and stability of such channels. Are there still channels of plant species that grew previously in that place?

However, these results are restricted by the observation, that large portions of the evaluated area are occupied by other fabric components. Small channels (Fig. 3c and d) cannot occur in
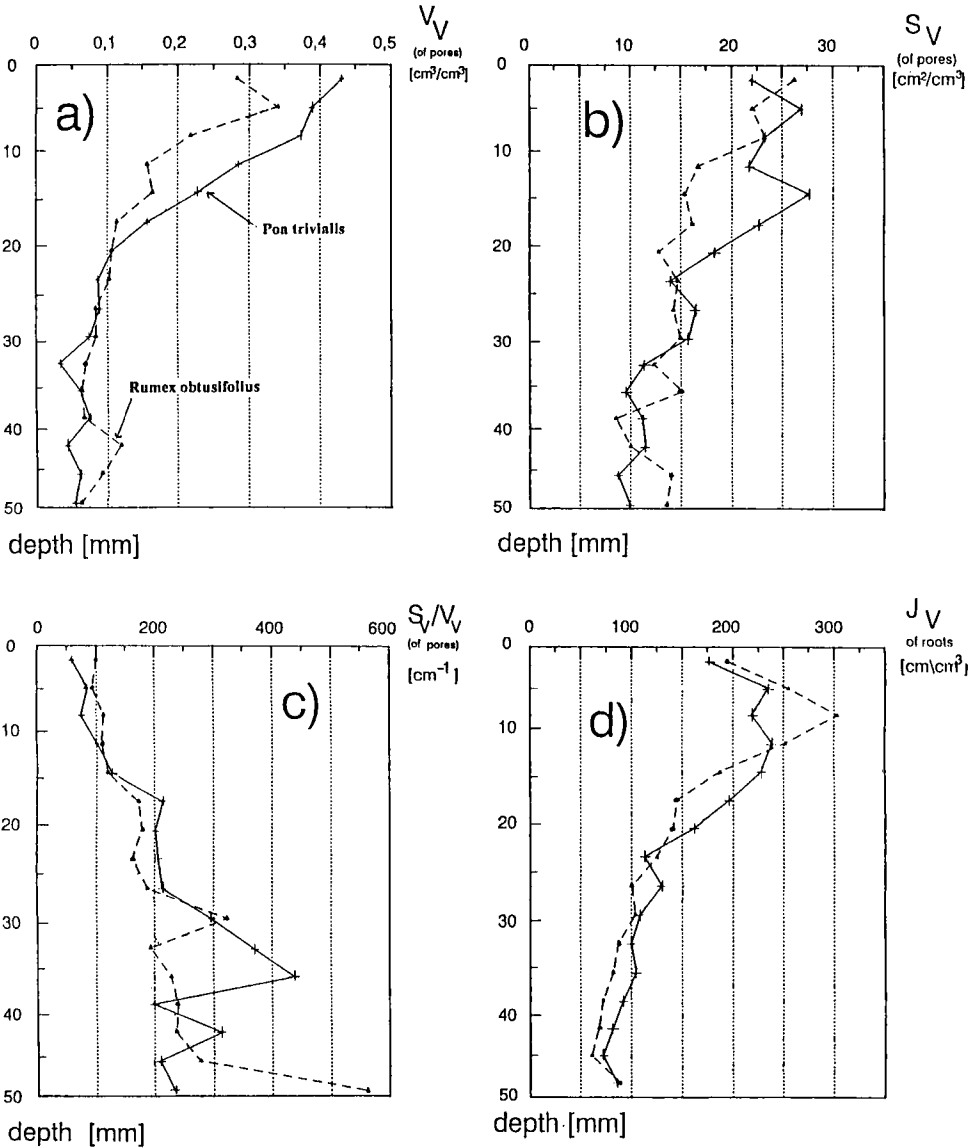
Fig. 1. a) Volume density V_V; b) surface density S_V; c) ratio S_V/V_V, of pores; and d) length density J_V of roots, in the top soil of a meadow under *Poa trivialis* (—) and *Rumex obtusifolius* (----) obtained on vertical polished blocks considering the dependency from the depth (average of 4 polished blocks per depth class and species).

areas occupied by large roots (Fig. 4a and b), large channels (Fig. 4c and d) or "other pores" (Fig. 4e and f). Small roots (Fig. 3a and b) cannot exist in areas, where large roots (Fig. 4a and
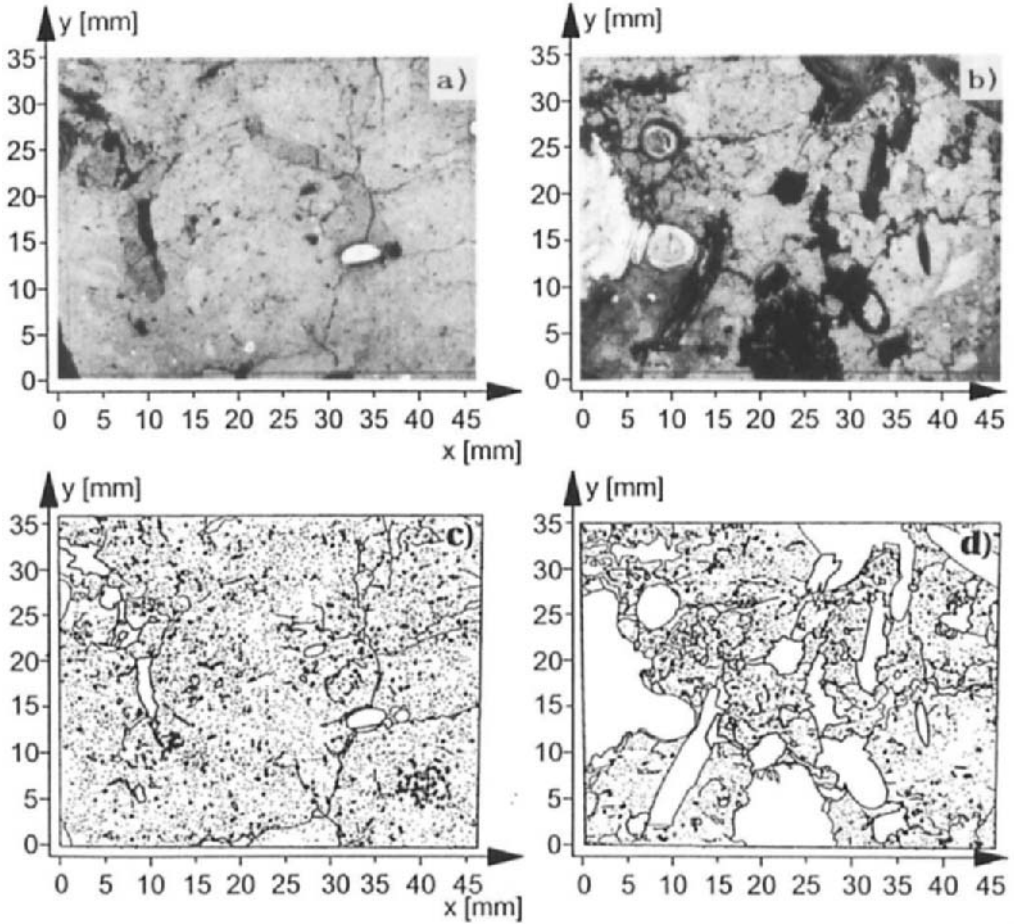
Fig. 2. **a)** and **b)** Photographs; and **c)** and **d)** digitized maps with 6 evaluated partial fabrics of the "hand-scanned" area (4.5 × 3.5 cm at a depth of 3 to 6.5 cm) of polished blocks prepared from a meadow (Fluvic Mollic Gleysol, loamy silt) under *Poa trivialis* (left) and *Rumex obtusifolius* (right). Legend for the digitized maps: small roots <200 μm (+), small channels <200 μm (•), cracks (   ), large roots >200 μm (   ), large channels >200 μm (   ), "other pores" (   ).

b) are found. The surface areas of the profiles of large roots and large channels are larger under *R. obtusifolius* (Fig. 4a, b and c, d). Therefore, the differences in the densities of small root profiles and small channel profiles between *P. trivialis* and *R. obtusifolius* might be less than that indicated in Table 2a, if the soil matrix is considered.

Table 2

Transection countings and boundary length measurements for some partial fabrics under two plant species obtained from the basic distribution maps, a) for the individual polished blocks (Fig. 3 and 4), and b) as mean values per 15.75 cm^2 of 4 polished blocks per plant species. Evaluated area of the polished blocks was 4.5 × 3.5 cm at a depth of 3 to 6.5 cm (Fig. 2a and 2b).

	a) data for indivividual polished blocks (Figs 2-5)		b) mean of four polished blocks	
	Poa trivialis	*Rumex obtusifolius*	*Poa trivialis*	*Rumex obtusifolius*
Transections of small roots	503	207	635	392
Transections of small channels	6330	3682	4114	2766
Ratio channels/roots	12.6	17.8	6.5	7.1
Total boundary length of large roots [mm]	117	286	131	153
Total boundary length of large channels [mm]	306	535	277	377
Total boundary length of "other" pores [mm]	169	438	332	374
Total length of cracks [mm]	254	305	347	443

Distribution patterns

The large amount of information makes it difficult to detect spatial relationships in the digitized maps of the six partial fabrics in Fig. 2c and d (compare with the photographs in Fig. 2a and b). Such relationships become apparent by regarding the individual partial fabric maps (basic distributions, Figs 3 and 4).

The small roots of *P. trivialis* appear randomly distributed, neglecting the two clusters, marked with an A in Fig. 3a. The map of small roots of *R. obtusifolius* (Fig. 3b) shows a decrease in root density along the vertical axis and groups with two or three roots (B) which might be more frequent than random. For both plant species, the basic distribution of small channels (Fig. 3c and d) is similar to the root distribution pattern (*e.g.* for *P. trivialis*, clusters (A, C) are visible in both patterns). The gaps in the map of *R. obtusifolius* (Fig. 3d) are explained by regarding Fig. 4b. As described previously, channels cannot be found in places (D) of large roots. Although interpretation of 2-dimensional crack patterns is restricted (Ringrose-Voase, 1991), the basic distributions of cracks with their clusters (Fig. 3e and f) give an idea of different extension of cracks, their degree of connection and their orientation patterns (many horizontal cracks in the map of *R. obtusifolius*, Fig. 3f).

Estimation of spatial relationships between two or more partial fabrics becomes possible by combining basic distribution patterns into one map. These relative distribution maps (Fig. 5) provide a basis for hypothesizing about fabric genesis. Fig. 5a shows, for *P. trivialis*, that there are no small channels in the clusters of small roots (A). This could imply that these roots grow mainly into old channels, due possibly to less mechanical resistance or better oxygen supply, and fill them so that they are not visible. Alternatively old channels are compacted while roots grow through the matrix, or destroyed by the activities of earthworms. However, no roots
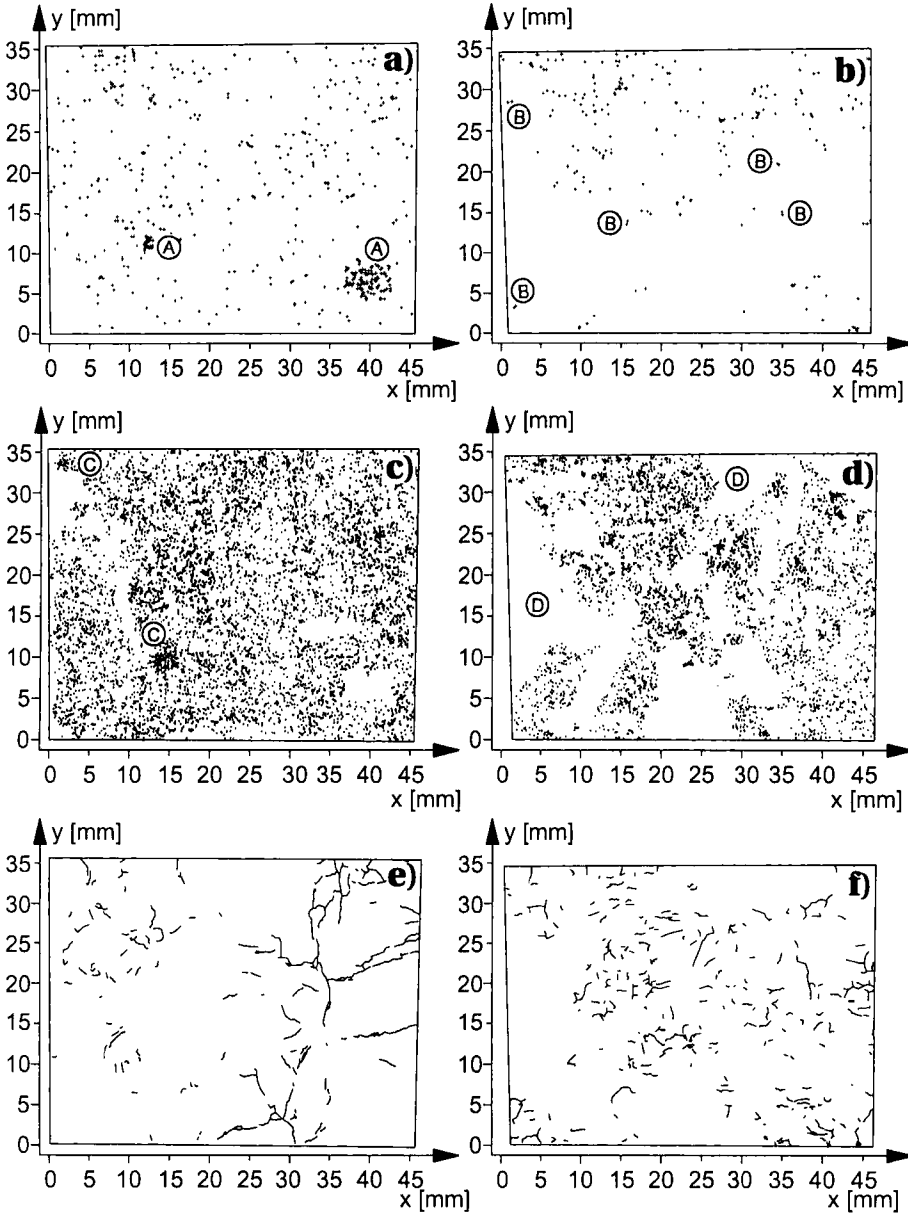
Fig. 3. Partial fabric maps (basic distribution patterns) of a) and b) small roots (<200 μm); c) and d) small channels (<200 μm); and e) and f) cracks of the evaluated polished block area (4.5 × 3.5 cm at a depth of 3 to 6.5 cm) under *P. trivialis* (left) and *R. obtusifolius* (right). Symbols A, B, C and D are explained in the text.
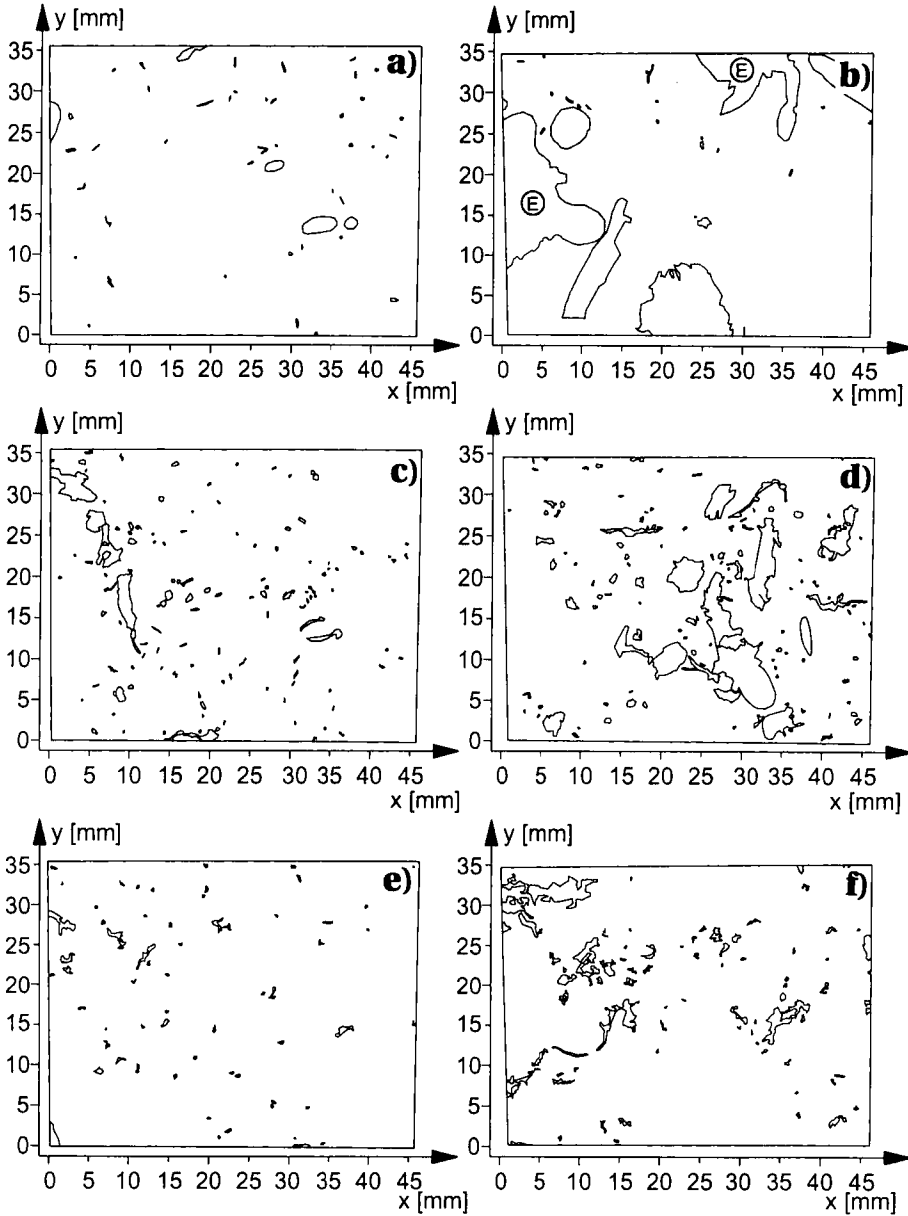
Fig. 4. Partial fabric maps (basic distribution patterns) of **a)** and **b)** large roots (>200 μm); **c)** and **d)** large channels (>200 μm); and **e)** and **f)** "other pores" of the evaluated polished block area (4.5 × 3.5 cm at a depth of 3 to 6.5 cm) under *P. trivialis* (left) and *R. obtusifolius* (right). Symbol E is explained in the text.
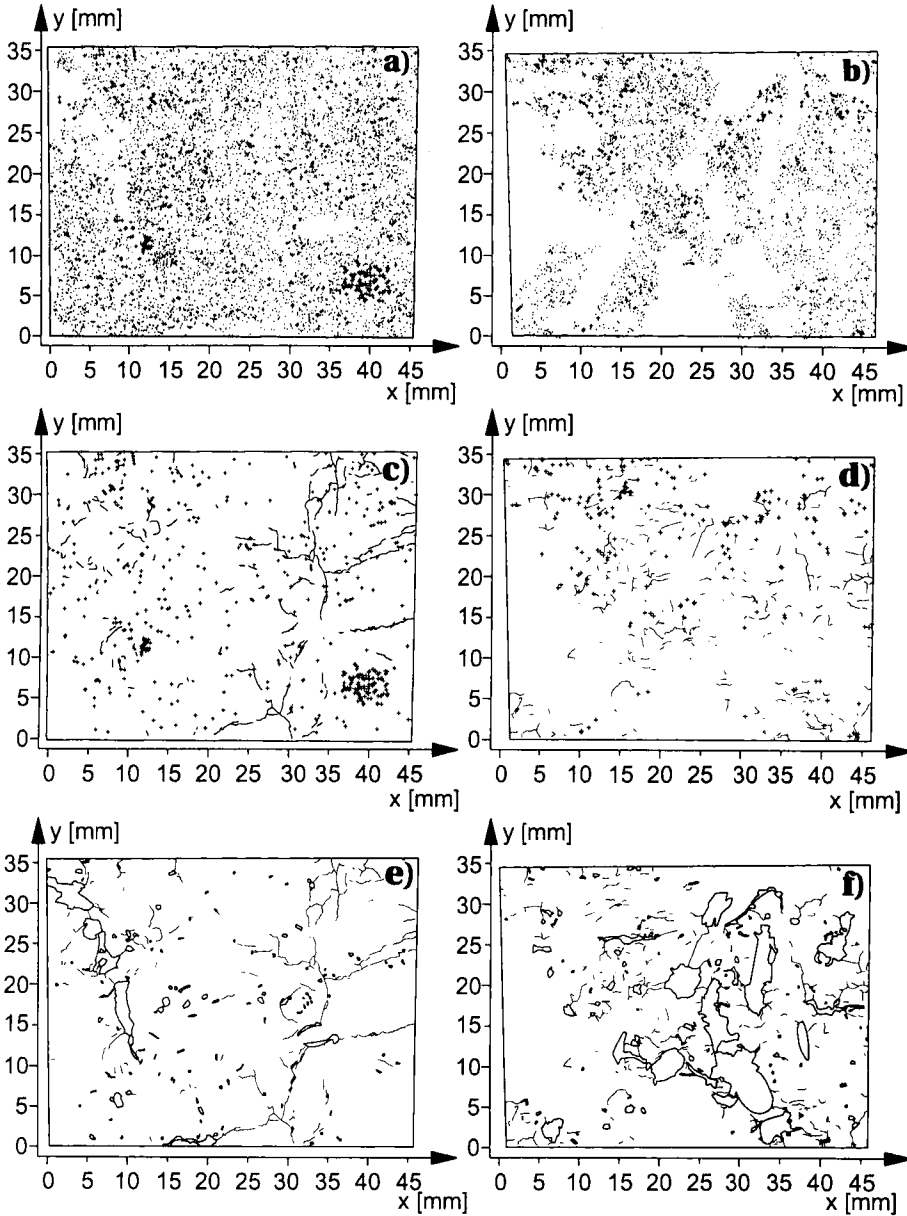
Fig. 5. Relative distribution patterns of **a)** and **b)** small roots and small channels as a combination of Figs. 3a/3c and 3b/3d, respectively), **c)** and **d)** small roots and cracks as a combination of Figs. 3a/3e and 3b/3f, respectively) and **e)** and **f)** cracks and large channels (as a combination of Figs. 3e/4c and 3f/4d, respectively). The evaluated polished block area was 4.5 × 3.5 cm at a depth of 3 to 6.5 cm under *P. trivialis* (left) and *R. obtusifolius* (right).

occur in the channel clusters (Fig. 5a (C)). Possible explanations for this are that the soil is too loose for root growing or the previous roots have exhausted the nutrient supply. For *P. trivialis* the relative distribution map in Fig. 5c shows no obvious relationship between cracks and small roots for the root density surrounding cracks and in areas without cracks is more or less the same. Even within or surrounding the root clusters (A) no cracks can be found, while for *R. obtusifolius* (Fig. 5d) a neighbourhood of cracks and roots might be more frequent. This could be checked by distance measurements. The relative distribution map of large channels/cracks (Fig. 5e and f) shows a high degree of connection between large channels and cracks for both plant species. Even in two dimensions, an impression of the continuity of pore systems becomes visible. This observation raises the issue as to whether cracks result from activities of earthworms and big roots (*e.g.* mechanical stress when they move through the soil under certain moisture conditions) or if earthworms and roots prefer to move into zones of weakness which are characterized by closed or open cracks. Both types of interdependence may occur. The formation of cracks and other small macropores at the surface of earthworm channels is shown by Babel and Kretzschmar (1994).

CONCLUSIONS

The storing of coordinates of individual partial fabric units from the microscopic image, using the computer based equipment described, allows several defined fabric components to be discriminated graphically into different partial fabrics. They can be investigated individually (basic distribution patterns). Graphical recombination of selected individual partial fabrics (relative distribution patterns) allows investigations of relationships between two or more partial fabrics. Because of the digitized character of the images, quantification of basic or relative distributions becomes possible. The procedure also elucidates, the importance of Sander's partial fabric concept (Sander, 1950) and the importance of hand drawings as a basis for many micromorphological fabric investigations for which automatical image analysis is not suitable. In either approach the degree of randomness, clustering or regularity can be discussed by evaluating basic distribution patterns. The comparison of individual units of different partial fabrics provides a basis for explaining apparent irregularities.

ACKNOWLEDGEMENTS

REFERENCES

Altemüller, H.-J. and Haag, T., 1983. Mikroskopische Untersuchungen an Maiswurzeln im ungestörten Bodenverband. Kali-Briefe, 16: 349-363.

Altemüller, H.-J. and Vliet-Lanoe, B. van, 1990. Soil thin section fluorescence microscopy. In: L.A. Douglas (Editor), Soil Micromorphology: A Basic and Applied Science. Proc. VIII Int. Working Meeting on Soil Mircromorphology, San Antonio, Texas, July 1988. Developments in Soil Science 19, Elsevier, Amsterdam, pp. 565-579.

Babel, U., 1990. Relativverteilung von Buchen- und Fichtenwurzeln zu Bodenhohlräumen. Allg. Forst- u. J.-Ztg., 161: 109-112.

Babel, U. and Krebs, M., 1991. Pflanzenartspezifische Mikrogefüge in Oberböden. Mitteilgn. Dtsch. Bodenkundl. Gesellsch., 66/II: 597-600.

Babel, U. and Kretzschmar, A., (1994). Micromorphological observations on casts and burrows of *Megascloides australis*. In: A.J. Ringrose-Voase and G.S. Humphreys (Editors), Soil Micromorphology: Studies in Management and Genesis. Proc. IX Int. Working Meeting on Soil Micromorphology. Developments in Soil Science, 22. Elsevier, Amsterdam, pp. 451-457.

Babel, U., Ehrmann, O. and Krebs, M., 1992. Relationships between earthworms and some plant species in a meadow. Soil Biol. Biochem., 24: 1477-1481.

Bengough, A.G. and Mullins, C.E., 1990. Mechanical impedance to root growth: a review of experimental techniques and root growth responses. J. Soil Sci., 41: 341-358.

Blevins, R.L., Holowaychuk, N. and Wilding, L.P., 1970. Micromorphology of soil fabric at tree root-soil interface. Soil Sci. Soc. Am. Proc., 34: 460-465.

Brewer, R., 1964. Fabric and Mineral Analysis of Soils. John Wiley and Sons, New York, 470 pp.

Geyger, E., 1964. Mikromorphometrische Untersuchungen über den Einfluß bestimmter Pflanzengemeinschaften auf die Strukturbildung im Boden. In: A. Jongerius (Editor), Soil Micromorphology. Proc. II Int. Working Meeting on Soil Micromorphology. Arnhem, The Netherlands, Sept. 1964. Elsevier, Amsterdam, 540 pp.

Helal, H.M., 1991. Bodengefüge, Wurzelentwicklung und Wurzelfunktionen. Z. Pflanzenernähr. Bodenk., 154: 403-407.

Krause, W. and Babel, U., 1984. Ätzung von Bodenanschliffen für stereologische Untersuchungen. Mitteilgn. Dtsch. Bodenkundl. Gesellsch., 39: 75-78.

McBratney, A.B. and Moran, C.J., 1990. A rapid method of analysis for soil macropore structure: II. Stereological model, statistical analysis, and interpretation. Soil Sci. Soc. Am. J., 54: 509-515.

McBratney, A.B., Moran, C.J., Stewart, J.B., Cattle, S.R. and Koppi, A.J., 1992. Modifications to a method of rapid assessment of soil macropore structure by image analysis. In: A.R. Mermut and D. Norton (Editors), Digitization, Processing and Quantitative Interpretation of Image Analysis. Geoderma, 53: 255-274.

Miedema, R., Pape, T. and van der Waal, G.J., 1974. A method to impregnate wet soil samples, producing high-quality thin sections. Neth. J. Agric. Sci., 22: 37-39.

Murphy, C.P., 1982. A comparative study of three methods of water removal prior to resin impregnation of two soils. J. Soil Sci., 33: 719-735.

Noordwijk, M. van. Concepts and methods for studying interactions of roots and soil structure. Geoderma, in press.

Passioura, J.B., 1991. Soil structure and plant growth. Aust. J. Soil Res., 29: 717-728.

Pfeffer, W., 1893. Druck und Arbeitsleistung durch wachsende Pflanzen. Abhandlungen der Königlich Sächsischen Gesellschaft der Wissenschaften, 33: 235-474.

Ringrose-Voase, A.J., 1991. Micromorphology of soil structure: Description, quantification, application. Aust. J. Soil Res., 29: 777-813.

Sander, B., 1950. Einführung in die Gefügekunde der geologischen Körper, Band II, Springer-Verlag, Wien und Innsbruck, 409 pp.

Vogel, H.-J. and Babel, U., 1994. Experimental relationship between the micromorphological pore size distribution and the soil water retention chararacteritic. In: A.J. Ringrose-Voase and G.S. Humphreys (Editors), Soil Micromorphology: Studies in Management and Genesis. Proc. IX Int. Working Meeting on Soil Micromorphology. Developments in Soil Science, 22. Elsevier, Amsterdam, pp. 591-600.

Vogel, H.-J., Weller, U. and Babel, U., 1993. Estimating orientation and width of channels and cracks at soil polished blocks - a stereological approach. In: L. Brussaard and M.J. Kooistra (Editors), Soil Structure/Soil Biota Interrelationships. Geoderma, 56: 301-316.

Weibel, E.R., 1979. Stereological Methods, Vol. 1: Practical Methods for Biological Morphometry. Academic Press, London, 415 pp.

Whiteley, G.M. and Dexter, A.R., 1984. The behaviour of roots encountering cracks in soil. Plant and Soil, 77: 141-149.

This Page Intentionally Left Blank

Micromorphological observations of casts and burrow walls of the Gippsland giant earthworm (*Megascolides australis*, McCoy, 1878)

U. Babel[1] and A. Kretzschmar[2]
[1]*Institut für Bodenkunde, Universität Hohenheim, (310), 70593 Stuttgart, Germany*
[2]*INRA-Zoologie, Laboratoire de Physique et Biologie des Sols, BP91, 84140 Montfavet, France*

ABSTRACT

Babel, U. and Kretzschmar, A., 1994. Micromorphological observations of casts and burrow walls of the Gippsland giant earthworm (*Megascolides australis*, McCoy, 1878). In: A.J. Ringrose-Voase and G.S. Humphreys (Editors), Soil Micromorphology: Studies in Management and Genesis. Proc. IX Int. Working Meeting on Soil Micromorphology, Townsville, Australia, July 1992. Developments in Soil Science 22, Elsevier, Amsterdam, pp. 451-457.

The earthworm *Megascolides australis* constructs large burrows (2 - 3 cm diameter , in which the microstructures of the burrow walls are relatively easier to observe than burrows of smaller species.

Samples of the soil with burrows and of cast material found within the burrows were selected during the description of the burrow system and prepared for polished blocks and thin sections.

Field observations together with microscopic studies of the structure of burrow walls show several phenomena:
- The presence of fissures parallel to the burrow wall, and of rare and thin stress cutans, can be interpreted as evidence of the low compaction effect due to burrowing activity.
- The ageing features of these galleries show the effects of abiotic and biotic processes on the degradation ot the burrow surface.
- The burrow wall surface, mainly after ageing, provides an increase in surface area and maintains connections to the pore system in the soil matrix. This implies that the burrow wall may facilitate water and gas exchange within the soil.

INTRODUCTION

Megascolides australis is the largest endogeic earthworm in Australia. In the past, it has been collected more as a curiosity and the total population seemed to decrease to such an extent that the species was declared "endangered". Recently, several investigations on its habitat, biology and behaviour have been conducted by the Museum of Victoria. In particular Van Praagh (1992) and Kretzschmar and Aries (1992), respectively, have described the distribution of this species, and provided a large scale reconstruction of its burrow system. The present study focuses on the micromorphological aspects of the cast and the burrow walls of *M. australis* in order to improve our understanding of the biology and ecology of this species.
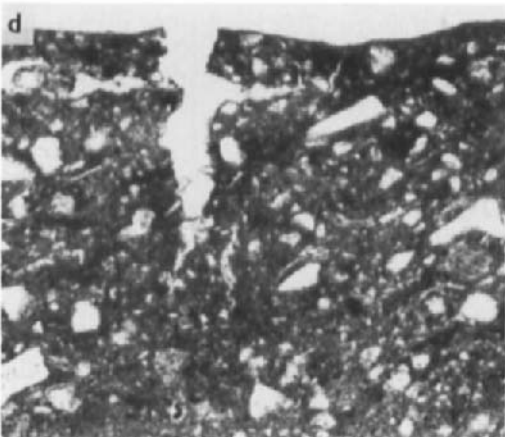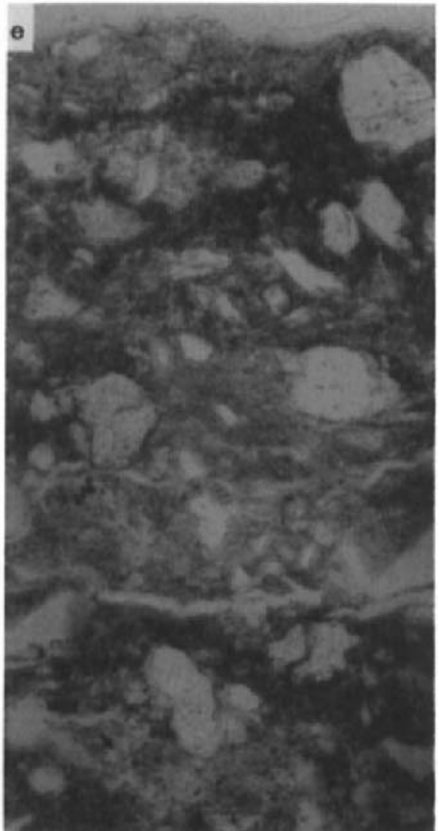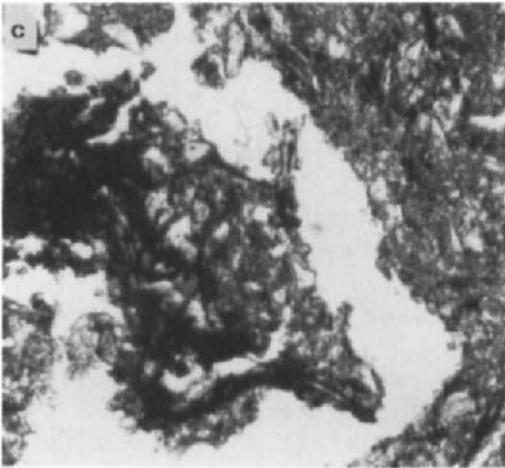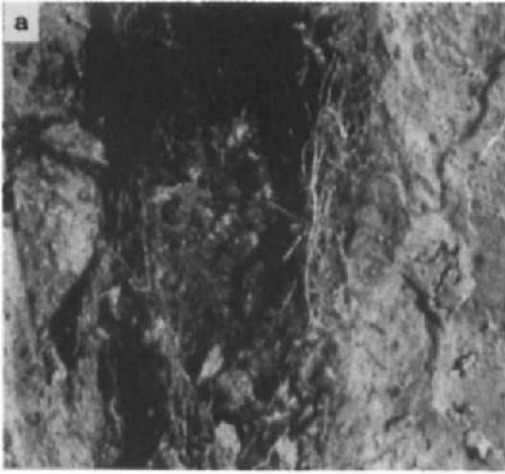
In addition, *M. australis* burrows are large (2-3 cm diameter), and it was thought that micromophological studies of the structure of the burrow wall could provide evidence of the mechanism of burrowing, the overall structure of the freshly made burrows, and the transformation of these structures with time. Furthermore, earthworm burrow walls provide a surface available for water and gas exchange (Kretzschmar, 1987) and it was anticipated that the study of a large species may lead to a better understanding of the role of the burrow systems in the soil tranfer properties.

MATERIAL AND METHODS

Populations of *M. australis* are generally found in loamy clay soils with waterlogging under permanent pasture in the Gippsland area, 100 km south-east of Melbourne, Victoria.

Adults of *M. australis* average *c.* 750 mm × 20 mm and range up to 380 g in weight. This species is active all year burrowing to about 1.5 m depth, though activity near the soil surface is, nevertheless, restricted to autumn and winter seasons. It is the only earthworm species at the site, occuring at a density of about three individuals per cubic metre.

Ten soil samples containing earthworm burrows and three containing casts were chosen within the same level of the profile (between 40 and 60 cm). The soil was nearly air dry at the time of sampling and completely air dried prior to transport to Stuttgart. Samples were then impregnated with the polyester resin Vestopal and cut to provide polished block (about 6 × 8 cm) and thin sections (about 2.5 × 4 cm). Staining was not used. Thin sections were examined under the microscope with plane and polarized transmitted light as well as with dark field incident light.

RESULTS AND DISCUSSION

The structure of casts.

M. australis does not produce surface casts at any time. Evidence of surface feeding was not observed in the biological studies of van Praagh (1992). Instead, morphological observation of casts in burrows, at different scales, were used to assess feeding behaviour and the ecological consequences of deep soil casting.

Many burrows filled with cast material and roots were observed in the profile (Fig. 1a). The casts seem to be rapidly colonized by small animals and roots. Initial root growth is

---

Fig. 1. **a)** Cast material and roots filling a burrow of *M. australis* in the profile wall. Cast material loosened by feeding activity of small animals and by roots. Roots concentrated in the gap between the cast material and the burrow wall. Burrow oriented quite steeply within a plane normal to the profile wall. Burrow diameter 23 mm. **b)** Matrix of cast (top) and of the surrounding soil, separated by a root, showing difference between matrices (compare with a). Thin section; transmitted light (TL), bright field (BF), frame width (FW) 1.28 mm. **c)** Irregular voids formed by high shrinkage of organic residues within the cast. Thin section, TL, BF, FW 1.51 mm. **d)** Burrow surface, oxidized and broken up after a period of waterlogging. Thin section, TL, dark field, FW 1.52 mm. **e)** Fissures in the burrow wall, more or less parallel to its surface (top), indicating stress during formation. Thin section, TL, BF, FW 0.32 mm.
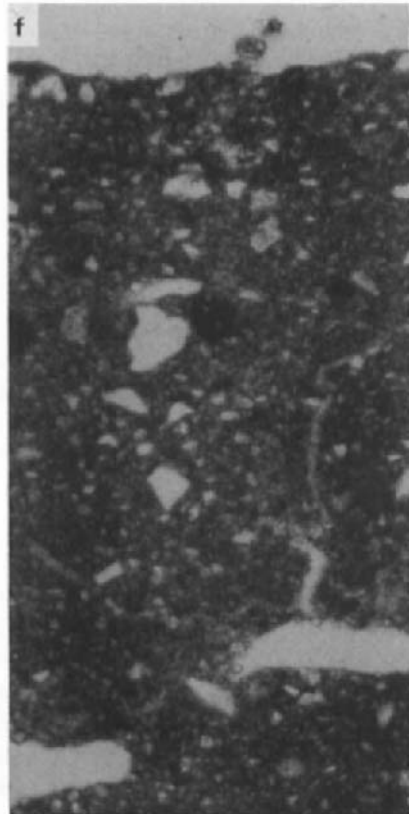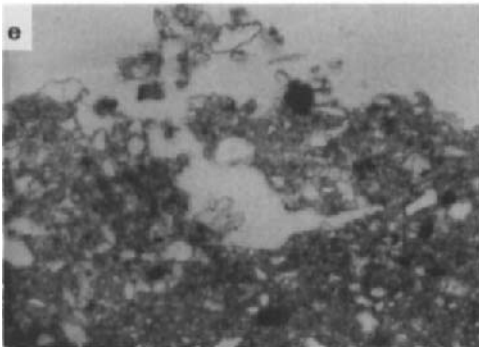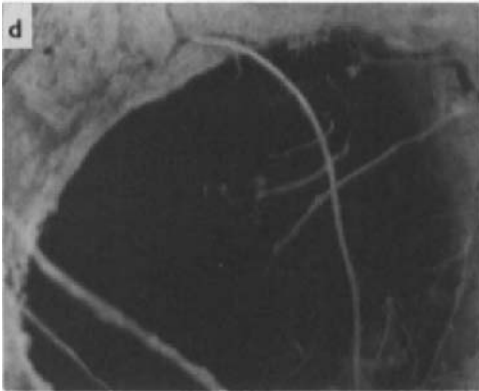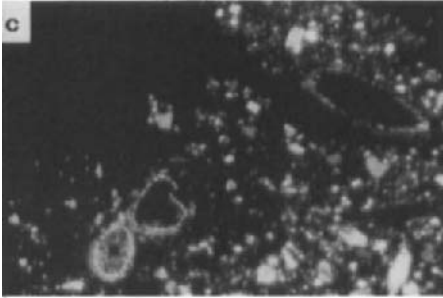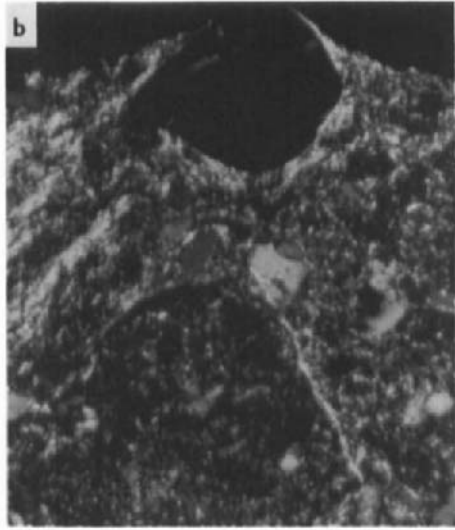
concentrated between casts and the burrow wall. The matrix of the cast is very different to that of the surrounding soil (Fig. 1b) with the high shrinkage of organic residues causing the development of many irregular voids (Fig. 1c). Plant material at all states of decomposition (*e.g.* leaf residues in the early alteration stage of browning, other residues in the further stage of blackening - which develops by lack of oxygen) can be observed in the cast. Leaf residues in the casts prove that *M. australis* - at least occasionally - consumes at or near the soil surface. On the surface of a few casts, traces of illuviation clay leptocutans (thickness about 3μm) can be found which may indicate water movement on this surface.

In contrast with the soil matrix, the casts deposited at depth in the soil profile show many signs of an intense biological activity. This may be enhanced by the high organic content in casts and by the preferential gas and water pathways in the gap between the cast and the burrow wall.

The formation of burrow walls

Particularly in view of the absence of surface casts, the mechanical stresses involved in opening the burrow should have an important effect on soil organisation at the vicinity of the burrow walls. Silt and sand sized particles, as well as fissures, might be expected to be oriented parallel to the burrow wall surface. But examples of this are rare and are restricted to the inner 1 mm of the wall (Fig. 1d and e). Also, thin stress cutans with clay orientation occurs just at the wall surface and only in places with iron reduction (Fig. 2a). This is surprising especially in a fabric where clay orientations, not related to the wall are frequent (Fig. 2b).

In the absence of any direct evidence, it seems that this soil is capable of absorbing temporary compaction at the time when burrows are first opened. On the other hand, the fact that many burrows are filled with casts proves that at least partially digging is done by feeding which is the common way for endogeic species. In any case, the absence of a zone of strong compaction means that the connection between burrows and soil matrix porosity is not strongly obstructed. This may prove to be important in preserving the transfer properties of this soil.

Near the burrow walls, wrapping cutans (Bal, 1973) occur in some places. They consist of cast material which is attached to the burrow surface. A similar feature was observed along the burrow wall of *Aporrectodea longa*, in an European temperate leached brown soil under pastures (Kretzschmar, 1987).

Fig. 2. **a)** Burrow surface with stress cutan with clay orientation parallel to the surface, in an area with iron reduction. Some mineral grains oriented parallel to the surface. Thin section, 45° XPL, FW 0.35 mm. **b)** Burrow surface with clay orientation unrelated to the surface (masepic, Brewer, 1964). Thin section, XPL, FW 0.35 mm. **c)** Burrow surface with roots from the lumen of the burrow (top) penetrating the soil matrix often along shrinkage fissures. Thin section; XPL, FW 1.4 mm. **d)** Abandoned burrow, serving as a pathway for roots which find places to enter the soil matrix. FW 19.1 mm. **e)** Burrow surface, roughened by the activity of soil animals, with aggregates on the surface composed of droppings of enchytraeids or collembola, transformed by welding and breaking apart. Thin section; TL, BF, FW 1.64 mm. **f)** Channels left by decomposition of roots that have followed a zone of weakness beneath the burrow surface (top) and parallel to it. Thin section; TL, BF, FW 1.24 mm.

Ageing of burrow walls

Other phenomena observed were interpreted as an effect of ageing. This term is used in a broader sense than that defined by Bal (1973). They may be arranged according to two types of processes. The first concerns processes of stabilization. Iron oxydation (Fig. 1d) as well as formation of illuvial clay leptocutans will act to stabilize and, at the same time, smooth the wall surface. Both processes are due to the burrow functioning as pathways for gases and liquids. The other type concerns processes of destabilisation. Here we have shrinkage (Fig. 1d), which also is an effect of gases (and liquids) transports in the burrows. The other destabilizing processes are due to the burrow functioning as pathways for roots (Figs. 1a and 2d) and soil organisms as both result in a roughening of the wall surface (Fig. 2c and e). Fig. 2f demonstrates that roots also make use of zones of weakness along walls. All the roughening processes of ageing interact which each other. For example, roots will penetrate into fissures and thereby enlarge them, and after death, animals will enter them, *etc.*

Rougher surfaces mean an increase in the exchange processes between burrow and soil matrix. Additionally it means provision of niches for small organisms (Kampichler and Hauser, 1993).

CONCLUSIONS

The absence of obvious compaction at a distance greater than about 1 mm from the burrow wall, seems to show that *M. australis* does not build up high stresses when digging. Hence, the burrow system retains a connection with the pore system of the soil matrix. Ageing processes improve this connection. If the compaction is not important around the burrow of a large earthworm species, there is a possibility that it does not occur in the vicinity of the burrows of other smaller species, too. This may prove to be an important result for the studies of preferential flows in soil which may have to consider earthworm burrow systems as a part of a larger potential exchange surface, connected with the fissure system and the soil surface.

The results presented here show the possibility of understanding the function of soil surfaces at a much smaller scale than that of the object itself. Corresponding micromorphological studies of surfaces of large cracks, which may also influence the transfer properties, should be undertaken.

ACKNOWLEDGEMENTS

REFERENCES

Bal, L., 1973. Micromorphological Analysis of Soils. Soil Survey Papers Netherlands. Soil Survey Institute, Wageningen.
Brewer, R., 1964. Fabric and Mineral Analysis of Soils. John Wiley and Sons, New York, 470 pp.

Kampichler, Ch. and Hauser, M., 1993. Roughness of soil pore surface and its effect on available habitat space of microarthropods. In: L. Brussaard and M.J. Koostra (Editors), Soil Structure/Soil Biota Interralationships. Geoderma, 56: 223-232.

Kretzschmar, A., 1987. Caractérisation microscopique de l'activité des lombriciens endogés. In: N. Fedoroff, L.M. Bresson and M.A. Coutry (Editors), Soil Micromorphology. Proc. VII Int. Working Meeting of Soil Micromorphology, Paris, July 1985. Association Française pour l'Etude du Sol, Plaisir, France, pp. 325-330.

Kretzschmar, A. and Aries, F., 1992. Analysis of the structure of the burrow system of the giant Gippsland earthworm Megascolides australis, Mc Coy (1878) using 3D-images. Soil Biol. Biochem., 24: 1583-1586.

van Praagh, B., (1992) The ecology, distribution and conservation of the giant Gippsland earthworm Megascolides australis, McCoy (1878). Soil Biol. Biochem., 24: 1363-1367.

This Page Intentionally Left Blank

Image processing and soil micromorphology

C.J. Moran

CSIRO Division of Soils, GPO Box 639, Canberra, ACT 2601, Australia.

ABSTRACT

Moran, C.J., 1994. Image processing and soil micromorphology. In: A.J. Ringrose-Voase and G.S. Humphreys (Editors), Soil Micromorphology: Studies in Management and Genesis. Proc. IX Int. Working Meeting on Soil Micromorphology, Townsville, Australia, July 1992. Developments in Soil Science 22, Elsevier, Amsterdam, pp. 459-482.

In the context of this paper, image processing in soil micromorphology is the use of digital images to study the form of soil features or parameters derived from these features. Emphasis is placed on colour image processing and display, and options available for image measurement, as these are perceived to be the areas dealt with least in the soil science literature. Finally, the field of modelling of soil attributes and processes using an image processing framework, herein called image modelling, is discussed and illustrated.

INTRODUCTION

In the context of this paper, image processing in soil micromorphology is the use of digital images to study the form of soil features or attributes derived from these features. Form is meant here in a most general sense, *i.e.* the structure, nature or pattern of a thing, *e.g.* morphology, size, spectral properties, spatial distribution, and inhibition or attraction relationships with other features. Estimates of attributes of features have conventionally been presented as tabulated and/or graphical summaries. Here attributes represented as images are included. These images have many origins. They can be; derived from one or more other images, *e.g.* a map of strong mottles or skeleton grains derived from images taken in various parts of the electromagnetic spectrum (Sweeney *et al.*, 1992); results from simulation of features, *e.g.* soil pore structure (McBratney and Moran, 1994) or simulation of processes, *e.g.* distribution of water on a flat soil surface as affected by straw cover (presented in this paper). No attempt is made to define the term image analysis as it means so many different things to different users. Image measurement is the generation of attributes of objects or connected components in an image. These image attributes can be interpreted as a reflection of the feature being measured and, therefore, be used to describe and/or model it quantitatively. Image modelling is the use of an image processing framework to simulate attributes of a system and/or to simulate processes that act on measured or simulated attributes.

The main objective of this paper is to transfer technology from the image processing literature to soil micromorphology. Specimen and image acquisition and segmentation are not dealt with here as a great deal of literature is already devoted to these subjects. A rudimentary understanding of colour in image processing is advantageous to effectively use the technological advance of colour digitising. An overview of colour implementation in computer

display devices is presented. Some of the colour representations that are available for manipulation in most modern software packages used for image processing are briefly explained. It is hoped that this will equip the interested reader with sufficient information to explore colour manipulation. This is followed by a section in which the issue of spatial context for data generated in micromorphology is raised. Two reviews which largely cover the history of image processing in soil micromorphology (Ringrose-Voase, 1991; Ringrose-Voase, in press) reveal that relatively few of the available image measurements have been explored by soil micromorphologists. Therefore, this paper gives a broad summary of the measurement options available and limited examples of their use; both in and out of micromorphology. Undoubtedly, some image measurements have been missed in this summary but the suite of references provided should allow the reader access to most of the current options. The selection of appropriate measurement procedures can be a difficult task, so a model to assist in this procedure is proposed. Finally, examples of image modelling of features, *i.e.* straw cover, and a dynamic process, *i.e.* water flow, are given.

Each year A. Rosenfeld publishes a bibliography of references relevant to image analysis and computer vision, arranged by subject matter, for that year. Prior to 1990 these appeared in the journal Computer Vision, Graphics and Image Processing which has now become CVGIP Image Understanding. This bibliography has now been published for 22 years and provides an unparalleled reference source for image processing.

IMAGE DISPLAY

This section concentrates on colour because it is likely that use of colour will continue to increase in image processing of soil micromorphological data. The main reasons for this are that colour display hardware and software are freely and cheaply available and colour digitising makes identification and quantification of many pedofeatures relatively easy. Consequently, we are attempting to present more information in images than in the past. More information can be represented in colour than in grey levels. It is useful to know how our machines represent colour and what options are available for its manipulation. Naturally, colour output devices are designed to allow humans to perceive colour. Protz *et al.* (1992), Sweeney *et al.* (1992) and Terribile and FitzPatrick (1992) presented colour segmentation and classification of pedological features as images and/or coloured maps derived from multi-plane images digitised using a variety of light sources and filters. This early success implies that quantification of the associations between different features should now proceed rapidly. Moran and Vezina (1993) showed examples of the use of colour, shading and texture mapping for simultaneously visualising soil, water and surface cover data in a study of surface aggregate breakdown through a sequence of simulated rainfall events.

Display hardware

A rudimentary summary of the predominant colour display system of today, the cathode ray tube (CRT) display, is presented to provide context for the discussion on colour (below). For a more complete description see Travis (1991).

The CRT produces a beam of electrons which are focussed and deflected onto the back of the phosphor-coated screen which fluoresces when struck by electrons. The smallest unit of fluorescent excitation on the screen is called a pixel. The simplest displays have a single

electron gun which can either display binary information by turning pixels on or may excite the pixels through a range of intensities. Colour is represented on a computer monitor as a mixture of the three display primaries: red, green and blue. This is achieved by having excitation sites for each primary close together, *i.e.* red, green and blue pixels. The spatial arrangement and delineation of individual pixels provides monitors of various properties, qualities and price.

CRT colour monitors have a digital-to-analogue convertor (DAC) and an electron gun for each of the colour primaries. Each colour is represented uniquely by a triplet of values; one for each primary. Triplets are placed in locations in memory used for display known as a video frame buffer. Positions in the video frame buffer are mapped to screen locations for display. Each time the frame buffer is read, each digit in the triplet is sent to a DAC which sends the appropriate voltage to the electron gun.

The range of colours that can be represented on a screen is controlled by the resolution of the DACs. The number of colours that can be displayed at any one time is controlled by the number of bits used for each pixel in the frame buffer. A large number of the image processing systems being used by soil micromorphologists have 8-bit frame buffers and 8-bit DACs. Therefore, they can display a maximum of 2^{24} colours but only 2^8 at any one time. A system with a 24-bit frame buffer and 8-bit DACs can display all 2^{24} colours at the same time (if there were sufficient pixels available). This is known as true-colour because 2^{24} colours is sufficient to match the spectral range and perception-resolution of the human eye.

It is possible to alter the colours represented on the screen without altering the contents of the frame buffer or transforming the image, by using look-up tables (LUTs). A LUT uses the input digit as an address into a table whose output value is sent to the DAC. Hence data can be transformed by substituting the LUTs which is much faster than rewriting the frame buffer. An image utility that operates interactively is provided with most image display packages. Also, many image formats allow storage of a LUT for the image; this is often referred to as the *colour map* of the image.

The main disadvantages of CRT displays are: that colour is non-uniform, the guns are rarely independent, it is sensitive to ambient illumination, screens are not flat, they require a lot of power to drive, and they are bulky because of the distance required to focus the electron beams. There are three main other technologies under development: electroluminescent, liquid crystal and plasma. These technologies and their advantages and disadvantages are summarised by Travis (1991).

Colour spaces

Any colour can be described by three digits which fall inside a 3D colour space which defines all colours. All colour spaces are 3D because colour vision is based on absorbtion by the three classes of cones; loosely red, green and blue. Colour spaces vary in how they represent the three digits. The use of a particular space depends on the aim of the use of colour. Some features that may be important are (Travis, 1991): (a) perceptual uniformity, equal steps in colour space are equally discriminable; (b) ease of access to particular colours or sequences; (c) resemblance to the visual system; (d) accurate colour specification; (e) ease of implementation on a colour display device. Often when one explores the display component of their image processing package several choices are offered for manipulation of colour. The main options are described and the relationships between them explained.
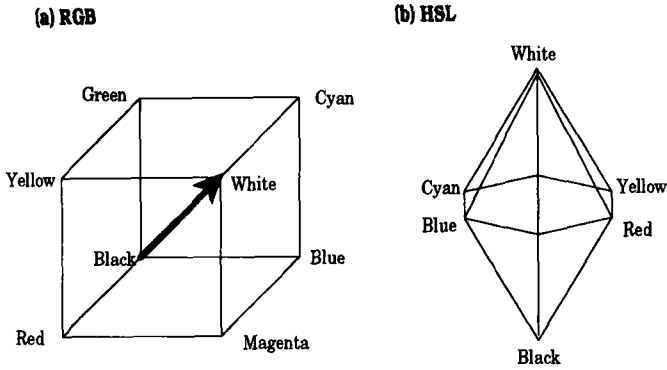
Fig. 1. The arrangement of the RGB cube and associated HSL colour space used for colour representation on CRT displays.

As was described above, implementation of colour on computers uses a RGB (red, green, blue) colour space for display (Fig. 1a). The axis of equal quantities of red, green and blue at each point defines a grey scale. It is simple to define a colour in RGB but one must become familiar with the mixtures which provide the desired colours. It is intuitive for some people to specify a colour by selecting the essence of the colour (hue) then fine-tuning it by choosing the pureness (saturation) and amount of white or black (lightness). Colour spaces which allow selection of colour in this manner are known as perceptual colour spaces. A perceptual space derived from the RGB space is the HSL space (Hue, Saturation, Value (HSV) is a similar alternative). This space is derived by rotating the RGB cube until the origin points down (Fig. 1b). The rotation places the fully-saturated (or pure) colours in the same horizontal plane in the centre of the space. Angles around this plane are known as hue angles; 0° being red. The vertical axis represents the lightness of the colour and the distance from the centre the saturation.

Monitors rarely have monochromatic primaries nor are the primaries the same on different monitors. Also, the phosphors and other electronics can alter the colours and some colours cannot be produced. The gamut of colours available on any given monitor will rarely, if ever, be well-represented by the cubic system of the RGB, *e.g.* often they are exaggerated in the red region. Thus, the colour space used by display devices should more aptly referenced as R'G'B' to distinguish it from RGB spaces based on monochromatic primaries. The same is true for computer implementations of HSL, *i.e.* H'S'L'.

The Commission Internationale de l'Eclairage CIE(X,Y,Z) colour space is a 3D RGB perceptual colour space which defines the gamut of colours of a person with normal colour vision. It is based on colour matching functions which are plots of the relative amounts of three primary lights (red, green and blue with wavelengths specified) needed to match a monochromatic light. The relative amounts of the primaries required to match a monochromatic source at a particular wavelength are known as tristimulus values. The colour matching functions are derived from human psychophysical studies. Any triplet of tristimulus values defines a colour within this space; each colour is perceived as the same by people with normal colour vision. Conversion from CIE(X,Y,Z) to R'G'B' is possible by assuming the monitor has standard phosphors as defined by the National Television System Committee (NTSC) (Pratt, 1988). The CIE(LUV) is a perceptually uniform colour space derived from the original CIE(X,Y,Z) colour space. Robertson (1988) provides useful information on the

definition, use and application of perceptual uniform colour spaces for visualisation of scientific information.

A colour order system is a rational plan of ordering and specifying object colours using a set of *material standards* displayed so as to represent all the colours under consideration (Wyszecki and Stiles, 1967). The Munsell colour system, used widely in soil science, is an example. The Munsell standards are selected to represent scales of constant hue, saturation (chroma) and lightness (value), each one spaced uniformly in accordance with an observer with normal colour vision. A modification of Munsell known as the Munsell renotation system provides values for a CIE colour space for Munsell hue, chroma and value. This allows specification of colour that can be represented on a display device by converting the CIE to R'G'B'.

The use of colour standards for representation of pedofeatures may become important as colour image processing in micromorphology becomes more extensive (Sweeney *et al.*, 1992). Even though it may seem easy to specify colour using R'G'B' or H'S'L' this is not a very sound communication tool. The CIE spaces provide unambiguous colour specification. The Munsell colour order system is also useful because soil scientists are familiar with Munsell and it is possible to convert to R'G'B' via CIE for CRT display.

Display of spatial information

Micromorphologists usually generate data at the micro-scale. Putting the data into context with the profile or the surrounding landscape may be difficult. This is not a problem of exact spatial location of pixels in images from thin sections by registering pixels onto a real scale, *e.g.* longitude and latitude.

Moran *et al.* (1988) measured the distance between zircon grains and their size in horizontal thin sections taken at several depths in a profile. Fig. 2 shows a random-process simulation of their data at various scales. Simulations of the distribution of individual zircon grains are shown on the left. This simulation was performed using the pore structure simulation model described by McBratney and Moran (1994). Each small image in the mosaic represents a simulation of a horizontal section. The sections are tilted at 90° for presentation. The depth of the section in the profile is indicated by the alignment of the centre of the image with the depth scale. Zircon grains were modelled as prolate spheroids, therefore their profile in section varies between circular and elipsoidal. In the figure, grains appear as the more or less aggregated light regions. Each pixel in this simulation is 10 μm. Given the density of grains measured on the thin sections, less than one grain would generally be observed in a field of view of the size shown. An advantage of simulation is that it is possible to increase the density of grains without changing the nature of spatial distribution of the point process guiding their location. To show such a distribution at the scale indicated, the intensity of the point process was magnified ten times. This provides a unique view of the grains as it is like examining a field of view ten times larger than the microscope can provide. Therefore, shape, orientation and distribution of grains can be visualised whilst maintaining sufficient size for the eye to accept that they are zircon grains.

In the middle of Fig. 2, the scale is such that grains are represented as points. The presentation is the same as described for the simulation of individual grains above. This simulation was generated by selecting points within the image from a completely random distribution until the density of points equalled that measured by Moran *et al.* (1988). This
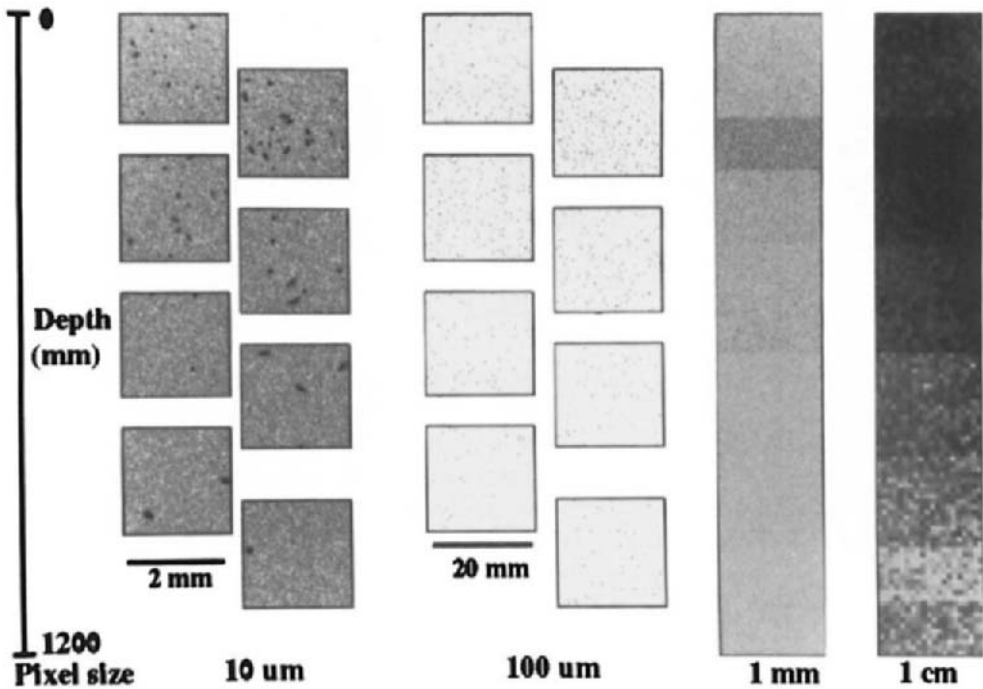
Fig. 2. Simulation of zircon grain distribution in a soil profile at various scales.

shows the distribution over a region of the thin section. Again, this provides a look at the data that is not physically possible because the grains would not be visible to the naked eye.

In the two profiles to the right, it is assumed that the distribution of grains in each horizon is isotropic and vertical sections are simulated at the millimetre and centimetre scales in which the depth of each horizon is shown proportionately. The size of each pixel is sufficiently large to accomodate more than one zircon grain. These simulations are effectively the same as the 100 μm simulation. The spatial scale is the same during the simulation, i.e. individual grains are still generated over a very large area divided into 100 μm pixels, but the position of each grain at the scale displayed in the figure is stored. This scaling obviates the need to create a huge image during the simulation and compute the average of regions afterwards to find the number of grains per unit area. The value of each pixel is the number of zircon grains per pixel. These values are normalised into 256 levels and displayed as a grey level image. These simulations provide a quantitative visualisation of the difference between sampled layers. We can now "see" a surrogate for the horizon density, i.e. concentration of zircon grains. A simulation model of a soil profile, albeit oversimplistic, has thus been developed directly from measurements made from thin sections.

This example illustrates a way of aggregating micromorphological data to provide the most powerful image processing device, the human eye and brain combination, an opportunity to see and interpret relationships in the data.

IMAGE MEASUREMENT

Recently, two reviews of 2-dimensional measurement of soil pore structure using digital images have been published (Ringrose-Voase, 1991; Ringrose-Voase, in press). Rather than duplicate these reviews a more general view of image measurement is presented. The image measurement literature is too vast for complete review but an attempt is made to cover the major measurement options and provide reference material with which the reader can begin exploration of new subject areas. Few texts on image measurement are available, however, Rosenfeld and Kak (1982), Levine (1985) and Russ (1990) contain a great deal relevant information.

Measurements are divided into those of objects in the image that can be considered as individuals and those of all or part of the image herein called image components. A limited number of examples of application of measurements are provided. A methodology for selection of appropriate attributes to measure is proposed and an example provided. Finally, a brief discussion of the evolution of image measurement, particularly of pore structure, and the utility of measurements is presented.

Measurement of individuals

The measurement of individual objects has been the dominant paradigm for image measurement in soil micromorphology. Measurement of several properties of individuals are outlined here: number, shape, roughness, size, and spatial distribution. Measurements of individuals should only be used when one is sure that the features in section are indeed individuals or when the implications of them perhaps not being individuals in 3D are understood. The measurement of pore structure by assuming pore outlines seen in section (poroids) are individual pores is an important case.

Number
The measurement of number of objects in an image is trivial. The 3D nature of soil should be considered if such measurements are to be interpreted as an estimate the number of objects in the soil (Weibel, 1980).

Shape and curvature
Description of object shape has been studied extensively for 2D measurement (*e.g.* Clark, 1981). Currently, there is much interest in rapid description of shape in 3D scenes particularly for robot vision and unmanned vehicle navigation (*e.g.* Wang, 1991). The majority of shape description in micromorphology has used primitive shape descriptors.

The elongation of objects can be estimated using the ratio of maximum to minimum Ferret diameter (*e.g.* Norton and Schroeder, 1987). The circularity of objects has been described by relationships between the area and the square of perimeter. This has formed the basis of much pore structure measurement since the early 'seventies (Ismail, 1975). The use of convex perimeter or convex hull instead of perimeter results in a measure less sensitive to object
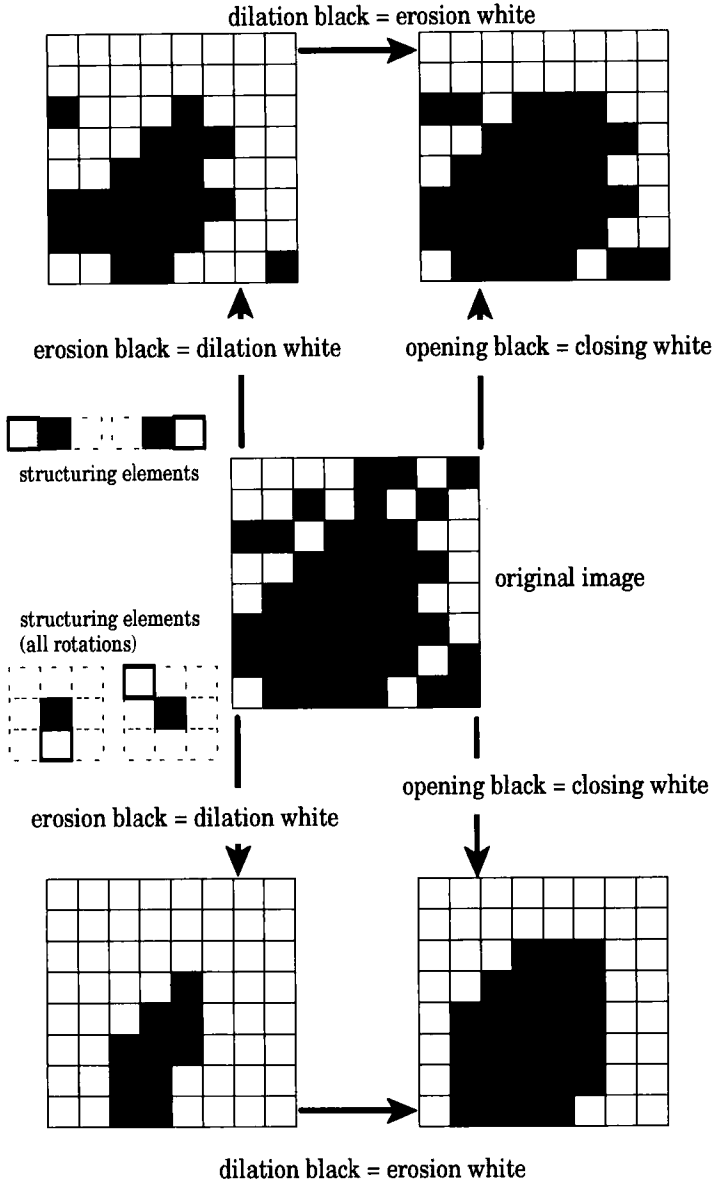
Fig. 3. Schematic examples of erosion, dilation, opening and closing with two different structuring elements.

boundary roughness (*e.g.* Ringrose-Voase and Bullock, 1984). Davis and Dexter (1972) characterised the asphericity of aggregates by comparing the difference in the length of a straight line between two points on the boundary to the distance between the points measured around the boundary.

Techniques using a Fourier transform of the boundary of an object (Schwarcz and Shane, 1969; Persoon and Fu, 1977) have the advantage that the transforms are reversible (Krzyzak *et al.*, 1989) and maintain an exact description of the objects assuming sufficient of the object boundary was digitised in the image. Davis and Dexter (1972) and Dexter (1985) found curvature and radius spectra generated using this technique successful for quantification of the shape of projections of soil aggregates.

Polygonal approximation of objects, emphasised in a discipline known as computational morphology (*e.g.* Toussaint, 1988), provides powerful shape descriptions. Objects are surrounded by lines until a polygon is formed. It is then possible to describe the nature of the polygon thereby quantifying the original object. The nature of the polygons can be controlled, *e.g.* controlling the minimum number of sides or the minimum length of any one side. Thus, the number distribution and orientation of line segments could be recorded, for example. The polygons may also be compared to other well-known shapes. This is in some ways analogous to circularity indices defined by comparison with a circle using area and perimeter (*e.g.* Ismail, 1975). Examples for micromorphology can be imagined. Hexagonal pore space formed in granodiorite saprolite may be formed by weathering of apatite. Sections through such pore space could be isolated by comparison with a hexagon. Detection of the number of sides needed to surround mineral grains in section may provide the basis for primary selection of some mineral species. The moments of an object, such as area, centre of gravity, orientation and moments of inertia, are fundamental attributes which are powerful shape descriptors (*e.g.* Teague, 1980). Moments can be transformed so that objects become scale, translation, rotation and reflection invariant (Hu, 1962). For example, one could use 3D polygonal approximation to describe soil aggregates of different shape. It may then be possible to study the movements of such aggregates under tillage by using invariant transformations of their moments.

A field which has gained greatly in application in image processing in the last few years is mathematical morphology, introduced formally by Serra (1982, 1988). Mathematical morphology is essestially a set-theory approach to image processing. The interactions between a template (known as a structuring element or kernel) and the image define set operations, *e.g.* intersections, unions. The template and the image are both treated as sets. Therefore, mathematical morphology is essentially for analysis of binary images. However, often there are grey level equivalents for the binary operations. The template is usually small compared to the size of the image to which it is being applied. The interaction of the image with a template lends objective meaning to the description (Shapiro *et al.*, 1987; Pitas and Venetsanopoulos, 1990). Different information about the same image can be generated by comparing it with different templates. The two most important operations are the erosion and dilation. The erosion operation removes pixels according to the template and the dilation adds pixels. If the template is symmetric, *i.e.* all neighbours are used, the erosion shrinks the image by one pixel everywhere and the dilation expands it (Fig. 3). The erosion of one of the binary components is the same as dilation of the other component. An opening is an erosion followed by a dilation of the resulting image; a closing is a dilation followed by an erosion. If the shape of the structuring element is changed the shape information is also changed (Fig. 3). The grey level equivalents of the erosion and dilation are the local neighbourhood minima and maxima, respectively. The examples presented in Fig. 3 do not consider edge effects.

An advantage of shape measurement is the ability to use shape definitions to define object classes (classify objects) and subsequently to allocate objects in the same or different images

into classes. If one has knowledge of the 3D shape of objects then the shapes that will be seen in section can sometimes be predicted. This is generally most useful for objects with simple shape, *e.g.* zircon grains assumed to be prolate spheroids (Moran *et al.* 1988). Schemes can then be designed to detect the 2D shapes. 3D parameters can then be estimated for shape classes using stereology (Weibel, 1979, 1980; Underwood, 1970). Ringrose-Voase and Bullock (1984) and Ringrose-Voase (1987) have applied these concepts to allocation of poroids in section. Poroids are assumed to be derived from cylindrical, sheet-like or irregular shapes in 3D. Parameters describing the nature of the 3D pores were estimated, using stereology, after allocation. Vogel *et al.* (1993) concluded that problems of automatically allocating shapes were prone to too much error. They developed a system that allowed the microscope operator to select pores of interest with the advantage of limited sight into the third dimension. The major features were recorded as circles and chords which formed the basis for a stereological analysis. Perhaps there is something to be gained for automatic pore allocation by examining two images; the first of which is focussed on the surface of the block and the second a little deeper to make a similar judgement.

Size

The frequency distribution of areas of objects can be used as an estimate of size distribution. A weighting of frequency may be necessary if objects are sampled from undisturbed sections as there is a greater probability of sectioning larger objects. Also, such a size distribution does not account for the nature of 3D objects represented in section. Stereological methods (Weibel, 1979, 1980; Underwood, 1970) can be used to "unfold" the 3D size distribution from the 2D distribution by making assumptions about the 3D shape of the objects. The 3D width distribution of cracks and length distribution of cylindrical pores, was unfolded in this manner by Ringrose-Voase and Nortcliff (1987). The chord size distribution has been used extensively in micromorphology to estimate sizes. Ringrose-Voase (1990) has discussed the relative merits of area and chord-length distributions for estimating pore size and recommends use of the latter.

Roughness

Measurement of roughness of objects in digital images can be confounded with image resolution issues. This may be especially apparent when comparing measurements of roughness of objects of different sizes. Simple estimates of roughness can be measured with little effort. The ratio of convex perimeter to perimeter, for example, is a shape-independent measure of the roughness of an object. This ratio has been used extensively in soil micropmorphology with success (*e.g.* Pagliai, 1987).

An estimator of roughness that has gained considerable attention in the last few years is the fractal dimension (Mandelbrot, 1967, 1977). This measure states that the length of a boundary (in the case of object roughness) is linearly related to the scale of measurement when considered on a log/log scale. Measurement of fractal dimension as an index of roughness involves measuring the same features several times, each time altering the resolution of the measuring device. A simple method involves counting the number of steps of fixed length required to surround an object; the beginning and end of each step must touch the boundary of the object. The same thing is repeated several times each time decreasing (or increasing) the length of the step. The number of steps is plotted against length of the step on a log/log scale and the slope of the line of best fit is used to estimate the fractal dimension. A manual method

similar to this was used by Young and Crawford (1992) to estimate the fractal dimension of line traces of fracture faces of soil aggregates. Alternatively one can alter the object rather than the measuring device. For example, when a morphological closing is performed on an object the boundary of the object is simplified. This simplification is result of removing edge lengths (or steps) of size one pixel; only those of size two pixels or greater remain. If a second closing is performed only step lengths greater than two remain, and so on. If the length of the perimeter of the object is measured after each closing the fractal dimension can be estimated from the slope of the log/log plot of closing number and perimeter. The use of the fractal dimension as an index of roughness is clearly justified. There have also been several attempts to attribute a more fundamental physical meaning to the fractal dimension (Tyler and Wheatcraft, 1989; Crawford *et al.*, 1993). Kaye (1989) provides a comprehensive account of methods for estimating the fractal dimension, its application and provides some sound cautionary words on the use of the dimension once measured.

Spatial distribution

The spatial spread of a set of points (known as a point process) can be quantified and described statistically (Diggle, 1983; Ripley, 1981; Upton and Fingleton, 1985; Cressie, 1991). The points themselves may be the original data, *e.g.* intersection of cracks and channels, or derived from a set of objects, *e.g.* centre of gravity of quartz grains. The points may be completely spatially random, regular, aggregated or non-stationary. A completely spatially random process is a realisation of a Poisson point process. Smettem and Collis-George (1985) measured such a process for distribution of biopores. A regular process is expressed as approximately the same distance between points. An aggregated process shows considerable clustering of points. Moran and McBratney (1992a) used this type of process to model the distribution of straws on the soil surface. A non-stationary process is a Poisson process which has an intensity gradient, *e.g.* fresh rock fragments may appear to be randomly distributed in sections taken down a profile but the average distance between fragments decreases with depth. A continuum exists between both random and regular processes and aggregated or clustered processes. Moran *et al.* (1988) tested the randomness and inhomogeneity of the distribution of zircon grains in thin sections and found some clustering in the parent material but a random distribution in the soil.

Estimates of the distance between points are used to test, measure and describe spatial distribution. Distances can be measured using point to point distances, *e.g,* distance to the nearest neighbour, the distance from points to some regular or random sampling grid, *e.g.* T-square sampling, or via a tesselation or triangulation of the points. Spatial distribution depends on the scale of observation and some caution should be exercised that spatial distribution is measured at the appropriate scale, *e.g.* biopores may appear Poisson over an area at one scale but over a wider area the occurrence may be clustered as certain organisms prefer an environmental niche. Eberhardt (1978) discusses a method based on line transects to estimate object density which may be considered a surrogate of distance for estimation of spatial distribution of objects rather than points.

Measurement of connected components

In this section images are considered to consist of two or more components. The aim of measurement is to gain information about each component and the interrelationships between components.

Quantity

The quantity of an image component is generally the proportion of the total number of pixels it occupies. It can be estimated by counting the pixels and dividing the sum by the total pixels in the image or the number of pixels of other components if a comparative measure is desired. This method was used by McBratney *et al.* (1992) to compute the area proportions (porosity) of surface-connected macropore space and total macropore space using 1D probes across each line in images of vertical sections based on the Delesse principle (Delesse, 1847).

Texture

"Image texture can be qualitatively evaluated as having one or more of the properties of fineness, coarseness, smoothness, granulation, randomness, lineation or being mottled, irregular, or hummocky" (Haralick, 1979). However, he also contends a formal approach or formal definition of texture does not exist even though it is widely and successfully used. The description of texture that is of most interest in soil micromorphology is identification and description of 2D patterns. There is a vast literature in this field; extensive reviews have been presented by Haralick (1979) and Wechsler (1980). The most widely accepted methods are based on spatial frequency analysis, first order statistics and higher order statistics and have been widely applied to medical and remotely-sensed image data.

Spatial frequency analysis is usually based on the spatial autocorrelation function, and the Fourier spatial domain or a mixture of both. The autocorrelation is a 2D function which describes the degree of correlation in an image at different distance offsets in both the x and y directions (Rosenfeld and Kak, 1982). Imagine two copies of the same image made on transparent film. One copy is kept stationary and the other is laid on top. The average transmission of light through the two copies is recorded as the first point in the resultant image. The top image is then shifted one pixel to the right and the transmission again recorded. The autocorrelation function is the image resulting from overlaying the top image over every pixel in the stationary copy. Fine-grained textures exhibit a high degree of correlation over short distances; the correlation length is longer for coarser fabrics. Periodicity in the texture appears as regular peaks in the function. Unfortunately, the autocorrelation function is not a very good discriminator of natural textures (Levine, 1985). However, Fourier analysis of the autocorrelation function has been more successful at discriminating texture using summaries of radial (frequency band) and angular components. Derbyshire *et al.* (1992) successfully quantified anisotropy patterns in sediment fabric using Fourier spatial domain representations.

Analysis of statistics, *e.g.* mean, variance, skewness and kurtosis, of neighbourhoods or other regions within images provide simple and often effective texture descriptions. Tovey and co-workers (*e.g.* Smart and Tovey, 1988; Tovey *et al.*, 1992) have published a great deal of work using methodology based on the grey level gradient in the local neighbourhood (local grey level differences) to quantify soil and sediment fabric orientation especially at the electron

microscope scale. It is likely that local statistics would be equally effective in distinguishing different soil fabric patterns at smaller scales.

Connectivity

A description of the connectivity of a three-dimensional object is the magnitude of its first topological dimension (also known as the genus, the first Betti number and the cyclomatic number). The genus is defined as the number of (non-self intersecting) cuts that may be made through an object without separating it into two disconnected parts (DeHoff *et al.*, 1972). The genus has been examined by Scott *et al.* (1988b) by quantifying serial sections of soil pore structure. They describe the genus as the number of passages in a network that can be blocked until only one passage remains through the network. The Euler number can be used as an estimate of the genus in images of 2D sections through 3D objects. The Euler number is the number of individual objects in the image less the number of holes in them. If one considers an image component to be isotropically distributed then it is possible to estimate its connectivity from a 2D section. If the assumption of isotropy is thought to hold locally then it may be reasonable to estimate the Euler number on sections taken locally. The interpolation of connectivity between the sections depends on the model assumed between sections. It would be interesting to compare the genus measured by Scott *et al.* (1988b) over an entire volume with estimates of the Euler number on individual sections.

Attempts have been made to estimate connectivity using markers of conducting pore space. The most common method has been use of Methylene blue (*e.g.* Bouma *et al.*, 1979). This has proved successful in some cases but adsorbtion of the dye and small areas for measurement cause some problems. Epoxy resin has also been used (Moran and McBratney, 1992b) to successfully quantify differences in connectivity due to long term cultivation and surface straw management.

Roughness

The measurement of roughness of a component is relatively easy using the fractal dimension (*e.g.* Bartoli *et al.*, 1991) (see above for more discussion on fractal dimension).

Size

Estimation of average size or size distribution of a component in an image is problematic. This is because area size measurement or separation into area size classes generally requires isolating individuals, which may not be desirable, *e.g.* connectivity of the component in the third dimension is unknown. It is possible to express size in terms of other attributes such as surface density or volume density. This obviates the need for description of individual objects as these attributes are expressed on a per unit volume (or area) basis. Chord (or intercept) lengths can also be used to estimate size distribution or average sizes.

The granulometry transformation from mathematical morphology (Serra, 1982) can be used to estimate size. This transformation consists of deriving all the erosions and dilations of a component, *i.e.* all the parts of a component of size one pixel are found by one erosion followed by a dilation (Fig. 3), parts of size two by two erosions followed by two dilations and so on. The histogram of the transformed image is the size distribution of the component. An estimate of the "average" size can be made by taking the size corresponding to the 50% frequency of the cumulative size distribution. This may provide an estimate of the median size rather than the mean if sizes are not normally distributed. The granulometry transform is not

IMAGE MEASUREMENT MODEL

Example
(McBratney & Moran, 1990)

| Aim of Measurement and Selection of Physical Process | **Aim**: Find potential infiltration throttles in seedbeds

Physical process: pore/solid structure |

↓

| Physical Process Model | **Dimensionality:**   **Statistical model:**
3D structure   horizontal isotropy
2 components   vertical heterogeneity
Information required about components :
Amount, size, contact and changes with depth |

↓

| Measurement Implementation Model | 2D vertical sections
Horizontal line probes
Stereology: Porosity, Surface density
Mathematical Morph.: Size |

Fig. 4. Flow diagram illustrating the proposed image measurement model and an example of its application.

stereologically equivalent to a volume distribution in 3D because the shape of the structuring element used for erosions and dilations imparts shape information into the transform. If assumptions regarding isotropy of the component in the third dimension are reasonable then a spherical structuring element (or the closest digital equivalent) provides a volume distribution estimate. Moran and McBratney (1992a) successfully used the granulometry transform to estimate the area of soil and straw patches in digitised photographs of the soil surface.

Association
    The association between two or more components is often the primary information required from an image. The perimeter between any two phases is a sensitive measure of association. The surface area density is a stereological measurement of the surficial contact between components estimated from the perimeter. The surface area density does not indicate the spatial relationship, however, unless some systematic sampling is used (*e.g.* McBratney and Moran, 1990).

Table 1
Evolution of image measurement.

	Individual features	**Structural parameters**	**Geometrical parameters and modelsfor physical models**
Date	1960's - present	1980's - present	1990's ->
Basis	counting, quantifying features related to pedofeatures *e.g.* number of large thin pores.	stereologically-based geometric parameters *e.g.* volumetric surface area.	physically meaningful geometric parameters *e.g.* diffusion radius.
Problems	No stereological basis	Assumptions of isotropy *etc.*	linkage between geometry and physical models

A useful measure of the association between two components in an image is the distribution of distances between the components in the image. This can be derived using the distance transform (Borgefors, 1986). This is equivalent to the granulometry transform mentioned above except that it represents the erosions only. Thus the expected distance from one component to another can be estimated from the 50% frequency of the cumulative erosion distribution. This can provide information such as the diffusion length from solid to pore space or distance from a root to pore space. McBratney and Moran (1990) measured the size of solid material and pore space in vertical sections using this method. The measure thus defined is known as the star length. The star length is equivalent to the length-weighted mean intercept length.

Image measurement model

As the review of measurement options above indicates there is a plethora of image measurement options available. It is not a simple task for the non-specialist to determine which measurements are best for the desired quantification. An image measurement model may assist in the selection of appropriate attributes (Fig. 4). A non-specialist in image processing should however know what information is desired. The first, and non-trivial, step is to establish the aim of the image measurement and decide which physical process needs to be quantified to achieve the stated aim. A model describing the nature of the physical process (or specific features) can then be formulated. Such a model provides a framework for the selection of appropriate measurements and its specification may also suggest a measurement methodology. The model specifies the dimensionality of the process, and a mathematical or statistical process description. It also lists the information required to fulfil the measurement aim. The measurement implementation model outlines a sampling strategy and specifies the measurement algorithms that are used to derive the information required for the physical process model. An image measurement expert could be consulted for the final stage. If the

other stages are completed reasonably well the specialist should have little trouble in guiding the soil scientist towards a set of tools which will fulfil the demand.

Evolution of image measurement

The evolution from inquisitiveness about image processing technology to the need for meaningful and reusable measurements can be traced through the measurement history of pore structure (Table 1). Initially, measurements were dictated by the capability of the new technology. Most early work in the Netherlands (Ismail, 1975) and at Rothamsted (Bullock and Thomasson, 1979) took output from the Quantimet and then attempted to relate measurements to physical processes. This amounted to quantifying and counting pedofeatures and is still successfully carried-out today (*e.g.* Gimenez *et al.*, 1992). Little consideration was given to the problem of measurement of a 3D network on 2D sections and outlines of pores in thin sections were considered to represent individual pores in the third dimension. Such measurements provide reasonable indices for comparison of treatments in field experiments, for example, but their applicability as a characterisation of the 3D network is at best limited.

Through the 1980's development of image measurement models began to progress. The use of stereology with appropriate assumptions regarding isotropy and heterogeneity consider the 3D nature of the physical process (*e.g.* Ringrose-Voase, 1987; McBratney and Moran, 1990). This indicates a development in description of structure and some maturing of our understanding of the relationship between 2D sections and the 3D pore structure. However, the re-usability of these measurements and their relationship with more conventional descriptions of structure using water or gas flow and storage are limited, *e.g.* empirical comparisons of moisture characteristics with results which vary greatly. Some work combining staining with Methylene blue and image measurement has succeeded in improving estimates of hydraulic conductivity (Bouma *et al.*, 1979). Unfortunately, there is little scope for dealing with the dynamics of pore structure, *e.g.* what are the implications for water flow that mean intercept length changes by 20% when water content changes by 20% - at best a semi-quantitative response to such a question could be attempted.

One measure, some say the only measure, of the utility of science is its predictive capability. Description of a physical process undoubtedly improves our predictive capacity. Another method is through the use of numerical models. Structure measurements which have both descriptive power and the potential for incorporation in models have been developed. The measurements of Scott *et al.* (1988a,b) have the advantage over others in that they are direct 3D measurements. Unfortunately, this work appears to have been discontinued and the development of structure simulations or process simulations, *e.g.* water flow, using these data has not occurred. Similarly, Yanuka *et al.* (1986) presented 3D measurement data using serial section analysis. This work also included simultaneous development of a simulation model from the measured information. This work consisted of locating points randomly within the measured 3D pore structure and recording the local information as the fit of a disc within the pore or solid space. Unfortunately, part two of this paper which was to compare the modelling results and the measured structures does not seem to have been published yet. A similar approach was used by Glaseby *et al.* (1991) who used spheres rather than discs. The sizes of spheres were controlled by statistical distributions rather than measurement of serial sections.

Recently, the world-wide interest in description of natural phenomena using fractal dimensions has been introduced into the soil micromorphology literature (Bartoli *et al.*, 1991;

Hatano *et al.*, 1992). The early success with these parameters indicates some potential for expanding our descriptive capabilites beyond one scale of observation. There is also some exciting work on the simultaneous development of a measurement and modelling framework (Crawford *et al.*, 1993; Rapoldt, 1990). In both these papers, estimates of structural attributes from thin sections and/or blocks have been included into simulation models for diffusion. The former paper uses a fractal approach using the ratio of two different estimates of fractal dimension; one for roughness the other for tortuosity. The latter paper introduces the diffusion radius a structural attribute estimated from sections. Combined measurement and modelling research such as this can potentially provide a link between more conventional physical measurements and information generated using micromorphological techniques.

All the descriptive and modelling methods published to date treat the soil at the scale of measurement as a binary process, *i.e.* each element is either pore or solid. This ignores our knowledge that the portion of material at any scale that is not resolvable as pore space often has a porosity greater than zero. This is addressed in the pore structure model proposed by McBratney and Moran (1994).

IMAGE MODELLING

Image modelling is the use of an image processing framework to simulate attributes of a system and/or to simulate processes that act on measured or simulated attributes. The intention here is to introduce image modelling and briefly discuss some of its potential. Examples of simulation of an attribute and a process are provided. More comprehensive examples of attribute modelling are available for soil surface cover (Moran and McBratney, 1992a) and for soil pore structure (McBratney and Moran, 1994).

Image modelling provides a framework for physical process modelling in more than one dimension. We can take advantage of many of the tools available for manipulating and visualising multi-dimensional images. Measured and simulated data can be mixed within the models relatively easily. We can study many combinations of attributes that are not feasible under physical experimental conditions. This can be used to aid selection of physical experiments. Image modelling facilitates examination of changes in measured attributes. Image processing tools for transformation, *e.g.* interpolation, are available and may be applied to some measured images. For example, a sequence of images measured at various time intervals can be interpolated to provide information on rate and an estimate of the condition of the attribute between the times measured.

Models can be used to test the descriptive quality of well-known measurements and to develop new measurements. Consider a simulation of a physical phenomenon; the statistical nature of the simulation is well known and understood. If attributes measured on the simulation provide a meaningful description of the simulation then one can have confidence that measurement of the same attributes on specimens of the real phenomenon are justified. It may also be possible to use simulations of processes to define attribute measurements. For example, if one developed a model for unsaturated flow through images of pore structures it would be possible to derive the conductivity vs water content relationship. This is an example where the functional attribute is already known in soil science but discovery of useful new relationships is also possible. Finally, an image processing framework is a convenient structure for implementation of models using massively parallel computers. This is important as
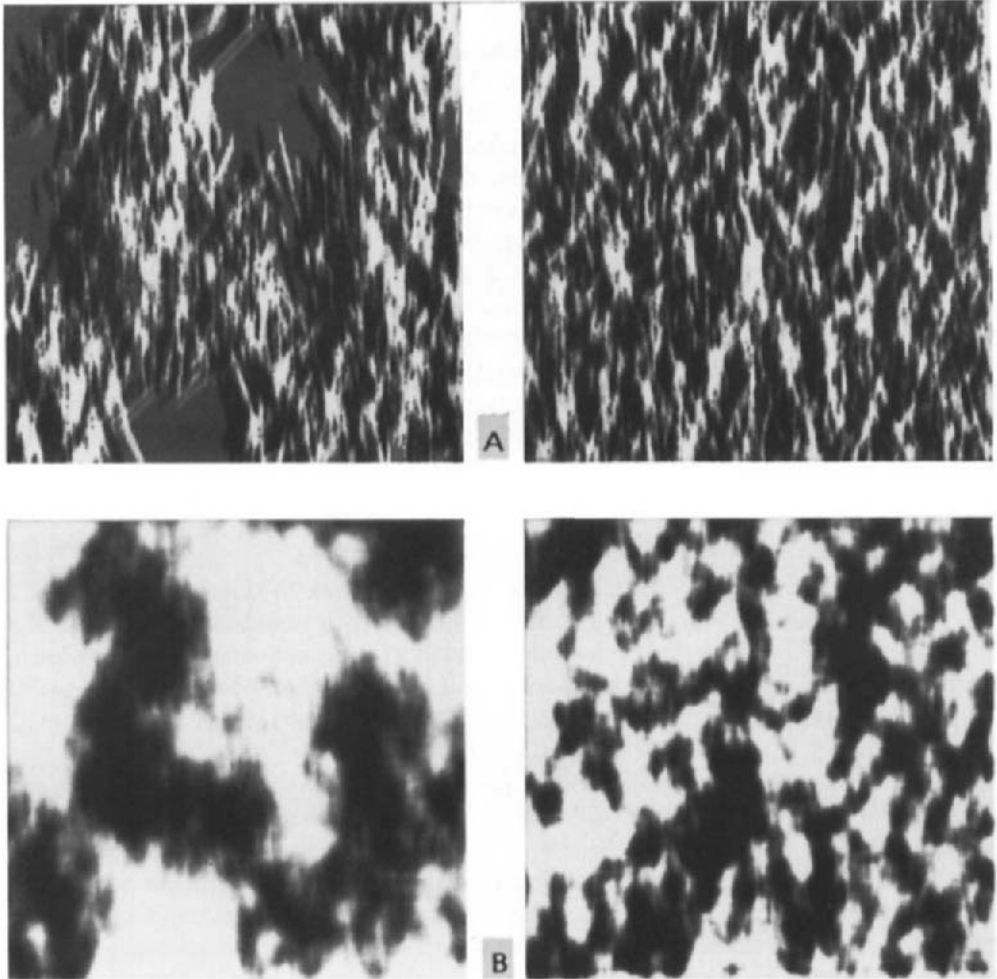
Fig. 5. A) Two examples of simulated binary straw cover. B) Conversion of the straw coverages in A) into hydraulic roughness maps.

simultaneous simulation of more than one physical process in more than one dimension can be computationally intensive.

Moran and McBratney (1992a) presented an image model for simulation of the 2D distribution of straw. The straw coverage was built-up by locating the centres of straws of length l in a random field and giving them orientation θ using a controlled clustering process. Several realisations of their model are shown in Fig. 5A. The same amount of cover is shown but with different spatial distributions.
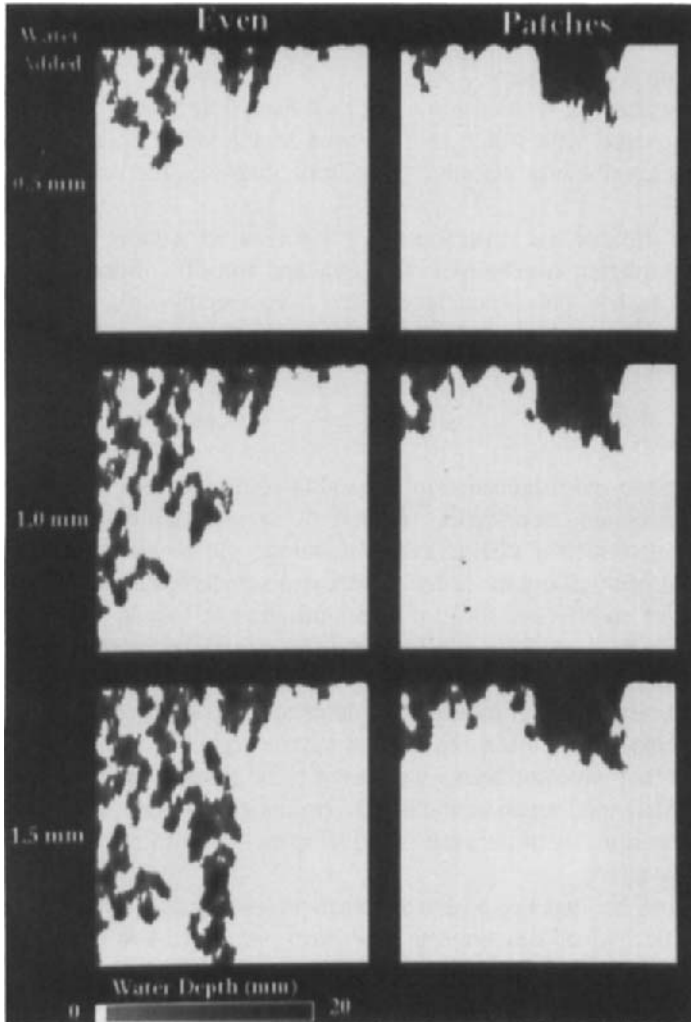
Fig. 6. Simplistic simulation of trickle water flow into the hydraulic roughness maps in Fig. 5B.

A simulation of the effect of the straw cover on surface water flow is used as an illustration of process modelling. The simulation is simplistic but will suffice as a more detailed example would be a paper in itself. First, the straw surface cover is converted to hydraulic roughness. This is achieved by giving the straw an arbitrary value of 1 and the soil 0. Next, a large (21 × 21) mean filter is passed over the straw image. The maximum thickness of stacked straw is assumed to be 50 mm. The mean image is then scaled by the maximum of the mean image divided by 50. The result is a hydraulic roughness image with a minimum of zero (soil) up to a maximum of 50 mm for stacked straw. This image is then treated as though is was an elevation image. Fig. 5B shows the two simulations from Fig. 5A as hydraulic roughness images with a shaded view provided to show the shape of the resulting roughness. A simplistic water flow algorithm, analogous to trickle flow, is applied in which water flows to the least rough parts of the image that are connected to the water entry point. The boundary condition

is that the edges of the hydraulic roughness image are infinitely large, thus water cannot flow off the surface. The effect of the two spatial distributions of straw on routing of water is shown for three stages of water accumulation in Fig. 6. The entry point for the water in both cases was every pixel along the top of the images.

An example of defining a new attribute relationship using such modelling would be to plot the proportion of the surface covered with water as a function of the water added to the surface. Such a function could describe how effectively the straw disperses the water if the model is valid.

This simulation is somewhat artificial but it demonstrates a portion of a more complete simulation which would include surface roughness, infiltration and run-off. Specification, implementation and validation of such models is not claimed here to be a simple task. Rather, it is a challenge for those interested in combining new technology and numerical solutions to difficult spatial and temporal problems.

CONCLUSIONS

Colour is an important descriptive and diagnostic tool for soil micromorphologists. Colour image processing capability is becoming accessible. Therefore, an understanding of how colour is perceived, how computers display colour and how colour can be manipulated is useful for its effective use. The Munsell colour order system is a standard, familiar to soil miromorphologists which provides an effective tool for communication of colour. Standard image display tools can be applied to images from micromorphology to provide context for the images and assist understanding of the data.

There are many options for measurement of individual features and connected components in images of soil. Some measurements have been exploited in micromorphology but there are many potentially useful methods that have not been widely used. The primary task of image measurement is to provide quantitative information about soil. An image measurement model, which takes into account the dimensionality of the system and its spatial properties, can aid the selection of appropriate measurements.

Soil attributes and processes can be modelled within an image processing framework. This is convenient for developing models which can simulate more than one process in more than one dimension simultaneously. This type of model is well-suited to current parallel computing technology because of the geometric structure of the images. Measurements which provide a reliable description of models whose statistical properties are known may also be effective in describing the process or attribute being modelled.

ACKNOWLEDGEMENTS

REFERENCES

Bartoli, F., Philippy, R., Doirisse, M., Niquet, S. and Dubuit, M., 1991. Structure and self-similarity in silty and sandy soils: the fractal approach. J. Soil Sci., 42: 167-185.

Borgefors, G., 1986. Distance transforms in digital images. Computer Vision Graphics and Image Processing, 34: 344-371.

Bouma, J., Jongerius, A. and Schoonderbeek, D., 1979. Calculation of saturated hydraulic conductivity of some pedal clay soils using micromorphometric data. Soil Sci. Soc. Am. J., 43: 261-264.

Bullock, P. and Thomasson, A.J., 1979. Rothamsted studies of soil structure II. Measurement and characterisation of macroporosity by image analysis and comparison with data from water rentention measurements. J. Soil Sci., 30: 391-413.

Clark, M.W., 1981. Quantitative shape analysis: a review. J. Math. Geol., 13: 303-320.

Crawford, J.W., Ritz, K. and Young, I.M., 1993. Quantification of fungal morphology, gaseous transport and microbial dynamics in soil: An integrated framework using fractal geometry. Geoderma, 56: 157-172.

Cressie, N.A.C., 1991. Statistics for Spatial Data. John Wiley and Sons, New York. 896pp.

Davis, P.F. and Dexter, A.R., 1972. Two methods for quantitative description of soil particle shape. J. Soil Sci., 23: 448-455.

DeHoff, R.T., Aigeltinger, E.H. and Craig, K.R., 1972. Experimental determination of the topological properties of three-dimensional microstructures. J. Microsc., 95: 69-91.

Delesse, M.A., 1847. Procédé mécanique pour déterminer la composition des roches. C.R. [Hebd. Séanc.] Acad. Sci., 25: 544-545.

Derbyshire, E., Unwin, D.J., Fang, X.M. and Langford, M., 1992. The Fourier frequency-domain representation of sediment fabric anisotropy. Computers and Geosciences, 18: 63-73.

Dexter, A.R., 1985. Shapes of aggregates from tilled layers of some Dutch and Australian soils. Geoderma, 35: 91-107.

Diggle, P.J., 1983. Statistical Analysis of Spatial Point Patterns. Academic Press, London, 148 pp.

Eberhardt, L.L., 1978. Transect methods for population studies. Journal of Wildlife Management, 42: 1-31.

Gimenez, D., Dirksen, C., Miedema, R., Eppink, L.A.A.J. and Schoonderbeek, D., 1992. Surface sealing and hydraulic conductances under varying-intensity rains. Soil Sci. Soc. Am. J., 56: 234-242.

Glaseby, C.A., Horgan, G.W. and Darbyshire, J.F., 1991. Image analysis and three-dimensional modelling of pores in soil aggregates. J. Soil Sci. 42: 479-486.

Haralick, R.M., 1979. Statistical and structural approaches to texture. Proceedings of the IEEE, 67: 786-804.

Hatano, R., Kawamura, N., Ikeda, J. and Sakums, T., 1992. Evaluation of the effect of morphological features of flow paths on solute transport by using fractal dimensions of methylene blue staining pattern. Geoderma, 53: 31-44.

Hu, M., 1962. Visual pattern recognition by moment invariants. IRE Trans. Inf. Theory, 8: 179-187.

Ismail, S.N.A., 1975. Micromorphometric soil-porosity characterisation by means of electro-optical image analysis (Quantimet 720). Soil Survey Paper No 9. Netherlands Soil Survey Institute, Wageningen.

Kaye, B.H., 1989. A Random Walk Through Fractal Dimensions. VCH Verlagsgesellschaft, 421 pp.

Krzyzak, A., Leung, S.Y. and Suen, C.Y., 1989. Reconstruction of two-dimensional patterns from Fourier descriptors. Machine Vision and Applications, 2: 123-140.

Levine, M.D., 1985. Vision in Man and Machine. McGraw-Hill Book Co., New York, 574 pp.

Mandelbrot, B.B., 1967. Fractals: Form, Chance and Dimension. W.H. Freeman and Co., San Francisco, 361 pp.

Mandelbrot, B.B., 1977. "How long is the coast of Britain?". Statistical self-similarity and fractional dimension. Science, 155: 636-638.

McBratney, A.B. and Moran, C.J., 1990. A rapid method of analysis for soil macropore structure. II. Stereological model, statistical analysis, and interpretation. Soil Sci. Soc. Am. J., 54: 509-515.

McBratney, A.B. and Moran, C.J., 1994. Soil pore structure modelling using fuzzy random pseudofractal sets. In: A.J. Ringrose-Voase and G.S. Humphreys (Editors), Soil Micromorphology: Studies in Management and Genesis. Proc. IX Int. Working Meeting on Soil Micromorphology. Developments in Soil Science, 22. Elsevier, Amsterdam, pp. 495-506.

McBratney, A.B., Moran, C.J., Stewart, J.S., Cattle, S. and Koppi, A.J., 1992. Modifications to a rapid method for analysis of soil pore structure. Geoderma, 53: 255-274.

Moran, C.J. and McBratney, A.B., 1992a. Image measurement and modelling of the two-dimensional spatial distribution of wheat straw. Geoderma, 53: 201-216.

Moran, C.J. and McBratney, A.B., 1992b. Acquisition and analysis of three-component digital images of soil pore structure. II. Application to seed beds in a fallow management trial. J. Soil Sci., 43: 551-566.

Moran, C.J. and Vezina, G., 1993. Visualising soil surfaces and crop residues. IEEE Computer Graphics and Applications, 13: 40-47.

Moran, C.J., McBratney, A.B. and Koppi, A.J., 1988. A micromorphometric method for estimating change in the volume of soil induced by weathering. J. Soil Sci., 39: 357-373.

Norton, L.D. and Schroeder, S.L., 1987. The effect of various cultivation methods on soil loss: A micromorphological approach. In: N. Fedoroff, L.M. Bresson and M.A. Coutry (Editors), Soil Micromorphology. Proc. VII Int. Working Meeting of Soil Micromorphology, Paris, July 1985. Association Française pour l'Etude du Sol, Plaisir, France, pp. 431-436.

Pagliai, M., 1987. Effects of different management practices on soil structure and surface crusting. In: N. Fedoroff, L.M. Bresson and M.A. Coutry (Editors), Soil Micromorphology. Proc. VII Int. Working Meeting of Soil Micromorphology, Paris, July 1985. Association Française pour l'Etude du Sol, Plaisir, France, pp. 415-421.

Persoon, E. and Fu, K.S., 1977. Shape discrimination using Fourier descriptors. IEEE Trans. Syst. Man Cyber., 7: 170-179.

Pitas, I. and Venetsanopoulos, A.N., 1990. Morphological shape decomposition. IEEE Transactions on Pattern Analysis and Machine Intelligence, 12: 38-45.

Pratt, W., 1978. Digital Image Processing. John Wiley and Sons, New York, 352 pp.

Protz, R., Sweeney, S.J. and Fox, C.A., 1992. An application of spectral image analysis to soil micromorphology, 1. Methods of analysis. Geoderma, 53: 275-287.

Rapoldt, C., 1990. The application of diffusion models to an aggregated soil. Soil Sci., 150: 645-661.

Ringrose-Voase, A.J., 1987. A scheme for the quantitative description of soil macrostructure by image analysis. J. Soil Sci., 38: 343-356.

Ringrose-Voase, A.J., 1990. One dimensional image analysis of soil structure. J. Soil Sci., 41: 499-512.

Ringrose-Voase, A.J., 1991. Micromorphology of soil structure: description, quantification, application. Aust. J. Soil Res., 29: 777-813.

Ringrose-Voase, A.J. Measurement of soil pore geometry by image analysis. In: A.J.M. Smucker and S.H. Anderson (Editors), Quantifying Root and Soil Dynamics. Am. Soc. Agron. Spec. Publ. (In Press).

Ringrose-Voase, A.J. and Bullock, P., 1984. The automatic recognition and measurement of soil pore types by image analysis and computer programs. J. Soil Sci., 35: 673-684.

Ringrose-Voase, A.J., and Nortcliff, S., 1987. The application of stereology to the estimation of soil structural properties: A preview. In: N. Federoff, L.M. Bresson and M.A. Courty (Editors), Soil Micromorphology, Proceedings of VIIth International Working Meeting on Soil Micromorphology, Paris, July 1985. L'Association Française pour l'Etude du Sol, pp. 81-88.

Ripley, B.D., 1981. Spatial Statistics. John Wiley and Sons, New York. 252 pp.

Robertson, P.K., 1988. Visualising colour gamuts: A user interface for the effective use of perceptual color spaces in data displays. IEEE Computer Graphics and Applications 8: 50-64.

Rosenfeld, A. and Kak, A.C., 1982. Digital Picture Processing. Academic Press, New York. 487 pp.

Russ, J.C., 1990. Computer-assisted Microscopy: The Measurement and Analysis of Images. Plenum, New York. 453 pp.

Schwarcz, H.P. and Shane, K.C., 1969. Measurement of particle shape by Fourier analysis. Sedimentology, 13: 213-231.

Scott, G.J.T., Webster, R. and Nortcliff, S., 1988a. Topology of pore structure in cracking clay soil. I. The estimation of numerical density. J. Soil Sci., 39: 303-314.

Scott, G.J.T., Webster, R. and Nortcliff, S., 1988b. Topology of pore structure in cracking clay soil. II. Connectivity density and its estimation. J. Soil Sci., 39: 315-326.

Serra, J., 1982. Image Analysis and Mathematical Morphology. Academic Press, London, 610 pp.

Serra, J., 1988. Image Analysis and Mathematical Morphology. Volume 2: Theoretical advances. Academic Press, London, 411 pp.

Shapiro, L.G., MacDonald, R.S. and Sternberg, S.R., 1987. Ordered structural shape matching with primitive extraction by mathematical morphology. Pattern Recognition, 20: 75-90.

Smart, P. and Tovey, N.K., 1988. Theoretical aspects of intensity gradient analysis. Scanning, 8: 75-90.

Smettem, K.R.J. and Collis-George, N., 1985. Statistical characterization of soil biopores using a soil peel method. Geoderma, 36: 27-36.

Sweeney, S.J., Protz, R. and Fox, C.A., 1992. An application of spectral image analysis to soil micromorphology, 2. Comparison of two soil profiles. Geoderma, 53: 341-355.

Teague, M., 1980. Image analysis via the general theory of moments. Journal of the Optical Society of America, 70: 121-134.

Terribile, F. and FitzPatrick, E.A., 1992. The application of multilayer digital image processing techniques to the description of soil thin sections. Geoderma, 55: 159-174.

Toussaint, G.T., 1988. Computational Morphology: A Computational Geometric Approach to the Analysis of Form. Elsevier, Amsterdam, 261 pp.

Tovey, N.K., Smart, P., Hownslow, M.W. and Leng, X.L., 1992. Automatic orientation mapping of some types of soil fabric. Geoderma, 53: 179-200.

Travis, D., 1991. Effective Color Displays: Theory and Practice. Academic Press, London, 301 pp

Tyler, S.W. and Wheatcraft, S.W., 1989. Application of fractal mathematics to soil water retention estimation. Soil Sci. Soc. Am. J. 53: 987-996.

Underwood, E.E. 1970. Quantitative Stereology. Addison Wesley, Reading, Mass. 378 pp.

Upton, G.J.G. and Fingleton, B., 1985. Spatial Data Analysis by Example. Volume I. Point Pattern and Quantitative data. John Wiley and Sons, Chichester, U.K., 409 pp.

Vogel, H.J., Weller, U. and Babel, U., 1993. Estimating orientation and width of channels and cracks at soil polished blocks - a stereological approach. Geoderma, 56: 301-316.

Wang, Y.F., 1991. Characterising three-dimensional surface structure from visual images. IEEE Transactions on Pattern Analysis and Machine Intelligence, 13: 52-60.

Wechsler, H, 1980. Texture analysis: A survey. Signal Processing, 2: 271-282.

Weibel, E.R., 1979. Stereological methods. Vol. 1. Practical Methods for Biological Morphometry. Academic Press, London, 415pp.

Weibel, E.R., 1980. Stereological Methods. Vol. 2. Theoretical Foundations. Academic Press, London, 340pp.

Wyszecki, G. and Stiles, W.S., 1967. Color Science: Concepts and Methods, Quantitative Data and Formulas. John Wiley and Sons, New York, 628 pp.

Yanuka, M., Dullien, F.A.L. and Elrick, D.E., 1986. Percolation processes and porous media I. Geometrical and topological model of porous media using a three-dimensional joint pore size distribution. Journal of Colloid and Interface Science, 112: 24-41.

Young, I.M. and Crawford, J.W. 1992. The analysis of fracture profiles of soil using fractal geometry. Aust. J. Soil Res., 30: 291-295.

Some principles to be observed in the quantitative analysis of sections of soil

A.J. Ringrose-Voase

CSIRO Division of Soils, GPO Box 639, Canberra, ACT 2601, Australia

ABSTRACT

Ringrose-Voase, A.J. 1994. Some principles to be observed in the quantitative analysis of sections of soil. In: A.J. Ringrose-Voase and G.S. Humphreys (Editors), Soil Micromorphology: Studies in Management and Genesis. Proc. IX Int. Working Meeting on Soil Micromorphology, Townsville, Australia, July 1992. Developments in Soil Science 22, Elsevier, Amsterdam, pp. 483-493.

Image analysis of sections can be used to derive quantitative information about the structure of opaque materials such as soil. Some basic stereological principles must be observed when measuring sections because the measurements are being made in less than three dimensions. Five topics of particular relevance to analysis of sections of soils are discussed.

Firstly, correct procedures must be observed at the edges of the frame in which measurements are being made. If discrete objects are being counted, a forbidden line along two adjacent edges should be used. Any object wholly or partly within the frame should be measured in its entirety unless it touches the forbidden line.

In order for the sampling scheme to be unbiased sections should be randomly positioned in the material and be oriented at different angles selected either randomly or systematically. The latter is necessary to avoid bias if the structure is anisotropic.

Measurements can be made in 0-D, 1-D or 2-D by using point counting, test lines or 2-D images, respectively. These are stereologically related to each other and to the true 3-D parameters defining the structure. The best strategy for choosing which measurements to make in 0-D, 1-D or 2-D is to first decide which 3-D parameters best describe the structure in question. It is sensible to consider carefully what shapes in 3-D gave rise to the objects being measured in 2-D, so that appropriate 2-D or 1-D measurements can be made.

One parameter to be treated with caution is the number of discrete objects per unit area of section, N_A. If the objects are discrete in 3-D, the value of N_A will depend not only on the number of objects per unit volume, N_V, but also on their size. In many cases, such as pore space, the 'discrete' objects seen in 2-D are interconnected in 3-D. N_A is not easily related to any 3-D parameter in this case, except where the structure is linear, such as channels, for which N_A is related to the length per unit volume.

Size distributions require a size parameter and an 'amount' parameter. Where the structure consists of discrete objects in 3-D, the size distribution can be expressed as N_V in each size class. For objects with simple geometric shapes, this can sometimes be estimated by measuring N_A of each size class in 2-D. In structures where N_A is difficult to interpret, alternative parameters to express the amount must be found.

INTRODUCTION

Sections provide a means of seeing the structure of an opaque material. Sections at a variety of magnifications can be used to investigate the structure and fabric of soils. Soil micromorphologists traditionally use thin sections observed under the petrological microscope. Sections can also be faces of polished blocks studied at the submicroscopic scale using SEM in back-scattered electron mode and at micro to mesoscopic scales using reflected light or fluorescent illumination. Sections also include horizontal ledges or vertical faces in soil pits for investigations at macroscopic scales.

In this context, sections are flat 2-D planes which cut through the structure. Sections do not include fracture surfaces as studied, for example, using SEM.

Sections are frequently analysed quantitatively or semi-quantitatively to allow statistical comparison between different soils or horizons or between soils subjected to different treatments. Image analysis of sections can be carried out manually or automatically in 2-D, in 1-D using test lines or in 0-D using point counting. However, measurements made in less than 3-D should be interpreted with care and are the subject of stereology. The principles of stereology as applicable to soil pore structure have been discussed previously by Ringrose-Voase and Nortcliff (1987). This paper attempts to highlight five topics which have particular relevance to the quantitative analysis of sections of soil. Whilst the stereology involved is well established, they are topics which have frequently been overlooked in soil micromorphology.

EDGE EFFECTS

A very basic, but nonetheless important procedural matter, concerns the measurement of objects that touch the edges of an image. The rules to avoid bias depend on whether the measurements relate to a given component in its entirety (*e.g.* the pore space) or to individual objects in the image (*e.g.* poroids). In the former case all parts of the component within the measuring frame are measured. For example, if the total area of the component in an image is being measured, then all the area within the frame is measured as shown in Fig. 1a.

When objects are being considered individually, it is necessary to use a 'forbidden' line along two adjacent edges of the frame as shown in Fig. 1b (Gundersen, 1977). Any object that falls wholly or partially within the frame should be measured in its entirety, unless it touches the forbidden line, in which case it is not measured as shown in Fig. 1b. The reasons for this are two fold. First, if all the objects within the frame are included whether or not they touch the frame, the number of objects per unit area will be overestimated. Similarly, the number of objects will be underestimated, if any object touching any edge is excluded. This can be illustrated by considering an image being measured using several adjacent frames as in Fig. 1b. If the forbidden line rule is followed then each object is only included in the measurement for one frame. Otherwise objects will be either counted twice or never counted. Second, if only those parts of objects within the frame are measured, the measurement will be underestimated for objects touching the frame, which will, in turn, cause the mean for all objects to be underestimated. Therefore it is also necessary to have a sufficiently large border region beyond those edges which are not part of the forbidden line so that objects crossing these edges can be measured without being truncated by the outer edges of the image.
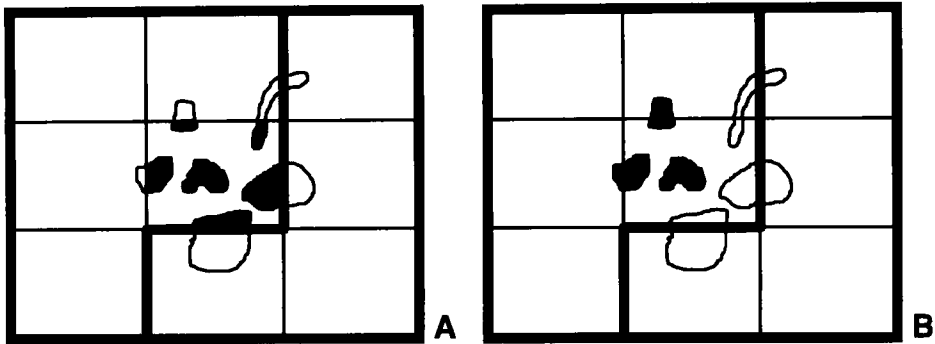
Fig. 1. Measurement of objects touching image edges. a) Measurement of the total area of a component should include all the component within the frame (filled areas). b) Measurements of individual objects should include only those not touching the forbidden line (shown thick).

SECTION ORIENTATION

Analysing anisotropic structures

Most traditional stereological methods assume that the component of the structure being measured is isotropic (*i.e.* with no preferred orientation) or that replicate sections at random orientations are being used. Soil structure is frequently anisotropic and estimates of 3-D parameters will be biased if measurements are made on sections at a single orientation using standard stereological formulae. This can be illustrated by considering the structure in Fig. 2 which consists of vertically oriented channels with length density[1] (length per unit volume), L_V, equal to 4. The standard stereological equation for estimating L_V from the 2-D intersect density (number of intersects per unit area), Q_A, is (Weibel, 1979, pp. 38):

$$L_V = 2Q_A \tag{1}$$

This assumes the channels have random orientation so that a section should on average have 2 channel intersects per unit area. However, in Fig. 2 vertical and horizontal sections will, on average, have Q_A equal to 0 and 4 respectively. Using Eqn. 1 measurements made only on horizontal or only on vertical sections will clearly over or underestimate L_V.

This problem can be overcome in one of three ways: using randomly oriented sections; using systematically oriented sections and modifying the stereological equations to take the anisotropy into account.

Randomly oriented sections

Selecting random orientations is analogous to selecting random sampling locations in a field. The orientation of a section is described by θ (the angle of its normal from the vertical) and ϕ

---

[1] In stereology, 'density' refers to a quantity (*e.g.* volume, area, number) per unit volume, unit area or unit length. These are denoted by subscript V, A and L respectively.
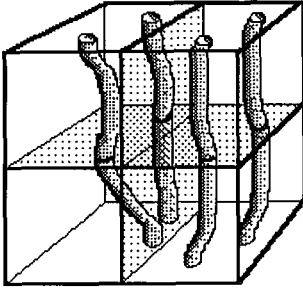
Fig. 2. Channels showing preferred vertical orientation (anisotropy). (From Ringrose-Voase and Nortcliff, 1987).

(the orientation of its normal in the horizontal plane). ϕ can be selected randomly or it can be assumed that there is no preferred orientation in the horizontal plane. However, values of θ must be chosen by selecting random values of $\cos\theta$. This is necessary because the probability of selecting a random orientation in 3-D is $d\theta(\sin\theta \cdot d\phi)$. (Imagine a globe with equally spaced lines of latitude, θ, and longitude, ϕ. The areas of each grid 'square', which are proportional to the probability of selecting those values of θ, ϕ, get smaller towards the poles). Therefore selecting random values of θ would cause low values (*i.e.* sections near to horizontal) to be over represented (see Weibel, 1980, pp. 41-47; Ringrose-Voase and Nortcliff, 1987).

Systematically oriented sections

The second option, selecting orientations systematically, is analogous to using grid sampling in the field and can be more efficient than random sampling (McBratney and Webster, 1983). ϕ can either be ignored, if there is no preferred orientation in the horizontal plane, or selected by regularly spaced values between 0 and 360°. Values of θ are selected by chosen regular intervals of $\cos\theta$ between 0 and 1, and taking the mid-point of each interval. If three values were appropriate, they would correspond to $\cos\theta$ of 1/6, 3/6 and 5/6 (*i.e.* 33.6°, 60.0° and 80.4°).

That these orientations give a correct estimate of L_V can be checked as follows using the structure in Fig. 2. The estimated number of vertical channels intersected by a section whose normal is at θ to the vertical is proportional to the projected area of the section in the horizontal plane, *i.e.* $A \cdot \cos\theta$, where A is the section area. The number intersected is $L_V \cdot A \cdot \cos\theta$. If $L_V=4$ units/unit^3 and the sections are of unit area, the number intersected by sections at 33.6°, 60.0° and 80.4° will be 3.33, 2.00 and 0.67 respectively. The mean Q_A is 2 and the estimate of L_V using Eqn. 1 is 4. Note that, although the mean of horizontal and vertical sections would also give approximately the correct estimate in this case, this is not always the case.

Assumption of anisotropic models

The final option, modifying the stereological equation, requires *a priori* knowledge of the anisotropy. For example, if it can be assumed in advance that the structure in Fig. 2 consists of vertical channels, the best strategy would be to use horizontal sections in order to maximise the number of channels sampled. Eqn. 1 is then modified to:

$$L_V = Q_A \tag{2}$$

1-D sections: test lines

Test lines are an efficient way of analysing many structures, especially manually. The stereological interpretation of measurements made using test lines assumes, as for 2-D section, that the structure or the test lines are isotropic. The same three options as for sections are available to ensure that estimates of 3-D properties are unbiased. Test lines usually consist of lines across a 2-D section. Baddeley *et al.* (1986) point out that it is possible to obtain a test line of any orientation, θ, ϕ, using vertical sections. The sample is sectioned vertically with the orientation of the cut in the horizontal plane being at ϕ. The test line is then drawn across it at an angle θ to the vertical. Hence the test line has a 3-D orientation of θ, ϕ. θ and ϕ are selected randomly or systematically as described for 2-D sections. Alternatively, Baddeley *et al.* (1986) suggest that the test lines consist of a pattern of regularly spaced cycloids drawn on a vertical section. Each cycloid consists of a quarter of a sine curve (*i.e.* between 0 and $\pi/2$ radians) turned through 90°. (This can be constructed as $y=1-\cos(x)$, where the height of each cycloid is 1 unit, the width $\pi/2$ units and the length 2 units). The cycloids are then positioned on the section in a grid pattern, such that the grid spacing is 2 units and there is a cycloid within every other grid square. This test line system automatically samples all values of θ with the correct weight.

STEREOLOGICAL RELATIONSHIPS

Relationships between 3-D parameters and measurements made in 2-D, 1-D or 0-D are shown in Table 1. These relationships can be visualised by considering the sheet-like component in Fig. 3. The derivations of such relationships can be found, for example, in Weibel (1979).

Measurements in 2-D sections

Fig. 3a is shown in section in Fig. 3b. The area of the component in the 2-D section is, in effect, a sample of the volume of the object. Hence its area per unit area of image, which is referred to as the area density, A_A, can be used to estimate the volume density in 3-D (volume per unit volume, V_V). Similarly, the boundary between the component and the background in 2-D is a sample of the component's surface area. The surface area density in 3-D (surface area per unit volume, S_V) can be estimated from the boundary length density in 2-D (length of boundary per unit area, B_A). The line drawn on one surface of the component in Fig. 3a appears as a point (transect) in 2-D in Fig. 3b. The length density of the line in 3-D, L_V, can be estimated from the transect density in 2-D (number of transects per unit area, Q_A).

Measurements along 1-D test lines

When 1-D sections (test lines) are used to analyse the structure, they generally consist of lines drawn across a 2-D section as in Fig. 3c. What these lines 'see' is a series of linear intercepts across the object (Fig. 3d). These intercepts are a sample of the volume of the component. The intercept length density (length of intercept per unit length of test line, L_L) can

Table 1.
Relationship of 3-D parameters to parameters measured in fewer dimensions. P_P is the proportion of points positioned in pore space when using point counting. Other symbols explained in text. (After Weibel, 1979)

3-D	2-D	1-D	0-D
V_V	A_A	L_L	P_P
S_V	$4/\pi \cdot B_A$	$2I_L$	-
L_V	$2Q_A$	-	-

be used to estimate V_V. Each end of an intercept is an intersect with the surface area of the component. The intersect density (number of such points per unit length of test line, I_L) can be used to estimate S_V. Test lines are not suitable for sampling linear components such as the line shown in Fig. 3a, because the probability of a test line hitting the line is negligible.

Measurement strategy

A general strategy for the quantitative analysis of a structure using sections is as follows. First decide which 3-D parameters are most appropriate to the shape of the component being measured. Then choose 2-D, 1-D or 0-D measurements from which the 3-D parameters can be estimated stereologically or which are at least related to the 3-D parameters where there is no established stereological method.

For example, the simplest way to characterise a sheet-like component, such as fissures in the soil, would be to estimate its volume density, V_V. A more sophisticated characterisation would be to estimate mean thickness of the fissures, $\bar{t}$, and their areal extent, $S_V(s)$, irrespective of their thickness. The area extent is equal to the surface area of one side of the fissure, *i.e.* $S_V/2$. Therefore:

$$V_V = \frac{\bar{t} \cdot S_V}{2} \tag{3}$$

To characterise the structure in this way using sections, it is necessary to measure A_A and B_A in 2-D to allow estimation of V_V and S_V respectively using the equations in Table 1. This allows $\bar{t}$ to be estimated as:

$$\bar{t} = \frac{\pi A_A}{2 B_A} \tag{4}$$

Alternatively, $\bar{t}$ can be estimated from the mean width of the fissures in the 2-D image, $\bar{w}$. Since $\bar{w} = 2A_A/B_A$:

$$\bar{t} = \frac{\pi}{4} \bullet \bar{w} \tag{5}$$
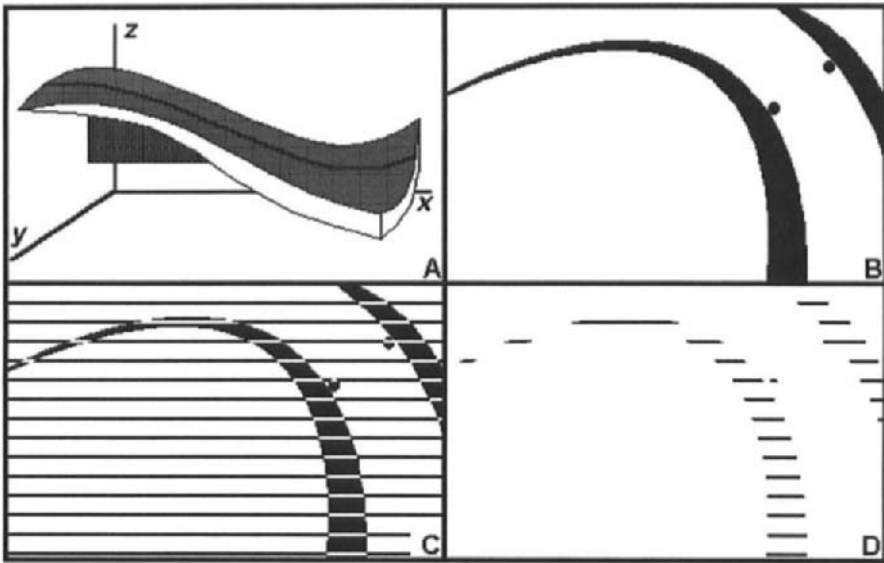
Fig. 3. Example of how a 3-D structure appears in 2-D and 1-D. a) A sheet-like 3-D structure of varying width with a line drawn on one surface. b) A horizontal, 2-D section through the structure. c) Test lines drawn on the section. d) The appearance of the structure in 1-D.

If the structure is to be analysed using test lines, it is necessary to measure L_L and I_L. These are used to estimate V_V and S_V respectively using equations in Table 1. Therefore:

$$\bar{t} = \frac{L_L}{I_L} \tag{6}$$

$\bar{t}$ can also be estimated from the mean intercept length, $\bar{l}$, since $\bar{l} = 2L_L/I_L$:

$$\bar{t} = \frac{\bar{l}}{2} \tag{7}$$

NUMBER PER UNIT AREA, N_A: A WARNING

Weibel (1979) refers to two basic types of structure. In non-particulate structures, the component being measured can have any shape and be interconnected to any degree. In particulate structures, the component consists of discrete particles[2]. When particulate structures are sectioned the component always appears as discrete profiles[3] in 2-D. When non-

---

[2] In stereology, 'particle' refers to any discrete, 3-D object. This should not be confused with 'particle' as commonly used in soil science. Hence, particular types of pore space can have 'particulate' structures if they consists of discrete pores such as vesicles. However, pore space generally has a non-particulate structure.

[3] In stereology, 'profile' refers to the image of a component on a section.
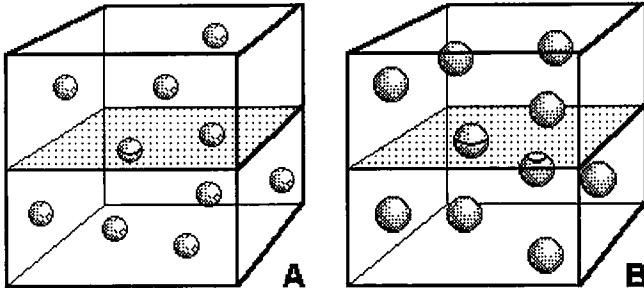
Fig. 4. Models of particulate structures, both with numerical densities, N_V, of 10 unit^{-3}. a) Spheres of diameter of 0.1 units; b) spheres of diameter 0.15 units.

particulate structures are sectioned, the component may also appear as discrete profiles in 2-D depending on its shape and connectivity in 3-D. In the latter case, it is important not to mistake the discrete profiles seen in 2-D as being derived from discrete objects in 3-D.

A frequently misused 2-D measurement is the numerical density of profiles, N_A, which is the number of discrete, 2-D objects per unit area in an image. N_A can be easily interpreted in only two situations.

N_A in sections of particulate structures

In sections through particulate structures, N_A can be used to estimate the number of particles per unit volume in 3-D, N_V. However, the number of profiles of particles appearing in a section depends not only on N_V but also on the size of the particles, because the probability of a section cutting through a particle depends on its projected diameter in the direction normal to the section. Hence, for convex particles of mean diameter $\overline{D}$:

$$N_A = N_V \cdot \overline{D} \tag{8}$$

Consider the two structures shown in Fig. 4. Both consist of spheres with numerical densities, N_V, of 10 unit^{-3}, but with diameters of 0.1 units and 0.15 units in Figs 4a and b respectively. When sectioned the mean number of particle profiles per unit area of section, N_A, will be 1.0 unit^{-2} and 1.5 unit^{-2} respectively.

It is important to realise that estimating N_V is one of the more difficult operations in stereology. Use of Eqn. 8 presupposes a knowledge of $\overline{D}$. However, $\overline{D}$ must itself be estimated from sections where the 2-D diameter of objects does not equal their 3-D diameter. This will be discussed further in the section on size distributions. Here it is sufficient to say that estimation of N_V is relatively simple for components with regular shapes such as spheres, but becomes very difficult as the shapes get more irregular. For a method to estimate N_V for particles of arbitrary shape, see Sterio (1984).

Q_A in sections of linear structures

The other situation in which the number per unit area can be easily interpreted is where the structure consists of a linear component such as the channels in Fig. 2. In this situation the profiles are actually transects through the linear structure. The number of transects is usually
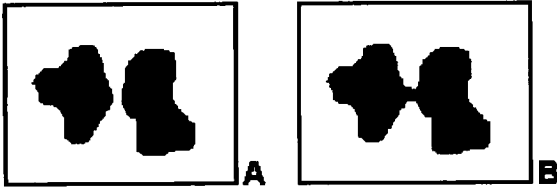
Fig. 5. Cross-sections of an inter-connected pore space, in which a small change in connectivity can have a large effect on the number and size of poroids seen in 2-D. The absence of one connection in (a) doubles N_A and halves the mean object area compared to (b). (From Ringrose-Voase, 1990).

referred to as Q rather than N. The transect density, Q_A, can be used to estimate the length per unit volume of the component, L_V, using Eqn. 1.

N_A *in sections of other structures*

Interpretation of N_A in sections of other structures is more difficult. If the component is highly interconnected, then N_V is not a meaningful parameter and N_A will depend on the width and degree of interconnection of the component. Ringrose-Voase (1990) gives an example (Fig. 5) of sections through interconnected pore space. In such sections, the number and size of poroids depends mainly on the degree of connectivity.

SIZE DISTRIBUTIONS

Sections are often made with the intention of estimating the size distribution of a particular component, such as the pore space. A size distribution consists of a parameter expressing the size of parts of the component and another expressing the amount of component of a particular size. Choosing which 2-D size distribution to measure requires some care so that it relates to the 3-D size distribution. The best strategy is first to decide which parameters best express the size distribution in 3-D, then to choose suitable 2-D or 1-D measurements.

Size distributions of particulate structures

For particulate structures size distributions are usually expressed in terms of the frequency, N_V, in particular diameter classes. The easiest size distribution to estimate is that for a population of spheres of varying sizes. To obtain the 3-D distribution from 2-D sections, it is first necessary to know the distribution of sizes in 2-D that is obtained by sectioning spheres of one size, D, in 3-D. The diameter, d, of the circular profile obtained by sectioning a single sphere of diameter, D, is always less than or equal to D depending on the position of the section. When a population of randomly positioned spheres of diameter, D, is sectioned, the number per unit area, N_A, of profiles of different diameters, d, can be predicted. Figs 6a and b show the size distributions in 2-D of the circular profiles obtained by sectioning the spheres shown in Figs 4a and b respectively.

N_A (units^{-2}) N_A (units^{-2})

Profile diameter in section (arbitrary units)
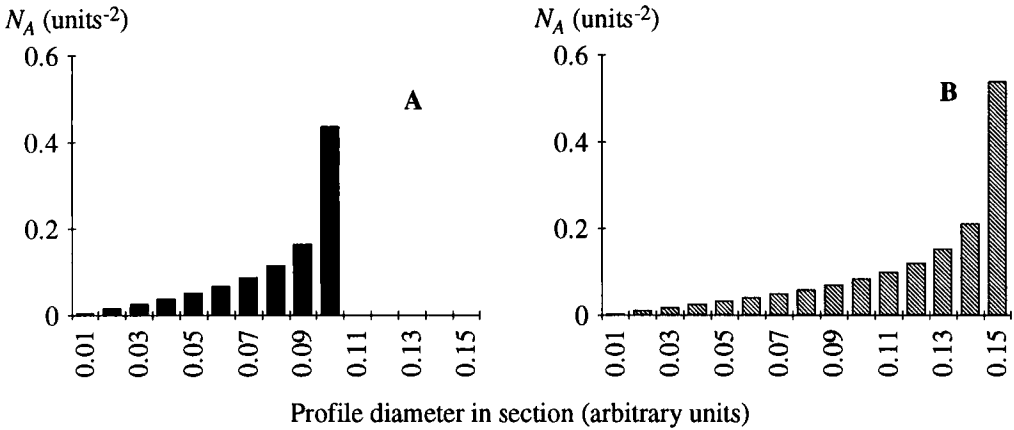
Fig. 6. 2-D diameter distributions of the circular profiles produced by sectioning a population of spheres: a and b correspond to those shown in Fig. 4a and b, respectively, and c to the addition of a and b.

When a population of spheres of varying distribution is sectioned, the 2-D diameter distribution can be 'unfolded' to obtain the 3-D distribution (Wicksell, 1925; Saltykov, 1958; Weibel, 1979, pp. 51-62). The procedure can be illustrated by considering a structure in which the spheres from Figs 4a and b are added together. The distribution of diameters in 2-D that would result from sectioning such a structure is shown in Fig. 6c. Since there can be no spheres with D larger than the largest d, the first step is to use N_A of the largest 2-D diameter class to predict N_V of the largest 3-D class. This then allows prediction of the number of circles in smaller classes that were derived from the largest sphere class. These circles are then subtracted from the 2-D distribution. The procedure is then repeated for the next largest class and so on until there are no circles remaining in the 2-D distribution.

Size distributions of non-particulate structures

For non-particulate structures other parameters must be found to express both size and amount. Instead of N_V to express the amount in each size class, volume density, V_V, areal extent, S_V, or length density, L_V, can be used where appropriate.

For example, an appropriate size distribution for fissures (Fig. 3) uses thickness, t, as a measure of size and the areal extent, $S_V(s)$, in each thickness class as a measure of amount. In 2-D, t is expressed as the width, w, and $S_V(s)$ as the length per unit area of fissures, $B_A(s)$.

Therefore, to estimate the 3-D distribution from 2-D, the length of fissure, $B_A(s)$, in each width class is measured. In 1-D, t is expressed as the intercept length, l, and $S_V(s)$ as the number of fissure intercepts per unit length, $I_L(s)$. The 3-D distribution can be estimated by measuring the number of intercepts in each length class. Clearly, both w and l must always be greater or equal to t. It is possible to predict the distribution of w or l that arise from sectioning fissures of a constant thickness. This information can then be used to estimate the 3-D thickness distribution for fissures of varying thickness using procedures (Cruz-Orive, 1979) similar in principle to the unfolding procedure for spheres. Note that neither the procedures for estimating from 2-D nor that for 1-D involve measurement of individual poroids in the image.

CONCLUSIONS

This paper has reviewed some basic stereological principles to be observed in the quantitative analysis of sections. The most important conclusion that can be drawn is necessity of having a conceptual model of the structure in 3-D before choosing which 2-D or 1-D measurements to make. The 3-D model allows parameters of interest to be chosen that are appropriate to the structure. It is then possible to determine how these 3-D parameters are expressed in 2-D or 1-D.

REFERENCES

Baddeley, A.J., Gundersen, H.J.G. and Cruz-Orive, L.M., 1986. Estimation of surface area from vertical sections. J. Microsc., 142: 259-276.

Cruz-Orive, L.M., 1979. Estimation of sheet thickness distribution from linear and plane sections. Biom. J., 21: 717-730.

Gundersen, H.J.G., 1977. Notes on the estimation of the numerical density of arbitrary profiles: the edge effect. J. Microsc., 111: 219-223.

McBratney, A.B. and Webster, R., 1983. How many observations are needed for regional estimation of soil properties? Soil Sci., 135: 177-183.

Ringrose-Voase, A.J., 1990. One dimensional image analysis of soil structure. I. Principles. J. Soil Sci., 41: 499-512.

Ringrose-Voase, A.J. and Nortcliff, S., 1987. The application of stereology to the estimation of soil structural properties: A preview. In: N. Fedoroff, L.M. Bresson and M.A. Courty (Editors), Soil Micromorphology. Proc. VII Int. Working Meeting on Soil Micromorphology, Paris, July 1985. Association Française pour l' Etude du Sol, 78370 Plaisir, France, pp. 81-88.

Saltykov. S.A., 1958. Stereometric Metallography. 2nd edition. State Publishing House for Metals and Sciences, Moscow.

Sterio, D.C., 1984. The unbiased estimation of number and sizes of arbitrary particles using the dissector. J. Microsc., 134: 127-136.

Weibel, E.R., 1979. Stereological Methods. Vol. 1. Practical Methods for Biological Morphometry. Academic Press, London, 415 pp.

Weibel, E.R., 1980. Stereological Methods. Vol. 2. Theoretical Foundations. Academic Press, London, 340 pp.

Wicksell, S.D., 1925. The corpuscle problem I. Biometrica, 17: 84.

This Page Intentionally Left Blank

Soil pore structure modelling using fuzzy random pseudofractal sets

A.B. McBratney[1] and C.J. Moran[2]

[1]Dept. of Agricultural Chemistry and Soil Science, University of Sydney, NSW 2006, Australia

[2]CSIRO Division of Soils, GPO Box 639, Canberra City, ACT 2601, Australia

ABSTRACT

McBratney, A.B. and Moran, C.J., 1994. Soil pore structure modelling using fuzzy random pseudofractal sets. In: A.J. Ringrose-Voase and G.S. Humphreys (Editors), Soil Micromorphology: Studies in Management and Genesis. Proc. IX Int. Working Meeting on Soil Micromorphology, Townsville, Australia, July 1992. Developments in Soil Science 22, Elsevier, Amsterdam, pp. 495-506.

Although much work has been done on measurement of soil pore structure at various scales, few attempts has been made to integrate these findings by building 2D or 3D geometric models. A two-dimensional pixel-based model of soil pore structure using fuzzy random fractal sets is presented. A coarse-scale model produces realisations of the fuzzy, random set "porosity" using the technique of simulated annealing. This produces a range of simple statistically homogeneous pore structures with aggregated circular, ellipsoidal and linear pore and solid aggregates of varying sizes at uniform, clustered or regularly spaced locations. Compound structures can be created by using the output from one realisation as input to a further generation of the model. A second model produces pseudofractal realisations at finer scales that preserves porosity in 3-by- 3 neighbourhoods at the coarsest scale. A variety of examples of pore structures produced by the models is presented. Possible applications include evaluating segmentation; cross-checking of 2D techniques and the use of pore models in physical process modelling. The extension to three dimensions is straightforward.

INTRODUCTION

Appropriate scale of measurement and modelling of soil physical processes is one of the greatest challenges facing those researching soil management. Soil pore structure models which encompass many or all scales provide unique methodology for understanding physical behaviour without inordinate measurement at each site of interest. Development of such 3-D models will allow realistic simulations which can be used in soil mechanical, fluid movement and plant growth models. Realistic simulations may allow estimation of pore structural attributes that cannot be readily obtained from sections or images thereof.

To date, although much work has been done on measurement at various scales, no real attempt has been made to integrate these findings by building 3-D geometric models. These have the added advantage of being useful for corroborating measurement techniques. Dexter (1976) developed a one-dimensional, fourth-order Markov chain model for horizontal transects through the soil. Two-dimensional analogues of this process are available – the Markov random-field models (Cross and Jain, 1983; Acuna, 1992). Soil structure is 3-D and it seems
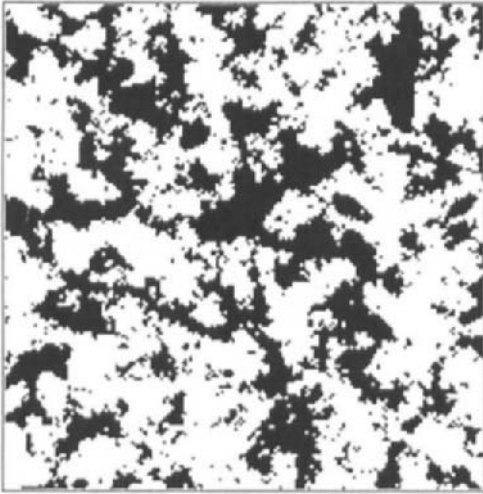
Fig. 1. A random set. The pore space, shown in black, shows a random outline suggesting a random rather than deterministic geometry.

more prudent to develop 3-D random-field models and then to take slices through them. The random-process model for surface straw developed by Moran and McBratney (1992) might be a more effective alternative. For example, packing pores can be modelled as Boolean processes (such as Serra, 1982, p.506) used for clay, sand and pore distribution in synthetic soil materials; biopores as randomly placed cylinders and cracks as random sheets. These individual components can be combined. The first work on 3-D soil pore structural modelling based on this idea has recently been published (Glaseby *et al.*, 1991).

There is no unique definition of soil structure. It is dependent on scale and the components or sets into which the soil volume is divided. The multiplicity of descriptive systems in micromorphology hinges on the subsets into which the volume is divided. Recalling McBratney *et al.* (1992), consider a three-dimensional volume of soil at some fixed time to be represented by a universal set T. Definitions of structure may be obtained by dividing the universal set T into subsets. For example, we can write,

$$T = P \cup S = P \cup P'$$

The conjoint sets P and S represent the pore or void and S the soil solid material respectively, $\cup$ is the set union operator and P' represents *not P* or, in other words, S. When we consider the soil in terms of these two subsets this may be termed the *soil pore structure* or, more fully, pore-solid structure as suggested by Fox and Teakle (1963). This definition leads away from ideas of 'structured' and 'structureless' soil because from the definition all soil has pore structure. Using this definition we can see clearly that it is the geometry and topology of the sets S and P which have to be described in order to measure pore structure.

The sets S and P do not have a deterministic geometry or topology. Indeed it is useful to treat P and S as *random* sets (Matheron, 1975; Serra, 1982), as shown in Fig. 1.

Moreover, this definition of randomness may include fractals (Tyler and Wheatcraft, 1989; Bartoli *et al.*, 1991) as shown in Fig. 2. Conventionally, attributes reflecting these properties have only been measured at a single scale. However, more recently the concept of the fractal dimension has been studied in pore structure measurement (Bartoli, *et al.*, 1991; Young and
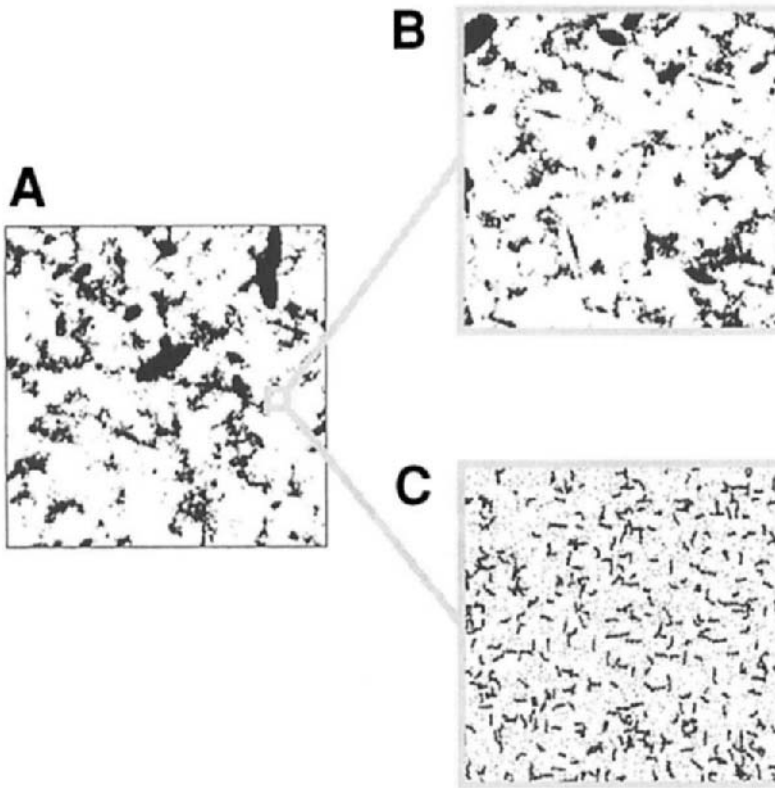
Fig. 2. Fractal random sets. **A)** A random set at a coarse spatial resolution. **B)** The set in (B) when shown magnified shows a similar geometry to that at the coarser scale - a self-similar fractal. **C)** The set in B) when shown magnified shows more detail but a different geometry to that at the coarser scale - a self-dissimilar or pseudofractal.

Crawford, 1992) and water flow characteristics (Tyler and Wheatcraft, 1989; Rieu and Sposito, 1991). Such work indicates that fractal dimensions may be used as a mechanism for scaling membership in P. It appears that the dimension varies between materials and also as the scale changes, the latter giving rise to pseudofractals (Fig. 2C).

Furthermore, at certain scales we may not be able to resolve P and S although we know they must exist. In that case we can consider membership to P and S and we have fuzzy (Kandel, 1986) random sets as depicted in Fig. 3. A seemingly natural fuzzy set to use is the fuzzy set 'pore' which has membership values ranging from zero to unity. The values of the membership to this fuzzy set are more commonly called porosity. In order to deal with all contingencies we require fuzzy, random fractal sets and that is what we shall deal with in this paper.

In all Figures in this paper degree of blackness represents increased membership in the fuzzy set 'pore'. Hence, white represents zero membership (solid) and black represents a membership of one.
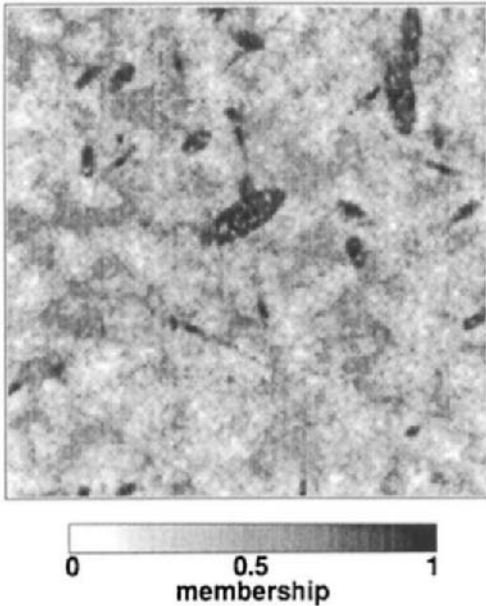
Fig. 3. A fuzzy set. An image of the fuzzy set 'pore' with memberships ranging from zero (white) to unity (black). The 0.5-level set (membership >0.5 shown as black) gives rise to the random set in Fig. 1 (membership >0.5 shown as black).

METHODS - THE GERM OF A MODEL

The following model, which is implemented in two dimensions, forms the basis for a possible three-dimensional pore structure model. It makes use of fuzzy, random (pseudo-) fractal sets. The model consists of two sub-models, one for creating a structure at the coarsest scale and another for producing structures at progressively finer scales while preserving features of the larger scale.

Coarse-scale structural model

The model uses the fuzzy set 'pore' as the principal variable. Values of the fuzzy set P are sampled at random from a statistical distribution and placed at the nodes of a n row by m column two-dimensional lattice. The lattice nodes are also called pixels. For all the examples in this paper, the values are sampled from a Gaussian distribution with mean 0.4 and variance 0.04. Figure 4A shows the shape of this distribution and Fig. 4B shows a realisation of this model for a 512×512 lattice. The values at neighbouring sites are independent and this gives rise to a homogeneous completely random isotropic structure reminiscent of a sandstone or sandy fabric. This is the base model for all the subsequent models described in this paper. In order to make models with exactly the same statistical distribution but with diverse spatial distributions a process of aggregation or inhibition based on swapping points around seed points was used. This type of procedure has been termed simulated annealing (Acuna, 1992) and was first proposed by Metropolis *et al.* (1953).

There are two main components controlling the types of structure produced. These are, (i) the seed types and (ii) the spatial distribution of their centroids.
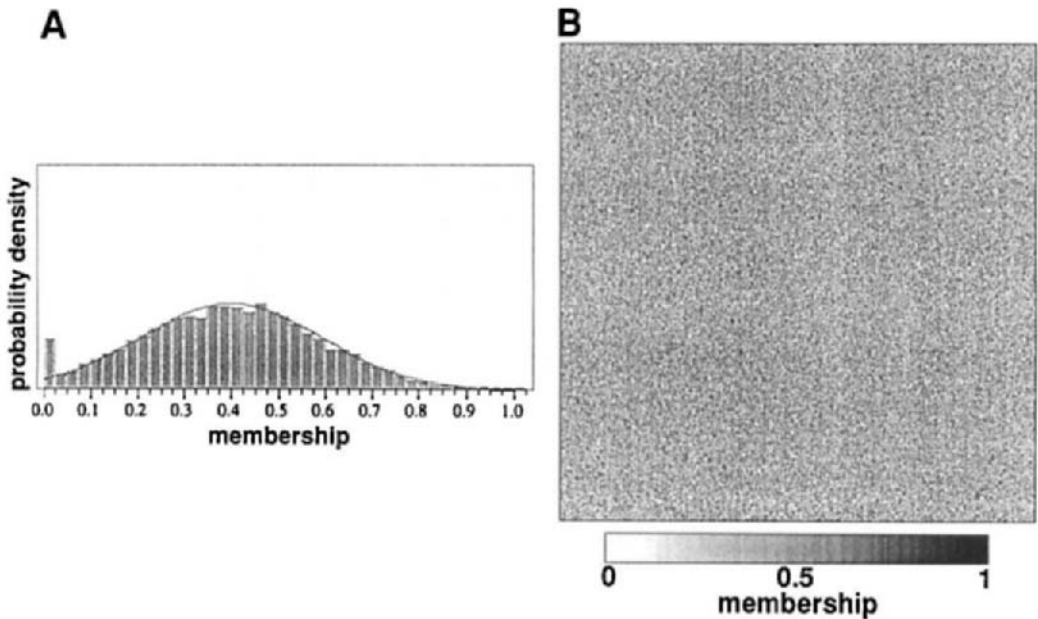
Fig. 4. A) The histogram and probability density function of membership to the fuzzy set 'pore'. B) Image of a realisation of the completely random model.

Seed types

Aggregation may apply to either solids (small membership of fuzzy set 'pore' clustered) or pores (large membership of fuzzy set 'pore' clustered). The model produces three types of aggregates from seed types with three main shapes: circular, ellipsoidal and linear. Circular pores or solids may have a uniform radius distribution up to a maximum size, or be distributed according to a Gaussian or log-Gaussian distribution. Ellipsoidal aggregates are similar to circular ones with an additional two sets of parameters. The first controls the ratio of major to minor axes, which can fixed or distributed statistically. The second controls the angle of the principal axis which may be uniformly distributed or sampled from a von Mises distribution. Linear aggregates of pores are created by joining two seed points, the angle and distance between them once again being controlled by statistical distributions.

Spatial distribution of seed centroids

The centroid of each seed (seed point) has a spatial point distribution which may be either random, clustered or regular. Random points are given co-ordinates from uniform distributions. Regular point patterns are created by sampling within grid cells and removing points that fall within a fixed radius from another point. Clustered points are produced by taking random seeds and from each seed producing daughter seeds with a fixed or uniformly distributed number (see Moran and McBratney, 1992 for further discussion). The second major parameter controlling the overall pattern of points is its intensity (the number of seed centroids per unit area).

Iterations

The program iterates beginning with a completely random distribution as in Fig. 4B. Given a set seed types, spatial distributions and intensities the program iterates by swapping randomly located pore or solid pixels from the structure to within a zone of influence for the seed type provided the swap increases the degree of aggregation within the zone of influence. For example for a circular aggregate of radius r, a point A is chosen at random within a radius r of the seed point of the aggregate, a second point B is chosen at random from the whole image. If the point B is more similar to the seed point than point A then the values are swapped, otherwise they remain the same. This process is iterated until the ratio of number swaps to number of attempted swaps reaches an equilibrium.

Structural types

The model is therefore capable of producing structures from the various seed types and their spatial distributions. They are classified by the spatial distribution of seed points:

Regular structures	regular solids
	regular pores
	regular aggregates structure (diffuse)
Random structures	random pores (or solids)
	anisotropic random
Clustered structures	isotropic clustered solids
	isotropic clustered pores
	isotropic linearly clustered pores

The structures listed above are constructed from a single seed type and are therefore called *unary* structures. *Compound* structures can be created by using the result of applying one seed type and distribution as the initial condition for another seed type. *Generational* structures can be produced by placing the output from one generation as input to the next.

Finer-scale model

From the earlier discussion it was felt necessary to produce a model capable of revealing finer scale structures. This is achieved by taking a subsample of the coarse-scale structure (say 64 × 64 pixels from a 512 × 512 image) and interpolating it to 512 × 512 pixels, which maintains continuity and the broad features of the previous scale. Porosity in the finer-scale image is preserved by the condition that in the finer-scale image the local porosity in a 3-by-3 window of the coarse-scale one has to be maintained. Currently this is done by adding random images to the interpolated image with the constraint that the porosity within certain regions of the image is fixed.

EXAMPLES

A range of structures is shown in Figs 5–8. All structures have the same porosity distribution as shown in Fig. 4A.

Fig. 5 shows four realisations of aggregated circular solids at clustered locations; the circular clusters have a density of 1 per 30 pixels with a maximum of 5 parents per cluster and a maximum cluster radius of 10 pixels. The clusters have an isotropic Gaussian radius distribution with a mean of 5 and a standard deviation of 1 pixels. Blacknesss represents degree of membership to the fuzzy set 'pore'.
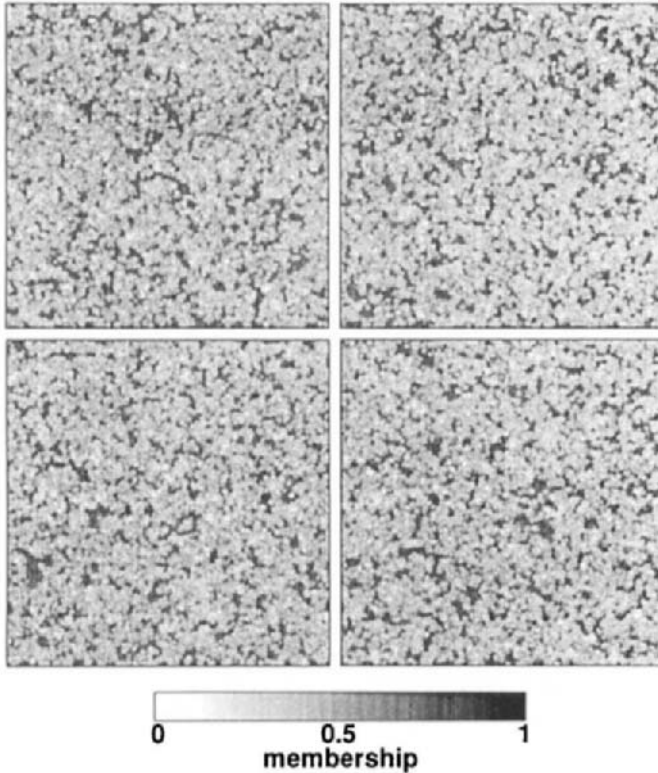
Fig. 5. Four realisations of aggregated circular solids at clustered locations.

Fig. 6 shows various pore structures created by the model. Fig. 6A shows ellipsoidal pores with regular spacing with a density of 1 per 2000 pixels, normally distributed radii (mean, 5 pixels; standard deviation, 2), uniformly distributed orientations and normally distributed major to minor axes (mean, 2.2; standard deviation, 2). Fig. 6B shows random linear pores or cracks. Fig. 6C depicts anisotropically clustered circular pores. The randomly spaced pore clusters have a density of 1 per 100 pixels, ellipsoidal radii distribution with a minimum of 3 pixels and maximum of 15 pixels, the maximum being at a fixed angle of 30°.

Fig. 7 shows compound structures as grey-level images representing degree of membership in the fuzzy set 'pore'. Fig. 7A is derived from Fig. 4B in a similar fashion to Fig 5. Fig. 7B is then derived from 7A by producing ellipsoidal, uniformly oriented pore clusters. Subsequently, the structure from Fig. 7B is used as input to produce randomly oriented linear pore clusters of mean length 50 pixels (Fig. 7C). Note that in these compound structures, previous features are destroyed to create later ones because of the fixed membership distribution.

Another type of compound structure, shown in Fig. 8, can be created by varying the number of generations of the same random process, the output from one generation being used as the starting condition for the next. In this example, the structure is based on ellipsoidal, uniformly oriented pore clusters. This is somewhat reminiscent of structures caused by annual faunal activity. It can be seen that there is little difference in structure between 100 and 1000 generations but the matrix has not been fully explored after only 10 generations.
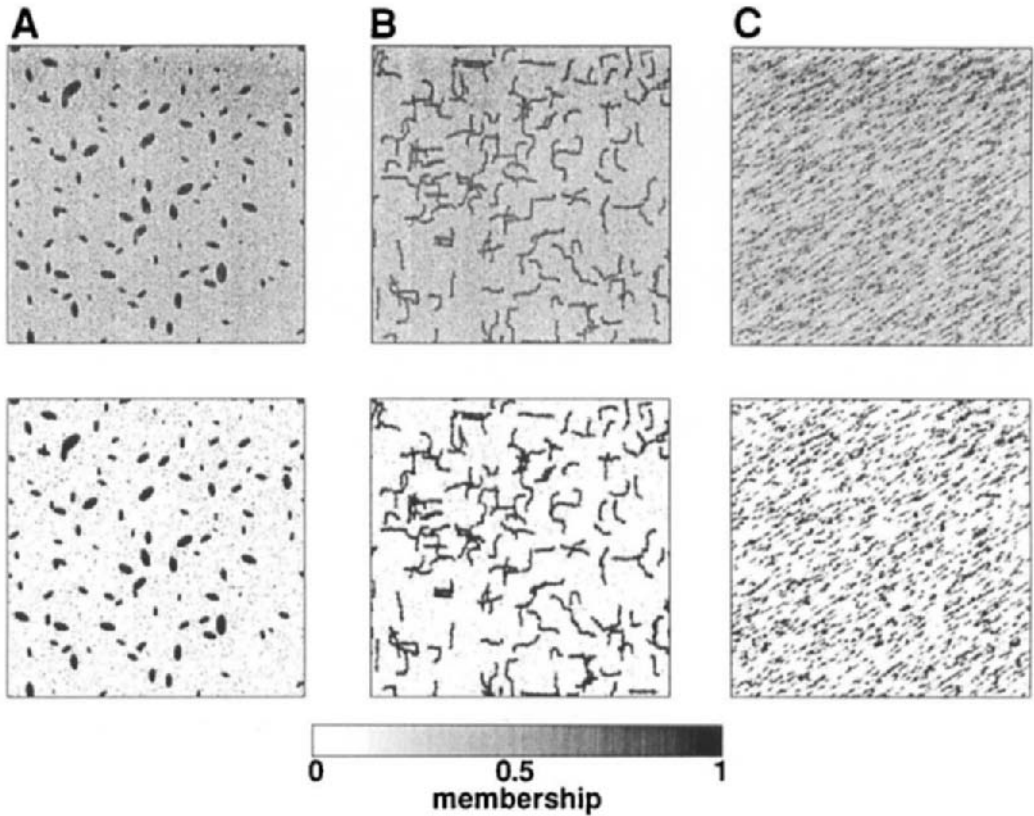
Fig. 6. Various pore structures created by the model. A) Ellipsoidal pores at regular locations; B) random cracks; C) oriented pores at random locations. The upper row shows fuzzy set 'pore' with larger membership values shown blacker. The lower row shows images with memberships over 0.5 shown in black.

Finer-scale model

The finer-scale model is a first attempt to produce fractal or pseudo-fractal structures. Pseudofractal structures at three levels of magnification are depicted in Fig. 9. Fig. 9A shows the structure at the coarsest level (nominally, 1× magnification) with finer levels indicated by inset squares. Figs 9B-E depict components of structure at 8× magnification. Fig. 9B shows the conditional porosity which must be maintained at a given locality in the final structure. Fig. 9C gives the final structure at 8× magnification. Fig. 9D is the structure magnified from 9A. Fig. 9E is the linearly interpolated structure from A. Figs 9F-I show components of structure at a magnification of 64×. Fig 9F shows the conditional porosity from 9C which is maintained in the final structure. Fig. 9G shows the structure at the third level. Fig. 9H is the structure magnified from A and Fig. 9I is the linearly interpolated structure from Fig. 9C. As can be seen, the model produces finer scale structures which have the gross features of the coarser scale ones but also have additional structures. Currently this is done by adding random images
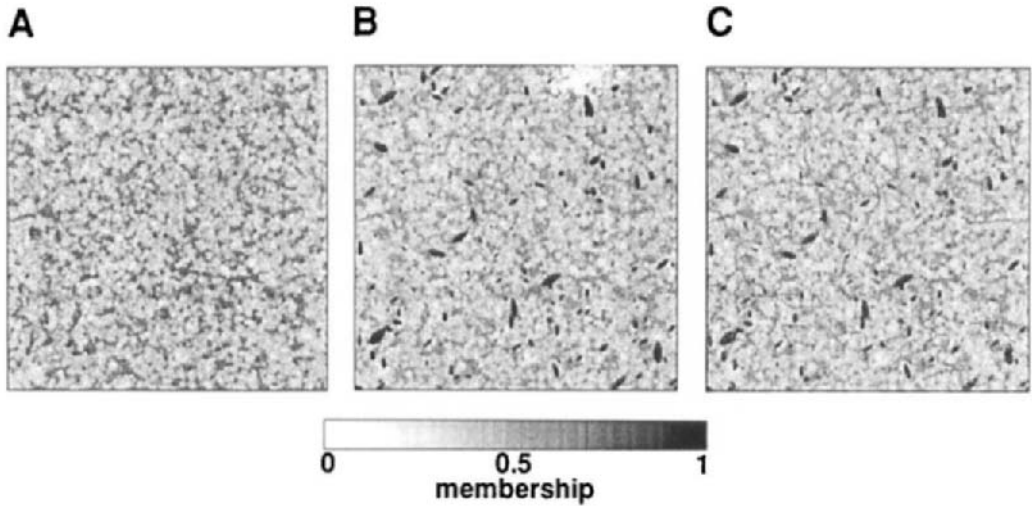
Fig. 7. Compound structures. **A)** Structure from Fig. 4. **B)** Structure from A is used as input to the model with ellipsoidal uniformly oriented pore clusters superimposed. **C)** Structure from B is used as input to model with randomly oriented linear pore clusters.

to the interpolated image with the added constraint that the porosity within certain regions of the image is fixed. The annealing algorithm is not used and therefore there is little control over finer-scale features. A version of the annealing model with local conditional porosity is required. The structures in Figs. 9A and 9C are not self-similar and therefore are pseudofractal. There is some hint of self-similarity between the structures in Fig. 9C and 9G. This is because the images were produced by the same random process.

DISCUSSION

Problems with model

Although the model is very flexible, it uses fairly simple seed types and spatial distributions. Work is needed on generating more angular aggregates. Modelling cracks is currently least effective. This is partly because the model does not allow increased porosity when cracks are generated, a feature that needs to be incorporated.

3-D extension

Because the model presented here is based largely on point processes in space the extension to three dimensions is theoretically straightforward. Clearly the 3-D model will be computationally more demanding and will require improved software tools for visualisation.

Applications

There are many possible applications of such models. Three are discussed briefly.
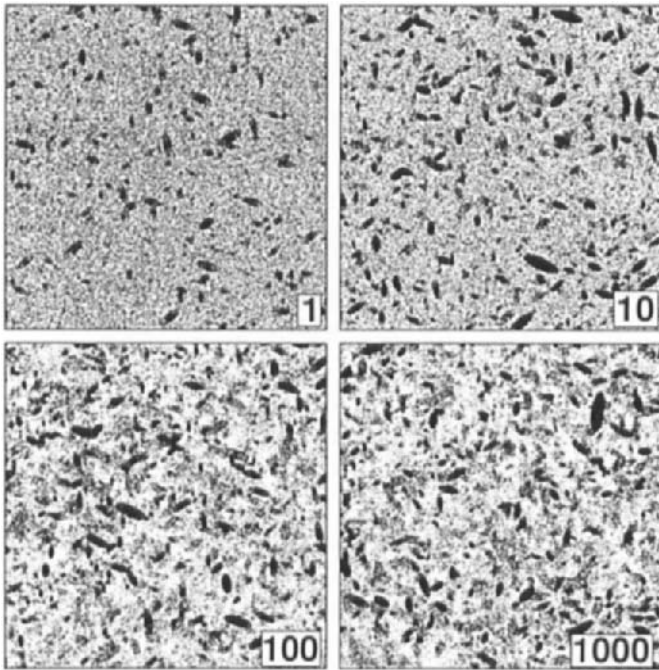
Fig. 8. 1, 10, 100 and 1000 generations of ellipsoidal, uniformly oriented pore clusters, the output from one generation being used as the starting condition for the next. The images depict the 0.5-level set with membership >0.5 shown as black.

Segmentation

Fig. 10B shows the bipartition segmentation of the pore structure in Fig. 10A with membership greater than 0.5 shown as black. Fig. 10C is segmented by membership all pixels in a 3-by-3 neighbourhood in fuzzy set greater than 0.5, pores shown as black. This corresponds to a Shannon-type segmentation which says that the smallest scale resolvable is twice the smallest sampling interval. Clearly the latter two are quite different with Fig. 10B containing many isolated pixels and this leads to questions of real resolution and its relation to segmentation.

Cross-checking of 2-D techniques

Three-dimensional data can be sectioned in any direction any number of times. This can be used to provide a basis for critical examination of stereological estimators used in 2-D activities. This, in turn, assists in developing optimum sampling procedures for selective sectioning and generation of stereological (or other) attributes.

Use of pore models in physical process modelling

Pore models can be used to quantify the mean and variance of properties over a range of scales. Using the models developed we can represent the quantity of pore space and solid at a given location at a range of scales. In order to use the model to examine structural effects on other soil properties, *e.g.* water flow properties, finite-element models will have to be developed. The models can then be run by random sampling at various scales to build up a relationship between expected flow and the variance of the flow and scale. This will indicate useful sample volumes for real measurement procedures.
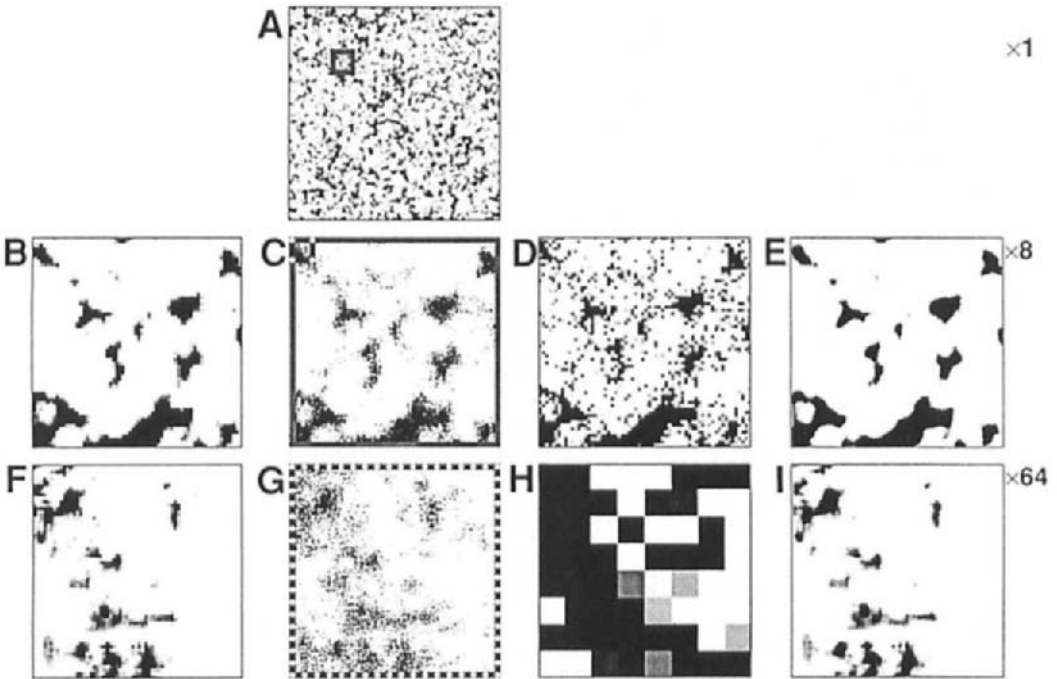
Fig. 9. Pseudofractal structures at three levels of magnification. **A)** Structure at coarsest level with finer levels indicated by inset squares. (B-E) Components of structure at second level. **B)** The conditional porosity. **C)** The structure at the second level. **D)** Structure magnified from A. **E)** Linearly interpolated structure from A. **F-I)** Components of structure at third level. **F)** The conditional porosity from C. **G)** The structure at the third level. **H)** Structure magnified from A. **I)** Linearly interpolated structure from C.

CONCLUSIONS

The two-dimensional model developed here within a mathematical framework of fuzzy, random fractal sets, shows promise for the development of quantitative soil pore structural studies. More work is required on improving the quality of the simulations with respect to real structures and there is a need for incorporation of structure-generating processes such as air-entry on shrinkage and compaction. Most effort should be expended on developing the model in three dimensions.

REFERENCES

Acuna, C.O., 1992. Texture modeling using Gibbs distributions. CVGIP: Graphical Models and Image Processing, 54: 210–222.

Bartoli, F., Philippy, R., Doirisse, M., Niquet, S. and Dubuit, M., 1991. Structure and self-similarity in silty and sandy soils: the fractal approach. J. Soil Sci., 42: 167–185.

Cross, G.R. and Jain, A.K., 1983. Markov random field texture models. IEEE Transactions on Pattern Analysis and Machine Intelligence, PAMI-5: 25–38.
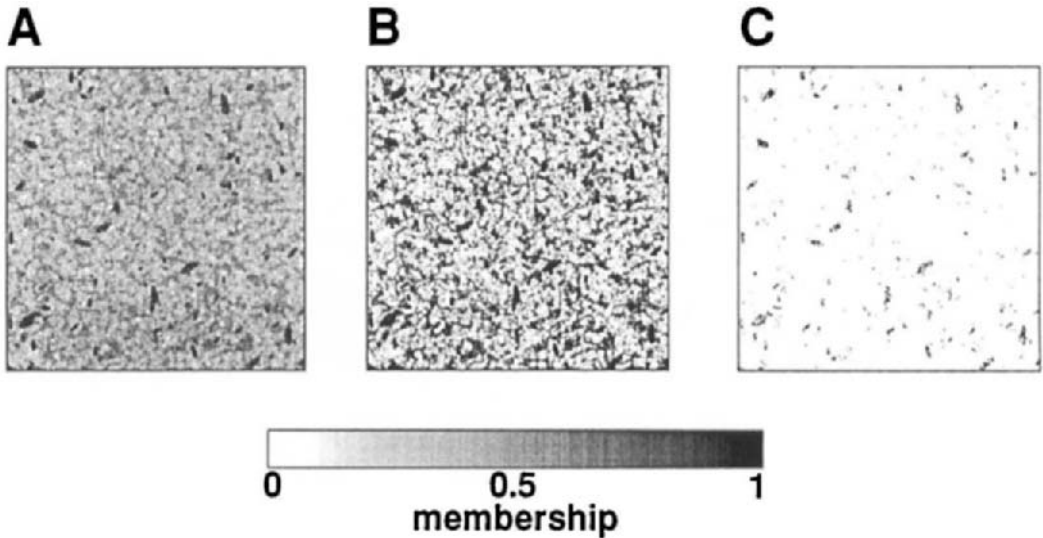
Fig. 10. Segmentation of pore structure. (A) fuzzy set 'pore' as grey levels. (B) Segmented by membership in fuzzy set greater than 0.5, pores shown as black. (C) Segmented by membership all pixels in 3-by-3 neighbourhood in fuzzy set greater than 0.5, pores shown as black.

Dexter, A.R., 1976. Internal structure of tilled soil. J. Soil Sci., 27: 267–278.

Fox, W.E. and Teakle, L.J.H., 1963. What is soil structure? Nature, 198: 1329–1330.

Glaseby, C.A., Horgan, G.W. and Darbyshire, J.F. 1991. Image analysis and three-dimensional modelling of pores in soil aggregates. J. Soil Sci., 42: 479–486.

Kandel, A., 1986. Fuzzy Mathematical Techniques with Applications. Addison–Wesley, New York, 274 pp.

Matheron, G., 1975. Random Sets and Integral Geomtery. John Wiley and Sons, New York, 261 pp.

McBratney, A.B., Moran, C.J., Cattle, S.R., Stewart, J.B. and Koppi, A.J., 1992. Modifications to a method of rapid assessment of soil macropore structure by image analysis. Geoderma, 53: 255–274.

Metropolis, N., Rosenbluth, A.W., Rosenbluth, M.N., Teller, A.G. and Teller, E., 1953. Equations of state calculations for fast computing machines. J. Chem. Phys., 21:1087-1091.

Moran, C.J. and McBratney, A.B., 1992. Image measurement and modelling of the 2-dimensional spatial distribution of surface wheat straw. Geoderma, 53: 201–216.

Rieu, M. and Sposito, G., 1991. Fractal fragmentation, soil porosity and soil water properties: I,II. Soil Sci. Soc. Am. J., 55: 1231–1244.

Serra, J., 1982. Image Analysis and Mathematical Morphology. Academic Press, London.

Tyler, S.W. and Wheatcraft, S.W., 1989. Application of fractal mathematics to soil water retention estimation. Soil Sci. Soc. Am. J., 53: 987–996.

Young, I.M. and Crawford, J.W., 1992. The analysis of fracture profiles of soil using fractal geometry. Aust. J. Soil Res., 30: 291–295.

Measurement of root distribution from sections through undisturbed soil specimens

J.B. Stewart[1,2], C.J. Moran[1] and A.B. McBratney[2]
[1]CSIRO Division of Soils, GPO Box 639, Canberra, ACT 2601, Australia
[2]Dept. of Agricultural Chemistry and Soil Science, University of Sydney, NSW 2006, Australia

ABSTRACT

Stewart, J.B., Moran, C.J. and McBratney, A.B. 1994. Measurement of root distribution from sections through undisturbed soil specimens. In: A.J. Ringrose-Voase and G.S. Humphreys (Editors), Soil Micromorphology: Studies in Management and Genesis. Proc. IX Int. Working Meeting on Soil Micromorphology, Townsville, Australia, July 1992. Developments in Soil Science 22, Elsevier, Amsterdam, pp. 507-514

Soil affects the distribution of plant roots. Measuring root systems is complicated by their concealment in soil. A method is given which allows roots to be measured in soil sections, preserving their *in situ* distribution.

Specimens of soil containing roots are partially impregnated with a fast-setting, epoxy-resin. The soil specimens are then sectioned and the roots detected by illuminating with ultra-violet radiation. Digital grey-level images are acquired and segmented. Root measurements are made on the resulting binary images.

Root systems are 3-D structures. Therefore they are only partially represented in the 2-D sections. Stereology offers a means of estimating 3-D root distribution attributes from these sections. Attributes measured are volume density, surface density, length density and mean root radius. Volume density, V_V (mm^3 mm^{-3}), is an estimate of the volume proportion of roots. Surface density, S_V (mm^2 mm^{-3}), is an estimate of the surface area of roots per unit volume. Length density, L_V (mm mm^{-3}), is an estimate of the length of roots per unit volume. Mean root radius, $\bar{r}$ (mm) is derived from S_V and L_V by assuming that roots are cylindrical.

The techniques of sample preparation, image acquisition and root measurement are outlined. Consideration is given to orientation of soil sections, and the consequences for root distribution measurements.

INTRODUCTION

In comparison to our understanding of plant shoots relatively little is known about roots. This is at least in part because roots are concealed in the soil, making it difficult to study their behaviour and measure their distribution.

The information required about root distribution must be specified before a measurement methodology can be selected. Commonly, soil cores are taken and the roots separated by washing. This allows length, number, density, and diameter of roots to be obtained (Mackie-Dawson and Atkinson, 1991). Washing roots is a time consuming and tedious task. It is

difficult in clayey soils for which a dispersing agent must often be used. Once separated from the soil material, root attributes can be determined either manually or by analysing images.

Measurements from core washings provide little information on the spatial distribution of the root system. Impregnating the soil sample with resin and cutting into sections, overcomes this limitation. Roots can be detected in the sections by applying stains prior to, or after impregnation, or by utilizing autofluorescence. Commins *et al.* (1991) tested a number of stains and found autofluorescence provided the best contrast between roots and resin-impregnated soil blocks.

Autofluorescence is the ability of plant cells to absorb short wave radiation and to emit radiation of longer wavelengths. In roots, the fluorescent compounds are commonly coumarins which fluoresce in the visible range when illuminated with ultra-violet radiation (Murray *et al.*, 1982). Roots are often observed in soil thin sections, due to their autofluorescence, but there are few descriptions of their nature or the environment in which they occur (FitzPatrick, 1990). Commins *et al.* (1991) and McBratney *et al.* (1992) used autofluorescence to obtain binary images for root measurement. Dyer and Brown (1983) monitored autofluorescence intensity as an indicator of elongation rate in soybean roots. They proposed using root fluorescence to evaluate the distribution of growth rates and nutrient absorption activities within a crop root system.

Stereology is used to obtain spatial information about roots from resin-impregnated sections. Stereology is defined by Weibel (1979) as "a body of mathematical methods relating three-dimensional (3-D) parameters defining the structure to two-dimensional (2-D) measurements obtainable on sections of the structure". Root systems generally exhibit a preferred orientation, or anisotropy, because they grow from a fixed point and are geotropic. This anisotropy needs to be considered when sectioning samples and estimating root attributes.

In this paper, a technique for sampling roots *in situ* and methods for measuring their distribution is described. Autofluorescence of oat roots (*Avena sativa* var. Cooba) is used to highlight the roots in soil sections which can be captured in an image. The method for detection of roots and measurement of attributes reflecting spatial distribution are illustrated with an example of roots grown in pots.

MEASUREMENT OF ROOT ATTRIBUTES

Volume density, V_V *(mm^3 mm^{-3})*

The volume density of roots in the sectioned soil was estimated by dividing the number of root pixels, N_R, by the total number of pixels, N_T:

$$V_V = \frac{N_R}{N_T} \tag{1}$$

Surface density, S_V *(mm^2 mm^{-3})*

The method of McBratney and Moran (1990) for pore structure was used to estimate S_V with the additional direction of 315°. Determining the number of intercepts in three directions takes into consideration the anisotropic nature of roots. Bias was avoided by weighting the intercepts according to the probability of their orientation and length of intercept line.

$$S_V = 2\left(\frac{\sin 90^\circ\, N_{90} + \sin 45^\circ\, N_{45} + \sin 315^\circ\, N_{315}}{L\sin 90^\circ + \sqrt{2}L\sin 45^\circ + \sqrt{2}L\sin 315^\circ}\right)$$

$$= 2\left(\frac{\sin 90^\circ\, N_{90} + \sin 45^\circ\, N_{45} + \sin 315^\circ\, N_{315}}{3L}\right) \tag{2}$$

N represents the number of intercepts at 90°, 45° and 315°. The length of the scan line, L is longer for the intercepts at 45° and 315° as they are measured on the diagonal.

Length density, L_V (mm mm^{-3})

Length density was estimated as a function of Q_A, the number of roots/unit area, such that:

$$L_V = \gamma_I^{-1}\, Q_A \tag{3}$$

Q_A is counted directly from the images assuming that each individual in the image is a section through a root. $\gamma_I^{-1} = 2.43$ after the results of Bengough *et al.* (1992) for L_V estimates on vertical sections.

Mean root radius, $\bar{r}$ (mm)

Assuming roots are long, gently curving cylinders of varying radii, mean root radius was determined by its relationship to S_V and L_V (Baddeley and Averback, 1983).

$$\bar{r} = \frac{S_V}{2\pi L_V} \tag{4}$$

$\bar{r}$ is limited by the resolution to half the pixel width.

Depth functions

The program STRUCTURA (Moran and McBratney, 1991) was used to determine the attributes V_V, S_V and soil star length with depth. Every horizontal raster line in the binary image was used as a test line. V_V and S_V were determined using equations (1) and (2).

Soil star length, l_s^* (the mean length-weighted intercept length) is a shape-independent measure of the size of the soil matrix. Alternatively it can be viewed as a measure of the distance between roots. l_s^* is the expected continuous length of non-root space (soil) in the horizontal plane that would be encountered in any direction from a random point at some fixed depth, z, in the soil (McBratney and Moran, 1990). It is computed from the erosion-length-density histogram, $P(l)$ which is derived by counting the total root and non-root pixels at each erosion. The number of erosions is dictated by the greatest continuous length of the same pixel type and may differ for each line (McBratney and Moran, 1990).

Soil star length was computed using equation (5):

$$l_s^* = \frac{2}{1 - V_V}\left(\frac{P(l_0)_s}{2} + \sum_{i=1}^{\max L} P(l_i)_s\right) \tag{5}$$

where $P(l_i)_s$ is the proportion of non-root (soil) pixels present after i erosions of one length (pixel), expressed in terms of the total length of pixels in the raster line.

The estimated values of V_V, S_V and l_s^* are presented by plotting them as functions of depth (McBratney and Moran, 1990). Robust, locally linear fits are used to smooth the data. $\frac{1}{20}$ of the data was used for smoothing at each depth.

SAMPLING

Appropriate sampling is required at each step in obtaining unbiased estimates. These are :
1) representative sample of the feature of interest;
2) sampling of each specimen via sectioning and;
3) attainment of measurements through statistical sampling.
Each of these steps has its associated errors.

A 2-D section is where a plane intersects a solid (Weibel, 1979). In stereology, estimates of 3-D parameters are determined by applying lower order probes; area (2-D), lines (1-D) or points (0-D). For unbiased estimates the section should be an isotropic uniform random (IUR) sample. This means that all section orientations in space must be equally likely (Weibel, 1979). An exception is the estimation of V_V.

For ease of sectioning, vertical sections are commonly taken in soil systems. This does not conform to IUR sectioning, but the bias is overcome by the use of IUR test lines (Baddeley *et al.*, 1986). Thus S_V can be estimated without bias from vertical sections.

As L_V must be estimated from the section (2-D probe), bias is introduced by using a vertical section. Several authors (Lang and Melhuish, 1970; Baldwin *et al.*, 1971; Cruz-Orive *et al.*, 1985; Sandau, 1989) have proposed methods to overcome this bias. They consider the direction of anisotropy by studying the elliptic profiles of the cut roots to determine the coefficient γ_1^{-1} in equation (3). Bengough *et al.* (1992) found γ_1^{-1} for vertical sections to be 2.43 (r = 0.940) by modifying the output of the 3-D root model ROOTMAP (Diggle, 1988).

Assuming that certain sampling conditions are met, statistical sampling errors for V_V, S_V and L_V are inversely proportional to the square of the number of observations (Hilliard, 1976).

EXAMPLE

The effect of a barrier on the root growth of oat seedlings (*Avena sativa* var. Cooba) was studied. A solid barrier was positioned at 28 mm depth, consisting of a plastic lid perforated with five evenly distributed 10 mm diameter holes. The pot was filled with sand (< 1 mm) and five pre-germinated oat seeds were sown into each 76 mm diameter × 88 mm (7×10^{-3} m^3) pot. The oat plants were grown for one month.

The pots were impregnated using an epoxy resin consisting of 170 g Base Resin (LC 191), 170 g Reactive Diluent (DY 026) and 160 g Hardener (LC 249) * (Moran *et al.*, 1989). To impregnate the pots, the bottoms were removed, and resin applied to the surface. The volume of resin applied to each pot was approximately twice the volume of pores in the soil material for thorough impregnation. After curing for about 24 hours, the pots were cut into a number of vertical sections, 10 - 20 mm wide, using a kerosene lubricated, circular diamond-cut saw. The sections were polished, washed with mineral turpentine and dried with an air gun.

---

* Products of Ciba-Geigy, distributed by Meury Enterprises Pty Ltd, Pendle Hill, NSW, Australia.
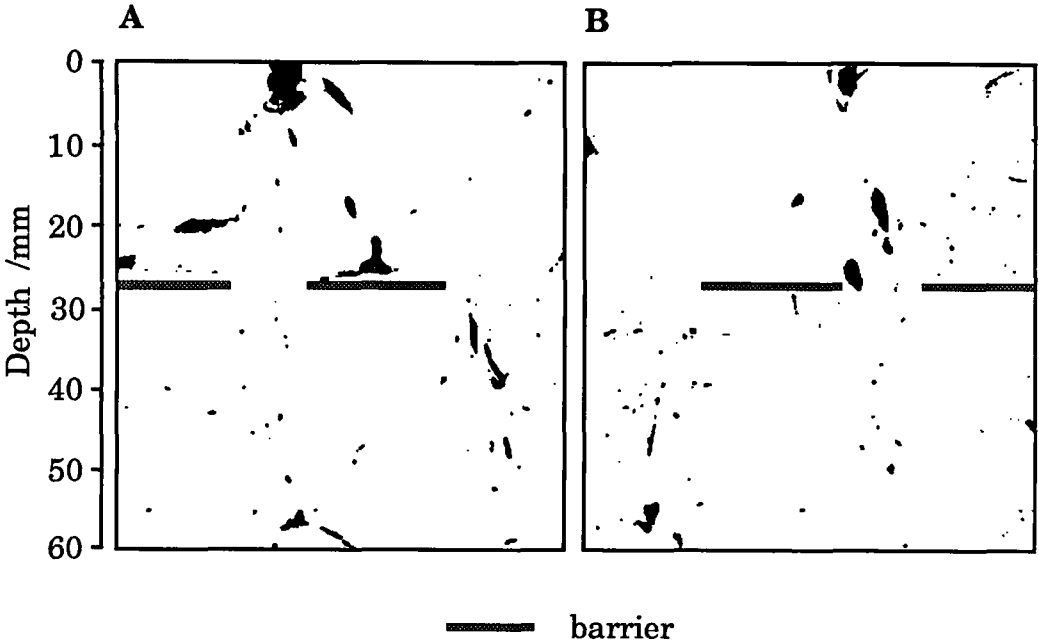
Fig. 1. Binary images of root growth in a pot containing a barrier, opposing faces A and B.

The roots were detected by autofluorescence. In the case of oat roots, the major contributor to the autofluorescence is the blue fluorescing compound, scopoletin (7-hydroxy-6-methoxy coumarin) (Goodwin and Kavanagh, 1949). Scopoletin is exuded upon root death into the soil (Sargent and Skoog, 1960). Thus the fluorescing roots captured in images for measurement were live roots.

The sections were illuminated with two 100 W UV lamps; the image captured with a CCD video camera and digitized to produce a grey-level image of 512×512 pixels. The length of each pixel represented 0.13 mm. The image was segmented using the procedure described by Moran *et al.* (1988) to obtain the binary image. A region of 412 pixels wide by 450 pixels long was selected from which root measurements were made.

DISCUSSION

Fig. 1 shows opposing faces of two vertical sections from the barrier pot experiment. Estimates of V_V, S_V, L_V and $\bar{r}$ of face A and B are given in Table 1. The length densities and mean root radius measurements correspond to that of a cereal first-order lateral to main axis root (Barley, 1970). Of more interest, is the manner in which the roots grow when they encounter the barrier. This is shown particularly in Fig. 1, Face A. When a root encounters the barrier, its growth changes to horizontal and its vertical growth is resumed when it grows through a hole.

The binary images in Fig. 1 were divided vertically into regions of "barriers" and "no barriers". These regions were then combined and smoothed depth functions plotted of V_V, S_V and soil star length, l_s^* (Fig. 2).

Table 1
Root measurements performed on the barrier binary images. Oat (var Cooba) plants were sampled 30 days-after-sowing.

Binary Image	Root Measurements			
	Volume density (mm^3 mm^{-3})	Surface density (mm^2 mm^{-3})	Length density (mm mm^{-3})	Mean root radius (mm)
Face A	0.03	0.10	0.06	0.27
Face B	0.02	0.08	0.07	0.17

Fig. 2 shows a decrease in V_V and S_V with a corresponding increase in l_s^* for the "barrier" regions below the barrier (> 28 mm). For the "no barrier" regions S_V increases while l_s^* decreases below the barrier. These data show that root growth below 28 mm is favoured in the "no barrier" regions.

It has been demonstrated that impregnation, sectioning and measurement of roots *in situ* to estimate root distribution attributes is possible. The example shows that different root growth patterns in laboratory conditions can be quantified. The technique allows examination of the relationship between the distribution of roots and soil features (*e.g.* the occurrence of a hard pan, changes in soil strength, water content, fertilizer placement, cracks, biopores). These data are required for realistic modelling of root growth. This technique must now be tried on field trials with a larger number of treatments and replicates.

CONCLUSIONS

Work is currently being conducted on applying the technique to field sampling of wheat plants. Wheat roots (*Triticum aestivum*, var. Kulin) also contain the fluorescing compound scopoletin. Successful impregnation of dense soil has proven difficult. The fast-setting, epoxy-resin seems to favour loosely aggregated soil material.

The γ_1^{-1} factor of Bengough *et al.* (1992) to estimate root L_V from vertical sections, was used for simplicity. Further work should address the new stereological methods available to estimate L_V from the distribution probabilities of the direction of anisotropy (*e.g.* Cruz-Orive *et al.*, 1985; Sandau, 1989). These methods would provide a measure of γ_1^{-1} for the particular root system under investigation.

Consideration should be given to the sampling errors of the stereological estimates. Hilliard (1976) proposes a procedure based on the error being inversely proportional to the square root of the number of observations. Care needs to be taken with this procedure that the test system used is representative of the features being measured. If the test lines are too closely spaced, individual features are counted more than once resulting in unrealistic low errors.

ACKNOWLEDGEMENTS
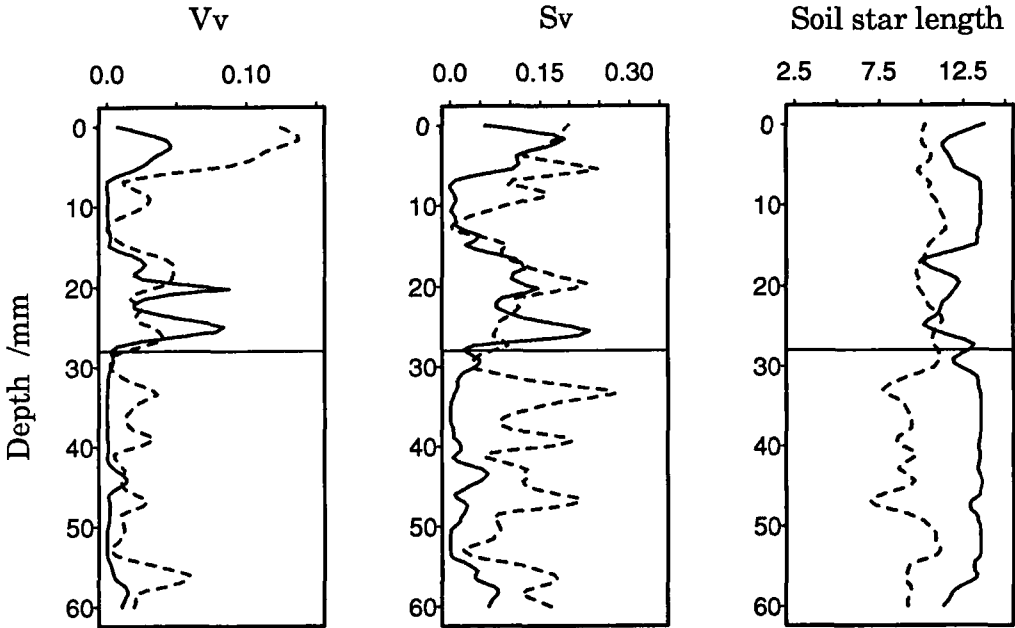
Fig. 2. Depth functions of volume density (V_V) in mm^3 mm^{-3}, surface density (S_V) in mm^2 m^{-3} and soil star length in mm, for images in Fig. 1 plotted as regions of barriers (solid line) and no barriers (dashed line). The line at 28 mm marks the position of the barrier.

REFERENCES

Baddeley, A. and Averback, P., 1983. Stereology of tubular structures. J. Microsc. 131: 323-340.

Baddeley, A.J., Gundersen, H.J.G. and Cruz-Orive, L.M., 1986. Estimation of surface area from vertical sections. J. Microsc., 142: 259-276.

Baldwin, J.P., Tinker, P.B. and Marriott, F.H.C., 1971. The measurement of length and distribution of onion roots in the field and laboratory. J. Appl. Ecol., 8: 543-551.

Barley, K.P., 1970. The configuration of the root system in relation to nutrient uptake. Adv. Agron., 22: 159-201.

Bengough, A.G., Mackenzie, C.J. and Diggle, A.J., 1992. Relations between root length densities and root intersections with horizontal and vertical planes using root growth modelling in 3-dimensions. Plant Soil, 145: 245-252.

Commins, P.J., McBratney, A.B. and Koppi, A.J., 1991. Development of a technique for the measurement of root geometry in the soil using resin-impregnated blocks and image analysis. J. Soil Sci., 42: 237-250.

Cruz-Orive, L.M., Hoppeler, H., Mathieu, O. and Weibel, E.R., 1985. Stereological analysis of anisotropic structures using directional statistics. Appl. Statist., 34: 14-32.

Diggle, A.J., 1988. ROOTMAP - a model in three-dimensional coordinates of the growth and structure of fibrous root systems. Plant Soil, 105: 169-179.

Dyer, D. and Brown, D.A., 1983. Relationship of fluorescent intensity to ion uptake and elongation rates of soybean roots. Plant Soil, 72: 127-134.

FitzPatrick, E.A., 1990. Roots in thin sections. In L.A. Douglas (Editor), Soil Micromorphology: A Basic and Applied Science. Proc. VIII Int. Working Meeting on Soil Micromorphology, San Antonio, Texas, July 1988. Developments in Soil Science 19, Elsevier, Amsterdam, pp. 9-15.

Goodwin, R.H. and Kavanagh, F., 1949. The isolation of scopoletin, a blue-fluorescing compound from oat roots. Bull. Torrey Bot. Club, 76: 255-265.

Hilliard, J.E., 1976. Assessment of sampling error in stereological analysis. In: E.E. Underwood, R. De Wit and G.A. Moore (Editors), Proceedings of the 4th International Congress on Stereology. National Bureau of Standards Special Publication No. 431, U.S. Gov. Printing Office, Washington, D.C., 547 pp.

Lang, A.R.G. and Melhuish, F.M., 1970. Lengths and diameters of plant roots in non-random populations by analysis of plane surfaces. Biometrics, 26: 421-431.

Mackie-Dawson, L.A. and Atkinson, D., 1991. Methodology for the study of roots in field experiments and the interpretation of results In: D Atkinson (Editor), Plant Root Growth: An Ecological Perspective. Blackwell Scientific Publications, Oxford, pp. 25-47.

McBratney, A.B. and Moran, C.J., 1990. A rapid method of analysis for soil macropore structure: II. Stereological model, statistical analysis, and interpretation. Soil Sci. Soc. Am. J. 54: 509-515.

McBratney, A.B., Moran, C.J., Stewart, J.B., Cattle, S.R. and Koppi, A.J., 1992. Modifications to a method of rapid assessment of soil macropore structure by image analysis. In: A.R. Mermut and L.D. Norton (Editors), Digitization, Processing and Quantitative Interpretation of Image Analysis in Soil Science and Related Areas. Geoderma, 53: 255-274.

Moran, C.J., Koppi, A.J., Murphy, B.W. and McBratney, A.B., 1988. Comparison of macropore structure of a sandy loam surface soil horizon subjected to two tillage treatments. Soil Use Manage., 4: 96-102.

Moran, C.J., McBratney, A.B. and Koppi, A.J., 1989. A rapid analysis method for soil pore structure. I. Specimen preparation and digital binary image production. Soil Sci. Soc. Am. J., 53: 921-928.

Moran, C.J. and McBratney, A.B., 1991. STRUCTURA: A C program for estimating attributes of two-phase, heterogeneous structures digitized from planar specimens. Computers and Geosciences, 17: 335-350.

Murray, R.D.H., Méndez, J. and Brown, S.A., 1982. The Natural Coumarins : Occurrence, Chemistry and Biochemistry. John Wiley & Sons Ltd, Chichester, 702 pp.

Sandau, K., 1989. Estimation of length- and surface density using information about directions. Acta Stereol., 8: 95-100

Sargent, J.A. and Skoog, F., 1960. Effects of IAA and kinetin on scopoletin-scopolin levels in relation to growth of tobacco in vitro. Plant Physiology, 35: 934-941.

Weibel, E.R., 1979. Stereological Methods. Volume 1. Practical Methods for Biological Morphometry. Academic Press, London, 415 pp.

On direct digital image acquisition from thin sections

L.-M. Bresson[1] and P. Guilloré[2]

[1]*Institut National Agronomique Paris-Grignon, 78850 Thiverval-Grignon, France*
[2]*CNRS, URA 12, Centre de Recherches Archéologiques, INA PG, 78850 Thiverval-Grignon, France*

ABSTRACT

Bresson, L.-M., and Guilloré, P., 1994. On direct digital image acquisition from thin sections. In: A.J. Ringrose-Voase and G.S. Humphreys (Editors), Soil Micromorphology: Studies in Management and Genesis. Proc. IX Int. Working Meeting on Soil Micromorphology, Townsville, Australia, July 1992. Developments in Soil Science 22, Elsevier, Amsterdam, pp. 515-520.

Image processing involves three stages: acquisition of a digital grey-level image, segmentation to a binary image, and generation of attributes. Image acquisition involves the digitizing of a soil thin section to a digital grey-level image. Sophisticated segmentation procedures may improve the binary image obtained from a poor quality grey-level image. However, the information contained within the grey-level image is controlled by the quality of the acquisition process. The latter mainly depends on the care taken by the user rather than on the image-processing software performance. A range of simple, practical procedures depending on the object studied and the features to be analyzed can improve image acquisition. A CCD black and white video camera was fitted either to a polarizing microscope or set up with a lens above a light table. The use of a dark cabinet which avoids interference of reflected light was found to be necessary. Cold light sources, optical fibres or IR filters should be used because most CCD video cameras are IR sensitive. Coloured filters can be used for increasing the contrast between areas of different colour. Different illumination modes, *i.e.* crossed polarized light, dark field, UV light, *etc.* can be used, and the different grey-level images can be combined for selecting different soil components. Gain and offset must be adjusted to get the optimum use of the 256 grey levels. This can be controlled using false colour look-up tables. Illumination heterogeneities due to the light source or induced by lens sphericity as well as by sensor deficiencies can be corrected in transmitted light mode. In this procedure, the image of the thin section is divided by the image of the source, leading to an "image" of the transmittance of the thin section. Examples illustrate the specific influence of these various procedures on the grey-level image and the segmented binary image.

INTRODUCTION

Image processing involves three stages: acquisition of a digital grey-level image, segmentation to a binary image and generation of attributes (Moran *et al.*, 1989). Sophisticated segmentation procedures may improve the binary image obtained from poor quality grey-level images, by extracting a larger proportion of the information contained within the grey-level image than the usual grey-level thresholding. For instance, the so called 'top-hat'
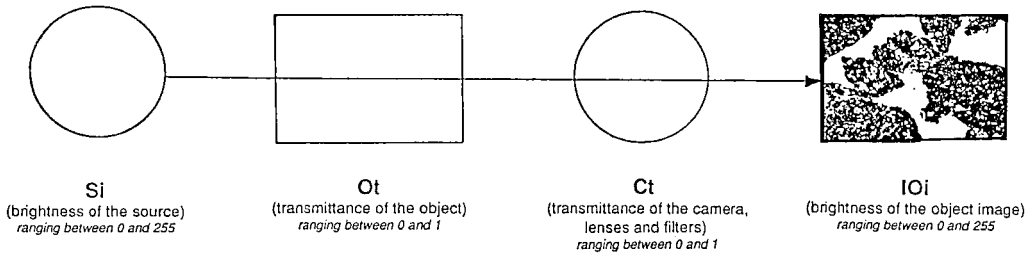
Fig. 1. Relationships between the transmittance of the object and the resulting grey-level image.

transformation (Serra, 1982) has been used to reveal the finest pores in an image without overestimating the largest pores (Moran *et al.*, 1989). However, the potential information which is available within the grey-level digital image is controlled by the quality of the acquisition process.

For the last twenty years, image analysis in soil micromorphology has usually involved image acquisition through an intermediate high-contrast photograph (Ismaïl, 1975; Bouma *et al.*, 1977; Murphy *et al.*, 1977; Ringrose-Voase, 1987; Bartoli *et al.*, 1991). Such a technique appeared to constitute a reasonable surrogate for both acquisition and segmentation when manufactured image analysis hardware and sofware were not well adapted to thin section images which usually were low-contrast images. For several years, however, video cameras with good resolution and high sensitivity have been available at a reasonable price. Therefore, image acquisition and segmentation should no more remain a "blind" process entrusted to a photographic laboratory.

This paper deals with image acquisition directly from thin sections. The quality of the resulting digital grey-level image mainly depends on the care taken by the user rather than on the performance of the image-processing software. Emphasis is laid on removal of optical artefacts rather than electronic artefacts. A range of simple, practical procedures are suggested for improving image acquisition which depend on the object studied and the features to be analyzed.

MATERIALS AND METHODS

A charged couple device (CCD) black and white video camera (Cohu 4700) was used. Its sensitivity was 0.1 lux, and its resolution 512×512 pixels. It was fitted either to a polarizing microscope or above a light table, which allowed coverage of a large range of magnifications. The thin sections which were digitized came from various soil materials and ranged from highly contasted transmittance (strongly coloured clayey B horizon) to poorly contasted transmittance (sandy white E horizon). We used a Matrox PIP 1024 digitizing board (512×512 pixels, 8 bits per pixel) and a IBM-compatible micro computer. The image processing software was Visilog 3.6 (Noésis).
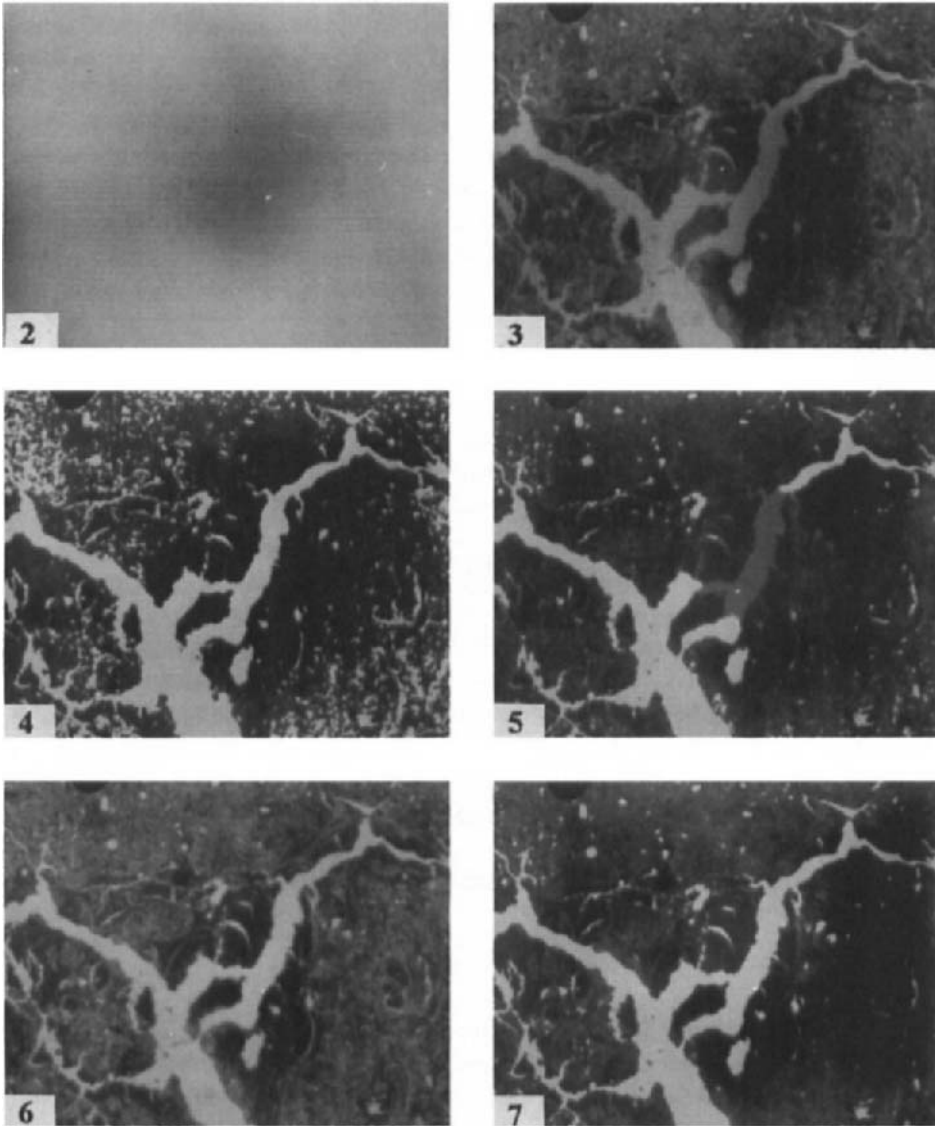
Fig. 2. Grey-level image of the light source (frame width 16 mm): for this experiment, brightness irregularities were deliberately increased.

Fig. 3. Grey-level image of the thin section (normalized): the appearance of pore space and matrix is affected by the brightness irregularities.

Figs 4 and 5. Poroids (white) were selected by thresholding the grey-level image (unselected 'solid' areas are displayed in half-tone gray). No satisfactory selection could be made: selecting most fissures induced an overestimation of the poroids within the matrix (Fig. 4) and adjusting to matrix poroids induced an underestimation of fissures (Fig. 5).

Fig. 6. Transmittance image of the object: Compare to Fig. 3.

Fig. 7. Poroids (white) selected from the transmittance image (unselected 'solid' areas are displayed in half-tone gray): compare to Figs 4 and 5.

RESULTS AND DISCUSSION

Dark cabinet

A dark cabinet was necessary to avoid interference from reflected light. This was especially obvious when digitizing thin sections under crossed-polarized or UV light, because the light intensity was low. The cabinet was useful, however, in all circumstances, because the pertinent threshold for image segmentation usually ranged in a narrow window of about 5 to 10 grey levels. External light could easily induce subtle, even unperceptible, variations that can result in artefacts after thresholding.

Light filtering

CCD video cameras, especially high sensitivity ones, are often significantly sensitive to infra-red light. Therefore, 'cold' light sources should be used, which can be easily achieved using optical fibres or adequate infra-red filters. This was especially relevant for cross-polarized light.

Coloured filters can be used with black and white video cameras for increasing the contrast between areas of different colours.

Gain and offset

An accurate segmentation by grey-level thresholding required getting optimum use of the full grey-level range (0 - 255). Moreover, both undersaturation of dense areas and oversaturation of pore space must be avoided because they prevent any differentiation of grey levels within the ranges concerned. Therefore, a good control of gain and offset is required, which can be easily assessed by using adequate look-up tables. False colour look-up tables which display the lowest grey levels in cold colours and the highest grey-levels in hot colours are especially convenient.

Transmittance image

It is very difficult to get even illumination of the field of view. Irregularities usually come from (1) the light source itself, including the condenser device, and (2) the sphericity aberration of the lenses of the video camera or microscope. Therefore, it is more convenient to get the transmittance image itself, which does not depend on the illumination conditions. This is possible by dividing the grey-level image of the thin section (Fig. 3) by the grey-level image of the source after removing the object (Fig. 2).

From the definition of transmittance:

$$IOi(x, y) = Si(x, y) \times Ot(x, y) \times Ct(x, y) \tag{1}$$

where IOi (brightness of the object image) and Si (brightness of the source) range between 0 and 255 and Ot (transmittance of the object) and Ct (transmittance of the camera) between 0 and 1 (Fig. 1).

Then,

$$Ot(x,y) = \frac{Ioi(x,y)}{Si(x,y) \times Ct(x,y)} \qquad (2)$$

If *ISi* is the image of the source and equals *Si(x,y)* × *Ct(x,y)*:

$$Ot(x,y) = \frac{IOi(x,y)}{Isi(x,y)} \qquad (3)$$

Multiplying by 255 allows visualization of the transmittance image (Fig. 6) using the full grey-level range: 0 for transmittance 0 (opaque) to 255 for transmittance 1 (transparent).

This procedure also partly overcomes some faults induced by the CCD sensor itself. The specific influence of this procedure on the grey-level image quality and on the resulting segmented binary image is illustrated in Figs 4, 5 and 7.

Such transmittance images cannot be obtained using video cameras with automatic gain control unless it can be disabled.

CONCLUSIONS

The practical procedures described above were found necessary to acquire good quality, digitized images from soil thin sections. The quality of the acquisition controls the amount of information within the grey-level image, which, in turn, controls the quality of the segmentated image and related attributes. Moreover, the pixel value of the transmittance image measures an intrinsic physical property of the object.

Good quality is of great importance in selecting different components within a thin section, because this usually involves the combination of several grey-level images acquired using different illumination modes (Ismail, 1975; Guilloré, 1987, Bui and Mermut, 1989).

The procedure is potentially applicable to colour images by applying the correction to the red, green and blue channels independently.

New technical improvements should be found for image acquisition in reflecting and emission modes.

REFERENCES

Bartoli, F., Philippy, R., Doirisse, M., Niquet, S. and Dubuit, M., 1991. Structure and self-similarity in sandy and silty soils: the fractal approach. J. Soil Sci., 42: 167-185.

Bouma, J., Jongerius, A., Boersma, O., Jager, A. and Schoonderbeek, D., 1977. The function of different types of macropores during saturated flow through four swelling soil horizons. Soil Sci. Soc. Am. J., 41: 945-950.

Bui, E.N. and Mermut, A.R., 1989. Quantification of soil calcium carbonates by staining and image analysis. Can. J. Soil Sci., 69: 677-682.

Guilloré, P., 1987. Analyse photographique à grand champ des lames minces. In: N. Fedoroff, L.M. Bresson and M.A. Coutry (Editors), Soil Micromorphology. Proc. VII Int. Working Meeting of Soil Micromorphology, Paris, July 1985. Association Française pour l'Etude du Sol, Plaisir, France, pp. 49-56.

Ismaïl, S.N.A., 1975. Micro-morphometric soil-porosity characterization by means of electro-optical image analysis (Quantimet 720). Soil Survey Papers, No. 9, Soil Survey Institute, Wageningen, The Netherlands.

Moran, C.J., McBratney, A.B. and Koppi, A.J., 1989. A rapid method for analysis of soil macropore structure. I. Specimen preparation and digital binary image production. Soil Sci. Soc. Am. J., 53: 921-928.

Murphy, C.P., Bullock, P. and Turner, R.H., 1977. The measurement and characterization of voids in soil thin sections by image analysis. Part I. Principles and techniques. J. Soil Sci., 28: 498-508.

Ringrose-Voase, A.J., 1987. A scheme for the quantitative description of soil macrostructure by image analysis. J. Soil Sci., 38: 343-356.

Serra, J., 1982. Image Analysis and Mathematical Morphology. Academic Press, London, 610 pp.

Description of the spatial interaction between earthworm burrows and cracks at the soil surface

J. Chadœuf[1], A. Kretzschmar[2], M. Goulard[1] and K.R.J. Smettem[3]

[1]INRA-Biométrie, BP 91, 84140 Montfavet, France
[2]INRA-Zoologie, Laboratoire de Physique et Biologie des Sols, BP 91, 84140 Montfavet, France
[3]CSIRO Division of Soils, PMB, Aitkenvale, 4814 QLD, Australia

ABSTRACT

Chadœuf, J., Kretzschmar, A., Goulard, M. and Smettem, K.R.J., 1994. Description of the spatial interaction between earthworm burrows and cracks at the soil surface. In: A.J. Ringrose-Voase and G.S. Humphreys (Editors), Soil Micromorphology: Studies in Management and Genesis. Proc. IX Int. Working Meeting on Soil Micromorphology, Townsville, Australia, July 1992. Developments in Soil Science 22, Elsevier, Amsterdam, pp. 521-530.

In order to investigate the spatial interaction between the distributions of earthworm burrows and cracks, the soil surface of a prepared soil box (0.5 m²) was observed after two successive periods of drying, between which the macroporosity of the soil surface was destroyed by raindrop impact and washing in of sediment by surface runoff. At each observation, the coordinates of earthworm burrows and the topology of cracks (from the skeleton of the crack pattern) were recorded. A scaling factor was estimated and the burrow coordinates were transformed to remove an observed edge effect.

More numerous burrows were observed after the second drying (256 compared to 183 at the first time) and they were longer and larger.

The distribution of earthworm burrows at increasing distances from the cracks was tested against a simulated random (non-stationary) distribution of burrows over the whole surface of the core (Poisson-like distribution).

A spatial relationship was found to exist. The number of burrows in the vicinity of cracks was higher in both observations than if they had been distributed at random. The strength of this relationship decreased with increasing distance from the cracks. Beyond a distance of 2 to 3 cm, there was no longer any difference between observed and random distributions.

It was also investigated if aggregative patterns in burrow distribution might modify the general relationship. The simulated distributions were conditioned so that a given burrow had a given number of neighbours at a fixed distance. In this case, there was no difference between simulated and observed distributions.

It was concluded that the spatial relationship between burrows and cracks was dependant only on the distance between burrow and cracks, with one exception *i.e.* the places where cracks and burrows occupied the same location were more numerous in the observed than with the simulated distribution. These burrows had been "captures" by the crack growth process.
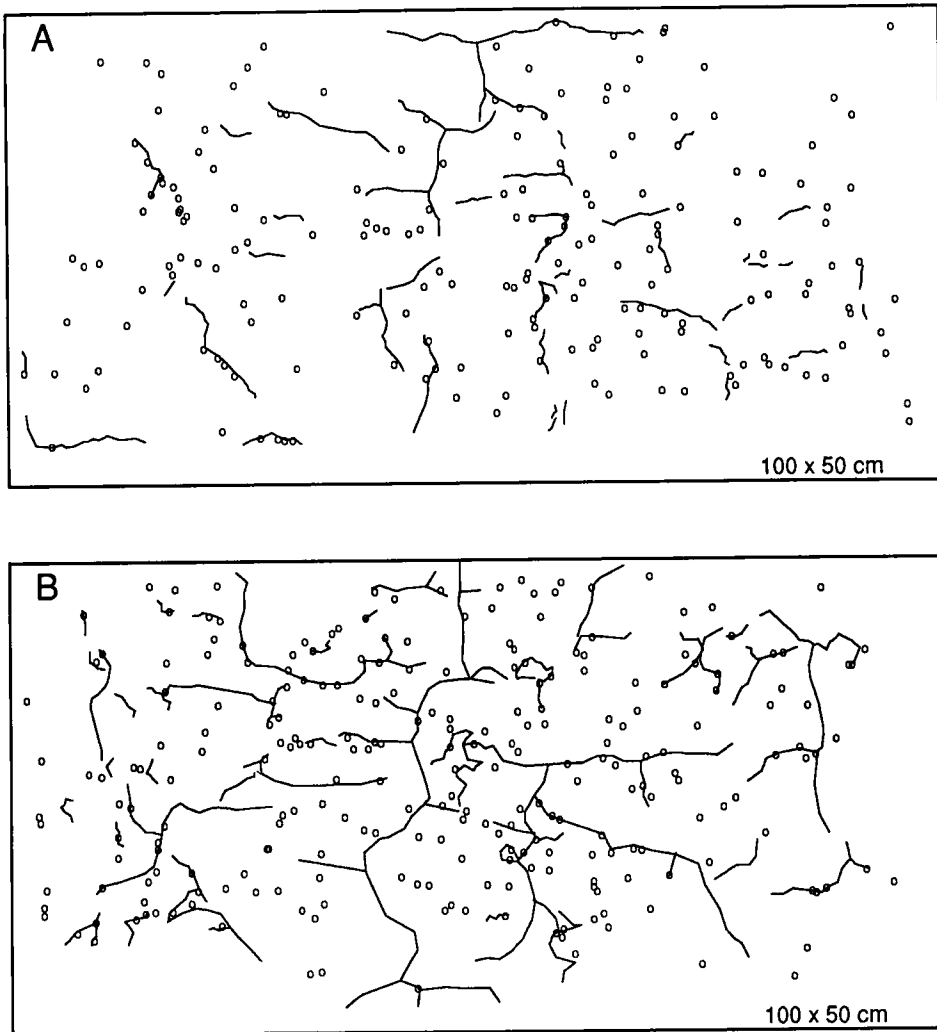
Fig. 1. Maps of cracks and burrows for the first (A) and the second (B) observations (dimension : 100 × 50 cm; O burrows; —— cracks).

INTRODUCTION

The spatial interactions of the main components of soil surface macroporosity (earthworm burrows and cracks) can be studied from different viewpoints:

(i)   The soil surface macroporosity might have a role in water infiltration after ponding and consequently on runoff and erosion.

(ii)   The spatial pattern of the distribution of these components may serve as a starting point for the description of the 3-D pattern of macropores within the soil profile.
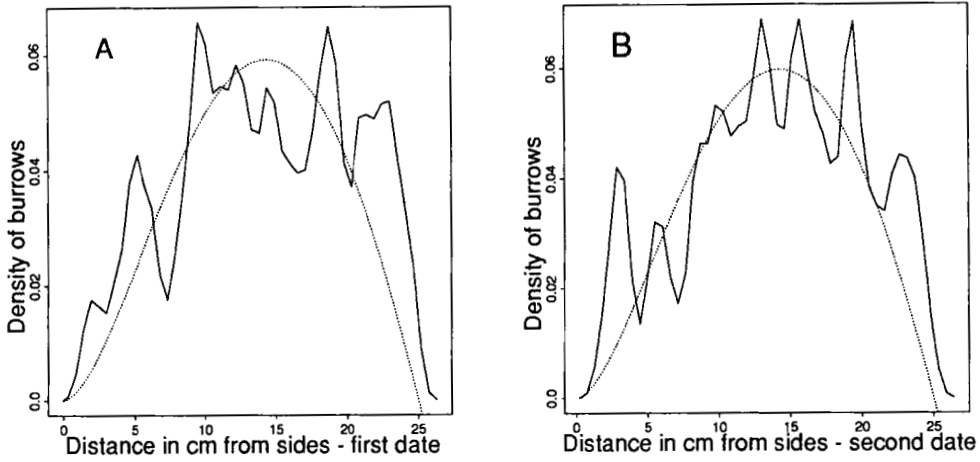
Fig. 2. Observed and simulated distribution of burrows versus the distance to the edges for the first (A) and the second (B) observations.
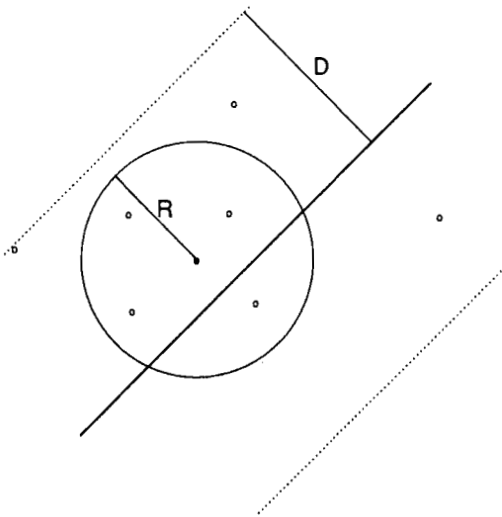
Fig. 3. Definition of R and D. + is an element of the point process situated in a zone at ± D from the crack (———) and having 4 neighbours (O) at a distance <R.

(iii)   Finally, this application may present an opportunity to assess a general method for studying the spatial interaction of point and fibre processes on a planar surface (Stoyan and Ohser, 1982).

The specific objectives of this study are:

(i)   Development of a model for the earthworm burrow distribution (a point process) which leads to a quantitative estimation of its interaction with the crack distribution (a fibre process).

Total number of burrows

Total number of burrows
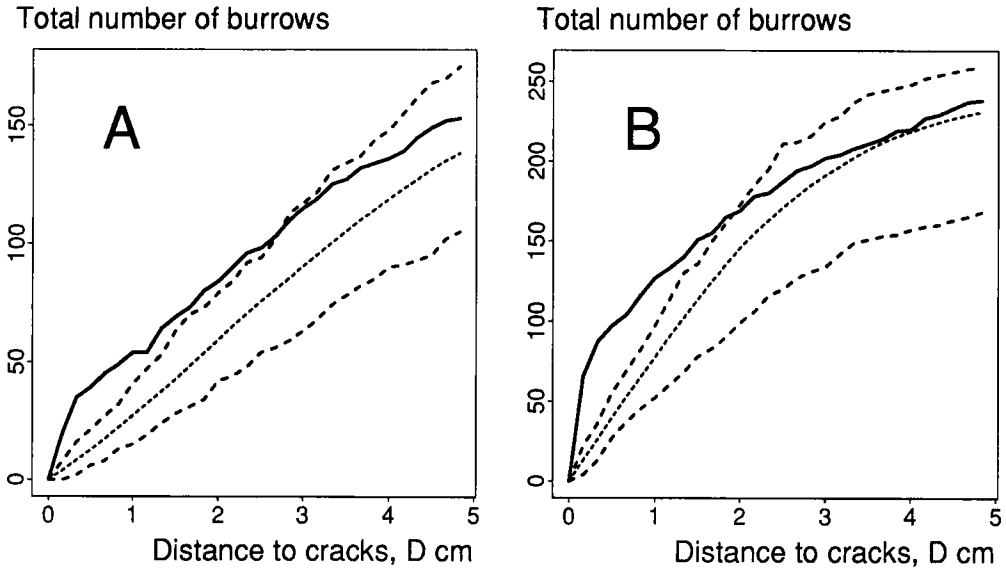
Fig. 4. Total interaction between cracks and burrows for the first (A) and the second (B) observations. Line symbols: − − − − − maximum and minimum curves of Monte Carlo simulations; − − − − − − − − − average curve of 99 simulations; ──────── observed data.

(ii)   To infer from the type of interaction a mechanism which governs the cracking dynamics in the presence of burrows, as burrow formation precedes cracking (the burrows occured during the wet phase and the cracks developed during the next drying phase).

Few data exist in the literature about the distribution of burrow openings at the surface. If mentioned (Beven and Germann, 1981; Smettem and Collis-George, 1985), the distribution is considered as random and stationary. The crack pattern at the soil surface has been studied *per se* as a tesselation process which implies consideration only of the closed cells. Moreover, they have been studied mainly in relation to clay surface crusts rather than to the general case of cracking at the surface of soils with low clay content.

The present study was set up as a preliminary investigation to understand the dynamics of the opening and closing of macropores at the soil surface as a conseqence of their spatial interactions. This study is based on a general method to estimate the interaction between point processes and fibre processes recently presented by Chadœuf *et al.* (in press).

MATERIALS AND METHODS

A calcareous sandy loam topsoil (Calcic Rhodoxeralf) was used in this study. Soil was collected from the surface 0.1 m, which had a texture of 11% clay, 19% silt (2 - 20 μm) and 69% sand. The soil organic carbon content was 1.4%.

Air-dried soil, crushed to pass through a 4.0 mm sieve, was packed at a bulk density of 1.3 Mg m^{-3} into a 0.5 × 1.0 m perspex tray to a depth of 90 mm over a 30 mm thick layer of

coarse sand. The soil tray was placed under a low energy rainfall sprinkler and irrigated. The movement of the wetting front was monitored to check its uniformity. After the soil was uniformly wet, earthworms were introduced to the tray. The surface was mulched with moistened, partially decomposed plant residues to encourage the development of surface connected burrows.

After two weeks burrowing activity, the mulch was removed by hand and all loosened surface casts were carefully removed with the aid of a small vaccum cleaner. The soil surface was then exposed to drying for a further two weeks, during which time a crack pattern developed.

The size and location of all surface vented burrows and dessication cracks at the soil surface were recorded with a marker pen on plastic sheets, when the crack patterns were stabilized.

The tray was then placed under the rainfall sprinkler for a second irrigation. This resulted in closure of all the surface macropores (worm channels and cracks) due to clogging by fine, transported sediment. After this irrigation, the experimental cycle described above was repeated and the burrow and crack system, when stabilized, were re-mapped.

RESULTS AND DISCUSSION

Burrow distribution model

Fig. 1 presents maps of the cracks and burrows, at the first (A) and the second (B) measurement dates. One can see, for both dates, that the distribution of burrows is not stationary (there are few burrows near the edge of the box). The distribution of burrows was then modelled using a non-stationary Poisson distribution:

$$p(x_1 \ldots x_n) = \frac{\lambda^n}{n!} \prod_{i=1}^{n} u_i^\alpha \exp(-\lambda g(\alpha))$$

where;
x = occurence of a burrow
$p(x_1 \ldots x_n)$ = probability of the occurence of a population of n burrows
n = number of burrows
u = distance to the edges

$$g(\alpha) = \int_0^{1/2} (L - 2u)(l - 2u)u^\alpha du$$

where L and l are the large and the small side lengths of the experimental blocks.
λ and α are estimated by the maximum likelihood method.

Fig. 2 shows the fitting of this distribution to the observed data for the first and second dates (A and B respectively). This non-stationary Poisson-like distribution appears to be a reasonable approximation of the observed data.

Interactions between burrows and cracks

The interaction was modelled using two spatial properties:
(i)   The variation of the density of burrows at a given distance D from the cracks when D varies from 0 to 5 cm.

No of burrows with 0 neighbours

No of burrows with 1 neighbour

No of burrows with 2 neighbours

No of burrows with 3 neighbours

R=1cm

R=3cm

R=5cm

Distance to cracks, D cm
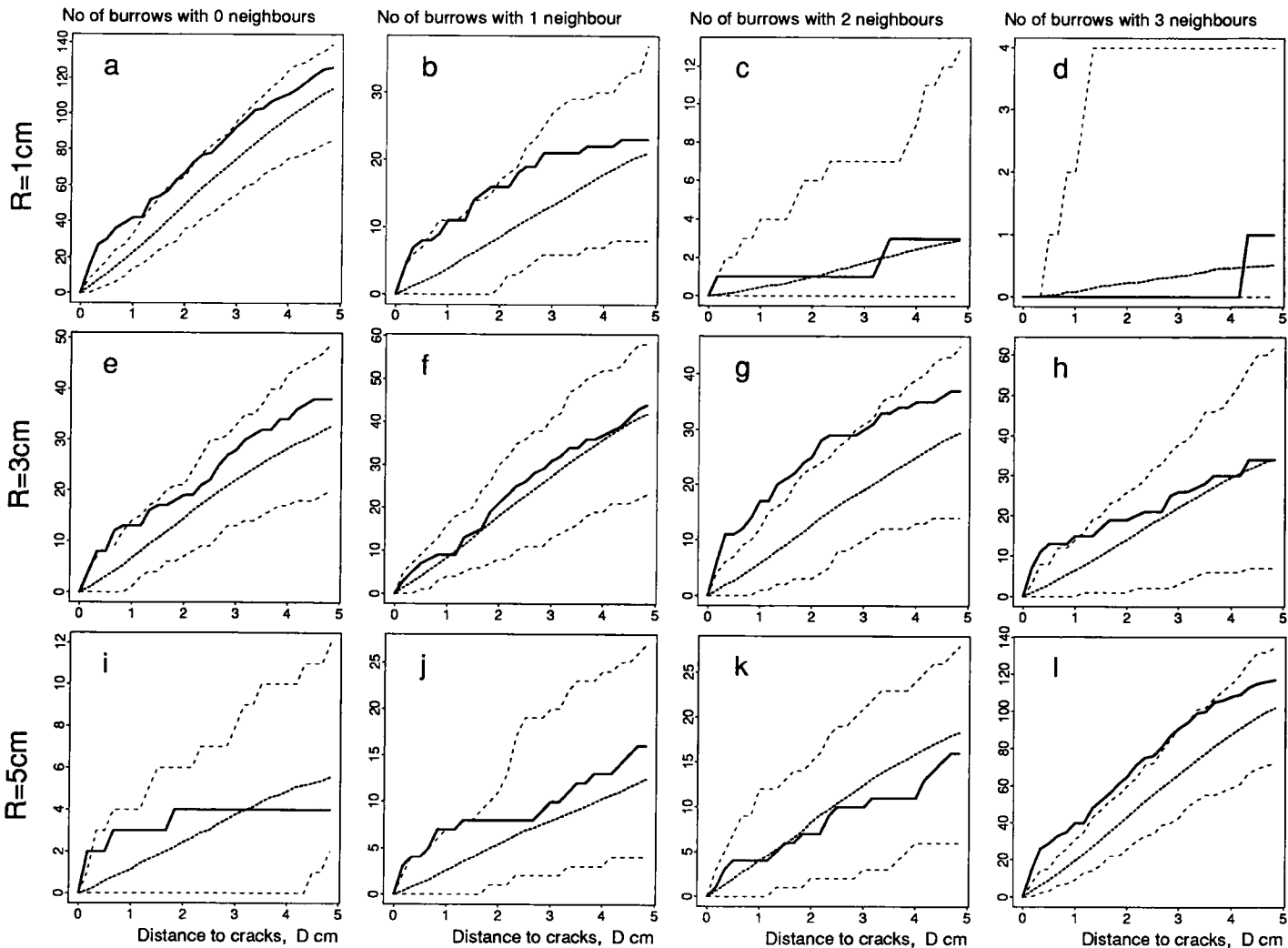
(ii)   The variation with D and R (Fig. 3) of the spatial density of burrows around a given burrow which is at distance, D, from a crack and which has 0, 1, 2, 3 or more neighbours within a radius R.

In the first case, the global interaction is estimated, whereas in the second, the method focuses on the local density near the cracks.

The estimation procedure was as follows: for each date, 99 simulations of a population of burrows (183 or 256 burrows were measured respectively for the first and second dates) were used to estimate the domain of independance of the interaction defined above. The global significance value of this test was 1% (Monte Carlo test; Diggle, 1983).

Fig. 4a and b show the total interaction for the first and the second dates respectively. The absence of interaction would be shown by the observed data falling within the area delimited by the minimum and maximum curves. Both figures clearly show an interaction because the number of burrows within 2 - 3 cm of the cracks is significantly greater than the independent distribution would admit.

Fig. 5 shows examples of the variation of the interaction depending on the distance and the local density (k = number of neighbours) in the case of R = 1, 3 or 5 cm for the first date. This figure shows that the interaction between burrows and cracks depends on the local density of burrows in the vicinity of the cracks. An interaction is clearly observed in a), g) and l). A small interaction, very close to the cracks, is shown in b), e), h), i) and j). The area delimited by the observed curve and the maximum curve (when the observed data are outside the domain of independance) is related to R and k. The interaction is maximum when the values of R and k lead to the highest number of burrows involved. This means the interaction occurs only when the global density of burrows reaches a given level. When there are few burrows, there is no interaction.

Conditional interaction

It must be asked now if the interaction depends on the local density of burrows $i.e.$ if the cracks are attracted by burrows when they are clustered.

To estimate if the interaction depends on the variation of local burrow density in the vicinity of cracks, the simulated distributions are then made conditional on the local density: the point density function of the simulated Poisson process at a given distance of the cracks now follows the density function as of the observed data. Fig. 6 gives evidence, for $R \leq 3$ cm, that the interaction, if it exists, is now only observed at a very short distance from the cracks.

This procedure demonstrates that the interaction between cracks and burrows relies only on the variation of burrow density which increases when the distance to the cracks decreases. It does not depend on local patterns of clustering of the burrows.

To demonstrate this global effect, the variation with D in the density function for burrow distribution is shown in Figs 7A and B for the first and second dates respectively. The interaction occurs at very short distances to the cracks indicating that burrows become the focus of cracks due to the presence of a zone of weakness.

Fig. 5. Interactions between cracks and burrows depending on the distance from the cracks and on the local density (number of burrows). a, b, c and d — R=1 cm; e, f, g and h — R=3 cm; i, j, k and l — R=5 cm. Line symbols as for Fig. 4.

No of burrows with 0 neighbours

R = 3cm

Distance to cracks, D cm

No of burrows with 1 neighbour

Distance to cracks, D cm

No of burrows with 2 neighbours

Distance to cracks, D cm

No of burrows with 3 neighbours

Distance to cracks, D cm
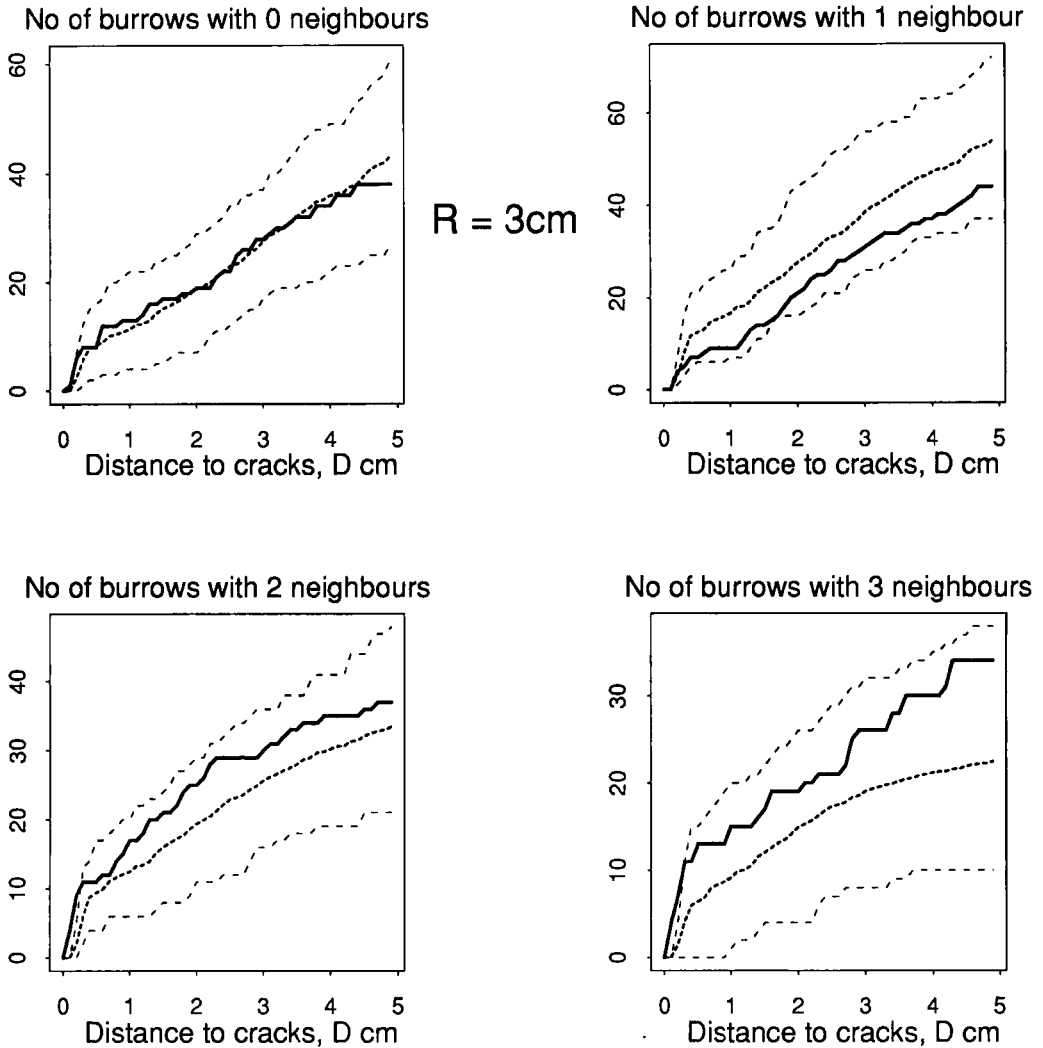
Fig. 6. Interactions between cracks and burrows with conditional density (R = 3 cm; first observation). Line symbols as for Fig. 4.

CONCLUSIONS

The description of the soil surface macropososity, using simple 2-D spatial distributions data, may lead to the formulation of an hypothesis for the dynamics of crack formation if the distribution patterns are precisely estimated. In the case of earthworm burrows and cracks, the successive estimations of the spatial interaction, using parameters derived from a Poisson-like distribution, show two stages of the interaction that correspond to two differents mechanisms:
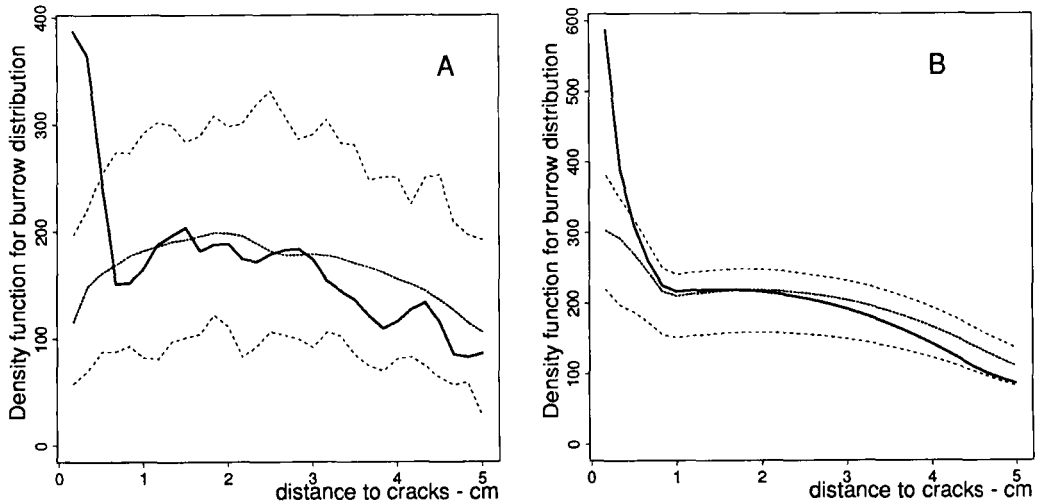
Fig. 7. Density function of burrow distribution related to the distance from the cracks for the first (A) and the second (B) observations. Line symbols as for Fig. 4.

(i)   The global non-stationarity of the Poisson-like distribution removes any experimentally induced "edge" effects and reveals the "attraction" between burrows and cracks within a domain surrounding the cracks;

(ii)   The "local-density-dependent" distribution reveals that the cracks are found mainly where the density of burrows is the highest; additionally, a significant part of that population of burrows is "captured" by the crack growth, leading to the formation of an interconnection between surface cracks and the burrow system underneath.

The topology of the soil surface macroporosity can be described by estimating the spatial interaction between the components.

This method is the basis of the quantitative study of the relative distribution of crack, roots, voids and channels at the microscopic scale (Krebs *et al.*, 1994). The measurement of spatial interaction should be a tool in the description of micromorphological features of soil fabrics.

The simulation of distribution patterns, which does not require computer image processing or image analysis, potentially allows quantitative estimation of spatial relationships and of the critical distance over which any interactions are effective. It may therefore be used as a basic model for interpreting the development of this particular type of macropore pattern.

REFERENCES

Beven, K. and Germann, P.F., 1981. Water flow in soil macropores. 2. A combined flow model. J. of Soils Sci., 32: 16-30.

Chadœuf , J., Kretzschmar, A., Goulard, M. and Smettem, K.R.J. Analyse de la liason entre un processus de galerie et la fissuration du sol. Biometrics (in press).

Diggle, P.J., 1983. Statistical Analysis of Spatial Point Patterns (Mathematics in Biology). Academic Press, London, 148 pp.

Krebs, M., Kretzschmar, A., Babel, U., Chadœuf, J. and Goulard, M., 1994. Investigations on distribution pattern in soil: basis and relative distributions of roots, channels and cracks. In: A.J. Ringrose-Voase and G.S. Humphreys (Editors), Soil Micromorphology: Studies in Management and Genesis. Proc. IX Int. Working Meeting on Soil Micromorphology. Developments in Soil Science, 22. Elsevier, Amsterdam, pp. 437-449.

Smettem, K.R.J. and Collis-George, N., 1985. Statistical characterization of soil biopores using a soil peel methods. Geoderma, 36: 27-36.

Stoyan, D. and Ohser, J., 1982. Correlation between planar random structures, with an ecological application. Biom. J., 24, 631-647.

Quantitative methods to determine microporosity in soils and sediments

N.K. Tovey[1], P. Smart[2] and M.W. Hounslow[1]

[1] *School of Environmental Sciences, University of East Anglia, Norwich, NR4 7TJ, UK*
[2] *Department of Civil Engineering, University of Glasgow, Glasgow, G12 8QQ, UK*

ABSTRACT

Tovey, N.K., Smart, P. and Hounslow, M.W., 1994. Quantitative methods to determine microporosity in soils and sediments. In: A.J. Ringrose-Voase and G.S. Humphreys (Editors), Soil Micromorphology: Studies in Management and Genesis. Proc. IX Int. Working Meeting on Soil Micromorphology, Townsville, Australia, July 1992. Developments in Soil Science 22, Elsevier, Amsterdam, pp. 531-539.

A new technique is described to quantify the porosity of soils using image analysis techniques. Unlike most previous studies, this method enables the porosity between clay size particles to be investigated. An essential pre-requisite is the use of Wiener filtering methods to remove some of the degradation inherent in all imaging systems. Segmentation of the images into binary form using a relative contrast histogram method provides a basis for the objective thresholding which can be used for automatic batch processing of images.

Bulk porosity measurements from image analysis are in good agreement with bulk porosity measurement. The intra-domain porosity may be studied by overlaying this porosity-segmented image with one which delineates the extent of different domains within the matrix. Domains which have particles aligned in a horizontal direction consistently have porosities which are greater than those domains with vertically orientated particles.

INTRODUCTION

It is well known that the micro-fabric and associated porosity play an important role in determining the macroscopic properties of soils and sediments, such as compression and shear behaviour, transmission of fluids, diagenesis and, also, crop yields. Assessment of the porosity within soils and sediments has usually used optical microscope methods (and sometimes low magnification electron microscopic methods) to observe and measure the larger pores within the sediment (Bisdom and Schoonderbeek, 1983; Pye, 1984; Dilks and Graham, 1985). In recent years, much research has been devoted to image analysis in an attempt to quantify the fabric changes seen.

A requirement for many of these studies has been a need to threshold or segment the images into patches which correspond to voids or particular particles of one mineral composition. Frequently, the sample has been impregnated with a fluorescent dye so that a sharp contrast between the solid and voids is obtained under ultra-violet light. Suitable images may also be obtained by transmission electron micrographs of ultra-thin sections of embedded clayey soils, and scanning electron microscope (SEM) images of polished blocks of embedded soils

observed in the back-scattered electron (BSE) mode. However, in neither of these cases is it easy to find a single threshold value which will adequately discriminate between the particles and voids. Operator intervention to "paint" areas of difficulty is far from satisfactory as this introduces subjectivity, creates problems when there are large numbers of features on a micrograph, and prevents the development of automatic batch processing routines. This latter aspect is important if sufficient images are to be analysed to provide statistically meaningful information about the pores and particles.

This paper describes a sequence of image processing and analysis steps which permits the objective quantification of batches of micrographs of certain types of soil fabric. The method may be extended to separate overall porosity into component parts within each individual domain or each group of domains. The technique is illustrated using samples of Speswhite Kaolin which were tested in the laboratory in both consolidation and shearing under known stress paths. The technique has also been used on a wide range of soils and sediments, although for soils where there is a wide range of particle sizes, it is often necessary to pre-process the images using the mineral segmentation techniques described by Tovey *et al.* (1994).

METHODS

Specimen Preparation

After testing in either consolidation or triaxial shear, the samples were impregnated with epoxy resin using techniques described in Smart and Tovey (1982), polished and coated with 10 nm carbon for viewing in the SEM. Both horizontal and vertical surfaces of each sample can be observed, but the majority of observations were on vertical surfaces. The kaolin particles have a higher average atomic number than the impregnating resin and thus the particles are brighter than the surrounding voids, when viewed using the BSE mode in the SEM. Digital images (512×512 pixels; 256 grey-levels) were captured using a dwell time of 51 µs per pixel, a pixel spacing of 0.11 µm (corresponding to a magnification of 2000× on the SEM used), operating voltages between 15 and 20 kV and working distances in the range 12 - 15 mm.

Image Processing and Analysis

Selection of suitable thresholds for images

Since the particles are of a different average atomic number from that of the resin, the BSE images should be ideally suited to segmenting the image into two components (particles and voids) by simple global thresholding. It was expected that, if the SEM intensities were carefully calibrated each time, the grey-level histogram would be bimodal with one peak representing the particles and the other the voids. The trough between the two would represent the value to select for the threshold. In reality, the histogram of grey-levels was unimodal, and global thresholding was not possible. This difficulty becomes particularly acute when the particles are small and near the limit of resolution. Others (*e.g.* Dilks and Graham, 1985), studied porosity in sandstones which have relatively large particles and thus do not have the same problem.

Image Restoration

All microscopes degrade the quality of the captured image as the microscope and capture system do not have infinite precision. Techniques to restore the image by removing the effects of the microscope are now in common use. In particular, it is noted that if the true image is represented by the two dimensional function $f(x,y)$ and the point spread function of the instrument by $h(x,y)$, then the image actually acquired, $g(x,y)$, is given by:

$$g(x,y) = f(x,y) \otimes h(x,y) + n(x,y)$$
Eqn. 1

where $\otimes$ is the convolution operator, and $n(x,y)$ indicates the noise function.

The aim of image reconstruction is to obtain the function $f(x,y)$ from the acquired image, $g(x,y)$. In the absence of noise, the Fourier Transform of the restored image may be obtained from:

$$F(u,v) = \frac{G(u,v)}{H(u,v)}$$
Eqn. 2

where $F(u,v)$, $G(u,v)$, $H(u,v)$ are the Fourier Transforms corresponding to $f(x,y)$, $g(x,y)$, and $h(x,y)$ respectively.

It is then a simple matter to invert this function $F(u,v)$ to produce a de-blurred image. This method of image reconstruction is not satisfactory because of the effects of noise (Gonzalez and Wintz, 1987). It is now common to use a Wiener filter, or other more complex, non-linear algorithms (Guan and Ward, 1989). The Wiener filter can be formalised in Fourier space as:

$$F(u,v) = G(u,v)\,Y(u,v)$$
Eqn. 3

where $F(u,v)$ is the best reconstruction, $G(u,v)$ is the image to reconstruct and $Y(u,v)$ is the Wiener filter and is a complex function involving both the point spread function and a noise function. To undertake such a reconstruction, it is necessary to know or measure both the point spread function and the noise function.

Practical procedures employed

A full discussion of the method may be found in Hounslow and Tovey (1994) but the following highlights the key points. The signal to noise ratio can be estimated for each group of digitised images by recording an image of the resin surrounding the sample. In these 'resin' images there should be no contrast variation. Any spread in intensities arises from noise.

The point spread function of the SEM was determined in this study by measuring the intensity profiles of point sources in the microscope at the working magnification of 2000×. Ten such point sources were observed and radial line profiles obtained at 30° intervals. These profiles were rotationally averaged and the composite mean from all 10 points was used to define the best fitting Gaussian intensity profile for use in all subsequent restoration work.

After the application of the Wiener filter, the original image (Fig. 1a) is considerably sharpened (Fig. 1b). However, if electrical interference effects are present in the Fourier Transform (a common occurrence), then these should be removed before final restoration (Hounslow and Tovey, 1994).
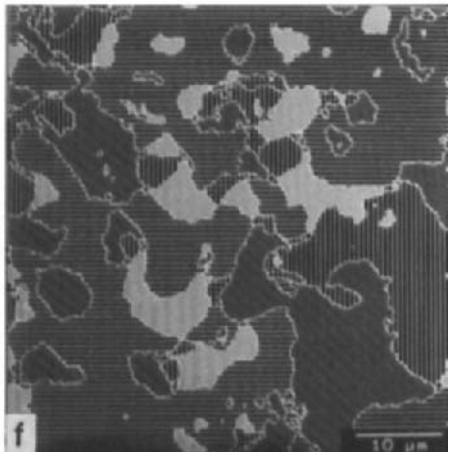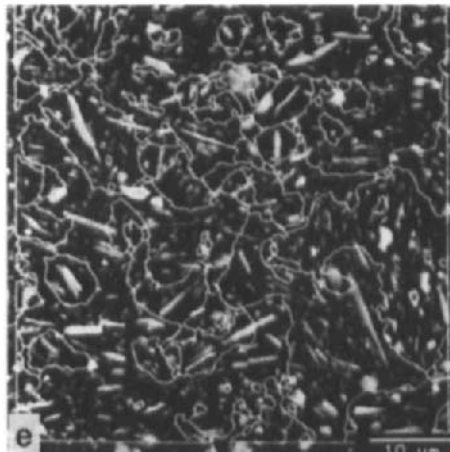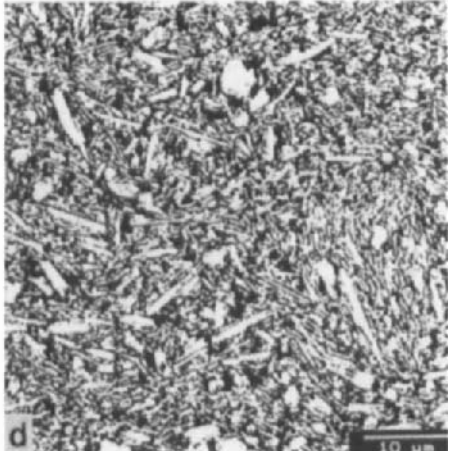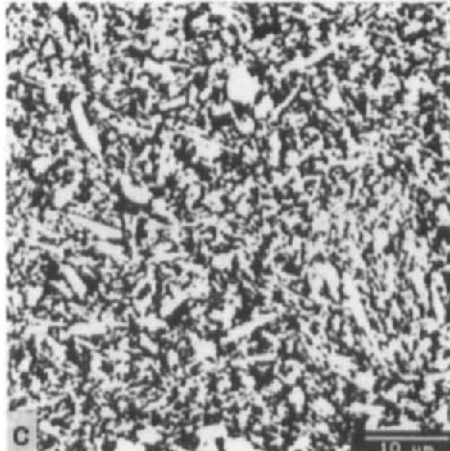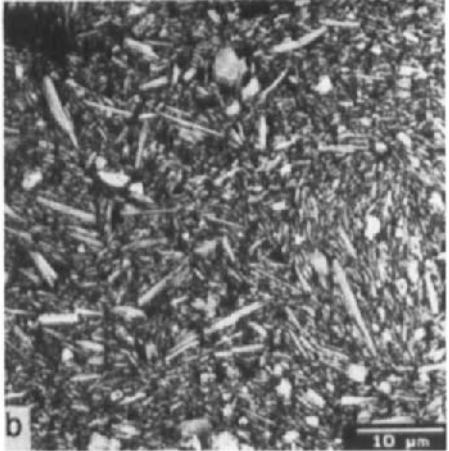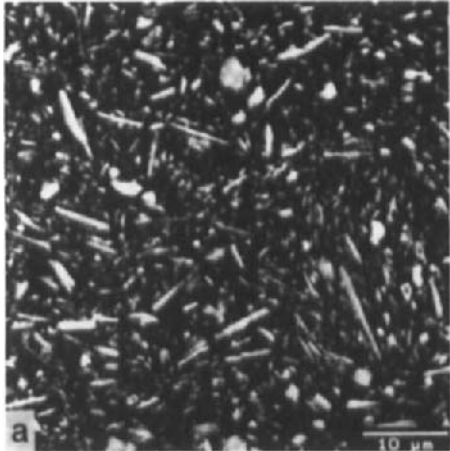
Selection of Best Global Threshold

While the Wiener filtered image is considerably sharpened, the grey-level histogram is still unimodal. Many algorithms, using Laplacian operators, and/or edge-detectors have been proposed to solve the thresholding problem. While some methods have proved very suitable in other applications (*e.g.* the method of White and Rohrer, 1983), they were generally unsuitable in this study, as there is no equivalent to the local consistency information of White and Rohrer, which could be included in a decision-making stage and which is applicable to a large range of soils.

The Relative Contrast Histogram method, first proposed by Kohler (1981), proved the most suitable method to select an objective threshold and was used throughout. The method examines the relative grey-level differences between a selected search threshold value and the intensities at adjacent pixels in either the x or y direction. If two adjacent pixel values are I_a and I_b (where $I_b \geq I_a$) and the search threshold level is T (where $I_a \leq T \leq I_b$, the contribution to the Relative Contrast Histogram, $C(t)$ from these two adjacent pixels is:

$$C(t) = \min(T - I_a, I_b - T)$$ Eqn. 4

This procedure is performed again for the same pair of pixels for each value of T from I_a to I_b. An output histogram for this pair of pixels is generated in the range I_a to I_b with a maximum value occurring at $C(I_a+I_b)/2$ (Fig. 2). The procedure is repeated across the whole image for each adjacent pair of pixels and the separate histograms summed to provide an aggregate histogram for the whole image. The resulting histogram has several peaks if the material is multi-phase (as for a natural soil), or a single peak if only two-phases are present as is the case here. The location of this peak then represents the optimum value for thresholding the Wiener filtered image. Fig. 1c, shows the binary image obtained using this technique on the original image, while Fig. 1d shows the effect of doing the same procedure, but this time with Wiener filtering. The improvement in the quality of Fig. 1d is immediately apparent.

RESULTS FROM POROSITY ANALYSIS

Overall Porosity

Once an image has been segmented, the evaluation of the porosity is a simple matter. Hounslow and Tovey (1994) showed that on the basis of nearly 2000 images from over 80 samples mechanically tested in a variety of ways, the porosity measured using image processing with initial Wiener filtering closely matched that determined from moisture content analysis on bulk samples. Only when the porosity became large was there a divergence in the results. This divergence was attributed to porosity associated with the ultra-fine voids which were beyond the resolution of the image.

Fig. 1. **a)** Back-scattered SEM image of consolidated kaolin (picture width 56 µm). **b)** Image restored after application of Wiener Filter. **c)** Binary image of a) using relative contrast histogram method. **d)** Binary image of b) computed using relative contrast histogram method. **e)** Domain-segmented image of a) showing boundaries overlaid on original. **f)** Classification of domains according to orientation (random domains are shown as a series of dots).
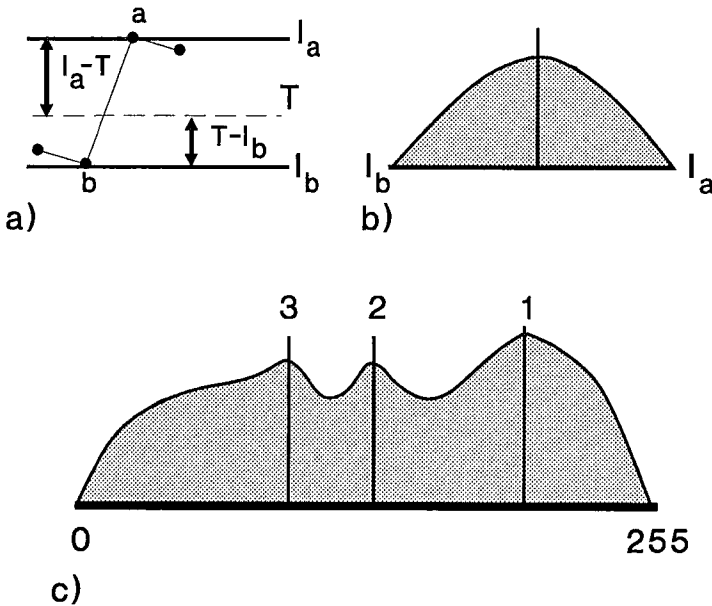
Fig. 2. a) Intensity waveform near two adjacent pixels; b) Relative Contrast Histogram for the two pixels; c) Cumulative Relative Contrast Histogram for a multi-phase image.

Porosity as a function of domain orientation

Smart and Tovey (1988) and Tovey *et al.* (1989) developed the intensity gradient technique as a means of automatically estimating orientation at each pixel within the image. This generates an *angles-coded* image. This intensity gradient analysis is done on the original image in preference to the Wiener filtered image as the algorithms adequately cope with any Gaussian degradation of the image. Regions with a particular general orientation can be automatically delineated using a large radius modal filter on the *angles-coded* image (Tovey *et al.*, 1992). The choice of radius is dependent on the material used. Extensive testing was done on images of the kaolin samples before a radius of 19 pixels was adopted. (This is consistent with the 0.11 μm pixel size used). For other pixel sizes, the radius is scaled appropriately. An automatic method for selection of this radius using mean chord length intercepts from the binary image is under development but was not used in this study although such a method would be generally applicable to a wide range of soils. The delineation of areas of similar general orientation is called *domain segmentation*. While it is normal to use 8, 12 or 16 basic orientation classes, only four are illustrated in the example given here for clarity. An additional fifth class is used for regions where there is no dominant direction. Fig. 1e shows the result of a four-direction domain-segmentation of the original image in which the domain boundaries are over-laid on the original, while in Fig. 1f, the dominant direction in each domain is indicated by the direction of the lines drawn on each domain area. For analysis purposes, each domain
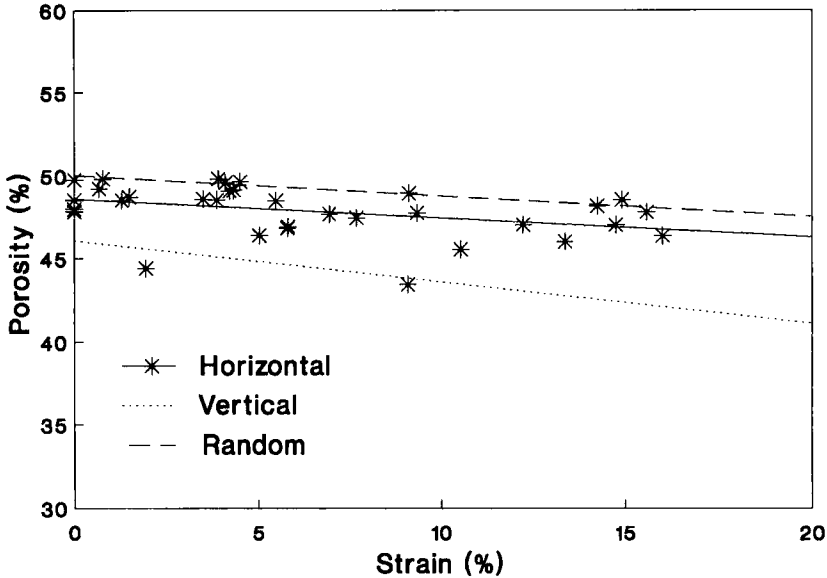
Fig. 3. Variation of porosity with strain for normally consolidated kaolin tested in drained triaxial shear. The horizontal domains are consistently more porous than the vertical ones.

class is conveniently assigned a particular pixel intensity value in the *domain- segmented* image (*e.g.* 1 for vertical domains, 2 for domains inclined from bottom left to top right, and so on).

The domain-segmented image and the binary image may be combined to examine the porosity in any one domain class or even within an individual domain. After analysing nearly 2000 images in this study, it was noted that the horizontal domains had, on average, a greater porosity than the vertical ones. The random areas, as expected, had the highest porosity. It had been expected that on consolidation the horizontal domains would compact further and the vertical domains would become more porous as a result of buckling. The reverse seems to be the case in practice. Further it was noted that the expected result that the horizontal domains would be less porous was seen in only about 2% of images.

It has also been possible to examine how porosity changes with amount of strain for normally consolidated samples (Fig. 3). The individual data points are shown only for the horizontal domains from which the extent of the scatter may be judged. These points were derived as follows. The mean porosity in all horizontal domains in each image was determined and then these computed values were averaged over the 24 separate images taken of each sample to give the values corresponding to a particular strain. For the other orientations, only the trend line is shown. This suggests that, contrary to expectations, the vertical domains are more compact than the horizontal ones for all strains with the inclined ones being somewhat intermediate. As expected, the ranom areas have the highest porosity at all strains. There are three possible reasons for this unexpected result. Firstly, the effect is real and a reconsideration of the mechanics of deformation need to be addressed. Secondly, it is an artifact associated with the extraction of the sample from the sampling rig or from the ground

or with the impregnation process. Finally, the explanation may be a manifestation of a stereological problem.

A possible mechanistic explanation may be that the vertical domains are in effect punched downwards through the other domains during deformation and become more compacted. In the case of sample preparation, it is known that in wet impregnation some swelling can take place, which can be greater in a direction perpendicular to the consolidation direction (see Smart and Tovey, 1982). This could be checked by examining samples which have been consolidated in a true three-dimensional manner.

Finally, the stereological effect arises because in a vertical section horizontal particles will always be horizontal while the 'vertical' ones could be inclined in the third direction. Some preliminary examination of mean effective particle widths in the different directions suggests that the stereological problem might contribute to the effects noticed, but cannot explain the full magnitude of the difference between the porosity of horizontal and vertical domains. Equally, as the random areas are always the most porous this would also suggests that stereological effects cannot be the full explanation. Clearly this aspect needs further investigation.

CONCLUSIONS

The techniques described in this paper provide an objective way to assess porosity from images of particulate samples. It is necessary to restore all the images using Wiener filtering methods. A Relative Contrast Histogram method has been developed and used with success to threshold large numbers of images both objectively and automatically. Combined with domain segmentation methods, investigations as to how the porosity varies within an individual image are now possible. None of the stages listed requires operator intervention, and it is thus possible to batch process large numbers of images so that statistically significant results from studies may be obtained.

In an extensive series of tests on kaolin samples deformed by differing amounts it was found that, contrary to expectations, the horizontal domains consistently, and at all levels of strain, had a higher porosity than those of the vertical domains. Further work is underway to examine how the particle spacing varies within each individual domain and within each domain class to explain this result.

Notwithstanding the possible doubt over comparing results from one class of domains with another, comparison of data within a particular class will be largely unaffected. The technique is readily extended to compare porosities and orientations between the individual domains in a particular class.

ACKNOWLEDGEMENTS

REFERENCES

Bisdom, E.B.A. and Schoonderbeek, D., 1983. The characterisation of the shape of mineral grains in thin sections by Quantimet and BSEI. Geoderma, 30: 303-322.

Dilks, A. and Graham, S.C., 1985. Quantitative mineralogical characterisation of sandstones by back-scattered electron image analysis. J. Sediment. Petrol., 55: 347-355.

Gonzalez, R.C. and Wintz, P., 1987. Digital Image Processing, (2nd edition). Addison-Wesley, Menlo Park, California, 503 pp.

Guan, L. and Ward, R.K., 1989. Restoration of randomly blurred images by the Wiener filter. IEEE Transactions of Acoustics, Speech, and Signal Proceedings, 37: 589-592.

Hounslow, M.W. and Tovey, N.K., 1994. Porosity measurement and domain segmentation of back-scattered SEM images of particulate materials. Scanning Microscopy, Supplement 6 (1992): 245-254.

Kohler, R., 1981. A segmentation system based on thresholding. Computer Graphics and Image Processing, 15: 319-338.

Pye, K., 1984. Rapid estimation of porosity and mineral abundance in back-scattered electron images using a simple SEM image analyser. Geological Magazine, 121: 81-136.

Smart, P. and Tovey, N.K., 1982. Electron Microscopy of Soils and Sediments - Techniques. Oxford University Press, 336 pp.

Smart, P., and Tovey N.K., 1988. Theoretical aspects of intensity gradient analysis. Scanning, 10: 115-121.

Tovey, N.K., Smart, P., Hounslow, M.W. and Leng, X.L., 1989. Practical aspects of automatic orientation analysis of micrographs. Scanning Microscopy, 3: 771-784.

Tovey N.K., Smart, P., Hounslow, M.W. and Leng, X.L., 1992. Automatic mapping of some types of soil fabric. Geoderma, 53: 179-200.

Tovey, N.K., Dent, D.L., Krinsley, D.H. and Corbett, W.M., 1994. Quantitative micro-mineralogy and micro-fabric of soils and sediments. In: A.J. Ringrose-Voase and G.S. Humphreys (Editors), Soil Micromorphology: Studies in Management and Genesis. Proc. IX Int. Working Meeting on Soil Micromorphology. Developments in Soil Science, 22. Elsevier, Amsterdam, pp. 541-547.

White, J.M. and Rohrer, G.D., 1983. Image thresholding for optical character recognition and other applications requiring character image extraction. IBM Journal of Research Development, 27: 400-411

This Page Intentionally Left Blank

Quantitative micro-mineralogy and micro-fabric of soils and sediments

N.K. Tovey[1], D.L. Dent[1], D.H. Krinsley[2] and W.M. Corbett[1]

[1]*School of Environmental Sciences, University of East Anglia, Norwich, NR4 7TJ, UK*
[2]*Department of Geological Sciences, University of Oregon, Eugene, Oregon, 97403, USA*

ABSTRACT

Tovey, N.K., Dent, D.L., Krinsley, D.H. and Corbett, W.M., 1994. Quantitative micro-mineralogy and micro-fabric of soils and sediments. In: A.J. Ringrose-Voase and G.S. Humphreys (Editors), Soil Micromorphology: Studies in Management and Genesis. Proc. IX Int. Working Meeting on Soil Micromorphology, Townsville, Australia, July 1992. Developments in Soil Science 22, Elsevier, Amsterdam, pp. 541-547.

An integrated package of techniques is described to quantify both the micro-fabric and the micro-mineralogy of soils and sediments. First, polished impregnated samples are prepared. Digital back-scattered electron images and digital X-ray distribution maps of key elements (silicon, iron *etc.*) are acquired. An initial estimate of the distribution of the various mineral species within the image is made using supervised multi-spectral classification methods on the X-ray distribution maps. Areas of doubtful classification, *e.g.* at mineral boundaries, are left unclassified. The back scattered electron image is then used to define the true outlines of the grains which, with further image processing, enables the remaining unclassified regions to be coded.

The resulting image may then be segmented into the different mineral species to ascertain grain size and shape within each species, something which is difficult or impossible to achieve by other means. The orientation of the fine-grained matrix as cutans or domains may also be quantified from this image using an intensity gradient method.

The techniques are illustrated using the Bt and 2C horizons of the Worlington Series, an argillic brown sand or Luvic Arenosol. Quantitative evidence from the distribution of calcium carbonate in the matrix indicates that as this is leached there is a removal of clay from the matrix.

INTRODUCTION

It has long been recognised that the microfabric of soils and sediments greatly influence their stress-strain behaviour. A knowledge of the soil microfabric can also provide insight into 1) diagenetic processes, 2) hydraulic behaviour, and 3) relationships between crops and soil. Early work in soil micromorpholgy began with the optical microscope observations of Kubiena (1938) for diagenetic and soil science applications, while Mitchell (1956) was the first to use optical microscopy for investigating stress-strain relationships. Besides optical microscopy, X-ray diffraction, transmission electron microscopy, and scanning electron microscopy have all been used extensively, although most observations have been qualitative and descriptive. A

comprehensive list of the early work on quantification may be found in Smart and Tovey (1982).

Many of the recent studies of microfabric have employed image analysis methods. However, there are problems which must be overcome before quantitative methods can be applied to all types of soils and sediments. Typical information for which quantitative data are required include: 1) the alignment of the platey clay particles, both in a general and a local sense; 2) the size distribution of the grains of each separate mineral; 3) the orientation of the different grains within each mineral species; 4) the size, shape and frequency of the large voids, and also the fine, intra-domain voids.

Digital acquisition of the image is an essential pre-requisite of image analysis. Typically, this is done with a grey-level resolution of 0 - 255 levels and a pixel resolution of 512 × 512. For most applications, it is necessary to discriminate between features present by image segmentation. Frequently this is achieved by thresholding the image into two or more distinct classes, each one containing an unique range of grey-level values. While this can be achieved for certain types of image, such as those in which there is high contrast between the two component parts (*e.g.* voids and particles), this separation cannot be achieved routinely for all applications. More often, two or more features have overlapping ranges of grey-scale values, for example quartz and feldspar grains (Tovey *et al.*, 1994a), so that simple thresholding methods cannot be used.

Alternative image analysis methods which involve computation of the intensity gradient vector (Smart and Tovey, 1988) provide fully automatic quantification of selected types of soil fabric, particularly those which are dominantly platey (Tovey *et al.*, 1994b). On the other hand, such methods are not so suitable when there is a large range of particle sizes.

Several different stages of processing and analysis are needed for a complete quantitative analysis. This paper summarises and combines the key stages, some theoretical aspects of which have been reported in more detail elsewhere (*e.g.* Tovey and Krinsley, 1991; Tovey *et al.*, 1992). Some of the steps require considerable processing, and these are described in detail in Tovey *et al.* (1994a). The techniques have been developed on a wide range of soils and sediments. They are illustrated here by a soil from East Anglia. Some additional analysis techniques are also discussed here.

SPECIMEN PREPARATION AND OBSERVATION

The soil studied was taken from the Worlington Series which is developed in well-sorted quartzose coversand, about 1 m thick, overlying chalky sand drift. The calcium carbonate content of the underlying drift varies from 25% to 80% while the remainder is a well-sorted sand having a median grain size of 200 μm. The coversand is acid, strongly leached, but at the junction with the chalky sand drift there is a sharply-defined, reddish brown Bt horizon. Samples discussed here are from the 2C and Bt horizons.

The samples were impregnated by successive replacement with acetone and finally with a mixture of Araldite AY18 and hardener HZ18 and allowed to harden. The impregnated blocks were cut to sizes of approximately 25 × 25 mm × 8 mm thick, ground and polished using increasingly fine grades of diamond paste down to 1 μm. (Experience has shown that the best surfaces for observation are obtained with a 1 μm paste rather than finer ones). The samples were coated with 20 nm of carbon and observed in the back-scattered electron mode (BSE) in the SEM at voltages between 10 and 20 kV. Contrast levels were adjusted on the BSE

detector using a calibration standard of quartz in resin to ensure that the full dynamic range of grey-levels was achieved. Digital BSE images were acquired using a dwell time of 51 μS, while the same area was scanned to generate X-ray maps of the key elements present in the sample.

X-ray map acquisition was done with a dwell time of 40 mS and a pixel resolution of 128 × 128. Typical elements scanned included aluminium, silicon, sulphur, potassium, calcium and iron, although other elements were scanned in some areas. Chlorine was also selected as the chlorine present in the resin can sometimes provide an indication of the distribution of the larger voids.

A typical BSE image of a sample of the chalky sand drift is shown in Fig. 1a, while the corresponding X-ray maps from selected elements are shown in Fig. 1b.

IMAGE PROCESSING AND ANALYSIS

Classification of the soil components

The individual X-ray maps were enlarged to the same scale as the BSE image and stacked with the BSE image into a multi-layer image. Training areas representative of each mineral group and the clay matrix were defined using the computer mouse. The relevant statistics within each defined training area and each layer were then computed to generate a covariance matrix. This matrix was used as the basis of a "Maximum Likelihood Classification" similar to that often used in classification of satellite images (Curran, 1985). During this classification it is prudent to leave areas of uncertainty as unclassified. In this analysis, pixels were assigned to a particular class only if the statistics for a particular pixel placed it within 2 standard deviations of the mean of that particular class. Thus, boundaries between grains were left unclassified, as were some regions within grains.

Unclassified regions at grain boundaries may be assigned to an appropriate class by defining the edges of the grains using an edge-detection routine, preferably one which also incorporates some filtering (for example, Tovey *et al.*, 1989). The classified regions within each feature are then dilated until they hit the nearest boundary. Some over-segmentation may be present from the edge-detection (*e.g.* additional lines within grains) and this may be removed by the techniques outlined in Tovey *et al.* (1994a).

Two types of voids are present in the sample: large voids which show as dark in the BSE images and small voids within the matrix which are not resolved at the current magnification of the instrument. For the large voids, an objective thresholding method should be used to define a binary image in which the voids are coded as zero, and all other regions are coded to unity. Probably the most robust automatic global thresholding method is the Relative Contrast Histogram method of Kohler (1981) which, essentially, computes the optimum threshold to maximise the number of edges. Once a binary image has been generated, it can be multiplied by the "classified image" to produce a final classification image (Fig. 1c).

Orientation analysis of the matrix

The nature of the fine-grained matrix is also of interest and may be analysed by generating a second binary image which is unity only within the matrix and zero elsewhere. This binary image is then used to mask the original BSE image. The resulting image is, in turn, used to
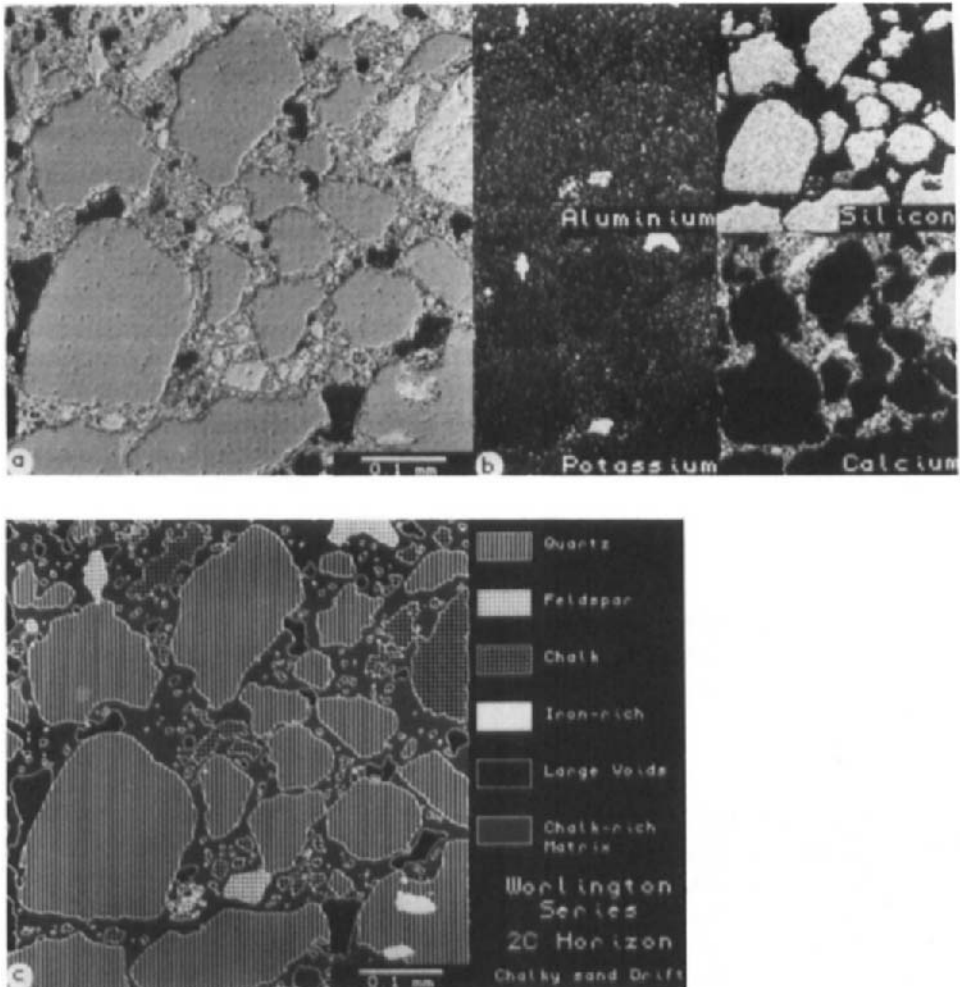
Fig. 1. SEM images of the 2C horizon of a Worlington Series Soil from East Anglia: a) BSE image; b) X-ray maps for the K_δ line spectra of aluminium, silicon, potassium and calcium; c) the final mineral classified image.

generate an *angles-coded* image in which the orientation at each pixel in the matrix has been determined using the Intensity Gradient method (Smart and Tovey, 1988; Tovey *et al.*, 1989). This *angles-coded* image has pixel values from 0 to 180 which represent the orientation in degrees of the features in the original image. In this sample, the matrix appears random with no preferred orientation, as confirmed by the rosette diagram (Fig. 2a).
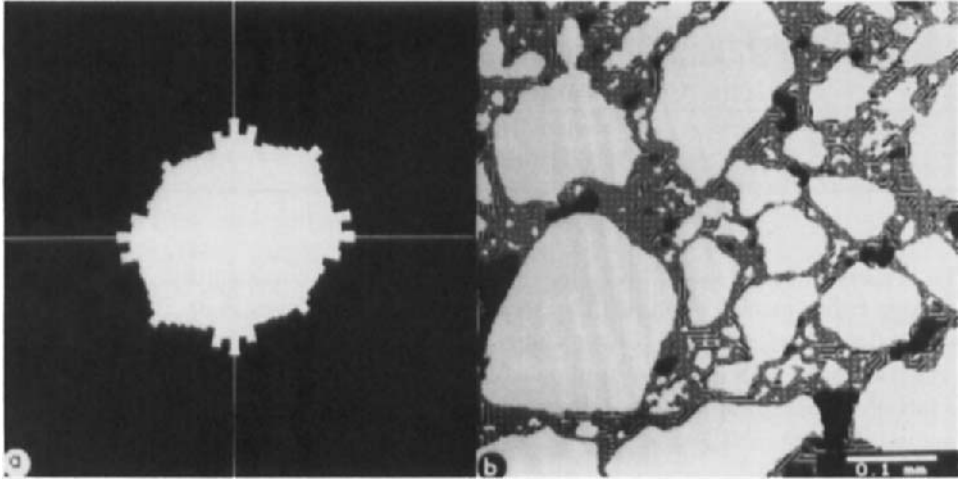
Fig. 2. Orientation patterns within the matrix of Fig. 1: a) rosette diagram showing distribution of orientation of features within the matrix; b) orientation patterns delineated using an automatic mapping algorithm. The hatched lines indicate the preferred orientation direction in the respective areas, while the areas covered by dots are the regions in which there is no dominant orientation.
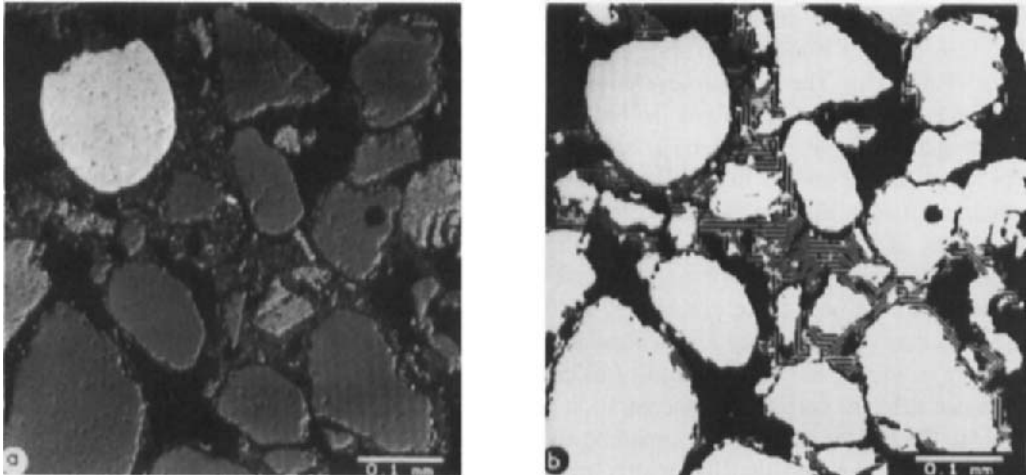
Fig. 3. SEM images of the Bt horizon of a Worlington Series Soil from East Anglia (taken from 3 mm above Fig. 1: a) BSE image; b) the orientation image.

Table 1.
Percentage of each image covered by skeleton grains, matrix and large voids.

	Skeleton grains	Matrix	Voids
2C Horizon (Fig. 1a)	59%	35%	6%
Bt Horizon (Fig. 3a)	55%	15%	30%

Finally, the *angles-coded* image is divided into regions of different dominant orientation by passing a large radius median filter over the *angles-coded* image (Tovey *et al.*, 1994b). From previous experience with this soil, a filter radius of 11 pixels was chosen. For clarity in the illustrations used here, only four dominant directions have been used (*i.e.* horizontal, vertical, and two inclined at 45°). It is normal practice, however, to analyse images using 8, 12, or more direction classes.

RESULTS AND DISCUSSION

Fig. 1a shows that the fabric of the 2C horizon is dominated by grains of medium sand up to 400 μm in diameter. This sand is mostly quartz, but both chalk and some feldspar are present. The non-matrix voids are few in number, irregular in shape, and generally less than 50 μm in width. The matrix between the sand-sized grains is mostly homogeneous and contains some fine discrete chalk fragments, but the majority is a chalk-rich clay.

Fig. 2b shows the matrix of the 2C horizon almost entirely classed as random. Only small regions of orientated clay are present, none of which appear to bear much relation to the position of the skeleton grain boundaries.

Fig. 3a shows the Bt horizon, only 3 mm above the previous sample. Compared with the 2C horizon, there is a lower proportion of matrix, almost balanced by a greater proportion of voids (Table 1). There is also evidence of alignment within the clay matrix in Fig. 3b which highlights the orientation patterns within this matrix.

The matrix of the 2C horizon is characterised by numerous fragments of chalk of silt size, which are less abundant in the Bt horizon. The concentration of calcium carbonate in the remaining matrix may be estimated as a proportion of the concentration in the larger chalk fragments. To achieve this, the chalk grains from the mineral-classified images (*e.g.* Fig. 1c) are used to generate a binary map to mask the calcium X-ray map so that the mean calcium concentration in only these grains may be determined. In addition, the binary mask defining only the matrix is combined in a similar way with the calcium X-ray maps to provide an estimate of the mean concentration of calcium in the matrix. In the image of the 2C horizon, the mean calcium carbonate concentration in the matrix is 52%, that of the chalk fragments, while in the Bt horizon the corresponding figure is 24%.

It may be surmised that the matrix remains stable while it is calcareous but, as leaching takes place and the calcium content decreases, the matrix flows out from between the skeleton grains. In this example, the Bt horizon appears to have lost clay. Further evidence of that flow of fine grained material is the alignment of the matrix parallel to the skeleton grains, thereby forming cutans (Fig. 3b). There are few regions in this image where the matrix is random.

The results discussed are based partly on the two images shown here and partly on supplementary studies on adjacent areas of the samples. They are, nevertheless, illustrative of the type of conclusion that can be made using the techniques described.

CONCLUSION

The combination of techniques described in this paper provide opportunities to make many quantitative measurements about both the micro-fabric and the micro-mineralogy of soils and sediments which facilitate more rigorous analysis than has been possible with qualitative visual observations. It has been possible to describe but a few of the many parameters which could be derived using these techniques.

ACKNOWLEDGEMENTS

REFERENCES

Curran, P.J., 1985. Principles of Remote Sensing. Longman, London, 282 pp.

Kohler, R., 1981. A segmentation system based on thresholding. Computer Graphics and Image Processing, 15: 319-338.

Kubiena, W.L., 1938. Micropedology. Collegiate Press, Ames, Iowa, 243 pp.

Mitchell, J.K., 1956. The fabric of natural clays and its relationship to engineering properties. Proc. Highways Research Board, 35: 693-713.

Smart, P. and Tovey, N.K., 1982. Electron Microscopy of Soil and Sediments: Techniques. Oxford University Press, Oxford, 264 pp.

Smart, P. and Tovey, N.K., 1988. Theoretical aspects of intensity gradient analysis. Scanning, 10: 115-121.

Tovey, N.K. and Krinsley, D.H., 1991. Mineralogical mapping of scanning electron micrographs. Sedimentary Geology, 75: 109-123.

Tovey, N.K., Smart, P., Hounslow, M.W. and Leng, X.L., 1989. Practical aspects of automatic orientation analysis of micrographs. Scanning Microscopy, 3: 771-784.

Tovey, N.K., Krinsley, D.H., Dent, D.L. and Corbett, W.M., 1992. Techniques to quantitatively study the microfabric of soils. Geoderma, 53: 217-235.

Tovey, N.K., Dent, D.L., Krinsley, D.H. and Corbett, W.M., 1994a. Processing multi-spectral SEM images for quantitative microfabric analysis. Scanning Microscopy, Suppl., 6: 269-282.

Tovey, N.K., Smart, P., Hounslow, M.W. and Desty, J.P., 1994b. Automatic orientation analysis of microfabric. Scanning Microscopy, Suppl., 6: 315-330.

This Page Intentionally Left Blank

Description of microcrack orientation in a clayey soil using image analysis

V. Hallaire

INRA Science du Sol, 65 rue de Saint-Brieuc, 35042 Rennes Cedex, France

ABSTRACT

Hallaire, V., 1994. Description of microcrack orientation in a clayey soil using image analysis. In: A.J. Ringrose-Voase and G.S. Humphreys (Editors), Soil Micromorphology: Studies in Management and Genesis. Proc. IX Int. Working Meeting on Soil Micromorphology, Townsville, Australia, July 1992. Developments in Soil Science 22, Elsevier, Amsterdam, pp. 549-557.

An image analysis method is proposed to describe microcrack orientation in clayey soils. Undisturbed soil cores were taken from vertical pit faces and their *in situ* orientation noted. In the laboratory the cores were impregnated with a fluorescent resin.

Image processing on sections of the cores was performed in three stages:

(i) *Extraction of the crack network*. A local threshold technique, capable of taking into account pore surroundings was used to segment the grey-level image, captured under ultra-violet light, into a binary image, clearly distinguishing cracks from solid.

(ii) *Disconnection of branches of the crack network*. Mathematical morphology (skeleton, pruning, triplepoint, SKIZ) was used to detect the junctions of the cracks in the network and divide the network at these points.

(iii) *Measurement of branch orientation*. An orientation index was calculated for each branch, using their second order moments and Feret diameters.

The results are presented as histograms showing the porosity of the cracks according to their orientation. An example of this method is given for a soil at decreasing water contents, which shows that the crack network is isotropic at first and becomes anisotropic with a preferential vertical orientation of the cracks.

INTRODUCTION

In clayey soils, the pattern of structural cracks can influence hydrological behaviour (Bouma *et al.*, 1977). For this reason the consequences of shrinkage on soil structure have been studied using physical (Bouma *et al.*, 1979; McIntyre and Sleeman, 1982) or morphological (Virgo, 1981; Scott *et al.*, 1988) methods.

Image analysis performed on soil sections allows soil structure to be quantified (Bullock and Thomasson, 1979; Ringrose-Voase, 1987; Warner *et al.*, 1989). However, a specific measurement of pore orientation has not often been carried out (Scott *et al.*, 1986; Bui and Mermut, 1989), in spite of the influence of this parameter on water flow in cracked soils.

The aim of this study is to propose a method of describing crack orientation in soil sections which involves extraction of the crack network from grey-tone images, disconnection of the
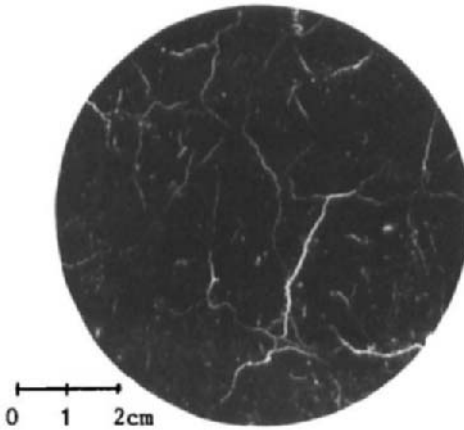
Fig. 1. A grey-tone image.

branches of the network and measurement of branch orientation from second order moments and Feret diameters. An example is given for a soil at different water contents.

METHODS

Samples collection and preparation

Undisturbed core samples were collected with cylinders, (100 mm diameter × 50 mm high). Cylinders were pushed horizontally into the faces of the pits and the orientation of the cores was recorded. In the laboratory, the samples were dehydrated using water/acetone exchange in liquid phase then impregnated with a polyester resin (Scott Bader Crystic) containing a fluorescent pigment (Ciba-Geigy Uvitex OB) at 1 g/l concentration.

Image acquisition and segmentation

Polished sections of the samples were captured with a CCD Camera, under ultra-violet light (Fig. 1). Images were digitized in 512 × 512 pixels, on a hexagonal grid, with a spectral resolution of 256 grey-levels. The spatial resolution was about 200 μm per pixel. As the captured windows were square and the observed samples were round, the captured images were multiplied by a binary circular mask, 480 pixels in diameter. The analyzed field had therefore an area of about 181,000 pixels.

The grey-level images were segmented in order to obtain a binary image by assigning each pixel to either pore or solid. Under ultra-violet light, pore space shows up bright on a dark background. However, the weakness of the signal (little distinction in grey-levels between pore and solid) and its variability within the image made it difficult to use simple bi-partitioning according to a grey-level threshold. In order to detect small, thin cracks whatever their surroundings, a local threshold technique from mathematical morphology, the top-hat transformation (Serra, 1982), was used. Although this technique only detects narrow objects it

Fig. 2. Binary segmented image.   Fig. 3. Skeleton of the binary shapes.

was not necessary to combine it with a bi-partitioning thresholding to detect larger objects (Moran *et al.*, 1988) because only cracks had to be detected. The top-hat transformation was performed using a morphological opening of size 3. Fig. 2 gives the segmented image using top-hat transformation and shows that this method was not faultness. It could overestimate the thickness of some cracks and disconnect other thin cracks. However, compared to other local threshold techniques such as the edge detector used by Moran *et al.* (1989), this transformation was found to give better results for the studied soil.

Binary image processing: disconnection of the branches of the crack network

It was necessary to isolate individual branches of the crack network, in order to measure their orientation. The following operations were used to detect the junctions of the cracks in the network and to divide it at these points.

Skeletonization of pore space image
This operation consisted in successive thinnings with rotation of the following structuring element until convergence:

$$\begin{array}{ccc} & 1 & 1 \\ X & 1 & X \\ & 0 & 0 \end{array}$$

where the value X stands for 0 or 1.

This operation is homotopic (*i.e.* does not change the topology) so that the resultant binary image (Fig. 3) has the same connectivity number as the original segmented image. In this image

Fig. 4. Pruned skeleton.
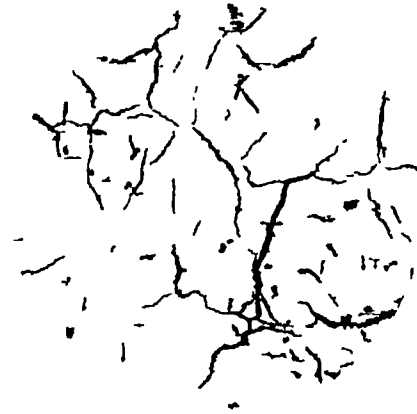
Fig. 5. Crack network reconstructed starting from the pruned skeleton.

the width of the cracks was 1 pixel, which was necessary to detect the junctions of the branches.

Pruning

This consisted of six successive thinnings with rotation of the following structuring element:

$$X \quad X$$
$$0 \quad 1 \quad 0$$
$$0 \quad 0$$

This non-homotopic operation removed from the skeleton branches smaller than 2 pixels, considered as "parasite" branches created by skeletonization; it also removed 2 pixels from the ends of longer branches and small individual skeletons (Fig. 4).

Reconstruction

The pore space image (Fig. 2) was reconstructed using a geodesic propagation of the pruned skeleton image (Fig. 4) within the connected components of the original segmented image (Fig. 2). The resultant binary image (Fig. 5) represents the crack network without any rounded bodies, whose skeletons were removed when pruning.

Detection of triple points

The junctions of the branches on the pruned skeleton (Fig. 4) were detected using the hit or miss transformation with the following neighbourhood configuration (up to one rotation):

Fig. 6. SKIZ of the branches of the network.

Fig. 7. Disconnected branches of of the network.

$$
\begin{array}{ccc}
& 1 & X \\
X & 1 & 1 \\
& 1 & X
\end{array}
\quad \text{or} \quad
\begin{array}{ccc}
1 & & 1 \\
X & 1 & X \\
1 & & X
\end{array}
$$

The resultant image was subtracted from the pruned skeleton, disconnecting the branches.

Skeletonization by zone of influence (SKIZ)

The zone of influence of each branch previously isolated was determined by successive thickenings with rotation of the following structuring element until convergence:

$$
\begin{array}{ccc}
X & & X \\
1 & 1 & 1 \\
0 & & 0
\end{array}
$$

The resultant image gives the boundaries between the different zones (Fig. 6).

Logical AND-NOT

This logical operation between the crack network image (Fig. 5) and the SKIZ of the pruned skeleton (Fig. 6) disconnected the branches of the cracks according to the junctions (Fig. 7). These branches were then labelled and analyzed individually.

Orientation measurement

The orientation of a crack in 3-D is given as the orientation of its normal in the vertical and the horizontal planes. In this study we assumed that the crack network was isotropic in the horizontal plane and measured the orientation of the cracks, θ, with respect to the vertical.

This means that the orientation in 3-D will always be greater than or equal to the orientation in 2-D.

Orientation indices based on Feret diameters (Murphy et al., 1977; Pagliai et al., 1983), rose of intercepts (Launeau et al., 1990) or rose of directions (Low et al., 1982; Daniel et al., 1987) provide an estimation of feature orientation. In a digital system these methods are not precise because of the limited number of intercept directions that can be chosen. In order to get more precise estimation, orientation was here defined as the direction of the major inertia axis of each branch in the resultant binary image. The index proposed by Noesis (1991) is given as the eigenvector of the largest eigenvalue of the inertia matrix and calculated from the second order moments of the object, according to the X and Y axes in the image:

$$\theta = \frac{1}{2}\arctan\left(\frac{2 \cdot \mathrm{Mom}\,XY}{\mathrm{Mom}\,X^2 - \mathrm{Mom}\,Y^2}\right) \qquad \text{Eqn. 1}$$

with:

$$\mathrm{Mom}\,X^2 = \frac{1}{N}\sum(X_n - \mathrm{Mom}\,X)^2 \qquad \text{Eqn. 2}$$

$$\mathrm{Mom}\,Y^2 = \frac{1}{N}\sum(Y_n - \mathrm{Mom}\,Y)^2 \qquad \text{Eqn. 3}$$

$$\mathrm{Mom}\,XY = \frac{1}{N}\sum(X_n - \mathrm{Mom}\,X)(Y_n - \mathrm{Mom}\,Y) \qquad \text{Eqn. 4}$$

where N is the number of pixels in the object, X_n and Y_n the coordinates of such points, MomX and MomY the moments of order 1, i.e. the mean or barycenters of the object.

Eqn. 1 gives an orientation between -45° and +45°, relative to either the X or Y axes. In order to distinguish to which axis the orientation is relative and correct all orientations so they are relative to the horizontal axis (0°), a correction using horizontal (Feret X) and vertical (Feret Y) Feret diameters was used:

orientation = -θ   if Feret Y ≤ Feret X Eqn. 5

or

orientation = 90°-θ   if Feret Y > Feret X Eqn. 6

This corrected index gives an orientation between 0° and 180°. These values are presented as angles relative to the vertical (i.e. between 0° and 90°, where 0° corresponds to a body with a horizontal inertia axis, 90° to a body with a vertical inertia axis) by converting the values from 90° to 180° to 180°-θ.

For each angle class, results are given as the porosity of the cracks. This is the area of the cracks (in pixels) divided by the image area (181,000 pixels). This area-weighted distribution is related to the volume of cracks in each orientation class and is preferred to a length-weighted distribution which does not give information about the width of the cracks.
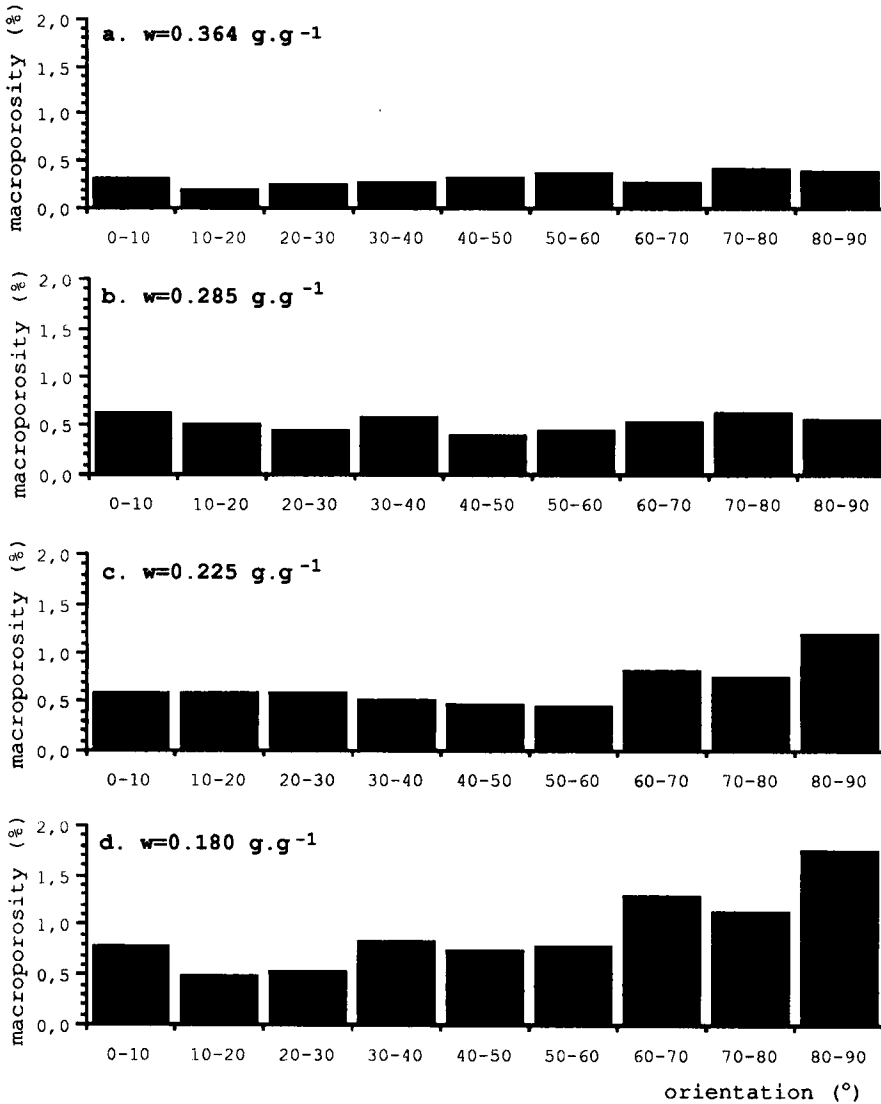
Fig. 8. Orientation histograms at 4 water content levels.

CASE STUDY

The studied soil was located in Courcival, 150 km west of Paris. Pedological (Specklin, 1983), hydrological (Zimmer, 1989) and physical (Hallaire, 1991) descriptions of this soil show the specific influence of the cracks on water transfer. In this study we analyzed crack

orientation at a depth of 0.45 m, in a clayey horizon (44% <2 μm; 11% 2 - 50 μm; 45% >50 μm).

Pits were dug under a winter wheat crop at different stages between March and July. At each stage, 5 to 10 cores were taken. Gravimetric water content, w, was determined on 10 samples collected at the same time as the cores.

Fig. 8 shows orientation histograms at four stages during drying. w varied from 36.4% (end of winter) to 18.0% (midsummer), which represented the range of moisture that can occur naturally in this horizon. At the beginning of the drying process there is an increase in crack porosity (2.8% in Fig. 8a, 4.7% in Fig. 8b) but cracks do not present any preferential orientation; the network is isotropic. Later in the drying process, crack porosity continues to increase (5.9% in Fig. 8c, 8.2% in Fig. 8d), but the network becomes more and more anisotropic with a preferential vertical orientation. In Fig. 8d, 40% of crack surface area is occupied by cracks with an orientation of between 70° and 90°.

This analysis confirms that the cracking of a clayey soil during drying occurs in two steps (Hallaire, 1988). First, shrinkage causes the soil to separate into a network of cracks in random orientations. Continued drying then causes sinking, creating a network of vertical cracks.

CONCLUSIONS

The use of image analysis to describe microcrack orientation on soil sections has led to: (i) the adaptation of a local threshold technique for the extraction of the crack network in sections even when the signal to be detected is weak compared with the light variation within the image; (ii) the development of an algorithm, using mathematical morphology, capable of detecting the junctions of the cracks in the network and to disconnect them at these points; (iii) a possible index for measuring the orientation of each branch.

It appears that cracks are generally organized in a network, so disconnection from the network is necessary when describing orientation. Each branch has to be analyzed individually.

Results show that this method can indicate the degree of anisotropy on a soil section. Furthermore it provides a precise characterization of crack evolution during drying in terms of crack size and orientation.

REFERENCES

Bouma, J., Jongerius, A., Boersma, Jager, A. and Schoonderbeek, D., 1977. The function of different types of macropores during saturated flow through four swelling soil horizons. Soil Sci. Soc. Am. J., 41: 945-950.

Bouma, J., Jongerius, A. and Schoonderbeek, D., 1979. Calculation of saturated hydraulic conductivity of some pedal soils using micromorphometric data. Soil Sci. Soc. Am. J., 43: 261-264.

Bui, E.N. and Mermut, A.R., 1989. Orientation of planar voids in vertisols and soils with vertic properties. Soil Sci. Soc. Am. J., 53: 171-178.

Bullock, P. and Thomasson, A.J., 1979. Rothamsted studies of soil structure. II. Measurement and characterization of macroporosity by image analysis and comparison with data from water retention measurements. J. Soil Sci., 30: 391-413.

Daniel, T., Gapais, D., Labit, C. and Le Corre, C., 1987. An application of textural and morphological image processing to deformation analysis within granitic rocks. In: J.L. Chermant (Editor), Proceedings of the 7th International Congress for Stereology. Acta Stereol., 6: 1041-1046.

Hallaire, V., 1988. La fissuration d'un sol argileux au cours du dessèchement. I. Description *in situ*. Agronomie, 8: 139-145.

Hallaire, V., 1991. Une méthode d'analyse bidimensionnelle du retrait d'échantillons naturels de sol. Science du Sol, 29: 147-158.

Launeau, P., Bouchez, J.L. and Benn, K., 1990. Shape prefered orientation of object population : automatic analysis of digitized images. Technophysics, 180: 201-211.

Low, A.J., Douglas, L.A. and Platt, D.W., 1982. Soil pore orientation and faults. Soil Sci. Soc. Am. J., 46: 789-792.

McIntyre, D.S. and Sleeman, J.R., 1982. Macropores and hydraulic conductivity in a swelling soil. Aust. J. Soil Res., 20: 251-254.

Moran, C.J., Koppi, A.J., Murphy, B.W. and McBratney, A.B., 1988. Comparison of the macropore structure of a sandy loam surface soil horizon subjected to two tillage treatments. Soil Use Manage., 4: 96-102.

Moran, C.J., McBratney, A.B. and Koppi, A.J., 1989. A rapid method for analysis of soil macropore structure. I. Specimen preparation and digital binary image production. Soil Sci. Soc. Am. J., 53: 921-928.

Murphy, C.P., Bullock, P. and Turner, R.H., 1977. The measurement and characterisation of voids in soil thin sections by image analysis. J. Soil Sci., 39: 65-70.

Noesis, 1991. A Tutorial on Image Processing. Noesis, Vélizy, France, 192 pp.

Pagliai, M., La Marca, M. and Lucamante, G., 1983. Micromorphometric and micromorphological investigations of a clay loam soil in viticulture under zero and conventional tillage. J. Soil Sci., 34: 391-403.

Ringrose-Voase, A.J., 1987. A scheme for the quantitative description of soil macrostructure by image analysis. J. Soil Sci., 38: 343-356.

Scott, G.J.T., Webster, R. and Nortcliff, S., 1986. An analysis of crack pattern in clay soil: its density and orientation. J. Soil Sci., 37: 653-668.

Scott, G.J.T., Webster, R. and Nortcliff, S., 1988. The topology of pore structure in cracking clay soil. I. The estimation of numerical density. J. Soil Sci., 39: 303-314.

Serra, J., 1982. Image Analysis and Mathematical Morphology. Academic Press, London, 628 pp.

Specklin, G., 1983. Etudes préliminaires en vue du drainage des terres agricoles du département de la Sarthe. Secteur de référence de l'Orne Saosnoise. ONIC, INRA, CEMAGREF, 127 pp.

Virgo, K.J., 1981. Observations of cracking in Somali vertisols. Soil Sci., 131: 60-61.

Warner, G.S., Nieber, J.L., Moore, I.D. and Geise, R.A., 1989. Characterizing macropores in soil by computed tomography. Soil Sci. Soc. Am. J., 53: 653-660.

Zimmer, D., 1989. Transferts Hydriques en Sols Drainés par Tuyaux Enterrés. Compréhension des Débits de Pointe et Essai de Typologie des Schémas d'Ecoulement. Thèse Univ. Paris VI, Etude du CEMAGREF, Hydraulique Agricole 5, 321 pp.

This Page Intentionally Left Blank

Image analysis of pore space morphology in soil sections, in relation to water movement

V. Hallaire and P. Curmi

INRA Science du Sol, 65 rue de Saint-Brieuc, 35042 Rennes Cedex, France

ABSTRACT

Hallaire, V. and Curmi, P., 1994. Image analysis of pore space morphology in soil sections, in relation to water movement. In: A.J. Ringrose-Voase and G.S. Humphreys (Editors), Soil Micromorphology: Studies in Management and Genesis. Proc. IX Int. Working Meeting on Soil Micromorphology, Townsville, Australia, July 1992. Developments in Soil Science 22, Elsevier, Amsterdam, pp. 559-567.

The aim of this study is to suggest a method of describing macroporosity in a Glossaqualf, in order to characterize the preferential paths of water transfer. A morphological description of the pores, using image analysis on undisturbed soil sections is proposed.

Water movement through four soil columns under saturated conditions was studied by staining the efficient porosity with methylene blue. The columns were then impregnated with a fluorescent resin and divided into horizontal and vertical sections. Image acquisition was carried out under ultra-violet illumination to identify the pore phase and in natural light conditions to identify stained areas. The efficient porosity was identified by superimposing these two images. A 2-D characterization of porosity was suggested using three variables *i.e.* size, shape and orientation. Changes of these parameters within the columns were observed section by section by establishing the spectral function of porosity for efficient and inefficient pores.

The results show that flow transfer is determined more by the shape of the macropores than their size. Biological channels, even the largest ones, do not allow water movement in the whole column, whereas cracks, because they are almost vertical and constitute a continuous network, are preferential pathways.

INTRODUCTION

Water movement in soils in saturated conditions is affected by macropores and depends mainly on their morphology (Bouma *et al.*, 1977; Scotter, 1978; Bouma, 1981; Germann and Beven, 1981; Douglas, 1986).

In this study, we tried to distinguish between macropores that function efficiently and inefficiently during saturated flow through the B horizon of a Glossaqualf (Soil Survey Staff, 1975), a degraded and leached soil. The horizon had a structural contrast between the silty clay loam matrix and tongues of silty loam with great differences in the size and shape of macropores. A method is suggested using (i) a coloured tracer for identification of the pathways followed by the water and (ii) image analysis on images captured under visible and ultra-violet light. By superimposing the two images obtained under these conditions, our

Table 1
Soil characteristics of matrix and tongues in Btgd horizon.

	Particle size analysis (%)					CEC	
	clay <2μm	fine silt 2-20 μm	coarse silt 20-50 μm	fine sand 50-200 μm	coarse sand 0.2-2 mm	meq/ 100 g soil	meq/ 100 g clay
Matrix	24.6	25.7	43.2	3.7	2.8	9.1	36
Tongues	11.1	28.3	52.1	6.2	2.3	2.7	24

purpose was to determine morphological parameters which would allow efficient and inefficient macropores to be distinguished.

MATERIALS AND METHODS

Soil materials

Four undisturbed cores, 90 mm in diameter and 200 - 250 mm high, were collected from the Btgd horizon of a Glossaqualf developed in a silt loam in the Noe-Luce wood, near Rennes (France, 48°05'N 1°41'W). This horizon (54 - 80/90 cm) is composed of a prismatic brown matrix (7.5YR 5.5/6) and sub-vertical grey tongues (10YR 7/1.5), 2 - 4 cm wide, which differ both in composition and in porosity (Diab *et al.*, 1988) (Table 1). Each core contained a tongue and the peripheral matrix. Permeability measured *in situ* was 6×10^{-5} m s^{-1}. In the laboratory, the cores were held in paraffin wax and the efficient porosity was stained with methylene blue dye (Bouma *et al.*, 1979). A 0.1 g l^{-1} methylene blue solution was added on the top of the core after saturation by capillarity. Percolation was stopped when the optical density of the effluent became stable, which occured in 4 to 9 weeks. After percolation, the cores were air-dried and impregnated with polyester resin. In order to visualize the macroporosity, a fluorescent dye (Ciba-Geigy Uvitex OB) was added to the resin. Three columns (A, B and C) were cut horizontally into ten blocks about 20 mm wide, the fourth one (D) was cut vertically into two blocks.

Image processing

Acquisition
Images were captured by reflected light on a face of the blocks. For each horizontal plane from columns A, B and C, five 16 mm square windows were captured under two light conditions: (i) ultra-violet, where the pore space shows up bright on a dark background (Fig. 1a), and (ii) visible light, where the areas coloured by the tracer show up dark on a light background (Fig. 1b). The complete width of stained pores (not only the walls) shows up dark, including even the centres of large pores, because of the thickness of the blocks observed. Images were digitized in 512×512 pixels, in a hexagonal grid, with a spectral resolution of 256 grey levels giving a pixel size of 31 μm.
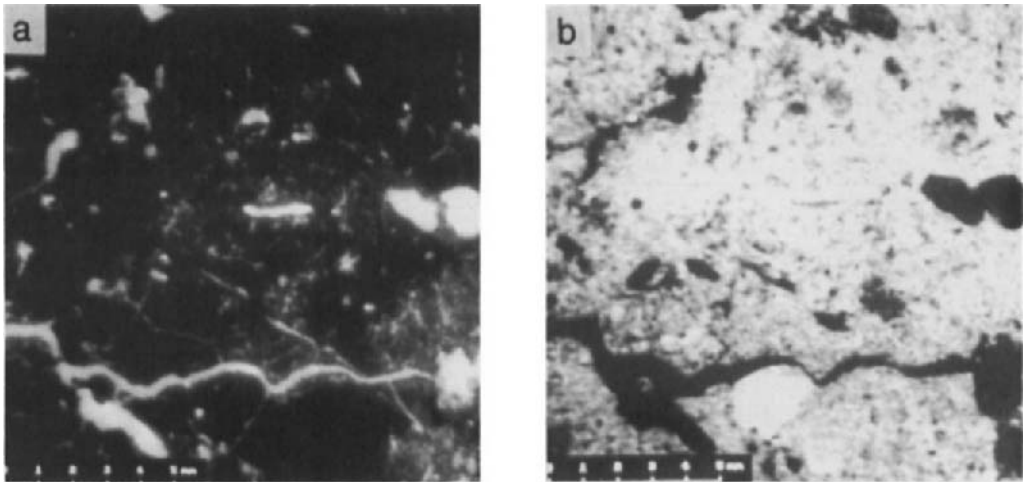
Fig. 1. Grey-tone images captured under : a) UV light b) visible light (Bar = 5 cm).

Segmentation

Identification of the pores or of the coloured areas on grey-tone images was performed according to a four step method derived from Moran *et al.* (1988). First, the largest pore bodies were detected by a simple partition thresholding. Second, the smallest and thinnest bodies were detected by a "tophat" transformation (Serra, 1982). This operation was found to be more efficient than the edge detector (morphological gradient between initial image and its eroded form) proposed by Moran *et al.* (1989) because the grey levels of the matrix and the tongues were very variable. Third, the two binary images obtained previously were combined using a logical OR operator. Finally, this image was thinned morphologically using a structuring element consisting of any rotation of:

$$
\begin{array}{ccc}
X & X & \\
0 \quad 1 & & 0 \\
0 & 0 &
\end{array}
$$

where the value X stands for 0 or 1. This operation removed from the previous image all occurrences of this configuration and counteracted any over-thickening of pore space.

Identification of stained and unstained macropores

The sides of the stained pores were coloured to a thickness of 0.5 - 1.5 mm due to methylene blue diffusion caused by the duration of the trials. The intersection of the two binary images (logical AND operator) obtained from the images captured under ultra-violet and visible light allowed the stained macroporosity to be identified. The image of unstained macroporosity was obtained using a logical subtraction between total and stained macroporosity.

Table 2
Mean values and standard deviations of macroporosity classified according to shape and size of poroids.

	column A		column B		column C		total	
	mean	std	mean	std	mean	std	mean	std
Rounded poroids								
R1	1.41	0.04	1.33	0.04	1.40	0.03	1.38	0.02
R2	0.79	0.02	0.80	0.02	0.80	0.02	0.80	0.01
R3	0.51	0.05	0.51	0.05	0.47	0.07	0.50	0.05
TOTAL	2.71		2.64		2.67		2.68	
Intermediate poroids								
I1	0.36	0.11	0.36	0.11	0.35	0.10	0.35	0.10
I2	0.91	0.05	0.90	0.08	0.85	0.05	0.89	0.03
I3	0.74	0.05	0.68	0.07	0.76	0.06	0.73	0.01
TOTAL	2.00		1.94		1.96		1.97	
Elongated poroids								
E1	0.14	0.03	0.15	0.02	0.12	0.02	0.14	0.01
E2	0.33	0.04	0.30	0.06	0.30	0.07	0.31	0.03
E3	1.06	0.20	1.02	0.20	1.03	0.17	1.02	0.03
TOTAL	1.52		1.47		1.45		1.47	
TOTAL	6.24		6.05		6.08		6.11	

Quantitative description of porosity

A 2-D characterization of individual pore outlines or "poroids" (Moran *et al.*, 1988) in an image was proposed. In this study poroids were described according to three variables, size, shape and orientation.

Many parameters are used in order to characterize pore structure (Murphy *et al.*, 1977; Bullock and Thomasson, 1979; Ringrose-Voase and Bullock, 1984; Edwards *et al.*, 1988; Bui *et al.*, 1989; McBratney and Moran, 1990). Ringrose-Voase (1990) showed that the poroid area can give an estimation of its size in 2-D but is not equal to the pore width in 3-D. In this work poroid area was used to estimate pore size, whatever the shape (Meng, 1989). Three size classes were defined: (1) area<100 pixels; (2) 100 pixels<area<500 pixels and (3) area>500 pixels.

The shape of the poroids was characterized by the lengthening index (Coster and Chermant, 1985):

$$lengthening\ index = \frac{(Perimeter)^2}{4\pi Area}$$

This index increases with poroid elongation. Poroids were classified into three classes: R (rounded poroids), lengthening index < 2, which consists mainly of channels; I (intermediate
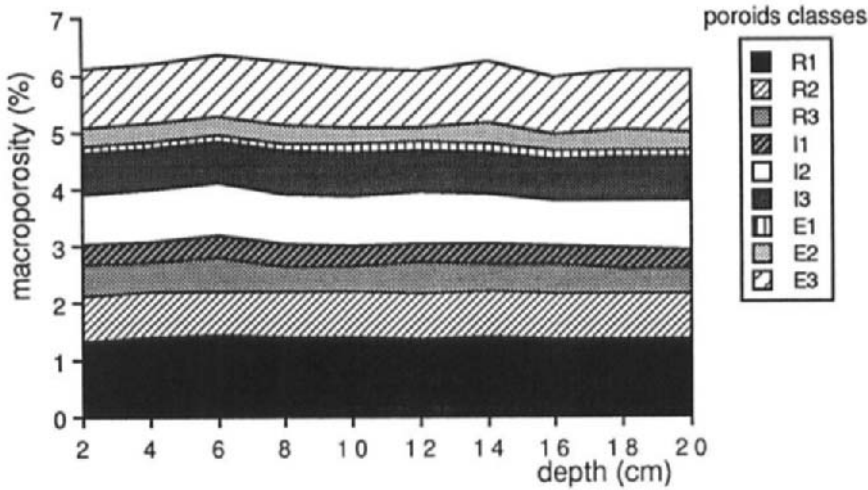
Fig. 2. Mean values profile of area of macropores in the columns.

poroids), 2 < lengthening index < 5, which consists mainly of vughs but can also consist of wide, short cracks; and E (elongated poroids), lengthening index > 5, which consists of cracks. By combining size and shape parameters the poroids could be classified into 9 classes.

The orientation index was calculated for the elongated poroids (class E) in the vertical sections (column D), after the branches of the crack network had been disconnected using the method of Hallaire (1994). This index gives an orientation between 0° and 90°, where 90° corresponds to the vertical.

RESULTS AND DISCUSSION

Total macroporosity

Table 2 gives the means and standard deviations of macroporosity for the nine classes of poroids for each column A, B and C (5 images per section, 10 horizontal sections) and for the three columns together (150 images). The results show that there is no significant difference between the three columns, so that the three columns can be studied together.

These results show that total macroporosity is about 6% of an image area (16,000 pixels). Rounded pores account for the most macroporosity (2.7%) followed by the intermediate pores (2.0%), and elongated pores (1.5%). These results agree with the pedological description of this horizon (Diab *et al.*, 1988) which noted many tubular and vesicular pores and moderately developed structural pores (cracks) along ped faces.

Fig. 2 shows the total macroporosity profile, from the top (2 cm depth) of the columns down to the bottom 20 cm depth: for each level, the values are calculated on 15 images (5 images per section, 3 columns). The macroporosity in each poroid class shows little variability.
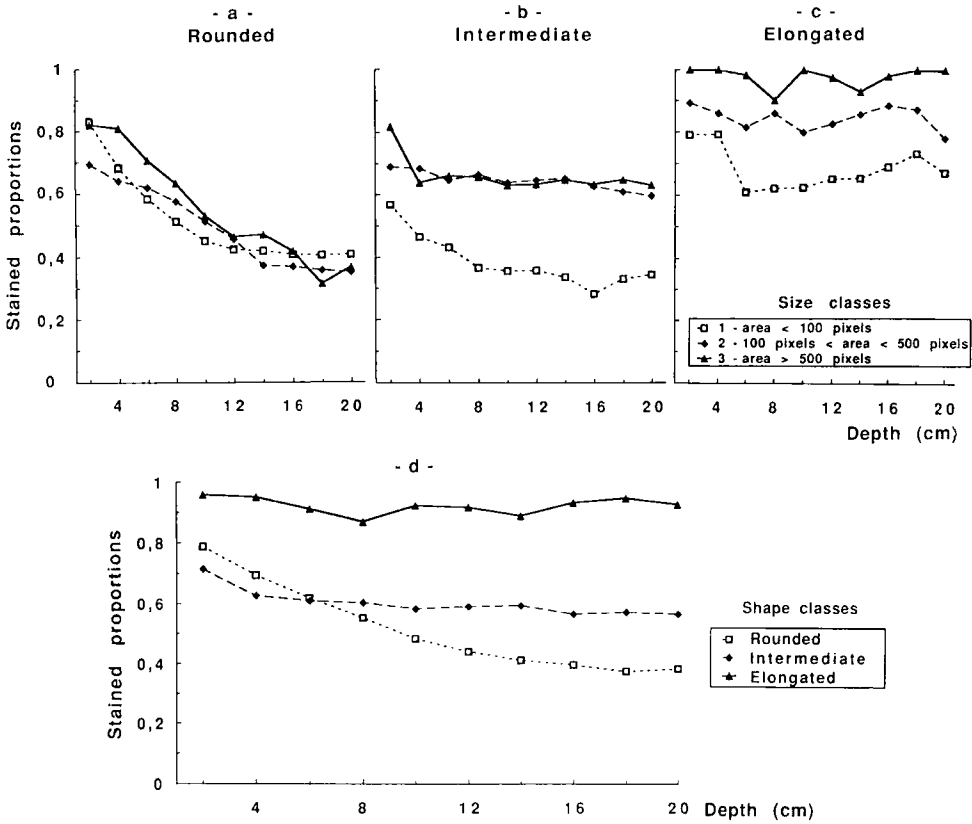
Fig. 3. Mean values profiles of stained proportion: a) rounded poroids; b) intermediate poroids; c) elongated poroids; d) overall proportion for each shape class of poroids.

Depth distribution of stained porosity on horizontal sections

Fig. 3a, b and c show the proportion of stained macroporosity within the columns (mean of columns A, B and C) for rounded, intermediate and elongated poroids respectively. Results are given for each size class.

For rounded poroids (Fig. 3a) there is a significant vertical gradient with stained porosity decreasing over the upper 10 cm. All size classes are affected including the largest rounded poroids (class R3). The influence of cylindrical macropores on water transfer is clearly confirmed (Smettem and Collis-George, 1985), but this influence appears to decrease after a few centimeters, because these channels - even the largest ones - are probably not interconnected or not vertical enough in comparison with the size of the column to allow water movement through the whole column.
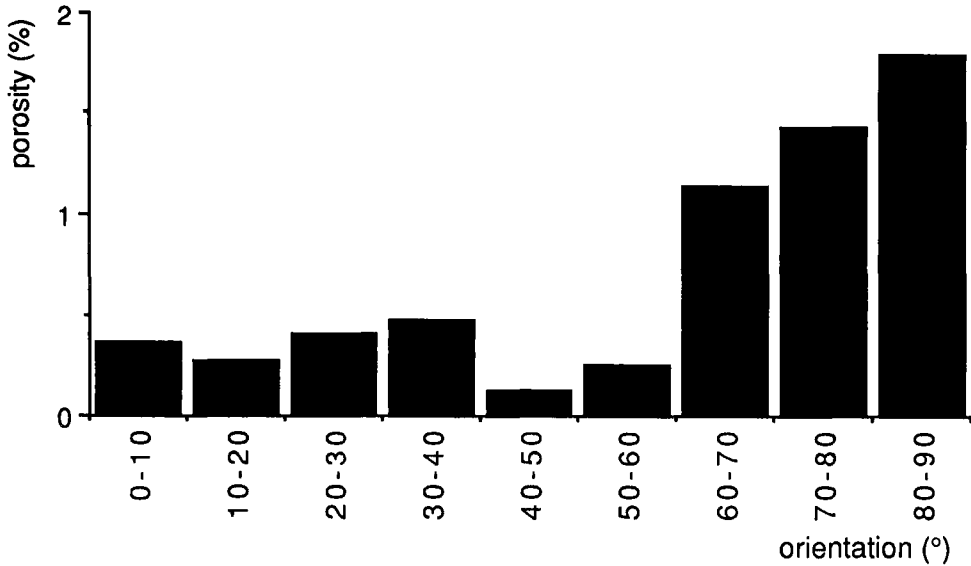
Fig. 4. Orientation histogram of elongated macropores on vertical soil sections.

For intermediate poroids (Fig. 3b) there is no vertical gradient. Stained porosity is about 1.5 times greater than unstained porosity. However the stained proportion varies with size with a greater proportion of larger poroids being stained.

For elongated poroids (Fig. 3c) there is no vertical gradient. Stained porosity is on average 12 times greater than unstained porosity. This ratio reaches 40 for size class 3, 7 for size class 2, and is greater than 2 even for size class 1 poroids. Cracks are therefore very efficient pores, whatever their size, through the whole column.

Fig. 3d summarizes the depth distribution of the proportion of stained macroporosity within the column, for each poroid shape class. For all rounded pores the stained proportion decreases with the depth: they are not efficient through the whole column. For intermediate pores it is necessary to distinguish between the size classes: the smallest ones are inefficient, the largest ones are efficient. For all elongated pores the stained proportion is high and does not decrease with the depth: they are efficient through the whole column.

Orientation of cracks on vertical sections

Fig. 4 presents the orientation of crack branches measured on the 10 images of column D. This figure shows that the cracks are mainly oriented between 70° and 90° (62% of the surface area of elongated pores belong to these classes), with a maximum at 90°. The crack network is anisotropic, with a preferential vertical orientation of its branches. This result could indicate a vertical continuity of the cracks and explain the preferential flow along them (Bouma, 1980).

CONCLUSIONS

Using image analysis of images captured under both visible and ultra-violet light and superimposing these two images allows stained poroids to be identified. This method makes it possible to analyze a great number of fields (150 images) and to propose for each of them a 2-D characterization according to size and shape. The studied horizon presents a large range in macropores (channels, vughs and cracks) without any vertical variation within the horizon.

Methylene blue staining shows differences of efficiency between macropores and allows their morphological characteristics to be measured. Transfer flow through macropores is more determined by their shape than by their size. Channels, even the largest ones, do not allow water movement in the whole column whereas cracks rapidly move water through the whole column because they are almost vertical and form a continuous, interconnected network.

REFERENCES

Bouma, J., 1980. Field measurement of soil hydraulic properties characterizing water movement through swelling clay soils. J. Hydrol., 45: 149-158.

Bouma, J., 1981. Soil micromorphology and preferential flow along macropores. Agric. Water Manage., 3: 235-250.

Bouma, J., Jongerius, A., Boersma, Jager, A. and Schoonderbeek, D., 1977. The function of different types of macropores during saturated flow through four swelling soil horizons. Soil Sci. Soc. Am. J., 41: 945-950.

Bouma, J., Jongerius, A. and Schoonderbeek, D., 1979. Calculation of saturated hydraulic conductivity of some pedal soils using micromorphometric data. Soil Sci. Soc. Am. J., 43: 261-264.

Bui, E.N., Mermut, A.R. and Santos, M.C.D., 1989. Microscopic and ultramicroscopic porosity of an oxisol as determined by image analysis and water retention. Soil Sci. Soc. Am. J., 53: 661-665.

Bullock, P. and Thomasson, A.J., 1979. Rothamsted studies of soil structure. II. Measurement and characterization of macroporosity by image analysis and comparison with data from water retention measurements. J. Soil Sci., 30: 391-413.

Coster, M. and Chermant, J.L., 1985. Précis d'Analyse d'Images. Editions du CNRS, Paris, 521 pp.

Diab, M., Mérot, Ph. and Curmi, P., 1988. Water movement in a glossaqualf as measured by two tracers. Geoderma, 43: 143-161.

Douglas, J.T., 1986. Macroporosity and permeability of some soil cores from England and France. Geoderma, 37: 221-231.

Edwards, W.M., Norton, L.D. and Redmond, C.E., 1988. Characterizing macropores that affect infiltration into nontilled soil. Soil Sci. Soc. Am. J., 52: 483-487.

Germann, P. and Beven, K., 1981. Water flow in soil macropores. I. An experimental approach. J. Soil Sci., 32: 1-13.

Hallaire, V., 1994. Description of microcrack orientation in a clayey soil using image analysis. In: A.J. Ringrose-Voase and G.S. Humphreys (Editors), Soil Micromorphology: Studies in Management and Genesis. Proc. IX Int. Working Meeting on Soil Micromorphology. Developments in Soil Science, 22. Elsevier, Amsterdam, pp. 549-557.

McBratney, A.B. and Moran, C.J., 1990. A rapid method for analysis of soil macropore structure. II. Stereological model, statistical analysis, and interpretation. Soil Sci. Soc. Am. J., 54: 509-515.

Meng, B., 1989. Image analysis of profiles to determine depth-dependent structural parameters of natural stone. In: M. Kalisnik and O. Leder (Editors), Proc. of the 5th European Congres for Stereolology. Acta Stereol., 8: 157-162.

Moran, C.J., Koppi, A.J., Murphy, B.W. and McBratney, A.B., 1988. Comparison of the macropore structure of a sandy loam surface soil horizon subjected to two tillage treatments. Soil Use Manage., 4: 96-102.

Moran, C.J., McBratney, A.B. and Koppi, A.J., 1989. A rapid method for analysis of soil macropore structure. I. Specimen preparation and digital binary image production. Soil Sci. Soc. Am. J., 53: 921-928.

Murphy, C.P., Bullock, P. and Turner, R.H., 1977. The measurement and characterisation of voids in soil thin sections by image analysis. J. Soil Sci., 39: 65-70.

Ringrose-Voase, A.J. and Bullock, P., 1984. The automatic recognition and measurement of soil pore types by image analysis and computer programs. J. Soil Sci., 35: 673-684.

Ringrose-Voase, A.J., 1990. One-dimensional image analysis of soil structure. I. Principles. J. Soil Sci., 41: 499-512.

Scotter, D.R., 1978. Preferential solute movement through larger soil voids. I. Some computations using simple theory. Aust. J. Soil Res., 16: 257-267.

Serra, J., 1982. Image Analysis and Mathematical Morphology. Academic Press, London, 628 pp.

Smettem, K.R.J. and Collis-George, N., 1985. The influence of cylindrical macropores on steady-state infiltration in a soil under pasture. J. Hydrol., 79: 107-114.

Soil Survey Staff, 1975. Soil Taxonomy. U.S. Dept. Agric. Handb. 436, U.S. Gov. Printing Office, Washington, D.C., 754 pp.

This Page Intentionally Left Blank

Degradation of structure and hydraulic properties in an Oxisol under cultivation (Brazil)

P. Curmi[1], F.F. Kertzman[2] and J.P. Queiroz Neto[3]

[1]*INRA-ENSA Laboratoire de Science du Sol, 65 rue de Saint Brieuc, 35042 Rennes Cedex, France*

[2]*Instituto de Pesquisas Technologicas de Sao Paulo, IPT-DIGEM, C.P. 7141, Sao Paulo, S.P., Brazil*

[3]*Universidade de Sao Paulo, Departamento de Geografia, Cidade Universitaria, C.P. 8105, 01000 S.P., Brazil*

ABSTRACT

Curmi, P., Kertzman, F.F. and Queiroz Neto, J.P., 1994. Degradation of structure and hydraulic properties in an Oxisol under cultivation (Brazil). In: A.J. Ringrose-Voase and G.S. Humphreys (Editors), Soil Micromorphology: Studies in Management and Genesis. Proc. IX Int. Working Meeting on Soil Micromorphology, Townsville, Australia, July 1992. Developments in Soil Science 22, Elsevier, Amsterdam, pp. 569-579.

Intensive farming and irrigation induce topsoil compaction in Oxisols which strongly reduces infiltration capacity and modifies soil water retention capacity. The aim of this work is to correlate the modification of soil structure and pore space distribution with degradation in hydraulic properties.

The soil studied was a "latossolo roxo" with a microgranular structure, developed on basalt near Guaira (Sao Paulo, Brazil). Two main horizons were identified: a compacted surface horizon in the top 40 cm (H2) and an undisturbed microgranular horizon below 40 cm (H1). Morphological description of the type and shape of macropores and their quantification by image analysis of thin sections were combined with volumetric pore space distribution determined by Hg porosimetry on centimetric bulk samples. Physico-chemical properties, water retention and K_{sat} measurements were performed on each horizon.

The pore space can be divided into three pore classes which are affected differently by compaction: (i) intra-aggregate pores (< 1 μm) unaffected by compaction; (ii) inter-aggregate pores ($1 - 100$ μm) with polyconcave shape whose size and total volume are reduced and (iii) tubular channels that disappear.

A geometric model showing strong correlation with the evolution of the physical properties was derived from the results. In the undisturbed horizon, organization of micro-aggregates can be modelled as a hexagonal network of spheres with tubular voids. The compacted horizon can be modelled as a compact hexagonal network of spheres.

INTRODUCTION

Intensive farming and irrigation can induce topsoil compaction in Oxisols which strongly reduces infiltration capacity and modifies soil water retention capacity. The aim of this study

Table 1
Chemical analyses of the secondary minerals (tri-acid method).

Depth	SiO_2	Al_2O_3	Fe_2O_3	TiO_2	MnO	Ki=SiO_2/Al_2O_3
cm			%weight fractions			molecular
H1:135-145	10.0	27.6	29.1	8.8	0.1	0.6

Table 2
Particle size distribution.

	pipette method			after Tamm pretreatment (1922)		
Depth	Clay	Silt	Sand	Clay	Silt	Sand
cm	< 2 μm	2 - 50 μm	50 - 2000 μm	< 2 μm	2 - 50 μm	50 - 2000 μm
H2: 0 - 20	25.6	19.6	54.9	33.0	29.3	37.7
H1: 40 - 60	30.2	19.3	50.5	40.6	30.4	29.0

was to determine the modifications of soil structure due to compaction and to correlate them with degradation of hydraulic properties (Spaans et al., 1989; Bresson and Zambaux, 1990). This was achieved by comparing two horizons of the same profile: a compacted surface horizon (H2) and an underlying undisturbed horizon (H1).

MATERIAL AND METHODS

The soil studied was a "latossolo roxo" (Camargo et al., 1987) with a microgranular structure, which developed on basalt near Guaira, Sao Paulo state, Brazil (21°S 48°W). Selective dissolution of the secondary minerals by using the tri-acid method (Harrison, 1933) (Table 1) shows high amounts of iron oxides and a molecular SiO_2/Al_2O_3 ratio Ki = 0.6 (Pédro, 1966). The sandy clay material was aggregated into 200 μm diameter micropeds formed by an association of kaolinite, gibbsite, iron oxides and quartz (Chauvel et al., 1978). This association was destroyed only after Tamm treatment (1922). Particle size analyses are presented in Table 2.

In the upper part of the deep soil profile, two main horizons were identified: a compacted surface horizon in the top 40 cm (H2) and an undisturbed microgranular horizon from 40 to 400 cm (H1). In this region, intensive farming, comprising 5 crops every two years, uses sprinkler irrigation and direct drilling of crops. Comparison with a soil under forest in a corresponding adjacent area confirmed the anthropogenic origin of the compacted horizon (I.P.T., 1987). Bulk density of the surface horizon increased from 0.96 to 1.46 g/cm³ between the two sites after ten years of intensive farming. Morphological and physical investigations were performed on undisturbed samples from H1 and H2 horizons.

Soil microstructure was observed on thin sections (90 × 160 mm) impregnated using a fluorescent dye (UVTex) after dehydration by acetone exchange (Murphy et al., 1977; Delaye, 1984). Three horizontal thin sections were made at 6, 14 and 29 cm depth for H2 and at 43, 52, 62 cm depth for H1. Image analysis was performed on 10 randomly chosen areas of

Table 3
Density measurements

Horizon	Density $\rho=Mass_{dry\ soil}/Vol_{total}$, g/cm³				Specific Volume $\upsilon = Vol_{pores}/Mass_{dry\ soil}$, cm³/g				
	ρ_{solid} ρ_s	ρ_{bulk} moist ρ_b	ρ'_{clod} moist ρ'_c	ρ_{clod} dry ρ_c	υ_{total} $1/\rho_b-1/\rho_s$	$\upsilon_{interclods}$ moist $1/\rho_b-1/\rho_c$	dry	$\upsilon_{intraclod}$ moist $1/\rho_c-1/\rho_s$	dry
H2	2.94	1.30	1.31	1.45	0.429	0.006	0.080	0.423	0.350
H1	2.98	1.02	1.14	1.14	0.645	0.103	0.103	0.542	0.542

120 mm² on every thin section using the VISILOG system. Images were digitized in 512×512 pixels, in a hexagonal grid, with a spectral resolution of 256 grey levels giving a pixel size of 21 μm. Identification of pores on images was performed using grey level thresholding. The porosity (mm³/mm³) was estimated as the proportion of pore pixels. This allowed quantification of total macroporosity and relative abundance of inter-aggregate pores and biological channels and vughs. The latter were identified on thin section and corresponded mainly to poroids (Moran et al., 1988) with areas larger than 1.1 mm². Therefore we used the area parameter to estimate pore size distribution despite the problems outlined in Ringrose-Voase (1990).

Physical measurements were done at 20 and 60 cm depth. Bulk density was determined on six replicates at two different scales by using 251 cm³ cylinders on wet soil and 2 - 5 cm³ clods on wet and air dried samples. Particle density was determined on oven dried samples using a water pycnometer. This allowed determination of both total and interclod porosity.

Pore size distribution, between 0.004 and 250 μm equivalent radii, was studied by mercury porosimetry (Micromeritics Pore Sizer 9310) on 2 - 4 cm³ clods (Pellerin, 1980; Fiès, 1984). Measurements were made on two replicates.

Water retention curves were obtained from undisturbed soil cylinders of 251 cm³ for low suction range (pF < 2) on suction table (Stakman et al., 1972) and from sieved samples for higher suctions, using Richard's apparatus (1947) on ten replicates.

Müntz infiltration tests (Colombani et al., 1972) were carried out in the field at 0 and 60 cm depth.

Comparison of data provided by these different techniques allowed determination of the evolution of each class of pores during compaction (Bruand and Prost, 1987) and their contribution to the hydraulic behaviour of soil (Grimaldi and Boulet, 1990).

RESULTS AND DISCUSSION

Pore space measurements obtained by the different methods (Tables 3 and 4) were compared at three different scales, i.e. whole soil, clod and microped. They are expressed volumetrically as porosity and gravimetrically as specific volume to compare pore space on samples of different or changing volumes.

Table 4
Comparision of pore space measurements by various methods

	Porosity $\varepsilon = V_{pores}/Vol_{total}$, cm³/cm³									Specific Volume $\upsilon = Vol_{pores}/Mass_{soil}$, cm³/g					
	ε_{total}	$\varepsilon_{interclods}$		$\varepsilon_{intraclod}$		$\varepsilon_{inter\text{-}aggreg.}$		$\varepsilon_{intra\text{-}aggreg.}$		$\upsilon_{intraclod}$		$\upsilon_{inter\text{-}aggreg.}$		$\upsilon_{intra\text{-}aggreg.}$	
		moist	dry	moist	dry	moist	dry	moist	dry	moist	dry	moist	dry	moist	dry
Density	$1-\rho_b/\rho_s$	$1-\rho_b/\rho_c$		$\rho_b(1/\rho_c-1/\rho_s)$						$1/\rho_c-1/\rho_s$					
H2	0.558	0.008	0.103	0.550	0.455					0.423	0.350				
H2	0.658	0.107	0.105	0.551	0.553					0.542	0.542				
Hg porosimetry				$A\,\rho_b$		$\rho_b(A\text{-}B)$		$B\,\rho_b$		A pores <250 µm		A - B		B pores <0.1 µm	
H2				0.450		0.233		0.217		**0.346**		0.179		**0.167**	
H1				0.496		0.314		0.182		**0.486**		0.308		**0.178**	
Water retention				$C\,\rho_b$		$\rho_b(C\text{-}D)$		$D\,\rho_b$		C V_{water} pF=0		C - D		D V_{water} pF=4.2	
H2				0.555		0.244		0.311		**0.427**		0.188		**0.239**	
H1				0.551		0.317		0.234		**0.540**		0.311		**0.229**	
Image analysis		E poroids> 1.1 mm²		F poroids< 1.1 mm²											
H2		**0.001**		**0.275**											
H1		**0.091**		**0.306**											

Measured data in bold characters
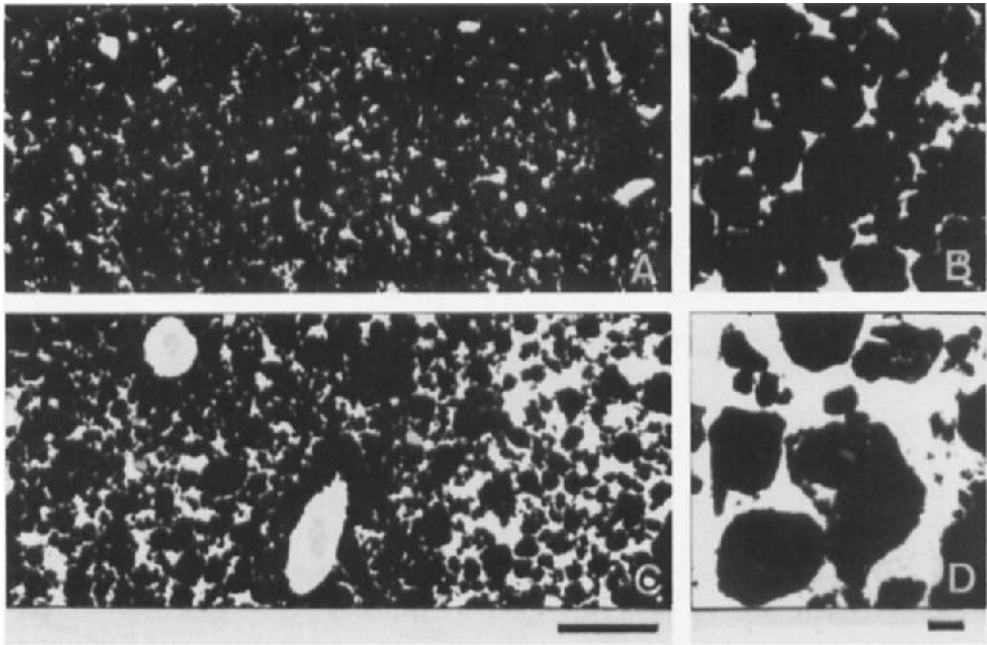
Fig. 1. Fluorescent micrographs of horizontal thin sections of H1 (C, D) and H2 (A, B) horizons at 52 cm and 14 cm depths respectively (A, C bar=1mm; B, D bar=100 mm).

Density measurements

Density measurements (Table 3) on whole soil and clod size samples showed that compaction induced a 33% reduction of total pore specific volume between H1 and H2 (0.22 cm^3/g). It corresponded to the disappearance of interclod voids (0.10 cm^3/g) and a decrease of intraclod voids (0.12 cm^3/g). No shrinkage occurred on clod size samples in H1 whilst 13% shrinkage occurred on H2 clods.

Light microscopy

Light microscopy examination showed that the arrangement of micropeds is denser in H2. than in H1. Thus, a large continuous void network is seen in H1, but only polyconcave voids loosely interconnected in 2-D are seen in H2 (Fig. 1A, C). This occurs without any modification of the size or shape of micropeds (Fig 1B, D). Moreover, biological channels and vughs showing compacted walls, abundant in H1, and absent in H2.

Image analysis

Image analysis was used to characterize and quantify this macroporosity. The macroporosity in H2 was 12% less than in H1, which corresponds to a relative decrease of
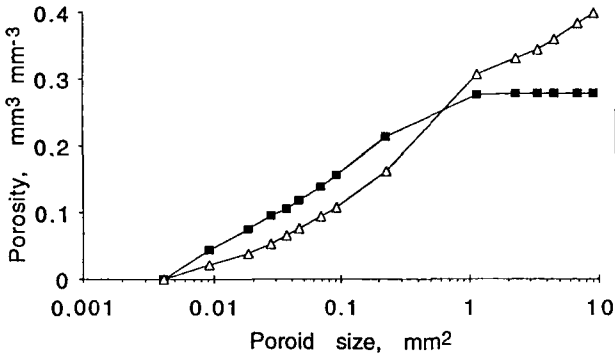
Fig. 2. Cumulative diagram of the different poroid area size classes obtained by image analysis.
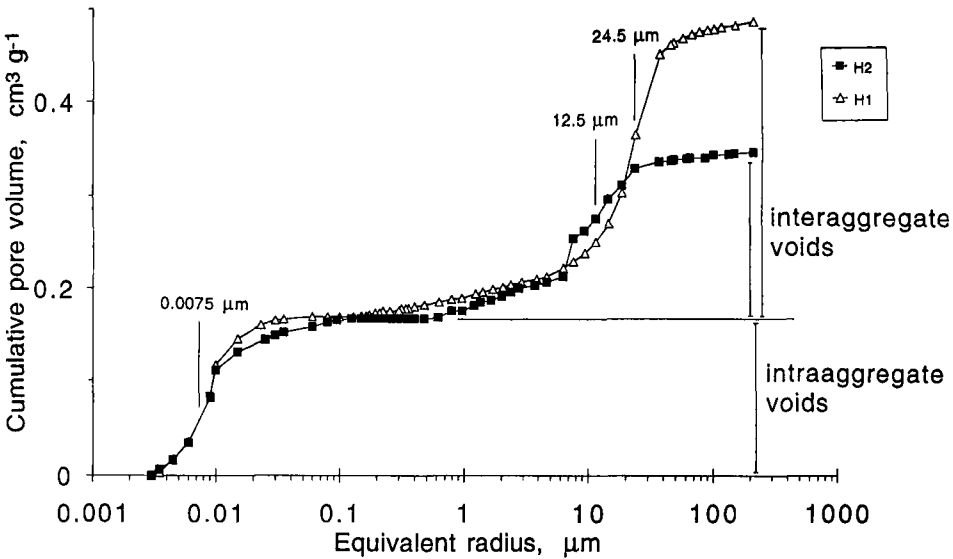
Fig. 3. Mercury injection curves.

30%. This decrease was due to the disappearance of poroids with areas more than 1.1 mm^2 which corresponded mainly to channels and vughs (Table 3, Fig. 1C), and a decrease in those smaller than 1.1 mm^2, which corresponded to inter-aggregate porosity. The latter corresponded also to a modification in pore space distribution with a fall in poroids between 1.1 and 0.2 mm^2 and an increase of poroids smaller than 0.03 mm^2 (Fig. 2). Quantitative estimation of coarse biological porosity by image analysis (0.09 mm^3/mm^3) agrees with interclod porosity estimated from density measurement (0.11 cm^3/cm^3) (Table 4).

Mercury porosimetry

Mercury porosimetry showed the soil had a bimodal pore size distribution (Fig. 3) similar to ferrallitic soils from Africa (Cambier and Prost, 1981). The first mode (voids < 0.1 µm) is
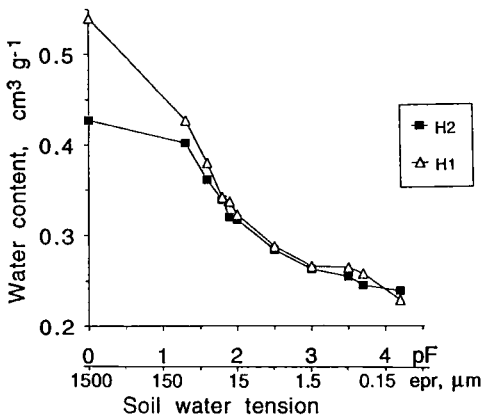
Fig. 4. Water retention curves, gravimetric water content.
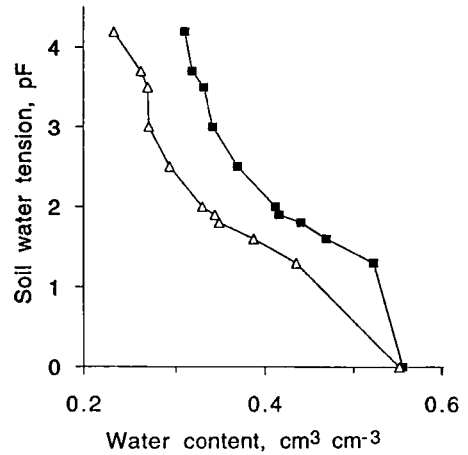
Fig. 5. Water retention curves, volumetric water content.

attributed to intra-aggregate porosity due to associations of clay particles and the second to inter-aggregate porosity (0.1 μm < voids < 250 μm).

Intra-aggregate voids were similar in H1 and H2 horizons, with a modal equivalent radius of 0.007 μm. The specific volume of intra-aggregate pores on a clay only basis was 0.44 and 0.51 cm^3/g of clay for H1 and H2, respectively, when referring to clay content after Tamm treatment (Table 2). This confirms the micromorphological observation that intra-aggregate voids were not affected by compaction.

Inter-aggregate voids were affected by compaction. Between H1 and H2, there was a 42% decrease in inter-aggregate specific volume and a reduction of the modal equivalent radius from 24.5 to 12.5 μm. Pore specific volume of clods as estimated by mercury porosimetry and by density measurements on dry samples was similar for H2 and not for H1. This indicates that intraclod pores were < 250 μm for H2 whilst the difference between these two techniques for H1 represents intraclod pores > 250 μm.

Water retention curves

Water retention curves for H1 and H2 (Fig. 4) are similar for pF > 2. The same water contents at pF = 4.2 are in agreement with the equal intra-aggregate pore specific volume shown by mercury porosimetry. Very different curve shapes for pF < 2 show the loss of inter-aggregate voids with equivalent radius > 80 μm in H2, corresponding to 40% decrease of inter-aggregate specific volume.

Comparison of intra-aggregate pore volumes estimated by water retention at pF = 2 and by mercury porosimetry showed a shrinkage of the micropeds in both horizons. Microped shrinkage did not affect clod volume in H1 whilst it corresponded to clod shrinkage in H2. This difference was probably due to larger contact surfaces between micropeds in the compacted horizon.

Table 5
Comparison of experimental data and data calculated according to two spherical packing models.

Horizon		Macroporosity[a]		Eqv. radius[b]	$K_{sat}{}^{c}$
		%	(σ)	μm	cm/h
H2	experimental data	27.60	(1.9)	12.5	6.6
	calculated data using compact hexagonal model	25.95		15.5	17.3
H1	experimental data	39.70	(1.1)	24.5	142.0
	calculated data using hexagonal model	39.54		41.4	22.2

Experimental data: [a] estimated from 2-D image analysis; [b] determined by Hg porosimetry; [c] determined by Müntz infiltration tests.

Calculated data: [a] and [b] using Graton and Faster formulae for 100 μm radius spheres; [c] using the equations of Scheidegger (1974) for compact hexagonal packing and hexagonal packing models.

Gravimetric water retention capacity at low suction range was strongly reduced by compaction (Fig. 4). Conversely, volumetric water retention capacity was higher in the compacted horizon H2 (da Silva *et al.*, 1986) from pF = 4.2 to pF = 1.3 mainly due to the water retention at pF = 4.2 being higher (Fig. 5).

An attempt was made to model the inter-aggregate pore space, based on the organization in micropeds, using a simple geometric model consisting of packed spheres of constant diameter (Vachier *et al.*, 1979). Two types of packing were tested:

    a) a hexagonal packing model to simulate the structure of H1;
    b) a compact hexagonal packing model to simulate the denser structure of H2.

Calculated and experimental data are compared in Table 5. Inter-aggregate porosity and equivalent radius were calculated for 100 μm radius spheres using the Graton and Fraser (1935) formulae. Saturated hydraulic conductivity was calculated according to Scheidegger (1974, in Humbel, 1976) as follows:

$$K_{sat} = 2.218 \times 10^7 \, R^2 \quad \text{for hexagonal packing model,}$$
$$K_{sat} = 1.725 \times 10^7 \, R^2 \quad \text{for compact hexagonal packing model,}$$

where R is the radius of the spheres.

The experimental values of inter-aggregate porosities used were derived from image analysis assuming isotropy. Experimental values of equivalent radii were determined by mercury porosimetry. K_{sat} values were obtained using the Müntz infiltration test.

The models are in agreement with experimental estimation of pore space characteristics of the two horizons, and of K_{sat} of H2. However, since coarse tubular porosity is not taken into account in these models, they failed in predicting K_{sat} for H1 where biological channels were abundant. Total macroporosity of H1 as determined by image analysis is in agreement with calculated data using hexagonal model. However, this macroporosity includes 23% coarse

biological channels and vughs with compacted walls as well as inter-aggregate packing voids. Therefore, these biological transformations of the macroporosity do not affect total macroporosity because the opening of large biological voids may be compensated by compaction of the surrounding soil.

CONCLUSIONS

A study of the soil pore space was conducted by combining morphological and physical approaches at different scales on undisturbed samples in order to characterize the complete range of pore sizes. The pore space of the Oxisols was divided in three types of voids: (i) fine intra-aggregate voids, (ii) inter-aggregate packing voids, (iii) coarse biological tubular voids. Compaction induced by cultivation resulted in a loss of 33% of the total pore specific volume. This reduction affected each void type differently. (i) Intra-aggregate voids were not modified. (ii) The volume of inter-aggregate packing voids decreased by 40% and their equivalent radius by a factor of two. (iii) Coarse biological tubular voids disappeared.

In the loose packing of microOEpeds of the undisturbed soil, local compaction related to shrinkage or bioturbation processes did not affect total porosity.

Denser packing of micropeds related to compaction strongly reduced gravimetric water retention capacity at low suction range and conversely increased volumetric water retention capacity.

The disappearance of biological tubular voids was responsible for a reduction in K_{sat}. This disappearance may be due to compaction or use of pesticides in this type of farming. The respective roles of these two factors on loss of coarse biological voids needs to be studied to improve water management.

Quantification of such large pores can only be achieved using volumetric measurements at different scales, including large samples, and image analysis of large sections (Hallaire, 1988a, b; Hallaire and Curmi, 1994).

Models of inter-aggregate pore space based on packed spheres predicted accurately the modification of several physical properties of these oxic horizons, with respect to the arrangement of micropeds.

ACKNOWLEDGEMENTS

REFERENCES

Bresson, L.M. and Zambaux, C., 1990. Micromorphological study of compaction induced by mechanical stress for a dystrochreptic fragiudalf. In: L.A. Douglas (Editor), Soil Micromorphology: A Basic and Applied Science. Proc. VIII Int. Working Meeting on Soil Micromorphology, San Antonio, Texas, July 1988. Developments in Soil Science 19, Elsevier, Amsterdam, pp. 33-40.

Bruand, A. and Prost, R., 1987. Effect of water content on fabric of a soil material: an experimental approach. J. Soil Sci., 38: 461-472.

Camargo, M.N., Klant, E. and Kauffman, J.H., 1987. Sisteme brasileiro de classificaçao de solos. Boletim informativo da Soc. Bras. de Ciencia do Solo, 12: 11-13.

Cambier, P. and Prost, R., 1981. Etude des associations argile-oxide: organisation des constituants d'un matériau ferrallitique. Agronomie, 1: 713-722.

Chauvel, A., Pedro, G. and Tessier, D., 1976. Rôle du fer dans l'organisation des matériaux kaolinitiques. Etudes expérimentales. Science du Sol, 2: 101-113.

Colombani, J., Lamagat, J.P. and Thiebaux, J., 1972. Mesure de la perméabilité des sols en place: un nouvel appareil pour la méthode Müntz. Une extension de la méthode Porcher aux sols hétérogènes. Cah. ORSTOM sér. Hydrol., vol. IX, 3: 15-46.

Delaye, R., 1984. Notes techniques sur la préparation des lames minces dans les matériaux meubles. Bull. Inst. Géol. Bassin d'Aquitaine, Bordeaux, 35: 135-158.

Fies, J.C., 1984. Analyse de la répartition du volume des pores dans les assemblages argile squelette: comparaison entre un modèle d'espace poral textural et les données fournies par la porosimétrie au mercure. Agronomie, 4: 319-355.

Graton, L.C. and Fraser, H.J., 1935. Systematic packing of spheres with a particular relation to porosity and permeability. J. Geol., 43: 785-909.

Grimaldi, M. and Boulet, R., 1990. Relation entre l'espace poral et le fonctionnement hydrodynamique d'une couverture pédologique sur socle de guyane francaise. Cah. ORSTOM, sér. Pédol., XXV: 263-275.

Hallaire, V., 1988a. La fissuration d'un sol argileux au cours du dessèchement. I Description in situ. Agronomie, 8: 139-145.

Hallaire, V., 1988b. La fissuration d'un sol argileux au cours du dessèchement. II Modélisation morphologique. Agronomie, 8: 273-280.

Hallaire, V. and Curmi, P., 1994. Image analysis of pore space morphology in soil sections, in relation to water movement. In: A.J. Ringrose-Voase and G.S. Humphreys (Editors), Soil Micromorphology: Studies in Management and Genesis. Proceedings of 9th International Working Meeting on Soil Micromorphology. Developments in Soil Science, 22. Elsevier, Amsterdam, pp. 559-567.

Harrison, J.B., 1933. The Katamorphism of Igneous Rocks under Humid Tropical Conditions. Imperial Bureau of Soil Science, Harpenden, U.K., 79 pp.

Humbel, F.X., 1976. L'espace poral des sols ferrallitiques du Cameroun: caractérisation et comportement en relation avec les régimes hydriques et bioclimats. Travaux et documents de l'ORSTOM 54, Paris: 306 pp.

I.P.T., 1987. Instituto de Pesqpuisas Tecnologicas de Sao Paulo: Apoio technologico à agricultura irrigada do municipio de Guaira, Sao Paulo. Relatorio n° 23966, Sao Paulo, Brazil.

Moran, C.J., Koppi, A.J., Murphy, B.W. and McBratney, A.B., 1988. Comparison of macropore structure of a sandy loam surface horizon subjected to two tillage treatments. Soil Use Manage., 4: 96-102.

Murphy, C.P., Bullock, P. and Turner, P.H., 1977. The measurement and characterization of voids in soil thin sections by image analysis. Part I - Principles and techniques. J. Soil Sci., 28: 498-508.

Pellerin, F.M., 1980. La porosimétrie au mercure appliquée à l'étude géotechnique des sols et des roches. Bull. Liaison Lab. Ponts Chaussées, 106: 106-116.

Pédro, G., 1966. Intérêt géochimique et signification minéralogique du paramètre moléculaire Ki = SiO_2/Al_2O_3 dans l'étude des latérites et bauxites. Bull. Gr. Franç. Argiles, XVIII, 13: 19-31.

Richards, L.A., 1947. Pressure-membrane apparatus - construction and use. Agric. Eng., 28: 451-454.

Ringrose-Voase, A.J., 1990. One-dimensional image analysis of soil structure. I. Principles. J. Soil Sci., 41: 499-512.

Silva, A.P. da, Libardi, P.L. and Camargo, O.A., 1986. Influencia da compactaçao nas propriedades fisicas de dois latossolos. R. Bras. Ci. Solo, 10: 91-95.

Spaans, E.J.A., Baltissen, G.A.M., Bouma, J., Miedema, R., Lansu, A.L.E., Schoonderbeek, D. and Wielemaker, W.G., 1989. Changes in physical properties of young and old volcanic surface soils in Costa Rica after clearing of tropical rain forest.

Stakman, W.P., Valk, G.A. and Harst, G.G. van der, 1972. Determination of soil moisture retention curves. I. Sand Box apparatus (range pF 0 - 2.7). Institute for Land and Water Management, Wageningen, 19 pp.

Tamm, O., 1922. Eine Methode zur Bestimmung der anorganischen Komponenten des Gel-Komplex in Boden. Medd. Statens Skogforsokanst, 19: 385-404.

Vachier, R., Cambier, P. and Prost, R., 1979. Structure d'un milieu poreux: la craie. Ann. Agron., 30: 247-263.

This Page Intentionally Left Blank

Study of soil porosity with mercury porosimetry and image analysis on backscattered electron scanning images (BESI). Application to tilled "crusting soils" in Zimbabwe

L.P. D'Acqui[1], A. Bruand[2] and M. Pagliai[3]*

[1]*CNR, Centro di Studio per i Colloidi del Suolo, P.le delle Cascine 28, 50144 Firenze, Italy.*
[2]*INRA Orléans, Service d'Etude des Sols et de la Carte Pédologique de France, Ardon, 45160 Olivet, France.*
[3]*CNR, Istituto per la Chimica del Terreno, Via Corridoni 78, 56100 Pisa, Italy.*

ABSTRACT

D'Acqui, L.P., Bruand, A. and Pagliai, M., 1994. Study of soil porosity with mercury porosimetry and image analysis on backscattered electron scanning images (BESI). Application to tilled "crusting soils" in Zimbabwe. In: A.J. Ringrose-Voase and G.S. Humphreys (Editors), Soil Micromorphology: Studies in Management and Genesis. Proc. IX Int. Working Meeting on Soil Micromorphology, Townsville, Australia, July 1992. Developments in Soil Science 22, Elsevier, Amsterdam, pp. 581-590.

Samples were collected from wheel-traffic and seed-line areas of a crusting soil in Zimbabwe. The pore-size distributions obtained by mercury porosimetry and image analysis of backscattered electron scanning images were compared. The two methods show: (i) a decrease in porosity under the wheel lines associated with hardening; (ii) two classes of pore, the first created by aggregate packing and biological activity, and the second by packing of skeleton particles with the porous clay phase; and (iii) no difference in volume of each pore class. However, the two pore-size distributions show a difference in the modal pore size of each class, which is higher in image analysis than in mercury porosimetry. This difference arises because mercury porosimetry shows the size of necks in the pore network whereas image analysis measures the size of randomly intersected pores.

INTRODUCTION

Mercury intrusion is widely used to analyse soil porosity. It enables study of the pore-size distribution over a large range of pore diameters (6×10^{-3} - 4×10^2 µm). However, this method gives no information on the shape of pores and on their organization in the groundmass. Another commonly used method for studying soil porosity consists of image analysis of thin sections under transmitted-light (Pagliai *et al.*, 1984; Kooistra *et al.*, 1984; Bullock *et al.*, 1985; Bui *et al.*, 1989). This approach allows the study of the shape and spatial distribution of the pores, but it is limited to pores larger than 30 µm because of the size limitation inherent in thin section thickness, although fluorescent photographs of polished cuts

---

through impregnated blocks (Geyger and Beckman, 1967) allow smaller pores to be photographed optically.

To date, results from mercury porosimetry and image analysis of thin sections have not been compared, except with respect to total pore volume rather than pore-size distribution (Fiès and Bruand, 1990). This is mainly because of the narrow range of pore sizes that can be measured by both methods. The aim of this study is to extend the range of pore sizes that can be studied in image analysis, thus allowing comparison of pore-size distributions determined with mercury porosimetry and image analysis.

SAMPLES AND METHODS

Samples were collected from a Chromic Luvisol (FAO-UNESCO, 1974) in Zimbabwe. These soils, which are prone to crusting, are found in areas of intensive commercial agriculture and are generally degraded by tillage practices (Nyamapfene, 1991). The degradation processes are mainly crusting of the soil surface and hardening of the tilled layer. Samples varying in their hardness were collected, during the dry season after soybean harvesting, in tilled horizons from the wheel-traffic (WT) and seed-line (SL) areas. The soil is a silty clay, but the clay content of WT samples was higher (36%) than that of the SL samples (31%).

Mercury porosimetry measures the pressure required to force mercury into the pores of a dry sample, as well as the volume of intruded mercury at each pressure (Lawrence, 1977; Vachier et al., 1979). Mercury intrusion was performed with a porosimeter (Micromeritics 9310) operating up to a maximum pressure of 200 MPa. The surface tension of mercury and its contact angle on the soil material were 0.484 Nm^{-1} and 130°, respectively (Fiès, 1984). Thus, the pore size volume distribution was measured for pores between 0.006 and 370 μm equivalent cylindrical diameter (D). Measurements were made on three replicate clods of 1 - 2 cm in size dried at 105°C for 24 hours. Pore volume was expressed on a mass basis ($cm^3 g^{-1}$). The cumulative pore volume (cpv) curve and its derivative pore volume distribution (pvd) curve, were used to discuss the results (Bruand and Prost, 1987).

Thin sections (5 × 3 cm) were obtained by impregnating oven-dried clods of 2 - 4 cm in size (40°C for a week) with a polyester resin diluted with 30 volume per cent of styrene monomer. The thin sections were polished and then carbon-coated prior to their examination with a scanning electron microscope (Cambridge 90 SEM), using backscattered electron emission. The backscattered electron mode gives micrographs, or BESI, with a high contrast between voids occupied by resin and the mineral phase, thus allowing pores down to 0.1 μm in diameter to be studied (Bisdom and Thiel, 1981; Chrétien and Bisdom, 1983; Fiès and Bruand, 1990).

Image analyses were made with a Quantimet 570 instrument. The image size was 510 × 510 pixels, and pixel sizes used were 0.2 and 3.25 μm, for 415× and 25× magnifications respectively. Twenty pictures were analysed to study representative areas at each magnification. The pore space was segmented by setting an appropriate grey-level threshold within the range of 256 levels. Measurements were made of the number, area and perimeter of individual poroids (after Moran et al., 1988) in the field of view (frame area) (Jongerius and Bisdom, 1981; Pagliai et al., 1983, 1984; Ringrose-Voase and Bullock, 1984). Poroids were classified according to the shape factor [perimeter^2/(4πarea)] into regular poroids (shape factor 1 - 2), irregular poroids (shape factor 2 - 5) and elongated poroids (shape factor >5). These classes correspond approximately to those used by Bouma et al. (1977). Poroids in each
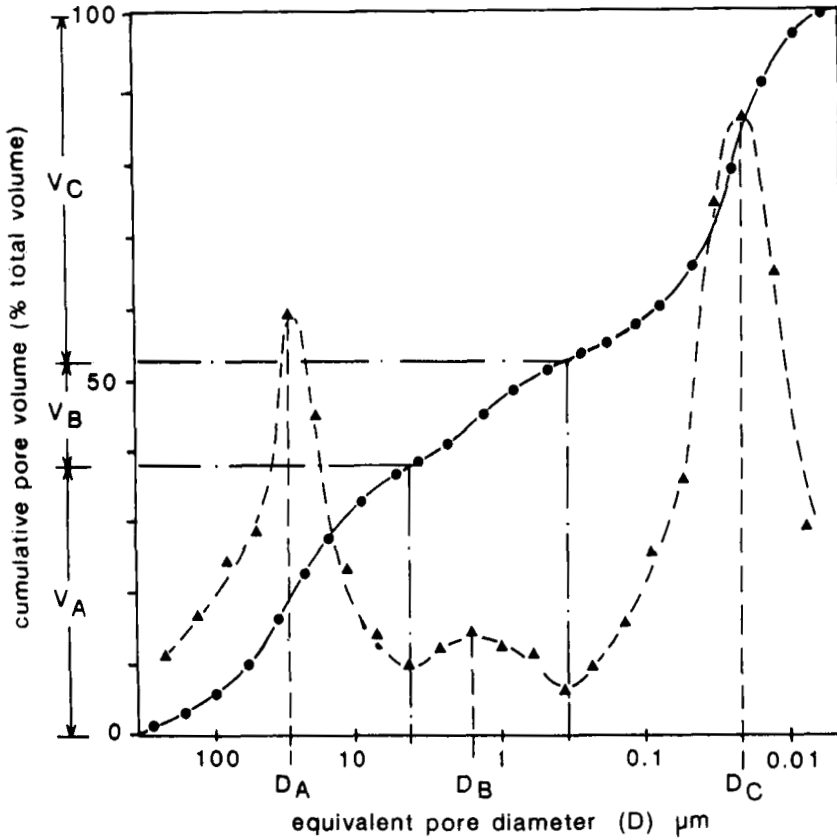
Fig. 1. Cumulative pore volume curve (dots) and derivative curve, $\Delta V/\Delta\log(D)$, which is the pore volume distribution (triangles), showing how size limits for pore volumes A, B and C are obtained.

Table 1
Total pore volume (V_{Hg}) and elementary pore volumes V_A, V_B and V_C obtained with mercury porosimetry on samples from wheel-traffic and seed-line areas (s.d. = standard deviation).

	Total pore volume		Elementary pore volumes					
	V_{Hg} cm^3 g^{-1}		V_A cm^3 g^{-1}		V_B cm^3 g^{-1}		V_C cm^3 g^{-1}	
	mean	s.d.	mean	s.d.	mean	s.d.	mean	s.d
Wheel-traffic	0.229	0.003	0.056	0.012	0.055	0.016	0.118	0.006
Seed lines	0.297	0.012	0.155	0.014	0.053	0.004	0.089	0.008
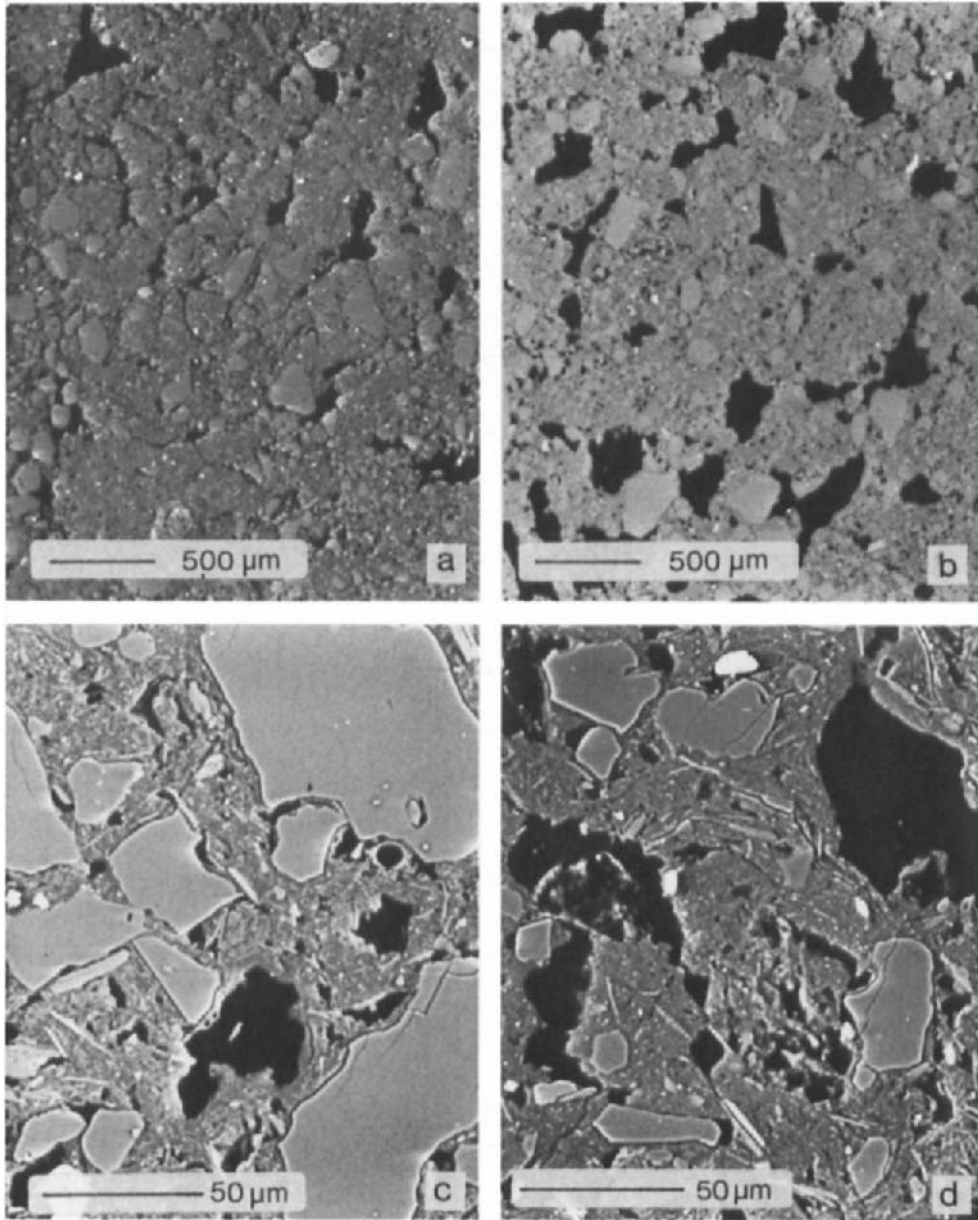
Fig. 2. Backscattered electron scanning images (BESI) of samples from wheel traffic areas (a: ×25 and c: ×415) and seed line areas (b: ×25 and d: ×415). Black areas are pores, grey areas are silt and sand particles, and dark grey areas are clay particles and associated pores.

group were further subdivided into size classes (S), calculated as equivalent diameter $\sqrt{4\,area/\pi}$, for regular and irregular poroids, and as width $[perimeter - \sqrt{perimeter^2 - 16\,area}]/4$ for elongated poroids. The pore-size distribution (psd) was obtained for S values from 0.5 to 320 μm, by combining the distributions for S in the range 0.5 - 10 μm and in the range 10 - 320 μm, obtained at magnifications of 415× and 25.5× respectively. The boundary of 10 μm corresponds to 50 pixels at 415× and 3.1 pixels at 25.5×.

RESULTS AND DISCUSSION

Pore volume distribution from mercury porosimetry

Mercury porosimetry allows different pore volumes to be identified. Each pore volume is defined by its modal diameter (D_m) and its volume-per-unit mass of solid (V). D_m corresponds to the "vertical" inflection point of the cumulative pore volume (cpv) curve, *i.e.* to maxima of the pore volume distribution (pvd) curve (Bruand and Prost, 1987; Coulon and Bruand, 1989) (Fig. 1). The limits defining pore volumes correspond to the "horizontal" inflection point of the cpv curve, *i.e.* to the minimum of the pvd curve.

The cpv curves show the total pore volume (V_{Hg}) consisted of three pore volumes V_A, V_B and V_C, corresponding respectively to pore size classes A, B and C. For the largest and smallest equivalent pore diameters (D), the cpv curve is asymptotic to the abscissa, indicating that the pores contributing to V_A and V_C were wholly taken into account by mercury porosimetry. D_m ranged from 60 to 30 μm for V_A, from 2 to 1 μm for V_B, and from 0.03 to 0.02 μm for V_C. The boundary between V_A and V_B corresponds to 5 μm and that between V_B and V_C to 0.3 μm. The mercury intrusion results show that V_{Hg} was less in WT than in SL samples (Table 1), mainly as a result of a lower V_A. Unimportant differences appear in class B. Class C, including pores <0.2 μm, can be attributed to the fabric of clay particles (Fiès and Bruand, 1990) and its variation is assumed to result from the higher clay content in WT (36%) than in SL samples (31%).

Poroid size distribution from image analysis

At low magnification, BESI show large poroids, that can be irregular, elongated and regular (Fig. 2a and b), which are related to aggregate packing and biological activity. The number unit area was less in WT samples (Fig. 2a). At higher magnification, BESI show pore space that results from the packing of skeleton particles with the porous clay fraction (Fig. 2c and d), which corresponds to lacunar pores defined by Fiès (1984) and Fiès and Bruand (1990).

The psd was established by plotting the pore-area density A_A(pore area/unit area) versus equivalent S, as calculated from image analyses (Fig. 3). The curves show a bimodal shape with two poroid size classes A and B, whose boundary is at 7 μm. Class B does not show any significant variation between WT and SL samples, either in porosity or in its distribution between the three poroid types. On the other hand, the porosity of class A is less in WT samples, mainly because of the absence of elongated poroids.
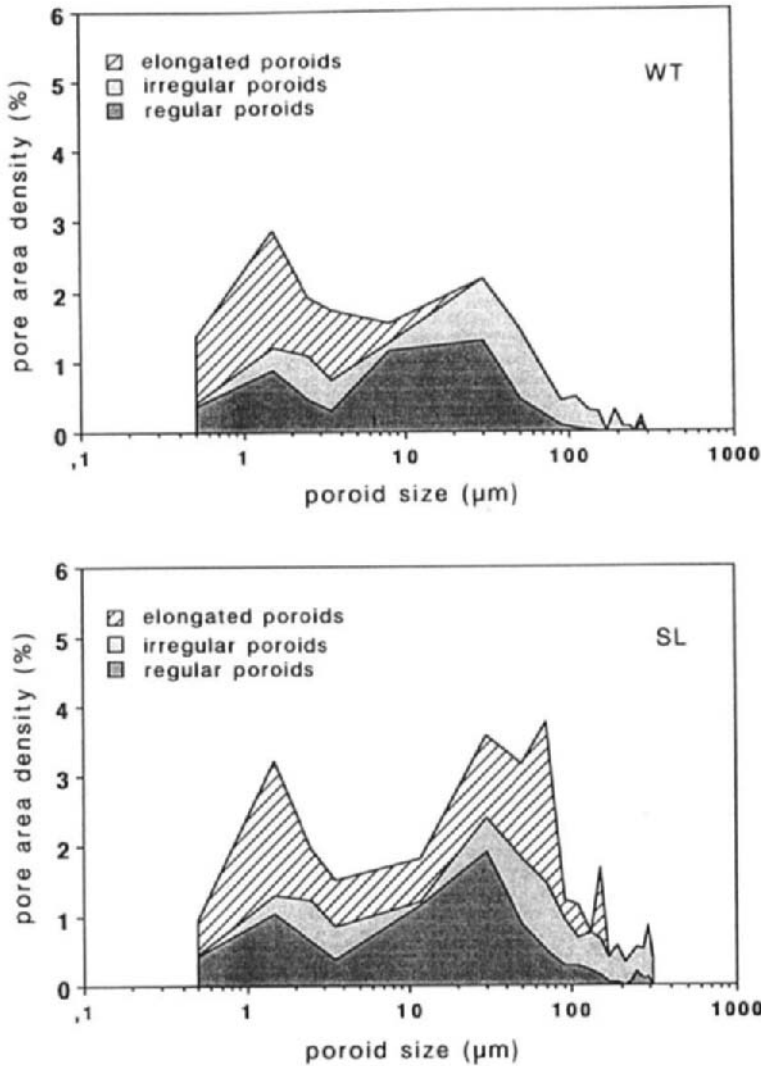
Fig. 3. Poroid size distribution determined by image analysis for samples from wheel-traffic (WT) and seed-line (SL) areas. The pore-area density percentage is plotted versus equivalent poroid size (S), which corresponds to an equivalent diameter for regular and irregular poroids, and to an equivalent width for elongated poroids.

Comparison of the two methods

The sections used for image analysis which give 2-D information are selected to be representative of the structure in 3-D because they are isotropic, uniform random (Weibel, 1979). Although the area proportions, A_A, in each size class bear an undefined relationship to

Table 2

Comparison of the results from mercury porosimetry and image analysis. Porosity is expressed as volume percentage for Hg porosimetry and as area density for image analysis (s.d. = standard deviation).

	Pore class A V_A %		Pore class B V_B %		Total pore volume $(V_A + V_B)$%
	mean	s.d.	mean	s.d.	
Mercury porosimetry					
Wheel traffic	9.3	2.0	9.1	2.6	18.4
Seed lines	24.0	2.2	8.2	0.6	32.2
Image analysis					
Wheel traffic	8.3	0.5	8.2	0.5	16.5
Seed lines	21.2	0.6	7.8	0.8	29.0

the volumetric proportions, V_V, in the same 3-D size class (Ringrose-Voase and Nortcliff, 1987; Ringrose-Voase, 1990), we compared the A_A results obtained from image analysis with the mercury intrusion results calculated volumetrically and using the bulk density of the mercury porosimetry samples (Fig. 4). The comparison concerns pore classes A and B alone, *i.e.* pores resulting from aggregate packing and biological activity, and pores resulting from packing of the skeleton and porous clay phase, since pores due to the clay fabric (class C) were not examined with BESI.

The distributions corresponding to pore classes A and B are in good agreement (Table 2). The porosity determined by mercury porosimetry is a little higher than the pore-area density obtained by image analysis. Differences in dehydration can explain a higher development of pore classes A and B in mercury porosimetry, because of higher shrinkage of the clay phase at 105°C.

The two psd curves show the modal size for classes A and B to be higher by image analysis than by mercury porosimetry (Fig. 4). For class B the model size from image analysis is 1-2 μm against 0.7 - 0.8 μm from mercury porosimetry, and for class A, it is 30 - 50 μm from image analysis against 10 - 15 μm from mercury porosimetry. For the latter method, the equivalent pore size corresponds to the size of necks of the pore network, thus explaining the lower modal sizes compared to the pore size determined over random sections through the pore network, as in image analysis.

CONCLUSIONS

Comparison of the mercury-porosimetry and image-analysis methods for porosity measurement shows that they give similar results for A and B pore classes, but that the modal size is greater in image analysis data.

The combined results from mercury porosimetry and image analysis on backscattered electron scanning images, comparing wheel-traffic and seed-line areas show: (i) a decrease in total porosity associated with soil hardening due to traffic; (ii) a pore class B unaffected
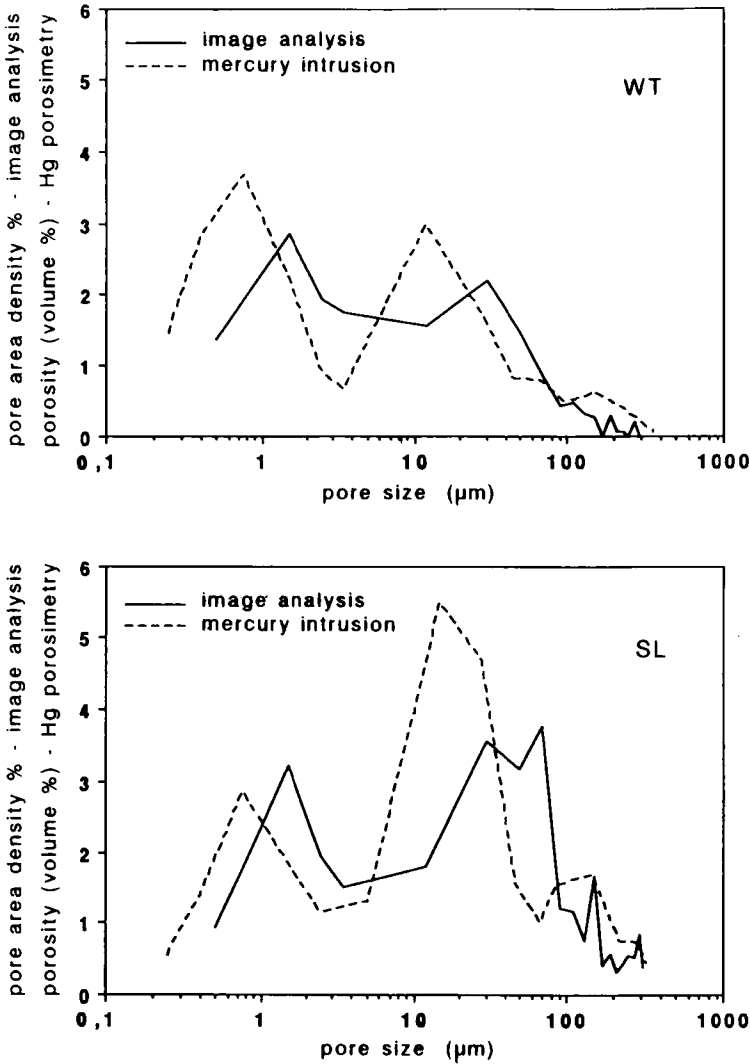
Fig. 4. Comparison of the pore volume distribution obtained by mercury porosimetry and poroid-size distribution by image analysis: samples from wheel-traffic (WT) and seed-line (SL) areas.

traffic and a class A whose porosity is significantly reduced by the impact of tillage; and (iii) a strong decrease in the porosity of elongated pores in class A under traffic areas.

ACKNOWLEDGEMENT

REFERENCES

Bisdom, E.B.A. and Thiel, F., 1981. Backscattered electron scanning images of porosities in thin sections of soils, weathered rocks and oil gas reservoir rocks using SEM-EDXRA. In: E.B.A. Bisdom (Editor), Submicroscopy of Soils and Weathered Rocks. 1st Workshop of the International Working Group on Submicroscopy of Undisturbed Soil Materials (IWGSUSM) 1980, Wageningen. Centre of Agricultural Publishing and Documentation (Pudoc), Wageningen, Netherlands, pp. 191-206.

Bouma, J., Jongerius, A., Boersma, O., Jager, A. and Schoonderbeek, D., 1977. The function of different types of macropores during saturated flow through four swelling soil horizons. Soil Sci. Soc. Am. J., 41: 945-950.

Bruand, A. and Prost, R., 1987. Effect of water content on the fabric of a soil material: an experimental approach. J. Soil Sci., 38: 461-472.

Bui, E.N., Mermut, A.R. and Santos, M.C.D., 1989. Microscopic and ultramicroscopic porosity of an Oxisol as determined by image analyses and water retention. Soil Sci. Soc. Am. J., 53: 661-665.

Bullock, P., Newman, A.C.D. and Thomasson, A.J., 1985. Porosity aspects of the regeneration of soil structure after compaction. Soil Tillage Res., 5: 325- 341.

Chrétien, J. and Bisdom, E.B.A., 1983. The development of soil porosity in experimental sandy soils with clay admixtures as examined by Quantimet 720 from BESI and by other techniques. Geoderma, 30: 285-302.

Coulon, E. and Bruand, A., 1989. Effects of compaction on the space geometry in sandy soils. Soil Tillage Res., 15: 137-152.

Fiès, J.C., 1984. Analyse de la répartition du volume de pores dans les assemblages argile squelette : comparaison entre un modèle d'espace poral textural et les données fournies par la porosimétrie à mercure. Agronomie, 4: 319-355.

Fiès, J.C. and Bruand, A., 1990. Textural porosity analysis of a silty clay soil using pore volume balance estimation, mercury porosimetry and quantified backscattered electron image (BESI). Geoderma, 47: 209- 219.

FAO-UNESCO, 1974. Soil Map of the World. Vol. I, Legend. UNESCO, Paris.

Geyger, E. and Beckmann, W., 1967. Apparate und Methoden der Mikromorphometrischen Strukturanalyse des Bodens. In: W.L. Kubiena (Editor), Die Mikromorphometrischen Bodenanalyse. Ferdinand Enke, Stuttgart, pp. 36-57.

Jongerius, A. and Bisdom, E.B.A., 1981. Porosity measurements using Quantimet 720 on backscattered electron scanning images of thin sections of soils. In: E.B.A. Bisdom (Editor), Submicroscopy of Soils and Weathered Rocks. 1st Workshop of the International Working Group on Submicroscopy of Undisturbed Soil Materials (IWGSUSM) 1980, Wageningen. Centre of Agricultural Publishing and Documentation (Pudoc), Wageningen, Netherlands, pp. 191-206.

Kooistra, M.J., Bouma, J., Boersma, O.H. and Jager, A., 1984. Physical and morphological characterization of undisturbed and disturbed ploughpans in sandy loam soil. Soil Tillage Res., 4: 405-417.

Lawrence, G.P., 1977. Measurement of pore size in fine textured soils: a review of existing techniques. J. Soil Sci., 28: 527-540.

Moran, C.J., Koppi, A.J., Murphy, B.W. and McBratney, A.B., 1988. Comparison of the macropore structure of a sandy loam surface soil horizon subjected to two tillage treatments. Soil Use Manage., 4: 96-102.

Nyamapfene, K., 1991. The Soils of Zimbabwe. Nehanda Publ., Harare, 179 pp.

Pagliai, M., La Marca, M. and Lucamente, G., 1983. Micromorphometic and micromorphological investigations of a clay loam soil in viticulture under zero and conventional tillage. J. Soil Sci., 34: 391-403.

Pagliai, M., La Marca, M., Lucamente, G. and Genovese, L., 1984. Effects of zero tillage on the length and irregularity of elongated pores in a clay loam soil under viticulture. Soil Tillage Res., 4: 433-444.

Ringrose-Voase, A.J. and Bullock, P., 1984. The automatic recognition and measurement of soil pore types by image analysis and computer programs. J. Soil Sci., 35: 673-684.

Ringrose-Voase, A.J. and Nortcliff, S., 1987. The application of stereology to estimation of soil structural properties: A preview, In: N. Fedoroff, L.M. Bresson and M.A. Coutry (Editors), Soil Micromorphology. Proc. VII Int. Working Meeting of Soil Micromorphology, Paris, July 1985. Association Française pour l'Etude du Sol, Plaisir, France, pp. 81-88.

Ringrose-Voase, A.J., 1990. One-dimensional image analysis of soil structure, I. Principles. J. Soil Sci., 41: 499-512.

Weibel, E.R., 1979. Stereological Methods. Vol. 1. Practical Methods for Biological Morphometry. Academic Press, London, 415 pp.

Vachier, P., Cambier, P. and Prost, R., 1979. Structure d'un milieu poreux: la craie. Ann. Agron., 30: 247-263.

Experimental relationship between the morphological pore-size distribution and the soil water-retention characteristic

H.J. Vogel and U. Babel
Institut für Bodenkunde und Standortslehre, Universität Hohenheim (310), 70593 Stuttgart, Germany

ABSTRACT

Vogel, H.J., and Babel, U., 1994. Experimental relationship between the morphological pore-size distribution and the soil water-retention characteristic. In: A.J. Ringrose-Voase and G.S. Humphreys (Editors), Soil Micromorphology: Studies in Management and Genesis. Proc. IX Int. Working Meeting on Soil Micromorphology, Townsville, Australia, July 1992. Developments in Soil Science 22, Elsevier, Amsterdam, pp. 591-600.

The pore-size distribution of soil is often derived from the water-retention characteristic. Since pore systems of soil cannot be considered to be continuous and of cylindrical shape, the water-retention characteristic is influenced by pore continuity and pore necks. Measurements of morphological pore-size distributions on polished blocks are independent of pore continuity or pore necks.

For measuring morphological pore-size distributions, the morphological width of pores is defined and a method, based on the distinction of different types of pore shape, is proposed.

Here, we compare the results of quantitative morphological measurements and the corresponding water-retention characteristics for 6 horizons of 2 soil profiles in Southern Germany.

The discrepancy between morphological pore-size distribution and the pore-size distribution derived from water retention curves is discussed in terms of pore continuity and methodological errors.

As might be expected, the pore-size distribution derived from water retention data is shifted towards smaller pores in comparison to the morphological method. However, the proportion of pores >300 µm, the largest category used here, was overestimated by the water retention method. This may be due to air entrapment and to methodological errors in the determination of particle density.

INTRODUCTION

Important functional properties of soils, such as translocation of liquid and gases or root penetration, are affected by the soil pore-size distribution. Determination of the water retention curve is one of the most frequently applied methods for characterization of soil pore-size distribution. The assumption of a cylindrical pore shape is usually adopted in order to estimate an 'equivalent' pore-size distribution. Interpretations of these results should take into account that the estimated pore-size distribution is influenced by pore continuity and pore necks (Klute, 1986; Lawrence, 1977).
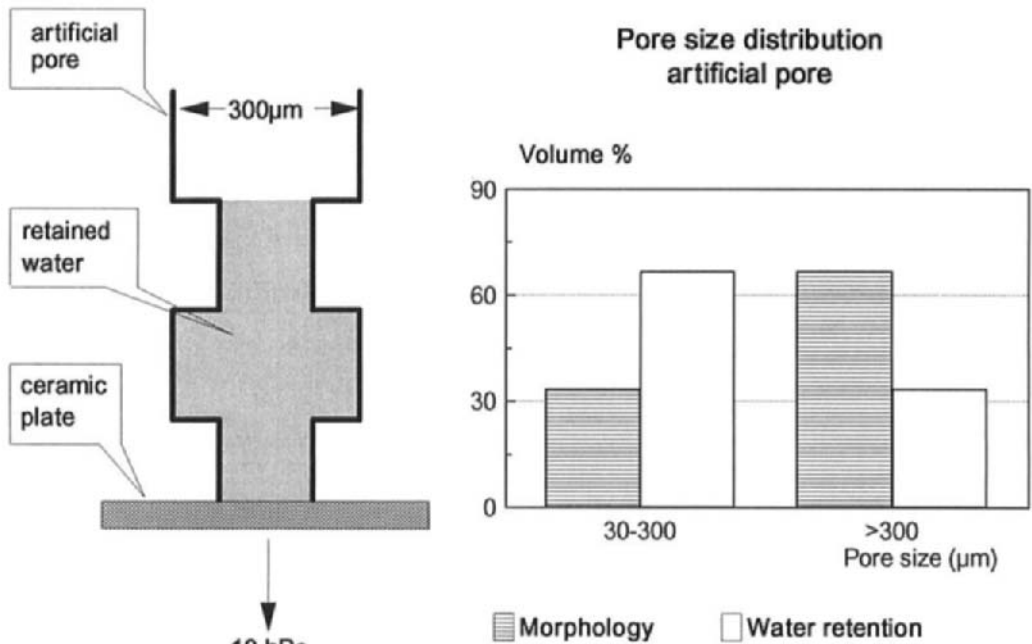
Fig. 1. Idealized pore necks and their effect on pore-size distribution derived from water retention data.

Pore sizes can also be investigated morphologically using polished blocks or thin sections of soil, in which case the results are not affected by pore continuity or neck sizes. It has to be expected that pore-size distributions derived from water retention data are shifted towards smaller pore sizes in comparison to those obtained morphologically. This effect was discussed by Bullock and Thomasson (1979) and Bui *et al.* (1989) and is illustrated for one simple pore in Fig. 1.

The main problem of the morphological approach is to relate the two dimensional cross section of pores to their three dimensional width. However, there are already some stereological methods available which are based on the distinction of different types of pore shape, namely channels, planar pores and other pores exhibiting a more or less irregular shape which will be referred to as irregular pores.

The aims of this paper are to consider: (1) methods of determination of a morphological pore-size distribution comparable to water retention data, (2) comparison of pore-size distributions obtained morphologically with those obtained from water-retention and (3) the results of sample comparisons in terms of pore continuity and possible methodological errors.

MATERIALS AND METHODS

Soil profiles investigated

Three horizons of a Terra Fusca (Mückenhausen, 1977) under forest and three horizons of a Pelosol (Mückenhausen, 1977) under meadow in southern Germany were investigated. They

Table 1
Texture, particle density, bulk density, air filled porosity at -10 kPa suction and volume density of pores > 30 μm.

Soil	Horizon	Texture			Core samples			Polished blocks
		clay <2 μm	silt 2-60 μm %	sand 60-2000 μm	particle density	bulk density g cm⁻³	air-filled porosity %	volume density %
Terra	Ah	43	34	23	2.60	1.05	18.3	16.8
Fusca	AhBv	52	31	17	2.65	1.27	14.7	14.0
	Bv	67	23	10	2.75	1.33	14.2	12.2
Pelosol	Ah	28	66	6	2.70	0.99	22.5	16.8
	AhBv	34	63	3	2.76	1.25	19.3	15.2
	Bvg	42	55	3	2.76	1.34	8.6	6.5

Note: The header row units should be read as: clay $<2\ \mu m$, silt $2\text{-}60\ \mu m$, sand $60\text{-}2000\ \mu m$ (all in %); particle density and bulk density in $g\ cm^{-3}$; air-filled porosity in %; volume density in %.

are briefly characterized in Table 1. Images of polished blocks at low magnification are shown in Fig. 2a and b.

Samples

For determination of water retention curves, six replicate undisturbed soil cores (100 cm³) were taken for each horizon. Care was taken to avoid any smearing on the upper side of the samples.

For morphological investigations, four replicate, undisturbed samples were taken with Kubiena boxes (40 × 60 × 80 mm) for each horizon at the same depths as the soil cores. After dehydration with acetone (FitzPatrick and Gudmundsson, 1978) and impregnation with a polyester resin (Vestopal 120L), one polished block (60 × 80 mm) was prepared in the vertical direction from each sample. After grinding and polishing, the surfaces of the polished blocks were etched with 10% fluoric acid to obtain good contrast between solid and pores when illuminated with oblique incident light.

Water retention measurements

After slow capillary saturation (10 days), the soil cores were progressively equilibrated on ceramic plates at potentials of 1, 3, 5 and 10 kPa with the corresponding equivalent pore diameters of 300, 100, 60 and 30 μm. The total pore volume was calculated from bulk density and particle density. The latter was measured with the pycnometer method using water as the liquid (Blake and Hartge, 1986).

Morphological pore sizes

The key to the morphological approach used in this study is to define the three-dimensional width suitable for comparison with water retention data at any place within the pore space. We
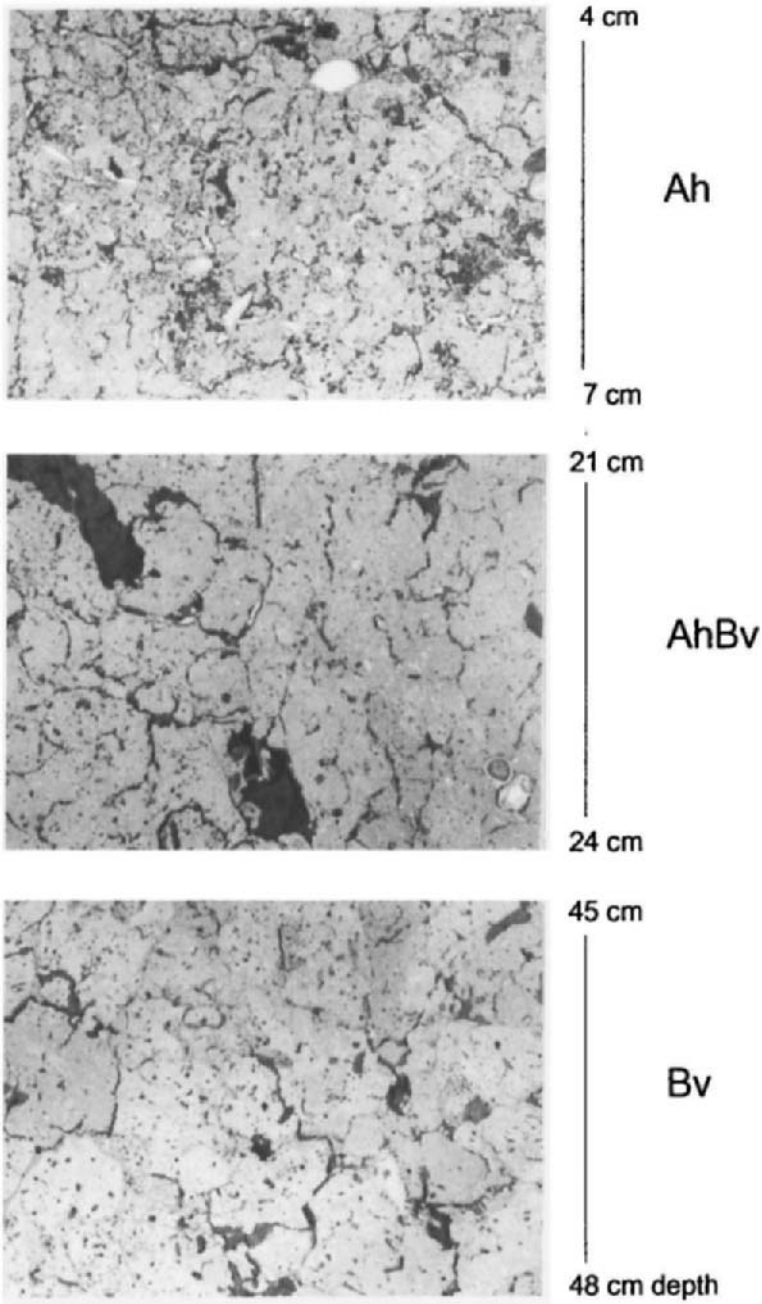
Fig. 2a. Photographs of polished blocks from horizons of a Terra Fusca.
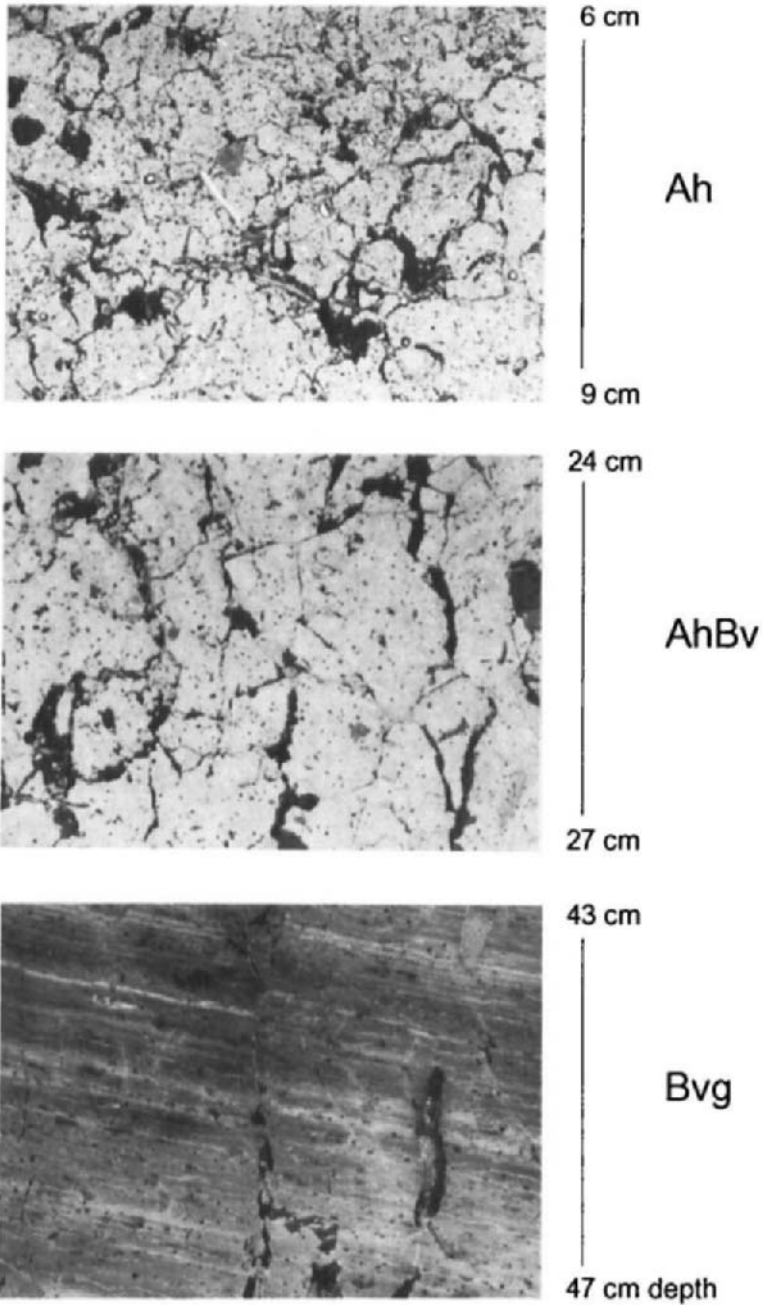
Fig. 2b. Photographs of polished blocks from horizons of a Pelosol.
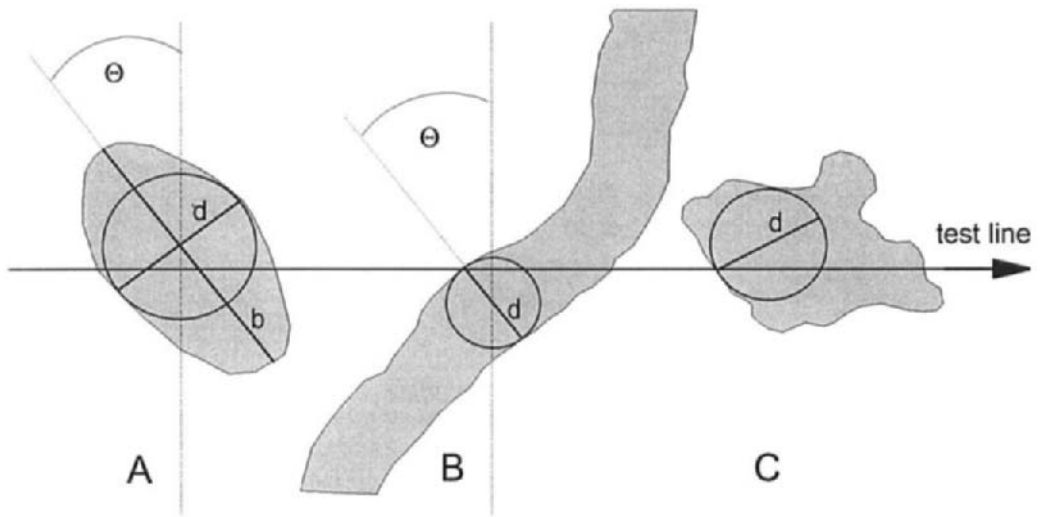
Fig. 3. Measurements of channel poroids (A), planar poroids (B) and irregular poroids (C) For further information see text.

used the following definition: The width at a point within the pore space is the diameter of the largest sphere which includes this point and which is completely part of the pore space.

In plane sections like polished blocks, the pore space appears as discrete individuals or as a more or less interconnected network, which will be referred to as poroids (Moran *et al.,* 1988) in the following description. Three basic types of pore shapes can be distinguished according to Brewer (1964):

- channels which give round to elliptical poroids in section,
- planar pores which give elongated poroids with almost parallel boundaries,
- packing voids and vughs, here called irregular pores, which give irregular poroids.

At least for channels and planar pores, there are realistic models of their three-dimensional geometry (Ringrose-Voase and Nortcliff, 1987; Ringrose-Voase, 1991). From these models it is evident that the relationship between the visible width in 2D and the 3D width according to the definition given above is different for these pore types. Consequently, we treated channels, planar pores and irregular pores separately.

Procedure

The method of measuring the pore space and the equipment used is described in detail by Vogel *et al.,* (1993). The polished blocks were observed with a stereomicroscope at a magnification of 40× illuminated with oblique incident light. Measurements were performed along horizontal and vertical test lines regularly distributed with a separation distance of 2 mm over an area (30 × 50 mm) centred on the polished block. In this way the total length of the testline was 150 cm per polished block, giving a total of 600 cm per horizon.

Widths and orientations were measured using a circle and a chord respectively. These were mirrored from a computer screen into the lightpath of the microscope and could be adapted by

the operator to the poroid being measured. Thereby, only pores larger than 30 μm were considered. At each transition point of the test line from solid to pore, the pore type was determined and measurements made as follows (Fig. 3):

- Channels: Small diameter (d), large diameter (b) and direction of the large diameter to the vertical axis (Θ).
- Planar poroids: Visible width (d) and direction of the planar poroid (Θ).
- Irregular poroids: Diameter of the largest circle touching the point of measurement and completely enclosed by the poroid.

CALCULATIONS

Channels

Assuming a more or less tortuous, cylindrical shape in 3D, the 3D-width of channels could be measured directly in the plane section as the small diameter (d) of the profile (Fig. 3). In addition, the large diameter (b) and its angle to the vertical axis (Θ) was measured to calculate the three-dimensional orientation distribution of the channels (these results will be published elsewhere). If the orientation distribution is known, the length density and volume density of different width classes can be estimated from the number of poroids intersected by the test line. These calculations were described in detail by Vogel *et al.* (1993).

Planar pores

The 3D-width of a planar pore can not be seen directly in a plane section. Depending on the orientation of the planar pores relative to the section plane the visible 2D width is always larger or equal to the 3D width. According to Sandau and Vogel (1993) the 3D width distribution was estimated from combined measurements of the visible 2D width and the angle of the profile to the vertical axis (Fig. 3).

Irregular pores

Unlike channels and planar pores there is no realistic model for the 3D geometry of irregular pores. Consequently there is no possibility to calculate the volume density for different size classes directly from the measured width distribution which is related to the surface density of these pores.

However, the total volume density of irregular pores can be quantified using the Delesse principle (Weibel, 1979). Assuming that the shape of irregular pores is self-similar or fractal for the different size-classes we used the V_V/S_V ratio, which is proportional to the pore diameter (d), to estimate the volume, V_{Vi}, of each size class, d_i:

$$V_{Vi}/S_{Vi} = x\, d_i$$

For a distinct shape x is constant (sphere: $x=1/6$; cylinder: $x=1/4$; sheet: $x=1/2$).

The total volume density, V_V, of irregular pores was estimated by point counting method (Weibel, 1979) using 3000 test points regularly distributed on each polished block.

The surface density S_{Vi} was obtained by:

$$S_{Vi} = 4\, I_i\, /\, L$$

where I_i is the number of points measured with width d_i and L the total lengths of the test line. Then:

$$x = \Sigma(d_i S_{Vi}) / V_V$$

In this way we found values of x between 0.26 and 0.34 for the different polished blocks. As a mean value we took 0.3 for the calculations:

$$V_{Vi} = 0.3 \, S_{Vi} \, d_i$$

As a first attempt, this calculation is based on the strong assumption that the distribution of d_i in 2D corresponds to the 3D width distribution according to the definition given above.

RESULTS AND DISCUSSION

The total pore volume >30 μm estimated by the two methods is shown in Table 1. In contradiction to the hypothesis, illustrated by Fig. 1, the results from the water-retention method were higher for all horizons.

The pore volumes of different size classes are shown in Figs 4 and 5. The standard deviations were calculated for four polished blocks and six core samples respectively.

Disregarding the largest category (>300 μm), the results obtained by the different methods were very close and the expected shifting of the physical results towards smaller pore sizes was equally detectable in all horizons.

The mean values of porosity >300 μm calculated from total pore volume and water retained at -1 kPa were generally higher than that calculated morphologically. However, the standard deviations are very high. In this pore size class the deviation between physical and morphological results may have been due to methodological problems:

- The volume of air entrapment within the whole pore space after saturation of the core samples is attributed to the largest pore size class which is calculated from the total porosity and the water retained at -1 kPa.
- In clayey soil, the pycnometer method may yield an over estimation of the particle density when water is used as liquid (Blake and Hartge, 1986).
- The morphological size distribution of irregular pores may yield an under estimation of large pores. Since the measurements are strictly connected to the outlines of the poroids, the measured pore diameters are decreased due to the roughness of the pore surface and this effect increases with increasing pore size.

One alternative for the measurement of morphological pore-size distribution could be the measurement of intercept lengths as frequently applied (Yanuka and Elrick, 1985; Bui *et al.*, 1987). However, with this method a systematic over estimation of large pores can not be excluded due to volume orientation, as shown by Odgaard *et al.*, (1990) for trabecular bone. For testing the hypothesis that physical measurements of pore-size distribution are shifted towards smaller pore sizes than obtained by morphological investigation, we preferred a morphological method which would tend to under estimate pore size.

With respect to the definition of the 3D pore size given above the opening size distribution (Serra, 1982) would probably give the best approximation.
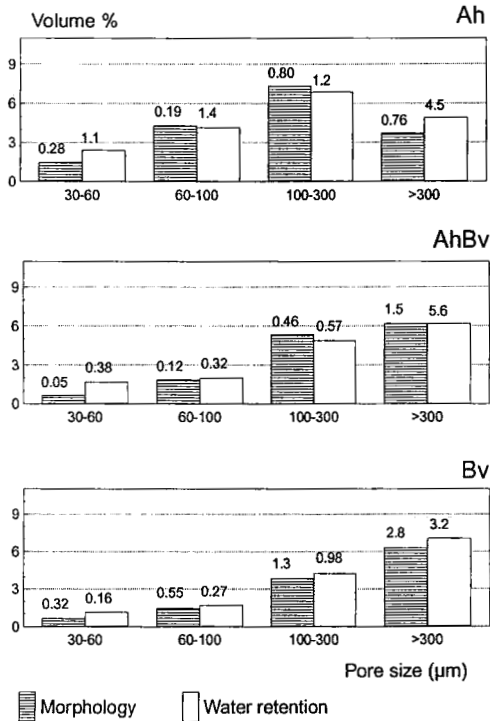
Fig. 4. Pore-size distribution of 3 horizons of a Terra Fusca: Morphological and physical results with standard deviations.
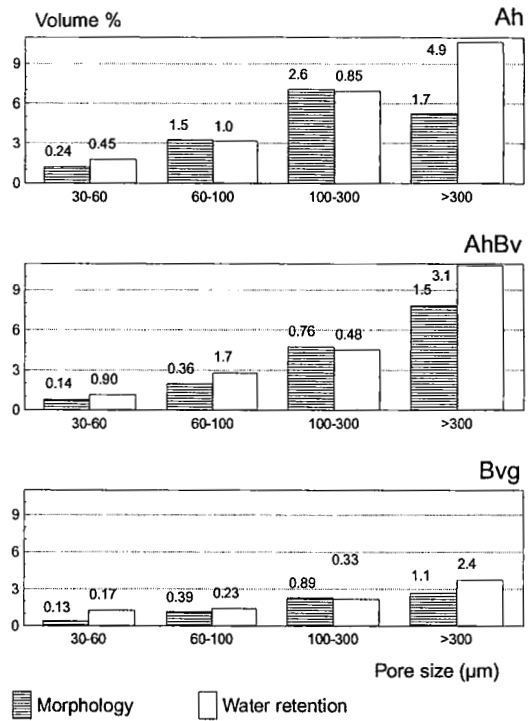
Fig. 5. Pore-size distribution of 3 horizons of a Pelosol: Morphological and physical results with standard deviations.

CONCLUSIONS

This investigation was focused upon a wide range of types of soil structure rather than intense replication. Nevertheless, based on these initial results, some cautious conclusions may be made:
- The morphometric measurements and the corresponding stereological calculations applied were quite sensitive for the determination of morphological pore-size distribution.
- Errors due to neck effects and pore continuity influencing the water-retention characteristics were detectable but not substantial in all investigated types of soil structure. Consequently we have some reason to assume that the pore systems were quite well connected in 3D.
- The evaluation of very large pores by the water-retention method is subject to methodological errors and requires larger sample volumes than applied here.

ACKNOWLEDGEMENTS

REFERENCES

Blake, G.R. and Hartge, K.H., 1986. Particle density. In: A. Klute (Editor), Methods of Soil
    Analysis. Part I. Am. Soc. Agron. and Soil Sci. Soc. Am., Madison, Wisconsin, pp. 377-
    381.
Brewer, R., 1964. Fabric and Mineral Analysis of Soils. John Wiley and Sons, New York,
    470 pp.
Bui, E.N., Mermut, A.R. and Santos, M.C.D., 1989. Microscopic and ultramicroscopic
    porosity of an Oxisol as determined by image analysis and water retention. Soil Sci. Soc.
    Am. J., 53: 661-665.
Bullock, P. and Thomasson, A.J., 1979. Rothamsted studies of soil structure. 2. Measurement
    and characterization of macroporosity by image analysis and comparison with data from
    water retention measurements. J. Soil Sci., 30: 391-413.
FitzPatrick, E.A. and Gudmundson, T., 1978. The impregnation of wet peat for the production
    of thin sections. J. Soil Sci., 29: 585-587.
Klute, A., 1986. Water retention: laboratory methods. In: A. Klute (Editor), Methods of Soil
    Analysis. Part I. Am. Soc. Agron. and Soil Sci. Soc. Am., Madison, Wisconsin, pp. 635-
    660.
Lawrence, G.P., 1977. Measurement of pore sizes in fine-textured soils: a review of existing
    techniques. J. Soil Sci., 28: 527-540.
Moran, C.J., Koppi, A.J., Murphy, B.W. and McBratney, A.B., 1988. Comparison of the
    macropore structure of a sandy loam surface soil horizon subjected to two tillage
    treatments. Soil Use Manage., 4: 96-102.
Mückenhausen, E., 1977. Entstehung, Eigenschaften und Systematik der Böden der
    Bundesrepublik Deutschland. DLG-Verlag Frankfurt/Main, 300 pp.
Odgaard, A., Jensen, E.B. and Gundersen, H.J.G., 1990. Estimation of structural anisotropy
    based on volume orientation. A new concept. J. Microsc., 157: 149-162.
Ringrose-Voase, A.J., 1991. Micromorphology of soil structure: description, quantification,
    application. Aust. J. Soil Res., 29: 777-813.
Ringrose-Voase, A.J. and Nortcliff, S., 1987. The application of stereology to the estimation
    of soil structural properties: A preview. In: N. Fedoroff, L.M. Bresson and M.A. Coutry
    (Editors), Soil Micromorphology. Proc. VII Int. Working Meeting of Soil Micromorpho-
    logy, Paris, July 1985. Association Française pour l'Etude du Sol, Plaisir, France, pp. 81-88.
Sandau, K. and Vogel, H.J., 1993. An estimation procedure for the joint distribution of spatial
    direction and thickness of flat bodies using vertical sections. Part II: An application in soil
    micromorphology. Biometrics, (in press).
Serra, J., 1982. Image Analysis and Mathematical Morphology. Academic Press, London,
    610pp.
Vogel, H.J., Weller, U. and Babel, U., 1993. Estimating orientation and width of channels and
    cracks at soil polished blocks - a stereological approach. Geoderma, 56: 301-316.
Weibel, E.R., 1979. Stereological Methods. Vol. 1. Practical Methods for Biological
    Morphometry. Academic Press, London, New York, 470 pp.
Yanuka, M. and Elrick, D.E., 1985. Application of microcomputerbased image digitization in
    soil and crop sciences. Comp. Electron. Agric., 1: 59-73.

The analysis of soil macropores and the flow of solutes

S. Nortcliff[1], V.L. Quisenberry[2], P. Nelson[1] and R.E. Phillips[3]

[1]*Department of Soil Science, University of Reading, Reading, RG1 5AQ, UK*
[2]*Department of Agronomy and Soils, Clemson University, Clemson, SC 29634, USA*
[3]*Department of Agronomy, University of Kentucky, Lexington, KY 40506, USA*

ABSTRACT

Nortcliff, S., Quisenberry, V.L., Nelson, P. and Phillips, R.E., 1994. The analysis of soil macropores and the flow of solutes. In: A.J. Ringrose-Voase and G.S. Humphreys (Editors), Soil Micromorphology: Studies in Management and Genesis. Proc. IX Int. Working Meeting on Soil Micromorphology, Townsville, Australia, July 1992. Developments in Soil Science 22, Elsevier, Amsterdam, pp. 601-612.

Recently there has been concern about the flow of water and solutes through soil and the possibility that these may pollute underlying materials, in particular groundwater. This study reports research undertaken in South Carolina and Kentucky, U.S.A to investigate the flow characteristics of soils using Cl⁻ as a tracer in relation to the nature and pattern of the macropores observed in impregnated soil blocks sampled after the leaching experiments. Sets of samples ($12.7 \times 16.5 \times 5$ cm) for impregnation using polyester resin with a UV dye, were taken at regular vertical intervals of approximately 10 cm to a depth of 1 m. Analysis of the macropore system involved serial sectioning through the block and analysis of the exposed surfaces. Measurements made on these blocks are, the area occupied by poroids with a cross sectional area >0.2, >3.0 and >7.0 mm^2 and the average distribution of these pores across the block. Flow characteristics of the soils have been investigated under artificial irrigation conditions in the laboratory using a sample collector placed at the base of a soil column, enabling the determination of breakthrough curves at 100 points across a cross-sectional area of 31×31 cm.

It is proposed that this analysis linking the nature and pattern of soil macropores and the flow characteristics of water and solutes through soils will provide the basis for a classification of soils into broad groups with respect to the likely occurrence of rapid solute transfer to underlying materials. Once established this approach would enable the rapid and relatively straightforward identification of soils susceptible to rapid leaching of applied materials through an analysis of their macropore characteristics.

INTRODUCTION

The research reported is part of a larger research programme to investigate the flow of solutes through soils to underlying materials and groundwaters and was initiated by the concern of both governments and industry to understand the processes whereby materials applied to the soil surface, either deliberately or accidentally, move through the soil. In particular, the concern is with why there often appears to be preferential movement of these

applied materials, which results in more of the applied material reaching the underlying strata at a faster rate than would be predicted by a standard 'uniform-displacement' type approach.

In this context, our eventual aim is the development of a soil classification system based upon soil macropore properties. We aim to use this classification to predict the behaviour of soils with respect to the leaching of solutes.

Whilst macropores are often taken as pores with diameters >60 μm, in reality it is often the larger pores which determine preferential flow events. We have therefore tentatively set a lower limit of pores with an equivalent spherical diameter of approximately 300 μm for this study.

A tentative classification of soils of South Carolina with respect to their leaching potential has been developed (Quisenberry *et al.*, 1993). Whilst there is some input from analysis of pore patterns for selected soils in this classification, we have at this stage focused upon an analysis based on field described structural types, referring extensively to the often much-ignored work of Brewer (1976), because of the dearth of pore structure information. Whilst the classification does not use information on soil macropore patterns, we suggest that further refinement of the tentative classification is probably only possible if soils are sampled and their macropore patterns described.

The focus in the practical side of this work is the study of:

    1. Solute flow-patterns in particular preferential flow;
    2. Soil-macropore characterisation.

The stages involved in the research are as follows:

    1. Measurement of water flow and solute breakthrough;
    2. Soil sampling, water exchange and impregnation;
    3. Elementary image analysis;
    4. Linking water and solute behaviour with soil macropore characterisation.

The eventual aim is to sample the soil through which the solute behaviour has flowed, but at this stage we are monitoring adjacent sites.

METHODS

As a *preliminary* study, and to enable the resolution of the methodologies for more extensive studies, we investigated a limited number of sites. Results are presented here for two soils:

Cecil sandy loam - Clayey, kaolinitic, thermic Kanhapludult (S. Carolina)
Maury silty loam - Fine, mixed mesic Typic Paleudalf (Kentucky)

At each site a pedestal 40 × 40 × 50 cm deep was carved. Thin, but rigid, sharp metal frames 30 × 30 × 2 cm deep in the Cecil and 32.5 × 32.5 × 2 cm in the Maury soil, were placed on the top of the pedestal. The frames were pushed slowly downward as the soil just ahead of the frame was carefully shaved with a knife. Levels were used to ensure the faces of the pedestal were vertical. A plywood box 32 cm high with internal dimensions of 31 × 31cm for the Cecil soil and 33.5 × 33.5 cm for the Maury soil was placed around the soil pedestal. Expandable polyurethane foam was poured between the box and soil. The foam completely filled the space between the box and soil including any voids created by irregular cutting and in the subsequent experiment minimised flow down the edges of the block. The foam was allowed to set overnight before the enclosed soil block with about 10 cm of soil extending
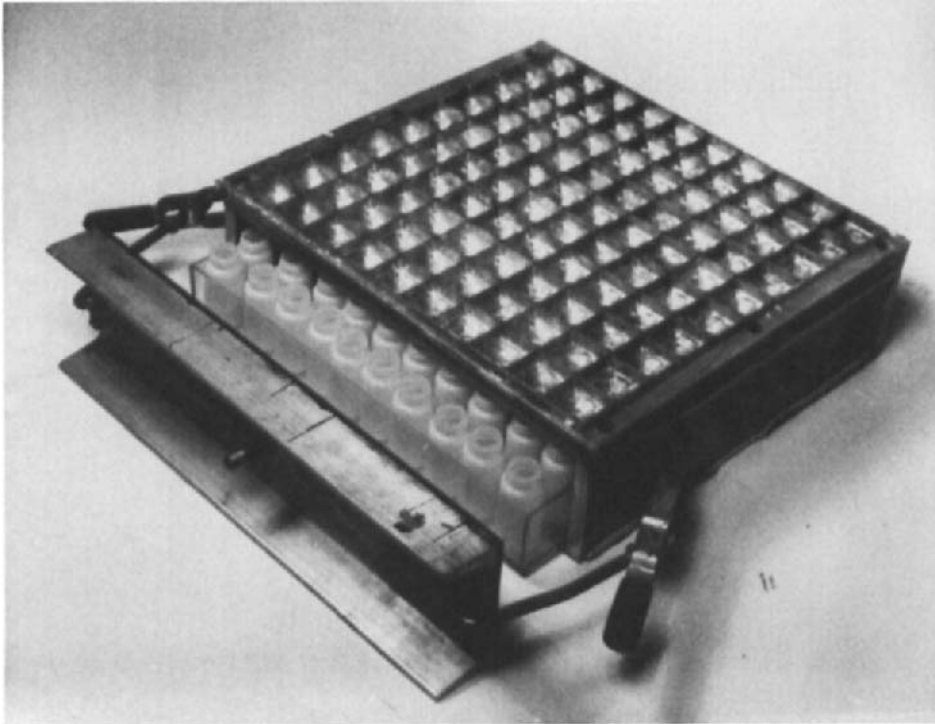
Fig. 1. The collection plate showing 100 cells.

below the box was removed and taken to the laboratory. In each case the top of the plywood box was at a depth of 30 cm from the original soil surface. In the Cecil soil the box contained 6 cm of BA horizon with weak fine to medium subangular blocky structure overlying part of the Bt_1 horizon, with a moderate to strong medium subangular blocky structure. In the Maury soil the box contained 3 cm of A1 horizon with moderate, fine granular structure overlying part of a $B_{21}t$ with moderate fine to medium subangular blocky structure.

In the laboratory the soil block was inverted, and the soil trimmed flush with the bottom of the plywood box. The soil block was placed upright on a collection plate and moved slightly to establish a good contact between sand and soil. A layer of sand approximately 2 cm thick was added to the surface to reduce the effects that repeated drops of water might have on infiltration. Silicon sealant was used at the contact of the box and collection unit.

Leaching experiment

For the leaching phase of the study a collection plate with 100 separate cells to collect drainage from the overlying column was developed (Fig. 1). Each cell has a cross-sectional area of 9.3 cm^2 at the top, but tapers to 3.0 mm. To minimise problems in drainage from the
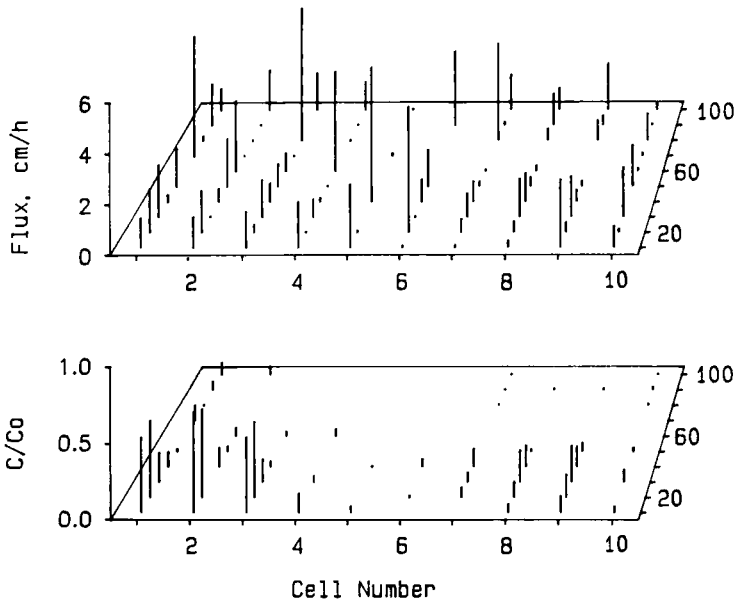
Fig. 2. Solute flux and relative Cl⁻ concentration in a Cecil soil after 2.34 cm of drainage with an application rate of 1.16 cm h^{-1}.

column, glasswool was placed in each cell and covered with fine sand. The sand was levelled slightly above the ribs of the sections. In order to maintain satisfactory hydraulic conditions at the plate/column interface a small tension (-1 to -2 kPa) was maintained at the bottom of the plate. For the Maury soil, the collection plate had 144 cells of the same dimensions. This allowed the solution to be collected in 100 cells while the soil-foam boundary was positioned over the outer row of cells. Whilst we believe that no edge effects existed at the soil-foam boundary, the addition of the outer rows of cells insured that we would have no wall effect within the 10 × 10 grid from which measurements were taken. The dimension of the undisturbed soil block was increased to 32.5 cm.

Water was applied from 100 25-gauge needles, arranged in a 10 × 10 grid, placed 20 cm above the surface. Each of the needles was located above the centre of a square cell in the collection plate. Flow rate was controlled by a peristaltic pump. Before the experiment began several pore volumes of water were applied to thoroughly wet the entire soil matrix. The column was allowed to drain under a tension of -1.5 kPa for 24 hours before Cl⁻ water was applied.

Water labelled with 300 mg l^{-1} of Cl⁻ as KCl, was applied at a rate of 1.16 cm h^{-1} for a total of 5.5 h in the Cecil soil and water labelled with 150 mg l^{-1} was applied at rates of 1.23 and 1.97 cm h^{-1} in the Maury soil. As the sand layer at the bottom of the soil column and the soil had bubbling pressures greater than -1.5 kPa, a small amount of air did flow through the column, but the quantity appeared to be negligible once water application commenced. Samples were collected from each cell in the collection plate in glass phials every 0.5 h in the
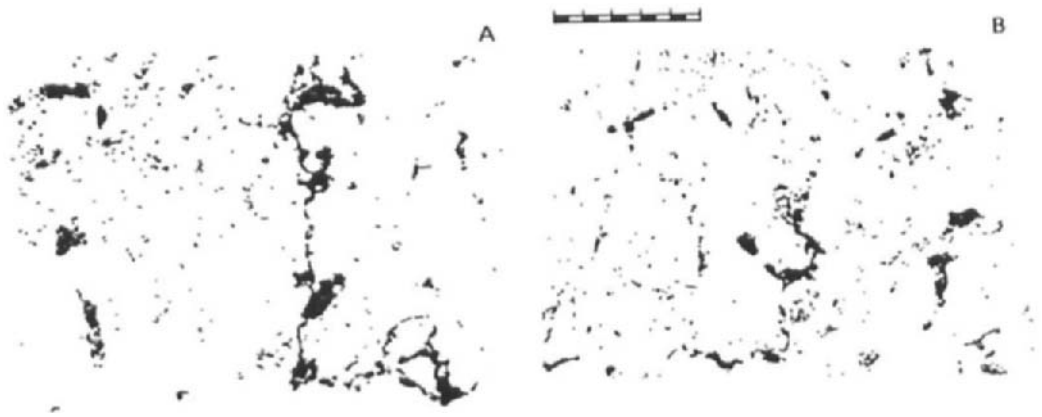
Fig. 3. Pores with a cross-sectional area >0.2 mm^2 in a Cecil soil sampled at 40 cm, horizontal images separated by a vertical distance of 2.5 cm (Bar = 5 cm).

Cecil soil and every 1 h in the Maury soil beginning 1 h after application commenced. This procedure took less than 20 s. Results presented here are for only one 0.5 h period for the Cecil soil and for 1 h periods for each of the application rates for the Maury soil. More thorough discussions are given for the Cecil soil by Quisenberry *et al.* (in press, a) and for the Maury soil by Quisenberry *et al.* (in press, b).

Macropore images

Undisturbed samples were taken horizontally with the upper surface at a depth of 40 cm, in Kubiena tins 12.7 × 16.5 × 5 cm. They were dehydrated by acetone replacement (Murphy, 1986), which was enhanced by the use of small bags of *'Water Grabber'* (cross linked Polyacrylamide) in the acetone to remove some of the water removed from the soil (Moran *et al.*, 1989). A two stage vacuum impregnation method using a polytite polyester resin containing a UV dye followed the procedures outlined by Murphy (1986).

Once hardened the blocks were cut horizontally using a large slab saw into slices 2.5 mm thick, with a cutting width of approximately 2.5 mm.

Image analysis of top and bottom faces of each slice was undertaken using a Cue 2 Image Analysis System (C-squared Corporation, Florida). Only pores occupying more than 4 pixels (0.2 mm^2) are analysed in this study.

RESULTS AND DISCUSSION

Cecil sandy loam

The spatial distribution of water flux and relative Cl$^-$ concentration after 3.5 h of application and the equivalent of 2.34 cm of solute had drained from the column is shown in Fig. 2. The fluxes are exceedingly variable. Six of the 100 cells had fluxes greater than 3.5 cm h^{-1}, but 16 cells had zero flux and 36 cells had flux less than 0.1 cm h^{-1}. Two characteristics of the flow
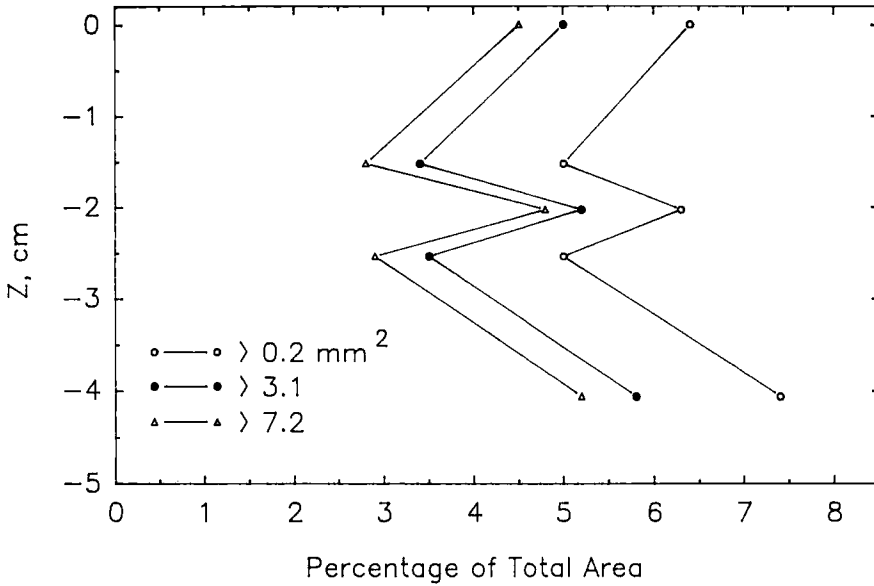
Fig. 4. Plots of the vertical distribution of the percentage of the total area occupied by pores with a cross-sectional area a) >0.2 mm^2 b) >3.1 mm^2 and c) >7.2 mm^2 in a Cecil soil. (Z measures the depth from the top of the impregnated block at 40 cm).
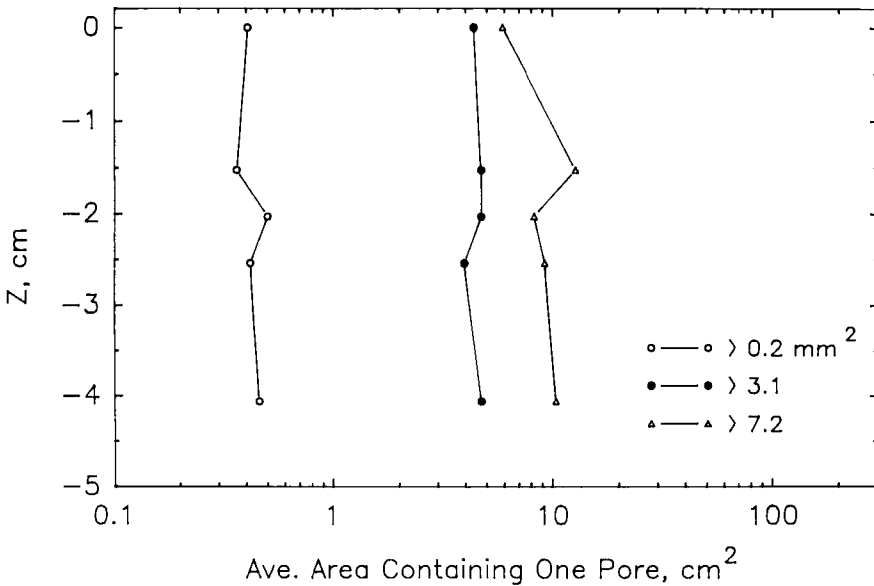
Fig. 5. Plots of the vertical distribution of the average cross-sectional area containing a single pore of a) >0.2 mm^2 b) >3.1mm^2 and c) >7.2mm^2 in a Cecil soil. (Z measures the depth from the top of the impregnated block at 40 cm).

distribution can be discerned: 1) zones of significantly high flux appear to be clustered and not isolated and 2) contiguous zones of zero flux are present. Quisenberry *et al.* (in press, a) showed that these characteristics persisted throughout a 5.5 h application.

The clustering of the relative Cl⁻ concentrations were even more pronounced. Two zones of significant Cl⁻ were measured: one in the front right and one in the front left of the plane. The back two quadrants had little or no Cl⁻ in the effluent after 2.34 cm of drainage and, as before, the pattern persisted throughout a 5.5 h application.

Fig. 3 shows pores with a cross-sectional area greater than 0.2 mm² in two blocks taken 1 cm apart vertically, with the upper section at 40 cm depth. We have suggested elsewhere (Quisenberry *et al.*, in press, a) that a significant amount of macropore flow in the argillic horizon of a Cecil soil occurs between tertiary structural units and that the spatial patterns of water and Cl⁻ flux could be related to these structural characteristics. The primary route of rapid transport are the macropore spaces between the tertiary structural units. Pore space between secondary units branch from the planar voids between tertiary units and, to a much lesser degree, voids between primary units branch from voids between secondary units. Hatfield (1988) and Nelson (1990) have shown that macropore flow in the Cecil sandy loam commences at the Ap-B interface. If voids between the tertiary units and branches from these voids are the primary macropore pathways, zones of high flux and zones of zero flux would be measured for transport through the Bt horizon. This suggested description of the pathways agrees with the data in Fig. 2 and that presented by Hatfield and Nelson.

The pore patterns shown in Fig. 3 appear to support this suggestion. Tertiary and secondary structural units are nearly completely coated with clay films, as are, to a considerably lesser degree, the primary peds. Impregnation of pore space within the primary peds would be difficult because of the clay films and the lack of connected pores. In the top image there is one large nearly continuous poroid that extends the breadth of the section. We believe this poroid is associated with the space between tertiary or secondary peds. Three major voids are shown on the left, but the section below it (images not shown) suggests they may be part of an interpedal void. There are also significant areas showing no measurable pores.

The lower image shows somewhat similar patterns. In the left centre, a partial outline of what could be a tertiary or secondary ped is shown. Within this ped few pores have been impregnated. Partial outlines of smaller structural units can be distinguished. Both images show a degree of pore connectivity and contiguous areas of no pores. It is possible that flow patterns through horizons such as this would exhibit similar general patterns as for pores. In both images the pore patterns indicate that the majority of the pores greater than 0.2 mm² are associated with pedal voids.

Fig. 4 shows that between 6 and 7% of the total cross-sectional area is associated with pores >0.2 mm². The decrease in porosity as the poroid area increases from 0.2 to 7.2 mm² is not nearly as great as in many other soils. Approximately 70% of the porosity associated with poroids with cross-sectional areas >0.2 mm² can be attributed to those >7.2 mm². If we assume a circular pore area of 0.2 mm², the bubbling pressure of such a pore would be approximately -0.6 kPa. Poroids of this area or larger probably account for most, if not all, the macropore flow. Our analyses indicate that most of the macroporosity occurs as planar voids which are quite connected to each other. The number of each pore size remains fairly constant throughout the sample and, although we recognise that no stereological interpretations of this nature may be made (Ringrose-Voase and Nortcliff, 1987), this might be taken as a broad
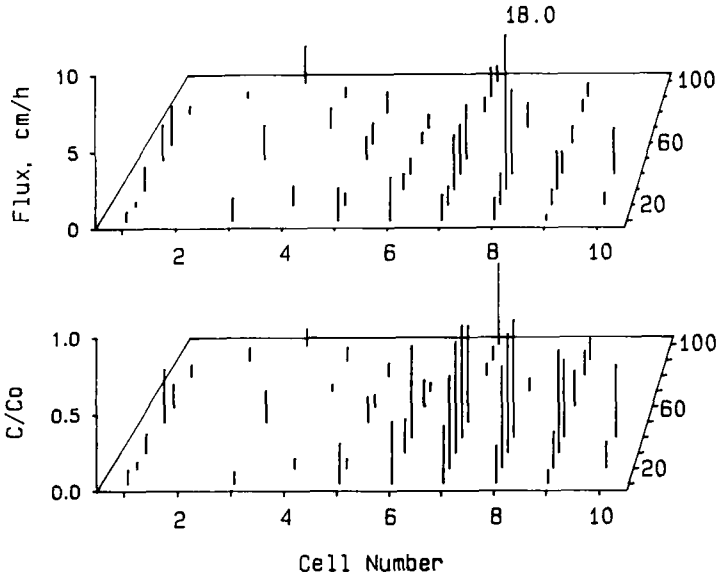
Fig. 6. Solute flux and relative Cl⁻ concentration in a Maury soil after 2.93 cm of drainage with an application rate of 1.23 cm h⁻¹.
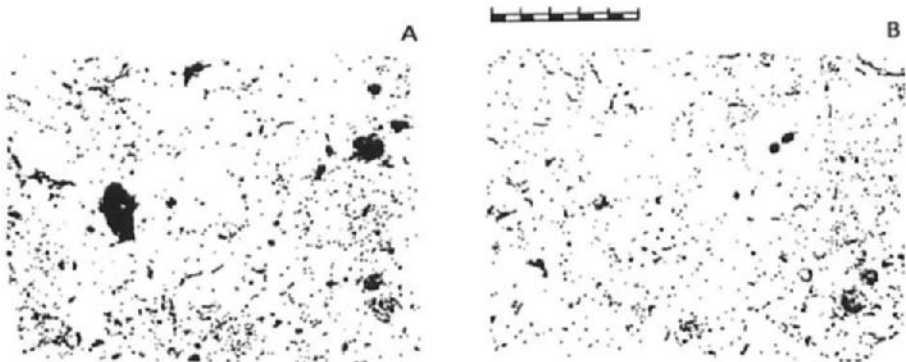
Fig. 7. Pores with a cross sectional area >0.2 mm² in a Maury soil sampled at 40 cm, horizontal images separated by a vertical distance of 1.5 cm (Bar = 5 cm).

indication that there is a degree of vertical pore continuity. Fig. 5 shows that each poroid with a cross-sectional area greater than 7.2 mm² was associated with approximately 10 cm² of the exposed surface. We realise that this value has to be interpreted with caution because one large pore extended over several cm depth of the block. The numbers do indicate however that the pores were as widely distributed as you would expect if they were associated with secondary and tertiary structural units.
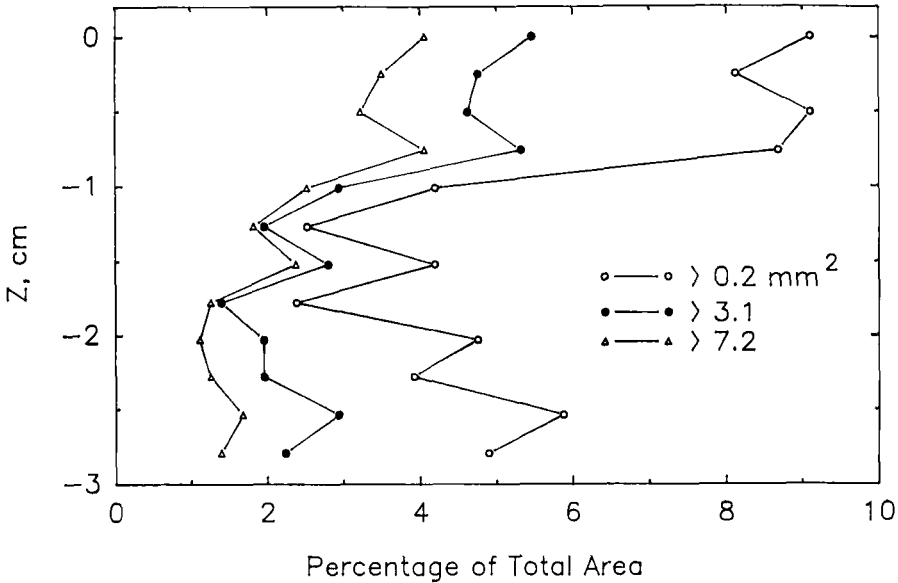
Fig. 8. Plots of the vertical distribution of the percentage of the cross-sectional area occupied by pores with cross section areas a) >0.2 mm^2 b) >3.1 mm^2 and c) >7.2 mm^2 in a Maury soil. (Z measures the depth from the top of the impregnated block at 40 cm).

Maury silt loam

Fig. 6 shows the spatial distribution of flux and relative Cl^- concentration for the application rate after application of approximately 3 cm to the Maury soil. The patterns are similar for the 1.97 cm h^{-1} application rate. The 1.23 cm h^{-1} distributions are broadly similar to those presented for the Cecil soil: 1) cells with high fluxes and Cl^- concentrations tend to be clustered not randomly distributed (50% of the water and Cl^- was collected from cells in the front right quadrant) and 2) large contiguous zones where zero or very low Cl^- concentrations were measured.

Fig. 7 shows the patterns of pores with a cross-sectional area >0.2 mm^2 from one impregnated block of the Maury soil sampled at 40 cm. In contrast to the Cecil, the Maury has many small pores somewhat more randomly distributed. These sections agree with field observations of the Maury soil, that it has primary, secondary and tertiary structural units, but that they are not as pronounced nor as well defined as in the Cecil. Clay films are not as thick nor as continuous around peds. In addition, total porosity is greater in the Bt of the Maury than in the Bt of the Cecil. Neither of the two images show the apparent tertiary unit faces of the Cecil, but do show clear outlines of what may be primary and possible secondary structural units.

Fig. 8 shows the much greater vertical variability in the Maury soil of the percentage of total area associated with the three poroid cross-sectional size classes. The mean porosity, considering only pores greater than 0.2 mm^2, was apparently greater in the Cecil than in the
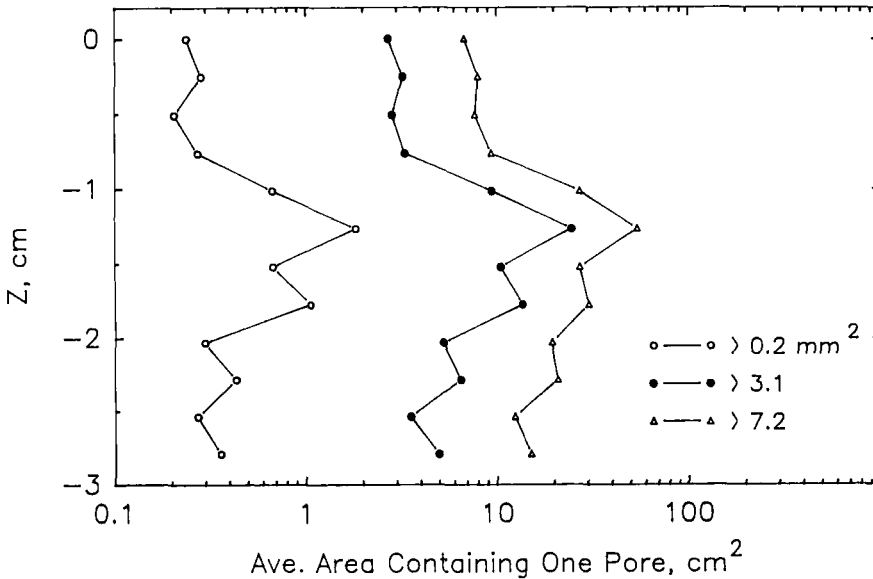
Fig. 9. Plots of the vertical distribution of the average cross sectional area containing a single pore of a) >0.2 mm^2 b) >3.1 mm^2 and c) >7.2 mm^2 in a Maury soil. (Z measures the depth from the top of the impregnated block at 40 cm).

Maury. This is in contrast to bulk density measurements that show greater total porosity in the Maury soil and is an indication of the problem of defining the representative elementary volumes for these soils. The larger porosity for the Cecil over the range considered arises due to the large voids between structural units; the Cecil seems to have more large continuous pores defining large and dense structural units. The vertical variation in the Maury probably reflects the dominance of much smaller structural units.

The variability in the average area associated with pores above the specified size limits resulting from the much smaller structural units in the Maury soil is shown in Fig. 9, with the larger poroids, greater than 7.2 mm^2, being more widely distributed across the section than in the Cecil. The greater variability among sections within the Maury as compared to the Cecil suggest that the continuity of macropores might be less. Further these differences in size and density of structural units might help explain the variations in the flow characteristics of these two soils.

CONCLUSIONS

The pore distributions in the Bt horizon of a Cecil soil were suggested to be in agreement with the suggested flow patterns of water and Cl$^-$ through an undisturbed column. The data suggest that voids between tertiary structural units may be the principal pathways of macropore flow. Branching from these voids will determine, to a degree, the amount of spreading of the percolating water.

Whilst the spatial distributions of water flux and Cl⁻ concentrations for the Maury soil were similar to those measured in the Cecil, pore distributions did not show the large continuous planar voids within the Maury. Phillips *et al.* (1989) have shown that for a simulated macropore, once macropore flow has been established, it can continue even after a positive head ceases to exist at the entrance to the macropore. No doubt continuous macropores do exist within the Maury. However the pore patterns measured indicate that the network of contiguous pores, and the mechanisms of flow may be more difficult to define than in the Cecil.

It is apparent that in many soils flow of water and solutes does not observe the simple 'piston flow' mechanism, rather there is considerable evidence that many soils, at least to a degree, exhibit a degree of preferential flow. If we consider the soil and soil related conditions which are likely to affect the occurrence of preferential flow we might include the following:- 1) soil water content, 2) water application rate, 3) characteristics of the Ap horizon for example, a. texture and b. structure, 4) Ap-B interface characteristics and 5) characteristic of the B horizon for example, a. texture and b. structure.

Of this list items 3, 4 and 5 broadly relate to soil structural properties and the nature and pattern of macropores, and it is our proposal that in order to predict the likely occurrence of preferential flow we must focus considerably more attention on these properties. Whilst field observation of soil structural properties is an important first step in this description, we believe that refinements of this predictive framework can be achieved by making simple observations of the macropore patterns in impregnated blocks. An initial attempt at classification of soils with respect to their susceptibility to preferential flow has been undertaken chiefly using field observations (Quisenberry *et al.*, 1993), but with the supplementation of these observations by macropore analysis and solute flow characteristics this classification would be much refined. We are confident this is the way forward and believe the simple observation of macropores to have a critical role in this framework to predict soils susceptible to preferential flow.

ACKNOWLEDGEMENTS

REFERENCES

Brewer, R., 1976. Fabric and Mineral Analysis of Soils. R.E. Kreiger, Huntingdon, New York, 470 pp.

Hatfield, M.W., 1988. Water and Anion Movement in a Typic Hapludult. Unpublished Ph.D. dissertation, Clemson University, USA.

Moran, C.J., McBratney, A.B., Ringrose-Voase, A.J. and Chartres, C.J., 1989. A method for the dehydration and impregnation of clay soil. J. Soil Sci., 40: 569-575.

Murphy, C.P., 1986. Thin Section Preparation of Soils and Sediments, AB Academic Publishers, Berkhamsted, U.K.

Nelson, P.A., 1990. Solute Movement and Root Distribution as Affected by Soil Structure. Unpublished Ph.D. dissertation, Clemson University, USA.

Phillips, R.E., Quisenberry, V.L., Zeleznik, J.M. and Dunn, G., 1989. Mechanisms of water entry into simulated macropores. Soil Sci. Soc. Am. J., 53: 1629-1635.

Quisenberry, V.L., Smith, B.R., Phillips, R.E, Scott, H.D. and Nortcliff, S., 1993. A soil classification system for describing water and chemical transport. Soil Science, 156: 306-315.

Quisenberry, V.L., Nortcliff, S., Phillips, R.E. and Smith, B.R. Spatial variability of water and chloride movement in an undisturbed column of cecil soil. Soil Sci. Soc. Am. J., (in press, a).

Quisenberry, V.L., Phillips, R.E. and Zeleznik, J.M. Spatial distribution of macropore flow of water and chloride in a well structured soil. Soil Sci. Soc. Am. J., (in press, b).

Ringrose-Voase, A.J. and Nortcliff, S., 1987. The application of stereology to the estimation of soil structural properties: a preview. In: N. Fedoroff, L.M. Bresson and M.A. Coutry (Editors), Soil Micromorphology. Proc. VII Int. Working Meeting of Soil Micromorphology, Paris, July 1985. Association Française pour l'Etude du Sol, Plaisir, France, pp. 81-88.

Structural pore pedofeatures: influence on some soil processes

L.A. Sullivan

Resource Science and Management, University of New England-Northern Rivers,
PO Box 157, Lismore, NSW 2480, Australia

ABSTRACT

Sullivan, L.A., 1994. Structural pore pedofeatures: influence on some soil processes. In: A.J. Ringrose-Voase and G.S. Humphreys (Editors), Soil Micromorphology: Studies in Management and Genesis. Proc. IX Int. Working Meeting on Soil Micromorphology, Townsville, Australia, July 1992. Developments in Soil Science 22, Elsevier, Amsterdam, pp. 613-622.

Individual structural pore pedofeatures (*e.g.* coatings around peds) may affect soil behaviour on a microscopic scale due to: 1) differences in the size and morphology of the pores within pedofeatures compared to those within the groundmass, 2) physical interactions between the components in pedofeatures and liquids and 3) chemical interactions between the components in pedofeatures and solutes. When structural pore pedofeatures are common within a soil material, the sum total of these microscopic effects can be important in influencing the macroscopic fluxes of liquids and solutes within that soil material. It is most likely that what are at present considered to be the effects of structural pores on soil behaviour are actually often the combined effects of two separate soil characteristics: 1) the nature of the structural pores *per se* and 2) the nature of the structural pore surfaces. Finally, the results of some submicroscopic studies show that thin coatings (*i.e.* < 5 μm) on structural pore surfaces are likely to be widely distributed in soils. These types of coatings cannot be detected in thin sections of these soils using light microscopy yet would also influence soil processes.

INTRODUCTION

Structural pores (*e.g.* channels, planar pores) are an important factor affecting the movement of liquids in soil. Kubiëna (1938) stated that "the soil solution follows elongated channels which we call conducting channels" and Bradfield (1937) considered that "water moves slowly into crumbs compared to water moving between crumbs". These early views were confirmed by later studies (Anderson and Bouma, 1973; Kissel *et al.*, 1973). In addition, Bouma and Anderson (1977) showed that the importance of structural pores to water flow varied according to the soil material in which those structural pores were found.

Structural pores also exert a large influence on the movement of gases within soils (Currie, 1961). Since plant roots tend to grow down pre-existing structural pores (Wang *et al.*, 1986), the surfaces of structural pores often constitute much of the immediate plant root environment.

Pedofeatures associated with structural pores (*e.g.* coatings, hypocoatings and quasi-coatings (Bullock *et al.*, 1985) have been extensively studied with regard to soil genesis. In contrast, there have been but few studies into the effects of these types of pedofeatures on soil processes such as the movement of liquids and solutes. Soileau *et al.* (1964) showed that the

presence of synthetic kaolinitic coatings around illite aggregates restricted the availability of potassium to plant roots. Similarly, Kalifa and Buol (1969) compared the growth of wheat on both clay-coated and uncoated peds and found that the plant uptake of both potassium and phosphorus was restricted by the presence of clay coatings. The detrimental effects of the clay coatings on plant nutrition were, in both of these studies, thought to be due to oriented clay coatings restricting the diffusion of nutrients from the soil matrix to the plant roots. This is supported by Lai and Mortland (1968) who found that the apparent diffusion coefficient across the basal plane of oriented clay aggregates was only 20% of that along the basal plane. Miller and Wilding (1972) considered that the presence of coatings of either iron oxides or calcium carbonates would, by causing precipitation, reduce the diffusion of phosphorus from within peds to roots.

This paper: 1) reviews some of the physical and chemical characteristics of structural pore pedofeatures such as coatings, hypocoatings and slickensides and 2) examines the probable mechanisms by which structural pore pedofeatures influence the movement of liquids, gases and solutes within soils. The abundance of these pedofeatures in soils is briefly examined.

STRUCTURAL PORE PEDOFEATURES AND SOIL PROCESSES

Structural pore pedofeatures may affect soil processes due to the following factors:
1) differences in the size and morphology of the pores within pedofeatures compared to those within the groundmass;
2) physical interactions between pedofeatures and liquids; and
3) chemical interactions between pedofeatures and solutes.

The effects of these factors will be addressed in turn with reference to a particular soil process.

Differences in the size and morphology of the pores within pedofeatures compared to those within the groundmass

The size, shape and orientation of the pores contained within structural pore pedofeatures may vary greatly when compared to those for the groundmass (where groundmass is as defined by Bullock *et al.*, 1985). The effect of three common types of structural pore pedofeatures - coatings, hypocoatings, and slickensides - in which the pores are generally smaller than in the adjacent groundmass, on the movement of liquids between structural pores and the groundmass will be discussed here.

Coatings composed of oriented clay around structural pores are good examples of this situation. Clay coatings contain pores which are mostly extremely small; have a planar morphology and are oriented essentially parallel to the structural pore surface (Fig. 1a and b). The pores within domains (*i.e.* stacks of oriented clay particles) are mainly less than 20nm (Russell, 1973), and it is reasonable to assume that the pores contained within coatings of oriented clay have similar dimensions.

Unless a clay-coated soil material is also totally composed of oriented clay (which would be an exceptional situation), we can reasonably assume that the pores within the clay coating are appreciably smaller and more tortuous than those in the groundmass. Under saturated flow conditions the relatively impermeable clay coatings act as a throttle against the movement of liquids into and out of the groundmass, in a similar fashion to the way that a crust on a

soilsurface decreases infiltration of ponded water into a soil. It is important to note that although clay coatings less than 1 μm thick would provide such an effect, the thicker the clay coating the greater the magnitude of the effect.

During unsaturated conditions the effect of clay coatings on the fluxes of liquids from a structural pore to the groundmass (and *vice versa*) are likely to be more complex. For example, the relationship between unsaturated hydraulic conductivity, $K(\tau)$, and matric potential, τ for a sandy loam material (Bridge, 1968) is shown in Fig. 2. The pores within coatings of oriented clay are both small and uniform in size. Therefore, the $K(\tau)$ vs τ relationship for flow across a clay coating is likely to be very flat with very low $K(\tau)$ values even near saturation. A likely $K(\tau)$ vs τ relationship for flow across a clay coating is shown in Fig. 2. In Fig. 2 there is a crossover point (A) where, at more negative matric potentials, the unsaturated hydraulic conductivities for flow across a clay coating are greater than that of the sandy loam. Therefore, in a sandy loam material in which structural pores are coated with oriented clay (*e.g.* Fig. 1c), the clay coating would, at matric potentials less negative than the crossover point, act as a throttle against the movement of water across the structural pore surface. At matric potentials more negative than this crossover point the clay coating would not appreciably restrict water movement.

The pores within hypocoatings will generally be smaller than those within the surrounding unimpregnated groundmass. For example, the manganese oxide hypocoating shown in Fig. 1d contains 15% MnO. This quantity of manganese oxides would probably cause a significant decrease in the pore sizes, the total porosity and the pore connectivity within this hypocoating. Such changes would affect the fluxes of liquids between the structural pores and the unimpregnated groundmass in much the same way as that described for clay coatings. The severity of the effect would depend upon the degree of the impregnation.

Slickensides are birefringent zones of parallel oriented clay particles lining planar pores (Bullock *et al.*, 1985). The similarities of their optical properties to those of oriented clay coatings suggest that the pores within slickensides are similar to those within clay coatings and would therefore have similar effects on the movement of liquids. Nuhfer *et al.* (1981), for example, considered that slickensides within some mudrocks would be a sufficient sealant to inhibit gas movement.

An extreme example of the effect of coatings on the movement of liquids across structural pores would be the effect of the thin (5 μm thick), non-porous, silica coating shown in Fig. 1e. Coatings such as these would effectively prevent any interchange of liquids and solutes between the structural pore and the adjacent groundmass.

Physical interactions between pedofeatures and liquids

One example of these interactions is the effect of organic matter coatings on the movement of liquids within soil materials. The hydrophobic properties of some soil organic matter coatings on structural pores may affect water movement: 1) directly, by reducing the pressure (and hence rate) with which water enters a soil pore (Robinson and Page, 1950; Emerson and Bond, 1963) and 2) indirectly, due to the increased air encapsulation that can occur when such organic matter coatings are non-uniformly distributed on the structural pores (Sullivan, 1990).

Organic matter matter pedofeatures within structural pores such as coatings, faecal pellets, roots and root remnants, fauna and faunal remains may also affect the movement of liquids
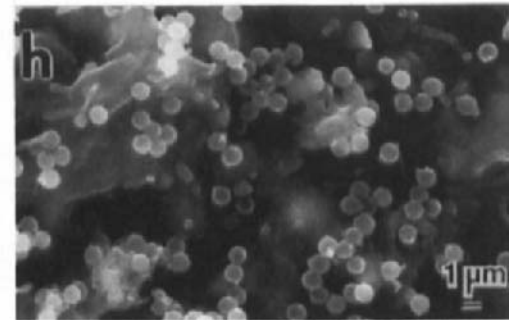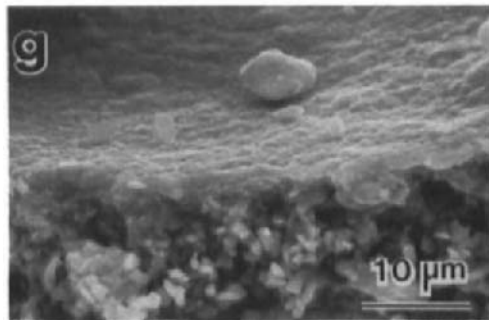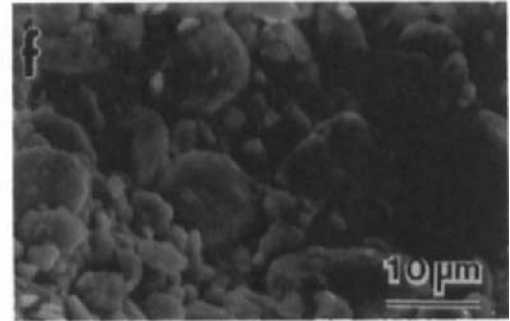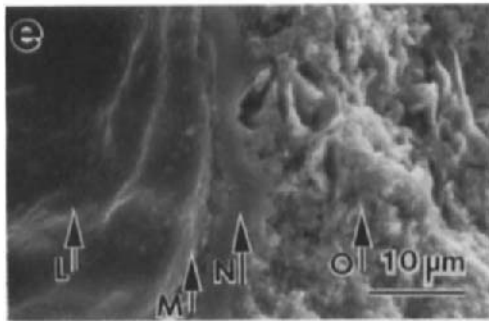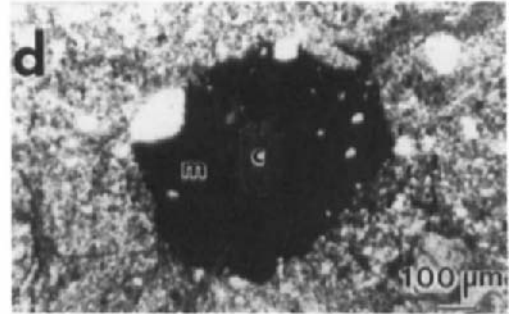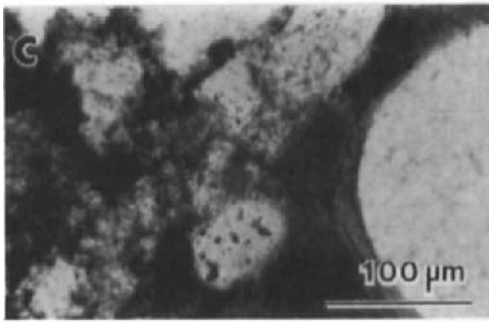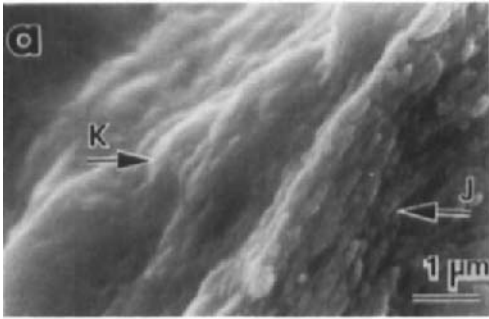
within soils by physical obstruction. For example, a single, large faecal pellet trapped near the ground surface within a channel may severely restrict the flow of water down the channel, even though the rest of the channel may be open. The effect of roots or root remains within channels or running across planar pores would have a similar effect.

Chemical interactions between pedofeatures and liquids

Components within structural pore pedofeatures may affect the movement of solutes within soils by adsorption, absorption or by causing precipitation of those solutes. For example, manganese oxides can be very efficient at accumulating elements such as Co, Cu, Ni, Zn, Ba and Pb, whilst iron oxides have the ability to retain Mn, Ni, Cu, Zn, As, Se and Mo (Norrish, 1975). Manganese oxides have a particularly high affinity for cobalt (Taylor *et al.*, 1964) and it is likely that the movement of cobalt will be inhibited by manganese oxide structural pore pedofeatures. Certainly, electron microprobe analysis of the manganese oxide coating in Fig. 1d determined that these features contained 9% CoO compared to only 0.02% CoO in the unimpregnated groundmass.

Structural pore pedofeatures in which iron and aluminium oxides are concentrated may similarly affect the movements of phosphate, sulphate, selenite, molybdate, flouride, silicate, benzoate and oxalate within soils (Miller and Wilding, 1972; Bowden *et al.*, 1973; Russell, 1973; Parfitt and Russell, 1977; Parfitt *et al.*, 1977; Tiller *et al.*, 1984; Barrow, 1983). Phosphate movement may also be greatly reduced across structural pore pedofeatures which contain significant quantities of calcium carbonates, due to the precipitation of calcium phosphates on these carbonates (Barrows *et al.*, 1966; Miller and Wilding, 1972).

Structural pore pedofeatures in which organic matter is concentrated may retard the movements of Cd and Mn within soils due to the high sorptivity of organic matter for these elements (Turner and Steele, 1988).

The degree of adsorption of solutes by soil components such as those mentioned above will be dependent upon many factors such as pH, solute concentration, temperature, the surface area of the adsorbants, the degree of saturation of adsorption sites and the degree of crystallinity of the adsorbants (Russell, 1973; Barrow, 1985; Borggaard, 1987).

Fig. 1. Scanning electron photomicrographs of: **a)** a fracture surface and the structural pore surface (indicated by arrows J and K, respectively) across an optically-oriented clay coating; **b)** a fracture surface across an optically-oriented clay coating; **e)** a structural pore surface (indicated by the arrow L) and a fracture surface across a composite coating consisting of a clay coating (indicated by arrow M), a silica coating (indicated by arrow N), and the adjacent groundmass (indicated by arrow O); **f)** a thin clay coating over, and bridging between, sand and silt grains on a vesicle; **g)** a thin clay coating over a silty groundmass adjacent a vesicle; **h)** an organic matter coating on a chamber surface populated by many micro-organisms. Photomicrographs of thin sections across: **c)** a clay coating over a sandy groundmass adjacent a structural pore, in plane polarised light; and **d)** a manganese oxide accumulation (m) around a channel (c), in circularly polarised light.
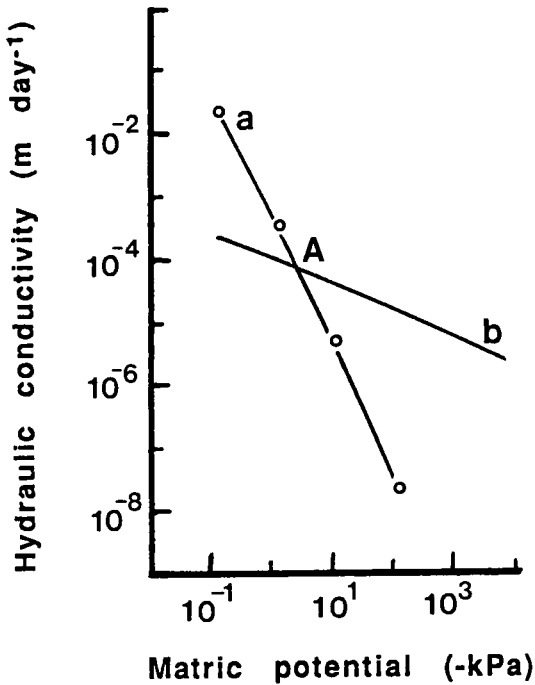
Fig. 2. Hydraulic conductivity, $K(\tau)$, - matric potential, τ, relationship for: a) a sandy soil material (Bridge, 1968) and b) a likely $K(\tau)$ - τ relationship for flow across a clay coating with the near-saturated value from McIntyre (1958).

Macroscopic effects of structural pore pedofeatures

The previous sections have largely focused on how individual structural pore pedofeatures can affect soil processes on a microscale. When such pedofeatures are common within a soil material the sum total of these microscopic effects may have an influence on the macroscopic fluxes of liquids and solutes within the soil. For example, the likely effects of relatively impermeable clay coatings surrounding permeable aggregates on solute flow through soil columns is illustrated in Fig. 3. Importantly, the current models of solute movement in soils (*e.g.* van Genuchten and Wierenga, 1976; Addiscott and Wagenet, 1985; Barraclough, 1989; Brusseau and Rao, 1990; Rappoldt, 1990; Youngs and Leeds-Harrison, 1990; Jarvis *et al.*, 1991) are all based on a conceptual model similar to that shown in Fig. 3a in which soil is an homogenous mixture of sand, silt, clay and organic matter with some superimposed macropores. However, soil micromorphology literature shows that soil patterns are usually much more complex than this. For example, clay coatings were observed in 112 of the 154 profiles examined in an extensive micromorphological review of Australian soils (Brewer *et al.*, 1983). It is most likely, therefore, that the effects on soil behaviour currently attributed to structural pores are actually often the combined effects of two separate soil characteristics:

1) the nature of the structural pores *per se* and
2) the nature of the structural pore surfaces ('Are there coatings of these surfaces?' 'Are there slickensides?').
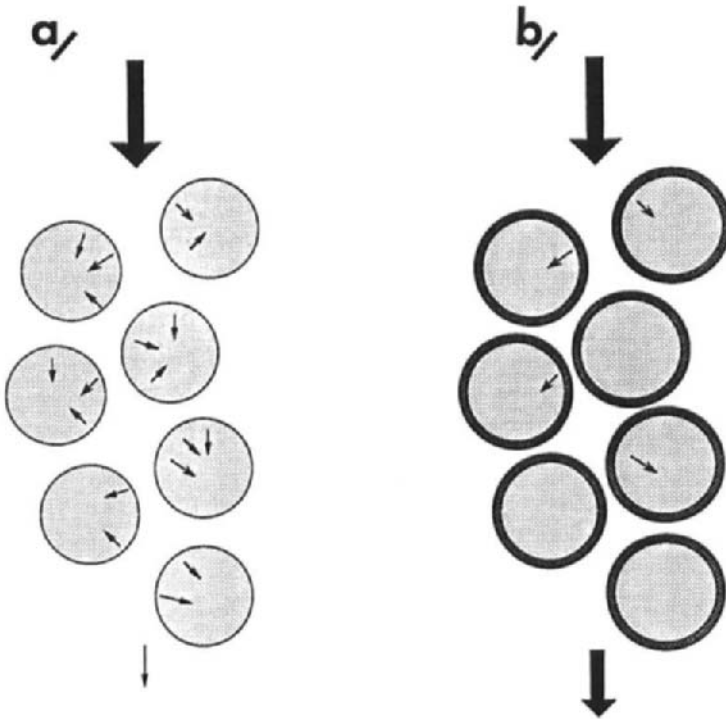
Fig. 3. Schematic illustration of the influence of relatively impermeable clay coatings (around permeable aggregates) on the movement of liquids and solutes during saturated flow within columns of aggregates: a) applied liquids and solutes quickly absorbed into uncoated aggregates resulting in little throughflow; b) applied liquids and solutes slowly absorbed into coated aggregates resulting in much throughflow.

ABUNDANCE OF STRUCTURAL PORE PEDOFEATURES

Structural pore pedofeatures are commonly observed. For example, in the review of Australian soil micromorphological studies by Brewer *et al.* (1983), 73% of the 154 examined soils contained clay coatings, 28% contained manganese oxide hypocoatings, 18% contained calcium carbonate coatings and 15% contained iron oxide quasi-coatings. Although the observation of clay coatings within a soil does not mean that all of the structural pores were thickly coated by oriented clay, it has been long known that pedofeatures such as thin clay coatings are difficult to recognize in soil thin sections (FitzPatrick, 1984). Certainly, the use of the standard 30 μm-thick soil thin section and light microscope to distinguish thin coatings (*i.e.* <5 μm thick) on structural pores is beset by the problem of poor resolution. Bullock *et al.* (1985) state that the lower size limit for recognition of pedofeatures (such as clay coatings) in thin sections using a petrological microscope is about 20 μm. Thus, thin coatings will effectively not be discernable in soil thin sections using light microscopy unless those coatings

contain components which are particularly conspicuous (as compared to the adjacent groundmass).

There are two reasons why some types of structural pore pedofeatures would rarely become thick enough for recognition (using soil thin sections and light microscopes) in certain soil types. Firstly, structural pore pedofeatures composed primarily of organic matter are unique (amongst these pedofeatures) in that they are a food source and, unless protected by being impregnated by aluminium or iron compounds or being situated in anaerobic conditions, would be decomposed by soil organisms before they become thick enough to be seen in soil thin sections. This is most likely the reason that organic matter coatings have only been observed with any regularity (when using light microscopy) in spodic horizons (Sullivan, 1988). Secondly, in any soils with active pedoturbation structural pore pedofeatures which are forming may be reincorporated into the groundmass before they are large enough to be resolved in thin section using light microscopy. The argillic horizons in which clay coatings are not recognisable in thin sections (Nettleton, 1972) would most likely represent a good example of this situation. These soils have high degrees of linear expansion which result in efficient pedoturbation and the destruction of any thin coatings formed by clay illuviation.

Thin structural pore pedofeatures that are too small to be observed in thin sections using light microscopy are often discernable in SEM studies of soils. Fig. 1f shows an example of a thin (around 1 µm) clay coating over and between sand and silt grains on a structural pore and Fig. 1g a similarly thin clay coating over a silty groundmass adjacent a vesicle. As mentioned previously, even 1 µm thick clay coatings around structural pores may affect the movement of liquids across structural pores surfaces. Sullivan and Koppi (1987), using SEM and low temperature ashing, observed very thin (much less than 1 µm) organic matter coatings over many of the structural pore surfaces of the three soil layers they examined: one was the B horizon of a Vertisol, one was the A horizon of an Alfisol and the other the B horizon of a different Alfisol. Although these coatings were very thin, the coated pore surfaces would have the physical and chemical properties of the organic matter rather than those of the underlying minerals. Some of these organic matter coatings were in the process of being decomposed by soil micro-organisms (Fig. 1h).

In the examples above, the thin structural pore pedofeatures were much more abundant than examination by thin section and light microscopy would have determined. It is likely that this is also the case for other soils and that structural pore pedofeatures are more common than observation by light microscopy alone would indicate.

REFERENCES

Addiscott, T.M. and Wagenet, R.J., 1985. Concepts of solute leaching in soils: a review of modelling approaches. J. Soil Sci., 36: 411-424.

Anderson, J.L. and Bouma, J., 1973. Relationships between saturated hydraulic conductivity and morphometric data of an argillic horizon. Soil Sci. Soc. Am. Proc., 37: 408-412.

Barraclough, D., 1989. A usable mechanistic model of nitrate leaching I. The model. J. Soil Sci., 40: 543-554.

Barrow, N.J., 1983. A mechanical model for describing the sorption and desorption of phosphate in soil. J. Soil Sci., 34: 733-740.

Barrows, H.L., Simpson, E.C. and Tu, H.Y., 1966. Formation of surface coatings on limestone particles in soils. Soil Sci. Soc. Am. Proc., 30: 317-320.

Borggaard, O.K., 1987. Influence of iron oxides on cobalt adsorption by soils. J. Soil Sci., 38: 229-238.

Bouma, J. and Anderson, J.L., 1977. Water and chloride movement through soil columns simulating pedal soils. Soil Sci. Soc. Am. J., 41: 766-770.

Bowden, J.W., Bolland, M.D.A., Posner, A.M. and Quirk, J.P., 1973. Generalised model for anion and cation adsorption at oxide surfaces. Nature, 245: 81-83.

Bradfield, R., 1937. Soil conservation from the view of soil physics. J. Am. Soc. Agron., 29: 85-92.

Brewer, R., Sleeman, J.R. and Foster, R.C., 1983. The fabric of Australian soils. In: Soils: An Australian Viewpoint. CSIRO, Melbourne/Academic Press, London, pp. 439-476.

Bridge, B.J., 1968. Soil Physical Properties as Influenced by Gypsum. M. Sc. Agr. Thesis. University of Sydney, Australia.

Brusseau, M.L. and Rao, P.S.C., 1990. Modelling solute transport in structured soils: a review. Geoderma, 46: 169-192.

Bullock, P., Fedoroff, N., Jongerius, A., Stoops, G., and Tursina, T., 1985. Handbook for Soil Thin Section Description. Waine Research Publications, Wolverhampton, U.K., 152 pp.

Currie, J.A., 1961. Gaseous diffusion in the aeration of aggregated soils. Soil Sci., 92: 40-45.

Emerson, W.W. and Bond, R.D., 1963. The rate of water entry into dry sand and calculations of the advancing contact angle. Aust. J. Soil Res., 1: 9-16.

FitzPatrick, E.A., 1984. Micromorphology of Soils. Chapman and Hall, London, 433 pp.

van Genuchten, M.Th. and Wierenga, P.J., 1976. Mass transfer in sorbing porous media I. Analytical solutions. Soil Sci. Soc. Am. J., 40: 473-480.

Jarvis, N.J., Jansson, P-E., Dik, P.E. and Messing, I., 1991. Modelling water and solute transport in macroporous soil. I. Model description and sensitivity analysis. J. Soil Sci., 42:59-70.

Kalifa, E.M. and Buol, S., 1969. Studies on clay skins in a Cecil (Typic Hapludult) soil: II. Effect on plant growth and nutrient uptake. Soil Sci. Soc. Am. Proc., 37: 421-24.

Kissel, D.E., Ritchie, J.T. and Burnett, E., 1973. Chloride movement in undisturbed swelling clay soil. Soil Sci. Soc. Am. Proc., 37: 421-24.

Kubiëna, W.L., 1938. Micropedology. Collegiate Press, Ames, Iowa, 470 pp.

Lai, T.M. and Mortland, M.M., 1968. Cationic diffusion in clay minerals: ii. Orientation effects. Clays and Clay Min., 16: 129-136.

McIntyre, D.S., 1958. Permeability measurements of soil crusts formed by raindrop impact. Soil Sci., 85: 185-189.

Miller, M.H. and Wilding, L.P., 1972. Micromorphological features of soils in relation to plant growth. In: R. Protz (Editor), Proceedings of a Symposium on Microfabrics of Soil and Sedimentary Deposits. CRD Publication No. 69, Guelph, Ontario, pp. 75-110.

Nettleton, W.D., 1972. Microfabric characteristics as applied to soil classification. In: R. Protz (Editor), Proceedings of a Symposium on Microfabrics of Soil and Sedimentary Deposits. CRD Publication No. 69, Guelph, Ontario, pp. 34-74.

Norrish, K., 1975. Geochemistry and mineralogy of trace elements. In: D.J.D. Nicholas and A.R. Egan (Editors), Trace Elements of the Soil-Plant-Animal Systems. Academic Press, New York, pp. 55-81.

Nuhfer, E.B., Vinopal, R.J. and Michael, M., 1981. Applications of SEM in petrology of mudrocks: results of studies of Devonian mudrocks from West Virginia and Virginia. In: E. Hohn and D.S. Klanderman (Editors), Scanning Electron Microscopy 1981/I. SEM. AMF, O'Hara, Chicago, Illinois, pp. 625-633.

Parfitt, R.L. and Russell, J.D., 1977. Adsorption on hydrous oxides. IV. Mechanisms of adsorption of various ions on goethite. J. Soil Sci., 28: 297-305.

Parfitt, R.L., Fraser, A.R., Russell, J.D. and Farmer, V.C., 1977. Adsorption on hydrous oxides. II. Oxalate, benzoate and phosphate on gibbsite. J. Soil Sci., 28: 40-47.

Rappoldt, C., 1990. The application of diffusion models to an aggregated soil. Soil Sci., 150: 645-661.

Robinson, D.O. and Page, J.B., 1950. Soil aggregate stability. Soil Sci. Soc. Am. Proc., 15: 25-29.

Russell, E.W., 1973. Soil Conditions and Plant Growth. Tenth Edition. Longmans, London, 849 pp.

Soileau, J.M., Jackson, W.A. and McCracken, R.J., 1964. Cutans (clay films) and potassium availability to plants. J. Soil Sci., 15: 117-123.

Sullivan, L.A., 1988. Surfaces and Pedological Features Associated with Planar Pores, Channels, Chambers, Vesicles and Cavities. Ph.D. Thesis, University of Sydney, Sydney, Australia.

Sullivan, L.A., 1990. Soil organic matter, air encapsulation and water stable aggregation. J. Soil Sci., 41: 529-534.

Sullivan, L.A. and Koppi, A.J., 1987. *In situ* soil organic matter studies using scanning electron microscopy and low temperature ashing. Geoderma, 40: 317-332.

Taylor, R.M., McKenzie, R.M. and Norrish, K., 1964. The mineralogy and chemistry of manganese in some Australian soil. Aust. J. Soil Res., 4: 29-39.

Tiller, K.G., Gerth, J. and Brummer, G., 1984. The relative affinities of Cd, Ni and Zn for different soil clay fractions and goethite. Geoderma, 34: 17-35.

Turner, R.R. and Steele, K.F., 1988. Cadmium and manganese sorption by soil macropore linings and fillings. Soil Sci., 145: 79-86.

Wang, J., Hesketh, J.D. and Woolley, J.T., 1986. Pre-existing channels and soybean rooting patterns. Soil Sci., 141: 432-437.

Youngs, E.G. and Leeds-Harrison, P.B., 1990. Aspects of transport processes in aggregated soils. J. Soil Sci., 41: 665-675.

Micromorphology and soil management

M. Pagliai[*]

Istituto per la Chimica del Terreno, C.N.R., Via Corridoni 78, 56100 Pisa, Italy

ABSTRACT

Pagliai, M., 1994. Micromorphology and soil management. In: A.J. Ringrose-Voase and G.S. Humphreys (Editors), Soil Micromorphology: Studies in Management and Genesis. Proc. IX Int. Working Meeting on Soil Micromorphology, Townsville, Australia, July 1992. Developments in Soil Science 22, Elsevier, Amsterdam, pp. 623-640.

The need to prevent the deterioration of soil structure caused by long-term intensive cultivation is one of the most important aims of soil researchers and agronomists. To evaluate the impact of management practices on the soil environment it is necessary to quantify the modifications of soil structure, which is one of the most important properties affecting crop production.

The quantification of soil porosity is fundamental to the characterization of soil structure and is made possible by image analysis of thin sections or impregnated soil blocks, prepared from undisturbed soil samples. Micromorphometric methods allow evaluation of the modifications of soil structure induced by management practices through quantification of parameters such as pore-size distribution, pore shape and relative position of aggregates and pores. Characterization of these parameters also allows quantification of different types of soil structure degradation, such as the formation of traffic pans, compaction of layers in cultivated profiles and crusting of the surface soil, all of which are strongly related to intensive soil management.

Generally, soils under intensive management practices have greater total porosity than soils under reduced tillage practices. However, the former show greater seasonal variations and the proportion of biopores and transmission pores, which are useful for water movement and root growth, are generally greater in soil under reduced tillage. Reduced cultivation practices generally seem most appropriate in the maintenance of favourable soil conditions and the prevention of soil structure degradation.

INTRODUCTION

Long-term intensive arable cultivations have negative effects on soil physical properties, particularly on soil structure, with possible effects on soil erodibility and crop yields. The need to check degradation of soil structure has caused farmers to consider no-till management as an alternative to conventional tillage. Additionally the abandonement of traditional farming

---

[*] Present address: Istituto Sperimentale per la Studio e la Difesa del Suolo, Piazza d'Azeglio 30, 50121 Firenze, Italy.

rotations and the adoption of intensive monocultures, without applications of farmyard manure or other organic materials to the soil, has decreased soil organic matter content with evident degradation of soil structure. The resulting soil porosity conditions are often unfavorable for crop growth (Pagliai *et al.*, 1983b, 1984, 1989a; Shipitalo and Protz, 1987).

To evaluate the impact of management practices on the soil environment it is necessary to quantify the modifications to soil structure. According to Greenland (1981), porosity is the best indicator of soil structure conditions. Crops require adequate "storage pores" (0.5 - 50 μm equivalent pore diameter, e.p.d.), which contain a reservoir of water for plants and microorganisms, as well as adequate "transmission pores" (continuous pores ranging from 50 to 500 μm e.p.d.), which allow water movement and easy root growth. Until recently, the necessary proportion of these pores has generally been inadequately defined and there has been a lack of knowledge of how pore space relates to crop yield due to the lack of methods allowing complete characterization of soil pore space. Micromorphometric analysis overcomes some of the problems associated with other methods of pore space analysis because aspects of pore space measured by image analysis in 2-D soil thin sections can be related to 3-D pore properties using the principles of stereology (Ringrose-Voase, 1991).

Recent research has shown that management practices can generally affect soil porosity (Kooistra *et al.*, 1990; Pagliai *et al.*, 1989a; Shipitalo and Protz, 1987). Management practices can also affect biological activity and thereby influence both the formation and preservation of biopores, which are important for water movement and root development (Kooistra, 1991).

This paper focuses on the application of micromorphology to the study of the impact of management practices on soil structure. In particular, the quantification of soil pore space will be discussed because it is fundamental to the evaluation of the soil as a rooting environment for crops and to the movement of water, air, nutrients and soil fauna through soil. Measurements of soil pore space also allow quantification of aspects of soil structure degradation such as the formation of traffic pans, compacted layers in the profile and surface crusts.

EFFECTS OF DIFFERENT TILLAGE PRACTICES ON SOIL PORE STRUCTURE

Pore space measurements are increasingly being used to quantify soil structure because it is the size, shape and continuity of pores that affect many of the important processes in soils (Lawrence, 1977). Possibilities now exist for improving shape models and for creating more accurate models of pore space in soils by using micromorphology coupled with image analysis of photographs of soil thin sections or of impregnated soil blocks (Murphy *et al.*, 1977a, b; Pagliai *et al.*, 1983a, b). This technique has the advantage that the measurement and characterization of the pore space can be combined with a visual appreciation of the type and distribution of the pores (Ringrose-Voase and Bullock, 1984).

Although the images analysed are only 2-D pictures, this method provides useful information on the complexity of pore patterns in soils, not obtainable using other common methods such as mercury intrusion, water retention, and nitrogen sorption. However, it is possible to apply stereology to 2-D image analysis results in order to characterize soil pore space in 3-D (Ringrose-Voase and Bullock, 1984; Ringroase-Voase and Nortcliff, 1987). This micromorphometric method based on image analysis can be used not only on soil thin sections but also on polished faces of large soil blocks impregnated directly in the field with (fairly cheap) materials such as paraffin wax (Dexter, 1988), plaster of Paris (FitzPatrick *et al.*, 1985) or resin (Moran *et al.*, 1989).
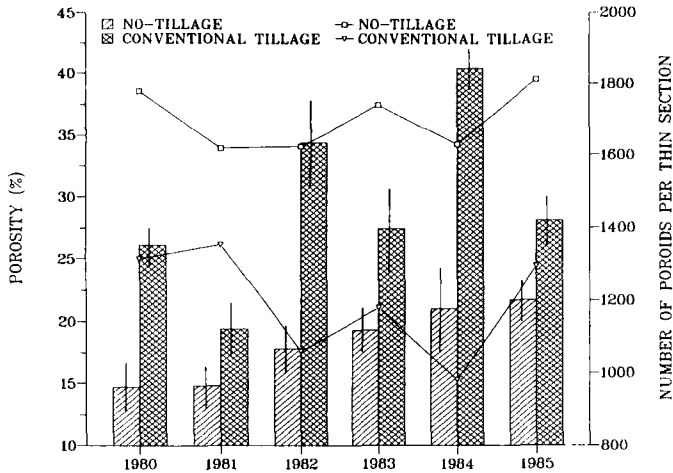
Fig. 1. Effects of two types of soil management on soil porosity, expressed both as a percentage of total area (histograms) and as number (lines) of poroids larger than 30 μm per thin section, of the surface layer (0 - 10 cm) of a clay loam soil under viticulture in the Po Valley (Italy). The analysed area of each thin section was 4.5 × 5.5 cm (1500 × 1833 pixels); means of six replicates. Bars represent confidence interval at P<0.05 (Data for 1980-1984 from Pagliai *et al.*, 1983, 1984; Pagliai, 1986, 1987a).

Total porosity

Tillage produces a loose and granular structure with increased macroporosity which is dominated by large packing pores separating aggregates or clods. On the other hand the microporosity (measured by mercury intrusion) does not seem to be strongly influenced by different tillage practices (Sparvoli *et al.*, 1989).

Granular structures produced by tillage are very unstable, especially near the surface and after the first rainfall and wetting and drying cycles, can be transformed into a more compact structure, often associated with the presence of a surface crust. This transformation is strongly related to soil type, organic matter content and aggregate stability. During the cultural cycle the soil structure changes. Therefore, when studying modifications induced by different tillage treatments, it is necessary to plan an appropriate sampling strategy during the crop cycle. Sampling in the period of crop ripening is particularly important because at that time, good soil conditions are critical for crop development (Pagliai *et al.*, 1989a). When studying the effect of different tillage treatments on crusting, it is very important to sample before seedling emergence.

In a long-term field experiment established in 1978 on a clay loam soil (Vertic Xerofluvent) under viticulture in the Po Valley (Italy), in which no-tillage and conventional tillage were compared, the total porosity, measured on thin sections from undisturbed samples collected every year at the end of July when grape ripening started, was always significantly higher (although very variable) in the conventionally tilled soil than in the untilled soil as shown in
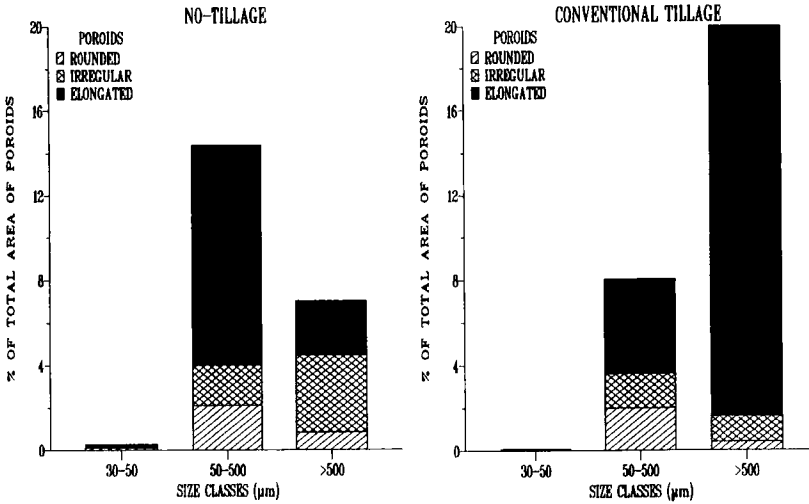
Fig. 2. Poroid shape and size distribution according to the equivalent poroid diameter for rounded and irregular poroids and to the width for elongated poroids from the same experiment as Fig. 1. Data refer to the sampling of the end of July 1985.

Fig. 1 (Pagliai *et al.*, 1983b, 1984; Pagliai, 1986 and 1987a). In contrast, the number of poroids[1] was significantly higher in samples of untilled soil, thus indicating a different pore-size distribution between the two management practices. The high variability of pore space in the conventionally tilled soil could be explained as the result of physical stresses, caused, for example, either by heavy rainfall that compacted the soil or by strong, dry winds that induced rapid soil drying, thus influencing soil shrinkage phenomena. The intensity of these natural events, which varies from year-to-year, can influence porosity in tilled soil. The untilled soil seemed to be more resistant to these physical stresses. In agreement with these observations, Mackie-Dawson *et al.* (1989) found that seasonal changes in macroporosity in untilled soil were smaller than in a neighbouring ploughed soil. The year by year increase of porosity in untilled soil is a clear symptom of the restoration of good soil structure.

Pore shape and size distribution

Fig. 2 reports the pore-size distribution of the above mentioned field experiment on a clay loam soil under viticulture (Pagliai *et al.*, 1983b, 1984; Pagliai, 1987a). The shapes of poroids were measured as the ratio of area, A, to perimeter squared, P^2, (A/P^2), and were classified into: more or less rounded poroids ($A/P^2 > 0.04$); irregular poroids ($0.015 < A/P^2 < 0.04$) and elongated poroids ($A/P^2 < 0.015$) (Bouma *et al.*, 1977). Poroids of each shape group were further subdivided into size-classes according to the equivalent pore diameter for rounded and

---

[1]When referring to individual discrete pore outlines in the 2-D image, Moran *et al.* (1988) suggested the term "poroid".
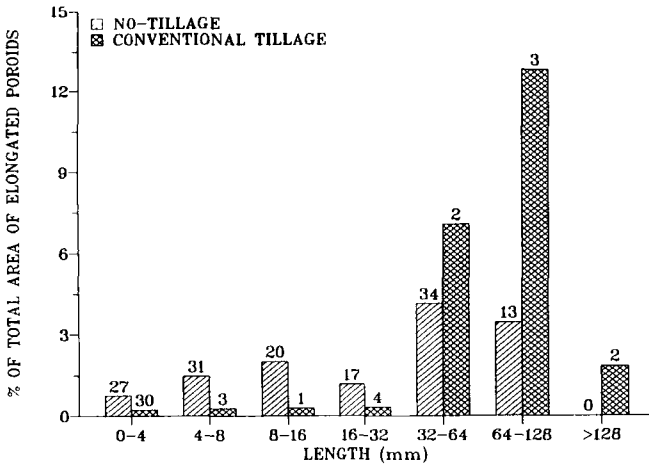
Fig. 3. Length distribution of elongated poroids from the same experiment as Fig. 1. Data refer to the sampling of the end of July 1985. Numbers refer to the number of elongated poroids for each class per thin section (4.5 × 5.5 cm analysed area) and are the mean of six replications.

irregular poroids and the width for elongated poroids (Pagliai *et al.*, 1983, 1984). The untilled soil showed strong differences to the conventionally tilled soil. In the latter, a higher proportion of total porosity was elongated poroids larger than 500 μm. The proportion of poroids ranging from 30 to 500 μm, which are considered the most important both in soil-water-plant relationships and in maintaining a good soil structure (Greenland, 1977; 1981), was higher in the untilled soil. Similar results were obtained in another no-tillage versus conventional tillage field experiment established on a clay soil (Typic Chromoxerert) in Sicily (Pagliai, 1987a). Sequi *et al.* (1985) and Pagliai and De Nobili (1993) found a positive correlation between soil enzyme activity and the amount of pore space in the 30 to 200 μm size range measured by image analysis of the thin sections from the viticulture experiment described above. Therefore, in the untilled soil, where the number of these pores was greater, the enzyme activity should be greater. Pagliai and De Nobili (1993) also showed that, in the same soil, the rooting potential in no-tilled soil was greater than in conventionally tilled soil. Roots were washed out of the soil (Bennie *et al.*, 1987) and the root length density (cm cm^{-3}) determined by image analysis as the root perimeter/2. The quantity of elongated poroids ranging from 50 to 500 μm was positively correlated with root density.

Microscopic observation revealed that the larger elongated poroids in the untilled soil (Fig. 2) were mostly biopores which are very important for water movement (Bouma, 1982; Edwards *et al.*, 1988). The larger elongated poroids in the conventionally tilled soil (Fig. 2) were planar pores surrounding or separating aggregates or clods formed by tillage. In agreement with these results, Shipitalo and Protz (1987) found that biopores formed by faunal activity were significantly higher in untilled soil than in conventionally tilled soil.

Length and irregularity of elongated pores

Fig. 3 reports the length of elongated poroids, which may reflect their continuity, measured by image analysis of thin sections from samples of the field experiment on clay loam soil under viticulture. The length of elongated poroids was calculated from their area and perimeter using a quadratic equation, assuming that elongated poroids are long narrow rectangles (Pagliai *et*
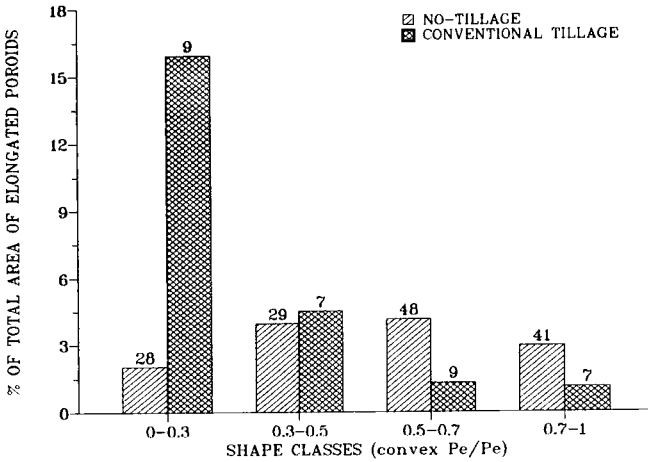
Fig. 4. Shape distribution of elongated poroids from the same experiment as Fig. 1. Data refer to the sampling of the end of July 1985. Numbers refer to the number of elongated poroids for each class per thin section (4.5 × 5.5 cm analysed area) and are the mean of six replications. Convex perimeter/perimeter decreases with increasing irregularity.

Table 1
Classification of elongated poroids according to their irregularity (convex perimeter/perimeter ratio). Modified from Pagliai *et al.*, 1984.

Shape-class	Morphology
0-0.3	Very irregular (Tortuous, curved, strongly digitate, U-shaped)
0.3-0.5	Moderately irregular
0.5-0.7	Moderately regular
0.7-1	Regular

al., 1984). Conventional tillage caused an increase in the length of elongated poroids with more than 90% of the elongated-pore area consisting of poroids greater than 32 mm in length. However, this high percentage was due to only a few elongated poroids. In contrast, the area-proportion of elongated poroids >32 mm in the untilled soil was about 50%, but this percentage was due to a higher number. This means that in the conventionally tilled soil the few longer elongated poroids were also wider. Some of them were represented by cracks caused by shrinkage, which was much more evident in the tilled than in the untilled soil (Pagliai *et al.*, 1983b). These cracks were interconnected and usually showed a vertical orientation.

In another loam soil, representative of the plain along the Tyrrhenian coast (Italy), used for autumn-sown wheat, Pagliai *et al.* (1989a) found that minimum tillage and chisel ploughing were the most appropriate tillage practices in maintaining favourable pore space in the soil. The pore space was more homogeneously distributed in the Ap horizon and the proportion and length of elongated poroids in the "transmission" range (50 - 500 μm) were greater than in conventionally ploughed (to a depth of 50 cm) plots.

In the viticulture experiment on clay loam soil, there were also great differences in the irregularity of elongated poroids between the untilled and conventionally tilled soil as shown in Fig. 4. The irregularity of elongated poroids was measured as convex perimeter/perimeter, which decreases with irregularity, tortuosity and re-entrancy. The elongated poroids were
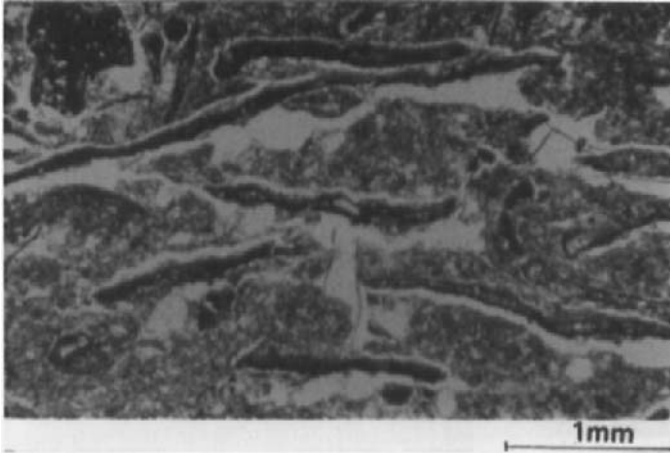
Fig. 5. Vertical thin section of untilled soil showing that abundant root remains (feeding roots) are present in the smaller planar pores in the surface layer (0-6 cm) from the same experiment as Fig. 1. Plain light. Pores appear white.

classified into four irregularity classes as shown in Table 1 (Pagliai *et al.*, 1984). In the conventionally tilled soil, the greatest area proportion of elongated poroids was accounted for by relatively few, longer and wider poroids in the very irregular class (0 - 0.3). In the untilled soil, the highest frequency of elongated poroids was in the moderately regular (0.5 - 0.7) and very regular (0.7 - 1) classes. Microscopic examination revealed that many of these moderately regular or regularly elongated poroids were >32 mm long and some of them traversed the full thin section. The high area percentage and number of moderately regular elongated poroids may be regarded as significant because their walls do not accomodate each other. Therefore, these pores permit passage of water even when the soil is wet and fully swollen. In contrast, flat and smooth poroids as found in the regular shape classes, which have accomodating faces, tend to seal when the soil is wet and thus prevent water movement. Furthermore, moderately regular elongated pores are not tortuous. From their length it was deduced that many of these pores were continuous and, therefore, act as growth paths for roots. Microscopic observation of the thin sections confirmed that root remains were more abundant in the untilled soil than in the conventionally tilled soil (Fig. 5) and were distributed in these moderately regular and continuous elongated poroids in the "transmission" pore space range (50 - 500 μm).

In field experiments examining the total and surface-connected macroporosity of a Vertisol in Queensland (Australia), under different management treatments, Moran and McBratney (1992) found, one week after sowing cereals, greater connectivity of pore space from the infiltrating surface to depth observed under zero-tillage than under conventional cultivation. In these experiments the pore structure was studied by image analysis of large blocks which had been resin-impregnated in the field.

Microstructure

The differences of soil pore space caused by different management practices, in the soils of the above cited experiments, can be visually appreciated by microscopic observation. After no-tillage and minimum tillage, an angular to subangular blocky microstructure (Bullock *et al.*, 1985a) was generally present and homogeneously distributed along the surface horizons (Fig.
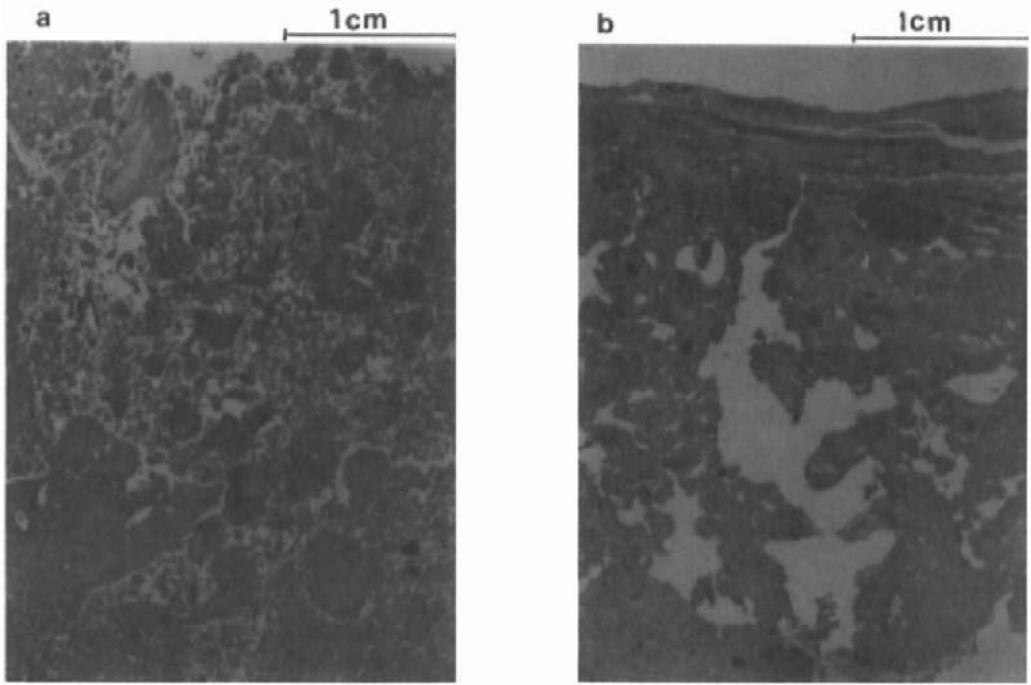
Fig. 6. Macrophotograph of vertically-oriented thin section from the surface of untilled (a) and tilled soils (b) from the same experiment as Fig. 1. Differences in the pore system and microstructure are very evident. The tilled soil (b) also has a surface crust, formed by thin layers of fine material intercalated by vertically discontinous elongated pores, and some vesicles. Plane light.

6a). In conventionally tilled soils, the microstructure was more complex. Immediately after tillage a crumbly microstructure could be recognized. However, such a microstructure was not stable and after several cycles of wetting and drying it was transformed into a platy structure in the topsoil (very often associated with surface crusting) with a vughy (Bullock *et al.*, 1985a) to massive microstructure in the layer below (Pagliai *et al.*, 1984, 1989a). These transformations can be ascribed to the low stability of soil aggregates which causes their breakdown and leads to a decrease in the proportion of storage (0.5-50 µm) and transmission (50-500 µm) pores (Fig. 6b).

Many results in the international literature seem to recommend the adoption of reduced tillage to prevent soil structure degradation. However, there are some soil types that have been found to be unsuitable. For example, Pagliai and Pezzarossa (1990) found that adopting reduced tillage on a clay soil developed on Pliocene marine clays (Typic Udorthent) produced a very compact massive structure, with few, if any elongated poroids. This creates a poor "habitat" for crop development and increasing the risks of erosion, since these pores are probably continuous and responsible for transmission of water. The main reasons for the poor
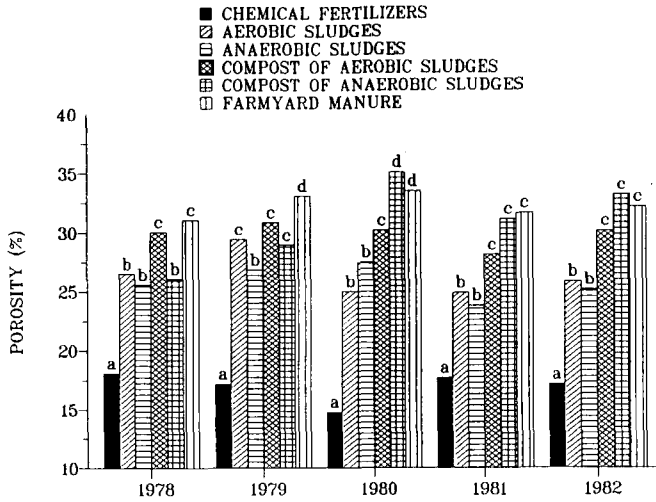
Fig. 7. Effect of aerobic sludges, anaerobic sludges, compost of aerobic sludge and the organic fraction of urban refuse (40 - 60%), compost of anaerobic sludges and the organic fraction of urban refuse (20 - 80%), farmyard manure and chemical fertilizers on soil porosity, expressed as a percentage of area occupied by poroids larger than 30 μm per thin section, of the surface layer (0 - 10 cm) of a sandy loam soil (Typic Psammaquent) located on an experimental farm near Pistoia, Tuscany. Means of six replicates. Within each year, mean values followed by the same lower case letter are not significantly different employing Duncan's Multiple Range test (Data for 1978-1980 from Pagliai *et al.*, 1981, 1983a).

physical properties of these soils are the low organic matter content (< 1%) and the high exchangeable sodium percentage (15%) which cause clay dispersion.

EFFECTS OF THE APPLICATION OF MANURES ON SOIL POROSITY

The application of organic materials to the soil has also been shown to enhance both soil porosity and pore-size distribution. Fig. 7 summarizes results obtained in a long-term field experiment established in 1978 on a sandy loam soil in which annual application of sewage sludges and composts from urban refuse were compared to the application of farmyard manure or chemical fertilizers (Pagliai *et al.*, 1981; 1983a). The application rates were calculated on the organic carbon basis and were equivalent to 50 metric tons/ha of manure. The soil was planted to corn and the tillage was the same for all treatments, *i.e.*, conventional ploughing to a depth of 25 cm. Data refer to the annual sampling during corn ripening. Soil pore space significantly increased in all years, after treatment with all organic materials compared to treatment with chemical fertilizer alone.

Pore shape and size distribution were also affected by to the application of organic materials. The proportion of storage (30-50 μm) and transmission pores (elongated poroids, 50-500 μm) was greater in soil treated with any type of organic material than in soil treated with chemical fertilizers only (Fig. 8). Similar results were obtained with the application of pig
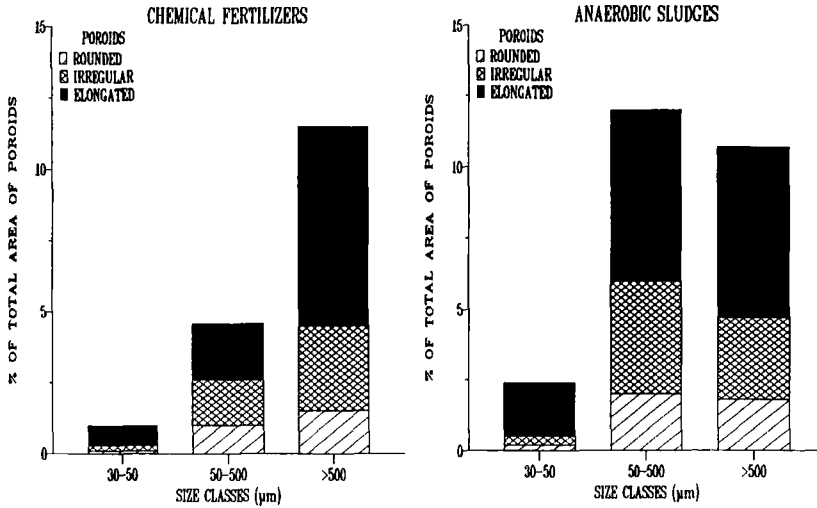
Fig. 8. Poroid size distribution according to the equivalent poroid diameter for rounded and irregular poroids and for the width for elongated poroids in soil treated with the anaerobic sludges in comparison with soil treated with the chemical fertilizers from the same experiment as Fig. 7. Data refer to the sampling of 1982.

slurry to a silty clay soil. In this experiment, a positive relationship between the rate of application and the increase of soil porosity was found. It also emerged that the time of application was important, with the best results being obtained for spring applications (Pagliai *et al.*, 1983a; 1985). The increase of pore space and the modification of the pore system in soil treated with these organic materials was associated with an increase of aggregate stability (Pagliai *et al.*, 1981). The data from these experiments provide clear evidence that sludges, composts and livestock effluents can improve the physical properties of soil in a similar way to manure.

EFFECTS OF MANAGEMENT PRACTICES ON SOIL WATER CONTENT AND WATER FLOW

Tillage and application of manures, through their effect on organic matter content and porosity, strongly influence the behaviour of water in the soil and its availability to plants. Van Ouwerkerk and Boone (1970) showed that soil water content at pF 2 could be influenced more by soil organic matter content than by total porosity. Therefore, if continuous tillage causes a decrease of soil organic matter, it can also have negative effects on its water holding capacity.

Ellis *et al.* (1982) found water content was always lower in conventionally tilled soils than in untilled or minimum tilled soils. This is probably because no-tillage and minimum tillage cause an increase in the proportion of storage pores even though the total porosity decreases (Pagliai *et al.*, 1983b).
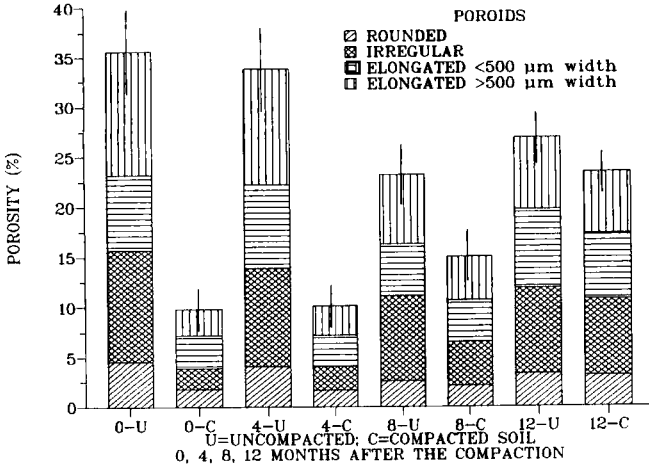
Fig. 9. Porosity and poroid shape distribution in the surface layer (0 - 10cm) of uncompacted and compacted clay loam soil located in the low Arno river basin, Tuscany. The experiment started in May 1985. Means of six replications. Bars represent confidence interval al P<0.05 of the total value of porosity. (After Pagliai *et al.*, 1987b).

Soil porosity and pore shape and size distributions can be also modified by depth of water table. Pagliai *et al.* (1989b) found that in a field experiment on a clay loam soil (Mollic Haplaquept) soil structure deteriorated in the long-term with shallower water tables, reducing soil pore space to an inadequate level for plant development. In this experiment the microporosity, measured by mercury intrusion, showed the same trend as porosity measured by image analysis *i.e.* it was lower in the soil where the water table was shallower. Ristori *et al.* (1989) confirmed that microporosity was strongly related to the water content and water potential.

Porosity measurements by image analysis can also be very useful in the calculation of hydraulic conductivity. As is known from field observations and deductions from physical studies, water flows preferentially through relatively large continuous pores. Macrostructure should allow such an estimation, but experience has shown that in several cases no correlation can be found between saturated hydraulic conductivity (K_{sat}) and macrostructure in swelling clay soils. To obtain a better insight into this correlation, undisturbed columns of clay soils that have been close to saturation for some time are percolated with a 0.1% solution of methylene-blue or another dye that is absorbed by the clay particles. Horizontal and vertical thin sections are prepared and measured by image analysis (Bouma *et al.*, 1977). Poroids are divided into three shape groups as already explained and the pore-size distribution calculated. For elongated poroids, the total area and the area and length with stained pore walls are measured. Particular attention should be paid to the measurement of the width of the necks of elongated pores because the hydraulic conductivity is determined by the necks in the flow system. Following this procedure the hydraulic conductivity (K_{sat}) can be calculated as proposed by Bouma *et al.* (1979).

EFFECT OF MANAGEMENT PRACTICES ON SOIL COMPACTION

Soil compaction is caused by a combination of natural and man-made forces. The latter are mainly related to vehicle wheel traffic and passage of tillage implements and generally have a much greater compactive effect than natural forces such as raindrop impact, soil swelling and
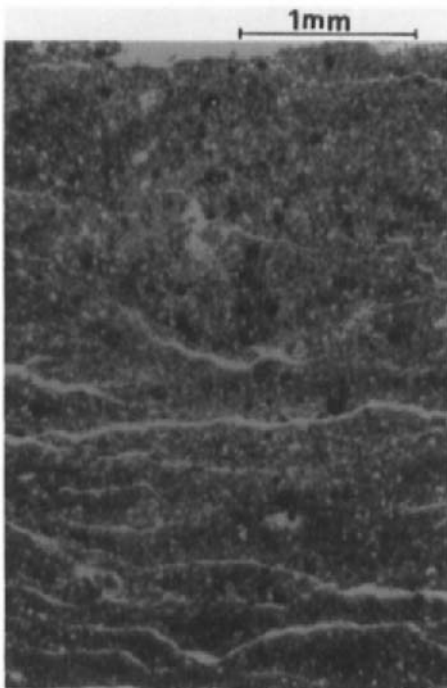
Fig. 10. Micrograph of vertically-oriented thin section from the surface layer (0 - 7 cm) of the compacted soil from the same experiment as Fig. 9. A platy structure is very evident. Plane light.
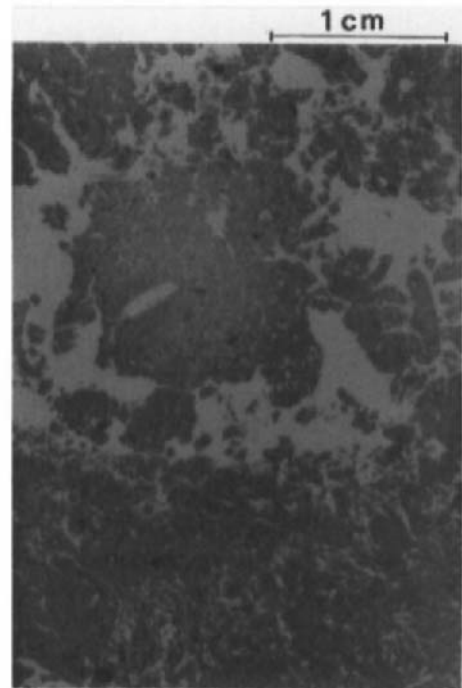
Fig. 11. Micrograph of vertically-oriented thin section of soil samples from the subsoil (23-30 cm) from the same experiment as Fig. 9. The lower limit of cultivation and the upper part of the ploughpan are visible. Plane light.

shrinking and root enlargement especially because trends in agricultural engineering over the last few decades have resulted in machines of a greater size and weight.

Fig. 9 shows the results of an experiment dealing with the modifications of soil porosity and structure induced by tractor wheels in a clay loam soil and for how long such modifications are apperent (Pagliai, 1987b). In the compacted topsoil, porosity greatly decreased, particularly that of irregular poroids. At the same time, the size of elongated poroids was reduced and other observations indicated a modification of their orientation. Microscopic observation revealed that these elongated poroids were thin fissures parallel to the soil surface, forming a platy structure, and had little vertical continuity (Fig. 10). As a consequence water infiltration was reduced, increasing the risk of soil erosion. After one year the modifications induced by compaction were no longer apparent with respect to the uncompacted topsoil. Bullock *et al.* (1985b) also found that soil structure could regenerate after compaction in clay soils, although over a period of some years. Bresson and Zambaux (1990) observed that a marked decrease in the porosity of biopores and fissures due to compaction was associated with increased pH and decreased organic matter due to continuous cultivation. They concluded that this may alter the
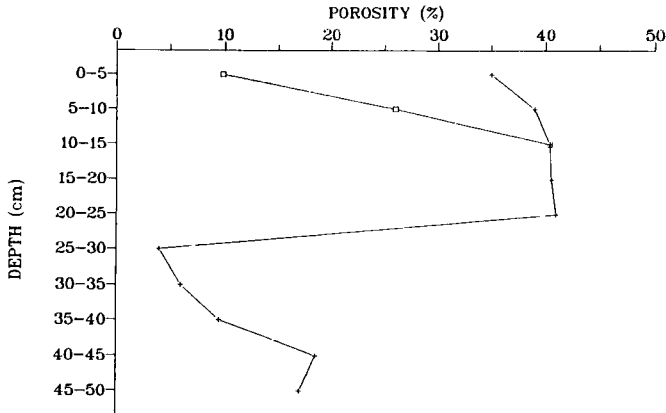
Fig. 12. Porosity as a percentage of total area of thin section at selected depths from the same experiment as Fig. 9 (After Pagliai, 1987b). + between wheel tracks; □ under wheel tracks.

cohesion of the isotropic ultramicrofabric and make compaction irreversible. Coulon and Bruand (1989) confirmed that compaction modified the pore space geometry and fabric of the elementary particles.

Continually ploughing the soil may cause the formation of a ploughpan (ploughsole) at the lower depth limit of cultivation (Fig. 11). Fig. 12 shows that the macroporosity, measured by image analysis, was high just above the ploughpan; decreased to a very low value in the ploughpan and slightly increased in uncultivated soil below. In this case the ploughpan was only a few centimetres deep but other studies have shown the thickness of its ploughpan can reach 10 cm. Microscopic observations revealed that in the first few centimetres of the ploughpan there were a few, very thin, elongated poroids parallel to the surface of the ploughpan. Some irregular poroids were present in the lower part of the plougpan. The presence of such dense layers at the lower depth limit of cultivation may greatly reduce water drainage and hamper root development at depth. Kooistra *et al.* (1984) observed that the continuity of large pores, made visible by staining, in thin sections of an undisturbed ploughpan in a sandy loam soil was greater than that in a ploughpan disturbed by deep rototilling, which had discontinuous (unstained) packing pores between the aggregates. This means that once the ploughpan is formed it is very difficult to recover a structure which allows good drainage.

Fig. 12 also shows that the effect of the wheel compaction can reach a depth of about 10 cm.

EFFECT OF MANAGEMENT PRACTICES ON SOIL CRUSTING

Surface crusts caused by raindrop impact are very common in tilled soils, especially on loamy soils with poor aggregate stability. Microscopic observations of thin sections prepared from surface soil show a thin layer of horizontally oriented plate-like particles at the soil surface. This thin, compact layer contains few, if any, large pores. In many tilled soils, the surface crust is formed by several layers of this kind (depositional crusts) (Chen *et al.*, 1980), intercalated by coarse materials, elongated pores and, sometimes, vesicles (Brewer, 1964) formed by air entrapped during the crusting process (Fig. 6b). From an agronomic point of view, the greatest disadvantages of soil crusts are their influence on seedling emergence and water infiltration. The latter problem can lead to increased run-off and greater risk of erosion.

In the long term field experiment on a clay loam soil under viticulture discussed previously (Pagliai *et al.*, 1983b), soil crusts were much less developed on untilled soil where layers of oriented particles were absent and pore space remained high even in the surface soil layers (Fig. 6a). This can be ascribed both to the greater aggregate stability of the surface soil in the untilled plots compared to that of the tilled plots and to reduced rain-drop impact due to grass residues killed by herbicide on the soil surface. Similar results were also obtained in the loam soil, representative of the plain along the Tyrrhenian coast (Italy), cultivated to grow autumn-sown wheat (Pagliai *et al.*, 1989a). In this soil, surface crusts were much less developed on minimum tilled and chisel ploughed soil than on ploughed soil. Norton and Schroeder (1987) also found that the different types of tillage practice can considerably affect soil loss, infiltration and run-off, soil porosity and surface crusting both in the short and in the long-term.

Soil crust formation is strongly related to low aggregate stability in the surface layer and is therefore associated with low organic matter content. In experiments carried out on sandy loam and silty clay soils, Pagliai *et al.* (1983a) found that application of sewage sludges, composts and livestock effluents played an important role in preventing soil crust formation. Surface crusts were much less developed in the treated than in untreated soils. Moreover, the addition of such organic materials enhanced both soil porosity and pore size distribution, even in the surface layers.

CONCLUSIONS

The results cited in this paper show that micromorphological techniques can make original contributions to the characterization of soil structure. Image analysis allows the quantification of soil structure by means of measurements of pore structure. Such quantification is useful to evaluate the impact of different management practices on the soil and to select practices that contribute, as much as possible, to the prevention of soil degradation. Moreover, quantification of soil structure allows assessment of the suitability of soil as a rooting environment; provision of a realistic basis for understanding water movement and the study the relationship between soil structure, soil biological and biochemical activity and the movement of soil organisms under different management practices.

Whilst image analysis of thin sections gives much useful information, the necessary sampling, drying and preparation of thin sections is time-consuming and labour-intensive. The number of thin sections necessary for experiments such as those described above is considerable. For example, considering only two treatments in a field experiment using a completely randomized block design with six replications and collecting six undisturbed samples for thin section preparation at one selected depth for each plot, requires preparation of 72 thin sections (6 samples × 6 plots × 2 treatments). This number increases depending on the number of variables (treatments, depths, time of sampling, *etc.*) taken into consideration.

With this in mind, a method for rapid image analysis of soil pore structure, developed by Moran *et al.* (1989), is very promising. This method consists of field impregnation with epoxy resin, followed by sawing, laboratory impregnation of the exposed face and grinding back to a smooth finish. After grinding, the face is digitized and the resulting digital image segmented to produce a binary image representing the soil macropore structure. Sample collection and preparation plus image processing can be completed in 4 to 5 days. A wide range of pore space size can be measured by changing the magnification of the optical apparatus, although the

combination of lens and video camera may limit resolution. Efforts should be made to overcome this possible limitation so that pore space 50 to 200 μm range can be thoroughly investigated, since it is important for root growth and water movement and is strongly affected by different management practices.

Micromorphological techniques can be used at many different scales. Even micropores with diameters as small as 0.1 μm can be measured by image analysis using backscattered electron scanning images (Bisdom and Thiel, 1981). The combination of submicroscopic techniques and image analysis has been very useful, for example, in studying the influence of waste organic matter on soil crusting and on soil microstructure (Pagliai et al., 1983a; Pagliai and Vittori Antisari, 1993).

The improvement of image analysis techniques, in particular, the use of mathematical morphology (Serra, 1982) in the characterization of soil pore structure and the availability of software packages for user-friendly image processing, can certainly improve the quantity and quality of results from applying micromorphology in agricultural research.

REFERENCES

Bennie, A.T.P., Taylor, H.M. and Georgen, P.G., 1987. An assessment of the core-break method for estimating rooting density of different crops in the field. Soil Tillage Res., 9: 347-353.

Bisdom, E.B.A. and Thiel, F., 1981. Backscattered electron scanning images of porosities in thin sections of soils, weathered rocks and oil-gas reservoir rocks using SEM EDXTRA. In: E.B.A. Bisdom (Editor), Submicroscopy of Soils and Weathered Rocks. Pudoc, Wageningen, pp. 207-216.

Bouma, J., 1982. Measuring the hydraulic conductivity of soil horizons with continuous macropores. Soil Sci. Soc. Am. J., 46: 438-411.

Bouma, J., Jongerius, A., Boersma, O., Jager, A. and Schoonderbeek, D., 1977. The function of different types of macropore during saturated flow through four swelling soil horizons. Soil Sci. Soc. Am. J., 41: 945-950.

Bouma, J., Jongerius, A. and Schoonderbeek, D., 1979. Calculation of saturated hydraulic conductivity of some pedal clay soils using micromorphometric data. Soil Sci. Soc. Am. J., 43: 261-264.

Bresson, L.M. and Zambaux, C., 1990. Micromorphological study of compaction induced by mechanical stress for a Dystrochreptic Fragiudalf. In: L.A. Douglas (Editor), Soil Micromorphology: A Basic and Applied Science. Proc. VIII Int. Working Meeting on Soil Mircromorphology, San Antonio, Texas, July 1988. Developments in Soil Science 19, Elsevier, Amsterdam, pp. 33-40.

Brewer, R., 1964. Fabric and Mineral Analysis of Soils. John Wiley and Sons, New York, 470 pp.

Bullock, P., Fedoroff, N., Jongerius, A., Stoops, G., and Tursina, T., 1985. Handbook for Soil Thin Section Description. Waine Research Publications, Wolverhampton, U.K., 152 pp.

Bullock, P., Newman, A.C.D. and Thomasson, A.J., 1985b. Porosity aspects of the regeneration of soil structure after compaction. Soil Tillage Res., 5: 325-341.

Chen, Y., Tarchitzky, J., Brouer, J., Morin, J. and Banin, A., 1980. Scanning electron microscope observation on soil crusts and their formation. Soil Sci., 130: 49-55.

Coulon, E. and Bruand, A., 1989. Effects of compaction on the pore space geometry in sandy soils. Soil Tillage Res., 15: 137-152.

Dexter, A.R., 1988. Advances in characterization of soil structure. Soil Tillage Res., 11: 199-238.

Edwards, W.M., Norton, L.D. and Redmond, C.E., 1988. Characterizing macropores that affect infiltration into nontilled soil. Soil Sci. Soc. Am. J., 52: 483-487.

Ellis, F.B., Christian, O.G. and Cannel, R.Q., 1982. Direct drilling, shallow tine-cultivation and ploughing on a silty-loam soil, 1974-1980. Soil Tillage Res., 2: 115-130.

FitzPatrick, E.A., Makie, L.A. and Mullins, C.E., 1985. The use of plaster of Paris in the study of soil structure. Soil Use Manag., 1: 70-72.

Greenland, D.J., 1977. Soil damage by intensive arable cultivation: temporary or permanent? Philosophical Trans. R. Soc. London, 281: 193-208.

Greenland, D.J., 1981. Soil management and soil degradation. J. Soil Sci., 32: 301-322.

Kooistra, M.J., 1991. Micromorphological approach to the interactions between soil structure and soil biota. Agric. Ecosystems Environ., 34: 315-328.

Kooistra, M.J., Bouma, J., Boersma, O.H. and Jager, A., 1984. Physical and micromorphological characterization of undisturbed and disturbed ploughpans in a sandy loam soil. Soil Tillage Res., 4: 405-417.

Kooistra, M.J., Juo, A.S.R. and Schoonderbeek, D., 1990. Soil degradation in cultivated alfisols under different management systems in south western Nigeria. In: L.A. Douglas (Editor), Soil Micromorphology: A Basic and Applied Science. Proc. VIII Int. Working Meeting on Soil Mircromorphology, San Antonio, Texas, July 1988. Developments in Soil Science 19, Elsevier, Amsterdam, pp. 123-148.

Lawrance, G.P., 1977. Measurement of pore size in fine textured soil: a review of existing techniques. J. Soil Sci., 28: 527-540.

Mackie-Dawson, L.A., Mullins, C.E., Goss, M.J., Court, M.N. and FitzPatrick, E.A., 1989. Seasonal changes in the structure of clay soils in relation to soil management and crop type. II. Effects of cultivation and cropping at Compton Beauchamp. J. Soil Sci., 40: 283-292.

Moran, C.J. and McBratney, A.B., 1992. Acquisition and analysis of three-component digital images of soil pore structure. II. Application to seed beds in a fallow management trial. J. Soil. Sci., 43: 551-566.

Moran, C.J., Koppi, A.J., Murphy, B.W. and McBratney, A.B., 1988. Comparison of the macropore structure of a sandy loam surface soil horizon subjected to two tillage treatments. Soil Use Manage., 4: 96-102.

Moran, C.J., McBratney, A.B. and Koppi, A.J., 1989. A rapid method for analysis of soil macropore structure. I. Specimen preparation and digital binary image production. Soil Sci. Soc. Am. J., 53: 921-928.

Murphy, C.P., Bullock, P. and Turner, R.H., 1977a. The measurement and characterization of voids in soil thin sections by image analysis: Part I. Principles and techniques. J. Soil Sci., 28: 498-508.

Murphy, C.P., Bullock, P. and Biswell, K.J., 1977b. The measurement and characterization of voids in soil thin sections by image analysis: Part II. Applications. J. Soil Sci., 28: 509-518.

Norton, L.D. and Schroeder, S.L., 1987. The effect of various cultivation methods on soil loss: a micromorphological approach. In: N. Fedoroff, L.M. Bresson and M.A. Coutry (Editors), Soil Micromorphology. Proc. VII Int. Working Meeting of Soil Micromorphology, Paris, July 1985. Association Française pour l'Etude du Sol, Plaisir, France, pp. 431-436.

Pagliai, M., 1986. Effetti della lavorazione e non lavorazione sulla porosità di un terreno franco-argilloso investito a vigneto. Riv. di Agron., 20: 178-183.

Pagliai, M., 1987a. Effects of different management practices on soil structure and surface crusting. In: N. Fedoroff, L.M. Bresson and M.A. Coutry (Editors), Soil Micromorphology. Proc. VII Int. Working Meeting of Soil Micromorphology, Paris, July 1985. Association Française pour l'Etude du Sol, Plaisir, France, pp. 415-421.

Pagliai, M., 1987b. Micromorphometric and micromorphological investigations on the effect of compaction by pressures and deformations resulting from tillage and wheel traffic. In: G. Monnier, M.J. Goss (Editors), Soil Compaction and Regeneration. A.A. Balkema, Rotterdam, pp. 31-38.

Pagliai, M. and De Nobili, M., 1993 Relationships between soil porosity, root development and soil enzyme activity in cultivated soils. In: L. Brussaard and P.J. Kooistra (Editors), Soil Structure/Soil Biota Interrelationships. Geoderma, 56: 243-256.

Pagliai, M. and Pezzarossa, B., 1990. Structure and porosity of silty clay and clay soils in relation to different management practices. Agr. Med., 120: 110-116.

Pagliai, M. and Vittori Antisari, L., 1993. Influence of waste organic matter on soil micro and macrostructure. Bioresource Technology, 43: 205-213.

Pagliai, M., Guidi, G., La Marca, M., Giachetti, M. and Lucamante, G., 1981. Effect of sewage sludges and composts on soil porosity and aggregation. J. Environ. Qual., 10: 556-561.

Pagliai, M., Bisdom, E.B.A. and Ledin, S., 1983a. Changes in surface structure (crusting) after application of sewage sludges and pig slurry to cultivated agricultural soils in northern Italy. Geoderma, 30: 35-53.

Pagliai, M., La Marca, M. and Lucamante, G., 1983b. Micromorphometric and micromorphological investigations of a clay loam soil in viticulture under zero and conventional tillage. J. Soil Sci., 34: 391-403.

Pagliai, M., La Marca, M., Lucamante, G. and Genovese, L., 1984. Effects of zero and conventional tillage on the length and irregularity of elongated pores in a clay loam soil under viticulture. Soil Tillage Res., 4: 433-444.

Pagliai, M., La Marca, M. and Lucamante, G., 1985. Relationship between soil structure and time of landspreading of pig slurry. In: J.H. Williams, G. Guidi and P. L'Hermite (Editors), Long-term Effects of Sewage Sludge and Farm Slurries Applications. Elsevier, Amsterdam, pp. 45-56.

Pagliai, M., Pezzarossa, B., Mazzoncini, M. and Bonari, E., 1989a. Effects of tillage on porosity and microstructure of a loam soil. Soil Technology, 2: 345-358.

Pagliai, M., Pezzarossa, B., Zerbi, G., Alvino, A., Pini, R. and Vigna Guidi, G., 1989b. Soil porosity in a peach orchard as influenced by water table depth. Agric. Water Manage., 16: 63-73.

Ringrose-Voase, A.J., 1991. Micromorphology of soil structure: description, quantification, application. Aust. J. Soil Res., 29: 777-813.

Ringrose-Voase, A.J. and Bullock, P., 1984. The automatic recognition and measurement of soil pore types by image analysis and computer programs. J. Soil Sci., 35: 673-684.

Ringrose-Voase, A.J. and Nortcliff, S., 1987. The application of stereology to the estimation of soil structural properties: a preview. In: N. Fedoroff, L.M. Bresson and M.A. Coutry (Editors), Soil Micromorphology. Proc. VII Int. Working Meeting of Soil Micromorphology, Paris, July 1985. Association Française pour l'Etude du Sol, Plaisir, France, pp. 81-88.

Ristori, G.G., Sparvoli, E. and Martelloni, C., 1989. Microstructure characterization of some italian soil at different water potential. Agr. Med., 119: 175-181.

Shipitalo, M.J. and Protz, R., 1987. Comparison of morphology and porosity of a soil under conventional and zero tillage. Can. J. Soil Sci., 67: 445-456.

Sequi, P., Cercignani, G., De Nobili, M. and Pagliai, M., 1985. A positive trend among two soil enzyme activities and a range of soil porosity under zero and conventional tillage. Soil Biol. Biochem., 17: 255-256.

Serra, J., 1982. Image Analysis and Mathematical Morphology. Academic Press, London, 610 pp.

Sparvoli, E., Ristori, G.G., Landi, L. and Martelloni, C., 1989. Influence of mineralogical composition on the porosity of two clay soils in relation to water content and tillage. Agr. Med., 119: 86-92.

Van Ouwerkerk, C. and Bonne, F.R., 1970. Soil physical aspects of zero-tillage experiments. Neth. J. Agric. Sci., 18: 247-261.

Structural degradation of a prairie soil from long-term management

R.G. Darmody[1] and L.D. Norton[2]

1Department of Agronomy, University of Illinois, Urbana, Illinois, USA
2USDA-ARS National Soil Erosion Res. Lab., W. Lafayette, Indiana, USA

ABSTRACT

Darmody, R.G. and Norton, L.D., 1994. Structural degradation of a prairie soil from long-term management. In: A.J. Ringrose-Voase and G.S. Humphreys (Editors), Soil Micromorphology: Studies in Management and Genesis. Proc. IX Int. Working Meeting on Soil Micromorphology, Townsville, Australia, July 1992. Developments in Soil Science 22, Elsevier, Amsterdam, pp. 641-649.

The Morrow Plots at the University of Illinois are the oldest agronomic research plots in the United States and include the oldest continuous maize (corn) plots in the world. These plots were established in 1876 to study the effect of crop rotations and fertilization on yield. There are three major plots remaining (continuous maize, maize and soybean in rotation, and maize-oats-clover in rotation) and a grass sod border area. Subplots within these plots have received variable rates of lime and NPK fertilizers. The objective of this study was to investigate the effect of long-term crop rotation and fertilization on soil fabric and structural properties.

Fertilization and lime inputs had little effect on aggregate properties or soil fabric. Crop rotations did make a considerable difference in both. Aggregate size and stability decreased in the order: grass sod, maize-oat-clover, maize-soybean, and continuous maize. Soil organic carbon decreased similarly. It was concluded that crop rotation has had a profound effect on structural properties whereas fertilization has not. Although greater biomass was produced with higher levels of fertilization, the type of residues appear more important in maintaining stable soil structure. However, all management systems have had a deleterious effect on soil structural properties and carbon content relative to the undisturbed grass sod soil.

INTRODUCTION

The Morrow Plots on the University of Illinois campus are the oldest agronomic research plots in the USA and include the oldest continuous maize (corn) plots in the world (Odell *et al.*, 1984). They were established in 1876 to study the effect of crop rotations and fertilization on yield and are now designated as a national historic landmark. Three major plots remain; continuous maize, maize-soybean rotation, and maize-oat-clover rotation, and a grass sod border area. Subplots are 101 m^2 and have received variable rates of lime and NPK fertilizers. Rates include: none, recommended level, and in excess of recommended level. The fertility levels (kg ha^{-1}) as established by soil tests are: N, 336 and 224; P, 112 and 45; K, 560 and 336 for the excessive and the recommended levels, respectively. The soil pH is maintained with lime at 6.5 on all fertilized plots. The medium fertilizer plots we studied had barnyard manure added equal to the crop dry matter residue removed each year from 1909-1966. The border is protected by a hedge and has been in grass sod since 1904 with no fertilizer applied. Analysis
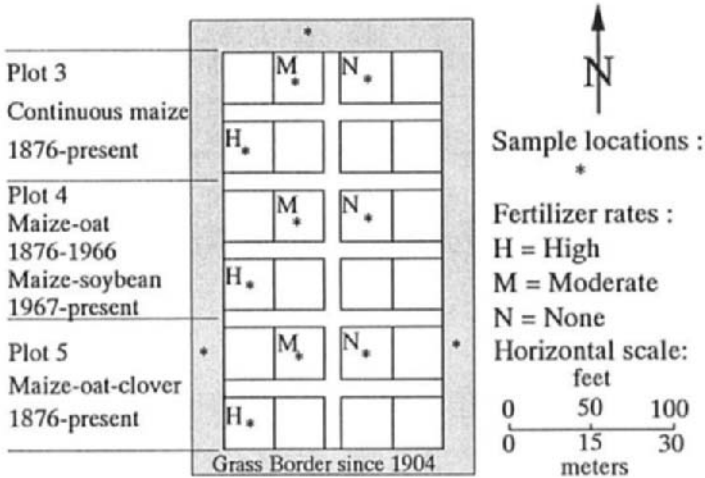
Fig. 1. Layout of Morrow Plots (40° 06'15"N, 88°13'32"W) showing sample locations, crop history, and fertilizer (LNPK) treatments.

of the treatment effects on the soil aggregation was previously done in 1940 by Stauffer *et al.* The crop yields on the plots were most recently compiled by T.R. Peck (pers. comm., 1992).

The climate in Urbana, Illinois is humid temperate continental, with mean monthly temperatures of -3° C in January and 24° C in July (Bryan and Wendland, 1987). The average annual precipitation is 864 mm with wide annual variations. About 85% of the precipitation falls from April through September. The number of frost-free days in a year ranges from 178 to 205. The elevation is about 225 m a.s.l. The soil of the plots is Flanagan silt loam, a fine, montmorillonitic, mesic Aquic Argiudoll (Fehrenbacher *et al.*, 1984). Slope is 1.5%. The mollic epipedon is about 46 cm thick. The soil developed under tall grass prairie vegetation in 102 to 152 cm of Peoria loess over late Wisconsinian age, calcareous loam glacial till.

The objective of this study was to investigate the effect of long-term crop rotation and fertilization on soil fabric and structural properties as compared to uncultivated adjacent areas.

MATERIALS AND METHODS

Samples were collected from selected subplots in September 1991. This was the one year out of six in the crop rotation scheme when all the plots were in maize (Fig. 1).

We wanted to assess the long-term and not recent condition, so we delayed sampling until the crop was mature but still standing to minimize effects of annual cultivation. The samples from the plots were collected from between the rows where there were no obvious wheel tracks. An additional set of samples were taken from the grass border around the plots. Four disturbed samples were taken from each sampled plot to analyze aggregate stability and size distribution and soil organic carbon content. Two *in situ* surface soil samples were taken from each plot by excavating a small (15 × 15 × 15 cm) pedestal which was encased in plastic insulating foam. The foam was sprayed into a moat around the pedestal, where it expanded as an annulus around the soil and dried quickly allowing excavation and transportation of the sample to the lab. This procedure was necessary because the soil was very dry, highly aggregated and very friable which made it difficult to retrieve undisturbed samples.
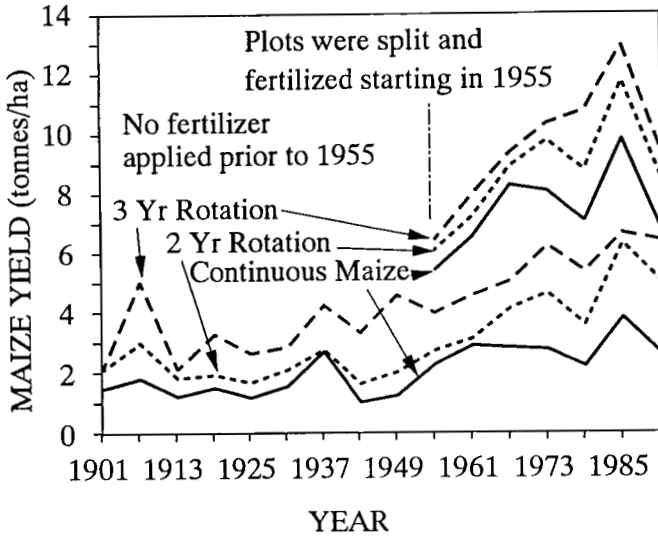
Fig. 2. Maize (corn) yields on the Morrow Plots, 1901-1991. (Source: T.R. Peck, pers. comm., 1992).
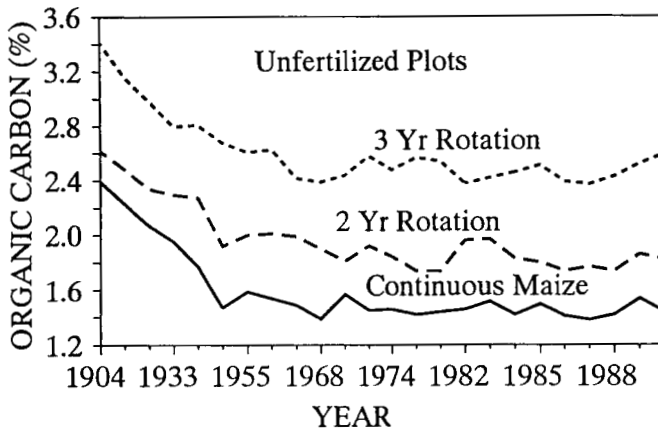
Fig. 3. Soil (0 - 15 cm) organic carbon content on the Morrow Plots, 1904-1990. Determined by wet combustion. (Source: T.R. Peck, pers. comm., 1992).

In the laboratory, the *in situ* samples were placed on moisture tension tables and equilibrated to 10 cm tension to increase soil cohesion. Following equilibrium, Kubiena tin (75 × 100 × 50 mm deep) samples were obtained from the upper surface. These were air dried then heated in steps at 40, 60, 95 and 105°C. Shrinkage was minimal and uniform in all samples. After drying, the samples were impregnated with epoxy resin containing fluorescent dye (Innes and Pluth, 1970). One 50 × 75 mm vertical thin section was taken from the center of each sample and prepared using standard petrographic techniques. Final polishing was on a Logitec lapping machine. These were the first thin sections known to be prepared from the Morrow Plots. Photomicrographs of the thin sections were made in plane polarized light.

Table 1
Aggregate size analysis of Morrow Plot soils (0 - 15 cm), 1991.

	Rotation			
	Continuous Maize	Maize-Soybean	Maize-Oat-Clover	Sod Border
D_{50}†	0.44‡	0.57	0.75	3.47
		Fertilizer treatment		
	High	Moderate	None	
D_{50}	0.61	0.54	0.60	

† Diameter (mm) of sieve passing 50% of the aggregates.
‡ All rotation effects are significantly different ($\alpha = 0.01$), but fertilizer effects are not significantly different ($\alpha = 0.10$) by Duncan's multiple range test.

Table 2
Soil (0 - 15 cm) organic C contents at the Morrow Plots, 1991.

Rotation	Fertilization	Organic C%	
Maize	None	1.45 c	Rotation Avg.
	Moderate	1.51 b	
	High	1.98 a	1.65 d
Maize/ Soybean	None	1.84 b	
	Moderate	1.99 a	
	High	2.01 a	1.95 c
Maize/ Oat/ Clover/	None	2.63 a	
	Moderate	2.43 b	
	High	2.58 a	2.55 b
Grass Border			4.56 a
Fertilizer Average	None	1.91 b	
	Moderate	2.03 b	
	High	3.06 a	

Means followed by same letter within a group are not significantly different by Duncan's multiple range test ($\alpha = 0.01$).
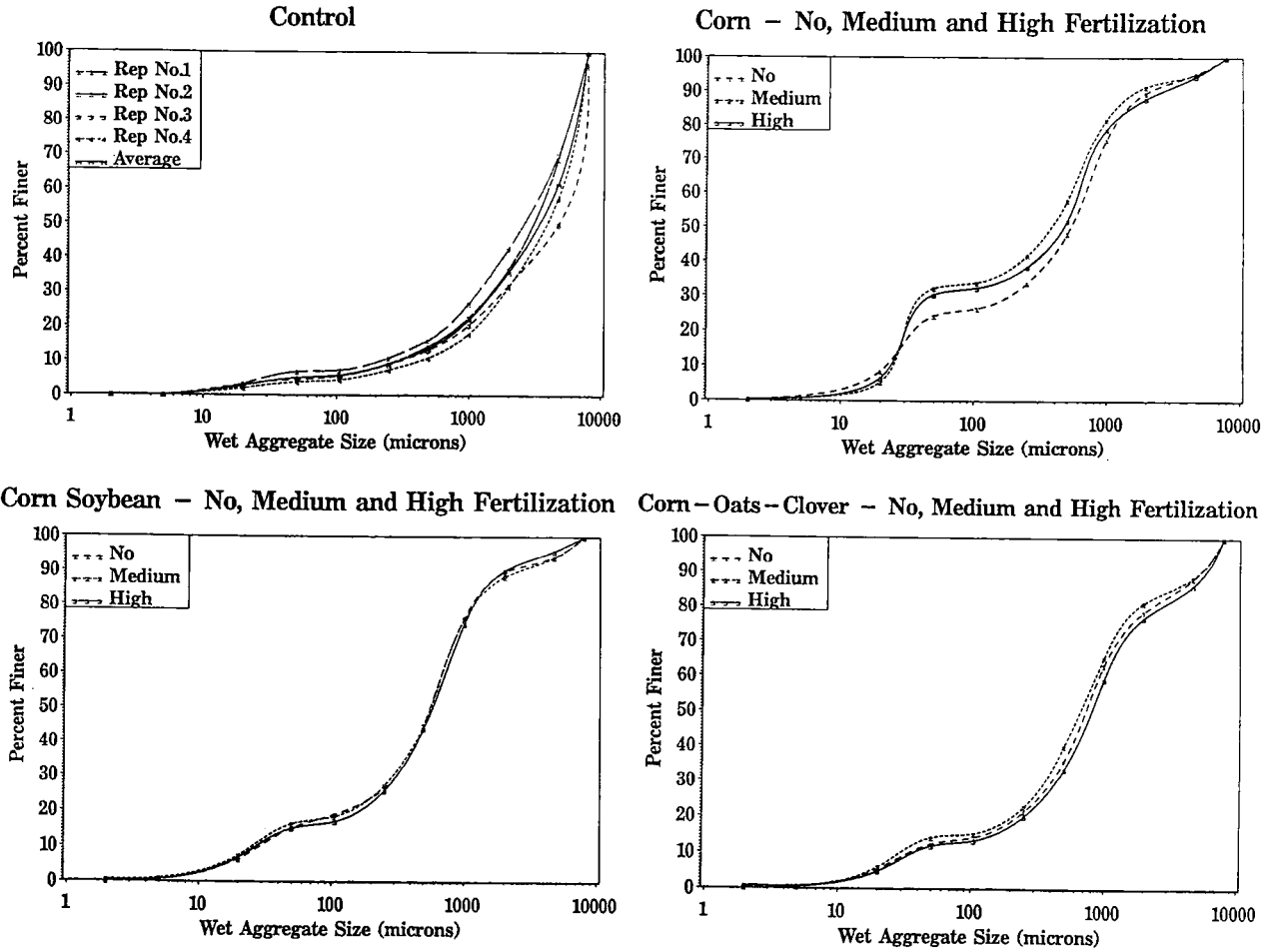
Fig. 4. Aggregate size distribution of Morrow Plot surface (0 - 15 cm) soils.
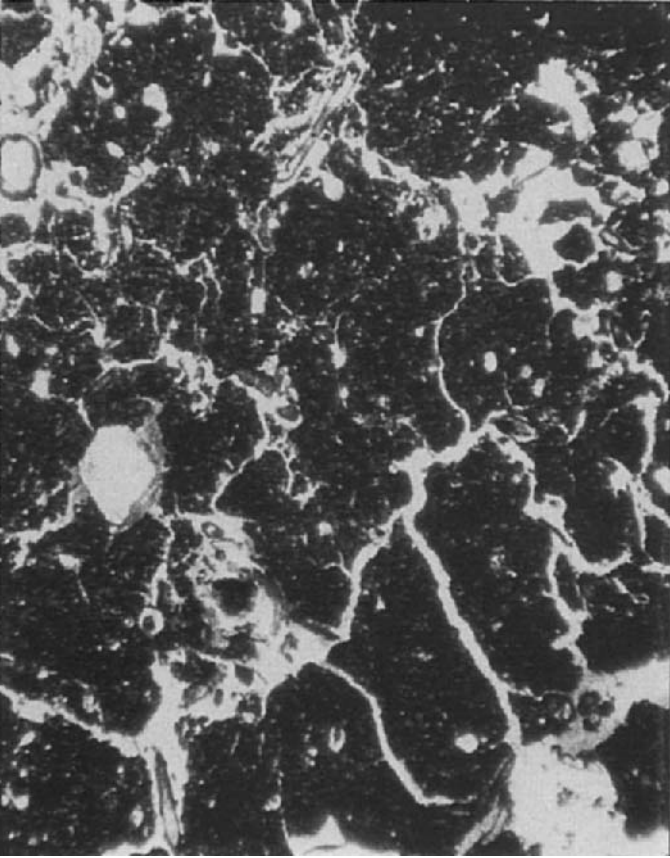
Fig. 5. Vertical thin sections of selected Morrow Plot surface soil, grass sod, no fertilizer. Plane polarized light (PPL); soil surface towards top; frame width 9 mm. Soil organic carbon is 4.56% and D_{50} is 3.47 mm.
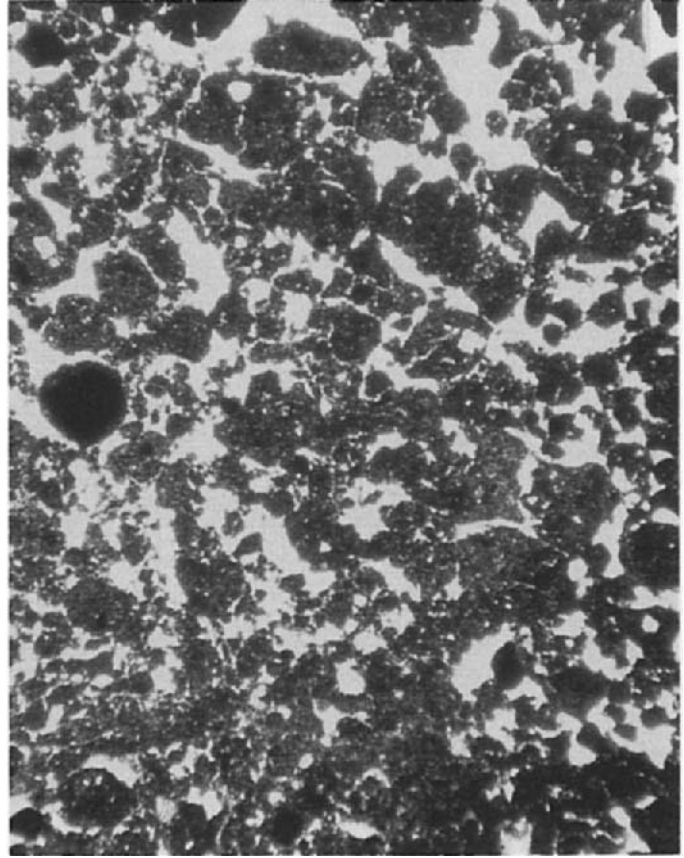
Fig. 6. Vertical thin sections of selected Morrow Plot surface soil, continuous maize, no fertilizer. PPL; soil surface towards top; frame width 9 mm. Soil organic carbon is 1.45% and D_{50} is 0.50 mm.
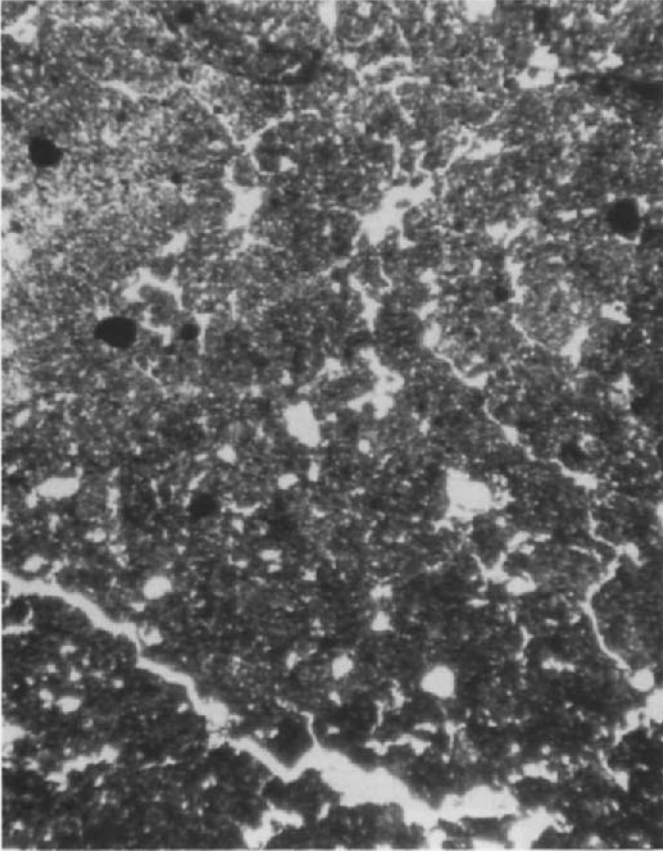
Fig. 7. Vertical thin sections of selected Morrow Plot surface soil, maize-soybean rotation, moderate fertilizer. PPL; soil surface towards top; frame width 9 mm. Soil organic carbon is 1.99% and D_{50} is 0.57 mm.
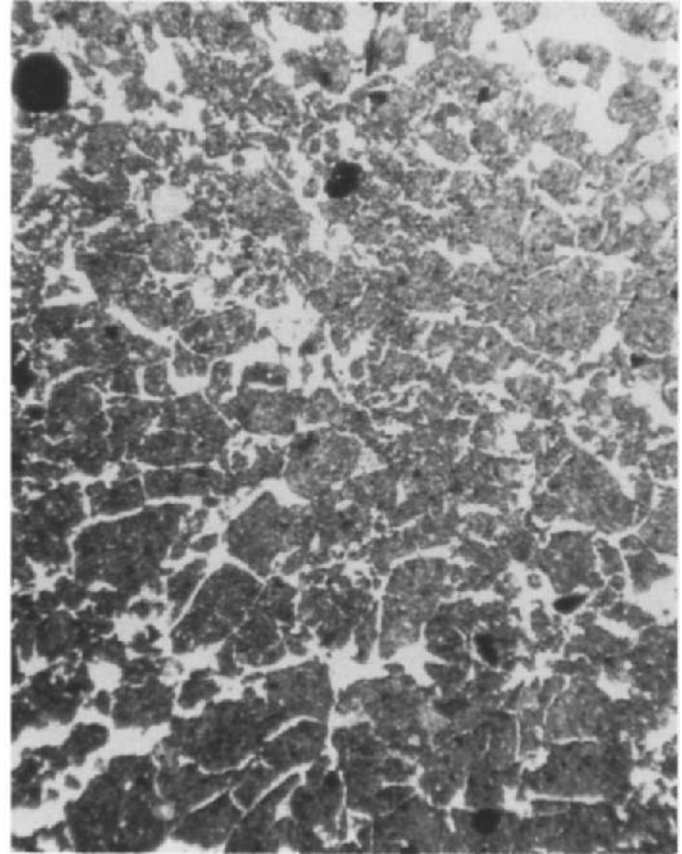
Fig. 8. Vertical thin sections of selected Morrow Plot surface soil, maize-oat-clover rotation, high fertilizer. PPL; soil surface towards top; frame width about 9 mm. Soil organic carbon is 2.58% and D_{50} is 0.78 mm.

Aggregate size and stability were determined by wet sieving (Kemper and Chepil, 1965). Soil organic carbon was determined by dry combustion (Allison, 1965). Results of the carbon and aggregate analyses were tested at a significance level of $\alpha = 0.01$ with Duncan's multiple range test for mean differences (SAS Institute, 1988).

RESULTS AND DISCUSSION

Crop rotation at the Morrow Plots has historically had a strong effect on crop yields. Maize yields are inversely related to frequency of maize in the rotation (Fig. 2). Addition of fertilizer in 1955 increased yields, but the effects of rotation still remained. Crop rotation has also influenced soil organic carbon content (Fig. 3). Soil samples taken in 1991 primarily show the effects of crop rotation. The soil from the grass border area had more large water stable aggregates and organic carbon (Fig. 4, Tables 1, 2) than the cropped areas.

The water stable aggregate content at 50% passing (D_{50}) was over three times greater in the grass border area than in the best crop rotation (maize-oat-clover). This is in general agreement with earlier results (Stauffer et al., 1940) indicating that most changes associated with cultivation occur rapidly. A decrease in water stable aggregation has been demonstrated to occur in one to three years after cultivation (Angers et al., 1992). Water stable aggregates have an important impact on soil erosion. High D_{50} values indicate high infiltration rates, lower runoff rates, lower erosion rates and greater root and air penetration.

Fertilizer treatments on the Morrow Plots had less effect than crop rotation on the measured parameters. Stauffer et al. (1940) also found that the rotation effect was greater than the fertilizer effect on aggregation and soil organic carbon on the Morrow Plots. A weak response to NPK fertilizer was also recently found by Hadas et al. (1990) who worked with a Typic Chromoxerert in Israel.

Thin sections of the surface (0 - 15 cm) soil of the Morrow Plots support the wet sieving and organic carbon data and predominately show rotation effects. The grass sod border (Fig. 5) is distinctly different from the cropped soils in pore-size distribution, pore continuity and s-matrix. The sod border microfabric is mullgranoidic (Pawluk and Bal, 1985) and the entire plasma forms discrete tightly packed mull-like units. The border is subjected to occasional traffic associated with tillage of the plots which may account for the tight packing. Soil organic carbon content of this sample was 4.56% and the D_{50} value was 3.47 mm.

The microfrabric of the unfertilized continuous maize plot (Fig. 6) reflects its low soil organic carbon content and unstable aggregates. Its microfrabric is mullgranoidic and the aggregates are smaller. Faecal pellets and Fe-Mn accumulations are distributed throughout the thin section. Soil organic carbon content of this sample was 1.45% and the D_{50} value was 0.50 mm. The maize-soybean (Fig. 7) and the maize-oat-clover (Fig. 8) thin sections are more similar to the mullgranoidic microfrabric and represent intergrades to the sod plot reflecting an increase in water stable aggregates and organic C. Soil organic carbon contents of these samples were 1.99 and 2.58% respectively. The D_{50} values were 0.57 and 0.78 mm respectively. Macropores may or may not be related to water stable aggregate size (D_{50}). However, there generally should be more large continuous pores capable of conducting air and water in soils with high D_{50}. Soils with well developed macropores also are more productive.

CONCLUSIONS

Fertilization and lime inputs had little effect on aggregate properties or soil fabric. Crop rotations did make a considerable difference in both. Aggregate size and stability decreased in the order: grass sod, maize-oats-clover, maize-soybean, and continuous maize. Soil organic carbon decreased similarly. It was concluded that crop rotation has had a profound effect on structural properties whereas fertilization has not. Although greater biomass was produced with higher levels of fertilization, the type of crop residues appear more important in maintaining stable soil structure. However, all management systems decrease soil organic carbon, aggregate stability, and macropore continuity relative to the undisturbed grass sod soil.

ACKNOWLEDGEMENTS

REFERENCES

Allison, L.E., 1965. Organic carbon. In: C.A. Black (Editor), Methods of Soil Analysis, Part 2. Agronomy 9, Am. Soc. Agron., Madison, Wisconsin, USA, pp. 1367-1378.

Angers, D.A., Pesant, A. and Vigneux, J., 1992. Early cropping-induced changes in soil aggregation, organic matter, and microbial biomass. Soil Sci. Soc. of Am. J., 56: 115-119.

Bryan, A.A. and Wendland, W.M, 1987. Local Climatological Data Summary Champaign-Urbana, Illinois 1888-1986. Illinois Water Survey Miscellaneous Publication 98, Illinois State Water Survey, Champaign, Illinois.

Fehrenbacher, J.B., Alexander, J.D., Jansen, I.J., Darmody, R.G., Pope, R.A., Flock, M.A., Voss, E.E., Scott, J.W., Andres, W.F. and Bushue, L.J., 1984. Soils of Illinois. Ag. Exp. Sta. Bull. 778, University of Illinois, Urbana, Illinois, 85 pp.

Hadas, A., Hadas, A. and Quinton, J., 1990. Long-term effects of high application rates of NPK fertilizer on tensile strength and water stability of the soil structure. Geoderma, 47: 381-392.

Innes, P.P. and Pluth, D.J., 1970. Thin section preparation using an epoxy impregnation for petrographic and electron microprobe analysis. Soil Sci. Soc. Am. Proc., 34: 483-485.

Kemper, W.D. and Chepil, W.S., 1965. Size distribution of aggregates. In: C.A. Black (Editor), Methods of Soil Analysis. Agronomy 9, Am. Soc. Agron., Madison, Wisconsin, pp. 499-510.

Odell, R.T., Walker, W.M., Boone, L.V. and Oldham, M.G., 1984. The Morrow Plots - A Century of Learning. Ag. Exp. Sta. Bull. 775, University of Illinois, Urbana, Illinois, 22 pp.

Pawluk, S. and Bal, L., 1985. Micromorphology of selected Mollic epipedons. In: L.A. Douglas and M.L. Thompson (Editors), Soil Micromorphology and Soil Classification. Soil Sci. Soc. Am. Special Pub. No. 15. Madison, Wisconsin, pp. 63-83.

SAS Institute, 1988. SAS/STAT Users Guide v. 6.03. SAS Institute, Cary, North Carolina, USA.

Stauffer, R.S., Muckenhirn, R.J. and Odell, R.T., 1940. Organic carbon, pH and aggregation of the soil of the Morrow Plots as affected by type of cropping and manurial addition. J. Am. Soc. Agron., 32: 819-832.

This Page Intentionally Left Blank

Micromorphological characteristics of soils of different fertility in north eastern China

Zi-qin Gao and Xi-ming Guan

Institute of Applied Ecology, Academia Sinica, Shenyang, P.R. China

ABSTRACT

Gao, Zi-qin and Guan, Xi-ming, 1994. Micromorphological characteristics of soils of different fertility in north eastern China. In: A.J. Ringrose-Voase and G.S. Humphreys (Editors), Soil Micromorphology: Studies in Management and Genesis. Proc. IX Int. Working Meeting on Soil Micromorphology, Townsville, Australia, July 1992. Developments in Soil Science 22, Elsevier, Amsterdam, pp. 651-658.

The micromorphology of north eastern China's cultivated soils with various levels of tillage and fertility were studied particularly those with differing cultivation and amelioration practices. The methods used were micro-aggregate composition and soil structure observations by petrological and scanning electron microscope. The results show that the fertility of north eastern China's cultivated soils, namely humidified black soils, low fertility black soils, ameliorated albic soils, and meadow type paddy soils can be identified by their micromorphology. Differentiating features of these soils include the iron-manganese content, the constitution of plasma materials, skeleton grains, aggregates, the void distribution pattern and plant residues. north eastern China has a frigid-temperate climate, where seasonal freezing and thawing plays an important role in the soil evolution process. Processes include oxidation-reduction, due to alternate drying and wetting, and organic matter decomposition. This is the major mechanism of soil aggregation and void creation.

INTRODUCTION

Black soil, albic soil, brown soil and meadow soil are the major soils used for the cultivation of wheat, corn and beans in north eastern China. In order to understand principles for management of soil productivity, the mechanisms by which these soils are productive needs to be fully understood. To this end research needs to consider not only the nutrient retention capacity, nutrient release and the interactions between soil temperature, water and atmosphere, but also soil microstructure. Microstructure characteristics include the degree of aggregation, microaggregate size distribution and the stability and arrangement of aggregates and pores. This paper investigates these characteristics for the above soils.

The micromorphological characteristics of the above soils, both in non-irrigated farmland and paddy fields, with various levels of fertility were investigated using the petrological (Brewer, 1972, 1974) and scanning electron microscopes (SEM) (Low and Stuart, 1974; Lynn and Frossmand, 1979).

SAMPLING

Samples were taken from cultivated soils (20 - 30 cm) developed in river or lake alluvial clay deposits. Their microaggregate and particle size distributions were measured (Table 1) and their structure coefficient calculated. The latter is the proportion of clay incorporated into microaggregates and defined as:

$$SC = \frac{a-b}{a} \cdot 100$$

where a is the clay content (*i.e.* particles <0.001 mm) and b the content of clay sized microaggregates <0.001 mm. The size distributions of water stable aggregates was also measured (Table 2).

Black soil is one of the major fertile soils in China. It has a thick humic layer (humus content 3 - 7%) and a high natural fertility which varies with the thickness of the humic layer.

Albic soil is of low fertility with poor soil properties and low yield. After forage legume cultivation and manuring its colour becomes grey to dark grey with improved soil microstructure and increased yield.

Brown soil and meadow soil have been cultivated to paddy field when they develop the fertility characteristics of paddy soils.

RESULTS

Experimental results show that the micro-structure characteristics of soils with different levels of productivity can be distinguished through micromorphological observation. The microstructure and porosity depend on texture, fertility, organic matter and soil water. Soil fertility conditions can be easily identified by the micro-structure and porosity of soils, which can be easily observed in thin sections.

Micromorphological characteristics Black soils

Black soil is one of the most productive cultivated soils in north eastern China. It has well developed microaggregates (Fig. 1a) in which humus is important as a stabilizing agent. Small aggregates are formed from 4 to 5 globes adhering together and larger ones by 10 to 20 globes. According to their size, these aggregates can be divided into three grades, namely primary, secondary and tertiary aggregates, together with many transition grades. These aggregates of adhering microaggregates form a loose but non-dispersed structure. They are coated by dark brown humus (Fig. 1b), which permeates their surface giving it a smooth appearance and imparting stability, which maitains porosity and water holding capacity.

In very fertile Black soils, the voids are well distributed and interconnected in a dendritic organization within and between the aggregates (Fig. 1b). Occasional macrovoids appear as branches of channels created by plant roots. Under SEM (Fig. 1c and d) the average size of microaggregates in the fertile Black soil is 1 - 5 μm mixed with some smaller microaggregates less than 0.5 μm. The aggregate surfaces appear wavy due to humus coatings. Surfaces take on a mamillate form due to the humus coating the inorganic fraction in the organic-inorganic clay complex.

Table 1.
Yield ranges of Black and Albic soils and their microaggregate and particle size distributions and structure coefficients (SC).

Soils		Wheat yield	Depth	Microaggregate size distribution (%)							SC
				Particle size distribution (%)							
				1.000 -0.500	0.500 -0.250	0.250 -0.050	0.050 -0.010	0.010 -0.005	0.005 -0.001	≤0.001	
		t/ha/y	cm				mm				%
Black soil	higher fertility	5.3-6.8	0-22	3.1	8.7	25.0	39.4	11.7	11.2	0.9	96
				2.4	4.1	3.9	34.7	8.8	23.0	23.2	
	lower fertility	2.3-3.0	0-18	2.5	7.3	14.7	42.9	13.7	14.2	4.7	86
				1.0	1.8	4.3	26.9	11.9	21.0	33.1	
Albic soil	ameliorated	2.3	0-18	2.7	2.5	12.8	47.6	16.2	17.8	0.4	98
				2.0	1.8	10.2	27.2	14.2	18.6	26.0	
	unameliorated	1.1	0-13	3.4	4.6	19.0	40.2	20.2	11.8	0.8	95
				2.8	3.3	11.3	37.2	12.8	15.8	16.2	

Table 2.
Water-stable aggregate size distribution.

Soils		Depth	Aggregate size distribution (%)					
		cm	>5	5-2	2-1	1-0.5	0.5-0.25	<0.25
					mm			
Black soils	higher fertility	0-22	1.1	7.4	36.4	10.4	16.2	28.5
	lower fertility	0-18	1.7	4.2	6.4	18.9	25.9	42.9
Albic soils	ameliorated	0-18	3.3	7.1	3.3	10.8	30.7	44.8
	unameliorated	0-13	5.2	9.7	2.2	7.5	14.4	61.0

By contrast, Black soils with low fertility possess a more compact microstructure. The microaggregates are more densely packed (Fig. 1e). Large, irregular particles (10 - 20 µm) consist of quartz grains and small, dark microaggregates and are separated by intersecting channels. Under SEM, these are polyhedral with rough, loosely adhering surfaces (Fig. 1f).

Micromorphology of Albic soils

Albic soils are very low yielding soils in north eastern China. Below the 20 cm deep plough layer, the soil is grey in colorand very compact with few roots able to penetrate. It is poorly drained and becomes anaerobic in the rainy season. Conversely, in the dry season it becomes very cracked and hardened with poor retention of available water. Micromorphological observation of the plough layer shows it consists chiefly of primary microaggregates (Fig. 2a) forming a loosely gelatinous structure and an agglomeritic fabric. The albic horizon chiefly consists of grey coloured fine silt with some dark brown ferrous humic particles of various
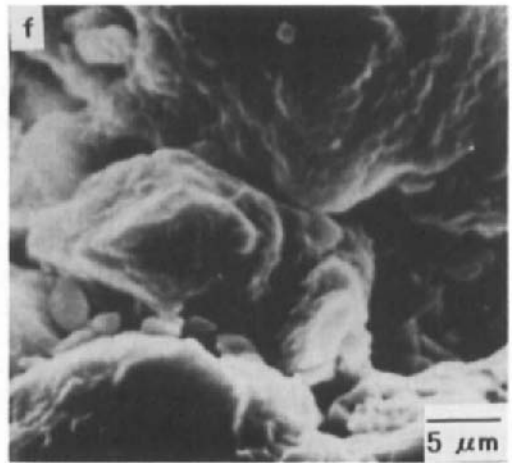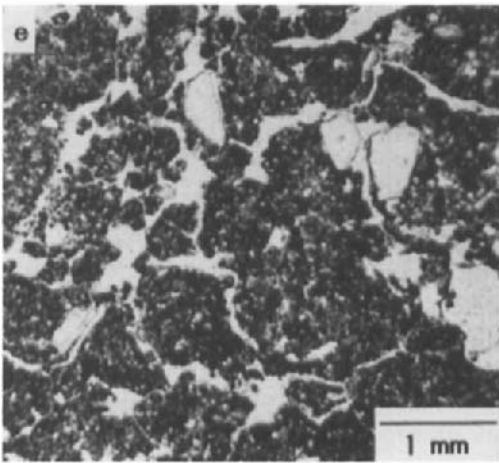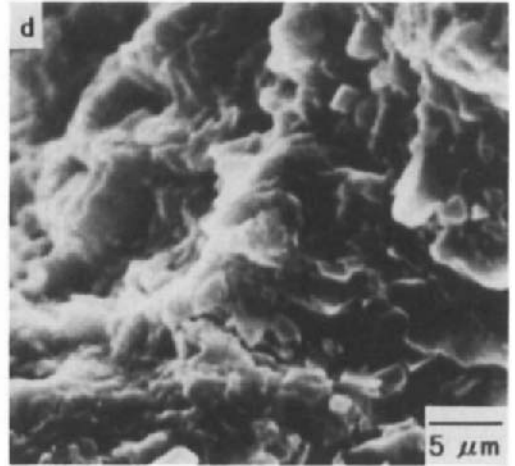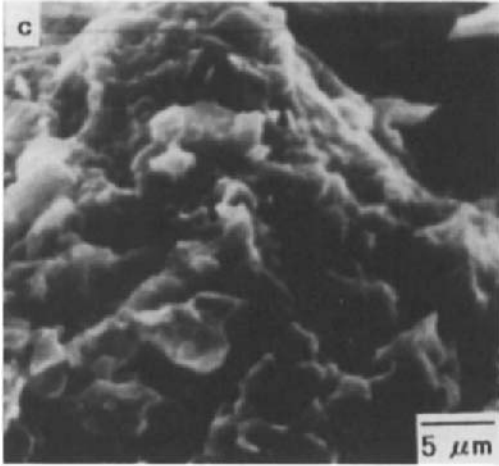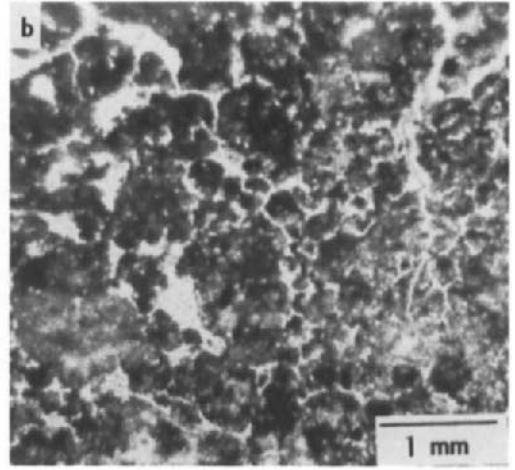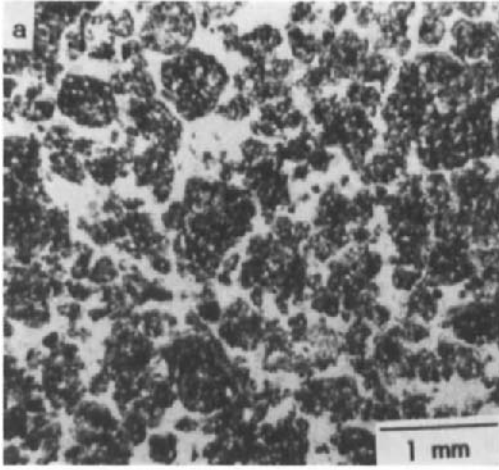
sizes (Fig. 2b). Under SEM it had a loose grain structure without gelatinous substances (Fig. 2c).

In soils which have been ameliorated by manuring, the plough layer has some humus colloids which appear to bridge the larger particles. There are few voids between the large aggregates (Fig. 2d). SEM observation confirms the thin sections findings and shows there are small soil particles with flocculated substances on their surfaces which bond the grains together.

Micromorphological characteristics of paddy soils

The micromorphological characteristics of paddy soil profiles are quite different to those of dryland soils. In natural conditions, their surface layers appear loose and unstructured. Under the influence of periodical wetting and drying, humus colloids and oxidized iron are often seen on the soil surface or at the bottom of a plough layer. In these situations, the voids are small fissures and horizontal cracks, resulting from freeze-thaw.

The meadow type paddy soils

Meadow paddy soils are heavy textured with good microstructure. Blocky structures develop with periodic drying and wetting cycles (Fig. 3a). Channels are formed by rice roots. There are many yellow-brown rust spots in the form of woollen gelatine substances, which wrap the surfaces of loose quartz particles, along void surfaces. These rust spots diffuse outwards from the voids with their colour gradually thinning (Fig. 3b). Often fine root residues occur in voids. In these fracture structures, there are clay particles and gelatinous coatings of oxides (Fig. 3c).

In less fertile paddy soils, there are tightly arranged particles with fewer root holes, fine voids and rust spots and streaks.

Brown type paddy soils

These soils are light textured. The porosity consits chiefly of fine voids with large voids or fissures in the soil profile. As a result of good oxidation conditions, there are many oxide deposits in the form of diffuse spots or stripes (Fig. 3d). There are gelatinous deposits of non-diffusion state in the plough sole. These flocculation substances disperse in the bottom layer, in the form of rust spot and small glutinous coatings in fractures.

Clearly, the difference between paddy soils and dryland soils is that, under flooded conditions, the glue action of humic and clay particles does not form aggregates but flocculated substances which wrap the skeleton particle surfaces. There is little flocculating material in poorer soils.

Fig. 1. Micrographs of the plough/surface layer of a thick Black soil: **a)** with lower fertility showing spongy, highly aggregated fabric with interconnecting dendroid voids (thin section, TS); **b)** with higher fertility showing typical spongy, highly aggregated fabric with gel substances accumulated on the aggregates and dendroid voids (TS); **c)** with higher fertility (SEM); **d)** in a virgin condition (SEM) and **e)** in a virgin condition showing spongy fabric with many sand grains and plant fragments between prismatic aggregates and network and channel voids (TS). **f)** SEM micrograph of the plough layer of a thin Black soil.
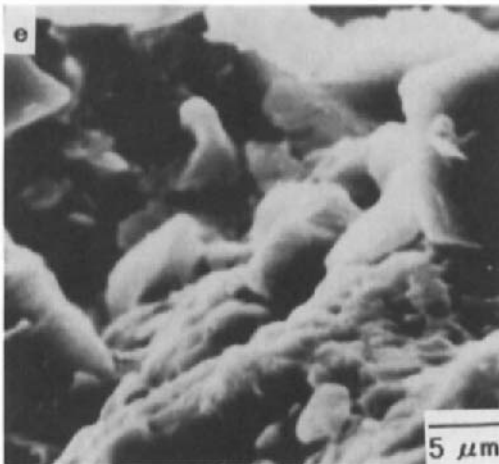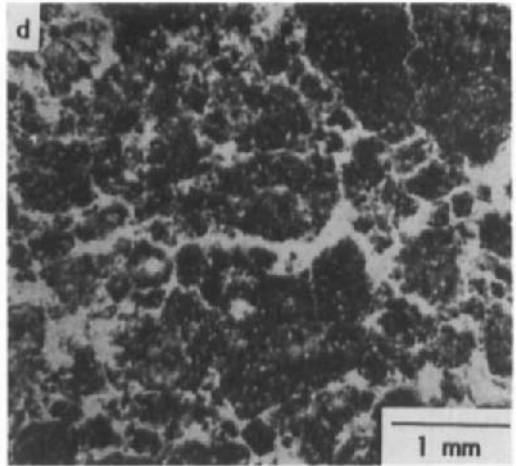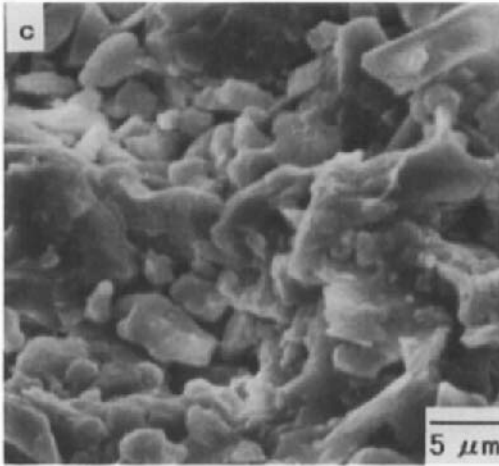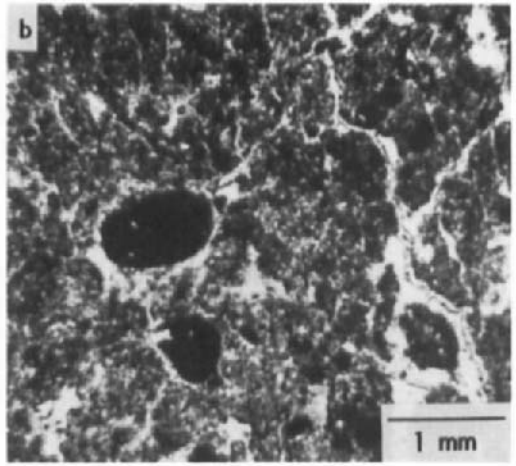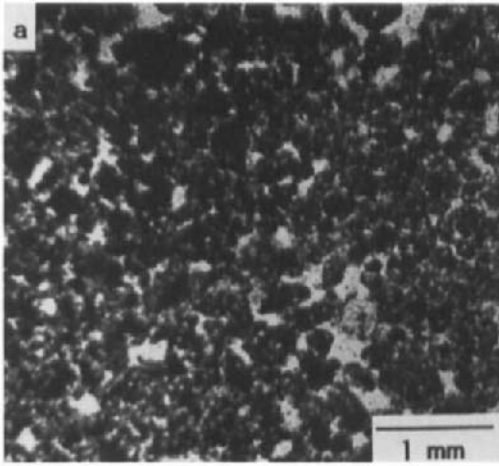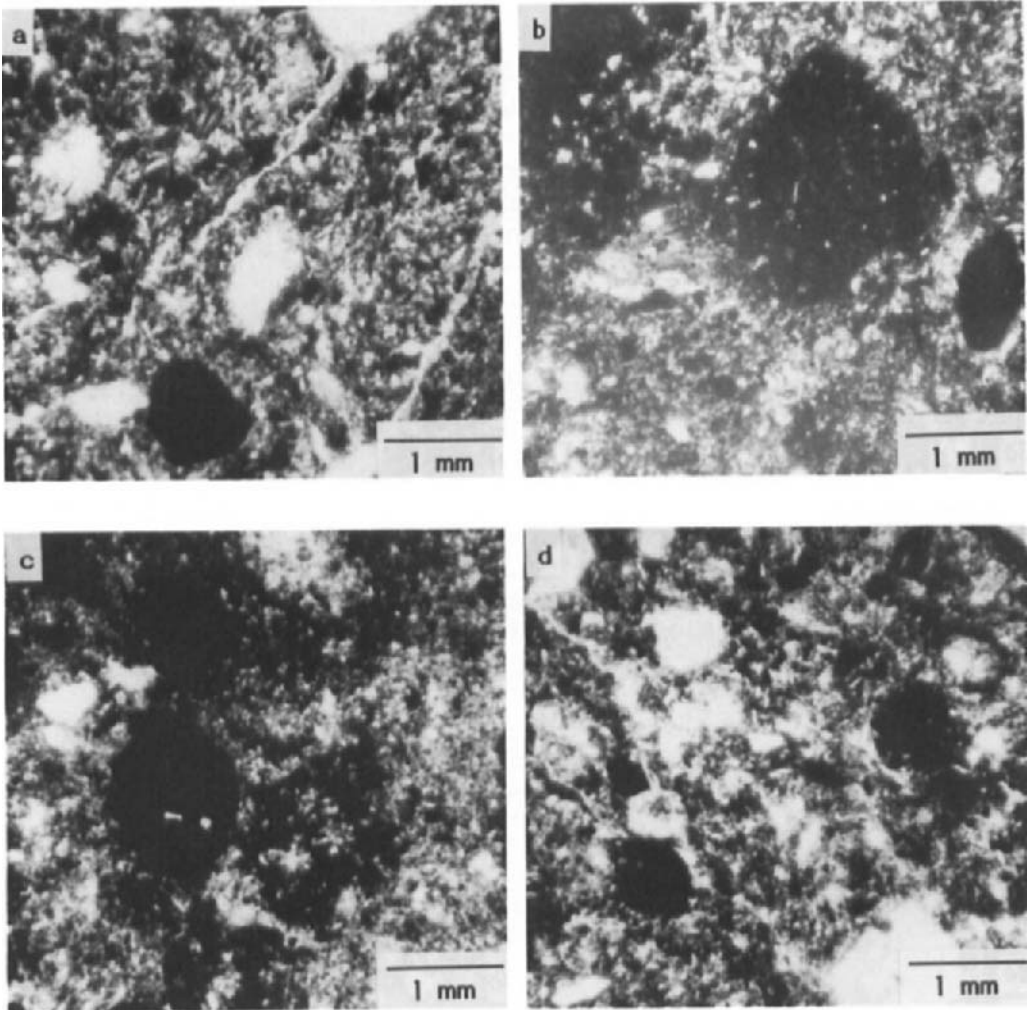
Fig. 3. Thin section micrographs of a meadow type paddy soil showing: **a)** channel voids (11 - 28 cm depth); **b)** rust spots (5.5 - 21 cm depth); **c)** coating (50 - 65 cm depth) and of **d)** a brown type paddy soil showing oxides (28 - 42 cm depth).

Fig. 2. Micrographs of an Albic soil: **a)** plough layer after amelioration showing agglomeritic, weakly aggregated fabric with many sand grains and iron oxide-humic concretions between the aggregates and few voids (TS); **b)** albic horizon showing bleached, unaggregated fabric with many iron oxide-humic concretions and sand grains and channel and chamber voids (TS); **c)** plough layer in unameliorated condition (SEM); **d)** plough layer after amelioration (TS); **e)** plough layer after amelioration (SEM).

CONCLUSION

The micromorphological characteristics of dry-land soils, namely the grade of aggregates, the size of voids and skeleton grains and the humus/organo-clay coatings can be used as an indicator of soil productivity. In paddy soils, which are under alternative drying and wetting, different parameters need to be used to indicate productivity namely mottle characteristics, the amount of the organo-complex and soil porosity. Such micromorphological characteristics allow evaluation of the structural condition of the soil and hence their productivity.

ACKNOWLEDGEMENTS

REFERENCES

Brewer, R., 1972. The basis of interpretation of soil micromorphological data, Geoderma, 8: 81-94.
Brewer, R., 1974. Some considerations concerning micromorphological terminology. In: G.K. Rutherford (Editor), Soil Microscopy. Proc. IV Int. Working Meeting on Soil Micromorphology, Kingston, Canada, August 1973. Limestone Press, Kingston, Canada, pp. 28-48.
Low, W.J. and Stuart, P.R., 1974. Micro-structure differences between arable and old grassland soils as shown in the scanning electron microscope. J. Soil Sci., 25: 135-137.
Lynn, W.C. and Frossmand, R.B., 1979. Observation of certain soil fabrics with the scanning electron microscope. Soil Sci. Soc. Am. Proc., 34: 645-648.

Soil structure transformations over the growing season - A micromorphological approach

N.W. Hall

Crop and Environment Research Centre, Harper Adams Agricultural College, Newport, Shropshire, TF10 8NB, UK

ABSTRACT

Hall, N.W., 1994. Soil structure transformations over the growing season - A micromorphological approach. In: A.J. Ringrose-Voase and G.S. Humphreys (Editors), Soil Micromorphology: Studies in Management and Genesis. Proc. IX Int. Working Meeting on Soil Micromorphology, Townsville, Australia, July 1992. Developments in Soil Science 22, Elsevier, Amsterdam, pp. 659-667.

The study investigates the frequency of occurrence of structures over the growing season in order to understand which structural attributes change in abundance over the season given that soil structure is a complex mixture of soil aggregate and air space characteristics.

Thin sections were prepared of arable soils on five different parent materials. The soils were Rendolls on Chalk, Typic Hapludalfs on clayey drift, Vertic and Mollic Haplaquepts on alluvium, and Psammentic Hapludalfs on sandstone.

Structure types were delineated on sections at the 1:1 scale and classified using four differentiating characteristics, namely degree of ped development, porosity, ped size (void size if apedal) and void type, and their percentage area measured.

The results show that peds become smaller (>50% peds <5 mm^2 and >80% <40 mm^2) and move into closer packing (10 - 20% voids) but do not loose their identity over the season. Sections showing a lack of ped development become increasingly less common over the season. The results show the role of improved ped packing through consolidation but with shrinkage and swelling maintaining structure particularly on the Chalk.

The paper integrates these findings with those published elsewhere on the influence of the length of time under tillage on structure and on calcium carbonate content, soil colour and interrelationships between structure and erosion. While aspects of good structure are not fully understood, structure changes over the season. This shows the need to optimise management to meet competing needs of agronomy, economy and sustaining the soil resource.

INTRODUCTION

There are two objectives in the physical management of arable soils; namely, creating a suitable seedbed, usually through tillage, and maintaining the number of coarse pores over the growing season (Wild, 1988, pp. 435-441). The latter is achieved by good soil management practices assisted or detracted from by intrinsic soil properties within a given climatic environment.

Table 1
Management classes sampled in the study.

Class 1.	Traditionally cultivated arable land during seed bed preparation and early stages of crop production. Winter crops sampled before mid November and spring crops before June.
Class 2.	As 1 above but at the end of the cycle of crop production or after harvesting but before autumn tillage. Sampled August and September.
Class 3.	Direct drilled cereals early in the annual cycle.
Class 4.	As 3 but late in the cycle.

Table 2
The classification of soil structure types (from Hall, 1990). A structure whose degree of ped development was class 1, whose porosity was class 2, whose ped size was class 2 and whose void type was class B would be denoted 1-2-2-B.

Differentiating Characteristics	Classes			
Degree of ped development	Class 1 Clearly defined peds	Class 2 Partially developed peds	Class 3 Secondary peds	Class 4 No peds
Porosity	Class 1 High	Class 2 Medium	Class 3 Low	
Ped size (or void size in the absence of peds)	Class 1 Large	Class 2 Small		
Void type	Class B Compound packing voids	Class C Curvo planar voids	Class D Planar voids	Class E Vughs

This paper attempts to elucidate structure transformations by investigating structural characteristics associated with arable land early in the annual cycle of crop production compared with late in the cycle.

THE SITES STUDIED AND METHODS USED

Two study areas were chosen which had a range of soils and management histories and had presented erosion problems. One is on the Berkshire Chalk Downland (National grid reference SU 554803) and the other in Oxfordshire (SU 454960). The Downland soils comprise silty clay loam Rendzina soils and clay loams on drift (Jarvis, 1973) which approximate to Typic Rendolls and Typic Hapludalfs (Soil Survey Staff, 1975). In Oxfordshire the soils are light sandy loams, sandy loam terrace soils and clayey alluvium which correspond to Psammentic Hapludalfs, Mollic Haplaquepts and Vertic Haplaquepts. Ninety six vertically orientated

Table 3
Table of results for structure --2-B (*i.e.* occurence or non-occurence of small peds and compound packing pores.

	Management classes (listed in Table 1)				
Structure --2-B	**1**	**2**	**3**	**4**	**TOTAL**
Occurrence	10	32	2	9	**53**
Non occurrence	17	4	4	6	**31**
TOTAL	**27**	**36**	**6**	**15**	**84**

Table 4.
Contingency table for structure --2-B. Frequencies for this structure late in the season versus all other management classes. Expected frequencies are given in parenthesis. *E.g.* the expected frequency of occurence in traditionally cultivated soils later in the season is $36 \times 53/84$ which is 23. In this example structure --2-B is strongly associated with the management class group.

	Management clases (listed in Table 1)		
	Traditional cultivation Late in the season	**All other classes**	**Total**
Occurrence	32 (23)	21 (30)	**53**
Non occurrence	4 (13)	27 (18	**31**
TOTAL	**36**	**48**	**84**

mammoth thin sections were prepared omitting visible wheelings over a three year period and representing the management classes shown in Table 1. The thin sections measured 8×10 cm and were taken from surface samples (0 - 10cm).

Areas of like structure were delineated on overlays at the 1:1 scale. Each area was then measured and classified using the system shown in Table 2. Each structure (*c.* 2 - 4 per section) was classified by visual comparison with reference sections which illustrate modes and ranges for each structure type (Hall, 1980). The definition of terms follows Bullock *et al.* (1985). Curvo-planar voids are transitional between compound packing voids and planar voids.

RESULTS

The structure type frequency data obtained were tested using the Chi square test. The null hypotheses used were based on the general expression that the frequency of occurrence (number of sections in which a structure type occurs) of a structure for a management class was similar to the frequencies expected from the number of times a structure occurred and the number of times each management group was represented. Table 3 shows an example table of results which was converted into the 2×2 contingency table shown in Table 4. This was
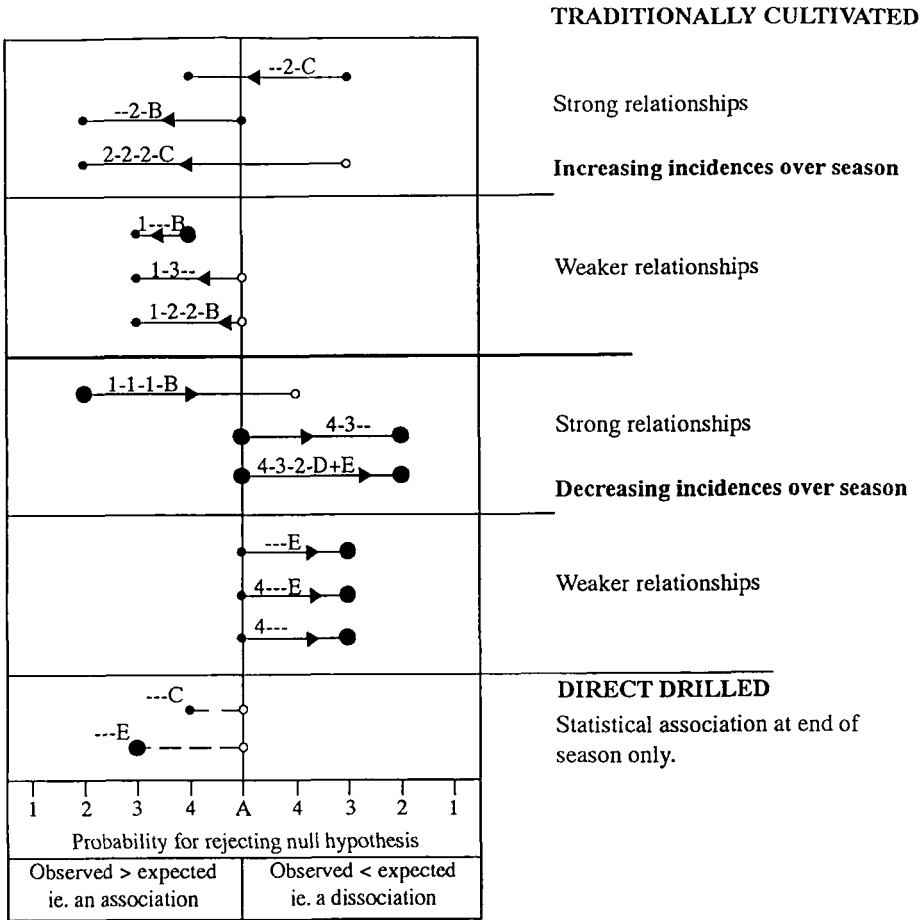
Fig. 1. Changes is soil structure over the growing season. Arrows denote changes from early to late in the cycle of crop production.

Probability % for rejecting the null hypothesis	Dot Size
	Each thin section was divided into areas of like structure, which were then measured. Dot size represents the mean area for each structure.

1 represents	>99.9		●	>	50% mean section area
2	"	99.9 - 99	•	<	50% mean section area
3	"	99 - 95	○		no rating due to low frequency
4	"	95 - 90			
A	"	<90			

Other structures tested and showing no associations or dissociations:
1---,   2----,   ---B,   --D, 1-2--,   2--C,   2--D,   2--B/C or D,   --1-D,   2-2-2-,   2-2--,   2-3--

repeated for all structures and management classes which met the Chi square requirements. This provided 45 Chi square probabilities for rejecting the null hypothesis for tilled land and 17 direct drilled land. Structures whose probability for rejecting the null hypothesis exceeded 90% and changed between early and late season are shown in Fig. 1. Strong relationships are where probability levels show large changes. This is illustrated by structure 2-2-2-C (*i.e.* partially developed peds with medium porosity, small peds and curvo-planar voids) which changed from an infrequent structure early in the season at the 95 - 99% level to a frequent structure late in the season at the 99 - 99.9% level. Approximately half of all structural associations tested gave statistically significant associations which changed between early and late in the cycle of crop production.

Fig. 1 includes information on the mean area (as a percentage of each section) occupied by a structure. Mean areas less that 50% tend to be mainly in the range 20 - 45% and more than 50% tend to be in the range 52 - 70%. In view of the large range of area values, areas are not discussed at length. A more intensive study would be needed. However, Fig. 1 suggests that structures which become more abundant over the season tend to involve areas less than 50% unlike structures whose incidence decreased over the season which tend to occupy large areas of thin sections.

Fig. 2 illustrates examples of the structures. In traditionally cultivated soils, the stronger relationships show that peds have become smaller. Ped size class 2 corresponds to more than 50% of peds less than 5 mm^2 and more than 80% less than 40mm^2. In addition peds move into closer packing - porosity class 2 corresponds with 10 - 20% voids with curvo-planar voids and to a lesser extent compound packing voids.

The weaker changes show the increasing importance over the season of clearly defined peds with combinations of medium porosity (30 - 50%), low porosity (<30%), small peds and compound packing voids.

Structures decreasing in abundance over the season comprise larger peds with large porosities (>50%) and also structures with no peds together with low porosities or these structures with small voids and planar voids or vughs. The less marked changes show a decreasing incidence of no clear peds and/or vughs.

A comparison between direct drilled and traditionally cultivated fields shows that none of the structures were associated specifically with direct drilling except the individual differentiating characteristics of curvo-planar voids or vughs. These structures were associated with direct drilling at the end of the season.

DISCUSSION AND INTERPRETATION

Individual differentiating characteristic classes do not reveal structural changes. The changes over the season involve two or more differentiating characteristics. In addition, the more significant changes include all the four differentiating characteristics showing that combinations of class groups within degree of ped development, porosity, ped size (or void size) and void type are important. Changes over the season involve *both* classes for soil solids together with classes for air spaces. This shows the importance of measuring a range of soil properties in soil studies. The results show that while peds become smaller and move into closer packing, pedality is maintained at least at the partially developed ped level. Structures with no clear peds become less abundant showing a maintenance of soil structure over the season unlike in some other soils (Dexter, 1976). The Downland site and sandy loam soils are
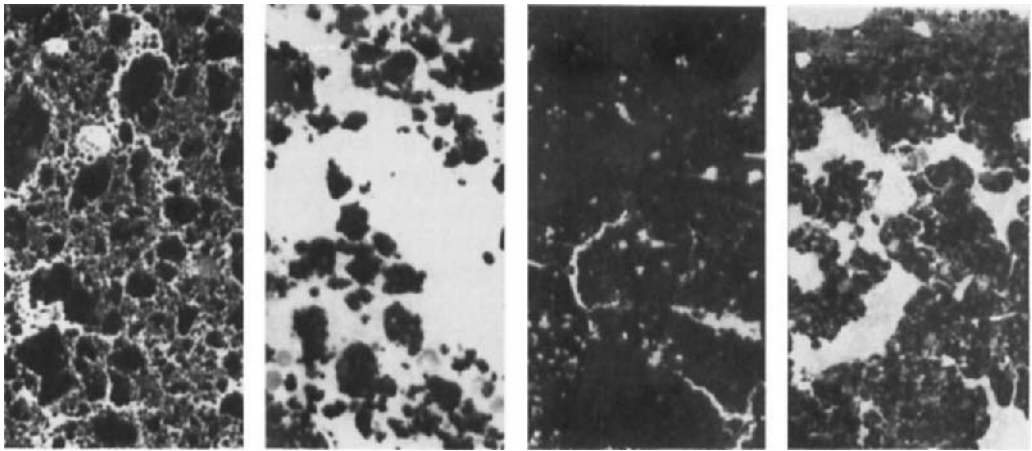
Classification

2-2-2-C/--2-C	1-1-1-B/1--B	4-3-2-D	---E
i.e. Partially developed peds, medium porosity smallpeds, curvoplanar voids.	*i.e.* clearly developed peds, large porosity, large peds, compound packing voids.	*i.e.* No clear peds, low porosity small planar voids.	*i.e.* Vughs
These structures are particularly associated with the end of the growing season.	The clearly developed peds together with the compound packing voids are associated with soils late in the season. These characteristics plus high porosity and large peds are dissociated from soils late in the season.	These structures become less common over the season due to fragmentation. Vughy structures do the same but become more common in direct drilled land later in the season.	

Fig. 2. Illustrations of the structures reported in Fig. 1. Frame width 10 mm.

well suited to sequential direct drilling (Cannell *et al.*, 1979) reflecting their ability to maintain seedbed characteristics through shrinkage over the season as shown in other soils by Mackie-Dawson *et al.* (1989). Adequate rooting should assist in water utilisation on the shallow Chalk soils even though upward movement of water is important on these soils (Gregory, 1989).
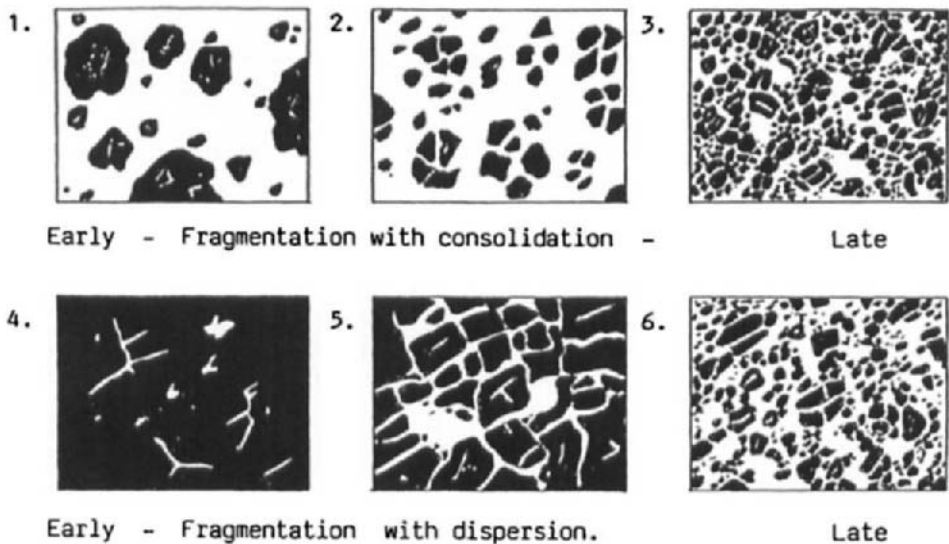
Fig. 3. Soil structure transformations.

Fig. 3 illustrates pathways of structural transformation through fragmentation with consolidation and fragmentation with dispersion possibly producing similar endpoints.

The results for within season changes at the Downland site can be compared with structural associations between long term tilled land (>70 years) and more recently tilled land (<35 years)(Hall, 1990). That study showed that clearly defined peds with compound packing voids or medium porosity are positively associated with long term tilled land. Thus as time elapses within the season, the structures move towards the closer packing of small peds with maintained pedality. This has similarities with the long term effects of tillage on Chalk soils. At the Downland site increasing calcium carbonate contents together with changing soil colour of these calcareous soils focuses on the maintenance of pedality at the partially isolated ped level. The results support the stabilising role of calcium carbonate in structure (Rimmer and Greenland, 1976) and the development of small peds which may be assisted by the lower tensile strength where exchange surfaces are highly dominated by calcium (Dexter and Chan, 1991).

The direct drilling results perhaps demonstrate that as these are surface samples they are disturbed through the action of drilling. Hence these soils have similarities with traditionally cultivated land. This is similar to Ap material shown by Pagliai *et al.* (1984) for a calcareous clay loam. That work demonstrated differences in structure between no till and conventionally tilled treatments but no specific structure exclusive to either. Differences were more in amounts of different voids rather than type of void *per se*.

MAFF (1992) has indicated the need for information on erosion. Relationships between structure types and the incidence of a water erosion fabric on these soils (Hall, 1987) can be applied to these results. In the 1987 study 25 structures occurred in association with an erosion fabric. 10% of these became more abundant over the season, for example partially

developed peds with medium porosity and small peds together with curvo-planar voids. However, 44% become less common over the season for example, structures with the vughly void class. This suggests that the erosion hazard is greatest early in the season supporting the findings of Mutter and Burnham (1990) for Chalk soils.

Structures favouring erosion tended to have large mean areas although their incidence decreased over the season. This suggests that erosion could focus or be initiated at specific points within fields later in the season. Visible wheelings, which were not sampled here, are likely to contain fewer peds and more planar voids (Bresson and Zambaux, 1990) and be the focus of water erosion. Avoiding erosion will require good soil and machinery management including tyre selection (Rusanov, 1991). Field observations and judicous interpretation of profile characteristics would seem to be important in utilising the soil's ability to maintain or improve its structure in an environment of seasonal variability and climatic change (Varallyay, 1990).

CONCLUSIONS

The results demonstrate the importance of both soil and void components and of using more than one parameter in soil structure studies. Peds became smaller over the season and pedality is maintained at the partially developed ped level as peds move into closer packing. This contrasts with the long term effects of tillage on the Chalk soils where increasing calcium carbonate contents through erosion are associated with even more strongly developed pedality and compound packing voids. Within season structural changes suggest that the water erosion hazard decreases over the season which focuses on the need for appropriate machinery management practices.

ACKNOWLEDGEMENTS

REFERENCES

Bresson, L.M. and Zambaux, C., 1990. Micromorphological study of compaction induced by mechanical stress for a Dystrochreptic Fragiudalf. In: L.A. Douglas (Editor), Soil Micromorphology: A Basic and Applied Science. Proc. VIII Int. Working Meeting on Soil Mircromorphology, San Antonio, Texas, July 1988. Developments in Soil Science 19, Elsevier, Amsterdam, pp. 33-40.

Bullock, P., Fedoroff, N., Jongerius, A., Stoops, G., and Tursina, T., 1985. Handbook for Soil Thin Section Description. Waine Research Publications, Wolverhampton, U.K., 152 pp.

Cannell, R.Q., Davies, D.B., Mackney, D and Pidgeon, J.D., 1979. Suitability of soils for sequential direct drilling of combine-harvested crops in Britain: a provisional classification. In: M.G. Jarvis and D. Mackney (Editors), Soil Survey Applications. Soil Survey Technical Monograph 13, Harpenden, Hertfordshire, U.K.

Dexter, A.R., 1976. Internal structure of tilled soils. J. Soil Sci., 27: 267-278.

Dexter, A.R. and Chan K.Y., 1991. Soil mechanical properties as influenced by exchangeable cations. J. Soil Sci., 42: 219-226.

Gregory, P.J., 1989. Depletion and movement of water beneath cereal crops grown on a shallow soil overlying Chalk. J. Soil Sci., 40: 513-523.

Hall, N.W., 1980. An Integrated Macro and Micro-pedological Approach to the Study of Soil Structure. Ph.D. thesis, University of Reading, U.K.

Hall, N.W., 1987. An application of micromorphology to evaluating the distribution and significance of soil erosion by water. In: N. Fedoroff, L.M. Bresson and M.A. Coutry (Editors), Soil Micromorphology. Proc. VII Int. Working Meeting of Soil Micromorphology, Paris, July 1985. Association Française pour l'Etude du Sol, Plaisir, France, pp. 437-443.

Hall N.W., 1990. Micromorphology and complementary assessments of soil structure description and their relationship to length of time under tillage and calcium carbonate contents. In: L.A. Douglas (Editor), Soil Micromorphology: A Basic and Applied Science. Proc. VIII Int. Working Meeting on Soil Mircromorphology, San Antonio, Texas, July 1988. Developments in Soil Science 19, Elsevier, Amsterdam, pp. 53-60

Jarvis, M.G., 1973. Soilsof the Wantage and Abingdon District. Memoirs of the Soil Survey of Great Britain, England and Wales, Harpenden, U.K., 200 pp.

Mackie-Dawson, L.A., Mullins, C.E., Fitzpatrick, E.A. and Court, M.N., 1989. Seasonal changes in the structure of clay soils in relation to soil management and crop type. 1. Effects of crop rotation at Cruder Bay, N.E. Scotland. J. Soil Sci., 40: 269-281.

MAFF, 1992. Ministry of Agriculture, Fisheries and Food, Research Strategy Requirements Document 1992-94. MAFF, London, pp. 29-30.

Mutter, G.M. and Burnham, C.P., 1990. Plot studies comparing water erosion on Chalky and non calcareous soils. In: J. Boardman, I.D.L. Foster and J.A. Dearing (Editors), Soil Erosion of Agricultural Land. John Wiley and sons, Chichester, U.K., pp.15-23.

Pagliai, M., La Marca, M., Lucamante, G. and Genovese, L., 1984. Effects of zero and conventional tillage on the length and irregularity of elongated pores in a clay loam soil under viticulture. Soil Tillage Res., 4: 433-444.

Rimmer, D. and Greenland, D.J., 1976. Effects of calcium carbonate on the swelling behaviour of a soil clay. J. Soil Sci., 27: 129-139.

Rusanov, V.A., 1991. Effects of wheel and track traffic on the soil and on crops growth and yield. Soil Tillage Res., 19: 131-143.

Soil Survey Staff, 1975. Soil Taxonomy. U.S. Dept. Agric. Handb. 436, U.S. Gov. Printing Office, Washington, D.C., 754 pp.

Varallyay, G.Y., 1990. Influence of climatic change on soil moisture regime, texture, structure and erosion. In: H.W. Scharpenseel, M. Schomaker and A. Ayoub (Editors), Soils of Warmer Earth. Developments in Soil Science, 20, Elsevier, Amsterdam, pp. 39-49.

Wild. A., (Editor), 1988. Russells Soil Conditions and Plant Growth. 11th ed., Longman, New York.

This Page Intentionally Left Blank

A pragmatic role for image analysis when assessing compaction in Vertisols

D.C. McKenzie[1], A.J. Koppi[2], C.J. Moran[3] and A.B. McBratney[2]

[1]NSW Agriculture, Biological and Chemical Research Institute, Rydalmere, NSW 2116, Australia

[2]Department of Agricultural Chemistry and Soil Science, University of Sydney, NSW 2006, Australia

[3]CSIRO Division of Soils, GPO Box 639, Canberra, ACT 2601, Australia

ABSTRACT

McKenzie, D.C., Koppi, A.J., Moran, C.J. and McBratney, A.B., 1994. A pragmatic role for image analysis when assessing compaction in Vertisols. In: A.J. Ringrose-Voase and G.S. Humphreys (Editors), Soil Micromorphology: Studies in Management and Genesis. Proc. IX Int. Working Meeting on Soil Micromorphology, Townsville, Australia, July 1992. Developments in Soil Science 22, Elsevier, Amsterdam, pp. 669-675.

Compaction and smearing of the subsoil of Vertisols is a major management problem which restricts root growth and causes cotton lint yield losses as great as 30%. Assessment procedures, for use by both research and advisory staff, to ascertain the severity of the problem are not well defined. An experiment was carried out in a Vertisol used for irrigated cotton production to compare a broad range of procedures for the measurement of soil structural form. Methods were considered in terms of the value of the information that they provided and their expense. We propose that a successful assessment scheme will have to describe both intra-aggregate aeration and strength, particularly within the larger units, and the nature of any continuous vertical macropores that allow roots to bypass inaccessible zones. The soil was studied under a wheeled furrow and below a well-structured ridge, on which the cotton plants are grown, to provide contrasting physical conditions. Examination of vertical and horizontal blocks of soil impregnated with resin containing a fluorescent dye provided evidence of features that are not shown clearly by the other methods, *i.e.* high variability of aggregate size to a depth of 250 mm under the ridge and the presence of fine cracks that may connect the strongly compacted furrow with relatively loose soil under the ridge. The SOILpak score, a semi-subjective, morphology-based measure of soil physical condition used routinely in the field as part of a soil management "expert system", correlated well with the measures of soil strength and aeration over 4 depths, but is prone to bias. Mesomorphological parameters - particularly macroporosity - that were obtained from image analysis of the impregnated blocks followed the same trends as the more conventional measures of soil structure.

INTRODUCTION

Most Australian cotton is grown on Vertisols. Subsoil compaction and remoulding are a major management problem on this soil type, causing lint yield losses as great as 30%. Damage

is due mainly to the adverse effects of traffic and tillage under wet conditions. However, compaction can also occur due to the natural collapse and excessive swelling of aggregates that contain large amounts of exchangeable sodium. Compaction and remoulding usually decrease cotton root growth and profitability due to:

(1) *Poor aeration* when the soil is wet.

(2) *High soil strength* at low water contents, applicable particularly to lateral roots and root hairs which have to extract water and nutrients from within soil aggregates.

(3) *Disruption of continuous vertical channels (macropores)* that allow roots - especially taproots - to bypass problem zones.

Assessment procedures - for use by both research and advisory staff - to ascertain the severity of the problem are not well defined. Methods are available to measure aeration, strength and macroporosity directly, although many of the procedures require complex equipment and are time consuming. When measuring *soil aeration*, oxygen flux density (Hodgson and MacLeod, 1989) is the most sensitive procedure. It is relevant to the biological processes taking place, but it is time consuming and requires expensive equipment. Air-filled porosity is a crude, but useful, first approximation. Hodgson and MacLeod (1989) found that significant oxygen diffusion only occurred when air-filled porosity exceeded 14% in cracking clays used for cotton near Narrabri, northern New South Wales. The most commonly used measuring devices for *soil strength* are penetrometers and shear vanes. These are easy to operate but soil water content needs to be measured at the same time in clay soil to standardise the results if between-site comparisons of the degree of compaction are required. Taylor and Ratliff (1969) have defined critical values of soil strength for cotton root growth. *Soil macropore structure* can be measured using the SOLICON image analysis system described by Moran *et al.* (1990), and modified recently by Koppi and McBratney (1991) to allow large, continuous soil monoliths to be impregnated with resin containing a fluorescent dye prior to video scanning. Vertical and horizontal sections of soil can be examined. Pore space with a diameter as small as 0.2 mm can be detected routinely. Indirect measures of soil structure, such as clod shrinkage indices (McGarry and Daniells, 1987), are also available but are not discussed here.

Unlike research staff, cotton advisors currently do not use such expensive procedures. They rate soil condition visually according to the fineness and hardness of aggregates and the frequency of shiny aggregate faces, using the *SOILpak score* (Daniells and Larsen, 1991). The larger the estimated values are on a scale ranging from 0 to 2, the better the soil structure with respect to cotton growth. Advisory staff use the information, via a soil management "expert system", to determine the most profitable land preparation procedures for the following cotton crop in individual fields. Methods available include deep ripping, gypsum application and minimum tillage. Advisory staff regard the SOILpak score as a useful first approximation, but there appears to be much scope for making their assessment more objective. In addition, the score needs to be related to aeration, strength and macroporosity.

We propose that a successful compaction assessment scheme, both for advisory and research staff, will have to describe both intra-aggregate aeration and strength, particularly within the larger units, and the nature of any continuous vertical macropores that allow roots to bypass inhospitable zones.

This paper describes part of an experiment that was carried out under moist conditions in a Vertisol used for irrigated cotton production. A broad range of procedures for the measurement of soil structural form (defined by Kay, 1990) were compared, in terms of the

value of the information that they provide and their expense, in an attempt to produce field-structure assessment packages. The role of image analysis in relation to other methods is emphasized.

MATERIALS AND METHODS

The site is on a grey clay (Stace *et al.*, 1968) (Entic Chromustert) near Warren (Auscott Ltd., Field 26), NSW, Australia (31°44'S, 147°53'E). Site elevation is 195 m and the mean annual rainfall is about 450 mm. The soil is a medium clay (clay content approximately 50%), and is near-neutral, non-sodic and non-saline, to a depth of 400 mm.

The field was first developed for furrow-irrigated cotton in 1967 after natural rainfed pasture. Numerous operations have since been carried out on the soil but the recent relevant ones are as follows. Following a wheat crop in 1989, before which the soil was in poor physical condition because of two consecutive wet harvests, the dry soil was chisel ploughed in February 1990 with the chisel point set at 350 mm. Shattering occurred between this depth and about 200 mm. In March 1990, 200 mm high ridges spaced 1 m apart were formed with a listing rig pulled by a 'Caterpillar® D8' crawler tractor. They are used to improve drainage in the upper part of the root zone and to direct the flow of irrigation water. Cotton was planted into these ridges in October 1990 under moist conditions which persisted during 2-3 mechanical weeding operations in the following months. In July 1991, after a dry harvest, a light lister was used to reform the ridges in preparation for another cotton crop. The depth of the lister point penetration in the furrows was approximately 120 mm. It should be noted that, before 1989, ridges and furrows were not always kept in the same place, ridges often being inadvertently positioned over old furrows after disc ploughing and re-listing.

When sampled in August 1991, the soil was near 'field capacity' (θ_g = 0.307 kg kg^{-1} ± 0.012; Number of samples (N) = 14), except for the surface 80 mm which was close to permanent wilting point (θ_g = 0.208 kg kg^{-1} ± 0.055 ; N = 2). The soil was studied in duplicate under a furrow, taken as depth zero at the surface, and at the same level below a well-structured ridge where the cotton plants were to be grown. The contrasting sites were within 3 m of each other. The soil was sampled from the sides of 1.5 m deep pits.

Blocks of soil, one vertical and one horizontal, were impregnated with epoxy resin containing a fluorescent dye at each of the 4 locations (Koppi and McBratney, 1991). Vertically oriented blocks were 400 mm high × 150 mm wide and horizontal ones 250 mm × 250 mm at a depth of 150 mm. The tops of the vertical blocks were positioned at the level of the furrow. The method used is the same as Method 1 described by Koppi and McBratney (1991), except that the profile was not sprayed with resin before attaching the backing boards.

The face of each block was ground flat using a disc grinder and scanned under UV light to produce a digital image. The pixel size was 195 × 195 µm for the vertical sections and 390 × 390 µm for the horizontal sections. Image segmentation and pore attribute data were obtained for the vertical images using the SOLICON system (Moran *et al.*, 1990). Mean values of macroporosity, macropore surface area, macropore star length and macrosolid star length were calculated using data from 5 mm wide × 100 mm long strips across each vertical block centred at depths of 50, 150, 250 and 350 mm. The strips contained 25 scan lines, each representing a depth increment of 0.2 mm.
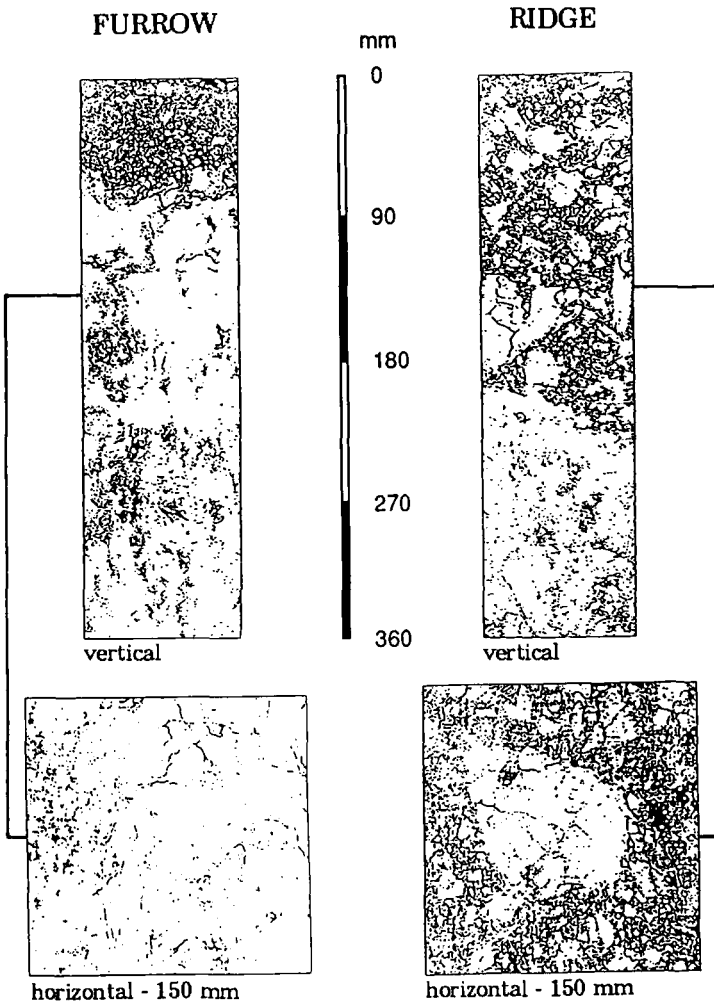
Fig. 1. Representative vertical (360 × 100 mm; pixel resolution 195 μm) and horizontal (200 × 200 mm; pixel resolution 390 μm) SOLICON images of a compacted furrow and an undamaged cotton ridge.

Bulk density, air-filled porosity and gravimetric water content were measured at 50, 150, 250 and 350 mm depth below the furrow level using single 50 mm long, 50 mm diameter thin walled rings. These cores were inserted vertically at each of the 16 sampling points using a large hammer. Soil strength (apparent cohesion) was assessed nearby in duplicate using a 'Geonor' hand-held shear vane. For the lower three depths the vane was inserted horizontally, but at 50 mm depth it was used vertically to avoid the separation and lifting of weakly bonded platey clods. The SOILpak score, described earlier, was also estimated. At each of the 16 sampling points these measurements, and the collection of vertical monoliths, were carried out within about 200 mm of each other.

Linear correlation was used to determine the degree of relationship between the image analysis parameters, air-filled porosity, shear strength and the SOILpak score.

RESULTS AND DISCUSSION

The upper half of Fig. 1 shows a pair of binary images from 2 of the 4 vertical monoliths. Under the furrow the greatest zone of compaction (smallest pore space, shown as black) extends from about 70 to 220 mm below the surface. Beneath this, the amount of pore space increases but there are still relatively large areas without pore space. This suggests that the compaction due to machinery traffic extended below the sample depth. The loose soil above about 70 mm has resulted both from self-mulching of the surface and from slumping of the adjacent ridges.

Under the ridge, above about 200 mm, the soil appears to have large surface area and short aggregate length between relatively large aggregate fragments that appear to have been dislodged by chisel ploughing. The regions of greatest surface area may offer root growth pathways which allow plants to avoid the potential detrimental effects of the massive areas. The more compacted zone below about 200 mm probably remains from the damage caused by the 2 consecutive wet harvests prior to 1990.

A horizontal section (200 × 200 mm) from the centre of the most compacted zone (150 mm depth) under the furrow (Fig. 1) indicates that there are infrequent, vertical cracks within relatively dense soil. These may facilitate water and root movement through a material that otherwise appears to be impermeable. The horizontal section from under the ridge at an equivalent depth (Fig. 1), like the vertical image, shows a large relatively massive lump and several smaller ones, that have persisted since chisel ploughing.

It should be noted that the images do not prove that the observed pore spaces are continuous and connect with the surface. Supplementary procedures, such as those described by Hulme et al. (1991) and Moran and McBratney (1992a, b), are required where dye solutions or resins are applied to the soil surface in the field prior to resin impregnation in the laboratory.

The regression analysis (Table 1) showed that the 4 structural attributes from the binary image parameters, macroporosity, macropore surface area, macropore star length, and macrosolid star length (shown in Table 2), related fairly well to the direct measures of aeration and strength, as did the SOILpak score. These conventional measures of soil compaction, also presented in Table 2, confirm that soil under the furrow was less well aerated and harder, when considered at a similar water content, than soil under the ridge.

CONCLUSIONS

The vertical and horizontal images provide a clear record of the soil structure in the field. The zones of large porosity could probably be used by roots to bypass damaged areas. The images indicate which depths are most crucial for further evaluation, and provide a good impression of the degree of variability. However, the good correlation between the binary image attributes and direct measures of aeration and strength suggest that this further testing may not be required because image measurements are sufficient. A greater range of field sites should be studied to test this conclusion more thoroughly. The SOILpak score, which is cheaper than the other procedures under consideration, also related well to these factors. This confirms its value as a first approximation for use by advisory staff, but the subjectivity of the scoring procedure means that some observers may introduce bias unless regular calibration takes place using more objective procedures such as image analysis.

Table 1

The degree of correlation between the 4 SOLICON binary image parameters, air-filled porosity, shear strength and the SOILpak score. The numbers shown are Pearson product-moment correlation coefficients ($\times$ 100).

VARIABLE	Binary image parameters				Air filled porosity	Shear Strength	SOILpak score
(N=14)	Macro-porosity	Macropore surface area	Macropore star length	Macro-solid star length			
Macro-porosity	100						
Macropore surface area	98	100					
Macropore star length	64	51	100				
Macrosolid star length	-76	-80	-54	100			
Air-filled porosity	64	63	28	-51	100		
Shear strength	-55	-51	-48	33	-70	100	
SOILpak score	75	72	60	-60	74	-77	100

NOTE. Data for the uppermost sampling points under the furrows (total of 2 points) have been excluded from the analysis because of their dryness.

Table 2

Mean soil macroporosity (V_{vp}, mm^3 mm^{-3}), macropore surface area (S_v, mm^2 mm^{-3}), macropore star length (l_p*, mm), macrosolid star length (l_s*, mm), bulk density (BD, Mg m^{-3}), gravimetric water content (θ_g, kg kg^{-1}), air-filled porosity (AFP mm^3 mm^{-3}), shear strength (SV, kPa) and SOILpak score (Spak) as a function of depth under the ridge and furrow.

Site	Depth mm	V_{vp}	S_v	l_p*	l_s*	BD	θ_g	AFP	SV	Spak
Ridge	50	0.17	1.05	0.97	8.74	1.23	0.30	0.18	3.5	1.7
Ridge	150	0.15	0.80	1.27	10.72	1.25	0.31	0.16	3.7	1.7
Ridge	250	0.07	0.49	0.93	17.87	1.24	0.32	0.15	3.7	1.4
Ridge	350	0.15	0.83	1.34	11.78	1.33	0.32	0.09	5.5	1.5
Furrow	50	0.42	1.34	3.06	3.06	1.14	0.21	0.33	9.9	0.2
Furrow	150	0.03	0.21	0.76	37.71	1.43	0.30	0.05	7.9	0.5
Furrow	250	0.06	0.49	0.75	15.72	1.39	0.30	0.07	6.8	1.1
Furrow	350	0.06	0.48	0.78	29.32	1.34	0.30	0.10	6.3	1.4

REFERENCES

Daniells, I.G. and Larsen, D., 1991. SOILpak β: a soil management package for cotton production on cracking clays. NSW Agriculture, Narrabri, Australia.

Hodgson, A.S. and MacLeod, D.A., 1989. Use of oxygen flux density to estimate critical air-filled porosity of a Vertisol. Soil Sci. Soc. Am. J., 53: 355-361.

Hulme, P.J., McKenzie, D.C., Abbott, T.S. and MacLeod, D.A., 1991. Changes in the physical properties of a Vertisol following an irrigation of cotton, as influenced by the previous crop. Aust. J. Soil Res., 29: 425-442.

Kay, B.D., 1990. Rates of change of soil structure under different cropping systems. Adv. Soil Sci., 12: 1-52.

Koppi, A.J. and McBratney, A.B., 1991. A basis for soil mesomorphological analysis. J. Soil Sci., 42: 139-146.

McGarry, D. and Daniells, I.G., 1987. Shrinkage curve indices to quantify cultivation effects on soil structure of a Vertisol. Soil Sci. Soc. Am. J., 51: 1575-1580.

Moran C.J. and McBratney, A.B., 1992a. Acquisition and analysis of three-component digital images of soil pore structure. I Method. J. Soil Sci., 43: 541-549.

Moran C.J. and McBratney, A.B., 1992b. Acquisition and analysis of three-component digital images of soil pore structure. II Application to seed beds in a fallow management trial. J. Soil Sci., 43: 551-566.

Moran, C.J., McBratney, A.B. and Koppi, A.J., 1990. The SOLICON soil imaging system: a description of the software. CSIRO Australia Div. Soils, Report No. 110.

Stace, H.C.T., Hubble, G.D., Brewer, R., Northcote, K.H., Sleeman, J.R., Mulcahy, M.J. and Hallsworth, E.G., 1968. A Handbook of Australian Soils. Rellim Technical Publications, Adelaide, South Australia, 435 pp.

Taylor, H.M. and Ratliff, L.F., 1969. Root elongation rates of cotton and peanuts as a function of soil strength and soil water content. Soil Sci., 108: 113-119.

This Page Intentionally Left Blank

Pore space degradation in Zimbabwean crusting soils

S. Carnicelli[1], G.A. Ferrari[1] and M. Pagliai[2*]

[1]Dip.to Scienza del Suolo, P.le Cascine 15, 50144 Firenze, Italy
[2]CNR, Ist. Chimica del Terreno, V. Corridoni 78, 56100 Pisa, Italy

ABSTRACT

Carnicelli, S., Ferrari, G.A. and Pagliai, M., 1994. Pore space degradation in Zimbabwean crusting soils. In: A.J. Ringrose-Voase and G.S. Humphreys (Editors), Soil Micromorphology: Studies in Management and Genesis. Proc. IX Int. Working Meeting on Soil Micromorphology, Townsville, Australia, July 1992. Developments in Soil Science 22, Elsevier, Amsterdam, pp. 677-686.

A micromorphological and image analysis study was made of three soils from Zimbabwe, showing evidence of structure degradation in the tilled horizon. The aim was to assess the kind of degradation processes operating, paying specific attention to the evolution of the pore system geometry.

Two sequences of porosity degradation were observed. The first involves the transformation of compound packing voids into rounded vughs. A different and independent degradation sequence can be described as an anisotropic compaction that produces planar voids. The first kind of degradation sequence extends far too deep to be attributable only to compaction by raindrop impact; it is most probably due to a hardsetting process. Pore degradation by elongation is clearly related to traffic in wet conditions.

Compaction in Zimbabwean "crusting" soils is thus a more complex process than simple surface crusting. Slaking and traffic in wet conditions are of primary importance and might be the starting point of all degradation phenomena.

INTRODUCTION

Many soils of tropical regions, under arable cultivation, face serious risks of structural degradation (Lal, 1987 pp. 565-617). Structural degradation, or soil compaction, are general terms, used to cover different processes as surface crusting, traffic compaction and hardsetting (Mullins *et al.*, 1987). These processes have different causes and require different remedial strategies. Mullins *et al.* (1990) outlined the need for a diagnostic approach, to identify the prevalent compaction processes in a given soil.

All compaction processes produce an alteration of soil pore space, adversely affecting many soil properties. Nevertheless, the kind of pore space degradation should be process-specific, allowing micromorphological observation and quantification to assist in the detection of active processes and estimation of their relative importance.

---

[*] Present address: Istituo Sperimentale per la Studio e la Difesa del Suolo, Piazza d'Azeglio 30, 50121 Firenze, Italy.

Table 1
Classification and main properties of the Ap horizon of the studied soils.

Soil	Classification	pH* (KCl)	Organic C %	CEC* (soil pH) cmol c+ kg-1	Sand % >53μm	Silt % 2-53μm	Clay % <2μm	Iron Oxides %
MWE	Rhodic Kandiustalf	5.1	0.97	7.6	24.0	45.5	30.6	3.7
SISI	TypicHaplustalf	6.1	1.01	10.8	18.9	53.7	26.4	1.6
BYO	LithicRhodustalf	5.3	1.50	13.3	31.3	33.2	35.6	4.5

*Data from M.T. Pardo, pers. comm., 1991

In Zimbabwe, soils showing serious compaction problems are widespread and are usually described as crusting soils (Nyamapfene and Hungwe, 1986). Field observation shows, however, that the whole Ap horizon is affected by the compaction process, suggesting either hardsetting or compaction by heavy mechanised traffic in wet conditions. This last hypothesis is the one usually put forward by land users, who are forced to carry out some operations, such as planting or herbicide treatments, on quite wet soils, in order to exploit substantial but erratic rains.

The micromorphological study described in this paper aimed to evaluate the relative importance of the different compaction processes in these soils and used image analysis methods to measure the effects of each process on pore space geometry.

MATERIALS AND METHODS

Three sites were selected as most representative of the compaction problems. Two sites, MWE and SISI, are large mechanised farms of north-east Zimbabwe. In these areas, arable cultivation has been established for several decades on all soils that are not too thin or too badly drained. The climate is characterised by a summer rainy season, with an average rainfall of 950 mm/year. In this area, climatic and economic constraints force the use, for cultural operations, of heavy tractors, operating either on dry or quite wet soil. The third site (BYO) is a peasant farm in the south-west region, where annual rainfall is about 690 mm. The soil here has been under cultivation for about five years, but similar, uncultivated soils were found to be seriously affected by overgrazing, with a compaction state not very different from that of cultivated soils.

For each site, a representative profile was described. Classification of soils, according to Soil Taxonomy (1990), and some of their main properties are summarised in Table 1.

Samples were taken in duplicate from each horizon in the profile, plus others from several points on the surface, according to surface morphology. A thin section (6 × 6 cm) was prepared from each air-dried sample and described using the nomenclature of Bullock et al. (1985). Photographs of the thin sections, obtained by multiple exposures with cross-polarised light at different orientations, were analysed (Pagliai et al., 1983) by a Quantimet 570 system equipped with Quic V01.02A software. Pixel size was 30.3 μm, but poroids, defined after Moran et al. (1988), of less than 10 square pixel area were filtered out prior to recording. The following geometrical parameters were measured directly or calculated by the instrument for
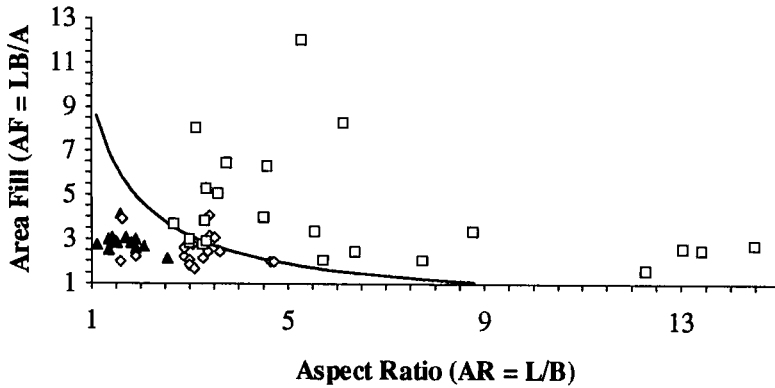
Fig. 1. Compound packing voids, planes and elongated vughs in the learning set plotted in the AF vs. AR pattern space. The hyperbola (—)represents the chosen discrimination line (*i.e.* P= 9.45). ▲ compound packing voids; ◊ elongated vughs; □ planar voids.

every poroid: area (A), perimeter (Pe), length (L) and breadth (B) (the maximum and minimum of 8 feret diameters, respectively) and shape factor ($S = Pe/(4\pi A)^{1/2}$).

On the basis of micromorphological observations, it was deemed necessary to define further shape indexes, to discriminate the following classes of pores: compound packing voids and polyconcave vughs (CPV), convexo-concave vughs (CCV, after Bresson and Boiffin, 1990), vesicles, elongated vughs (EV, vughs having one axis clearly longer than the others), planes (PLN). For this purpose, a learning set was built by using typical poroids from the samples under study: 18 vesicles, 19 convexo-concave vughs, 18 elongated vughs, 24 planes and 14 polyconcave vughs and compound packing voids. The latter two classes of voids were grouped together because an objective criterion for separating them could not be found.

The shape factor, S, was quite effective in discriminating compound packing voids and polyconcave vughs, which have values greater than 5. Distinguishing convexo-concave vughs from vesicles was more difficult, as small deviations from circularity cause vesicles to have S values similar to those of smooth vughs. Therefore, smooth vughs and vesicles were grouped into a single class, regular voids, defined by values of $S < 2.5$. Other convexo-concave vughs were classified as irregular vughs with $2.5 < S < 5$.

Elongated vughs and planes could easily be discriminated from other voids by having aspect ratio (AR) values greater than 2.5, where:

$$AR = \frac{L}{B} \tag{1}$$

AR did not allow effective discrimination between these two classes, because some planar poroids are not rectilinear, but curved, zigzag-shaped or branching. In these cases AR does not estimate correctly the elongation of the poroid. However, it was observed that non-straight planes occupy a small fraction of the area defined by a circumscribed rectangle so that the area fill index, AF, defined as:

$$AF = \frac{LB}{A} \tag{2}$$

might be an effective discriminator. The compound packing voids, planes and elongated vughs classes are plotted in the AF versus AR pattern space in Fig. 1.

Clearly, planes tend to plot above and to the right of a hyperbola whose coefficient, P, equals 9.45 where:

$$P = AF \cdot AR = \left(\frac{LB}{A}\right)\left(\frac{L}{B}\right) = \frac{L^2}{A} \tag{3}$$

This occurs because, whilst AR is high and AF low for straight planes, AR decreases and AF increases as planes become less straight. P, or planarity index, is therefore suitable for discriminating planar pores.

Every poroid was then classified in accordance with the following scheme:

Planes:	poroids with $P > 9.45$
Elongated vughs:	poroids with $P < 9.45$ and $AR > 2.5$
Compound packing voids:	poroids with $P < 9.45$, $AR < 2.5$ and $S > 5$
Irregular vughs:	as above but $2.5 < S < 5$
Regular voids (smooth vughs and vesicles):	as above but $S < 2.5$

This system of void classification was adopted in place of the more refined one proposed by Ringrose-Voase and Bullock (1984) to enable inclusion of compound packing voids and elongated vughs as a separate class and to avoid special-purpose computer programming, since all calculations could be performed on commercial spreadsheet programs.

RESULTS

Field observations

The soil surface at the three sites showed a pattern of narrow ridges, corresponding to crop rows, and depressed inter-rows, still possessing a significant microrelief. Sedimentary crusts were observed in low-lying areas, while in the high-standing ones crusts were of the structural type, either with or without thin sealing layers.

Profile descriptions revealed that structural degradation, indicated by structureless or weak structure states and hardness when dry, involves the whole Ap horizon, which usually extends down to about 30 cm. The tilled horizons in MWE and SISI sites were also observed to be very sensitive to slaking, as clods of all sizes were readily destroyed by immersion in water. These horizons met the criteria reported in Mullins et al. (1987) for hardsetting behaviour in most, but not all the observed volume.

Biological activity, mostly by termites, was observed to be very intense in horizons below the cultivation layer.

Micromorphology

In all three soils, the microstructure of the deep, uncompacted B horizon is dominated by well developed granules and crumbs. It appears that termites play the role of the main structuring agent, binding soil components in stable granules. The level of termite activity
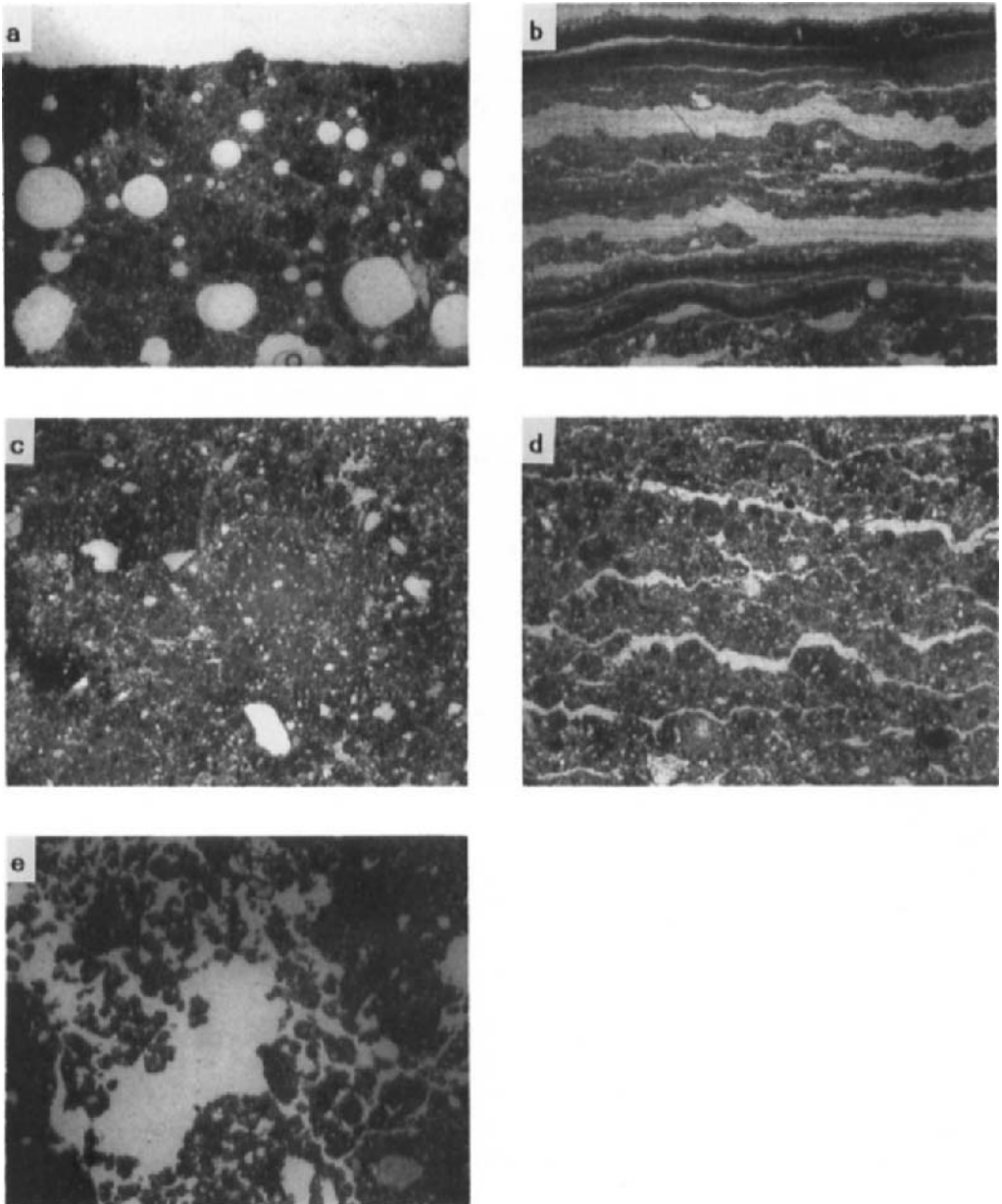
Fig. 2. Microstructure and porosity of typical micro-horizons. a) L1a, b) L1b, c) L2a, d) L2b, e) L4. Plane polarized light. Frame width 5.9 mm.

creates a porosity dominated by compound packing voids, with rare channels and no planar pores. Given the absence of comparable uncompacted soils, the microstructure of the deep

horizons was used as the closest available approximation to an undegraded structure and taken as reference for the estimation of the kind and extent of compaction in cultivated horizons.

In the compacted Ap horizons, different microstructures often coexist in a sample, generally in superimposed layers, or micro-horizons. The following micro-horizon types were recognized:

L1a: (Fig. 2a) Apedal vesicular structure with some depletion of fine materials and relative accumulation of fine sand and silt; stable zoogenic granules still visible, but embedded in the coarser-grained matrix without compound packing voids.

L1b: (Fig 2b) Sedimentary crust, with multiple size-sorted layers and apedal crack structure; planar voids oriented parallel to the surface.

The L1a and L1b micro-horizons are only present at the SISI and MWE sites, where they represent a typical, well separated, surface crust. They characterise, respectively, the sealing layer and the sedimentary crust observed in the field and their depth does not usually exceed 2 cm.

At the BYO site, in a sample from the MWE site (MWE 6) and in two from the SISI site (SISI 4 and SISI 5), no such micro-horizon was observed. In these cases, the structure at the surface still appeared apedal, with low porosity dominated by either vughs or planes. Although these might be termed structural crusts, observations evidenced no unambiguous basis to discriminate this microstructure from that deeper in the Ap. Consequently, structural crusts were considered as type L2 together with all strongly compacted areas in the Ap horizon. Two kinds of L2 micro-horizons were identified (Fig. 2c - d):

L2a: Vughy structure, with either well rounded or convexo-concave vughs.

L2b: Crack structure, with fewer and finer planes than L1b, mostly oriented parallel to the surface.

The L2b micro-horizon is much less common than the L2a, never appearing below 5 cm. When they are both present, L2a is below L2b.

Other micro-horizon types identified were:

L3: Micro-horizons occurring usually below 5 cm depth and showing less severe evidence of compaction, with weakly or moderately expressed crumb structure, some compound packing voids and common vughs.

L4: Uncompacted microstructure of uncultivated horizons (Fig. 2e).

Two processes of pore space degradation were hypothesised by comparing the microstructure of tilled horizons with that of deep, uncompacted horizons. The first is a substitution of compound packing voids with irregular, initially, and then regular vughs that might be termed *isotropic compaction* and was described by Bresson and Boiffin (1990). The second process appears to entail a stretching of the voids along the horizontal axis to create elongated vughs and planar pores and may be defined as *anisotropic compaction*.

Image analysis

Thin sections showing micro-horizonation were subdivided accordingly and each micro-horizon measured separately. Details of sample identity and general structural and porosity character are given in Table 2.

The porosity in each void class in each micro-horizon is shown in Table 3. In both tables, one sample from an uncompacted horizon of each soil is shown for comparison. The area-weighted mean S was calculated excluding planes, on the assumption obtained from visual

Table 2
Sample identities, micro-horizons and general structural and porosity characters.

Sample	Location	Micro-horizon type	Depth[*], cm (upper-lower)	Pedality	Mean S	Total voids %
MWE 1	Surface	L1b	0-1	Apedal	2.2	29.7
MWE 1	=	L2b1	1-3	Apedal	3.1	16.5
MWE 1	=	L2b2	3-6	Apedal	4.1	14.2
MWE 2	=	L1b	0-1	Apedal	2.0	19.0
MWE 2	=	L2a1	1-4	Apedal	2.6	10.4
MWE 2	=	L2a2	4-6	Apedal	2.8	6.0
MWE 3	=	L1a	0-0.6	Apedal	1.8	12.6
MWE 3	=	L2a	0.6-3	Apedal	3.0	5.6
MWE 3	=	L3	3-6	Moderate	13.5	14.9
MWE 4	=	L2a	0-6	Apedal	2.9	10.3
MWE 5	Ap horizon	L2a	27-33	Apedal	2.7	13.0
MWE 6	Ap horizon	L2a	19-25	Weak	5.1	8.5
MWE 7	Ap2 horiz.	L2a	47-53	Apedal	2.3	5.6
MWE 8	Bt2 horiz.	L4	87-93	Strong	18.1	23.1
SISI 1	Surface	L1a	0-3	Apedal	2.2	13.3
SISI 2	=	L1a	0-3	Apedal	2.5	13.1
SISI 3	=	L1b	0-2	Apedal	5.1	19.2
SISI 3	=	L2a1	2-4	Apedal	3.2	9.4
SISI 3	Surface	L2a2	4-6	Apedal	2.1	6.1
SISI 4	=	L2a	0-5	Apedal	2.6	5.0
SISI 5	=	L2b	0-3	Apedal	4.9	12.0
SISI 5	=	L2a	3-6	Apedal	3.2	7.9
SISI 6	Ap horizon	L2a1	3-5	Apedal	3.3	14.6
SISI 6	=	L2a2	5-7	Apedal	2.5	6.7
SISI 6	=	L3	7-9	Moderate	9.0	21.0
SISI 7	=	L3	4-10	Moderate	8.9	10.7
SISI 8	Bt horizon	L4	77-83	Moderate	4.6	14.3
BYO 1	Surface	L2a	0-5	Moderate	6.4	18.4
BYO 2	=	L2a	0-5	Apedal	3.2	10.9
BYO 3	=	L2a	0-5	Moderate	7.2	16.4
BYO 4	Bt horizon	L4	45-50	Strong	50.1	34.9

[*] Averages for non straight limits

observation, that planes do not represent structural porosity in these samples. A comparison between mean S and visual evaluation of void interconnection, estimated from pedality (Bullock et al., 1985), supports the hypothesis by Bresson and Boiffin (1990) that pore shape roughness and interconnection are related.

It appears that in compacted micro-horizons the dominant porosity is due to either regular vughs or planes. The intermediate classes, irregular vughs and elongated vughs, are always less important.

Fig. 3 shows the percentage of total porosity occupied by regular voids versus that for planar voids. L3 and L4 micro-horizons, rich in compound packing voids, plot towards the origin, while compacted micro-horizons tend to scatter close to the axes. L1a and L2a micro-horizons scatter close to x axis while L1b and L2b micro-horizons scatter close to the y axis.

Table 3
Porosity due to each void class in each micro-horizon, in percent of measured void area.

Sample	Micro-horizon	Regular voids %	Irregular vughs %	Compound packing voids %	Elongated vughs %	Planar voids %
MWE 1	L1b	2.7	1.7	0.0	2.3	93.3
MWE 1	L2b1	19.4	10.3	5.5	12.7	52.1
MWE 1	L2b2	18.3	5.7	9.1	3.5	63.4
MWE 2	L1b	4.7	0.0	0.0	2.7	92.6
MWE 2	L2a1	40.8	21.4	0.0	16.4	21.4
MWE 2	L2a2	56.6	21.7	6.7	11.7	3.3
MWE 3	L1a	79.4	14.3	0.0	6.3	0.0
MWE 6	L2a	41.7	11.9	24.9	14.3	7.2
MWE 7	L2a	60.7	16.1	10.7	12.5	0.0
MWE 8	L4	11.3	12.6	68.0	7.4	0.4
SISI 1	L1a	77.5	14.3	2.1	5.3	0.8
SISI 2	L1a	66.9	14.7	7.7	6.9	3.8
SISI 3	L1b	25.0	13.0	12.5	3.6	45.8
SISI 3	L2a1	55.3	19.1	16.0	9.6	0.0
SISI 3	L2a2	64.4	14.6	0.0	11.3	9.7
SISI 4	L2a	36.0	36.0	0.0	16.0	12.0
SISI 5	L2b	14.2	20.8	30.8	4.2	30.0
SISI 5	L2a	45.6	25.3	6.3	20.3	2.5
SISI 6	L2a 1	52.1	20.5	17.1	9.6	0.7
SISI 6	L2a 2	54.4	19.7	6.1	13.7	6.1
SISI 6	L3	21.0	9.9	45.2	21.0	2.9
SISI 7	L3	22.2	13.8	47.3	11.1	5.6
SISI 8	L4	22.9	29.1	15.4	31.9	0.7
BYO 1	L2a	30.6	23.5	30.6	3.3	12.0
BYO 2	L2a	40.4	27.5	11.9	3.7	16.5
BYO 3	L2a	21.2	12.1	49.1	4.3	13.3
BYO 4	L4	6.9	4.3	85.4	3.4	0.0

The central region is empty. It appears, then, that each portion of the tilled horizons was mainly subjected to one of the two types of pore space degradation.

The effects of isotropic compaction were detected throughout the Ap, while anisotropic compaction only appears in surface samples and was not detected at the BYO site.

DISCUSSION

In L1b micro-horizons, the dominance of planar porosity is clearly linked to the genesis of the sedimentary crust. In contrast, micromorphological observation shows that L2b micro-horizons do not belong to the surface crust proper and are the product of some other kind of compaction process. It is highly probable that the genesis of this kind of microstructure is linked to the effect of high axle loads on wet soil, as shown by the experiments of Slowinska-Jurkiewicz and Domzal (1991) and Bresson and Zambaux (1990). However, L2b micro-
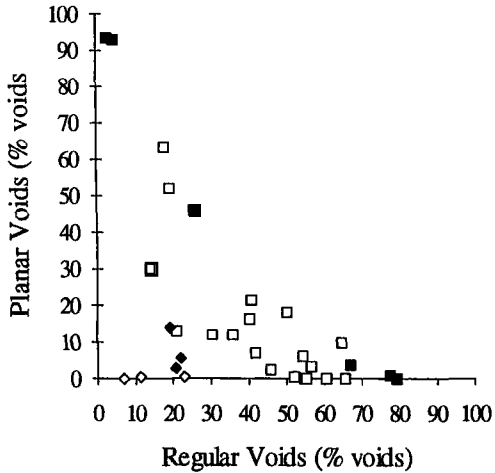
Fig. 3. Percentage of total porosity due to regular voids vs. percentage due to planar voids in the different sampling units. ■ L1; □ L2; ♦ L3 and ◊ L4 microhorizons.

horizons were observed in relatively few samples, which seems to indicate that heavy traffic on wet soil is not the predominant compaction agent in these soils.

The prevailing process of pore space degradation instead appears to be the substitution of compound packing voids by regular vughs, implying a reduction in both the interconnection and roughness of pores. This process can be caused by physico-chemical processes, like slaking and dispersion, as indicated by Mullins *et al.* (1987) as the basis of hardsetting behaviour, or by the action of raindrop impact.

Raindrop impact has been observed to be effective in inducing compaction down to about 5 cm (Bresson and Boiffin, 1990). Therefore, it may be the main compaction process in SISI and BYO soils. In MWE soil, however isotropic compaction extends, without significant differences in magnitude and nature, down to 30 cm. The strong susceptibility to slaking of this soil points to a hardsetting type process. Mobilisation of fine materials and slumping, both typical of hardsetting, should actually be very effective in inducing the kind of pore space modifications typical of isotropic compaction.

CONCLUSIONS

Crusting soils of Zimbabwe undergo structural degradation caused by the actions of different agents that extend beyond the classical definition of crusting. The development of management techniques for improving the structural state of the soils should take into account all the different causes.

The simple system of void classification developed has shown that it is possible to distinguish different types of pore space alteration, each caused by different processes. This allows evaluation of the importance of each process involved in compaction of a soil, which may help in the development of a diagnostic approach for soil compaction.

Isotropic compaction (*i.e.* loss of pore interconnection and smoothing of pore walls) appears, when extended to the whole cultivated horizon, to be the typical kind of pore space degradation associated with the hardsetting process.

Hardsetting seems to be a major compaction process in many Alfisols and Ultisols of the tropical regions. The problem of susceptibility to slaking seems of major importance in dealing with structural degradation of these soils.

ACKNOWLEDGEMENTS

REFERENCES

Bresson, L.M. and Boiffin, J., 1990. Morphological characterization of soil crust development stages on an experimental field. Geoderma, 47: 301-325.
Bresson, L.M. and Zambaux, C., 1990. Micromorphological study of compaction induced by mechanical stresses for a Dystrochreptic Fragiudalf. In: L.A. Douglas (Editor), Soil Micromorphology: A Basic and Applied Science. Proc. VIII Int. Working Meeting on Soil Mircromorphology, San Antonio, Texas, July 1988. Developments in Soil Science 19, Elsevier, Amsterdam, pp. 33-40.
Bullock, P., Fedoroff, N., Jongerius, A., Stoops, G., Tursina, T. and Babel, U., 1985. Handbook for Soil Thin Section Description. Waine Research Publications, Wolverhampton, U.K., 152 pp.
Lal, R., 1987. Tropical Ecology and Physical Edaphology. John Wiley and Sons, Chichester, U.K., 732 pp.
Moran, C.J., Koppi, A.J., Murphy, B.W. and McBratney, A.B., 1988. Comparison of the macropore structure of a sandy loam surface soil horizon subjected to two tillage treatments. Soil Use Manage., 4: 96-102
Mullins, C.E., Macleod, D.A., Northcote, K.H., Tisdall, J.M. and Young, I.M., 1990. Hardsetting soils, behaviour, occurrence and management. In: R. Lal and B.A. Stewart (Editors), Soil Degradation. Advances in Soil Science, 11. Springer Verlag, New York, pp. 37-108.
Mullins, C.E., Young, I.M., Bengough, A.G. and Ley, G.J., 1987. Hardsetting soils. Soil Use Manage., 3: 79-83.
Nyamapfene, K.W. and Hungwe, A.P., 1986. Nature, distribution and management of crusting soils in Zimbabwe. In: F. Callebaut, D. Gabriels and M. De Boodt (Editors), Assessment of Soil Surface Sealing and Crusting. Flanders Research Center for Soil Erosion and Soil Conservation, Ghent, pp. 320-329.
Pagliai, M., La Marca, M. and Lucamante, G., 1983. Micromorphometric and micromorphological investigations of a clay loam soil in viticulture under zero and conventional tillage. J. Soil Sci., 34: 391-403.
Ringrose-Voase, A.J. and Bullock, P., 1984. The recognition and measurement of soil pore types by image analysis and computer programs. J. Soil Sci., 35: 673-84.
Slowinska-Jurkiewicz, A. and Domzal, H., 1991. The structure of the cultivated horizon of soil compacted by the wheels of agricultural tractors. Soil Tillage Res., 19: 215-226.
Soil Survey Staff, 1990. Keys to Soil Taxonomy. 4th edition. SMSS Technical Monograph No. 6, Virginia Polytechnic Institute and State University, Blacksburg, 422 pp.

Changes in sandy Oxisols microfabric after mechanical up-rooting of an oil palm plantation

C. Hartmann[1], D. Tessier[2] and G. Pédro[2]
[1]ORSTOM, BP 181, Brazzaville, Congo
[2]Science du Sol, INRA, 78026 Versailles, France

ABSTRACT

Hartmann, C., Tessier, D. and Pédro, G., 1994. Changes in sandy Oxisols microfabric after mechanical up-rooting of an oil palm plantation. In: A.J. Ringrose-Voase and G.S. Humphreys (Editors), Soil Micromorphology: Studies in Management and Genesis. Proc. IX Int. Working Meeting on Soil Micromorphology, Townsville, Australia, July 1992. Developments in Soil Science 22, Elsevier, Amsterdam, pp. 687-695.

In the savannah of Dabou (Southern Ivory Coast) large oil palm plantations have been established on sandy Oxisols from the 1950's. They were mechanically uprooted after 25 years and replanted. Yield dropped as a result of the use of heavy machinery, accompanied by decreased soil porosity and increased hardness , especially in the AB horizon (40/50 cm). Thin soil sections were observed under ultra-violet light to allow description of the porosity and the organisation of the constituents. In the original plantation, clayey aggregates juxtaposed to the quartz grains were clearly shown. In the re-planted site, 15 years after replanting, the plasma covered the quartz grains, giving a continuous solid phase. TEM observations indicated that the clay crystal arrangement was associated with the location of organic matter. In the original plantation organic matter filled up the pore space of the clay matrix while in the re-planted site organic matter mainly disappeared. Consequences for the management and rejuvenation of sandy Oxisols are discussed.

INTRODUCTION

Soils cultivated in tropical areas may be subject to rapid modifications, not only of their chemical composition but also, maybe more importantly, of their physical properties. The use of machinery can reduce the volume of pores and result in soil deterioration. Such soil degradation was clearly shown on Oxisols, particularly those containing more than 50% clay (Chauvel *et al.*, 1991). Sandy Oxisols have a relative resistance to compaction due to the presence of a rigid skeleton. Nevertheless, this "low" compaction can induce huge changes in soil properties.

Sandy Oxisols of the Southern Ivory Coast are a good example of changes in soil organisation due to mechanical usage. Oil palm trees were first planted in the 1950's on virgin savannah and were replanted after mechanically uprooting the initial palm trees. After re-plantation a decrease of soil porosity of about 10 - 15% was observed and soil water retention was reduced. Furthermore, yield decreased by 20 - 30% at R. Michaud's plantation (Dufour and Olivin, 1985; Caliman *et al*, 1987). However, no structural differences could be seen in the

Table 1

Particle size distribution and some physico-chemical properties of the soil from the original plantation (FP) and the re-planted site (RP).

	Particle size distribution %				Organic C g/100g	pH	CEC mEq/100g
	< 2μm	2-50μm	50-200μm	200-2000μm			
Ap (0-10)							
FP	10.5	4.1	22.2	63.3	2.4	4.5	4.3
RP	11.9	3.4	26.1	58.6	1.2	3.9	1.5
AB (40/50)							
FP	16.1	3.4	18.5	62.0	1.0	4.3	1.2
RP	16.5	2.7	21.0	59.8	0.7	4.2	1.1
B							
FP (150 cm)	19.3	4.4	24.7	51.6	0.5	4.0	1.0
RP (100 cm)	18.1	4.8	22.9	54.2	0.4	4.3	0.9

profile, although hampered root development indicated the formation of a hardened horizon after replanting, with hardness increasing especially in dry conditions (Caliman *et al.*, 1987; Caliman, 1990). Sub-soiling was tested, but induced no yield increase and the hardened horizon is still present.

The aim of this study was to identify changes in soil structure and porosity at different scales of their organisation so as to understand better the changes in both soil physical and mechanical properties after using heavy machinery. Emphasis was put on potential reversibility of the sandy soil deterioration process.

EXPERIMENTAL SITES AND METHODS

Two situations were studied in R. Michaud's plantation at Dabou, 60 km of Abidjan (5°N 4° E). The climate is tropical and annual rainfall varies widely from 1000 to 2500 mm per year.

The soils of the plantation (3.5 km^2) are Oxisols developed on sandy sediments (Tertiary period) with very low field variability. To identify the changes due to the action of heavy machinery four toposequences were studied: two in original plantations (palm trees after savannah) and two on replanted sites (palm trees after up-rooting of the original plantation). On each toposequence, 3 to 4 profiles were studied in different topographic positions (Hartmann, 1991). Comparison was made of two profiles representative of the original plantation (20 years old) and replanted site (15 years old) sampled in similar topographic positions, *i.e.* mid-slope on a gentle slope of approximately 5%.

The soils of the whole plantation are sandy (10% clay in the first horizon) and the clay content increases slightly with depth (30% below 3 m).

In the original plantation the Ap horizon (0 - 30 cm) is very dark grey (10YR3/1) with a weakly developed structure consisting of very fine subangular blocky peds (<5 mm) as a consequence of high biological activity. The AB horizon (30 to 100/130 cm) is very dark greyish-brown (10YR 3/2) with a massive structure containing fine biological channels a few millimeters in diameter.
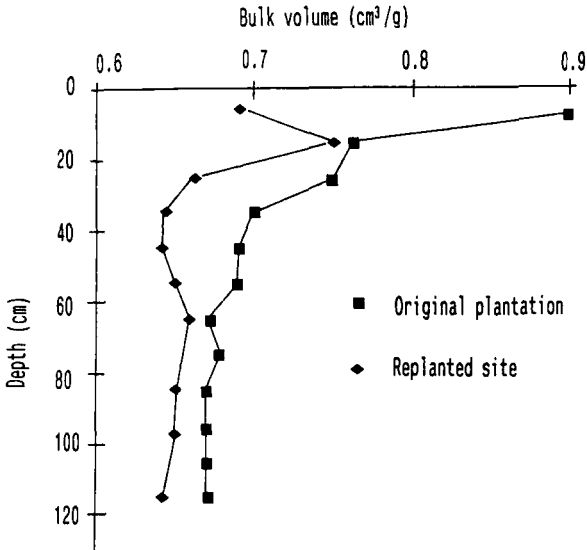
Fig. 1. Bulk volume (cm³/g) of soil samples in original and re-plantation site. Note that the root zone is located between 10 and 30 cm.

In the re-planted site, the Ap horizon is similar. The AB horizon is less developed (30 cm depth to 80/100 cm) with a massive structure containing fewer biological channels. Despite having the same massive structure, cohesion is more important than in the initial plantation, especially when the soil dries. Moreover, during rainfall events, run-off can be seen over the re-planted sites (measurements have not been made).

The results of the mechanical and physico-chemical analysis of these profiles are presented in Table 1.

The specific volume was measured with cylinders (3 replicates) and the results expressed as bulk volume on a dry mass basis (cm³ g^{-1}) *i.e.* the reciprocal of the bulk density. The bulk volume of the replanted soil decreased at all depths, especially between 40 to 50 cm (Fig. 1).

Undisturbed samples of different horizons in all profiles of the 4 toposequences were air-dried and impregnated with a polyester resin containing a fluorescent dye (Uvitex, Ciba-Geigy). Thin sections were observed using incident ultra-violet (UV) light for examining porosity, or using transmitted visible light and incident UV light simultaneously for studying the soil fabric (Hartmann *et al.*, 1992). Only the photographs obtained in the 40/50 cm horizon of the previously described profiles are presented.

On these two thin sections fragments of plasma were taken and embedded in an epoxy resin (Spurr, 1969; Tessier, 1984). After hardening, thin sections of the plasma fragments, 50 nm thick, were prepared with a diamond knife. Electron micrographs at low (10,000×) magnification were obtained using a Philips Model 420 scanning/transmission electron microscope.

RESULTS

When using incident UV light, the sample from the AB horizon of the original plantation was very porous with fine, regularly distributed pores (Fig. 2a). The re-plantation sample, on the contrary, showed less pores, many resembling cracks (Fig. 2b).
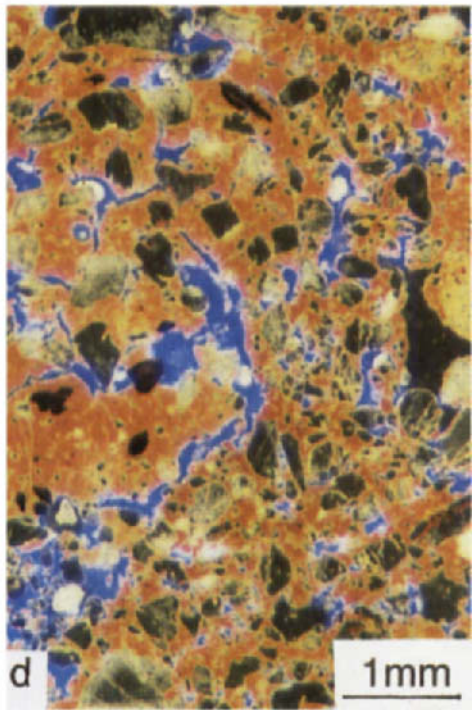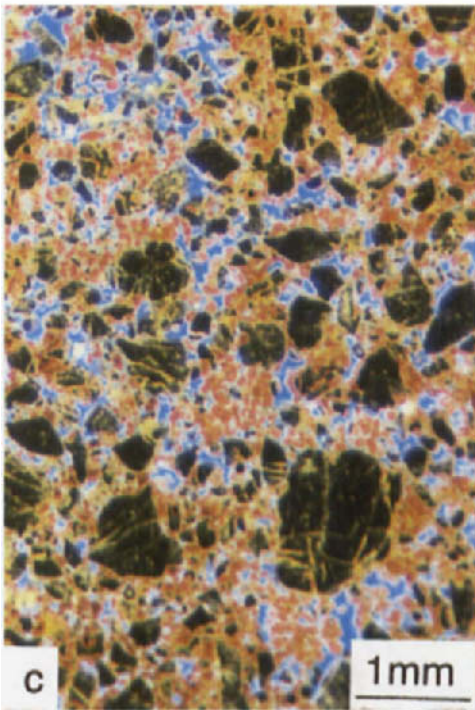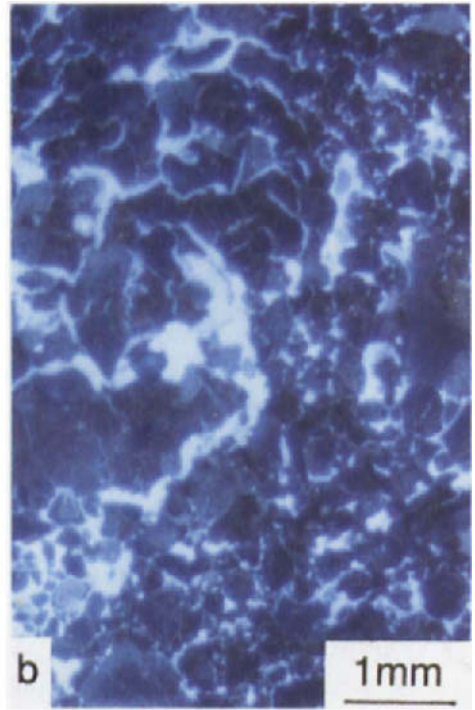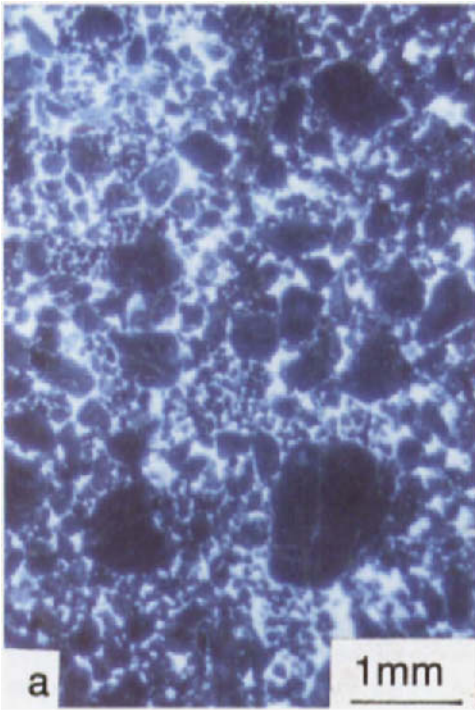
Observation with UV and visible light simultaneously (Hartmann *et al.*, 1992) allowed the pore space (blue), the plasma (dark brown to orange-red) and the quartz grains (black) to be distinguished. In the original plantation, the clay matrix consisted of spheroidal clay micropeds between the quartz grains (enaulic/porphyric intergrade) so that the pore space was mainly interaggregate (Figs 2c and 3a). In the re-planted site, the related distribution pattern was porphyric and the pore space consisted of cracks in the clay matrix (Figs 2d and 3b). These cracks formed during the drying of the sample in the laboratory. Contrary to the original plantation, the pore system was no longer continuous while the clay matrix appeared mainly continuous.

At higher magnifications, the organisation of the clay matrix was seen more clearly (Fig. 3a and b). The thin section of the original plantation showed a predominance of spheroidal clay micropeds, 50 μm in diameter. Clay did not embed the quartz grains. In the re-planted site, the clay embeds the skeleton grains as a matrix.

The arrangement of the clay particles in each thin section could be seen with TEM (Fig. 4a and b). The kaolinite crystals were grey and iron oxides (hematite) black. Organic matter could be differentiated from pores by its milky appearance. In the original plantation, clay particles were randomly oriented and the intercrystal pore space was largely filled by organic matter. In the re-planted site, the clay crystals were oriented face-to-face. The particle frequency, *i.e.* the amount of particles per unit area, increased sharply in the re-planted situation.

DISCUSSION

The use of heavy machinery during re-planting resulted in differences between original and re-planted sites including: increased soil hardness, soil compaction and the appearance of run-off due to decreased water retention (Caliman *et al.*, 1987; Hartmann, 1991).

Our results indicated that, in the original plantation, clay particles were organised into micropeds between quartz grains. Thin sections showed a continuous pore space which could explain the high permeability of the soil, which behaved as an assemblage of sand-like particles and therefore was soft. In this case, all constituents, *i.e.* quartz grains and micropeds, behaved as individuals. As a consequence, the soil hardness did not increase very much during drying.

After replanting, there was a complete change in the organisation of microstructure. The degradation of sandy Oxisols involved a rearrangement of soil components from the microscopic to ultramicroscopic scale. At the microscopic scale, the quartz grains were embedded by the clay matrix and the solid phase (skeleton and clay matrix) was mainly continuous. Soil cohesion, especially after drying, increased. Permeability decreased and root penetration was hampered.

In the Oxisols of R. Michaud's plantation the clay content and quartz particle size were similar in each situation, *i.e.* 16% and 80%. Changes in soil physical properties could not be related to clay content but rather to clay location and its local concentration around skeleton grains. Thus, the soil physical properties of these sandy Oxisols could not be interpreted only

Fig. 2. Micrographs of original plantation sample (a and c) and re-planted site sample (b and d) with UV light (a and b), UV and visible light simultaneously (c and d).
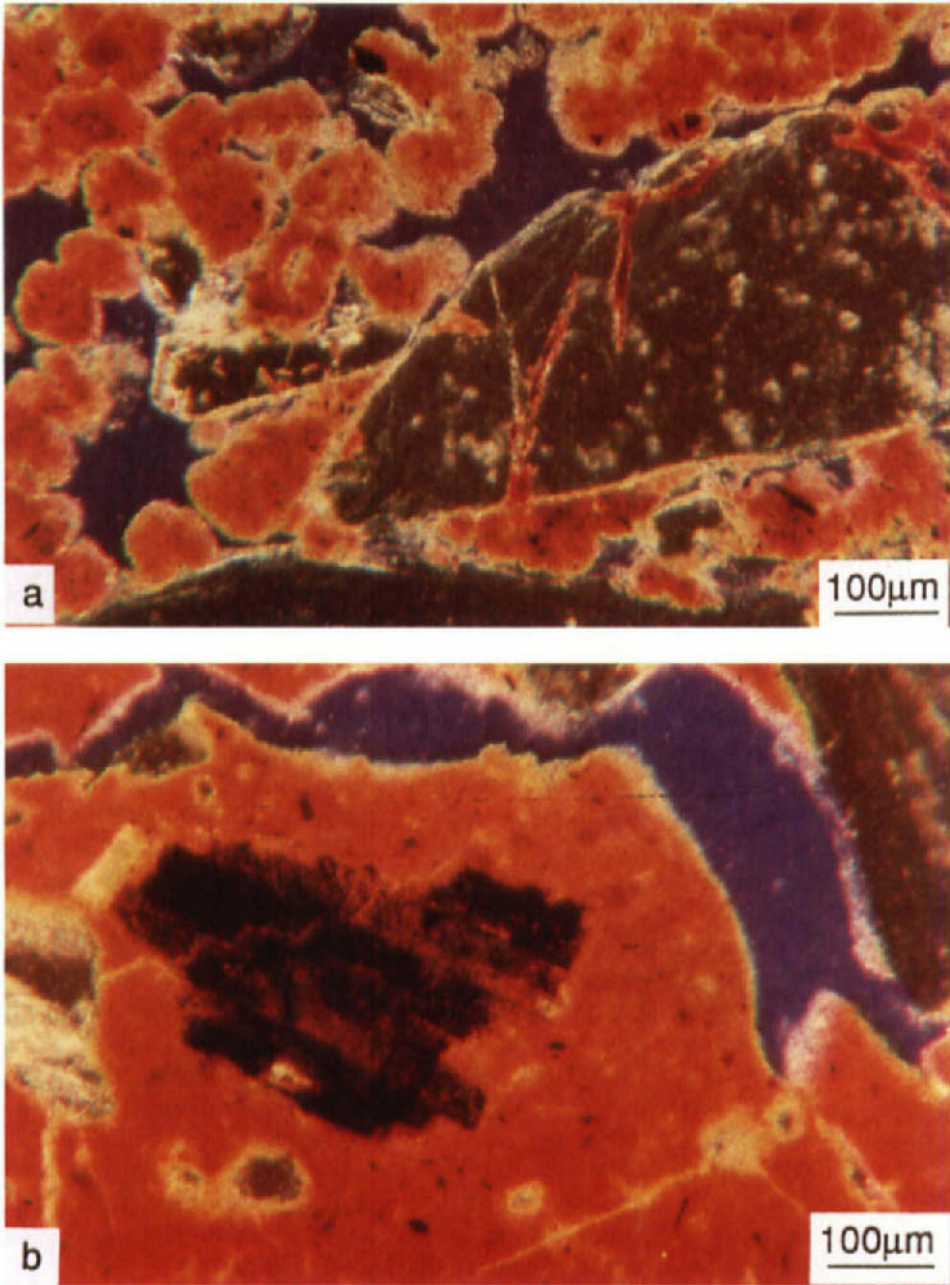
Fig. 3. Thin section observation of the original plantation sample (a) and re-planted site sample (b) at higher magnification.
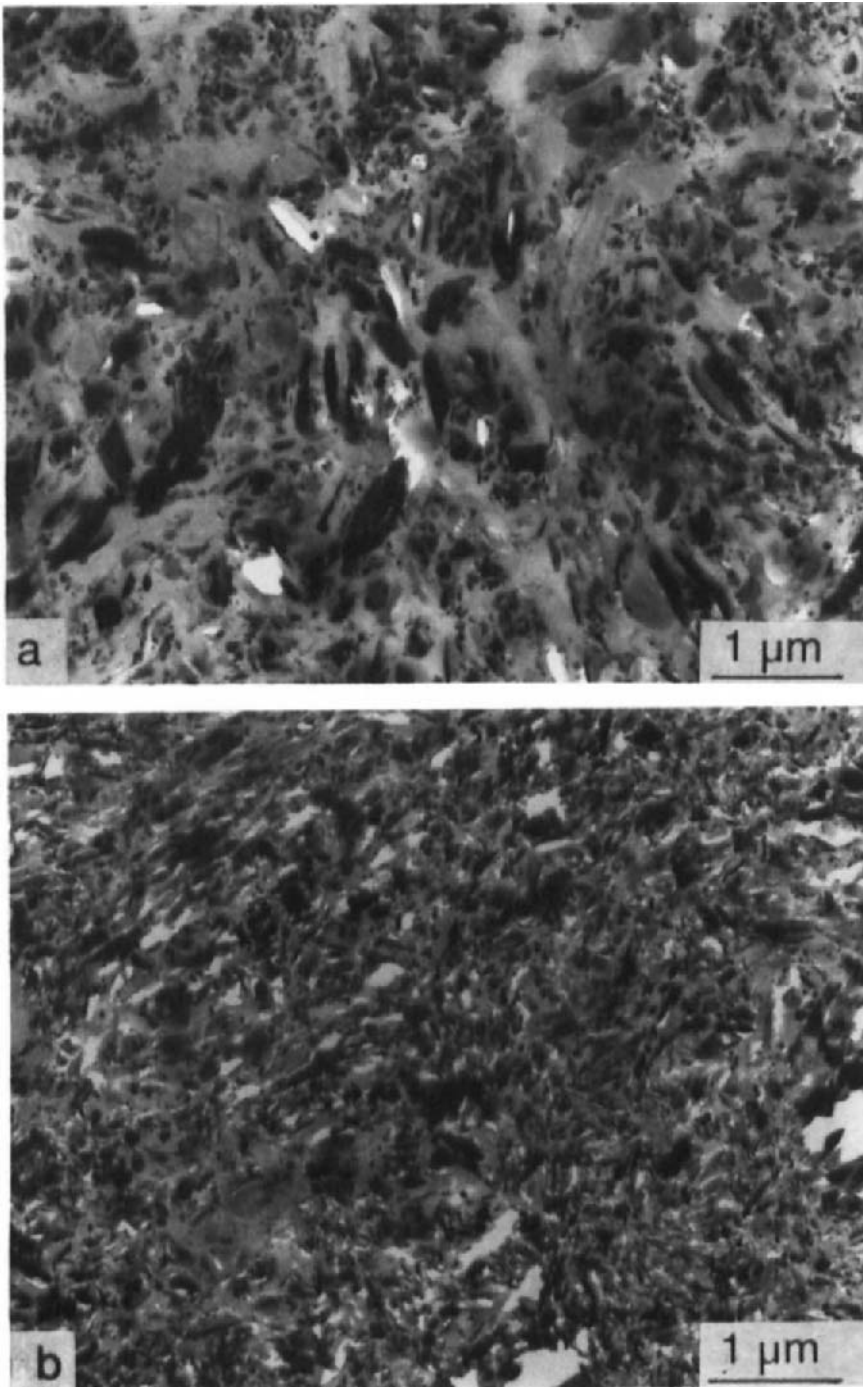
Fig. 4. TEM observation of clay matrix fragments taken on the original plantation thin section (a) and re-planted site thin section (b).

on the basis of their clay content. After the action of heavy machinery, when clay embedded skeleton grains, the soil behaved as a clayey material with low macropore continuity, and much higher cohesion in the dry state. On the other hand, its clay content was too low to induce shrink-swell phenomena and, therefore, to aid regeneration of soil structure.

TEM revealed that, in the microaggregates of the original plantation, organic matter filled up the pore space of the clay matrix. The mean distance between clay crystals was then considerably larger than in the re-plantation where the clay particles were mainly in contact face-to-face. Although the amount of organic matter was similar in original and re-planted situations, 1% and 0.7% respectively, its presence in the clay matrix seemed to play a major role in determining clay particle arrangement, *i.e.* microaggregation (Chenu and Guerif, 1991). As a consequence, organic matter can also play a major role in soil fabric and physical properties.

As the soil physical properties are mainly related to the clay microfabric, the key to soil rejuvenation appears to be associated with the genesis of a micropedal microstructure. As deep ploughing or subsoiling change the structure at much higher levels of organisation, they are not suitable techniques for the rejuvenation of those tropical sandy Oxisols. Only appropriate management of plant residues and high bioactivity appear capable of incorporating organic matter at the scale of the clay particle arrangement and of maintaining a micropedal structure (Tisdall *et al.*, 1978; Garnier Sillam *et al.*, 1987).

CONCLUSIONS

Even in sandy Oxisols with a kaolinitic clay content of approximately 16% and organic matter content of 1%, the clay matrix plays a major role in soil structure and physical properties. These physical properties must therefore be interpreted on the basis of the clay location around skeleton grains.

The micropedal structure in the original plantation, characteristic of the sandy Oxisols of Dabou, does not differ from other Oxisols. Degradation of these sandy Oxisols involves a complete rearrangement of clay particles and organic matter at microscopic scales as it has been shown for temperate soils (Stengel *et al.*, 1984; Coulon and Bruand, 1989).

Management of sandy Oxisols must thus take into account changes at the smallest scale. Under tropical conditions, only bioactivity is likely to regenerate soil structure and help in developing sustainable agriculture.

REFERENCES

Caliman, J.P., 1990. Dégradation de Propriétés Physiques Conditionnant la Fertilité sous Culture de Palmier à Huile en Côte d'Ivoire. Essais de Correction. Thesis Univ. of Dijon. 219 pp.

Caliman, J.P., Olivin, J. and Dufour, O., 1987. Dégradation des sols ferrallitiques sableux en culture de palmiers à huile par acidification et compaction. Oléagineux, 42: 393-401.

Chenu, C. and Guerif, J., 1991. Mechanical strength of clay minerals as influenced by an adsorbed polysaccharide. Soil Sci. Soc. Am. J., 55: 1076-1080.

Chauvel, A., Grimaldi, M. and Tessier, D., 1991. Changes in soil pore-space distribution following deforestation and revegetation. An example from the Central Amazon Bassin, Brazil. Forest Ecology and Management, 38: 259-271.

Coulon, E. and Bruand, A., 1989. Effects of compaction on the pore space geometry in sandy soils. Soil Tillage Res., 15: 137-152.

Dufour, O. and Olivin, J., 1985. Evolution des sols de la plantation de palmiers à huile sur savane. Oléagineux, 40: 113-124.

Garnier Sillam, E., Villemin, G., Toutain, F. and Renoux, J., 1987. Contribution à l'étude du rôle des termites dans l'humification des sols forestiers tropicaux. In: N. Fedoroff, L.M. Bresson and M.A. Coutry (Editors), Soil Micromorphology. Proc. VII Int. Working Meeting of Soil Micromorphology, Paris, July 1985. Association Française pour l'Etude du Sol, Plaisir, France, pp. 330-336.

Hartmann, C., 1991. Evolution et Comportement de Sols Sablo-Argileux Ferrallitiques sous Culture de Palmiers à Huile. Cas de la Plantation R. Michaux à Dabou (Côte d'Ivoire). Thesis Univ. Paris VI., 201 pp.

Hartmann, C., Tessier, D. and Wilding, L.P., 1992. Simultaneous use of transmitted and ultraviolet light in describing soil microfabrics. Soil Sci. Soc. Am. J., 56: 1867-1870.

Spurr, A.R., 1969. A low-viscosity epoxy resin embedding medium for electron microscopy. Ultrastructure Research, 26á: 31-43.

Stengel, P., Douglas, J.T., Guerif, J., Goss, M.J., Monnier, G. and Cannel, R.Q., 1984. Factors influencing the variation of some properties of soils in relation to their suitability for direct drilling. Soil Tillage Res., 4: 35-53.

Tessier, D., 1984. Etude Expérimentale de l'Organisation des Matériaux Argileux. Hydratation, Gonflement et Structuration au Cours de la Dessication et de la Réhumectation. Thesis Univ. Paris VII, 361 pp.

Tisdall, J.M., Cockroft, B. and Uren, N.C., 1978. The stability of soil aggregates as affected by organic materials, microbial activity and physical disruption. Aust. J. Soil Res., 16: 9-17.

This Page Intentionally Left Blank

Biological and physical amelioration of poached soils

R.A. Kemp, J.A. Lee, D.A. Thompson and A.Prince

Department of Geography, Royal Holloway University of London, Egham, Surrey TW20 OEX, UK

ABSTRACT

Kemp, R.A., Lee, J.A., Thompson, D.A and Prince, A., 1994. Biological and physical amelioration of poached soils. In: A.J. Ringrose-Voase and G.S. Humphreys (Editors), Soil Micromorphology: Studies in Management and Genesis. Proc. IX Int. Working Meeting on Soil Micromorphology, Townsville, Australia, July 1992. Developments in Soil Science 22, Elsevier, Amsterdam, pp. 697-706.

A poached area of land on a dairy farm in Berkshire (United Kingdom) has had trampling pressures largely removed by relocation of the gate. Vertical and horizontal macroporosity images, produced from resin-impregnated blocks of soil, illustrate the soil structural changes that have taken place at the site over a one year period since gate relocation. Rapid production of a more continuous macropore network, largely in response to biological activity, has led to a significant improvement in water infiltration rate. Further time, however, is clearly required for complete structural regeneration. Changes in recorded maximum past consolidation pressures experienced by the soil provide further insights into the processes of amelioration.

INTRODUCTION

Permanent grassland, grazed by dairy cattle, is the traditional landuse associated with heavy soils developed on London Clay in south-east England (Jarvis *et al.*, 1984). Winter and early spring housing of the livestock is essential to avoid poaching of these moisture-retentive clayey soils. Grazing too late in the year or too early in the spring, when the moisture content is relatively high and the soil strength correspondingly low, may lead to compression and/or shearing of the soil. The associated increase in water retention, a consequence of the diminished permeability, leads to a reduction in strength of the soils, making them even more susceptible to further damage by grazing animals (Scholefield and Hall, 1985; Batey, 1988; Briggs and Courtney, 1989).

Soil structural damage to areas of fields where cattle congregate, *e.g.* around gates and water troughs, is virtually impossible to restrict. Here, there are not only high trampling intensities, but also increased moisture levels due to excessive urine inputs. Briggs and Courtney (1989) suggest that the loss of yield over such small areas is inconsequential: more important are the associated problems of hygiene, animal cleanliness and health. Rather than attempting 'patchwork' repairs, local farmers often periodically remove cattle pressures from the relevant areas and rely on natural biological and physical processes of structural regeneration to ameliorate soil conditions.

There have been several studies concerned with detailed monitoring of the 'natural' amelioration of soils compacted by agricultural vehicles (*e.g.* Voorhees, 1983; Blackwell *et al.*,

1985; Hodara and Domzal, 1991). Gradual regeneration of soil structure has been demonstrated by reference to macroporosity images produced from resin-impregnated soil blocks photographed under UV light (Bullock *et al.*, 1985; Pagliai, 1987). To date, such techniques have not been utilised to examine the processes of structural recovery after cattle poaching. A monitoring programme on a dairy farm in Berkshire (United Kingdom) has been initiated by the present authors to assess these ameliorative processes. This paper reports on the first year results, concentrating particularly on changes in macroporosity patterns and rates of water infiltration. Other effects of amelioration are monitored using a technique developed by civil engineers to estimate the maximum consolidation pressures experienced and *still recorded* by materials. Values from agricultural soils should reflect the net balance between compression and processes of decompression or reorganisation. This measurement, although it does not directly take into account all forces active in poaching, provides a different and potentially more dynamic viewpoint of stress history than can be obtained by considering 'static' parameters such as shear strength.

MATERIALS AND METHODS

Site details

The field study was based at Woodside Dairy Farm (grid reference: SU 979736), Old Windsor, 30 km west of central London. Mean annual temperature and rainfall are about 10°C and 650 mm respectively (Jarvis *et al.*, 1979) The soil is a typical stagnogley of the Wickham series (Jarvis *et al.*, 1979) developed in a thin cover of silty drift over London Clay. The upper 25 cm has an organic carbon content of about 6% and a clay loam texture (27% sand (2 - 0.06 mm), 52% silt (0.06 - 0.002 mm), 21% clay (<0.002 mm)). Such soils have clay fractions dominated by randomly interstratified mica-smectites (Loveland, 1984).

Between 55 and 65 cows are normally housed on the farm between late November and early April. During the rest of the year they are rotated around the fields according to grass growth and grazing requirements. All the fields retain the original tile drainage dating back at least 40 years. The land is fertilised regularly and shallow chain-harrowed to remove thatch when necessary. There is no attempt, however, to modify *directly* the physical fertility of the soil. The farmer considers that poaching is not a major problem, except around gates. The latter is controlled by periodically changing the location of the gate, thus removing the pressure and allowing time for the damaged area to recover naturally.

The study was concentrated in a flat, 4 hectare field which has been under permanent pasture of ryegrass since 1973. In February 1991 the area around the gate was very wet, poached and largely devoid of grass. The farmer therefore moved the gate 50 m to east, where it has remained for the duration of the monitoring period.

Field and laboratory methods

Two 15 × 5 m areas of the field were marked out in February 1991. One was in the centre, well away from areas of congregation and visible signs of soil or grass damage (FIELD site). The other was within the poached area adjacent to the previous location of the gate (GATE site). Infiltration rates were measured at five random locations within each area by the falling head method using double ring infiltrometers (ring diameters: 290 mm and 450 mm). The
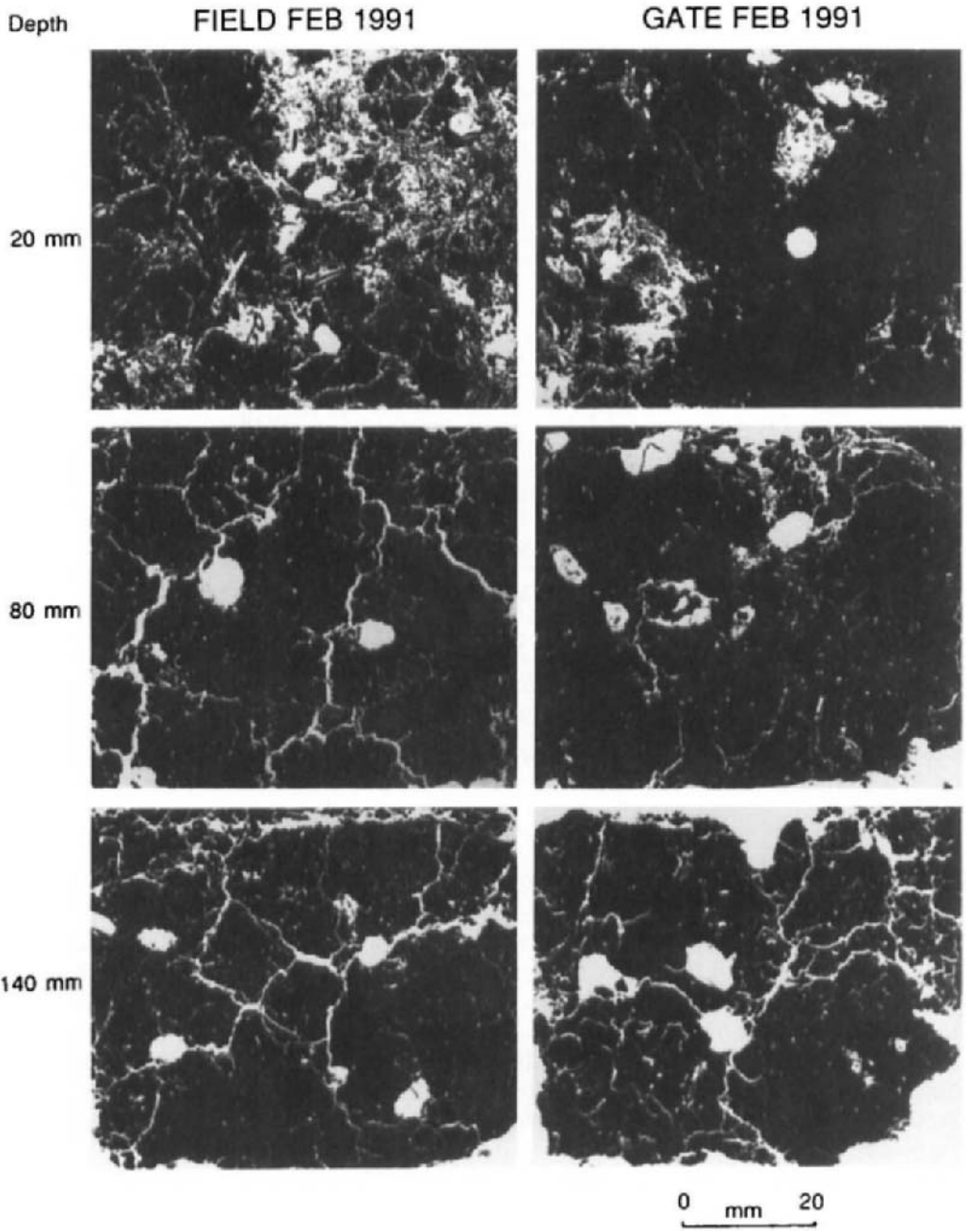
Fig. 1. Representative images of horizontal resin-impregnated blocks from the soils at the field and gate sites in February 1991. Voids are shown in white.

Table 1
Intercept densities of planar voids and channels on the horizontal porosity images from Figs 1 and 3.

		Planar voids, No. dm^{-1}		Channels, No. dm^{-1}	
		1991	1992	1991	1992
Field	20 mm	3.490	3.470	0.440	0.540
Field	80 mm	4.050	7.400	0.260	0.250
Field	140 mm	4.700		0.500	
Gate	20 mm	0.980	2.200	0.360	1.500
			2.890		0.630
Gate	80 mm	3.600	5.030	0.740	0.600
Gate	140 mm	4.320		1.000	

Table 2
Mean infiltration rates at the field and gate sites in 1991 and 1992.

	Mean infiltration rate ($\times 10^{-4}$ m^{3}s^{-1})	
	1991	1992
Field	2.35 a (z)	1.73 a (z)
Gate	0.38 b (y)	1.09 a (z)

Means followed by the same letter within each column, or in parentheses within each row, are not significantly different at 95% level.

reported values represent the final infiltration rates: these were obtained after 1 - 2 hours and remained constant thereafter (ADAS, 1982). Up to eight 38 mm and 100 mm diameter core samples were taken at each site for oedometer tests. Undisturbed 70 × 60 × 40 mm samples were taken in Kubiena tins from three random locations within each site. Two vertical blocks (0 - 70 and 70 - 140 mm) and three horizontal blocks (0 - 40, 60 - 100 and 120 - 160 mm) were obtained from each location.

The farm was revisited in April 1991 after the cows had been returned to the land for grazing and additional Kubiena tin samples were collected. Further visual inspection was made in September 1991. The complete field sampling and measurement programme was repeated in February 1992.

Oedometer tests were undertaken and consolidation curves constructed in accordance with the method given by B.S. 1377 (1990). The maximum past consolidation pressures were estimated from these curves using the techniques of Casagrande (1936) and Schmertmann (1955). The maximum consolidation pressure to which the sample had been subjected previously is approximately equivalent to the point on the curve where the rate of consolidation versus pressure becomes much steeper. Kubiena tin samples were acetone-dried, impregnated with crystic resin, cut, polished and surfaces photographed under UV light (Lee

and Kemp, 1992). Differences in quantities of planar voids (>0.25 mm) and channels (>1 mm) on selected enlarged (×2) porosity images were quantified by manually counting intercept densities according to the methods of Ringrose-Voase and Bullock (1984) and A.J. Ringrose-Voase (pers. comm., 1993). Perpendicular semi-circular transects (n = 74) and regular grid transects (n = 116) were used for counting the planar voids and channels respectively.

RESULTS AND DISCUSSION

The soil just below the surface (20 mm) at the field site in February 1991 had a mixture of vertically-oriented biological channels, vughs/compound packing voids associated with excrements and organic matter fragments and a moderately-developed planar void system defining sub-angular and sub-rounded aggregates (Fig. 1 and Table 1). A more extensive and continuous network of planar voids, often linked to individual inter- and intra-aggregate vertically-oriented channels, was present at 80 mm and 140 mm. Similar structures were apparent from the lower depths at the gate site, although the images taken from 80 mm displayed a less developed pedal structure and planar void network. Major differences between the sites were at 20 mm, with the poached soil at the gate having few defined aggregates and only occasional channels, vughs and irregular compound packing voids.

The difference in macroporosity patterns (Fig. 1) between the two sites can be attributed to compression and shearing of the soil at the gate by congregating livestock. The consequential differences in macropore quantity, type and presumably continuity in the upper few centimetres were responsible for the significantly lower infiltration rates recorded at the gate site in February 1991 (Table 2).

By February 1992 the infiltration rate at the gate had increased to such an extent that it was statistically indistinguishable from the field site (Table 2). This dramatic change in drainage potential was accompanied by an improvement in the soil as a growth medium, as evidenced by the patchy yet more extensive grass cover at the site compared to the previous year. The role of physical and biological processes in this amelioration can be inferred from the sequence of vertical porosity images taken at 0 - 70 mm depth from the soil at the gate site at intervals during the monitoring period (Fig. 2). In February 1991 the soil had a dense fabric which was sometimes separated into platey aggregates by horizontally-aligned planar voids. These presumably formed in response to compressive and shear forces and were perhaps enhanced by ice growth during the earlier part of the winter. Worm activity in the spring (April 1991) led to substantial, yet only localised, reworking of the upper layers and creation of numerous macrochannels. Faunal modification diminished during the hot, dry summer and an extensive network of desiccation cracks (vertically-aligned planar voids) were observed in September 1991. However, the size of the cracks (50 - 100 mm depth and 10 - 20 mm width) meant that it was impossible to take Kubiena tin samples. Autumn rains led to swelling of the soil and renewed faunal and root activity. These processes, possibly combined with minimal frost action during the subsequent mild winter, removed all evidence of the desiccation phase. Mackie-Dawson et al. (1989) have illustrated how seasonal variation in generative processes may cause major cyclical changes in aggregate forms and void patterns of clay soils under grass. Significant changes, therefore, can only be assessed by comparing samples taken at equivalent times of the year. The vertical images in February 1992, twelve months after the initial sampling, indicate that the net changes in structure of the upper few centimetres of the soil at the gate site were of varying extent and mainly attributable to worm and root activity. The

FIELD FEB 1992   GATE FEB 1992
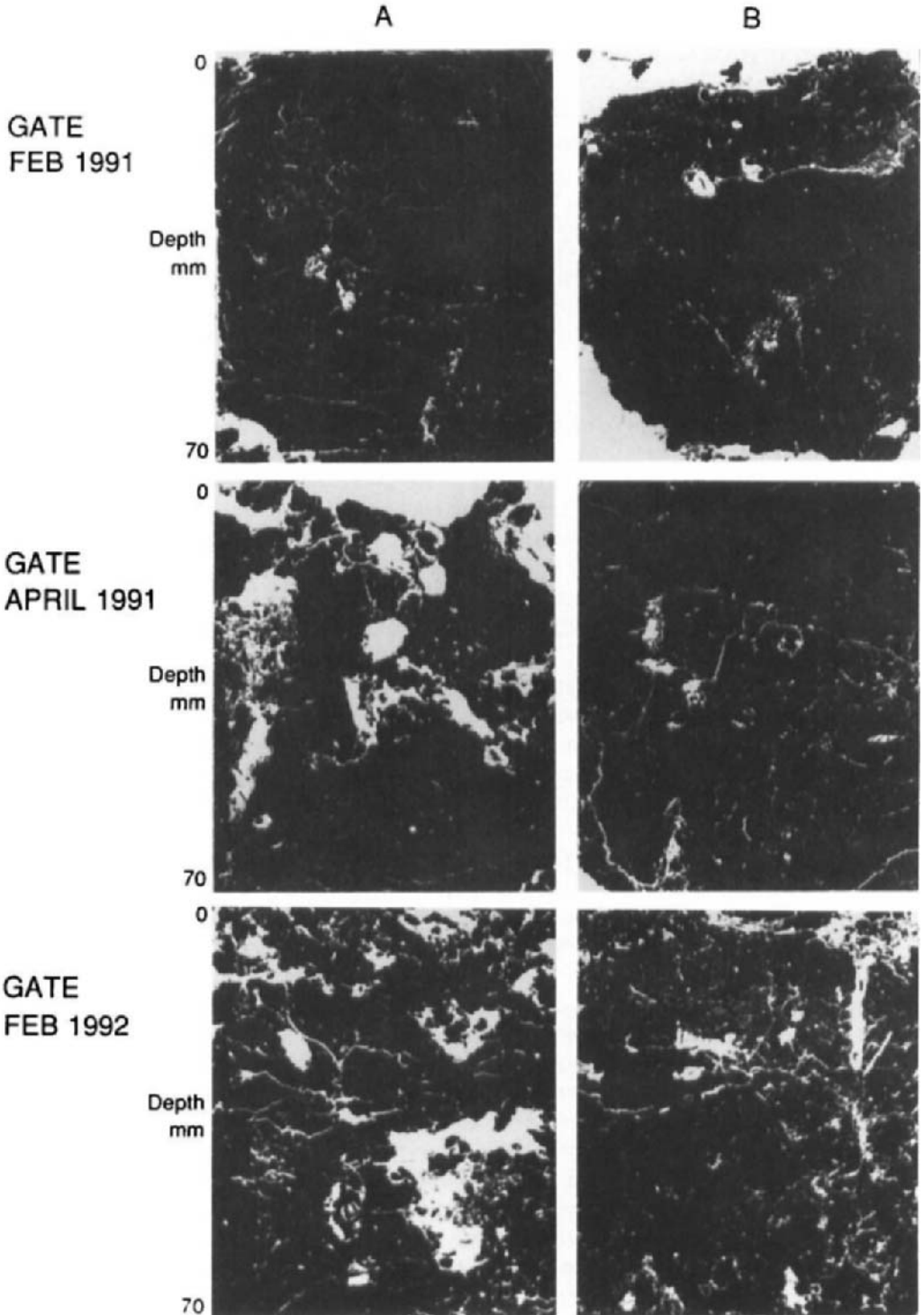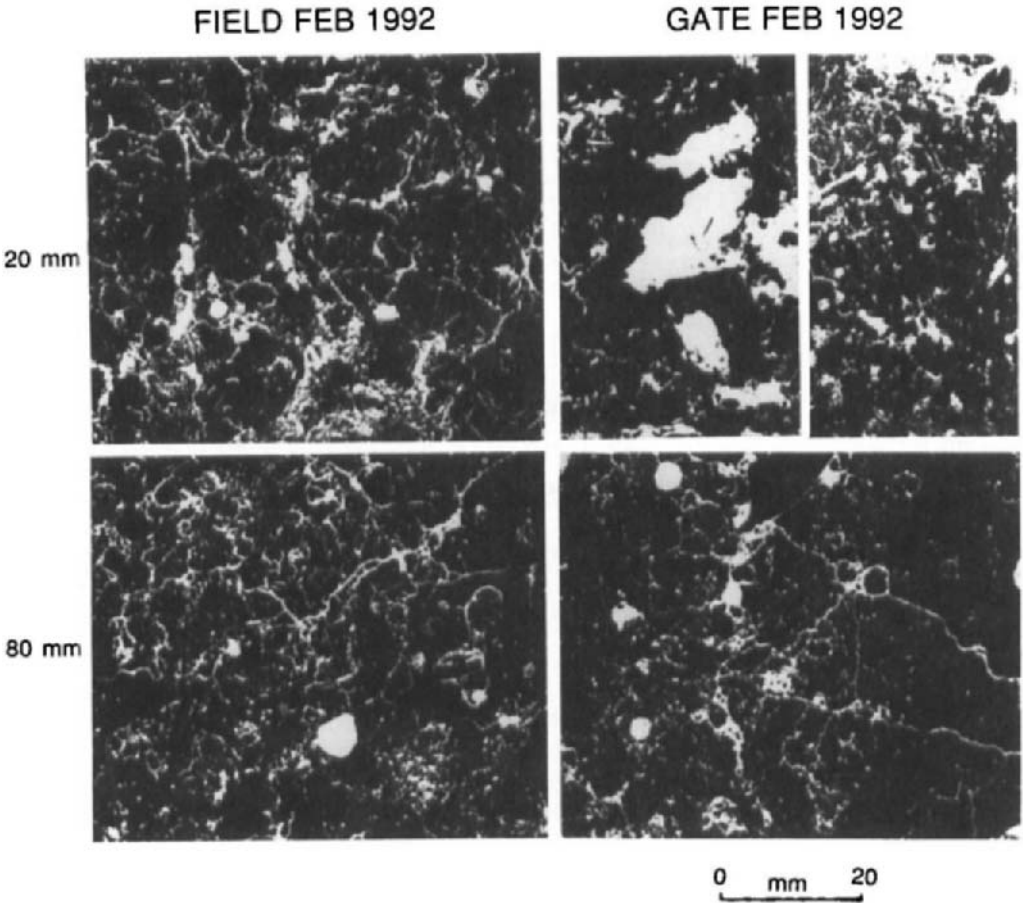
Fig. 3. Representative images of horizontal resin-impregnated blocks from the soils at the field and gate sites in February 1992. Voids are shown in white.

improved surface infiltration of water was clearly a consequence of the newly-created macrochannel network.

Despite the recorded improvements in infiltration rate and grass growth at the gate site over the year, it is apparent from Fig. 3 and Table 1 that soil structure had not recovered sufficiently throughout the upper eighty millimetres to reach the level of development exhibited by the field site. Such differences in structural development could affect post-drought water transmission

Fig. 2. Images of vertical resin-impregnated blocks from the soil at two locations (A, B) at the gate site (February 1991, April 1991, February 1992). Voids are shown in white.
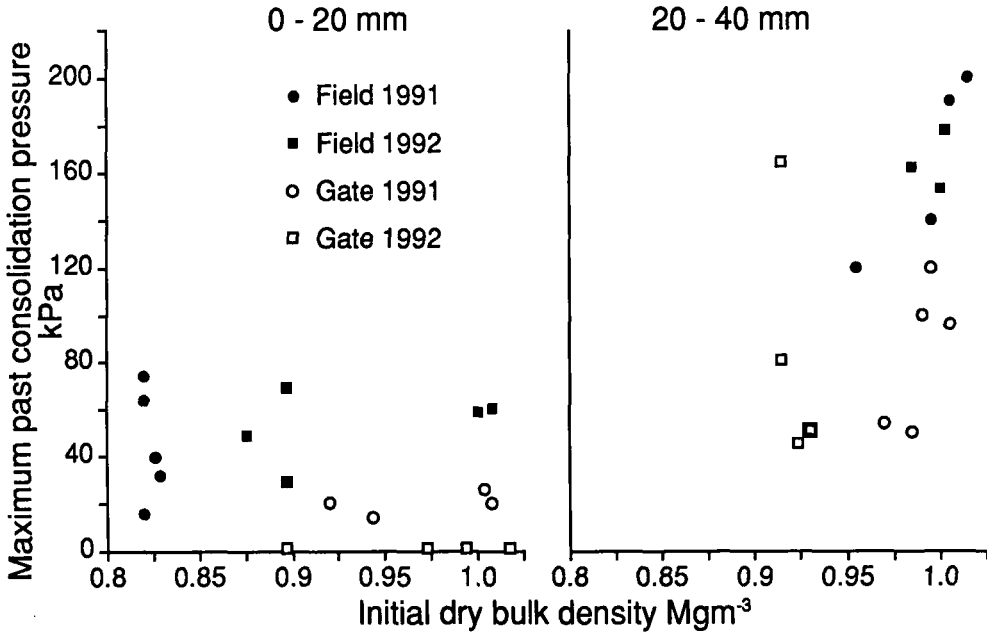
Fig. 4. Plots of maximum past consolidation pressures against initial dry bulk densities for the soils at the field and gate sites in 1991 and 1992.

and retention (Reid and Parkinson, 1984). Generation of a network of stable aggregates and associated interlinked voids clearly requires a longer period of time than considered so far in the monitoring programme.

Plots of maximum past consolidation pressures against dry bulk densities (Fig. 4) provide further insights into the transformations taking place in the soil over the monitoring period. The high, although variable, past consolidation pressures recorded at the field site in both years reflect a state of dynamic equilibrium between compression, shearing (both associated with livestock trampling) and biological and/or physical amelioration processes. Values were considerably lower in the 0 - 20 mm layer than the 20 - 40 mm layer, an indication of the greater impact of shearing and ammelioration processes closer to the surface. The increase in bulk density in the 0 - 20 mm layer of soil at the field site between 1991 and 1992 suggests the dominance of compression, although the changes are not clearly substantiated by the macroporosity images (Figs 1 and 3).

Bulk densities were variable at the gate site and do not appear to have changed significantly with time, except perhaps in the 20 - 40 mm layer (Fig. 4). Maximum past consolidation pressures in 1991 were generally lower at the gate than the field, particularly at 20 - 40 mm depth, presumably a consequence of greater remolding and shear deformation by the cattle hooves at the gate site. Amelioration processes over the next year, however, removed all traces of the stress history previously recorded in the 0 - 20 mm layer. This 'zeroing' of the stress history, combined with the absence of appreciable grazing and trampling at the gate site in

1992, ensured that the maximum consolidation pressures recorded at 0 - 20 mm were very low (<1 kPa). Similar changes, however, do not appear to have occurred at the lower depth.

SUMMARY AND CONCLUSIONS

The changes in macroporosity patterns, infiltration rates and recorded maximum past consolidation pressures over the course of a single year clearly demonstrate the important role that biological and physical processes may have in encouraging soil structural recovery after cattle poaching. Continued monitoring at this site will aim to provide further insights into the details and rates of these ameliorative processes.

ACKNOWLEDGEMENTS

REFERENCES

ADAS, 1982. Techniques for Measuring Soil Physical Properties. Ministry of Agriculture, Food and Fisheries Reference Book 441.
Batey, T., 1988. Soil Husbandry. Soil and Land Use Consultants, Aberdeen, 157 pp.
Blackwell, P.S., Ward, M.A., Lefevre, R.N. and Cowan, D.J., 1985. Compaction of a swelling clay soil by agricultural traffic; effects upon conditions for growth of winter cereals and evidence for some recovery of structure. J. Soil Sci., 36: 633-650.
Briggs, D.J. and Courtney, F.M., 1989. Agriculture and Environment. Longman, Harlow, 442 pp.
B.S. 1377, 1990. British Standard Methods of Test for Soils for Civil Engineering Purposes.
Bullock, P., Newman, A.C.D. and Thomasson, A.J., 1985. Porosity aspects of the regeneration of soil structure after compaction. Soil Tillage Res., 5: 325-341.
Casagrande, A., 1936. The determination of the pre-consolidation load and its practical significance. In: Proc. I International Conference on Soil Mechanics and Foundation Engineering, Cambridge, Massachusetts, p. 60.
Hodara, J. and Domzal, H., 1991. A preliminary study on the durability of the effects of compaction on a brown soil developed from loess. Soil Tillage Res., 19: 255-262.
Jarvis, M.G., Hazelden, J. and Mackney, D., 1979. Soils of Berkshire. Soil Survey of England and Wales Bulletin 8, Harpenden, Herts, U.K.
Jarvis, M.G., Allen, R.H., Fordham, S.J., Hazelden, J., Moffat, A.J. and Sturdy, R.G., 1984. Soils and Their Use in South East England. Soil Survey of England and Wales Bulletin 15, Harpenden, Herts, U.K.
Lee, J.A. and Kemp, R.A.,1992. Thin Sections of Unconsolidated Sediments and Soils: A Recipe. Centre for Environmental Analysis and Management Technical Monograph, Royal Holloway University of London 2.
Loveland, P.J., 1984. The soil clays of Great Britain: 1. England and Wales. Clay Minerals, 19: 681-707.

Mackie-Dawson, L.A., Mullins, C.E., FitzPatrick, E.A. and Court, M.N., 1989. Seasonal changes in the structure of clay soils in relation to soil management and crop type. I. Effects of crop rotation at Cruden Bay, NE Scotland. J. Soil Sci., 40: 269-282.

Pagliai, M., 1987. Micromorphometric and micromorphological investigations on the effect of compaction by pressures and deformations resulting from tillage and wheel traffic. In: G. Monnier and M.J. Goss (Editors), Soil Compaction and Regeneration. Balkema, Rotterdam, pp. 31-38.

Reid, I. and Parkinson, R.J., 1984. The wetting and drying of a grazed and ungrazed clay soil. J. Soil Sci., 35: 607-614.

Ringrose-Voase, A.J. and Bullock, P., 1984. The automatic recognition and measurement of soil pore types by image anlysis and computer programs. J. Soil Sci., 35: 673-684.

Scholefield, D. and Hall, D.M., 1985. A method to measure the susceptibility of pasture soils to poaching by cattle. Soil Use Manage., 1: 134-138.

Schmertmann, J.M., 1955. The undisturbed consolidation of clay. Transactions American Society Civil Engineers, 120: 1201.

Voorhees, W.B., 1983. Relative effectiveness of tillage and natural forces in alleviating wheel-induced soil compaction. Soil Sci. Soc. Am. J., 47: 129-133.

Micromorphological study of compacted mine soil in east Texas

L. Yao and L.P. Wilding

Department of Soil and Crop Sciences, Texas A&M University, College Station, Texas, USA

ABSTRACT

Yao, L. and Wilding, L.P., 1994. Micromorphological study of compacted mine soil in east Texas. In: A.J. Ringrose-Voase and G.S. Humphreys (Editors), Soil Micromorphology: Studies in Management and Genesis. Proc. IX Int. Working Meeting on Soil Micromorphology, Townsville, Australia, July 1992. Developments in Soil Science 22, Elsevier, Amsterdam, pp. 707-718.

Soil compaction by reclamation vehicles is a potential hazard and constraint to the performance of reclaimed surface mines in Texas. The objectives of this paper are to assess compaction effects on soil micromorphology and the quality of postmined soils. Compaction reference plots were established in 1990 from mixed lignite overburden materials with three treatments: Treatment A: soil reclaimed by conventional reclamation practices using scraper to back fill the mined sites and dozer to level the surface; Treatment B: mixed spoil compacted at 30 cm depth with successive passes of a scraper with a total load force of about 0.2 MPa; Treatment C: mixed spoil compacted at 60 cm depth using the same method as above.

A large variety of micromorphological features was observed in mine soil from East Texas which had high spatial variability. Most of the macropores were oriented horizontally in both compacted and conventionally treated zones, indicating mechanical and shear stress due to compaction. Horizontally oriented pores impeded infiltration and percolation of water. Compacted soils had dense porphyroskelic s-matrix (porphyric) with insepic (stipple speckled b-fabric), silasepic (stipple speckled b-fabric), mosepic (mosaic-speckled b-fabric) and skelsepic (granostriated b-fabric) plasmic fabrics. Total macroporosity was very low and ranged from 2% in compacted soils to about 20% in conventionally reclaimed soils. The mean of total macroporosity is 5.3% and standard error of 2.73. A large volume of shale fragments showing various degrees of disintegration was observed. Some were bent, indicative of mechanical stress during compaction. Lignite was also observed in thin sections in small amounts (about 2 - 3%). Cone index (penetration resistance) ranged from 10 MPa in the most compacted zones to as low as 2 MPa in reclaimed uncompacted surface soils. In the surficial 10 - 20 cm depth, significantly higher cone indices were observed in the conventionally reclaimed treatment than in similar materials in the compacted treatments. Hydraulic conductivities ranged from 2.1×10^{-7} to 1.1×10^{-6} m/s in the surface horizons in all treatments and from 8.1×10^{-9} to 6.7×10^{-8} m/s in compacted zones. This study indicates soil physical properties and micro-structures were adversely affected by compaction. These conditions enhanced surface runoff, decreased rates of water movement and decreased plant growth and productivity.

INTRODUCTION

Successful reclamation requires favourable soil chemical and physical conditions for plant growth, including optimum ranges for pH, bulk density, soil texture, soil moisture, lack of compaction and sufficiency of plant nutrients. Several studies have indicated that mixed overburden spoil in the Gulf Coast sediments of Texas could form postmined soils that have greater plant available water than nearby undisturbed soils (Hons, 1978). Absence of a restrictive clay subsoil in mine soils favoured greater rooting depth and higher root density than in undisturbed soils of the same material (Bearden, 1984). This work also indicated that water retention and root penetration were generally more favourable for plant growth in mixed overburden materials than in the soils before mining.

Fig. 1. Location of research site.

Most research of Texas mine soils has focused on the oxidation of pyrite and corresponding chemical and biological effects that release acidity and lead to low pH conditions that are toxic to revegetation (Arora et al., 1978; Pugh et al., 1981; Doolittle, 1986). Surface mining has also brought attention to the undesirable attribute of soil compaction. Little research is available, however, that documents comprehensively the effects of compaction on the success of the reclamation process.

Compaction refers to the increase in density of a soil as a result of applied stress. Mechanically applied stresses are the major cause of compaction in postmine reclamation (Jansen et al., 1986). Compaction results in reorientation of soil particles, a change in pore-size distribution and an increase in density (Bradford and Gupta, 1986; Bresson and Zambaux, 1990). Compaction causes large pores to collapse. These pores become partially filled with solid particles, or become very fine pores that are less effective in transmitting air and water. Compaction also reduces the permeability of the soil to water and restricts root elongation and proliferation (Baver et al., 1972). Plant rooting depth in these soils tends to be shallow. Most of the roots present are confined to desiccation cracks and there is a tendency for roots to stop or turn and grow laterally at each compacted interface. Such soils have a relatively low available water storage capacity and much of the water retained is unavailable for the restricted root systems. This impairs the ability of row crops to survive and flourish during periods of high moisture demand (Jansen, 1977). In Texas, reclaimed soils consist of mixed overburden materials from various premined soils and geologic strata. Because postmined soils have more clay in surface zones than undisturbed soils (Hossner, 1980), they are highly susceptible to compaction, slaking and structure degradation, especially if levelled during periods when moisture contents favour compaction.
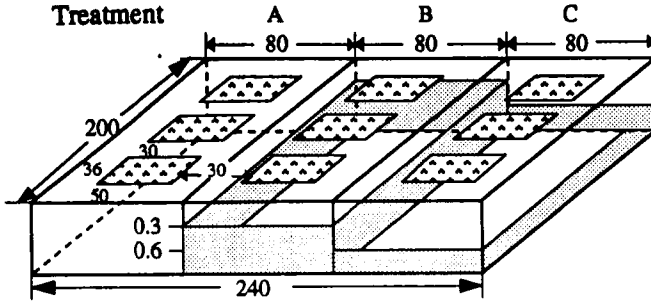
Fig. 2. Experimental design with 3 management areas in each treatment. Units in metres. Shaded areas were compacted.

MATERIALS AND METHODS

The research site is located at Freestone County, East Texas (Fig. 1). The site was reclaimed in 1988 and is located on a convex summit landscape position with 2-3% slope. Three treatments were constructed on this site. Treatment A was constructed by the conventional reclamation process. The overburden materials were transported by scrapers and downloaded to restore roughly the original topography. The materials were later levelled by bulldozers to meet the topography requirements. For the treatment B, on the reclaimed site, the surface 30 cm overburden materials were scraped off and piled outside the treatments. The exposed surface at 30 cm depth was compacted by successive passes of a loaded scraper weighing about 80 tons. Treatment C was constructed by the same method as treatment B but compacted at 60 cm depth. Three plots (50 × 36 m) were set up as measurement areas in each treatment. The experimental design is illustrated in Fig. 2.

To remove the differences in revegetation caused by soil chemical conditions such as pH and nutrient contents, the experimental area was treated with lime and fertilizers to optimal levels. After plots were designed, the whole area was sprigged with coastal bermudagrass (*Cynodon dactylon* L. Pers.) which is a commonly used species in reclamation efforts in this area. The site was enclosed by a fence that makes it inaccessible to grazing animal traffic.

Soils from compacted and conventionally treated plots were sampled for soil chemical, particle size and bulk density analyses. Undisturbed samples were collected in August (1990) in Kubiena tins of 16 × 8 × 5 cm and marked with the orientation. Three tins were collected at each depth (0-30, 30-60 and 60-90 cm) within each plot. Twenty seven tins were collected for each treatment. Acetone replacement of the water in the samples (Miedema *et al.*, 1974) was not feasible because of the swelling problem of the materials in acetone. Instead, samples were freeze-dried in liquid nitrogen (Jongerius and Heintzberger, 1986) to remove water. The freeze-dried samples were heated to 70°C and impregnated with a plastic resin with a fluorescent dye. Three samples for thin sections were collected in each of the surface and subsurface horizons of conventionally reclaimed soil and in induced compaction treatments. Thin sections cut from these samples were described and studied under cross- and plane-polarized lights on a petrographic microscope (Brewer, 1976). The size of macropore is defined as 75 μm (Brewer, 1976).

The impregnated blocks were used for macroporosity measurement (Puentes, 1990). Vertical faces (5 × 8 cm) were cut through the impregnated samples, polished and photographed under UV light. A SEM/IPS image processing system was used for analysis of

Table 1.
Morphological descriptions of mine soils *.

Grouping of horizons**	Colour dry	moist	Texture	Structure	Consistence dry	moist	Boundary	Special features
k	10YR 5/2	10YR 4/3	cl	f gr-sbk	ds-dsh	mfr		few roots and lignite; common shale
l	10YR 5/2	10YR 3/3 10YR 4/2	l	ma-abk	dvh-deh	mf-mvf	ci-gi	many lignite and shale
m	10YR 5/3	10YR 3/3 10YR 3/2	cl	f gr-sbk	ds-dsh -dh	mfr-mf		few roots and lignite; common shale
n	10YR 5/3 10YR 6/2	10YR 3/3 10YR 3/1 10YR 4/2	l	ma-abk -sbk	dvh-deh	mf-mvf	ci	few to common lignite; and common shale

* Abbreviations from Soil Survey Staff (1951, pp. 139-140).
** k - Surface 15 cm A horizons of treatment A.
    l - Subsurface 15 - 90 cm C horizons of treatment A.
    m - Surface A horizons of 0 - 30 cm in treatment B and 0 - 60 cm in treatment C.
    n - Subsurface C horizons of 30 - 90 cm in treatment B and 60 - 90 cm in treatment C.

Table 2
Selected physical properties.

Grouping of Horizons *	Bulk density (g/cm3)	Total porosity (%)	Macroporosity (%)	Cone index (MPa)	Ksat (10⁻⁸ m/s)
k	1.44 (9) **	46 (9)	10 (7)	2.7 (30)	29 (5)
l	1.67 (9)	36 (9)	3 (7)	5.0 (240)	6 (5)
m	1.60 (9)	39 (9)	5 (7)	3.4 (270)	25 (10)
n	1.68 (9)	35 (9)	3 (7)	5.8 (270)	2 (10)

* k - Surface 15 cm A horizons of treatment A.
    l - Subsurface 15 - 90 cm C horizons of treatment A.
    m - Surface A horizons of 0 - 30 cm in treatment B and 0 - 60 cm in treatment C.
    n - Subsurface C horizons of 30 - 90 cm in treatment B and 60 - 90 cm in treatment C.
** Numbers in parentheses are the number of observations.

the pore space in the negatives. Measurements of the macroporosity, maximum and minimum diameters and the orientation of elongated voids were performed. Total soil porosity was derived from bulk density data assuming a soil particle density of 2.6 Mg/m^3.

Soil penetration resistance was measured at approximately 1 cm intervals to a depth of 90 cm using a recording penetrometer (Hooks and Jansen, 1986; Morrison, 1987). It was mounted on a truck and driven down by a hydraulic probe at a constant speed. Nine penetration resistance profiles were measured in each treatment. Data were averaged over depths of 0 - 30, 10 - 30, 30 - 60 and 60 - 90 cm for statistical analysis.
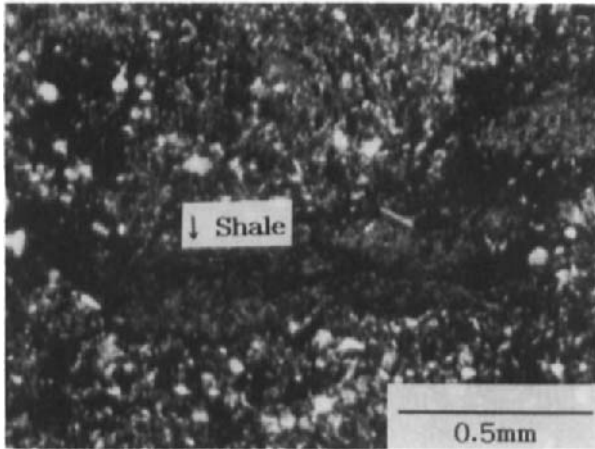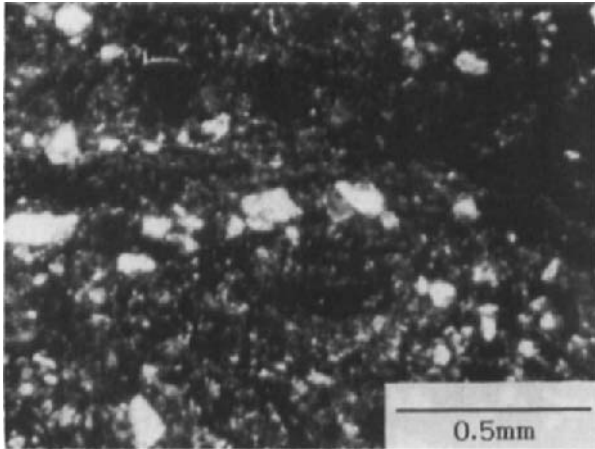
Fig. 3. Thin sections from (a) uncompacted surface of treatment A and (b) induced compacted zone of treatment C (cross-polarized light).

A single ring infiltrometer with a constant water head (Bouma, 1982) was used for hydraulic conductivity measurements. Six measurements were taken in both surface and subsurface horizons of each treatment.

RESULTS AND DISCUSSION

Mine soil field morphology

The reclaimed mine soils are classified as fine-loamy, mixed, nonacid, thermic, Typic Ustorthents. A brief profile description of the groups of horizons for the respective treatments is given in Table 1. Soil layers are grouped by their treatments and status of compaction. These groups will be used throughout the discussion.

The soil in treatment A has a relatively thin uncompacted surface layer about 10 cm thick. This layer had been ploughed after the reclaimed materials were levelled. Soil materials are soft and friable except for large fragments of shale, lignite and clay-textured hard overburden materials. Although lignite and shale fragments are present in all layers in mine soil profiles, the subsurface soil in treatment A is characterized by large amounts of unweathered shale and lignite fragments. It is structureless and hard to very hard when dry. Soil in this layer is dry or only slightly moist most of the year.

Treatments B and C have induced compaction pans at about 30 cm and 60 cm, respectively. Most of the upper 30 cm (treatment B) and 60 cm (treatment C) layers are friable to firm. Some parts are firm to very firm due to the variability in composition of the materials. The induced compaction zones are dense and very hard to extremely hard when dry. Compaction also results in the massive structure in these layers. These induced compaction zones have an abrupt upper boundary and can be identified morphologically in the field.

Micromorphological study

Although mine soils differ in degree of compaction, they have many morphological features in common. Thin sections show that s-matrix fabric of mine soils are porphyroskelic (porphyric). They vary from open porphyric to single spaced porphyric. Most of plasmic fabrics are insepic (stipple speckled b-fabric), silasepic (stipple speckled b-fabric), mosepic (mosaic-speckled b-fabric) and skelsepic (granostriated b-fabric) with some argillasepic (stipple speckled b-fabric), masepic (parallel striated b-fabric) and vosepic (porostriated b-fabric) in places depending on rock compositions and induced stresses upon reclamation. Most voids are irregular ortho vughs, with a few meta and ortho skew planes. Mine soils are more porous in the uncompacted surface layers than the compacted zones which have a dense massive structure (Fig. 3a and b). The rearrangement of the soil particles caused by compaction is manifested by the decrease in macroporosity in the compaction zones. The average macroporosity from polished blocks is 10% in the surface horizon of the conventionally reclaimed treatment (group k, Table 2) and decreases to 3% in the subsurface of the same treatment (group l). This is significantly different at 0.01 level. For the induced compaction treatment, macroporosity dropped from 5% in the surface uncompacted layers (group m) to 3% in the induced compacted layers (group n).

Large amounts of shale fragments were observed in each horizon throughout soil profiles. They differ in colour, size, shape and degrees of disintegration. Some were bent and broken due to compaction by mechanical stress when scraper and blade reclamation equipment weighing over 50 tons crossed the plots. Shale fragments account for 17 - 36% of mine soil (by weight) in >2 mm coarse fraction and 20 - 30% (by volume) in soil thin sections. Lignite was also observed in thin sections in small amounts (about 2 - 3%). There is great spatial variability at micro- and macro scales both vertically and horizontally. Local occurrence of hard materials identified in the field either as compacted overburden or inherited as overconsolidated overburden are common not only in the compacted subsurface (groups l and n), but also in the uncompacted surface zones (groups k and m).

Micropedological features observed in both uncompacted and compacted zones include: argillans, ferrans, mangans, ferriargillans, papules and diffuse and sharp Fe-Mn nodules. Since the site was only recently reclaimed in 1988, these features were inherited from mixed
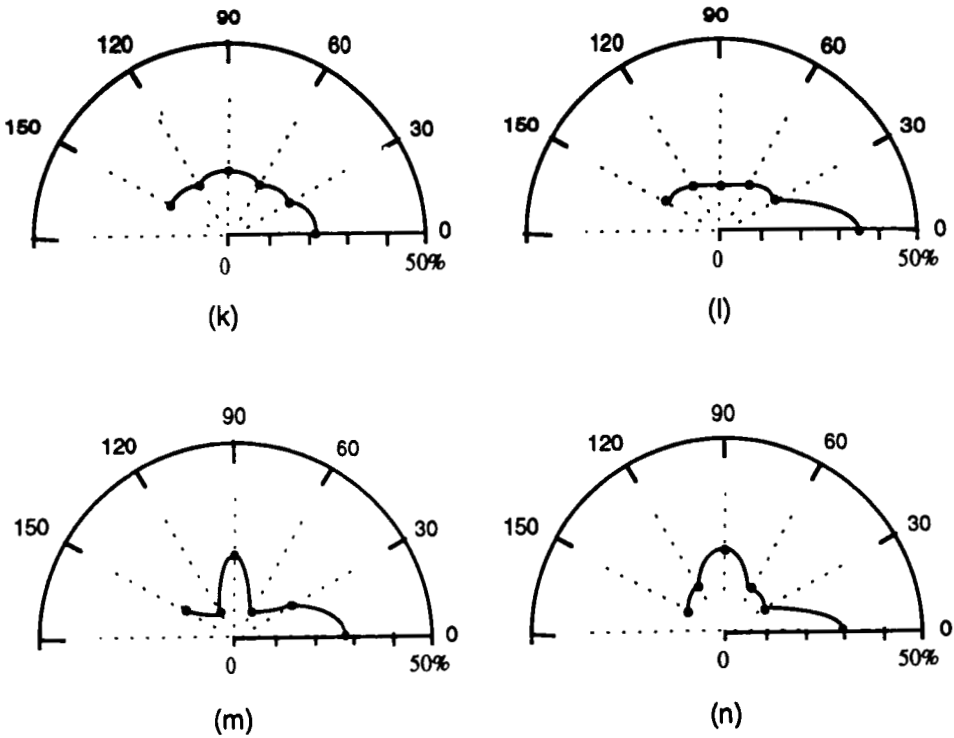
Fig. 4. Orientation patterns of macropores. (k), (l), (m) and (n) are the groups of horizons as identified in Table 1 (7 observations for each group).

premined soil and overburden materials. They are considered as pedorelicts in these reclaimed soils. Few weatherable minerals were observed in mine soils.

The orientation of elongated pores exhibits complex patterns. Fig. 4 shows the relative areas of macropores at different orientations. Horizontal orientation is given as $0°$ and the vertical as $90°$. Data for corresponding complementary angles (e.g. $0°$ and $180°$; $30°$ and $150°$; $60°$ and $120°$; etc.) are equal because the azimuth orientation of the samples were not recorded when the samples were collected. In the uncompacted surface horizons of conventionally reclaimed mine soils (group k, Fig. 4k), macropores are randomly distributed and are not dominated by a specific orientation. However, in compacted subsurface layers of the same treatment (group l, Fig. 4l), about 35% of macropores are oriented horizontally as a result of compaction. In the induced compaction treatments (B and C), both uncompacted surface layers and compacted subsurface layers (groups m and n, Fig. 4m and n) have a dominance of horizontal pores with a secondary dominance of vertical pores. The low hydraulic conductivity in the compacted zones (Table 2) can be attributed to the lack of macropores and the dominant horizontal orientation of macropores present. This is probably a consequence of compaction.

Table 3
Duncan's mean comparisons and F tests of cone indices (MPa).

Depth (cm)	Treatment			F	CV(%)	Number of obs.
	A	B	C			
0-10	2.7 b *	2.8 d	2.3 d	3.75	72	30
	x/y**	x	y			
10-30	4.9 a	3.5 c	3.8 c	56	25	60
	x	z	y			
30-60	5.1 a	5.2 b	4.7 b	23	31	90
	x	x	y			
60-90	5.0 a	6.2 a	6.1 a	31	31	90
	y	x	x			
F	85	86	57			
CV(%)	20	28	37			

* a, b, c, and d are classes of Duncan's mean comparisons for depth differences (Duncan, 1955). Same letter means non-significantly different at 0.01 probability level.
** x, y, and z are classes for treatment differences.

There is not a satisfactory explanation for the evident large percentage of vertical pores in the compacted treatment shown in Fig. 4m and Fig. 4n. In addition to the compaction factor introduced while constructing the site, several other factors may contribute to the orientation of the elongated pores. First, desiccation cracks associated with bedding planes of randomly distributed shale and lignite fragments tend to add a random element to pore orientation patterns. Second, multiple compaction process may occur when the overburden materials were handled during mining and reclamation processes. Consolidation and compaction might have occurred before site levelling and construction of the research plots. Last, the amount of short elongated craze and skew planes arising from desiccation cracks may contribute significantly to the random orientation. These factors add complexity to the patterns and make interpretation more difficult.

Correlation of total and macroporosity with selected physical properties

Selected physical properties of mine soils such as bulk density, cone index and saturated hydraulic conductivity were measured. These compaction and morphology-related soil properties serve as indicators for quantification of the effects of compaction.

Penetration resistance values also reflect compaction. Dense, massive soil materials have greater cone indices than loose well-structured soils. Great spatial variability is observed both within and between treatments in penetration resistance. The statistical analysis of penetration resistance data collected in August 1990 is illustrated in Table 3. Some of the "noise" and "spikes" observed in cone indices may be due to fragments of shale and lignite encountered in addition to the difference in cohesivety of matrices and/or moisture interactions. Compacted layers were identified by the significantly higher cone index in the table.
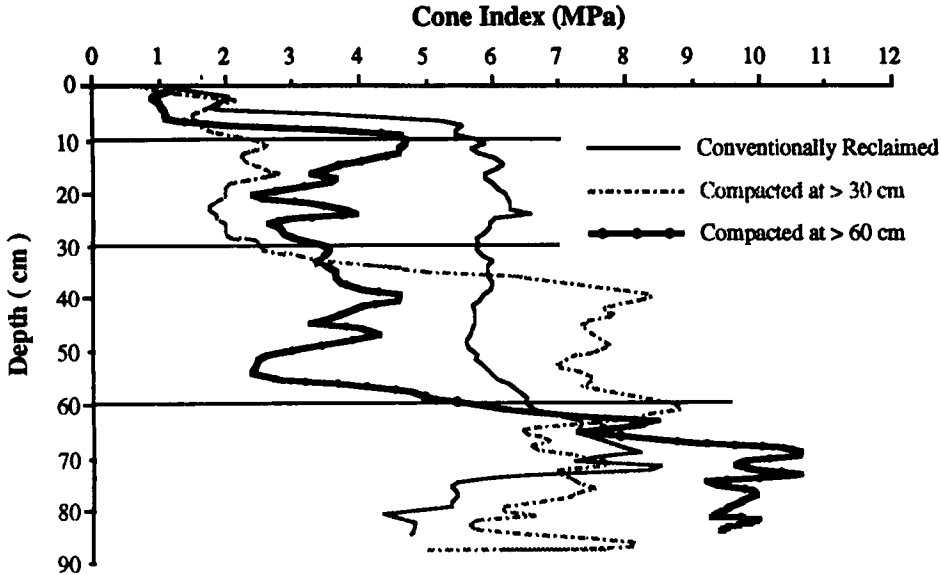
Cone Index (MPa)

Fig. 5. Penetration resistance profiles of the 3 treatments.

Significant differences at 0.01 probability level in cone index were observed between depths in conventionally reclaimed soil. Although surface layers of treatments A, B and C were all reclaimed by conventional methods, they vary significantly in degree of compaction. Conventionally reclaimed treatment A has a restrictive layer starting at about 10 cm depth (Table 3 and Fig. 5). At 10 - 30 cm, cone indices in treatment A is significantly higher than the other two treatments at 0.01 probability level (see F values and Duncan's mean comparisons). At 30 - 60 cm, significantly higher cone indices are observed in treatments A and B than in treatment C. The high cone indices for treatment B can be attributed to the induced compaction, whereas in treatment A it is probably caused by conventional reclamation operations. At 60 - 90 cm, treatment A has lower cone indices than the induced compaction zones of treatments B and C, presumably due to the induced compaction conditions.

Typical penetration resistance profiles for these three treatments are presented in Fig. 5. More than one compaction zone could be formed by conventional reclamation, in this case, with a second one starting at about 60 cm depth. The limiting cone index for root growth was reported by Taylor (1971) to be between 1 MPa and 2.5 MPa. Cone indices of all the subsurface zones of all treatments far exceed these limits (Table 3 and Fig. 5) and provide a physical constrain to the quality of these reclaimed mine soils.

A direct consequence of the decrease in soil macroporosity and horizontal orientation of macropores is the low saturated hydraulic conductivities (K_{sat}) measured in the compacted zones (Table 2). They range from 2.1×10^{-7} to 1.1×10^{-6} m/s with an average of 2.7×10^{-7} m/s on uncompacted surface layers (group k and m). It decreases to an average of 6.0×10^{-8} m/s in the 15 - 90 cm layers of treatment A (group l). The compacted zone in treatments B and C (group n) have the lowest values, ranging from 8.1×10^{-9} to 6.7×10^{-8} m/s with an average
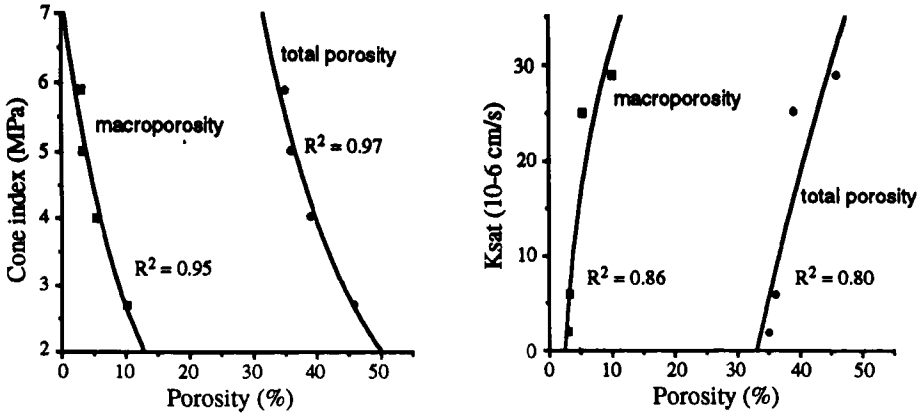
Fig. 6. Correlation of macro and total porosities to cone index and saturated hydraulic conductivity (K_{sat}).

of 2.0×10^{-8} m/s which is about 10 times slower than the surface layers. The reduction of macropores by compaction is responsible for the decreased saturated hydraulic conductivity.

Regression curves were established between soil macroporosity (ε_m), total porosity (ε) and cone indices (CI) and saturated conductivity (Fig. 6).

The following regression equations were obtained:

$$CI = 7.26 \times 10^{(-0.0292\varepsilon_m)} \qquad R^2 = 0.95$$
$$CI = 58.16 \times 10^{-0.0292\varepsilon} \qquad R^2 = 0.97$$
$$K_{sat} = -19.65 + 51.53 \log(\varepsilon_m) \qquad R^2 = 0.86$$
$$K_{sat} = -344.33 + 226.52 \log(\varepsilon) \qquad R^2 = 0.80$$

The cone indices are well correlated to macroporosity and total porosity. When total and macroporosity decrease, soil particles become more closely packed and the dense s-matrix results in high penetration resistance. Reduction of preferential flow pathways in the soil due to low porosities, especially macroporosity, together with horizontal orientation of elongated macropores, is the main cause of the sharp decrease in saturated hydraulic conductivities of conventionally reclaimed subsoils and induced compaction zones in these soils.

CONCLUSIONS

Compaction by conventional reclamation operations and induced simulated conditions result in undesirable physical constraints to these materials. Compaction results in formation of massive structure, a decrease in total porosity via rearrangement of soil particles and a reduction of soil macropores. Stress cutans and bent and broken shale fragments are indicative of mechanical stress and shear stress induced by the heavy weight of the reclamation vehicles. Soil cone indices and hydraulic conductivities also reflect these adverse attributes and are well correlated to soil macroporosity and total porosity. Decreases in macroporosity and horizontal orientation of the macropores by compaction result in decreased rates of water movement. A

probable consequence of these effects are enhanced surface runoff. Compaction also restricts root penetration and proliferation into the compacted zones and thus decreases plant growth and productivity.

REFERENCES

Arora, H.S., Dixon, J.B. and Hossner, L.R., 1978. Pyrite morphology in lignite coal and associated strata of East Texas. Soil Sci., 125: 151-159.

Baver, L.D., Gardner, W. H. and Gardner, W. R., 1972. Soil Physics. John Wiley and Sons, New York.

Bearden, E.D., 1984. A Comparison of Variability of Undisturbed and Surface Mined Soils in Freestone County, Texas. MSc. Thesis, Texas A&M University, College Station, Texas.

Bouma, J., 1982. Measuring the hydraulic conductivity of soil horizons with continuous macropores. Soil Sci. Soc. Am. J., 46: 438-441.

Bradford, J.M. and Gupta, S.C., 1986. Compressibility. In: A. Klute (Editor), Methods of Soil Analysis, Part 1: Physical and mineralogical methods. Am. Soc. Agron. and Soil Sci. Soc. Am. Monograph No. 9, pp. 479-480.

Bresson, L. M. and Zambaux, C., 1990. Micromorphological study of compaction induced by mechanical stress for a dystrochreptic Fragiudalf. In: L.A. Douglas (Editor), Soil Micromorphology: A Basic and Applied Science. Proc. VIII Int. Working Meeting on Soil Mircromorphology, San Antonio, Texas, July 1988. Developments in Soil Science 19, Elsevier, Amsterdam, pp 33-40.

Brewer, R., 1976. Fabric and Mineral Analysis of Soil. R.E. Krieger Publ., New York, 182 pp.

Doolittle, J. J., 1986. Pyrite Oxidation in a Minespoil Environment: A Lysimeter Study. M.Sc. Thesis, Texas A&M University, College Station, Texas.

Duncan, D.B., 1955. Multiple range and multiple F tests. Biometrics, 11: 1-42.

Hons, F.M., 1978. Chemical and Physical Properties of Lignite Spoils and Their Influence Upon Successful Reclamation. Ph.D. Dissertation, Texas A&M University, College Station, Texas.

Hooks, C.L. and Jansen, I.J., 1986. Recording cone penetrometer developed in reclamation research. Soil Sci. Soc. Am. J., 50: 10-12.

Hossner, L.R. (Editor)., 1980. Reclamation of Surface-Mined Lignite Spoil in Texas. Texas Agri. Exp. Sta. Bull. RM-10, College Station, Texas.

Jansen, I.J., 1977. Research toward reclamation of surface-mined land for row-crop production. In: Papers presented before the Fifth Symposium on Surface Mining and Reclamation. National Coal Association, pp. 25-27.

Jansen, I.J. and Melsted, S.W., 1986. Land shaping and soil construction. In: L.R. Hossner (Editor), Reclamation of Surface-Mined Lands. CRC Press, Boca Raton, Florida. pp. 125-136

Jongerius, A. and Heintzberger, G., 1975. Methods in Soil Micromorphology: A Technique for the Preparation of Large Thin Sections. Soil Survey Papers No. 10, Neth. Soil Survey Institute, Wageningen, p. 48.

Miedema, R., Pape, Th. and van der Waal, J.J., 1974. A method to impregnate wet soil samples, producing high-quality thin sections. Neth. J. Agri. Sci., 22: 37-39.

Morrison, J.E., Jr. and Bartek, L.A., 1987. Design and field evaluation of a hand pushed digital soil penetrometer with two cone materials. Transactions of the ASAE, 30: 646-651.

Puentes, R., 1990. Soil Structure Restoration in Vertisols Under Pastures in Texas. Ph.D. Dissertation, Texas A&M University, College Station, Texas.

Pugh, C.E., Hossner, L.R. and Dixon, J.B., 1981. Pyrite and marcasite area as influenced by morphology and particle diameter. Soil Sci. Soc. Am. J., 45: 979-982.

Soil Survey Staff, 1951. Soil Survey Manual. U.S. Dept. Agric. Handb. 18, U.S. Gov. Printing Office, Washington, D.C., 503 pp.

Taylor, H.M., 1971. Effects of soil strength on seedling emergence, root growth and crop yield. In: K.K. Barnes (Editor), Compaction of Agricultural Soils. American Society of Agricultural Engineering Monograph, pp. 292-305.

Effects of simulated seismic acceleration on silty clay soil horizons: a submicroscopic, micromorphological and geotechnical approach

D. Magaldi[1], P. Rissone[2] and G. Totani[1]

[1]Dipartimento di Ingegneria delle Strutture delle Acque e del Terreno, University of L'Aquila, 67100 L'Aquila, Italy

[2]Dipartimento di Meccanica e Tecnologie Industriali University of Firenze, 50100 Firenze, Italy

ABSTRACT

Magaldi, D., Rissone, P. and Totani, G., 1994. Effects of simulated seismic acceleration on silty clay soil horizons: a submicroscopic, micromorphological and geotechnical approach. In: A.J. Ringrose-Voase and G.S. Humphreys (Editors), Soil Micromorphology: Studies in Management and Genesis. Proc. IX Int. Working Meeting on Soil Micromorphology, Townsville, Australia, July 1992. Developments in Soil Science 22, Elsevier, Amsterdam, pp. 719-728.

In order to study the deformation of microstructure and microfabric of silty clay soils induced by earthquakes, some air-dried samples from C horizons of two Ustorthents from Pescara, Italy were subjected to simulated seismic acceleration. Induced shear stress was simulated via an equivalent inertial load using an acceleration root mean square value of 9.8 m/s^2 for 180 s.

A micromorphological analysis of the samples was carried out on large thin sections. Scanning electron microscopic (SEM) observations were performed on small air dried soil fragments. Measurement of the mechanical properties was carried out by uniaxial or "unconfined" compressive strength test. Strain-gauges were used to measure the deformations.

SEM and micromorphological observations and geotechnical tests, carried out on both virgin and stressed samples, suggest that seismic-like acceleration should bring about the following induced effects:

1. Development of collapsed clay platelet fabrics (from previous cardhouse fabrics) and formation of shear planes at submicroscopic level (5000 to 10,000×);
2. No significant changes to the basic orientation pattern of clay domains and of other micromorphological aspects;
3. A decrease (10 - 20%) in the unconfined compressive strength.

INTRODUCTION

The effects of earthquakes on bedrock and deep, loose, unconsolidated materials have been known for some time (Hunt, 1984; Vucetic and Dobry, 1988). The effects on soil horizons, however, are little appreciated largely because of their lesser importance in engineering practice. Therefore, a submicroscopic and micromorphological analysis of samples from C horizons of silty clay soils was carried out with application of simulated seismic acceleration to determine the effects on microstructural properties. In addition, some geotechnical
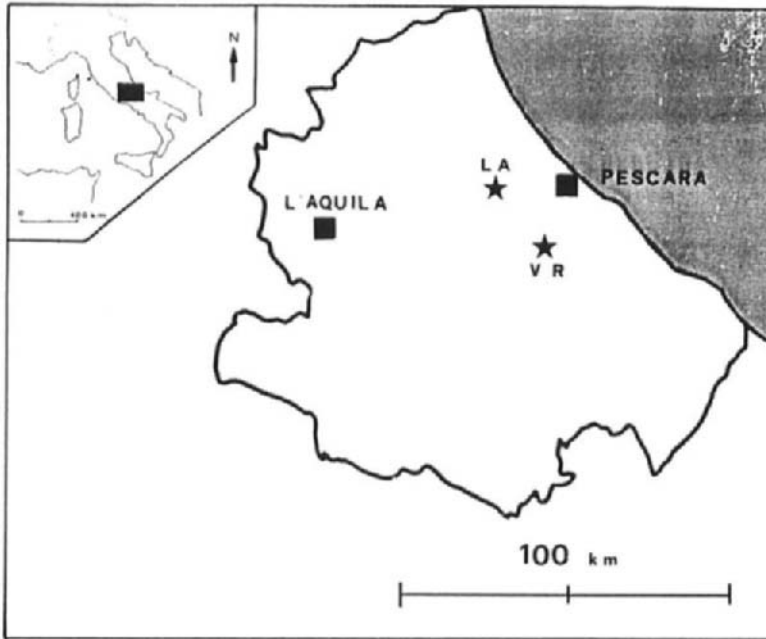
Fig. 1. Location of sample sites.

Table 1
Mineralogical composition of clay-size fractions.

Sample	Clay Mineral Composition (%)					
	SM	IS	CL	CV	IL	KA
Villa Reia	30	10	15	15	10	20
Loreto Aprutino	25	10	20	10	15	20

SM = smectite, IS = illite smectite, CL = chlorite, CV = chlorite vermiculite,
IL = illite chorite, KA = kaolinite

characteristics of the soil were examined. Research appeared to be useful for obtaining more information on the effects of the acceleration on mechanical soil properties in relation to shallow foundations and slope stability problems (Mitchell, 1956; Veniale, 1985; Crespellani, 1988).

Simulated acceleration takes advantage of the fact that an approximate value may be given to the energy released during an earthquake by examining the maximum acceleration reached during the quake (Hunt, 1984).
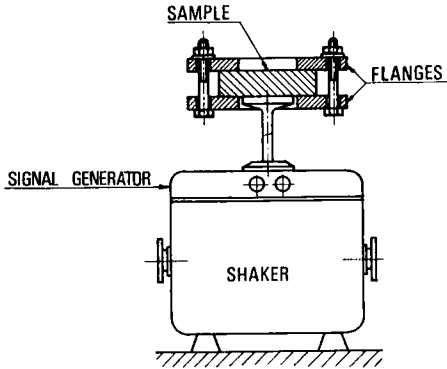
Fig. 2. Apparatus for the seismic acceleration simulation.

MATERIALS AND METHODS

The soils were developed in the surface formation of normally consolidated Pliocene clay in the Province of Pescara (Central Italy), one near Villa Reia (VR) and the other near Loreto Aprutino (LA) (Fig. 1), where seismic activity is almost absent. Approximately 10 kg undisturbed block samples were taken from each site at a depth of about 2 - 3 m in order to avoid the consequences of mechanized agriculture, erosion and rapid wetting and drying cycles. The samples, collected in an almost dry state, were representative of the deep C horizons of Ustorthents (Soil Survey Staff, 1975) found in this area and were silty clay. The moist colours were light grey (5Y 6.5/1) for Villa Reia and grey (2.5Y 5/0) for Loreto Aprutino. Their clay mineral composition was almost identical (Table 1). Each sample was air-dried and divided, at testing time, into smaller undisturbed samples on which the various tests and analyses described below were carried out.

Seismic simulation

The conditions of seismic simulation were established on the basis of data obtained from the most important seismic events worldwide (Hunt, 1984) and on the information collected and analysed by Carrara *et al.* (1989) from central and southern Italy. The acceleration values referred for real earthquakes worldwide range 0.03 to 11.8 m/s^2. The acceleration used was 9.8 m/s^2, which corresponds to point 9 - 10 on the Mercalli Scale. The duration of the vibrations was set at 180 s which is rarely encountered naturally except in extreme circumstances, *e.g.* the 1964 earthquake at Anchorage in Alaska. Taking into consideration that the research was in early stages, these very severe conditions were selected in order to amplify the effects on the microfeatures induced by acceleration.

The experimental setup was developed mainly to obtain information about the capabilities of the proposed approach since the samples came from soil horizons, we assumed that the dynamic inertial loads were far more important than other forces such as the weight of soil above the sampling depth. No confining stresses were imposed in order to reproduce the conditions of materials at soil surface. Therefore, the simplest experimental procedure was used which applied a shear load to the sample. Such a stress would typically arise from
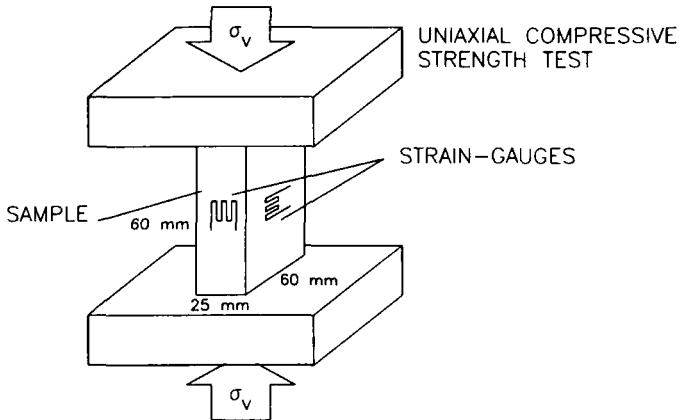
Fig. 3. Apparatus for measuring uniaxial compressive strength on rectangular parallelepiped soil specimens.

reciprocal movements among soil strata. The load was applied using the device shown in Fig. 2.

The samples (in the form of a rectangular parallelepiped $60 \times 60 \times 25$ mm) were placed at the same orientation as in the field, between two confining plates each with a central hole 35 mm in diameter. The mass of the plates was 1 kg in order to provide sufficient inertial load. Vibration was induced by a shaker resting on the free opposite surface of the sample. Acceleration (root mean square value) was achieved by a random signal with a cutoff frequency 1 to 25 Hz. Under this standard condition a nominal shear stress of 0.4 N/cm^2 was calculated in the cylindrical section of the sample corresponding to the hole. The value is quite rough because the boundary effects derived by the contact between sample and confining plates were not well known.

The subsequent analyses and observations were undertaken on both stressed and virgin samples.

Scanning Electron Microscope (SEM) Observations

Polyhedral fragments which had been air-dried and coated with gold were examined using a Philips SEM (model 505). Observations were carried out on the central parts in contact with the vibrating head and on those around the sides. SEM descriptions were made using the terminologies of Smart and Tovey (1981) and Cotecchia *et al.* (1982).

Thin Section Observations

Thin sections were made from undisturbed samples which had been air-dried and impregnated with polyester resin. Micromorphological descriptions were made using the terminologies of Bullock *et al.* (1985) and partly of Brewer (1964). Orientation analysis of the clay domains was also undertaken following the method outlined by Magaldi (1987). This analysis is based on the variation of light intensity over 5 fields of view (1 mm in diameter) per section, obtained by submitting the section to a full rotation under crossed polarizers. Readings are taken after every 20° of rotation by means of a Nikon photomicrographic device (Microflex). Similar values over a complete rotation indicate random distribution of the
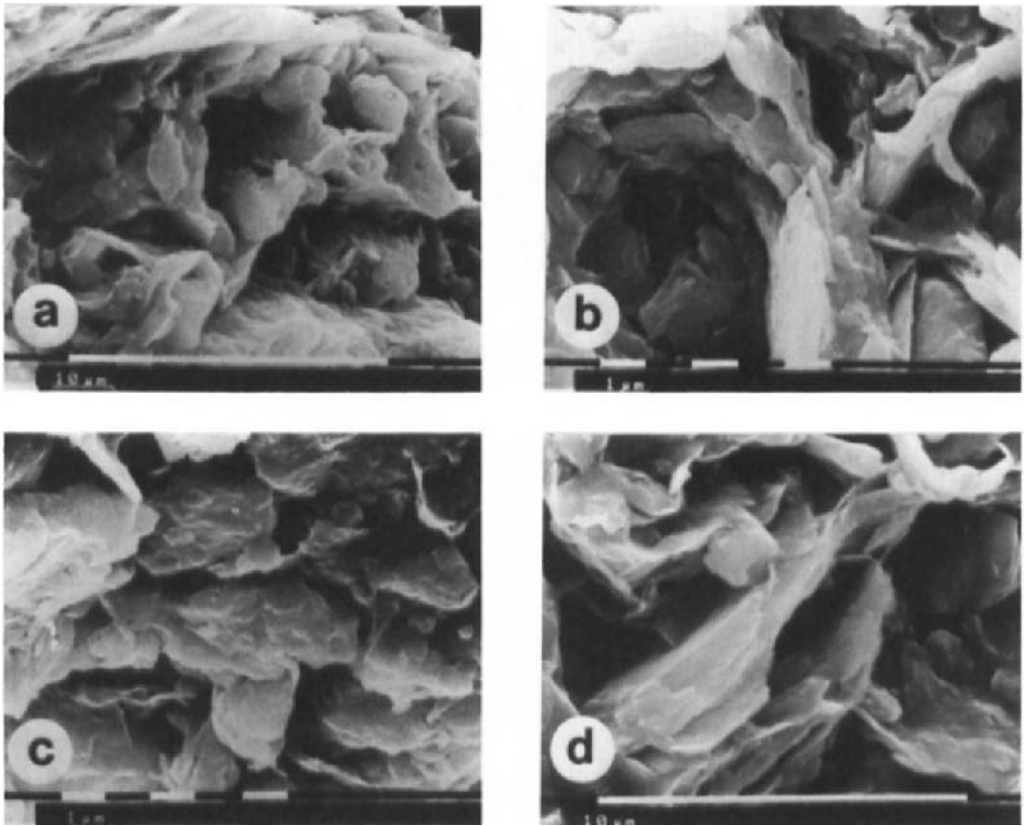
Fig. 4. SEM micrographs of untreated (virgin) clay samples showing: face-to-face and edge-to-edge aggregation, common equant voids, diffuse cardhouse fabric and some oriented clay platelets. (a, c, d, Villa Reia; b, Loreto Aprutino).

domains. A small number of periodically recurring values similar to each other, but different from the rest, indicate one or more directions of preferential orientation. The fields of view were selected among more clayey areas excluding those where coarser mineral grains occurred. The degree of orientation can be roughly quantified by means of Pearson's coefficient of relative variability, equal to the ratio of standard deviation and arithmetic mean. This was calculated for 20 fields of view for each sample.

Geotechnical tests

In view of the small size of the samples prepared for the simulation and the conditions under which the test was conducted (air-dried samples), it was decided that only a simple, undrained compression test could provide a sufficient quantity of data to show up any eventual behavioural differences between virgin samples and stressed samples.

Table 2
Submicroscopic effects of simulated seismic acceleration on samples. Sample location: LA, Loreto Aprutino; VR, Villa Reia. Location of observation within accelerated samples: "centre", adjacent to shaking rod; "side 1" and "side 2", edges. Fabric: CH, cardhouse; pl, clay platelets.

Sample	Acceleration	Aggregation	Voids	Fabric
LA	undisturbed	face to face common; edge to face scarce	equant, common	CH, some oriented pl.
LA side 1	9.8 m/s^2 for 180s	face to face common; edge to face scarce	prolate/irregular, common	CH, many oriented pl.
LA side 2	"	face to face common; edge to face scarce	prolate/irregular, polygonal, common	CH, some oriented pl.
LA centre	"	face to face with some disturbed particles	prolate/irregular, few	collapsed CH, with many oriented pl.
VR	undisturbed	face to face, edge to edge	equant, rounded, common,	CH, no oriented pl.
VR side 1	9.8 m/s^2 for 180s	face to face, edge to edge	prolate/irregular, common	collapsed CH, with many oriented pl.
VR side 2	"	face to face, edge to edge	prolate/irregular, rounded, common	collapsed CH, with some oriented pl.
VR centre	"	face to face, edge to edge, some deformed platelets	prolate/irregular, common	collapsed fabric, few oriented pl.

A compression testing machine with parallel plates was used for the test, enabling a vertical load to be applied to the samples. The latter were in the form of a rectangular parallelepiped $60 \times 60 \times 25$ mm and placed as shown in Fig. 3. Two strain gauges were applied to each 60×60 face and one to each 60×25 face to measure, respectively, the degree of axial and lateral deformation. The strain gauges (K = 2.05 ± 1%) were connected to a data acquisition device in order to record continuously the data. The axial load was applied at a constant velocity of approximately 200 kPa/s and measured by means of an electronic load cell (K = 0.2%).

RESULTS AND DISCUSSION

SEM Observations

The virgin samples of both soils (Fig. 4) show face-to-face aggregations of clay platelets or, less commonly, face-to-edge or edge-to-edge, generally arranged as a cardhouse fabric, in the broad sense of the term. Voids delimited by the clay aggregates were common and usually had equant shapes. The microstructure observed after simulated vibration (Fig. 5) was similar in both sample groups and at different locations within the individual samples.
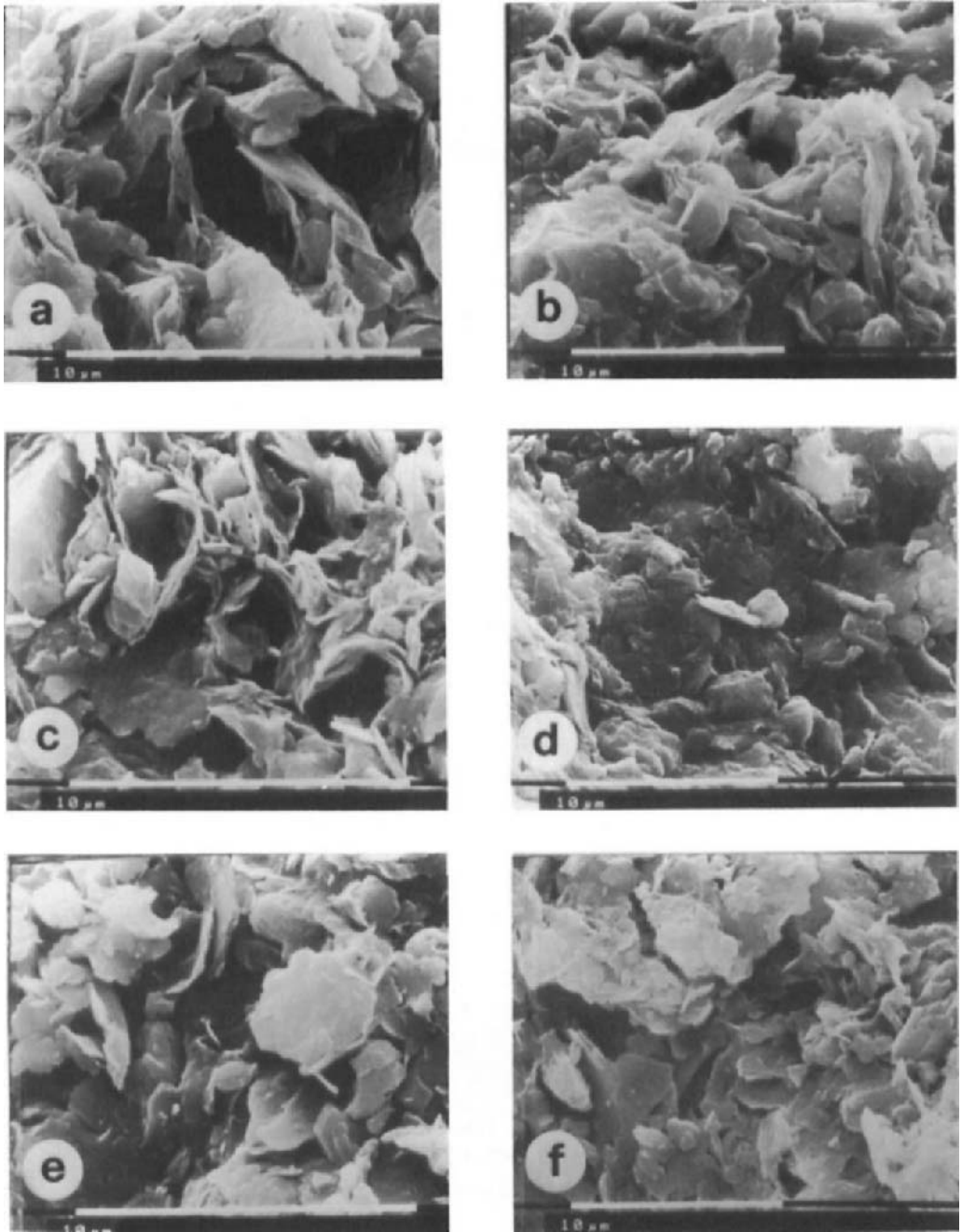
Fig. 5. SEM micrographs of stressed clay samples showing: frequent deformed and collapsed fabrics, disturbed clay aggregates, reduced void sizes and common oriented clay platelets. (a, d, f, Loreto Aprutino; b, c, e, Villa Reia).

STRESS—STRAIN BEHAVIOUR OF
VIRGIN AND STRESSED SOILS
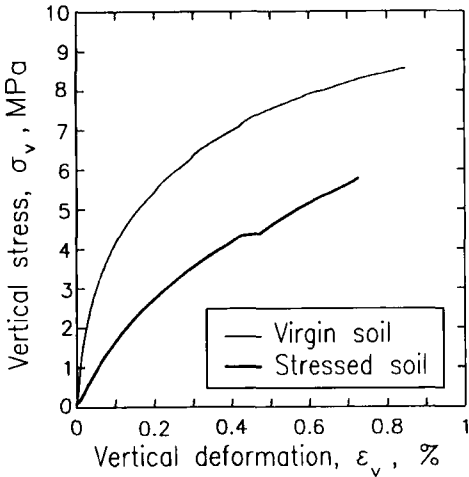
Fig. 6. Typical stress-strain behaviour of virgin and stressed soils measred by unconfined compression test. Results relate to a sample from Villa Reia. σ_v, vertical stress; ε_v, vertical deformation (percent reduction in thickness).

mainly involved alterations or collapse of the microstructure and creation of preferential planes of orientation. In some cases there was a marked change in the shape of the voids together with a reduction in their size. The shape of voids changes from equant or round types to more prolate and irregular types. The results obtained for the various samples are presented in summary form in Table 2.

Thin Section Observations

Thin sections from both locations, both before and after application of stress, were very similar except for minor   variations in constituents and some pedological features. The micromorphology was described as follows:

Microstucture. Predominantly massive with 2 - 5% visible porosity; few vughs (50 - 500 μm), with irregular walls and random basic distribution; very few planar voids.

Basic mineral components: c/f limit 20 μm; c/f ratio 10:90. Coarse fraction of subangular, very fine sand sized of quartz with some detrital calcite and muscovite; few grains of altered biotite and chlorite; all with random basic distribution. Fine fraction mostly of fine silt and clay sized clay minerals mixed with fine calcitic material; speckled pale brown in plane light.

Basic organic components. Small amount of fine, amorphous, possibily carbonized, organic material; occasional, well preserved foraminiferal tests.

Groundmass. Open spaced porphyric related distribution; stipple speckled to crystallitic and undifferentiated b-fabric.

Pedofeatures. Crystalline pedofeatures include common, single euhedral fine sand sized calcite crystals, equant ones with a sharp boundary. Amorphous pedofeatures include very few, typic and concentric, coarse sand sized brown to dark red Fe nodules usually rounded and occasionally with a core filled with silicatic and Ca carbonate anorthic material.

The degree of orientation calculated from light intensity measurement was low (coefficient of variability, 4 - 5%) in both soils, both before and after stress application.

Geotechnical Results

The stressed samples had lower uniaxial compressive strength (10 - 20% less on average) and lower strain moduli than the virgin samples (Fig. 6). These differences appear to substantiate the assertion that vibration causes the partial destruction of the original clay microstructure.

CONCLUSIONS

The methodology here used promises to be a useful tool for interpreting the genesis of some microstructures found in unweathered and weathered fine textured material. Of the tests carried out, only the micromorphological analysis did not show up the microstructural differences. It is possible that the induced alterations were on too small a scale to be observed in thin section. It must be concluded that fine sized soils and sediments, although dried, may be altered by seismic-like vibrations, with the collapse of clay aggregates, collapse of cardhouse fabrics, formation of shear micro-planes and the probable reduction of very fine porosity. These changes are mirrored at a macroscopic level by the deterioration of their mechanical properties (destructuration of the clay, decrease of compression strength, and perhaps, decrease of shear strength).

REFERENCES

Brewer, R., 1964. Fabric and Mineral Analysis of Soils. John Wiley and Sons, New York, 470 pp.

Bullock, P., Fedoroff, N., Jongerius, A., Stoops, G. and Tursina, T., 1985. Handbook for Soil Thin Section Description. Waine Research Publications, Wolverhampton, U.K., 178 pp.

Carrara, C., Magri, G., Margottini, C., Molin, D. and Narcisi, B., 1989. Aspetti principali della sismicita' storica. In: Elementi di Tettonica Pliocenico-Quaternaria ed Indizi di Sismicita' Olocenica nell'Appennino Laziale-Abruzzese. Guida all'Escursione, Società Geologica Italiana. pp. 11-19.

Crespellani, T., 1988. Meccanismi ed effetti indotti dal terremoto nei pendii naturali. In: P. Canuti and E. Pranzini (Editors), La Gestione delle Aree Franose. Edizioni delle Autonomie, Rome, pp. 165-197.

Cotecchia, V., Federico, A. and Trizzino, R., 1982. Microtessiture di sedimenti argillosi, analisi delle tipologie e terminologie ed applicazioni nel campo della geotecnica. Geol. Applicata e Idrogeologia, 2: 1-34.

Hunt, R.E., 1984. Geotechnical Engineering Investigations Manual. McGraw-Hill, New York, 983 pp.

Magaldi, D., 1987. Degree of soil plasma orientation in relation to age in some hydromorphic soils of Tuscany. In: N. Fedoroff, L.M. Bresson and M.A. Coutry (Editors), Soil Micromorphology. Proc. VII Int. Working Meeting of Soil Micromorphology, Paris, July 1985. Association Française pour l'Etude du Sol, Plaisir, France, pp. 605-609.

Mitchell J.K., 1956. The fabric of natural clays and its relation to engineering properties. Proc. Highway Research Board, 35: 693-713.

Smart, P. and Tovey, N.K., 1981. Electron Microscopy of Soils and Sediments: Examples. Clarendon Press, Oxford, 178 pp.

Soil Survey Staff, 1975. Soil Taxonomy: A Basic System of Soil Classification for Making and Interpreting Soil Surveys. U.S. Dept. Agric. Handb. 436, U.S. Gov. Printing Office, Washington, D.C., 754 pp.

Veniale, F., 1985. The role of microfabric in clay soil stability. In: A. Pozzuoli (Editor), Clays and Clay Minerals. Mineralogica et Petrographica Acta 29-A, Bologna, pp. 101-119.

Vucetic, M. and Dobry, R., 1988. Degradation of marine clays under cyclic loading. Journal Geotechnical Engineering Division, American Society Civil Engineering, 114: 133-149.

Microstructure of desert soils related to swelling behaviour

J.M. Marcoen[1], D. Tessier[2] and Y. Zaczek[3]
[1]Faculté des Sciences Agronomiques, B 5030 Gembloux, Belgium
[2]Science du Sol, Inra, 78026 Versailles, France
[3]Tractebel Engineering, Av. Ariane, B 1200 Brussels, Belgium

ABSTRACT

Marcoen, J.M., Tessier, D. and Zaczek, Y., 1994. Microstructure of desert soils related to swelling behaviour. In: A.J. Ringrose-Voase and G.S. Humphreys (Editors), Soil Micromorphology: Studies in Management and Genesis. Proc. IX Int. Working Meeting on Soil Micromorphology, Townsville, Australia, July 1992. Developments in Soil Science 22, Elsevier, Amsterdam, pp. 729-736.

The apparently anomalous geotechnical behaviour related to uncontrolled irrigation of aridic soils with relatively low clay content is explained on the basis of a case history in the Riyadh area, Saudi Arabia. The classical swelling tests (ASTM D4546) failed to pinpoint the presence of expansive soils at this site. However, mineralogical identification by XRD indicated evidence for smectite among hormite, illite and kaolinite as the clay fraction in a quartz and calcite matrix. Micromorphological studies (thin section micrography, SEM, electron microprobe elemental analysis, TEM and electron diffraction) have been carried out on undisturbed samples. The results clearly explain the geotechnical instability of the soil: smectite swelling at low water potential followed by loss of cohesion at high water content.

INTRODUCTION

The destructive impact of expansive soil movement is listed as one of the major natural hazards along with earthquakes, landslides, hurricanes, tornadoes and floods (Wiggins, 1978). In 1976, soil investigations were performed by well qualified contractors on the site for a very large building complex ($\sim$500,000 m^2) to be erected on desert soil located approximately 20 km NE of Riyadh, Saudi Arabia. The presence of potentially swelling soils was unknown in this region at the time of construction and for some time afterwards. (Chen, 1975, 1988; Ruwaih, 1988).

Damage to buildings, observed toward the end of 1985 but then unexplained, was attributed to soil heaving. It was thought that water, from excessive irrigation of the numerous gardens and patios with trees and flowerbeds, had reached the underlying soil with the result of heave and localized superficial soil collapses. This interpretation was still being mooted up until mid-1988.

Throughout this period, the classical swelling tests (ASTM D4546) had failed to detect any expansive behaviour in the silty-sandy soil at this site, although subsequent mineralogical studies by XRD (after soft decarbonation) indicated the presence of smectite as a swelling component (Marcoen and Zaczek, 1988, 1989). This result was in agreement with other studies undertaken on different profiles in the region from agricultural and pedological
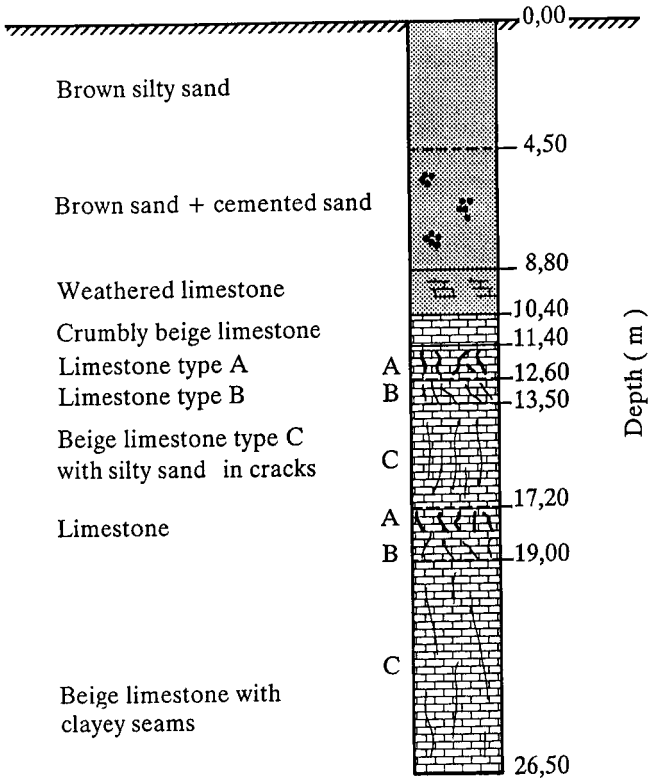
WEATHERING LEVEL :
A = VERY WEATHERED
B = MODERATELY WEATHERED
C = LITTLE WEATHERED

Fig. 1. Typical soil profile
from borehole records.

viewpoints (Lee *et al.*, 1983; Shafdan and Mashhady, 1985). The aim of the present study was to utilize recent developments in hydrated clayey soil systems and micromorphology to help understand the soil response mechanism of a major geotechnical problem.

GEOLOGY

The affected zone lies towards the centre of the Arabian shield basement of Precambrian age which is covered by a thick sedimentary sequence ranging in age from Cambrian to Cretaceous. The sedimentary rocks, mainly limestone, are covered by younger aeolian sand and water deposited superficial materials from the Quaternary. To the west of the site is the Al Jubayl escarpment, formed from the Sulaiyl limestone formation (Thamana group, lower Cretaceous). On the site, the subsurface materials consist of beige limestone more or less weathered (types A, B and C) as indicated by the continuous boring described in Fig. 1. The topsoil consists of reddish brown fine to very fine sand with some silt and fine gravel of Quaternary age. This material is in a medium dense to very dense state of compaction.

GEOTECHNICAL DATA

Soil and foundation investigations were performed in 1976, at the design stage. No groundwater was encountered in any of the borings. The grain-size analyses indicated sandy soils with none to very few clay particles. The Atterberg limits were very low reflecting the sandy composition with no potential for heaving. Following geomechanical test results, the proposed structures were designed to be supported by conventional shallow-spread footings which allowed for a 0.2 to 0.3 MPa bearing pressure. It was recommended that ponding of water in excavated footings be avoided so as not to soften the bearing surface, since this could have induced settlement. At the design and soil investigation stages, no evidence of swelling was discovered by the classical geotechnical tests that are normally applied.

As a consequence of uncontrolled irrigation, made some years after the construction, the moisture content reached 14% down to a depth of 3.5 m with an average around 7% down to 15 m. Beyond the depth of 16 m the water content was measured around 4%. The natural soil density was quite high, around 20 to 21 kN/m^3, for the dry samples.

ANALYTICAL PROCEDURES

Mineralogy

Mineral identification was performed by X-Ray diffraction (XRD) on randomly oriented powder of whole samples and of oriented mounts of the clay size fraction (<2 μm) after selective decarbonatation by NaOAc at pH 5.

Water potential and swelling

Natural clods, between 5 to 10 cm^3 in size, were progressively wetted at water potentials from -1.6 MPa to -1.0 kPa or were equilibrated with 50% relative humidity (RH) using the filtration device described by Tessier and Berrier (1979). Apparent volume was determined by the kerosene method (Tessier and Berrier, 1979). Dry weight was determined by reference to heating at 105°C.

Micromorphology

Micrographs of thin sections 30 μm thick were taken on samples embedded under vacuum using Epofix resin with Epodye (Struers) and observed with a petrographic microscope.

Scanning Electron Microscopy (SEM) was achieved using a SEM Phillips 525 equipped with a cryogenic system Oxford CT 1500 and a Link Energy-dispersive X-Ray spectrometer (EDX). The microstructure of the hydrated material was preserved by freeze-drying samples, about 1 mm^2, in nitrogen paste at about -210°C in order to limit water crystal growth (followed by ice sublimation at -90°C).

Transmission Electron Microscopy (TEM) of drops of clay suspensions deposited on carbon-coated grids were obtained with a Phillips 420 STEM scanning transmission electron microscope, equipped with an High Energy Electron Diffraction (HEED) device.
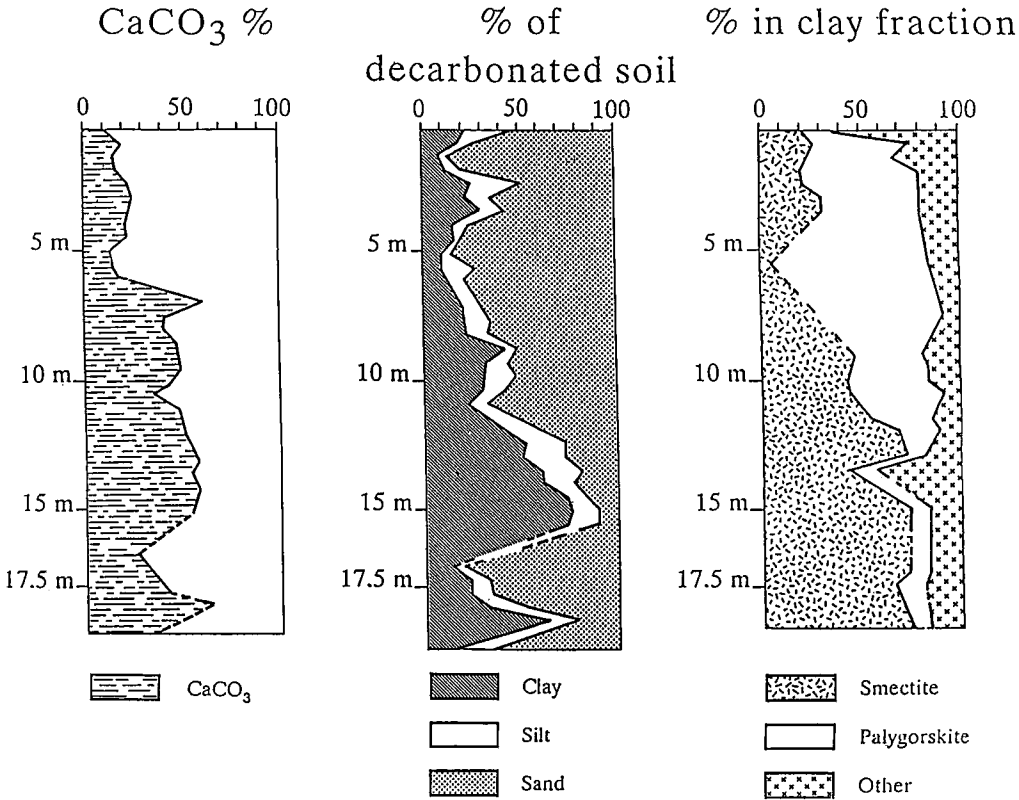
Fig. 2. Relative contents of minerals in the core boring.

RESULTS

Micrographs of thin sections of samples at 5.0 m and 12.7 m depth, have granular microfabrics with scattered quartz grains in a micritic calcite cement, without clear evidence of clay features. Porosity decreases with depth.

Fig. 2 shows the relative contents of minerals in the core boring. It is only with XRD, using the soft decarbonation treatment, that the presence of smectite as a swelling mineral among palygorskite, illite and kaolinite in the clay fraction of a quartz and calcite matrix was detected.

According to water potential studies (Table 1), the volume change for a sample of dry soil taken at 8.0 m depth gives a macroscopic swelling of 25%. This is calculated as follows:

$$S = \frac{e_{(-1kPa)} - e_0}{1 + e_0} \times 100 \qquad\qquad 1$$

where S (in %) is the macroscopic swelling, e_0 the void ratio and $e_{(-1kPa)}$ the water ratio at -1 kPa.

Table 1.
Physical data: bulk density (g cm^{-3}), water content (g g^{-1} × 100), void ratio (void volume/solid volume) and water ratio (water volume/ solid volume), at 50% RH and at -1 kPa.

Samples	Bulk density (g cm^{-3})	Void ratio e_0	Water content w(%)	Water ratio $e_{(-1 kPa)}$
Natural	2.23 ± 0.04	0.08	2.3	0.06
Hydrated (at -1 kPa)	1.96 ± 0.04	0.35	12.6	0.33

SEM observations show fibrous clay particles oriented around skeleton grains (Fig. 3a) and along large fracture planes that cross the microstructure (Fig. 3b). TEM reveals planar crystals that closely interbed the large fibres (Fig. 3c). Electron diffraction of planar crystals indicates a pseudohexagonal structure typical of 2:1 minerals (Fig. 3d).

Chemical micro-analysis of planar clay particles shows an elemental composition of Si-Al clay minerals such as smectite (Fig. 4a). On the other hand, the magnesium content of the fibrous minerals is more compatible with palygorskite composition (Fig. 4b).

DISCUSSION

The natural water content of the never-before irrigated soils was very low, as a result of the dry conditions. Following irrigation, the soil exhibited two different behaviours: (1) swelling; (2) local collapsing.

In the first step of moistening, i.e. with low water potential (negative suction pressure), swelling forces of clays are strong while the cohesion forces induced by negative pressure acting between particles can prevent the rupture of the soil.

At higher water potentials, i.e. with water pressure close to atmospheric pressure, the clay continues to swell, and cohesion forces become very weak resulting in the rupture of the material. In the studied soil, smectite is systematically interbedded between palygorskite fibres. TEM observations have shown a very small lateral extension and thickness of smectite crystals, compared to natural Ca-montmorillonites (Tessier, 1984). It is well known that the presence of smectite can lead to substantial swelling and that the smaller the clay particle size, the greater the swelling (Tessier, 1991). However, because the clay plasma is located mainly between skeleton grains a situation exists that maximizes swelling. This is associated with loss of cohesion of the material due to shearing as water content increases.

CONCLUSIONS

The features examined in this investigation explain both the swelling and mechanical instability of the material under question. The swelling behaviour of this soil has been clearly demonstrated by the micromorphological studies conducted on samples with monitored water potentials.

The lesson to be learned from this study is that the swelling behaviour of this particular soil was difficult or impossible to detect without the additional information obtained from clay mineralogy and micromorphology to compliment the geotechnical investigations. As there are situations where heaving soil behaviour cannot be detected by classical geotechnical tests
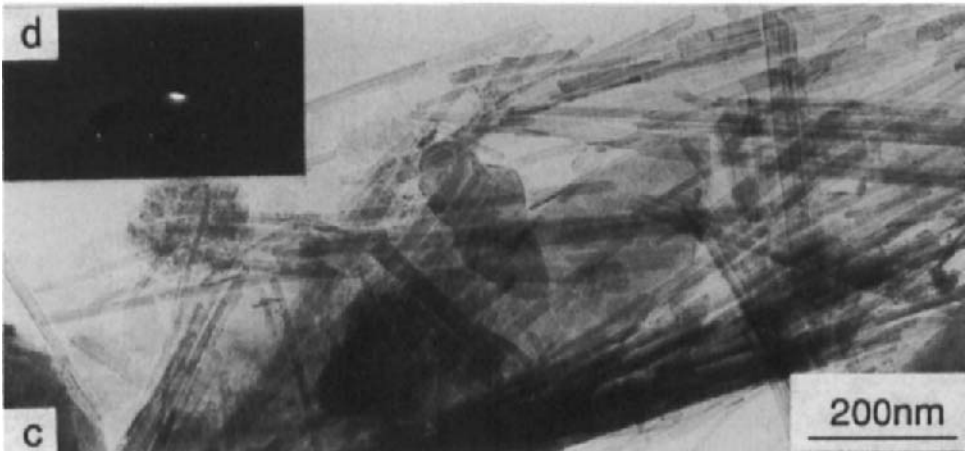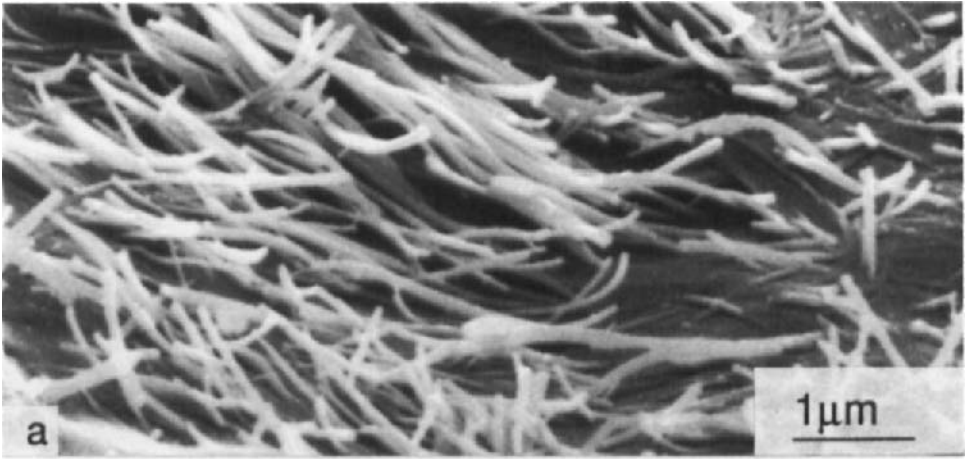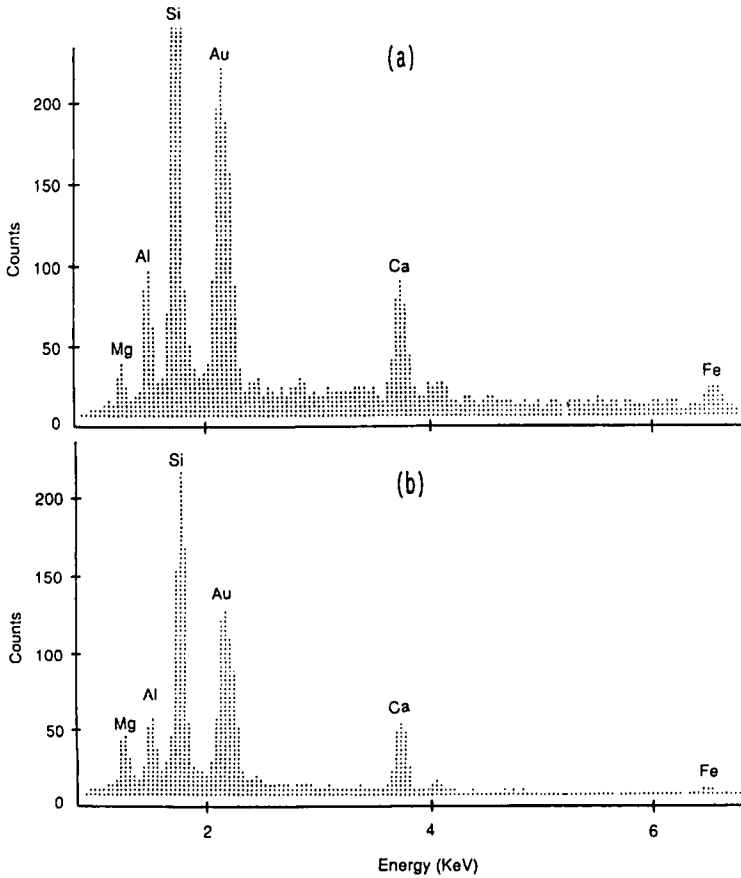
Fig. 4. EDX chemical micro-analyses of: a) smectite plates; b) palygorskite fibres.

(Atterberg, swelling tests *etc.*) it is necessary to modify the standard swelling test (ASTM D4546). A new test standard should involve the evaluation of the response to mechanical loading on samples moisturized at negative water pressures for this will show any tendency to swell.

ACKNOWLEDGMENTS

Fig. 3. SEM micrographs of: **a)** clays surrounding skeleton grains; **b)** clays oriented along fracture planes. **c)** TEM micrographs of planar crystals interbedded with fibres. **d)** HEED pattern of pseudohexagonal 2:1 mineral structure.

this study.

REFERENCES

ASTM D4546, 1989. Standard test methods for one-dimensional swell or settlement potential of cohesive soils. Annual Book of ASTM Standards, Vol. 04.08: 743-749.

Chen, F.H., 1975. Foundations on Expansive Soils. Devel. in Geotechnical Engineering, Vol 12. Elsevier, Amsterdam, 280 pp.

Chen, F.H., 1988. Foundations on Expansive Soils. Devel. in Geotechnical Engineering, Vol 54. Elsevier, Amsterdam, 463 pp.

Lee, S.Y., Dixon, J.B. and Aba-Husayn, M.M., 1983. Mineralogy of Saudi Arabian soils: eastern region. Soil Sci. Soc. Am. J., 47: 321-326.

Marcoen, J.M. and Zaczek, Y., 1988, 1989. Mineralogical and Geotechnical Investigations of Soils of Saudi Arabia (NE of Riyadh). Expert reports to the Ministry of Public Works and Housing, Saudi Arabia.

Ruwaih, I.A., 1988. Experiences with expansive soils in Saudi Arabia. In: Proceedings 6th International Conference on Expansive Soils, Dec. 1987, New Delhi, India. Vol 1. A.A. Balkema, Rotterdam, pp. 317-322.

Shafdan, H. and Mashhady, A.S., 1985. Distribution of palygorskite in sediments and soils of eastern Saudi Arabia. Soil Sci. Soc. Am. J., 49: 243-250.

Tessier, D., 1984. Etude Expérimentale de l'Organisation des Matériaux Argileux. Hydratation, Gonflement et Structuration au Cours de la Dessiccation et de la Réhumectation. Thèse, Univ. Paris VII. INRA Versailles Ed., 361 pp.

Tessier, D., 1991. Behaviour and microstructure of clay minerals. In: M. De Boodt, M. Hayes and A. Herbillon (Editors), Soil Colloids and Their Associations in Aggregates. Plenum Publishing, New York, pp. 387-415.

Tessier, D. and Berrier, J., 1979. Utilisation de la microscopie électronique à balayage dans l'étude du sol. Observation de sols humides soumis à différents pF. Science du Sol, 1: 67-82.

Wiggins, J.H., 1978. Building Losses from Natural Hazards: Yesterday, Today and Tomorrow. Report for National Science Foundation, USA, Grant No ENV.77.08435.

Soil surface crust formation: contribution of micromorphology

L.-M. Bresson[1] and C. Valentin[2]

[1]*Institut National Agronomique Paris-Grignon, 78850 Thiverval-Grignon, France and Visiting Scientist at CSIRO Division of Soils, Canberra, Australia*

[2]*ORSTOM, B. P. 11416, Niamey, Niger*

ABSTRACT

Bresson, L.-M. and Valentin, C., 1994. Soil surface crust formation: contribution of micromorphology. In: A.J. Ringrose-Voase and G.S. Humphreys (Editors), Soil Micromorphology: Studies in Management and Genesis. Proc. IX Int. Working Meeting on Soil Micromorphology, Townsville, Australia, July 1992. Developments in Soil Science 22, Elsevier, Amsterdam, pp. 737-762.

Surface crusting is due to the breakdown of surface aggregates into finer fragments and/or primary particles which are then redistributed on the surface or within the top few millimetres. Microscopic investigations of such thin layers have been found useful for more than fifty years. To assess the specific contribution of micromorphology, a literature review of the period 1939-1991 (54 papers, including only 8 pre-1980) was carried out. The main features of the experiments were analyzed, *e.g.* soil material properties, soil initial state and rainfall characteristics. Techniques for monitoring crust development and standards of description and illustration were also examined. A limitation of many experiments was the lack of recognition of crusting stages. Many crusts described seemed to be actually depositional or erosion crusts, which might explain contradictions in the literature about structural crust formation. Initial conditions, such as the soil water content before rainfall or the aggregate size distribution, were often not quoted or taken into account in the discussion. The lack of clear description, good illustration and definition of diagnostic features induced misunderstanding of widely used concepts, *e.g.* "washing-in". Nevertheless, microscopy has played a major role in our understanding of the various processes involved in both aggregate breakdown and redistribution of the resulting particles, according to soil, climatic and management conditions. In the field, crusts developing during surface degradation are genetically related and form specific time- and space-dependent sequences (structural, erosion and depositional crusts). Microscopically-defined crust types can be identified in the field using morphological diagnostic features. These help to assess the crusting rate and allow indentification of the processes involved. Methodological recommendations for future micromorphological studies are made. Research opportunities are also suggested, including the study of: (1) some crusting processes, *e.g.* dispersion in sodic environments and compaction on sandy soils; (2) the complex evolution of crusts for months (cultivated fields) or years (rangelands); (3) the development of crust strength according to the related distribution of coarse and fine particles and (4) the detachability and erodibility of various crusts.

INTRODUCTION

Structural degradation of the soil surface (crusting) strongly reduces the infiltration rate, which decreases water storage in the soil and triggers runoff and hence soil erosion. Therefore, its agricultural and environmental effects are severe, although in arid areas runoff inducement can be involved in water harvesting management. Moreover, surface crusts can induce failure of seedling emergence and hamper stand establishment. Predicting actual surface degradation in the field and preventing its consequences requires the knowledge of the processes which take place in a given soil material according to the prevailing management practices and the expected climatic conditions (Bresson and Boiffin, 1990).

Surface crust formation under rainfall or irrigation involves two stages. The first is the breakdown of surface aggregates into finer fragments and/or primary particles and involves various processes such as slaking due to entrapped air compression and physico-chemical dispersion of clay. The second is the redistribution of the resulting particles and/or fragments both laterally on the surface by splash and/or overland flow or vertically within the top few millimeters by the infiltrating water. Microscopic investigations of such thin layers have been found useful for more than fifty years (Duley, 1939) and at least 54 papers involving micromorphology have been published. Various types of crusts and/or microlayers have been described, including skin seal and washed-in layers (McIntyre, 1958a), structural and depositional crusts (Chen *et al.*, 1980), sieving crusts (Valentin, 1986), washed-out layers (Norton, 1987), coalescing crusts (Bresson and Boiffin, 1990), erosion pavements (Valentin, 1991) and infilling crusts (Bresson and Cadot, 1992).

Sometimes, the same name has been used to qualify different crusts or microlayers, *e.g.* 'skin seal' or 'washed-in layer'. Conversely, different names were used to qualify the same feature, *e.g.* 'depositional' and 'sedimentational', or 'filtration pavement' and 'three-layered structural crust'. This has induced some confusion in the literature so that Mualem *et al.* (1990) stated that "too much was left undisclosed under the common definition of soil seal leaving too much room for personal interpretation". Despite some apparent contradictions, however, micromorphology greatly contributed to our present understanding of crust formation. Recently, West *et al.* (1992) summarized the morphological characteristics of surface crusts and their genesis in relation to soil, rainfall and topographic characteristics.

The aim of this critical review paper is: (1) to assess the specific contribution of micromorphology; (2) to get a better understanding of how the main results could be obtained; and (3) to suggest research opportunities. First, the main features of the experiments were analyzed, *e.g.* soil material properties, soil initial state and rainfall characteristics. In addition, techniques for monitoring crust development, and the standards of description and illustration were examined. Then, the main formation processes were discussed and integrated within the general framework of the crusting model suggested by Boiffin (1986), Valentin and Ruiz-Figueroa (1987), Bresson and Boiffin (1990) and Valentin and Bresson (1992).

MAIN FEATURES OF THE REVIEWED PAPERS

The first paper dealing with soil surface crust and including micromorphological observations was published in 1939 (Duley). Forty years later, only 8 such papers had been published. Within 5 years, between 1986 and 1990, 28 micromorphological studies of crusting were studied. This review included 54 papers, involving 93 authors. One Australian author

contributed to 6 papers and a French one to 5 papers. Four authors, from Australia, France, The Netherlands and Israel, contributed to 4 papers and five others to 3 papers (France, Israel, Italy and USA). Seventeen authors contributed to two papers, and 65 to only one paper.

Objectives

The aim of most papers (83%) was to determine the processes involved in surface crusting. Half of them also dealt with the hydrological and/or mechanical behaviour of crusts. Few studies only considered the behaviour of the crust (9%). Sometimes the main objective of the study was not surface crusting alone but the overall degradation of the cultivated layer, including slumping or compaction (Dexter *et al.*, 1983; Pagliai, 1987; Moran *et al.*, 1988; Kooistra *et al.*, 1990).

Materials and methods

Soil material properties
The particle size distribution of the soil materials studied showed a very wide range: 1.7 - 60.4% clay, 1 - 87.2% silt, 1.2 - 89% sand (the limit between the silt and sand fractions sometimes differed, but this could not be taken into account). First studies dealt with sandy loams and silt loams (Duley, 1939); clay loams and silty clay loams were studied 30 years later (Evans and Buol, 1968) as well as loams (Ahmad and Roblin, 1971). Then, sandy clay loams (Figueira and Stoops, 1983), silty clays (Pagliai *et al.*, 1983), clays (Gal *et al.*, 1984), sands (Valentin, 1986) and silts (West *et al.*, 1990) were investigated. Valentin (1986) considered the most sandy soil material (89%), West *et al.* (1990) the most silty (82.2%). The highest clay contents were around 60%, with sand contents ranging from 5% (Moss, 1991) to 30% (Norton, 1987). No study dealt with sandy clays.

The amount of organic matter was given in only 45% of the papers reviewed. The first was Ahmad and Roblin (1971). Organic carbon ranged between 0.05% and 5%.

Gal *et al.* (1984) were the first to consider the ESP of the soil material studied. Usually, ESP was not indicated, which probably means that the soil material studied was not sodic. Therefore, 85% of the soil studied had an ESP < 5, and 15% an ESP > 15 (up to ESP = 88, Greene *et al.*, 1988)

In 54% of the papers reviewed, no additional information was given about the soil material. Clay mineralogy or ECC were often given (26%), as well as aggregate stability index (20%).

Different soil materials were studied in only 39% of the papers reviewed. The range of textures greatly varied, but was usually wider for the sand fraction (> 10% in 95%) than for the clay fraction (> 10% in 65%). Evans and Buol (1968) were the first to study soils with significant differences in clay content.

Surface characteristics
Fifty two percent of the papers reviewed dealt with seedbeds studied in the field; 39% with soil samples packed in the laboratory and 13% with rangeland soil surfaces (the first being Valentin, 1986). In some cases (7%), different types are compared (the first being Chen *et al.*, 1980).

Usually, the aggregate size distribution was not indicated (93%). Ahmad and Roblin (1971) were the first to consider the sorting degree. The upper limit of the aggregate size was quoted

in 39% of the reviewed papers. It ranged between 2 and 40 mm and only seven studies dealt with aggregates coarser than 4 mm.

The area of the studied plots ranged between 15 and 100,000 cm^2. The slope of the soil surface was indicated in 31% of the papers reviewed and ranged between 1.5 and 9%.

The initial moisture content of the soil before rainfall was not quoted in 59% of the reviewed papers, but in most cases a dry initial state could be assumed. Therefore, only one third of the studies dealt with moist or wet soils (the first being Tackett and Pearson, 1965). Only five papers compared different initial moisture contents: Valentin (1986), Valentin and Ruiz-Figueroa (1987), Helalia *et al.* (1988), Le Bissonnais *et al.* (1989) and Valentin (1991).

Rainfall characteristics

Most studies were carried out using simulated rainfall (63%) compared to natural rainfall (35%). Sometimes, flood irrigation was considered (6%). Only 7% of the reviewed papers considered various water application modes: Falayi and Bouma (1975), Casenave and Valentin (1989), Le Souder *et al.* (1990) and Bresson and Valentin (1990).

Rainfall intensity, when quoted (56%), was generally high with an average of 63 mm h^{-1} and a standard deviation of 38. Chen *et al.* (1980) were the first to use a moderate simulated rainfall intensity (26 mm h^{-1}) and Mücher *et al.* (1981) a very low intensity (7 mm h^{-1}). The kinetic energy was first quoted by Falayi and Bouma (1975), but few studies did the same (20%). Few studies (15%) considered various intensities like McIntyre and even fewer dealt with various kinetic energies (Valentin and Ruiz-Figueroa, 1987; Levy *et al.*, 1988; Valentin, 1991).

Most studies dealing with simulated rainfall did not specify the characteristics of the water used (92%) and only two considered various electrical conductivities (Tarchitzky *et al.*, 1984; Helalia *et al.*, 1988).

Monitoring crust development

Most studies (65%) dealt with only one sampling time, which means that the development of the crust could not be studied. The first study which monitored crust development was carried out by Chen *et al.* (1980). The closest monitoring (16 sampling times) was done by Luk *et al.* (1990), which allowed them to describe a complex sequence of sub-processes, including four successive generations of vesicles during 30 min rainfall.

The sampling time was generally determined by the duration of the experiment. In most studies dealing with simulated rainfall, this duration was fixed in such a way to get the so-called "final infiltration rate". In field studies under natural rainfall, however, no criteria for the sampling time was given in relation to climatic events or crop development. Time to ponding or runoff was sometimes the criterium for sampling time (9%). In some studies (9%), the development of the crust was monitored using the morphological aspect of the soil surface, according to the method suggested by Boiffin (1986).

Physical characterizations

Infiltration rate was assessed in 52% of the papers reviewed, most often from runoff measurements (68%). Boiffin and Bresson (1987) gave drip infiltrometer measurements. Other physical characteristics are sometimes given, such as the bulk density of the soil surface (13%) or the penetration resistance of the crust (11%). Le Bissonnais *et al.* (1989) studied

crust porosity using mercury injection and the modulus of rupture of the crusts was measured by Evans and Buol (1968) and Greene *et al.* (1988).

Micromorphological observations

Microscopy was the main tool for 60% of the reviewed papers. Thin sections of impregnated crusts were studied in most papers (81%), although Duley (1939) did not observe thin sections but microprofiles of crusts. Scanning electron microscopy of bulk samples was commonly used (41%), following Chen *et al.* (1980). Both techniques were often used simultaneously (20%), the first being Pagliai *et al.* (1983).

Magnifications ranged between ×1 and ×10,000. Half of the reviewed papers exhibited illustrations or descriptions at different magnifications and the ratios between the lowest magnification and the highest one ranged from 2 to 2,500.

Descriptions were generally of moderate quality. Mücher *et al.* (1981) were the first to provide quite full and global descriptions and the first detailed descriptions could be found in Chartres *et al.* (1985). Illustrations were not always very informative. Crossed or semi-crossed polarized images of thin sections, as well as SEM micrographs, were often disappointing. The photographs given by Duley (1939) were of great quality.

Image analysis was used in 30% of the reviewed papers, mainly for porosity characterization.

Results

Type of the crust studied

Structural crusts were observed in 41% of the reviewed papers. Most were named as such following Chen *et al.* (1980) but others were named using different terms although the formation processes invoked were typical of structural crusts. In addition, the crusts described and/or illustrated in some studies (20%) also seemed to be structural crusts.

So-called "depositional crusts" (Chen *et al.*, 1980), or crusts explicitly corresponding to this concept suggested by Evans and Buol (1968), were observed in 44% of the reviewed papers. In addition, crusts described and/or illustrated in some studies (20%) also seemed to be depositional crusts.

Erosion crusts (Mücher *et al.*, 1981) were described in 15% of the papers reviewed, namely by Valentin and Ruiz-Figueroa (1987), Escadafal and Fedoroff (1987), Mücher *et al.* (1988), Poss *et al.* (1989), Casenave and Valentin (1989), Kinnell *et al.* (1990) and Valentin (1991). In addition, so-called "cryptogamic crusts" were described by Mücher *et al.* (1988) and by Chartres and Mücher (1989).

Concepts developed

Generally, the main conclusions of the reviewed papers dealt with the processes involved in crust formation (78%). Nevertheless, the concept of typical microlayers often arose (43%). The role of microtopography in crust differentiation was only occasionally considered (22%), namely by Falayi and Bouma (1975), Valentin (1986) and his associates, Boiffin (1986) and his associates, Norton (1987) and Levy *et al.* (1988). The concept of crusting stages could be found in 32% of the reviewed papers, but this global proportion overestimates the actual use of this essential concept. In fact, the number of authors concerned was few: Tarchitzky *et al.* (1984), Valentin (1986) and his associates, Boiffin (1986) and his associates, Norton (1987)

Table 1
Main mechanisms suggested in the reviewed papers: frequency, first quotation and main
references.

Mechanisms suggested	Papers involved (%)	First quotation	Main references
Slaking	39	McIntyre (1958b)	Tarchitzky *et al.* (1984); Valentin (1986); Le Bissonnais *et al.* (1989)
Dispersion	35	McIntyre (1958a)	Greene *et al.* (1988); Helalia *et al.* (1988)
Compaction	30	McIntyre (1958a)	Moss (1991)
Coalescence	12	Ahmad and Roblin (1971)	Dexter *et al.* (1983); Bresson and Boiffin (1990)
Splash	11	McIntyre (1958a)	McIntyre (1958a); Mücher *et al.* (1981)
Washing-in	37	McIntyre (1958a)	Greene *et al.* (1990); Bresson and Cadot (1992)
Washing-out	39	Duley (1939)	Norton (1987); Radcliffe *et al.* (1991); West *et al.* (1990)
Sedimentation	44	Evans and Buol (1968)	Mücher and De Ploey (1977); Mücher *et al.* (1988); Bresson and Boiffin (1990)
Role of cryptogams	7	Mücher *et al.* (1988)	Mücher *et al.* (1988); Chartres and Mücher (1989); Greene *et al.* (1990)

and Luk *et al.* (1990). Chen *et al.* (1980) distinguished different stages in structural crust formation, but did not suggest any relationship with the depositional crust. Tarchitzky *et al.* (1984) related different crust morphologies to the hydrological conditions at the soil surface *i.e.* before runoff, after runoff and steady state infiltration rate. The genetic relationships between structural and depositional crusts were first described by Valentin (1981) and Boiffin (1984).

Mechanisms suggested
The main mechanisms suggested in the reviewed papers are listed in Table 1.

INTEGRATED DISCUSSION

Crust formation processes

Skin seal formation
The term 'skin seal' was used by McIntyre (1958a) to describe "a dense layer 0.1 mm thick which contained no visible pore under high magnification". This skin seal "apparently formed by compaction due to impact" (McIntyre, 1958a). Even though no description or illustration was provided, such a layer might be depleted of clay, because it was opposed to "the 'washed-in' region of decreased porosity" which could be observed underneath. Many authors used the term of 'skin seal' with reference to McIntyre but to describe another type of layer, enriched in clay particles compared to the underlying material. For instance, Chen *et al.* (1980) described

"a dense 'skin' 0.1 mm thick composed almost solely of fine particles". Norton (1987) and Arshad and Mermut (1988) also described as skin seal a very thin and fine textured layer observed at the surface of some crusts. However, such plasmic seals can result from two different processes: (1) preferential erosion of the coarse particles, which form the top of the crust, by overland flow (Chen *et al.*, 1980; Valentin and Ruiz-Figueroa, 1987) or (2) deposition of clay particles dispersed in turbulent water flow when rain stops (Pagliai *et al.*, 1983; Norton, 1987; Arshad and Mermut, 1988).

According to the process involved, *i.e.* compaction, erosion or deposition, the impact of the crust on the hydrological behaviour of the soil surface might be different. Compacted seals and erosion plasmic seals seem to have a great effect on the permeability of the soil surface (McIntyre, 1958; Valentin, 1991). Conversely, 'after rain deposits' (Pagliai *et al.*, 1983) which form after overland flow stops, may have little effect on the infiltration rate during the rainfall event. This apparent confusion in the literature may explain why Mualem *et al.* (1990) stated that "no universal seal (such as 'skin' 0.1 mm) can accurately represent a real seal layer". Micromorphology, however, is a unique tool for identifying these different types of microlayers.

Washed-in layer formation

McIntyre (1958a) defined the concept of 'washing-in' as the "plugging of the large pores by washed-in material". This concept has been so widely adopted that, when no washed-in layer could be observed, this was often noted (Chen *et al.*, 1980; Tarchitzky *et al.*, 1984; Norton *et al.*, 1986; Boiffin and Bresson, 1987; Mücher *et al.*, 1988). Moreover, analyzing the results of Chen *et al.* (1980), Mualem *et al.* (1990) claimed that "to our best judgement, the presence of washed-in material under the 'skin' was evident", despite the fact that the former authors pointed out the lack of such a layer. Sometimes, the presence or absence of a washed-in layer can be explained easily because crusting involves different processes controlled by soil and environmental conditions (Bresson and Boiffin, 1990; Valentin and Bresson, 1992). For instance, such an illuviation of fine material can hardly occur on initially dry seedbeds because slaking induces a rapid breakdown of the aggregate framework which seals the surface and prevents any further illuviation of fine particles (Bresson and Cadot, 1992). Difficulties in identifying small amounts of washed-in fine material against the matrix were also invoked to explain that a washed-in layer could not always been recognized (West *et al.*, 1990; Luk *et al.*, 1990).

However, some confusion in the literature arises because the washing-in process is still not clearly defined, especially the size and composition of the washed particles. McIntyre (1958a) used the expression 'fine particles' and not 'clay particles', even though he pointed out the role of physico-chemical dispersion. This may mean that this fine material consisted of fragments of aggregates as well as primary particles. Unfortunately, McIntyre did not give any information about this. Despite the prominent role of micromorphology in the elaboration of the washing-in concept, the thin section description was laconic: "considerably reduced porosity, to a depth of 1.5 to 3 mm, due to plugging of the larger pores by washed-in material". Moreover, no illustration was presented. However, most later authors, quoting McIntyre clearly considered the washing-in process as clay particle illuviation, which involves different mechanisms and conditions. Rather surprisingly, they did not provide clear evidence of clay illuviation. Bertrand and Sor (1962), using a labeling method, showed that 1% of the clay moved down to 3 cm depth and Helalia *et al.* (1988) measured significant amounts of clay in percolating water. Only

a few convincing illustrations of clay coatings (related to crusting) can be found in the literature (Greene *et al.*, 1988; Bresson and Cadot, 1992).

Yet, these two different concepts of washing-in involve different mechanisms and conditions. Some clarification is all the more needed because washing-in was invoked in many papers which did not involve micromorphology. Discussing their results, Agassi *et al.* (1981) explained that, using distilled water, "the dispersed particles are washed into the soil with the infiltrating water, and the pores immediately beneath the surface become clogged". Yet, no observation was made and the only data given were infiltration rates. Later, Levy *et al.* (1986) gave Agassi *et al.* (1981) as the first reference when summarizing the washing-in process in their introduction.

Washed-out layer formation

Duley (1939) stated that "in many cases, the compact layer which forms at the surface will contain a higher percentage of coarse material", because "the finer material is brought in suspension in the runoff water and carried down the slope". Such coarse textured surface microlayers were frequently described later, often using the term 'washing-out' (Norton, 1987) which was introduced by Onofiok and Singer (1984). The mechanism invoked was usually clay depletion (Gal *et al.*, 1984), which was supported by the sorted laminae, composed of 10 - 30 μm grains, observed in simulated erosional environments by Mücher *et al.* (1981). However, Chen *et al.* (1980) observed that this layer formed during the earlier stage of structural crust formation and was then eroded. More recently, West *et al.* (1990) and Radcliffe *et al.* (1991) suggested another mechanism. They observed that such layers occurred in slightly depressed areas, which showed that they were actually depositional features. Valentin (1991) described another type of coarse textured upper layer in sandy soils and related it to a sieving process. Therefore, some discernment is required when using so-called washed-out layers as diagnostic features for identifying the conditions which induced their formation.

Sieving crust formation

In arid sandy soils, Valentin (1986, 1991) described stuctural crusts with a surface layer of loose skeleton grains, overlying a thin plasmic layer (Fig. 1). Using a close time-dependent sequence of sampling, this author showed that textural differentiation mainly results from mechanical winnowing and sieving so that the finer the particles, the deeper they are deposited. Moreover, the downward translocation of clay through the coarse grained top layer can be enhanced by percolating water. Fine particles then accumulate, probably due to entrapped air within the underlying layers (Kooistra and Siderius, 1986). Raindrop impact plays the main role in sieving crust formation, so that mulching is effective in limiting the development of such crusts (Collinet and Valentin, 1985). In tropical areas, such sieving crusts have been observed in cultivated sandy soils (Poss *et al.*, 1989). Some of the coarse textured top layers described in the literature, especially when developed on sandy soils, seem to be similar to sieving crusts (Duley, 1939; Chen *et al.*, 1980; Collins *et al.*, 1986; Kinnell *et al.*, 1990). This type of crust has also been called 'filtration pavement' (Valentin, 1991) or 'layered structural crust' (Casenave and Valentin, 1992).

In arid areas, pebbles are often embedded within a crust similar to the sieving crust described above (Valentin, 1986, 1991) with a pronounced vesicular structure, especially below the coarse fragments (Springer, 1958). Such a crust, called 'coarse pavement crust', can be considered as a peculiar form of sieving crust.
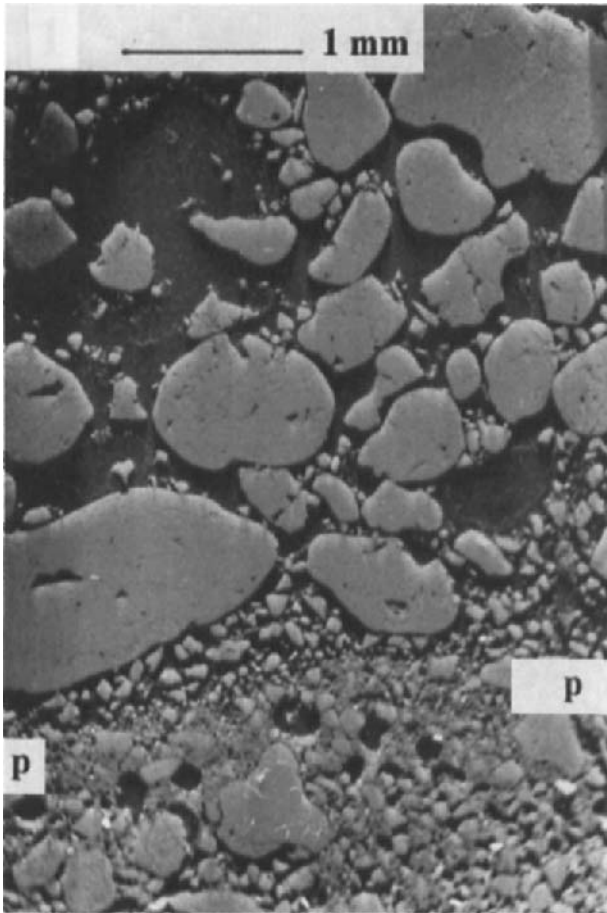
Fig. 1. Structural crust: Sieving crust on a sandy soil (vertical polished section, BESI mode): loose skeleton grains overlaying a thin plasmic layer (p).

Infilling crust formation

Boiffin and Bresson (1987) described in the field a structural crust with net-like infillings of bare silt grains (Fig. 2). Further laboratory studies (Le Bissonnais *et al.*, 1989) showed that such features developed only if the soil was wet before rainfall and that, with air dried samples, a slaking crust quickly sealed the surface. Such crusts were clearly due to silt illuviation. Raindrop impact, rather than physico-chemical dispersion, induces textural separation at the top of surface aggregates and the resulting separated silt grains illuviate a few millimetres deeper into the interaggregate packing voids (Bresson and Cadot, 1992). Contrary to slaking crusts, infilling crusts develop slowly. As a result, they occur only when the soil and/or climatic conditions are unfavourable for more rapid processes such as slaking due to entrapped air compression or aggregate coalescence due to plastic deformation.
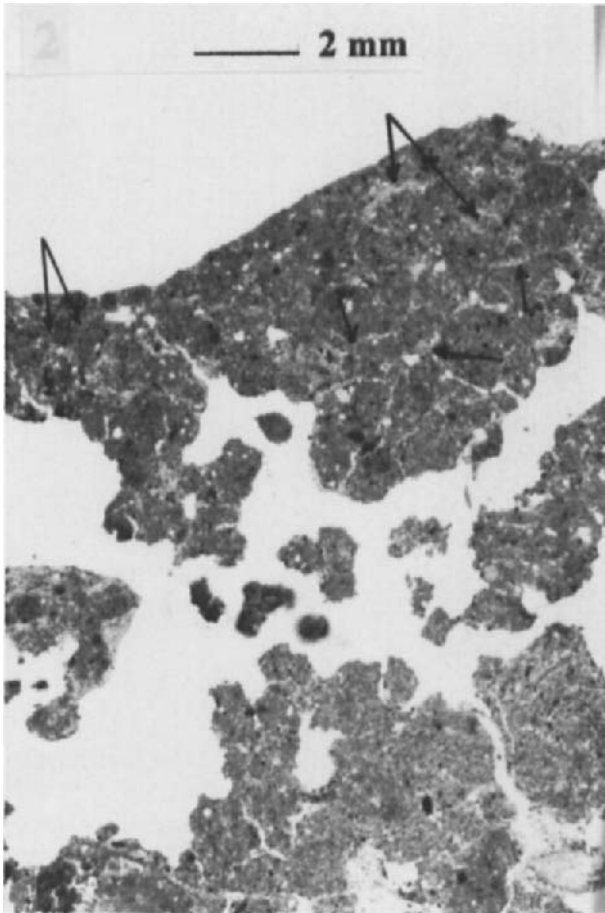
Fig. 2. Structural crust: Infilling crust on a loamy soil (vertical thin section, plain light): net-like infillings of bare silt grains (arrow) within inter-aggregate packing voids.

Slaking crust formation

Slaking was one of the breakdown processes invoked by McIntyre (1958b). Ahmad and Roblin (1971) described a crust where the structure of the top 2 mm of soil had completely disintegrated. Aggregate slaking due to entrapped air compression was well documented by Robinson and Page (1950), but few clear micromorphological illustrations of slaking-induced crusts were given before Le Bissonnais *et al.* (1989) and Le Souder *et al.* (1991). Tarchitzky *et al.* (1984) defined slaking as caused either by swelling or the pressure of entrapped air, but suggested that it played a minor role compared to raindrop impact. In the early stage of the crust formation, Onofiok and Singer (1984) described a reduction in the size of the aggregates in the upper 0.4 mm and a corresponding increase in micropores, which is good evidence of the model of aggregate breakdown suggested by Valentin (1981) and Farres (1987). Typically, slaking crusts (Fig. 3) consist of a thin, dense layer which do not show clear textural separation between coarse particles (skeleton) and fine particles (plasma), even in sodic soils (Valentin
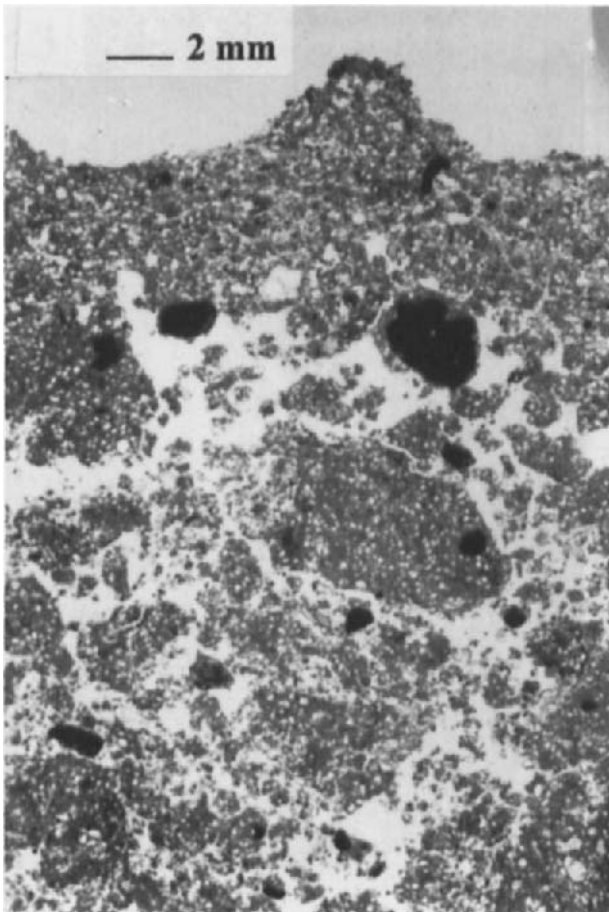
Fig. 3. Structural crust: Slaking crust on a loamy soil (vertical thin section, plane light).

and Bresson, 1992). Slaking crusts predominate when the soil is dry before rainfall (Valentin, 1981; Boiffin, 1986; Norton, 1987; Le Bissonnais *et al.,* 1989). Hydrophobic conditioners are effective in delaying slaking crust formation (Le Souder *et al.,* 1990, 1991), but mulching is not (Valentin and Ruiz-Figueroa, 1987), which is consistent with the process involved.

'Swelling crusts', observed in arid loamy soils (Valentin, 1991), can be considered as a peculiar form of slaking crust (Valentin and Bresson, 1992). Such crusts are characterized by the banded distribution of skeleton grains within superficial parts of clods. Upon wetting, clay lattices expand, turn into a slurry and fill the interstices between clods (Valentin, 1991). The latter process can be related to coalescing, as well as to the early stage of depositional crust formation ('muddy flow'; Bresson and Boiffin, 1990).

Coalescing crust formation

Bresson and Boiffin (1990) described structural crusts which were rather porous and showed a diffuse boundary with the underlying undisturbed layer (Fig. 4). Macropores were
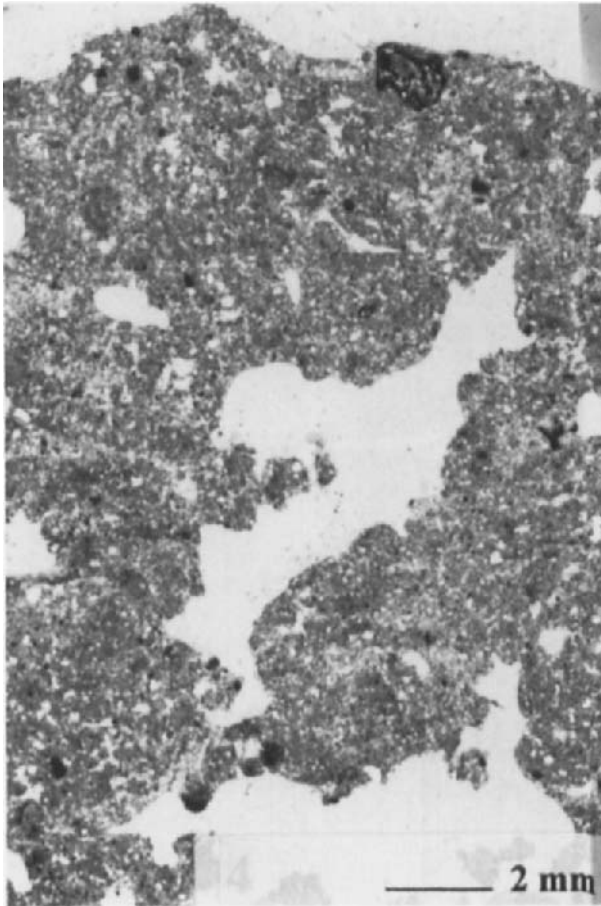
Fig. 4. Structural crust: Coalescing crust on a loamy soil (vertical thin section, plane light): rather thick crust showing a diffuse boundary with the underlying porous layer; convexities of packing voids gradually increase towards the surface.

typical polyconcave packing voids at the bottom, but their amount and roughness gradually decreased towards the surface, as convexities developed. The main process involved was a gradual coalescence of the initial aggregates by raindrop compaction under plastic conditions. Coalescing crusts occur on soils which are wet before rainfall and are most developed in sodic soil (Bresson and Boiffin, 1990). Coalescence of aggregates was described by Ahmad and Roblin (1971) below a 2 mm thick very dense surface layer. Moss (1991b) also described crusts where compaction was mainly due to aggregate deformation. However, studying the overall slumping of seedbeds, Dexter et al. (1983) suggested an internal soil erosion process with dispersed material from the finer aggregates welding the coarser aggregates at their points of contact. Some of the crusts described in the literature are similar to coalescing crusts (Evans and Buol, 1968; Moss, 1991b). Remley and Bradford (1989) displayed a thin section micrograph which shows some morphological features of a coalescing crust. However, they did not identify any crust, because the matrix did not show any particle size segregation with depth.

Silt-layer induced compaction

Compaction by raindrop impact was invoked by McIntyre (1958a), but was not well documented in later micromorphological studies. Thirty three years later, Moss (1991a and b) provided new concepts. Studying crust formation under simulated rainfall, Moss (1991a) carried out a very close micromorphological monitoring of the process and sampled the early stage after 30 s (0.33 mm rainfall). Craters developed first, then, at 1 min, a thin layer of tightly packed silt grains spread on the surface. After 8 min, the silt layer, 200 μm to 3000 μm thick, covered the surface and compaction was visible to 3 - 5 mm depth. Further experiments involving various kinetic energies as well as local shielding of the surface and telescopic observations, suggested that the silt layer played the major role in compaction of so-called 'rain impact' crusts (Moss, 1991a and b). Three stages could be distinguished: (1) 10 - 50 μm particles are concentrated at the surface by preferential removal of other sizes in the airsplashing environment; (2) the resulting silt grains are spread over the surface by lateral outflow sheets of the drops and deposit as tightly packed bed-load sediments; (3) this layer is dilatant, resists deformation by raindrop impact and prevents water penetration because its pores are < 15 μm. Therefore, the underlying layer may be compacted by stress waves (Moss, 1991a and b).

Such a silt layer may be similar to the washed-out layer described in the literature or to the sieving crusts observed on arid sandy soils by Valentin (1986, 1991) and Poss *et al.* (1989). However, it has never been observed on temperate cultivated loamy soils in France. Contrary to Moss's assertion, silt-layer compaction does not seem to be "widespread". Moss's experiments dealt with pre-wetted soils, which might prevent slaking, and with poorly aggregated soil materials, which might prevent silt infilling and could not involve aggregate coalescence. Besides, using a wider range of soil materials, Moss (1991b) also described plastic deformation of aggregates and washing-in of fine particles. Therefore, the innovative conception of compaction suggested by Moss seems to be compatible with the model of structural crust formation suggested by Bresson and Valentin (1990). Further studies are required for determining the conditions which lead to silt layer induced compaction, especially in the field.

Erosion crust formation

Erosion crusts were defined by Valentin (1981, 1991) as thin, smooth surface layers enriched in fine particles (Fig. 5). The fine particles are usually poorly oriented. Voids are generally restricted to some cracks and vesicles. The thickness of this plasmic layer is rather regular and is not related to the surface microtopography. Some skin seals described in the literature may be similar (Chen *et al.*, 1980). Kinnell *et al.* (1990) observed that, after erosion of the first top millimetres, the remnants were mainly argillaceous layers. Such crusts often result from erosion of the coarse textured top layer of sieving crusts (Valentin, 1986). They form a rather resistant surface against further wind or water erosion, and therefore often cover large areas. Erosion crusts form first on the higher points, then expand over the surface as the global surface roughness diminishes. Formation of an erosion crust from other structural crusts, which do not show any textural differentiation, may involve the preferential erosion of coarser particles by high energy raindrops (Chen *et al.*, 1980; Valentin, 1991). Erosion crusts can be recognized from after rain deposits and eroded depositional crusts using not only their spatial distribution in the field but also micromorphological features of their plasmic surface layer, namely (1) the poor orientation of the fine particles and (2) the absence of relationship
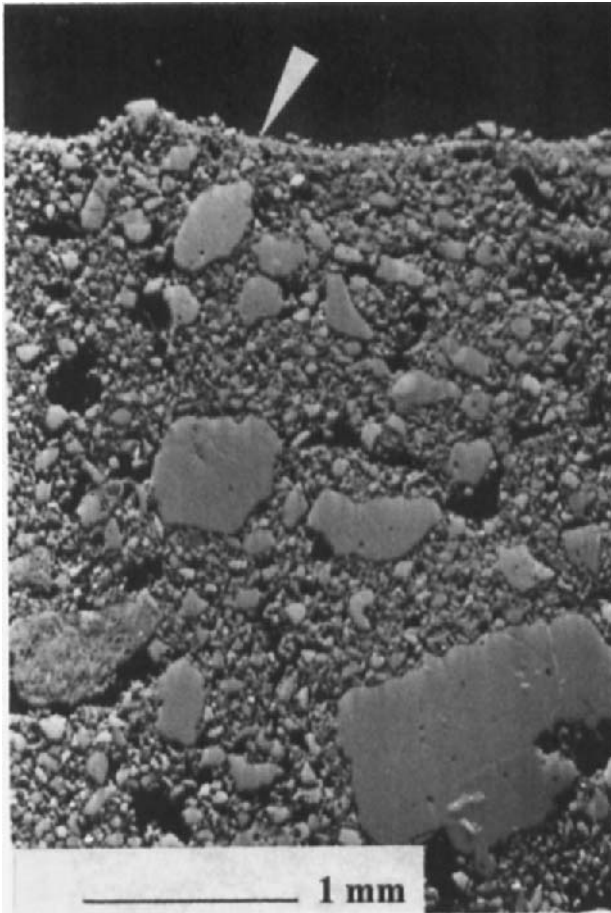
Fig. 5. Erosion crust on a sandy soil (vertical polished section, BESI mode): smooth plasmic surface layer (arrow).

between the layer thickness and the surface microtopography. However, the term 'erosion crust' might be confusing because most crusts affected by erosion processes are not 'erosion crusts'.

Erosion crusts are usually more developed in arid rangeland areas rather than in cultivated fields, presumably because the velocity of overland flow is not limited by the surface roughness of the seedbed. Moreover, rangeland crusts are not rejuvenated by tillage practices and often develop over many years (Valentin and Bresson, 1992).

Depositional crust formation

Crusts formed by deposition of the particles suspended in overland flow (Fig. 6) were recognized by Evans and Buol (1968). The term 'depositional crust' was later introduced by Chen *et al.* (1980). The micro-sedimentation process involved (Bishay and Stoops, 1975) was studied by Mücher and De Ploey (1977). Sedimentology provided the basic concepts which were transposed to the microenvironment of crust formation. Micromorphology was found a
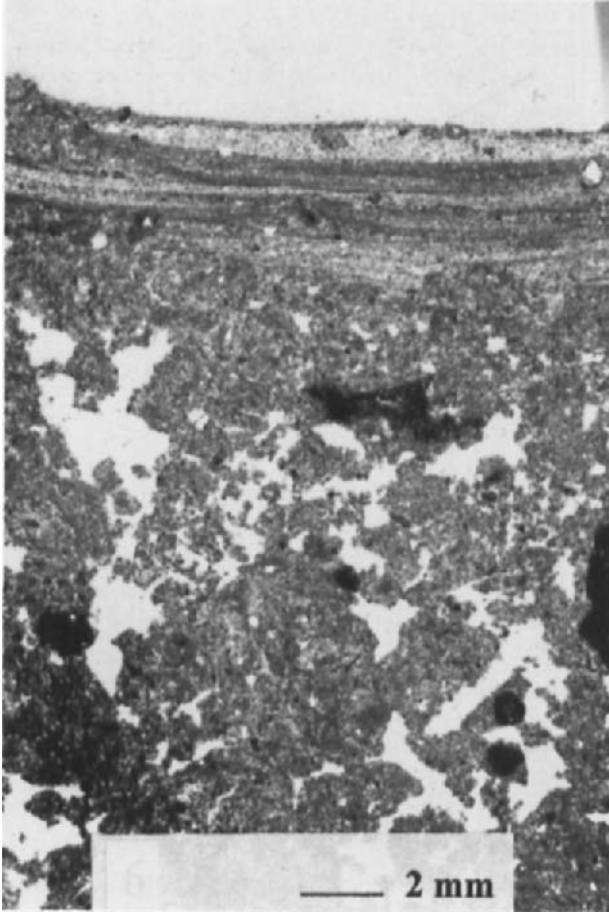
Fig. 6. Depositional crust on a loamy soil (vertical thin section, plane light): microbedded layers overlying a structural crust.

very useful tool for determining the main diagnostic characters, *i.e.* microbedding, particle sorting and orientation.

Sorting of basic particles was studied by Mücher *et al.* (1981) in both erosional and depositional environments. Deposits resulting from turbulent rainwash generally lead to laminae with 10 - 50 μm grains. Conversely, afterflow deposits show laminae with a greater percentage of particles smaller than 30 μm. Pure splash deposits do not show any lamination or particle sorting (Mücher *et al.*, 1981). The presence of aggregates within depositional crusts was also described (Falayi and Bouma, 1975). Mücher *et al.* (1988) observed loose aggregates at the top of crusts, and suggested they were deposited by afterflow. Conversely, microbeds observed at the bottom of depositional crusts, filling in small pocket-like depressions in former structural crusts, contained small aggregates included within a densely packed material. This was related to a muddy flow process which induced short-distance translocation of particles (Bresson and Boiffin, 1990).

Orientation of the deposited particles is related to the degree of dispersion. Studying the effect of electrolyte concentration on the micromorphology of artificial depositional crusts, Southard *et al.* (1988) showed that only suspensions prepared with distilled water produced crusts with high birefringence.

Various *distribution patterns of microbeds* have been described, *e.g.* 'rill' and 'finger-like' (Kooistra and Siderius, 1986; Mücher *et al.*, 1988) and 'deltaic' (Bresson and Boiffin, 1990). Superposition of different patterns has been used to assess the succession of different hydrodynamic conditions at the soil surface during crust development (Bresson and Boiffin, 1990). Moreover, studying a long-term experimental field to which various fertilizers and amendments had been applied, Bresson and Boiffin (1990) suggested that the size and duration of puddles played the main role in the characteristics of the depositional crust which, in turn, appeared to be partly controlled by the properties of the underlying structural crust. This applied to all the studied soils, including a sodic soil.

Cryptogamic crusts

Cryptogamic crusts have been recognized for many years in rangeland areas (Fletcher and Martin, 1948). However, the first microscopic characterization of such crusts were carried out only recently in Australia (Mücher *et al.*, 1988; Chartres and Mücher, 1989; Greene *et al.*, 1990; Kinnell *et al.*, 1990). Cryptogams develop preferentially on argillaceous materials containing carbonates and Ca-oxalate crystals exuded from plant roots during stable periods without deposition or erosion (Mücher *et al.*, 1988). Amorphous gel-like organic material has been observed near or associated with algal sheaths, and sometimes fungal hyphae extend a few millimetres below surface cryptogams (Greene *et al.*, 1990). Individual algae, which often live in juxtaposition with lichens, contribute to aggregate stabilization by secreting cementing gums (Bond and Harris, 1964), reinforcing the aggregation effect of associated fungal hyphaes (Greene and Tongway, 1989).

The effect of cryptogamic crusts on the hydrological behaviour of the surface, however, is not well understood, and may be either beneficial or detrimental (van der Watt and Claassens, 1990). Generally, such crusts are considered as a good protection against erosion due to their higher cohesion (Fletcher and Martin, 1948; Greene and Tongway, 1989). Destruction of the cryptogam cover by fire gives very clear evidence of its protective effect (Chartres and Mücher, 1989; Greene *et al.*, 1990; Kinnell *et al.*, 1990). However, Greene *et al.* (1990) found that runoff could be greater from cryptogam mats than from bare surfaces and removal of the cryptogamic crust increased infiltration rate four times (Greene *et al.*, 1990). This may be explained by the properties of the underlying layers which may control infiltration rate. Cryptogamic cover were observed on various types of crusts, erosion crusts and depositional crusts (Valentin and Bresson, 1992). Therefore, cryptogams should be considered as a micro vegetal-cover rather than a micro soil-layer, and thus should not be studied alone but in relation with the crust they colonize.

Vesicle formation

Vesicles have been described in various crust types and in various environments. Springer (1958) suggested that vesicles form by air entrapment. When the saturated crust dries out it loses fluidity so that escaping gases form cavities. The production of carbon dioxide liberated by biological activity from organic material may also play a role in vesicle formation (Pagliai *et al.*, 1983). Figueira and Stoops (1983) described particular vesicles which showed micro-

erosion of the walls and micro-deposition on the bottom by the action of a descending water front. Usually, vesicles are more numerous and larger as the number of wetting and drying cycles increases. Miller (1971) showed that wetting and drying cycles first induced a platy structure in which vesicles then gradually form due to capillary pressure on wetting. However, Figueira and Stoops (1983) suggested that the platy structure is mainly determined by fissures interconnecting the large vesicles previously formed. On the other hand, Bresson and Boiffin (1990) suggested that the genesis of vesicles may be ascribed to compaction of initial packing voids due to plastic strain under semi-liquid conditions. Although vesicle formation should be better documented, vesicle microlayers can be successfully used as a predicting criterion of very low infiltrability (Casenave and Valentin, 1989).

Crusting model

Valentin (1981) and Boiffin (1984) suggested essential concepts for crusting studies, which were adopted and developed in the following papers: Boiffin, (1986), Valentin (1986), Boiffin and Bresson (1987), Valentin and Ruiz-Figueroa (1987), Le Bissonnais *et al.* (1989), Poss *et al.* (1989), Casenave and Valentin (1989), Le Souder *et al.* (1990), Bresson and Boiffin (1990), Bresson and Valentin (1990), Le Souder *et al.* (1991), Valentin (1991), Bresson and Cadot (1992), Casenave and Valentin (1992) and Valentin and Bresson (1992). According to these authors, the main different types of crusts are genetically related, and form time- and space-dependent sequences.

Time- and space-dependant variations

Time- and space-dependent variability were mainly studied by Valentin (1986) and his associates and by Boiffin (1986) and his associates. Chen *et al.* (1980), Norton (1987) and Luk *et al.* (1990) distinguished different stages in structural crust formation, but did not suggest any relationship to depositional crusts. Tarchitzky *et al.* (1984) related different crust morphologies to the hydrological conditions at the soil surface, *i.e.* before runoff, after runoff and steady state infiltration rate. The genetic relationships between structural and depositional crusts were first described by Valentin (1981, 1986) and Boiffin (1984, 1986). The role of microtopography in crust differentiation was seldom considered by other authors. Falayi and Bouma (1975) were the first, followed by Norton (1987) and Levy *et al.* (1988).

Crusting stages. Crusting is a dynamic process which follows the same general pattern: (1) sealing of the surface by a structural crust, then (2) development of a depositional crust (Fig. 7). The change from the first to the second stage mainly depends on a decrease in infiltration rate due to the structural crust properties, which induces microrunoff (Valentin, 1981; Boiffin, 1984, 1986). These two stages can be identified in the field, using simple macroscopic features (Boiffin, 1984; Bresson and Boiffin, 1990) which can also be used to quantify the crusting rate (Boiffin, 1986).

Spatial variability. Structural crusts generally develop faster where aggregates are finer, which explains why crusts observed in the field do not uniformly cover the seedbed surface (Boiffin, 1984; Boiffin and Bresson, 1987). Depositional crusts first form in microdepressions or interstices between large clods. As the soil surface flattens, the deposited microbeds become thinner but tend to expand more extensively over the former structural crust (Bresson and Boiffin, 1990). In sandy soils, the surface roughness is usually more transitory and the spatial variability of crusts occurs at a larger scale: structural crusts being observed upslope, erosion

Seedbed   Structural   Depositional
                           crust   crust
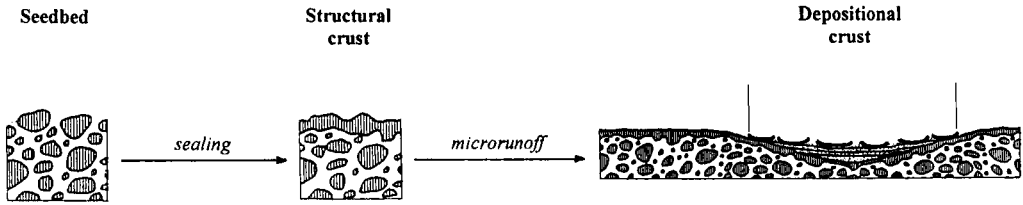
Fig. 7. Time- and space-dependent sequence of crusts in a loamy cultivated field: (1) sealing of the soil surface by a structural crust, then (2) development of a depositional crust.

crusts midslope and depositional crusts downslope (Valentin, 1991; Valentin and Bresson, 1992).

Crust typology

From their studies of loamy and sandy soils, which involved more than 400 thin sections from more than 100 soils, Valentin and Bresson (1992) suggested a typology of crusts based on macro- and micro-morphological characterization: (1) structural crusts including slaking (and swelling), infilling, coalescing and sieving (and coarse pavement) sub-types; (2) erosion crusts and (3) depositional crusts, with two sub-types, runoff- and still-. Such a morpho-genetic classification of crusts appeared to be relevant to the prediction of infiltrability (Boiffin and Monnier, 1986; Bresson and Boiffin, 1990; Casenave and Valentin, 1992; Valentin and Casenave, 1992).

This typology seems to account for most of the crusts described in the literature except the silt layer (or clay depleted layer). Skin seal can be related to erosion crusts, depositional crust or silt layer, depending on their morphology. Washed-in layers, if well identified, may be part of sieving crusts. Washed-out layers can be related to silt layers or depositional crusts or may be sieving crusts. Cryptogamic crusts can be considered as crusts of whatever type (according to the properties of the underlying layers) colonized by a peculiar vegetal cover.

CONCLUSIONS

"The long-term benefit of applied research, even if recognized, was sacrificed to meet the short term 'practical' objective. Consequently, soil sealing is still understood in concepts suggested by McIntyre, 1958" (Mualem *et al.*, 1990). The current critical review of 54 papers involving microscopic investigations of soil crusts shows that the latter statement is far fetched. The contribution of micromorphology to our present understanding of crust formation has been prominent. Various crusting processes have been clearly identified or elucidated thanks to microscopic observations, *e.g.* depositional, coalescing, infilling, sieving and slaking crust formation and silt-layer compaction. Diagnostic macro- and microscopic features have been found which allow recognition of the processes involved in the formation of the various types of crusts (Valentin and Bresson, 1992). Moreover, even though Mualem *et al.* (1990) considered that "there are serious doubts about the validity of the identification of the seal layer, formed during rainfall, with the crust layer visually observed afterward", these microscopically defined crust types helped to assess the crusting rate as well as to predict

infiltrability (Boiffin and Monnier, 1986; Bresson and Boiffin, 1990; Casenave and Valentin, 1992). Micromorphology also helped to assess the role of initial moisture content and initial aggregate size distribution in controlling the nature and the kinetics of crusts. Moreover, the general pattern of soil surface crust development was partly elaborated thanks to microscopic studies. Therefore, micromorphology appears to be a unique tool for predicting and controlling crust development.

Some suggestions for further studies arise from the current critical review.

Methodological suggestions

Soil initial state and rainfall event characteristics

In most studies (87%), the *initial moisture content before rainfall* was neither specified, nor taken into account in the discussion. The same situation generally prevailed (93%) for the *initial aggregate size distribution*. These two factors, however, partly control the crusting rate as well as the type and the properties of the crust which forms (Falayi and Bouma, 1975; Boiffin, 1986; Valentin and Ruiz-Figueroa, 1987; Le Bissonnais, 1988; Bresson and Cadot, 1992). Underestimating their role may have led to apparent contradictions in the literature. Moreover, controlling the initial state of the seedbed is a realistic method for farmers to delay structural crust formation especially when slaking by air entrapment compression is the main soil degradation process.

In most field studies under natural rainfall (87%), the crust samples studied were not referred to the *climatic events* which induced their formation. Such data, however, are required for relating the morphological features observed to the physical conditions of their formation, *e.g.* rainfall intensity, cumulative kinetic energy, dry periods, *etc.* (Boiffin, 1984, 1986; Bresson and Boiffin, 1990).

Dynamics of crust development

Close monitoring. Many studies (64%) dealt with only one sampling time. A closer monitoring is required to take into account the dynamic aspect of crust formation. This is of great practical importance because the impact of crusting on seedling emergence is closely related to the development rate of the crust compared to the emergence and establishment rate of the crop.

Reference to the crusting stage. In most studies (72%), crust samples were not referred to the development stage they characterized. However, such a reference is needed for reliable comparison of crusting in soils of different composition, climatic environment and land use and management (Bresson and Boiffin, 1990). This is especially important when a close monitoring cannot be done.

Specific problems of simulated environments

Simulated seedbeds. Usually, crusts were sampled after runoff had started, *i.e.* after the formation of the structural crust. Because the surface of repacked seedbeds was usually very smooth and because a slope was generally set up to prevent ponding, such crusts actually formed under constant erosional conditions. Yet, such experiments were used not only to study erosional processes but also to discuss the formation of structural crusts. On the other hand, most of the crusts formed in the laboratory from repacked samples did not actually seem to correspond to any of the natural crusts described in the field. There is a very close relationship

between the so-called washed-out layers and this type of experiment. Among the papers describing washed-out layers, 84% dealt with repacked seedbeds and, among those dealing with repacked seedbeds, 76% described a washed-out layer. Among the five papers which did not describe washed-out layers, two seemed to have stopped the experiment before runoff (Ahmad and Roblin, 1971; Le Bissonnais *et al.*, 1989). McIntyre did not describe any washed-out layer but his thin sections, which he did not examine himself (McIntyre, 1958a) and which are held by the CSIRO Division of Soils in Canberra, clearly show similar coarse textured top layers (Bresson, unpublished). This suggests that more realistic simulation of the conditions which prevail in the field should be considered, including (1) aggregate size distribution and (2) microtopography. Moreover, formation of structural crusts should be only studied using crusts sampled before runoff.

Simulated rainfalls. Recent studies showed that varying intensity rains should also be used. Giménez *et al.* (1992) observed that the hydraulic properties of the seal were mainly determined by the rainfall intensities prior to ponding and during intensity peaks. They suggested that the rainfall pattern partly controlled the balance between crust formation and crust erosion.

Research opportunities

Rheology

According to many scientists studying soil surface crusting, it is evident that crust formation is associated with clay dispersion and movement in the soil (Agassi *et al.*, 1981). Describing a thin section micrograph which seems to be a coalescing crust, Remley and Bradford (1989) did not identify any crust, because the matrix did not show any particle size segregation with depth. This is an example of the close conceptual relationship between crusting and dispersion. However, on a sodic soil, Bresson and Boiffin (1990) could not find any textural separation in structural crusts. Conversely, in a non-sodic environment, clear textural separation occurred, with silt grains illuviating just below the surface aggregates and clay particles depositing a few millimetres deeper. This was related to the remaining aggregate framework (Bresson and Cadot, 1992). El Morsy *et al.* (1991) also suggested that conditions leading to dispersion provided a rapid crust formation which reduced the potential for illuviation. Therefore, textural separation should not be related to dispersive conditions. Moreover, the current critical review showed that in many cases other mechanisms control the nature and the development rate of crusts. Even on sodic soils, swelling and deformation under plastic conditions could play the main role (Bresson and Boiffin, 1990). Gypsum reduced crust formation more efficiently on soils with smectitic rather than kaolinitic clays (Chartres *et al.*, 1985; Greene *et al.*, 1988), which suggests that swelling occurred rather than real dispersion.

As a matter of fact, physico-chemical dispersion, swelling and deformation under plastic conditions do not constitute different processes but different levels of the same process, *i.e.* hydration. Therefore, crust development in clayey and sodic environments should be related to global rheological properties rather than to the physico-chemical dispersability *sensu stricto*.

Long-term evolution

Most of the reviewed studies dealt with the development of crust during the few weeks after sowing, which was pertinent to the impact of crusting on seedling emergence. However, the final state of the crust, after harvesting, greatly controls the ability of the soil to store water

until the next sowing. Moreover, this final state may also control the tillage conditions and hence the properties of the next seedbed. In this respect, the mid-term (several months) evolution of crusts should be considered, which requires taking account of the succession of climatic events. Field scale studies are required to predict runoff and water intake. Nevertheless, simulated environments which deal with erosional conditions could also be relevant.

Natural crusts in rangeland areas involved the same processes as crusts developing in cultivated soils. However, they result from a much longer evolution because they are not rejuvenated by tillage practices. Moreover, velocity of overland flow in rangelands is not limited by the surface roughness induced by tillage (Valentin and Bresson, 1992). As a result, rangeland crusts involve a complex succession of erosion, sedimentation and bioturbation periods (Valentin, 1986; Mücher *et al.*, 1988; Casenave and Valentin, 1989). Micromorphology should help to recognize such different phases (Courty, 1986), and to identify specific processes, if any.

Mechanical properties

Few micromorphological studies dealt with the mechanical properties of crusts, and the applicability of the typology suggested in this paper to the prediction of mechanical impedance is yet to be assessed. Micromorphology should be especially useful to study the relationships between mechanical properties and the relative distribution of the coarse and fine particles.

Crust erodibility

Crusts greatly control runoff and soil loss. In many studies, the morphology of crusts was related to their hydrological behaviour, *i.e.* infiltration rate and runoff inducement. On the contrary, very little is known about the relationship between detachability and the type and the morphology of crusts. Applicability of the typology presented in this paper should be tested and new research on crust detachability and erodibility should be carried out involving microscopic investigations.

REFERENCES

* *Papers including microscopic study and reviewed here.*
*Ahmad, N. and Roblin, A.J., 1971. Crusting of River Estate soil, Trinidad, and its effect on gaseous diffusion, percolation, and seedling emergence. J. Soil Sci., 22: 23-31.
Agassi, M., Shainberg, I. and Morin, J., 1981. Effect of electrolyte concentration and soil sodicity on infiltration rate and crust formation. Soil Sci. Soc. Am. J., 45: 848-851.
*Arshad, M.A. and Mermut, A.R., 1988. Micromorphological and physico-chemical characteristics of soil crust types in northwestern Alberta, Canada. Soil Sci. Soc. Am. J., 52: 724-729.
Bertrand, A.R. and Sor, K., 1962. The effects of rainfall intensity on soil structure and migration of colloidal material in soils. Soil Sci. Soc. Am. J., 26: 297-300.
Boiffin, J., 1984. La dégradation structurale des couches superficielles du sol sous l'action des pluies. Ph.D. Thesis, Institut National Agronomique Paris-Grignon, Paris, 320 pp.
Boiffin, J., 1986. Stages and time-dependency of soil crusting *in situ*. In: F. Callebaut, D. Gabriels and M. De Boodt (Editors), Assessment of Soil Surface Sealing and Crusting. Flanders Research Center for Soil Erosion and Soil Conservation, Ghent, pp. 91-98.

*Boiffin, J. and Bresson, L.-M., 1987. Dynamique de formation des croûtes superficielles: apport de l'analyse microscopique. In: N. Fedoroff, L.M. Bresson and M.A. Coutry (Editors), Soil Micromorphology. Proc. VII Int. Working Meeting of Soil Micromorphology, Paris, July 1985. Association Française pour l'Etude du Sol, Plaisir, France, pp. 393-399.

Boiffin, J. and Monnier, G., 1986. Infiltration rate as affected by soil surface crusting caused by rainfall. In: F. Callebaut, D. Gabriels and M. De Boodt (Editors), Assessment of Soil Surface Sealing and Crusting. Flanders Research Center for Soil Erosion and Soil Conservation, Ghent, pp. 210-217.

Bond, R.D. and Harris J.R., 1964. The influence of the microflora on physical properties of soils. I. Effects associated with filamentous algae and fungi. Aust. J. Soil Res., 2: 111-122.

*Bresson, L.-M. and Boiffin, J., 1990. Morphological characterization of soil crust development stages on an experimental field. Geoderma, 47: 301-325.

Bresson, L.-M. and Cadot, L., 1992. Illuviation and structural crust formation on loamy temperate soil. Soil Sci. Soc. Am. J., 56: 1565-1570.

*Bresson, L.-M. and Valentin, C., 1990. Comparative micromorphological study of soil crusting in temperate and arid environments. Trans. 14th Congress of I.S.S.S., Kyoto, Japan, VII: 238-243.

*Bishay, B.G. and Stoops, G., 1975. Micromorphology of irrigation crusts formed on a calcareous soil of the mechanized farm, north-west Egypt. Pédologie, 25: 143.

*Casenave, A. and Valentin, C., 1989. Les États de Surface de la Zone Sahélienne. Influence sur l'Infiltration. ORSTOM, Paris, France, 230 pp.

Casenave, A. and Valentin, C., 1992. A runoff capability classification system based on surface features criteria in semi-arid areas of West Africa. J. Hydrol., 130: 231-249.

*Chartres, C.J. and Mücher, H.J., 1989. The effects of fire on the surface properties and seed germination in two shallow monoliths from a rangeland soil subjected to simulated raindrop impact and water erosion. Earth Surf. Proc. Landforms, 14: 407-417.

*Chartres, C.J., Greene, R.S., Ford, G.W. and Rengasamy, P., 1985. The effect of gypsum on macroporosity and crusting of two red duplex soils. Aust. J. Soil Res., 23: 467-479.

*Chen, Y., Tarchitzky, J., Brouwer, J., Morin, J. and Banin, A., 1980. Scanning electron microscope observations on soil crusts and their formation. Soil Sci., 130: 49-55.

Collinet, J. and Valentin, C., 1985. Evaluation of factors influencing water erosion in West Africa using rainfall simulation. In: Challenges in African Hydrology and Water Resources, IAHS, No. 144, pp. 451-461.

*Collins, J.F., Smillie, G.W. and Hussain, S.M., 1986. Laboratory studies of crust development in Irish and Iraqi soils. III. Micromorphological observations of artificially-formed crusts. Soil Tillage Res., 6: 337-350.

*Courty, M.-A., 1986. Morphology and genesis of soil surface crusts in semi-arid conditions (Hissar region, north-west India). In: F. Callebaut, D. Gabriels and M. De Boodt (Editors), Assessment of Soil Surface Sealing and Crusting. Flanders Research Center for Soil Erosion and Soil Conservation, Ghent, pp. 32-39.

*Dexter, A.R., Radke, J.K. and Hewitt, J.S., 1983. Structure of a tilled soil as influenced by tillage, wheat cropping, and rainfall. Soil Sci. Soc. Am. J., 47: 570-575.

*Duley, F.L., 1939. Surface factors affecting the rate of intake of water by soils. Soil Sci. Soc. Am. Proc., 3: 60-64.

El Morsy, E.A., Malik, M. and Letey, J., 1991. Interactions between water quality and polymer treatment on infiltration rate and clay migration. Soil Technology, 4: 221-231.

*Escadafal, R. and Fedoroff, N., 1987. Apport de la micromorphologie à une étude multiscalaire de la surface des sols en région aride (Tunisie méridionale). In: N. Fedoroff, L.M. Bresson and M.A. Coutry (Editors), Soil Micromorphology. Proc. VII Int. Working Meeting of Soil Micromorphology, Paris, July 1985. Association Française pour l'Etude du Sol, Plaisir, France, pp. 409-413.

*Evans, D.D. and Buol, S.W., 1968. Micromorphological study of soil crusts. Soil Sci. Soc. Am. Proc., 32: 19-22.

*Falayi, O. and Bouma, J., 1975. Relationships between the hydraulic conductance of surface crusts and soil management in a Typic Hapludalf. Soil Sci. Soc. Am. Proc., 39: 957-963.

Farres, P.J., 1987. The dynamics of rainsplash erosion and the role of soil aggregate stability. Catena, 14: 119-130.

*Figueira, H. and Stoops, G., 1983. Application of micromorphometric techniques to the experimental study of vesicular layer formation. Pédologie, 33: 77-89.

Fletcher, J.E. and Martin, W.P., 1948. Some effects of algae and molds on the rain crust of desert soils. Ecology, 29: 95-100.

*Gal, M., Arcan, L., Shainberg, I. and Keren, R., 1984. Effect of exchangeable sodium and phosphogypsum on crust structure - scanning electron microscope observations. Soil Sci. Soc. Am. J., 48: 872-878.

Giménez, D., Dirksen, C., Miedema, R., Eppink, L.A.A.J. and Schoonderbeek, D., 1992. Surface sealing and hydraulic conductances under varying-intensity rains. Soil Sci. Soc. Am. J., 56: 234-242.

Greene, R.S.B. and Tongway, D.J., 1989. The significance of (surface) physical and chemical properties in determining soil surface condition of red-earths in rangelands. Aust. J. Soil Res., 27: 213-225.

*Greene, R.S.B., Rengasamy, P., Ford, G.W., Chartres, C.J. and Millar, J.J., 1988. The effect of sodium and calcium on physical properties and micromorphology of two red-brown earth soils. J. Soil Sci., 39: 639-648.

*Greene, R.S.B., Chartres, C.J. and Hodgkinson, K.C., 1990. The effects of fire on the soil in a degraded semi-arid woodland. I. Cryptogam cover and physical and micromorphological properties. Aust. J. Soil Res., 28: 755-777.

*Helalia A.M., Letey, J. and Graham, R.C., 1988. Crust formation and clay migration effects on infiltration rate. Soil Sci. Soc. Am. J., 52: 251-255.

*Kinnell, P.I.A., Chartres, C.J. and Watson, C.L., 1990. The effects of fire on the soil in a degraded semi-arid woodland. II. Susceptibility of the soil to erosion by shallow rain-impacted flow. Aust. J. Soil Res., 28: 779-794.

*Kooistra, M.J. and Siderius, W., 1986. Micromorphological aspects of crust formation in a savanna climate under rainfed subsistence agriculture. In: F. Callebaut, D. Gabriels and M. De Boodt (Editors), Assessment of Soil Surface Sealing and Crusting. Flanders Research Center for Soil Erosion and Soil Conservation, Ghent, pp. 9-17.

*Kooistra, M.J., Juo, A.S.R. and Schoonderbeek, D., 1990. Soil degradation in cultivated alfisols under different management systems in southwestern Nigeria. In: L.A. Douglas (Editor), Soil Micromorphology: A Basic and Applied Science. Proc. VIII Int. Working Meeting on Soil Mircromorphology, San Antonio, Texas, July 1988. Developments in Soil Science 19, Elsevier, Amsterdam, pp. 61-69.

Le Bissonnais, Y., 1988. Analyse des Mécanismes de Désagrégation et de la Mobilisation des Particules de Terre sous l'Action des Pluies. Ph.D. Thesis, Université d'Orléans, Orléans, 225 pp.

*Le Bissonnais, Y., Bruand, A. and Jamagne, M., 1989. Laboratory experimental study of soil crusting: Relation between aggregate breakdown mechanisms and crust structure. Catena 16: 377-392.

*Le Souder, C., Le Bissonnais, Y., Robert, M. and Bresson, L.-M., 1990. Prevention of crust formation with a mineral conditioner. In: L.A. Douglas (Editor), Soil Micromorphology: A Basic and Applied Science. Proc. VIII Int. Working Meeting on Soil Mircromorphology, San Antonio, Texas, July 1988. Developments in Soil Science 19, Elsevier, Amsterdam, pp. 81-88.

*Le Souder, C., Le Bissonnais, Y. and Robert, M., 1991. Influence of a mineral conditioner on the mechanisms of disaggregation and sealing of a soil surface. Soil Sci., 152: 395-402.

Levy, G., Shainberg, I. and Morin, J., 1986. Factors affecting the stability of soil crusts in subsequent storms. Soil Sci. Soc. Am. J., 50: 196-201.

*Levy, G.H., Berliner, P.R., Du Plessis, H.M. and Van der Watt, H.v.H., 1988. Microtopographical characteristics of artificially formed crusts. Soil Sci. Soc. Am. J., 52: 784-791.

*Luk, S.H., Dubbin, W.E. and Mermut, A.R., 1990. Fabric analysis of surface crusts developed under simulated rainfall on loess soils, China. In: R.B. Bryan (Editor), Soil Erosion - Experiments and Models. Catena Verlag, Cremlingen, Germany, pp. 29-40.

*McIntyre, D.S., 1958a. Permeability measurements of soil crusts formed by raindrop impact. Soil Sci., 85: 185-189.

McIntyre, D.S., 1958b. Soil splash and the formation of a surface crusts by raindrop impact. Soil Sci., 85: 261-266.

*Miller, D.E., 1971. Formation of vesicular structure in soil. Soil Sci. Soc. Am. Proc., 35: 635-637.

*Moran, C.J., Koppi, A.J., Murphy, B.W. and McBratney, A.B., 1988. Comparison of the macropore structure of a sandy loam surface soil horizon subjected to two tillage treatments. Soil Use Manage., 4: 96-102.

*Moss, A.J., 1991a. Rain-impact soil crust. I. Formation on a granite-derived soil. Aust. J. Soil Res., 29: 271-289.

*Moss, A.J., 1991b. Rain-impact soil crust. II. Some effects of surface-slope, drop-size and soil variation. Aust. J. Soil Res., 29: 291-309.

Mualem, Y., Assouline, S. and Rohdenburg, H., 1990. Rainfall induced soil seal. A. A critical review of observations and models. Catena, 17: 185-203.

*Mücher, H.J. and De Ploey, J., 1977. Experimental and micromorphological investigation of ersion and redeposition of loess by water. Earth Surf. Proc., 2: 117-124.

*Mücher, H.J., De Ploey, J. and Savat, J., 1981. Response of loess material to simulated translocation by water: micromorphological observation. Earth Surf. Proc. Landforms, 6: 331-336.

*Mücher, H.J., Chartres, C.J., Tongway, D.J. and Greene, R.S.B., 1988. Micromorphology and significance of the surface crusts of soils in rangelands near Cobar, Australia. Geoderma, 42: 227-244.

*Norton, L.D., 1987. Micromorphological study of surface seals developed under simulated rainfall. Geoderma, 40: 127-140.

*Norton, L.D., Schroeder, S.L. and Moldenhauer, W.C., 1986. Differences in surface crusting and soil loss as affected by tillage methods. In: F. Callebaut, D. Gabriels and M. De Boodt (Editors), Assessment of Soil Surface Sealing and Crusting. Flanders Research Center for Soil Erosion and Soil Conservation, Ghent, pp. 64-71.

*Onofiok, O. and Singer, M.J., 1984 Scanning electron microscope studies of surface crusts formed by simulated rainfall. Soil Sci. Soc. Am. J., 48: 1137-1143.

*Pagliai, M., 1987. Effects of different management practices on soil structure and surface crusting. In: N. Fedoroff, L.M. Bresson and M.A. Coutry (Editors), Soil Micromorphology. Proc. VII Int. Working Meeting of Soil Micromorphology, Paris, July 1985. Association Française pour l'Etude du Sol, Plaisir, France, pp. 415-421.

*Pagliai, M., Bisdom, E.B.A. and Ledin, S., 1983. Changes in surface structure (crusting) after application of sewage sludge and pig slurry to cultivated agricultural soils in northern Italy. Geoderma, 30: 35-53.

*Pagliai, M., La Marca, M. and Lucamente, G., 1983. Micromorphological investigation of the effect of sewage sludges applied to soil. In: P. Bullock and C.P. Murphy (Editors), Soil Micromorphology, volume 1: Techniques and Applications, Proc. VI Int. Working Meeting on Soil Micromorphology, London, July 1981, AB Academic Publishers, Berkhamsted, U.K., pp. 219-225.

*Poss, R., Pleuvret, C. and Saragoni, H., 1989. Influence des réorganisations superficielles sur l'infiltration dans les terres de Barre (Togo méridional). Cahiers de l'ORSTOM, série. Pédologie, XXV: 405-415.

*Radcliffe, D.E., West, L.T., Hubbard, R.K. and Asmussen, L.E., 1991. Surface sealing in coastal plains loamy sands. Soil Sci. Soc. Am. J., 55: 223-227.

*Remley, P.A. and Bradford, J.M., 1989. Relationship of soil crust morphology to inter-rill erosion parameters. Soil Sci. Soc. Am. J., 53: 1215-1221.

Robinson, D.O. and Page, J.B., 1950. Soil aggregate stability. Soil Sci. Soc. Am. Proc., 14: 25-29.

*Southard, R.J., Shainberg, I. and Singer, M.J., 1988. Influence of electrolyte concentration on the micromorphology of artificial depositional crust. Soil Sci., 145: 278-288.

Springer, M.E., 1958. Desert pavement and vesicular layer of some soils of the desert of the Lahonton Basin, Nevada. Soil Sci. Soc. Am. Proc., 22: 63-66.

*Tackett, J.L. and Pearson, R.W., 1965. Some sharacteristics of soil crusts formed by simulated rainfall. Soil Sci., 99: 407-413.

*Tarchitzky, J., Banin, A., Morin, J. and Chen, Y., 1984. Nature, formation and effects of soil crusts formed by water drop impact. Geoderma, 33: 135-155.

Valentin, C., 1981. Organisations Pelliculaires Superficielles de Quelques Sols de Région Subdésertique (Agadez, Rép. du Niger). Dynamique de formation et conséquences sur l'économie en eau. Ph.D. Thesis, Univ. Paris VII, Paris, 213 pp.

*Valentin, C., 1986. Surface crusting of arid sandy soils. In: F. Callebaut, D. Gabriels and M. De Boodt (Editors), Assessment of Soil Surface Sealing and Crusting. Flanders Research Center for Soil Erosion and Soil Conservation, Ghent, pp. 40-47.

*Valentin, C., 1991. Surface crusting in two alluvial soils of northern Niger. Geoderma, 48: 201-222.

*Valentin, C. and Ruiz Figueroa, J.F., 1987. Effects of kinetic energy and water application rate on the development of crusts in a fine sandy loam soil using sprinkling irrigation and rainfall simulation. In: N. Fedoroff, L.M. Bresson and M.A. Coutry (Editors), Soil Micromorphology. Proc. VII Int. Working Meeting of Soil Micromorphology, Paris, July 1985. Association Française pour l'Etude du Sol, Plaisir, France, pp. 401-408.

Valentin, C. and Bresson, L.M., 1992. Morphology, genesis and classification of surface crusts in loamy and sandy soils. Geoderma, 55: 225-245.

Valentin, C. and Casenave, A., 1992. Infiltration into sealed soils as influenced by gravel cover. Soil Sci. Soc. Am. J., 56: 1167-1173.

*van der Watt, H.v.H. and Claassens, A.S., 1990. Effect of surface treatments on soil crusting and infiltration. Soil Technology, 3: 241-251.

*West, L.T., Bradford, J.M. and Norton, L.D., 1990. Crust morphology and infiltrability in surface soils from the southeast and midwest U.S.A. In: L.A. Douglas (Editor), Soil Micromorphology: A Basic and Applied Science. Proc. VIII Int. Working Meeting on Soil Mircromorphology, San Antonio, Texas, July 1988. Developments in Soil Science 19, Elsevier, Amsterdam, pp. 107-113.

West, L.T., Chiang, S.C. and Norton, L.D., 1992. The morphology of surface crusts. In: M.E. Sumner and B.A. Stewart, Soil Crusting: chemical and Physical Processes, Proc. 1st Int. Symposium on Soil Crusting. Lewis Publishers, Boca Raton, pp. 73-92.

Micromorphological and hydraulic properties of surface crusts formed on a red earth soil in the semi-arid rangelands of eastern Australia

R.S.B. Greene[1]* and A.J. Ringrose-Voase[2]

[1]CSIRO, Division of Wildlife and Ecology, PO Box 84, Lyneham, ACT 2602, Australia.
[2]CSIRO, Division of Soils, GPO Box 639, Canberra, ACT 2601, Australia.

ABSTRACT

Greene, R.S.B. and Ringrose-Voase, A.J., 1994. Micromorphological and hydraulic properties of surface crusts formed on a red earth soil in the semi-arid rangelands of eastern Australia. In: A.J. Ringrose-Voase and G.S. Humphreys (Editors), Soil Micromorphology: Studies in Management and Genesis. Proc. IX Int. Working Meeting on Soil Micromorphology, Townsville, Australia, July 1992. Developments in Soil Science 22, Elsevier, Amsterdam, pp. 763-776.

Measurements were made of the micromorphological and hydraulic properties of surface crusts occurring on a Xerollic Haplargid soil (massive red earth) in the semi-arid rangelands of eastern Australia. The crusts were formed on hard, stony, runoff areas in a semi-arid mulga woodland on soil surfaces devoid of any plant or litter cover. The following treatments were used: (i) natural surface during a dry period, (ii) ponded infiltration using a disc permeameter, (iii) simulated rainfall, and (iv) simulated rainfall with protection against raindrop impact.

Micromorphological examination of the surface crusts distinguished four main categories of surfaces in each treatment, *i.e.* a matric crust, skelic crust, porphyric crust and a disturbed crust. The crusts were shown to be spatially variable and dynamic, with the proportion of the four categories related to the amount of wetting, raindrop impact, and surface flow received by the surfaces during each treatment. Wetting settles the disturbed category; impact creates skelic crust from some of the porphyric crust material and flow breaks up and mixes some of the skelic crust.

As these processes reduce the infiltration rate of the surface, the structural properties of these crusts have a major effect on surface hydrology and hence on vegetation distribution in semi-arid rangelands.

INTRODUCTION

The infiltration of rainfall and redistribution of runoff are critical in determining the long term stability of rangelands. They affect the subsequent spatial variation in available soil-water and hence have significant effects on diversity and production in the rangelands (Noy-Meir, 1973). Excessive runoff enhances soil-erosion hazards on sloping land and can cause off-site water and sediment damage downslope (Römkens *et al.*, 1990).

---

* Present address: Department of Geography, Australian National University, Canberra, ACT 0200, Australia
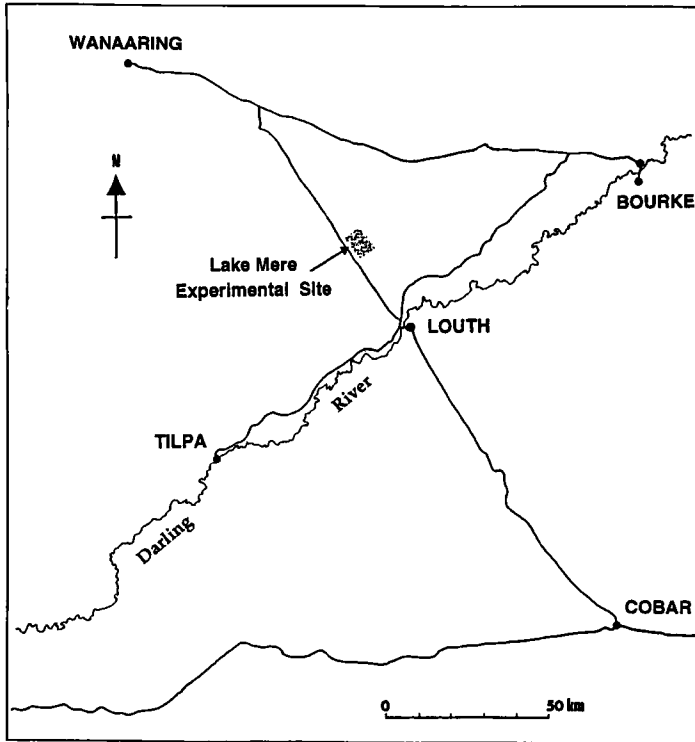
Fig. 1. Location of the 'Lake Mere' study site in the semi-arid rangelands of eastern Australia.

The formation of surface crusts or seals during rainfall events in the arid and semi-arid rangelands can have a major impact on infiltration and run-off processes. In addition to increasing runoff and severely reducing infiltration, surface crusts can alter erodibility at the soil surface, affect air movement and interfere with seedling emergence (Moss, 1991).

There have been several earlier studies on the effects of management on crusting in red earth soils in the semi-arid rangelands. For example, Mott *et al.* (1979), Mücher *et al.* (1988) and Greene and Tongway (1989) have investigated the effects of over-grazing on the formation of surface crusts. Chartres and Mücher (1989), Greene *et al.* (1990) and Kinnell *et al.* (1990) also measured the physical, chemical and micromorphological properties of surface crusts occurring on soils that had been subjected to various fire treatments. These studies indicated that crusts result from a combination of processes such as raindrop impact, deposition of material, colonisation by cryptogams and bioturbation. Work by Greene (1992) and Greene and Sawtell (1992) on crusts formed on a red earth soil near Louth, N.S.W., Australia, also showed that these surface crusts or seals are usually very dense, have a high mechanical resistance and low infiltration rates.

The study reported here was undertaken as part of a larger investigation into the effects of grazing and climatic factors, *i.e.* rainfall, on the structural properties of red earth surface soils in a semi-arid mulga woodland, near Louth. This paper describes the micromorphological and hydraulic properties of surface crusts formed under various experimental conditions. The relationship of these crusts to naturally occurring surface crusts in rangelands is briefly discussed.

Table 1.
Some physical and chemical properties of the < 2.0 mm fraction from the 0 - 20 mm layer of a typical stony runoff zone at the Lake Mere Experimental site.

Particle size analysis (%)					pH [a]	EC [a]	Total C
<2μm	2-20μm	20-63μm	63-200μm	200-2000μm		(μS cm^{-1})	(%)
24.4	8.4	19.1	36.4	10.2	6.0	84.7	1.2

[a] pH and EC (electrical conductivity) in 1:5 soil - water extracts.
Clay mineralogy: Kaolinite dominant, with minor amounts of illite, quartz and iron oxides.

METHODS

The Study Site

The study was conducted on 'Lake Mere' station (144°54'E, 30°17'S), 35 km north of Louth, New South Wales (Fig. 1). It was in an area of semi-arid mulga woodland that was comprised of a patterned sequence of groves and intergroves (Tongway and Ludwig, 1990). The vegetation on the study site is dominated by mulga *(Acacia aneura)* in the groves and contains a wide variety of perennial grasses scattered throughout the landscape. The study site was situated on the Landsdowne land system (Walker, 1991) which is comprised of undulating stony ridges of Cretaceous sandstones and shales and low tablelands of Tertiary silcretes. Relief is up to 20 m, with narrow to broad dendritic drainage lines and slopes of less than 0.5%.

The median rainfall at the site is 275 mm, which is evenly distributed throughout the year. However, high intensity, short duration storms commonly occur each year, causing major redistributions of water from the intergrove areas into the mulga groves (Greene, 1992). All measurements described in this paper were carried out in runoff areas (named runoff zones by Tongway and Ludwig, 1990) in the intergroves during the period March to July 1991.

The soil at the site was classified as a massive red earth Gn2.12 (Northcote, 1979) or a Xerollic Haplargid (Soil Survey Staff, 1975). It consists of a red-brown loamy surface soil over a massive red clay B horizon. Analysis of the total soil from the 0 - 20 mm layer of a typical stony runoff zone indicated 54% of it consists of stones and gravel > 2.0 mm. Some analytical data for the < 2.0 mm fraction from the 0 - 20 mm layer is given in Table 1.

Soil surface treatments and sampling

The following four treatments were used: (i) natural surface during a dry period, (ii) ponded infiltration using a disc permeameter, (iii) simulated rainfall, and (iv) simulated rainfall with protection against raindrop impact. In each case the soil surface was sampled in a bare condition without litter or vegetation. Although some stones usually occurred at the surface, they were usually < 5% of the area. Details of the treatments are as follows:

(i) Natural surface after dry period

Samples were taken of the surface in July 1991 after an extended dry period in which only 12.3 mm rainfall was recorded in the preceding 9 weeks, and only 35.2 mm in the preceeding 24 weeks.

(ii) Surface wetted by ponding
The surface was wetted using a disc permeameter (200 mm diameter) that supplied water at a potential of +10 mm (ponded condition) to the soil surface (Perroux and White, 1988). The final, 3-D infiltration rate was recorded when there was a quasi-steady outflow rate from the disc. This usually occurred after 30 - 45 minutes. Immediately after the infiltration measurement, the infiltrometer ring was removed, excess water allowed to drain off and samples of the moist soil collected for preparation of thin sections. These samples were intended to show by comparison with the dry samples (i) above, the effects of wetting the surface without raindrop impact or surface flow.

(iii) Surface wetted by simulated rainfall
A rotating disc rainfall simulator (Grierson and Oades, 1977) was used to apply a steady rainfall rate of 30 mm h^{-1} to a 1 m^2 quadrat on the soil surface until a constant runoff rate was attained (approx. 50 min). Runoff samples were collected at minute intervals for determination of infiltration and erosion rates. Simulation measurements were carried out in duplicate. Infiltration rate was calculated as the difference between the application rate (30 mm h^{-1}) and the final runoff rate. At the end of each simulation run, tins for thin section samples were inserted into the soil whilst it was still moist. A complete description of the rainfall simulator and method of collecting runoff and erosion is given by Greene and Sawtell (1992).

These samples aimed to show, by comparison with the dry surface, the effect of a single rainfall event on dry soil. They would also show, by comparison with the ponded samples, the effects of raindrop impact and surface flow additional to those of wetting alone.

(iv) Surface wetted by simulated rainfall with protection
The surface was wet as above with simulated rainfall but was protected from direct raindrop impact by shade cloth (approx. 0.25 mm mesh). Measurements of runoff and erosion rates and samples for thin sections were taken as above. By comparing these samples with the rainfall wetted samples (iii) above, the effects of raindrop impact additional to those of wetting and surface flow, would be shown.

Preparation of samples for micromorphological examination

Duplicate samples, 160 × 90 × 50 mm depth, were taken by pushing tins vertically into the soil surface for each treatment. After drying at 40°C, the samples were impregnated with polyester resin. Two, vertically oriented thin sections (60 × 40 mm) were then produced from each sample with the longer dimension parallel to the surface, except for samples from the dry treatment for which only one section was produced.

Micromorphological description of thin sections

In rangeland situations, the surface at any one time is a product not only of the most recent rainfall event, but also of previous rainfall, runoff, erosion, deposition and drying events and bioturbation. This leads to quite complex patterns in the upper layers of the soil. In order to study the effects of the applied experimental treatments, only the immediate soil surface was described in detail. This is in marked contrast to what happens to a seedbed of aggregates in a recently cultivated soil, where the effects of one rainfall event can extend to a depth of several centimeters (see for example Norton, 1987).
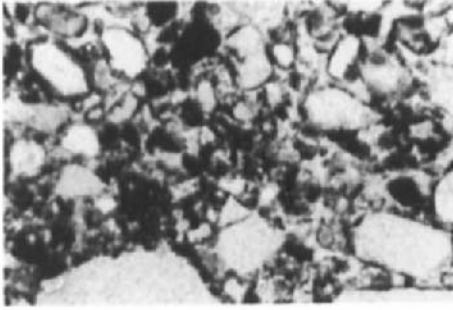
a) Well aggregated matrix just below surface (OL, FW 1.0 mm)

b) Argillans on quartz grains just below surface (XP, FW 1.0 mm)
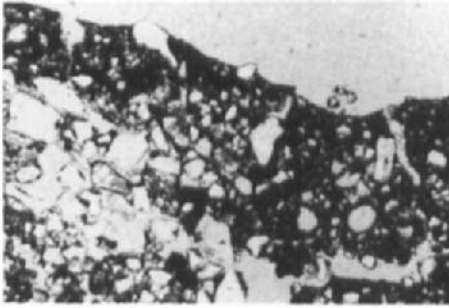
c) Matric crust (OL, FW 4.0 mm)
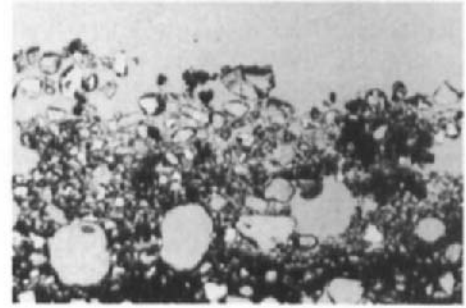
d) Skelic crust + vesicles (OL, FW 4.0 mm)
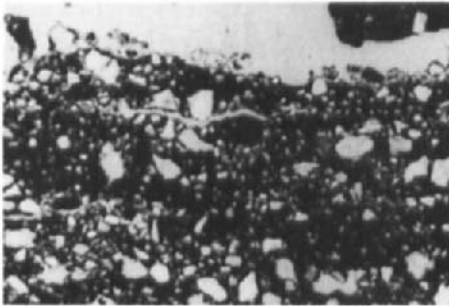
e) Porphyric crust (OL, FW 4.0 mm)
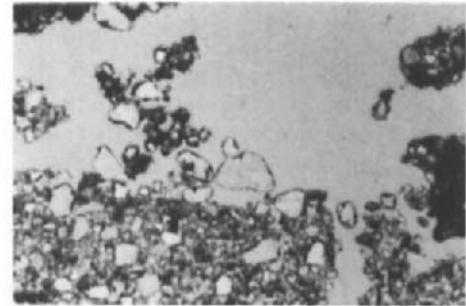
f) Distrurbed crust (OL, FW 4.0 mm)

Fig. 2. Vertical sections of various features immediately below the soil surface (a and b) and of the four surface categories (c, d, e and f). (OL: ordinary light; XP: crossed polarised illumination; FW: frame width)

Table 2.
Percentage of surface in the various categories after various treatments. (Totals may not equal
100% due to rounding). Values in parentheses have been rounded to nearest 20%. Standard
error of differences calculated on 10 degrees of freedom.

Category	Proportion of surface (%) after treatment				S.E.(difference)	
	Dry	Disc permeameter	Simulated rainfall (bare)	(covered)	between any 2 treatments	between 'dry' treatment and
	[Dry]	[Disc]	[Rain]	[Cover]	except 'dry'	any other
Matric crust	16 (20)	21 (20)	25 (20)	28 (20)	8.7	10.7
Skelic crust	18 (20)	39 (40)	A43 (40)	13 (20)	9.3	11.4
Disturbed	47 (40)	4 (0)	18 (20)	14 (20)	9.6	11.7
Porphyric crust	19 (20)	37 (40)	14 (20)	45 (40)	7.4	9.1

A After this treatment, part of the quartz crust equal to 9% of the total surface had a distinct
vesicular layer, which was absent after the other treatments.

Initial examination indicated that four categories of surface could be distinguished in
sections from all treatments. Different treatments appeared to show differences in the
proportions at the surface belonging to the various categories. Hence, the surface visible in
each thin section was examined in short segments, each about 1.125 mm long (equal to
approximately one quarter of the frame width). The segments were allocated to one of the
categories, and the overall proportions for each treatment were calculated from all segments
from all thin sections for that treatment.

RESULTS

Micromorphological properties

At low magnifications the matrix immediately below the surface in all treatments appears
solid with a porphyric fabric. However, at higher magnification the matrix can be seen to
consist of strongly aggregated clay (Fig. 2a). This could be the wind-blown clay referred to as
parna that mantles much of the region to the south of the experimental site (Butler, 1956).
Most quartz grains have argillans with sharp boundaries with the surrounding matrix (*i.e.* not
skelsepic) (Fig. 2b). The argillans are thinnest at sharp edges of the grains. These observations
suggest that the quartz grains are aeolian in origin and have been abraded during transport.
Four main categories of surface morphology were distinguished at the immediate soil
surface in the thin sections. Presumably their relative positions are dependent on microrelief.
They were described after Brewer and Sleeman (1988).
  A. *Matric crust:* concentration of clay at surface as a very thin crust of clay micro-
      aggregates (50 μm thick); possibly darkened by organic matter; no dispersion; vughy,
      monospaced porphyric distribution fabric below (Fig. 2c).
  B. *Skelic crust:* (500 - 800 μm thick); concentration of sand-sized quartz grains at surface;
      occasional vesicles; porphyric distribution fabric below (Fig. 2d).
  C. *Porphyric crust:* no fraction concentrated at surface; crusted, monospaced porphyric
      distribution fabric; vughy (Fig. 2e).

Table 3.
Comparison of soil hydraulic properties of surface crusts formed with disc permeameter and a rainfall simulator.

Infiltration measurement	Soil Hydraulic Properties		
	Infiltration Rate (mm h^{-1})	Runoff Rate (mm h^{-1})	Erosion Rate (g h^{-1} m^{-2})
Rainfall simulator[a] (bare surface)	6.7 ($\pm$2.0)[b]	23.3($\pm$2.0)	6.41($\pm$0.33)
Rainfall simulator (shade cloth)	12.7($\pm$1.4)	17.3($\pm$1.4)	1.28($\pm$0.38)
Disc permeameter (ponded infiltration)	24.4($\pm$4.6)	-	-

[a] Aplication rate: 30 mm h^{-1} [b] Mean and standard error

D. Disturbed crust: crust broken up, sometimes containing organic matter (Fig. 2f).
Because the categories are based only on the very surface layer, it is not always possible to relate them to crust categories used by other workers. Nevertheless, the matric crust and skelic crust described above relate to the erosion crust and sieved structural crust respectively of Valentin and Bresson (1992).

Table 2 shows how the surface is partitioned between the different categories after the various treatments. The skelic crust after simulated rainfall contained a definite vesicular layer in places (approx. 9% of total surface). The results for each treatment form a one dimensional matrix, called [Dry] for the surface after a dry period; [Disc] for that after wetting by disc permeameter; [Rain] for that after simulated rainfall and [Cover] for that after simulated rainfall with protection. For example, if A, B, C and D are the proportions in each category:

$$[\mathbf{Dry}] = \begin{bmatrix} A \\ B \\ C \\ D \end{bmatrix}_{\mathbf{Dry}}$$

Hydraulic properties

Table 3 shows the hydraulic properties of the soil surface measured with a rainfall simulator (with and without shade cloth) and a disc permeameter. Using a rainfall simulator, the final infiltration rate measured under shade cloth was 12.7 mm h^{-1}, which was double that of a bare surface (6.7 mm h^{-1}). The erosion rate from the bare surface (6.4 g h^{-1}) was 5 times that of the surface covered with shade cloth (1.3 g h^{-1}). The final infiltration rate measured with the disc permeameter (24.4 mm h^{-1}) was considerably higher than that measured under shade cloth with the simulator.

Table 4
The effects of various actions on the proportions (percent) of the surface belonging to the various categories, expressed as treatment differences. A simple determination of the significance of treatment differences using Student's t-test (10 degrees of freedom) is shown. *** Significant at 95% probability; ** at 90%; * at 80%; ns, not significant.

Category	Treatment differences				
	[Δrain] = [Rain]-[Dry]	[Δwet] = [Disc]-[Dry]	[Δimpact] = [Rain]-[Cover]	[Δflow$_2$] = [Cover]-[Disc]	[Δdry] = [Dry]-[Rain]
Matric crust	9 ns	5 ns	-3 ns	8 ns	-9 ns
Skelic crust	25 **	21 *	30 ***	-26 ***	-25 **
Disturbed	-29 ***	-43 ***	4 ns	10 *	29 ***
Porphyric crust	-5 ns	18 *	-31 ***	8 ns	5 ns

DISCUSSION

Cyclical nature of stable crusts

The results show that the surface crust is both spatially variable and dynamic, with the proportions in the various categories changing as the soil is subjected to rainfall followed by periods of drying. The simulated rainfall event in the experiment is only the most recent of many rainfall events to which the surface has been subjected. However, significant changes occur during this event as can be seen by comparing the proportions after rainfall, [Rain], with those after a dry period, [Dry]. This shows that a single event increases the proportion of skelic crust at the expense of the disturbed category (Table 2). Since this soil is fairly stable with a well developed seal formed over a long period (Greene et al., in press), such changes could not occur with every event unless they were reversed in the intervening dry periods.

Therefore, it is probable that in this soil the crust morphology observed after a single, significant rainfall event gradually reverts during a dry period to a condition similar to that found before the event. This implies that the morphological and hydraulic properties of surface crusts are cyclical over time. Seasonally cyclic patterns in soil properties have also been observed in grazed pastures in West Africa (Casenave and Valentin, 1989) and in Texas, U.S.A. (Thurow et al., 1988). This situation contrasts with changes in cultivated seedbeds during rainfall (e.g. Valentin and Bresson, 1992), which are largely irreversible (except by further cultivation). However, even in the latter situation, the surface probably reaches a stable cycle if left long enough.

Factors affecting surface morphology

The action of rain falling on the surface and running off has three components: wetting, raindrop impact and surface flow. The individual effects of these three components on surface morphology, i.e. that of wetting, [Δwet], raindrop impact, [Δimpact], and surface flow, [Δflow], can be determined by examining the differences between various pairs of treatments as shown in Table 4. For example, [Δwet] = [Disc] - [Dry]. Expanded this becomes:
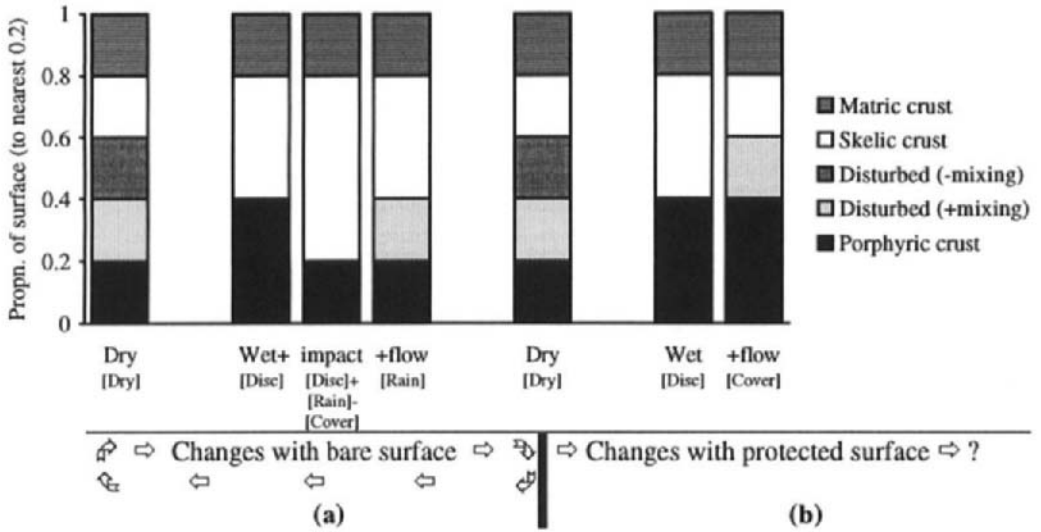
Fig. 3. Schematic diagram depicting how the different categories of surface crust are partitioned between the treatments (rounded to 20%). (a) simulated rainfall on a bare surface. (b) simulated rainfall with protection against raindrop impact. In (a) the values for + impact have been calculated as discussed in the text. The partition of the undisturbed category into mixed and unmixed is hypothetical and not based on observation (see text).

$$
\begin{bmatrix} \Delta A \\ \Delta B \\ \Delta C \\ \Delta D \end{bmatrix}_{\Delta wet} = \begin{bmatrix} A \\ B \\ C \\ D \end{bmatrix}_{Disc} - \begin{bmatrix} A \\ B \\ C \\ D \end{bmatrix}_{Dry}
$$

where ΔA, ΔB, ΔC and ΔD are the changes in the proportions of each of the four surface categories. The four treatments [Dry], [Disc], [Rain] and [Cover] are shown schematically in Fig. 3, where the proportions of each category have been rounded to the nearest 20%. The surface morphology after any of the treatments ([Disc], [Rain], and [Cover]) can be calculated as the sum of the effects of the particular processes ([Δwet], [Δimpact], [Δflow]) acting during the treatment, as follows.

[Disc]:
The surface after ponded infiltration using a disc permeameter includes only the effect of: rapid wetting on ponding [Δwet]. Therefore:

$$[\text{Disc}] = [\text{Dry}] + [\Delta\text{wet}] \tag{1}$$

[Rain]:
The surface after simulated rainfall on bare ground includes the effects of: (i) wetting by rotating disc [Δwet]; (ii) raindrop impact [Δimpact] and (iii) strong raindrop detachment and

transport after runoff begins [Δflow$_1$]. Moss and Green (1983) showed that this component causes significant erosion. Therefore:

$$[\mathbf{Rain}] = [\mathbf{Dry}] + [\mathbf{\Delta wet}] + [\mathbf{\Delta impact}] + [\mathbf{\Delta flow_1}] \qquad (2)$$

The effects of the two methods of wetting the soil in treatments [Disc] and [Rain] are assumed to be the same. Even though ponding water from a disc permeameter results in rapid wetting at the soil surface, the rotating disc also causes the soil surface to be wet quickly as the rain is applied as discrete bursts of water.

[Cover]:
The surface after simulated rainfall with protection against raindrop impact includes the effects of: (i) wetting under shade cloth [Δwet] (assumed to be the same as in treatments [Disc] and [Rain]); (ii) reduced raindrop impact (assumed to be zero) and (iii) reduced raindrop detachment and transport after runoff begins [Δflow$_2$]. Therefore:

$$[\mathbf{Cover}] = [\mathbf{Dry}] + [\mathbf{\Delta wet}] + [\mathbf{\Delta flow_2}] \qquad (3)$$

Although the runoff rates were similar with and without cover (Table 3), the process of particle detachment due to the interaction of surface flow and raindrops cannot be assumed to be equal because the drops in the treatment without cover have greater energy and would cause greater detachment.

The effects of the various factors are discussed below in the context of a stable cycle of crust morphology. Some mechanisms to account for the observed changes are also suggested.

Wetting: [Δwet]:
The effect of wetting can be calculated by rearranging Eqn. 1.

$$[\mathbf{\Delta wet}] = [\mathbf{Disc}] - [\mathbf{Dry}] \qquad (4)$$

Wetting the soil results in a significant increase in both skelic crust and porphyric crust ([Δwet] Table 4) at the expense of the disturbed category which is reduced almost to zero ([Disc] Table 2). Wetting alone is unlikely either to concentrate quartz grains at the surface or to mix existing laminae. This suggests that the disturbed portion of the surface in a dry state consists of skelic crust or porphyric crust material that has been broken up at earlier stages of the cycle (see below) and simply settles back to its original morphology when wetted.

Raindrop impact: [Δimpact]:
The effect of raindrop impact on a bare surface is calculated by subtracting Eqn. 3 from 2.

$$[\mathbf{\Delta impact}] + [\mathbf{\Delta flow_1}] - [\mathbf{\Delta flow_2}] = [\mathbf{Rain}] - [\mathbf{Cover}] \qquad (5)$$

Although as discussed [Δflow$_1$]$\neq$[Δflow$_2$], for the purposes of this discussion it will be assumed that [Δimpact]$>>$[Δflow$_1$]-[Δflow$_2$]. In Table 4 [Δimpact] shows the effect of raindrop impact additional to that of wetting is to create skelic crust from porphyric crust. It was also observed that a portion of the skelic crust after rain had a distinct vesicular layer, that

was absent from the other treatments. This is consistent with observations by Valentin and Bresson (1992) that impact creates sieved, structural crusts, with larger particles concentrated at the surface. [Δimpact] might be better obtained by sampling the surface before runoff occurs. The theoretical state of a surface subjected to wetting and impact is shown in Fig. 3a and calculated as:

$$[\text{Disc}] + [\Delta\text{impact}] = [\text{Disc}] + [\text{Rain}] - [\text{Cover}] \tag{6}$$

Surface flow [Δ flow]:
The effect of surface flow can be calculated by subtracting Eqn. 1 from Eqn. 3.

$$[\Delta\text{flow}_2] = [\text{Cover}] - [\text{Disc}] \tag{7}$$

The effect of surface flow [Δflow] is to loose some of the skelic crust and create disturbed crust. The skelic crust may be lost by mixing with sediment entrained by the interaction of raindrops and surface flow. This portion of disturbed crust is maintained through the drying phase and disappears on wetting. It is shown separately in Fig. 3a to the remainder of the disturbed crust created during drying (see below), although no distinction was recorded during micromorphological examination. This type of disturbed crust would probably become porphyric crust on wetting since mixing would have destroyed the layered structure at the surface.

Dry period [Δdry]:
The final stage of the proposed cycle is drying, which returns the surface to the original condition found before rain. Drying involves a breakup of the skelic crust to increase further the proportion in the disturbed category, [Dry]. A number of factors could be involved, such as shrinkage, faunal activity, microbial activity or wind. Utomo and Dexter (1982) showed that, in a non-aggregated soil, wetting and drying cycles increased water stable aggregation by creating planes of weakness, which provide the initial faces of aggregates. Whitford *et al.* (1992) discuss how soil invertebrates create pores in these soils and Hagen (1991) how saltation disturbs crusts.

The portion of disturbed crust created in this phase of the cycle is shown separately to that created by surface flow as discussed above. Hypothetically, the mechanism that is acting does not mix the layers so that on re-wetting this portion settles back into skelic crust.

In summary, wetting settles the disturbed category; impact creates skelic crust from some of the porphyric crust material and the interaction of raindrops and surface flow breaks up and mixes some of the skelic crust. The matric crust category seems to be largely unaffected by these factors.

Effects of surface cover

The effect of treatment with simulated rainfall on a protected surface is shown schematically in Fig. 3b. Comparison with Fig. 3a shows that removal of raindrop impact by the introduction of shade cloth causes an increase in the proportion of porphyric crust surface at the expense of the skelic category. Thus cover disrupts the hypothetical cycle (Fig. 3a). Further experiments

Table 5
Effects of high intensity rainfall on infiltration measured using a disc permeameter on bare runoff areas in a semi-arid mulga woodland at Lake Mere. Each value is a mean of 36 reps (Greene, unpublished data).

Date of Measurement	Climatic Conditions	Infiltration Rate (mm h^{-1})
1986	Dry condition (drought)	24.0
1988	Immediate post-rain (183 mm)	5.1
1991	Dry condition (drought)	23.0

are needed to establish the effects of a subsequent dry period and whether the surface morphology reaches a new, stable surface morphology cycle after several rainfall/dry period cycles.

Effects of crusts on hydraulic properties

On first examination, the relative infiltration rates measured using the disc permeameter and the rainfall simulator with and without cover (Table 3) do not appear to correlate well with the proportion of any crust category. One reason for this is that infiltration is affected by more than the immediate surface included in the crust categories. The infiltration rates for each treatment are better understood with reference to the processes involved in crust formation as shown in Figs 3a and 3b.

The reduction in infiltration rates (relative to that measured with a disc permeameter) that occurred when simulated rainfall was applied to a bare or a protected surface is probably partly caused by entrained sediment blocking pores immediately below the surface. Agassi *et al.* (1981) also found that, when simulated rainfall was applied to a sandy loam surface soil, dispersed soil particles were washed into the soil with the infiltrating water where they blocked pores immediately beneath the surface and reduced infiltration. In our experiments, application of simulated rainfall to a protected surface reduced infiltration by a factor of 0.52 (*i.e.* 12.7/24.4) compared to the disc permeameter. The largest reduction in infiltration occurred with rain falling on a bare surface and is associated with the effects both of impact, which creates skelic crust and associated compact layers (*e.g.* Valentin and Bresson, 1992), and of surface flow. The additional effect of impact is to reduce infiltration by a further 0.53 (*i.e.* 6.7/12.7).

These results suggest infiltration rate is reduced by processes that actively re-arrange the layers of particles near the surface and presumably block the larger pores in doing so. These processes are impact, which concentrates skeleton grains near the surface, and surface flow, which mixes finer material with quartz crust. By contrast, wetting does not seem to change the layering of particles and blocks fewer pores.

Some additional infiltration measurements at the site (Greene, unpublished data) provide further evidence that crusts have a cyclic nature and that infiltration decreases during rain and increases during dry periods. Table 5 shows that after a series of high intensity rainfall events the infiltration rate dropped to 5.1 mm h^{-1} (similar to the value for simulated rain in Table 3). During the subsequent dry period the rate returned to the value before the events and similar to that shown for the disc permeameter in Table 3.

CONCLUSIONS

The crusts investigated in this study are both heterogeneous and dynamic. Changes in surface morphology can be quite dramatic after treatment by wetting, raindrop impact, surface flow and various combinations of these. Since the crusts are stable in the long-term, the changes due to a single rainfall event must be reversed during a dry period, suggesting that the morphology is cyclical. Various mechanisms to account for the changes in morphology and hydraulic properties have been suggested, but need verification by further study.

ACKNOWLEDGMENTS

REFERENCES

Agassi, M., Shainberg, I. and Morin, J., 1981. Effect of electrolyte concentration and soil sodicity on infiltration rate and crust formation. Soil Sci. Soc. Am. J., 45: 848-851.

Brewer, R. and Sleeman, J.R., 1988. Soil Structure and Fabric. CSIRO Australia, Adelaide, 173 pp.

Butler, B.E., 1956. Parna, an aeolian clay. Aust. J. Sci., 18: 145-151.

Casenave, A. and Valentin, C., 1989. Les états de surface de la zone sahélienne. Influence sur l'infiltration. ORSTOM, Paris, Collection Didactiques, 230 pp.

Chartres, C.J. and Mücher, H.J., 1989. The response of burned and unburned rangeland soil surfaces to simulated raindrop impact and water erosion. Earth Surf. Proc. Landf., 14: 407-417.

Greene, R.S.B., 1992. Soil physical properties of three geomorphic zones in a semi-arid woodland. Aust. J. Soil Res., 30: 55-69.

Greene, R.S.B. and Sawtell, G.R., 1992. A collection system for measuring runoff and soil erosion with a mobile rainfall simulator on sealed and stony red earth soils. Aust. J. Soil Res., 30: 457-463.

Greene, R.S.B. and Tongway, D.J., 1989. The significance of (surface), physical and chemical properties in determining soil surface condition of red-earths in rangelands. Aust. J. Soil Res., 27: 213-225.

Greene, R.S.B., Chartres, C.J. and Hodgkinson, K.C., 1990. The effects of fire on the soil in a degraded semi-arid woodland. I. Cryptogam cover and physical and micromorphological properties. Aust. J. Soil Res., 28: 755-777.

Greene, R.S.B., Kinnell, P.I.A. and Wood, J.T. Role of plant cover in runoff and soil erosion in the semi-arid wooded rangelands. Aust. J. Soil Res., (in press).

Grierson, I.E. and Oades, J.M., 1977. A rainfall simulator for field studies of runoff and soil erosion. J. Agric. Res., 22: 37-44.

Hagen, L.J., 1991. Wind erosion mechanics: abrasion of aggregated soil. Trans. Am. Soc. Ag. Eng., 34: 831-837.

Kinnell, P.I.A., Chartres, C.J. and Watson, C.L., 1990. The effects of fire on the soil in a degraded semi-arid woodland. II. Susceptibility of the soil to erosion by shallow rain-impacted flow. Aust. J. Soil Res., 28: 779-794.

Moss, A.J., 1991. Rain-impact soil crust. I. Formation on a granite-derived soil. Aust. J. Soil Res., 29: 271-289.

Moss, A.J. and Green, P., 1983. Movement of solids in air and water by raindrop impact. Effects of drop-size and water-depth variations. Aust. J. Soil Res., 21: 257-269.

Mott, J.J., Bridge, B.J. and Arndt, W., 1979. Soil seals in tropical tall grass pastures of northern Australia. Aust. J. Soil Res., 30: 483-494.

Mücher, H.J., Chartres, C.J., Tongway, D.J. and Greene, R.S.B., 1988. Micromorphology and significance of the surface crusts of soils in rangelands near Cobar, Australia. Geoderma, 42: 227-244.

Northcote, K.H., 1979. A Factual Key for the Recognition of Australian Soils: 4th Ed. Relim Tech. Publ., Glenside, South Aust.

Norton, L.D., 1987. Micromorphological study of surface seals developed under simulated rainfall. Geoderma, 40: 127-140.

Noy-Meir, I., 1973. Desert ecosystems: environment and producers. Ann. Ecol. and Syst., 4: 25-51.

Perroux, K.M. and White, I., 1988. Designs for disc permeameters. Soil Sci. Soc. Am. J., 52: 1205-1215.

Römkens, M.J.M., Prasad, S.N. and Whisle, F.D., 1990. Surface sealing and infiltration. In: M.G. Anderson and I.P. Burt (Editors), Process Studies in Hillslope Hydrology. John Wiley and Sons, New York, pp. 127-172.

Soil Survey Staff, 1975. Soil Taxonomy: A Basic System of Soil Classification for Making and Interpreting Soil Surveys. USDA Agric. Handbk. No. 436. Govt. Printer, Washington D.C.

Thurow, T.L., Blackburn, W.H. and Taylor, C.A., 1988. Infiltration and interrill erosion responses to selected livestock grazing strategies, Edwards Plateau. Texas. J. Range Manage., 41: 296-302.

Tongway, D.J. and Ludwig, J.A., 1990. Vegetation and soil patterning in semi-arid mulga lands of eastern Australia. Aust. J. Ecol., 15: 23-34.

Utomo, W.H. and Dexter, A.R., 1982. Changes in soil aggregate water stability induced by wetting and drying cycles in non-saturated soil. J.Soil Sci., 33: 623-637.

Valentin, C. and Bresson, L.-M., 1992. Morphology, genesis and classification of surface crusts in loamy and sandy soils. Geoderma, 55: 225-245.

Walker, P.J. 1991. Land Systems of Western NSW. Technical Report No. 25. Dept. Conserv. Land Manage, NSW.

Whitford, W.G., Ludwig, J.A. and Noble, J.C., 1992. The importance of subterranean termites in semi-arid ecosystems in south-eastern Australia. J. Arid Environ., 22: 87-91.

Fabric changes during reclamation of a scalded, red duplex soil by waterponding

A.J. Ringrose-Voase[1] and S.G. McClure[2]

[1]CSIRO Division of Soils, GPO Box 639, Canberra, ACT 2601, Australia
[2]CSIRO Division of Soils, PMB No. 2, Glen Osmond, SA 5064, Australia

ABSTRACT

Ringrose-Voase, A.J. and McClure, S.G., 1994. Fabric changes during reclamation of a scalded, red duplex soil by waterponding. In: A.J. Ringrose-Voase and G.S. Humphreys (Editors), Soil Micromorphology: Studies in Management and Genesis. Proc. IX Int. Working Meeting on Soil Micromorphology, Townsville, Australia, July 1992. Developments in Soil Science 22, Elsevier, Amsterdam, pp. 777-786.

In semi-arid New South Wales, large areas of red duplex soils were scalded by wind and water erosion exacerbated by overgrazing and drought, leaving them devoid of vegetation. On slopes of less than 0.5%, waterponds (about 0.5 ha) enclosed by horseshoe shaped banks have been successful in reclaiming scalds.

The macro- and micromorphology and chemical and physical properties of profiles under scald and under 7 month old and 22 year old waterponds were compared. The silt loam A horizon of the scald profiles was thin (<3 cm) with a vesicular crust, which hindered both infiltration and seedling emergence. The B horizon was saline and sodic with well developed peds (<20 mm). The clay fraction was 25% smectite. Leaching had occurred under recent ponds but few other changes.

The surface of old ponds was comparatively well vegetated. The B horizon had become massive with shrinkage cracks extending from the surface to 25 cm depth, which greatly increased infiltration. The horizon was non-saline but still sodic resulting in lower aggregate stability. Microscopically, the fabric showed more birefringent clay and some argillans in the upper part of the horizon. At sub-microscopic scales, the fabric had changed from a dense mixture of quartz grains and clay matrix to a spongy fabric where clay appeared to coat the quartz grains, leaving pore space between them.

It was concluded that early stages of revegetation resulted from water retention and later stages from improved infiltration due to restructuring the B horizon accompanied by formation of large cracks. Restructuring resulted from destabilizing the clay which remained sodic after leaching of soluble salts. Although leaching is rapid, restructuring takes several years, possibly due to the absence of any mechanical input.

INTRODUCTION

In semi-arid regions of New South Wales used for extensive sheep and cattle grazing, overgrazing during droughts in the early part of the century caused wind and water erosion of large areas of red duplex soils (Dr1.22, Northcote, 1974; Typic Haplargids, Soil Survey Staff, 1975). These soils have a coarse textured A horizon overlying a clay B horizon and are found

on the flood plain of the Murray and Darling Rivers and their tributaries. Erosion has removed the sandy A_1 horizon and exposed the silty clay loam A_2 horizon, which forms a dense crust due to rain-drop impact. In other places, the crust consists of deposited material possibly cemented by dispersed clay. These crusts prevent revegetation by inhibiting seedling emergence and greatly reducing the infiltration rate. They also prevent further erosion. Such bare, crusted areas are called 'scalds' (Beadle, 1948).

One successful technique for reclaiming scalds is waterponding (Jones, 1967). This involves laying out ponds of about 0.5 ha to contain natural rainfall (Rhodes, 1987b). On gentle slopes (<0.5%) the ponds are partly enclosed by horse-shoe shaped banks constructed by road grader or bulldozer, which pond water to a maximum depth of about 10 cm. On flat areas, the ponds are completely enclosed. Revegetation by grasses, saltbush (*Atriplex* spp.) and copperburr (*Sclerolaena* spp.) usually occurs after about 5 years of average rainfall (Rhodes, 1987a). Waterponds are long-term structures and give more consistent reclamation than other methods such as checkerboard ploughing, which require rapid establishment of vegetative cover to prevent the furrows slaking and reverting to scald (Jones, 1967). Ponding is economically feasible even on land which can support only 0.4 - 0.7 sheep ha^{-1} after reclamation.

In the short term, waterponding appears to work by retaining rainfall that would otherwise run off (Ringrose-Voase et al., 1989a). In the longer term, waterponding dramatically improves the infiltration rate so that rainfall is stored in the subsoil where it is protected from evaporation. This improvement in infiltration is caused by the development of vertical cracks, which act as preferential pathways for rainfall to enter the subsoil bypassing the surface crust (Jones, 1969; Ringrose-Voase et al., 1989a).

Ringrose-Voase et al. (1989a) studied the macro- and micromorphology of profiles under scalds and waterponds to understand the processes occurring during reclamation. In addition, the study aimed to determine which soil properties are necessary for waterponding to be successful so that the efficacy of the techniques on other soil types can be assessed. This paper expands on the micromorphological aspects of the study and the mechanisms of structural change that account for the long-term improvement in infiltration.

METHODS

Sampling

The site investigated is 100 km north on Nyngan, New South Wales on the Bogan River/Marra Creek/Macquarie River flood plain complex. The area consists of a complex pattern of prior and current drainage lines. The red soils affected by scalding are located adjacent to these drainage lines (Jones, 1966) and form a mosaic with grey clays which are located further from the drainage lines.

The region has an average annual rainfall between 405 mm (Gongolgon) and 425 mm (Nyngan), with 30% more falling in the summer months than in the rest of the year. The summers are hot (mean January maximum of 34°C at Nyngan) with high evaporation rates. The land is used for extensive grazing by sheep and some cattle of native pastures, including grasses, perennial and annual saltbush (*Atriplex* spp.) and copperburr (*Sclerolaena* spp.).

Sampling was carried out at two sites, A and B, 500 m apart. Waterponds were 22 years old at site A and 7 months old at site B. The ponds at site A were revegetated with grasses and annual saltbush forming about 50% ground cover. Those at site B were bare except for

Table 1
Particle size data and summary of the field description of macrostructure and segregations (according to McDonald *et al.*, 1984).

Horizon	Depth	Percent			Macrostructure[A]	Segregations
	cm	Clay <2	Silt 2-20 μm	Sand >20		
					AS: Site A, scald	
A_{21}	0.0 - 0.5	25	34	41	Massive	
A_{22}	- 3.0	34	32	34	Weak platy (<2mm)	
B_{21}	- 5.5	54	25	21	Strong, subangular blocky (<10mm)	
$B_{22}n$	- 16.5	63	23	16	Strong, subangular blocky (<10mm)	Fe/Mn ped coatings
B_{23}	-24.5 ± 3.5	59	23	15	Strong, angular to subangular blocky (<20mm)	
B_{24}	-37.5 ± 7.5	55	26	16	Strong, angular blocky (<50mm)	Ca concretions
B_3	- 100.0+	52	30	15	Massive to moderate, prismatic (<100mm)	Ca concretions to 80cm, gypsum below
					BS: Site B, scald	
A_2	0.0 - 1.5	17	45	37	Massive	
B_{21}	- 6.0	46	40	14	Strong, subangular blocky (<10mm)	Mn/Fe ped coatings
$B_{22}n$	- 19.0	56	34	11	Moderate, subangular blocky (<20mm)	Mn/Fe ped coatings
B_{23}	- 40.0	59	31	10	Weak, subangular blocky (<20mm)	Ca concretions
B_3	- 90.0+	52	40	7	Massive	Ca concretions to 70cm, gypsum below
					AP: Site A, 22 year old pond	
A_2	0.0 - 3.0	24	35	39	Massive; vertical cracks (width <20mm)	
B_{21}	- 8.0	45	25	29	Strong, subangular blocky (<20-50mm); vertical cracks (width < 10mm)	
B_{22}	- 25.0	60	28	15	Strong, prismatic (<100mm) breaking to weak, subangular blocky (<20mm); vertical cracks (width <10mm)	
B_{23}	- 47.0	57	26	16	Weak, prismatic (<20mm)	Ca concretions
B_3	- 90.0+	50	32	15	Massive	Ca concretions to 80cm, gypsum below
					BP: Site B, 7 month old pond	
A_{21}	0.0 - 1.0	22	37	40	Massive	
A_{22}	- 3.0	32	35	33	Massive	
B_{21}	- 7.0	50	31	21	Strong, subangular blocky (<10mm)	Mn/Fe ped coatings
$B_{22}n$	- 17.0	54	28	17	Moderate, subangular blocky (<20mm)	Mn/Fe ped coatings
B_{23}	- 45.0	54	30	14	Weak, subangular blocky (<20mm)	Ca concretions
B_3	- 100.0+	52	36	10	Massive	Ca concretions to 70cm, gypsum below

[A] Strong, moderate and weak refer to the degree of ped development.

small patches of vegetation which existed before waterponding. The gradient at both sites was less than 0.11%. Profiles were described and sampled in the centre of a pond at each site (profiles AP and BP respectively) and under the adjacent undisturbed scald (profiles AS and BS). Both profiles at site B were located under bare areas. Profile descriptions are summarised in Table 1 and can be found in full in Ringrose-Voase et al. (1989b).

Chemical, Particle size and Mineralogical Analyses

Particle size analyses were carried out using the plummet method (McIntyre and Loveday, 1974). Results are given in Table 1. Cation exchange capacity and exchangeable cations were measured by the silver-thiourea method (Pleysier and Juo, 1980). Exchangeable sodium percent (ESP) and electrical conductivity (EC) of the 1:5 extract are shown in Figs 1 and 2. A full account of the data collected can be found in Ringrose-Voase et al. (1989a, b). The clay mineralogy of the $B_{22}n$ and B_3 horizons of profile AS was determined by X-ray diffraction. The density of small peds from the B_{21} and B_{22} horizons was measured by coating them in a thin layer of wax and weighing them in air and in water.

Micromorphological Analysis

Undisturbed samples ($155 \times 90 \times 50$ mm) were taken from each profile at depth of 0 - 5, 5 - 10 and 15 - 20 cm. Thin sections were prepared from these samples after they had been air dried and impregnated under vacuum with polyester resin. Descriptive terms below are from Brewer and Sleeman (1988). In addition, small peds from the B_{21} and B_{22} horizons of profiles AS and AP were examined by scanning electron microscope (SEM).

RESULTS

Macromorphology and mineralogy

All profiles had a thin, crusted, silty clay loam A horizon, but the surface of profile AP had considerable microrelief, whereas that of the others was smooth. The upper, silty clay B horizon of profiles AS, BS and BP had a strongly developed subangular blocky structure, with prominent manganiferous ped coatings. The clay fraction consisted of approximately equal proportions of smectite, illite and kaolinite. In profile AP, the equivalent horizon had a prismatic structure without ped coatings. This profile had large vertical cracks extending from the surface to 25 cm depth. It is these cracks that improve infiltration by allowing rainfall to bypass the crust and enter the subsoil, which results in the long term success of waterponding.

Chemistry and ped density

The subsoils of all profiles were sodic (Fig. 1). The ECs of the subsoil of the untreated profiles (AS and BS) indicated they were also saline (EC of 1:5 extract greater than 0.625 dS m^{-1}, which according to Talsma (1968), is equivalent to Richards' (1954), threshold of 4 dS m^{-1} for the saturation extract). Fig. 2 shows that soluble salts have been leached from the profile AP and are being leached from profile BP. Aggregate stability data in Ringrose-Voase et al. (1989a) indicate that the combination of high ESP and low soluble salts decrease;
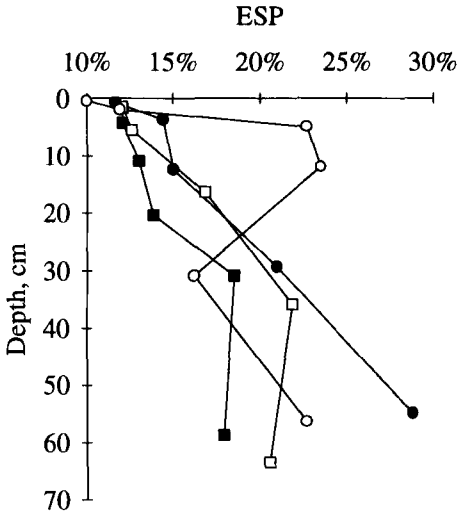
Fig. 1. Exchangeable sodium percentage (ESP) of four profiles: ■ Scald, site A; ● Scald, site B; □ 22 year old pond, site A; ○ 7 month old pond, site B.
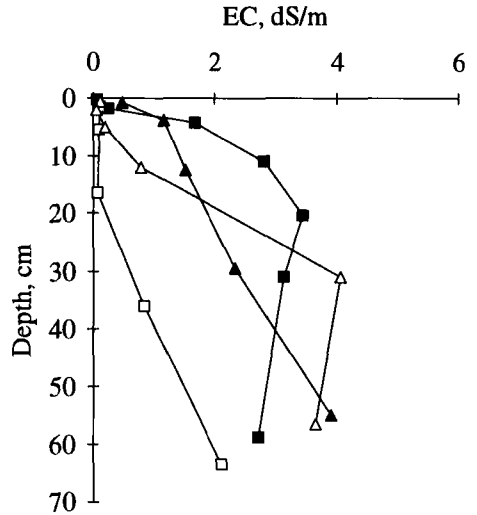
Fig. 2. Electrical conductivity (EC) (1:5 extract) of four profiles: ■ Scald, site A; ▲ Scald, site B; □ 22 year old pond, site A; △ 7 month old pond, site B.

significant at P = 0.999. This difference implies a loss of solid material of 4% by volume (assuming a particle density of 2.6 g cm^{-3}).

Micromorphology and Submicroscopy

In the scald profiles, AS and BS, the upper 1 mm of the surface crust had an adporphyric distribution fabric with a densely packed mixture of fine sand and silt grains with silt-sized clay aggregates (Fig. 3a). The surface was smooth. In places there were vesicles indicating the crust had been formed by rain drop impact. In other places, there were laminae indicating deposition of eroded material. Below this layer there were laminae of material similar to above interspersed with more clayey material with a porphyric distribution fabric and insepic orientation fabric. In profile BP, the surface was similar, but had a layer of strongly oriented clay on the surface, which had presumably settled out of suspension in the pond. In profile AP, the surface layer was still dense, but had a rougher surface and incorporated plant material and no vesicles (Fig. 3b).

The B horizon of all profiles had a fragmoidic physical fabric with units 0.5 - 5.0 mm at 5 - 10 cm depth (Fig. 3c) becoming more weakly developed (aporic-fragmoidic) at 15 - 20 cm depth (Fig. 3e). Macropore space consisted of occasional large fissures and metavughs. The distribution fabric was porphyric. The orientation fabric of the B horizon of profiles AS, BS and BP was [skel-bima]-insepic. In profile AP, it was [skel]-bima-mo-insepic, indicating greater alignment of clay by stress (Fig. 3f). Associated structures included few ferro-

Scald profiles (AS and BS)   **Profile AP under 22 year old waterpond**
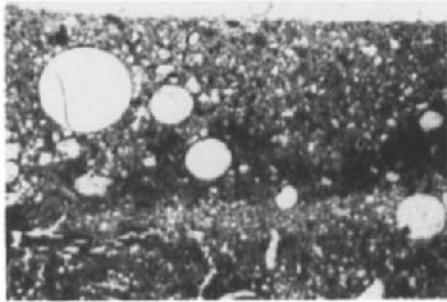
a) Surface, BS (OL, FW 3.0 mm)
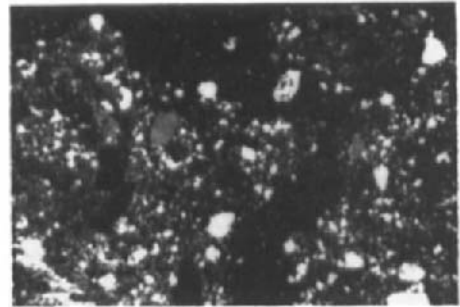
b) Surface (XP, FW 3.0 mm)
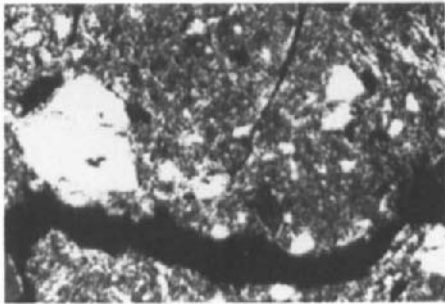
c) B_{21} horizon, AS (XP, FW 1.19 mm)
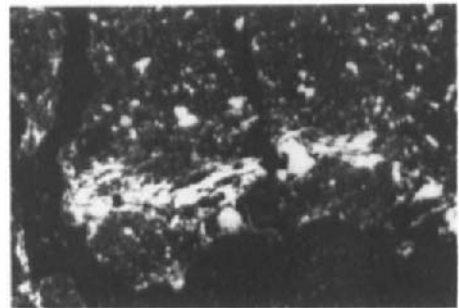
d) B_{21} horizon (XP, FW 3.0 mm)

e) B_{23} horizon, AS (XP, FW 0.75 mm)
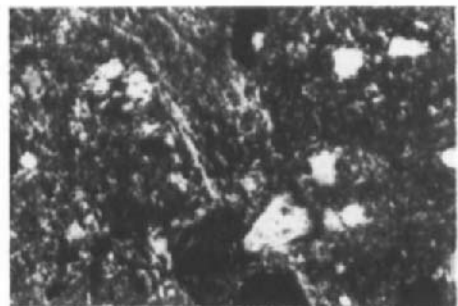
f) B_{22} horizon (XP, FW 0.75 mm)

Fig. 3. Micrographs of vertical thin sections of profiles under scald and 22 year old waterpond (OL: ordinary light; XP: cross-polarised light; FW: frame width)

manganese veins and nodules and very few void argillans, which were more common in profile AP (Fig. 3d), indicating that ponding had encouraged dispersion and translocation of clay.

Examination of small peds from the upper B horizon of profiles AS and AP by SEM revealed quite different fabrics (Fig. 4). Fracture surfaces of peds from under the untreated scald (Fig. 4a, b, c, d) revealed a dense fabric in which the quartz grains were completely embedded in clay, as would be expected for a porphyric distribution fabric. After 22 years waterponding, the fabric appeared spongy (Fig. 4e, f, g, h). The clay matrix no longer completely embedded the quartz grains, but instead coated them, leaving small pores between them. The clay coats formed bridges in some instances (Fig. 4h). In places there were more extensive clay skins and in others completely naked, silt sized quartz grains (Fig. 4g).

DISCUSSION

After 22 years of waterponding the fine, sub-angular blocky macrostructure of the B horizon had been replaced by a coarser, prismatic structure with large cracks, which extend through the thin, crusted A horizon and greatly improve the infiltration rate. The starting point for the structural changes was the leaching of soluble salts by waterponding which lowered the aggregate stability due to the sodicity of the clay. After some time this destabilisation caused a reorganisation of the clay. Some clay dispersion and translocation occurred at the microscopic scale as shown by the increased frequency of argillans in profile AP and the decrease in ped density. However, these are probably not enough to account for the gross change in the macrostructure nor the increase in porosity of the pore size seen by SEM. Changes at a submicroscopic scale suggest a more widespread reorganisation of the clay fabric. A possibility is that clay has dispersed and been redeposited locally in a more compact arrangement (*i.e.* face to face, with less pore space between the clay plates) as coats on fine sand and silt sized quartz grains and as bridges between them, leaving a network of interstitial pores. This would involve a shift in the pore size distribution rather than a change in total porosity. (This arrangement cannot be seen in thin section because the pores and coats are smaller than the section thickness). Although there appears to be a link between the submicroscopic reorganisation of the fabric and the changes in macrostructure, the mechanism is not known.

The change in structure occurred over a period of years and was only evident under long established waterponds (*i.e.* in profile AP but not BP). However, leaching of soluble salts occurred over a period of months and had occurred in profile BP as well as AP. The delay between leaching the soluble salts, which destabilised the clay, and the changes in structure could be a result of the lack of mechanical input to provide the 'activation energy' to start the structural changes. The only physical disturbance the system receives is that of shrink/swell activity due to the greater magnitude of wetting/drying cycles under ponding and the increased shrink/swell potential caused by the lower soluble salt concentration. The differences in orientation fabric in profile AP provide some evidence of greater shrink/swell activity in profile AP. The magnitude of this disturbance is small compared to the disturbance that would occur during cultivation. Comparison can be made with coastal clay soils of England and the Netherlands, which are sodic and saline. The structure of these soils is stable when the land is used for permanent pasture, but rapidly collapses due to clay dispersion if the land is drained and cultivated for arable farming (Loveland *et al.*, 1984). In the latter case, it is possible that the relatively rapid structural collapse was brought about by the greater disturbance of tillage.
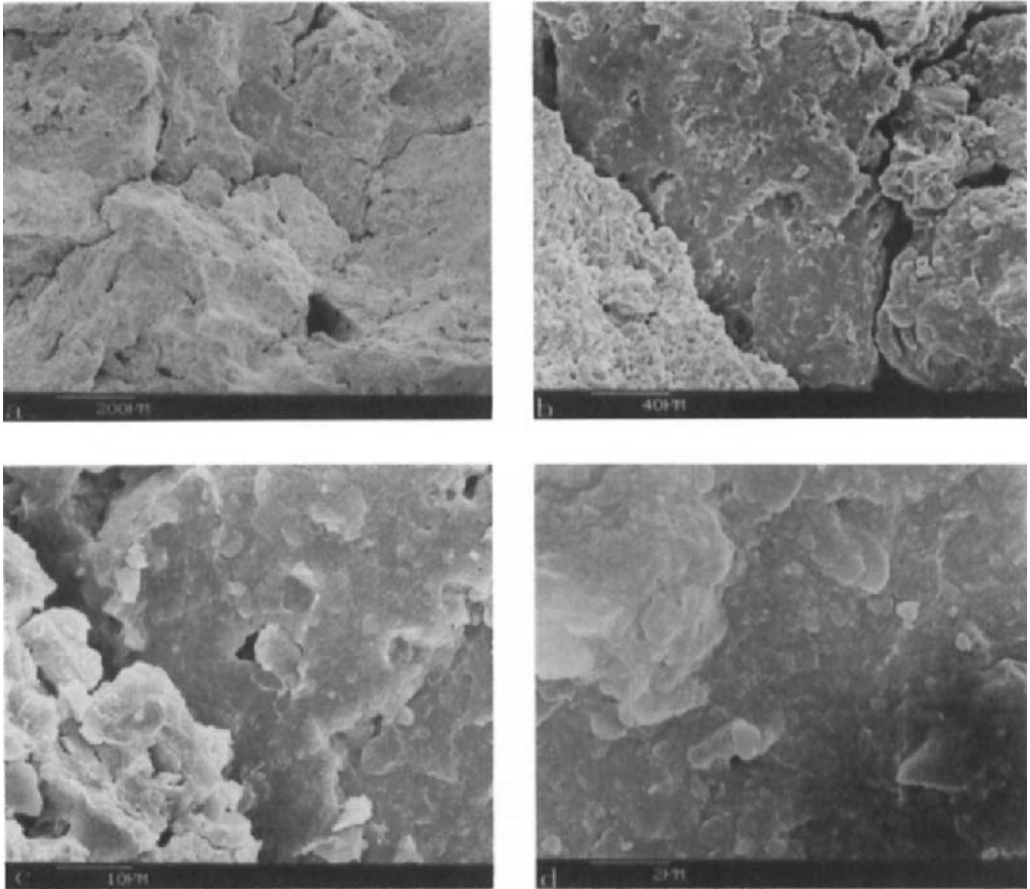
Fig. 4. a, b, c and d. SEM micrographs of peds from the upper B horizon of profile AS under scald at various magnifications.

CONCLUSIONS

The success of waterponding in increasing the infiltration rate is caused by the formation of vertical cracks which appears to be linked to a reorganisation of the clay fabric of the B horizon. This reorganisation is itself a result of the sodic clay in the B horizon becoming unstable as soluble salts are leached by waterponding. This suggests that this treatment will only be successful where scalds occur on texture contrast soils with saline/sodic clay subsoils.

The restructuring process takes several years after the salts have been leached, possibly because of the lack of physical disturbance apart from shrink/swell activity. This suggests that the clay fraction should contain some swelling clays for the restructuring to happen.
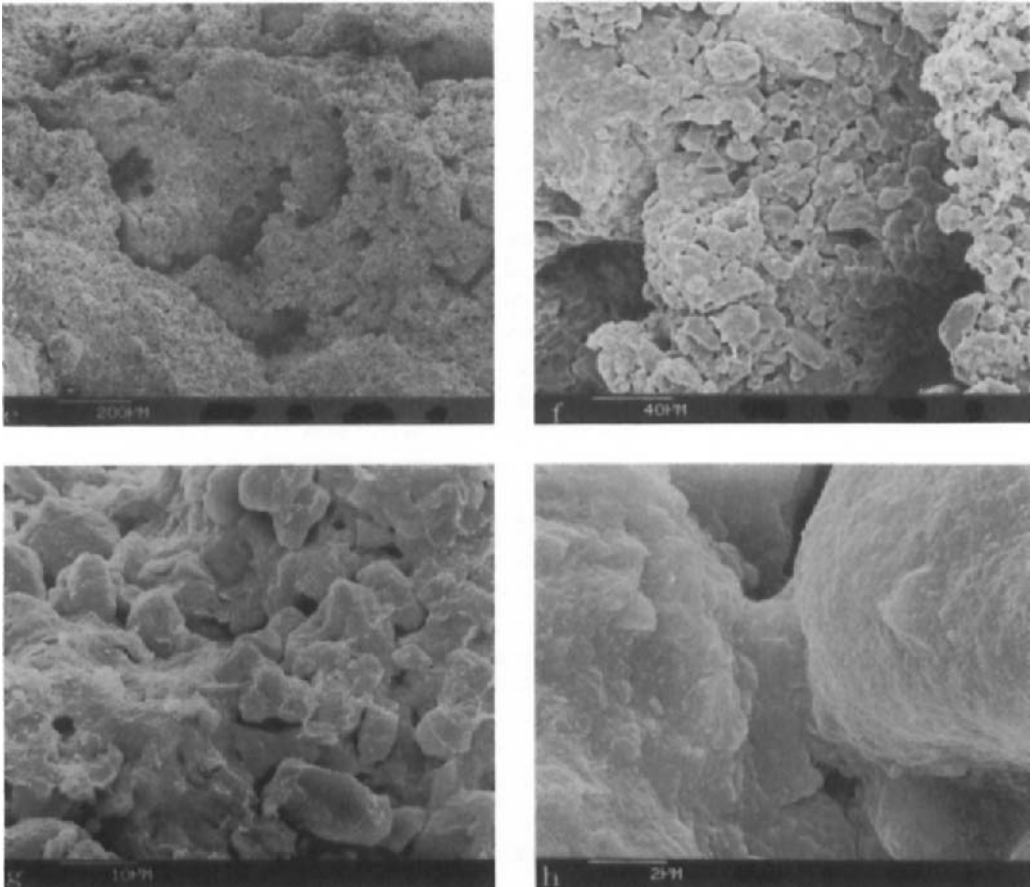
Fig. 4 e, f, g and h. SEM micrographs of peds from the upper B horizon of profile AP under 22 year old waterpond. Magnifications of e, f, g and h are the same as Fig. 4a, b, c and d respectively

REFERENCES

Beadle, N.C.W., 1948. Studies in wind erosion. Part I. The origin, general appearance and classification of scalds. J. Soil Conserv. N.S.W., 4: 30-35.

Brewer, R. and Sleeman, J.R., 1988. Soil Structure and Fabric. CSIRO Aust., Adelaide.

Jones, R.M., 1966. Scald reclamation studies in the Hay district, N.S.W. Part I. Natural reclamation of scalds. J. Soil Conserv. N.S.W., 22: 147-160.

Jones, R.M., 1967. Scald reclamation studies in the Hay district, N.S.W. Part III. Reclamation by ponding banks. J. Soil Conserv. N.S.W., 23: 57-71.

Jones, R.M., 1969. Scald reclamation studies in the Hay district, N.S.W. Part IV. Scald soils: Their properties and changes with reclamation. J. Soil Conserv. N.S.W., 25: 104-120.

Loveland, P.J., Sturdy, R.G. and Hazelden, J., 1984. Soils and solute patterns in reclaimed esturine marshland in south-east England. In: J. Bouma and P.A.C. Raats (Editors), Proceedings of the ISSS Symposium on Water and Solute Movement in Heavy Clay Soils. International Institute for Land Reclamation and Improvement Publication 37, Wageningen, The Netherlands, pp. 252-256.

McDonald, R.C., Isbell, R.F., Speight, J.G., Walker, J. and Hopkins, M.S., 1984. Australian Soil and Land Survey: Field Handbook. Inkata Press, Melbourne.

McIntyre, D.S. and Loveday, J., 1974. Particle size analysis. In: J. Loveday (Editor), Methods for Analysis of Irrigated Soils. Commonwealth Bureau of Soils Tech. Commun. No. 54. Commonwealth Agricultural Bureaux, Farnham Royal, U.K., pp. 88-89.

Northcote, K.H., 1974. Factual Key for the Recognition of Australian Soils. 3rd Ed. Rellim, Glenside, South Australia.

Pleysier, J.L. and Juo, A.S.R., 1980. A single-extraction method using silver-thiourea for measuring exchangeable cations and effective CEC in soils with variable charge. Soil Sci., 129: 205-211.

Rhodes, D.W., 1987a. Vegetation response and productivity improvements under waterponding. J. Soil Conserv. N.S.W., 43: 62-67.

Rhodes, D.W., 1987b. Waterponding banks - design, layout and construction. J. Soil Conserv. N.S.W., 43: 80-83.

Richards, L.A., 1954. Saline and Alkaline Soils. U.S. Dept. Agric. Handb. No. 60. U.S. Gov. Printing Office, Washington, D.C.

Ringrose-Voase, A.J., Rhodes, D.W. and Hall, G.F., 1989a. Reclamation of a scalded, red duplex soil by waterponding. Aust. J. Soil Res., 27: 779-795.

Ringrose-Voase, A.J., Thompson, R., Beatty, H.J., Chapman, G. and Rhodes, D.W., 1989b. Soil properties of scalded, red duplex soils before and after reclamation by waterponding. CSIRO Aust. Div. Soils Tech. Mem. 4/89.

Soil Survey Staff, 1975. Soil Taxonomy. U.S. Dept. Agric. Handb. No. 436. U.S. Gov. Printing Office, Washington, D.C.

Talsma, T., 1968. Environmental studies of the Colleambally Irrigation Area and surrounding districts. Part III. Soil salinity. Water Conservation and Irrigation Commission, N.S.W. Bull. No. 2 (Land Use Series).

Bowl-structures: a composite depositional soil crust

G.S. Humphreys

*Research School of Pacific and Asian Studies, Australian National University, Canberra,
ACT 0200, Australia*

ABSTRACT

Humphreys, G.S., 1994. Bowl-structures: a composite depositional soil crust. In: A.J. Ringrose-Voase and G.S.
Humphreys (Editors), Soil Micromorphology: Studies in Management and Genesis. Proc. IX Int. Working
Meeting on Soil Micromorphology, Townsville, Australia, July 1992. Developments in Soil Science 22,
Elsevier, Amsterdam, pp. 787-798.

Bowl-structures are ephemeral concave-up features commonly found in the upper 50 mm of
the soil in the Sydney Basin, N.S.W. They form when rainwash transports *Eucalyptus* leaves,
which are then buried by sandy sediment. The size and shape of bowls are controlled by the
dimensions of leaf fragments and the degree of curling induced by desiccation prior to burial.
Bowls are typically 25 - 70 mm long and 5 - 20 mm thick. Internally, bowls are mostly apedal
with grain support fabrics but in thin section a variety of discrete sedimentological features are
recognisable. These include: graded beds, reverse graded beds, graded interstitial beds, current
crescents and imbricate patterns. Some of these features are identifiable as different types of
soil crusts and hence bowl-structures can be considered as a 'composite depositional soil crust'.

INTRODUCTION

During an investigation of some coarse textured biomantles in the Sydney Basin a variety of
depositional surface features were observed. The largest of these consisted of ant and termite
mounds (Humphreys, 1981; Humphreys and Mitchell, 1983; and Cowan *et al.*, 1985) and
arcuate bands of litter - termed *litter dams*. The litter dams develop on relatively bare surfaces
and are created by runoff following bush fires when floating load is detained or otherwise
deposited to form walls of organic debris 30 - 50 mm high (Mitchell and Humphreys, 1987).
Bedload is trapped by these dams when water ponding occurs, forming microterraces. These
microterraces are 10 - 30 mm thick and commonly consist of laminations of finer organic
material and clean sands in which various types of depositional and structural crusts occur (*cf.*
Valentin and Bresson, 1992).

In addition to litter dams and microterraces, however, there is another type of feature with a
distinct concave-up shape that occurs only in the upper-most part of the mineral soil. These
features, herein termed 'bowls' or 'bowl-structures', are another form of depositional crust. This
paper describes their formation by using a quasi-sedimentological approach which was
successful in the evaluation of litter dams and microterraces (Mitchell and Humphreys, 1987;
following in part the observations of Emmett, 1970; Moss and Walker, 1978; Moss *et al.*,
1979).
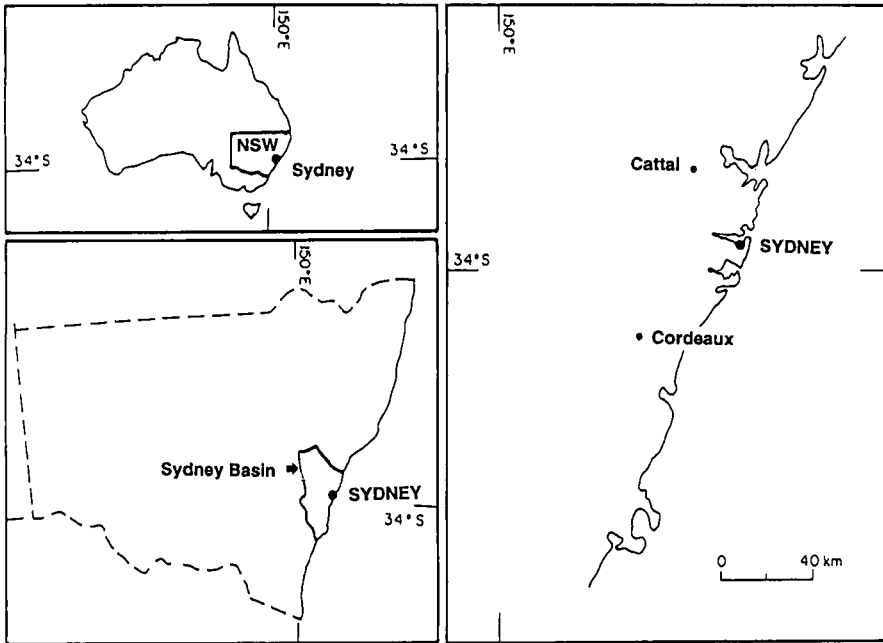
Fig. 1. Location of the two study areas.

SITE CONDITIONS AND METHODS

Study Sites

Five soil profiles were examined from two localities within the Sydney Basin: Cattai and Cordeaux, 39 km NW and 64 km SW of Sydney, respectively (Fig. 1). Both sites are positioned on upper ridge crests of quartzose Hawkesbury Sandstone and support open forest dominated by *Eucalyptus* spp. with an understorey of proteaceae shrubs. Rainfall averages 900 - 1,000 mm annually but is highly variable on a yearly basis. The topsoil at both sites consists of 200 - 400 mm of apedal, loamy sand to fine sandy loam overlying either clayey or loamy subsoils to produce texture contrast soils (Haplohumult, Soil Survey Staff, 1975; Yellow Podzolic, Stace *et al.*, 1968) and shallow earths (Quartzipsamments, Soil Survey Staff, 1975; Earthy Sands, Stace *et al.*, 1968). Additional site details are contained in Humphreys and Mitchell (1983).

Surface Flow Conditions

On both sites slopes are generally < 6° and sediment transport over the surface is primarily via rainwash (which includes a combination of rainsplash, slopewash, *cf.* Mücher and De Ploey, 1977; and sediment rafting). An anastomosing flow pattern of shallow channels (*e.g.* Emmett, 1970) commonly develops with raindrop induced turbulent flow. This is maintained even

during heavy rainfall events due to the impact of gravity drops (*cf.* Moss and Green, 1987) and to the maintenance of surface roughness by protuberances such as ant mounds and plant stems. This flow is sufficient to separate the floating load of charcoal, leaves and other organic fragments from the suspended load of clay and silt, and the bedload of quartz sand. Site observations are supported by similar field based accounts by Moss and Walker (1978) in the Canberra region (160 km SW of Cordeaux) and in part by associated experimental work (*e.g.*. Moss *et al.*, 1979; Moss, 1988; Kinnell, 1988). These flow conditions are most obvious on bare surfaces following fire when hydrophobicity is well developed (Mitchell and Humphreys, 1987) but it also occurs well after plant regeneration providing the litter layer is not too thick.

Methods

A variety of techniques spanning meso to micro-scales of investigation were adopted for fabric analysis. This included careful trenching to obtain undisturbed, oriented samples in Kubiena tins which were examined under a dissecting microscope or impregnated with polyester resin. Impregnated blocks (150 × 80 × 50 mm) were serially sectioned and all pedological features > 3 - 4 mm^2 in size were mapped though sometimes smaller entities were distinguished also, and selected areas thin sectioned for petrographic analysis. In total 17 blocks were sectioned, of which 8 included the upper 50 mm of soil and the remainder contained some portion within 150 mm of the surface. More than 25 thin sections were examined. X-ray radiography (Radifluor 360 instrument) was undertaken on sections 3 - 6 mm thick to help define the shape of bowl-structures following the procedure in Bouma (1969). Scanning electron microscopy (JEOL T20 instrument) was undertaken to examine the matrix fabric of bowls on carefully extracted, undisturbed air-dried samples which had been mounted on aluminium stubs and gold splattered.

Grain size analysis of sands involved dispersion of a bulk sample with Sodium hexametaphosphate followed by wet sieving through a 63 μm screen. The retained portion was oven-dried and sieved at half phi intervals. The pipette method (Folk, 1974) was used on a subsample of the untreated soil for material < 63 μm.

CHARACTERISTICS OF BOWLS

Occurrence

Bowls-structures are found within the upper 20 - 50 mm of the mineral soil with faint traces extending to 110 mm, *i.e.* into the zone of active bioturbation (Fig. 2A and B). They are mostly associated with microterraces (*cf.* Mitchell and Humphreys, 1987) or within the outwash zone surrounding ant and termite mounds. When present they generally extend to the surface though in some situations a thin (*c.* 5 mm) sheet of sand covers them. The bowls have no easily recognisable surface expression and were first detected in serially sectioned blocks of impregnated soil.

Morphology

The results of the meso-scale mapping on eight examples from different profiles are used in the following description, although only three examples are shown in Fig. 2. Individual bowls are
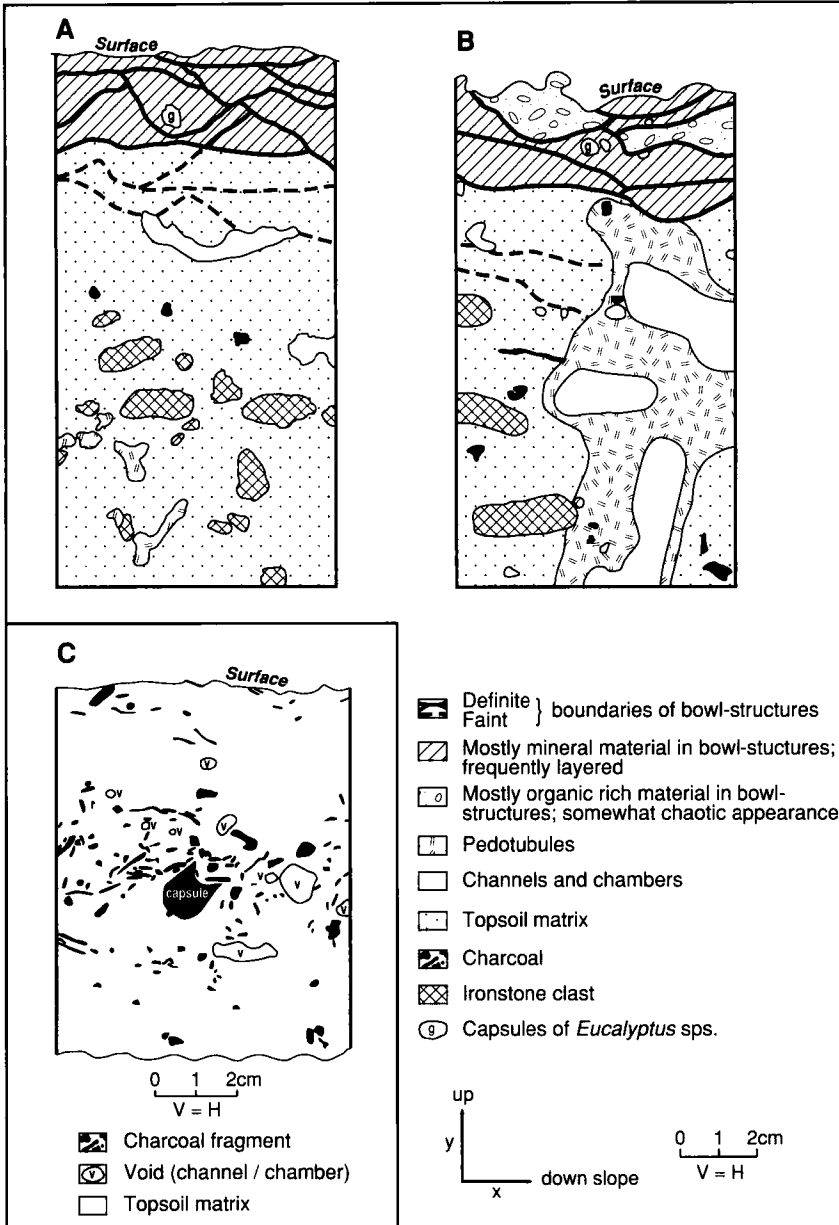
Fig. 2. Meso-scale maps of features in the uppermost soil at Cattai. The chambers, channels and pedotubules below the bowls in 'A' are due to the funnel ant (*Aphaenogaster longiceps*) and in 'B' the sugar ant (*Camponotus consobrinus*). The distribution of charcoal fragments in 'C' displays an imbricate arrangement on the upslope side of the *Eucalyptus* capsule.

stacked in an overlapping arrangement sub-parallel to the surface to form a discrete layer. Isolated bowls were not observed. The bowls are mostly 25 - 70 mm long (L) orientated downslope (X-Y plane of Allen, 1968), 10 - 30 mm wide, and 5 - 20 mm or more thick (T), though some larger examples occur. Typically the L:T ratio varies between 3:1 and 7:1. They are concave-up, often lens-like in shape and have a tendency for a tail to develop downslope. Curvature of the base varies from being fairly planar to distinctly 'V'-shaped.

The base of each bowl is often defined by a leaf or leaf fragment of *Eucalyptus* spp., which imparts a sharp, smooth character to the boundary (Fig. 3A and B). The overlying sediment is normally in contact with the upper surface of the leaf. On the underside, however, there is often a pronounced elongated void, about 1 mm or more thick and 10 - 20 mm or more long. These voids closely parallel the leaf, normally being in contact with it. Hence, they tend to be planar to sinuous in long-section (X-Y plane) and similar in shape to the leaf (Fig. 3C). Otherwise, individual bowls or parts of bowls can be recognised by discontinuities following grain boundaries (Fig. 3D; *cf.* Conybeare and Crook, 1968).

Individual bowls contain a wedge of moderately to poorly sorted clean sediment or zones of more organic rich material. The sediment consists of quartz sand with the ratio of the -1 to 4 phi size fraction to mud (*i.e.* < 4 phi *cf.* Folk, 1974) > 3:1. The organic material also contains some quartz sand but there is an abundance of charcoal < 2 mm (-1 phi) in size, which imparts a darker colour. Sometimes these two sediment types occur in what appears to be a facies relationship over distances up to 20 mm within a single bowl.

The bowls, or the facies within them, are apedal with denser and more porous varieties of grain (*i.e.* skeletal) support fabrics (Fig. 4A). This can be seen in hand specimen under a stereo-microscope and/or under a low magnification scanning electron microscopy (Fig. 3D). Where plasma occurs it appears to include some clay and abundant organic matter including invertebrate faecal pellets. Flecked and striated extinction patterns are observed (silasepic to insepic plasmic fabrics of Brewer, 1976). However, it is not always clear whether these patterns are due to clay mineral and/or anisotropic plant fragments, especially in the case of faecal pellets where mineral soil and comminuted plant fragments form highly heterogeneous masses. An enaulic related distribution pattern dominates between plasma and grains (c/f 2 μm) within bowls but the full range varies from monic phytoquartzopsam to gefuric and rare porphyric psammi/phytohumopelisil (*cf.* Stoops and Jongerius, 1975).

In comparison to the immediate underlying soil, bowl-structures are noted for their absence of gravel (ironstone clasts), large biopores in the shape of channels and chambers, and pedotubules (Figs 2A and B). However, smaller elliptical (2 - 5 mm) voids (not packing voids) are occasionally present. Charcoal occurs throughout, though it may be concentrated in bands (*e.g.* Fig. 2C). Any capsules (gumnuts) of the dominant tree (*Eucalyptus*), whether carbonised or not, are restricted to these bowl-structures (Figs 2A - B, 3A - B).

Other Associated Features

Within bowls an array of sedimentary features are recognisable in thin section. These features are described using the terminology of Conybeare and Crook (1968) unless indicated otherwise.

(i) Graded bedding: These are fining upward sequences that commonly occur in various depositional environments. This feature is often found within troughs (*i.e.* lowest part of
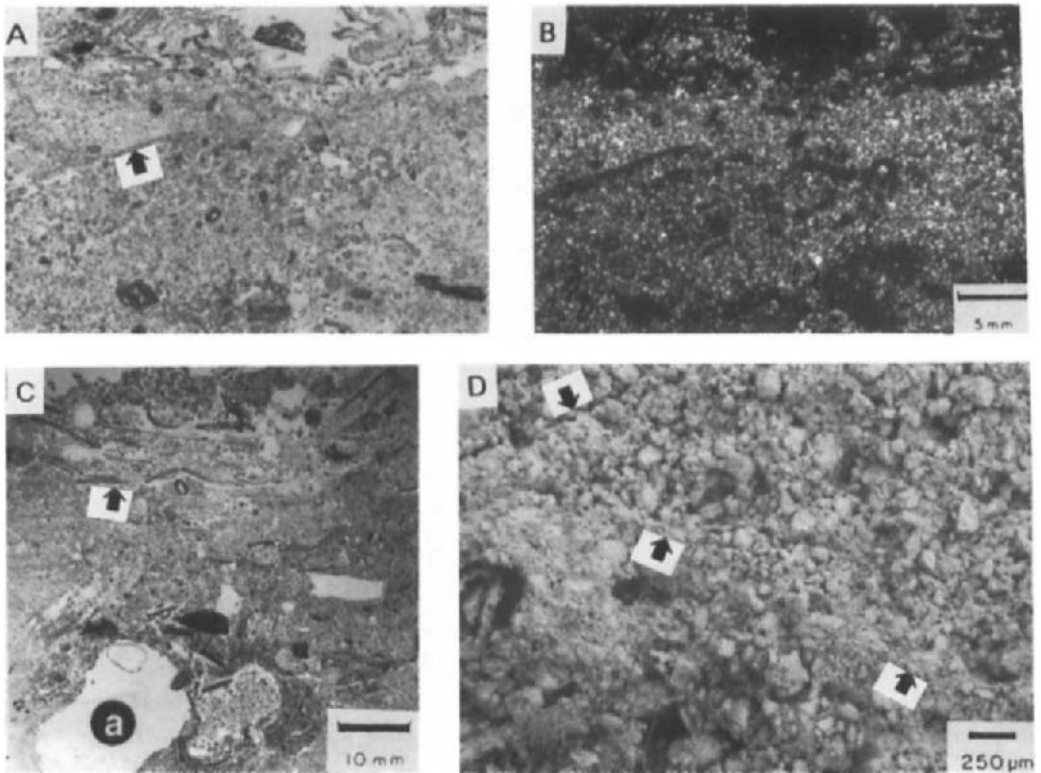
Fig. 3. A) and B) Bowl-structures. Note the basal leaf fragment (arrow) and overlying lens of sediment to the left and the abundance of organic fragments. Upper 0 - 20 mm. A) Plane polarised light (PPL), B) Cross polarised light (XPL). C) Several bowls are evident forming a distinct layer about 20 mm thick (arrow points to the base of deepest bowl). Bioturbation by the sugar ant (a) occurs below these bowls. D) Scanning electron micrograph of bowl-structures. These discrete depositional units can be distinguished on a fabric and compositional basis also. For example, the central unit is more densely packed than those above and below. In this case the bowl shapes are defined by discontinuities following grain boundaries (arrows). Upper 50 mm.

bowl) but they are laterally discontinuous, < 5 mm high and not always well developed (Fig. 4C).

(ii) Reverse graded bedding: These sequences coarsen upwards and occur as discrete units similar in size to graded beds (Fig. 4D). However, they are mostly located above larger particles such as a pieces of charcoal or the basal leaf in a trough.

(iii) Graded interstitial beds: These are beds in which the grain size distribution of the bulk of the bed remains uniform, but where there is a decrease in the content of interstitial material away from the base (see Lowe and LoPiccolo, 1974). This feature (Fig. 4E) is much less common and limited in extent compared with graded or reverse graded bedding.
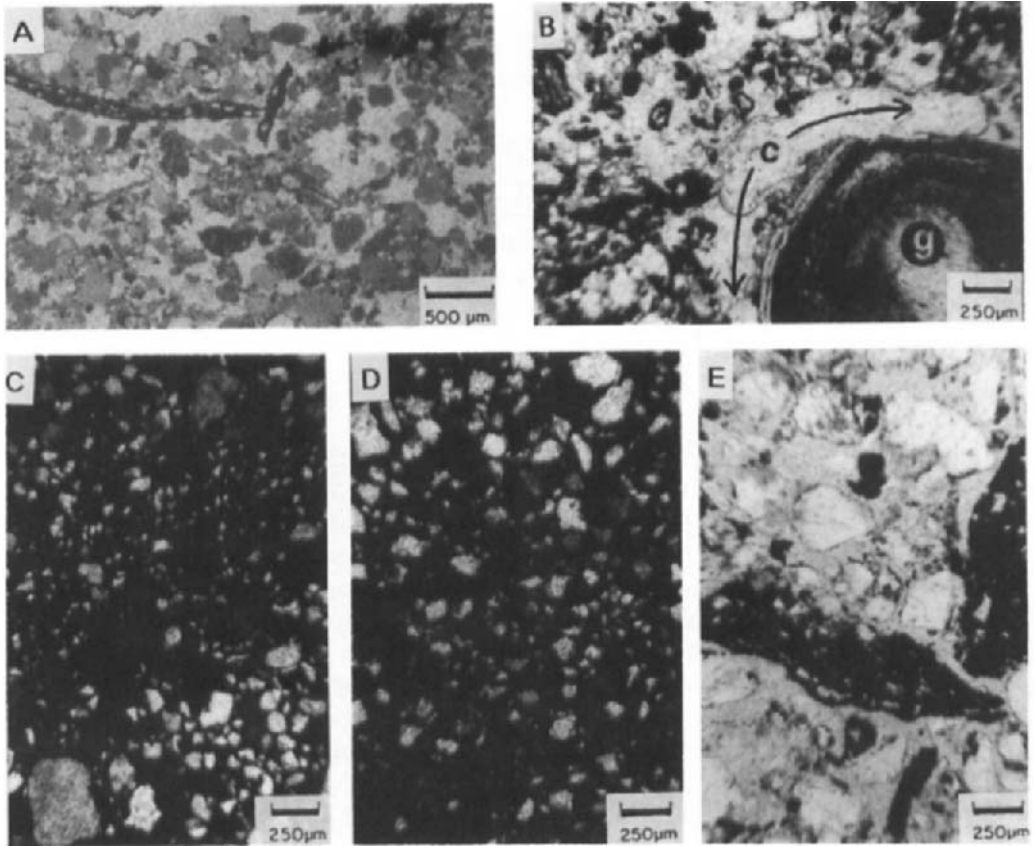
Fig. 4. Thin sections A to F from bowl-structures. **A)** Close-up of part of the surface of a recent bowl-structure shown in Figs 3A and B. Note the very open arrangement of the particles showing little if any compaction. **B)** The large arcuate void (marked c) is thought to represent a current crescent formed around a gumnut (g, lower right corner). The current flowed from left to right. PPL. **C)** Part of a graded bedded sequence. The grains are coarser at the base of the photo. XPL. **D)** Reverse graded bedding. The particles coarsen upwards. XPL. **E)** Graded interstitial beds. The finer grains, trapped between larger uniformly sized quartz grains, decrease in concentration upwards. The large black sub-horizontal particle is charcoal. PPL.

(iv) Cross-sections of apparent 'current crescents': These are scour marks around objects, such as capsules (Fig. 4B), gravel, *etc*. This feature is frequently observed on the surface of microterraces.

(v) Imbricate arrangement: These are particles (especially platey ones) arranged in a loose to somewhat stacked pattern, with dips pointing upslope. Fig. 2C shows a good example involving carbonised plant fragments upslope of a capsule (*Eucalyptus eximia*).

(vi) Small-scale ripple-like features: These resemble 'ripples', in the sense of Allen (1968), whereby the down-current side is bounded by a narrower and more steeply inclined face than the up-current side. They tend to occur in isolation above the basal boundary, attaining heights of only 2 - 3 mm.

Two other features associated with bowl-structures also help to characterise them; stacked plant fragments and denser packing over barriers. The former is somewhat similar to imbricate structures, but they are parallel to the surface and are composed of plant fragments and leaves of varying degrees of carbonisation and fragmentation on or near the surface. They resemble an 'edgewise conglomerate' when platey clasts are so arranged. The second feature refers to the concentration of mineral and organic grains overlying barriers such as leaf and charcoal fragments.

ORIGIN

It is apparent from the description and the environmental setting that bowl-structures can be classed as primary depositional features: they are located in the uppermost zone of the mineral soil where rainwash has been observed and measured at both sites (Humphreys and Mitchell, 1983) and they are often, though not always, found with microterraces. Organic-rich bowls appear to be incipient litter dams that ceased forming during the waning stage of a flow event and/or when starved of a suitable debris supply. Sandy bowls seem to result from bedload transport under shallow flow conditions over short distances. In this situation the separation of plasma would be restrained, leading to little sorting. It is also conceivable that some of the sand has moved by rafting, in which case little sorting is to be expected. Furthermore, it is possible to explain the origin of other features observed within bowl-structures in terms of contemporary sediment transporting processes.

Graded bedding can be expected when material is deposited into ponded zones and during the waning stage of rainwash events when increasingly smaller particles are transported and deposited. Reverse graded bedding requires special circumstances. One site where this can occur is on the surface of sand lenses where continued rainsplash promotes a coarser, better sorted upper layer. Particle size analysis of two samples from sand lenses - with raindrop impact craters - showed that this material is coarser and better sorted than the underlying soil (Table 1). This is an example of a sieving-crust (Valentin and Bresson, 1992) which they attributed to rainsplash whereby finer particles move downwards in a manner resembling a nested set of sieves. This interpretation differs from Mücher and De Ploey (1977) who, on the basis of experiments on loess, indicate that rainsplash or rainwash impart little or no change to sorting - a result that is not unexpected given the apparent uniform grain size used. On similar loessic material, however, Norton (1987) reports a washed-out zone where colloids have been removed to leave a silty layer that presumably became better sorted. The presence of current crescents probably indicates streaming behaviour as water is deflected around objects that have become stationary during the waning stages of a flow event. It is difficult to account for imbricated small plant fragments other than by concluding that it is another manifestation of sediment transport and flow velocity. Hence, a direct analogy to gravel beds of river channels, which they closely resemble, cannot be valid. The small-scale ripple-like feature may or may not be a ripple though Moss and Walker (1978) record ripples with foreset heights of 1 - 2 mm that developed in pools when flow became subcritical. Graded interstitial beds and the dense packing arrangement of material above a barrier of leaf fragments, charcoal, *etc.*, could be

Table 1
Grain size measures of sandy lenses and the underlying soil

Material	Gravel	Sand	Mud	Ratio	M_z	σ_I
	(> 2 mm)	(0.063 - 2 mm)	(< 0.063 mm)	S:M	(ϕ)	(ϕ)
Sand lens	0.8	98.9	0.3	357.9	1.06	0.49
Soil	0.8	93.5	5.7	16.3	1.31	1.05
Sand lens	2.0	88.9	9.1	9.79	2.07	1.03
Soil	17.9	64.9	17.2	3.76	2.90	1.96

M_z = Graphic mean
S_I = Inclusive graphic standard deviation (*i.e.* a measure of sorting)
Both M_z and S_I are defined by Folk (1974) and in these examples refer to material < 2 mm
using the phi-scale (ϕ).

manifestations of the same feature. They may represent a primary depositional feature in which fines have been trapped with the coarser grains. Alternatively, this feature may be coupled to the development of sieving-crusts, *i.e.* as the repository of the pervected (*cf.* Paton, 1978, p. 59) finer grains. It could also represent a form of infilling-crust (*cf.* Valentin and Bresson, 1992) or washed-in zone (McIntyre, 1958; Norton, 1987) though Chartres and Mücher (1989) and others have questioned the efficacy of a washing-in mechanism. Finally, the absence of interstitial material above a zone of concentration may be due to dewatering.

However, the issue of bowl shape remains. An important feature of many bowl-structures is the distinctive base which is commonly delineated by leaf fragments. The partial burial of leaves within trapped sand lenses has already been commented upon. However, this is not the only site of burial. Leaves near mesofauna mounds are commonly buried totally or partly, due either to direct mound construction and/or the erosion of mound material by rainwash. Commonly, burial is concentrated on part of a leaf first. This promotes a concave-up form as desiccation of the exposed leaf portion leads to contraction and curling. Leaves at an advanced stage of desiccation tend to fragment when subjected to the impact of rainsplash. This interpretation would seem to offer a simple, yet serviceable explanation of the irregular concave-up shape of the bowls in which the contact between successive bowls is simply the stacking of leaves separated by transported sediment.

DISCUSSION AND CONCLUSION

Similar features to bowl-structures have been reported elsewhere and to avoid any equivocation it is necessary to consider these alternatives. To varying degrees bowl-structures resemble both 'cut and fill' sequences and 'dish structures' in the sedimentological literature. Cut and fill events of the size demanded were never observed on the soil surface at the study sites, and the presence of basal leaf fragments is inconsistent with this process. There are, however, several points in common between bowl-structures and dish structures (described by Lowe and LoPiccolo, 1974; Allen, 1982, pp. 367-374). Features similar to both include: dimensions; grain size; a dark sharp base; reverse graded bedding; graded interstitial beds; pale clean sands; and in part, shape and arrangement. In terms of shape, dish structures show an up-

sequence change starting as very open features which are slightly concave and gradually developing pronounced concavity. In comparison, bowl-structures show a similar range in shape but there is no gradual change from one type to the other. Furthermore, in dish structures the upward pointing limbs do not make contact with the base of the overlying dish, whereas in bowl-structures this is common. An additional difference is the presence of a 'pillar' within many dish structures (Lowe and LoPiccolo, 1974). These pillars consist of circular columns of massive or swirled sand, the diameter of which varies from 1 mm to as much as 1 m or more in extreme cases. They can occur independently of dish structures or in almost any relationship with them. To date dish structures have been recorded in a variety of recent and ancient sediments, including alluvial deposits, delta fronts, volcanic ash and flysch sequences.

Two mechanisms have been advanced to explain dish structures. Lowe and LoPiccolo (1974) argue that they are a secondary feature resulting from a gradual dewatering of quick or under-consolidated beds; the water being forced laterally beneath semi-permeable laminations. Furthermore, they consider that pillars result from the same basic process but that water movement is at higher velocities. Allen (1982) also favours a secondary origin. He suggests, however, that during early stages of sand compaction, a situation can be reached where partly consolidated and slightly cohesive sand coexists with sand that has remained non-cohesive. When this state is achieved an unstable situation results with the more cohesive sand body tending to sink under the influence of gravity. In turn, this initiates failure in the underlying non-cohesive sand and leads to the eventual formation of dish structures in which the upturned limbs define a concave shape.

Regardless of which hypothesis is favoured for the development of dish structures it is clear that they have a different origin to bowl-structures. Hence, to avoid confusion the new term has been introduced. In essence, bowl-structures are a primary depositional feature that can be subjected to secondary reorganisation in which a variety of crusts may develop (cf. Valentin and Bresson, 1992). In this sense bowl-structures are considered a 'composite depositional soil crust' consisting of a nested set of crust-elements, which in turn may form part of larger depositional features such as microterraces and the outwash zone around ant and termite mounds. In this environment soil crusts are probably best considered as part of these larger depositional features rather than as discrete entities.

This study has also highlighted the potential importance of organic debris in influencing the type of deposits that form at the surface as a result of rainsplash and rainwash. Previously, Mitchell and Humphreys (1987) noted that litter dams developed best when there was an abundant supply of acicular shaped litter (e.g. leaves of Hakea spp., Casuarina spp. and Pinus spp.) even though other materials are included. Litter dams were rarely formed by Eucalyptus leaves, but it is these lanceolate shaped leaves that define the shape and size of bowls. This suggests that the geometry of plant fragments may have a controlling influence on the style of deposition, and hence should be considered with other variables known to be important in soil crust development such as particle size and flow conditions.

The presence of bowl-structures in the study areas indicates that sediment movement at the surface is an ongoing process that is not dependent on episodic bush fires as is required by litter dams and microterraces. A suitable source of material is provided by mounds of various organisms, especially the funnel ant, Aphaenogaster longiceps, which deposits loose aggregates at rates > 500 g m^{-2}y^{-1} (Humphreys, 1981; Humphreys and Mitchell, 1983). Like microterraces and litter dams, however, bowl-structures are not preserved in the soil as they are quickly destroyed by bioturbation. Observations suggest that individual bowls may last a

few months only. Because of their ephemeral nature it is unknown whether or not bowl-structures alter the hydrological conditions at the surface, other than showing that sediment movement takes place on gentle slopes. Though the banding pattern of shrubs and grasses appears to be associated with litter dams in these study areas (cf. Mitchell and Humphreys, 1987) there is no evidence to suggest that bowl-structures *per se* have an equivalent effect.

ACKNOWLEDGMENTS

REFERENCES

Allen, J.R.L., 1968. Current Ripples: Their Relation to Patterns of Water and Sediment Motion. North-Holland Publ. Amsterdam, 443 pp.

Allen, J.R.L., 1982. Sedimentary Structures, Their Character and Physical Basis. Vol.II. Elsevier, Amsterdam, 663 pp.

Bouma, A.H., 1969. Methods for the Study of Sedimentary Structures. John Wiley and Sons, New York, 458 pp.

Brewer, R., 1976. Fabric and Mineral Analysis of Soils. Reprinted by R.E. Kreiger Co., New York, 482 pp.

Chartres, C.J. and Mücher, H.J., 1989. The effects of fire on the surface properties and seed germination in two shallow monoliths from a rangeland soil subjected to simulated raindrop impact and water erosion. Earth Surf. Proc. Landf., 14: 407-417.

Conybeare, C.E.B. and Crook, K.A.W., 1968. Manual of Sedimentary Structures. Bull. Bur. Min. Res. Geol. and Geophys., 102, Aust. Dept. Nat. Devel., Canberra, 327 pp.

Cowan, J.A., Humphreys, G.S., Mitchell, P.B. and Murphy, C.L., 1985. An assessment of pedoturbation by two species of mound-building ants, *Camponotus intrepidus* (Kirkby) and *Iridomyrmex purpureus*, (F. Smith), Aust. J. Soil Res., 22: 95-107.

Emmett, W.W., 1970. The Hydraulics of Overland Flow on Hill Slopes. USGS Prof. Pap. 662A, 68 pp.

Folk, R.L., 1974. Petrology of Sedimentary Rocks. 2nd. Ed., Hemphill Pub. Co., Texas, 182 pp.

Humphreys, G.S., 1981. The rate of ant mounding and earthworm casting near Sydney, New South Wales. Search, 12: 129-131.

Humphreys, G.S. and Mitchell, P.B., 1983. A preliminary assessment of the role of bioturbation and rainwash on sandstone hillslopes in the Sydney Basin. In: R.W. Young and G.C. Nanson (Editors), Aspects of Australian Sandstone Landscapes. Aust. and NZ Geom. Gp. Spec. Publn. No. 1., pp. 66-80.

Kinnell, P.I.A., 1988. The influence of flow discharge on sediment concentrations in raindrop induced flow transport. Aust. J. Soil Res., 26: 575-582.

Lowe, D.R. and LoPiccolo R.D., 1974. The characteristics and origins of dish and pillar structures. J. Sed. Petr., 44: 484-501.

McIntyre, D.S., 1958. Permeability measurements of soil crusts formed by raindrop impact. Soil Sci., 85: 185-189.

Mitchell, P.B. and Humphreys, G.S., 1987. Litter dams and microterraces formed on hillslopes subject to rainwash in the Sydney Basin, Australia. Geoderma, 39: 331-357.

Moss, A.J.,1988. Effects of flow-velocity variation on rain-driven transportation and the role of rain impact in the movement of solids. Aust. J. Soil Res., 26: 443-450.

Moss, A.J. and Green, T.W., 1987. Erosive effects of the large drops (gravity drops) that fall from plants. Aust. J. Soil Res., 25: 9-20.

Moss, A.J and Walker, P.H., 1978. Particle transport by continental water flows in relation to erosion, depositional, soils, and human activities. Sediment. Geol., 20: 81-139.

Moss, A.J., Walker, P.H. and Hutka, J., 1979. Raindrop-stimulated transportation in shallow water flows: an experimental study. Sediment. Geol., 22: 165-184.

Mücher H.J. and De Ploey, J., 1977. Experimental and micromorphological investigation of erosion and redeposition of loess by water. Earth Surf. Proc., 2: 117-124.

Norton, L.D., 1987. Micromorphological study of surface seals developed under simulated rainfall. Geoderma, 40: 127-140.

Paton, T.R., 1978. The formation of soil material. George Allen and Unwin, London, 143 pp.

Soil Survey Staff, 1975. Soil Taxonomy, U.S. Dept. Agric. Handb. No. 436, U.S. Gov. Printing Office, Washington, D.C., 754 pp.

Stace, H.T.C., Hubble, G.P., Brewer, R., Northcote, K.H., Sleeman, J.R., Mulcahy, M.J. and Hallsworth, E.G., 1968. A Handbook of Australian Soils. Rellim Tech. Publ., Glenside, South Australia, 435 pp.

Stoops, G. and Jongerius, A., 1975. Proposal for a micromorphological classification of soil materials. I. A classification of related distribution of coarse and fine particles. Geoderma, 13: 189-200.

Valentin, C. and Bresson, L-M., 1992. Morphology, genesis and classification of surface crusts in loamy and sandy soils. Geoderma, 55: 225-245.

Mineralogy and micromorphology of salt crusts from the Punjab, Pakistan

S.A. Shahid[1] and D.A. Jenkins[2]

[1]*Dept. Soil Science, Univisity of Agriculture, Faisalabad, Pakistan*
[2]*Soil Science - SAFS, University of Wales, Bangor, UK*

ABSTRACT

Shahid, S.A. and Jenkins, D.A., 1994. Mineralogy and micromorphology of salt crusts from the Punjab, Pakistan. In: A.J. Ringrose-Voase and G.S. Humphreys (Editors), Soil Micromorphology: Studies in Management and Genesis. Proc. IX Int. Working Meeting on Soil Micromorphology, Townsville, Australia, July 1992. Developments in Soil Science 22, Elsevier, Amsterdam, pp. 799-810.

Salt crusts are a feature of poorly drained saline-sodic soils (natric camborthids) in the semi-arid Punjab region of Pakistan, forming by capillary rise and surface evaporation. These crusts have been studied using XRDA to establish their mineralogy, together with thin section microscopy/EPMA and SEM/EDXRA to reveal their micromorphology and confirm their chemical composition. They have been compared to crusts produced experimentally in the laboratory.

Of 25 samples collected between 1985-87, all qualified as saline or strongly saline, with pH ranging from 9.4-10+ and water chemistry dominated by $SO_4^{2-}>Cl^->HCO_3^-$ and $Na^+>Ca^{2+}$. XRDA established that the mineralogy was dominated by thenardite in 13 crusts, by mirabilite in 8 and by halite in 4. Accompanying these minerals in smaller, variable amounts were calcite, nahcolite, thermonatrite, trona, burkeite, and gaylussite, together with occasional traces of sylvite, hexahydrite and natron. Variations were shown within and between sites and with season, year and depth. For the more common minerals, all combinations seem possible other than that of mirabilite with nahcolite or gaylussite. In thin section halite, thenardite and calcite were observed in a variety of habits and crystallisation sequences as well as in a range of microfabrics. Using also EPMA and SEM/EDXRA, bassanite, trona and possibly nahcolite, glauberite and thermonatrite were also recorded. The heterogeneity of salt mineralogy within these samples has implications for root environment and thus for management.

INTRODUCTION

It has been estimated (Szabolcs, 1989) that salt-affected soils occupy some 0.9×10^6 ha on the world's land surface. These occur principally in the hot arid and semi-arid regions although they have also been recorded in polar regions. In the northern Indus plain region of Pakistan, salt accumulation is accentuated and the area involved has been calculated at 19% (5.5×10^6 ha; Muhammed, 1978). Soil salinity imposes important limits on current pressures to expand agricultural production into such areas of potentially irrigatable land. This makes an understanding of the nature and properties of these soils particularly necessary with mineralogy
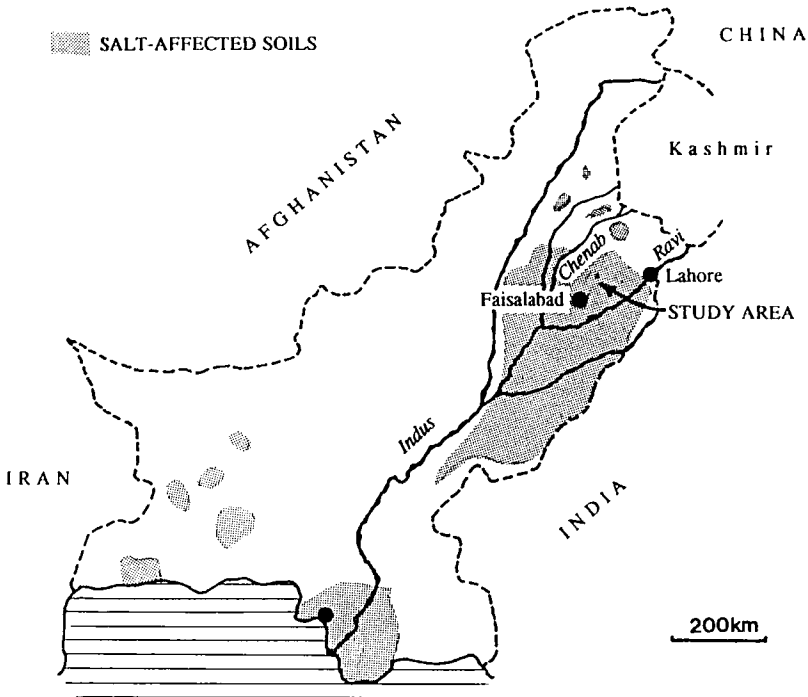
Fig. 1: Location of study area in relation to salt-affected soils in Pakistan.

and micromorphology playing important roles. As one part of a more general investigation of these soils in the Punjab (Shahid, 1988), specific attention was paid to the nature of the surface salt crusts which are an obvious manifestation of the more extreme effects of salinity. This paper reports on the mineralogical and micromorphological results of that study; other aspects will be reported elsewhere.

The detailed micromorphology of saline soils generally (cf. Allen, 1985), and of salt crusts specifically, has attracted only limited attention relative to that paid to features in temperate agricultural soils. This is partly because of their relative inaccessibility, but it is also due to problems in their routine sampling and analysis caused by the solubility of the minerals involved and their often ephemeral nature. Nevertheless, the essential chemistry of these "efflorescences" and its expression in "modal" mineralogy was established by Richards (1954), by Braitsch (1962) and summarised by Donar and Lynn (1989). Subsequently, detailed studies using SEM and micromorphology by, amongst others, Driessen and Schoorl (1973), Eswaran and Carrera (1980), Vergouwen (1980), Gumuzzio et al. (1982) and Mees and Stoops (1991) have described the mineralogical assemblages of salt crusts and the habits of specific minerals (e.g. sulphates - Stoops et al., 1978; halite - Eswaran et al., 1980). The objective of this study has been to characterise the mineralogy, morphology and chemistry of salt crusts from the Punjab, a region that has not previously been reported on.

Table 1
Composition of solutions used in leaching columns.

	Na^+	Ca^{2+}	Mg^{2+}	HCO_3^-	Cl^-	SO_4^{2-}	EC	SAR	pH_c
				$me.l^{-1}$					
A	48.5	5.0	6.5	1.5	43.5	15.0	6.0	20	7.9
B	56.1	1.9	2.0	1.5	43.5	15.0	6.0	40	8.3

MATERIALS AND METHODS

The *Khurrianwala Series* was selected for detailed study since this is the soil most strongly affected by salinity in the region around Faisalabad in the Punjab (Fig. 1). This soil series has lain barren for many years due to the lack of good quality irrigation water necessary for reclamation and it develops a characteristic salt crust in early summer and winter due to capillary rise and surface evaporation. It has formed in alluvial silty loams and occupies the margins of shallow depressions on otherwise flat older river terraces which now form interfluves (*Bari* and *Rechni doabs*) in the upper Indus plain. The profile is calcareous (3 - 10% $CaCO_3$) throughout and has a sandy silt loam surface (0 - 5 cm) which is white (10YR 8/1) when dry and brown (10YR 5/3) when moist, and is often distinctively vesicular, implying successive wetting/drying cycles (Evenari *et al.*, 1974). This passes down into a pale brown (10YR 6/3), dense, silty clay loam at 25 cm depth which shows evidence of some clay illuviation. It has a surface pH_s of 8.8, increasing to 9.7 at 45 - 70 cm depth, and an EC_e of 140 decreasing to 47 dS m^{-1} at 5 - 10 cm depth. As such it qualifies as a "dense saline-sodic soil" (Rafiq, 1975) and would be classified as a *Natric Camborthid* in the USDA scheme (Ahmad and Amin 1986) and as a *solonchak* on the FAO/UNESCO scheme.

Salt crusts were sampled from 8 sites in the summer of 1985, further samples being taken from one of these sites in the winters of 1985-6 and 1986-87 (*see* Table 2). They were of the order of 1 - 5 cm thick, well defined with a smooth surface and porous. Bulk samples were collected for chemical (pH, $EC_{1.5}$, soluble Na^+, K^+, Ca^{2+}, Mg^{2+}, CO_3^{2-}, HCO_3^-, Cl^- and SO_4^{2-}) and mineralogical analysis. X-ray diffraction analyses of the 25 natural crust samples and 3 created experimentally were obtained using Philips equipment (PW 1011/1048 using $Cu_{K\alpha\alpha}$ generated at 40 kV/20 mA) and the mineralogy identified from the XRD spectra of the total samples by reference to standard minerals and ASTM files. Estimates of abundance were made from the relative peak heights.

The micromorphological context of a selection of these minerals was investigated both optically in thin section and also by SEM. Undisturbed samples of the crust were taken for examination by SEM (Hitachi S520 + EDAX 702A), following gold or carbon coating; one sample was also analysed by energy dispersive X-ray analysis (EDXRA) using a 9800 EDAX attachment. Undisturbed samples were also taken for the preparation of vertical thin sections following impregnation with an acetone-diluted ("Crystic") monostyrene resin. Thin sections were polished successively with 6, 3 and 1 μm diamond pastes and initially covered with oil-mounted cover slips to allow subsequent electron probe microanalysis (EPMA) of selected samples on a JEOL.JXA3A instrument, following photography and carbon coating. Features

Table 2
Mineralogical composition[1] of 25 Salt Crusts from the Punjab.

Site sample[2]	No. 1 a b c c'	No. 2 a	No. 3 a b c d	No. 4 a b c d	No. 5 a b c d	No. 6 a b c d	No. 7 a b c	No. 8 a
Thenardite Na_2SO_4; (orh)[3]	4 3 4 -	4	4 1 4 4	- - 4 -	4 4 3 3	3 4 4 3	3 3 3	4
Mirabilite $Na_2SO_4.10H_2O$; (mcl)	- - - 4	.	- - - -	4 4 - 4	- - 4 4	- - - 4	4 - -	-
Halite NaCl; (cub)	- 4 1 -	-	- 4 2 2	- - - -	3 - - -	1 - 1 2	- 4 3	1
Nahcolite $NaHCO_3$; (mcl)	- 1 1 -	-	2 1 1 -	- - 3 -	- - - -	1 - - -	- 1 -	1
Natron $Na_2CO_3.10H_2O$; (mcl)	- - - -	.	- - - -	- - - -	- - - -	- - - -	1 1 -	-
Thermonatrite $Na_2CO_3.H_2O$; (orh)	1 2 - 1	1	- 1 1 2	- - 1 -	1 - - -	- 1 1 -	1 - 1	1
Trona $Na_3H(CO_3)_2.2H_2O$; (mcl)	- 2 2 3	3	1 1 2 -	3 3 - -	1 - - -	2 - 3 -	1 - 1	1
Burkeite $Na_6CO_3(SO_4)_2$; (orh)	- 2 1 1	1	1 1 2 1	1 1 1 1	1 - - -	3 - 1 -	1 1 1	-
Gaylussite $Na_2Ca(CO_3)_2.5H_2O$; (mcl)	- 1 - -	-	1 1 1 1	- - - -	- - - -	1 - - -	1 1 1	1
Glauberite[4] $Na_2Ca(SO_4)_2$; (mcl)	1 - . .	.	. . . .	. . . .	. . . .	. . . .	. . .	.
Calcite $CaCO_3$; (trig)	1 1 1 2	1	2 2 2 2	2 2 2 1	1 2 2 2	1 1 1 1	2 1 1	1
Bassanite[5] $CaSO_4.\frac{1}{2}H_2O$; (trig)	- 1 . .	.	. . . .	. . . .	. . . .	. . . .	. . .	.
Hexahydrite $MgSO_4.5H_2O$; (mcl)	- - - -	-	- 1 - -	- - - -	- - - -	- - - -	- - -	-
Sylvite KCl; (cub)	- - - -	-	- - - -	- - - -	- - - -	- - - -	- - -	1

[1] Abundances from relative XRDA peak heights: 4 dominant; 3 major; 2 minor; 1 trace; - not detected; . not analysed.

[2] Surface samples (0 - 3 cm) except for 1c' which was collected at 4 - 6 cm depth, and all collected in winter 1986/7 except for 1a (summer 85), 1b and 2a (winter 1985/6).

[3] Crystal system: (orh) - orthorhombic; (mcl) - monoclinic; (cub) - cubic; (trig) - trigonal

[4] Identified by SEM/EDRA only.

[5] Identified by optical microscopy/EPMA only.

observed optically in thin-section were investigated further by SEM following removal of the resin by low temperature ashing ("LTA": Jenkins, 1980).

Salt crusts were successfully prepared in the laboratory by capillary rise and surface evaporation in columns (30 mm Ø × 200 mm long) of *Khurrianwala Series* soil (<2 mm), fed in through a wide bore funnel to avoid stratification. The columns underwent 5 wetting/drying cycles, each comprising 24 hours of immersion of the lower 30 mm followed by 24 hours of drying the surface with a forced draught at 40°C. Two solutions of very high sodicity and

Table 3
Chemical compositions of the salt crusts.

Site &	Na^+	K^+	Ca^{2+}	Mg^{2+}	HCO_3^-	CO_3^{2-}	Cl^-	SO_4^{2-}	pH_c	EC
sample				Water soluble (1:5) ions me.l^{-1}						dS/m
1a	1650	3.89	1.6	0.67	4.75	20.1	19.5	1610	10.2	129
1b	1430	3.99	0.9	0.33	194	602	158	487	9.8	116
1c	782	6.39	2.3	0.67	22.1	51.0	138	583	9.8	68
1c'	101	0.31	0.9	0.17	2.30	0.87	0.34	96.7	9.6	9
2a	1320	3.89	1.0	0.50	9.03	17.9	178	1275	9.8	110
3a	298	0.92	0.6	0.17	26.8	59.9	59.2	154	10.1	24
3b	400	1.48	0.5	0.33	31.2	145	80.7	145	10.1	31
3c	821	3.58	2.0	0.67	68.3	260	139	361	9.9	70
3d	400	1.28	1.5	0.50	18.9	100	44.6	240	10.2	30
4a	361	1.08	1.2	0.33	1.90	1.67	<0.05	360	9.7	28
4b	98	0.41	1.5	0.33	2.33	<0.10	6.03	91.7	9.8	9
4c	164	0.51	1.4	0.33	2.10	0.38	2.20	161	9.6	14
4d	109	0.41	0.3	0.17	3.15	2.33	4.62	100	9.8	10
5a	800	2.92	4.2	1.00	1.57	0.53	224	583	9.4	72
5b	878	7.77	0.3	0.17	19.7	49.4	38.5	779	9.8	73
5c	930	7.77	0.8	0.17	16.0	50.0	41.1	829	9.8	78
5d	1050	5.01	1.0	1.33	5.86	7.13	13.0	1033	9.8	86
6a	701	9.87	1.9	0.50	49.2	305	86.3	274	10.2	62
6b	1770	3.79	2.6	0.67	5.24	15.7	15.9	1740	10.0	135
6c	1320	3.79	1.2	0.33	10.8	20.5	25.0	1270	9.7	107
6d	800	7.06	1.3	3.50	9.97	19.9	84.6	696	10.0	71
7a	948	3.79	1.9	0.33	15.0	14.7	10.5	913	9.4	79
7b	1120	39.4	1.2	0.33	64.6	195	491	413	9.7	105
7c	974	11.2	1.2	0.50	36.1	212	209	525	10.1	87
8a	913	16.8	1.2	0.67	72.5	205	266	393	9.8	84

salinity (Table 1), comparable to local irrigation waters, were used together with a third solution of NaCl (60 me.l^{-1}) to study specifically the morphology of halite.

RESULTS AND DISCUSSION

The results of this investigation are presented in Tables 2 (relative abundances of the minerals identified) and 3 (chemical composition of salt crust extracts), and they are illustrated in Figs 2 (optical micrographs), 3 (EPMA analyses) and 4 (SEM micrographs). They will be discussed first in terms of mineral assemblages and then in terms of morphology as assessed by optical and scanning electron microscopy. Finally, a brief account of the nature of the experimental salt crusts will be given.
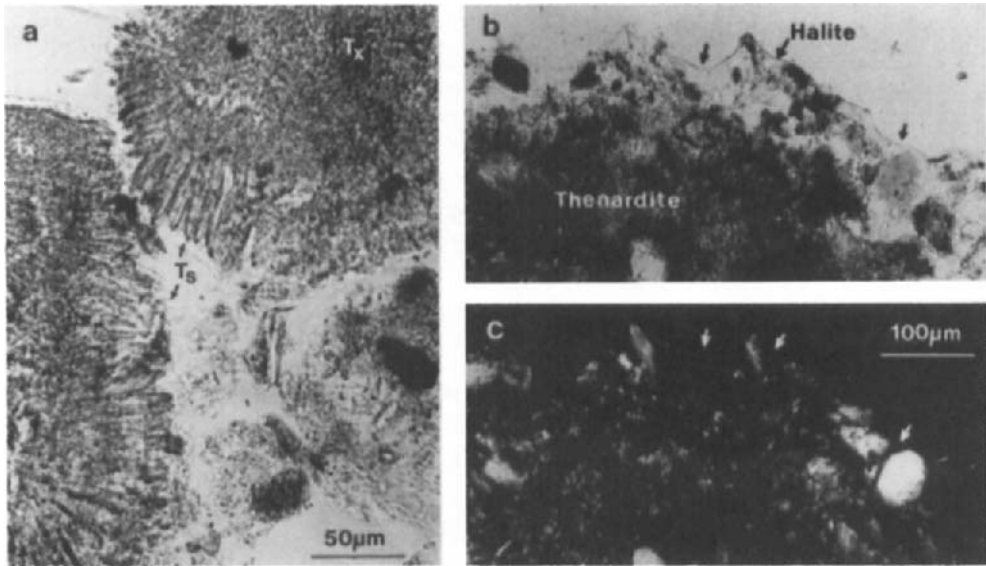
Fig. 2. **a)** Stellate thenardite (t$_s$) lining a void, and in fine granular form (t$_x$) in a xenotopic matrix (Sample 1a; Plane polarized light, PPL; **b)** Massive halite encrusting thenardite (Sample 1a; PPL); **c)** View of (b) between crossed polars showing isotropic halite.

Mineralogy

The mineralogical composition of the 25 salt crusts was found to be variable and dominated (or co-dominated) by thenardite in 13 samples, by mirabilite in 8, and by halite in 4 samples (Table 2).   The general dominance of sodium sulphates in the crusts is illustrated in the composition of the water soluble extract quoted for the sites   (Table 3)   and overall this mineralogy compares to that of halite-trona-thenardite±burkeite assemblage reported from Peru by Mees and Stoops (1991), though certain minerals (*i.e.* eugsterite and pirssonite) are missing and others (*e.g.* mirabilite, nahcolite and gaylussite) present.   The variations in mineralogy can be considered in terms of site and, in one instance (site 1), in terms of season and depth.   Between sites differences are evident.   For example, gaylussite is consistently present at site 3 but only in two samples from the other 7 sites; burkeite is absent from 3 of the samples at site 5;   traces of sylvite, hexahydrite and natron were only detectable at one site each.   By contrast, calcite is ubiquitous in trace or minor amounts, which could indicate an aeolian origin.   However, there are also clear variations within sites. For example, samples 3a, 4c, 5a, 6d and 7a (Table 2) all differ markedly from the other 2 or 3 samples from the same site.   This would result from fractional crystallisation and zonation and makes intersite interpretations difficult with the limited amount of data available at this stage.

Relationships can also be sought from the mineralogical assemblages. All combinations of the common mineral species occur except that of mirabilite and nahcolite or gaylussite.   There is also a predictable inverse relationship shown between mirabilite and its anhydrous version, thenardite.   The latter has been commented on by previous workers (*e.g.* Tursina, 1980) who suggested that mirabilite is readily transformed to thenardite in, for example, the surface layer.

This suggestion is consistent with the presence of the former in the sub-surface layer 1c' and its replacement by the latter in the surface layer 1c. A similar relationship is hinted at by the distribution of thermonatrite and the anhydrous carbonate nahcolite in these two samples, and also by the presence of gaylussite rather than its lesser-hydrated (.2H$_2$O cf. .5H$_2$O) equivalent pirssonite. The vulnerability of mirabilite might imply its transformation between sampling and analysis, but special care was taken in this respect and the presence of dominant mirabilite in 8 surface samples would indicate its survival. A different situation has been reported by Mees and Stoops (1991) for salt efflorescences in Peru, where the absence of mirabilite was related to the transition temperature to thenardite of 17.9°C for NaCl-saturated solutions proposed by Braitsch (1971), a temperature, however, also exceded in the surface horizons of soils in the Punjab. Clearly, the relationship between such minerals of differing hydration has yet to be fully elucidated.

Site 1 was also sampled during different seasons and in successive years. The assemblage in the summer of 1985 (sample 1a) is depleted compared to the assemblages in the winters of 1985/6 and 1986/7 (samples 1b and 1c), in which an additional 4 to 5 minerals respectively could be identified. The latter two samples differ in their halite and thermonatrite contents. Without further data it is again difficult to ascribe these observed differences in mineralogy specifically to season or year in view of the intra-site variations noted above.

Such assemblages ultimately reflect solute chemistry. Within limits, this may be expressed in phase diagrams as constructed by, for example, Eugster and Smith (1965) for the thenardite-trona-halite system. Although the mineralogy in this present study reflects the chemistry, there are discrepancies evident in the detection of K$^+$ (sylvite) and Mg^{2+} (hexahydrite) minerals in only one sample each, neither of which corresponds to the highest levels found of these two elements. This may be due to the heterogenous distribution of less common minerals at the scale of sample analysis (c. 10 g). Such discrepancies were also noted by Mees and Stoops (1991), with whose data those in Table 3 are comparable for Na$^+$, SO$_4^{2-}$, HCO$_3^-$ and CO$_3^{2-}$, although values of Mg^{2+}, Ca^{2+} and Cl$^-$ are somewhat lower, and some values of K$^+$ higher.

Thin section Micromorphology and EPMA

The micromorphology of the less common minerals in salt crusts is not yet well known. Some are isotropic but of differing, negative, low relief (halite µ = 1.54; sylvite µ = 1.49), whilst others also show a range of negative relief (RI. 1.43 - 1.54) and birefringence (0.01 - 0.13) and tend to be prismatic, either orthorhombic (*e.g.* burkeite, thenardite, thermonatrite) or monoclinic (*e.g.* hexahydrite, mirabilite, nahcolite, natron, trona). Optical identification is aided by qualitative EPMA where elemental associations are indicative of groups of minerals, *e.g.* Na only - nahcolite, natron, thermonatrite, trona; Na and Ca - gaylussite; Na and Cl - halite; Na and S - burkeite, mirabilite, thenardite; Na, Ca and S - eugsterite, glauberite *etc.*

In the complexity of the soil thin section, only halite and thenardite were positively identified. Of the particular samples examined, however, one (1a) had a restricted mineralogy and in the other (1b) burkeite, thermonatrite and trona, identified by XRDA, were not detected probably due to their absence in the three sections of this sample which were examined. The thenardite formed conspicuous encrustations of stellate lath-like crystals (up to 10 × 100 µm) on void and ped surfaces (Fig. 2a "thenardans"), as well as a fine anhedral granular (≤5 µm) matrix displaying a dense xenotopic fabric, both forms together comprising 46% of the volume by point count analysis. Conversely halite occurred sparsely (1.8%) as more massive coatings with
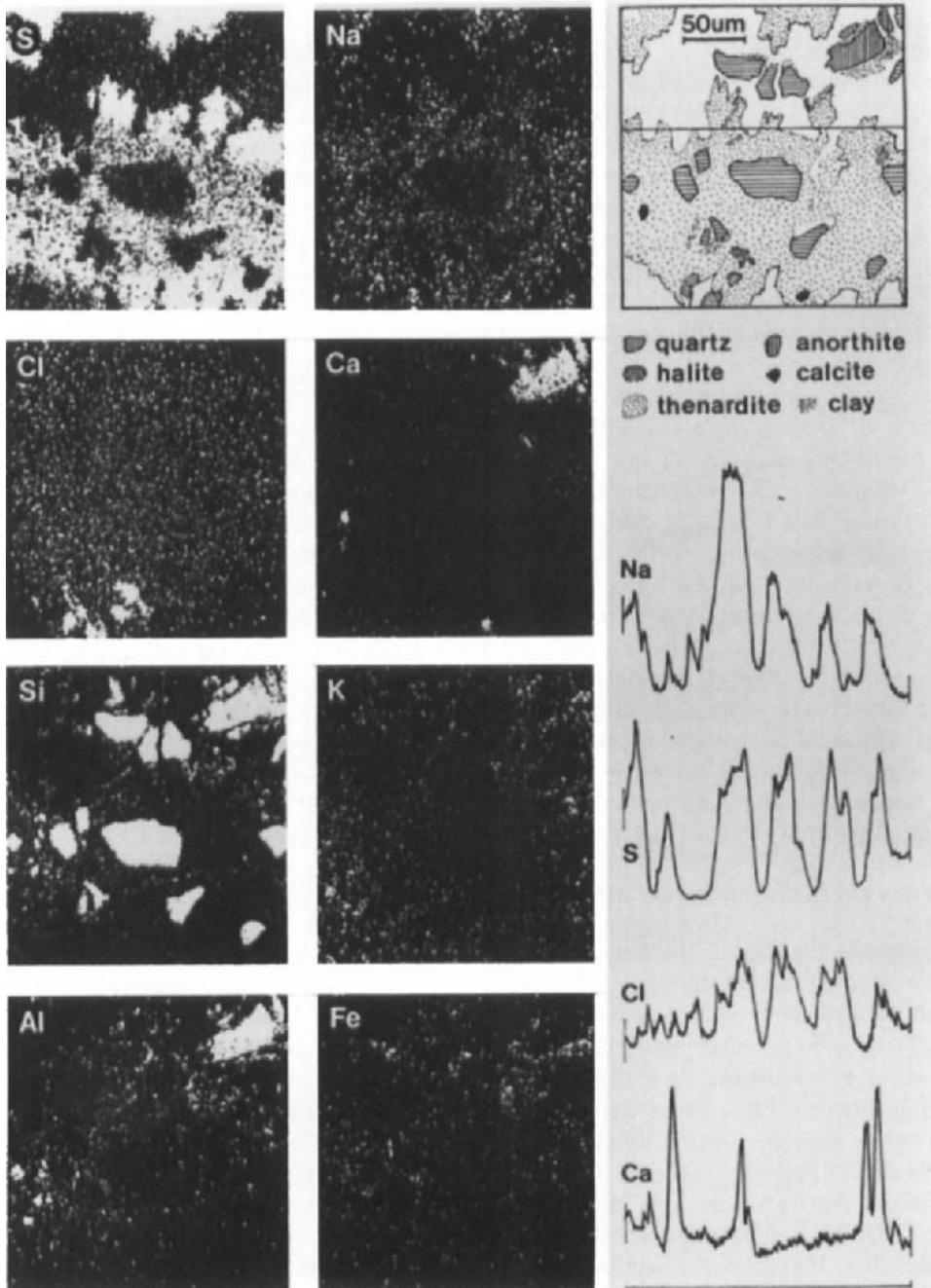
Fig. 3. X-Ray images and line scans of a thenardan in a salt crust (Sample 1a).

smooth surfaces probably resulting from dissolution (Fig. 2b-c). X-ray images and line scans of a thenardan are presented in Fig. 3, which also shows traces of halite and detrital Ca-feldspar with a coating of Fe/clay.

Calcite was present in the crusts in the granular form common throughout these profiles, whilst at depths greater than 25 cm it also occured as distinctive acicular "lublinite", up to a maximum of 4% at 65 - 70 cm. In addition, a stellate form occured in the winter 1985/6 crust (sample 1b), with EPMA confirming the presence of Ca alone (*i.e.* $CaCO_3$). Another mineral observed within voids in the winter 1985/6 crust occurred as a finely granular material with a distinctive blueish grey interference colour, comparable to the bassanite [$CaSO_4.\frac{1}{2}H_2O$] illustrated by Bullock *et al.* (1985, Fig. 73e). This identification was further strengthened by SEM/EDXRA indicating the presence of Ca and S only. This mineral did not survive LTA and its detailed morphology could not therefore be studied by SEM.

SEM/EDXRA observations

The observation of salt crusts from Site 1 under the SEM revealed a variety of thenardite habits, together with occasional crystals of thermonatrite, trona, halite and glauberite, as inferred from EDXRA data. Thenardite was observed as radial euhedral bladed crystals lining a void (Fig. 4a), as cushions of radiating acicular crystals (Fig. 4b, *cf.* Buringh, 1979), as stellate clusters (Fig. 4c, *cf.* Stoops *et al.*, 1978) and in granular form (Fig. 4d, *cf.* Vergouwen, 1980). Mirabilite was sought in the subsurface sample (Site 1c') where it was found as an aggregate of small (≤ 5 μm) acicular-planar crystals (Fig. 4e), but it proved a difficult mineral to study by SEM because of surface charging and instability due to dehydration. Trona and thermonatrite were identified (EDXRA - Na only) as stellate acicular and acicular-planar crystals (Fig. 4f and g). Nahcolite was inferred (EDXRA - Na only) for a parallel cluster of acicular-planar crystals (Fig. 4h), since natron - an alternative possibility - was not detected in these soils. Analysis of another group of planar crystals (Fig. 4i) indicated the presence of Na, Ca and S suggesting the presence glauberite [$Na_2Ca(SO_4)_2$] rather than eugsterite [$Na_4Ca(SO_4)_3.3H_2O$] which has an acicular habit (Vergouwen, 1980).

Experimental salt crusts

Mineralogical analysis of the salt crusts produced with the simulated irrigation waters revealed an assemblage dominated by halite and with traces of trona and thermonatrite. Where the higher SAR solution was used (40 *cf.* 20) there were, in addition, traces of calcite, nahcolite and thenardite. This assemblage is generally similar to that observed in natural crusts, but differs in the dominance of halite and in the presence of major gypsum, which was not detected in the field samples. An unidentified flaky mineral containing Na, Cl and S (EDXRA) was also noted.

Gypsum occurred as typical lenticular crystals, subhedral where embedded in massive halite but euhedral where associated with cubic halite. Halite also occured in anhedral granular and skeletal forms and in the massive surface form, which showed polygonal cracking and was underlain by a curved fibrous form, a sequence similar to that reported by Eswaran *et al.* (1980). All these various habits of halite were also produced in the crust formed by the evaporation of NaCl solution in the laboratory columns.
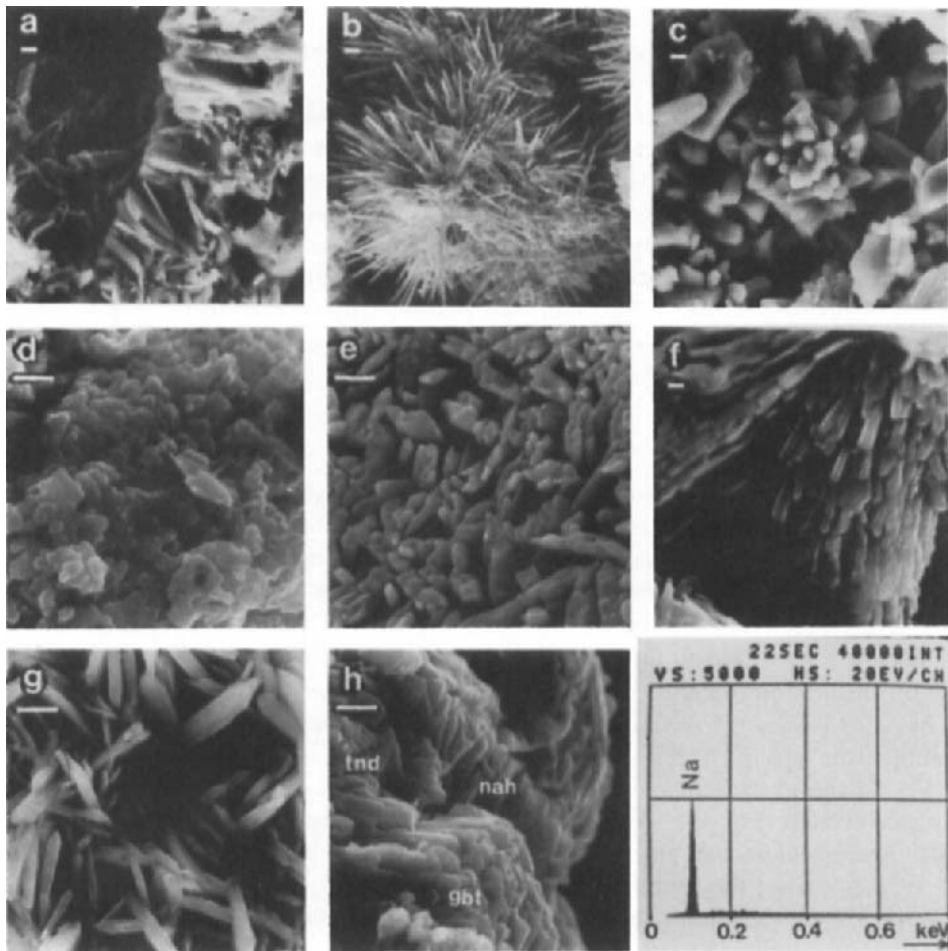
Fig. 4. SEM micrographs of salt minerals: **a-d)** different habits of thenardite; **e)** mirabilite; **f)** trona with (below) EDXRA spectrum showing Na only; **g)** nahcolite (nah), glauberite (gbt) and thenardite (tnd), (scale bar = 2μm in each case; a, b, f, g and h from sample 1a; c, d and e from sample 1c).

CONCLUSIONS

A distinctive assemblage of minerals has been recorded for natural salt crusts, dominated by Na^+ and SO_4^{2-} in the form of either thenardite or mirabilite and accompanied by various combinations of 12 other minerals. These have been identified in bulk material by XRDA and, with less certainty, within soil microfabric   by morphology/elemental composition using SEM/EDXRA. There are variations in assemblage composition both between and within sites and also, in the individual cases examined, with season, year and depth.   More data will be

needed to resolve the relative significance of factors and further samples are being collected for this purpose. A variety of habits has also been recorded for the main minerals and some of these have been reproduced in experimental crusts. By virtue of its habit, thenardite results in a loose soil fabric whilst halite forms a compact cemented surface. Mirabilite has been identified within a few centimetres of the surface, suggesting it is more stable than previously considered.

Salt crusts are a visible symptom of salinity and they have implications, both direct and indirect, for reclamation, management and crop growth. The most obvious of these for the soils studied is the dominance of the mineral thenardite. This casts doubt on the routine screening of crops for salt tolerance in hydroponic NaCl solutions, as does the observed heterogeneity of salt mineralogy exposed at the surfaces of the voids which constitute the root environment.

REFERENCES

Ahmad, M. and Amin, R., 1986. Distribution of higher categories of soil taxonomy in Pakistan. In: M. Ahmad, M. Akram, M.S. Baig, M.Y. Javed and R. Amin (Editors), Proceedings of the XII International Forum on Soil Taxonomy and Agrotechnology Transfer. Soil Survey of Pakistan, Lahore, pp. 31-44

Allen, B.L., 1985. Micromorphology of aridisols. In: L.A. Douglas and M.L. Thompson (Editors), Soil Micromorphology and Soil Classification. Soil Sci. Soc. Am. Spec. Publ., 15, Madison, Wisconsin, pp. 197-216

Braitsch, O., 1962. Entstehung und Stoffbestand der Salzlagerstatten. Min. und Petr. in Einzeldarstellungen, 3, Springer Verlag, Berlin.

Braitsch, O., 1971. Salt Deposits. Their Origin and Composition. Springer, Berlin, 297pp.

Bullock, P., Federoff, N., Jongerius, A., Stoops, G., Tursina, T. and Babel, U., 1985. Handbook for Soil Thin Section Description. Waine Research Publications, Wolverhampton, U.K.

Buringh, P., 1979. Arid and semi-arid soils. In: P. Buringh (Editor), An Introduction to the Study of Soils in Tropical and Subtropical Regions. C.A.P.D., Wageningen, pp. 17-28.

Donar, H.E. and Lynn, W.C., 1989. Carbonate, halide, sulphate and sulphide minerals. In: J.B. Dixon and S.B. Weed (Editors), Minerals in the Soil Environment. 2nd Ed. Soil Sci. Soc. Am., Madison, Wisconsin, pp.75-98.

Driessen, P.M. and Schoorl, R., 1973. Mineralogy and morphology of salt efflorescences on saline soils in the Great Konya Basin, Turkey. J. Soil Sci., 24: 436-442.

Eswaran, H. and Carrera, M., 1980. Mineralogical zonation in salt crusts. In: Int. Symp. on Salt Affected Soils. Central Soil Salinity Research Institute, Karnal, India, pp. 20-30.

Eswaran, H., Stoops, G. and Abatahi, A., 1980. SEM morphologies of halite (NaCl) in soils. J. Microsc., 120: 343-352.

Eugster, H.P. and Smith, G.I., 1965. Mineral equilibria in the Searles Lake evaporites, California. J. Petrol. 6: 473-522.

Evenari, M., Yaalon, D.H. and Gutterman, Y., 1974. Note on soils with vesicular structure in deserts. Z. Geomorph. N.F., 18: 162-172

Gumuzzio, J., Battle, J. and Casa, J., 1982. Mineralogical composition of efflorescences in a typic salorthid, Spain. Geoderma, 28: 39-51.

Jenkins, D.A., 1980. The transition from optical microscopic to scanning electron microscopic studies on soils. In: E. Bisdom (Editor), Submicroscopy of Soils and Weathered Materials. IPAC, Wageningen, The Netherlands, pp. 237-248.

Mees, F. and Stoops, G., 1991. Mineralogical study of salt efflorescences on soils of the Jequetepeque Valley, northern Peru. Geoderma, 49: 255-272

Muhammed, S., 1978. Salt affected soils of Pakistan. In: R.H. Qureshi, S. Muhammed and M. Aslam (Editors), Proc. Workshop on Biophysics and Salt Tolerance in Plants. Faisalabad, Pakistan, pp. 47-64.

Palasche, C., Berman, H. and Frondel, C., 1951. The System of Mineralogy (Dana). Vol II. Halides, Nitrates, Phosphates etc. 7th Ed. John Wiley and Sons, New York.

Rafiq, M., 1975. Saline, saline-alkali and waterlogged soils of the Indus plains - their characteristcs, causes of formation and measures needed for reclamation. In: N.M. Awan (Editor), Proc. Int. Conf. Waterlogging and Salinity. Lahore, Pakistan. pp. 308-321.

Richards, L.A. (Editor), 1954. Diagnosis and Improvement of Saline and Alkaline soils. U.S. Dept. Agric. Handb. No. 60, U.S. Gov. Printing Office, Washington DC.

Shahid, S.A., 1988. Studies on the Micromorphology of Salt-Affected Soils in Pakistan. Ph.D. thesis, University of Wales.

Stoops, G., Eswaran, H. and Abtahi, A., 1978. Scanning electron microscopy of authigenic minerals in soils. In: M. Delgado (Editor), Micromorfologia del Suelos, Proc. V Int. Working Meeting on Soil Micromorphology, Granada, Spain, pp. 1093-1113

Szabolcs, I., 1989. Salt Affected Soils. CRC Press, Boca Raton, Fl. p. 274

Tursina, T., 1980. The microstructure and the origin of new salt formation of salt affected soils. In: Proc. Int. Conf. Salt-Affected Soils. Central Soil Salinity Research Institute, Karnal, India, pp. 35-43.

Vergouwen, L., 1980. Scanning electron microscopy applied on saline soils from the Konya Basin in Turkey and from Kenya. In: E. Bisdom (Editor), The Submicroscopy of Soils and Weathered Rocks. CAPD, Wageningen, The Netherlands, pp. 237-248.

Micromorphology of silica cementation in soils

L.D. Norton

USDA-Agricultural Research Service, National Soil Erosion Research Laboratory, Purdue University, West Lafayette, Indiana 47906, USA

ABSTRACT

Norton, L.D., 1994. Micromorphology of silica cementation in soils. In: A.J. Ringrose-Voase and G.S. Humphreys (Editors), Soil Micromorphology: Studies in Management and Genesis. Proc. IX Int. Working Meeting on Soil Micromorphology, Townsville, Australia, July 1992. Developments in Soil Science 22, Elsevier, Amsterdam, pp. 811-824.

Soils containing various degrees of cementation by silica occur in many parts of the world, from humid to arid moisture regimes. In some areas, soils containing silica cementation can be quite extensive in area. Such cements have been reported in hard-setting (A/E) horizons and soils with subsurface fragipans (Bx) and duripans (Bqm). These cements contribute to the adverse properties associated with these types of horizons such as poor water movement and rooting limitations and therefore, have ramifications to landuse. Cemented or partially cemented horizons occur in many parent materials, and most commonly those which are medium textured and have an abundant supply of skeletal grains available to be cemented. Soils high in clay-sized materials typically do not have horizons with silica cementation.

The degree of silica cementation in soils is highly variable. Some weakly cemented soils have peds that slake easily in water whereas more indurated horizons such as duripans do not. Selective dissolution studies have shown that cemented horizons contain enriched levels of amorphous silica. However, the amount and the Si/Al ratios of cements are highly variable. Other destructive studies have shown that silica cementation may be associated with silicate clays, carbonates or iron oxides. Energy dispersive X-ray analyses have confirmed that cemented horizons have Si enriched bridges at the contact points of skeletal grains, and also show that these bridges have highly variable compositions. Little is known about the mineralogy of these silica rich phases.

Typically, the micromorphology of cemented horizons is characterized by grainy bridging structures with isotic to undulic fabric in a silasepic groundmass. Also reported are isotropic bridges between skeletal grains, isotropic cutans and fine-grained cutans with isotropic areas. Other bridging structures range from isotic to isotic with flecks of birefringent materials to highly birefringent indicating that clay minerals may be occluded. Submicroscopic (SEM) studies show definite bridges between quartz grains.

INTRODUCTION

Soils

Complete cementation of soil, such that it becomes an impervious material, is obviously a detrimental process for both plant growth and water movement. Partial cementation may be

beneficial for some soil uses or adverse for others. Partial cementation may bind clay and silt particles into larger more stable aggregates which resist surface sealing and erosion and make plant growth easier. Conversely, partial cementation of a complete horizon (*e.g.* fragipans) may actually restrict root growth and severely impede downward water movement. Complete induration of soil horizons greatly reduces soil erosion to such an extent that it may actually affect landscape development (Flach *et al.*, 1969). Several materials have been identified as natural cementing agents in soils. The best known are sesquioxides (petroferric or lateritic horizons), carbonates (petrocalcic horizons or caliche layers) and silica (duripans, silcretes, duracrusts *etc.*). The focus of this paper will be on the latter and, in particular, the role micromorphology may have in elucidating the role of silica in soil cementation.

Historical Perspective

An understanding of cementation of materials has been a key factor in the development of civilization. Cements have been used for thousands of years in masonry construction and later in concretes. The ancient Egyptians calcined gypsum and limestone to produce cements. They were mixed with sands and gravels to produce mortar. Some sands and gravels were found to produce stronger, longer lasting mortars. Such materials included tuffs and volcanic ashes. Historic examples include materials from the Grecian island of Santorin and the town of Pozzuoli near Mt. Vesuvius in Italy, hence the name of "Pozzolan" for naturally occurring cementing materials. The Romans found that mixing these materials with sand, gravel, lime and a minimal amount of water, produced concrete. The Roman knowledge of concrete allowed the construction of the Colosseum and the Pantheon which have lasted for two thousand years. The understanding of cements contributed greatly to their success.

Naturally occurring pozzolanic materials are generally highly siliceous, but vary considerably in composition. Typically, the more opaline and finely divided the material, the more the pozzolanic activity (Mielenz, 1949). In thin section, most pozzolanic materials have a considerable amount of isotropic material presumed to be silica in some form. Recent volcanic ashes near Vesuvius have weak pozzolanic activity whereas older ashes are much more active. Presumably some amount of weathering and soil formation is responsible for development of the cementing activity of these materials. Possibly, induration and silica cementation that occurs naturally in soils forms by mechanisms similar to those that occur in pozzolanic materials.

SILICON, SILICATES AND SILICA

Silicon

Elemental silicon (L. *silex, silicis*, at. wt. 28 m.p. 1410°C; sp. gr. 2.33) is the second most abundant element on earth next to oxygen (25.7 % of earth's crust). Silicon is one of the most important elements on earth and silicates are the most abundant minerals in soils and sediments. Elemental Si is not found in nature, but occurs as the oxide and as silicates. Quartz, hornblende, feldspars, micas and opal are just a few examples of the silicates. Although to the chemist these minerals are considered insoluble in cold water, they may weather in soil environments and produce monosilicic acid and soluble silicate salts, which may then dehydrate and form silicate cements in soils. These cements are known to be involved in

the induration of soils with duripans and are also suspected to be involved in the partial cementation of fragipans and soils with hard-setting characteristics. Hydrated species of silicates and alumnosilicates are important components of andisols.

Silicate Minerals

Silicate minerals are the dominant minerals of most soils and sediments (Schultze, 1989). The main building block is the silicon tetrahedron (SiO_4). Silicate minerals are built up by linkage of these tetrahedra. The manner by which they are linked determines their classification into one of six groups of silicates. These are: nesosilicates, sorosilicates, inosilicates, cyclosilicates, phyllosilicates and tectosilicates.

When the tetrahedra are linked together by a metal cation such as Fe or Mg in olivine ((Mg, $Fe)_2SiO_4$) the structure is called a nesosilicate. The next group of silicates are characterized by two tetrahedral units sharing a common oxygen atom. This "pair" may then be bonded together by cations in minerals such as epidote ($Ca_2MgSi_2O_7$). These minerals are called sorosilicates. The next level of complexity occurs when the tetrahedra share two common oxygen atoms. This configuration produces chains of tetrahedra such as the pyroxene group of which enstatite ($MgSiO_3$) is an example. This group is called the inosilicates. Two straight chains of pyroxene type chains may "polymerize" or share a common oxygen. The ratio of Si/O is 4/11 and is typical of the amphibole group. These chain silicates are called inosilicates. Hornblende ($Ca_2(Mg,Fe)_5(OH)_2Si_8O_{22}$) is an example of a double chain inosilicate.

When the two shared oxygen atoms are bonded at angles and form polyhedra or form a closed chain the group is called cyclosilicates. Beryl and tourmaline are examples of this type of mineral of which larger crystals are semiprecious stones. This group of silicates is not very important in soils or sediments. Many chains of silica tetrahedra may condense and extend in two dimensions in the form of sheets. These minerals are called phyllosilicates and have a Si/O ratio of 2/5. In these minerals, three of the four oxygen atoms of the silicon tetrahedra are shared between adjacent tetrahedra. The primary mineral, muscovite ($K_2Al_4(OH)_4(Si,Al)_8O_{20}$), is an example of this group of minerals. Many of the clay minerals found in soils and sediments are phyllosilicates that are secondary in origin (*e.g.* kaolinite).

The last group of silicate minerals are those where all four oxygen atoms are shared in a 3-D framework. This group is called the tectosilicates. Quartz (SiO_2), the second most common mineral in the earth's crust, is the best example of this group of minerals. Feldspars, the most common minerals in the earth's crust, are also tectosilicates. They exhibit substitution of Al for Si in the framework. This leads to a permanent negative charge on the structure which must be counter balanced with cations. Counter ions typically are Na^+, K^+, or Ca^{2+}, as well as other cations. There may be a variable amount of the counter cation ranging from mostly K, to mostly Ca or mostly Na, which constitute end members in a solid solution series. The end members are, orthoclase ($KAlSi_3O_8$), anorthite ($CaAl_2Si_2O_8$) and albite ($NaAlSi_3O_8$), all of which are tectosilicates, but have variable properties.

Weathering resistance and mineral stability of the silicates are closely related to their structure (*i.e.* degree of tetrahedron polymerization). Olivine is the most weatherable whereas tourmaline and quartz the least weatherable in most soil environments. Silicates weather mainly by hydrolysis, the rate of which may be affected by a number of factors as discussed later. The hydrolysis of all silicates produces monomeric silicic acid which may precipitate or
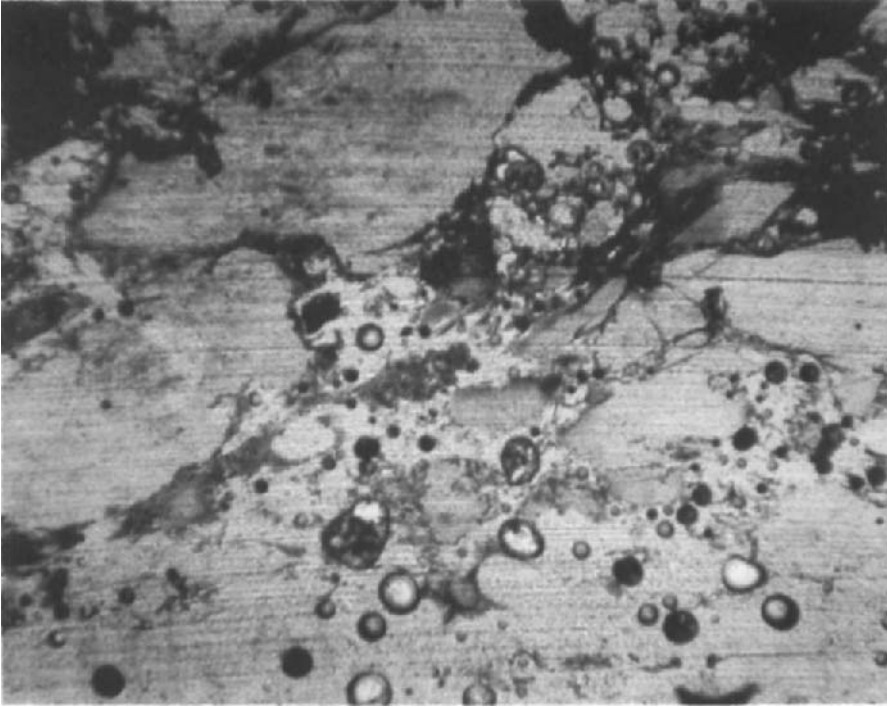
Fig. 1. Micrograph of a thin section of pyroclastic material from Rotorua, New Zealand showing weatherable pozzolanic material.; plane polarized light (PPL); frame width (FW) 15.8 mm.

polymerize in the soil to form a number of minerals depending on the environmental conditions. These phases may or may not cement skeletal grains together upon precipitation.

Silica

Silica (SiO_2) may occur naturally as one of seven polymorphs (Drees *et al.*, 1989). They are: quartz, cristobalite, tridymite, coesite, stishovite, lechatelerite (silica glass) and opal. Silica glass and opal are considered to be amorphous. Coesite and stishovite are not important polymorphs in soils and sediments and tridymite is also rare. Of the remainder, quartz (as stated before) is the most abundant, whereas opal is the most soluble and comprises biogenic opal and diatomaceous earths. Quartz has a highly ordered structure and is easily identified in thin section with optical techniques. Biogenic opal is istotropic but assumes the shape of the cells of the organism. Diatoms and sponge spicules composed of silica, likewise, may also be identified based on morphology. Volcanic glass is a very soluble phase in some soils, also has a characteristic morphology and is easily identified with optical techniques.

Opal may be divided into three phases. The most disordered (Opal-A) is X-ray amorphous and occurs in duripans. Opal-C is the most ordered being similar to the cristobalite structure, and is found in pyroclastic materials (Fig. 1). Opal-CT has randomly interstratified layers
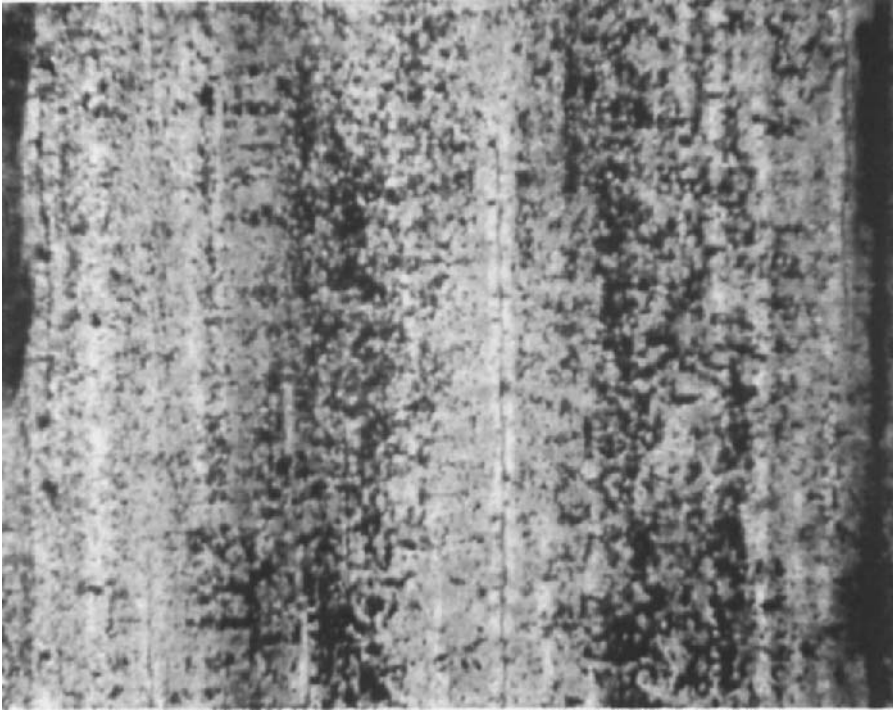
Fig. 2. Micrograph of thin section of petrified wood from the Bryan Formation, College Station, Texas, U.S.A. showing complete induration by silica; PPL; FW 15.8 mm.

similar to both cristobalite and tridymite. It is commonly found as the cementing agent in duripans and silicretes (Drees *et al.*, 1989) and also in cherts and fossilized wood (Senkayi *et al.*, 1985; Fig. 2).

SOURCES OF SILICA IN SOILS

Weathering of silicates

The weathering of silicate minerals is governed by factors that affect the solubility (*e.g.* pH, particle-size, solution chemistry *etc.*). Water soluble silica levels have been reported as high as 300 ppm in strongly alkaline soils (Kelly and Brown, 1939). Amorphous silica may release 120 ppm SiO_2 in normal soil pH ranges, but soil solutions and river waters typically range from 3 - 20 ppm (Keller, 1968). Karathanasis (1989) found soil solution levels of silica near the solubility level of amorphous silica in fragipan horizons and proposed that amorphous silica is a bonding agent in fragipans.

Quartz has low solubility at normal temperatures, whereas amorphous silica may quickly release 50 - 60 mg Si l^{-1} (Krauskopf, 1979). Other silicates may hydrolyze very quickly and produce an abundant source of monosilicic acid, particularly those containing iron and
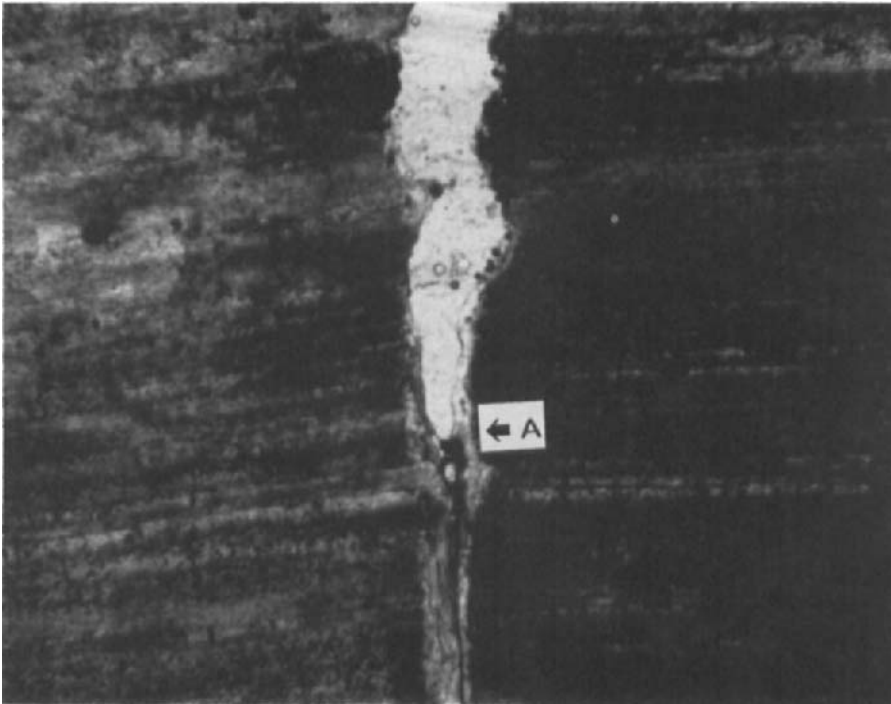
Fig. 3. Micrograph of thin section of petrified wood from the Bryan Formation, College Station, Texas, U.S.A. showing conversion of quartz to opal-A (A); PPL; FW 15.8 mm.

magnesium. The presence of acids (organic and inorganic) speeds the weathering and increases the supply of monosilicic acid. Particle size of the mineral also has an effect on dissolution. This is the reason quartz is rarely found in the finer clay fractions of soils.

Quartz can also be converted to different polymorphs during weathering. Senkayi *et al.* (1985) reported that cryptocrystalline quartz observed in the weathering of petrified wood could be converted to opal-CT and ultimately to opal-A. Such a conversion sequence along a weathering crack in petrified wood can be seen in Fig. 3.

The soil environment and the degree of leaching and plant uptake have an effect on the soluble silica level. In a study of etch pits from orthoclase and pyribole grains from a loess catena, Cremeens *et al.* (1992) found that the more poorly drained soil contained the smallest and most numerous etch pits in both minerals than the better drained soils (Fig. 4). The number of etch pits decreased with depth in both well drained and poorly drained profiles. The mechanism of etch pit growth differed for the two minerals in the same soil environment indicating that silicate weathering is a very complex phenomena. A decrease of etch pit density on quartz surfaces with depth in a soil profile was interpreted as being caused by an increase in the Si concentration in pore fluids with depth (Brantley *et al.*, 1986).
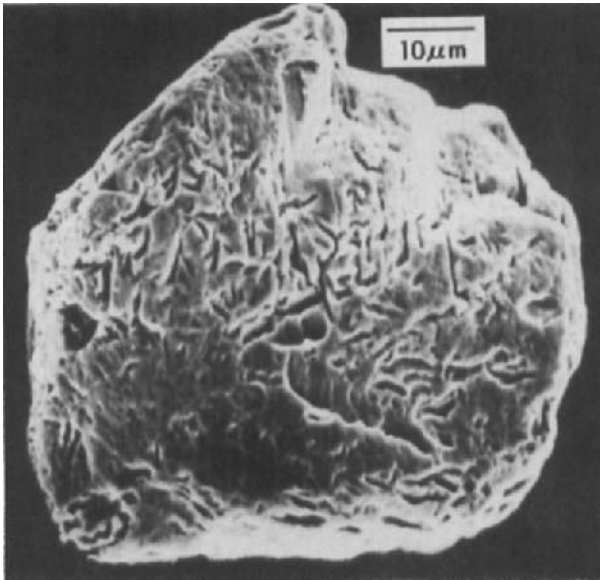
Fig. 4. Scanning electron micrograph of a pyribole grain showing weathering etch pits from which monosilicic acid was released.
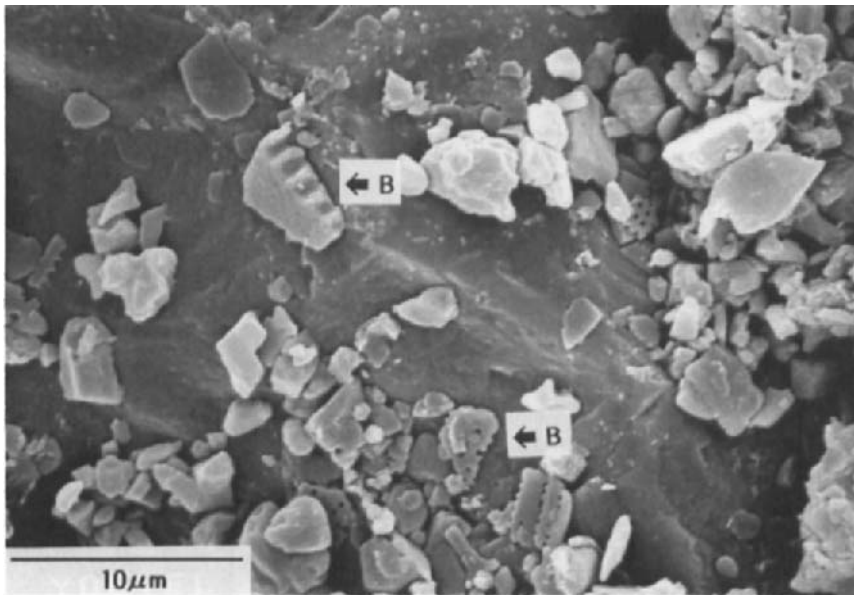
Fig. 5. Scanning electron micrograph of biogenic silica from a duric horizon of a soil from near Yeoval, New South Wales, Australia (*e.g.* B).

As this water is extracted by plants, some of which exclude silica, the water may become supersaturated with silica and precipitation in some form may occur (Franzmeier *et al.*, 1989).
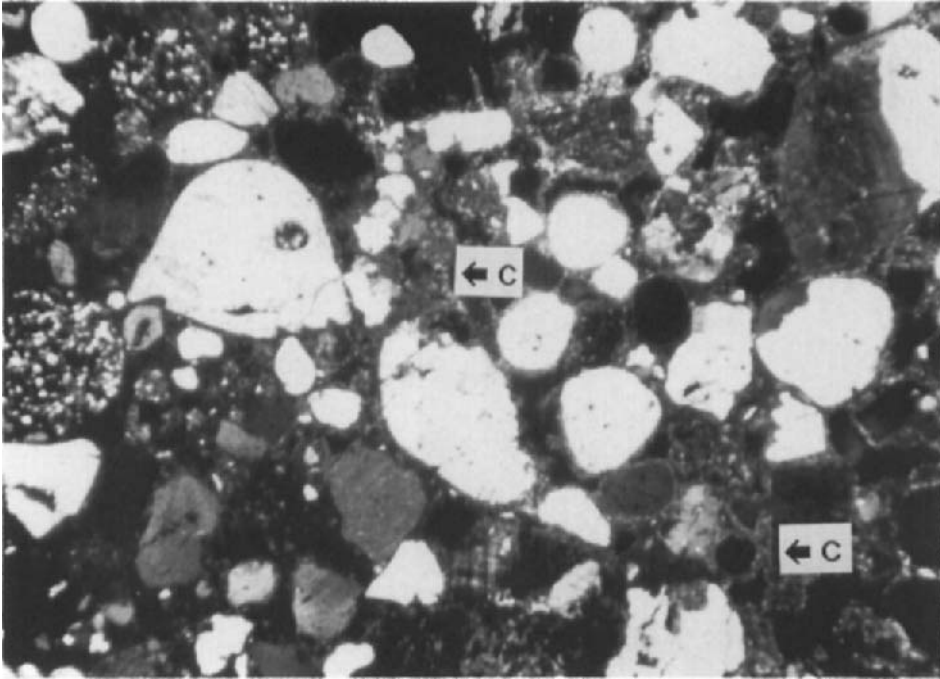
Fig. 6. Micrograph of thin section of carbonate cemented outwash from River Falls, Wisconsin, USA showing open-porphyric fabric with calcite (*e.g.* C) cementing grains; crossed polarized light (XPL); FW 15.8 mm.

According to Iler (1979) soluble silica precipitates in the presence of salts and will redissolve if the salt is of a monovalent metal, but is insoluble when precipitated by a polyvalent metal.

Precipitation of silica has also been implicated in surface crusting by Uehara and Jones (1972). They presented transmission electron microscopy (TEM) evidence for coatings of amorphous silica gel on a wide variety of mineral grains. They further suggested that such gels could form bridges and, upon loss of water, become rigid and cause crusting. The silica content found in citrate-bicarbonate-dithionite extracts of soils has been discounted as viable cement because of being too low in Si (DeKimpe *et al.*, 1972). However, Uehara and Jones (1972) argue that, if one considers the alkali soluble silica determined by the method of Hashimoto and Jackson (1960), the amount is greater by several weight percent SiO_2 and more than sufficient to act as a cementing agent. Gillford and Thran (1972) found that alkali free glass beads would be cemented by adding distilled water (ionic strength similar to rain water) and allowing them to dry. The bead strength was found to be around 1.5 bars. By adding 10 ppm and 100 ppm silica solutions, the strength increased to 3.2 and 3.4 bars, respectively, in a single wetting cycle. Thus very little cementing material is apparently necessary to bond particles together.
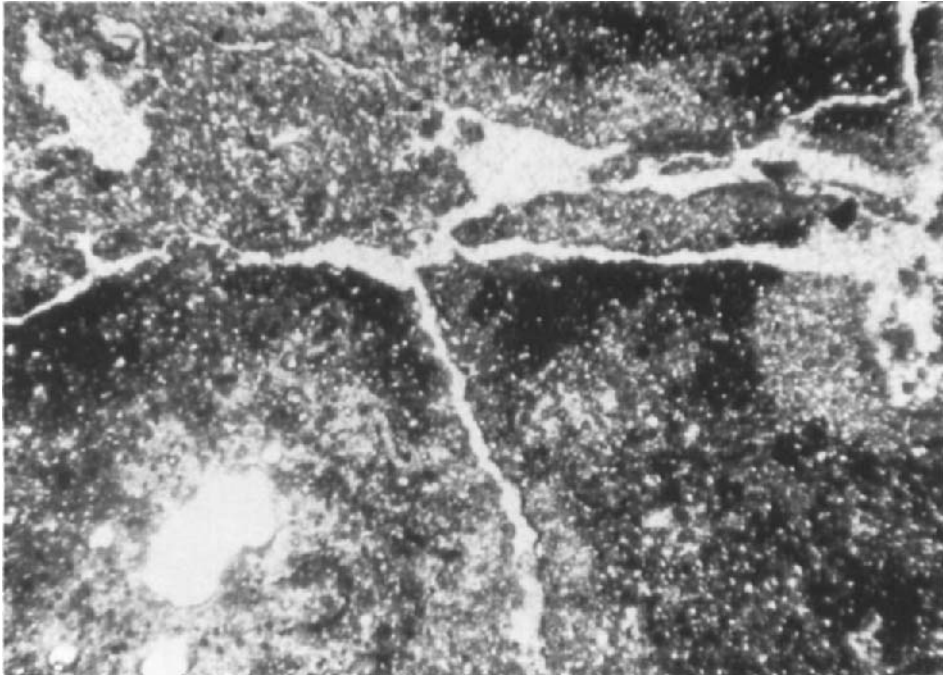
Fig. 7. Micrograph of thin section from Maranhao State, Brazil showing close-porphyric related distribution patterns; PPL; FW 15.8 mm.

Biogenic silica

Monosilicic acid (H_4SiO_4) produced by weathering of silicates accumulates within many terrestrial plants and is deposited in cellular structures of the organism as opal-A. The silica assumes the size, shape and configuration of the cell in which it is deposited (Fig. 5) and can be somewhat resistant to decomposition and cycling in soil systems. Some species take up considerable amounts of silica whereas others exclude its uptake (Geis, 1973). According to Jones and Handreck (1967) plants may be classified into three classes: those that actively take up silica such as rice (*Oryza sativa* L.); grasses (monocotyledons) which passively take up silica; and dicotyledons which actively exclude silica. Rice may contain 100 to 150 g kg^{-1} SiO_2 in the straw while grasses contain 15-20 g kg^{-1} and Dicotyledons usually less than 5 g kg^{-1} SiO_2. The SiO_2 content of dicots varies widely among species (Geis, 1973) and depends greatly on the concentration of monosilicic acid in the soil solution and the plant species. Leaves from 36 species of deciduous angiosperms were found by Geis (1973) to contain from a trace to 3.79% by dry weight biogenic opal.

DIFFERENCES AMONG NATURAL CEMENTS

Cements constitute a continuum from small adhesive bridges at grain contact points to a continuous matrix. In cases such as petrified wood, the entire mass is the cementing material
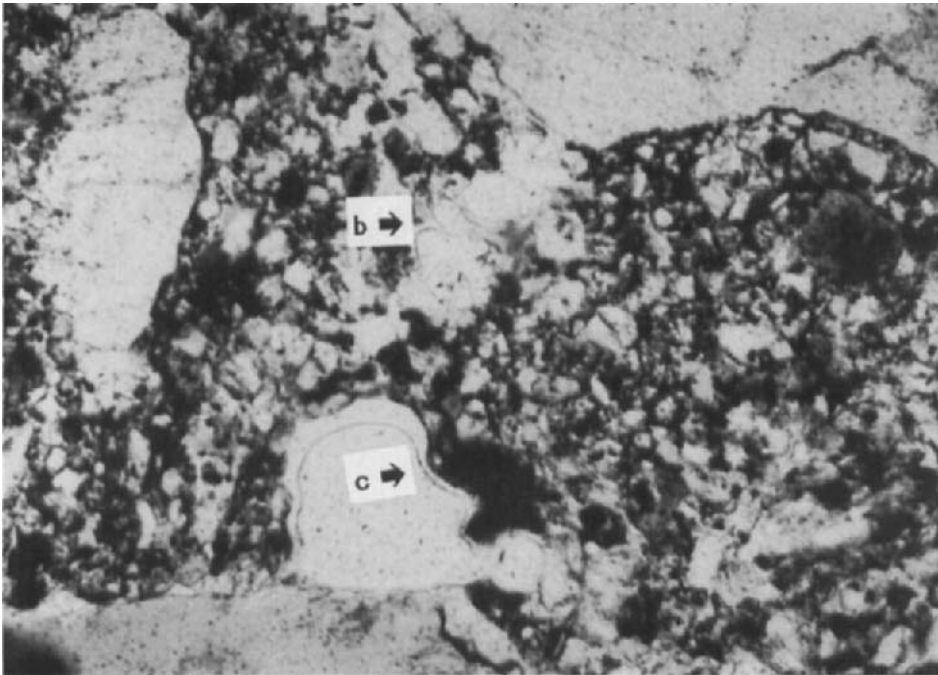
Fig. 8. Micrograph of thin section from a duric horizon of a soil from near Yeoval, New South Wales, Australia showing an isotropic cutan (c) and grains with isotropic bridges (b); PPL: FW 15.4 mm.

(Fig. 3). Chadwick and Nettleton (1990) identified cements as being adhesive or cohesive. They reported that ionically bonded calcite (petrocalcic horizons) and gypsum (petrogypsic horizons) produced open-porphyric related distribution patterns (Fig. 6) whereas covalently bonded silica, iron, aluminum and organic matter produced close-porphyric related-distribution-patterns (Fig. 7). The hypothesis was that covalent bonding favoured adhesion of the cement to skeletal grains whereas ionic bonding favoured cohesion of the cement to itself. Uehara and Jones (1972) concluded that sesquioxides of iron and aluminum do not act as cementing agents in soils until they form a continuous matrix whereas silica can cement materials without forming a continuous matrix (Fig. 8).

Gillford and Thran (1972) found that smaller silica bridges were actually stronger than larger ones. They found that the bridges were not actually solid cylinders between grains but an irregular hollow cylinder with only 33 to 78% connection. The smaller the bridge the greater the percentage of solid and therefore the greater strength. They described the steps in cementation from their observations as follows. First, when the volume of water decreases, a volume of minimum surface area is assumed between particles. The water further dries and becomes cloudy at or near the final diameter of the cementing bridge. Continued drying takes place on the surface of a cylinder which eventually ruptures from internal pressure. Continued evaportation leaves a hollow cylinder with one or more break points in the wall.

Fig. 9. Micrograph of thin section from a duric horizon of a soil from near Yeoval, New South Wales, Australia showing a channel filled with amorphous silica (s); PPL; FW 15.8 mm.

SILICA CEMENTED HORIZONS

Duripans are diagnostic subsurface horizons known to be cemented by silica. The brittle nature of fragipans is probably caused in part by silica cementation (Norton et al., 1984). The "hard-setting" soils of Australia are near-surface or subsurface horizons also suspected of containing amorphous silica cements (Chartres et al., 1990). In duric horizons, coatings and fillings of amorphous silica can clearly be seen in thin section (Fig. 9), whereas in fragipans and hard-setting horizons they generally cannot (Fig. 10). Because of the difficulty in finding direct evidence of silica cementation in fragipans and hard-setting horizons techniques other than optical microscopy have been used. Selective dissolution studies have shown that fragipans (Franzmeier et al., 1989) and hard-setting horizons (Chartres et al., 1990) have greater amounts of extractable silica than adjacent horizons.

In duripans, Chadwick et al. (1987) proposed a model for silica cementation in arid/semiarid soils by which silica adsorbed on skeletal grains serves as a template for further adsorption upon subsequent drying of the soil solution and precipitation of opaline silica. The polymers formed bonds between adjacent grains without plugging the interparticle voids. Franzmeier et al. (1989) proposed a similar mechanism in humid fragipan soils, in which desiccation and silica precipitation is driven by water extraction and exclusion of silica by the tree roots.
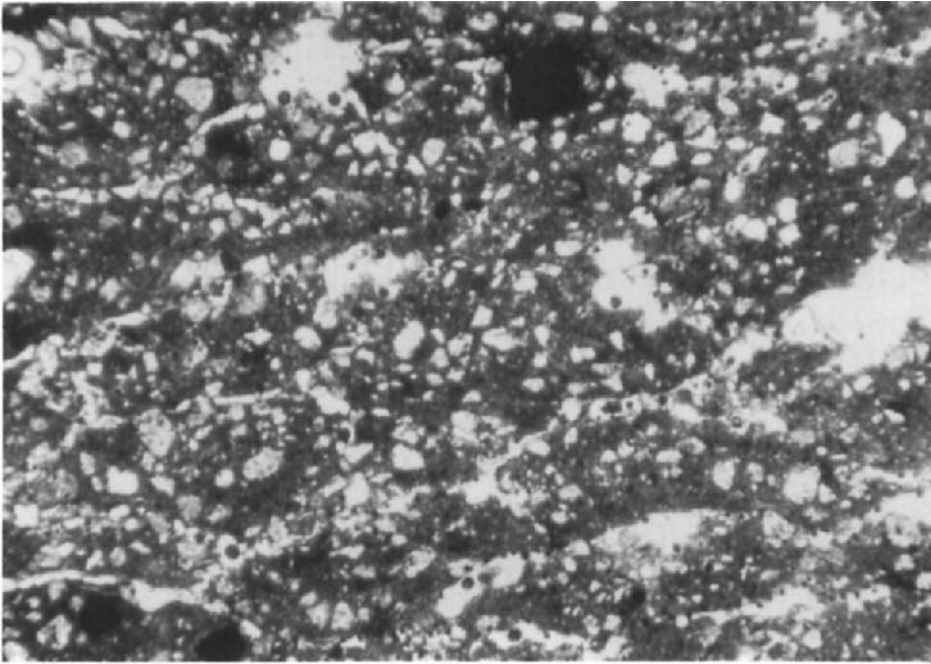
Fig. 10. Micrograph of thin section from a fragipan from near Brazil, Indiana, U.S.A. showing lack of any bonding observable; PPL; FW 15.8 mm.

Norton *et al.* (1984) found direct evidence for bridging of grains by alumnosilicates in fragipans using etched thin-sections and scanning electron microscopy. The Si/Al ratio was highly variable in the bridging structures. Chartres *et al.* (1990) concluded that amorphous silica was the major cementing agent in hard-setting soils. They found imogolite-like aluminosilicate, a feldspathoid mineral and possibly a silica-Fe complex involved in the cementation. A mechanism of formation similar to that proposed for duripans and fragipans probably occurs in hard-setting soils.

CONCLUSIONS

Cementation by silica is a very important process in a number of soil horizons. Silica cementation is involved in the genesis of surface crusts, hard-setting horizons, fragipans, and duripans. Micromorphology is a useful tool in some cases for observing the cementation, but in many cases small bridges cannot be seen. When the volume of cementing material is significant, such as in duripans, optical microscopy is very useful. Other complimentary techniques such as selective dissolution studies and electron microscopy are useful in determining the nature of the cementing materials. Such studies have shown that only small amounts of silica cementing materials are required to significantly increase soil strength. Compared to carbonate and iron cements, very little silica cementing material is required to produce the strength increase. This increase is due to small bridging structures with isotic to

undulic character. The composition of the bridging material is highly variable, but generally is highly siliceous. In the case of fragipans and hard-setting horizons, the bridging material seems to dissolve reversibly and precipitate resulting in their characteristic low strength when wet and high strength when dry. Potentially, a better understanding of these siliceous, naturally occurring cements will lead to development of low cost, locally available cements for construction purposes in addition to development of amelioration techniques for soils where cementation is problematic.

ACKNOWLEDGMENTS

REFERENCES

Brantley, S.L., Crane, S.R., Crerar, D.A., Hellman, R. and Stallard, R., 1986. Dissolution at dislocation etch pits in quartz. Geochem. Cosmochim Acta., 50: 2349-2361.

Chadwick, O.A. and Nettleton, W.D., 1990. Micromorphologic evidence of adhesive and cohesive forces in soil cementation. In: L.A. Douglas (Editor), Soil Micromorphology: A Basic and Applied Science. Proc. VIII Int. Working Meeting on Soil Mircomorphology, San Antonio, Texas, July 1988. Developments in Soil Science 19, Elsevier, Amsterdam, pp. 207-212.

Chadwick, O.A., Hendricks, D.M. and Nettleton, W.D., 1987. Silica in duric soils: I. A depositional model. Soil Sci. Soc. Am. J., 51: 975-982.

Chartres, C.J., Kirby, J.M. and Raupach, M., 1990. Poorly ordered silica and aluminosilicates as temporary cementing agents in hard-setting soils. Soil Sci. Soc. Am. J., 54: 1060-1067.

Cremeens, D.L., Darmody, R.G. and Norton, L.D., 1992. Etch-pit size and shape distribution on orthoclase and pyriboles in a loess catena. Geochem. Cosmochim Acta., 56: 3423-3434.

DeKimpe, C., Baril, R.W. and Rivard, R., 1972. Characterization of a toposequence with fragipan: The Leeds-Ste. marie-Brompton series of soil, Province of Quebec. Can. J. Soil Sci., 52: 135-170.

Drees, L.R., Wilding, L.P., Smeck, N.E. and Senkayi, A.L., 1989. Silica in soils: Quartz and disordered silica polymorphs. In: J.B. Dixon and S.B. Weed (Editors), Minerals in Soil Environments, 2nd Edition. Soil Sci. Soc. Am., Madison, Wisconsin, pp. 913-974.

Flach, K.W., Nettleton, W.D., Gile, L.H. and Cady, J.G., 1969. Pedocementation: Induration by silica, carbonates, and sesquioxides in the Quaternary. Soil Sci., 107: 442-453.

Franzmeier, D.P., Norton, L.D. and Steinhardt, G.C., 1989. Fragipan formation in loess of the midwestern United States. In: N.E. Smeck and E.J. Chiolkosz (Editors), Fragipans: Their Occurrence, Classification, and Genesis. Soil Sci. Soc. Am. Spec. Publ. No. 24, Madison, Wisconsin, pp. 69-97.

Geis, J.W., 1973. Biogenic silica in selected species of deciduous angiosperms. Soil Sci., 116: 113-119.

Gillford, R.O and Thran, D.F., 1972. Bonding mechanisms for soil crusts: Strength of silica cementation. In: J.W. Cary and D.D. Evans (Editors), Soil Crusts. Univ. Arizona Agric. Exp. Sta. Tech. Bull. 214, Tucson, Arizona., pp. 28-30.

Hashimoto, I., and Jackson, M.L., 1960. Rapid dissolution of allophane and Kaolinite-halloysite after dehydration. Clays and Clay Minerals, 7: 102-113.

Iler, R.K., 1979. Chemistry of Silica. Wiley Interscience, New York, 324 pp.

Jones, L.H.P. and Handreck, K.A., 1967. Silica in soils, plants, and animals. Adv. Agron., 19: 107-194.

Karathanasis, A.D., 1989. Solution chemistry of fragipans-Thermodynamic approach to understanding fragipan formation. In: N.E. Smeck and E.J. Chiolkosz (Editors), Fragipans: Their Occurrence, Classification, and Genesis. Soil Sci. Soc. Am. Spec. Publ. No. 24, Madison, Wisconsin, pp. 113-139.

Keller, W.D., 1968. Principles of Chemical Weathering. Lucas Bros. Printing, Columbia, Missouri., 111 pp.

Kelly, W.P. and Brown, S.W., 1939. An unusual alkali soil. J. Am. Soc. Agron., 31: 41-43.

Krauskopf, K., 1979. Introduction to Geochemistry. McGraw-Hill, New York, 617 pp.

Mielenz, R.D., 1949. Materials for Pozzolan: A Report for the Engineering Geologist. Petrographic Laboratory Report No. Pet-90A, Research and Engineering Div., U.S. Dept. of Interior, Bureau of Reclamation, Denver, Colorado, 25 pp.

Norton, L.D., Hall, G.F., Smeck, N.E. and Bigham, J.M., 1984. Fragipan bonding in a late-Wisconsinan loess-derived soil East-central Ohio. Soil Sci. Soc. Am. J., 48: 1360-1366.

Schultze, D.G., 1989. An Introduction to Soil Mineralogy. In: J.B. Dixon and S.B. Weed (Editors), Minerals in Soil Environments, 2nd Edition. Soil Sci. Soc. Am., Madison, Wisconsin., pp. 1-34.

Senkayi, A.L., Dixon, J.B., Hossner, L.R., Yerima, B.P.K. and Wilding, L.P., 1985. Replacement of quartz by opaline silica during weathering of petrified wood. Clays and Clay Minerals, 33: 525-531.

Uehara, G., and Jones, R.C., 1972. Bonding mechanisms for soil crusts: Particle surfaces and cementing agents. In: J.W. Cary and D.D. Evans (Editors), Soil Crusts. Univ. Arizona Agric. Exp. Sta. Tech. Bull. 214, Tucson, Arizona, pp. 17-28.

Micromorphological and chemical properties of Australian soils with hardsetting and duric horizons

C.J. Chartres[1] and L.D. Norton[2]

[1]CSIRO Division of Soils, GPO Box 639, Canberra, ACT 2601, Australia
[2]USDA-Agricultural Research Service, National Soil Erosion Research Laboratory,
Purdue University, West Lafayette, Indiana 47906, USA

ABSTRACT

Chartres, C.J. and Norton, L.D., 1994. Micromorphological and chemical properties of Australian soils with hardsetting and duric horizons. In: A.J. Ringrose-Voase and G.S. Humphreys (Editors), Soil Micromorphology: Studies in Management and Genesis. Proc. IX Int. Working Meeting on Soil Micromorphology, Townsville, Australia, July 1992. Developments in Soil Science 22, Elsevier, Amsterdam, pp. 825-834.

Three Alfisol pedons with hardsetting properties and one with duripan horizons were identified on the basis of dry strength in the field. Thin-sections (75 × 55 mm) were made from A, E and upper B horizon samples. Subsamples were also examined using a scanning electron microscope with energy dispersive X-ray detector. Chemical analyses (CBD, oxalate and acid-alkali dissolution) were performed to determine the presence of possible cementing agents.

There was a strong relationship between A and E horizon hardsetting properties and densely packed fine sand and silt particles, low macroporosity and little biological activity. A feature of these materials is the occurrence of grainy (< 2 μm) s-matrix materials with isotic to undulic fabric. Relatively high concentrations of opal phytoliths were commonly observed in hardsetting horizons suggesting that conditions were more conducive to silica accumulation rather than dissolution compared with other parts of the profiles. High acid/alkali extractable Si concentrations are associated with the hardest field structural conditions. SEM data indicated the presence of bridging materials consisting of fine quartz and clay minerals. Some clay zones had Si/Al ratios of up to approximately 10:1 suggesting the presence of amorphous silica coatings.

The data presented indicate that soil chemical cementation by compounds of silica and aluminium plays a role in hardsetting as well as physical properties including massive structure and dense packing of sand and silt grains. It is hypothesized that in such materials the close proximity of skeleton grains and the coating of grain surfaces by s-matrix materials as a result of effective stress processes may be conducive to the development of additional strength due predominantly to amorphous silica and also possibly to aluminosilicate precipitation. In the seasonally wet and dry environments studied, opportunities exist for such processes to take place as the soils desiccate through plant water uptake in spring.

INTRODUCTION

Hardsetting horizons have been recognised in a large number of Australian soils occurring in seasonally wet and dry climates. Hardsetting is a property originally defined by Northcote

(1979) for surface horizons, characterised by the development of strong to rigid consistence (McDonald *et al.*, 1990; Mullins *et al.*, 1990) when dry. On wetting, however, hardsetting materials will eventually slake and sometimes disperse. The aim of this paper is to describe the micromorphological and chemical properties of four soils with hardsetting and, in one case, duric horizons and to examine their similarities with fragipans and duripans described elsewhere.

SITE LOCATIONS AND ANALYTICAL METHODS

Four profiles in southeastern Australia were selected for detailed investigation. Soil classifications are given in Table 1. All the sites occur in the 450 - 550 mm rainfall belt, in xeric moisture regimes, although the two more northerly sites at Yeoval and Beni State Forest can have significant summer rainfall occurring as intense storms. Field descriptions were made following McDonald *et al.* (1990). 75 × 55 mm thin sections were made following impregnation with polyester resin. Small fracture samples were collected for analysis using scanning electron microscopy (SEM) and energy dispersive X-ray analysis (EDXRA). Electrical conductivity and pH were determined in 1:5 soil to water suspensions following shaking for 1 hr. Exchangeable cations and CEC were determined at pH 7.0 following methods in Loveday (1974). Organic carbon was determined using a modified Walkely-Black procedure. Fe, Al, and Si were determined using both citrate-dithionite-bicarbonate (CBD) and acid oxalate (pH 3.5). Sequential extractions of Fe, Al and Si were also made using 0.5M KOH and 6N HCl following the method of Karathanasis (1987). In all cases, Fe and Al were determined by atomic absorption spectroscopy and Si colormetrically (Weaver, 1968).

FIELD PROPERTIES

Profile descriptions are given in Table 1. Properties similar to hardsetting were observed below 60 cm at Beni, 94 - 120 cm at Temora and 82 - 90 cm at The Rock. Duripans (designated m horizons) occurred in the Yeoval profile at 20 - 25 cm and from 48 - 55 cm (the latter was not analysed chemically because of its extreme induration). Subsurface horizons with properties similar to hardsetting as defined by McDonald *et al.* (1984) are designated x (fragipan; Soil Survey Staff, 1975), although the horizons described here often lack the vertical bleached planes common in fragipans overseas. In common with fragipans, the local horizons slake slowly in water, or may rupture under applied pressure when moist. Apart from the A1 horizons a significant feature of the indurated and hardsetting horizons was a lack of evidence of bioturbation and macroporosity.

THIN SECTION AND SEM/EDXRA PROPERTIES OF HARDSETTING AND DURIC HORIZONS

Beni State Forest

The Ex horizon has a porphyric related distribution pattern and has silasepic plasmic fabric. Rare yellowish, limpid ferriargillans were observed in voids. These tended to have poor orientation with some zones being isotic. The B21x horizon is characterized by a greater clay content and insepic plasmic fabric. Common reddish-orange ferriargillans occur in voids and

Table 1
Soil descriptions and classification.

Beni State Forest (Arenic Natrustalf)

A1		Grayish brown (10YR 5/2 dry), massive fine sandy loam. Common roots. Gradual slightly wavy boundary.
E	20-60cm	Very pale brown (10YR 7/3 dry) massive to weakly laminated (lower 5 cm) coarse loamy sand. Common roots. Few Fe-Mn nodules. Abrupt, slightly wavy boundary.
Ex	60-65cm	White (10YR 7/2 dry), common, faint, medium, light red (2.5YR 6/6 dry) mottles, massive sandy loam. Organic matter stains on vertical faces. Abrupt, slightly wavy boundary.
B21x	65-95cm	Light reddish brown (2.5YR 6/4 dry), faint fine bleached faces to peds, common medium faint-distinct light red mottles (2.5YR 6/6 dry) columnar to weak medium subangular blocky sandy clay loam. Organic stains down root channels. Gradual smooth boundary.
B22x	95+cm	Mottled 50% weak red (2.5YR 5/2 dry) 50% strong brown (7.5YR 5/8) light clay.

Yeoval (Natric Durixeralf)

A1	0-6cm	Light yellowish brown (10YR 6/4 dry) laminated loamy coarse sand. Clear smooth boundary.
A1b	6-12cm	Yellowish brown (10YR 5/4 dry) loamy coarse sand. Gradual boundary.
E	12-20cm	Light brownish gray (10YR6/2 dry) massive vesicular sandy loam. Abrupt smooth boundary.
Em	20-25cm	Light brownish gray (10YR 6/2 dry) duripan layer. Abrupt smooth boundary.
B2	25-48cm	Light brownish gray (10YR 6/2 moist) medium subangular blocky sandy clay loam. Organic stains on ped faces. Abrupt smooth boundary.
Bm	48-55cm	Light gray (2.5Y 7/2 dry) massive clay loam. Gradual smooth boundary.
IIB2	55+cm	Light gray (2.5Y 6/2), subangular blocky to prismatic sandy light clay. Ped faces stained grayish brown (10YR 5/2).

Temora (Typic Fragixeralf)

A	0-6cm	Brown (7.5YR 5/4 dry), massive, very firm silt loam. Clear wavy boundary.
B21	6-38cm	Yellowish red (5YR 5/6 dry) weak medium subangular blocky, very firm silty clay loam. Gradual wavy boundary.
B22	38-56cm	Strong brown (7.5YR 6/6-6/8 dry) weak subangular blocky, very firm light clay. Gradual wavy boundary.
B23	56-69cm	Light yellowish brown (10YR 6/4 dry), common medium distinct red (2.5YR 4/8 dry) mottles, few fine distinct pale brown (10YR 4/3 dry) mottles, medium to fine subangular blocky, very firm light to medium clay. Clear wavy boundary.
IIB2	69-94cm	Pink (7.5YR 7/4 dry), few fine faint yellowish red (5YR 5/8 dry) mottles, massive, very firm sandy clay. Gradual wavy boundary.
IIBx	94-120cm	Very pale brown (10YR 7/3 dry), few fine distinct strong brown (7.5YR 5/8 dry) mottles, massive, hard loam. Gradual wavy boundary.
IIBC	120-130cm	As above, except weak subangular blocky structure and very firm consistence.

The Rock (Typic Natrixeralf)

A1	0-14 cm	Pale brown (10YR 6/3 dry) massive fine sandy loam. Gradual wavy boundary.
E21	14-60cm	Light gray (10YR 7/2 dry) massive, soft, loamy sand. Gradual smooth boundary.
E22	60-82cm	Light gray (10YR 7/2 dry) massive hard loamy sand. Abrupt smooth boundary.
Bx	82-90cm	Brownish yellow (10YR 6/6 dry), very few fine yellowish brown mottles (10YR 5/6 dry). Very hard. Gradual smooth boundary.
Bt	90-150cm	Brown (7.5YR 5/4 dry) medium subangular blocky clay. Hard. Few faint medium yellowish red (5YR 5/8) mottles.
C?	150+cm	Mottled 50% yellowish red (5YR 5/8 dry), 50% pinkish gray (7.5YR 6/2 dry) medium to large subangular blocky clay.
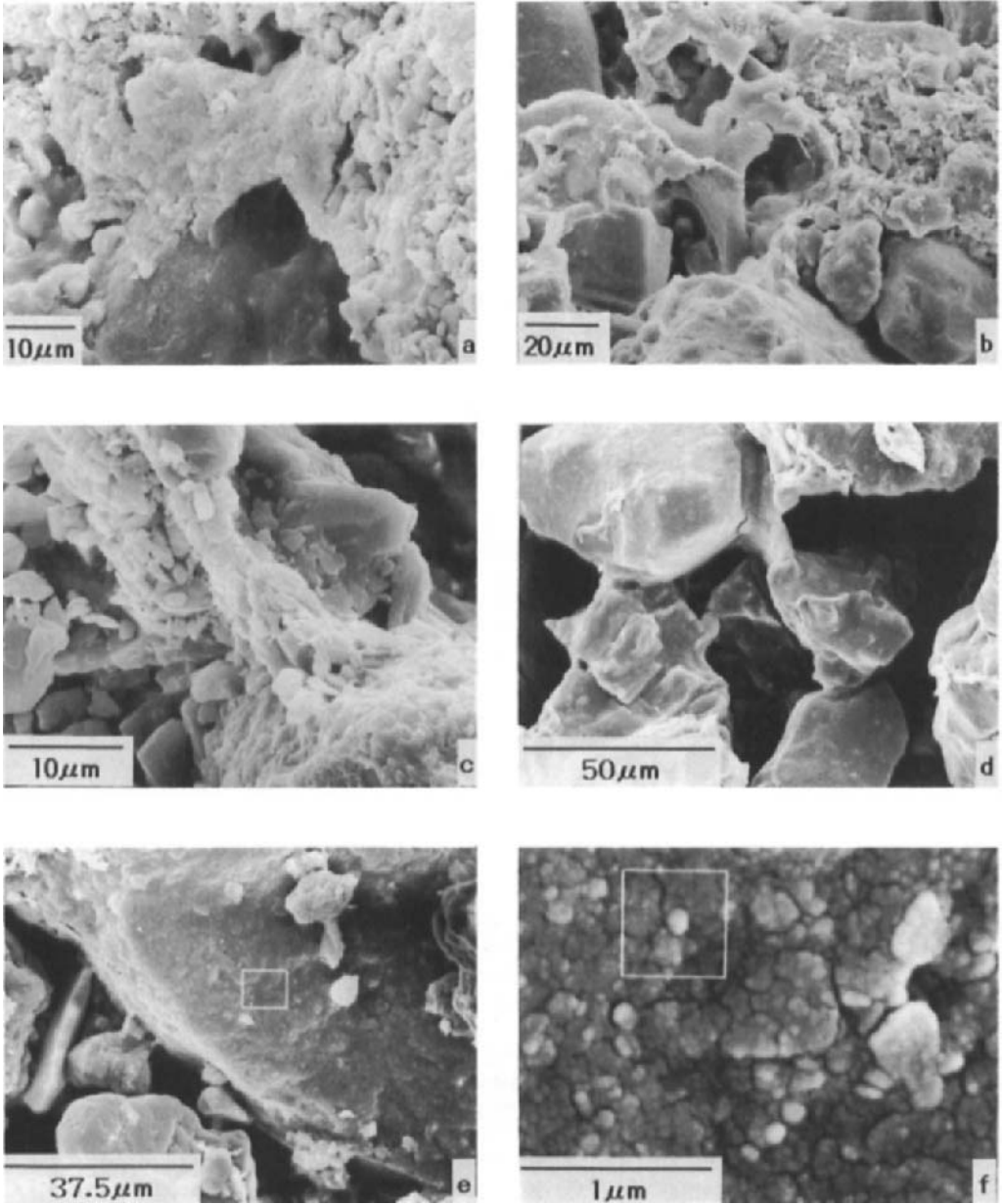
Fig. 1. SEM features of hardsetting and duric horizons: **a)** Beni B22; clay and fine silt cutan; **b)** Yeoval Bm; silicified void coating; **c)** the Rock E22/Bx boundary; fine quartz; **d)** Yeoval Bm; silicified bridges; **e)** the Rock Bx; quartz grain; **f)** enlargement of (e) showing amorphous silica and clay cutan spherules.

channels. Rare blackish grainy (Chartres, 1988) void cutans, which are isotic in crossed polarized light were also observed. SEM analyses showed common bridges consisting predominantly of fine silt and clays (Fig. 1a).

Yeoval

Both duripan layers (20 - 25 cm and 48 - 55 cm) are porphyric and silasepic. Many areas of the matrix are characterised by very fine grained (< 2 μm) grainy material, which has a 'dirty' grayish appearance in plane polarized light and has undulic to isotic extinction in cross polarized light (Fig. 2a). Similar material was observed in cutans in the bottom of voids. Void and channel argillans were rare and a few contained grainy zones with similar properties to the matrix materials described (Fig. 2b). SEM/EDXRA and thin section observations demonstrated the occurrence of common, predominantly siliceous features which, on the basis of their morphology, were probably phytoliths. Other areas examined had cutan-like structures, which were also silica-rich (Fig. 1b and Fig. 3). Bridging structures consisting of some clay minerals and grainy material were common adjacent to many voids with clay-like materials consisting predominantly of Si (Fig. 1d), with Si/Al EDXRA ratios of between 3:1 and 12:1.

Temora

The hardsetting horizon (94 - 120 cm) at this site was also porphyric and silasepic. Areas of dirty grayish, grainy materials occur in the matrix and lining the lower margins of some voids. Yellowish, laminated ferriargillans are common. SEM/EDXRA observations were not made on these samples.

The Rock

The micromorphological properties of the hardsetting horizon (82 - 90 cm) are similar to those described at the other sites. A few zones of fine grayish grainy material could be observed at the macroscopic scale in the thin section and under magnification could be seen to both line channels and occur within the matrix (Figs 2c and 2d). This material appears to contain some very fine quartz and has an appearance somewhat similar to a very fine grained siltstone. However, some of the material has undulic to isotic extinction and may be amorphous. SEM observations (Fig. 1c) indicated similar features to those observed at Beni. In some instance some very fine (< 1 mm) almost filamentous cementing materials were seen bridging matrix materials. In other instances opaline silica was observed precipitated as spherules on grain surfaces (Fig. 1e and f).

CHEMICAL PROPERTIES

Results of chemical analyses are shown in Table 2 and Fig. 4. pH levels are everywhere below 7 except at Yeoval, where levels rise from 7.3 at 10 - 20 cm to 8 and above at greater depths and in the Temora IIBC horizon. In all hardsetting horizons and the Em duripan at Yeoval (the Bm horizon was not chemically analysed because of its lithified nature) exchangeable sodium percentages exceeded 9. Oxalate extractable Fe, Al and Si are generally very low in both hardsetting, duric and other horizons (data not shown). Dithionite extractable Si increases from E to B horizons and are at or near maximum values in the hardsetting and
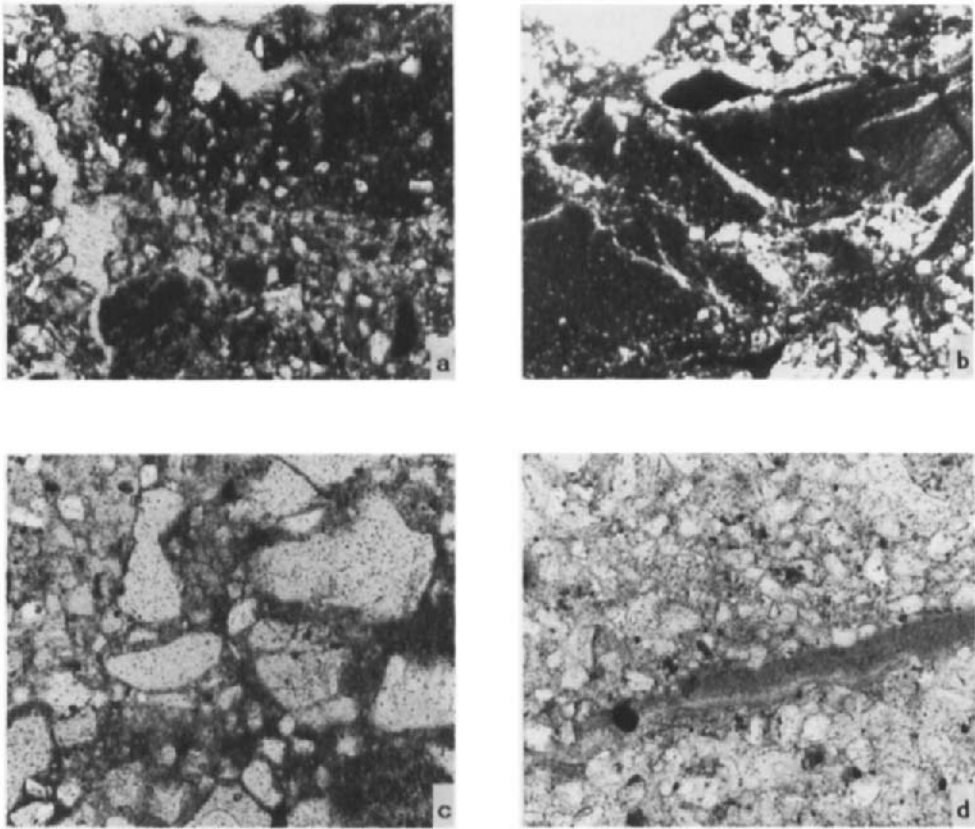
Fig. 2. Thin section micrographs: **a)** Yeoval Em; grainy matrix; plane polarized light (PPL); frame width (FW) 1.5 mm; **b)**Yeoval Em; degraded cutan with isotic properties; crossed polarized light; FW 0.9 mm; **c)** the Rock Bx; grainy matrix materials; PPL; FW 0.9 mm; **d)** The Rock Bx; degraded, grainy cutan; PPL; FW 0.9 mm.

duripan horizons. (Fig. 4). Si extractable in sequential alkali and acid extracts is generally high in the hardsetting and duric horizons except at Temora, where there is little change with depth (Table 2). Molar Si (Si/Si+Al) values are generally highest in the soil A and E horizons except at Temora where they are high in both E and IIBx and IIBC horizons (Fig. 4).

DISCUSSION

Hardsetting has been shown by previous studies (Mullins *et al.*, 1990) to be primarily a physical process possibly resulting from effective stresses as the soil dries out. The current results also indicate that all the hardsetting and duripan horizons are characterised by generally
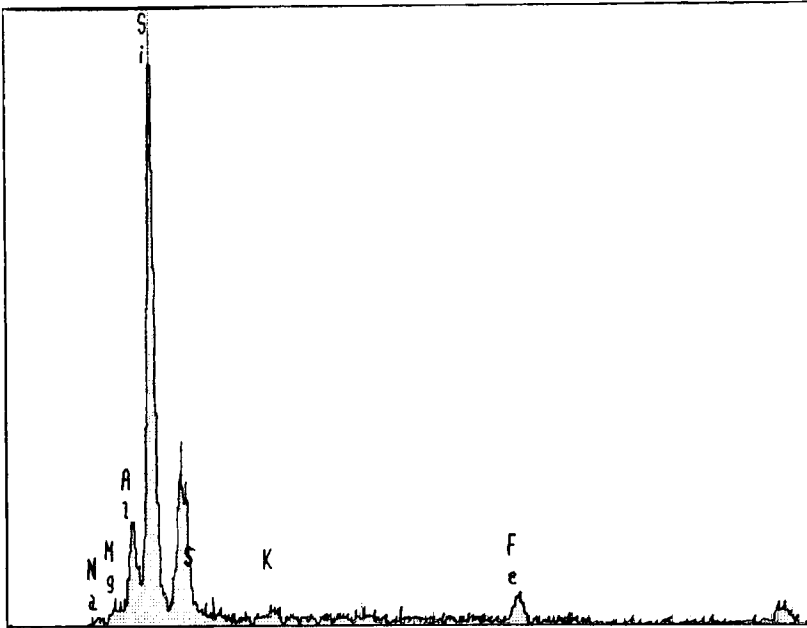
Fig. 3. EDXRA trace of analysis taken at the top of the silicified void coating from the Yeoval Bm horizon shown in Fig. 1b.

densely packed sands and silts and limited amounts of clay. They lack evidence of much biological activity and organic matter.

Micromorphologically, the occurrence of dirty, grainy zones, consisting of very fine particles generally < 2 mm diameter, is common to both the duripans and hardsetting horizons investigated. Observations indicate that these materials consist of some very fine quartz grains and apparently amorphous particles and coatings of silica. These materials occur both in voids and within the matrix itself. EDXRA analyses indicate that Si/Al ratios are generally higher than those found in layer silicate minerals and that Fe and Ti are commonly associated with these materials (Chartres, 1988). These properties indicate that the grainy materials are most probably weathering residues left following decomposition of cutans and s-matrix clays. An alternative hypothesis is that the grainy zones represent accumulation of very fine particles leached down the profile although the occurrence of grainy zones sometimes crossing depositional laminae supports a weathering rather than sedimentary origin. A combination of relatively long periods of time for soil formation and current seasonal waterlogging above the B horizons would also favour this hypothesis.

Chemical analyses indicate that dithionite extractable Si contents increase in or just above duripan and hardsetting horizons. This result parallels findings for fragipans in the U.S.A. (Norton *et al.* 1984). However, the low concentrations of dithionite Si even in the duripan horizons compared with higher amounts of acid/alkali extractable Si indicate that the former is not a good indicator of the presence of soil cementing agents. Dithionite preferentially extracts semi-crystalline iron oxides and Si extracted may be primarily bound in these

Table 2
Chemical properties of the soils.

Sample	Depth	E.C.	pH	Org.C	CEC	ESP	Si extr. in KOH/HCl	Dithionite extractable			Si_{ox}/Al_{ox}
					cmol(+)			Fe	Al	Si	
	cm	mS/cm		%	kg^{-1}		µg g^{-1}		µg g^{-1}		
Beni											
A1	0-10	0.017	5.4	1.59	9.2	6	5232	9039	1182	400	0.12
E	40-50	0.009	6.2	0.04	0.76	11	3010	2475	150	144	0.21
Ex	60-65	0.030	6.6	0.11	6.9	25	4001	3175	373	743	0.36
B21x	70-80	0.168	6.4	0.11	8.4	31	6050	11290	898	1065	0.49
B22	90-100	0.194	6.3	0.13	9.4	33	6650	13516	959	944	0.48
Yeoval											
A1	0-05	0.021	5.5	1.37	5.3	8	5746	3313	455	835	0.12
E	10-20	0.036	7.2	0.29	4.4	19	6122	1163	212	511	0.37
Em	20-25	0.068	7.8	0.16	4.4	33	7341	981	232	553	0.39
B2x	25-35	0.155	8.3	0.23	13.9	31	10959	2039	435	1426	0.73
B2x	35-45	0.291	8.2	0.15	20.0	33	11097	2640	417	1692	0.72
IIB2	55-65	0.329	8.0	0.04	18.3	28	8505	4976	400	1611	0.41
Temora											
A1	0-6	0.043	6.4	1.10	10.0	2	5286	8933	882	428	0.13
B21	6-38	0.040	6.3	0.36	5.4	0.2	5375	8939	859	387	0.25
B22	38-56	1.07	5.7	0.28	8.3	5	5616	15969	1842	507	0.35
B23	56-69	1.14	5.7	0.14	17.4	5	7111	14189	2144	728	0.41
IIB2	69-94	0.223	6.7	0.06	10.3	1	5347	7921	593	1098	0.58
IIBx	94-120	0.182	6.7	0.04	6.6	9	4393	5587	375	1087	0.43
IIBC	120-130	0.260	7.4	0.04	12.6	13	5343	5536	709	1518	0.54
The Rock											
A1	0-10	0.047	6.0	0.78	11.2	6	5577	6429	893	1220	0.37
E21	30-40	0.051	6.3	0.29	3.6	13	3339	2424	282	298	0.24
E22	60-70	0.080	6.4	0.08	1.7	8	2955	2731	261	265	0.36
Bx	80-90	0.440	5.7	0.12	13.0	12	5897	7399	954	1434	0.45
Bt	90-100	0.424	5.7	0.19	14.7	8	5644	8843	1175	1289	0.55
C	150-160	0.868	4.8	0.08	8.1	12	5766	7559	842	642	0.29

materials. Very small amounts of oxalate extractable Si (< 400 µg g^{-1}) were also detected and these also peaked in the indurated horizons. Si/Al ratios of the oxalate extracts in the indurated horizons were between 0.5 - 0.7, suggesting that very small amounts of allophane-like materials could be present. Total acid plus alkali extractable Si contents generally paralleled dithionite extractable Si contents except at Temora where the former are highest in the lower B horizon. The data (Table 2) also indicate that as total Si contents increase the molar Si values indicate a decrease in silicon to aluminium (Fig. 4). This could be due to dissolution of unstable phyllosilicate minerals by the extracting reagents, or may indicate a change in the mineralogy of the forms of silica and aluminium found in most hardsetting and duric horizons (Chartres *et al.*, 1990). Whilst the acid/alkali extraction method may dissolve some layer lattice silicate clays, Karathanasis (1987) suggests that it predominantly dissolves amorphous coatings on and between other soil constituents. Thus, the current data may be interpreted to indicate that such coatings in the A and E horizons are Si rich, but that in hardsetting and
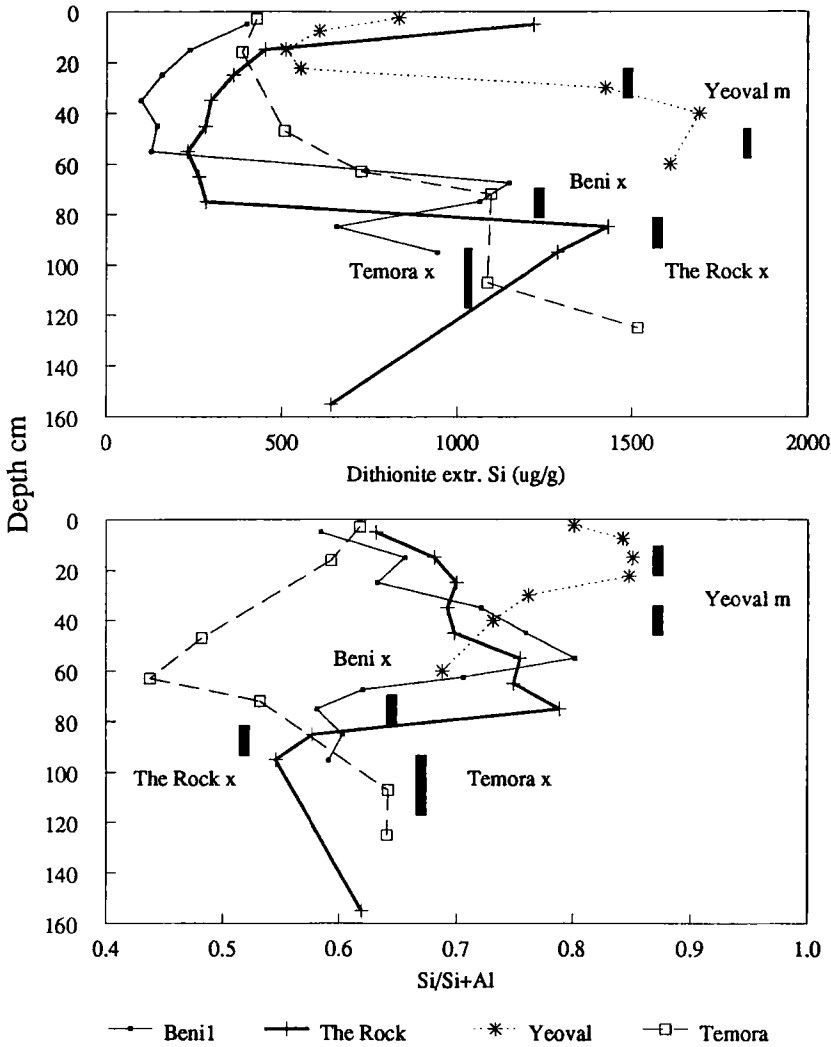
Fig. 4. Dithionite extractable Si and molar Si (Si/Si+Al) depth functions for the four sites. The solid bars indicate approximate depths of respective duripan (m) and hardsetting (x) horizons.

duripan horizons they contain a larger proportion of Al.   Karathansis postulated albite weathering as the source of
the amorphous cements in the fragipans he investigated.   Whilst feldspars occur in the Australian soils examined, they generally appear to be more severely weathered and the sources of silica and aluminium in the amorphous cements detected are uncertain. However, it is likely that under the seasonally wet and dry conditions experienced Si and Al will be concentrated from solution as the soils dry out. There may also be further accumulation of

silica and aluminium in some hardsetting and duric horizons due to leaching from A horizons, or other overlying materials. As in the U.S.A. examples, there is an apparent relationship between high Si concentrations and exchangeable sodium accumulation.

It is concluded that the grainy dark zones observed in thin section are probably the products of prolonged weathering under seasonal wet and dry conditions and that a small proportion of the silicon and aluminium weathering products have been precipitated to form amorphous cements. These coat and bridge grains of quartz and clay minerals affording considerable strength to the soil horizons affected. Hardsetting horizons contain considerably less silica-rich bridging materials and evidence of amorphous silica precipitates than the duripans examined, but the optical and SEM evidence does suggest that amorphous or mineralogically poorly ordered precipitates may play some role in the development of their strength on drying. The coating of crystalline materials with these precipitates may also explain the undulic to isotic properties of features observed in thin-section.

Previously the term hardsetting has been applied to surface horizons. However, the current results indicate that similar properties to those exhibited by surface hardsetting horizons are found in E and B horizons. Whilst the increased hardness and strength of the E and B horizons at Beni, Temora and the Rock are most probably predominantly the result of physical factors, chemical agents appear to be involved as well. Whilst the horizons designated x in these three soils are somewhat analogous with fragipans, they do not exhibit all the properties commonly associated with the latter (Soil Survey Staff, 1975). It is therefore suggested that the term hardsetting as defined by McDonald et al. 1990) be used for subsoil as well as surface horizons.

REFERENCES

Chartres, C.J., 1988. The composition and formation of grainy void cutans in some soils with textural contrast in southeastern Australia. Guelder, 39: 209-233.

Chartres, C.J., Kirby, M.J. and Raupach, M., 1990. Poorly ordered silica and aluminosilicates as temporary cementing agents in hardsetting soils. Soil Sci. Soc. Am. J., 54: 1060-1067.

Karathanasis, A.D., 1987. Thermodynamic evaluation of amorphous aluminosilicate binding agents in fragipans of western Kentucky. Soil Sci. Soc. Am. J., 51: 819-824.

Loveday, J. (Editor), 1974. Methods for Analysis of Irrigated Soils. Commonwealth Bureau of Soils Tech. Commun. 54, Commonwealth Agricultural Bureaux, Farnham Royal, U.K.

McDonald, R.C., Isbell, R.F., Speight, J.G., Walker, J. and Hopkins, M.S., 1990. Australian Soil and Land Survey Field Handbook. 2nd Ed. Inkata Press, Melbourne. 198 pp.

Mullins, C.E., MacLeod, D.A., Northcote, K.H., Tisdall, J.M and Young, I.M., 1990. Hardsetting soils: behaviour, occurrence and management. Advances in Soil Science, 11: 37-108.

Northcote, K.H., 1979. A Factual Key for the Recognition of Australian Soils. Rellim Technical Publications, Adelaide.

Norton, L.D., Hall, G.F., Smeck, N.E. and Bigham, J.M., 1984. Fragipan bonding in a late Wisconsinan loess-derived soil in east central Ohio. Soil Sci. Soc. Am. J.,48: 1360-1366.

Soil Survey Staff, 1975. Soil Taxonomy. U.S. Dept. Agric. Handb. No. 436. U.S. Govt. Printing Office, Washington, D.C.

Weaver, R.M., Syers, J.K. and Jackson, M.L., 1968. Determination of silica in citrate-dithionite bicarbonate extracts of soils. Soil Sci. Soc. Am. Proc., 32: 497-501.

Nature and origin of a duripan in a Durixeralf-Duraqualf toposequence: micromorphological aspects

I.D. Hollingsworth and R.W. Fitzpatrick

CSIRO Division of Soils, Private Bag No. 2, Glen Osmond, SA, 5064, Australia

ABSTRACT

Hollingsworth, I.D. and Fitzpatrick, R.W., 1994. Nature and origin of a duripan in a Durixeralf-Duraqualf toposequence: micro morphological aspects. In: A.J. Ringrose-Voase and G.S. Humphreys (Editors), Soil Micromorphology: Studies in Management and Genesis. Proc. IX Int. Working Meeting on Soil Micromorphology, Townsville, Australia, July 1992. Developments in Soil Science 22, Elsevier, Amsterdam, pp. 835-844.

A duripan occurs below clayey B horizons in some soils in the Warren Reservoir catchment in the Adelaide Hills of South Australia. This feature has not previously been described in this region. The nature of the duripan, iron-rich nodules and soil horizons was investigated using micromorphological, physical, chemical, mineralogical and electron optical methods.

The duripan occurs in a toposequence of Xeralfs and Aqualfs formed in carbonate-free contiguous polypedons on colluvial fans at the base of rolling low hills of Cambrian mica schist. A fine, kaolinitic, mesic, Aquic Durixeralf soil profile occurs on convex crests and a loamy, siliceous, mesic Albic Duraqualf (proposed new subgroup) profile occurs in concave drainage depressions on the surface of the fan, which is underlain by kaolinised mica schist bed rock. This micro relief has an amplitude of 2 m.

The duripan has a massive microstructure. Dominantly smooth, poorly sorted, subangular blocky, single quartz grains dominate the coarse fraction. Fragments of subrounded, blocky sandstone and schist comprise 2% of the coarse fraction. Grains and fragments are fresh or weakly altered. The duripan has a porphyric related distribution with stipple speckled b-fabric and porostriated partial fabrics around pores and incomplete macropore infillings of silt, clay and amorphous silica. Ferruginous nodules in the A-B horizon have an embedded grain structure of poorly sorted, subangular blocky quartz grains cemented by optically opaque hematite, goethite and maghemite. One in ten ironstone fragments has a compound structure of older nodules where the silica grains are deeply etched.

The presence of compound rock fragments of metasandstone and schist in the duripan indicate that the substrate is transported material. Clay coatings on particles and in pores identify illuviation of kaolinite into the matrix and pores of the duripan. Silicification of the clay matrix and pore linings by amorphous silica to form the duripan is possibly associated with: (a) the redoximorphic/weathering processes which released silica when the ferricrete formed, (b) solubilization of poorly sorted, siliceous colluvium and (c) kaolinisation of the underlying bed rock. Relict ferricretes occur on footslopes 15 m higher in the landscape. The compound ferruginous nodules in the A-B horizon of the Durixeralfs contain several generations of ferruginous structures derived from the breakup of the ferricrete.

INTRODUCTION

Soils with a duripan (Bqm) have not been previously described in the Adelaide Hills region. The climate is mediteranean and the mean annual precipitation in the Warren catchment study area is 730 mm. The duripan was identified by observing that fragments of the indurated horizon did not slake after prolonged soaking in water or 1N HCl.

The duripan underlies Xeralfs (crest) and Aqualfs (drainage depression) that occur on colluvial fans at the base of rolling low hills of Cambrian mica schist. This is a complex soil-landscape comprising mottled pallid zones, ferruginous glæbules in A-B horizons and ferricretes. The exact relationship between these ancient weathering features and the immediately adjacent relatively younger soils is not clearly understood.

The colluvial fan landform is very gently inclined (1 - 3% slope) and has surface micro-relief with a 2 m vertical interval and 50 m horizontal interval. The parent materials for the pedons with duripans are poorly sorted sandy colluvia from Cambrian meta-sandstone, schist and pegmatite.

Two sites in a toposequence comprising crest and drainage depression landform elements, located at Australian Map Grid reference 319840 East 6155425 North in Map Zone 54, at an elevation of 430 - 437 m a.s.l., were sampled for micromorphological analysis. A soil profile on the crest in this toposequence was classified as a fine, kaolinitic, mesic, Aquic Durixeralf. A soil profile in the drainage depression was classified as a loamy, siliceous, mesic Albic Duraqualf. Fitzpatrick *et al.* (1992) have recently proposed Albic as a new subgroup to Soil Taxonomy (Soil Survey Staff, 1992).

These pedons overlie a mottled pallid zone. Ferricrete outcrops occur upslope of the Durixeralf/Duraqualf toposequence with reworked ferruginous ironstone fragments occurring as a stone line in and above the argillic horizons of soils in the toposequence. The original *Eucalyptus camaldulensis* woodland was cleared before 1936 (Gordon, 1969).

The objectives of this study were to assess the micromorphology of:

a) the duripan underlying two soils in a toposequence (Xeralfs and Aqualfs), as well as the duripan material outcropping in the study area,

b) ferruginous nodules in A-B horizons of soils and ferricrete outcropping on footslopes upslope from the Xeralf-Aqualf toposequence,

c) soil matrices from selected horizons in the Xeralf-Aqualf toposequence.

for the purpose of identifying the cementing agents in the duripan and developing a pedogenetic model for this soil.

METHODS

Soil and landscape features

Soil and landscape features were described according to McDonald *et al.* (1990).

Chemical, physical and mineralogical analyses

Duripan fragments sampled below both pedons and from outcrops were subjected to prolonged soaking in water and 1N HCl and observed for evidence of slaking.

Analyses for particle size, exchangeable cations, soluble ion and organic carbon were conducted on all soil material that could be lightly crushed with a mortar and pestle and passed

through a 2 mm sieve. X-ray diffraction (XRD) patterns were obtained from specimens ground to a fine powder in an agate mortar and packed in random orientation into aluminium holders. Major and minor element abundances in the samples were determined by X-ray fluorescence spectrometry (XRS) using the techniques of Norrish and Hutton (1969). Simultaneous differential thermal analyses (DTA) and thermogravimetric analyses (TGA) were made.

Thin section preparation and technique

Oriented undisturbed samples (10 × 10 × 5 cm) of the duripan, Btg horizon and A-B horizon iron-rich nodules were impregnated with Escon 4527 polyester resin thinned with 2 parts methyl methacrylate monomer with a cumene hydroperoxide catalyst (0.5% wt) and methylethylkeytone peroxide accelerator (1 drop per 100 g) in a vacuum chamber at -30 kPa pressure for 24 hours. Samples were cured for 1 day at 35°C and a second day at 65°C. Thin sections were slabbed from indurated samples using a gem cutting saw, then stuck onto slides (45 × 25 mm) with epoxy and polished with 0.1 μm diamond grit.

Micromorphological description

The soil fabrics produced by pedogenic deposits of silica and clay were studied at progressively greater magnifications using a 40× polarizing microscope and an SEM equipped with an EDS microprobe. Pedogenic opaline silica was identified by its birefringence in cross polarised light and its light grey colour in plane light (Kerr, 1977). Interpretations were confirmed by using molar ratios derived from electron microprobe analyses on thin sections. Micromorphological features of interest were photographed at successively higher magnifications using a scanning electron microscope (SEM). The SEM provided greater detail of specific features.

RESULTS

Profile Morphology

The main macromorphological features of the two soils studied are: (i) the sharp texture change between the E and Bt horizons and (ii) the presence of a duripan below the Bt horizons. The Duraqualf profile, in the drainage depression, has an albic horizon abruptly overlying a strongly prismatic Btg horizon typical of a natric horizon. However, this horizon is acid and does not have enough exchangeable sodium to qualify as natric (Table 1). The Btg2 horizon has matrix colours with chromas of less than 2 and mottles with bright orange colours (7.5YR 5/8) indicating seasonally redoximorphic conditions.

Duripan

The powder XRD patterns from ground whole samples of the duripan showed sharp strong quartz peaks and a broad diffraction band in a region centred between 0.39 and 0.41 μm (see arrowed band in Fig. 1a) indicative of amorphous silica. There are minor peaks indicating relatively lesser amounts of kaolinite (between 10 and 20%), illite, anatase and plagioclase. The mineralogy and chemistry of the duripan did not differ appreciably in samples from the two soil profiles being studied.

Table 1.
Soil profile physical and chemical properties.

Horizon	Depth	Particle sizes (%)				pH	EC	Exchangeable cations					CEC	ESP
	cm	Clay	Silt	Fine sand	Coarse sand	1:5 soil:H$_2$O	dS/m		(pH 7.0) cmol(+)/kg				(NH$_4$) cmol(+)	%
		<0.002 mm	0.002- 0.02mm	0.02- 0.2mm	0.2- 2.0mm			Ca	Mg	Na	K	Total	/kg	
fine,kaolinitic,mesic Aquic Durixeralf														
A11	0-5	6	5	54	35	6.0	0.20	6.20	1.63	0.22	0.96	9.0	10.2	2
A12	5-10	6	5	55	33	5.0	0.06	1.80	0.37	0.03	0.30	2.5	5.0	<1
E	10-30	5	2	52	40	5.0	0.04	0.61	0.18	0.07	0.15	1.0	1.8	4
Bt1	30-35	65	2	18	12	5.0	0.05	4.69	6.47	0.48	0.46	12.1	17.0	3
Bt2	35-50	73	3	13	9	5.0	0.06	4.26	8.45	0.59	0.34	13.6	16.0	4
Btg	50-80	53	3	22	19	4.5	0.06	1.83	6.34	0.71	0.25	9.1	14.2	5
Btg2	80-95	52	4	22	18	4.5	0.06	1.61	8.43	1.07	0.27	11.4	17.6	6
Bqm	95													
loamy, silicious, mesic Albic Duraqualf*														
A1	0-4	11	12	47	29	5.5	0.25	7.80	1.77	0.77	0.82	11.2	15.1	5
E1	4-10	13	14	47	27	5.0	0.09	2.73	0.97	0.32	0.17	4.2	8.3	4
E2	10-20	12	14	43	30	4.0	0.05	1.75	0.82	0.30	0.20	3.1	5.1	6
EB	20-30	14	15	39	33	4.5	0.04	1.35	1.08	0.29	0.24	3.0	4.4	6
Btg1	30-35	22	12	40	25	5.5	0.05	2.01	2.11	0.49	0.29	4.9	7.2	7
Btg2	35-40	31	6	30	33	5.5	0.06	3.12	3.59	0.67	0.39	7.8	10.3	6
Bqm	40													

*new subgroup proposed by Fitzpatrick *et al.* (1992)

Ferruginous nodules and ferricrete

The powder XRD patterns from whole ground samples of A-B horizon nodules (Fig. 1b) and ferricrete fragments (Fig. 1c) show sharp strong quartz peaks (25 to 35% quartz), peaks for hematite, maghemite and kaolinite. Small amounts of goethite were also identified in both samples.

Bt horizon

The Bt horizon of the Duraqualf profile has a weakly developed microstructure with very angular blocky peds and undulating irregular ped faces that are partially accommodated with incompletely separated planar voids.

Coarse mineral components (>50 μm) are smooth and subangular, moderately sorted grains with variable sphericity and composed dominantly of quartz with rarely occurring, generally weakly weathered feldspars, acicular micas and opaques. There are no compound mineral grains or rock fragments.

The fine mineral component (25 μm) consists of speckled and dotted clay with iron oxides with a strongly variable degree of impregnation giving colours ranging from grey to yellowish brown in transmitted plane light.

The groundmass of the thin section shows a speckled b-fabric. The groundmass has a very clear single and double spaced porphyric c/f related distribution. Amorphous pedofeatures of
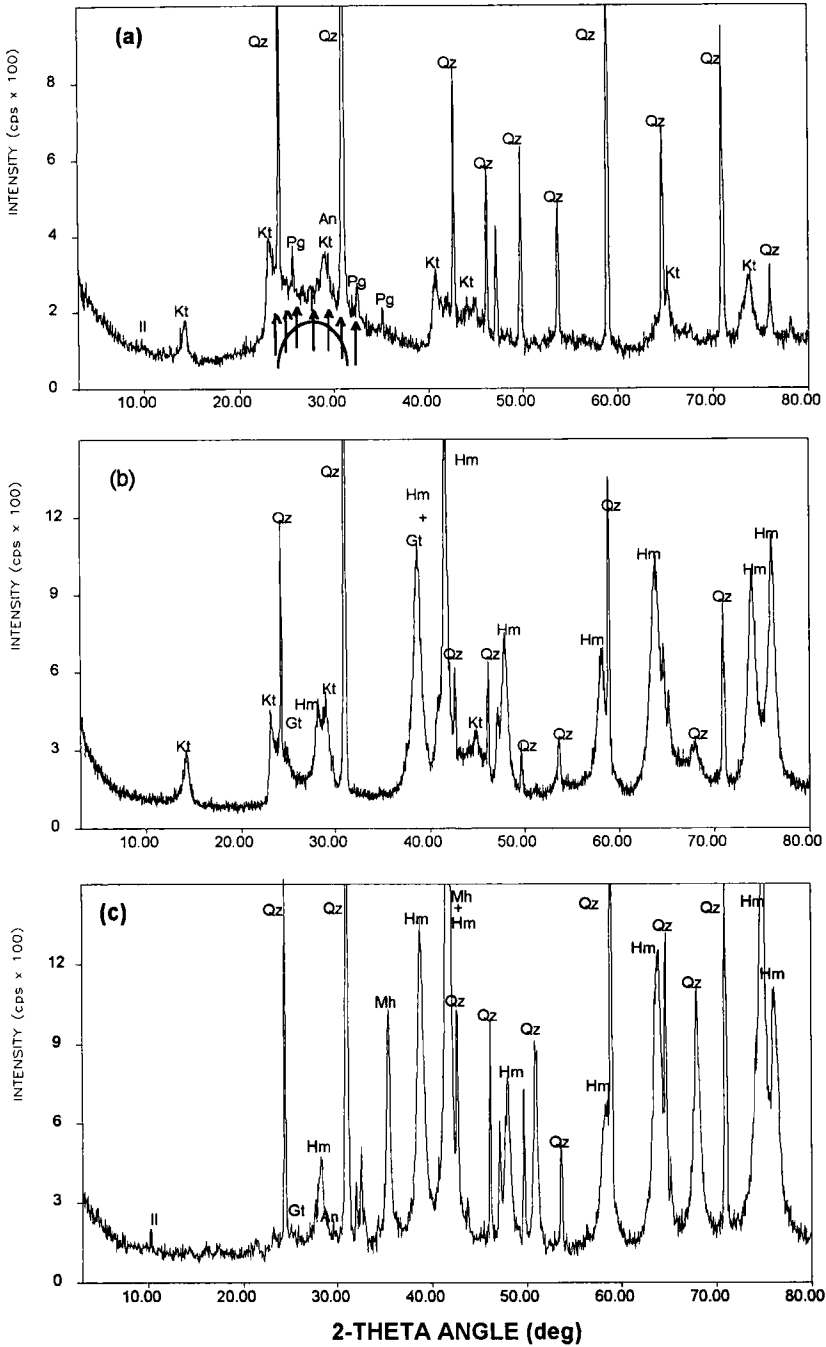
Fig. 1.   Powder X-ray diffraction patterns of: (a) columnar duripan in strongly weathered mottled colluvium/saprolite, (b) iron-rich glæbules in A-B horizon of Aquic Durixeralf, (c) ferricrete. Qz, quartz; Kt, kaolinite; Hm, hematite; Mh, maghemite; Gt goethite; Il, Illite; Pg, plagioclase; An, anatase.
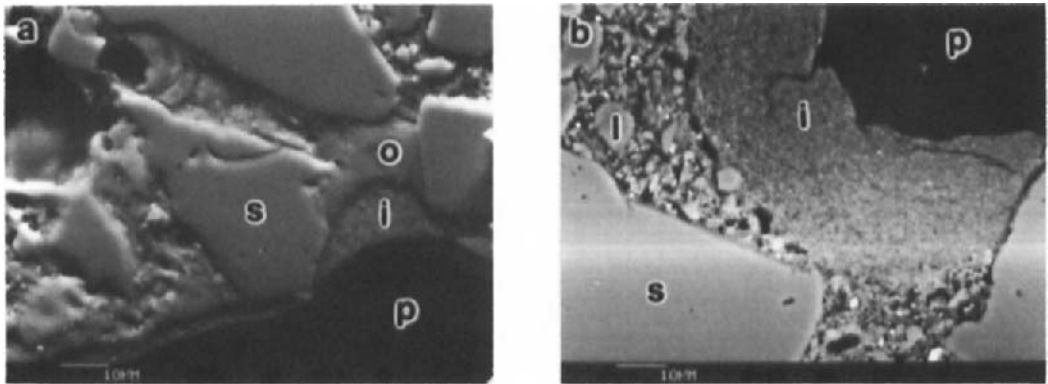
Fig. 2. SEM backscatter micrographs of polished thin sections of duripan material from a loamy, siliceous, mesic Albic Duraqualf showing **a)** pitted quartz sand grains (S), outer pore rind (O), inner pore rind (I), soil pore (P), and **b)** an area with (I) inner rind, silt sized quartz (L), sand sized quartz (S) and soil pore (P).

subrounded, impregnated iron nodules (50 - 500 μm diameter) with sharp boundaries comprise 1% of the matrix, are randomly distributed and are unreferred.

The fabric has passage features 50 - 100 μm thick with diffuse boundaries. Textural pedofeatures occur as clay coatings (0.02 - 0.05 mm thick) on grains and voids. Depletion hypocoatings occur as mottles of variable size depleted of iron oxides. These features are normally associated with planar voids and channels. Boundaries with the adjacent groundmass are normally very sharp and with prominent contrast. Depletion of iron oxides is also present in textural pedofeatures.

Duripan

The duripan typically has a coarse mineral component consisting of smooth, poorly sorted sub angular, single mineral grains. Composition is dominated by quartz with unevenly distributed but infrequently occurring feldspars, rock fragments and acicular micas. Rock fragments comprise 2 % of the coarse fragments and are subrounded blocky fragments of sandstone and schist 1 to 2 mm diameter with smooth surfaces. Grains and fragments are fresh or slightly altered. The surfaces of quartz sand fragments show some pitting and etching. The mineral components have a c/f limit at 10 μm. The c/f ratio is 30:70.

The fine mineral material is limpid yellow-brown, mainly clay sized material containing optically amorphous iron oxides. The yellow brown material has a speckled appearance in transmitted plane polarized light. The material has a speckled appearance in cross polarised light with laminar interference patterns along voids.

The groundmass in the thin section from the Duraqualf profile has a stipple speckled b-fabric and porostriated partial fabrics around pores and infillings. The ground mass shows a very clear single and double spaced porphyric c/f related distribution in some areas. In other
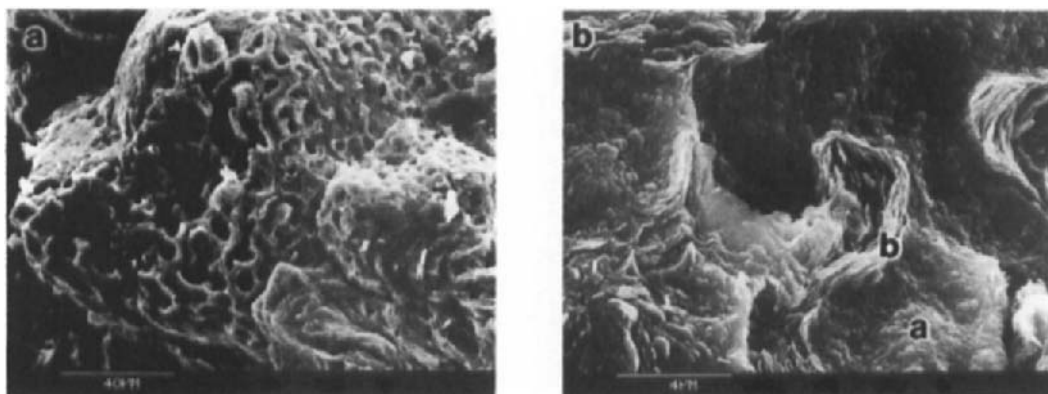
Fig. 3. SEM backscatter micrographs of a fracture surface of a fragment of duripan showing **a)** the pockmarked surface and **b)** pockmarking at higher magnification showing oriented clay bridges between grains (B) and surface deposits of amorphous silica (A).

areas there is a bridged grain structure with stipple speckled silica cement bridging grains and partial pore infillings of oriented clay which is strongly birefringent in cross polarised light.

The scanning electron micrograph of the polished thin section cut from outcropping duripan adjacent to the Durixeralf profile (Fig. 2a) shows pitted quartz sand grains embedded in a matrix of silt sized quartz grains with pore infillings of clay and clay-sized quartz. The pore lining has an inner rind of quartz and clay-sized quartz and an outer rind of clay cemented with amorphous silica, which is more resistant to the polishing process and stands out topographically from the inner rind (Fig. 2b). The inner rind increases in silica content (EDAX analyses - not shown) from the inner surface to its contact with the matrix in the bottom left hand side of the pore shown in Fig. 2a. At higher magnification (Fig. 2b) the backscattered image reveals the coarser grained texture (*i.e.* reflects an increase in the amount of quartz particles) towards the outer part of the rind at this point. There are minor mineral occurrences of muscovite, ilmenite and rutile.

Scanning electron micrographs of a fracture surface of a fragment of duripan material from the Duraqualf profile show pock-marked surface features (Fig. 3a) which at higher magnification (Fig. 3b) appears as oriented layer silicates bridging (cementing) silt sized grains in the matrix of the duripan.

Ferruginous nodules in A-B horizons of the Durixeralf

A-B horizon nodules have a vesicular microstructure. One in 10 nodules have a strongly developed granular structure of older nodules. The coarse mineral component is dominantly poorly to moderately sorted subangular blocky, sand sized single mineral grains with rare acicular mica fragments. Nodules with a strongly developed granular structure have rough, digitate, subangular grains. The fine mineral component is optically opaque with small patches which are highly reflective under cross polarised light.
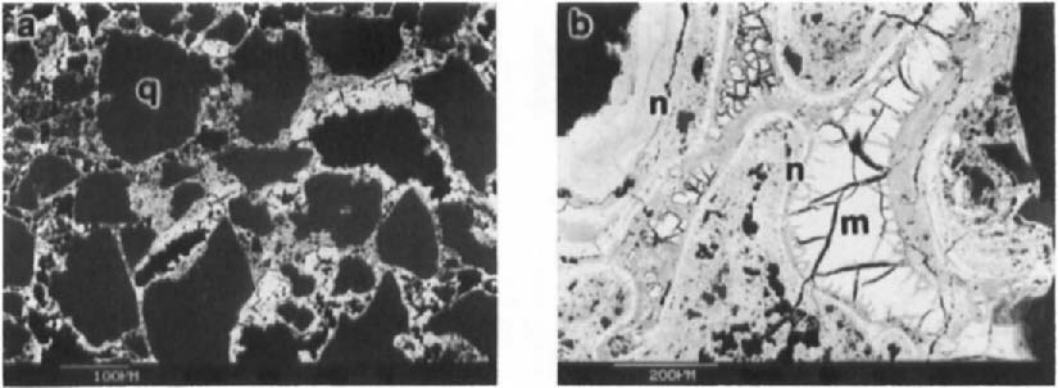
Fig. 4. SEM backscatter micrographs of A-B horizon nodules from the Aquic Durixeralf showing: (a) etched quartz grains (Q) in a hematite/maghemite matrix (M), (b) primary iron nodules (N) cemented together in a hematite/maghemite matrix (M).

Scanning electron micrographs of polished thin sections of A-B horizon nodules show highly etched quartz grains in an iron rich matrix (Fig. 4a).   Nodules with a compound structure have bright and dark iron oxide cementing materials (Fig. 4b). The darker cement is lower in iron content and has some kaolinite mixed in with the hematite and maghemite cement. The darker matrix is considered to be a more recent infill of cracks in the bright matrix.

DISCUSSION AND CONCLUSIONS

The duripan has a narrow landscape context in the Warren Catchment associated with colluvial fans. The presence of compound rock fragments of metasandstone and schist in the duripan indicates that the duripan has formed in siliceous transported material (colluvium).

The clay coatings and X-ray diffraction patterns identified illuviation of kaolinite into the matrix and pores of the duripan. The sand sized skeletal grains and silt size groundmass of the duripan are bridged by and embedded in infillings and coatings of iron oxides, silt and clay.

Silicification of the matrix and pore linings by amorphous silica to form the duripan is associated with weathering processes within and outside of these soil profiles. The mono silicic acid produced by weathering is adsorbed throughout the plasma phase, where it is precipitated in contact with high surface area clay, sesquioxide, and weathered primary mineral surfaces (Chadwick et al., 1987).

Large amounts of silica could be released in the process of the forming ferricrete 15 m higher in the landscape and the kaolinisation of the underlying silicate rocks (Stephens, 1971). Also, within a seasonally water logged soil profile, ferrolytic destruction of 2:1 layer silicates in the B horizon can release silica, iron and aluminium. The model of the process in seasonally wet soils results in either chloritization of the clay or a very low clay content Brinkman (1970). This would account for the low clay content in the B horizon of the Duraqualf profile compared with the Durixeralf profile.

The deep etching of quartz grains in ferruginous nodules of the B horizon (Fig. 4a) is evidence for silica solubilization from quartz grain surfaces during the process of nodule formation. The compound ferruginous nodules in the AB horizon of the Durixeralfs contain several generations of ferruginous nodular structures which indicate multiple stages of breakup, colluviation (causing rounding) and recementing of ferricrete.

Pitting of the sand sized, quartz skeletal grains in the scanning electron micrograph of the duripan (Fig. 2a) shows that there has been solubilization of silica *in situ*. The large weatherable surface area of quartz, with a matrix of silt sized quartz grains and pore infillings of clay and clay sized quartz evident in Fig. 2a and b is further evidence for *in situ* mobilisation and deposition of amorphous silica in formation of the duripan.

Stephens (1971) determined that duripans and ferricretes in the Mid-North Region of South Australia occurred in association with ancient river terraces. Alley (1977) put these in the narrower environmental context of a lake system formed by fault uplift of the basement rocks and a thick podocarp forest cover in the mid to late Tertiary period. He found that duripans overlaid kaolinised bedrock while the ferricretes, slightly higher in the landscape, did not. The duripan and associated kaolinised bedrock occurred in the higher parts of pediments and there was greater weathering here, where the water table was generally low but fluctuated considerably owing to variations in inflow, than on valley floors.

The age of weathering of the kaolinised bed rock is uncertain and several weathering events may be superimposed. Oxygen isotope data from kaolinite in weathered pegmatite exposed in the Warren Catchment are consistent with a mid to late -Tertiary age for kaolinisation of bedrock under the duripan (Bird and Chivas, 1989).

The ferricrete and duripan surfaces slope down towards the present valley floor. Consequently, the present drainage system was already established at the time when the ferricrete and duripan were forming. This indicates the stability of this landform and the long period of time available for the solution and precipitation processes that formed the duripan.

The broad scenario for duripan formation with the silica being released by deep kaolinisation of the underlying bedrock, ferricrete formation and the *in situ* weathering of siliceous colluvium in a poorly drained part of the landscape may be applied to the formation of the duripans in the Warren Catchment, in the Adelaide Hills of South Australia.

ACKNOWLEDGMENTS

REFERENCES

Alley, N.F., 1977. Age and origin of laterite and silcrete duripans and their relationship to episodic tectonism in the Mid-north of South Australia. J. Geol. Soc. Aust., 24: 107-116.

Bird, M.I. and Chivas, A.R., 1989. Stable-isotope geochronology of the Australian regoloty. Geochem. Cosmochim. Acta, 59: 3239-3256.

Brinkman, R., 1970. Ferrolysis, a hydromorphic soil forming process. Geoderma, 3: 199-206.

Chadwick, O.A., Hendricks, D.M. and Nettleton, W.D., 1987. Silica in duric soils: I. A depositional model. Soil Sci. Soc. Am. J., 51: 975-982.

Fitzpatrick R.W., Hudnall, W.H., Lowe, D. J., Maschmedt, D.J. and Merry, R.H., 1992. Proposed changes in the classification of Histosols, Alfisols, Andisols, Aridisols, Inceptisols, Entisols and Spodosols in South Australia. CSIRO (Australia) Division of Soils Technical Report No. 51/1992. 33 pp.

Gordon, S., 1969. History of the Mount Crawford Area. Williamstown Historical Society Monograph.

Hollingsworth, I.D. and Fitzpatric, R.W. The nature and origin of a duripan in an Aquic Durixeralf-Duraqualf toposequence: 1. Soil landscape relationships. Aust. J. Soil Res. (in press)

Kerr, P.F., 1977. Optical Mineralogy. McGraw-Hill Book Co., New York.

McDonald, R.C., Isbell, R.F., Speight, J.G., Walker, J. and Hopkins, M.S., 1990. Australian Soil and Land Survey Field Handbook. 2nd Ed. Inkata Press, Melbourne.

Norrish, K. and Hutton, J.T., 1969. An accurate X-ray spectrographic method for the analysis of a wide range of geological samples. Geochem. Cosmochim. Acta, 33: 431-453.

Soil Survey Staff, 1992. Keys to Soil Taxonomy, fifth edition. SMSS Technical Monograph No. 19. Pocahontas Press, Blacksburg, Virginia, 556 pp.

Stephens, C.G., 1971. Laterite and silcrete in Australia: A study of the genetic relationships of laterite and silcrete and their companion materials, and their collective significance in the formation of the weathered mantle, soils, relief and drainage of the Australian continent. Geoderma, 5: 5-52.

Micromorphology and composition of silica accumulations in a hardpan

L.A. Sullivan

*Resource Science and Management, University of New England-Northern Rivers,
PO Box 157 Lismore, NSW 2480, Australia*

ABSTRACT

Sullivan, L.A., 1994. Micromorphology and composition of silica accumulations in a hardpan. In: A.J. Ringrose-Voase and G.S. Humphreys (Editors), Soil Micromorphology: Studies in Management and Genesis. Proc. IX Int. Working Meeting on Soil Micromorphology, Townsville, Australia, July 1992. Developments in Soil Science 22, Elsevier, Amsterdam, pp. 845-853.

The morphology and composition of silica coatings and silica impregnations in a hardpan underlying a desert loam (Haplic Durargid) from north-western New South Wales were examined. Optical properties and electron microprobe analyses indicate that these features were composed of opal-A. The coatings were remarkably pure being 99.1% SiO_2 (excluding water). X-ray maps indicate that the silica impregnations were also calcite depletion pedofeatures. Even at high magnifications in an SEM (*i.e.* up to ×5,000), the silica coatings had a dense, vitreous appearance with few voids. These voids often contained spheroids of silica up to 1 μm in size. The original plant cell structure in silicified root remnants was remarkably well preserved and often contained silicified actinomycete hyphae.

INTRODUCTION

Soils with silica-indurated subsoil layers - termed hardpan horizons - occupy a large portion of the semi-arid and arid regions of Australia (Stace *et al.*, 1968) and occur within a wide variety of soil types (Chartres, 1985). Silica is considered to be the main cementing agent within these horizons with both coatings and impregnations of silica around voids having been observed in soil thin sections (Brewer *et al.*, 1983; Chartres, 1985).

Despite the widespread distribution of hardpan horizons in Australia, there have been only few detailed micromorphological studies, and no detailed submicromorphological studies of these horizons. This study examines the morphology and composition of the silica accumulations in a hardpan layer using light microscopy, electron microscopy and electron analytical techniques. The relationships of silica to other soil components in the hardpan were also examined.

METHODS AND MATERIALS

Undisturbed lumps of soil, approximately 800 cm^3, were obtained from the 40 - 45 cm layer of a hardpan horizon (20 - 60cm depth) beneath a desert loam soil (Haplic Durargid; Soil Survey Staff, 1975) (Dr1.55; Northcote, 1979) from a site (latitude 29°16'S, longitude 141°
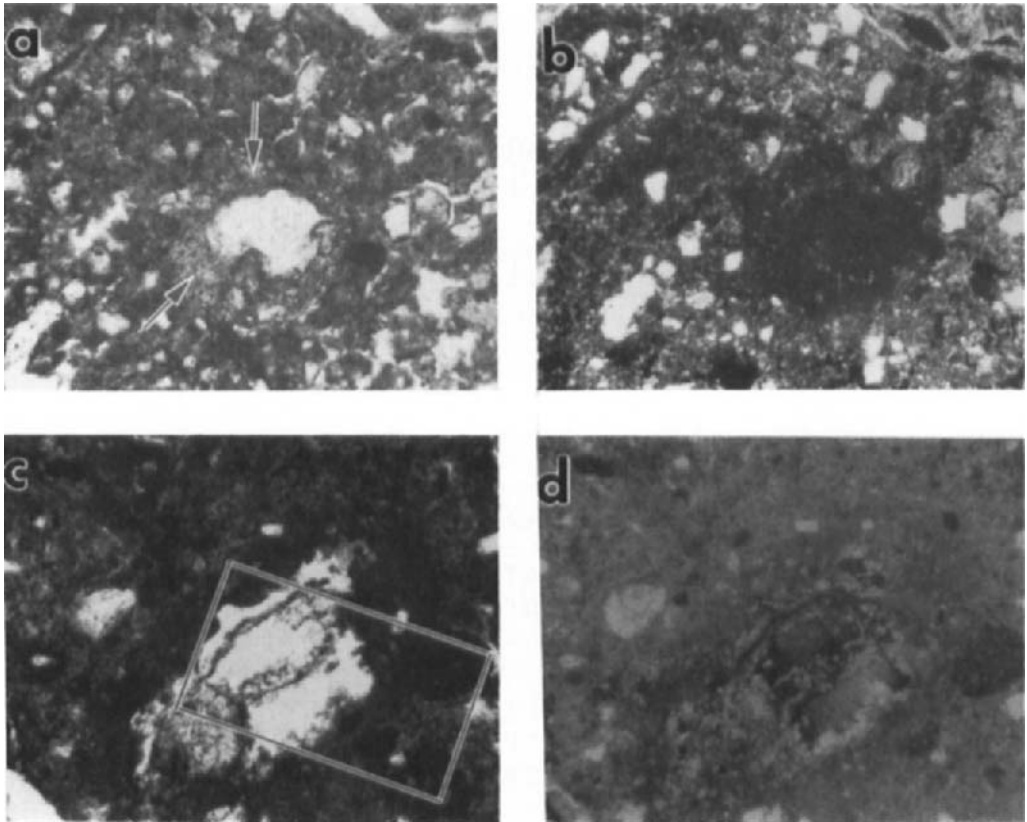
Fig. 1. Photomicrographs of: (*a* - *b*) a thin section across a thick silica coating around a channel in plane polarized and circularly polarized light, respectively; (*c* - *d*) a thin section across a silica coating and impregnation around a channel in plane polarized and circularly polarised light, respectively. Frame width is 0.83 mm.

41'E) near Tibooburra, N.S.W., Australia. This horizon consisted of nine wavy laminar structural units all of which were visually similar: the 40 - 45 cm layer was one of these. The site, with an average rainfall of 214 mm, was on the middle of a long, gentle (*i.e.* <2°) slope with vegetation absent for a distance of at least 5 m. The soil was in a dry state when sampled.

Vertically-oriented thin sections of the 40 - 45 cm layer were made by the method of FitzPatrick (1984). These were then examined using both an optical microscope and, after carbon coating, an ETEC microprobe equipped with three wavelength dispersive spectrometers. The electron microprobe analyses were performed at an accelerating voltage of 15 kV with a regulated specimen current of 38 nA.

Fragments of soil material less than 2.5 cm in maximum dimension from the 40-45 cm layer were fixed to 2.5 cm diameter aluminium discs, carbon coated and examined in a Philips 505
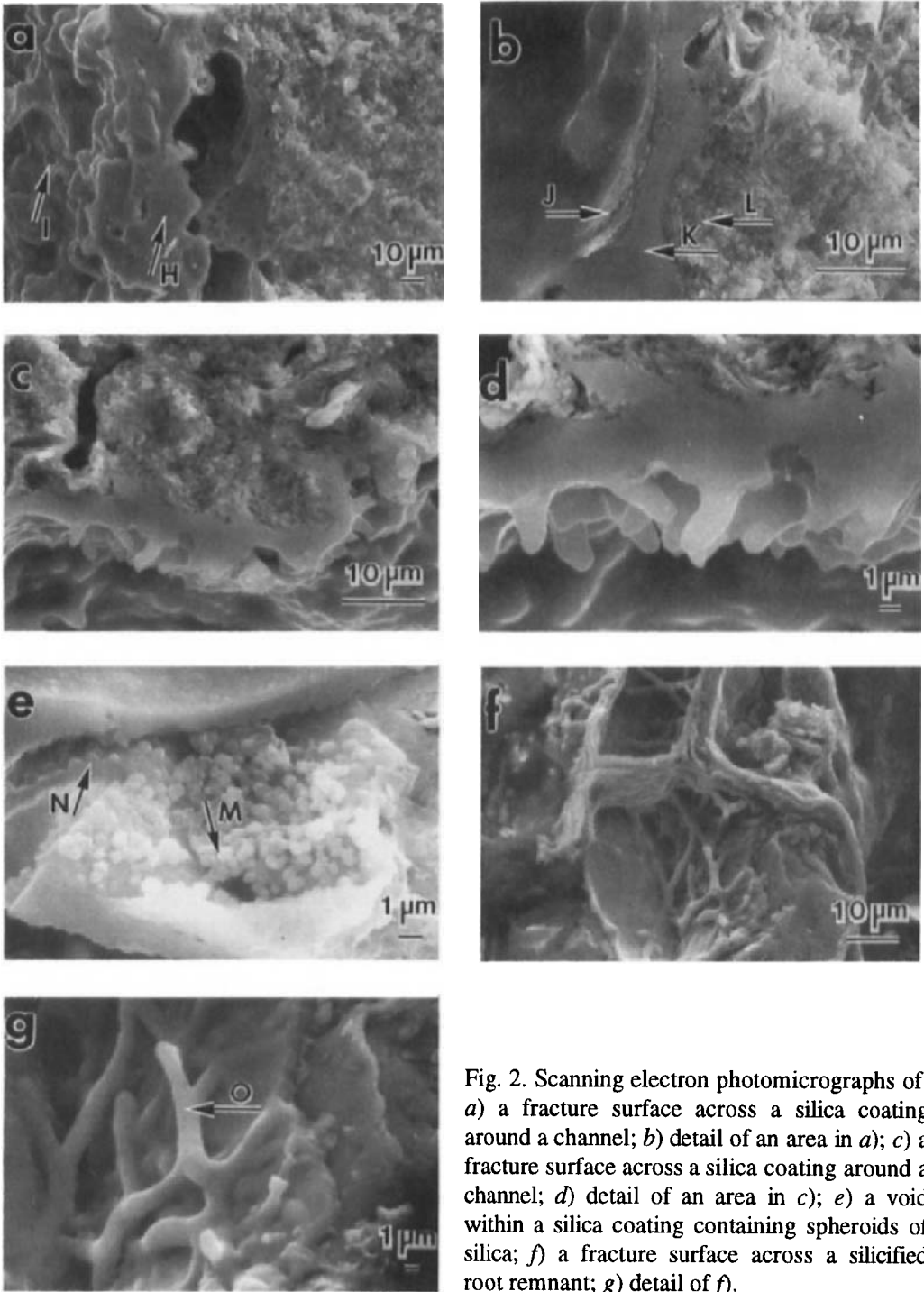
Fig. 2. Scanning electron photomicrographs of: *a*) a fracture surface across a silica coating around a channel; *b*) detail of an area in *a*); *c*) a fracture surface across a silica coating around a channel; *d*) detail of an area in *c*); *e*) a void within a silica coating containing spheroids of silica; *f*) a fracture surface across a silicified root remnant; *g*) detail of *f*).
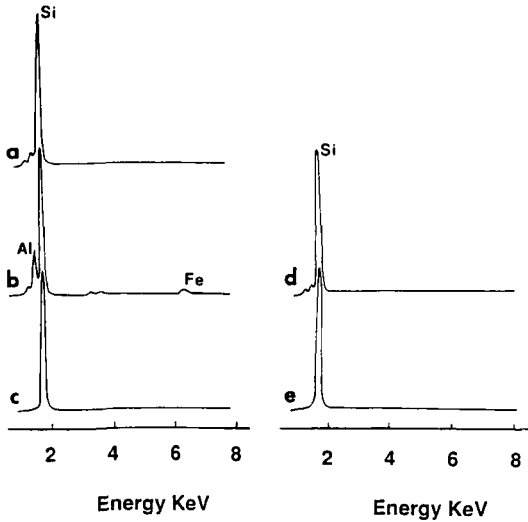
Fig. 3. EDXRA spectra from an electron beam (15 kV accelerating voltage) focussed on: a) the point indicated by arrow M in Fig. 2e; b), c) and d), the points indicated by arrows J, K, and L, respectively, in Fig. 2b, and; e) the point indicated by arrow O in Fig. 2g.

scanning electron microscope (SEM) equipped with an energy dispersive X-ray analyser (EDXRA).

A micromorphological description of the soil thin sections using the terminology of FitzPatrick (1984) is given in the Appendix.

RESULTS AND DISCUSSION

Light microscopy

Fracture surfaces across thick (up to 100 μm) silica coatings around the channels in the hardpan layer had a clear vitreous appearance using a stereomicroscope. In thin section, these silica coatings (*e.g.* the coating indicated by the arrows in Fig. 1a) had a clear to grey appearance in transmitted plane polarized light and were isotropic (Fig. 1b), whereas the silica impregnations surrounding the coatings had a dark grey appearance in both transmitted plane (Fig. 1c) and transmitted circularly polarized light (Fig. 1d), and a white appearance in reflected plane light.

The root remnant in the channel shown in Fig. 1c was silicified (see Fig. 4) and, like many of the silica coatings in the hardpan layer, was coated with calcite crystals and alumino-silicate clay.

Scanning electron microscopy

Fig. 2a shows a portion of a fracture surface across a silica coating (up to 70 μm thick) in the SEM. The pore surface of the silica coating (indicated by arrow I in Fig. 2a) was undulating. Fracture surfaces across silica coatings (*e.g.* area indicated by indicated by arrow H in Fig. 2a) were very smooth and vitreous and had a generally massive appearance, even at high magnifications (*e.g.* Fig 2b), with only occasional voids. These voids often contained spheroids of silica up to 1 μm in size (Fig. 2e, an EDXRA analysis from the point indicated by

arrow M in Fig. 2e shown in Fig. 3a). All of these spheroids appeared to be fused onto the surface of the coating (*e.g.* see area indicated by arrow N in Fig. 2e) and were morphologically similar to the inorganic opaline spheres on the quartz grains shown in Drees *et al.* (1989). Finger-shaped protuberances of silica up to 2 μm wide and 5 μm long were occasionally observed projecting from silica coatings into channels (Fig. 2c and d).

Like many of the other silica coatings in the hardpan layer, a thin (up to 5 μm) layer of clay (indicated by arrow J in Fig. 2b) coated the silica coating in Fig. 2a. EDXRAs of the points indicated by the arrows J, K and L in Fig. 2b are shown in Fig. 3b, c and d, respectively).

As shown in Fig. 1b, silicified root remnants often had hollow centres which had probably been consumed by soil fauna prior to silicification. However, the outer cell layers of the root were remarkably well preserved. Fig. 2f shows an area of this silicified root remnant in which there are solid branching 'ropes', around 2 μm in diameter, within the silicified root cells. These are shown in greater detail in Fig. 2g. An EDXRA analysis from the point indicated by arrow O in Fig. 2g is shown in Fig. 3e, and indicates that these 'ropes' were composed of silica. These silica features were morphologically similar to the vegetative hyphae of actinomycetes observed by Mayfield *et al.* (1972), and are most probably silicified actinomycete hyphae. Actinomycetes are known to colonize root cells extensively subsequent to cell lysis (Martin, 1978).

Electron microprobe analysis (EMA)

X-ray images for Al, Si, and Ca of the region of the silica accumulation within the box in Fig. 1c are shown in Fig. 4. The backscattered electron image (BSE) and Si X-ray image in Fig. 4 show that there was a thin (approximately 10 μm) coating of silica lining this channel. The mean SiO_2 content of ten unnormalized EMAs of non-porous regions of this silica coating was 91.92% indicating that these features had a hydration of approximately 8%. This hydration content, the massive and occasionally spheroidal SEM morphology and isotropic light optical properties indicate that the silica in these accumulations is composed of opal-A (Drees *et al.*, 1989). Opaline spheroids were not apparent within the non-porous silica coatings even at high magnifications in the SEM. It is likely that the silica spheroids, of which opal-A is composed (Drees *et al.*, 1989), within the coatings were either (1) smaller than could be resolved at ×5,000 (*i.e.* <150 nm in diameter) or (2) cemented together by gels similar to those in silica extracted from duricrusts as observed by Blank and Fosberg (1991) using transmission electron microscopy.

The mean composition of non-porous regions of the silica coating shown in Fig. 4 (from ten EMAs and normalised to 100%) was as follows: SiO_2, 99.09%; Na_2O, 0.04%; MgO, 0.06%; Al_2O_3, 0.29%; P_2O_5, 0.04%; K_2O, 0.02%; CaO, 0.26%; TiO_2, 0.02%; Cr_2O_3, 0.02%; FeO, 0.15% and SO_3, 0.02%. These EMAs show that the silica coatings in this soil were remarkably pure which agrees with previous analytical studies of inorganic opal-A (Drees *et al.*, 1989; Blank and Fosberg, 1991) and opaline silcrete (Smale, 1973).

The Ca, Al and Si X-ray maps in Fig. 4 indicate that the silica coating was coated in some places with calcite crystals and by a thin layer of aluminosilicate clay. Fig. 5 shows the normalised concentrations of SiO_2 in the boxes shown in Fig. 4 and of the silica coating adjacent to box 1. Both Fig. 5 and the silicon x-ray image in Fig. 4 show that adjacent to the silica coating was an impregnation of silica (up to 20% SiO_2 enrichment) of approximately
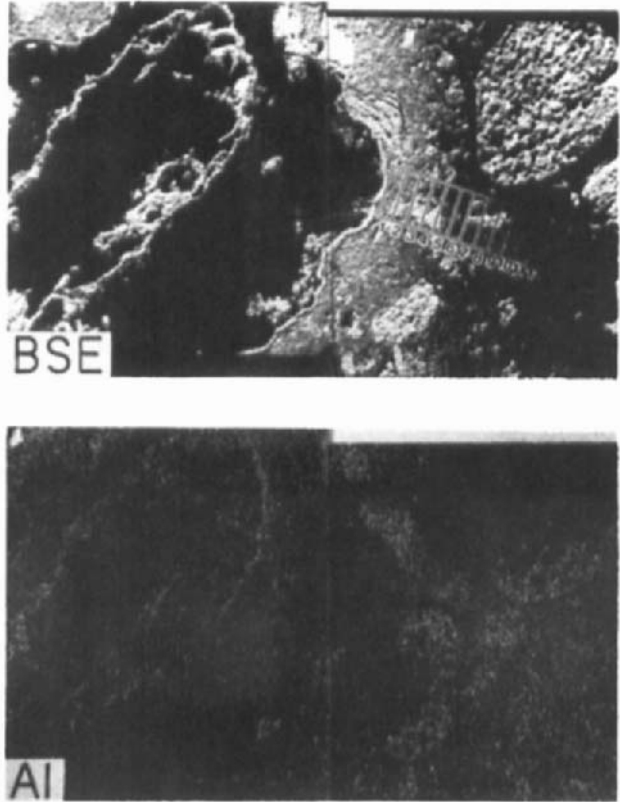
Fig. 4. A backscattered electron image (BSE) and aluminum (Al), silicon (Si) and calcium (Ca) X-ray maps of the area across the channel defined by the box in Fig. 1c. The length along each image is 690 μm.

100 μm thickness (up to box 6). This impregnation of silica corresponds to the areas which have a milky white appearance in reflected plane light (Fig. 1d).

The silica impregnation in Fig. 1b was depleted of calcium (see Fig. 4) as were other impregnations of silica around channels in this soil layer. Two mechanisms might account for the lower concentrations of calcium (most probably in the form of calcite, Sullivan, 1988). Calcite might have been removed from these regions during or prior to silica impregnation. Alternatively, if the precipitation of the calcite within these had been excluded simply because of inaccessibility. Since the soil matrix in the silica impregnation material was quite porous even after impregnation (e.g. the mean unnormalised EMA total for the 12 elements analysed in the boxes 1, 2, 3 and 4 in Fig. 4 was only 66%), it is most probable that the period of calcite depletion occurred during, or prior to, silica impregnation. The shared zone of calcite depletion and silica enrichment evident in Fig. 4 suggests a close association between the processes of calcite depletion and silica enrichment. Certainly, mechanisms for silica precipitation accompanied by calcite dissolution have been proposed (Siever, 1962) and the replacement of calcites by silica has been commonly observed in limestones (Smale, 1973) as well as in dolomites (Dietrich et al., 1963) and geodes (Hayes, 1964). Therefore, the calcite depletion pedofeatures most probably resulted from the dissolution of the calcite in these regions by silica-precipitating solutions.
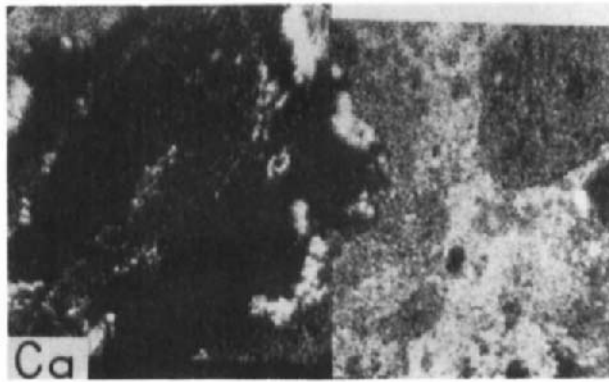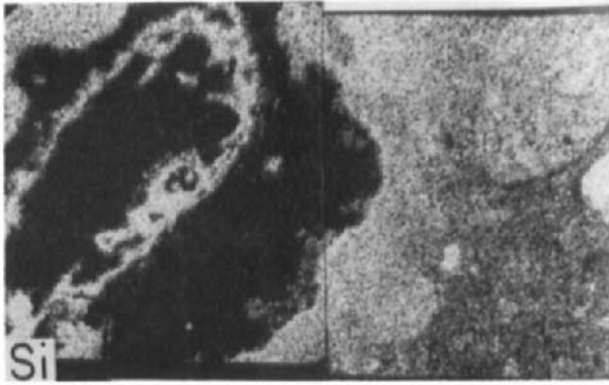
Fig. 4. Continued.
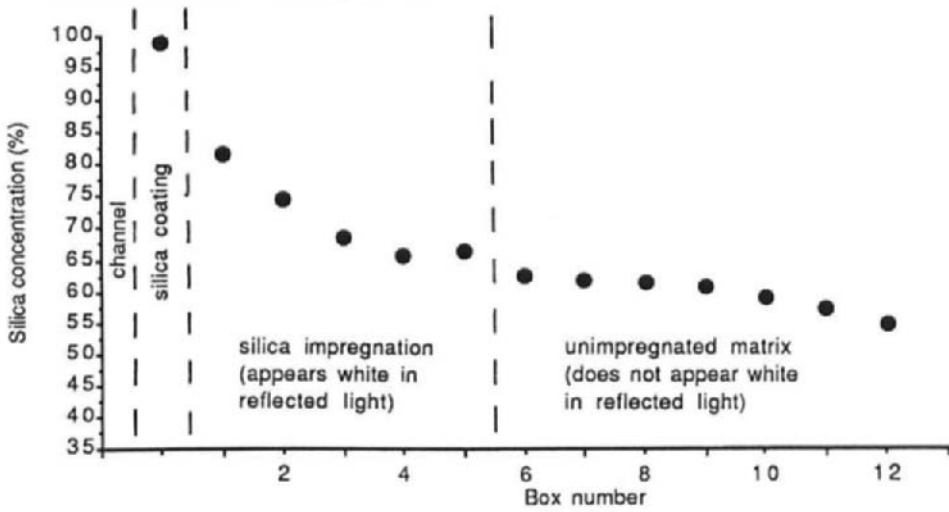
Fig. 5. The normalised SiO_2 concentrations in the boxes shown in Fig. 4 and of the silica coating adjacent to box 1 in Fig. 4.

CONCLUSIONS

1. Even at high magnifications in an SEM, the silica coatings had a dense, vitreous appearance. The occasional voids that did occur within silica coatings often contained spheroids of silica up to 1 μm in size. The original plant cell structure in silicified root remnants was well preserved and contained silicified actinomycete hyphae.
2. The optical properties and EMAs of the silica accumulations indicate that these features were composed of opal-A and were remarkably pure being 99.1% silica (excluding water).
3. EMAs indicate that the silica impregnations around channels were also calcite depletion pedofeatures. These calcite depletion pedofeatures most probably resulted from the dissolution of the calcite by silica-precipitating solutions.

REFERENCES

Blank, R.R. and Fosberg, M.A., 1991. Duripans of the Owyhee Plateau region of Idaho: genesis of opal and sepiolite. Soil Sci., 152: 116-133.
Brewer, R., Sleeman, J.R. and Foster, R.C., 1983. The fabric of Australian soils. In: Soils: An Australian Viewpoint. CSIRO, Melbourne/Academic Press, London, pp. 439-476.
Chartres, C.J., 1985. A preliminary investigation of hardpan horizons in north-west New South Wales. Aust. J. Soil Res., 23: 325-337.
Dietrich, R.V., Hobbs, C.R.B. (Jr.) and Lowry, W.D., 1963. Dolomitization interrupted by silicification. J. Sediment. Petrol., 33: 646-663.
Drees, L.R., Wilding, L.P., Smeck, N.E. and Senyaki, A.L., 1989. Silica in soils: quartz and disordered silica polymorphs. In: J.B. Dixon and S.B. Weed (Editors), Minerals in Soil Environments. 2nd Ed. Soil Sci. Soc. Am., Madison, Wisconsin, pp. 913-973.
FitzPatrick, E.A., 1984. Micromorphology of Soils. Chapman and Hall, London, 433 pp.
Hayes, J.B., 1964. Geodes and concretions from the Mississippian Warsaw Formation, Keokuk Region, Iowa, Illinois, Missouri. J. Sediment. Petrol., 34: 123-133.
Mayfield, C.I., Williams, S.T., Ruddick, S.M. and Hatfield, H.L., 1972. Studies on the ecology of actinomycetes in soil. IV. Observations on the form and growth of streptomycetes in soil. Soil Biol. Biochem., 4: 79-91.
Northcote, K.H., 1979. A Factual Key for the Recognition of Australian Soils. Rellim Technical Publications, Adelaide, 123 pp.
Siever, R.L., 1962. Silica solubility 0-200°C and the diagenesis of siliceous sediments. J. Geol., 61: 127-149.
Smale, D., 1973. Silcretes and associated silica diagenesis in Southern Africa and Australia. J. Sediment. Petrol., 43:1077-1089.
Soil Survey Staff, 1975. Soil Taxonomy. U.S. Dept. Agric. Handb. 436, U.S. Gov. Printing Office, Washington, D.C., 754 pp.
Stace, H.C.T., Hubble, G.D., Brewer, R., Northcote, K.H., Sleeman, J.R., Mulcahy, M.J. and Hallsworth, E.G., 1968. A Handbook of Australian Soils. Rellim Technical Publications, Glenside, South Australia, 429 pp.
Sullivan, L.A., 1988. Surfaces and Pedological Features Associated with Planar Pores, Channels, Chambers, Vesicles and Cavities. Ph.D. Thesis, University of Sydney, N.S.W., 355 pp.

APPENDIX

A micromorphological description using the terminology of FitzPatrick (1984) of thin sections of the 40 - 45 cm laminar unit of the hardpan horizon follows.

The laminar structural unit varied in thickness from 50 to 20 mm. The upper and lower surfaces were wavy and moderately to strongly accordant with the surfaces of adjacent structural units. The unit had a complex structure with non-indurated composite coatings both above and below.

The upper composite coating was from 1 to 11 mm thick and consisted of (mainly) highly convoluted clay coatings and regions of clay pellets, commonly from 100 - 200 μm in size, similar to those described by Chartres (1985). Crystals of strontiobarytes, acicular calcium carbonate and gypsum were frequently found in the pores between the clay pellets. The lower composite coating was from 1 to 5 mm thick and consisted of regions of clay pellets, and thick (< 600 μm), highly convoluted clay coatings.

The silica-indurated material comprised $c.70\%$ of the laminar unit and was up to 35 mm thick. It was separated (moderately accordantly) from the upper composite coating by a planar pore space up to 150 μm wide. The silica indurated material was composed of laminar aggregates up to 10 mm by 30 mm in size. All of the surfaces of these aggregates were rough and covered by wavy to convoluted coatings of oriented clay up to 300 μm thick. Micrite was often found on the surfaces of these clay coatings. Clusters of acicular calcium carbonate crystals were often found in the inter-aggregate and the intra-aggregate pore space in this zone.

Towards the top of the silica indurated material, roughly parallel with the uppermost surface of this zone, was a layer of anisotropic silica up to 50 μm thick which had a dirty grey appearance in plane polarized light and a milky white appearance in reflected light.

Channels up to 1 mm in diameter occupied 2-5% of the area in this zone. Most of these channels were coated with a thick (< 100 μm) coating of a clear to dirty grey coloured (in plane polarized light), isotropic silica. Some of these silica coatings exhibited coralloid outgrowths of clear isotropic silica into the channel pore space. The walls surrounding channels coated with silica were impregnated with isotropic silica. These silica impregnations had a milky-white appearance in reflected light and a dirty grey appearance in plane polarized light. Coatings or accumulations of micrite and thin coatings of oriented clay lined many of the silica coated channels. Most of the silica-coated channels also contained silicified root remnants.

The <2 mm size fraction consisted of about 85% rounded quartz grains up to 800 μm in size, about 5% rounded wustenquartz and about 10% rounded grains of either isotropic siliceous material or ironstone.

The fine matrix had a light brown appearance in plane polarized light and was strongly anisotropic with randomly oriented, very short and narrow, anisotropic units which appeared to be calcite, as well as clay domains.

This Page Intentionally Left Blank

Strength characteristics of spodic horizons in soils of the Atlantic Coastal Plain, U.S.A.

M.C. Rabenhorst and R.L. Hill

University of Maryland, College Park, MD 20742, USA

ABSTRACT

Rabenhorst, M.C. and Hill, R.L., 1994. Strength characteristics of spodic horizons in soils of the Atlantic Coastal Plain, U.S.A. In: A.J. Ringrose-Voase and G.S. Humphreys (Editors), Soil Micromorphology: Studies in Management and Genesis. Proc. IX Int. Working Meeting on Soil Micromorphology, Townsville, Australia, July 1992. Developments in Soil Science 22, Elsevier, Amsterdam, pp. 855-863.

During late Pleistocene and Holocene times, eolian sands were redistributed as dunal deposits along portions of the Atlantic Coastal Plain. Under poorly drained conditions, soils formed in these sandy deposits commonly have spodic horizons. Spodic horizons of these Haplaquods (Alaquods) exhibit a range in moist consistence with some containing strongly indurated ortstein. This investigation was undertaken to elucidate the cause of ortstein induration. Field estimates of moist consistence were compared with measurements of soil strength using modulus of rupture for air dry samples and unconfined penetrometer under saturated conditions. The strength of the ortstein samples is not due to cementation by either Si or Fe, and soil strength appears to be inversely related to total organic C. Strength appears to be most closely related to the presence of monomorphic coatings of fine materials bridging framework sand grains. A pyrophosphate extractable Al phase may be present in the bridging material, but silicate clays identified in coatings in the ortstein may be partially responsible for the greater strength. Overall, the microfabric is more informative concerning the strength of the materials, than chemical characteristics of the samples.

INTRODUCTION

On the lower Delmarva peninsula there are areas with sandy deposits which have water tables at or near the land surface for significant periods each year. In such areas, soils may develop spodic horizons or subsoil zones enriched with illuvial organic materials which would lead to their classification as Aquods (Soil Survey Staff, 1990). In some instances these zones (Bh or spodic horizons) become strongly indurated (presumably cemented) which has important implications for the use of these soils. These soils are of limited extent on the Delmarva Peninsula but they occur throughout the Atlantic coastal plain and, in some states, are very extensive (Daniels *et al.*, 1975; Collins, 1992).

On the Delmarva Peninsula, Aquods seem to occur primarily in sediments which were initially of fluvial origin, but were later reworked during late Pleistocene or Holocene times by eolian activity. These eolian sands are reported to have been deposited during a major period of climatic change in late Pleistocene time (10 - 30,000 years ago) (Denny and Owens, 1979).

There is, however, some evidence that eolian activity has occurred on the Delmarva Peninsula at various points throughout the Holocene.

Ortstein is a common occurrence in Aquods. Lee *et al.*, (1988a) observed the presence of ortstein associated with spodic horizons in Aquods in the coastal plain of Florida (1000 km south of Maryland) and sought to determine the cause of the induration. They concluded that the principal reason for the induration was cementation of the coarser sand grains by Al-rich materials, and that the Al in the cemented horizons was mainly complexed by fulvic acid (Lee *et al.*, 1988b). McHardy and Robertson (1983) also identified Al as a major constituent of coatings in cemented spodic horizons in the U.K., but in addition found lower levels of Fe and higher levels of Ca than in more weakly cemented materials.

In a recent review of microscopy in Spodosols, McSweeney and FitzPatrick (1990) cite the work of several others who have related cementation in spodic horizons (development of ortstein) to various microfabrics. In general, the presence of coatings of organic-rich material (presumably complexed with Fe or Al) are indicative of a spodic horizon, and are nearly always present if the sample is indurated.

Based on the work of others as well as our own preliminary research, hypotheses on the cause of induration in these spodic horizons were developed. Possible cementing agents, include Fe or Al compounds, Si compounds or complex organic compounds. The objective of this study was to test these hypotheses regarding the major cause of cementation in indurated spodic horizons by correlating chemical extractions and micromorphological observations to strength measurements of spodic horizon materials.

METHODS AND MATERIALS

Samples for this study were collected from sites identified during an earlier study of Aquods occurring on dunal landscapes of the lower Delmarva Peninsula (Fig. 1) (Condron, 1990). The two pedons (termed sites A and B) from which samples were collected for this study were both classified as sandy, siliceous, mesic Typic Haplaquods (Soil Survey Staff, 1990) or as Typic Alaquods following recent proposed revisions to the classification of Spodosols (ICOMOD, 1991).

The soils in this study were similar in nature to those examined by Daniels *et al.*, (1975) in that they possessed very strongly expressed spodic horizons, some of which were >2 m in thickness (Condron, 1990). Within the upper meter of the spodic horizons, the soil materials ranged in moist consistence from friable through very firm to indurated. The indurated zones were considered to be ortstein and were generally discontinuous within the horizons. Soil zones of intermediate consistence (firm-brittle) were also identified. Clods, approximately 15 to 20 cm in diameter, were collected and grouped into one of three classes, "friable", "intermediate" or "cemented." Three to six clods from each of the two pedons, were collected from each consistence class.

Using a circular saw with an abrasive blade, moist clods were cut into slabs and trimmed to a size (*c.* 1 × 3 × 7 cm) appropriate for strength measurements using the modulus of rupture (MOR) equipment. Three to eight slabs were prepared from each clod and air dried. Strength determinations were made on each of the slabs using the modulus of rupture method of Reeve (1965). The mean air dry moisture content of the soils during this determination was 1.6% and ranged from 0.3 to 4.9%. Once the slabs were broken during the MOR determination, half of
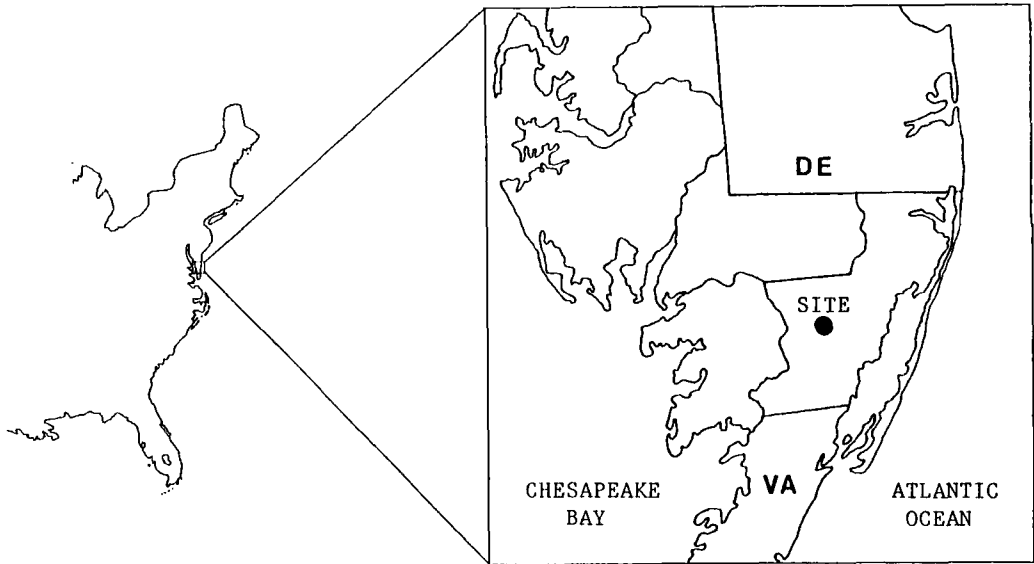
Fig. 1. Location of study site on the Delmarva Peninsula, Atlantic Coastal Plain.

each broken slab was brought to saturation with distilled water, and a measurement of unconfined strength was made using a hand held penetrometer.

Selected slabs were analyzed for bulk density using the paraffin-coated clod method. Total organic C was determined using dry combustion. Aluminum was determined on 0.2M sodium pyrophosphate (pH 9.5) extracts using atomic absorption spectroscopy.

Soil thin sections were prepared from selected slabs representing the median strength determination for each clod. Air dried samples were impregnated using a 60:40 mixture of Castolite:monomeric styrene. After about 1 week, the samples were hardened by exposing them to a 5 Mrad dose of γ radiation. Thin sections were analyzed by transmitted light microscopy and scanning electron microscopy using a JEOL model JXA-840A electron microscope/microprobe equipped with an energy dispersive spectrometer.

The statistical design used in data analysis was completely randomized in which a group composed of a friable, an intermediate, and a cemented clod was treated as a replication. The location sites and the qualitative strength field assessments (*i.e.* friable, intermediate or cemented) were the main class variables. Multiple determinations from the slabs obtained from the same clods were used in the analysis. The determination error associated with the multiple determinations was partitioned from the general experimental error so as not to bias the analysis. Determination and experimental error were pooled when they were not significantly different (p > 0.25). A general linear model (GLM) procedure was used to perform analysis of variance on penetrometer, MOR, C, Al and bulk density measurements. Type III sums of squares were used for comparisons in the analysis of variance to account for unequal sample sizes where it was not possible to have complete groupings of five replications of friable, intermediate, and cemented clods. A minimum of three replications were used at all times.

Table 1
Summary of Statistical Significance.

	Penetrometer Strength	Modulus of Rupture Strength	Total Carbon	Pyrophosphate Extractable Aluminum	Bulk Density
Site	**	**	**	**	*
Consistence Group	**	**	**	*	*
Site × Group Interaction	**		**	*	NS

*, ** indicates statistical significance at 0.05 and 0.01 respectively; ns indicates non-significance at the 0.05 level.

Table 2
Comparisons of means of various parameters arranged by site and field moist consistence grouping. Values within the same row which are followed by the same letter are not significantly different at the 0.05 level.

Parameters	Site B			Site A		
	Friable	Intermediate	Cemented	Friable	Intermediate	Cemented
Penetrometer Strength (kg/cm^2)	0.126^a	0.217^a	0.533^b	0.184^a	0.582^b	1.377^c
Modulus of Rupture	0.415^{ab}	0.232^a	0.700^c	0.650^c	0.464^{bc}	0.843^d
Total Carbon	1.91^{bc}	1.20^a	1.40^{ab}	3.40^d	3.57^d	2.04^c
Aluminum (pyrophosphate)	0.39^a	0.35^a	0.40^a	0.76^b	0.96^c	0.94^c
Bulk Density	1.54^{bc}	1.57^{bc}	1.75^c	1.28^a	1.38^{ab}	1.58^{bc}

Means were compared following a significant F-statistic using student's t-tests. A correlation analysis was performed to determine if consistent patterns were occurring among the dependent variable measurements. All statistical procedures were performed using the SAS system for analysis (SAS, 1985).

RESULTS AND DISCUSSION

Strength Measurements

When penetrometer strength measurements (saturated soils) were compared for the various field (moist) consistence groups from two sites, significant differences ($\alpha = 0.05$) were found between the groups (Table 2). At a given site, the strength of groups were ordered, as expected, as cemented > intermediate > friable. There were also significant differences between the sampling sites (Table 1). As previously suggested, we postulate that the increased strength in the indurated samples is due to some sort of cementation.
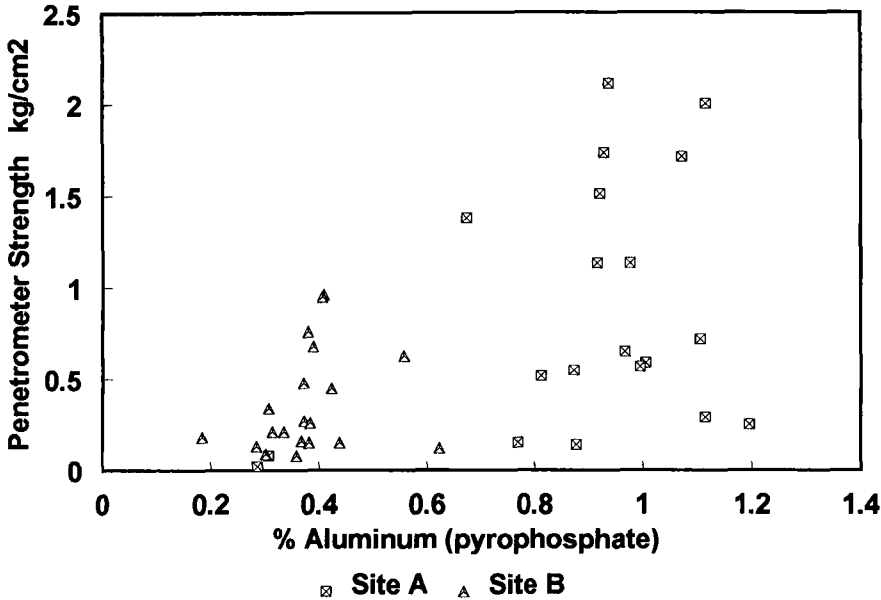
Fig. 2. Pyrophosphate extractable aluminum vs. strength (kg/cm^2) of saturated soil as determined by penetrometer. The correlation coefficient was only 0.54, but still significant at the 0.01 level.

Significant differences between groups were also observed in strength determinations using Modulus of Rupture (Table 2). At a given site, the "cemented" samples always had significantly greater strength than the other two groups. The friable group, however, had greater strength (though not significantly so) than the intermediate group. This contrast in strength measurements between the penetrometer and the modulus of rupture is likely related to differences in the moisture content at the time of measurement. The penetrometer determinations were done at saturation while the MOR determinations were done at air dryness. It is postulated that greater quantities of organic matter (Table 2) or clay in the friable (when moist) samples may yield additional strength under air dry conditions.

Chemical Extractions

Silica
Some workers have suggested that some forms of Si, such as allophane, may be constituents of grain coatings in spodosols. Silica was therefore measured in selected samples which were extracted using the dithionite-citrate-buffer (DCB) procedure (Kittrick and Hope, 1963). The quantities of Si determined were generally below the detection limit. Therefore, the hypothesis that Si might be an important cementing agent was discarded and Si determinations were not made for the remainder of the samples.
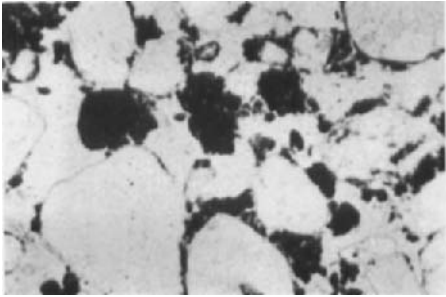
Fig. 3. Intergrain microaggregate microstructure and an enaulic related distribution pattern of friable sample from site A; plane polarized light (PPL); frame width (FW) 1.2 mm.

Iron

Because Fe is a common constituent in spodic horizons of better drained spodosols, some have postulated that secondary Fe may contribute to the cementation and strength characteristics of these soils. The poorly drained (reducing) and highly permeable (sandy) nature of the Aquods on the Delmarva Peninsula have resulted in extractable Fe levels (DCB, pyrophosphate and acid ammonium oxalate) which commonly approach the detection limit of the analysis (<0.1g kg^{-1}). Levels in the horizons sampled in this study ranged from 0.0 to 0.2 g kg^{-1}. We concluded, therefore, that Fe was not responsible for the induration observed in these materials.

Total Carbon

As commonly occurs in spodic horizons, the C content in these materials was high (Table 2) (mean %C = 2.2 and ranging from 0.6 to 5.7%). Within a given site there appears to be an inverse relationship between total C and moist (penetrometer) strength. Furthermore, the strongest significant differences in organic C levels were found between sites (Table 1). Therefore, while total organic C is an important component of spodic horizons, this parameter cannot explain the induration of ortstein in these soils.

Aluminum

Previous work had shown that sodium pyrophosphate and acid ammonium oxalate both extract similar amounts of Al from these spodosols (Condron, 1990) Pyrophosphate extractable Al was significantly correlated with penetrometer strength although there were clear effects caused by differences between sites (Fig. 2 and Tables 1 and 2). While this relationship was significant at the 0.01 level, the correlation coefficient was only 0.54 indicating that there is a great deal of variability in strength which is not related to the Al content of the samples.

As indicated in Table 2, the mean values for extractable Al were not significantly different between consistence classes at site B although there were significant differences between the cemented and friable samples in site A. Aluminum levels in samples analyzed from sites B and A in this study ranged from 0.39 to 0.76 and from 0.40 to 1.38, respectively. These values were generally higher and more variable than those observed by Lee *et al.*, (1988a) for samples in Florida. They observed a significant difference in Dithionite-Citrate-Bicarbonate (DCB) extractable Al between indurated and friable materials with the ortstein ranging from 0.25 to
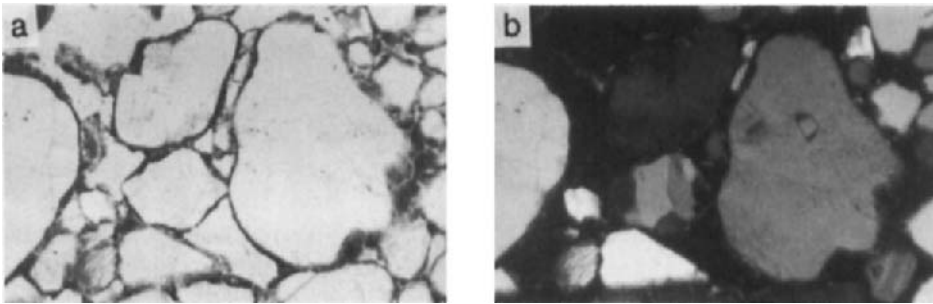
Fig. 4. Pellicular or bridged grain microstructure and a chitonic-gefuric related distribution pattern of ortstein sample from site A; a) PPL; b) cross polarized light; FW 1.2 mm.
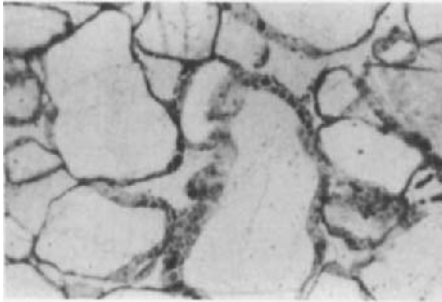
Fig. 5. Cracked organic-rich fine material coating sand grains in ortstein sample from site B, constituting a chitonic-gefuric related distribution pattern; PPL; FW 1.2 mm.

0.65% extractable Al and the friable materials ranging from 0.04 to 0.15% Al. Thus, many friable samples had higher levels of extractable Al than the ortstein samples in Florida.

Micromorphology

Microscopic observations were very enlightening and provided insight into fundamental differences between the cemented and friable samples. The friable samples were characterized by an intergrain microaggregate microstructure and an enaulic related distribution pattern (Fig. 3). The framework sand grains were largely uncoated. The fine material consisted of polymorphic organic material (or black or dark brown monomorphic fine material) with some small amounts of silt and clay. The fine material was loosely aggregated into silt and fine sand sized, irregularly shaped aggregates, which in some cases formed bridges between the framework grains.

In distinct contrast, the ortstein samples had a pellicular or bridged grain microstructure and a chitonic or gefuric related distribution pattern (Fig. 4a). In plane light, the fine material appeared as brown or reddish-brown monomorphic organic material which coated the framework grains. Some of the coatings showed cracking patterns (Fig. 5) commonly reported by others (McSweeney and FitzPatrick, 1990). More commonly, the coatings were continuous

and fairly thin (10 - 50 μm). In cross polarized light, the bulk of the coatings were isotropic, but within some, a thin coating that appears to be weakly oriented silicate clay was visible (Fig. 4b). This birefringent material was generally adjacent to the sand grains and interior to the amorphous organic-rich coatings.

Scanning Electron Microscopy

Some workers studying ortstein have suggested that the material coating and bridging framework grains is enriched in Al and have concluded that the cementing material is an Al rich amorphous compound (Lee *et al.*, 1988a; McHardy and Robertson, 1983). In an attempt to test this hypotheses, thin sections were selected which had been prepared from contrasting samples collected from site A. One was from a strongly indurated ortstein (1.38 kg/cm^2) and the other from a friable sample (0.14 kg/cm^2). The fine materials coating (ortstein) or surrounding (friable) the framework sand grains were compared using SEM and EDX microchemical analyses. Using an analytical computer program coupled with the EDX system, Al and Si were quantified and Al:Si ratios were calculated at 8 to 12 points on each slide. The mean Al:Si ratios for the ortstein and friable samples were 0.47 (range 0.36 to 0.56) and 0.36 (range 0.27 to 0.43), respectively. Although there is considerable overlap in the range in Al:Si ratio, a means comparison test indicated that the Al:Si ratios of these samples were significantly different at the 0.01 level. This observation, in conjunction with data on extractable Al, might lead one to conclude that an Al cementing agent might be involved in the greater strength of the ortstein.

In examining the illuvial clay from the lamellae in a Bt horizon of a somewhat excessively drained soil formed in similar eolian sands approximately 1 km away, the Al:Si ratio of was determined to be 0.594, considerably higher than the fine materials in either of the two spodic horizons examined. Assuming that this clay was similar in mineralogy to the weakly oriented clay in the grain coatings of the ortstein sample (Fig. 4b), the higher Al:Si ratio in the ortstein coatings might be attributed, in part, to the presence of silicate clays.

CONCLUSIONS

The field classification of moist consistence of spodic horizon materials corresponds well with the unconfined saturated strength determinations by penetrometer. The indurated nature of the ortstein samples is not a result of cementation by either Si or Fe, and strength of the soil materials appears to be inversely related to total organic C content. Strength of the indurated materials is most closely related to the presence of monomorphic coatings of fine materials bridging framework sand grains. These coatings are expressed micromorphologically as chitonic-gefuric related distribution patterns. A pyrophosphate extractable Al phase may be present in the bridging material, but the levels of total Al (and Al:Si ratios) are not dramatically different from the intergranular fine material in the friable materials. Silicate clays identified in coatings in the ortstein may be partially responsible for the greater strength of these materials. Ignorance of the presence of silicate clays within the coatings may lead to the erroneous interpretation of EDX data, resulting in overestimations of the importance of amorphous Al compounds in the formation of ortstein. Overall, the related distribution of the coarse and fine materials (microfabric) is much more informative concerning the strength of the materials, than chemical characteristics of the samples.

REFERENCES

Collins, M.E., 1990. Aquods. In: J.M. Kimble and R.D. Yeck (Editors), Proceedings from the Fifth International Soil Correlation Meeting (ISCOM V) Characterization, Classification, and Utilization of Spodosols. USDA, SCS, Lincoln, Nebraska, pp. 105-122.

Condron, M.A., 1990. Soils with Spodic Characteristics on the Eastern Shore of Maryland. M.S. Thesis. University of Maryland at College Park. 109 pp.

Daniels, R.B., Gamble, E.E. and C.S. Holzhey., 1975. Thick Bh horizons in the N. Carolina coastal plains: Morphology and relations to texture and soil ground water. Soil Sci. Soc. Am. Proc., 39: 1177-1181.

Denny, C.S. and Owens, J.P., 1979. Sand dunes on the central Delmarva Peninsula, Maryland and Delaware. U.S. Geol. Survey Prof. Paper 1067-A.

ICOMOD, 1991. Circular letter #10 of the International Committee on Spodosols, with proposed modifications to Keys to Soil Taxonomy. USDA-SCS, National Technical Center, Lincoln, Nebraska.

Kittrick, J.A. and Hope, E.W., 1963. A procedure for the particle size separation of soils for XRD analysis. Soil Sci., 96: 319-323.

Lee, F.Y., Yuan, T.L. and Carlisle, V.W., 1988a. Nature of cementing materials in ortstein horizons of selected Florida Spodosols: I. Constituents of cementing materials. Soil Sci. Soc. Am. J., 52: 1411-1418.

Lee, F.Y., Yuan, T.L. and Carlisle, V.W., 1988b. Nature of cementing materials in ortstein horizons of selected Florida Spodosols: II. Soil properties and chemical form(s) of aluminum. Soil Sci. Soc. Am. J., 52: 1796-1801.

McHardy, W.J. and Robertson, L., 1983. An optical scanning microscopic and microanalytical study of cementation in some podzols. Geoderma, 30: 160-171.

McSweeney, K. and FitzPatrick, E.A., 1990. Microscopic characterization of the spodic horizon. In: J.M. Kimble and R.D. Yeck (Editors), Proceedings from the Fifth International Soil Correlation Meeting (ISCOM V) Characterization, Classification, and Utilization of Spodosols. USDA, SCS, Lincoln, Nebraska, pp. 211-220.

Reeve, R.C. 1965. Modulus of rupture. In: C.A. Black (Editor), Methods of Soil Analysis, Part 1. Agron. Monogr. 9. Am. Soc. Agron., Madison, Wisconsin, pp. 466-471.

SAS, 1985. SAS User's Guide: Statistics. Version 5 Edition, Statistical Analysis Inst., Cary, North Carolina.

Soil Survey Staff, 1990. Keys to Soil Taxonomy. SMSS Technical Monograph No.6, 4th editon. Virginia Polytechnic Institute and State University, Blacksburg, Virginia, 422 pp.

This Page Intentionally Left Blank

Author index

Subject index

(Entries refer to the first page of relevant papers)